ISSN 2307-8960 (online)

World Journal of *Clinical Cases*

World J Clin Cases 2022 June 26; 10(18): 5934-6340



Published by Baishideng Publishing Group Inc

WJCC

World Journal of Clinical Cases

Contents

Thrice Monthly Volume 10 Number 18 June 26, 2022

MINIREVIEWS

5934 Development of clustered regularly interspaced short palindromic repeats/CRISPR-associated technology for potential clinical applications

Huang YY, Zhang XY, Zhu P, Ji L

5946 Strategies and challenges in treatment of varicose veins and venous insufficiency

Gao RD, Qian SY, Wang HH, Liu YS, Ren SY

5957 Diabetes mellitus susceptibility with varied diseased phenotypes and its comparison with phenome interactome networks

Rout M, Kour B, Vuree S, Lulu SS, Medicherla KM, Suravajhala P

ORIGINAL ARTICLE

Clinical and Translational Research

5965 Identification of potential key molecules and signaling pathways for psoriasis based on weighted gene co-expression network analysis

Shu X, Chen XX, Kang XD, Ran M, Wang YL, Zhao ZK, Li CX

5984 Construction and validation of a novel prediction system for detection of overall survival in lung cancer patients

Zhong C, Liang Y, Wang Q, Tan HW, Liang Y

Case Control Study

6001 Effectiveness and postoperative rehabilitation of one-stage combined anterior-posterior surgery for severe thoracolumbar fractures with spinal cord injury

Zhang B, Wang JC, Jiang YZ, Song QP, An Y

Retrospective Study

6009 Prostate sclerosing adenopathy: A clinicopathological and immunohistochemical study of twelve patients

Feng RL, Tao YP, Tan ZY, Fu S, Wang HF

6021 Value of magnetic resonance diffusion combined with perfusion imaging techniques for diagnosing potentially malignant breast lesions

Zhang H, Zhang XY, Wang Y

6032 Scar-centered dilation in the treatment of large keloids

Wu M, Gu JY, Duan R, Wei BX, Xie F

6039 Application of a novel computer-assisted surgery system in percutaneous nephrolithotomy: A controlled study

Qin F, Sun YF, Wang XN, Li B, Zhang ZL, Zhang MX, Xie F, Liu SH, Wang ZJ, Cao YC, Jiao W

World Journal of Clinical Cases

Thrice Monthly Volume 10 Number 18 June 26, 2022

Contents

6050 Influences of etiology and endoscopic appearance on the long-term outcomes of gastric antral vascular ectasia

Kwon HJ, Lee SH, Cho JH

Randomized Controlled Trial

6060 Evaluation of the clinical efficacy and safety of TST33 mega hemorrhoidectomy for severe prolapsed hemorrhoids

Tao L, Wei J, Ding XF, Ji LJ

6069 Sequential chemotherapy and icotinib as first-line treatment for advanced epidermal growth factor receptor-mutated non-small cell lung cancer

Sun SJ, Han JD, Liu W, Wu ZY, Zhao X, Yan X, Jiao SC, Fang J

Randomized Clinical Trial

6082 Impact of preoperative carbohydrate loading on gastric volume in patients with type 2 diabetes

Lin XQ, Chen YR, Chen X, Cai YP, Lin JX, Xu DM, Zheng XC

META-ANALYSIS

6091 Efficacy and safety of adalimumab in comparison to infliximab for Crohn's disease: A systematic review and meta-analysis

Yang HH, Huang Y, Zhou XC, Wang RN

CASE REPORT

6105 Successful treatment of acute relapse of chronic eosinophilic pneumonia with benralizumab and without corticosteroids: A case report

Izhakian S, Pertzov B, Rosengarten D, Kramer MR

6110 Pembrolizumab-induced Stevens-Johnson syndrome in advanced squamous cell carcinoma of the lung: A case report and review of literature

Wu JY, Kang K, Yi J, Yang B

6119 Hepatic epithelioid hemangioendothelioma after thirteen years' follow-up: A case report and review of literature

Mo WF, Tong YL

6128 Effectiveness and safety of ultrasound-guided intramuscular lauromacrogol injection combined with hysteroscopy in cervical pregnancy treatment: A case report

Ye JP, Gao Y, Lu LW, Ye YJ

6136 Carcinoma located in a right-sided sigmoid colon: A case report

Lyu LJ, Yao WW

6141 Subcutaneous infection caused by *Mycobacterium abscessus* following cosmetic injections of botulinum toxin: A case report

Deng L, Luo YZ, Liu F, Yu XH

World Journal of Clinical Cases

Thrice Monthly Volume 10 Number 18 June 26, 2022

Contents

6148 Overlapping syndrome of recurrent anti-N-methyl-D-aspartate receptor encephalitis and anti-myelin oligodendrocyte glycoprotein demyelinating diseases: A case report

Yin XJ, Zhang LF, Bao LH, Feng ZC, Chen JH, Li BX, Zhang J

6156 Liver transplantation for late-onset ornithine transcarbamylase deficiency: A case report

Fu XH, Hu YH, Liao JX, Chen L, Hu ZQ, Wen JL, Chen SL

6163 Disseminated strongyloidiasis in a patient with rheumatoid arthritis: A case report

Zheng JH, Xue LY

6168 *CYP27A1* mutation in a case of cerebrotendinous xanthomatosis: A case report

Li ZR, Zhou YL, Jin Q, Xie YY, Meng HM

6175 Postoperative multiple metastasis of clear cell sarcoma-like tumor of the gastrointestinal tract in adolescent: A case report

Huang WP, Li LM, Gao JB

6184 Toripalimab combined with targeted therapy and chemotherapy achieves pathologic complete response in gastric carcinoma: A case report

Liu R, Wang X, Ji Z, Deng T, Li HL, Zhang YH, Yang YC, Ge SH, Zhang L, Bai M, Ning T, Ba Y

6192 Presentation of Boerhaave's syndrome as an upper-esophageal perforation associated with a right-sided pleural effusion: A case report

Tan N, Luo YH, Li GC, Chen YL, Tan W, Xiang YH, Ge L, Yao D, Zhang MH

6198 Camrelizumab-induced anaphylactic shock in an esophageal squamous cell carcinoma patient: A case report and review of literature

Liu K, Bao JF, Wang T, Yang H, Xu BP

6205 Nontraumatic convexal subarachnoid hemorrhage: A case report

Chen HL, Li B, Chen C, Fan XX, Ma WB

6211 Growth hormone ameliorates hepatopulmonary syndrome and nonalcoholic steatohepatitis secondary to hypopituitarism in a child: A case report

Zhang XY, Yuan K, Fang YL, Wang CL

6218 Vancomycin dosing in an obese patient with acute renal failure: A case report and review of literature

Xu KY, Li D, Hu ZJ, Zhao CC, Bai J, Du WL

6227 Insulinoma after sleeve gastrectomy: A case report

Lobaton-Ginsberg M, Sotelo-González P, Ramirez-Renteria C, Juárez-Aguilar FG, Ferreira-Hermosillo A

6234 Primary intestinal lymphangiectasia presenting as limb convulsions: A case report

Cao Y, Feng XH, Ni HX

6241 Esophagogastric junctional neuroendocrine tumor with adenocarcinoma: A case report

Kong ZZ, Zhang L

World Journal of Clinical Cases

Thrice Monthly Volume 10 Number 18 June 26, 2022

Contents

6247 Foreign body granuloma in the tongue differentiated from tongue cancer: A case report

Jiang ZH, Xv R, Xia L

6254 Modified endoscopic ultrasound-guided selective N-butyl-2-cyanoacrylate injections for gastric variceal hemorrhage in left-sided portal hypertension: A case report

Yang J, Zeng Y, Zhang JW

6261 Management of type IIIb dens invaginatus using a combination of root canal treatment, intentional replantation, and surgical therapy: A case report

Zhang J, Li N, Li WL, Zheng XY, Li S

6269 Clivus-involved immunoglobulin G4 related hypertrophic pachymeningitis mimicking meningioma: A case report

Yu Y, Lv L, Yin SL, Chen C, Jiang S, Zhou PZ

6277 *De novo* brain arteriovenous malformation formation and development: A case report

Huang H, Wang X, Guo AN, Li W, Duan RH, Fang JH, Yin B, Li DD

6283 Coinfection of *Streptococcus suis* and *Nocardia asiatica* in the human central nervous system: A case report

Chen YY, Xue XH

6289 Dilated left ventricle with multiple outpouchings — a severe congenital ventricular diverticulum or left-dominant arrhythmogenic cardiomyopathy: A case report

Zhang X, Ye RY, Chen XP

6298 Spontaneous healing of complicated crown-root fractures in children: Two case reports

Zhou ZL, Gao L, Sun SK, Li HS, Zhang CD, Kou WW, Xu Z, Wu LA

6307 Thyroid follicular renal cell carcinoma excluding thyroid metastases: A case report

Wu SC, Li XY, Liao BJ, Xie K, Chen WM

6314 Appendiceal bleeding: A case report

Zhou SY, Guo MD, Ye XH

6319 Spontaneous healing after conservative treatment of isolated grade IV pancreatic duct disruption caused by trauma: A case report

Mei MZ, Ren YF, Mou YP, Wang YY, Jin WW, Lu C, Zhu QC

6325 Pneumonia and seizures due to hypereosinophilic syndrome—organ damage and eosinophilia without synchronisation: A case report

Ishida T, Murayama T, Kobayashi S

6333 Creutzfeldt-Jakob disease presenting with bilateral hearing loss: A case report

Na S, Lee SA, Lee JD, Lee ES, Lee TK

LETTER TO THE EDITOR

6338 Stem cells as an option for the treatment of COVID-19

Cuevas-González MV, Cuevas-González JC

Contents

ABOUT COVER

Editorial Board Member of *World Journal of Clinical Cases*, Cristina Tudoran, PhD, Assistant Professor, Department VII, Internal Medicine II, Discipline of Cardiology, "Victor Babes" University of Medicine and Pharmacy Timisoara, Timisoara 300041, Timis, Romania. cristina13.tudoran@gmail.com

AIMS AND SCOPE

The primary aim of *World Journal of Clinical Cases* (*WJCC*, *World J Clin Cases*) is to provide scholars and readers from various fields of clinical medicine with a platform to publish high-quality clinical research articles and communicate their research findings online.

WJCC mainly publishes articles reporting research results and findings obtained in the field of clinical medicine and covering a wide range of topics, including case control studies, retrospective cohort studies, retrospective studies, clinical trials studies, observational studies, prospective studies, randomized controlled trials, randomized clinical trials, systematic reviews, meta-analysis, and case reports.

INDEXING/ABSTRACTING

The *WJCC* is now indexed in Science Citation Index Expanded (also known as SciSearch®), Journal Citation Reports/Science Edition, Scopus, PubMed, and PubMed Central. The 2021 Edition of Journal Citation Reports® cites the 2020 impact factor (IF) for *WJCC* as 1.337; IF without journal self cites: 1.301; 5-year IF: 1.742; Journal Citation Indicator: 0.33; Ranking: 119 among 169 journals in medicine, general and internal; and Quartile category: Q3. The *WJCC*'s CiteScore for 2020 is 0.8 and Scopus CiteScore rank 2020: General Medicine is 493/793.

RESPONSIBLE EDITORS FOR THIS ISSUE

Production Editor: *Ying-Yi Yuan*; **Production Department Director:** *Xu Guo*; **Editorial Office Director:** *Jin-Lei Wang*.

NAME OF JOURNAL

World Journal of Clinical Cases

ISSN

ISSN 2307-8960 (online)

LAUNCH DATE

April 16, 2013

FREQUENCY

Thrice Monthly

EDITORS-IN-CHIEF

Bao-Gan Peng, Jerzy Tadeusz Chudek, George Kontogeorgos, Maurizio Serati, Ja Hyeon Ku

EDITORIAL BOARD MEMBERS

https://www.wjgnet.com/2307-8960/editorialboard.htm

PUBLICATION DATE

June 26, 2022

COPYRIGHT

© 2022 Baishideng Publishing Group Inc

INSTRUCTIONS TO AUTHORS

https://www.wjgnet.com/bpg/gerinfo/204

GUIDELINES FOR ETHICS DOCUMENTS

https://www.wjgnet.com/bpg/GerInfo/287

GUIDELINES FOR NON-NATIVE SPEAKERS OF ENGLISH

https://www.wjgnet.com/bpg/gerinfo/240

PUBLICATION ETHICS

https://www.wjgnet.com/bpg/GerInfo/288

PUBLICATION MISCONDUCT

https://www.wjgnet.com/bpg/gerinfo/208

ARTICLE PROCESSING CHARGE

https://www.wjgnet.com/bpg/gerinfo/242

STEPS FOR SUBMITTING MANUSCRIPTS

https://www.wjgnet.com/bpg/GerInfo/239

ONLINE SUBMISSION

https://www.f6publishing.com

© 2022 Baishideng Publishing Group Inc. All rights reserved. 7041 Koll Center Parkway, Suite 160, Pleasanton, CA 94566, USA

E-mail: bpgoffice@wjgnet.com https://www.wjgnet.com

World Journal of Clinical Cases

Submit a Manuscript: https://www.f6publishing.com

World J Clin Cases 2022 June 26; 10(18): 5934-5945

DOI: 10.12998/wjcc.v10.i18.5934

ISSN 2307-8960 (online)

MINIREVIEWS

Development of clustered regularly interspaced short palindromic repeats/CRISPR-associated technology for potential clinical applications

Yue-Ying Huang, Xiao-Yu Zhang, Ping Zhu, Ling Ji

Specialty type: Biochemistry and molecular biology

Provenance and peer review: Unsolicited article; Externally peer reviewed.

Peer-review model: Single blind

Peer-review report's scientific quality classification

Grade A (Excellent): 0
Grade B (Very good): B
Grade C (Good): C
Grade D (Fair): 0
Grade E (Poor): 0

P-Reviewer: Asmamaw M, Ethiopia; Cho YS, South Korea

Received: November 3, 2021
Peer-review started: November 3, 2021
First decision: December 27, 2021
Revised: January 10, 2022
Accepted: April 24, 2022
Article in press: April 24, 2022
Published online: June 26, 2022

Yue-Ying Huang, Xiao-Yu Zhang, Ping Zhu, School of Medical Laboratory, Weifang Medical University, Weifang 261053, Shandong Province, China

Ling Ji, Department of Laboratory Medicine, Peking University Shenzhen Hospital, Shenzhen 518035, Guangdong Province, China

Corresponding author: Ling Ji, Doctor, Chief Technician, Department of Laboratory Medicine, Peking University Shenzhen Hospital, No. 1120 Lianhua Road, Futian District, Shenzhen 518035, Guangdong Province, China. 1120303921@qq.com

Abstract

The clustered regularly interspaced short palindromic repeats (CRISPR)-CRISPR-associated (Cas) proteins constitute the innate adaptive immune system in several bacteria and archaea. This immune system helps them in resisting the invasion of phages and foreign DNA by providing sequence-specific acquired immunity. Owing to the numerous advantages such as ease of use, low cost, high efficiency, good accuracy, and a diverse range of applications, the CRISPR-Cas system has become the most widely used genome editing technology. Hence, the advent of the CRISPR/Cas technology highlights a tremendous potential in clinical diagnosis and could become a powerful asset for modern medicine. This study reviews the recently reported application platforms for screening, diagnosis, and treatment of different diseases based on CRISPR/Cas systems. The limitations, current challenges, and future prospectus are summarized; this article would be a valuable reference for future genome-editing practices.

Key Words: CRISPR-Cas; Gene editing; Molecular diagnostics; Gene targeting

©The Author(s) 2022. Published by Baishideng Publishing Group Inc. All rights reserved.

Core Tip: This review mainly discusses and explores the potential clinical applications of the clustered regularly interspaced short palindromic repeats (CRISPR)/CRISPR-associated (Cas) technology. The detection technologies for nucleic acids and small molecules of different pathogens based on the CRISPR/Cas system are summarized. The advantages and disadvantages of the CRISPR/Cas technology from the aspects of gene editing, disease treatment, multi-drug resistance, and treatment are enumerated, asserting that CRISPR/Cas system has unlimited potential in clinical applications with certain challenges.

Citation: Huang YY, Zhang XY, Zhu P, Ji L. Development of clustered regularly interspaced short palindromic repeats/CRISPR-associated technology for potential clinical applications. *World J Clin Cases* 2022; 10(18): 5934-5945
URL: https://www.wjgnet.com/2307-8960/full/v10/i18/5934.htm
DOI: https://dx.doi.org/10.12998/wjcc.v10.i18.5934

INTRODUCTION

The clustered regularly interspaced short palindromic repeats (CRISPR)/CRISPR-associated (Cas) system, an adaptive immune system present in numerous bacteria and archaea, is a nucleic acid-targeted defense mechanism composed of numerous short and conserved repeat regions and spacers that protect themselves from exogenous mobile genetic elements such as plasmids and phages. A similar arrangement in the chromosomes of Gram-negative bacteria (*Escherichia coli, E. coli*) was also reported by Ishino *et al* in 1987 and was again confirmed in 2010[1]. The type II CRISPR/Cas system from *Streptococcus pyogenes* could specifically recognize and cleave target DNA guided by gRNA[2]; thus, laying the foundation for the development and utilization of the CRISPR/Cas system. Over the past few years, several CRISPR/Cas systems belonging to Cas proteins with different characteristics have been developed, which in turn have produced many CRISPR/Cas system-related toolboxes, offering functional robustness, efficiency, and ease of implementation in multiple organisms[3]. Various gene-editing tools based on CRISPR/Cas9 were introduced in 2013[4], followed by successful implementation in the modern medical field. Within a few years, CRISPR/Cas technology gradually made crucial breakthroughs and is now widely employed in gene-editing, treatment of genetic diseases, clinical diagnosis of common pathogenic molecules, and alleviating antimicrobial resistance. This review compiles the recent advancements in CRISPR technology and summarizes the achievements of CRISPR/Cas technology in clinical applications to provide opportunities for programmable genomic editing for translational medicine.

CLASSIFICATION OF CRISPR/CAS SYSTEM

In CRISPR/Cas systems, researchers have discovered various Cas proteins with different characteristics. There are two classes of CRISPR/Cas systems based on the composition of their effector subunits, Classes 1 and 2 (Table 1). Class 1 system contains numerous RNA-effector complexes, and Class 2 system comprises a solitary protein like Cas 9 that conducts all effector complex activities[4]. The Class 1 CRISPR–Cas system includes type I, III, and putative IV subtypes. The type I subtype contains the signature gene Cas3 encoding a single-stranded DNA (ssDNA), which acts as a candidate for guiding cascade in type I CRISPR module like Cas8 for DNA invasion, but this theory has not been thoroughly investigated. The type III CRISPR-Cas system containing gene Cas10 includes nonspecific degradation of both ssDNA and RNA molecules and requires the target DNA transcription for immunity[5,6]. The Cas10 subunit cleaves the transcribed ssDNA and activates the Csm6 nonspecific-RNase activity, while as the Csm^3 cleaves the RNA target, the RuvC domain introduces staggered double-stranded DNA (dsDNA) breaks[7-9]. Since the Cas10 subunit HD domain cleaves ssDNA from the transcription bubble [10-12], due to activation of the Palm domain, ATP is converted into four or six-member cyclic oligoadenylate (CoA) rings. These six-member CoA rings then act as a secondary messenger and activate Csm6 by binding to its CARF (CRISPR-Associated Rossman Fold) domain, causing activation of the Higher Eukaryotes and Prokaryotes Nucleotide-binding (HEPN) domain and unleashing nonspecific RNA cleavage[13-15]. Putative type IV CRISPR/Cas systems include a large subunit, Csf1, Cas5, and Cas7 (a solitary unit), and usually lack the known Cas proteins involved in adaptation and target cleavage[16].

Class 2 effectors are composed of a single Cas unit that associates with the CRISPR RNAs (crRNA) for gene targeting in various biotechnological applications. This class includes CRISPR types II, V, and VI. Type II uses the mature crRNA directed CRISPR-associated protein Cas9 base-paired to trans-activating crRNA (tracrRNA) while introducing double-stranded breaks (DSB) in target DNA (Figure 1). Although Cas9 also harbors RuvC and HNH domains, at sites complementary to the crRNA-guide sequence, the

Table 1 Features of clustered regularly interspaced short palindromic repeats/CRISPR-associated system

CRISPR type		Specific cleavage	Collateral cleavage	Secondary messenger	CRISPR inhibitors	Ref.
Class 1	I (Cas8)	DNA	Not identified to date	Not identified to date	Yes	[4]
	III (Cas10)	RNA	RNA, ssDNA	cOA	Not identified to date	[6-8]
	IV (Csf1)	Not studied yet	Not studied yet	Not studied yet	Not studied yet	[16]
Class 2	II (Cas9)	DNA	Not identified to date	Not identified to date	Yes	[4,5,16-20]
	V (Cas12, Cas14)	DNA	ssDNA	Not identified to date	Yes	[21-23]
	VI (Cas13)	RNA	RNA	Not identified to date	Not identified to date	[24-26]

CRISPR: Clustered regularly interspaced short palindromic repeats; ssDNA: Single-stranded DNA; cOA: Cyclic oligoadenylate.

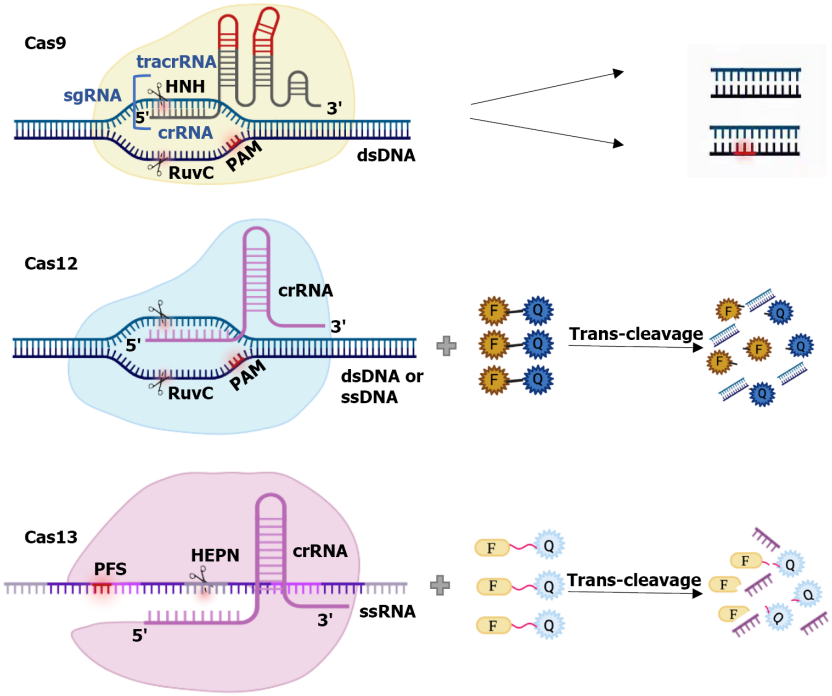

DOI: 10.12998/wjcc.v10.i18.5934 **Copyright** ©The Author(s) 2022.

Figure 1 Collateral activity of Cas9, Cas12 and Cas13. PAM: Protospacer adjacent motif; dsDNA: Double-stranded DNA; ssDNA: Single-stranded DNA; crRNA: Clustered regularly interspaced short palindromic repeats RNAs; HEPN: Higher Eukaryotes and Prokaryotes Nucleotide-binding.

Cas9 HNH nuclease domain cleaves the complementary strand. In contrast, the Cas9 RuvC-like domain cleaves the noncomplementary strand, thereby stressing the fact that target recognition by Cas9 requires both a seed sequence in the crRNA as well as a GG dinucleotide-containing protospacer adjacent motif (PAM) sequence adjacent to the crRNA-binding region in the DNA target[2,16-20]. The majority of type V CRISPR modules can recognize dsDNA targets. For instance, a single crRNA processed by Cas12 RNase domain guides Cas12 with a T-rich PAM sequence to cleave dsDNA targets, generating sticky ends[21] (Figure 1). Cas12a cleaves both the target and non-target strands of a targeted dsDNA by a single active site in the RuvC catalytic pocket[22]. Besides Cas12, Cas14 is the smallest RNA-guided nuclease discovered to date with 400-700 amino acids and does not require a target sequence such as PAM in the ssDNA substrate[23]. Lastly, Cas13 (also named C2c2) belongs to type VI recognizing RNA targets. A study discovered that Cas13 has two HEPN domains commonly associated with ribonucleases (RNases)-one for cutting its RNA target and the other for processing the crRNA[24-26] (Figure 1). It is also suggested that both type V and VI CRISPR modules work collaterally, *i.e.*, Cas12 and Cas14 can cleave ssDNA nonspecifically. In contrast, Cas13 can initiate nonspecific RNA cutting[16], which has not been observed when Cas12, Cas14, and Cas13 have been applied in either human or plant cell lines[27,28].

CLINICAL APPLICATION OF CRISPR/CAS TECHNOLOGY

Application of CRISPR/Cas technology in clinical disease diagnosis

Application of CRISPR/Cas technology in pathogen detection: Zhang *et al*[24] developed a detection platform called Specific High-sensitivity Enzymatic Reporter Unlocking (SHERLOCK) that combined isothermal amplification and Cas13a technology for the detection of either single DNA or RNA molecules. As activated Cas13 cleaves quenchable fluorescent RNA, it produces a quantifiable signal indicating the presence of the target nucleic acid (Figure 1). SHERLOCK was demonstrated to detect closely related Zika virus and dengue virus due to its property of rapidly detecting nucleic acids with high sensitivity. Subsequently, SHERLOCK was updated to SHERLOCKv2, based on simple four-channel multiplexing with orthogonal nucleic acid sequences of LwaCas13a, PsmCas13b, CcaCas13b, and AsCas12a[29], breaking through the quantitative and fluorescence limitations of SHERLOCK. SHERLOCKv2 uses fewer primers during the pre-amplification process to achieve better quantification without affecting sensitivity. Furthermore, the introduction of the test strip aids in determining whether the target DNA or RNA is present in the sample by visualization. SHERLOCKv2, due to its efficiency, specificity, ease of use, and portability, can detect ssRNA of dengue or Zika virus, as well as mutations in liquid biopsy samples from patients by the lateral flow assay system. Chen *et al*[30] also reported that Cas12a could be used as a potential nucleic acid detection platform and developed DNA endonuclease-targeted CRISPR trans reporter (DETECTR), whose working principle was similar to that of SHERLOCK as this platform used isothermal amplification and Cas12a ssDNase activation for detection (Figure 1). Their system could specifically identify two human papillomavirus strains [Human papillomavirus (HPV16) and HPV18] from human SiHa and HeLa cells with higher accuracy.

However, as the above-mentioned nucleic acid detection processes require repeated uncapping and extraction, Joung *et al*[31] introduced the "one-pot" detection technology, while updating the COVID-19 detection technology, in which RNA does not need to be purified from patient samples. Moreover, the reaction steps required to detect COVID-19 are done in a tube during the test. It was then named SHERLOCK Testing in One Pot (STOP). While STOP employs loop-mediated isothermal amplification (LAMP) as a method to amplify RNA and utilizes AapCas12b, an enzyme that can remain active at 60 °C (the temperature required for the LAMP reaction), the steps of RNA extraction were simplified enough that could easily detect viral RNA only by adding viral lytic releasers to throat wipes or saliva samples containing new crown viruses without purifying and isolating RNA.

Although STOP simplifies the complexity of the detection process and reduces the contamination caused by reagent transfer, it also requires heating, amplification, and other steps when compared with SHERLOCKv2. To overcome these hindrances, a new system, CRISPR-Cas9-assisted DNA detection (CADD), was developed. This system employed the Beads-HCR method, in which a pair of dCas9-single-guide RNA (sgRNA), after being attached to the target DNA, was captured by the bead surface, followed by the addition of two hybridization chain reaction (HCR) hairpins (hairpin 1 and hairpin 2). Since the hairpin was labeled with fluorescein, HCR could produce a fluorescent signal on the bead's surface. As the hairpin was connected continuously, the fluorescence signal became brighter in the positive direction, thereby making it easier to detect the fluorescence signals to the greatest extent without amplifying the target gene[32].

Due to the advantages of simple design, high efficiency, convenience, and a wider scope of application, CRISPR-Cas systems have become the most frequent genome editing technology in molecular biology while simultaneously promoting the development of basic scientific research, molecular innovations, and advanced clinical approaches. Freije *et al*[33] combined the Cas13 antiviral activity with its diagnostic ability and established a powerful and rapidly programmable diagnostic and antiviral system, named Cas13-assisted restriction of viral expression and readout. This system could detect RNA-based viruses such as influenza A virus in human cells within two hours on the test strip itself. Fozouni *et al*[34] also developed a COVID-19 detection technology connected to a smartphone that took only 15-30 min from sampling to reporting results on a mobile phone. This technique omitted the reverse transcription and pre-amplification steps and used CRISPR to directly detect viral RNA. It was a new diagnostic test that, apart from producing positive or negative results, could also measure the viral load in a given sample. Since Csm6 can sense the presence of RNA small loops and cleaves various RNA molecules, Liu *et al*[35] utilized Cas13, Csm6, and their activators in combination to create a tandem nuclease method for detecting COVID-19. This method avoided the original amplification of RNA and the possibility of sample cross-contamination caused by amplification (Table 2).

Application of CRISPR/Cas technology in tumor pathogenesis monitoring: Tumor monitoring is still an important parameter of global chronic disease monitoring. In recent years, due to complicated operations, long detection time, and low specificity, genetic sequencing for tumor marker detection has lost its popularity. To overcome this recurrent issue, Chow *et al*[36] developed *in vivo* CRISPR screening that identified both oncogenes and tumor suppressors that are the regulators of tumor immunotherapy in the tissue microenvironment[37]. This method could be suitable for personalized cancer modeling and tumor-driven analysis in the future to provide guidance for precision medicine. In recent years, as microRNAs have been reported to be associated with tumorigenesis, diagnosis, and prognosis, the CRISPR/Cas technology promises great potential for an early diagnosis of miRNA-related disease[38,

Table 2 Clustered regularly interspaced short palindromic repeats-based pathogen nucleic acid detection system

Nucleic acid detection system	Cas	Target DNA	Amplification method	Test method	Time	Sensitivity	Specificity	Ref.
SHERLOCK	Cas13a	Zika virus *etc.*	RPA	Fluorescence	2-5 h	2×10^{-8} M	High	[26]
SHERLOCKv2	Cas13a, Cas12a, Csm6	Zika virus, Gordon fever virus, yellow fever virus, *etc.*	RPA	FluorescenceTest strip	0.5-4.0 h	8×10^{-21} M	High	[29]
DETECTR	Cas12a	HPV	RPA	Fluorescence	1 h	10^{-18} M	High	[30]
STOP	Cas12b	2019-nCoV	LAMP	Fluorescence	1 h	100 copies	High	[31]
CADD	Cas9	HPV	-	Fluorescence	30 min	10^{-15} M	High	[32]
CARVER	Cas13a	Influenza A	RPA	Test strip	2 h	-	High	[33]
Smartphone testing	Cas13a	2019-nCoV	-	Fluorescence	15-30 min	10^{-4} M	High	[34]
Tandem nuclease	Cas13a + Csm6	2019-nCoV	-	Fluorescence	20 min	3.1×10^{-5} M	High	[35]

Cas: CRISPR-associated protein; RPA: Recombinase Polymerase Amplification; SHERLOCK: Specific high-sensitivity enzymatic reporter unlocking; STOP: SHERLOCK Testing in One Pot; CADD: CRISPR-Cas9-assisted DNA detection; CARVER: LAMP: Loop-mediated isothermal amplification; 2019-nCoV: 2019 novel coronavirus; HPV: Human papillomavirus.

39]. Qiu *et al*[40] developed the RCA-CRISPR-split-HRP (RCH) detection system based on dCas9, which facilitated CRISPR/Cas9 technology in miRNA detection for the first time. It offers great advantages such as a low detection cost and significant genetic effects. To demonstrate the potential application value of RCH, it was applied to detect circulating let-7a in serum samples from patients with non-small cell lung cancer (NSCLC) and healthy volunteers. As it was reported that since the expression of circulating let-7a was significantly down-regulated in patients with NSCLC, it could become a useful biomarker for NSCLC[41]. It was also discovered that the detection results were highly consistent with RT-PCR results and the literature reports, suggesting that this method could be used for the screening and diagnosis of tumors in the near future. Simultaneously, Lee *et al*[42] developed CRISPR-mediated Ultrasensitive Detection of Target DNA)-PCR (CUT) using Cas9/sgRNA for specific cleavage of wild-type DNA in blood samples from colorectal cancer patients, which in turn enriched the circulating tumor DNA content in plasma to improve the specificity and sensitivity of early tumor diagnosis. While the SHERLOCK and SHERLOCKv2 molecular detection platforms can detect the BRAF V600E mutation in simulated circulating DNA samples and the EGFR L858R mutation in liquid biopsy samples from adenocarcinoma patients[26,29,43], the DETECTR method can also be used to rapidly detect tumor mutations in the reproductive system[30]. For example, human papillomavirus, closely related to the occurrence of cervical cancer, is detected in human anal wipe DNA extracts[41]. The development of this technology is expected to bring a significant breakthrough in the early screening of cervical cancer (Table 3).

Application of CRISPR/Cas technology in gene-editing disease therapy

In clinical medicine, gene-editing has changed from a niche research technique to an extensive and highly precise tool for disease treatment[44], which has shown surprising results in the treatment of a variety of clinical diseases, such as genetic disorders[45] and cancer immunotherapy[46].

Application of the CRISPR/Cas9 System in gene editing disease therapy: An *in vitro* study by Egelie *et al*[47] observed that Cas9 protein could target and edit genes in bacterial cells, human stem cells, zebrafish, and human cell lines. In the targeting phase, Cas9 is guided to the DNA target site beside the PAM (spacer sequence adjacent motif) site (3′ GGN) by gRNA. The Cas9 nuclease domains like RuvC and HNH cleave single strands of DNA to form DNA DSBs. Although non-homologous end joining is subsequently activated in the host for repair, resulting in frameshift mutations, the body can also perform precise repair by homologous recombination repair in the presence of homologous sequences [48]. Lately, the CRISPR/Cas9-mediated gene therapy has become a quick and effective gene-editing tool as it corrects single-gene mutations, thus saving the disease phenotypes by achieving prompt treatment[49]. Leber congenital amaurosis (LCA) is an autosomal recessive retinopathy with both early and severe onset, causing severe visual loss due to premature transcription termination due to the presence of point mutations in the CEP290 gene at the intron branch point, followed by complete loss of pyramidal cell function in both eyes at birth or within one year of birth in infants[50,51]. Many previous studies on LCA disclosed that the adeno-associated virus type 5 (AAV5) vector delivers Cas9 and CEP290-specific gRNAs to the retina by targeting the point mutation region to invert or delete it as a

Table 3 Clustered regularly interspaced short palindromic repeats-based tumor diagnostic system

System	Cas	Tumor type	Sensitivity	Specificity	Ref.
RCH	Cas9	NSCLC	10^{-15} M	High	[40]
CUT	Cas9	Colorectal cancer	< 0.01%	High	[41]
SHERLOCK	Cas13a	NSCLC	0.1%	High	[26]
SHERLOCKv2	Cas13a, Cas12a, Csm6	NSCLC	8×10^{-21} M	High	[29]
DETECTR	Cas12a	HPV	10^{-18} M	High	[30]

RCH: RCA-CRISPR-split-HRP; NSCLC: Non-small cell lung cancer; HPV: Human papillomavirus; CUT: CRISPR-mediated Ultrasensitive Detection of Target DNA-PCR; SHERLOCK: Specific high-sensitivity enzymatic reporter unlocking; DETECTR: DNA endonuclease-targeted CRISPR trans reporter.

whole, thereby restoring the normal expression of CEP290 gene[52-54]. Although still in the early clinical trial stage, this recent approach is currently being used to treat type 10 congenital mongolism patients[55]. It has also been suggested that using mRNAs encoding nucleases, like CRISPR/Cas9 and gRNA, and their DNA editing property in target cells has the potential to be effective in Cystic fibrosis (CF) patients with the impact of potential mutations[56]. Many past literary insights reported that an adeno-associated virus vector might be used to express the Cas9 of *Campylobacter jejuni* with adenine deaminase activity as well as the corresponding sgRNA to achieve accurate correction of oncogenic mutations in the telomerase gene promoter region of glioma cells[57].

Additionally, numerous prior studies have also demonstrated that CRISPR/Cas9 technology also has application prospects in the treatment of hematological diseases: For example, when congenital glucose-6-phosphatase-dehydrogenase (G6PD) deficiency patients ingest fava beans, acute hemolytic anemia with several manifestations occur along with sickle cell anemia and β-thalassemia, a condition caused by mutations in the β-globin gene (HBB). Wu *et al*[45] effectively corrected G6PD and HBB point mutations by giving composite injections into single-cell human embryos in Cas9-sgRNA and homologous donors [58,59], thereby demonstrating that CRISPR/Cas9 might also become a valuable therapeutic tool in human genetic diseases.

Application of the CRISPR/Cas12 System in gene editing therapy: In 2015, Zetsche *et al*[21] characterized the Cas12a protein and identified two candidate enzymes from Eosinophilaceae and Lactobacillaceae, and demonstrated that Cas12a protein was able to conduct effective genome editing activity in human cells. Unlike Cas9, the crRNA used by cas12a has only 42 nt[21], which offers many advantages in design and facilitates delivery and simplification of the multiplex gene-editing process[60]. According to Verwaal, LbCas12a and FnCas12a show editing efficiency comparable to Cas9 in yeast cells and are expected to be good alternatives to Cas9 in the future[61]. However, it is not widely used in practice, so there are very few instances of genome editing for disease treatment. Recently, some researchers engineered wild-type AsCas12a and designed a nuclease called enAsCas12a[62], which can show better gene editing activity at the TTT PAM site, greatly improving the editing efficiency of base C to base T. DeWeirdt *et al*[63] also applied enAsCas12a for genetic screening in human cells, and in the future, the CRISPR/Cas12 system might also play a larger role in disease treatment.

Application of the CRISPR/Cas13 System in gene editing therapy: On the contrary, the Cas13 protein family also seems to be promising in RNA knockout and editing, as reported by Cox *et al*[64]. In their study, catalytically inactive Cas13 (dcas13) was combined with ADAR2 to target transcripts to mammalian cells for editing of RNA bases A to I and correcting certain mutations in genetic diseases[27,64]. Recently, Li *et al*[65] also developed a brand-new CRISPR/Cas gene-editing technology using dCas13, called RESCUE, in which ADAR2 enzyme targeted both base C in RNA and unwanted base C in tRNA and precisely modified them to base U, thereby achieving the purpose of changing the protein without modifying the DNA by altering the mRNA injunctions.

N^6-methyladenosine (m^6A) is a common post-transcriptional RNA methylation modification in eukaryote mRNA responsible for mRNA modifications, which sometimes in an abnormal state can trigger a series of diseases[66]. This was also confirmed by Wilson *et al*[67] using an m6A RNA editing tool constructed by phase fusion of dCas13 and gRNA, and precisely edited m^6A in the nucleus and cytoplasm. It could correct the methylase abnormality, bringing the latest breakthroughs in RNA editing. Thus, CRISPR/Cas technology can provide broader research ideas and application prospects for the treatment of many diseases by precisely editing genes and rectifying the diversity of gene variants that cause diseases.

In recent years, CRISPR/Cas technology has emerged as a potentially powerful tool in cancer research and treatment. It offers genetic screening of oncogenic mutations and can alter expressions of tumor suppressor genes[68]. It can be applied in CAR-T cell immunotherapy and immune checkpoint blocking therapy[46,69,70], thereby exploring and validating novel therapeutic targets in several

preclinical studies involving tumors.

Application of CRISPR/Cas technology in multi-drug resistance analysis and treatment

CRISPR/Cas technology can be utilized to assess the surmounting multi-drug resistance (MDR) that has emerged as a serious public health threat due to inappropriate clinical antibiotic usage[71]. MDR usually occurs due to horizontal gene transfer of antibiotic resistance genes mediated by plasmids into other pathogenic bacterial forms[72]. Guk *et al*[73] discovered a significant negative correlation between CRISPR/Cas loci in bacteria and detected the acquired antibiotic resistance by sequencing the *Enterococcus faecalis* genome. It was revealed that strains without CRISPR/Cas loci were more likely to acquire external resistance genes than strains with CRISPR/Cas loci[74].

Nearly 26000 Enterobacteriaceae infections per year in China are caused by extended-spectrum β-lactamases (ESBLs) producing *E. coli*[72]. Bader *et al*[75] developed a technique called Re-Sensitization to Antibiotics from Resistance (ReSAFR). In this technique, the CRISPR/Cas9 system facilitates the intracellular delivery of antimicrobials, followed by sgRNA-guided Cas9 specific cleavage of resistance-mediating genes present on the same plasmid as the target genes so that antibiotic-resistant cells become re-sensitive to antibiotics. As ReSAFR improves the practical value of the CRISPR/Cas9 system, it might become an effective approach to curb the formation of multidrug-resistant bacteria[72,76]. Since in recent years, methicillin-resistant *Staphylococcus aureus* (MRSA) has become a major nosocomial pathogen worldwide, Guk *et al*[73] developed a simple, rapid, and highly sensitive method to detect MRSA, *i.e.*, DNA-FISH to rapidly and reliably detect MRSA and provide effective treatment. In this technique, the dCas9/sgRNA complex is used as the targeting material and a nucleic acid stain SYBR Green I as the fluorescent probe to capture the MRSA DNA by specifically recognizing the mecA gene sequence with sgRNA. It offers a detection sensitivity of 10 CFU/mL, which is sufficient for effective detection of MRSA as the mecA gene, mainly present in resistant bacteria, is the prime underlying cause of MRSA resistance to β-lactam antibiotics. Therefore, MRSA can be promptly identified based on the mecA gene for effective antimicrobial therapy[77]. Kiga *et al*[78] also reported a positive outcome while developing the CRISPR-Cas13a-based antimicrobials capable of sequence-specific killing of MRSA, which is expected to be put into practical use as a therapeutic agent. Many of the emerging technologies mentioned above have tremendous potential to combat some of our most critical clinical predicaments in world public health problems.

Challenges to the application of CRISPR/Cas technology

CRISPR/Cas technology is indeed a convenient, easy-to-use biomedical tool having a wide range of potential applications, but at the same time, there are certain unsolved problems in its application that should be accurately recognized.

Off-target effect

CRISPR has proven to be a highly versatile gene-editing tool with great potential in a wide range of problems such as gene therapy, drug discovery, and gene modification in plant technology. However, the accuracy and reliability of CRISPR technology might be severely hampered by off-target effects due to unintended cleavage at untargeted genomic loci that do not match sgRNA, thus resulting in severe genomic aberrations[79].

When CRISPR technology is used for nucleic acid detection, the presence of an off-target effect can cause false positive or false negative results, affecting the accuracy of clinical diagnosis. The off-target effect is the main limiting factor affecting the application of CRISPR technology in clinical practice. In 2019, Grünewald *et al*[80] reported that the Cas9-based DNA editor experienced a severe off-target phenomenon while editing single bases and mutating a large number of unrelated DNA and RNA. A correct interpretation of genomic data, along with the strategies for the detection of off-target mutations and minimizing off-target cleavage efficiency, are still some of the urgent problems that need to be addressed at present. For example, technologies such as GUIDE-seq[81], Digenome-seq[77], and CIRCLE-seq[82] have been widely used to detect off-target effects. In recent years, after an in-depth study of the factors affecting off-target effects, it has been found that the current strategies to solve off-target effects mainly include: (1) Predicting off-target sites: Using CRISPOR, CHOPCHOP, and other tools, gRNAs can be designed online to analyze potential off-target sites, so that researchers can select gRNAs with low off-target effects as much as possible. The recently introduced DISCOVER-Seq technology[83] can identify the exact site of CRISPR cutting genome with simple processes and accurate results. In addition, the structure of sgRNAs and the activity of Cas protein are closely related to the off-target effects[84]; (2) optimizing the design strategy of sgRNAs: Doench *et al*[85] found a significant reduction in off-target effects after establishing new sgRNA design rules by optimizing the composition of sgRNAs; and (3) altering the structure of the Cas enzyme: Slaymaker *et al*[86] improved the binding rate to the target sequences using mutants of the Cas9 protein.

Safety and ethical issues

Recently, a study reported that a large number of unnecessary repetitive fragments appear when gene insertion is performed in mice using the CRISPR/Cas technology, which cannot be detected using the

standard PCR analysis[87]. On the other hand, it was also proposed that in human embryonic cells, frequent DNA breakage can lead to the loss of the entire chromosome or sometimes a large part of the chromosome, which can pose significant challenges for mutation corrections[88]. Another therapeutic intervention is the usage of AAV vectors that are often used with CRISPR/Cas9 for targeted gene editing. They are sometimes unable to load larger genes and might adversely affect the functioning of AAV vectors carrying exogenous DNA fragments inserted into human chromosomes due to insertional mutagenesis. Henceforth, all combined efforts should be directed towards implementing the strong gene-editing abilities of CRISPR/Cas technology for the treatment of related diseases, while preventing any untoward genome-editing behaviors and similar negative events, as well as avoiding irreversible and unethical mutational consequences.

Quantitative and high-throughput detection and sample pretreatment

As CRISPR/Cas technology accurately conducts a quantitative analysis of target nucleic acids, it is deemed important for providing rapid and ultrasensitive data relevant for prompt disease management and treatment. However, HOLMES and DETECTR, two detected CRISPR-Cas effectors, might not be capable of precise target quantification for Cas12-based detection platforms[30,89]. In addition to that, multi-channel detection is also very crucial for distinguishing different pathogens as well as single-base polymorphisms for an accurate diagnosis, but only SHERLOCKv2 contains multi-channel detection ability at present[29], highlighting its innate potential as a rapid and quantitative detection platform.

With the more and more extensive application of CRISPR/Cas technology in clinical diagnosis, the sample sources, as well as the influencing factors within the samples, will be gradually expanded and diversified[90]. Therefore, it is very important to select a simple, efficient and economical sample pretreatment strategy for opening up novel avenues to tackle genetic diseases in a precise manner.

Despite significant technical improvements, the above-mentioned challenges should be further addressed for optimizing genomic stability in future studies.

CONCLUSION

As stated by Barrangou *et al*[91], "The potential for CRISPR/Cas technology applications is enormous, affecting almost all aspects of life and providing inspiration for future technological breakthroughs". CRISPR/Cas technology may revolutionize diagnostic and therapeutic research in clinical diseases and become a versatile tool in practice in the field of clinical medicine as a pathogen detection platform due to its high efficiency, portability, and low-cost factor. Moreover, the developed diagnostic tools based on the CRISPR/Cas system are highly suitable for large-scale screening tasks in the frontline, community hospitals, and resource-limited environments[90], thereby initiating rapid and accurate detection and further promoting the development of point-of-care testing. Simultaneously, emerging CRISPR/Cas technology is being used with renewed efforts for discovering new therapeutic targets and detecting biomarkers to provide more accurate and scientific avenues for the early diagnosis and clinical treatment of oncological diseases[38,69,70]. Since the application of CRISPR/Cas technology in bacterial resistance detection has the advantages of simplicity, rapidity, and sensitivity, the recently developed platform can be more optimized by applying more detection methods for discovering various pathogens, which will be essential to prevent the spread of drug-resistant bacterial infections in hospitals[73,78].

Owing to the fact that as CRISPR/Cas technology has an undeniable tremendous potential in clinical applications and scientific research technology, many long-term clinical studies are required to elucidate biological mechanisms behind disease development and progression. This will make CRISPR/Cas technology an emerging discipline that provides better health care and improves human health more efficiently. It is also suggested that CRISPR will certainly provide more exciting results in the future, bringing us unlimited possibilities, thus providing novel molecular therapies and promoting the development of the life sciences.

FOOTNOTES

Author contributions: Huang YY contributed to the conception of the study; Zhang XY designed the work; Zhu P contributed to the acquisition of the case; Ji L revised the manuscript critically for important intellectual content; all authors have read the manuscript and gave their final approval of the version to be published.

Supported by the Shenzhen Science and Technology R&D Fund, No. JCYJ20190809095203586.

Conflict-of-interest statement: The authors declare that they have no conflict of interest.

Open-Access: This article is an open-access article that was selected by an in-house editor and fully peer-reviewed by external reviewers. It is distributed in accordance with the Creative Commons Attribution NonCommercial (CC BY-

NC 4.0) license, which permits others to distribute, remix, adapt, build upon this work non-commercially, and license their derivative works on different terms, provided the original work is properly cited and the use is non-commercial. See: https://creativecommons.org/Licenses/by-nc/4.0/

Country/Territory of origin: China

ORCID number: Yue-Ying Huang 0000-0002-9591-0490; Xiao-Yu Zhang 0000-0002-8887-4946; Ping Zhu 0000-0002-2787-1522; Ling Ji 0000-0003-4088-2514.

S-Editor: Chen YL
L-Editor: Webster JR
P-Editor: Chen YL

REFERENCES

1 **Garneau JE**, Dupuis MÈ, Villion M, Romero DA, Barrangou R, Boyaval P, Fremaux C, Horvath P, Magadán AH, Moineau S. The CRISPR/Cas bacterial immune system cleaves bacteriophage and plasmid DNA. *Nature* 2010; **468**: 67-71 [PMID: 21048762 DOI: 10.1038/nature09523]
2 **Bharathkumar N**, Sunil A, Meera P, Aksah S, Kannan M, Saravanan KM, Anand T. CRISPR/Cas-Based Modifications for Therapeutic Applications: A Review. *Mol Biotechnol* 2022; **64**: 355-372 [PMID: 34741732 DOI: 10.1007/s12033-021-00422-8]
3 **Hidalgo-Cantabrana C**, Goh YJ, Barrangou R. Characterization and Repurposing of Type I and Type II CRISPR-Cas Systems in Bacteria. *J Mol Biol* 2019; **431**: 21-33 [PMID: 30261168 DOI: 10.1016/j.jmb.2018.09.013]
4 **Liu X**, Hussain M, Dai J, Li Y, Zhang L, Yang J, Ali Z, He N, Tang Y. Programmable Biosensors Based on RNA-Guided CRISPR/Cas Endonuclease. *Biol Proced Online* 2022; **24**: 2 [PMID: 35067222 DOI: 10.1186/s12575-021-00163-7]
5 **Varble A**, Marraffini LA. Three New Cs for CRISPR: Collateral, Communicate, Cooperate. *Trends Genet* 2019; **35**: 446-456 [PMID: 31036344 DOI: 10.1016/j.tig.2019.03.009]
6 **Deng L**, Garrett RA, Shah SA, Peng X, She Q. A novel interference mechanism by a type IIIB CRISPR-Cmr module in Sulfolobus. *Mol Microbiol* 2013; **87**: 1088-1099 [PMID: 23320564 DOI: 10.1111/mmi.12152]
7 **Javaid N**, Choi S. CRISPR/Cas System and Factors Affecting Its Precision and Efficiency. *Front Cell Dev Biol* 2021; **9**: 761709 [PMID: 34901007 DOI: 10.3389/fcell.2021.761709]
8 **Staals RH**, Zhu Y, Taylor DW, Kornfeld JE, Sharma K, Barendregt A, Koehorst JJ, Vlot M, Neupane N, Varossieau K, Sakamoto K, Suzuki T, Dohmae N, Yokoyama S, Schaap PJ, Urlaub H, Heck AJ, Nogales E, Doudna JA, Shinkai A, van der Oost J. RNA targeting by the type III-A CRISPR-Cas Csm complex of Thermus thermophilus. *Mol Cell* 2014; **56**: 518-530 [PMID: 25457165 DOI: 10.1016/j.molcel.2014.10.005]
9 **Tamulaitis G**, Kazlauskiene M, Manakova E, Venclovas Č, Nwokeoji AO, Dickman MJ, Horvath P, Siksnys V. Programmable RNA shredding by the type III-A CRISPR-Cas system of Streptococcus thermophilus. *Mol Cell* 2014; **56**: 506-517 [PMID: 25458845 DOI: 10.1016/j.molcel.2014.09.027]
10 **Elmore JR**, Sheppard NF, Ramia N, Deighan T, Li H, Terns RM, Terns MP. Bipartite recognition of target RNAs activates DNA cleavage by the Type III-B CRISPR-Cas system. *Genes Dev* 2016; **30**: 447-459 [PMID: 26848045 DOI: 10.1101/gad.272153.115]
11 **Estrella MA**, Kuo FT, Bailey S. RNA-activated DNA cleavage by the Type III-B CRISPR-Cas effector complex. *Genes Dev* 2016; **30**: 460-470 [PMID: 26848046 DOI: 10.1101/gad.273722.115]
12 **Kolesnik MV**, Fedorova I, Karneyeva KA, Artamonova DN, Severinov KV. Type III CRISPR-Cas Systems: Deciphering the Most Complex Prokaryotic Immune System. *Biochemistry (Mosc)* 2021; **86**: 1301-1314 [PMID: 34903162 DOI: 10.1134/S0006297921100114]
13 **Han W**, Stella S, Zhang Y, Guo T, Sulek K, Peng-Lundgren L, Montoya G, She Q. A Type III-B Cmr effector complex catalyzes the synthesis of cyclic oligoadenylate second messengers by cooperative substrate binding. *Nucleic Acids Res* 2018; **46**: 10319-10330 [PMID: 30239876 DOI: 10.1093/nar/gky844]
14 **Huang F**, Zhu B. The Cyclic Oligoadenylate Signaling Pathway of Type III CRISPR-Cas Systems. *Front Microbiol* 2020; **11**: 602789 [PMID: 33552016 DOI: 10.3389/fmicb.2020.602789]
15 **Rouillon C**, Athukoralage JS, Graham S, Grüschow S, White MF. Control of cyclic oligoadenylate synthesis in a type III CRISPR system. *Elife* 2018; **7** [PMID: 29963983 DOI: 10.7554/eLife.36734]
16 **Pinilla-Redondo R**, Mayo-Muñoz D, Russel J, Garrett RA, Randau L, Sørensen SJ, Shah SA. Type IV CRISPR-Cas systems are highly diverse and involved in competition between plasmids. *Nucleic Acids Res* 2020; **48**: 2000-2012 [PMID: 31879772 DOI: 10.1093/nar/gkz1197]
17 **Smits JPH**, Meesters LD, Maste BGW, Zhou H, Zeeuwen PLJM, van den Bogaard EH. CRISPR-Cas9–Based Genomic Engineering in Keratinocytes: From Technology to Application. *JID Innov* 2022; **2**: 100082 [PMID: 35146483 DOI: 10.1016/j.xjidi.2021.100082]
18 **Dort EN**, Tanguay P, Hamelin RC. CRISPR/Cas9 Gene Editing: An Unexplored Frontier for Forest Pathology. *Front Plant Sci* 2020; **11**: 1126 [PMID: 32793272 DOI: 10.3389/fpls.2020.01126]
19 **Burmistrz M**, Pyrć K. CRISPR-Cas Systems in Prokaryotes. *Pol J Microbiol* 2015; **64**: 193-202 [PMID: 26638527 DOI: 10.5604/01.3001.0009.2114]
20 **Sapranauskas R**, Gasiunas G, Fremaux C, Barrangou R, Horvath P, Siksnys V. The Streptococcus thermophilus CRISPR/Cas system provides immunity in Escherichia coli. *Nucleic Acids Res* 2011; **39**: 9275-9282 [PMID: 21813460 DOI: 10.1093/nar/gkr606]

21 **Zetsche B**, Gootenberg JS, Abudayyeh OO, Slaymaker IM, Makarova KS, Essletzbichler P, Volz SE, Joung J, van der Oost J, Regev A, Koonin EV, Zhang F. Cpf1 is a single RNA-guided endonuclease of a class 2 CRISPR-Cas system. *Cell* 2015; **163**: 759-771 [PMID: 26422227 DOI: 10.1016/j.cell.2015.09.038]

22 **Dronina J**, Samukaite-Bubniene U, Ramanavicius A. Towards application of CRISPR-Cas12a in the design of modern viral DNA detection tools (Review). *J Nanobiotechnology* 2022; **20**: 41 [PMID: 35062978 DOI: 10.1186/s12951-022-01246-7]

23 **Aquino-Jarquin G**. CRISPR-Cas14 is now part of the artillery for gene editing and molecular diagnostic. *Nanomedicine* 2019; **18**: 428-431 [PMID: 30935995 DOI: 10.1016/j.nano.2019.03.006]

24 **Zhang D**, Li Z, Yan B, Li JF. A novel RNA-guided RNA-targeting CRISPR tool. *Sci China Life Sci* 2016; **59**: 854-856 [PMID: 27436421 DOI: 10.1007/s11427-016-0192-5]

25 **Aquino-Jarquin G**. Recent progress on rapid SARS-CoV-2/COVID-19 detection by CRISPR-Cas13-based platforms. *Drug Discov Today* 2021; **26**: 2025-2035 [PMID: 34147688 DOI: 10.1016/j.drudis.2021.06.005]

26 **Caliendo AM**, Hodinka RL. A CRISPR Way to Diagnose Infectious Diseases. *N Engl J Med* 2017; **377**: 1685-1687 [PMID: 29069564 DOI: 10.1056/NEJMcibr1704902]

27 **Abudayyeh OO**, Gootenberg JS, Essletzbichler P, Han S, Joung J, Belanto JJ, Verdine V, Cox DBT, Kellner MJ, Regev A, Lander ES, Voytas DF, Ting AY, Zhang F. RNA targeting with CRISPR-Cas13. *Nature* 2017; **550**: 280-284 [PMID: 28976959 DOI: 10.1038/nature24049]

28 **Li SY**, Cheng QX, Liu JK, Nie XQ, Zhao GP, Wang J. CRISPR-Cas12a has both cis- and trans-cleavage activities on single-stranded DNA. *Cell Res* 2018; **28**: 491-493 [PMID: 29531313 DOI: 10.1038/s41422-018-0022-x]

29 **Priya Swetha PD**, Sonia J, Sapna K, Prasad KS. Towards CRISPR powered electrochemical sensing for smart diagnostics. *Curr Opin Electrochem* 2021; **30**: 100829 [PMID: 34909513 DOI: 10.1016/j.coelec.2021.100829]

30 **Chen JS**, Ma E, Harrington LB, Da Costa M, Tian X, Palefsky JM, Doudna JA. CRISPR-Cas12a target binding unleashes indiscriminate single-stranded DNase activity. *Science* 2018; **360**: 436-439 [PMID: 29449511 DOI: 10.1126/science.aar6245]

31 **Joung J**, Ladha A, Saito M, Segel M, Bruneau R, Huang MW, Kim NG, Yu X, Li J, Walker BD, Greninger AL, Jerome KR, Gootenberg JS, Abudayyeh OO, Zhang F. Point-of-care testing for COVID-19 using SHERLOCK diagnostics. *medRxiv* 2020 [PMID: 32511521 DOI: 10.1101/2020.05.04.20091231]

32 **Xu X**, Luo T, Gao J, Lin N, Li W, Xia X, Wang J. CRISPR-Assisted DNA Detection: A Novel dCas9-Based DNA Detection Technique. *CRISPR J* 2020; **3**: 487-502 [PMID: 33346711 DOI: 10.1089/crispr.2020.0041]

33 **Freije CA**, Myhrvold C, Boehm CK, Lin AE, Welch NL, Carter A, Metsky HC, Luo CY, Abudayyeh OO, Gootenberg JS, Yozwiak NL, Zhang F, Sabeti PC. Programmable Inhibition and Detection of RNA Viruses Using Cas13. *Mol Cell* 2019; **76**: 826-837.e11 [PMID: 31607545 DOI: 10.1016/j.molcel.2019.09.013]

34 **Fozouni P**, Son S, Díaz de León Derby M, Knott GJ, Gray CN, D'Ambrosio MV, Zhao C, Switz NA, Kumar GR, Stephens SI, Boehm D, Tsou CL, Shu J, Bhuiya A, Armstrong M, Harris AR, Chen PY, Osterloh JM, Meyer-Franke A, Joehnk B, Walcott K, Sil A, Langelier C, Pollard KS, Crawford ED, Puschnik AS, Phelps M, Kistler A, DeRisi JL, Doudna JA, Fletcher DA, Ott M. Amplification-free detection of SARS-CoV-2 with CRISPR-Cas13a and mobile phone microscopy. *Cell* 2021; **184**: 323-333.e9 [PMID: 33306959 DOI: 10.1016/j.cell.2020.12.001]

35 **Liu TY**, Knott GJ, Smock DCJ, Desmarais JJ, Son S, Bhuiya A, Jakhanwal S, Prywes N, Agrawal S, Díaz de León Derby M, Switz NA, Armstrong M, Harris AR, Charles EJ, Thornton BW, Fozouni P, Shu J, Stephens SI, Kumar GR, Zhao C, Mok A, Iavarone AT, Escajeda AM, McIntosh R, Kim S, Dugan EJ; IGI Testing Consortium, Pollard KS, Tan MX, Ott M, Fletcher DA, Lareau LF, Hsu PD, Savage DF, Doudna JA. Accelerated RNA detection using tandem CRISPR nucleases. *Nat Chem Biol* 2021; **17**: 982-988 [PMID: 34354262 DOI: 10.1038/s41589-021-00842-2]

36 **Chow RD**, Chen S. Cancer CRISPR Screens In Vivo. *Trends Cancer* 2018; **4**: 349-358 [PMID: 29709259 DOI: 10.1016/j.trecan.2018.03.002]

37 **Song CQ**, Li Y, Mou H, Moore J, Park A, Pomyen Y, Hough S, Kennedy Z, Fischer A, Yin H, Anderson DG, Conte D Jr, Zender L, Wang XW, Thorgeirsson S, Weng Z, Xue W. Genome-Wide CRISPR Screen Identifies Regulators of Mitogen-Activated Protein Kinase as Suppressors of Liver Tumors in Mice. *Gastroenterology* 2017; **152**: 1161-1173.e1 [PMID: 27956228 DOI: 10.1053/j.gastro.2016.12.002]

38 **Shan Y**, Zhou X, Huang R, Xing D. High-Fidelity and Rapid Quantification of miRNA Combining crRNA Programmability and CRISPR/Cas13a trans-Cleavage Activity. *Anal Chem* 2019; **91**: 5278-5285 [PMID: 30873832 DOI: 10.1021/acs.analchem.9b00073]

39 **Durán-Vinet B**, Araya-Castro K, Calderón J, Vergara L, Weber H, Retamales J, Araya-Castro P, Leal-Rojas P. CRISPR/Cas13-Based Platforms for a Potential Next-Generation Diagnosis of Colorectal Cancer through Exosomes Micro-RNA Detection: A Review. *Cancers (Basel)* 2021; **13** [PMID: 34572866 DOI: 10.3390/cancers13184640]

40 **Qiu XY**, Zhu LY, Zhu CS, Ma JX, Hou T, Wu XM, Xie SS, Min L, Tan DA, Zhang DY, Zhu L. Highly Effective and Low-Cost MicroRNA Detection with CRISPR-Cas9. *ACS Synth Biol* 2018; **7**: 807-813 [PMID: 29486117 DOI: 10.1021/acssynbio.7b00446]

41 **Cook PJ**, Ventura A. Cancer diagnosis and immunotherapy in the age of CRISPR. *Genes Chromosomes Cancer* 2019; **58**: 233-243 [PMID: 30382614 DOI: 10.1002/gcc.22702]

42 **Lee SH**, Yu J, Hwang GH, Kim S, Kim HS, Ye S, Kim K, Park J, Park DY, Cho YK, Kim JS, Bae S. CUT-PCR: CRISPR-mediated, ultrasensitive detection of target DNA using PCR. *Oncogene* 2017; **36**: 6823-6829 [PMID: 28846115 DOI: 10.1038/onc.2017.281]

43 **Granados-Riveron JT**, Aquino-Jarquin G. CRISPR-Cas13 Precision Transcriptome Engineering in Cancer. *Cancer Res* 2018; **78**: 4107-4113 [PMID: 30021724 DOI: 10.1158/0008-5472.CAN-18-0785]

44 **Bak RO**, Gomez-Ospina N, Porteus MH. Gene Editing on Center Stage. *Trends Genet* 2018; **34**: 600-611 [PMID: 29908711 DOI: 10.1016/j.tig.2018.05.004]

45 **Wu Y**, Zeng J, Roscoe BP, Liu P, Yao Q, Lazzarotto CR, Clement K, Cole MA, Luk K, Baricordi C, Shen AH, Ren C, Esrick EB, Manis JP, Dorfman DM, Williams DA, Biffi A, Brugnara C, Biasco L, Brendel C, Pinello L, Tsai SQ, Wolfe SA, Bauer DE. Highly efficient therapeutic gene editing of human hematopoietic stem cells. *Nat Med* 2019; **25**: 776-783

[PMID: 30911135 DOI: 10.1038/s41591-019-0401-y]

46 **Qasim W**, Zhan H, Samarasinghe S, Adams S, Amrolia P, Stafford S, Butler K, Rivat C, Wright G, Somana K, Ghorashian S, Pinner D, Ahsan G, Gilmour K, Lucchini G, Inglott S, Mifsud W, Chiesa R, Peggs KS, Chan L, Farzeneh F, Thrasher AJ, Vora A, Pule M, Veys P. Molecular remission of infant B-ALL after infusion of universal TALEN gene-edited CAR T cells. *Sci Transl Med* 2017; **9** [PMID: 28123068 DOI: 10.1126/scitranslmed.aaj2013]

47 **Egelie KJ**, Graff GD, Strand SP, Johansen B. The emerging patent landscape of CRISPR-Cas gene editing technology. *Nat Biotechnol* 2016; **34**: 1025-1031 [PMID: 27727218 DOI: 10.1038/nbt.3692]

48 **Nishiga M**, Liu C, Qi LS, Wu JC. The use of new CRISPR tools in cardiovascular research and medicine. *Nat Rev Cardiol* 2022 [PMID: 35145236 DOI: 10.1038/s41569-021-00669-3]

49 **Khadempar S**, Familghadakchi S, Motlagh RA, Farahani N, Dashtiahangar M, Rezaei H, Gheibi Hayat SM. CRISPR-Cas9 in genome editing: Its function and medical applications. *J Cell Physiol* 2019; **234**: 5751-5761 [PMID: 30362544 DOI: 10.1002/jcp.27476]

50 **Cideciyan AV**, Jacobson SG. Leber Congenital Amaurosis (LCA): Potential for Improvement of Vision. *Invest Ophthalmol Vis Sci* 2019; **60**: 1680-1695 [PMID: 31009524 DOI: 10.1167/iovs.19-26672]

51 **Maeder ML**, Stefanidakis M, Wilson CJ, Baral R, Barrera LA, Bounoutas GS, Bumcrot D, Chao H, Ciulla DM, DaSilva JA, Dass A, Dhanapal V, Fennell TJ, Friedland AE, Giannoukos G, Gloskowski SW, Glucksmann A, Gotta GM, Jayaram H, Haskett SJ, Hopkins B, Horng JE, Joshi S, Marco E, Mepani R, Reyon D, Ta T, Tabbaa DG, Samuelsson SJ, Shen S, Skor MN, Stetkiewicz P, Wang T, Yudkoff C, Myer VE, Albright CF, Jiang H. Development of a gene-editing approach to restore vision loss in Leber congenital amaurosis type 10. *Nat Med* 2019; **25**: 229-233 [PMID: 30664785 DOI: 10.1038/s41591-018-0327-9]

52 **Yu W**, Wu Z. Use of AAV Vectors for CRISPR-Mediated In Vivo Genome Editing in the Retina. *Methods Mol Biol* 2019; **1950**: 123-139 [PMID: 30783971 DOI: 10.1007/978-1-4939-9139-6_7]

53 **Ruan GX**, Barry E, Yu D, Lukason M, Cheng SH, Scaria A. CRISPR/Cas9-Mediated Genome Editing as a Therapeutic Approach for Leber Congenital Amaurosis 10. *Mol Ther* 2017; **25**: 331-341 [PMID: 28109959 DOI: 10.1016/j.ymthe.2016.12.006]

54 **Wang D**, Tai PWL, Gao G. Adeno-associated virus vector as a platform for gene therapy delivery. *Nat Rev Drug Discov* 2019; **18**: 358-378 [PMID: 30710128 DOI: 10.1038/s41573-019-0012-9]

55 **Ledford H**. CRISPR treatment inserted directly into the body for first time. *Nature* 2020; **579**: 185 [PMID: 32157225 DOI: 10.1038/d41586-020-00655-8]

56 **Da Silva Sanchez A**, Paunovska K, Cristian A, Dahlman JE. Treating Cystic Fibrosis with mRNA and CRISPR. *Hum Gene Ther* 2020; **31**: 940-955 [PMID: 32799680 DOI: 10.1089/hum.2020.137]

57 **Li X**, Qian X, Wang B, Xia Y, Zheng Y, Du L, Xu D, Xing D, DePinho RA, Lu Z. Programmable base editing of mutated TERT promoter inhibits brain tumour growth. *Nat Cell Biol* 2020; **22**: 282-288 [PMID: 32066906 DOI: 10.1038/s41556-020-0471-6]

58 **Tang L**, Zeng Y, Du H, Gong M, Peng J, Zhang B, Lei M, Zhao F, Wang W, Li X, Liu J. CRISPR/Cas9-mediated gene editing in human zygotes using Cas9 protein. *Mol Genet Genomics* 2017; **292**: 525-533 [PMID: 28251317 DOI: 10.1007/s00438-017-1299-z]

59 **Park SH**, Lee CM, Dever DP, Davis TH, Camarena J, Srifa W, Zhang Y, Paikari A, Chang AK, Porteus MH, Sheehan VA, Bao G. Highly efficient editing of the β-globin gene in patient-derived hematopoietic stem and progenitor cells to treat sickle cell disease. *Nucleic Acids Res* 2019; **47**: 7955-7972 [PMID: 31147717 DOI: 10.1093/nar/gkz475]

60 **Jiang DJ**, Xu CL, Tsang SH. Revolution in Gene Medicine Therapy and Genome Surgery. *Genes (Basel)* 2018; **9** [PMID: 30486314 DOI: 10.20944/preprints201810.0010.v1]

61 **Verwaal R**, Buiting-Wiessenhaan N, Dalhuijsen S, Roubos JA. CRISPR/Cpf1 enables fast and simple genome editing of Saccharomyces cerevisiae. *Yeast* 2018; **35**: 201-211 [PMID: 28886218 DOI: 10.1002/yea.3278]

62 **Kleinstiver BP**, Sousa AA, Walton RT, Tak YE, Hsu JY, Clement K, Welch MM, Horng JE, Malagon-Lopez J, Scarfò I, Maus MV, Pinello L, Aryee MJ, Joung JK. Engineered CRISPR-Cas12a variants with increased activities and improved targeting ranges for gene, epigenetic and base editing. *Nat Biotechnol* 2019; **37**: 276-282 [PMID: 30742127 DOI: 10.1038/s41587-018-0011-0]

63 **DeWeirdt PC**, Sanson KR, Sangree AK, Hegde M, Hanna RE, Feeley MN, Griffith AL, Teng T, Borys SM, Strand C, Joung JK, Kleinstiver BP, Pan X, Huang A, Doench JG. Optimization of AsCas12a for combinatorial genetic screens in human cells. *Nat Biotechnol* 2021; **39**: 94-104 [PMID: 32661438 DOI: 10.1038/s41587-020-0600-6]

64 **Cox DBT**, Gootenberg JS, Abudayyeh OO, Franklin B, Kellner MJ, Joung J, Zhang F. RNA editing with CRISPR-Cas13. *Science* 2017; **358**: 1019-1027 [PMID: 29070703 DOI: 10.1126/science.aaq0180]

65 **Li G**, Wang Y, Li X, Huang X, Gao J, Hu X. Developing PspCas13b-based enhanced RESCUE system, eRESCUE, with efficient RNA base editing. *Cell Commun Signal* 2021; **19**: 84 [PMID: 34380502 DOI: 10.1186/s12964-021-00716-z]

66 **Tang F**, Chen L, Gao H, Xiao D, Li X. m^{6}A: An Emerging Role in Programmed Cell Death. *Front Cell Dev Biol* 2022; **10**: 817112 [PMID: 35141221 DOI: 10.3389/fcell.2022.817112]

67 **Wilson C**, Chen PJ, Miao Z, Liu DR. Programmable m^{6}A modification of cellular RNAs with a Cas13-directed methyltransferase. *Nat Biotechnol* 2020; **38**: 1431-1440 [PMID: 32601430 DOI: 10.1038/s41587-020-0572-6]

68 **Moses C**, Garcia-Bloj B, Harvey AR, Blancafort P. Hallmarks of cancer: The CRISPR generation. *Eur J Cancer* 2018; **93**: 10-18 [PMID: 29433054 DOI: 10.1016/j.ejca.2018.01.002]

69 **Yin H**, Xue W, Anderson DG. CRISPR-Cas: a tool for cancer research and therapeutics. *Nat Rev Clin Oncol* 2019; **16**: 281-295 [PMID: 30664678 DOI: 10.1038/s41571-019-0166-8]

70 **Wang G**, Chow RD, Bai Z, Zhu L, Errami Y, Dai X, Dong MB, Ye L, Zhang X, Renauer PA, Park JJ, Shen L, Ye H, Fuchs CS, Chen S. Multiplexed activation of endogenous genes by CRISPRa elicits potent antitumor immunity. *Nat Immunol* 2019; **20**: 1494-1505 [PMID: 31611701 DOI: 10.1038/s41590-019-0500-4]

71 **Gupta D**, Bhattacharjee O, Mandal D, Sen MK, Dey D, Dasgupta A, Kazi TA, Gupta R, Sinharoy S, Acharya K, Chattopadhyay D, Ravichandiran V, Roy S, Ghosh D. CRISPR-Cas9 system: A new-fangled dawn in gene editing. *Life Sci* 2019; **232**: 116636 [PMID: 31295471 DOI: 10.1016/j.lfs.2019.116636]

72 **Kim JS**, Cho DH, Park M, Chung WJ, Shin D, Ko KS, Kweon DH. CRISPR/Cas9-Mediated Re-Sensitization of Antibiotic-Resistant Escherichia coli Harboring Extended-Spectrum β-Lactamases. *J Microbiol Biotechnol* 2016; **26**: 394-401 [PMID: 26502735 DOI: 10.4014/jmb.1508.08080]

73 **Guk K**, Keem JO, Hwang SG, Kim H, Kang T, Lim EK, Jung J. A facile, rapid and sensitive detection of MRSA using a CRISPR-mediated DNA FISH method, antibody-like dCas9/sgRNA complex. *Biosens Bioelectron* 2017; **95**: 67-71 [PMID: 28412663 DOI: 10.1016/j.bios.2017.04.016]

74 **Wang G**, Song G, Xu Y. Association of CRISPR/Cas System with the Drug Resistance in *Klebsiella pneumoniae*. *Infect Drug Resist* 2020; **13**: 1929-1935 [PMID: 32606841 DOI: 10.2147/IDR.S253380]

75 **Bader MS**, Loeb M, Leto D, Brooks AA. Treatment of urinary tract infections in the era of antimicrobial resistance and new antimicrobial agents. *Postgrad Med* 2020; **132**: 234-250 [PMID: 31608743 DOI: 10.1080/00325481.2019.1680052]

76 **Shabbir MAB**, Shabbir MZ, Wu Q, Mahmood S, Sajid A, Maan MK, Ahmed S, Naveed U, Hao H, Yuan Z. CRISPR-cas system: biological function in microbes and its use to treat antimicrobial resistant pathogens. *Ann Clin Microbiol Antimicrob* 2019; **18**: 21 [PMID: 31277669 DOI: 10.1186/s12941-019-0317-x]

77 **Kim D**, Bae S, Park J, Kim E, Kim S, Yu HR, Hwang J, Kim JI, Kim JS. Digenome-seq: genome-wide profiling of CRISPR-Cas9 off-target effects in human cells. *Nat Methods* 2015; **12**: 237-243, 1 p following 243 [PMID: 25664545 DOI: 10.1038/nmeth.3284]

78 **Kiga K**, Tan XE, Ibarra-Chávez R, Watanabe S, Aiba Y, Sato'o Y, Li FY, Sasahara T, Cui B, Kawauchi M, Boonsiri T, Thitiananpakorn K, Taki Y, Azam AH, Suzuki M, Penadés JR, Cui L. Development of CRISPR-Cas13a-based antimicrobials capable of sequence-specific killing of target bacteria. *Nat Commun* 2020; **11**: 2934 [PMID: 32523110 DOI: 10.1038/s41467-020-16731-6]

79 **Wang DC**, Wang X. Off-target genome editing: A new discipline of gene science and a new class of medicine. *Cell Biol Toxicol* 2019; **35**: 179-183 [PMID: 31030279 DOI: 10.1007/s10565-019-09475-7]

80 **Grünewald J**, Zhou R, Garcia SP, Iyer S, Lareau CA, Aryee MJ, Joung JK. Transcriptome-wide off-target RNA editing induced by CRISPR-guided DNA base editors. *Nature* 2019; **569**: 433-437 [PMID: 30995674 DOI: 10.1038/s41586-019-1161-z]

81 **Höijer I**, Emmanouilidou A, Östlund R, van Schendel R, Bozorgpana S, Tijsterman M, Feuk L, Gyllensten U, den Hoed M, Ameur A. CRISPR-Cas9 induces large structural variants at on-target and off-target sites in vivo that segregate across generations. *Nat Commun* 2022; **13**: 627 [PMID: 35110541 DOI: 10.1038/s41467-022-28244-5]

82 **Tsai SQ**, Nguyen NT, Malagon-Lopez J, Topkar VV, Aryee MJ, Joung JK. CIRCLE-seq: a highly sensitive in vitro screen for genome-wide CRISPR-Cas9 nuclease off-targets. *Nat Methods* 2017; **14**: 607-614 [PMID: 28459458 DOI: 10.1038/nmeth.4278]

83 **Fu R**, He W, Dou J, Villarreal OD, Bedford E, Wang H, Hou C, Zhang L, Wang Y, Ma D, Chen Y, Gao X, Depken M, Xu H. Systematic decomposition of sequence determinants governing CRISPR/Cas9 specificity. *Nat Commun* 2022; **13**: 474 [PMID: 35078987 DOI: 10.1038/s41467-022-28028-x]

84 **Pattanayak V**, Lin S, Guilinger JP, Ma E, Doudna JA, Liu DR. High-throughput profiling of off-target DNA cleavage reveals RNA-programmed Cas9 nuclease specificity. *Nat Biotechnol* 2013; **31**: 839-843 [PMID: 23934178 DOI: 10.1038/nbt.2673]

85 **Doench JG**, Fusi N, Sullender M, Hegde M, Vaimberg EW, Donovan KF, Smith I, Tothova Z, Wilen C, Orchard R, Virgin HW, Listgarten J, Root DE. Optimized sgRNA design to maximize activity and minimize off-target effects of CRISPR-Cas9. *Nat Biotechnol* 2016; **34**: 184-191 [PMID: 26780180 DOI: 10.1038/nbt.3437]

86 **Slaymaker IM**, Gao L, Zetsche B, Scott DA, Yan WX, Zhang F. Rationally engineered Cas9 nucleases with improved specificity. *Science* 2016; **351**: 84-88 [PMID: 26628643 DOI: 10.1126/science.aad5227]

87 **Skryabin BV**, Kummerfeld DM, Gubar L, Seeger B, Kaiser H, Stegemann A, Roth J, Meuth SG, Pavenstädt H, Sherwood J, Pap T, Wedlich-Söldner R, Sunderkötter C, Schwartz YB, Brosius J, Rozhdestvensky TS. Pervasive head-to-tail insertions of DNA templates mask desired CRISPR-Cas9-mediated genome editing events. *Sci Adv* 2020; **6**: eaax2941 [PMID: 32095517 DOI: 10.1126/sciadv.aax2941]

88 **Zuccaro MV**, Xu J, Mitchell C, Marin D, Zimmerman R, Rana B, Weinstein E, King RT, Palmerola KL, Smith ME, Tsang SH, Goland R, Jasin M, Lobo R, Treff N, Egli D. Allele-Specific Chromosome Removal after Cas9 Cleavage in Human Embryos. *Cell* 2020; **183**: 1650-1664.e15 [PMID: 33125898 DOI: 10.1016/j.cell.2020.10.025]

89 **Li SY**, Cheng QX, Wang JM, Li XY, Zhang ZL, Gao S, Cao RB, Zhao GP, Wang J. CRISPR-Cas12a-assisted nucleic acid detection. *Cell Discov* 2018; **4**: 20 [PMID: 29707234 DOI: 10.1038/s41421-018-0028-z]

90 **Li Y**, Li S, Wang J, Liu G. CRISPR/Cas Systems towards Next-Generation Biosensing. *Trends Biotechnol* 2019; **37**: 730-743 [PMID: 30654914 DOI: 10.1016/j.tibtech.2018.12.005]

91 **Barrangou R**, Doudna JA. Applications of CRISPR technologies in research and beyond. *Nat Biotechnol* 2016; **34**: 933-941 [PMID: 27606440 DOI: 10.1038/nbt.3659]

World Journal of Clinical Cases

Submit a Manuscript: https://www.f6publishing.com

World J Clin Cases 2022 June 26; 10(18): 5946-5956

DOI: 10.12998/wjcc.v10.i18.5946

ISSN 2307-8960 (online)

MINIREVIEWS

Strategies and challenges in treatment of varicose veins and venous insufficiency

Rong-Ding Gao, Song-Yi Qian, Hai-Hong Wang, Yong-Sheng Liu, Shi-Yan Ren

Specialty type: Medicine, research and experimental

Provenance and peer review: Invited article; Externally peer reviewed.

Peer-review model: Single blind

Peer-review report's scientific quality classification

Grade A (Excellent): 0
Grade B (Very good): B
Grade C (Good): C
Grade D (Fair): 0
Grade E (Poor): 0

P-Reviewer: Kumar S, India; Yoshida S, Japan

Received: December 3, 2021
Peer-review started: December 3, 2021
First decision: March 15, 2022
Revised: March 26, 2022
Accepted: April 26, 2022
Article in press: April 26, 2022
Published online: June 26, 2022

Rong-Ding Gao, Shi-Yan Ren, Department of Laser and Vascular Surgery, Aviation General Hospital, China Medical University, Beijing 100012, China

Song-Yi Qian, Department of Cardiac Surgery, Zhongshan Hospital (Xiamen Brach), Fudan University, Xiamen 361015, Fujian Province, China

Hai-Hong Wang, Department of Peripheral Vascular Disease, The Affiliated Hospital of Shanxi University of Chinese Medicine, Taiyuan 030024, Shanxi Province, China

Yong-Sheng Liu, Department of Dermatology, Aviation General Hospital, China Medical University, Beijing 100012, China

Corresponding author: Shi-Yan Ren, MD, PhD, Chief Doctor, Vascular Surgeon, Department of Laser and Vascular Surgery, Aviation General Hospital, China Medical University, No. 2 Beiyuan Road, Chaoyang District, Beijing 100012, China. rens66@126.com

Abstract

Patients with varicose veins can be treated with conservative or surgical approaches based on the clinical conditions and patient preferences. In the recent decade, the recommendations for managing symptomatic varicose veins have changed dramatically due to the rise of minimally invasive endovascular techniques. The literature was systematically searched on Medline without language restrictions. All papers on the treatment of varicose veins and venous insufficiency with different procedures were included and reviewed. Endovenous laser ablation (EVLA) and radiofrequency ablation (RFA) both are same safe and effective in terms of occlusion rate, and time to return to normal activity. In comparison with RFA or EVLT, Cure conservatrice et Hemodynamique de l'Insufficience Veineuse en Ambulatoire (CHIVA) may cause more bruising and make little or no difference to rates of limb infection, superficial vein thrombosis, nerve injury, or hematoma. In terms of recurrence of varicose veins, there is little or no difference between CHIVA and stripping, RFA, or EVLT. Great saphenous vein recanalization is highest in the ultrasound-guided foam sclerotherapy (FS) group (51%) during 1 year of follow-up. The 2013 National Institute for Health and Care Excellence clinical guidelines recommend surgery as a third-line therapeutic option after EVLA or RFA and sclerotherapy. Although the mechano-chemical endovenous ablation (MOCA) is a non-thermal, non-tumescent option and appears to be of similar efficacy to stab avulsion with no potential risk of nerve damage, the overall success rate of MOCA is lower than those of other procedures such as EVLA, RFA, or high ligation and stripping. EVLA is the most

cost-effective therapeutic option, with RFA being a close second for the treatment of patients with varicose veins. Endovenous thermal ablation (EVLA or RFA) is recommended as a first-line treatment for varicose veins and has substituted the high ligation of saphenofemoral junctional reflux and stripping of varicose veins. Ultrasound-guided FS is associated with a high recurrence rate and can be used in conjunction with other procedures. MOCA and cyanoacrylate embolization appear promising, but evidence of their effectiveness is required.

Key Words: Varicose veins; Venous insufficiency; High ligation and stripping; Endovenous laser ablation; Radiofrequency ablation; Cure conservatrice et Hemodynamique de l'Insufficience Veineuse en Ambulatoire

©The Author(s) 2022. Published by Baishideng Publishing Group Inc. All rights reserved.

Core Tip: Endovenous laser ablation (EVLA) is the most cost-effective therapeutic option, with radiofrequency ablation (RFA) being a close second for the treatment of patients with varicose veins. Endovenous thermal ablation (EVLA or RFA) is recommended as a first-line treatment for varicose veins and has substituted the high ligation of saphenofemoral junctional reflux and stripping of varicose veins. In terms of recurrence of varicose veins, there is little or no difference between Cure conservatrice et Hemodynamique de l'Insufficience Veineuse en Ambulatoire and EVLA, RFA, or stripping. Ultrasound guided foam sclerotherapy is associated with a high recurrence rate and can be used in conjunction with other procedures. Mechanochemical endovenous ablation and cyanoacrylate embolization appear promising, but evidence on their effectiveness is warranted.

Citation: Gao RD, Qian SY, Wang HH, Liu YS, Ren SY. Strategies and challenges in treatment of varicose veins and venous insufficiency. *World J Clin Cases* 2022; 10(18): 5946-5956
URL: https://www.wjgnet.com/2307-8960/full/v10/i18/5946.htm
DOI: https://dx.doi.org/10.12998/wjcc.v10.i18.5946

INTRODUCTION

Varicose veins are tortuous, twisted, or elongated veins dilated to at least 3 mm in diameter evaluated when a patient in standing status with a prevalence of 10% in the population[1], and serious conditions such as deep venous thrombosis (DVT) and pulmonary embolism may occur if untreated[2,3]. Patients with varicose veins can be treated with conservative or surgical options based on the clinical conditions and patient preferences[4-6]. In the recent decade, there has been a dramatic change in the recommendations for managing symptomatic varicose veins due to the rise of minimally invasive endovascular techniques[6,7]. Therefore, we searched the literature and summarize the strategies and challenges in the treatment of varicose veins and venous insufficiency.

STRATEGIES IN TREATMENT OF VARICOSE VEINS AND VENOUS INSUFFICIENCY

The decision and the choice of treatment for varicose veins are based on the severity of the venous insufficiency, cost, risk of postoperative complications, and patient preferences. Management options for varicose veins include conservative treatment and surgical intervention. Asymptomatic patients with varicose veins are initially managed with conservative treatment options that include medicine, compression therapy, and lifestyle modifications, while symptomatic patients are suggested to consider surgical options[1] that include endovenous laser ablation (EVLA), radiofrequency ablation (RFA), high ligation and stripping (HL/S) of the incompetent great saphenous vein (GSV), Cure conservatrice et Hemodynamique de l'Insufficience Veineuse en Ambulatoire (CHIVA), mechanochemical ablation (MOCA), cyanoacrylate embolization (CAE), *etc.* (Table 1)[6-8].

COMPRESSION THERAPY

Compression therapy is the mainstay of conservative management and is effective in the treatment of varicose veins with venous ulcers[9]. Compression bandaging helps manage ankle edema. However, many patients can barely tolerate bandaging because of itching, pain, and difficulty in putting on shoes. Thus, medical stockings are more welcomed than compression bandaging[10]. Compression stockings

Table 1 Strategies for management of varicose veins

Name of treatment	Mechanism
Conservative	
Medicine	Enhancing venous tone and reducing inflammation
Compression	External pressure, bandages, or graduated stockings
Surgery	
HL/S	Ligation of the conjunction of reflux, stripping veins
AP	Removal of veins *via* small incision
CHIVA	Ligation of the escape point and preserving veins
HIPP	Destroying veins and sucking out with vaccum pressure
Thermal	
EVLA	Sealing the veins by laser energy
RFA	Sealing the veins by radiofrequency
Nontheramal	
Sclerotherapy	Destroying the venous wall by sclerosants or chemical agents and sealing veins by external pressure
MOCA	Rotating the venous wall and sealing veins with a clue
CAE	Sealing veins with a clue

HL/S: High ligation and stripping; EVLA: Endovenous laser ablation; RFA: Radiofrequency ablation; MOCA: Mechanochemical ablation; CAE: Cyanoacrylate embolization; CHIVA: Cure conservatrice et Hemodynamique de l'Insuffiсience Veineuse en Ambulatoire.

with graduated compression produce graded external compression directly to the legs and oppose the venous blood pressure.

When choosing compression stockings, patients are educated to prefer compression stockings with graduated compression to non-graded ones. Patients with varicose veins involving the main axial superficial veins above and below the knee should choose thigh-length graduated compression stockings rather than knee-length ones. Stockings with moderate pressure (20-30 mmHg) are recommended for patients with varicose veins (C2 to C3), stockings with pressure around 30 to 40 mmHg for people with skin change or an ulcer (C4 to C6), and stockings with a pressure between 40 and 50 mmHg for patients with a recurrent ulcer as an adjuvant treatment to prevent ulcer recurrence [10,11].

At least 1-wk compression stocking therapy after EVLA is suggested because a long time (1-2 wk) of using compression therapy is better than a short-term (24-48 h) of application in terms of reducing postoperative pain at 1 wk and recovery for work[11]. Yet, a trial of compression therapy is unnecessary before endovenous thermal ablation[9] as there is no strong evidence to support compression stockings in the cure of varicose veins C1-C4[9]. Limitations to the use of compression stockings include arterial insufficiency, application difficulty, and patient preferences.

MEDICAL THERAPY

Venoactive drugs are prescribed for symptomatic patients with varicose veins, ankle swelling, and venous ulcers to improve venous tone and capillary permeability. The commonly used drugs are spooning, *e.g.*, horse chestnut seed extract, the micronized purified flavonoid fraction (MPFF), and flavonoids[12-14]. Pentoxifylline is reported to target inflammatory cytokine release, leukocyte activation, and platelet aggregation at the microcirculatory level. The use of pentoxifylline or MPFF in combination with compression therapy may improve the closure of venous ulcers compared with compression and placebo[13]. A Cochrane meta-analysis shows that vasoactive drugs may relieve pain and swelling caused by chronic venous insufficiency, but their precise mechanism is not clear. Long-term studies of the safety and effectiveness of phlebotomists are warranted[12-15].

SURGICAL THERAPY

Historically, surgery with high ligation of saphenofemoral junction (SFJ) or saphenopopliteal junction with or without vein stripping (HL/S) has been the gold standard of care for varicose veins[1]. Specifically, following general or lumbar anesthesia, an incision is made at the groin or upper calf, the GSV is located and incised, the proximal end is ligated below the SFJ, a stripping wire with a probe is put into the GSV and advanced distally, and the proximal part of the GSV is tied to the wire and stripped. Recently, a growing number of research data do not consistently favor surgery as the standard treatment option due to postoperative complications, and the 2013 National Institute for Health and Care Excellence clinical guidelines recommend surgery as a third-line therapeutic option after EVLA or RFA and sclerotherapy[8,16-18].

HL/S of the GSV and their respective junctions are indicated when the saphenous veins themselves dilate greater than 1 cm in diameter. In a cohort study, Navarroet al[19] evaluated the relationship of GSV diameter measured in the thigh and calf to the clinical severity of reflux in 112 legs of 85 consecutive patients with SFJ and truncal GSV incompetence[19] and found that a GSV diameter of 5.5 mm or less predicted having no abnormal reflux, with a sensitivity of 78%, specificity of 87%, positive and negative predictive values of 78%, and accuracy of 82%[19].

The surgical outcome of HL/S is relatively satisfactory; HL/S is associated with higher anatomic closure rates at 30 d and 5 years than RFA and ultrasound-guided foam sclerotherapy (UGFS)[8,16]. HL/S has similar long-term saphenous vein closure rates with EVLA at 5 years[8,16-18]. However, the postoperative complications are DVT, bleeding, hematoma, ecchymosis, wound infection, nerve injury, pain, and delayed return to normal activity. The injury of femoral arteries, such as ligation and or stripping of the femoral artery, occurred in the hands of inexperienced operators, which is underreported. Ligation alone is usually associated with a high recurrence rate of the varicose vein that may necessitate re-operation[20]. Stripping of the GSV below the knee or the SSV is not usually performed to avoid the risk of nerve injury.

AMBULATORY PHLEBECTOMY

Ambulatory phlebectomy (AP), also known as hook phlebectomy, mini-phlebectomy, microphlebectomy, or stab phlebectomy, is a minimally invasive procedure operated under local anesthesia as an outpatient procedure, and it can excise most varicose veins except the proximal long saphenous vein [21]. AP has a technically better outcome in terms of recurrence of GSV and SFJ reflux than UGFS in the long term. Specifically, a small stab wound or puncture is made to remove varicose veins. Administering a certain volume of saline around the target veins before making a stab may help retrieve a longer section of unwanted veins. AP is usually performed in conjunction with other procedures.

Notwithstanding, recurrence rates can be high if the junctional reflux is untreated[21]. The junctional reflux should be managed by HL/S or EVLT rather than simple AP[21]. Patients can walk right away after AP. The proportion of complications associated with AP such as localized thrombophlebitis and hemorrhage is much lower than that of HL/S. The postoperative complications are reduced dramatically after the application of broad compression pads over the wounds following AP.

CHIVA

CHIVA is ambulatory conservative hemodynamic management of varicose veins that preserves deliberately the saphenous vein and collaterals based on venous hemodynamics[22]. CHIVA is an office-based treatment for varicose veins performed under local anesthesia. The main advantages are the preservation of the saphenous vein, local anesthesia, low cost, low pain, and less bruising, nerve damage, and recurrence than stripping saphenectomy[23] (Figure 1). CHIVA seemed to have superior clinical benefits in long-term efficacy for treating varicose veins[24]. Practically, CHIVA procedure is most likely similar to AP. Patients can walk out of the theatre immediately after CHIVA surgery and go home following observing for a while.

However, the recent Cochrane review[25] included six randomized controlled trials (RCTs) with 1160 patients and compared CHIVA with RFA, vein stripping, and EVLT, respectively, for their effects. In terms of recurrence of varicose veins, there is little or no difference between CHIVA and stripping, RFA, or EVLT. In comparison with RFA or EVLT, CHIVA may cause more bruising and make little or no difference to rates of limb infection, superficial vein thrombosis, nerve injury, or hematoma. Three RCTs comparing CHIVA with vein stripping showed that CHIVA may reduce slightly nerve injury and hematoma in the legs, but make little or no difference to the side effects of limb infection, and superficial vein thrombosis or bruising[25]. One RCT comparing CHIVA with compression dressings in patients with venous ulcers shows uncertainty on whether CHIVA can reduce recurrence.



DOI: 10.12998/wjcc.v10.i18.5946 **Copyright** ©The Author(s) 2022.

Figure 1 A 56-year-old man had varicose veins for 20 years and received day surgery with Cure conservatrice et Hemodynamique de l'Insufficience Veineuse en Ambulatoire procedure, and the varicose veins disappeared on day 5 (Figures are provided by Dr. Shi-Yan Ren).

It is necessary to map and find the escape point (EP) of the veins before CHIVA. Most (82.3%) EPs are located below the knee, and 65.8% are located from the knee to midcalf. The diameter of tributary veins (TVs) near the EP is about 90% of that of the GSV. Thermal ablations of the below-knee varicose vein may damage the nerve[26].

TRANSILLUMINATION POWERED PHLEBECTOMY

Transilluminated powered phlebectomy (TIPP) is reported as a minimally invasive procedure that is often performed under spinal or general anesthesia for the treatment of varicose veins[27], and it was once considered cosmetic for veins less than 2.5 mm in diameter due to few incisions. However, TIPP has been associated with a higher incidence of hematoma, postoperative pain, and paresthesia[28] due to damage to tissue and nerve around the veins; it has not been proven to be superior to other procedures to remove varicose veins[27]. Aremu *et al*[27] compared conventional stab avulsions to TIPP and found that recurrence at 52 wk in the TIPP group is higher than that in the stab avulsion group (21.2% *vs* 6.2%)[28].

TIPP cannot be performed for all the varicose veins, especially for truncal varicose veins. In combination with RFA, a more satisfactory outcome at a 1-year follow-up[29] can be achieved. Passman *et al*[30] divided their patients into three groups to evaluate the effect of TIPP: Saphenous stripping-stab avulsion phlebectomy (STRIP-AP), combined saphenous vein stripping-TIPP (STRIP-TIPP), and combined EVLT-TIPP. The rate of complications was higher in procedures involving TIPP (STRIP-AP 5.6%, STRIP-TIPP 6.5%, and EVAB-TIPP 2.0%; P = NS), and more hematomas occurred in procedures involving TIPP (STRIP-AP 5.6%, STRIP-TPP 16.3%, and EVAB-TPP 6.9%; $P < 0.05$)[30].

ENDOVENOUS THERMAL ABLATION THERAPY

Endovenous thermal ablation (EVLA or RFA) is recommended as a first-line treatment and has substituted the surgical procedure to destroy the veins by heat and occlude the veins for symptomatic varicose veins[9,31,32].

EVLA was initially reported by Dr. Carlos Bone for the treatment of varicose veins at the International Union of Phlebology in 1999. The laser fiber is inserted into the target vein, a heat generator emits laser energy, and the thermal light emitting out of the fiber tip induces local thermal injury to the veins, leading to vein contraction, blood thrombosis, and venous fibrosis. EVTA with or without HL/S appeared to be a safe and effective treatment for patients with incompetent saphenous veins[33].

One systematic evidence review reported that the occlusion rates of the GSV and small saphenous vein within 6 mo after EVLA were all greater than 90%[20]. A study by Wallace *et al*[34] showed that the SFJ anatomical success closure rate detected by DUS 5 years after treatment is similar between HL/S

(85%) and EVLA (93%). A meta-analysis by Kheirelseid *et al*[35] demonstrated no significant differences between HL/S in comparison to EVLA and RFA after 5 years[35].

A range of laser wavelengths can be used to achieve occlusion, and the radial fibers and lasers with high wavelengths (1470–1940 nm) are introduced for homogeneous damage of the vein wall to improve the efficacy and reduce the side effect of procedures[36]. The temperature produced by a 1470-nm laser with a radial probe is 120–140 °C (± 20 °C)[36], and less pain is noticed in the first week after the use of a 1470-nm wavelength fiber than a 940-nm fiber. At the 48-mo follow-up, the recurrence rate of treated veins followed by ultrasound was less with the 1470-nm wavelength laser than with 940-nm fibers (8.3% *vs* 15.9%, $P = 0.017$)[37]. Another RCT indicated that patients treated with the 1470-nm catheter had a higher occlusion rate than those with the 1920-nm system (94.7%*vs* 87.5%; $P = 0.05$) at 1-year follow-up. Patients treated with the 1920-nm EVLA catheter had less ecchymosis, induration, and analgesic use.

However, a systematic review and meta-analysis show that commonly used EVLA parameters do not influence efficacy, no particular wavelength is superior to any other[20], and no statistically significant differences were found for wavelengths [short (810, 940, and 980 nm), long (1470, 1500, and 1920 nm)], high or low administered energy (≤ 50 J/cm and > 50 J/cm), or follow-up (≤ 1 year and > 1 year). The overall success rate of EVLA was 92%[38]. An RCT study by Malskat *et al*[39] showed that treatment success and adverse event rates between a 1470-nm wavelength fiber and a 940-nm fiber for the treatment of varicose veins were similar[39].

The common complications after EVLA are bruising (24%-75%), thrombophlebitis (5%), superficial vein thrombosis, DVT, hematomas and ecchymoses, skin burn, pigmentation, nerve injury, recurrence, and retained fragment of catheter[40,41]. Arteriovenous fistula has been reported after perforator ablation. The risk of nerve lesions increases when the endovenous treatment is carried out on the lower leg. Recurrence can be treated with the second ablation, and the occlusion rate was 93.3% 1 year after the second ablation[42,43].

RFA

RFA is an ultrasonography-guided minimally invasive treatment that ablates the refluxing vein segment using thermal energy delivered through a radiofrequency catheter. RFA can be segmental procedures that induce heat to 120 °C. Ultrasonography is used to guide to insert a guidewire into the target vein, and an introducer sheath is advanced through the guidewire which will be pulled away followed by inserting the RFA catheter into the sheath into the target position.

A tumescent anesthetic solution is injected around GSV to reduce pain, provide good hemostasis, and prevent burn and nerve damage. After injection of a tumescent solution, the RF generator is then activated and the catheter is slowly pulled along the length of the vein. Compression therapy is used to reduce the risk of vein thrombosis, postoperative bruising, and tenderness. Patients are encouraged to walk immediately after RFA[44].

There is a difference among the RFA devices. F-Care (F Care Systems, Antwerp, Belgium) is a relatively new RFA technique for the treatment of venous insufficiency. The 30-d total occlusion rates in the F-Care and Closurefast groups were 96.2% and 98.1%, respectively ($P = 0.5$). The 1-year full occlusion rates in the F-Care and Closurefast groups were 71.7% and 90.6%, respectively ($P = 0.013$)[45]. The 3-RF trial is the first RCT of Venefit, radiofrequency induced thermal therapy (RFITT), and endovenous radiofrequency (EVRF) to compare outcomes of RFA devices. At 6 mo, complete GSV closure was significantly better after Venefit and RFITT treatment (100% and 98%, respectively) compared with EVRF treatment (79%, $P < 0.001$). However, clinical outcomes did not differ significantly at 1 year[46].

RFA is associated with a high satisfaction rate and quality of life score. Although operative time in RFA was significantly longer than that in surgery, recovery after RFA was significantly quicker than that after surgery in terms of returning to usual activity and work in 1 wk with fewer major adverse events. Complete obliteration of GSV was obtained in 98.2% of 135 patients (164 limbs) at a median follow-up of 11 mo[47]. RFA was shown to be non-inferior in terms of recurrence of CHIVA and HL/S 2 years after treatment. No differences in postoperative complications or pain were found among HL/S, RFA, and CHIVA[48].

COMPARISON OF RFA AND EVLA

EVLA and RFA seem to be the same safe and effective modalities in clinical efficacy in terms of occlusion rate, time to return to normal activity, and complications such as thrombophlebitis, hematoma, and recanalization[31,49,50]. A 10-year follow-up with duplex ultrasound for 240 patients treated with a 1470-nm diode laser with radial fibers found stable and valuable long-term results[36]. EVLA is the most cost-effective therapeutic option, followed by RFA, in patients with the incompetence of the GSV[8]. EVLA can manage almost all the varicose veins both above and below the knee; in contrast, RFA is used to ablate the truncal varicose vein above the knee, and cannot treat the varicose

veins below the knee that can be managed by EVLA. Thus, RFA is usually performed in conjunction with other procedures such as HIPP to achieve a better outcome[29].

An RCT comparing the endovenous treatment of primary GSV in 159 patients using RFA or 810 nm EVLT showed complete occlusion (100%) by duplex ultrasound in both groups at 1 wk, and 97% for RFA and 96% for EVLT at 3 mo follow-up. No significant adverse event was observed. Even though RFA showed less pain, ecchymosis, and hematomas[50,51], EVLA and RFA demonstrated comparable outcomes in terms of venous occlusion rates and return to normal activities. Both radiofrequency-powered segmental ablation and EVLA using bare-tip fibers have similarly high GSV obliteration rates in the first 5 years, and the treatments are equally effective clinically and have similar minimal postoperative pain scores and short recovery times[52].

SCLEROTHERAPY

Sclerotherapy is a less invasive percutaneous approach to administering sclerosants into the target veins [52] that will be closed subsequently after immediate external pressure. Anesthesia is generally not required during sclerotherapy. Compression stockings or bandages should be applied immediately after sclerotherapy. Patients are encouraged to walk to reduce the complications of sclerotherapy.

Sclerotherapy is recommended to treat varicose tributaries or the incompetent saphenous vein[9] and is considered cosmetic for treatment of veins less than 2.5 mm in diameter and all other indications. As sclerotherapy alone has not been proven to be effective for the treatment of SFJ or saphenopopliteal junctions reflux, patients with reflux should be treated with EVLA or HL/S to reduce the risk of recurrence.

Currently available sclerosants include detergents (*e.g.*, polidocanol and sodium morrhuate), osmotic agents, and chemical agents. No reliable evidence is available to support that one type of sclerosant is better than any other. Instead of using sclerosant as a liquid, foam sclerotherapy (FS) is performed using mixed sclerosant with air (usually 1:4) with or without UGFS, and it is used primarily or in conjunction with other procedures. The closure rate of veins with FS is higher (68%) than that with liquid sclerotherapy (17.5%) at 12 mo of follow-up[53]. UGFS is associated with faster recovery and less postoperative pain compared with EVLA and surgical stripping. The common complications are superficial venous thromboembolism, recurrence, hyperpigmentation, telangiectasia matting, *etc.* Patients often complain of nodular or linear hardness alone in the varicose veins with tenderness. DVT, tissue necrosis, or even arterial thrombosis has been observed after FS, especially with the use of liquid sodium morrhuate.

GSV recanalization was highest in the UGFS group (51%) during 1 year of follow-up[53]. A prospective RCT involving more than 580 legs compared four treatments: EVLA, RFA, UGFS, and surgical stripping for GSVs. UGFS was associated with a higher technical failure (16.3%) compared with other treatments ($P < 0.001$) at the 5-year follow-up. A total of 288 limbs of 233 patients were treated with UGFS, and the mean follow-up interval was 37.8 mo. Occlusion was achieved for 89.6% of the incompetent veins in two sessions of UGFS. The internal diameters of the treated veins were reduced to 66.9% at 3 mo and 32.7% at 12 mo. It is worthy to know that UGFS is unable to seal incompetent GSV segments completely and may be repeated several times in cases of recurrence[54].

MECHANOCHEMICAL ENDOVENOUS ABLATION

MOCA was conducted in 2010 using the ClariVein device. A wire tip is introduced into the targeted veins and rotated to abrase the intimal layer of the venous wall mechanically (3500 rpm), and a liquid sclerosant is simultaneously injected into the damaged venous wall below the catheter tip to seal the veins.

The MOCA is a non-thermal-non-tumescent option (NTNT) and appears to be of similar efficacy with stab avulsion with no potential risk of nerve damage.

A recent multi-center randomized study comparing MOCA with RFA for truncal vein reflux demonstrated that MOCA was significantly less painful than RFA ($P = 0.003$). There were no significant differences between MOCA and RFA for occlusion rates, clinical severity scores, time to return to normal activities, and adverse effects such as DVT and superficial thrombophlebitis[55].

The anatomical closure rate of MOCA is higher with 3% POL liquid than with 2% POL liquid at the 6-mo follow-up. A multicenter RCA study showed that the technical success rate at 6 mo was 69.8% in the 2%-group *vs* 78.0% in the 3%-group ($P = 0.027$). The overall closure rate was higher in GSVs < 5.9 mm than in GSVs > 5.9 mm (84.3% *vs* 59.5%, $P < 0.001$). Regardless of the concentration of sclerosant, the overall success rate of MOCA is lower than that of EVAL, RFA, or HL/S[55].

CAE

CAE is a novel endovascular NTNT ablation technique for treatment of incompetent truncal veins with *n*-butyl-2-cyanoacrylate (NBCA) glue[56-58]. Multiple studies have shown the effectiveness of CAE since its first use in 2013. Current available two techniques are the VenaSealTM Closure System and the VariCloseR vein sealing system[56]. A catheter used is pulled back segmentally in a former system or, continuously in the latter technique. NBCA glue is an adhesive that rapidly polymerizes during endovenous treatment to cause rapid occlusion of veins and initiate vein fibrosis.

In a review of 2910 patients (3220 veins) in 17 studies, 1981 patients received NBCA, 445 RF, and 484 EVLA. The mean followed-up was 12.3 mo (1–36 mo). Two-year occlusion rates were 93.7, 90.9, and 91.5% for NBCA, RFA, and EVLA, respectively[58]. CAE had higher anatomic closure rates at 30 d than EVLA[16]. Patients treated with CAE had less postoperative ecchymosis than those with RFA ($P < 0.01$). Pain during the procedure was comparable for both groups. Patients treated with NBCA had the fewest complications, *e.g.*, bruising, phlebitis, and pain. NBCA is simple to administer, safe, and effective even without compression stockings[58].

However, complications of CAE treatment are phlebitis, cellulitis, and DVT. The adhesive is presumably not degraded and remains in the vein over many years. In rare instances, cyanoacrylate glue embolization can extravasate and cause chronic foreign body reactions necessitating surgical intervention[57,58]. A thread-like thrombus extension has been reported with the VenaSeal system, which resolved spontaneously without additional adjunctive treatment after 6 mo of follow-up. Occlusion of the treated vein is incomplete with recanalization in the peripheral region after CAE. In this case, USFS can be used to achieve the complete occlusion of the veins. MOCA and CAE appear promising but evidence of their effectiveness is needed[8].

CONCLUSION

EVLA is the most cost-effective therapeutic option, with RFA being a close second for the treatment of patients with varicose veins. Endovenous thermal ablation (EVLA or RFA) is recommended as a first-line treatment for varicose veins and has substituted the high ligation of saphenofemoral junctional reflux and stripping of varicose veins. The 2013 National Institute for Health and Care Excellence clinical guidelines recommend surgery as a third-line therapeutic option after EVLA or RFA and sclero-therapy. In terms of recurrence of varicose veins, there is little or no difference between CHIVA and EVLA, RFA, or stripping. Ultrasound-guided FS is associated with a high recurrence rate and can be used in conjunction with other procedures. Currently, no strong evidence is available to show whether MOCA or cyanoacrylate embolization is similar or superior to any other procedures in the treatment of varicose veins.

FOOTNOTES

Author contributions: Qian SY and Gao RD contributed equally to this manuscript by composing the manuscript; Ren SY searched and studied the references and designed, wrote, revised, and submitted the manuscript; Wang HH and Liu YS discussed the manuscript; all authors have read and approved the final manuscript.

Conflict-of-interest statement: No conflict of interest exists.

Open-Access: This article is an open-access article that was selected by an in-house editor and fully peer-reviewed by external reviewers. It is distributed in accordance with the Creative Commons Attribution NonCommercial (CC BY-NC 4.0) license, which permits others to distribute, remix, adapt, build upon this work non-commercially, and license their derivative works on different terms, provided the original work is properly cited and the use is non-commercial. See: https://creativecommons.org/Licenses/by-nc/4.0/

Country/Territory of origin: China

ORCID number: Rong-Ding Gao 0000-0002-4516-1575; Song-Yi Qian 0000-0001-9258-5621; Hai-Hong Wang 0000-0002-7126-7138; Yong-Sheng Liu 0000-0002-9560-5875; Shi-Yan Ren 0000-0003-4528-2307.

S-Editor: Fan JR
L-Editor: Wang TQ
P-Editor: Fan JR

REFERENCES

1 **Medical Advisory Secretariat**. Endovascular radiofrequency ablation for varicose veins: an evidence-based analysis. *Ont Health Technol Assess Ser* 2011; **11**: 1-93 [PMID: 23074413]
2 **Raetz J**, Wilson M, Collins K. Varicose Veins: Diagnosis and Treatment. *Am Fam Physician* 2019; **99**: 682-688 [PMID: 31150188]
3 **Lin F**, Zhang S, Sun Y, Ren S, Liu P. The management of varicose veins. *Int Surg* 2015; **100**: 185-189 [PMID: 25594661 DOI: 10.9738/INTSURG-D-14-00084.1]
4 **Li X**, Yang B, Li X, Ren S. Prospective Comparison of Effect of Ligation and Foam Sclerotherapy with Foam Sclerotherapy Alone for Varicose Veins. *Ann Vasc Surg* 2018; **49**: 75-79 [PMID: 29428536 DOI: 10.1016/j.avsg.2018.01.004]
5 **Sun Y**, Li X, Chen Z, Ren S. Feasibility and safety of foam sclerotherapy followed by a multiple subcutaneously interrupt ligation under local anaesthesia for outpatients with varicose veins. *Int J Surg* 2017; **42**: 49-53 [PMID: 28419883 DOI: 10.1016/j.ijsu.2017.04.023]
6 **Li X**, Fan L, Ren S, Li X. Outcomes of Foam Sclerotherapy plus Ligation *vs* Foam Sclerotherapy Alone for Venous Ulcers in Lower Extremities. *Ann Vasc Surg* 2017; **45**: 160-165 [PMID: 28648655 DOI: 10.1016/j.avsg.2017.06.055]
7 **Liu P**, Ren S, Yang Y, Liu J, Ye Z, Lin F. Intravenous catheter-guided laser ablation: a novel alternative for branch varicose veins. *Int Surg* 2011; **96**: 331-336 [PMID: 22808616 DOI: 10.9738/cc44.1]
8 **Epstein D**, Bootun R, Diop M, Ortega-Ortega M, Lane TRA, Davies AH. Cost-effectiveness analysis of current varicose veins treatments. *J Vasc Surg Venous Lymphat Disord* 2022; **10**: 504-513.e7 [PMID: 34450353 DOI: 10.1016/j.jvsv.2021.05.014]
9 **Gloviczki P**, Comerota AJ, Dalsing MC, Eklof BG, Gillespie DL, Gloviczki ML, Lohr JM, McLafferty RB, Meissner MH, Murad MH, Padberg FT, Pappas PJ, Passman MA, Raffetto JD, Vasquez MA, Wakefield TW; Society for Vascular Surgery; American Venous Forum. The care of patients with varicose veins and associated chronic venous diseases: clinical practice guidelines of the Society for Vascular Surgery and the American Venous Forum. *J Vasc Surg* 2011; **53**: 2S-48S [PMID: 21536172 DOI: 10.1016/j.jvs.2011.01.079]
10 **Todd M**. Compression therapy for chronic oedema and venous leg ulcers: CoFlex TLC Calamine. *Br J Nurs* 2019; **28**: S32-S37 [PMID: 31242115 DOI: 10.12968/bjon.2019.28.12.S32]
11 **Chou JH**, Chen SY, Chen YT, Hsieh CH, Huang TW, Tam KW. Optimal duration of compression stocking therapy following endovenous thermal ablation for great saphenous vein insufficiency: A meta-analysis. *Int J Surg* 2019; **65**: 113-119 [PMID: 30959134 DOI: 10.1016/j.ijsu.2019.03.024]
12 **Gohel MS**, Davies AH. Pharmacological agents in the treatment of venous disease: an update of the available evidence. *Curr Vasc Pharmacol* 2009; **7**: 303-308 [PMID: 19601855 DOI: 10.2174/157016109788340758]
13 **Ulloa JH**. Micronized Purified Flavonoid Fraction (MPFF) for Patients Suffering from Chronic Venous Disease: A Review of New Evidence. *Adv Ther* 2019; **36**: 20-25 [PMID: 30758743 DOI: 10.1007/s12325-019-0884-4]
14 **Akhmetzianov RV**, Bredikhin RA. Clinical Efficacy of Conservative Treatment with Micronized Purified Flavonoid Fraction in Female Patients with Pelvic Congestion Syndrome. *Pain Ther* 2021; **10**: 1567-1578 [PMID: 34537951 DOI: 10.1007/s40122-021-00312-6]
15 **Krasinski Z**, Krasińska A, Markiewicz S, Zieliński M. Patients with chronic venous insufficiency in the times of COVID-19 and the risk of thrombus formation - suggestions on conservative treatment of such patients based on the principles of pathophysiology. *Pol Przegl Chir* 2021; **93**: 43-52 [PMID: 33949321 DOI: 10.5604/01.3001.0014.8500]
16 **Farah MH**, Nayfeh T, Urtecho M, Hasan B, Amin M, Sen I, Wang Z, Prokop LJ, Lawrence PF, Gloviczki P, Murad MH. A systematic review supporting the Society for Vascular Surgery, the American Venous Forum, and the American Vein and Lymphatic Society guidelines on the management of varicose veins. *J Vasc Surg Venous Lymphat Disord* 2021 [PMID: 34450355 DOI: 10.1016/j.jvsv.2021.08.011]
17 **Snyder D**, Sullivan N, Margolis D, Schoelles K. Skin Substitutes for Treating Chronic Wounds [Internet]. Rockville (MD): Agency for Healthcare Research and Quality (US); 2020-Feb-2 [PMID: 32101391]
18 **Mazzei S**, Sindoni A, Fama F, Buizon NJ, Shafei MA. Dehydrated human amnion/chorion membrane treatment of venous leg ulcers. *Indian J Dermatol Venereol Leprol* 2020; **86**: 212-214 [PMID: 31997789 DOI: 10.4103/ijdvl.IJDVL_175_19]
19 **Navarro TP**, Delis KT, Ribeiro AP. Clinical and hemodynamic significance of the greater saphenous vein diameter in chronic venous insufficiency. *Arch Surg* 2002; **137**: 1233-1237 [PMID: 12413308 DOI: 10.1001/archsurg.137.11.1233]
20 **MSAC**. Endovenous laser therapy (ELT) for varicose veins. Assessment report. MSAC Application 1113 Canberra, ACT: MSAC; March. 2008
21 **MSAC**. Consultation Decision Analytic Protocol (DAP) to guide the assessment of radiofrequency ablation for the treatment of varicose veins due to chronic venous insufficiency. MSAC Application 1166 Canberra, ACT: MSAC; November 11. 2011
22 **Faccini FP**, Arendt AL, Pereira RQ, de Oliveira AR. CHIVA to spare the small and great saphenous veins after wrong-site surgery on a normal saphenous vein: a case report. *J Vasc Bras* 2019; **18**: e20180077 [PMID: 31191627 DOI: 10.1590/1677-5449.007718]
23 **Faccini FP**, Ermini S, Franceschi C. CHIVA to treat saphenous vein insufficiency in chronic venous disease: characteristics and results. *J Vasc Bras* 2019; **18**: e20180099 [PMID: 31191629 DOI: 10.1590/1677-5449.009918]
24 **Guo L**, Huang R, Zhao D, Xu G, Liu H, Yang J, Guo T. Long-term efficacy of different procedures for treatment of varicose veins: A network meta-analysis. *Medicine (Baltimore)* 2019; **98**: e14495 [PMID: 30762775 DOI: 10.1097/MD.0000000000014495]
25 **Bellmunt-Montoya S**, Escribano JM, Pantoja Bustillos PE, Tello-Díaz C, Martinez-Zapata MJ. CHIVA method for the treatment of chronic venous insufficiency. *Cochrane Database Syst Rev* 2021; **9**: CD009648 [PMID: 34590305 DOI: 10.1002/14651858.CD009648.pub4]
26 **Yun S**. Ultrasound-based topographic analysis of tributary vein connection with the saphenous vein during ambulatory conservative hemodynamic correction of chronic venous insufficiency. *J Vasc Surg Venous Lymphat Disord* 2019; **7**: 356-

363 [PMID: 30777672 DOI: 10.1016/j.jvsv.2018.09.011]
27 **Aremu MA**, Mahendran B, Butcher W, Khan Z, Colgan MP, Moore DJ, Madhavan P, Shanik DG. Prospective randomized controlled trial: conventional *vs* powered phlebectomy. *J Vasc Surg* 2004; **39**: 88-94 [PMID: 14718823 DOI: 10.1016/j.jvs.2003.09.044]
28 **de Zeeuw R**, Wittens C, Loots M, Neumann M. Transilluminated powered phlebectomy accomplished by local tumescent anaesthesia in the treatment of tributary varicose veins: preliminary clinical results. *Phlebology* 2007; **22**: 90-94 [PMID: 18268858 DOI: 10.1258/026835507780346141]
29 **Liao CJ**, Song SH, Li T, Zhang Y, Zhang WD. Randomized clinical trial of radiofrequency-induced thermotherapy combined with transilluminated powered phlebectomy *vs* high ligation and stripping for the treatment of lower limb varicose veins. *J Vasc Surg Venous Lymphat Disord* 2021; **9**: 95-100 [PMID: 32454239 DOI: 10.1016/j.jvsv.2020.04.028]
30 **Passman MA**, Dattilo JB, Guzman RJ, Naslund TC. Combined endovenous ablation and transilluminated powered phlebectomy: is less invasive better? *Vasc Endovascular Surg* 2007; **41**: 41-47 [PMID: 17277242 DOI: 10.1177/1538574406296207]
31 **Kabnick LS**, Sadek M, Bjarnason H, Coleman DM, Dillavou ED, Hingorani AP, Lal BK, Lawrence PF, Malgor R, Puggioni A. Classification and treatment of endothermal heat-induced thrombosis: Recommendations from the American Venous Forum and the Society for Vascular Surgery This Practice Guidelines document has been co-published in *Phlebology* [DOI: 10.1177/0268355520953759] and *Journal of Vascular Surgery: Venous and Lymphatic Disorders* [DOI: 10.1016/j.jvsv.2020.06.008]. The publications are identical except for minor stylistic and spelling differences in keeping with each journal's style. The contribution has been published under a Attribution-Non Commercial-No Derivatives 4.0 International (CC BY-NC-ND 4.0), (https://creativecommons.org/Licenses/by-nc-nd/4.0/). *Phlebology* 2021; **36**: 8-25 [PMID: 32998622 DOI: 10.1177/0268355520953759]
32 **Mohammadi Tofigh A**, Tahmasebi H, Zebarjadi J. Comparing the Success Rate and Side Effects of Endovenous Laser Ablation and Radiofrequency Ablation to Treat Varicose Veins in the Lower Limbs: A Randomized Clinical Trial. *J Lasers Med Sci* 2020; **11**: S43-S48 [PMID: 33995968 DOI: 10.34172/jlms.2020.S7]
33 **Hamann SAS**, van der Velden SK, De Maeseneer MGR. Safety and Effectiveness of Endovenous Thermal Ablation for Incompetent Saphenous Veins with an Aneurysm Close to the Junction. *Eur J Vasc Endovasc Surg* 2019; **58**: 244-248 [PMID: 31153734 DOI: 10.1016/j.ejvs.2018.12.007]
34 **Wallace T**, El-Sheikha J, Nandhra S, Leung C, Mohamed A, Harwood A, Smith G, Carradice D, Chetter I. Long-term outcomes of endovenous laser ablation and conventional surgery for great saphenous varicose veins. *Br J Surg* 2018; **105**: 1759-1767 [PMID: 30132797 DOI: 10.1002/bjs.10961]
35 **Kheirelseid EAH**, Crowe G, Sehgal R, Liakopoulos D, Bela H, Mulkern E, McDonnell C, O'Donohoe M. Systematic review and meta-analysis of randomized controlled trials evaluating long-term outcomes of endovenous management of lower extremity varicose veins. *J Vasc Surg Venous Lymphat Disord* 2018; **6**: 256-270 [PMID: 29292115 DOI: 10.1016/j.jvsv.2017.10.012]
36 **Pavei P**, Spreafico G, Bernardi E, Giraldi E, Ferrini M. Favorable long-term results of endovenous laser ablation of great and small saphenous vein incompetence with a 1470-nm laser and radial fiber. *J Vasc Surg Venous Lymphat Disord* 2021; **9**: 352-360 [PMID: 32599308 DOI: 10.1016/j.jvsv.2020.06.015]
37 **Arslan Ü**, Çalık E, Tort M, Yıldız Z, Tekin Aİ, Limandal HK, Kaygın MA, Dağ Ö, Erkut B. More Successful Results with Less Energy in Endovenous Laser Ablation Treatment: Long-term Comparison of Bare-tip Fiber 980 nm Laser and Radial-tip Fiber 1470 nm Laser Application. *Ann Vasc Surg* 2017; **45**: 166-172 [PMID: 28647634 DOI: 10.1016/j.avsg.2017.06.042]
38 **Malskat WSJ**, Engels LK, Hollestein LM, Nijsten T, van den Bos RR. Commonly Used Endovenous Laser Ablation (EVLA) Parameters Do Not Influence Efficacy: Results of a Systematic Review and Meta-Analysis. *Eur J Vasc Endovasc Surg* 2019; **58**: 230-242 [PMID: 31230868 DOI: 10.1016/j.ejvs.2018.10.036]
39 **Malskat WS**, Giang J, De Maeseneer MG, Nijsten TE, van den Bos RR. Randomized clinical trial of 940- *vs* 1470-nm endovenous laser ablation for great saphenous vein incompetence. *Br J Surg* 2016; **103**: 192-198 [PMID: 26661521 DOI: 10.1002/bjs.10035]
40 **Nemoto H**, Mo M, Ito T, Inoue Y, Obitsu Y, Kichikawa K, Yamaki T, Ogawa T; Japanese Endovenous Ablation Committee for Varicose Veins. Venous thromboembolism complications after endovenous laser ablation for varicose veins and role of duplex ultrasound scan. *J Vasc Surg Venous Lymphat Disord* 2019; **7**: 817-823 [PMID: 31540837 DOI: 10.1016/j.jvsv.2019.06.014]
41 **Ren S**, Liu P, Wang W, Yang Y. Retained foreign body after laser ablation. *Int Surg* 2012; **97**: 293-295 [PMID: 23294067 DOI: 10.9738/CC155.1]
42 **Rodriguez Santos F**, Loson V, Coria A, Marquez Fosser C, Dotta M, Katsini R, Pared C, Bauzá Moreno H, Martínez H. Secondary Ablation of Recanalized Saphenous Vein after Endovenous Thermal Ablation. *Ann Vasc Surg* 2020; **68**: 172-178 [PMID: 32339689 DOI: 10.1016/j.avsg.2020.04.017]
43 **Müller L**, Alm J. Feasibility and technique of endovenous laser ablation (EVLA) of recurrent varicose veins deriving from the sapheno-femoral junction-A case series of 35 consecutive procedures. *PLoS One* 2020; **15**: e0235656 [PMID: 32628724 DOI: 10.1371/journal.pone.0235656]
44 **Somasundaram SK**, Weerasekera A, Worku D, Balasubramanian RK, Lister D, Valenti D, Rashid H, Singh Gambhir RP. Office Based Endovenous Radiofrequency Ablation of Truncal Veins: A Case for Moving Varicose Vein Treatment out of Operating Theatres. *Eur J Vasc Endovasc Surg* 2019; **58**: 410-414 [PMID: 31351830 DOI: 10.1016/j.ejvs.2019.05.020]
45 **Bitargil M**, Kılıç HE. Ablation of the great saphenous vein with F-care *vs* Closurefast endovenous radiofrequency therapy: Double-blinded prospective study. *Phlebology* 2020; **35**: 561-565 [PMID: 32192407 DOI: 10.1177/0268355520913389]
46 **Nyamekye IK**, Dattani N, Hayes W, Harding D, Holloway S, Newman J. A Randomised Controlled Trial Comparing Three Different Radiofrequency Technologies: Short-Term Results of the 3-RF Trial. *Eur J Vasc Endovasc Surg* 2019; **58**: 401-408 [PMID: 31351832 DOI: 10.1016/j.ejvs.2019.01.033]
47 **Borghese O**, Pisani A, Di Centa I. Endovenous radiofrequency for chronic superficial venous insufficiency: Clinical outcomes and impact in quality of life. *J Med Vasc* 2021; **46**: 3-8 [PMID: 33546819 DOI: 10.1016/j.jdmv.2020.11.003]

48 **González Cañas E**, Florit López S, Vilagut RV, Guevara-Noriega KA, Santos Espí M, Rios J, Soto SN, Giménez Gaibar A. A randomized controlled noninferiority trial comparing radiofrequency with stripping and conservative hemodynamic cure for venous insufficiency technique for insufficiency of the great saphenous vein. *J Vasc Surg Venous Lymphat Disord* 2021; **9**: 101-112 [PMID: 32353592 DOI: 10.1016/j.jvsv.2020.04.019]

49 **He G**, Zheng C, Yu MA, Zhang H. Comparison of ultrasound-guided endovenous laser ablation and radiofrequency for the varicose veins treatment: An updated meta-analysis. *Int J Surg* 2017; **39**: 267-275 [PMID: 28119106 DOI: 10.1016/j.ijsu.2017.01.080]

50 **Izzo L**, Pugliese F, Pieretti G, Izzo S, Izzo P, Florio G, Del Papa M, Messineo D. High ligation of sapheno-femoral junction and thermal ablation for lower limb primary varicosity in day hospital setting. *Ann Ital Chir* 2020; **91**: 61-64 [PMID: 32180575]

51 **Florio G**, Carnì P, D'Amata G, Crovaro M, Musmeci L, Manzi L, Del Papa M. Thermal ablation combined with high ligation of sapheno-femoral junction for lower limb primary varicosity. *G Chir* 2019; **40**: 413-416 [PMID: 32003720]

52 **Lawson JA**, Gauw SA, van Vlijmen CJ, Pronk P, Gaastra MTW, Tangelder MJ, Mooij MC. Prospective comparative cohort study evaluating incompetent great saphenous vein closure using radiofrequency-powered segmental ablation or 1470-nm endovenous laser ablation with radial-tip fibers (Varico 2 study). *J Vasc Surg Venous Lymphat Disord* 2018; **6**: 31-40 [PMID: 29248107 DOI: 10.1016/j.jvsv.2017.06.016]

53 **Epstein D**, Onida S, Bootun R, Ortega-Ortega M, Davies AH. Cost-Effectiveness of Current and Emerging Treatments of Varicose Veins. *Value Health* 2018; **21**: 911-920 [PMID: 30098668 DOI: 10.1016/j.jval.2018.01.012]

54 **Chen CH**, Chiu CS, Yang CH. Ultrasound-guided foam sclerotherapy for treating incompetent great saphenous veins--results of 5 years of analysis and morphologic evolvement study. *Dermatol Surg* 2012; **38**: 851-857 [PMID: 22540961 DOI: 10.1111/j.1524-4725.2012.02408.x]

55 **Lam YL**, Alozai T, Schreve MA, de Smet AAEA, Vahl AC, Nagtzaam I, Lawson JA, Nieman FHM, Wittens CHA. A multicenter, randomized, dose-finding study of mechanochemical ablation using ClariVein and liquid polidocanol for great saphenous vein incompetence. *J Vasc Surg Venous Lymphat Disord* 2021 [PMID: 34781008 DOI: 10.1016/j.jvsv.2021.10.016]

56 **Chan SS**, Tang TY, Chong TT, Choke EC, Tay HT. Retrograde technique for great saphenous vein ablation using the VenaSeal™ closure system - Ideal approach for deep seated or small below the knee refluxing truncal veins. *Phlebology* 2020; **35**: 102-109 [PMID: 31132940 DOI: 10.1177/0268355519853412]

57 **Langridge BJ**, Onida S, Weir J, Moore H, Lane TR, Davies AH. Cyanoacrylate glue embolisation for varicose veins - A novel complication. *Phlebology* 2020; **35**: 520-523 [PMID: 31992129 DOI: 10.1177/0268355520901662]

58 **Dimech AP**, Cassar K. Efficacy of Cyanoacrylate Glue Ablation of Primary Truncal Varicose Veins Compared to Existing Endovenous Techniques: A Systematic Review of the Literature. *Surg J (N Y)* 2020; **6**: e77-e86 [PMID: 32577526 DOI: 10.1055/s-0040-1708866]

World Journal of Clinical Cases

Submit a Manuscript: https://www.f6publishing.com

World J Clin Cases 2022 June 26; 10(18): 5957-5964

DOI: 10.12998/wjcc.v10.i18.5957

ISSN 2307-8960 (online)

MINIREVIEWS

Diabetes mellitus susceptibility with varied diseased phenotypes and its comparison with phenome interactome networks

Madhusmita Rout, Bhumandeep Kour, Sugunakar Vuree, Sajitha S Lulu, Krishna Mohan Medicherla, Prashanth Suravajhala

Specialty type: Endocrinology and metabolism

Provenance and peer review: Invited article; Externally peer reviewed.

Peer-review model: Single blind

Peer-review report's scientific quality classification

Grade A (Excellent): 0
Grade B (Very good): 0
Grade C (Good): C, C, C
Grade D (Fair): D
Grade E (Poor): 0

P-Reviewer: Lei Y, China; Wang W, China; Zeng Y, China

Received: December 27, 2021
Peer-review started: December 27, 2021
First decision: January 23, 2022
Revised: February 2, 2022
Accepted: April 22, 2022
Article in press: April 22, 2022
Published online: June 26, 2022

Madhusmita Rout, Department of Pediatrics, University of Oklahoma Health Sciences Centre, Oklahoma City, OK 73104, United States

Madhusmita Rout, Krishna Mohan Medicherla, Department of Biotechnology and Bioinformatics, Birla Institute of Scientific Research, Jaipur 302001, Rajasthan, India

Bhumandeep Kour, Sugunakar Vuree, Department of Biotechnology, Lovely Professional University, Phagwara 144001, Punjab, India

Sajitha S Lulu, Department of Biotechnology, Vellore Institute of Technology, Vellore 632014, Tamil Nadu, India

Prashanth Suravajhala, Amrita School of Biotechnology, Amrita Vishwa Vidyapeetham, Vallikavu PO, Amritapuri, Clappana, Kollam 690525, Kerala, India

Corresponding author: Prashanth Suravajhala, PhD, Principal Scientist, Department of Biotechnology, Amrita School of Biotechnology, Amrita Vishwa Vidyapeetham, Vallikavu PO, Amritapuri, Clappana, Kollam 690525, Kerala, India. prash@bioclues.org

Abstract

An emerging area of interest in understanding disease phenotypes is systems genomics. Complex diseases such as diabetes have played an important role towards understanding the susceptible genes and mutations. A wide number of methods have been employed and strategies such as polygenic risk score and allele frequencies have been useful, but understanding the candidate genes harboring those mutations is an unmet goal. In this perspective, using systems genomic approaches, we highlight the application of phenome-interactome networks in diabetes and provide deep insights. LINC01128, which we previously described as candidate for diabetes, is shown as an example to discuss the approach.

Key Words: Type 1 diabetes; Gestational diabetes mellitus; Prostate cancer; Phenome; Type 2 diabetes; Pleiotropy

©The Author(s) 2022. Published by Baishideng Publishing Group Inc. All rights reserved.

Core Tip: Comprehensive genome-wide phenome-interactome networks are essential to identify candidate biomarkers such as LINC01128.

Citation: Rout M, Kour B, Vuree S, Lulu SS, Medicherla KM, Suravajhala P. Diabetes mellitus susceptibility with varied diseased phenotypes and its comparison with phenome interactome networks. *World J Clin Cases* 2022; 10(18): 5957-5964
URL: https://www.wjgnet.com/2307-8960/full/v10/i18/5957.htm
DOI: https://dx.doi.org/10.12998/wjcc.v10.i18.5957

INTRODUCTION

Diabetes mellitus occurs as a result of insufficient insulin production or impaired insulin sensitivity, and it has become a serious threat to people's health[1,2]. It is a heterogeneous problem with numerous aetiologies comprising three main types, *viz*., type 1 diabetes mellitus (T1DM), type 2 diabetes mellitus (T2DM), and gestational diabetes mellitus (GDM). Understanding the biological mechanisms associated would allow us to identify candidate proteins and genes[3]. The emergence of genome-wide association studies (GWASs) has substantially enhanced our understanding of the genetic basis of disease risk in the past few years. Prior to the introduction of GWASs in 2006, very little information was available about the genes that influence common complicated or multifactorial diseases and quantitative traits. These research findings imply that susceptibility to prevalent diseases is influenced by a variety of genetic topologies, including common genetic variants with minimal effects and uncommon variants with substantial impact sizes[4-6]. Nevertheless, the combination of candidate T2DM genes discovered using GWASs does not fully confirm established features of disease pathogenesis. Several system-level approaches have been used to bridge the gap between genome and phenome correlation[7]. Computational analyses of disease linked genes using interactome and toxicogenomic data help us to connect T2DM candidate genes found in GWAS with disease pathophysiology, including abnormal pancreatic cell formation and function, and insulin sensitivity. On the other hand, computational predictions of potential proteins/genes are less expensive and time-saving than experimental methods[8,9]. In order to unravel the genetic roots of common disorders, it is necessary to understand the complexity of the gene–phenotype connection. Recent research employing the human interactome and phenome has uncovered not just common phenotypic and genetic overlap between diseases but also a modular architecture of the genetic landscape of human diseases, opening up new avenues for reducing the complexity of human diseases[10,11]. Because diseases are rarely caused by the malfunction of a single protein, a more comprehensive and robust interactome is essential for identifying groups of interconnected proteins associated with disease aetiology[12].

PHENOME INTERACTION NETWORKS

The phenome interaction networks are used to study a wide range of phenotypic traits based on the analysis of the complete genome; it follows a genotypic to phenotypic approach in order to analyse the phenotypic traits[13]. The diseases with overlapping clinical signs can be predicted because of the mutation in different genes which are playing a role in similar functions. More recently, the studies on humans as well as model organisms have revealed that the primary or secondary association between proteins can also be one of the reasons of the same phenotype that means the mutation in particular protein along with its direct or indirect association with a single or multiple proteins can be responsible for overlapping of the clinical manifestations[14]. The opposite scenario can also be analysed using a phenome-interactome network, in case of pleiotropy, the cases in which a single gene is responsible for different phenotypic traits[15]. The protein-protein interaction (PPI) network models are used to analyse the phenomic traits, which in turn is helpful in understanding cell signalling and drug development in the diseased as well as normal cell physiology; basically, it is important to understand almost every process of the cell. PPI networks are the mathematical representation of physical interaction between similar or different proteins for the analysis of phenomes. The mathematical representation of interaction among different proteins in PPIs is based upon graph theory where the proteins are represented as nodes and edges to depict the type of interaction between two different interacting proteins[16]. PPI networks help to find the genes for a particular disease with a huge accuracy and when PPIs are implemented on the large datasets, it could lead to prediction of novel gene candidates[11]. The phenome interaction networks are quite important to understand and mine the genes associated with a particular disease. The genes that are responsible for similar functions have a higher chance of having the same phenotypes; therefore, understanding phenotypic as well as genotypic data is a must in order to understand the origination and development of a disease at the systems biology level for the better

treatment[17]. The origin and cause of several complex diseases including cancer, diabetes, and obesity can be understood by PPI network analysis[18].

GDM

GDM is categorised as insulin resistance leading to hyperglycemia during pregnancy, which mostly retracts after parturition. According to the World Health Organization, the prevalence rate is 15.8% accounting to about 20.4 million live births, with the majority of cases in pregnant women above the age of 35 years. The International Diabetes Federation in 2019 estimated a prevalence of 28.5% in India with incidence varying in each state due to challenges in screening strategies and paucity of consensus among physicians and healthcare providers in prepartum and postpartum management of GDM[19]. The diagnostic criteria may differ worldwide, and understanding the pathophysiology is crucial as it affects both the mother and the fetus during gestation, delivery, and later stages of life making them susceptible to diabetes, obesity, and cardiovascular complications in the long term[20]. Major challenges that have governed this disease are the guidelines for screening and diagnosis. The testing criteria are different with varying forms of oral glucose tolerance test being followed worldwide[21]. Management of GDM is another challenge as both the mother and fetus are at risk in their current milieu. Studies have highlighted the importance of treating GDM, reducing the risk of perinatal morbidity and improving post-delivery outcomes[22]. Glucose intolerance leads to the manifestation of the disease, hence the benchmark of GDM treatment should be glycaemic control which is achieved through lifestyle intervention such as diet and exercise, pharmacological intervention such as insulin, oral drugs, and herbal medicines, and finally postnatal management[23].

Pregnant women with GDM have an inherent risk of developing T2DM post-delivery or later on in life. The offspring is also susceptible to any form of diabetes postnatally or in the long term. The genetic factors responsible for GDM and future risk of developing T2DM through epidemiological and physiological studies reveal commonality in susceptibility loci, which implies that most of the diabetes genes are involved in causing GDM. The few key genes that share common variants are *KCNJ11*, *GCK*, *HNF1A*, *TCF7L2*, *CDKAL1*, *KCNQ1*, *CDKN2A*, *MTNR1B*, *SRR*, *HHEX*, *TCF2*, *SLC30A8*, and *IGF2BP2*[24, 25]. Genetic similarities between T1DM and GDM is less studied, and a study among Asian Indian women with GDM showed the presence of pancreatic autoantibodies like GAD which is a biomarker for T1DM[26]. Maturity onset diabetes of young (MODY) has different types and each type is characterised by a single gene, and few studies have shown that mutations in *HNF1A* and *HNF4A* are MODY genes which predispose to GDM[27].

Integrating phenotypic data with genotypic data through a computationally created high-confidence interaction network to analyse human diseases concurrently defines a phenome-interactome network [14]. An organized study on genes expressed in thigh subcutaneous adipose tissue of Asian Indian Type 2 Diabetes Mellitus revealed evidence of "sick thigh fat" as a causative disease. The phenome-interactome network had a significant correlation of differentially expressed genes (DEGs) and hub proteins with its phenotypic traits obtained at the clinical, biochemical, and radiological, cellular, and molecular levels, thus enumerating their role in T2DM, T1DM, and obesity[28]. RNA-seq analysis enables identification of differentially expressed genes and their role in a disease. The depth of the literature available on RNA-seq analysis performed on pregnant ladies with GDM is negligible. The GDM is a condition in which the intrauterine milieu, especially the placenta, plays a central role in altering the course of the fetus. Hence, having an understanding of the key genes regulated in the placenta is paramount for the disease diagnosis. Most of the literature available on RNA-seq analysis is centred on identifying DEGs in the placenta, umbilical cord, and amniocytes[29-32]. Studies have identified that non-coding RNAs such as long non-coding (lnc)RNAs, microRNAs, and circular RNAs play a central role in GDM pathogenesis. MicroRNAs have been identified as non-invasive early diagnostic biomarkers for GDM[33]. LncRNA-associated feed-forward loops network had a strong correlation between dysregulated glucose metabolism and hormone regulation in GDM cases[34]. The mechanism governing the pathophysiology of the disease is still not clear and the studies available are limited. Hence, the current problem is to understand the genetic background that affects both the mother and fetus with changes in the intrauterine environment and thus identify early diagnostic biomarkers. GDM is associated with a number of comorbidities due to the multifactorial nature of the disease. A study to identify key genes involved in GDM maternal and placental milieu revealed associations with T2DM, T1DM, obesity, hyperglycaemia, preeclampsia, neonatal diabetes, MODY, neurological disorders, cardiovascular disease, preeclampsia, hepatitis C, rheumatoid arthritis, and neoplasms[35]. Hence, the need to identify genes governing this disease and the variations that might affect the phenotype needs to be understood.

PROSTATE CANCER AND DIABETES, LINCO1128

As glucose level in the body is regulated by insulin, a hormone (peptide) which increases the glucose uptake and its assimilation. However, insulin resistance is stated when it becomes unable to perform this function in a diabetic patient. On the other hand, the beta cell continuously secretes insulin to make up and maintain balance but it results in hyperinsulinemia[36]. This increased level will trigger the production of IGF-1 from liver cells. IGF-1 will then bind to its tyrosine kinase receptor IGF-1R and stimulate various metabolic and mitogenic signalling pathways to control processes like cancer cell proliferation, differentiation, and apoptosis. Later, some downstream targets like PI3KB and rat sarcoma-mitogen-activated protein kinase/extracellular signal regulated kinase signaling pathways get stimulated. PI3KB signaling has a role in cancer cell survival and migration, while the rat sarcoma mitogen-activated protein kinase/extracellular signal regulated kinase signaling pathway controls cancer cell proliferation and metabolism[37]. Hence, patients who have diabetes show increased levels of IGF-1, bringing in them more susceptibility towards a higher risk of developing different cancers like breast, prostate, and colorectal cancer[38]. However, the growth factor IGF-II which shares locus with lncH19 (IGF-II/H19) forms an imprinted gene. This silencing is found disrupted in different cancers including prostate cancer. The association of adipose tissue and obesity is a known risk factor for both T2DM and prostate cancer by disturbing cellular environments. As a result, hyperglycaemia or inflammatory metabolic situations are hypothesized to be the cause of this loss of imprinting (LOI)[39]. Differentially expressed lncRNA (LINC01128) is already known to increase the rate of cervical cancer progression and is also predicted as a biomarker of gestational hypertension[40,41]. Similarly, Pradeep Tiwari *et al*[28] in 2019 suggested that LINC01128 could serve as a biomarker for diabetes diagnosis and prognosis (Figure 1). Metformin, an antidiabetic drug from several studies, has been proved to not only effect on glucose metabolism but also show interactions with androgen receptors. It plays a role in stabilizing prostate specific antigen (PSA) levels[42]. In certain therapy, another commonly used method for T2DM, it is reported that glucagon-like peptide-1 receptor expression plays an anti-prostate cancer effect. It is helping in attenuating cell cycle progression. So, its forceful activation to express can be a potential therapeutic approach[43]. Therefore, both metformin and certain therapies help in blocking cell cycle progression by reducing mTOR activity[44]. Hypogonadism (decrease in level of testosterone) is also found associated with both diabetes and prostate cancer (PCa). A fall in its serum level is capable of causing high graded PCa. Hence, T2DM is suggested to be a crucial predictor of high graded PCa especially with benign prostatic hyperplasia[45]. For early possible detection, PSA levels are broadly used, but its concentration shows variation due to several other comorbidities, age, and lifestyle, which makes it to demand more precise analysis of test results. Based on a linear aggression analysis, there is a fall in PSA in patients who are taking antidiabetics and obese people on hemodilution. This establishes an inverse relationship between diabetes obesity and PSA level. Such study suggests to deliberately check the PSA level, especially in diabetic and obese patients[46]. Both PCa and DM incidence is rising parallel with age. Despite the fact diabetes mellitus reduces the risk of PCa, DM can also increase its mortality[47]. The understanding of association between DM and PCa is still insufficient. Moreover, obesity makes its pathophysiology a more complex situation[48].

LINC01128

In a study, GEO datasets of osteosarcoma (OS) were analysed for LINC01128 expression to clear its oncogenic role. It revealed that increased expression of LINC01128 in OS patients is accompanied with their shorter survival. However, its knockdown turned down the proliferation, migration, and invasion. In OS, LINC01128 is identified to work as a sponge in triggering Wnt/β-Catenin signaling by promoting MMP2 expression through miR-299-3p[49]. In promoting cervical cancer development again, it functions as a sponge for miR-383-5p[50]. In cervical cancer tissues, the expression of LINC01128 is found significantly high and its fall suggests that it might lower the SFN (stratifin) at both the mRNA and protein levels. SFN, a known potential biomarker in cervical cancer, is also majorly expressed in the early stage of lung adenocarcinomas. It clearly explains how LINC01128 could accelerate cell processes like cell proliferation, migration, and invasion and even can inhibit the apoptosis through SFN upregulation and release by binding miR-383-5p and also working as its antagonist[51,52]. miR-383 is under regulation of LINC01128. However, overexpression of miR-383 in T2DM serum reverses the cell apoptosis under high glucose in mouse β cells by *TLR4* and *APOC3* suppression[53]. Also, high LINC01128 was seen in stage III-IV CRC and mediated PRMT5 function, which is a mediator of methylation of proteins[54]. In pancreatic cancer, it was found as an EMT-LPS (epithelial mesenchymal transition related lncRNA prognostic signature) molecule[55].

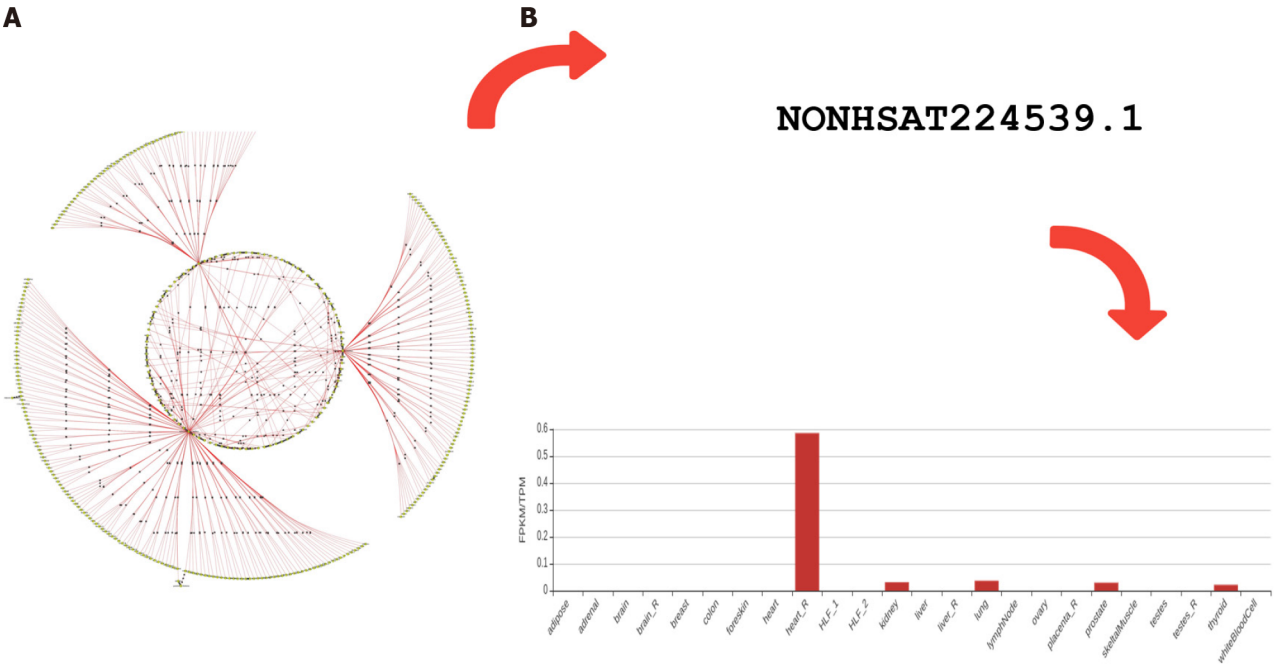

DOI: 10.12998/wjcc.v10.i18.5957 **Copyright** ©The Author(s) 2022.

Figure 1 Researchers have chosen interesting genes based on *P* value, heuristics, and contextuality, and then used CHAT analysis to find high-dimensional gene expression data for confirmation. Many critical genes, as well as their enriched pathways, were discovered to be involved in the molecular processes of obesity, lupus, adipose tissue, and fatty acid pathways. A: Phenome interactome networks of diabetes represented earlier (Tiwari *et al* [28], 2018); B: LncRNANONHSAT224539.1 (LINC01128 representative) expression in various tissues, largely seen in the heart, thyroid, kidney, and prostate.

CONCLUSION

The phenome-interactome networks have been a powerful approach to understand and characterize networks. There is a greater scope of relevance underlying the pathophysiology mentioned above. To fully comprehend the importance of phenome-interactome networks and diabetes associated metabolism, it is vital to ensure that there is a healthy diet regimen followed which also addresses the clinical implications of its absorption, bioavailability, and human health benefits. Integrated systems approaches can be used to discover the novel genes and pathways with an emphasis on the molecular physiological insights gained through systems/nutrigenomic modules and thereby candidate DEGs could be detected. Furthermore, standard operating procedures, recommendations, and guidelines in consideration of the aforementioned diabetes phenotypes for better dissemination of phenome-interactome predictions will help avoid the risk of over/under treatment. In addition, post next generation sequencing, a large focus nowadays should be on the development of NGS/genotyping panels which can set a precedent for a global consortium effort bridging the gap between the nutritional deficiency diseases and diabetes.

ACKNOWLEDGEMENTS

The authors gratefully acknowledge Arvinpreet Kaur, Mehak Chopra, Berenice, Kiran Telukunta, Anshu Bharadwaj, Harpreet Singh, and Purnima Sharma for subtle scientific deliberations.

FOOTNOTES

Author contributions: Rout M wrote the first draft; Kour B wrote the sections on diabetes; Suravajhala P proofread the manuscript with sections on phenome-interactome networks; all authors chipped in laterally; Kour B and Rout M are equal contributing first authors.

Conflict-of-interest statement: The authors declare no conflict of interest for this article.

Open-Access: This article is an open-access article that was selected by an in-house editor and fully peer-reviewed by external reviewers. It is distributed in accordance with the Creative Commons Attribution NonCommercial (CC BY-NC 4.0) license, which permits others to distribute, remix, adapt, build upon this work non-commercially, and license

their derivative works on different terms, provided the original work is properly cited and the use is non-commercial. See: https://creativecommons.org/Licenses/by-nc/4.0/

Country/Territory of origin: India

ORCID number: Madhusmita Rout 0000-0001-6011-5887; Bhumandeep Kour 0000-0003-2961-9272; Sugunakar Vuree 0000-0002-3262-434X; Sajitha S Lulu 0000-0002-3392-4168; Krishna Mohan Medicherla 0000-0001-7099-7721; Prashanth Suravajhala 0000-0002-8535-278X.

S-Editor: Liu JH
L-Editor: Wang TQ
P-Editor: Liu JH

REFERENCES

1 **Stumvoll M**, Goldstein BJ, van Haeften TW. Type 2 diabetes: principles of pathogenesis and therapy. *Lancet* 2005; **365**: 1333-1346 [PMID: 15823385 DOI: 10.1016/S0140-6736(05)61032-X]
2 **Brunetti A**, Chiefari E, Foti D. Recent advances in the molecular genetics of type 2 diabetes mellitus. *World J Diabetes* 2014; **5**: 128-140 [PMID: 24748926 DOI: 10.4239/wjd.v5.i2.128]
3 **Tang X**, Hu X, Yang X, Fan Y, Li Y, Hu W, Liao Y, Zheng MC, Peng W, Gao L. Predicting diabetes mellitus genes *via* protein-protein interaction and protein subcellular localization information. *BMC Genomics* 2016; **17** Suppl 4: 433 [PMID: 27535125 DOI: 10.1186/s12864-016-2795-y]
4 **Gibson G**. Rare and common variants: twenty arguments. *Nat Rev Genet* 2012; **13**: 135-145 [PMID: 22251874 DOI: 10.1038/nrg3118]
5 **Visscher PM**, Brown MA, McCarthy MI, Yang J. Five years of GWAS discovery. *Am J Hum Genet* 2012; **90**: 7-24 [PMID: 22243964 DOI: 10.1016/j.ajhg.2011.11.029]
6 **Hirschhorn JN**, Gajdos ZK. Genome-wide association studies: results from the first few years and potential implications for clinical medicine. *Annu Rev Med* 2011; **62**: 11-24 [PMID: 21226609 DOI: 10.1146/annurev.med.091708.162036]
7 **Jain P**, Vig S, Datta M, Jindel D, Mathur AK, Mathur SK, Sharma A. Systems biology approach reveals genome to phenome correlation in type 2 diabetes. *PLoS One* 2013; **8**: e53522 [PMID: 23308243 DOI: 10.1371/journal.pone.0053522]
8 **Prokopenko I**, McCarthy MI, Lindgren CM. Type 2 diabetes: new genes, new understanding. *Trends Genet* 2008; **24**: 613-621 [PMID: 18952314 DOI: 10.1016/j.tig.2008.09.004]
9 **Florez JC**. Newly identified loci highlight beta cell dysfunction as a key cause of type 2 diabetes: where are the insulin resistance genes? *Diabetologia* 2008; **51**: 1100-1110 [PMID: 18504548 DOI: 10.1007/s00125-008-1025-9]
10 **Wu X**, Liu Q, Jiang R. Align human interactome with phenome to identify causative genes and networks underlying disease families. *Bioinformatics* 2009; **25**: 98-104 [PMID: 19010805 DOI: 10.1093/bioinformatics/btn593]
11 **Oti M**, Snel B, Huynen MA, Brunner HG. Predicting disease genes using protein-protein interactions. *J Med Genet* 2006; **43**: 691-698 [PMID: 16611749 DOI: 10.1136/jmg.2006.041376]
12 **Alanis-Lobato G**. Mining protein interactomes to improve their reliability and support the advancement of network medicine. *Front Genet* 2015; **6**: 296 [PMID: 26442112 DOI: 10.3389/fgene.2015.00296]
13 **Hebbring SJ**. The challenges, advantages and future of phenome-wide association studies. *Immunology* 2014; **141**: 157-165 [PMID: 24147732 DOI: 10.1111/imm.12195]
14 **Lage K**, Karlberg EO, Størling ZM, Olason PI, Pedersen AG, Rigina O, Hinsby AM, Tümer Z, Pociot F, Tommerup N, Moreau Y, Brunak S. A human phenome-interactome network of protein complexes implicated in genetic disorders. *Nat Biotechnol* 2007; **25**: 309-316 [PMID: 17344885 DOI: 10.1038/nbt1295]
15 **Cronin RM**, Field JR, Bradford Y, Shaffer CM, Carroll RJ, Mosley JD, Bastarache L, Edwards TL, Hebbring SJ, Lin S, Hindorff LA, Crane PK, Pendergrass SA, Ritchie MD, Crawford DC, Pathak J, Bielinski SJ, Carrell DS, Crosslin DR, Ledbetter DH, Carey DJ, Tromp G, Williams MS, Larson EB, Jarvik GP, Peissig PL, Brilliant MH, McCarty CA, Chute CG, Kullo IJ, Bottinger E, Chisholm R, Smith ME, Roden DM, Denny JC. Phenome-wide association studies demonstrating pleiotropy of genetic variants within FTO with and without adjustment for body mass index. *Front Genet* 2014; **5**: 250 [PMID: 25177340 DOI: 10.3389/fgene.2014.00250]
16 **Agapito G**, Guzzi PH, Cannataro M. Visualization of protein interaction networks: problems and solutions. *BMC Bioinformatics* 2013; **14** Suppl 1: S1 [PMID: 23368786 DOI: 10.1186/1471-2105-14-S1-S1]
17 **Li Y**, Patra JC. Genome-wide inferring gene-phenotype relationship by walking on the heterogeneous network. *Bioinformatics* 2010; **26**: 1219-1224 [PMID: 20215462 DOI: 10.1093/bioinformatics/btq108]
18 **Sun J**, Zhao Z. A comparative study of cancer proteins in the human protein-protein interaction network. *BMC Genomics* 2010; **11** Suppl 3: S5 [PMID: 21143787 DOI: 10.1186/1471-2164-11-S3-S5]
19 **Morampudi S**, Balasubramanian G, Gowda A, Zomorodi B, Patil AS. The Challenges and Recommendations for Gestational Diabetes Mellitus Care in India: A Review. *Front Endocrinol (Lausanne)* 2017; **8**: 56 [PMID: 28392778 DOI: 10.3389/fendo.2017.00056]
20 **McIntyre HD**, Catalano P, Zhang C, Desoye G, Mathiesen ER, Damm P. Gestational diabetes mellitus. *Nat Rev Dis Primers* 2019; **5**: 1-9 [PMID: 31296866 DOI: 10.1038/s41572-019-0098-8]
21 **Mpondo BC**, Ernest A, Dee HE. Gestational diabetes mellitus: challenges in diagnosis and management. *J Diabetes Metab Disord* 2015; **14**: 42 [PMID: 25977899 DOI: 10.1186/s40200-015-0169-7]
22 **Crowther CA**, Hiller JE, Moss JR, McPhee AJ, Jeffries WS, Robinson JS; Australian Carbohydrate Intolerance Study in

Pregnant Women (ACHOIS) Trial Group. Effect of treatment of gestational diabetes mellitus on pregnancy outcomes. *N Engl J Med* 2005; **352**: 2477-2486 [PMID: 15951574 DOI: 10.1056/NEJMoa042973]

23 **Langer O**. A spectrum of glucose thresholds may effectively prevent complications in the pregnant diabetic patient. *Semin Perinatol* 2002; **26**: 196-205 [PMID: 12099309 DOI: 10.1053/sper.2002.33962]

24 **Huerta-Chagoya A**, Vázquez-Cárdenas P, Moreno-Macías H, Tapia-Maruri L, Rodríguez-Guillén R, López-Vite E, García-Escalante G, Escobedo-Aguirre F, Parra-Covarrubias A, Cordero-Brieño R, Manzo-Carrillo L, Zacarías-Castillo R, Vargas-García C, Aguilar-Salinas C, Tusié-Luna T. Genetic determinants for gestational diabetes mellitus and related metabolic traits in Mexican women. *PLoS One* 2015; **10**: e0126408 [PMID: 25973943 DOI: 10.1371/journal.pone.0126408]

25 **Watanabe RM**. Inherited destiny? *Genome Med* 2011; **3**: 18 [PMID: 21457499 DOI: 10.1186/gm232]

26 **Unnikrishnan R**, Shanthi Rani CS, Anjana RM, Uthra SC, Vidya J, Sankari GU, Venkatesan U, Rani SJ, Mohan V. Postpartum development of type 1 diabetes in Asian Indian women with gestational diabetes. *Indian J Endocrinol Metab* 2016; **20**: 702-706 [PMID: 27730084 DOI: 10.4103/2230-8210.190562]

27 **Weng J**, Ekelund M, Lehto M, Li H, Ekberg G, Frid A, Aberg A, Groop LC, Berntorp K. Screening for MODY mutations, GAD antibodies, and type 1 diabetes--associated HLA genotypes in women with gestational diabetes mellitus. *Diabetes Care* 2002; **25**: 68-71 [PMID: 11772903 DOI: 10.2337/diacare.25.1.68]

28 **Tiwari P**, Saxena A, Gupta N, Medicherla KM, Suravajhala P, Mathur SK. Systems Genomics of Thigh Adipose Tissue From Asian Indian Type-2 Diabetics Revealed Distinct Protein Interaction Hubs. *Front Genet* 2018; **9**: 679 [PMID: 30671081 DOI: 10.3389/fgene.2018.00679]

29 **Cao M**, Zhang L, Lin Y, Li Z, Xu J, Shi Z, Chen Z, Ma J, Wen J. Circular RNA expression profiles in umbilical cord blood exosomes from normal and gestational diabetes mellitus patients. *Biosci Rep* 2020; **40** [PMID: 33146699 DOI: 10.1042/BSR20201946]

30 **Magee TR**, Ross MG, Wedekind L, Desai M, Kjos S, Belkacemi L. Gestational diabetes mellitus alters apoptotic and inflammatory gene expression of trophobasts from human term placenta. *J Diabetes Complications* 2014 [PMID: 2476820 DOI: 10.1016/j.jdiacomp.2014.03.010]

31 **Pinney SE**, Joshi A, Yin V, Min SW, Rashid C, Condon DE, Wang PZ. Exposure to Gestational Diabetes Enriches Immune-Related Pathways in the Transcriptome and Methylome of Human Amniocytes. *J Clin Endocrinol Metab* 2020; **105** [PMID: 32687192 DOI: 10.1210/clinem/dgaa466]

32 **Wang H**, She G, Zhou W, Liu K, Miao J, Yu B. Expression profile of circular RNAs in placentas of women with gestational diabetes mellitus. *Endocr J* 2019; **66**: 431-441 [PMID: 30814439 DOI: 10.1507/endocrj.EJ18-0291]

33 **Zhu Y**, Tian F, Li H, Zhou Y, Lu J, Ge Q. Profiling maternal plasma microRNA expression in early pregnancy to predict gestational diabetes mellitus. *Int J Gynaecol Obstet* 2015; **130**: 49-53 [PMID: 25887942 DOI: 10.1016/j.ijgo.2015.01.010]

34 **Fu X**, Cong H, Zhao S, Li Y, Liu T, Sun Y, Lv N. Construction of Glycometabolism- and Hormone-Related lncRNA-Mediated Feedforward Loop Networks Reveals Global Patterns of lncRNAs and Drug Repurposing in Gestational Diabetes. *Front Endocrinol (Lausanne)* 2020; **11**: 93 [PMID: 32210913 DOI: 10.3389/fendo.2020.00093]

35 **Rout M**, Lulu S S. Molecular and disease association of gestational diabetes mellitus affected mother and placental datasets reveal a strong link between insulin growth factor (IGF) genes in amino acid transport pathway: A network biology approach. *J Cell Biochem* 2018 [PMID: 30335885 DOI: 10.1002/jcb.27418]

36 **Godsland IF**. Insulin resistance and hyperinsulinaemia in the development and progression of cancer. *Clin Sci (Lond)* 2009; **118**: 315-332 [PMID: 19922415 DOI: 10.1042/CS20090399]

37 **Poloz Y**, Stambolic V. Obesity and cancer, a case for insulin signaling. *Cell Death Dis* 2015; **6**: e2037 [PMID: 26720346 DOI: 10.1038/cddis.2015.381]

38 **Adekola K**, Rosen ST, Shanmugam M. Glucose transporters in cancer metabolism. *Curr Opin Oncol* 2012; **24**: 650-654 [PMID: 22913968 DOI: 10.1097/CCO.0b013e328356da72]

39 **Kingshott G**, Biernacka K, Sewell A, Gwiti P, Barker R, Zielinska H, Gilkes A, McCarthy K, Martin RM, Lane JA, McGeagh L, Koupparis A, Rowe E, Oxley J, Holly JMP, Perks CM. Alteration of Metabolic Conditions Impacts the Regulation of IGF-II/H19 Imprinting Status in Prostate Cancer. *Cancers (Basel)* 2021; **13** [PMID: 33669311 DOI: 10.3390/cancers13040825]

40 **Xue F**, Song X, Zhang S, Niu M, Cui Y, Wang Y, Zhao T. Long non-coding RNA TMPO-AS1 serves as a tumor promoter in pancreatic carcinoma by regulating miR-383-5p/SOX11. *Oncol Lett* 2021; **21**: 255 [PMID: 33664819 DOI: 10.3892/ol.2021.12517]

41 **Xu J**, Fan L, Qi F, Xiu X. Screening of Biomarkers for Hypertension Susceptibility in Pregnancy Proc Anticancer Res. 2020; 4

42 **Taussky D**, Delouya G. Impact of diabetes and metformin use on prostate cancer. *Scand J Urol* 2020; **54**: 508-509 [PMID: 32787660 DOI: 10.1080/21681805.2020.1806355]

43 **Shigeoka T**, Nomiyama T, Kawanami T, Hamaguchi Y, Horikawa T, Tanaka T, Irie S, Motonaga R, Hamanoue N, Tanabe M, Nabeshima K, Tanaka M, Yanase T, Kawanami D. Activation of overexpressed glucagon-like peptide-1 receptor attenuates prostate cancer growth by inhibiting cell cycle progression. *J Diabetes Investig* 2020; **11**: 1137-1149 [PMID: 32146725 DOI: 10.1111/jdi.13247]

44 **Lin E**, Garmo H, Van Hemelrijck M, Adolfsson J, Stattin P, Zethelius B, Crawley D. Association of type 2 diabetes mellitus and antidiabetic medication with risk of prostate cancer: a population-based case-control study. *BMC Cancer* 2020; **20**: 551 [PMID: 32539807 DOI: 10.1186/s12885-020-07036-4]

45 **Ohwaki K**, Endo F, Shimbo M, Fujisaki A, Hattori K. Comorbidities as predictors of incidental prostate cancer after Holmium laser enucleation of the prostate: diabetes and high-risk cancer. *Aging Male* 2017; **20**: 257-260 [PMID: 28332895 DOI: 10.1080/13685538.2017.1301417]

46 **Kobayashi M**, Mizuno T, Yuki H, Kambara T, Betsunoh H, Nukui A, Abe H, Fukabori Y, Yashi M, Kamai T. Association between serum prostate-specific antigen level and diabetes, obesity, hypertension, and the laboratory parameters related to glucose tolerance, hepatic function, and lipid profile: implications for modification of prostate-specific antigen threshold. *Int J Clin Oncol* 2020; **25**: 472-478 [PMID: 31440861 DOI: 10.1007/s10147-019-01527-6]

47 **Knura M**, Garczorz W, Borek A, Drzymała F, Rachwał K, George K, Francuz T. The Influence of Anti-Diabetic Drugs on Prostate Cancer. *Cancers (Basel)* 2021; **13** [PMID: 33921222 DOI: 10.3390/cancers13081827]

48 **Kelkar S**, Oyekunle T, Eisenberg A, Howard L, Aronson WJ, Kane CJ, Amling CL, Cooperberg MR, Klaassen Z, Terris MK, Freedland SJ, Csizmadi I. Diabetes and Prostate Cancer Outcomes in Obese and Nonobese Men After Radical Prostatectomy. *JNCI Cancer Spectr* 2021; **5** [PMID: 34169227 DOI: 10.1093/jncics/pkab023]

49 **Yao Q**, Chen T. LINC01128 regulates the development of osteosarcoma by sponging miR-299-3p to mediate MMP2 expression and activating Wnt/β-catenin signalling pathway. *Journal of cellular and molecular medicine* 2020; **24**: 14293-14305 [PMID: 33108067 DOI: 10.1111/jcmm.16046]

50 **He J**, Ling L, Liu Z, Ren X, Wan L, Tu C, Li Z. Functional interplay between long non-coding RNAs and the Wnt signaling cascade in osteosarcoma. *Cancer Cell International* 2021; **21**: 1-7 [PMID: 34130697 DOI: 10.1186/s12935-021-02013-8]

51 **Hu Y**, Ma Y, Liu J, Cai Y, Zhang M, Fang X. LINC01128 expedites cervical cancer progression by regulating miR-383-5p/SFN axis. *BMC Cancer* 2019; **19**: 1157 [PMID: 31779593 DOI: 10.1186/s12885-019-6326-5]

52 **Li X**, Yuan J, Cao Q, Xie A, Chen J. MicroRNA-383-5p inhibits the proliferation and promotes the apoptosis of gastric cancer cells by targeting cancerous inhibitor of PP2A. *Int J Mol Med* 2020; **46**: 397-405 [PMID: 32626915 DOI: 10.3892/ijmm.2020.4603]

53 **Cheng X**, Huang Y, Yang P, Bu L. miR-383 ameliorates high glucose-induced β-cells apoptosis and hyperglycemia in high-fat induced diabetic mice. *Life Sci* 2020; **263**: 118571 [PMID: 33058915 DOI: 10.1016/j.lfs.2020.118571]

54 **Zhao Z**, Yang YB, Li XY, Li XG, Chu XD, Lin ZB, Zhang YR, Guo YG, Ding H, Pan YL, Wang L, Pan JH. Comprehensive Analysis of N6-Methyladenosine-Related lncRNA Signature for Predicting Prognosis and Immune Cell Infiltration in Patients with Colorectal Cancer. *Dis Markers* 2021; **2021**: 8686307 [PMID: 34745388 DOI: 10.1155/2021/8686307]

55 **Deng Y**, Hu H, Xiao L, Cai T, Gao W, Zhu H, Wang S, Liu J. Identification of EMT-Related lncRNAs as a Potential Prognostic Biomarker and Therapeutic Targets for Pancreatic Adenocarcinoma. 2021

World Journal of Clinical Cases

Submit a Manuscript: https://www.f6publishing.com

World J Clin Cases 2022 June 26; 10(18): 5965-5983

DOI: 10.12998/wjcc.v10.i18.5965

ISSN 2307-8960 (online)

ORIGINAL ARTICLE

Clinical and Translational Research

Identification of potential key molecules and signaling pathways for psoriasis based on weighted gene co-expression network analysis

Xin Shu, Xiao-Xia Chen, Xin-Dan Kang, Min Ran, You-Lin Wang, Zhen-Kai Zhao, Cheng-Xin Li

Specialty type: Medicine, research and experimental

Provenance and peer review: Unsolicited article; Externally peer reviewed.

Peer-review model: Single blind

Peer-review report's scientific quality classification

Grade A (Excellent): 0
Grade B (Very good): 0
Grade C (Good): C, C
Grade D (Fair): 0
Grade E (Poor): 0

P-Reviewer: Bhargava S, India; Grigoras A, Romania
A-Editor: Yao QG, China

Received: February 17, 2022
Peer-review started: February 17, 2022
First decision: March 29, 2022
Revised: March 30, 2022
Accepted: May 22, 2022
Article in press: May 22, 2022
Published online: June 26, 2022

Xin Shu, Department of Dermatology, The Third Medical Center of Chinese PLA General Hospital, Beijing 100039, China

Xin Shu, Chinese PLA Medical School, Beijing 100853, China

Xiao-Xia Chen, Department of Radiology, The Third Medical Center of Chinese PLA General Hospital, Beijing 100039, China

Xin-Dan Kang, Department of Comprehensive Surgical, The Second Medical Center of Chinese PLA General Hospital, Beijing 100089, China

Min Ran, Department of Endocrine, The Third Medical Center of Chinese PLA General Hospital, Beijing 100039, China

You-Lin Wang, Zhen-Kai Zhao, Cheng-Xin Li, Department of Dermatology, The First Medical Center of Chinese PLA General Hospital, Beijing 100853, China

Corresponding author: Cheng-Xin Li, Doctor, Department of Dermatology, The First Medical Center of Chinese PLA General Hospital, No. 28 Fuxing Road, Haidian District, Beijing 100853, China. dr_xincheng@163.com

Abstract

BACKGROUND

Psoriasis is a chronic inflammatory skin disease, the pathogenesis of which is more complicated and often requires long-term treatment. In particular, moderate to severe psoriasis usually requires systemic treatment. Psoriasis is also associated with many diseases, such as cardiometabolic diseases, malignant tumors, infections, and mood disorders. Psoriasis can appear at any age, and lead to a substantial burden for individuals and society. At present, psoriasis is still a treatable, but incurable, disease. Previous studies have found that microRNAs (miRNAs) play an important regulatory role in the progression of various diseases. Currently, miRNAs studies in psoriasis and dermatology are relatively new. Therefore, the identification of key miRNAs in psoriasis is helpful to elucidate the molecular mechanism of psoriasis.

AIM

To identify key molecular markers and signaling pathways to provide potential basis for the treatment and management of psoriasis.

METHODS
The miRNA and mRNA data were obtained from the Gene Expression Omnibus database. Then, differentially expressed mRNAs (DEmRNAs) and differentially expressed miRNAs (DEmiRNAs) were screened out by limma R package. Subsequently, DEmRNAs were analyzed for Gene Ontology and Kyoto Encyclopedia of Genes and Genomics functional enrichment. The "WGCNA" R package was used to analyze the co-expression network of all miRNAs. In addition, we constructed miRNA-mRNA regulatory networks based on identified hub miRNAs. Finally, *in vitro* validation was performed. All experimental procedures were approved by the ethics committee of Chinese PLA General Hospital (S2021-012-01).

RESULTS
A total of 639 DEmRNAs and 84 DEmiRNAs were identified. DEmRNAs screening criteria were adjusted *P* (adj. *P)* value < 0.01 and |logFoldChange| (|logFC|) > 1. DEmiRNAs screening criteria were adj. *P* value < 0.01 and |logFC| > 1.5. KEGG functional analysis demonstrated that DEmRNAs were significantly enriched in immune-related biological functions, for example, toll-like receptor signaling pathway, cytokine-cytokine receptor interaction, and chemokine signaling pathway. In weighted gene co-expression network analysis, turquoise module was the hub module. Moreover, 10 hub miRNAs were identified. Among these 10 hub miRNAs, only 8 hub miRNAs predicted the corresponding target mRNAs. 97 negatively regulated miRNA-mRNA pairs were involved in the miRNA-mRNA regulatory network, for example, hsa-miR-21-5p-claudin 8 (CLDN8), hsa-miR-30a-3p-interleukin-1B (IL-1B), and hsa-miR-181a-5p/hsa-miR-30c-2-3p-C-X-C motif chemokine ligand 9 (CXCL9). Real-time polymerase chain reaction results showed that IL-1B and CXCL9 were up-regulated and CLDN8 was down-regulated in psoriasis with statistically significant differences.

CONCLUSION
The identification of potential key molecular markers and signaling pathways provides potential research directions for further understanding the molecular mechanisms of psoriasis. This may also provide new research ideas for the prevention and treatment of psoriasis in the future.

Key Words: Psoriasis; MicroRNAs; Weighted gene co-expression network analysis; Functional enrichment; MicroRNA-mRNA regulatory network

©The Author(s) 2022. Published by Baishideng Publishing Group Inc. All rights reserved.

Core Tip: Psoriasis is a common chronic, recurrent, immune-regulatory skin and joint disease. Although psoriasis is widespread and has significant negative impact on patients' life quality, it has not yet been fully diagnosed and treated. Moreover, it is also associated with many other diseases. So far, psoriasis is still a treatable, but incurable, disease. We use weighted gene co-expression network analysis to identify key modules and microRNAs (miRNAs) related to psoriasis and explore potential key pathways related to psoriasis through the targeting relationship of miRNA-mRNA. This provides new research ideas for the prevention and treatment of psoriasis in the future.

Citation: Shu X, Chen XX, Kang XD, Ran M, Wang YL, Zhao ZK, Li CX. Identification of potential key molecules and signaling pathways for psoriasis based on weighted gene co-expression network analysis. *World J Clin Cases* 2022; 10(18): 5965-5983
URL: https://www.wjgnet.com/2307-8960/full/v10/i18/5965.htm
DOI: https://dx.doi.org/10.12998/wjcc.v10.i18.5965

INTRODUCTION

Psoriasis is a common chronic, recurrent, immune-regulatory skin and joint disease. It has a variety of clinical skin manifestations, but the most common clinical manifestations are erythematous, scaling papules, and plaques[1]. Previous studies have found that psoriasis is affected by family history and age [2]. Mechanical stress, air pollutants, sun exposure, infection, lifestyle, obesity, dyslipidemia, and mental stress are associated with the progression of psoriasis[3]. The pathogenesis of psoriasis is more complicated and often requires long-term treatment. Mild to moderate psoriasis can be treated topically with a combination of glucocorticoids, vitamin D analogues, and phototherapy. Moderate to severe psoriasis usually requires systemic treatment[4]. Psoriasis is also associated with many diseases, for

example cardiometabolic diseases, malignant tumors, infections and mood disorders[5]. So far, psoriasis is still a treatable, but incurable, disease. Therefore, identification of key genes and signaling pathways are of great significance for understanding the molecular mechanism of psoriasis and provides potential basis for the treatment and management of psoriasis.

MicroRNAs (miRNAs) are a class of small non-coding single-stranded RNAs that regulate gene expression[6]. MiRNAs play a vital role in the progression of diseases, for example cancer, infectious diseases, and immune diseases[7]. MiRNAs can regulate cell proliferation, keratinocyte differentiation, apoptosis, and atypical immune activation in psoriasis[8]. Previous studies have found that miR-187 can inhibit the proliferation of keratinocytes by targeting B7 homolog 3 protein. In addition, in the mouse model of psoriasis, overexpression of miR-187 can reduce acanthosis and reduce the severity of the disease[9]. MiR-183-3p can inhibit the proliferation and migration of keratinocytes in psoriasis by inhibiting growth factor receptor binding 2-associated binding protein 1[10]. MiR-320b negatively regulates keratinocyte proliferation in psoriasis by targeting AKT serine/threonine kinase 3[11]. The low expression of miR-31 in dermal mesenchymal stem cells (DMSCs) in patients with psoriasis results in the increased expression of some of its target genes, which in turn promotes the activation of T lymphocyte by inhibiting the proliferation of DMSCs, thereby contributing to the pathogenesis of psoriasis[12]. Previous studies have found that miR-146 regulates inflammatory responses in keratinocytes and skin fibroblasts, which may affect the pathogenesis of psoriasis[13]. Furthermore, in human keratinocytes, the expression of miR-146a is induced by pro-inflammatory cytokines tumor necrosis factor-α (TNF-α), interleukin-1B (IL-1B), and IL-17a, and the expression of miR-146b is induced by interferon-γ (IFN-γ) and IL-22. MiR-203 promotes keratinocyte proliferation by targeting liver X receptor-α and peroxisome proliferator-activated receptor-γ in psoriasis[14]. MiR-125 regulates keratinocytes proliferation by regulating targeted genes[15,16]. MiR-197 over expression inhibits keratinocytes proliferation induced by IL-22 and keratinocytes migration[17]. In addition, miR-99 also plays an important role in regulating the abnormal proliferation and differentiation of keratinocytes in psoriasis[18]. These studies demonstrate that miRNAs play a vital role in the pathogenesis of psoriasis. Currently, miRNAs studies in psoriasis and dermatology are relatively new. Therefore, the identification of key miRNAs in psoriasis is helpful to elucidate the molecular mechanism of psoriasis.

Weighted gene co-expression network analysis (WGCNA) can be used for finding clusters (modules) of highly correlated genes[19]. WGCNA has been used to identify key genes for many diseases, including cancer[20], cardiovascular disease[21], and immunological diseases[22]. In addition, WGCNA has also been used to identify key mRNAs and long noncoding RNAs in psoriasis. So far, we have not found studies that use WGCNA to identify key miRNAs in psoriasis. Therefore, we use WGCNA to identify key modules and miRNAs related to psoriasis and explore potential key pathways related to psoriasis through the targeting relationship of miRNA-mRNA.

MATERIALS AND METHODS

Data sources and processing

The miRNA and mRNA data were obtained from the Gene Expression Omnibus (GEO) database[23]. The keyword we searched in the GEO database was "psoriasis". Cell line or animal level studies and single-sample studies were excluded. Five datasets GSE13355, GSE66511, GSE145054, GSE142582, and GSE129373 were involved in this study (Table 1). All data were derived from skin samples. GSE13355 and GSE66511 were mRNA data from GPL570 and GPL16288 platform, respectively. GSE145054, GSE142582, and GSE129373 were miRNA data from GPL19117, GPL20301, and GPL11154, respectively. The gene expression matrix files in GSE13355 and GSE145054 were downloaded. The GPL annotation file was used to annotate the expression matrix. The probe ID was converted to the gene symbol. Multiple probes correspond to the same gene, taking the average value. The probe that corresponds to multiple genes was removed. The original data of gene expression profile in GSE66511, GSE142582, and GSE129373 were downloaded, and performed by logarithm processing. Then, the combat function in "sva" R package was used to remove batch effects.

Differential expression analysis

After the above pretreatment, differentially expressed mRNAs (DEmRNAs) and differentially expressed miRNAs (DEmiRNAs) were screened out by limma R package[24]. DEmRNAs screening criteria were adjusted *P* (adj. *P*) value < 0.01 and |logFoldChange| (|logFC|) > 1. DEmiRNAs screening criteria were adj. *P* value < 0.01 and |logFC| > 1.5.

Functional enrichment analysis

To investigate the possible involvement of DEmRNAs in the biological processes related to psoriasis, we performed Gene Ontology (GO) and Kyoto Encyclopedia of Genes and Genomics (KEGG) functional enrichment analyses. David database was used for the enrichment analysis of DEmRNAs[25], and the screening criterion was $P < 0.05$. GO enrichment analysis, which is comprised of biological processes (BP), cellular components (CC), and molecular functions (MF). The "GOplot" R package was used to

Table 1 Details of five datasets

GEO ID	Samples, Normal:Case	Platforms	Author	Type	Source
GSE13355	64:58	GPL570	Gudjonsson JE	mRNA	Skin
GSE66511	12:12	GPL12688	Keermann M	mRNA	Skin
GSE145054	4:4	GPL19117	Mildner M	miRNA	Skin
GSE142582	5:5	GPL20301	Yu Z	miRNA	Skin
GSE129373	9:9	GPL11154	Srivastava A	miRNA	Skin

visualize the enrichment results.

Construction of weighted gene co-expression network

The "WGCNA" R package was used to analyze the co-expression network of all miRNAs. To detect outliers, the "hclust" function was used to cluster the sample data. Subsequently, to construct a scale-free topology, the "pickSoftThreshold" function was used to select an appropriate soft threshold power regulator (height 0.90, β value 2). Calculate the adjacency matrix based on the kernel value. The adjacency matrix was transformed into topological overlap matrix (TOM) and corresponding dissimilarity matrix (1-TOM). Genes with similar expression patterns were gathered together, and modules were divided according to the function of "cutreeDynamic" with default parameters. Since the modules identified by the dynamic tree cutting algorithm may be similar, they are combined with a truncation of 0.25 height[26].

Hub modules and miRNAs

To identify the important modules associated with psoriasis, the module eigengene (ME) of each module was calculated using the "moduleEigengenes" function. Then, the correlation between ME and psoriasis was analyzed using Pearson method. Subsequently, the module with the highest correlation with psoriasis was identified as the hub module. According to module connectivity (MM) and clinical trait relationship (GS) of each gene in the hub module, the candidate hub miRNAs were screened out [27]. The screening criteria were MM > 0.8 and GS > 0.5. Finally, the intersection of candidate hub miRNAs and DEmiRNAs were selected as real hub miRNAs.

MiRNA-mRNA network

To explore the correlation between miRNA and mRNA, we constructed a miRNA-mRNA regulatory network. Target mRNAs of miRNAs were predicted using miRDB (http://mirdb.org) database. MiRNA-mRNA pairs involved in common DEmRNA and negatively regulated were selected to construct the network. Cytoscape (www.cytoscape.org/) was used to visualize the miRNA-mRNA regulatory network.

In vitro validation

We collected skin tissue samples from healthy control individuals and patients with psoriasis. Basic information (including age, sex, *etc*) of patients and healthy controls were recorded in detail during sample collection (Table 2). The specific inclusion criteria of patients with psoriasis: (1) Patients had at least one well-circumscribed erythematous and squamous lesion, which had been confirmed by at least two dermatologists; (2) Patient's pathological tissues were confirmed by clinical histopathology; (3) Patients had no systemic anti-psoriatic treatment 2 wk before the skin biopsy; and (4) Patients had no topical anti-psoriatic treatment 1 wk before the skin biopsy. Patients with psoriasis who were treated with immune-related drugs before sampling and whose clinical information was incomplete were excluded. The individuals in the normal control group were sex and age matched with the psoriasis group, and without history of psoriasis or other autoimmune diseases.

According to screening criteria, 7 normal and 7 patient skin tissue samples were obtained. Firstly, total RNA of the samples was extracted using TRIzol. Then, fastKing cDNA first strand synthesis kit and miRNA first strand cDNA synthesis kit (Tailing Reaction) were used for mRNA and miRNA reverse transcription, respectively. Subsequently, SuperReal PreMix Plus (SYBR Green) and miRNA quantitative PCR kit (SYBR Green Method) were used to perform real-time polymerase chain reaction (RT-PCR) validation of mRNA and miRNA, respectively. GAPDH, ACTB, and hsa-U6 were internal reference. ABI7300 fluorescence quantitative PCR instrument was used for detection. Finally, the $2^{-\Delta\Delta Ct}$ method was used for relative quantitative analysis of the data[28]. This study complied with the Declaration of Helsinki. Informed consent was obtained from the participants. All experimental procedures were approved by the ethics committee of Chinese PLA General Hospital, No. S2021-012-01.

Table 2 Clinical information of healthy control individuals and patients with psoriasis in vitro validation

Group	Sample number	Sampling location	Sex	Age	Height, cm	Body weight, kg	BMI	Smoking	Drinking	History of ASCVD	History of hypertension	History of hyperlipidemia	History of diabetes	Psoriatic arthritis	Severity index, PASI	Whether to collect non-lesion parts
Normal control group	C1	Right forearm extension side	Female	47	158	54	21.6	No	No	No	No	No	No			
	C2	Right sole of the foot	Male	60	178	70	22.1	Yes	Yes	No	No	No	No			
	C3	Left sole of the foot	Male	59	183	81	24.2	No	No	No	No	No	No			
	C4	Left armpit	Female	27	160	52	20.3	No	Yes	No	No	No	No			
	C7	Left forearm extension side	Female	18	160	50	19.5	No	No	No	No	No	No			
	C9	Right shoulder	Female	27	161	62	23.9	No	No	No	No	No	No			
	C11	Right calf	Female	60	156	55	22.6	No	No	No	No	No	No			
Psoriasis group	E2-2	Right forearm	Male	19	177	58	18.5	No	No	No	No	No	No	No	10.5	Yes
	E3-2	Back	Female	58	157	58	23.5	No	No	No	No	Yes	No	No	8	Yes
	E5-2	Left calf stretched side	Male	55	176	68	22	No	No	No	Yes	No	Yes	No	13.4	Yes
	E6-2	Outer left thigh	Female	44	166	67	24.3	No	No	No	No	No	No	No	11.9	Yes
	E7-2	Right thigh internal test	Male	62	170	66	22.8	Yes	No	No	No	No	No	No	8.6	Yes
	E8-2	Right forearm extension side	Male	48	170	58	20.1	Yes	No	No	No	No	No	No	15.4	Yes
	E10-2	Back	Male	18	172	60	20.3	Yes	No	No	No	No	No	No	22.2	Yes

ASCVD: Arteriosclerotic cardiovascular disease; BMI: Body mass index.

Statistical analysis

All statistical analyses were performed using R software. Limma R package was used to screen for DEmRNAs and DEmiRNAs. Pearson's method was used to analyze the correlation between ME and psoriasis. RT-PCR validation data were statistically analyzed by one-way ANOVA. $P < 0.05$ was statistically significant.

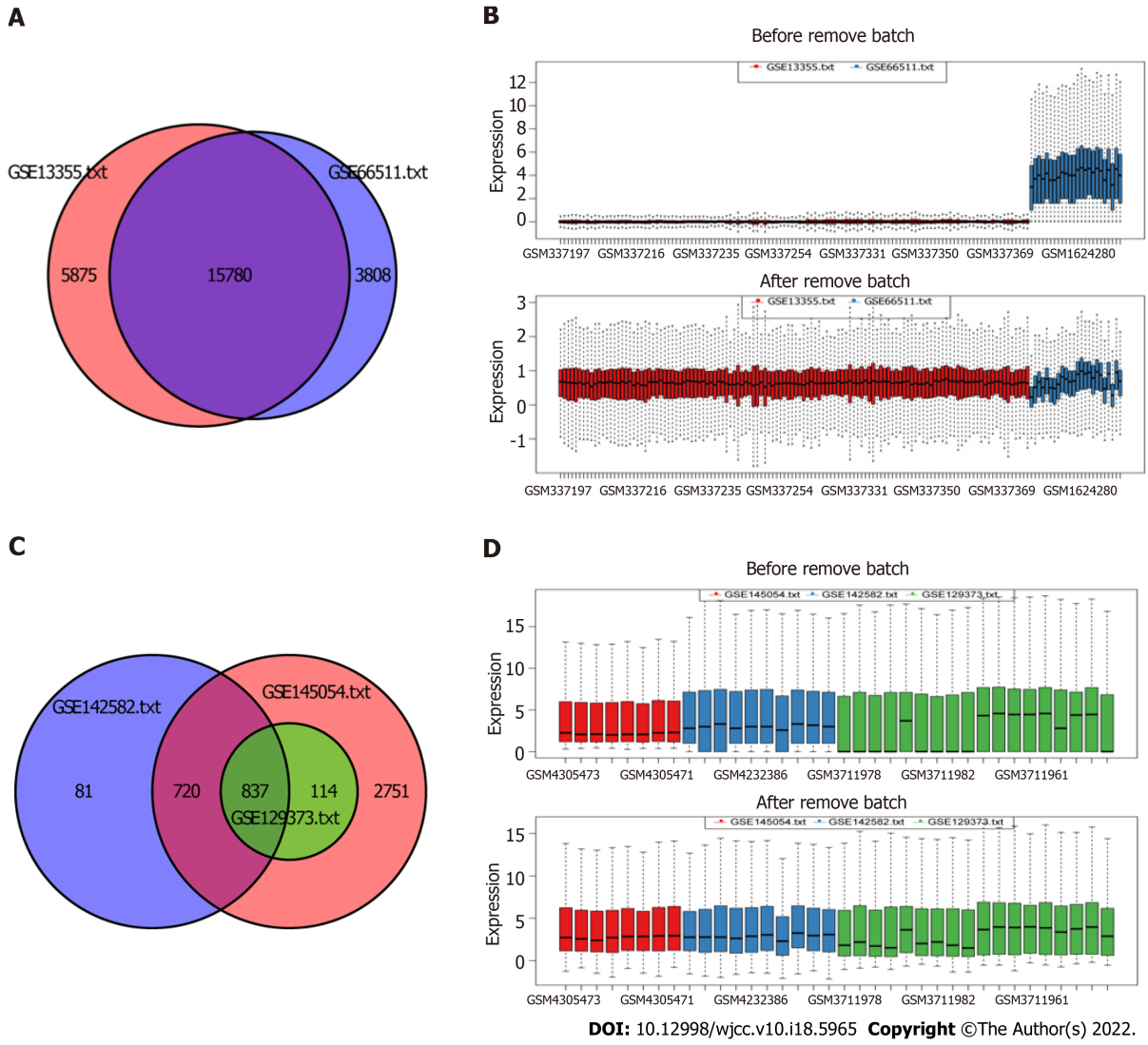

DOI: 10.12998/wjcc.v10.i18.5965 **Copyright** ©The Author(s) 2022.

Figure 1 Removal of data batch effect. A: Ven diagram of batch effect of mRNA; B: Boxplot of batch effect of mRNA; C: Ven diagram of batch effect of miRNA; D: Boxplot of batch effect of miRNA.

RESULTS

Analysis of DEmRNAs and DEmiRNAs

After pretreatment of the raw data, 15780 mRNAs and 837 miRNAs were screened out (Figure 1). Compared with the control group, 639 DEmRNAs were identified in the psoriasis group (adj. *P* value < 0.01 and |logFC| > 1). Among them, 497 were up-regulated and 142 were down-regulated. Compared with the control group, 84 DEmiRNAs were identified in the psoriasis group (adj. *P* value < 0.01 and |logFC| > 1.5). Among them, 70 were up-regulated and 14 were down-regulated. Heat maps showed that there were significant differences of mRNA (Figure 2A) and miRNA (Figure 2B) expression between psoriasis group and control group. The volcano maps of DEmRNAs and DEmiRNAs were shown in Figure 2C and D.

Analysis of biological functional

Functional analysis of 639 DEmRNAs was performed using David database ($P < 0.05$). GO enrichment results showed that most of the DEmRNAs were distributed in inflammatory response (GO:BP), immune response (GO:BP), cytosol (GO:CC), extracellular exosome (GO:CC), protein homodimerization activity (GO:MF), and other biological functions (Figure 3A-C). KEGG enrichment results demonstrated that DEmRNAs were significantly enriched in metabolic pathways, influenza A, chemokine signaling pathway, and cytokine-cytokine receptor interaction (Figure 3D and Table 3).

WGCNA

WGCNA was performed on 837 miRNAs. The samples were clustered to remove abnormal samples (GSM3711960 and GSM3711959) (Figure 4A and B). After calculation, when the soft threshold β was 2, it

Table 3 Kyoto Encyclopedia of Genes and Genomics function enrichment of differentially expressed mRNAs

Category	hsa	Term	Count	*P* value	Genes
KEGG_PATHWAY	hsa03320	PPAR signaling pathway	14	3.07E-06	*GK, MMP1, ADIPOQ, LPL, FADS2, ACADL, ACOX2, FABP5, FABP7, ACSBG1, PLIN1, ANGPTL4, SLC27A4, PPARD*
KEGG_PATHWAY	hsa05164	Influenza A	22	1.05E-05	*NLRX1, RSAD2, DDX58, STAT1, TMPRSS4, MX1, MAPK13, PYCARD, CXCL10, SOCS3, OAS1, OAS2, IL-1B, OAS3, TNFSF10, IRF7, CCL2, PRSS3, KPNA2, PRSS2, MYD88, IRF9*
KEGG_PATHWAY	hsa05133	Pertussis	12	2.56E-04	*PYCARD, C1QB, CASP7, NOS2, CALML5, IL-1B, IRF1, IRF8, CALML3, FOS, MYD88, MAPK13*
KEGG_PATHWAY	hsa05162	Measles	16	4.14E-04	*DDX58, STAT1, MX1, CD3G, CD3D, OAS1, CCNE2, CCNE1, OAS2, IL-1B, OAS3, TNFSF10, IRF7, PRKCQ, MYD88, IRF9*
KEGG_PATHWAY	hsa04668	TNF signaling pathway	14	4.87E-04	*MLKL, CCL20, CXCL1, FOS, NOD2, SELE, MMP9, MAPK13, CXCL10, SOCS3, CASP7, IL-1B, CCL2, JUNB*
KEGG_PATHWAY	hsa04062	Chemokine signaling pathway	19	7.44E-04	*LYN, CXCL9, CCL22, STAT1, CCL20, CXCR4, CXCL1, CXCL13, CXCL10, HCK, CCL8, PLCB4, CXCR2, RAC2, CCL2, CCR7, CCL19, CCL18, CCL27*
KEGG_PATHWAY	hsa04060	Cytokine-cytokine receptor interaction	21	0.002838	*CXCL9, IL20, IL4R, CCL22, CCL20, CXCR4, IL19, CXCL1, CXCL13, CXCL10, CCL8, IL-1B, CXCR2, TNFSF10, CCL2, CCR7, CCL19, IL7R, CCL18, CCL27, TNFRSF21*
KEGG_PATHWAY	hsa05160	Hepatitis C	14	0.003635	*DDX58, STAT1, IFIT1, CLDN1, MAPK13, SOCS3, OAS1, OAS2, IRF1, OAS3, CLDN8, IRF7, CLDN17, IRF9*
KEGG_PATHWAY	hsa00590	Arachidonic acid metabolism	9	0.003655	*PLA2G2F, HPGDS, GPX2, PLA2G4D, PLA2G2A, PLA2G3, ALOX12B, CYP2E1, CYP4F8*
KEGG_PATHWAY	hsa04110	Cell cycle	13	0.00555	*BUB1B, TTK, CDC6, CDC25B, CCNA2, CDC20, CCNB2, CCNB1, CCNE2, PTTG1, CCNE1, CDK1, MAD2L1*
KEGG_PATHWAY	hsa05142	Chagas disease (American trypanosomiasis)	11	0.011418	*C1QB, GNA15, PLCB4, NOS2, IL-1B, CCL2, CD3G, FOS, CD3D, MYD88, MAPK13*
KEGG_PATHWAY	hsa04114	Oocyte meiosis	11	0.017478	*CDC20, CCNB2, CCNB1, PTTG1, CALML5, CCNE2, CCNE1, CDK1, CALML3, MAD2L1, AURKA*
KEGG_PATHWAY	hsa00592	Alpha-Linolenic acid metabolism	5	0.018996	*PLA2G2F, FADS2, PLA2G4D, PLA2G2A, PLA2G3*
KEGG_PATHWAY	hsa05168	Herpes simplex infection	15	0.020979	*DDX58, STAT1, TAP1, FOS, IFIT1, SOCS3, OAS1, OAS2, IL-1B, OAS3, IRF7, CDK1, CCL2, MYD88, IRF9*
KEGG_PATHWAY	hsa04380	Osteoclast differentiation	12	0.021031	*FOSL1, SOCS3, FCGR3B, STAT1, LCK, IL-1B, BLNK, ACP5, FOS, JUNB, IRF9, MAPK13*
KEGG_PATHWAY	hsa04064	NF-kappa B signaling pathway	9	0.028614	*LYN, BCL2A1, DDX58, LCK, IL-1B, BLNK, PRKCQ, CCL19, MYD88*
KEGG_PATHWAY	hsa04621	NOD-like receptor signaling pathway	7	0.028679	*PYCARD, IL-1B, CARD6, CCL2, CXCL1, NOD2, MAPK13*
KEGG_PATHWAY	hsa00591	Linoleic acid metabolism	5	0.031316	*PLA2G2F, PLA2G4D, PLA2G2A, PLA2G3, CYP2E1*
KEGG_PATHWAY	hsa00120	Primary bile acid biosynthesis	4	0.031945	*CYP39A1, CH25H, ACOX2, CYP7B1*
KEGG_PATHWAY	hsa00140	Steroid hormone biosynthesis	7	0.033377	*SULT2B1, HSD11B1, STS, HSD3B1, HSD17B2, CYP2E1, CYP7B1*
KEGG_PATHWAY	hsa01100	Metabolic pathways	64	0.037857	*ST6GALNAC1, GDA, GLDC, PIK3C2G, PYGL, HK2, SMPD3, IL4I1, HPGDS, PNP, ACADL, SPTLC2, KYNU, NAMPT, LIPG, HYAL4, PGM2, TK1, UPP1, AASS, PLA2G4D, ARG1, GPT2, AMPD3, NME1, ALDH3A1, PLCB4, ACOX2, CMPK2, ACSBG1, CYP2E1, IDO1, PLA2G3, ALOX12B, FUT2, CYP2C18, FUT1, FUT3, TYMP, HSD11B1, UGCG, RDH12, HSD17B2, RDH16, ATP6V0A4, XDH, HAO2, PLA2G2F, GALNT6, RRM2, GK, GCH1, NOS2, PLA2G2A, HSD3B1, CYP4F8, ALDH4A1, SQLE, HAL, AKR1B10, DHRS9, POLE2, POLR3G, HPSE*
KEGG_PATHWAY	hsa05143	African trypanosomiasis	5	0.047416	*PLCB4, IL-1B, SELE, MYD88, IDO1*

was approximately a scale-free topology (Figure 4C). After determining the soft threshold, the cluster tree graph was constructed. Subsequently, with the minimum number of genes for modules set to 20, the modules with dissimilarity < 25% merged using the dynamic tree cutting method. Finally, 6 modules were determined (Figure 4D).

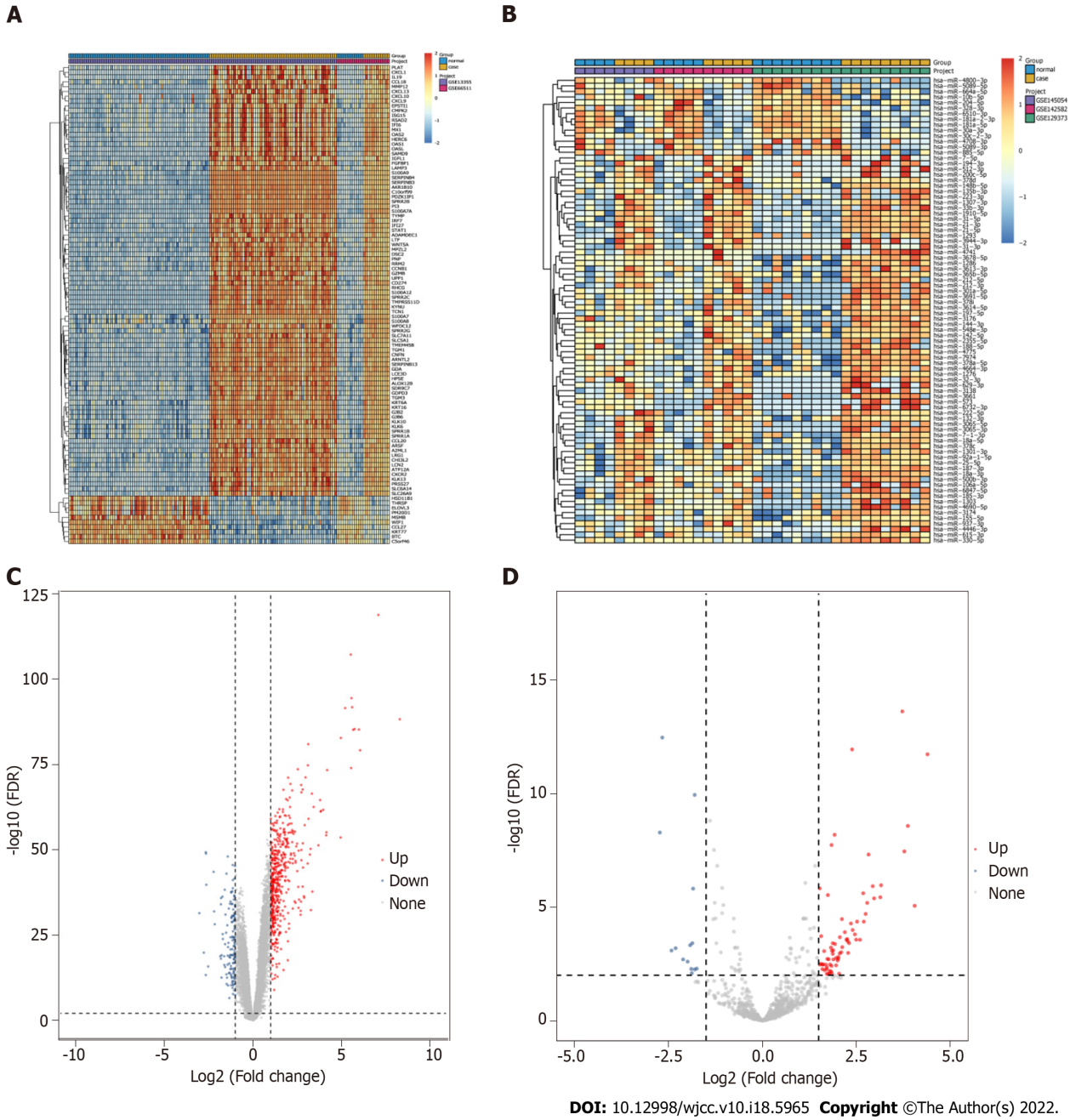

DOI: 10.12998/wjcc.v10.i18.5965 **Copyright** ©The Author(s) 2022.

Figure 2 Identification of differentially expressed mRNAs and differentially expressed miRNAs. A: Heat map of top 100 differentially expressed mRNAs (DEmRNAs). Complete linkage method combined with Euclidean distance was used to construct clustering; B: Heat map of differentially expressed miRNAs (DEmiRNAs); C: Volcano map of DEmRNAs. Blue, red, and gray points represent down-expressed, up-expressed, and not DEmRNAs, respectively; D: Volcano map of DEmiRNAs.

Uncovering of hub modules and miRNAs

The correlation between modules and psoriasis was analyzed by Pearson's method. The results showed that turquoise module had the highest correlation with psoriasis (r = 0.96) (Figure 5A). Therefore, turquoise module was considered the hub module. Subsequently, 21 miRNAs were screened out from the turquoise module as candidate hub miRNAs (MM > 0.8 and GS > 0.5) (Figure 5B). Intersection of DEmiRNAs and candidate hub miRNAs was obtained (Figure 5C). Ten intersecting miRNAs were identified as real hub miRNA. Among them, 5 hub miRNAs were up-regulated (hsa-miR-21-3p, hsa-miR-21-5p, hsa-miR-31-5p, hsa-miR-18a-5p, and hsa-miR-33b-3p) and 5 hub miRNAs were down-regulated (hsa-miR-181a-2-3p, hsa-miR-181a-5p, hsa-miR-6510-3p, hsa-miR-30a-3p, and hsa-miR-30c-2-3p).

MiRNA-mRNA regulatory network

Target mRNAs of 10 hub miRNAs were predicted using miRDB database, but only 8 hub miRNAs (4 up-regulated and 4 down-regulated) were predicted to the corresponding target mRNAs. Eleven target

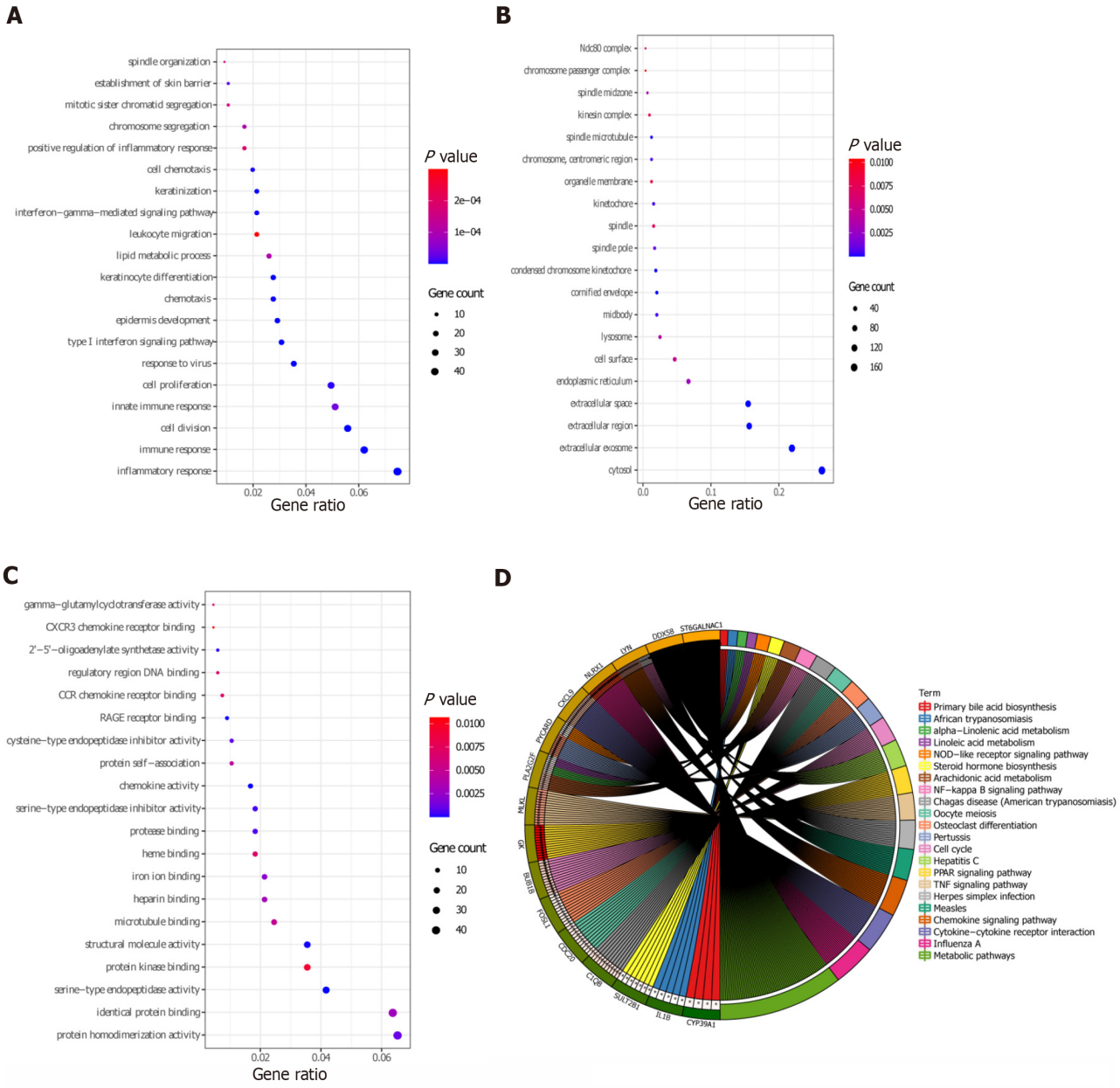

DOI: 10.12998/wjcc.v10.i18.5965 **Copyright** ©The Author(s) 2022.

Figure 3 Gene Ontology and Kyoto Encyclopedia of Genes and Genomics analysis of differentially expressed mRNAs. A: Biological processes terms were enriched of differentially expressed mRNAs (DEmRNAs) by Gene Ontology (GO) function analysis; B: Cellular components terms were enriched of DEmRNAs by GO function analysis; C: Molecular functions terms were enriched of DEmRNAs by GO function analysis; D: Kyoto Encyclopedia of Genes and Genomics enrichment of DEmRNAs.

mRNAs of up-regulated hub miRNAs (hsa-miR-21-3p, hsa-miR-21-5p, hsa-miR-18a-5p, and hsa-miR-33b-3p) were matched with DEmRNAs, and 72 target mRNAs of down-regulated hub miRNAs (hsa-miR-181a-2-3p, hsa-miR-181a-5p, hsa-miR-30a-3p, and hsa-miR-30c-2-3p) were matched with DEmRNAs. Ninety-seven negatively regulated miRNA-mRNAs were involved in the miRNA-mRNA regulatory network (Figure 6); for example, hsa-miR-21-3p/hsa-miR-18a-5p-F3, hsa-miR-21-5p-claudin 8 (CLDN8), hsa-miR-33b-3p-PLCB4, hsa-miR-30a-3p-IL-1B, hsa-miR-181a-5p-C-C motif chemokine ligand 8 (CCL8), hsa-miR-181a-5p/hsa-miR-30c-2-3p-C-X-C motif chemokine ligand 9 (CXCL9), and hsa-miR-30c-2-3p-KYNU.

Functional enrichment of target DEmRNAs

Functional analysis of 83 target DEmRNAs was performed using David database ($P < 0.05$). GO enrichment results demonstrated that most of the target DEmRNAs were distributed in signal transduction (GO:BP), immune response (GO:BP), integral component of membrane (GO:CC), plasma membrane (GO:CC), ATP binding (GO:MF), and other biological functions (Figure 7A-C). KEGG enrichment results demonstrated that the target DEmRNAs were significantly enriched in influenza A, hepatitis C, measles, and chemokine signaling pathway (Figure 7D and Table 4).

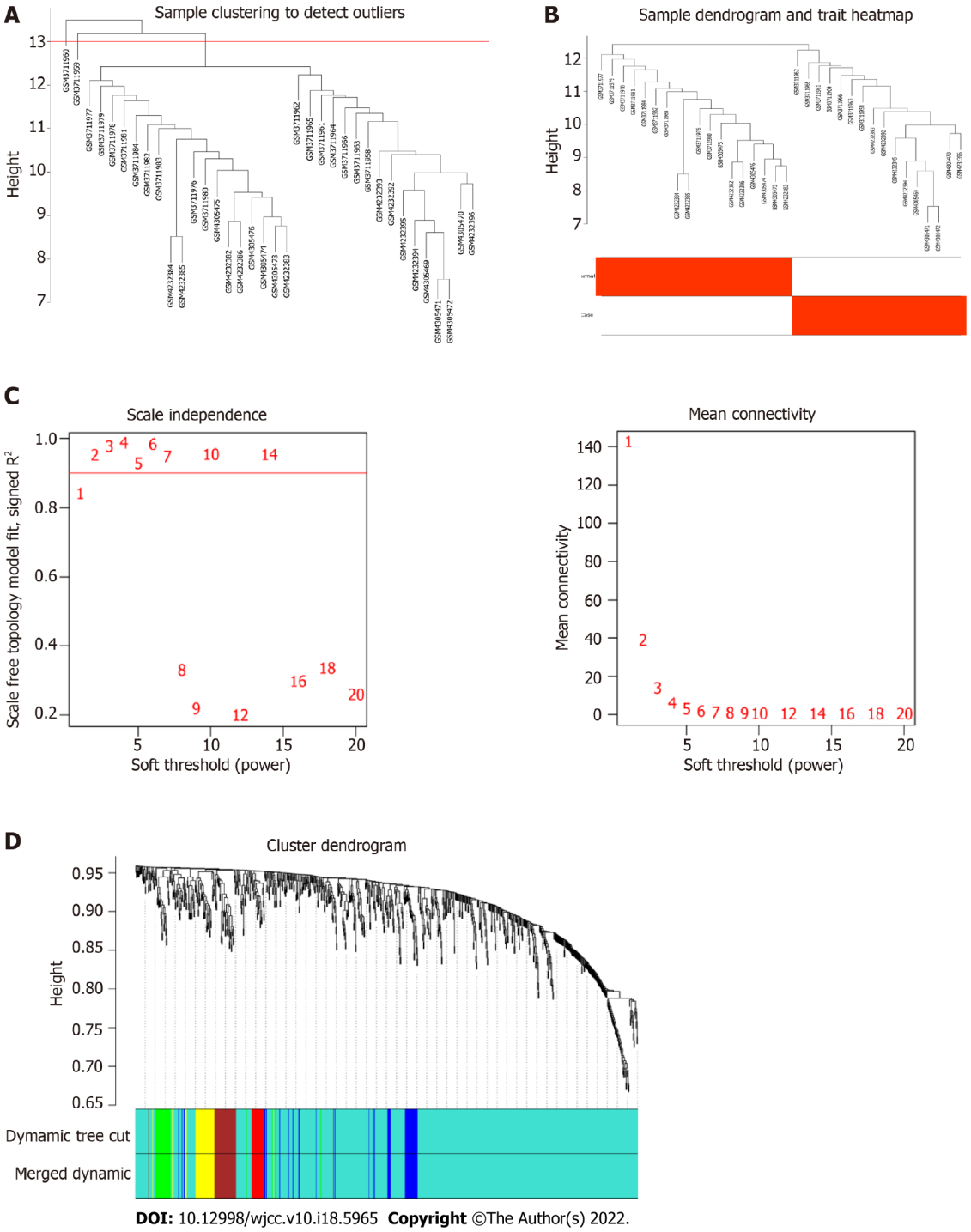

DOI: 10.12998/wjcc.v10.i18.5965 **Copyright** ©The Author(s) 2022.

Figure 4 Construction of weighted gene co-expression network. A: Sample screening dendrogram; B: Sample dendrogram and trait heat map; C: Scale-free fit index of different soft threshold power (β) and mean connectivity of various soft threshold power; D: The cluster dendrogram of the miRNAs. Each branch represents one gene, and every color below represents one module.

RT-PCR validation

IL-1B, CXCL9, CLDN8, CCL8, hsa-miR-181a-5p, hsa-miR-30a-3p, and hsa-miR-21-5p related to psoriasis were selected from hub miRNAs and target DEmRNAs for *in vitro* validation. Primers for each mRNAs and miRNAs were shown in Table 5. IL-1B, CXCL9 and CCL8 were up-regulated and CLDN8 and hsa-miR-181a-5p were down-regulated in psoriasis tissues (Figure 8). Among them, IL-1B, CXCL9, and CLDN8 showed significant difference in expression levels. In addition, we found that expression trends of hsa-miR-30a-3p and hsa-miR-21-5p were contrary to the results of bioinformatics analysis. The reason for the inconsistency between RT-PCR and bioinformatics analysis results may be the small sample size. Further research is needed.

Table 4 Kyoto Encyclopedia of Genes and Genomics function enrichment of target differentially expressed mRNAs

Category	hsa	Term	Count	*P* value	Genes
KEGG_PATHWAY	hsa05164	Influenza A	6	0.002804	*STAT1, OAS2, IL-1B, OAS3, TNFSF10, MAPK13*
KEGG_PATHWAY	hsa05160	Hepatitis C	5	0.006506	*STAT1, OAS2, CLDN8, OAS3, MAPK13*
KEGG_PATHWAY	hsa05162	Measles	5	0.006506	*STAT1, OAS2, IL-1B, OAS3, TNFSF10*
KEGG_PATHWAY	hsa04062	Chemokine signaling pathway	5	0.020355	*CXCL9, CCL8, PLCB4, CCL22, STAT1*
KEGG_PATHWAY	hsa04620	Toll-like receptor signaling pathway	4	0.021751	*CXCL9, STAT1, IL-1B, MAPK13*
KEGG_PATHWAY	hsa04060	Cytokine-cytokine receptor interaction	5	0.047526	*CXCL9, CCL8, CCL22, IL-1B, TNFSF10*

Table 5 Primer sequence in the real-time polymerase chain reaction

Primer name	Primer sequence, 5' to 3'
GAPDH-F (internal reference)	5-GGAGCGAGATCCCTCCAAAAT-3
GAPDH-R (internal reference)	5-GGCTGTTGTCATACTTCTCATGG-3
ACTB-F (internal reference)	5-CATGTACGTTGCTATCCAGGC-3
ACTB-R (internal reference)	5-CTCCTTAATGTCACGCACGAT-3
IL-1B-F	5-TTCGACACATGGGATAACGAGG-3
IL-1B-R	5-TTTTTGCTGTGAGTCCCGGAG-3
CXCL9-F	5-CCAGTAGTGAGAAAGGGTCGC-3
CXCL9-R	5-AGGGCTTGGGGCAAATTGTT-3
CCL8-F	5-TGGAGAGCTACACAAGAATCACC-3
CCL8-R	5-TGGTCCAGATGCTTCATGGAA-3
CLDN8-F	5-CTACAGGCAGCCAGAGGACT-3
CLDN8-R	5-ACAGGGATGAGCACCACCAT-3
hsa-U6 (internal reference)	
hsa-miR-30a-3p	5-CTTTCAGTCGGATGTTTGCAGC-3
hsa-miR-181a-5p	5-AACATTCAACGCTGTCGGTGAGT-3
hsa-miR-21-5p	5-TAGCTTATCAGACTGATGTTGA-3

DISCUSSION

Although psoriasis is widespread and has significant negative impact on patients' quality of life, it has not yet been fully diagnosed and treated. In the research, we used the WGCNA method to identify 10 hub miRNAs that may be related to the pathogenesis of psoriasis. Then, target mRNAs of hub miRNAs were predicted by using miRDB database. Only 8 hub miRNAs were predicted to the corresponding target mRNAs. Subsequently, to understand the key biological functions involved in DEmRNAs and target DEmRNAs, we performed GO and KEGG functional analysis. Results demonstrated that they were significantly enriched in immune-related biological functions, for example, immune response, cell chemotaxis, and chemokine signaling pathway.

Hsa-miR-21-5p is abnormally expressed in psoriasis, but the specific molecular mechanism remains unclear[29]. In this study, results demonstrated that hsa-miR-21-5p expression was up-regulated and negatively regulated with CLDN8. CLDN8 is down-regulated in psoriasis and has an important molecular regulatory role[30]. CLDN8 has also been identified as a key downstream component of the IL-9 and IL-23 inflammatory cascade[31,32]. In addition, KEGG functional enrichment analysis showed that CLDN8 was enriched in hepatitis C. Cohen *et al*[33] found that psoriasis is associated with hepatitis C[33]. Cathelicidin, toll like receptor 9 (TLR9), IFN-γ, and TNF-α are inflammatory cytokines. Hepatitis C may increase susceptibility to psoriasis by up-regulating these inflammatory factors[34,35]. Thus, we hypothesized that hsa-miR-21-5p may play a vital regulatory role in hepatitis C through regulating CLDN8 and, thus, affect the pathogenesis of psoriasis.

Hsa-miR-30a-3p can affect the migration and proliferation of cancer cells by targeting related genes [36,37]. Hsa-miR-30a-3p is also contacted with platelet apoptosis and adhesion in immune thrombocyt-

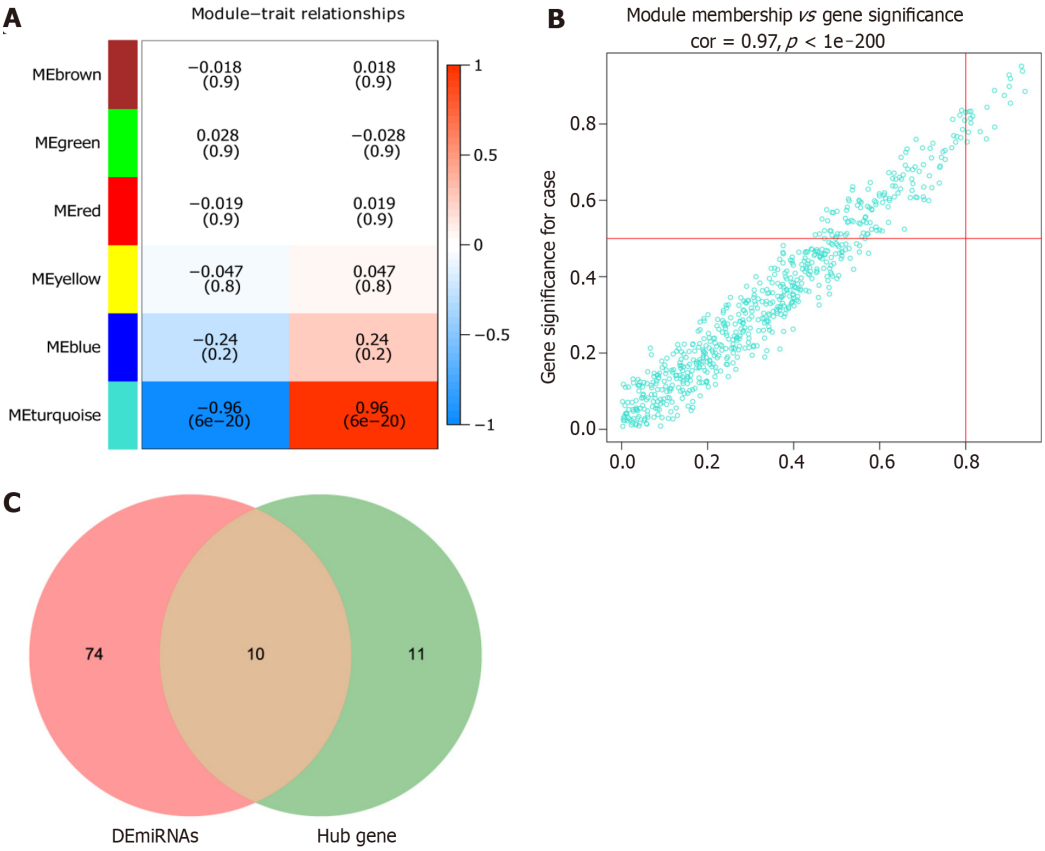

DOI: 10.12998/wjcc.v10.i18.5965 **Copyright** ©The Author(s) 2022.

Figure 5 Hub module and hub miRNAs. A: Heat map of the correlation between module eigengene and psoriasis. The correlation between turquoise module and psoriasis was highest; B: Scatter plot of miRNAs in the turquoise module. MiRNAs with module connectivity > 0.8 and clinical trait relationship > 0.5 were selected as candidate hub miRNAs; C: The 10 intersecting miRNAs were identified as real hub miRNAs.

openia[38]. However, we have not found any report about hsa-miR-30a-3p in psoriasis. In this study, we found that hsa-miR-30a-3p was up-regulated and negatively regulated with multiple DEmRNAs in psoriasis. It may play a vital regulatory role in psoriasis by targeting these DEmRNAs. We found the pro-inflammatory factor IL-1B in target DEmRNAs of hsa-miR-30a-3p. IL-1B has been found to play an important role in autoimmune or autoinflammatory conditions[39]. IL-1B is abundant in the tissue fluid of psoriasis and participates in the disease progression through dual effects[40]. First, it induces insulin resistance through p38 mitogen-activated protein kinase (p38MAPK), preventing insulin-dependent differentiation of keratinocytes, while IL-1B promotes keratinocyte proliferation, both hallmarks of psoriasis. Through KEGG functional enrichment analysis, we also found that IL-1B participates in multiple signal pathways, for example, measles, toll-like receptor signaling pathway, and cytokine-cytokine receptor interaction. Measles can relieve psoriasis through an immunosuppressive effect[41]. Toll-like receptor signaling pathway play an important role in psoriasis by affecting keratinocyte production[42]. The cytokine-cytokine receptor interaction is related to the occurrence and progression of psoriasis through combined transcriptomic analysis[43], which is consistent with our analysis. Thus, we hypothesized that hsa-miR-30a-3p may play a vital molecular role in the progression of psoriasis by targeting DEmRNAs to regulate multiple biological signaling pathways.

Hsa-miR-181a-5p is involved in the catabolic pathway of chondrocytes and oxidative stress in osteoarthritis[44]. Hsa-miR-181a-5p can also regulate the pathogenesis of sepsis-related inflammation through CRNDE/hsa-miR-181a-5p/TLR4 pathway[45]. In a case-control study, hsa-miR-181a-5p was significantly down-regulated in psoriasis[29]. The miRNA-mRNA regulatory network results demonstrated that hsa-miR-181a-5p was negatively regulated with multiple DEmRNAs. Among these DEmRNAs, we found inflammatory mediators CXCL9 and CCL8. CXCL9 is an important chemokine involved in T cell recruitment and is up-regulated in the plasma of patients with psoriasis[46,47]. Increased CXCL9 expression can aggravate the progression of psoriasis[48]. CXCL9 and hsa-miR-30c-2-3p were also negatively regulated in the miRNA-mRNA regulatory network. Oncology studies have shown that hsa-miR-30c-2-3p play a vital role in tumor pathogenesis by regulating the proliferation, apoptosis, migration, and invasion of cancer cells[49,50]. So far, we have not found any studies on hsa-miR-30c-2-3p in psoriasis. This article may be the first to report that hsa-miR-30c-2-3p plays a role in the pathogenesis of psoriasis. As a chemokine, CCL8 is involved in immune regulation and inflammatory processes in a variety of diseases[51-53]. Although no relevant studies on CCL8 have been found in

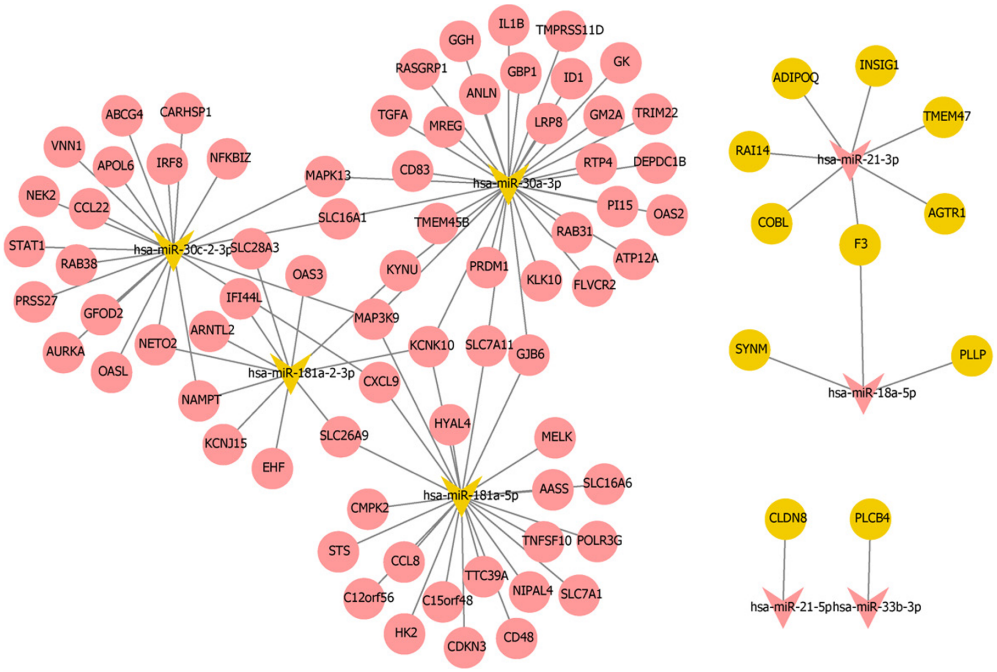

DOI: 10.12998/wjcc.v10.i18.5965 **Copyright** ©The Author(s) 2022.

Figure 6 Regulatory network of miRNA-mRNA. Red, yellow, oval, and V-shaped represent up-regulated, down-regulated, differentially expressed mRNAs, and hub differentially expressed miRNAs, respectively.

psoriasis, the expression of CCL8 is up-regulated in atopic dermatitis[54]. In addition, CXCL9 and CCL8 were found to be enriched in chemokine signaling pathway and cytokine-cytokine receptor interaction by functional analysis. Therefore, this further suggests that hsa-miR-181a-5p and hsa-miR-30c-2-3p may play a regulatory role in psoriasis by targeting DEmRNAs to mediate multiple biological signaling pathways.

Current research results highlighted that silencing hsa-miR-181a-2-3p could enhance cadmium-induced inflammatory response and activation of inflammasome[55]. In the research, we found that hsa-miR-181a-2-3p was negatively regulated with multiple DEmRNAs. Among these DEmRNAs, OAS3 was found to be involved in hepatitis C and measles in KEGG functional enrichment. Some researchers have found that the OAS3 is concerned with the occurrence and progression of psoriasis through transcriptomic analysis, which is consistent with our analysis[56,57]. Thus, we hypothesized that hsa-miR-181a-2-3p may play a regulatory role in the progression of psoriasis by targeting OAS3 to mediate hepatitis C and measles. This provides potential molecular research directions for further research on the pathogenesis of psoriasis.

The expression of hsa-miR-21-3p in psoriasis was significantly increased[58]. Moreover, hsa-miR-21-3p plays a pro-inflammatory role in keratinocytes, and high expression in the skin is concerned with psoriasis[59]. So far, we have not found relevant reports about hsa-miR-18a-5p in psoriasis. However, hsa-miR-18a-5p promotes the proliferation and migration of pulmonary smooth muscle cells by targeting notch receptor 2[60]. Oncology studies have shown that hsa-miR-18a-5p promotes melanoma cell proliferation by targeting EPH receptor A7 signaling[61]. Hsa-miR-18a-5p can affect keratinocytes apoptosis by targeting B-cell lymphoma/leukemia-2-like protein 10 in patients with toxic epidermal necrolysis and is related to the skin erythema or erosion area of drug eruptions[62]. The miRNA-mRNA regulatory network regulatory network result demonstrates that hsa-miR-21-3p and hsa-miR-18a-5p jointly negatively regulate coagulation factor III, tissue factor (F3). This finding provides new research ideas for the pathogenesis of psoriasis in the future.

Results of previous studies demonstrate that down-regulation of interleukin 1 receptor associated kinase 3 by hsa-miR-33b-3p can alleviate the inflammation and apoptosis induced by IL-1B in CHON-001 cells[63]. As a key miRNA of major depression disorder and Kawasaki disease, hsa-miR-33b-3p play an important role in their pathogenesis[64,65]. Hsa-miR-33b-3p has also been reported in cancer[66]. In the miRNA-mRNA regulatory network, phospholipase C beta 4 (PLCB4) is the only negatively regulated target DEmRNA of hsa-miR-33b-3p. Neutrophils are an important part of the innate immune system and an early line of defense against microbial invasion. PLCB4 can regulate the number of neutrophils[67]. In addition, KEGG functional analysis result demonstrated that PLCB4 was enriched in chemokine signaling pathway. Thus, we hypothesized that hsa-miR-33b-3p may play a vital molecular role in psoriasis by targeting PLCB4 to regulate chemokine signaling pathway.

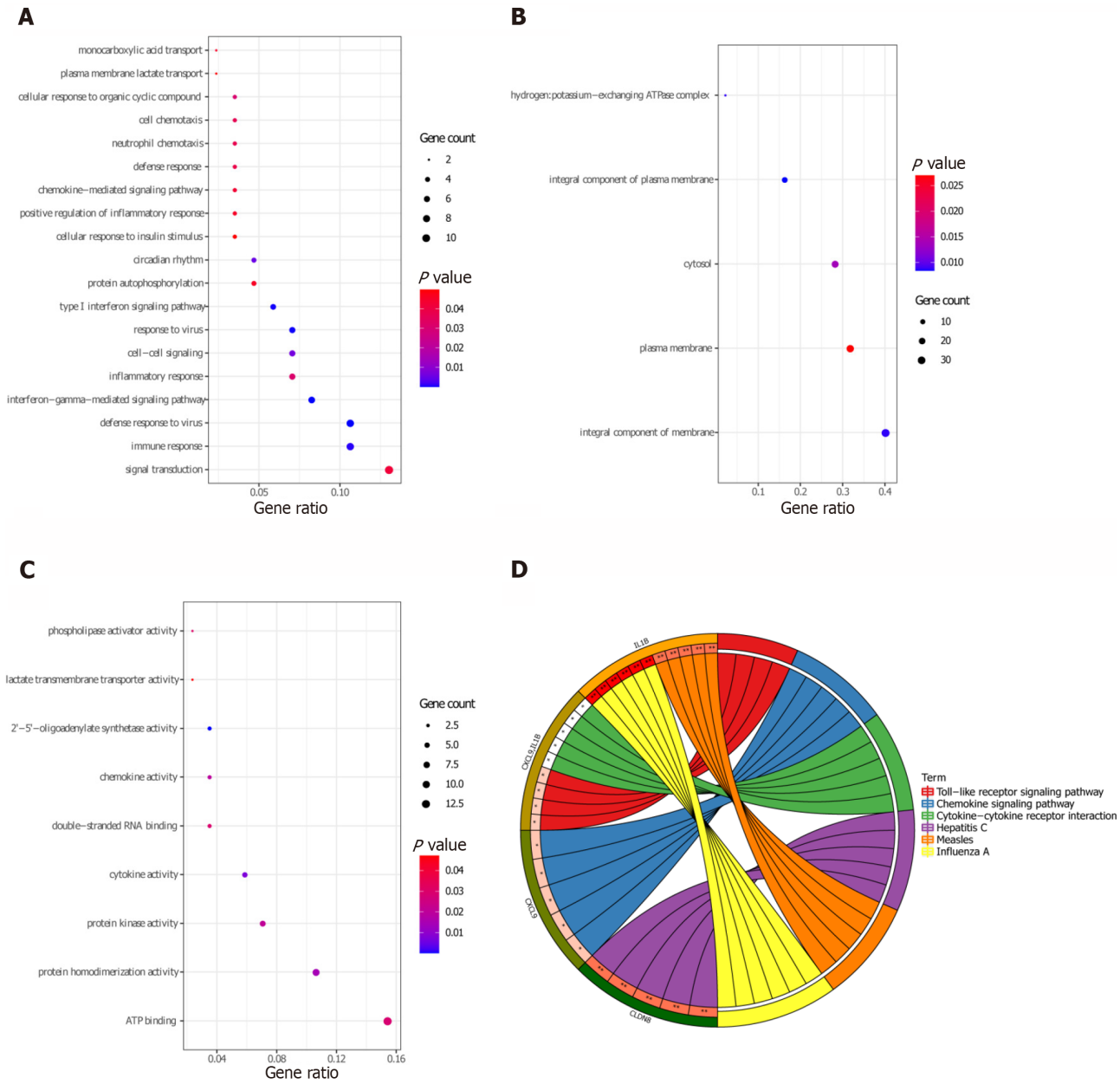

DOI: 10.12998/wjcc.v10.i18.5965 **Copyright** ©The Author(s) 2022.

Figure 7 Gene Ontology and Kyoto Encyclopedia of Genes and Genomics analysis of target differentially expressed mRNAs. A: biological processes terms were enriched of target differentially expressed mRNAs (DEmRNAs) by Gene Ontology (GO) function analysis; B: Cellular components terms were enriched of target DEmRNAs by GO function analysis; C: Molecular functions terms were enriched of target DEmRNAs by GO function analysis; D: Kyoto Encyclopedia of Genes and Genomics enrichment of target DEmRNAs.

This study has some limitations. First, sample size of *in vitro* validation was small, leading to a certain degree of error between RT-PCR validation results and bioinformatics analysis results. Further studies with a larger sample size are needed. Secondly, the specific regulatory mechanism of the identified genes and signaling pathways in psoriasis remain unclear, so further research is needed.

CONCLUSION

In conclusion, identification of potential key molecular markers and signaling pathways provides potential molecular research directions for further understanding the pathological mechanisms of psoriasis. This may also provide new research ideas for the prevention and treatment of psoriasis in the future.

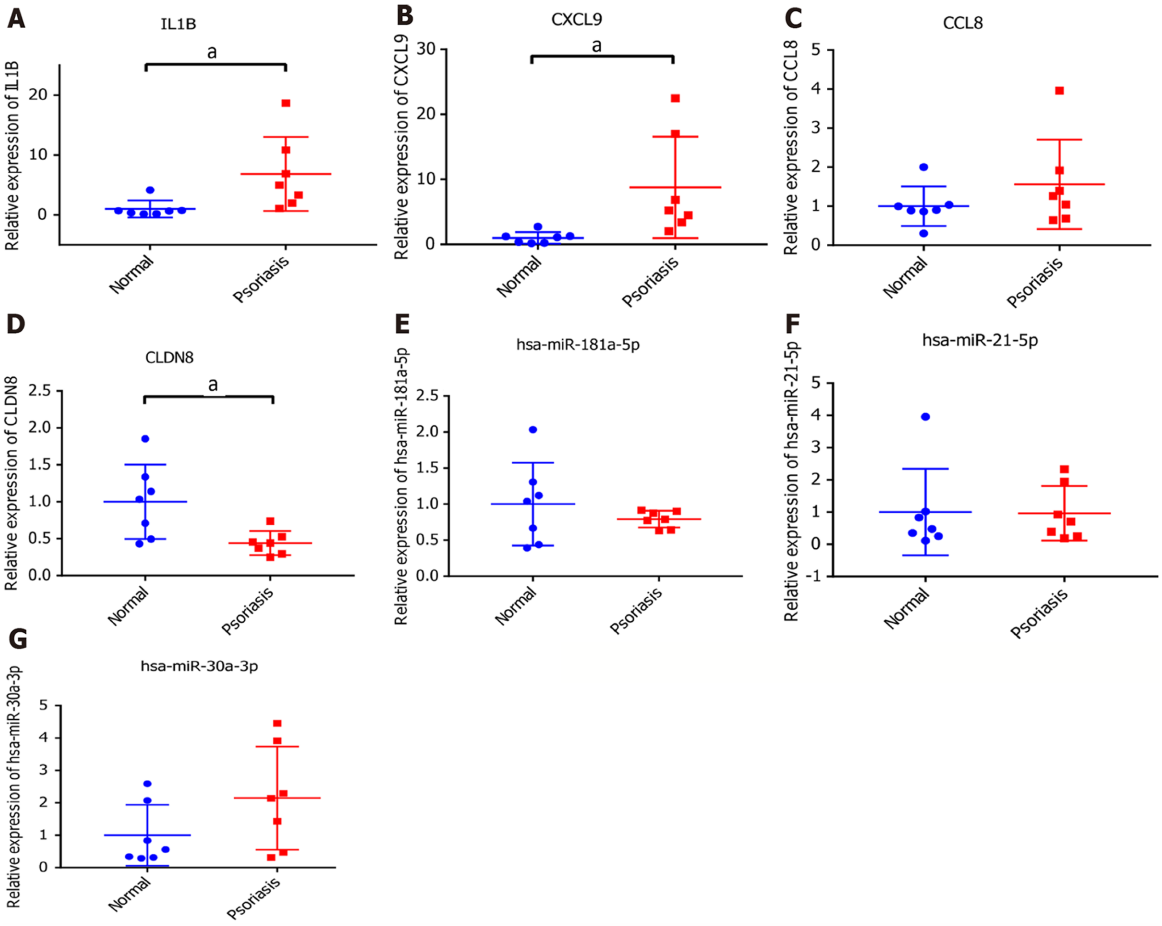

DOI: 10.12998/wjcc.v10.i18.5965 **Copyright** ©The Author(s) 2022.

Figure 8 Real-time polymerase chain reaction validation. A: Interleukin-1β; B: C-X-C motif chemokine ligand 9; C: C-C motif chemokine ligand 8; D: Claudin 8; E: hsa-miR-181a-5p; F: hsa-miR-21-5p; G: hsa-miR-30a-3p. $^{a}P < 0.05$, $P < 0.05$ was considered significant.

ARTICLE HIGHLIGHTS

Research background

Previous studies have found that microRNAs (miRNAs) play an important regulatory role in the progression of various diseases. Currently, miRNAs studies in psoriasis and dermatology are relatively new.

Research motivation

Although psoriasis is widespread and has significant negative impact on patients' life quality, it has not yet been fully diagnosed and treated.

Research objectives

Identification of key miRNAs in psoriasis is helpful to elucidate the molecular mechanism of psoriasis.

Research methods

Differentially expressed mRNAs (DEmRNAs) and differentially expressed miRNAs were screened out by limma R package. DEmRNAs were analyzed for Gene Ontology and Kyoto Encyclopedia of Genes and Genomics functional enrichment. The "Weighted gene co-expression network analysis (WGCNA)" R package was used to analyze the co-expression network of all miRNAs. We constructed miRNA-mRNA regulatory networks based on identified hub miRNAs.

Research results

We identified a large number of DEmRNAs and screened possible signaling pathways related to psoriasis, for example, toll-like receptor signaling pathway, cytokine-cytokine receptor interaction, and chemokine signaling pathway. Ten hub miRNAs were identified by WGCNA. Eight hub miRNAs predicted the corresponding target mRNAs. Ninety-seven negatively regulated miRNA-mRNA pairs were involved in the miRNA-mRNA regulatory network, for example, hsa-miR-21-5p-CLDN8, hsa-miR-

30a-3p-IL-1B and hsa-miR-181a-5p/hsa-miR-30c-2-3p-CXCL9.

Research conclusions

The identification of potential key molecular markers and signaling pathways provides potential research directions for further understanding the molecular mechanisms of psoriasis.

Research perspectives

This study provide new research ideas for the prevention and treatment of psoriasis in the future.

FOOTNOTES

Author contributions: Shu X contributed to the conception and design; Li CX performed the administrative support; Wang YL and Kang XD provide materials and samples; Shu X, Ran M, and Chen XX contributed to the data collection and collation; Shu X and Zhao ZK contributed to the data analysis and interpretation; All authors read and approved the final version of the manuscript.

Institutional review board statement: All experimental procedures were approved by the ethics committee of Chinese PLA General Hospital, No. S2021-012-01.

Conflict-of-interest statement: All the authors report no relevant conflicts of interest for this article.

Data sharing statement: All data generated or analyzed during this study are included in this published article.

Open-Access: This article is an open-access article that was selected by an in-house editor and fully peer-reviewed by external reviewers. It is distributed in accordance with the Creative Commons Attribution NonCommercial (CC BY-NC 4.0) license, which permits others to distribute, remix, adapt, build upon this work non-commercially, and license their derivative works on different terms, provided the original work is properly cited and the use is non-commercial. See: https://creativecommons.org/Licenses/by-nc/4.0/

Country/Territory of origin: China

ORCID number: Cheng-Xin Li 0000-0001-9862-031X.

S-Editor: Fan JR
L-Editor: Filipodia
P-Editor: Qi WW

REFERENCES

1 **Langley RG**, Krueger GG, Griffiths CE. Psoriasis: epidemiology, clinical features, and quality of life. *Ann Rheum Dis* 2005; **64** Suppl 2: ii18-23; discussion ii24 [PMID: 15708928 DOI: 10.1136/ard.2004.033217]
2 **López-Estebaranz JL**, Sánchez-Carazo JL, Sulleiro S. Effect of a family history of psoriasis and age on comorbidities and quality of life in patients with moderate to severe psoriasis: Results from the ARIZONA study. *J Dermatol* 2016; **43**: 395-401 [PMID: 26460276 DOI: 10.1111/1346-8138.13157]
3 **Kamiya K**, Kishimoto M, Sugai J, Komine M, Ohtsuki M. Risk Factors for the Development of Psoriasis. *Int J Mol Sci* 2019; **20** [PMID: 31491865 DOI: 10.3390/ijms20184347]
4 **Rendon A**, Schäkel K. Psoriasis Pathogenesis and Treatment. *Int J Mol Sci* 2019; **20** [PMID: 30909615 DOI: 10.3390/ijms20061475]
5 **Takeshita J**, Grewal S, Langan SM, Mehta NN, Ogdie A, Van Voorhees AS, Gelfand JM. Psoriasis and comorbid diseases: Epidemiology. *J Am Acad Dermatol* 2017; **76**: 377-390 [PMID: 28212759 DOI: 10.1016/j.jaad.2016.07.064]
6 **Saliminejad K**, Khorram Khorshid HR, Soleymani Fard S, Ghaffari SH. An overview of microRNAs: Biology, functions, therapeutics, and analysis methods. *J Cell Physiol* 2019; **234**: 5451-5465 [PMID: 30471116 DOI: 10.1002/jcp.27486]
7 **Bhaskaran M**, Mohan M. MicroRNAs: history, biogenesis, and their evolving role in animal development and disease. *Vet Pathol* 2014; **51**: 759-774 [PMID: 24045890 DOI: 10.1177/0300985813502820]
8 **Timis TL**, Orasan RI. Understanding psoriasis: Role of miRNAs. *Biomed Rep* 2018; **9**: 367-374 [PMID: 30402223 DOI: 10.3892/br.2018.1146]
9 **Tang L**, He S, Zhu Y, Feng B, Su Z, Liu B, Xu F, Wang X, Liu H, Li C, Zhao J, Zheng X, Sun C, Lu C, Zheng G. Downregulated miR-187 contributes to the keratinocytes hyperproliferation in psoriasis. *J Cell Physiol* 2019; **234**: 3661-3674 [PMID: 30607907 DOI: 10.1002/jcp.27135]
10 **Liu T**, Zhang X, Wang Y. miR-183-3p suppresses proliferation and migration of keratinocyte in psoriasis by inhibiting GAB1. *Hereditas* 2020; **157**: 28 [PMID: 32650835 DOI: 10.1186/s41065-020-00138-w]
11 **Wang Y**, Yu X, Wang L, Ma W, Sun Q. miR-320b Is Down-Regulated in Psoriasis and Modulates Keratinocyte Proliferation by Targeting AKT3. *Inflammation* 2018; **41**: 2160-2170 [PMID: 30136020 DOI: 10.1007/s10753-018-0859-7]
12 **Wang Q**, Chang W, Yang X, Cheng Y, Zhao X, Zhou L, Li J, Zhang K. Levels of miR-31 and its target genes in dermal

mesenchymal cells of patients with psoriasis. *Int J Dermatol* 2019; **58**: 198-204 [PMID: 30198149 DOI: 10.1111/ijd.14197]

13 **Hermann H**, Runnel T, Aab A, Baurecht H, Rodriguez E, Magilnick N, Urgard E, Šahmatova L, Prans E, Maslovskaja J, Abram K, Karelson M, Kaldvee B, Reemann P, Haljasorg U, Rückert B, Wawrzyniak P, Weichenthal M, Mrowietz U, Franke A, Gieger C, Barker J, Trembath R, Tsoi LC, Elder JT, Tkaczyk ER, Kisand K, Peterson P, Kingo K, Boldin M, Weidinger S, Akdis CA, Rebane A. miR-146b Probably Assists miRNA-146a in the Suppression of Keratinocyte Proliferation and Inflammatory Responses in Psoriasis. *J Invest Dermatol* 2017; **137**: 1945-1954 [PMID: 28595995 DOI: 10.1016/j.jid.2017.05.012]

14 **Xiao Y**, Wang H, Wang C, Zeng B, Tang X, Zhang Y, Peng Y, Luo M, Huang P, Yang Z. miR-203 promotes HaCaT cell overproliferation through targeting LXR-α and PPAR-γ. *Cell Cycle* 2020; **19**: 1928-1940 [PMID: 32594829 DOI: 10.1080/15384101.2020.1783934]

15 **Xu N**, Brodin P, Wei T, Meisgen F, Eidsmo L, Nagy N, Kemeny L, Ståhle M, Sonkoly E, Pivarcsi A. MiR-125b, a microRNA downregulated in psoriasis, modulates keratinocyte proliferation by targeting FGFR2. *J Invest Dermatol* 2011; **131**: 1521-1529 [PMID: 21412257 DOI: 10.1038/jid.2011.55]

16 **Su F**, Jin L, Liu W. MicroRNA-125a Correlates with Decreased Psoriasis Severity and Inflammation and Represses Keratinocyte Proliferation. *Dermatology* 2021; **237**: 568-578 [PMID: 33735868 DOI: 10.1159/000510681]

17 **Lerman G**, Sharon M, Leibowitz-Amit R, Sidi Y, Avni D. The crosstalk between IL-22 signaling and miR-197 in human keratinocytes. *PLoS One* 2014; **9**: e107467 [PMID: 25208211 DOI: 10.1371/journal.pone.0107467]

18 **Chen CL**, Liu XM, Xiong-Ming PU, Wei-Dong WU. Research Advances of miRNA Differential Expression in Psoriasis. Medical Recapitulate 2016.

19 **Langfelder P**, Horvath S. WGCNA: an R package for weighted correlation network analysis. *BMC Bioinformatics* 2008; **9**: 559 [PMID: 19114008 DOI: 10.1186/1471-2105-9-559]

20 **Song ZY**, Chao F, Zhuo Z, Ma Z, Li W, Chen G. Identification of hub genes in prostate cancer using robust rank aggregation and weighted gene co-expression network analysis. *Aging (Albany NY)* 2019; **11**: 4736-4756 [PMID: 31306099 DOI: 10.18632/aging.102087]

21 **Niu X**, Zhang J, Zhang L, Hou Y, Pu S, Chu A, Bai M, Zhang Z. Weighted Gene Co-Expression Network Analysis Identifies Critical Genes in the Development of Heart Failure After Acute Myocardial Infarction. *Front Genet* 2019; **10**: 1214 [PMID: 31850068 DOI: 10.3389/fgene.2019.01214]

22 **Zhao X**, Zhang L, Wang J, Zhang M, Song Z, Ni B, You Y. Identification of key biomarkers and immune infiltration in systemic lupus erythematosus by integrated bioinformatics analysis. *J Transl Med* 2021; **19**: 35 [PMID: 33468161 DOI: 10.1186/s12967-020-02698-x]

23 **Edgar R**, Domrachev M, Lash AE. Gene Expression Omnibus: NCBI gene expression and hybridization array data repository. *Nucleic Acids Res* 2002; **30**: 207-210 [PMID: 11752295 DOI: 10.1093/nar/30.1.207]

24 **Ritchie ME**, Phipson B, Wu D, Hu Y, Law CW, Shi W, Smyth GK. limma powers differential expression analyses for RNA-sequencing and microarray studies. *Nucleic Acids Res* 2015; **43**: e47 [PMID: 25605792 DOI: 10.1093/nar/gkv007]

25 **Huang da W**, Sherman BT, Lempicki RA. Systematic and integrative analysis of large gene lists using DAVID bioinformatics resources. *Nat Protoc* 2009; **4**: 44-57 [PMID: 19131956 DOI: 10.1038/nprot.2008.211]

26 **Zhong S**, Chen C, Liu N, Yang L, Hu Z, Duan P, Shuai D, Zhang Q, Wang Y. Overexpression Of hsa-miR-664a-3p Is Associated With Cigarette Smoke-Induced Chronic Obstructive Pulmonary Disease Via Targeting FHL1. *Int J Chron Obstruct Pulmon Dis* 2019; **14**: 2319-2329 [PMID: 31632001 DOI: 10.2147/COPD.S224763]

27 **Lin J**, Yu M, Xu X, Wang Y, Xing H, An J, Yang J, Tang C, Sun D, Zhu Y. Identification of biomarkers related to $CD8^+$ T cell infiltration with gene co-expression network in clear cell renal cell carcinoma. *Aging (Albany NY)* 2020; **12**: 3694-3712 [PMID: 32081834 DOI: 10.18632/aging.102841]

28 **Livak KJ**, Schmittgen TD. Analysis of relative gene expression data using real-time quantitative PCR and the 2(-Delta Delta C(T)) Method. *Methods* 2001; **25**: 402-408 [PMID: 11846609 DOI: 10.1006/meth.2001.1262]

29 **Alatas ET**, Kara M, Dogan G, Akın Belli A. Blood microRNA expressions in patients with mild to moderate psoriasis and the relationship between microRNAs and psoriasis activity. *An Bras Dermatol* 2020; **95**: 702-707 [PMID: 32811699 DOI: 10.1016/j.abd.2020.07.001]

30 **He H**, Bissonnette R, Wu J, Diaz A, Saint-Cyr Proulx E, Maari C, Jack C, Louis M, Estrada Y, Krueger JG, Zhang N, Pavel AB, Guttman-Yassky E. Tape strips detect distinct immune and barrier profiles in atopic dermatitis and psoriasis. *J Allergy Clin Immunol* 2021; **147**: 199-212 [PMID: 32709423 DOI: 10.1016/j.jaci.2020.05.048]

31 **Li L**, Huang S, Wang H, Chao K, Ding L, Feng R, Qiu Y, Feng T, Zhou G, Hu JF, Chen M, Zhang S. Cytokine IL9 Triggers the Pathogenesis of Inflammatory Bowel Disease Through the miR21-CLDN8 Pathway. *Inflamm Bowel Dis* 2018; **24**: 2211-2223 [PMID: 29788092 DOI: 10.1093/ibd/izy187]

32 **Wang H**, Chao K, Ng SC, Bai AH, Yu Q, Yu J, Li M, Cui Y, Chen M, Hu JF, Zhang S. Pro-inflammatory miR-223 mediates the cross-talk between the IL23 pathway and the intestinal barrier in inflammatory bowel disease. *Genome Biol* 2016; **17**: 58 [PMID: 27029486 DOI: 10.1186/s13059-016-0901-8]

33 **Cohen AD**, Weitzman D, Birkenfeld S, Dreiher J. Psoriasis associated with hepatitis C but not with hepatitis B. *Dermatology* 2010; **220**: 218-222 [PMID: 20185894 DOI: 10.1159/000286131]

34 **Chun K**, Afshar M, Audish D, Kabigting F, Paik A, Gallo R, Hata T. Hepatitis C may enhance key amplifiers of psoriasis. *J Eur Acad Dermatol Venereol* 2017; **31**: 672-678 [PMID: 27184185 DOI: 10.1111/jdv.13578]

35 **Imafuku S**, Naito R, Nakayama J. Possible association of hepatitis C virus infection with late-onset psoriasis: a hospital-based observational study. *J Dermatol* 2013; **40**: 813-818 [PMID: 23961783 DOI: 10.1111/1346-8138.12240]

36 **Zhou K**, Cao D, Wang Y, Wang L, Meng X. Hsa-miR-30a-3p attenuates gastric adenocarcinoma proliferation and metastasis *via* APBB2. *Aging (Albany NY)* 2021; **13**: 16763-16772 [PMID: 34182542 DOI: 10.18632/aging.203197]

37 **Zhong B**, Guo S, Zhang W, Zhang C, Wang Y. Bioinformatics prediction of miR-30a targets and its inhibition of cell proliferation of osteosarcoma by up-regulating the expression of PTEN. *BMC Med Genomics* 2017; **10**: 64 [PMID: 29141684 DOI: 10.1186/s12920-017-0300-3]

38 **Deng G**, Yu S, He Y, Sun T, Liang W, Yu L, Xu D, Li Q, Zhang R. MicroRNA profiling of platelets from immune thrombocytopenia and target gene prediction. *Mol Med Rep* 2017; **16**: 2835-2843 [PMID: 28677771 DOI:

10.3892/mmr.2017.6901]
39 **Swindell WR**, Beamer MA, Sarkar MK, Loftus S, Fullmer J, Xing X, Ward NL, Tsoi LC, Kahlenberg MJ, Liang Y, Gudjonsson JE. RNA-Seq Analysis of IL-1B and IL-36 Responses in Epidermal Keratinocytes Identifies a Shared MyD88-Dependent Gene Signature. *Front Immunol* 2018; **9**: 80 [PMID: 29434599 DOI: 10.3389/fimmu.2018.00080]
40 **Buerger C**, Richter B, Woth K, Salgo R, Malisiewicz B, Diehl S, Hardt K, Boehncke S, Boehncke WH. Interleukin-1β interferes with epidermal homeostasis through induction of insulin resistance: implications for psoriasis pathogenesis. *J Invest Dermatol* 2012; **132**: 2206-2214 [PMID: 22513786 DOI: 10.1038/jid.2012.123]
41 **Chakravarti VS**, Lingam S. Measles induced remission of psoriasis. *Ann Trop Paediatr* 1986; **6**: 293-294 [PMID: 2435240 DOI: 10.1080/02724936.1986.11748460]
42 **Chen JQ**, Szodoray P, Zeher M. Toll-Like Receptor Pathways in Autoimmune Diseases. *Clin Rev Allergy Immunol* 2016; **50**: 1-17 [PMID: 25687121 DOI: 10.1007/s12016-015-8473-z]
43 **Gao Y**, Yi X, Ding Y. Combined Transcriptomic Analysis Revealed AKR1B10 Played an Important Role in Psoriasis through the Dysregulated Lipid Pathway and Overproliferation of Keratinocyte. *Biomed Res Int* 2017; **2017**: 8717369 [PMID: 29204449 DOI: 10.1155/2017/8717369]
44 **Xue J**, Min Z, Xia Z, Cheng B, Lan B, Zhang F, Han Y, Wang K, Sun J. The hsa-miR-181a-5p reduces oxidation resistance by controlling SECISBP2 in osteoarthritis. *BMC Musculoskelet Disord* 2018; **19**: 355 [PMID: 30286747 DOI: 10.1186/s12891-018-2273-6]
45 **Wang Y**, Xu Z, Yue D, Zeng Z, Yuan W, Xu K. Linkage of lncRNA CRNDE sponging miR-181a-5p with aggravated inflammation underlying sepsis. *Innate Immun* 2020; **26**: 152-161 [PMID: 31604377 DOI: 10.1177/1753425919880946]
46 **Duarte GV**, Boeira V, Correia T, Porto-Silva L, Cardoso T, Macedo MN, Oliveira MF, Carvalho E. Osteopontin, CCL5 and CXCL9 are independently associated with psoriasis, regardless of the presence of obesity. *Cytokine* 2015; **74**: 287-292 [PMID: 25972108 DOI: 10.1016/j.cyto.2015.04.015]
47 **Costa MC**, Paixão CS, Viana DL, Rocha BO, Saldanha M, da Mota LMH, Machado PRL, Pagliari C, de Oliveira MF, Arruda S, Carvalho EM, Carvalho LP. Mononuclear Phagocyte Activation Is Associated With the Immunopathology of Psoriasis. *Front Immunol* 2020; **11**: 478 [PMID: 32269570 DOI: 10.3389/fimmu.2020.00478]
48 **Wang H**, Chen W, He J, Xu W, Liu J. Network analysis of potential risk genes for psoriasis. *Hereditas* 2021; **158**: 21 [PMID: 34134787 DOI: 10.1186/s41065-021-00186-w]
49 **Tang CT**, Liang Q, Yang L, Lin XL, Wu S, Chen Y, Zhang XT, Gao YJ, Ge ZZ. RAB31 Targeted by MiR-30c-2-3p Regulates the GLI1 Signaling Pathway, Affecting Gastric Cancer Cell Proliferation and Apoptosis. *Front Oncol* 2018; **8**: 554 [PMID: 30534536 DOI: 10.3389/fonc.2018.00554]
50 **Zhang HD**, Jiang LH, Hou JC, Zhou SY, Zhong SL, Zhu LP, Wang DD, Yang SJ, He YJ, Mao CF, Yang Y, Wang JY, Zhang Q, Xu HZ, Yu DD, Zhao JH, Tang JH, Ji ZL. Circular RNA hsa_circ_0072995 promotes breast cancer cell migration and invasion through sponge for miR-30c-2-3p. *Epigenomics* 2018; **10**: 1229-1242 [PMID: 30182731 DOI: 10.2217/epi-2018-0002]
51 **Abu El-Asrar AM**, Berghmans N, Al-Obeidan SA, Gikandi PW, Opdenakker G, Van Damme J, Struyf S. The CC chemokines CCL8, CCL13 and CCL20 are local inflammatory biomarkers of HLA-B27-associated uveitis. *Acta Ophthalmol* 2019; **97**: e122-e128 [PMID: 30242977 DOI: 10.1111/aos.13835]
52 **Asano K**, Takahashi N, Ushiki M, Monya M, Aihara F, Kuboki E, Moriyama S, Iida M, Kitamura H, Qiu CH, Watanabe T, Tanaka M. Intestinal CD169(+) macrophages initiate mucosal inflammation by secreting CCL8 that recruits inflammatory monocytes. *Nat Commun* 2015; **6**: 7802 [PMID: 26193821 DOI: 10.1038/ncomms8802]
53 **Zhang X**, Chen L, Dang WQ, Cao MF, Xiao JF, Lv SQ, Jiang WJ, Yao XH, Lu HM, Miao JY, Wang Y, Yu SC, Ping YF, Liu XD, Cui YH, Zhang X, Bian XW. CCL8 secreted by tumor-associated macrophages promotes invasion and stemness of glioblastoma cells *via* ERK1/2 signaling. *Lab Invest* 2020; **100**: 619-629 [PMID: 31748682 DOI: 10.1038/s41374-019-0345-3]
54 **Brunner PM**, Suárez-Fariñas M, He H, Malik K, Wen HC, Gonzalez J, Chan TC, Estrada Y, Zheng X, Khattri S, Dattola A, Krueger JG, Guttman-Yassky E. The atopic dermatitis blood signature is characterized by increases in inflammatory and cardiovascular risk proteins. *Sci Rep* 2017; **7**: 8707 [PMID: 28821884 DOI: 10.1038/s41598-017-09207-z]
55 **Kim J**, Kim DY, Heo HR, Choi SS, Hong SH, Kim WJ. Role of miRNA-181a-2-3p in cadmium-induced inflammatory responses of human bronchial epithelial cells. *J Thorac Dis* 2019; **11**: 3055-3069 [PMID: 31463135 DOI: 10.21037/jtd.2019.07.55]
56 **Gao LJ**, Shen J, Ren YN, Shi JY, Wang DP, Cao JM. Discovering novel hub genes and pathways associated with the pathogenesis of psoriasis. *Dermatol Ther* 2020; **33**: e13993 [PMID: 32648291 DOI: 10.1111/dth.13993]
57 **Keermann M**, Kõks S, Reimann E, Prans E, Abram K, Kingo K. Transcriptional landscape of psoriasis identifies the involvement of IL36 and IL36RN. *BMC Genomics* 2015; **16**: 322 [PMID: 25897967 DOI: 10.1186/s12864-015-1508-2]
58 **Li X**, Li J, Lu F, Cao Y, Xing J, Hou R, Yin G, Zhang K. Role of SPRED1 in keratinocyte proliferation in psoriasis. *J Dermatol* 2020; **47**: 735-742 [PMID: 32396270 DOI: 10.1111/1346-8138.15369]
59 **Degueurce G**, D'Errico I, Pich C, Ibberson M, Schütz F, Montagner A, Sgandurra M, Mury L, Jafari P, Boda A, Meunier J, Rezzonico R, Brembilla NC, Hohl D, Kolios A, Hofbauer G, Xenarios I, Michalik L. Identification of a novel PPARβ/δ/miR-21-3p axis in UV-induced skin inflammation. *EMBO Mol Med* 2016; **8**: 919-936 [PMID: 27250636 DOI: 10.15252/emmm.201505384]
60 **Miao R**, Liu W, Qi C, Song Y, Zhang Y, Fu Y, Lang Y, Zhang Z. MiR-18a-5p contributes to enhanced proliferation and migration of PASMCs *via* targeting Notch2 in pulmonary arterial hypertension. *Life Sci* 2020; **257**: 117919 [PMID: 32585247 DOI: 10.1016/j.lfs.2020.117919]
61 **Guo Y**, Shi W, Fang R. miR18a5p promotes melanoma cell proliferation and inhibits apoptosis and autophagy by targeting EPHA7 signaling. *Mol Med Rep* 2021; **23** [PMID: 33236144 DOI: 10.3892/mmr.2020.11717]
62 **Ichihara A**, Wang Z, Jinnin M, Izuno Y, Shimozono N, Yamane K, Fujisawa A, Moriya C, Fukushima S, Inoue Y, Ihn H. Upregulation of miR-18a-5p contributes to epidermal necrolysis in severe drug eruptions. *J Allergy Clin Immunol* 2014; **133**: 1065-1074 [PMID: 24184144 DOI: 10.1016/j.jaci.2013.09.019]
63 **Tao T**, Zhang Y, Wei H, Heng K. Downregulation of IRAK3 by miR-33b-3p relieves chondrocyte inflammation and

apoptosis in an *in vitro* osteoarthritis model. *Biosci Biotechnol Biochem* 2021; **85**: 545-552 [PMID: 33590831 DOI: 10.1093/bbb/zbaa105]

64 **Wu C**, Zhao Y, Liu Y, Yang X, Yan M, Min Y, Pan Z, Qiu S, Xia S, Yu J, Yang P, Wan B, Shao Q. Identifying miRNA-mRNA regulation network of major depressive disorder in ovarian cancer patients. *Oncol Lett* 2018; **16**: 5375-5382 [PMID: 30214617 DOI: 10.3892/ol.2018.9243]

65 **Chen Y**, Ding YY, Ren Y, Cao L, Xu QQ, Sun L, Xu MG, Lv HT. Identification of differentially expressed microRNAs in acute Kawasaki disease. *Mol Med Rep* 2018; **17**: 932-938 [PMID: 29115644 DOI: 10.3892/mmr.2017.8016]

66 **Xu N**, Li Z, Yu Z, Yan F, Liu Y, Lu X, Yang W. MicroRNA-33b suppresses migration and invasion by targeting c-Myc in osteosarcoma cells. *PLoS One* 2014; **9**: e115300 [PMID: 25546234 DOI: 10.1371/journal.pone.0115300]

67 **Okada Y**, Kamatani Y, Takahashi A, Matsuda K, Hosono N, Ohmiya H, Daigo Y, Yamamoto K, Kubo M, Nakamura Y, Kamatani N. Common variations in PSMD3-CSF3 and PLCB4 are associated with neutrophil count. *Hum Mol Genet* 2010; **19**: 2079-2085 [PMID: 20172861 DOI: 10.1093/hmg/ddq080]

World Journal of Clinical Cases

Submit a Manuscript: https://www.f6publishing.com

World J Clin Cases 2022 June 26; 10(18): 5984-6000

DOI: 10.12998/wjcc.v10.i18.5984

ISSN 2307-8960 (online)

ORIGINAL ARTICLE

Clinical and Translational Research

Construction and validation of a novel prediction system for detection of overall survival in lung cancer patients

Cheng Zhong, Yun Liang, Qun Wang, Hao-Wei Tan, Yan Liang

Specialty type: Oncology

Provenance and peer review: Unsolicited article; Externally peer reviewed.

Peer-review model: Single blind

Peer-review report's scientific quality classification

Grade A (Excellent): 0
Grade B (Very good): B
Grade C (Good): C
Grade D (Fair): 0
Grade E (Poor): 0

P-Reviewer: Miranda LA, Brazil; Mizuno N, Japan

Received: February 21, 2022
Peer-review started: February 21, 2022
First decision: March 23, 2022
Revised: March 30, 2022
Accepted: April 29, 2022
Article in press: April 29, 2022
Published online: June 26, 2022

Cheng Zhong, Qun Wang, Hao-Wei Tan, Department of Respiratory, Fenghua District People's Hospital, Ningbo 315000, Zhejiang Province, China

Yun Liang, Yan Liang, Department of Hematology and Oncology, Fengdu People's Hospital, Chongqing 408200, China

Corresponding author: Yun Liang, MD, Attending Doctor, Department of Hematology and Oncology, Fengdu People's Hospital, No. 33 Lutang Street, Sanhe Town, Chongqing 408200, China. dr_ly123@163.com

Abstract

BACKGROUND

Many factors have an aberrant effect on the overall survival of lung cancer (LC) patients. In recent years, remarkable progress has been made in immunotherapy, targeted treatment, and promising biomarkers. However, the available treatments and diagnostic methods are not specific for all patients.

AIM

To establish a system for predicting poor survival in patients with LC.

METHODS

The expression matrix and clinical information for this study were obtained from The Cancer Genome Atlas and Gene Expression Omnibus databases. After the differential analysis of all screened genes, weighted gene coexpression network analysis was performed to analyze hub genes related to patient survival. A logistic regression model was used to construct the scoring system. The expression of the hub genes was verified by performing quantitative reverse transcription-polymerase chain reaction.

RESULTS

A total of 5007 differentially expressed genes were selected for the Weighted Gene Co-expression Network Analysis algorithm. We found that the turquoise module showed the highest correlation with patient prognosis. The gene module with the greatest positive correlation with patient survival was located in the turquoise area. The Gene Ontology and Kyoto Encyclopedia of Genes and Genomes analyses performed for the genes contained in the turquoise module indicated the potential roles of the selected genes in the regulation of LC development. In addition, protein–protein interaction analysis was performed to screen hub genes,

which identified 100 hub genes located in the core area of the network. We then intersected the 100 hub genes with 75 key genes sorted by module members to identify real hub genes associated with prognosis. Forty-one genes were finally selected. We then used a logistic regression model to determine 11 independent risk genes, namely *CCNB2*, *CDC20*, *CENPO*, *FOXM1*, *HJURP*, *NEK2*, *OIP5*, *PLK1*, *PRC1*, *SKA1*, *UBE2C* and *SPARC*.

CONCLUSION

We constructed a predictive model based on 11 independent risk genes to establish a system predicting the survival status of patients with non-small-cell lung carcinoma.

Key Words: Lung cancer; Weighted Gene Co-expression Network Analysis; Hub genes; prognosis; Logistic regression

©The Author(s) 2022. Published by Baishideng Publishing Group Inc. All rights reserved.

Core Tip: This was a bioinformatics-based study aimed at identifying a novel system for predicting overall survival in lung cancer patients. We constructed a predictive model using Weighted Gene Co-expression Network Analysis, protein-protein interaction network, and least absolute contraction and selection operator-logistic regression analysis. And the expression of hub genes was verified by polymerase chain reaction, immunohistochemistry in lung cancer cell lines, and patient samples.

Citation: Zhong C, Liang Y, Wang Q, Tan HW, Liang Y. Construction and validation of a novel prediction system for detection of overall survival in lung cancer patients. *World J Clin Cases* 2022; 10(18): 5984-6000
URL: https://www.wjgnet.com/2307-8960/full/v10/i18/5984.htm
DOI: https://dx.doi.org/10.12998/wjcc.v10.i18.5984

INTRODUCTION

Lung cancer (LC) is one of the most common malignant tumors and one of the leading causes of cancer-related deaths worldwide. In 2012, the deaths caused by LC were approximately 1.6 million, accounting for 19% of the total global cancer deaths[1,2]. Despite advancement in its treatment, surgery is the primary therapy for patients with non-small-cell lung carcinoma. However, the overall survival rate of LC patients remains low.

Many factors have an aberrant effect on the overall survival of LC patients. The main reason is that patients who are diagnosed with advanced and metastasis LC cannot undergo radical surgery. Therefore, the development of more advanced diagnosis and predictive biomarkers is a promising direction for cancer diagnosis and treatment[3,4].

In recent years, remarkable progress has been made in immunotherapy, targeted treatment, and promising biomarkers. However, the available treatments and diagnostic methods are not specific for all patients[5]. A high recurrence rate is observed after such treatment because of the complexity of cancer. Identification of new diagnostic and therapeutic biomarkers for cancer treatment is urgent[6].

The development of high-throughput technology has made important contributions to the identification of a large number of target genes in various diseases[7]. At the same time, as an emerging cross-discipline, bioinformatics analysis is widely used in the discovery of disease-related genes, new drug molecular targets, drug design, and functional analysis, which is helpful for the discovery of disease mechanisms[8]. Xie *et al*[9] performed bioinformatics analysis to analyze tumorigenesis-related genes and their target miRNAs in colon cancer, which facilitated the exploration of the potential targets for diagnosis, prognosis and treatment of colon carcinoma. Using RNA-Seq and bioinformatics methods, several key genes including *ID1*, *ID3* and *SMAD9* were identified in esophageal squamous cell carcinoma[10]. Many genes associated with LC progression and invasion have been identified by a combination of bioinformatics analysis and high-throughput sequencing[11-13].

The identification of differentially expressed genes (DEGs) has garnered considerable scientific attention. However, this method does not consider genes with similar expression patterns. Weighted Gene Co-expression Network Analysis (WGCNA) is a new algorithm that evaluates the correlation between gene modules and clinical features by constructing a scale-free gene coexpression network. In this study, we combined the WGCNA algorithm with DEGs to identify pivotal genes associated with clinicopathological characteristics and to provide insights into targeted therapy of LC.

MATERIALS AND METHODS

Data collection

The clinical and expression data of LC patients were derived from the Gene Expression Omnibus (GEO) and The Cancer Genome Atlas (TCGA) databases (https://portal.gdc.cancer.gov/; http://www.ncbi.nlm.nih.gov/geo/). GEO data contains two cohorts (GSE30129 and GSE50081). The sva package was used to normalize the Meta-GEO data. Next, we used the TCGA data (LogFC > 0.5, $P < 0.05$) to identify the DEGs and combined these DEGs with all GEO genes. Finally, 5007 genes were selected for the subsequent analyses.

Construction of WGCNA

WGCNA R package was used to analyze the coexpression networks. We determined the threshold of β = 5 to establish the optimal weighted network by Pearson's correlational analysis. The adjacent matrix was transformed into a topological overlap measure matrix *via* topological overlapping dissimilarity to estimate its connectivity property in the network. We set the minimum number of module genes to 100, and the threshold for merging similar modules was set to 0.25. $P < 0.05$ was considered to indicate statistical significance. After the modules of interest were selected, the key genes were selected according to the gene signature (GS) and module membership (MM) of each module.

Gene Ontology and Kyoto Encyclopedia of Genes and Genomes analyses

The functional analysis of core genes was performed using the Gene Ontology (GO) and Kyoto Encyclopedia of Genes and Genomes (KEGG). Through the R language clusterProfiler and ggplot2 packages, several important pathways have been discovered so far. The cut-off criteria were defined as count > 2 and $P < 0.05$.

Protein–protein interaction network

We employed the STRING database to analyze the interaction between the module genes and set the confidence score to ≥ 0.9. The Cytohubba plug-in of Cytoscape software (version 3.7.0) was used to identify the core genes in the network.

Construction of predictive model

All patients were assigned to training and validation sets in the ratio of 6:4. The least absolute contraction and selection operator (LASSO) reduced the data dimensionality, and Cox regression analysis was applied to construct a patient prognostic evaluation model. The predictive efficacy of the model was evaluated by the receiver operating characteristic (ROC) curve. A nomogram was used to visualize the scoring system through the rms package in the R software.

Cell culture

A549 and H1299 LC cells, and human lung fibroblasts were purchased from the Cancer Cell Repository (Shanghai Cell Bank, Shanghai, China). The medium used for cell culture was 10% Dulbecco's modified eagle's medium (supplemented with fetal bovine serum and penicillin/streptomycin). The cells were cultured in an incubator under 5% CO_2 at 37 °C.

Quantitative real-time polymerase chain reaction

We use 1 mL TRIzol (Invitrogen, Grand Island, NY, United States) and 200 μL chloroform to extract the total RNA from 2 × 10^6 cells in LC cells. Total RNA was reverse transcribed into cDNA (TaKaRa Bio, Shiga, Japan). The cDNA, primers, and the SYBR Green PCR Master Mix (TOYOBO, Osaka, Japan) were quantitatively detected by PCR. The primer sequences of all genes are depicted in Table 1. The gene expression level was evaluated by the $2^{-\Delta\Delta Ct}$ method. All experiments were repeated three times.

Statistical analyses

All data in this study were analyzed using GraphPad Prism 5 and R software. The data were expressed as mean ± SD. A two-tailed *t* test was applied for quantitative real-time polymerase chain reaction (qRT-PCR) analysis among different groups. The results were considered to be significant at $P < 0.05$.

RESULTS

Identification of intersecting genes between GEO cohort and TCGA dataset

We screened DEGs based on the TCGA dataset by including $1037^{tumor}/108^{normal}$ samples. A total of 10 970 DEGs were selected based on the criteria of $P < 0.05$ and $|\log 2\ FC| > 1$. The top 30 up- and downregulated genes are shown in Figure 1A. We then intersected DEGs of TCGA with all genes in the GEO dataset and found 5007 common genes for further WGCNA.

Table 1 Sequence of polymerase chain reaction primers used in this study

Gene	Forward primer sequence (5'-3')	Reverse primer sequence (5'-3')
CCNB2	CCGACGGTGTCCAGTGATTT	TGTTGTTTTGGTGGGTTGAACT
CDC20	GCACAGTTCGCGTTCGAGA	CTGGATTTGCCAGGAGTTCGG
CENPO	AGTGAGCAGATCCCGTAAACA	GGTTGGGTTCTACATTGGCAATA
FOXM1	CGTCGGCCACTGATTCTCAAA	GGCAGGGGATCTCTTAGGTTC
HJURP	CCACGCTGACCTACGAGAC	CTCACCGCTTTTTGAATCGGC
GADPH	ACAACTTTGGTATCGTGGAAGG	GCCATCACGCCACAGTTTC
NEK2	TGCTTCGTGAACTGAAACATCC	CCAGAGTCAACTGAGTCATCACT
OIP5	TGAGAGGGCGATTGACCAAG	AGCACTGCGTGACACTGTG
PLK1	AAAGAGATCCCGGAGGTCCTA	GGCTGCGGTGAATGGATATTTC
PRC1	ATCACCTTCGGGAAATATGGGA	TCTTTCTGACAGACGGATATGCT
SKA1	CCTGAACCCGTAAAGAAGCCT	TCATGTACGAAGGAACACCATTG
UBE2C	GACCTGAGGTATAAGCTCTCGC	TTACCCTGGGTGTCCACGTT

WGCNA

To determine the roles of common DEGs associated with prognosis and other clinicopathological characteristics of LC patients, WGCNA was performed to construct a coexpression network. As shown in Figure 1B and C, the correlation coefficient was converted to the adjacent coefficient according to the optimal parameter (β = 5). Thereafter, highly correlated samples and delete discrete samples were clustered (Figure 1E). A threshold of 0.25 and a minimum gene number of 150 were considered to merge similar modules. Figure 1D shows eight modules that were finally selected on the basis of the filter criteria. The hierarchical clustering of module hub genes is shown in Figure 1F.

Identification of highly correlated modules

The topological overlap matrix plot (Figure 1G) indicated the correlation between the genes of the eight modules sorted using the clustering tree. The turquoise module showed a positive correlation of about 0.31 with LC patient survival, followed by the green module (0.28) and yellow module (0.23) (Figure 2A and B). The turquoise module contained 1673 genes. We then selected 75 key genes from the turquoise module with MM > 0.8 (Figure 2C). Taken together, the turquoise module was finally selected for further analysis.

GO and KEGG analyses in modules

GO enrichment analysis experiments showed that the turquoise module genes mainly encoded for ATPase, helicase, 3′-5′ DNA helicase, DNA-dependent ATPase, DNA helicase, ATP-dependent DNA helicase, and ATP-dependent helicase and associated with the binding of many molecules including DNA replication origin, single-stranded DNA, and tubulin. KEGG analysis indicated that many signaling pathways involved in Fanconi anemia and the p53 signaling pathway were correlated with turquoise module genes. In addition, other important pathways such as metabolism of carbon, pyrimidine, cysteine, and methionine, cell cycle, and DNA repair were also found in the turquoise module. These results indicated that the mechanism that affects the survival of LC patients may be closely related to the molecular binding mechanism and several important signaling pathways (Figure 2D).

Establishment of protein–protein interaction networks and selection of module genes

To determine which cluster of genes in the turquoise module have a pivotal effect on the prognosis of LC, we constructed protein–protein interaction networks using the STRING database (Figure 3A) and Cytoscape software and found 100 hub genes located in the core area of the network (Figure 3B). We then intersected the 100 hub genes with 75 key genes sorted by MM to identify real hub genes associated with prognosis (Figure 3C).

Construction of the hub-genes-based scoring system

Subsequently, we performed a LASSO-logistic analysis of real hub genes to establish a prognostic evaluation model. Finally, 11 prognostic genes were selected in the predictive model in the training dataset, namely *CCNB2*, *CDC20*, *CENPO*, *FOXM1*, *HJURP*, *NEK2*, *OIP5*, *PLK1*, *PRC1*, *SKA1*, *UBE2C* and *SPARC* (Figure 4A). The risk score = 4.43 (Intercept) + CCNB2-expression × 0.552 + CDC20-expression × 0.037 CENPO-expression × 0.287 + FOXM1-expression × 0.106 + HJURP-expression × 0.229 + NEK2-

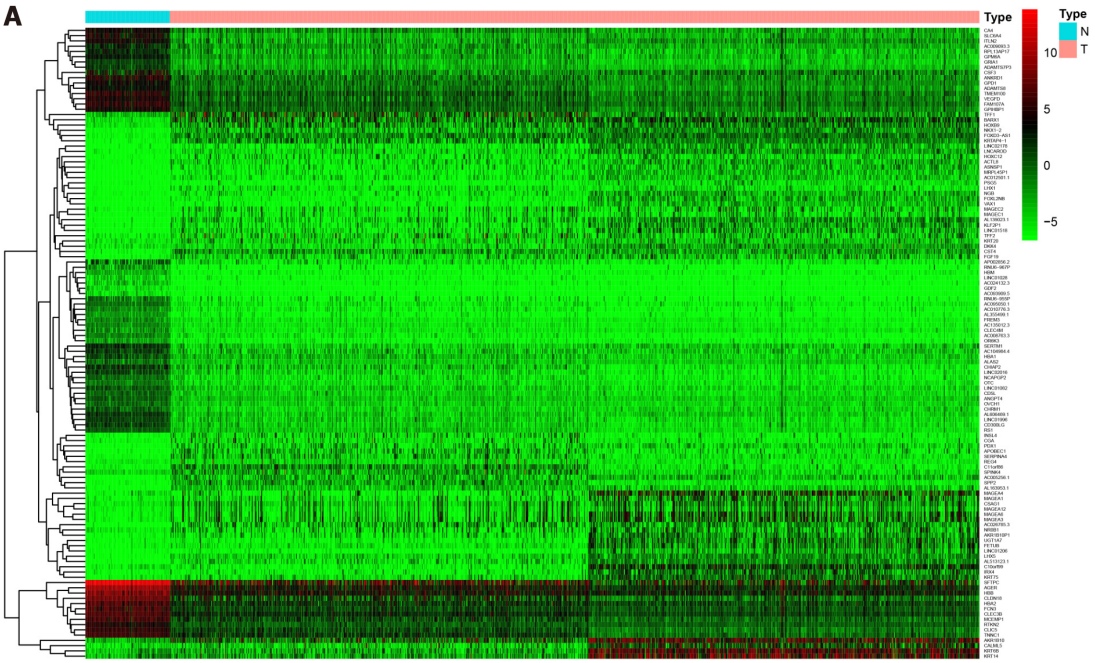
A
Type
N
T
10
5
0
−5

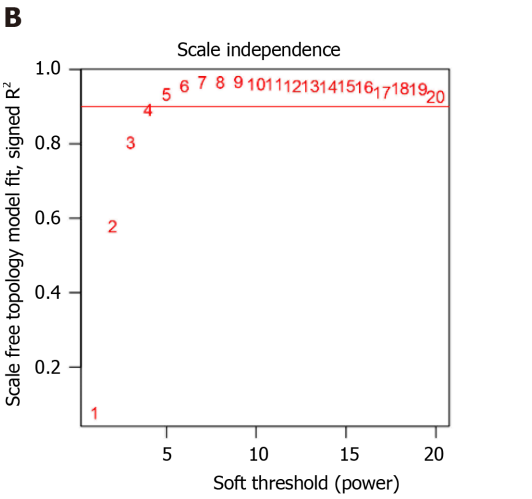
B
Scale independence
Scale free topology model fit, signed R²
Soft threshold (power)

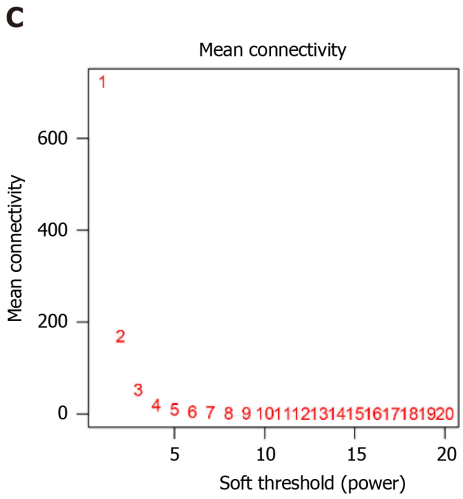
C
Mean connectivity
Mean connectivity
Soft threshold (power)

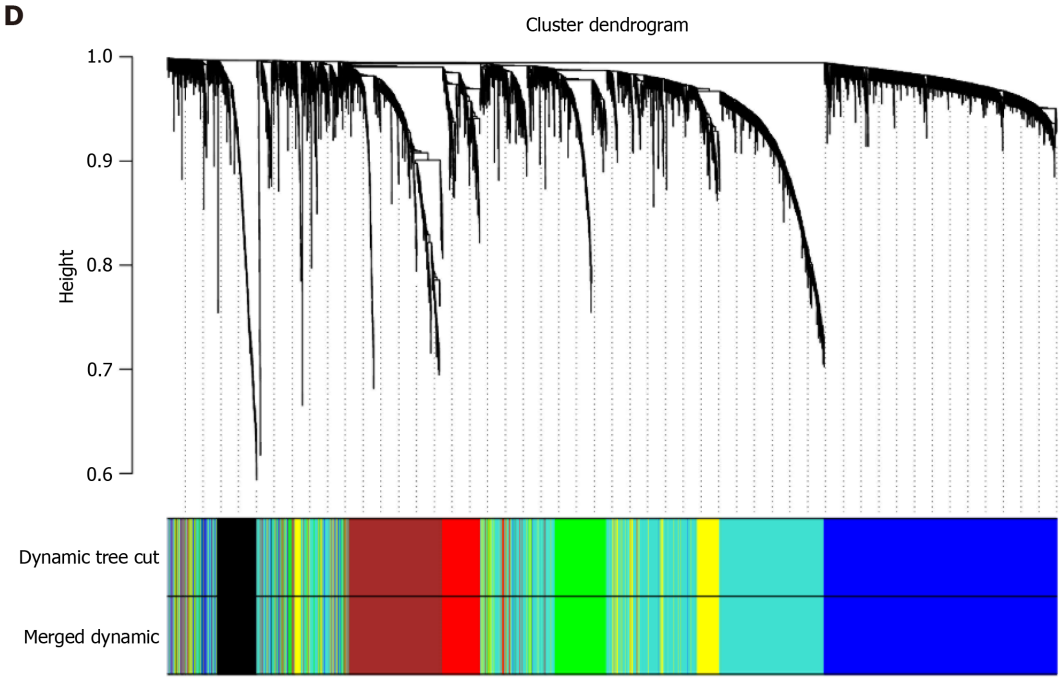
D
Cluster dendrogram
Height
Dynamic tree cut
Merged dynamic

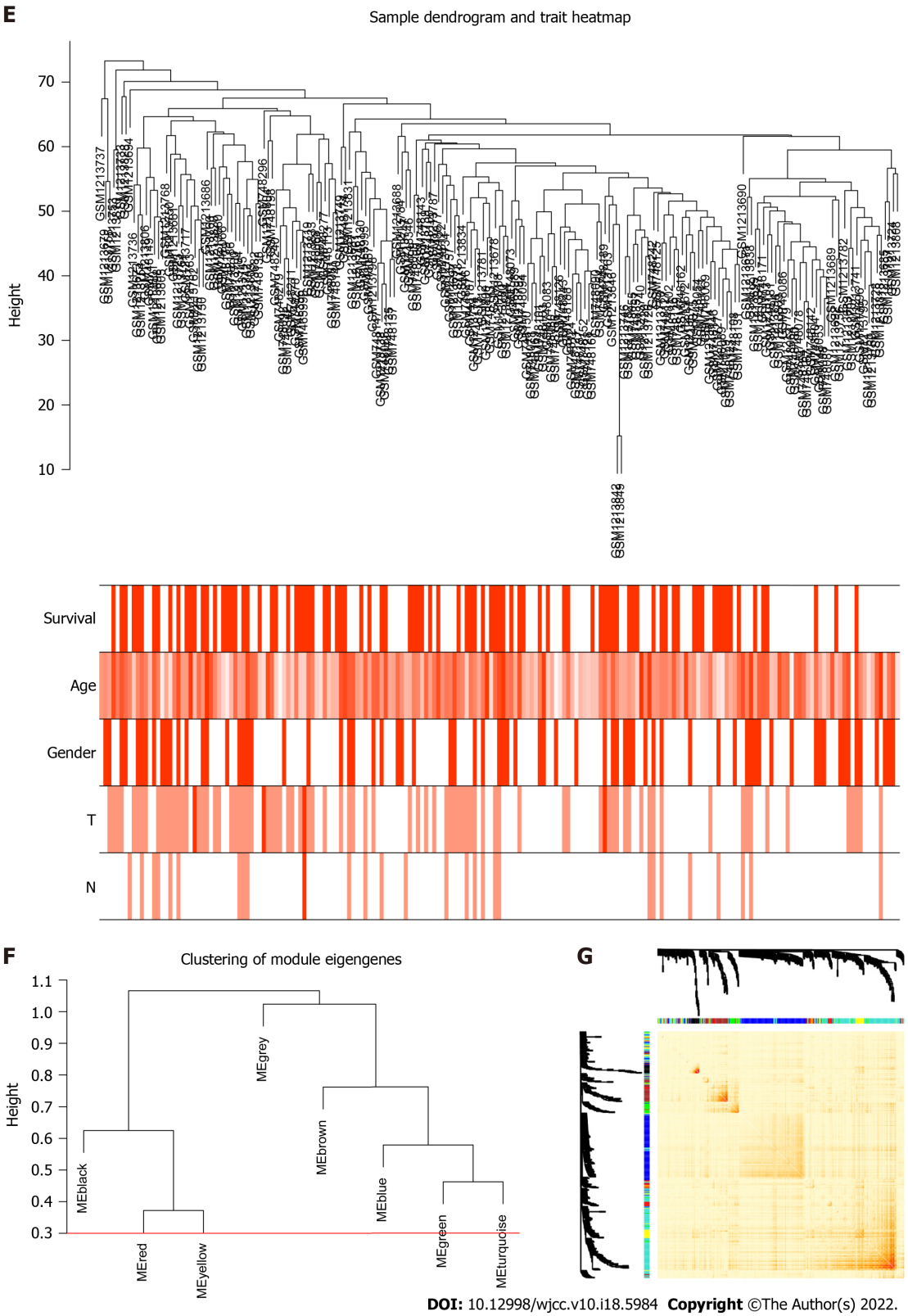

DOI: 10.12998/wjcc.v10.i18.5984 **Copyright** ©The Author(s) 2022.

Figure 1 Identification of differentially expressed genes and Weighted Gene Co-expression Network Analysis. A: The differentially expressed genes analyzed in The Cancer Genome Atlas dataset. Top 30 upregulated and downregulated genes are shown; B and C: Soft-threshold power analysis revealed the scale-free fit index and the mean connectivity of network topology; D: Hierarchical cluster analysis of the coexpression module based on the dissimilarity measurement; E: Sample clustering based on expression data used to detect the outliers; F: Dendrogram of consensus module eigen genes. Groups of eigen genes below the red line merged owing to their similarity; G: The topological overlap matrix heatmap showing the overlap between the co-expression genes.

expression × 0.083 OIP5-expression × 0.020 PLK1-expression × 0.520 + PRC1-expression × 0.192 SKA1-expression × 0.110 + UBE2C-expression × 0.263. Subsequently, we evaluated the reliability of the model by the ROC curve. The results showed that the area under the curve of the training set and test set were 0.754 and 0.626, respectively (Figure 4B). Cox regression analysis showed that risk score was an

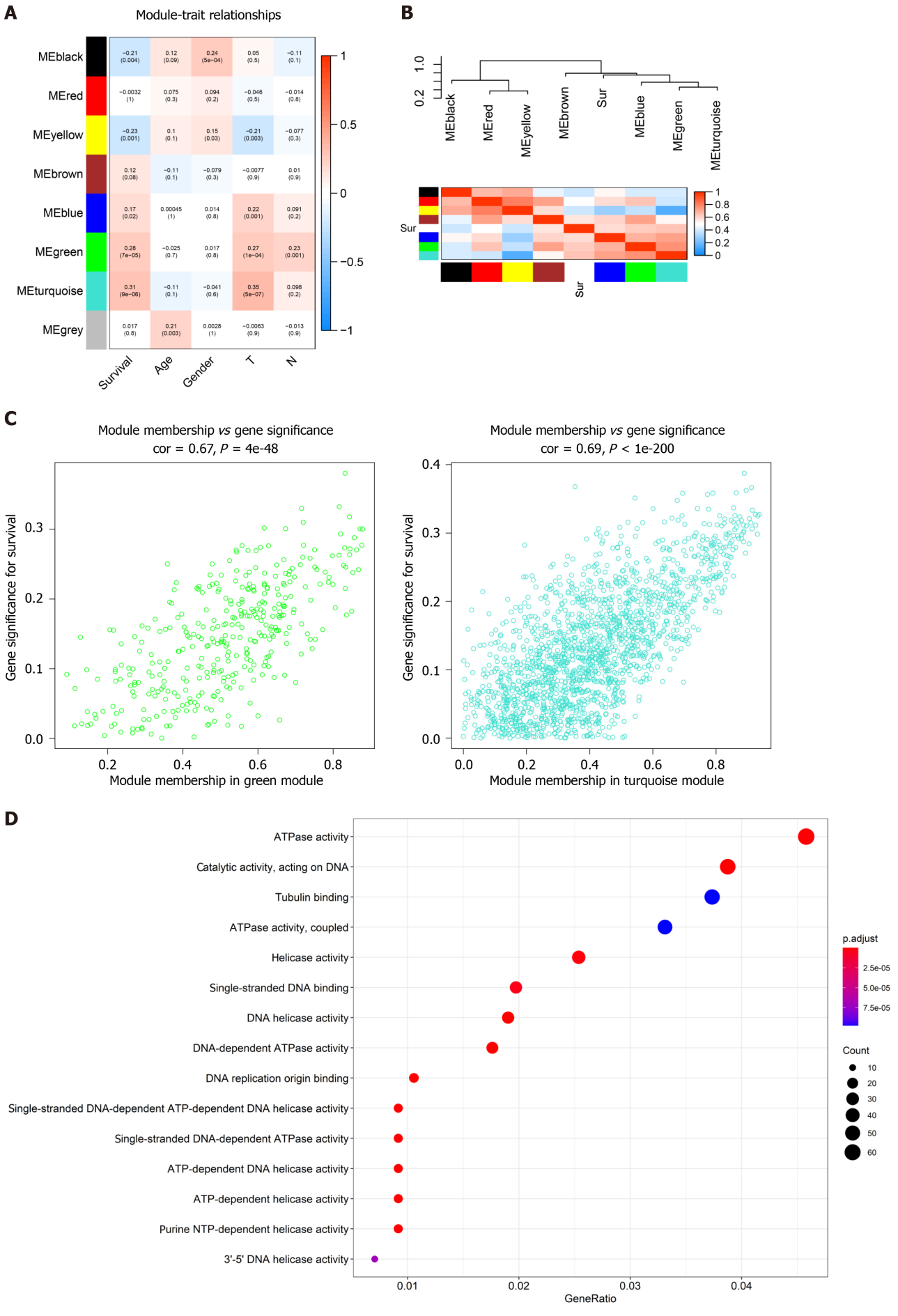
A
Module-trait relationships
MEblack
MEred
MEyellow
MEbrown
MEblue
MEgreen
MEturquoise
MEgrey
Survival
Age
Gender
T
N
1
0.5
0
−0.5
−1
B
1.0
0.2
MEblack
MEred
MEyellow
MEbrown
Sur
MEblue
MEgreen
MEturquoise
Sur
Sur
1
0.8
0.6
0.4
0.2
0
C
Module membership vs gene significance
cor = 0.67, P = 4e-48
Gene significance for survival
Module membership in green module
Module membership vs gene significance
cor = 0.69, P < 1e-200
Gene significance for survival
Module membership in turquoise module
D
ATPase activity
Catalytic activity, acting on DNA
Tubulin binding
ATPase activity, coupled
Helicase activity
Single-stranded DNA binding
DNA helicase activity
DNA-dependent ATPase activity
DNA replication origin binding
Single-stranded DNA-dependent ATP-dependent DNA helicase activity
Single-stranded DNA-dependent ATPase activity
ATP-dependent DNA helicase activity
ATP-dependent helicase activity
Purine NTP-dependent helicase activity
3'-5' DNA helicase activity
GeneRatio
p.adjust
2.5e-05
5.0e-05
7.5e-05
Count
10
20
30
40
50
60

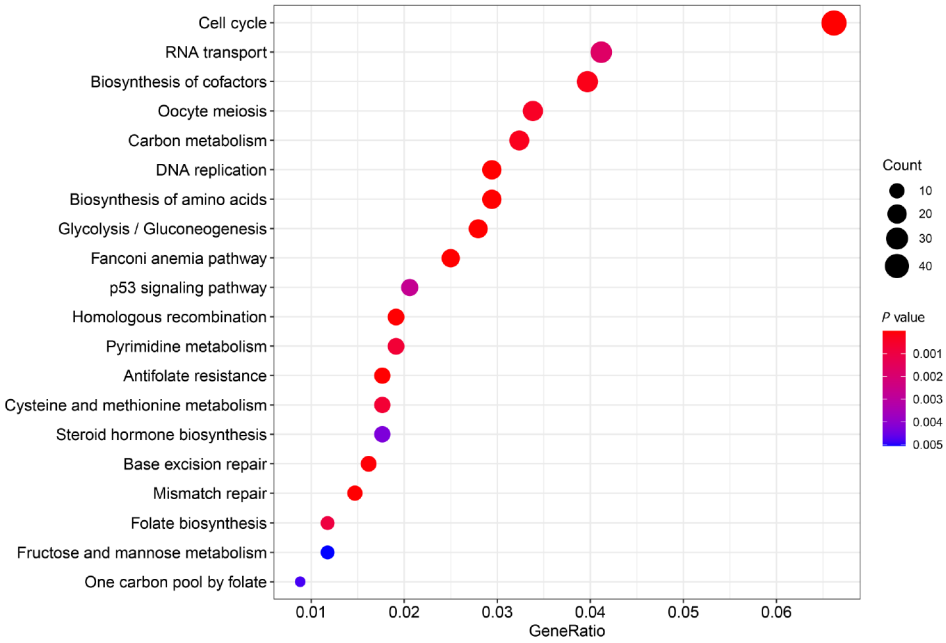

DOI: 10.12998/wjcc.v10.i18.5984 **Copyright** ©The Author(s) 2022.

Figure 2 Identification of highly correlated gene modules by Weighted Gene Co-expression Network Analysis. A: Correlation between eight module genes and the clinical features. Turquoise module indicating a high correlation with the patient's overall survival ($P < 0.001$, $r = 0.31$); B: Heatmap plot showing the adjacent modules and survival traits; C: The gene signature and module membership of turquoise and green modules; D: Significantly enriched Gene Ontology items and the Kyoto Encyclopedia of Genes and Genomes pathways in turquoise module with top 20 count number of genes shown.

independent risk factor for predicting the poor prognosis of LC patients (Figure 4C). To further evaluate the prognosis of LC, we constructed a nomogram based on risk factors (Figure 4D and E).

After the construction of the scoring system in the GEO dataset, we determined the effect of 11 genes in the TCGA dataset. As shown in Figure 5A, all genes were differentially expressed in LC patients compared with normal samples. Moreover, all genes were significantly correlated with patient prognosis except for *CCNB2* and *SKA1* (Figure 5B).

To validate the expression of the 11 hub genes, we performed an immunohistochemistry experiment obtained from the Protein Atlas database. Immunohistochemistry indicated that the protein levels of CDC20, FOXM1, HJURP, PRC1, UBE2C and CCNB2 were increased in the LC samples compared with the normal samples, whereas those of OIP5, PLK1 and SKA1 were decreased (Figure 5C). To explore the mRNA expression levels of these genes, we performed qRT-PCR analysis and found that the mRNA levels of *CCNB2*, *CDC20*, *FOXM1*, *HJURP*, *NEK2*, *PRC1*, *SKA1* and *UBE2C* were increased in the LC cell lines, whereas those of *CENPO*, *OIP5* and *PLK1* was decreased (Figure 5D).

DISCUSSION

LC treatments include a combination of radical surgery, radiation therapy, chemotherapy, and precise targeted therapy[14]. Despite advancement in LC treatment and diagnosis, the 5-year overall survival rate remains low[15]. The main reason is that patients who are diagnosed with advanced and metastasis LC cannot undergo radical surgery. Therefore, more specific and sensitive biomarkers are needed to facilitate early diagnosis and prediction of overall survival.

Recently, several therapeutic targets and prognostic biomarkers have been identified using advanced high-throughput sequencing technology and integrative bioinformatics analysis. Previous studies have reported many prognostic biomarkers in LC by performing a combined analysis using TCGA and GEO datasets and validated by *in vitro* experiments. Sun *et al*[16] reported the role of C-type lectin domain family 3 member B (CLEC3B) in tumor progression, prognosis, and immune responses in LC by performing RNA-Seq and bioinformatics analysis; the expression and methylation of CLEC3B were also validated by qRT-PCR analysis. miRNA-144-3p, an important noncoding RNA, was identified and validated as an independent risk factor for LC prognosis by performing bioinformatics analysis and qRT-PCR[17]. However, because of the insufficient sample size, biological heterogeneity, and different statistical methods, highly effective genes are not found in clinical practice. Moreover, the prediction efficiency in tumor patients could be limited by simply using a single GS instead of a multi-GS. Therefore, more biological markers and more effective prediction models are required for the prevention and treatment of LC.

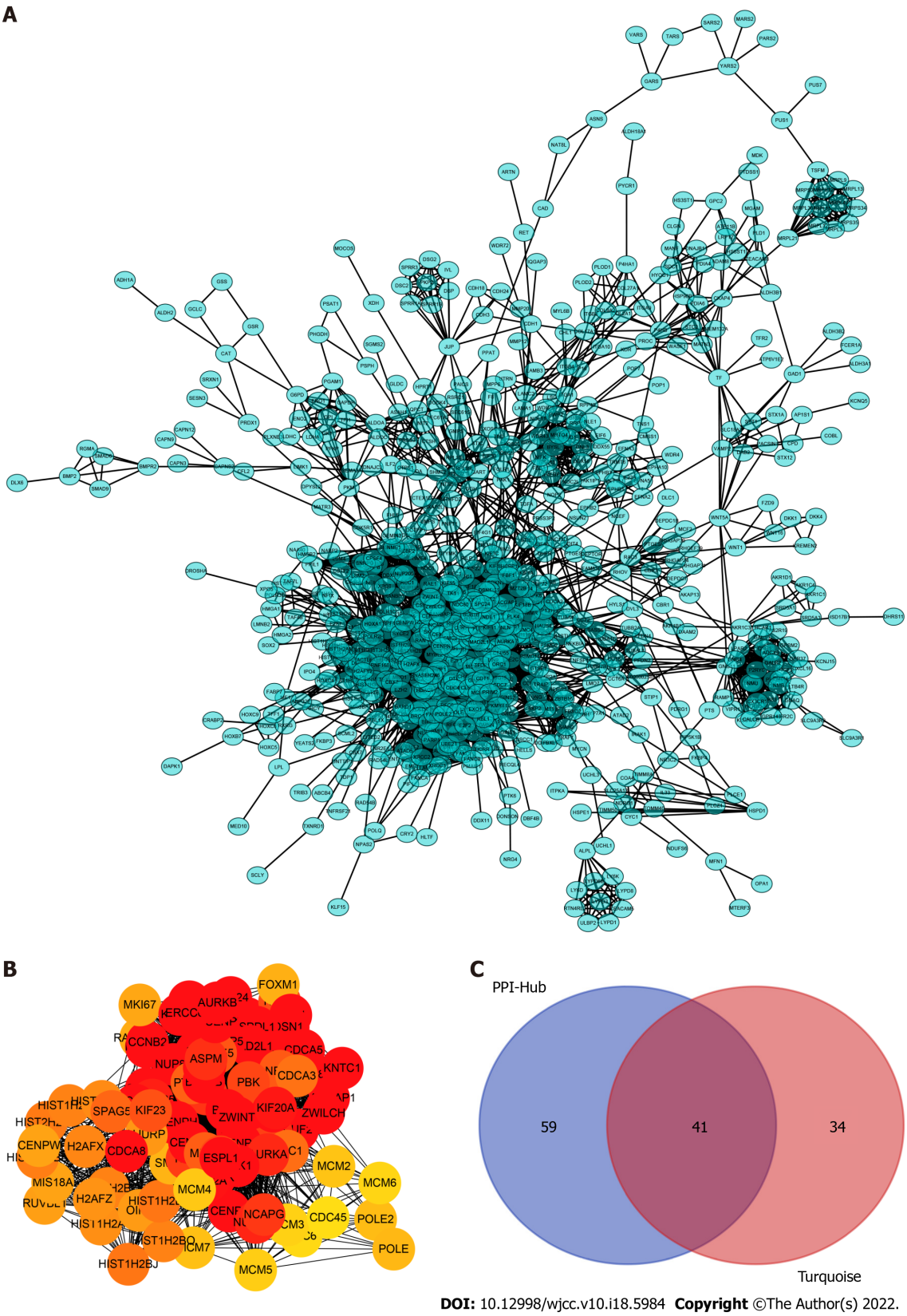

DOI: 10.12998/wjcc.v10.i18.5984 **Copyright** ©The Author(s) 2022.

Figure 3 Construction of the protein–protein interaction networks of turquoise module genes and the selected hub genes. A: Network of all turquoise module genes excluding the low connectivity genes; B: The cytohubba algorithm used to identify the top 100 hub genes located in the core area of the turquoise module; C: Venn diagram showing an overlap between the protein–protein interaction hub and gene signature/module membership-key genes in the turquoise module. A total of 41 real hub genes finally selected for further analyses.

In the present study, we initially detected DEGs based on the TCGA dataset and intersected these DEGs with all GEO cohort genes to obtain an expression profile. We used the WGCNA algorithm to identify core genes in GEO expression data and that were highly related to clinical features. WGCNA

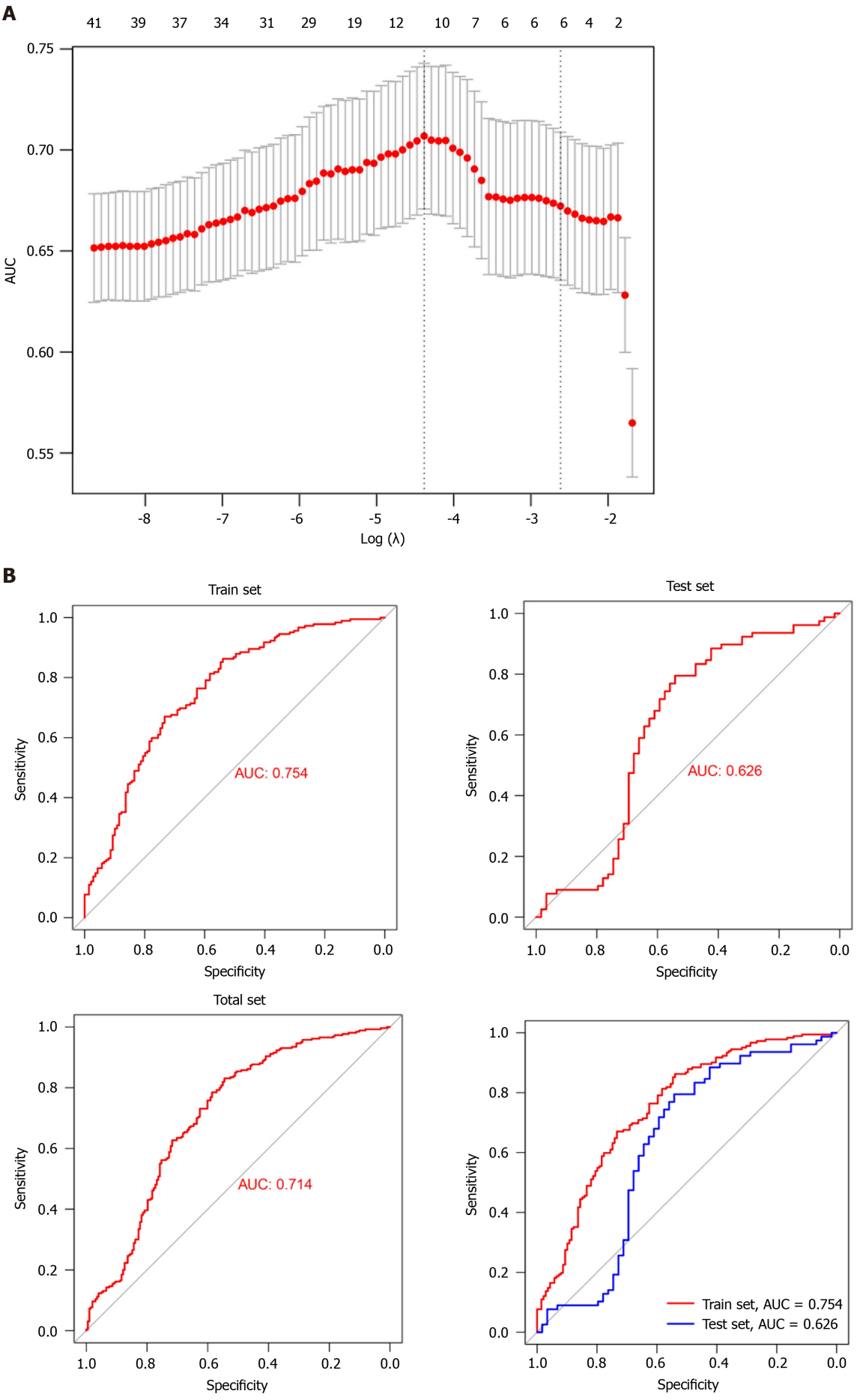
A
41 39 37 34 31 29 19 12 10 7 6 6 6 4 2
0.75
0.70
0.65
0.60
0.55
AUC
-8 -7 -6 -5 -4 -3 -2
Log (λ)
B
Train set
AUC: 0.754
Test set
AUC: 0.626
Total set
AUC: 0.714
Sensitivity
Specificity
1.0 0.8 0.6 0.4 0.2 0.0
Train set, AUC = 0.754
Test set, AUC = 0.626

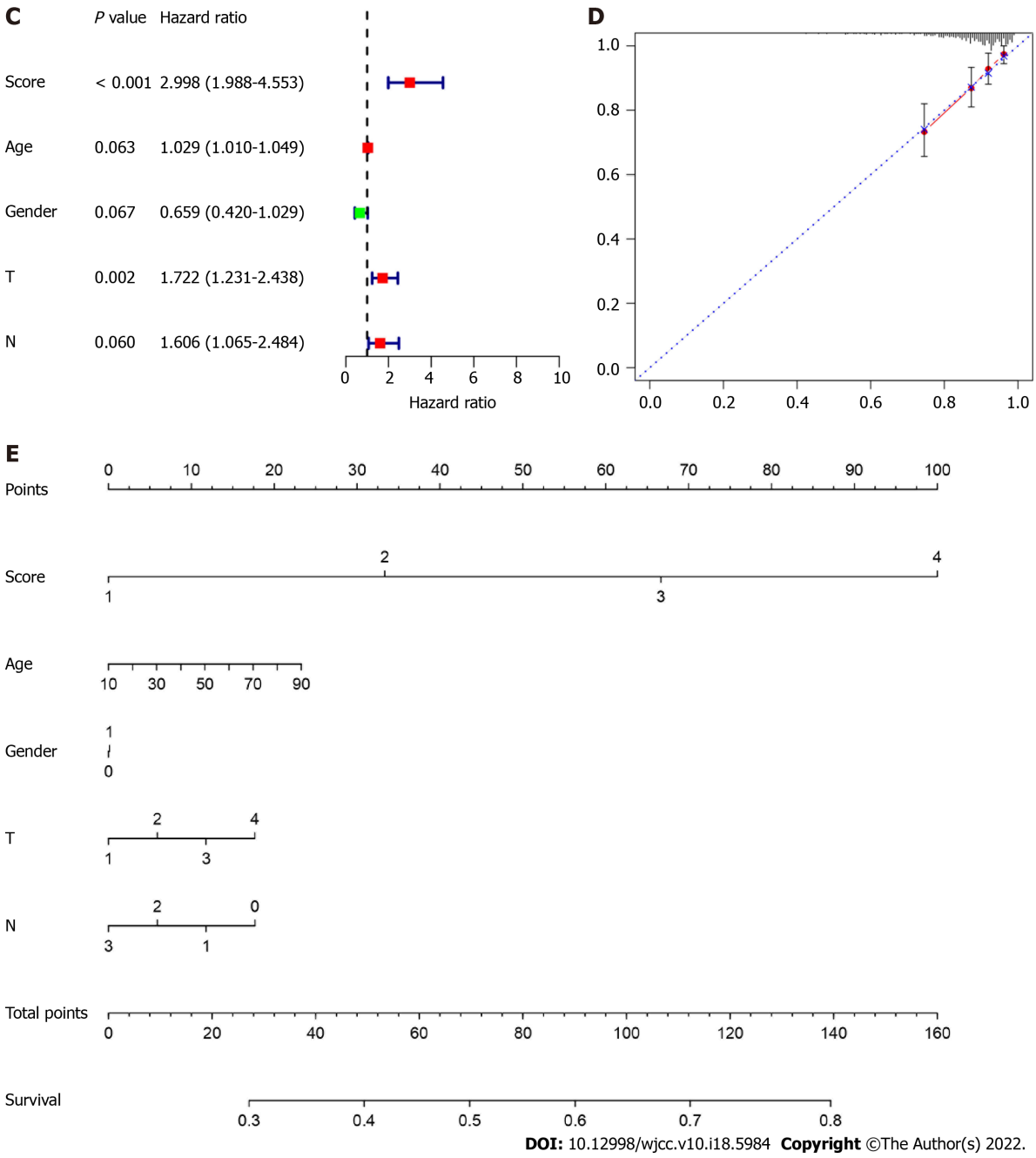

DOI: 10.12998/wjcc.v10.i18.5984 **Copyright** ©The Author(s) 2022.

Figure 4 Construction of a prognostic predictive model using real hub genes. A: Area under the curve measurement performed to select the optimal candidate genes for the scoring system construction; B: Receiver operating characteristic curve showing the prediction efficiency of the scoring system in the training, test, and all dataset; C: Risk-score served as an independent risk factor in predicting patients' survival; D and E: Development of nomograms and calibration curves for prognosis in the total dataset.

classified eight modules and subsequently correlated the modules with clinical characteristics. In these modules, the turquoise module contained 1673 genes that showed the highest correlation with LC patient prognosis. We then performed GO enrichment and KEGG pathway analyses of the turquoise module genes and found that the function of these genes was mainly related to activation of enzymes including ATPase, helicase, 3′-5′ DNA helicase, DNA-dependent ATPase, DNA helicase, ATP-dependent DNA helicase, and ATP-dependent helicase and binding of many molecules including DNA replication origin, single-stranded DNA, and tubulin and activation of signaling pathways involved in Fanconi anemia and p53 signaling pathway. Subsequently, we performed a protein–protein interaction network analysis of the genes contained in the yellow module and intersected the network hub genes with MM > 0.8. Forty-one genes were selected and subjected to LASSO-logistic regression. We finally identified 11 prognostic genes, namely *CCNB2*, *CDC20*, *CENPO*, *FOXM1*, *HJURP*, *NEK2*, *OIP5*, *PLK1*, *PRC1*, *SKA1*, *UBE2C* and *SPARC*. Among these genes, *FOXM1* and *PLK1* are the most studied genes in LC. FOXM1, an important family member of the FOX family, plays a pivotal role in a series of biological processes, including facilitating cell proliferation, differentiation, and organ development[18]. FOXM1

A

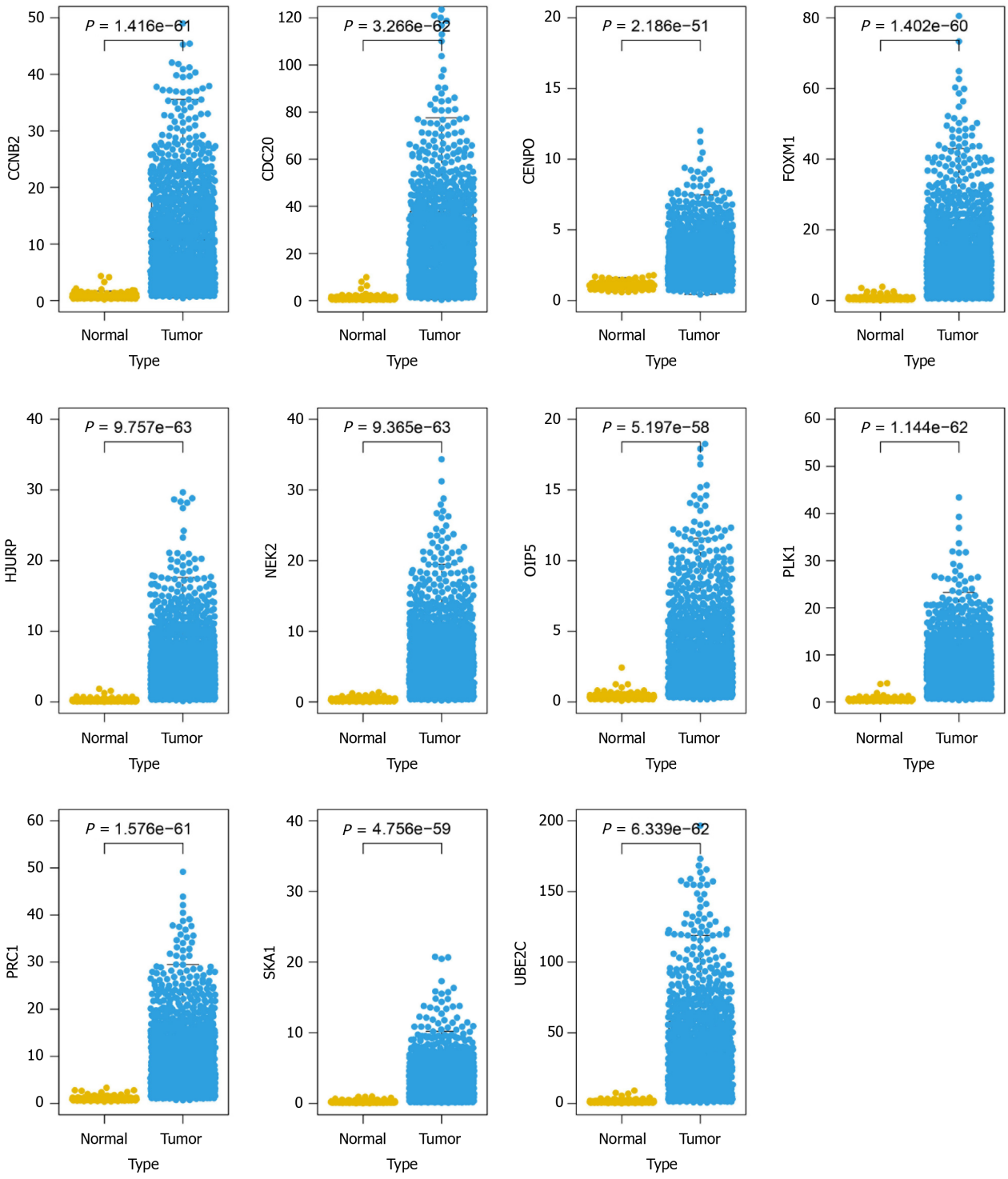
CCNB2
P = 1.416e−61
CDC20
P = 3.266e−62
CENPO
P = 2.186e−51
FOXM1
P = 1.402e−60
HJURP
P = 9.757e−63
NEK2
P = 9.365e−63
OIP5
P = 5.197e−58
PLK1
P = 1.144e−62
PRC1
P = 1.576e−61
SKA1
P = 4.756e−59
UBE2C
P = 6.339e−62
Normal
Tumor
Type

B

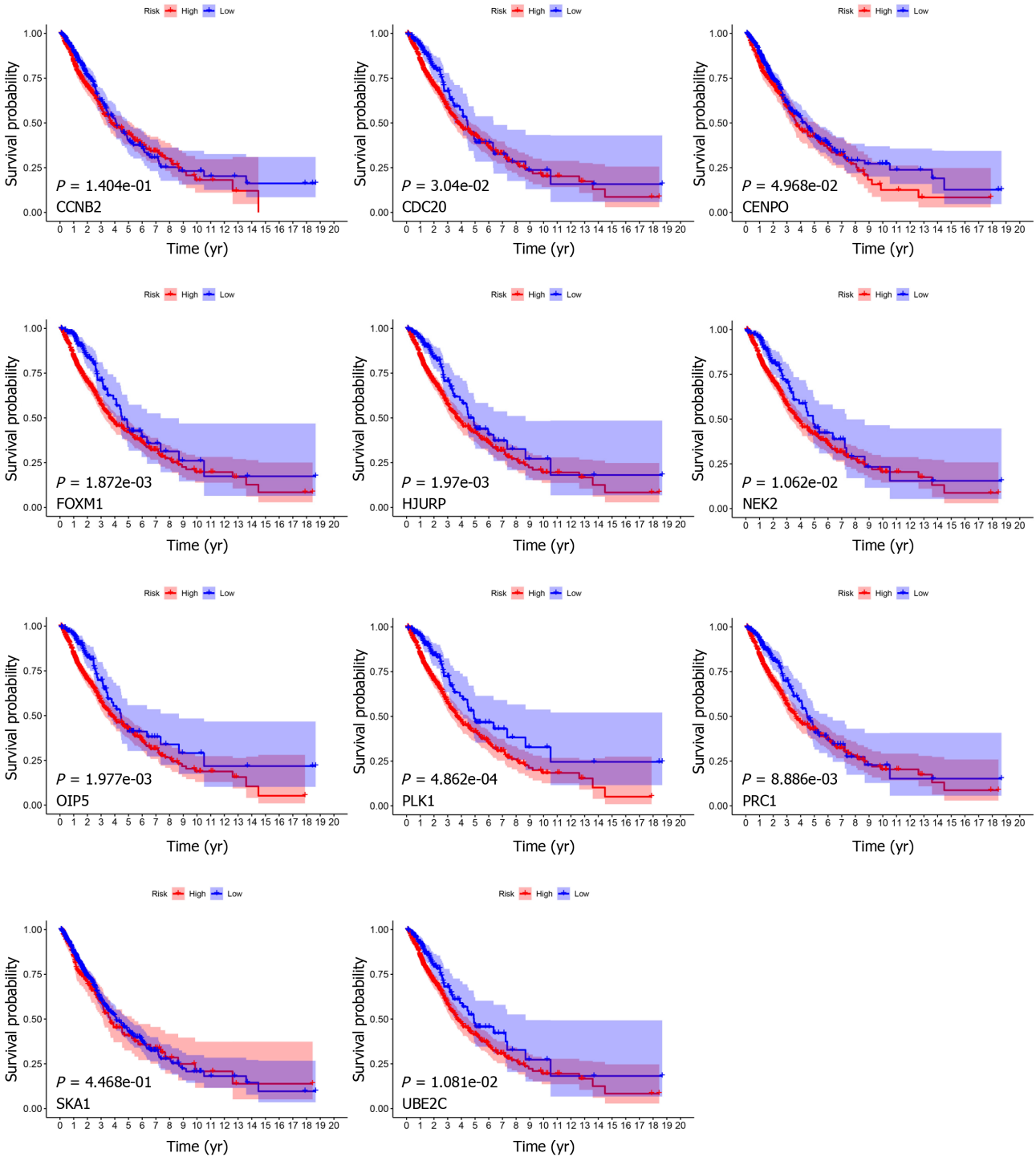
Risk High Low
Survival probability
Time (yr)
P = 1.404e-01
CCNB2
P = 3.04e-02
CDC20
P = 4.968e-02
CENPO
P = 1.872e-03
FOXM1
P = 1.97e-03
HJURP
P = 1.062e-02
NEK2
P = 1.977e-03
OIP5
P = 4.862e-04
PLK1
P = 8.886e-03
PRC1
P = 4.468e-01
SKA1
P = 1.081e-02
UBE2C

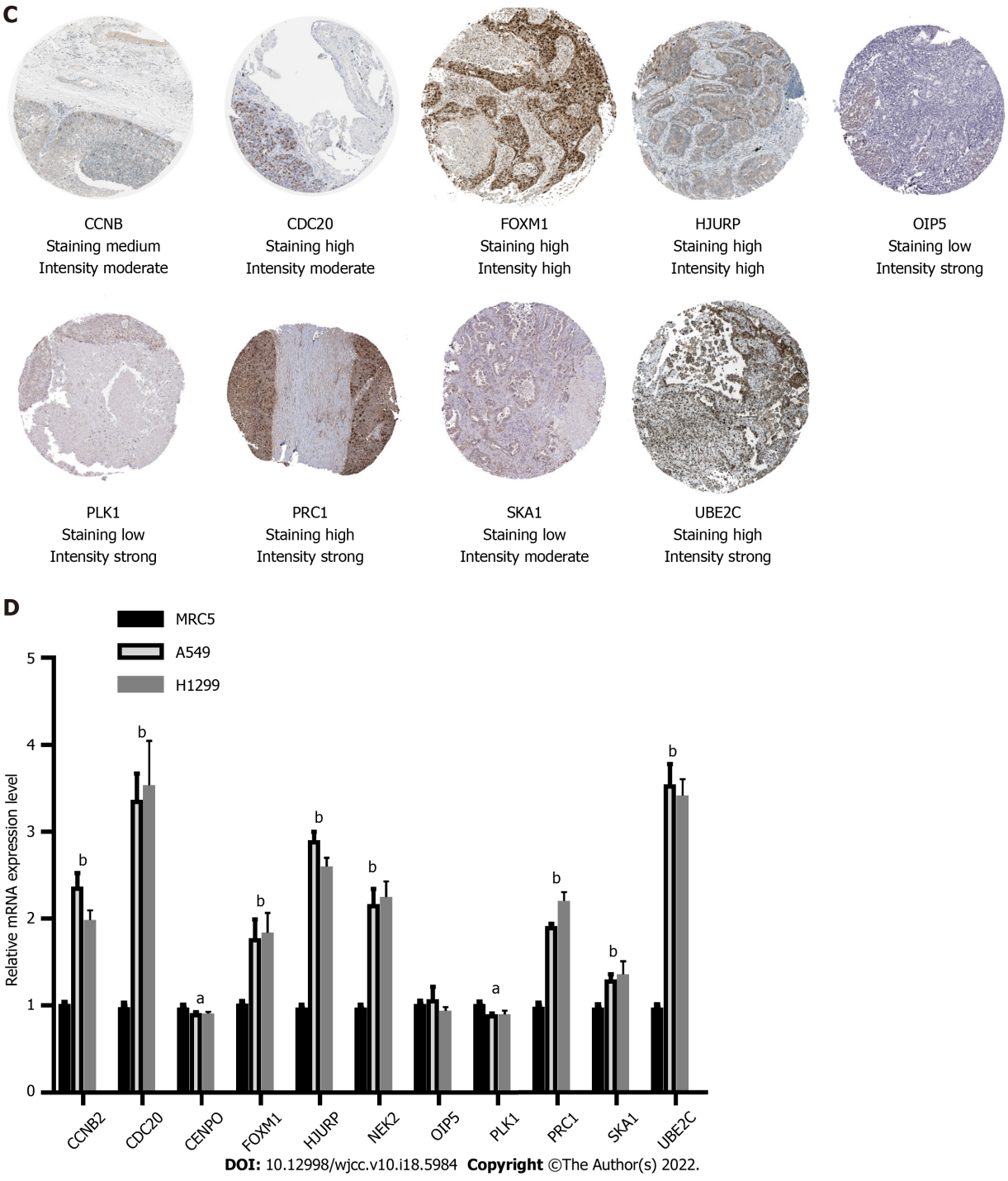

DOI: 10.12998/wjcc.v10.i18.5984 **Copyright** ©The Author(s) 2022.

Figure 5 Expression and survival curve of 11 genes in The Cancer Genome Atlas dataset and the validation of the 11 genes' expression by immunohistochemistry and quantitative real-time polymerase chain reaction analyses. A: Expression of 11 genes in The Cancer Genome Atlas (TCGA) dataset; B: Correlation of 11 genes and the survival rate in the TCGA dataset; C: Expression profile of 11 genes in tumor tissues obtained from the Protein Atlas database; D: Quantitative real-time polymerase chain reaction analysis indicating the expression of 11 genes in lung cancer cell lines when compared with that in normal lung bronchial cells. $^{a}P < 0.05$, $^{b}P < 0.01$.

level is significantly increased in LC cells and could be regulated by miR-216b, which promotes cancer progression and epithelial–mesenchymal transition in LC cells[19]. Moreover, FOXM1 could directly regulate the radiosensitivity of LC cells *via* interacting with KIF20A, suggesting that FOXM1 might be a novel therapeutic target for LC treatment. FOXM1 could also be regulated by other important molecules. The family with sequence similarity 188-member B is a member of the novel putative deubiquitinase family and directly binds to FOXM1, which promotes LC progression[20]. PLK1 is highly correlated with LC progression. PLK1 can target and regulate the transforming growth factor β signaling pathway, and then amplify its metastatic activity by positive feedback[20]. PLK1 is also regulated by long noncoding RNAs. For instance, miR-296-5p decreases the ability of cell invasion and migration by directly targeting PLK1 in LC cells[21]. However, other genes have not been actively

researched, especially with regard to the mechanism of progression in LC. Therefore, in-depth knowledge of these genes will help develop new biomarkers for early LC diagnosis and prediction of prognosis.

After the scoring system was constructed, we further evaluated the performance of the model in LC patients. The ROC curve showed that the model had an excellent predictive performance. In addition, the risk predictor of the model can be considered an independent risk factor for predicting LC prognosis. To conclude, this study showed the potential of prognostic genes in LC patients using WGCNA combined with the established predictive model. However, this study also had some limitations. Firstly, LC patients were from public databases, thus the number of samples was limited. In future studies, we will collect samples from our hospital to expand the sample size to validate the predictive model. Second, the molecular biological mechanism by which the hub gene affects the prognosis of patient needs to be further explored.

CONCLUSION

This study used the WGCNA algorithm to identify functional modules highly correlated with LC prognosis. After construction of the predictive model, we screened and validated 11 prognostic genes, which might be considered new therapeutic targets for the diagnosis and treatment of LC. This study also had some limitations. The mechanisms of the effect of the 11 prognostic genes on cancer progression need to be studied in the future.

ARTICLE HIGHLIGHTS

Research background

Many factors have an aberrant effect on the overall survival of lung cancer (LC) patients. In recent years, remarkable progress has been made in immunotherapy, targeted treatment, and promising biomarkers. However, the available treatments and diagnostic methods are not specific for all patients.

Research motivation

Identifying new diagnostic and therapeutic biomarkers for cancer treatment is urgent.

Research objectives

We aimed to establish a system for predicting poor survival in patients with LC.

Research methods

Weighted Gene Co-expression Network Analysis (WGCNA), functional enrichment analysis, quantitative real-time polymerase chain reaction, and other bioinformatics analysis were used in this study.

Research results

A total of 5007 differentially expressed genes were selected for the WGCNA algorithm. The turquoise module showed the highest correlation with patient prognosis. The gene module with the greatest positive correlation with patient survival was located in the turquoise area. Gene Ontology and Kyoto Encyclopedia of Genes and Genomes analyses performed for the genes contained in the turquoise module indicated the potential roles of the selected genes in the regulation of LC development. In addition, protein–protein interaction analysis was performed to screen hub genes, which identified 100 hub genes located in the core area of the network. We intersected the 100 hub genes with 75 key genes sorted by module members to identify real hub genes associated with prognosis. Forty-one genes were finally selected. We used a logistic regression model to determine 11 independent risk genes, namely *CCNB2*, *CDC20*, *CENPO*, *FOXM1*, *HJURP*, *NEK2*, *OIP5*, *PLK1*, *PRC1*, *SKA1*, *UBE2C* and *SPARC*.

Research conclusions

We constructed a model based on 11 independent risk genes to establish a system to predict the survival status of patients with non-small-cell lung carcinoma.

Research perspectives

The new predictive model could play a role in overall survival.

FOOTNOTES

Author contributions: Zhong C and Liang Y conceptualized and designed the article; Zhong C and Wang Q analyzed and interpreted the data; Zhong C drafted of the article; Liang Y and Tang HW were responsible for critical revision of the article for important intellectual content.

Institutional review board statement: This study was approved by the Ethics Committee of the Fenghua District People's Hospital.

Clinical trial registration statement: This study does not involve the clinical trials, so the clinical trial registration is not required.

Informed consent statement: The data that support the findings of current study are publicly available, so the signed informed consent document is not required.

Conflict-of-interest statement: The authors have no conflicts of interest to declare.

Data sharing statement: No additional data are available.

Open-Access: This article is an open-access article that was selected by an in-house editor and fully peer-reviewed by external reviewers. It is distributed in accordance with the Creative Commons Attribution NonCommercial (CC BY-NC 4.0) license, which permits others to distribute, remix, adapt, build upon this work non-commercially, and license their derivative works on different terms, provided the original work is properly cited and the use is non-commercial. See: https://creativecommons.org/Licenses/by-nc/4.0/

Country/Territory of origin: China

ORCID number: Cheng Zhong 0000-0002-4077-2676; Yun Liang 0000-0003-3759-2997; Qun Wang 0000-0003-2258-4791; Hao-Wei Tan 0000-0001-6188-9294; Yan Liang 0000-0002-8608-0229.

S-Editor: Gong ZM
L-Editor: Kerr C
P-Editor: Gong ZM

REFERENCES

1 **Torre LA**, Bray F, Siegel RL, Ferlay J, Lortet-Tieulent J, Jemal A. Global cancer statistics, 2012. *CA Cancer J Clin* 2015; **65**: 87-108 [PMID: 25651787 DOI: 10.3322/caac.21262]
2 **Chen W**, Zheng R, Baade PD, Zhang S, Zeng H, Bray F, Jemal A, Yu XQ, He J. Cancer statistics in China, 2015. *CA Cancer J Clin* 2016; **66**: 115-132 [PMID: 26808342 DOI: 10.3322/caac.21338]
3 **Villalobos P**, Wistuba II. Lung Cancer Biomarkers. *Hematol Oncol Clin North Am* 2017; **31**: 13-29 [PMID: 27912828 DOI: 10.1016/j.hoc.2016.08.006]
4 **Di X**, Jin X, Li R, Zhao M, Wang K. CircRNAs and lung cancer: Biomarkers and master regulators. *Life Sci* 2019; **220**: 177-185 [PMID: 30711537 DOI: 10.1016/j.lfs.2019.01.055]
5 **Ciliberto D**, Staropoli N, Caglioti F, Gualtieri S, Fiorillo L, Chiellino S, De Angelis AM, Mendicino F, Botta C, Caraglia M, Tassone P, Tagliaferri P. A systematic review and meta-analysis of randomized trials on the role of targeted therapy in the management of advanced gastric cancer: Evidence does not translate? *Cancer Biol Ther* 2015; **16**: 1148-1159 [PMID: 26061272 DOI: 10.1080/15384047.2015.1056415]
6 **Tsoukalas N**, Kiakou M, Tsapakidis K, Tolia M, Aravantinou-Fatorou E, Baxevanos P, Kyrgias G, Theocharis S. PD-1 and PD-L1 as immunotherapy targets and biomarkers in non-small cell lung cancer. *J BUON* 2019; **24**: 883-888 [PMID: 31424637]
7 **Moncho-Amor V**, Pintado-Berninches L, Ibañez de Cáceres I, Martín-Villar E, Quintanilla M, Chakravarty P, Cortes-Sempere M, Fernández-Varas B, Rodriguez-Antolín C, de Castro J, Sastre L, Perona R. Role of Dusp6 Phosphatase as a Tumor Suppressor in Non-Small Cell Lung Cancer. *Int J Mol Sci* 2019; **20** [PMID: 31027181 DOI: 10.3390/ijms20082036]
8 **Kulasingam V**, Diamandis EP. Strategies for discovering novel cancer biomarkers through utilization of emerging technologies. *Nat Clin Pract Oncol* 2008; **5**: 588-599 [PMID: 18695711 DOI: 10.1038/ncponc1187]
9 **Xie B**, Zhao R, Bai B, Wu Y, Xu Y, Lu S, Fang Y, Wang Z, Maswikiti EP, Zhou X, Pan H, Han W. Identification of key tumorigenesisrelated genes and their microRNAs in colon cancer. *Oncol Rep* 2018; **40**: 3551-3560 [PMID: 30272358 DOI: 10.3892/or.2018.6726]
10 **Zhao Y**, Zhu J, Shi B, Wang X, Lu Q, Li C, Chen H. The transcription factor LEF1 promotes tumorigenicity and activates the TGF-β signaling pathway in esophageal squamous cell carcinoma. *J Exp Clin Cancer Res* 2019; **38**: 304 [PMID: 31296250 DOI: 10.1186/s13046-019-1296-7]
11 **Zhao T**, Khadka VS, Deng Y. Identification of lncRNA biomarkers for lung cancer through integrative cross-platform data analyses. *Aging (Albany NY)* 2020; **12**: 14506-14527 [PMID: 32675385 DOI: 10.18632/aging.103496]
12 **Xue L**, Xie L, Song X. Identification of potential tumor-educated platelets RNA biomarkers in non-small-cell lung cancer by integrated bioinformatical analysis. *J Clin Lab Anal* 2018; **32**: e22450 [PMID: 29665143 DOI: 10.1002/jcla.22450]

13 **Liu L**, Ahmed T, Petty WJ, Grant S, Ruiz J, Lycan TW, Topaloglu U, Chou PC, Miller LD, Hawkins GA, Alexander-Miller MA, O'Neill SS, Powell BL, D'Agostino RB Jr, Munden RF, Pasche B, Zhang W. SMARCA4 mutations in KRAS-mutant lung adenocarcinoma: a multi-cohort analysis. *Mol Oncol* 2021; **15**: 462-472 [PMID: 33107184 DOI: 10.1002/1878-0261.12831]

14 **Hensing T**, Chawla A, Batra R, Salgia R. A personalized treatment for lung cancer: molecular pathways, targeted therapies, and genomic characterization. *Adv Exp Med Biol* 2014; **799**: 85-117 [PMID: 24292963 DOI: 10.1007/978-1-4614-8778-4_5]

15 **Li F**, He H, Qiu B, Ji Y, Sun K, Xue Q, Guo W, Wang D, Zhao J, Mao Y, Mu J, Gao S. Clinicopathological characteristics and prognosis of lung cancer in young patients aged 30 years and younger. *J Thorac Dis* 2019; **11**: 4282-4291 [PMID: 31737313 DOI: 10.21037/jtd.2019.09.60]

16 **Sun J**, Xie T, Jamal M, Tu Z, Li X, Wu Y, Li J, Zhang Q, Huang X. CLEC3B as a potential diagnostic and prognostic biomarker in lung cancer and association with the immune microenvironment. *Cancer Cell Int* 2020; **20**: 106 [PMID: 32265595 DOI: 10.1186/s12935-020-01183-1]

17 **Chen YJ**, Guo YN, Shi K, Huang HM, Huang SP, Xu WQ, Li ZY, Wei KL, Gan TQ, Chen G. Down-regulation of microRNA-144-3p and its clinical value in non-small cell lung cancer: a comprehensive analysis based on microarray, miRNA-sequencing, and quantitative real-time PCR data. *Respir Res* 2019; **20**: 48 [PMID: 30832674 DOI: 10.1186/s12931-019-0994-1]

18 **Zhang Y**, Qiao WB, Shan L. Expression and functional characterization of FOXM1 in non-small cell lung cancer. *Onco Targets Ther* 2018; **11**: 3385-3393 [PMID: 29928129 DOI: 10.2147/OTT.S162523]

19 **Wang L**, Wang Y, Du X, Yao Y, Wang L, Jia Y. MiR-216b suppresses cell proliferation, migration, invasion, and epithelial-mesenchymal transition by regulating FOXM1 expression in human non-small cell lung cancer. *Onco Targets Ther* 2019; **12**: 2999-3009 [PMID: 31114243 DOI: 10.2147/OTT.S202523]

20 **Choi YE**, Madhi H, Kim H, Lee JS, Kim MH, Kim YN, Goh SH. FAM188B Expression Is Critical for Cell Growth *via* FOXM1 Regulation in Lung Cancer. *Biomedicines* 2020; **8** [PMID: 33142744 DOI: 10.3390/biomedicines8110465]

21 **Xu C**, Li S, Chen T, Hu H, Ding C, Xu Z, Chen J, Liu Z, Lei Z, Zhang HT, Li C, Zhao J. miR-296-5p suppresses cell viability by directly targeting PLK1 in non-small cell lung cancer. *Oncol Rep* 2016; **35**: 497-503 [PMID: 26549165 DOI: 10.3892/or.2015.4392]

World Journal of Clinical Cases

Submit a Manuscript: https://www.f6publishing.com

World J Clin Cases 2022 June 26; 10(18): 6001-6008

DOI: 10.12998/wjcc.v10.i18.6001

ISSN 2307-8960 (online)

ORIGINAL ARTICLE

Case Control Study

Effectiveness and postoperative rehabilitation of one-stage combined anterior-posterior surgery for severe thoracolumbar fractures with spinal cord injury

Bo Zhang, Jin-Chao Wang, Yu-Zhen Jiang, Qing-Peng Song, Yan An

Specialty type: Orthopedics

Provenance and peer review: Unsolicited article; Externally peer reviewed.

Peer-review model: Single blind

Peer-review report's scientific quality classification

Grade A (Excellent): 0
Grade B (Very good): B, B
Grade C (Good): 0
Grade D (Fair): 0
Grade E (Poor): 0

P-Reviewer: Goudeau YR, United States; Middleton AH, United States

Received: December 27, 2021
Peer-review started: December 27, 2021
First decision: January 25, 2022
Revised: February 24, 2022
Accepted: April 25, 2022
Article in press: April 25, 2022
Published online: June 26, 2022

Bo Zhang, Jin-Chao Wang, Yu-Zhen Jiang, Qing-Peng Song, Yan An, Department of Spine Surgery, Beijing Jishuitan Hospital, Beijing 100035, China

Corresponding author: Bo Zhang, MD, Chief Doctor, Neurosurgeon, Professor, Surgeon, Department of Spine Surgery, Beijing Jishuitan Hospital, No. 31 East Street, Xinjiekou, Xicheng District, Beijing 100035, China. jishuitanjizhu@163.com

Abstract

BACKGROUND

Thoracolumbar fractures are generally combined with spinal cord injury to varying degrees, which may cause deterioration of the patients' condition and increase the difficulty of clinical treatment. At present, anterior or combined anterior-posterior surgery is preferred for severe thoracolumbar fractures.

AIM

To investigate the effectiveness and postoperative rehabilitation of one-stage combined anterior-posterior surgery for severe thoracolumbar fractures with spinal cord injury.

METHODS

One-hundred-and-twenty patients who received surgery for severe thoracolumbar fractures with spinal cord injury at our hospital from February 2018 to February 2020 were randomly enrolled. They were randomly divided into group 1 (one-stage combined anterior-posterior surgery, $n = 60$) and group 2 (one-stage anterior-approach surgery, $n = 60$). Treatment efficacy was compared between the two groups.

RESULTS

Blood loss was greater and the operation time was longer in group 1 than in group 2, and the differences were statistically significant ($P < 0.05$). Incision length, intraoperative X-rays, and length of hospital stay were not significantly different between the two groups ($P > 0.05$). Preoperative function of the affected vertebrae was not significantly different between the two groups ($P > 0.05$). In each group, the patients showed significant improvement after surgery. The anterior vertebral height ratio and the posterior vertebral height ratio in group 1 after surgery were significantly higher than those in group 2. The Cobb angle after

surgery was significantly lower in group 1 than in group 2 ($P < 0.05$). The canal-occupying ratio of the affected vertebrae was not significantly different between the two groups ($P > 0.05$). Before surgery, there was no significant difference in the quality of life scores between the two groups ($P > 0.05$). The above indicators were significantly improved after surgery compared with before surgery in each group. In addition, these indicators were markedly better in group 1 than in group 2 after surgery ($P < 0.05$ for each).

CONCLUSION

One-stage combined anterior-posterior surgery effectively improves the function of the affected vertebrae and the life quality of patients with severe thoracolumbar fractures and spinal cord injury. This surgical approach is worthy of popularization in clinical use.

Key Words: Thoracolumbar fracture; Spinal cord injury; Combined anterior-posterior surgery; Postoperative rehabilitation; Quality of life

©The Author(s) 2022. Published by Baishideng Publishing Group Inc. All rights reserved.

Core Tip: One-stage combined anterior-posterior surgery can effectively improve the function of affected vertebrae and the life quality of patients with severe thoracolumbar fractures and spinal cord injury. This surgical approach is worthy of popularization in clinical use. The one-stage combined anterior-posterior approach effectively restored the height of the affected vertebrae and corrected kyphosis. The one-stage combined anterior-posterior approach also allows for sufficient anterior decompression, and the simple anterior approach does not enable temporary fixation, auxiliary reduction, and three-column fixation according to Denis' three-column concept.

Citation: Zhang B, Wang JC, Jiang YZ, Song QP, An Y. Effectiveness and postoperative rehabilitation of one-stage combined anterior-posterior surgery for severe thoracolumbar fractures with spinal cord injury. *World J Clin Cases* 2022; 10(18): 6001-6008

URL: https://www.wjgnet.com/2307-8960/full/v10/i18/6001.htm

DOI: https://dx.doi.org/10.12998/wjcc.v10.i18.6001

INTRODUCTION

Thoracolumbar fractures refer to fractures at the thoracolumbar spine, which are mainly featured by local thoracic spinal pain and swelling and muscle tension on both sides of the fracture. Patients with thoracolumbar fractures may have difficulty in standing and turning over. Some may even suffer from movement disorder and significant impairment of daily life activities. The incidence of thoracolumbar fractures is relatively high, and is a common trauma at the Department of Orthopedics. The diagnosis of this disorder has become easier and faster in China due to the continuous improvement in medical technology[1,2]. Thoracolumbar fractures are generally combined with spinal cord injury to varying degrees, which may cause deterioration of the patients' condition and increase the difficulty of clinical treatment. The reasons for this are as follows: The fractured blocks and the intervertebral disc tissues protrude into the spinal canal, resulting in spinal cord contusion and compression. Therefore, fracture reduction, spinal compression, and spinal fixation and fusion at the affected segments are crucial steps in surgery[3]. China has witnessed a rapid development of medical science in recent years, and the diagnosis of thoracolumbar fractures is more rapid, while the selection of an appropriate treatment has become a primary concern[4]. At present, anterior or combined anterior-posterior surgery is preferred for severe thoracolumbar fractures. In this study, the application value, advantages, and disadvantages of these two surgical approaches were compared by reviewing the data of patients with thoracolumbar fractures treated at our hospital.

MATERIALS AND METHODS

Patients

The present study was approved by the hospital ethics committee. One hundred and twenty patients with severe thoracolumbar fractures and spinal cord injury treated at our hospital from February 2020 to February 2021 were randomly enrolled. The random sampling method was used to divide the patients into two groups, namely, group 1 and group 2, with 60 patients in each group. Informed

consent was obtained from all patients. The two groups were not different significantly in terms of the basic information ($P > 0.05$) (Table 1).

Inclusion criteria: (1) No conscious disturbance; (2) complete medical records; (3) thoracolumbar fractures confirmed by computed tomography (CT) or X-rays, combined with nerve injury; (4) fractured blocks occupying over 50% of the spinal canal; (5) patients tolerant to surgery; and (6) the degree of vertebral compression greater than 50%.

Exclusion criteria: (1) Cognitive impairment to varying degrees; (2) recent history of acute and chronic infections; (3) hearing impairment or incapable of communication; (4) pathological fractures caused by tumors, infections, or osteoporosis; (5) severe spinal degenerative diseases; and (6) history of drug dependence or drug allergy.

Methods

Patients in group 2 received anterior decompression plus bone grafting with internal fixation. General anesthesia was performed in the lateral position. A lateral-anterior extra-pleuroperitoneal approach was adopted to expose the affected vertebrae and the adjacent vertebrae. The ribs were resected selectively to prepare the bone graft. The lateral portion of the pedicle of the affected vertebral body was resected to expose the dural sac and nerve root sleeve fully. The posterior 3/4 portion of the vertebral body was resected, along with the superior and inferior intervertebral discs and the endplate cartilage. Decompression was performed to the medial margin of the contralateral pedicle. Extra care was taken not to injure the spinal cord. Further inspection was conducted to confirm that the compression was completely removed and the deformity was corrected. Next, an autologous tricortical iliac bone graft of an appropriate length was inserted between the superior and inferior vertebral bodies. The titanium plate was mounted and immobilized. The residual fractured blocks were placed into the iliac bone and the lateral gaps. Thorough hemostasis was performed, followed by washing with normal saline. The incision was sutured layer by layer.

Patients in group 1 received surgery *via* the combined anterior-posterior approach: The same steps were followed for anterior decompression as in group 2. The incision was maintained at a length of 10-12 cm as no anterior fixation would be performed. Grafting with large iliac bone blocks was performed for the fusion. If the harvested iliac bone blocks were thin, the fusion was performed using a titanium mesh cage. Posterior fixation was performed *via* the intermuscular space. Therefore, no damage would be caused to the posterior complex structure (Figure 1). The GSS-II rod-screw system and Depuy pedicle screw system were used. It was unnecessary to perform canal decompression. Lateral fenestration of the vertebral body was performed if the superior and inferior intervertebral discs of the affected vertebra were not damaged, which was followed by intravertebral bone grafting. A closed thoracic drainage tube was indwelled for all patients receiving thoracotomy. The drainage tube was removed after confirming that there was no effusion or pneumatosis in the thoracic cavity. Costal bone was introduced for patients who received fusion using large iliac bone blocks. The fractured blocks harvested by spinal decompression were regrafted.

The early interventions after surgery were the same in both groups. Patients with nerve injury were treated with hormones and mannitol 4-5 d after surgery and with antibiotics 5-7 d after surgery. Fluid replacement was given to maintain electrolyte and acid-base balance. The indication for blood transfusion was assessed based on intraoperative blood loss and postoperative routine blood tests. Patients with osteoporosis received anti-osteoporosis treatment within 1 mo after surgery, and only then were they allowed to get out of bed. The time to ambulation was prolonged to 1.5 mo after surgery for those with severe osteoporosis. In addition, these patients were required to wear waist braces within the first 3 mo of ambulation.

Observation indicators

The observation indicators were blood loss, incision length, operation time, intraoperative X-rays, length of hospital stay, anterior vertebral height ratio, posterior vertebral height ratio, Cobb angle, and canal-occupying ratio of the affected vertebra.

Quality of life (QOL) was scored in the two groups before treatment and at 2 mo after surgery. The total score of each item ranged from 0 to 60: scores < 20, extremely poor; 20-50, fair; and 51-60, good[5].

Statistical analysis

All statistical analyses were performed using SPSS 22.0 software. Measurements were expressed as mean ± SD and analyzed by the *t*-test. Counts were expressed as *n* (%) and analyzed by the χ^2 test. $P < 0.05$ indicated a significant difference.

Table 1 Comparison of basic information

Groups	Male/female	Age (yr)	Causes of injury (Falling injury/traffic accidents/falling from heights)	Preoperative ASIA grade(B/C/D)	Frankel classification (A/B/C/D)	Preoperative AO classification (A3/B3/C2)	BMI (kg/m^2)
Group 1 (n = 60)	35/25	45.37 ± 4.24	13/32/15	13/22/25	13/18/15/14	13/35/12	23.75 ± 1.69
Group 2 (n = 60)	29/31	45.26 ± 4.09	16/29/15	12/20/28	15/20/12/13	15/30/15	23.84 ± 1.76
χ^2/t value	1.205	0.145	0.4579	0.305	0.619	0.861	0.286
P value	0.272	0.885	0.7954	0.859	0.892	0.650	0.776

ASIA: American Spinal Injury Association; BMI: Body mass index.

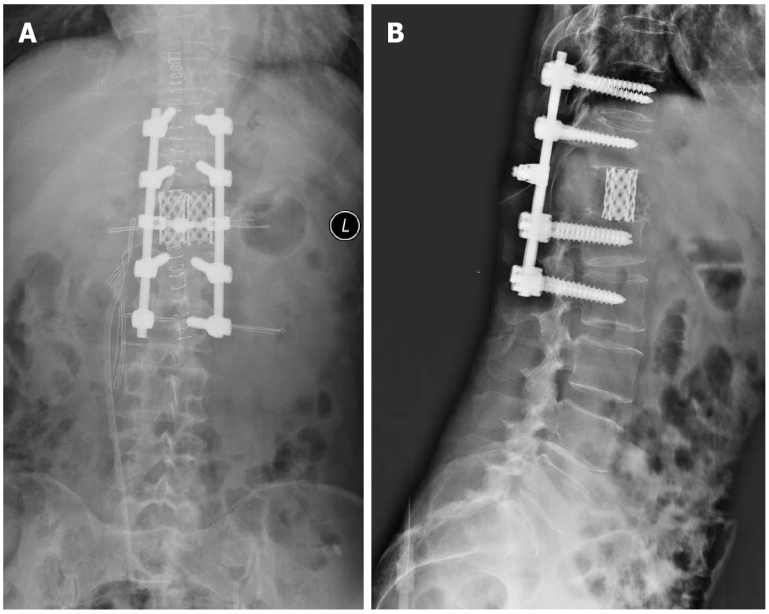

DOI: 10.12998/wjcc.v10.i18.6001 **Copyright** ©The Author(s) 2022.

Figure 1 The intraoperative X-ray of group 1. A, B: The titanium mesh cage and pedicle screw and rod were in good position, and the decompression was sufficient.

RESULTS

Comparison of surgical indicators

Blood loss was greater and the operation time was longer in group 1 than in group 2, with significant difference (P < 0.05). Incision length, intraoperative X-rays, and length of hospital stay were not significantly different between the two groups (P > 0.05) (Table 2).

Comparison of the function of the affected vertebrae

There were no significant differences in the preoperative function of the affected vertebrae between the two groups (P > 0.05). Significant improvement was achieved in both groups after surgery. The anterior vertebral height ratio and the posterior vertebral height ratio in group 1 after surgery were significantly higher than those in group 2. The Cobb angle after surgery was significantly lower in group 1 than in group 2 (P < 0.05). The canal-occupying ratio of the affected vertebrae was not significantly different between the two groups (P > 0.05) (Table 3).

Comparison of the QOL scores between the two groups

Before surgery, there was no significant difference in the QOL scores between the two groups (P > 0.05). The above indicators in each group were significantly improved after surgery compared with before surgery. In addition, these indicators were much better in group 1 than in group 2 after surgery (P < 0.05) (Table 4).

Table 2 Comparison of the surgical indicators (mean ± SD)

Groups	Blood loss (mL)	Incision length (cm)	Operating time (min)	Intraoperative X-rays	Length of hospital stay (d)
Group 1 (n = 60)	748.28 ± 74.69	6.97 ± 0.62	145.79 ± 14.63	18.77 ± 1.63	12.89 ± 1.67
Group 2 (n = 60)	625.71 ± 62.43	7.14 ± 0.75	125.28 ± 12.07	19.05 ± 1.52	12.48 ± 1.43
t value	9.753	1.353	8.376	0.973	1.444
P value	0.001	0.179	0.001	0.332	0.151

Table 3 Comparison of the function of the affected vertebrae (mean ± SD)

Group	Anterior vertebral height ratio of the affected vertebra (%)		Posterior vertebral height ratio of the affected vertebra (%)		Cobb angle (°)		Canal-occupying ratio of the affected vertebra (%)	
	Before	After	Before	After	Before	After	Before	After
Group 1 (n = 60)	61.86 ± 6.20	91.97 ± 7.12	89.74 ± 8.51	97.52 ± 1.66	27.54 ± 2.71	5.11 ± 0.53	66.12 ± 6.17	13.09 ± 1.23
Group 2 (n = 60)	61.57 ± 6.25	89.20 ± 6.16	89.43 ± 8.62	95.40 ± 2.35	27.68 ± 2.62	7.09 ± 0.75	66.63 ± 6.41	12.87 ± 1.45
t value	0.255	2.279	0.198	5.708	0.288	16.700	0.444	0.896
P value	0.799	0.024	0.843	0.001	0.774	0.001	0.658	0.372

Table 4 Comparison of the quality of life scores between the two groups (mean ± SD)

Group	Activities of daily living		Spirit		Sleep		Appetite	
	Before	After	Before	After	Before	After	Before	After
Group 1 (n = 60)	35.78 ± 5.61	51.13 ± 2.04	32.91 ± 6.23	48.72 ± 5.45	36.47 ± 4.52	50.87 ± 1.69	33.96 ± 5.12	52.41 ± 1.37
Group 2 (n = 60)	36.02 ± 5.77	44.81 ± 3.62	33.80 ± 6.14	42.36 ± 5.22	36.68 ± 4.31	45.12 ± 2.78	34.03 ± 5.08	46.89 ± 2.65
t value	0.200	10.203	0.683	5.653	0.226	11.856	0.065	12.413
P value	0.842	0.001	0.497	0.001	0.822	0.001	0.948	0.001

DISCUSSION

Severe spinal fractures caused by high-energy trauma have become increasingly common in recent years. Spinal fractures, damaged spine structure, spinal dislocation, and space occupation by a large number of fractured blocks in the spinal canal may cause spinal cord compression and nerve injury[6,7]. At present, the clinical treatment for such a disorder aims to achieve sufficient spinal decompression, restore the support and immobilize the vertebrae, and hence promote bone union and recovery of nerve function. However, the conventional posterior approach may fail to achieve these goals[8,9].

Surgical treatment for thoracolumbar fractures is usually intended to reconstruct the normal spinal structure and spinal stability, relieve compression, prevent late-stage thoracolumbar deformity and secondary nerve injury, and offer mechanical protection for recovery of nerve function[10,11]. Posterior spinal surgery is an invasive surgery, and the surgical indications of patients should be carefully assessed to prevent complications and ensure surgical success[12,13]. Given these facts, posterior open spinal surgery is generally intended to treat thoracolumbar fractures with spinal instability. Spinal instability is a disorder where the spine does not maintain normal anatomy when resisting loads. As a result, the nerve roots may have a secondary injury or mechanical injury, which further changes the spine structure and induces fracture malunion[14,15]. Certain rules should be followed during surgery, and the surgical approach is selected depending on the position of spinal compression. In addition, a pedicle screw-rod internal fixation system is used to improve surgical outcomes[16,17]. The present study showed that blood loss was greater and the operation time was longer in group 1 than in group 2 ($P < 0.05$). Incision length, intraoperative X-rays, and length of hospital stay were not significantly different between the two groups ($P > 0.05$). In each group, the patients' condition was significantly improved after surgery compared with before surgery. The anterior vertebral height ratio and the posterior vertebral height ratio in group 1 after surgery were significantly higher than those in group 2. The Cobb angle after surgery was significantly lower in group 1 than in group 2 ($P < 0.05$). However, the canal-occupying ratio of the affected vertebra was not significantly different between the two groups

($P > 0.05$). Each group of patients achieved significant improvement after surgery. All of the relevant indicators in group 1 were significantly higher than those in group 2 after surgery ($P < 0.05$). The reasons for these results might be due to the larger incision, greater blood loss, longer operation time, and difficulty in vertebral exposure. Anterior spinal surgery has the following advantages compared with the posterior approach: More thorough spinal decompression, lower risk of fixation loosening and disruption, removal of the fixation system after artificial joint fusion is unnecessary, and less likelihood of vertebral deformity, paralysis and sequelae after surgery[18,19]. The following defects have been reported for posterior spinal surgery: Degeneration and stenosis of the affected vertebrae and the superior adjacent intervertebral disc; multiple micromovements of the pedicle screws under excessive loading, which further causes loosening before bony fusion[20,21]; postoperative cutting of the screws within the cancellous bone, leading to reduction loss in those for whom osteoporosis is not confirmed before surgery; and fatigue fracture of the pedicle screws and implants due to overload[9]. Despite the above defects, posterior spinal surgery also has the following advantages. It is easier to perform surgery *via* this approach; only the superior and inferior adjacent segments of the affected vertebrae are immobilized with pedicle screws. In this way, the number of segments to be immobilized is reduced, while the motor function of the spine is preserved maximally[17]. This approach allows for posterior laminectomy with direct decompression. In addition, a well-designed implant enables sufficient stretching of the anterior and posterior longitudinal ligaments of the fibrous ring under the physiological curvature through three-dimensional adjustment. The implant can effectively achieve the reduction of fractured blocks in the vertebral canal in burst fractures through traction. Hence, indirect decompression is achieved without further damaging the stability of the bony structure[16]. The posterior approach not only allows bone grafting for fusion, but also fusion of the anterior affected bone *via* the pedicle. The combined anterior-posterior surgery integrates the advantages of both the anterior and posterior approaches. The combined approach can directly manage the displacement of a posterior column fracture and offer pre-support to assist in anterior reduction. The adjacent segments can be temporarily stabilized. In addition, the cage for anterior bone fusion can be conveniently placed by pressurizing and tightening. Moreover, excessive tilting or subsidence of the titanium mesh cage can be prevented. Therefore, the normal physiological loading state before the injury can be best reproduced [22]. Our study showed that the combined anterior-posterior surgery outperformed the posterior spinal surgery in promoting the functional recovery of the affected vertebrae and improved the patients' QOL. The combined approach effectively restored the height of the affected vertebrae and corrected kyphosis. The combined approach also allows for sufficient anterior decompression, and the simple anterior approach does not enable temporary fixation, auxiliary reduction, and three-column fixation according to Denis' three-column concept. Therefore, the latter is usually associated with an unfavorable microenvironment for callus regeneration.

However, our study also has some limitations. First, this was a single-center study with limited number of patients enrolled, and the novel surgical approach is still expected to be attempted in more centers. Second, the follow-up was short in our study, and the long-term efficacy of the novel surgical approach remains to be further documented.

CONCLUSION

One-stage combined anterior-posterior surgery can effectively improve the function of affected vertebrae and the life quality of patients with severe thoracolumbar fractures and spinal cord injury. This surgical approach is worthy of promotion in clinical use.

ARTICLE HIGHLIGHTS

Research background

Thoracolumbar fractures are usually accompanied by spinal cord injury, and anterior or combined anterior-posterior surgery is preferred for severe thoracolumbar fractures.

Research motivation

We have performed one-stage combined anterior-posterior surgery for severe thoracolumbar fractures with spinal cord injury at our center, and the outcomes are expected to be reported.

Research objectives

This study aimed to investigate the effectiveness and postoperative rehabilitation of one-stage combined anterior-posterior surgery for severe thoracolumbar fractures with spinal cord injury.

Research methods

One hundred and twenty patients with severe thoracolumbar fractures and spinal cord injury treated at our hospital from February 2020 to February 2021 were randomly enrolled, which were randomly divided into group 1 (one-stage combined anterior-posterior surgery) and group 2 (one-stage anterior-approach surgery). Blood loss, incision length, operation time, intraoperative X-rays, length of hospital stay, anterior vertebral height ratio, posterior vertebral height ratio, Cobb angle, canal-occupying ratio of the affected vertebra, and quality of life scores were compared between the two groups.

Research results

Blood loss was greater and the operation time was longer in group 1 than in group 2, with significant difference. Incision length, intraoperative X-rays, and length of hospital stay were not significantly different between the two groups. Preoperative function of the affected vertebrae was not significantly different between the two groups. In each group, the patients showed significant improvement after surgery. The anterior vertebral height ratio and the posterior vertebral height ratio in group 1 after surgery were significantly higher than those in group 2. The Cobb angle after surgery was significantly lower in group 1 than in group 2. The canal-occupying ratio of the affected vertebrae was not significantly different between the two groups. Before surgery, there was no significant difference in the quality of life scores between the two groups. The above indicators were significantly improved after surgery compared with before surgery in each group. In addition, these indicators were markedly better in group 1 than in group 2 after surgery.

Research conclusions

One-stage combined anterior-posterior surgery effectively improves the function of the affected vertebrae and the life quality of patients with severe thoracolumbar fractures and spinal cord injury.

Research perspectives

One-stage combined anterior-posterior surgery is worthy of popularization in clinical use.

FOOTNOTES

Author contributions: Conceptualization: Zhang B contributed the conceptualization of the study; An Y, Wang JC, Song QP and Jiang YZ collected the data; An Y and Wang JC Formal analyzed the data; Wang JC, Song QP and Jiang YZ wrote the manuscript; Wang JC, Song QP and Zhang B reviewed and edited the manuscript.

Institutional review board statement: The study was reviewed and approved by the Ethics Committee of Beijing Jishuitan Hospital (Approval No. 202110-05).

Informed consent statement: All study participants, or their legal guardian, provided informed written consent prior to study enrollment.

Conflict-of-interest statement: The authors declare that they have no conflicts of interest concerning this article. No benefits in any form have been or will be received from any commercial party related directly or indirectly to the subject of this study.

Data sharing statement: No additional data are available.

STROBE statement: The authors have read the STROBE Statement - checklist of items, and the manuscript was prepared and revised according to the STROBE Statement - checklist of items.

Open-Access: This article is an open-access article that was selected by an in-house editor and fully peer-reviewed by external reviewers. It is distributed in accordance with the Creative Commons Attribution NonCommercial (CC BY-NC 4.0) license, which permits others to distribute, remix, adapt, build upon this work non-commercially, and license their derivative works on different terms, provided the original work is properly cited and the use is non-commercial. See: https://creativecommons.org/Licenses/by-nc/4.0/

Country/Territory of origin: China

ORCID number: Bo Zhang 0000-0002-6320-7258; Jin-Chao Wang 0000-0003-0423-750X; Yu-Zhen Jiang 0000-0003-2248-7211; Qing-Peng Song 0000-0002-2146-6913; Yan An 0000-0003-4919-2106.

S-Editor: Wang JL
L-Editor: A
P-Editor: Wang JL

REFERENCES

1 **Zhang ZW**, Rao XH, Tian JQ. One-stage combined anterior and posterior approach for severe thoracolumbar and lumbar spine fracture. *Zhonguo Jizhu Jisui Zazhi* 2010; **20**: 228-234 [DOI: 10.3969/j.issn.1004-406X.2010.03.13]

2 **Fu TY**, Liu Y, Zhang W. Comparison of efficacy of the anterior and posterior approaches for surgical treatment of thoracolumbar fractures with spinal cord injury. *Zhongguo Zhongyi Gushangke Zazhi* 2020; **28**: 76-79

3 **Allain J**. Anterior spine surgery in recent thoracolumbar fractures: An update. *Orthop Traumatol Surg Res* 2011; **97**: 541-554 [PMID: 21820378 DOI: 10.1016/j.otsr.2011.06.003]

4 **Wang J**, Liu P. Analysis of surgical approaches for unstable thoracolumbar burst fracture: minimum of five year follow-up. *J Pak Med Assoc* 2015; **65**: 201-205 [PMID: 25842559]

5 **Jiang XY**, Zhang ZB. Analysis of the short-term efficacy of simple short posterior segmental percutaneous pedicle screw fixation for type A1-A3 thoracolumbar fractures. *Shiyong Linchuang Yixue* 2021; **18**: 139-142

6 **Jiang P**, Li NH, Wei C. Observational study on the treatment of ankylosing spondylitis with thoracolumbar fracture with posterior long segmental percutaneous fixation. *Zhonguo Jizhu Jisui Zazhi* 2019; **29**: 303-309

7 **He RK**, Cao Y. Research progress in the surgical treatment of thoracolumbar fractures *via* the posterior approach. *Guoji Gukexue Zazhi* 2020; **41**: 100-103

8 **Liu FQ**, Zhang SM. An observation of the clinical effect of posterior single segmental pedicle screw internal fixation in the affected vertebra to treat thoracolumbar fractures. *Zhonghua Yixue Zazhi* 2020; **55**: 753-756

9 **Ko S**, Choi W, Lee J, Song S, Nam J. Relationship between the time from injury to surgery and the degree of fracture reduction by ligamentotaxis in a posterior instrumentation without fusion for thoracolumbar unstable burst fracture: a retrospective cohort study. *Curr Orthop Pract* 2021; **32**: 124-129 [DOI: 10.1097/BCO.0000000000000976]

10 **Kapoen C**, Liu Y, Bloemers FW, Deunk J. Pedicle screw fixation of thoracolumbar fractures: conventional short segment versus short segment with intermediate screws at the fracture level-a systematic review and meta-analysis. *Eur Spine J* 2020; **29**: 2491-2504 [PMID: 32529525 DOI: 10.1007/s00586-020-06479-4]

11 **Wang W**, Duan K, Ma M, Jiang Y, Liu T, Liu J, Hao D. Tranexamic Acid Decreases Visible and Hidden Blood Loss Without Affecting Prethrombotic State Molecular Markers in Transforaminal Thoracic Interbody Fusion for Treatment of Thoracolumbar Fracture-Dislocation. *Spine (Phila Pa 1976)* 2018; **43**: E734-E739 [PMID: 29189568 DOI: 10.1097/BRS.0000000000002491]

12 **Gumussuyu G**, Islam NC, Kose O, Gungor M, Ozcan H. Comparison of Two Segment Combined Instrumentation and Fusion versus Three Segment Posterior Instrumentation in Thoracolumbar Burst Fractures: A Randomized Clinical Trial with 10 Years of Follow Up. *Turk Neurosurg* 2019; **29**: 555-563 [PMID: 30900733 DOI: 10.5137/1019-5149.JTN.25025-18.3]

13 **Spiegl UJ**, Devitt BM, Kasivskiy I, Jarvers JS, Josten C, Heyde CE, Fakler HM. Comparison of combined posterior and anterior spondylodesis versus hybrid stabilization in unstable burst fractures at the thoracolumbar spine in patients between 60 and 70 years of age. *Arch Orthop Trauma Surg* 2018; **138**: 1407-1414 [PMID: 30008109 DOI: 10.1007/s00402-018-2993-y]

14 **Yang M**, Zhao Q, Hao D, Chang Z, Liu S, Yin X. Comparison of clinical results between novel percutaneous pedicle screw and traditional open pedicle screw fixation for thoracolumbar fractures without neurological deficit. *Int Orthop* 2019; **43**: 1749-1754 [PMID: 29909584 DOI: 10.1007/s00264-018-4012-x]

15 **Harding AT**, Weeks BK, Lambert C, Watson SL, Weis LJ, Beck BR. Exploring thoracic kyphosis and incident fracture from vertebral morphology with high-intensity exercise in middle-aged and older men with osteopenia and osteoporosis: a secondary analysis of the LIFTMOR-M trial. *Osteoporos Int* 2021; **32**: 451-465 [PMID: 32935171 DOI: 10.1007/s00198-020-05583-x]

16 **Morrissey PB**, Shafi KA, Wagner SC, Butler JS, Kaye ID, Sebastian AS, Schroeder GD, Kepler CK, Aarabi B, Oner FC, Vaccaro AR. Surgical Management of Thoracolumbar Burst Fractures: Surgical Decision-making Using the AOSpine Thoracolumbar Injury Classification Score and Thoracolumbar Injury Classification and Severity Score. *Clin Spine Surg* 2021; **34**: 4-13 [PMID: 32657842 DOI: 10.1097/BSD.0000000000001038]

17 **Piccone L**, Cipolloni V, Nasto LA, Pripp C, Tamburrelli FC, Maccauro G, Pola E. Thoracolumbar burst fractures associated with incomplete neurological deficit in patients under the age of 40: Is the posterior approach enough? *Injury* 2020; **51**: 312-316 [PMID: 31917009 DOI: 10.1016/j.injury.2019.12.031]

18 **Park SJ**, Lee CS, Park JS, Lee KJ. Should Thoracolumbar Junction Be Always Avoided as Upper Instrumented Vertebra in Long Instrumented Fusion for Adult Spinal Deformity? *Spine (Phila Pa 1976)* 2020; **45**: 686-693 [PMID: 31842105 DOI: 10.1097/BRS.0000000000003364]

19 **Li T**, Zheng YH, Xu ZW, Hao DJ, Qian LX. Outcomes of Thoracolumbar Burst Fracture in Patients With Osteoporosis Without Neurologic Symptoms: Analysis of Three Different Surgical Approaches. *J Biomater Tissue Eng* 2019; **9**: 1052-1057 [DOI: 10.1166/jbt.2019.2111]

20 **Jang HD**, Bang C, Lee JC, Soh JW, Choi SW, Cho HK, Shin BJ. Risk factor analysis for predicting vertebral body re-collapse after posterior instrumented fusion in thoracolumbar burst fracture. *Spine J* 2018; **18**: 285-293 [PMID: 28735766 DOI: 10.1016/j.spinee.2017.07.168]

21 **Wang W**, Pei B, Pei Y, Shi Z, Kong C, Wu X, Wu N, Fan Y, Lu S. Biomechanical effects of posterior pedicle fixation techniques on the adjacent segment for the treatment of thoracolumbar burst fractures: a biomechanical analysis. *Comput Methods Biomech Biomed Engin* 2019; **22**: 1083-1092 [PMID: 31225742 DOI: 10.1080/10255842.2019.1631286]

22 **He D**, Wu L, Chi Y, Zhong S. Facet joint plus interspinous process graft fusion to prevent postoperative late correction loss in thoracolumbar fractures with disc damage: finite element analysis and small clinical trials. *Clin Biomech (Bristol, Avon)* 2011; **26**: 229-237 [PMID: 21115215 DOI: 10.1016/j.clinbiomech.2010.10.009]

World Journal of Clinical Cases

Submit a Manuscript: https://www.f6publishing.com

World J Clin Cases 2022 June 26; 10(18): 6009-6020

DOI: 10.12998/wjcc.v10.i18.6009

ISSN 2307-8960 (online)

ORIGINAL ARTICLE

Retrospective Study

Prostate sclerosing adenopathy: A clinicopathological and immunohistochemical study of twelve patients

Run-Lin Feng, Yan-Ping Tao, Zhi-Yong Tan, Shi Fu, Hai-Feng Wang

Specialty type: Pathology

Provenance and peer review: Unsolicited article; Externally peer-reviewed.

Peer-review model: Single-blind

Peer-review report's scientific quality classification

Grade A (Excellent): 0
Grade B (Very good): B
Grade C (Good): C
Grade D (Fair): 0
Grade E (Poor): 0

P-Reviewer: Cassell III AK, Liberia; Marickar F, India

Received: November 2, 2021
Peer-review started: November 2, 2021
First decision: April 7, 2022
Revised: April 19, 2022
Accepted: April 30, 2022
Article in press: April 30, 2022
Published online: June 26, 2022

Run-Lin Feng, Department of Pathology, The Second Affiliated Hospital of Kunming Medical University, Kunming 650101, Yunnan Province, China

Yan-Ping Tao, Department of Emergency, Kunming Third People's Hospital, Kunming 650000, Yunnan Province, China

Zhi-Yong Tan, Shi Fu, Hai-Feng Wang, Department of Urology, The Second Affiliated Hospital of Kunming Medical University, Kunming 650101, Yunnan Province, China

Corresponding author: Hai-Feng Wang, PhD, Chief Doctor, Department of Urology, The Second Affiliated Hospital of Kunming Medical University, No. 374 Yunnan-Burma Avenue, Kunming 650101, Yunnan Province, China. wanghaifeng@kmmu.edu.cn

Abstract

BACKGROUND

Although sclerosing adenopathy of the prostate is a very rare benign disease, an effective differential diagnosis is required. Here, we report the clinicopathological and immunohistochemical morphological features of 12 cases of sclerosing adenopathy of the prostate to improve understanding of the disease.

AIM

To investigate the clinicopathological features, diagnosis, and immunohistochemical phenotypes that distinguish prostate sclerosing adenopathy from other conditions.

METHODS

The clinical data, laboratory tests, pathological morphology, and immunohistochemical phenotypes of 12 cases of prostatic sclerosing adenopathy were retrospectively analyzed, and the relevant literature was reviewed.

RESULTS

All patients were elderly men (mean age, 71.7 years; 62–83 years). Eleven of them had hematuria, urinary frequency, urinary urgency, difficulty in urination, and serum total prostate-specific antigen values within the normal range. One patient had increased blood pressure. Enlarged prostates with single to multiple calcifying foci were observed. Moreover, prostate tissue hyperplastic changes were observed in all patients. Small follicular hyperplastic nodules without an obvious envelope, with a growth pattern mimicking the infiltration pattern of

"prostate adenocarcinoma" were noted. Basal cells expressed AR, CKH, P63, and CK5/6, and myoepithelial markers, such as calponin, S100, and smooth muscle actin. No recurrence or exacerbation of the lesions was observed, except for one case of death due to bladder cancer.

CONCLUSION

Prostatic sclerosing adenopathy is highly misdiagnosed as prostate adenocarcinoma or other tumor-like lesions. Therefore, it should attract the attention of clinicopathologic researchers.

Key Words: Clinicopathology; Immunohistochemistry; Prostate disease; Sclerosing adenopathy

©The Author(s) 2022. Published by Baishideng Publishing Group Inc. All rights reserved.

Core Tip: Sclerosing prostatic adenopathy is a rare pseudoadenocarcinoma proliferative lesion with a unique histomorphology and immunohistochemical phenotype. Compared to the common prostate adenocarcinoma, the incidence of sclerosing prostatic adenopathy is low, and we are under-recognized and have a high rate of misdiagnosis. Meanwhile, there are no large samples of data available to clinicopathologic to date because it is a rare lesion. To further our understanding of prostatic sclerosing adenopathy, this study aimed to investigate the histopathological morphology and immunohistochemical phenotype of this very rare prostate lesion and to further explore its associated biological significance.

Citation: Feng RL, Tao YP, Tan ZY, Fu S, Wang HF. Prostate sclerosing adenopathy: A clinicopathological and immunohistochemical study of twelve patients. *World J Clin Cases* 2022; 10(18): 6009-6020
URL: https://www.wjgnet.com/2307-8960/full/v10/i18/6009.htm
DOI: https://dx.doi.org/10.12998/wjcc.v10.i18.6009

INTRODUCTION

Sclerosing adenopathy of the prostate is a rare pseudomalignant proliferative lesion with a distinct histomorphological and immunohistochemical phenotype that often resembles acinar adenocarcinoma but may also resemble sarcomatoid carcinoma[1]. It can manifest as single or multiple lesions, in which good small glands and scattered single-cell components can be seen, forming the impression of cell-like features. These lesions are benign pseudotumor hyperplasia lesions that are very similar to those of small alveolar prostate adenocarcinoma and are often misdiagnosed as prostate cancer by primary pathologists due to their characteristic interstitial spindle cell proliferation and small glandular architecture. They are observed in 2% of the transurethral prostatectomy or prostatectomy specimens and are rare in small samples derived from prostate needle biopsy[2-4]. The glandular components show nuclear atypia, including nuclear enlargement and prominent nucleoli. However, sclerosing adenopathy tends to be a more focal lesion than sarcomatoid carcinoma, which is thought to arise from the myoepithelial cells surrounding the prostate, high molecular weight cytokeratins. Moreover, the lesions are often positive for muscle-specific actin staining. Compared with that prostate adenocarcinoma, sclerosing adenopathy has a lower incidence and a higher misdiagnosis rate. Furthermore, since it is a rare lesion, to date, no large samples have been available for clinical pathology experiments. In clinical treatment, surgical resection is still the best treatment option for sclerosing adenopathy of the prostate. To further understand this condition, we aimed to investigate the histopathological morphology and immunohistochemical phenotype of this very rare prostate lesion and to further explore its associated biological significance and underlying mechanisms.

MATERIALS AND METHODS

Thirteen patients with prostate sclerosing adenopathy that visited the Second Affiliated Hospital of Kunming Medical University from January 2015 to November 2021 were enrolled and followed up. Their clinical history, imaging data, and disease were analyzed and further confirmed *via* the relevant immunohistochemical analysis. Twelve specimens were routinely fixed using 4% neutral formaldehyde, paraffin-embedded, and tissue-sectioned to a thickness of 4 μm, followed by HE staining and immunohistochemical analysis. The HE-stained slides were reviewed by three pathologists to confirm the diagnosis. We reviewed the gross specimen characteristics and read the immunohistochemical product instructions, the expiration dates of the antibodies, the localization of the positive antibodies, and the staining intensity interpretation criteria in detail. The required immunohistochemistry AR, CKH, P63,

CD56, CK5/6, calponin, S100, P504S, prostate-specific antigen (PSA), PSAP, P53, and Ki-67 markers were obtained from the Fujian Meixin Company, China, and the procedures were carried out strictly according to the instructions, and positive and negative controls were routinely set up.

The immunohistochemistry results were interpreted by two senior pathologists using a double-blind reading method in strict accordance with the immunohistochemistry interpretation criteria. In case of disagreement between the two pathologists, the reading was interpreted by a third senior pathologist. A standard reading was performed using a semi-quantitative counting method by randomly selecting 10 representative fields at high magnification (400× field of view) and calculating the cell positivity rate (the number of positive tumor cells divided by the total number of cells) × 100%, for which a cell positivity rate below and above 10% was considered as negative and positive, respectively. The staining results were based on the percentage of stained cells: When < 25%, in the 25%–50% range, in the 50%–75% range, and > 75%, the result was negative (-), weakly positive (+), moderately positive (++), and strongly positive (+++), respectively. AR, P63, P53, and Ki-67 were found in the cytosol, and CKH, CD56, CK5/6, calponin, S100, P504S, PSA, and PSAP were found in the cytoplasm or cytosol, and precise color localization was considered positive.

None of the 12 patients in this study had received prior radiotherapy, chemotherapy, immunotherapy, or drug therapy. Complete clinical and pathological data were obtained for all 12 patients, and intraoperative histological specimens were obtained. The study was approved by the Ethics Committee of the Second Affiliated Hospital of Kunming Medical University (approval number: trial-PJ-2021-142). Since the study was performed using medical records and biological specimens obtained from previous clinical consultations, all conditions were met to exempt patients from informed consent.

RESULTS

Clinical data

A total of 7674 surgically resected prostate specimens were collected between January 2015 and November 2021, including 625 radical prostatectomy specimens, 1155 prostate puncture specimens, and 5894 transurethral electrodesiccation prostate specimens. A re-read of the 7674 prostate specimens revealed 12 cases of sclerosing adenopathy (0.2%), 2 of which were found in radical prostatectomy specimens, and 10 were found in transurethral resection specimens, with no lesions found in the prostate puncture specimens. The clinical data, laboratory tests, pathological morphology, and immunohistochemical phenotype of these 12 cases of prostatic sclerosing adenopathy were analyzed and are summarized in Table 1.

All 12 patients were elderly men with an average age of 71.7 years (age range, 62–83 years). In terms of clinical symptoms, 11 patients presented varying degrees of hematuria, urinary frequency, urinary urgency, and difficulty in urination, and one patient had increased blood pressure. After admission to the hospital, the laboratory tests revealed that 11 of the 12 patients had serum total prostate-specific antigen (PSA) values within the normal reference range, and only one patient had a slightly higher than normal value. Rectal finger examination showed hyperplastic changes in all the prostate tissues, with varying degrees of prostatic hyperplasia visible intraoperatively, mainly in both lobes and on the right wall. Among the 12 cases, transurethral resection of the prostate was performed in 10 of them, and total cystectomy and bowel replacement with total cystectomy and double ureterostomy for bladder cancer was performed in two cases, respectively.

Imaging features

In the 12 patients, the computed tomography examination results showed an enlarged prostate with single to multiple calcified foci and, in three cases, localized protrusion into the bladder trigone with uneven enhancement (Figure 1). The preoperative ultrasonography results showed an enlarged prostate morphology, an enlarged inner gland, a thinning of the outer gland under pressure, and inhomogeneous parenchyma with one to multiple strong echogenic spots in all the 12 patients (Figure 2, Table 2).

Histopathological findings

Specimen analysis showed that 10 cases presented a fragmented prostate tissue, two cases presented the complete cystoprostate tissue, which was grayish-red, along with a tissue multi-sectional cut that was tough. No obvious nodules or masses were seen. The microscopic observation results revealed that all 12 cases of prostate sclerosing adenopathy presented modularly distributed lesions indicative of benign prostatic hyperplasia. The lesions only had a few millimeters, had a nodular shape with varying degrees of small alveolar hyperplasia, without an obvious envelope, and with a growth pattern that mimicked the infiltration pattern of "prostate adenocarcinoma" (Figure 3A). The hyperplastic mesenchyme extruded the gland into ductal (Figure 3B), lacunar, and linear (Figure 3C) forms, and the glandular epithelium was covered with eosinophilic spike-like cells. Some of the glands were extruded to form vacuoles, and the increased number of vacuolated cells could form a structure similar to that of printed ring cells (Figure 3D). The interstitium was collagenous or mucinous and consisted of cells with a mild

Table 1 Clinical characteristics of patients with prostate sclerosing adenopathy

Case	Age of onset (yr)	Clinical symptoms	Difficulty urinating	PSA check value (ng/mL)	Imaging diagnosis	Surgical findings	Surgical approach	Follow up
1	76	Difficulty urinating	Without	2.43	Benign prostatic hyperplasia	The lobes on both sides of the prostate protrude and protrude into the bladder, and the urethral cavity is narrowed	Transurethral plasma resection of the prostate	Survival and good, normal rectal examination, 73 mo
2	62	Hematuria	Bladder papilloma	5.21	Bladder cancer, invasion of the prostate	Irregular hyperplasia of the right side of the bladder, invading the adjacent prostate	Total cystectomy and double-layer ureterostomy	Died from bladder cancer, 27 mo
3	63	Frequent urination, difficulty urinating	Cholecystectomy; history of hypertension	1.73	Prostate cancer	The lobes on both sides of the prostate proliferate and protrude into the bladder	Transurethral plasma resection of the prostate	Survival and good, normal rectal examination, 69 mo
4	68	Gross hematuria	History of gastrectomy	3.36	Bladder Cancer	Prostatic hyperplasia, multiple neoplastic new organisms are seen in the bladder triangle and right wall	Total cystectomy and intestinal replacement for new bladder	Alive, 46 mo
5	67	Frequent urination, urgency	Without	1.34	Benign prostatic hyperplasia	Irregular hyperplasia of the lobes on both sides of the prostate	Transurethral plasma resection of the prostate	Survival and good, normal rectal examination, 24 mo
6	83	Frequent urination, difficulty urinating	History of hypertension, diabetes	3.81	Benign prostatic hyperplasia	Irregular hyperplasia of the lobes on both sides of the prostate	Transurethral plasma resection of the prostate	Survival and good, normal rectal examination, 21 mo
7	67	High blood pressure	History of prostatitis, appendix surgery	2,76	Prostatic hyperplasia with calcification	Enlargement of the right side wall of the prostate	Transurethral plasma resection of the prostate	Survival and good, normal rectal examination, 2 mo
8	83	Hematuria with frequent urination and urgency	Right inguinal hernia repair	4.91	Prostatic hyperplasia with calcification	Significant enlargement of the bilateral and middle lobes of the prostate	Transurethral resection of the prostate	Survival and good, 3 mo
9	72	Frequent urination, urgency	History of hypertension, diabetes	2.21	Prostatic hyperplasia with calcification	The lobes on both sides of the prostate proliferate and protrude into the bladder	Transurethral resection of the prostate	Survival and good, normal rectal examination, 6 mo
10	68	Difficulty urinating	Without	2.39	Benign prostatic hyperplasia	Irregular hyperplasia of the lobes on both sides of the prostate	Transurethral resection of the prostate	Survival and good, normal rectal examination, 13 mo
11	81	Frequent urination, urgency	Bladder papilloma	3.31	Benign prostatic hyperplasia	Irregular hyperplasia of the lobes on both sides of the prostate	Transurethral resection of the prostate	Survival and good, normal rectal examination, 19 mo
12	71	Difficulty urinating	Without	3.07	Prostatic hyperplasia with calcification	Irregular hyperplasia of the lobes on both sides of the prostate	Transurethral resection of the prostate	Survival and good, normal rectal examination, 24 mo

PSA refers to the detection of total prostate-specific antigen, the reference range is 0.00-4.00 ng/mL.

Table 2 Ultrasound appearance of patients with prostate sclerosing adenopathy

Case	prostate size	Ultrasound image performance
1	5.8 cm × 5.0 cm × 5.8 cm	Full shape, regular margins, normal ratio of internal and external glands, uneven echo, and sonographic image of benign prostatic hyperplasia
2	3.5 cm × 4.1 cm × 3.2 cm	The shape is normal, the edges are regular, the ratio of internal and external glands is normal, and there is a strong echogenic spot in the parenchyma, with a long diameter of about 0.2 cm
3	4.7 cm × 4.5 cm × 3.6 cm	The volume increases, the shape is plump, the internal glands are enlarged, the external glands are compressed and thinned, the parenchyma echoes uniformly, and multiple hyperechoic spots are detected in the parenchyma
4	4.3 cm × 4.3 cm × 4.4 cm	The volume increases, the shape is plump, the internal glands are enlarged, the external glands are compressed and thinned, the parenchymal echo is uneven, and a strong echogenic spot is detected in the parenchyma, with a long diameter of about 0.5 cm
5	5.5 cm × 4.0 cm × 3.7 cm	Enlarged volume, plump shape, enlarged internal glands, thin external glands under compression, uniform parenchymal echo, and sonographic image of benign prostatic hyperplasia
6	5.1 cm × 3.7 cm × 3.2 cm	Enlarged volume, plump shape, enlarged internal glands, thin external glands under compression, uniform parenchymal echo, and sonographic image of benign prostatic hyperplasia
7	4.1 cm × 5.5 cm × 4.7 cm	Full-bodied, enlarged internal glands, thin external glands under pressure, uneven parenchymal echo, and multiple hyperechoic spots within the parenchyma
8	5.7 cm × 5.4 cm × 4.6 cm	The volume increased, the shape was plump, the edges were still regular, the internal glands were enlarged, the external glands were compressed and thinned, and a strong echogenic spot was detected in the parenchyma, with a long diameter of about 0.1cm
9	5.3 cm × 5.1 cm × 3.2 cm	The volume increased, the shape was plump, the edges were still regular, the internal glands were enlarged, the external glands were compressed and thinned, and a strong echogenic spot was detected in the parenchyma, with a long diameter of about 0.6 cm
10	4.9 cm × 4.3 cm × 3.2 cm	Enlarged volume, plump shape, enlarged internal glands, thin external glands under compression, uniform parenchymal echo, and sonographic image of benign prostatic hyperplasia
11	5.5 cm × 4.0 cm × 3.7 cm	Enlarged volume, plump shape, enlarged internal glands, thin external glands under compression, uniform parenchymal echo, and sonographic image of benign prostatic hyperplasia
12	5.5 cm × 4.6 cm × 4.1 cm	The volume increased, the shape was plump, the edges were still regular, the internal glands were enlarged, the external glands were compressed and thinned, and a strong echogenic spot was detected in the parenchyma, with a long diameter of about 0.4 cm

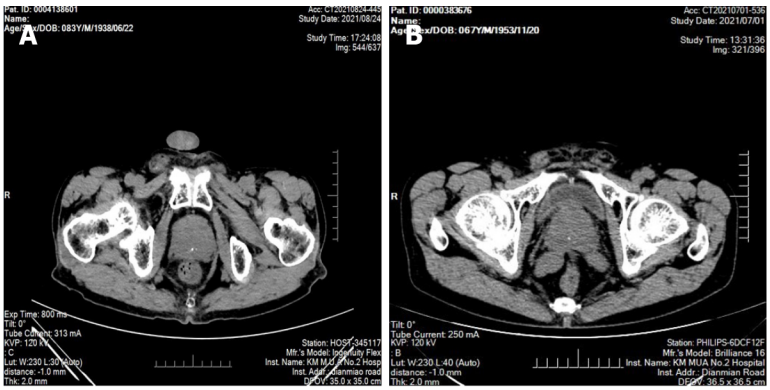

DOI: 10.12998/wjcc.v10.i18.6009 **Copyright** ©The Author(s) 2022.

Figure 1 Computed tomography images of sclerosing adenopathy of the prostate. A: Computed tomography (CT) showing an enlarged prostate with multiple calcifications; B: CT showing that the prostate was enlarged and calcified, partially protruding into the trigone of the bladder, and the enhancement was not uniform.

spindle-like morphology (Figure 3E). Observation at high magnification showed an eosinophilic cytoplasm with nuclei located at the base and small nucleoli but no nuclear division (Figure 3F).

Immunohistochemical phenotype

The basal cells of all the 12 cases of prostatic sclerosing adenopathy expressed molecules such as AR (Figure 4A), CKH (Figure 4D), P63 (Figure 4E), and CK5/6 (Figure 4C) to varying degrees, and also myoepithelial markers such as calponin (Figure 4B), S100 (Figure 4H), and smooth muscle actin (SMA) (Figure 4G). Nine of the 12 cases did not express P504S (Figure 4F), and the remaining three cases showed only a weakly positive expression of P504S. In addition, the prostate-specific markers PSA and PSAP were also expressed, P53 was not expressed, and the Ki67 proliferation index was in the 1%–3%

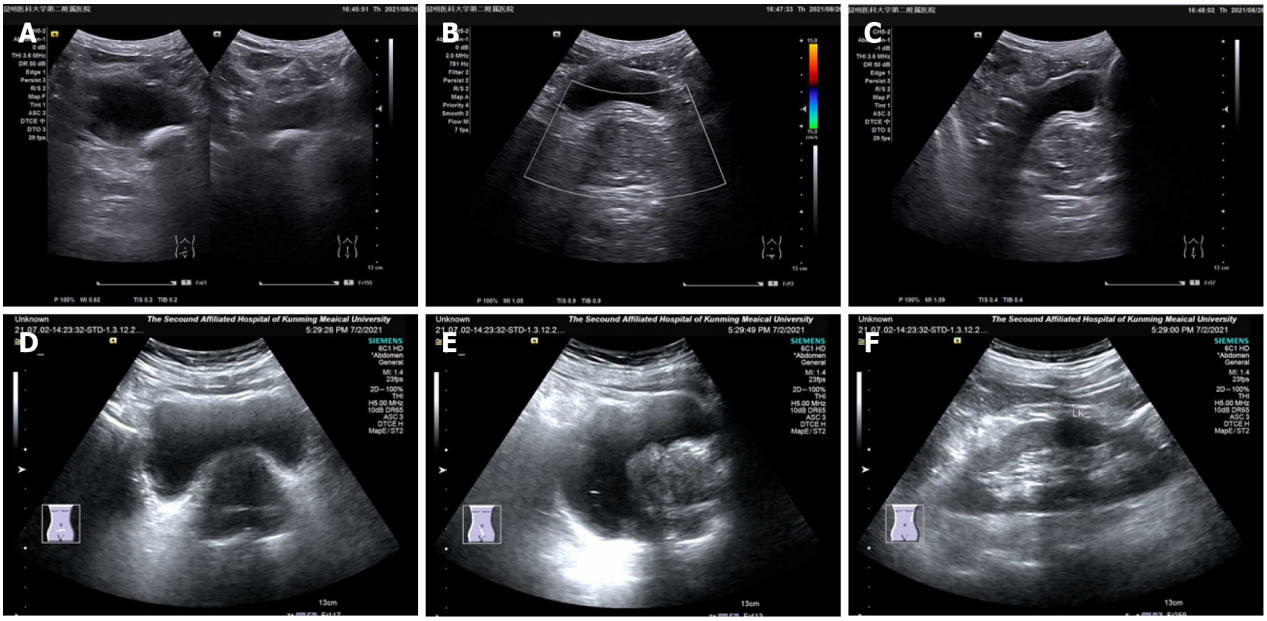

DOI: 10.12998/wjcc.v10.i18.6009 **Copyright** ©The Author(s) 2022.

Figure 2 Ultrasound image of sclerosing adenopathy of the prostate. A-C: The prostate shape was full, showing regular margins, a normal ratio of internal to external glands, an uneven echo, and a sonographic image of benign prostatic hyperplasia; D-F: The prostate gland was enlarged, its shape was plump, the internal gland was enlarged, the external gland was compressed and thinned, the parenchymal echo was not uniform, and the parenchyma was probed with multiple hyperechoic spots.

range (Table 3).

Follow-up results

The mean follow-up time was 27.6 mo (3–73 mo), and 11 of the 12 patients survived well with normal rectal examinations and no recurrence or exacerbation of the disease. One patient died 26 mo after surgery due to bladder cancer.

DISCUSSION

In 1983, Chen and Schiff reported a prostate lesion that they considered most notably similar to an adenomatous tumor[5]. Therefore, it was named sclerosing adenopathy[6]. Sclerosing adenopathy of the prostate, first reported in 1987 by Young *et al*[7], was previously known as an adenomatous prostate tumor, prostatic pseudoadenoma, and fibroepithelial nodules[8-10]. It was originally used to express the similarity of the lesions to testicular adenomatous tumors but was abandoned due to the recognition that the lesions were of prostatic origin based on the immunoreactivity of PSA in acinar cells. It was subsequently found that sclerosing adenopathy is superficially similar to the breast lesion of the same name, is composed of prostate epithelial cells rather than mesothelial cells, and is characterized by glandular hyperplasia of varying sizes in the intercellular substance[11-14]. Sclerosing adenopathy is well characterized both immunohistochemically and ultrastructurally, and there are currently several case reports and small series of this lesion[15,16].

Sclerosing adenopathy is a rare benign proliferative lesion of the small alveoli without a markedly sclerotic stroma that occurs most occasionally after transurethral resection of the prostate, simple prostatectomy, or radical prostatectomy based on benign prostatic hyperplasia. It is detected by pathologists but occurs very rarely[17,18]. The histopathological pattern of sclerosing lymphadenopathy of the prostate is very similar to that of mammary sclerosing lymphadenopathy; however, unlike mammary sclerosing lymphadenopathy, prostatic sclerosing lymphadenopathy results in small lesions, usually with only a few millimeters[19]. It can result in single or multiple lesions, and it mostly occurs in the peripheral area of the prostate. It is difficult to detect the lesion *via* rectal ultrasound, and it cannot be touched *via* digital rectal examination. In addition, the serum PSA value is not high; thus, it is very difficult to measure it in clinical practice. In this group of 12 cases of prostate sclerosing lymphadenopathy, ultrasonography and rectal examination showed no abnormalities, and the serum PSA value did not increase. With the continuous improvement of ultrasound-guided technology, the probability of finding prostate sclerosing lymphadenopathy in biopsy tissue samples will increase; however, the possibility of it being misdiagnosed as prostate cancer will also increase. Research analysis found that 2% of the cases with this condition were diagnosed as prostate cancer. T1a stage prostate cancer was

Table 3 Immunohistochemical expression of sclerosing adenopathy

Case	AR	CK5/6	P63	CKH	S100	SMA	Calponin	P504S
1	+	+	++	+++	+	+	-	+
2	+++	+++	+	+	++	++	+	-
3	++	+	+	+	++	+	++	+
4	-	++	++	+++	+	+	++	-
5	-	++	+	++	-	++	+	-
6	+	+	++	+	+	+	+	-
7	++	++	+	+	++	++	+	+
8	+	++	++	+++	+	+	-	-
9	++	++	+	-	+	+	-	++
10	++	+	+	+	+	++	-	++
11	+	++	++	+	+	+	-	+
12	++	+	+	++	+	++	-	++

The interpretation adopted a semi-quantitative counting method, randomly selects 10 representative fields under high magnification (400 x field of view), and calculates the positive rate of cells (the number of positive tumor cells divided by the total number of tumor cells) × 100%, the positive rate of cells Less than 10% is negative, and more than 10% was positive. For positive cells, the percentage of stained cells in the cell count was negative (-), 25%-50% was weakly positive (+), 50%-75% Was medium positive (++), > 75% was strong positive (+++).

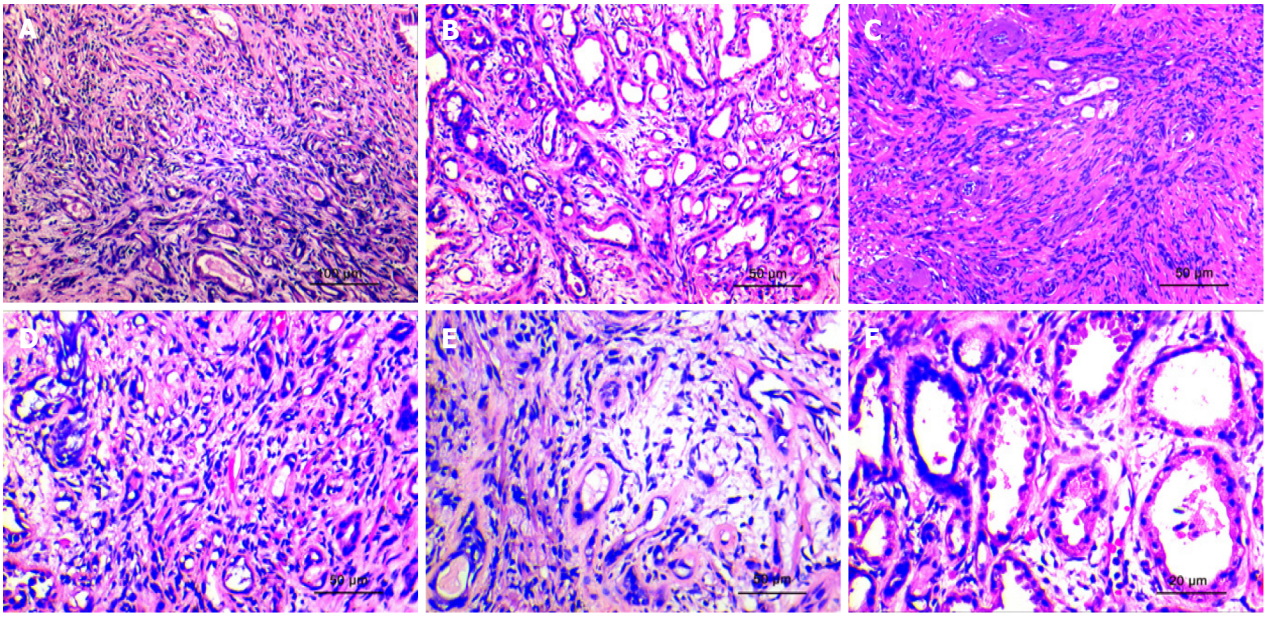

DOI: 10.12998/wjcc.v10.i18.6009 **Copyright** ©The Author(s) 2022.

Figure 3 Histopathological morphological characteristics. A: The lesions are distributed uniformly, have a nodular shape, without obvious capsules, and the simulated prostate adenocarcinoma presents an "invasive growth" pattern. (HE × 100; scale bar, 100 μm); B: The hyperplastic stroma squeezes the glands to form glandular tubes of varying sizes. Eosinophilic shoed spike-like protrusions can be seen in part of the lumen (HE × 200; scale bar, 50 μm); C: The glands of sclerosing adenopathy are squeezed into a cord-like, thread-like, or even single-cell-like arrangement, and the cells have a shuttle-like shape (HE × 200; scale bar, 50 μm); D: When the glandular transition is squeezed, it can form a vacuole-like structure, and the increase in the number of vacuole-like cells leads to a signet ring-like morphology (HE × 200; scale bar, 50 μm); E: The interstitium of the disease was composed of mildly morphological spindle cells, often with collagenous or mucinous changes (HE × 200; scale bar, 50 μm); F: At high power, the glandular epithelium and the compressed myoepithelial components can be seen, the cell cytoplasm is eosinophilic, and the nucleus is located at the base (HE × 400; scale bar, 20 μm).

confirmed to be prostate sclerosing adenopathy *via* reexamination[20]. Therefore, surgeon pathologists should consider prostate biopsy specimens as of great importance to avoid overdiagnosis of sclerosing adenopathy as prostate cancer.

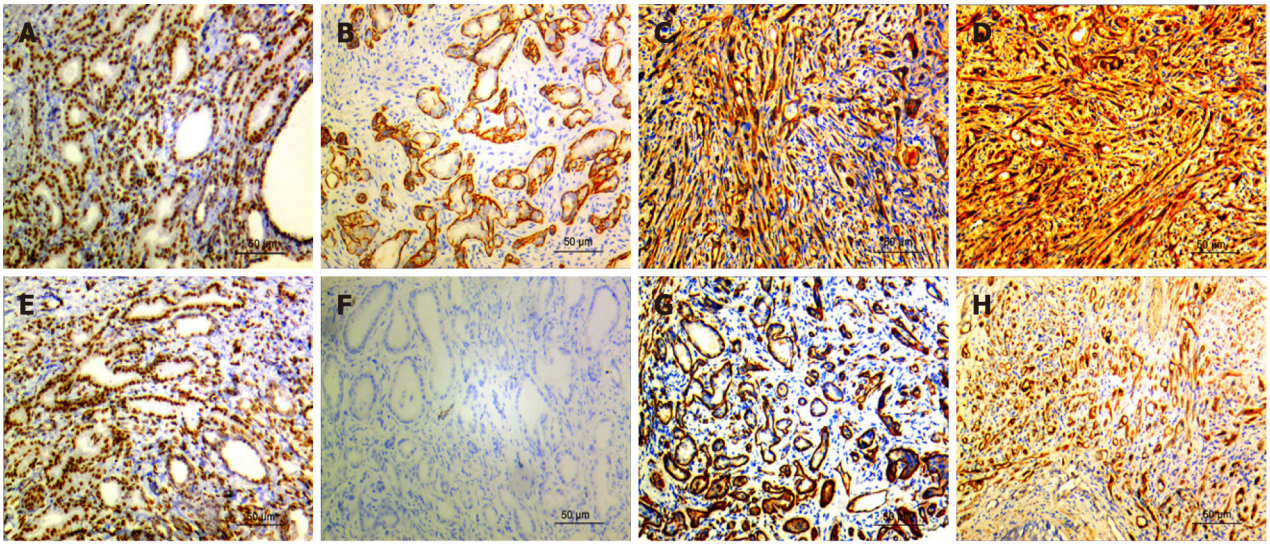

DOI: 10.12998/wjcc.v10.i18.6009 **Copyright** ©The Author(s) 2022.

Figure 4 Immunohistochemistry results. A: AR was strongly expressed in prostate sclerosing adenopathy (Immunohistochemistry; magnification, × 200; scale bar, 50 μm); B: Calponin is positively expressed in prostate sclerosing adenopathy (Immunohistochemistry; magnification, × 200; scale bar, 50 μm); C: CK5/6 is positively expressed in prostate sclerosing adenopathy (Immunohistochemistry; magnification, × 200; scale bar, 50 μm); D: CKH was strongly expressed in prostate sclerosing adenopathy (Immunohistochemistry; magnification, × 200; scale bar, 50 μm); E: P63 was moderately expressed in prostate sclerosing adenopathy (Immunohistochemistry; magnification, × 200; scale bar, 50 μm); F: P504S is not expressed in prostate sclerosing adenopathy (Immunohistochemistry; magnification, × 200; scale bar, 50 μm); G: SMA is moderately expressed in prostatic sclerosing adenopathy (Immunohistochemistry; magnification, × 200; scale bar, 50 μm); H: S100 is strongly expressed in prostate sclerosing adenopathy (Immunohistochemistry; magnification, × 200; scale bar, 50 μm).

Sclerosing adenopathy of the prostate has clear demarcation, is associated with small and concentrated lesions, nodular growth, no obvious capsule, and an infiltrative growth trend to the surrounding normal prostate tissue, similar to the growth pattern of prostate adenocarcinoma, but in the scope of growth-restricted lesions[21]. On the surface, it has a worrying appearance, with morphological distortions that can form stripes, threads, clusters, nests, and even single-cell arrangements. When the gland overproliferates, it may expand into a cyst, in which the amyloid material disappears and is replaced by a crystalline or myxoid material that is suggestive of prostate cancer[9,12]. In addition, several authors have described the lesion as presenting mild atypia and even small nucleoli, but generally no apparent large nucleoli. When individual cases are accompanied by moderate heterogeneity, heterogeneity, such as large and deep nuclear staining and prominent nucleoli, they are likely misdiagnosed as prostate adenocarcinoma. There is no evidence of the underlying malignancy of this lesion, although follow-up in our cases and others documented in the literature is admittedly limited.

In daily clinical practice, immunohistochemical markers are relied upon to help determine when lesions are morphologically atypical or when cellular heterogeneity occurs. Moreover, prostate basal cells are not considered myoepithelial cells[22], contrary to the notion of the myoepithelial origin of salivary gland myoepithelial cells, since they do not have actin filaments. S100 protein and smooth muscle actin are not expressed in normal prostate basal cells[23,24]; in contrast, the presence of the S100 protein and SMA immunoreactivity in basal cells of sclerosing adenopathy suggests that they present myoepithelial differentiation, a characteristic feature based on which sclerosing adenopathy is diagnosed. In addition, some scholars have confirmed the existence of microfilaments in the cytoplasm of basal cells of sclerosing adenopathy using electron microscopy, which is consistent with the presence of actin filaments[25]. In rare cases, S100 protein immunoreactivity can be seen in prostate basal cell hyperplasias, such as adenoid basal cell carcinoma, adenoid cystic carcinoma, and atypical basal cell hyperplasia[26]. In addition, we have recently found that D2-40 is a sensitive marker of prostate basal cells[27]; therefore, D2-40 and the combination of P63 and cytokeratin can be used to differentiate sclerosing adenopathy from prostate cancer. However, in practice, due to the severe extrusion of basal cells and myoepithelial cells, the immunohistochemical expression results are not ideal, and some sclerosing adenopathy cases will express P504S to varying degrees, overlapping with the immunohistochemistry results of patients with prostate cancer, posing great challenges during pathological diagnosis.

Sclerosing adenopathy of the prostate is considered a rare variant of adenopathy whose biological behavior remains uncertain, and the research on the risk of prostate cancer following a diagnosis of sclerosing adenopathy is very limited. Sclerosing adenopathy might be one of the precursors of prostate adenocarcinoma; however, this is unlikely because of its rarity and lack of other evidence linking its clinic features or pathology to cancer. When patients with sclerosing adenopathy present with cellular atypia, it is considered atypical sclerosing adenopathy; however, we should emphasize the use of the

term "atypical sclerosing adenopathy" does not imply that these lesions are precancerous. Some scholars have found that DNA aneuploidy occurs in some atypical sclerosing adenopathy cases, but all typical sclerosing adenopathy cases are DNA diploid[28]. Whether sclerosing adenopathy can be used as an independent feature to predict the risk of prostate cancer in men is not yet clear, and a large multi-institutional prospective study is needed for confirmation.

Sclerosing adenopathy has a similar histological pattern to that of the following lesions and is easily misdiagnosed as one of them. In this group of 12 patients with sclerosing adenopathy, two were misdiagnosed as having prostate adenocarcinoma and one was misdiagnosed as having nephrogenic adenoma by the primary pathologist. Therefore, prostate adenocarcinoma sclerosing adenopathy should be distinguished from the following lesions[1]. Prostate adenocarcinoma, which is the most likely misdiagnose. The identification points include: (1) Sclerosing adenopathy is mainly located in the peripheral area, with small and concentrated lesions, unlike cancer, that spreads and whose growth is invasive; (2) Sclerosing adenopathy is glandular hyperplasia with interstitial hyperplasia that is mucoid or fibrous; (3) An eosinophilic basement membrane material is seen around the ducts of patients with sclerosing adenopathy; (4) Mild-to-moderate dysplasia of the glandular epithelium may lead to subnucleation without significantly enlarged nucleoli; (5) There is no amyloid but a myxoid in the glandular follicular lumen. Furthermore, prostate cancer acini are lined with a layer of cuboidal or columnar cells without a distinctly flattened basal cell layer, as evidenced by the negative immunoreactivity for keratin 903[29,30]; and (6) Nephrogenic adenomas differentiate from sclerosing adenomas when they are tubular or solid. Nephrogenic adenomas are usually confined to the lamina propria, covering a single layer of short columnar or subcubical epithelial cells, among which some are shoe-stud-like cells, with round or oval nuclei, visible nucleoli, and most express markers such as CK7, CKH, CKL, and CEA, whereas they do not express the markers P63, PSA, PSAP, GATA3, and CK5/6. Atypical adenomatous hyperplasia is also nodular hyperplasia with clear borders; however, the lesions are often interspersed with a small number of large acinar with a normal structure in the proliferating small glands[31].

In addition, there are no studies that show that the PSA value is related to the occurrence and development of prostate sclerosing adenopathy. In this study, the PSA value of the vast majority of patients with sclerosing adenopathy was within the reference range. Therefore, patients with sclerosing adenopathy should be informed that long-term follow-up and observation are required. If the PSA value increases significantly compared to the original value, and clinical symptoms such as frequent urination, urgency, dysuria, hematuria, and dysuria appear, patients should promptly consult their doctor, since they may have prostate cancer.

CONCLUSION

In conclusion, sclerosing adenopathy of the prostate is a morphological abnormality with characteristic histological features and immunohistochemical profiles. All the available evidence indicates that it is a benign condition that does not require treatment and is not a precancerous condition of prostate cancer. It is important to note, however, that many of the cases encountered to date have had a short follow-up period, and that it may often co-exist with other unrelated cancers in older men. The pathogenesis of this lesion is unclear, but its most striking feature seems to be the ability of cells to differentiate and proliferate. Studying and better understanding the features of sclerosing adenopathy should lead to its appropriate conservative management.

Sclerosing adenopathy of the prostate is a morphological abnormality with characteristic histological features and immunohistochemical profiles. All the available evidence indicates that it is a benign condition that does not require treatment and is not a precancerous condition of prostate cancer. It is important to note, however, that many of the cases encountered to date have had a short follow-up period, and that it may often co-exist with other unrelated cancers in older men. The pathogenesis of this lesion is unclear, but its most striking feature seems to be the ability of cells to differentiate and proliferate. Studying and better understanding the features of sclerosing adenopathy should lead to its appropriate conservative management.

ARTICLE HIGHLIGHTS

Research background

Sclerosing adenopathy of the prostate is a focal proliferative lesion, and the same name is also proposed for the prostate lesion due to its similarity in appearance to sclerosing adenopathy of the breast. Due to the presence of dense small acini in the proliferative stroma, the morphology is similar to that of prostate adenocarcinoma, which brings great challenges to both imaging diagnosis and pathological diagnosis. In addition, a small proportion of sclerosing adenopathy of the prostate co-exists with adenocarcinoma, which makes the diagnosis of this lesion more difficult. So far, there is still a lack of a large number of clinical data sample libraries for clinical pathologists to study in-depth, and further

exploration is needed in the future. Since we are aware of the importance of this lesion morphology, the clinical features, pathological morphology, and immunohistochemical phenotype of prostate sclerosing lesions were retrospectively analyzed in this study to further increase the importance of this lesion.

Research motivation

The objective is to investigate the clinicopathological features, diagnosis, and immunohistochemical phenotypes that distinguish prostate sclerosing adenopathy from other conditions.

Research objectives

This study explores the clinicopathological features, diagnosis, and immunohistochemical phenotypes that distinguish prostate sclerosing adenopathy from other conditions. We believe that our study makes a significant contribution to the literature because we show that this condition is benign, does not require treatment, and is not a precancerous condition of prostate cancer. However, notably, many of the cases encountered to date have had a short follow-up period, and this condition may often co-exist with other unrelated cancers in older men.

Research methods

The clinical data, laboratory tests, pathological morphology, and immunohistochemical phenotypes of 12 cases of prostatic sclerosing adenopathy were retrospectively analyzed, and the relevant literature was reviewed.

Research results

The authors summarized the age, clinical symptoms, medical history, serum total prostate-specific antigen (PSA) value, surgical findings, surgical methods, follow-up time, and follow-up results of 12 patients with prostate sclerosing adenopathy in detail (Table 1). The results of the study showed that the patients were all elderly men, with an average age of 71.7 years. The patients had symptoms of hematuria, frequent urination, urgency, and dysuria to varying degrees. Different degrees of prostate hyperplasia was seen during digital rectal examination and surgery, and the bladder was the most common. Lateral lobe hyperplasia is predominant. The mean postoperative follow-up time was 27.6 mo, and only 1 patient died of bladder cancer. In addition, 11 of the 12 patients had PSA values within the normal reference range. From the above description, it is not difficult to find that the clinical features of sclerosing adenopathy of the prostate are similar to those of benign prostatic hyperplasia and prostate cancer, and most of the patients' PSA values are Within the normal range, suggesting that sclerosing adenopathy may be a benign lesion. Pathologically, the lesions are very complex, with single or mixed glandular tubular, cord-like and linear structures, and focal distribution in benign prostate glands. Unlike prostate adenocarcinoma, immunohistochemical Expression of the basal cell (such as P63, CK5/6) and myoepithelial (Calponin, S100, SMA) markers, provides a very meaningful value for the identification of the two. In practice, when it is difficult to identify prostate sclerosing adenopathy and prostate cancer, we can use immunohistochemical markers to distinguish them. In addition, we can also use immunohistochemical PSA, and PSAP to identify sclerosing adenopathy and other neoplastic lesions such as nephrogenic adenoma. The above pathological characteristics can provide effective help for the follow-up in-depth study of the prostate. However, even though we performed a comprehensive systematic analysis of sclerosing adenopathy of the prostate, this study has some limitations. First, although we predicted a certain relationship between sclerosing adenopathy of the prostate and PSA values, there is still a lack of direct evidence for the two relevance of the person. Secondly, the sample size of this study is too small, and it is necessary to further supplement the sample size and explore it in depth. Finally, whether sclerosing adenopathy is a precancerous lesion of prostate cancer also lacks direct evidence to further prove. These issues need to be further explored in future work.

Research conclusions

Sclerosing adenopathy of the prostate is a morphological abnormality with characteristic histological features and immunohistochemical profiles. All the available evidence indicates that it is a benign condition that does not require treatment and is not a precancerous condition of prostate cancer. It is important to note, however, that many of the cases encountered to date have had a short follow-up period, and that it may often co-exist with other unrelated cancers in older men. The pathogenesis of this lesion is unclear, but its most striking feature seems to be the ability of cells to differentiate and proliferate. Studying and better understanding the features of sclerosing adenopathy should lead to its appropriate conservative management.

Research perspectives

Patients should be informed that long-term follow-up and observation are required. If the PSA value increases significantly compared to the original value, and clinical symptoms such as frequent urination, urgency, dysuria, hematuria, and dysuria appear, patients should promptly see their doctor, since they may have prostate cancer.

FOOTNOTES

Author contributions: Feng RL and Tan ZY contributed equally to this work; Feng RL, Tao YP, Fu S, and Wang HF designed the study; Tan ZY and Tao YP contributed new reagents and analytical tools; Tao YP, Fu S and Wang HF analyzed data; Feng RL and Tan ZY wrote the manuscript. All authors have read and approved the final manuscript.

Institutional review board statement: The study was authorized by the Ethics Committee at The Second Affiliated Hospital of Kunming Medical University.

Conflict-of-interest statement: The authors declared that no competing interests exist.

Data sharing statement: On reasonable request, the corresponding author will provide the analyzed datasets generated during the study.

Open-Access: This article is an open-access article that was selected by an in-house editor and fully peer-reviewed by external reviewers. It is distributed by the Creative Commons Attribution-NonCommercial (CC BY-NC 4.0) license, which permits others to distribute, remix, adapt, build upon this work non-commercially, and license their derivative works on different terms, provided the original work is properly cited and the use is non-commercial. See: https://creativecommons.org/Licenses/by-nc/4.0/

Country/Territory of origin: China

ORCID number: Run-Lin Feng 0000-0002-3532-9450; Yan-Ping Tao 0000-0001-8868-7166; Zhi-Yong Tan 0000-0002-7771-0962; Shi Fu 0000-0003-4023-7195; Hai-Feng Wang 0000-0002-0891-5120.

S-Editor: Ma YJ
L-Editor: A
P-Editor: Ma YJ

REFERENCES

1 **Hansel DE**, Herawi M, Montgomery E, Epstein JI. Spindle cell lesions of the adult prostate. *Mod Pathol* 2007; **20**: 148-158 [PMID: 17170745 DOI: 10.1038/modpathol.3800676]
2 **Jones EC**, Clement PB, Young RH. Sclerosing adenosis of the prostate gland. A clinicopathological and immunohistochemical study of 11 cases. *Am J Surg Pathol* 1991; **15**: 1171-1180 [PMID: 1720930 DOI: 10.1097/00000478-199112000-00008]
3 **Sakamoto N**, Tsuneyoshi M, Enjoji M. Sclerosing adenosis of the prostate. Histopathologic and immunohistochemical analysis. *Am J Surg Pathol* 1991; **15**: 660-667 [PMID: 1711794 DOI: 10.1097/00000478-199107000-00007]
4 **Grignon DJ**, Ro JY, Srigley JR, Troncoso P, Raymond AK, Ayala AG. Sclerosing adenosis of the prostate gland. A lesion showing myoepithelial differentiation. *Am J Surg Pathol* 1992; **16**: 383-391 [PMID: 1373581 DOI: 10.1097/00000478-199204000-00007]
5 **Chen KT**, Schiff JJ. Adenomatoid prostatic tumor. *Urology* 1983; **21**: 88-89 [PMID: 6823716 DOI: 10.1016/0090-4295(83)90138-3]
6 **Gleason DF**. Atypical hyperplasia, benign hyperplasia, and well differentiated adenocarcinoma of the prostate. *Am Surg Pathol* 1985; **9**: 53-67
7 **Young RH**, Clement PB. Sclerosing adenosis of the prostate. *Arch Pathol Lab Med* 1987; **111**: 363-366 [PMID: 2435261]
8 **Helpap B**. The biological significance of atypical hyperplasia of the prostate. *Virchows Arch A Pathol Anat Histol* 1980; **387**: 307-317 [PMID: 7456316 DOI: 10.1007/BF00454834]
9 **Sesterhenn IA**, Mostofi FK, Davis CJ. Fibroepithelial nodules of the prostate simulating carcinoma. Lab Investig 1988; 58: 83A
10 **Chen KT**. Adenomatoid prostatic tumor versus sclerosing adenosis of the prostate. *Am J Surg Pathol* 1990; **14**: 989 [PMID: 1698343 DOI: 10.1097/00000478-199010000-00014]
11 **Young RH**, Clement PB. 'Pseudoadenomatoid' tumour of prostate. *Histopathology* 1990; **16**: 420 [PMID: 1694514 DOI: 10.1111/j.1365-2559.1990.tb01155.x]
12 **Ronnett BM**, Epstein JI. A case showing sclerosing adenosis and an unusual form of basal cell hyperplasia of the prostate. *Am J Surg Pathol* 1989; **13**: 866-872 [PMID: 2476945 DOI: 10.1097/00000478-198910000-00006]
13 **O'Malley FP**, Grignon DJ, Shum DT. Usefulness of immunoperoxidase staining with high-molecular-weight cytokeratin in the differential diagnosis of small-acinar lesions of the prostate gland. *Virchows Arch A Pathol Anat Histopathol* 1990; **417**: 191-196 [PMID: 1696762 DOI: 10.1007/BF01600133]
14 **Srigley JR**, Dardick I, Hartwick RW, Klotz L. Basal epithelial cells of human prostate gland are not myoepithelial cells. A comparative immunohistochemical and ultrastructural study with the human salivary gland. *Am J Pathol* 1990; **136**: 957-966 [PMID: 1691595 DOI: 10.1016/S0015-7368(90)73325-7]
15 **Collina G**, Botticelli AR, Martinelli AM, Fano RA, Trentini GP. Sclerosing adenosis of the prostate. Report of three cases with electronmicroscopy and immunohistochemical study. *Histopathology* 1992; **20**: 505-510 [PMID: 1376714 DOI: 10.1111/j.1365-2559.1992.tb01035.x]
16 **Parker C**, Muston D, Melia J, Moss S, Dearnaley D. A model of the natural history of screen-detected prostate cancer, and

the effect of radical treatment on overall survival. *Br J Cancer* 2006; **94**: 1361-1368 [PMID: 16641912 DOI: 10.1038/sj.bjc.6603105]

17 **Evans AJ**, Henry PC, Van der Kwast TH, Tkachuk DC, Watson K, Lockwood GA, Fleshner NE, Cheung C, Belanger EC, Amin MB, Boccon-Gibod L, Bostwick DG, Egevad L, Epstein JI, Grignon DJ, Jones EC, Montironi R, Moussa M, Sweet JM, Trpkov K, Wheeler TM, Srigley JR. Interobserver variability between expert urologic pathologists for extraprostatic extension and surgical margin status in radical prostatectomy specimens. *Am J Surg Pathol* 2008; **32**: 1503-1512 [PMID: 18708939 DOI: 10.1097/PAS.0b013e31817fb3a0]

18 **Cheng L**, Bostwick DG. Atypical sclerosing adenosis of the prostate: a rare mimic of adenocarcinoma. *Histopathology* 2010; **56**: 627-631 [PMID: 20459573 DOI: 10.1111/j.1365-2559.2010.03525.x]

19 **Luque RJ**, Lopez-Beltran A, Perez-Seoane C, Suzigan S. Sclerosing adenosis of the prostate. Histologic features in needle biopsy specimens. *Arch Pathol Lab Med* 2003; **127**: e14-e16 [PMID: 12562286 DOI: 10.5858/2003-127-e14-SAOT]

20 **Bostwick DG**, Chang L. Overdiagnosis of prostatic adenocarcinoma. *Semin Urol Oncol* 1999; **17**: 199-205 [PMID: 10632121]

21 **Berney DM**, Fisher G, Kattan MW, Oliver RT, Møller H, Fearn P, Eastham J, Scardino P, Cuzick J, Reuter VE, Foster CS; Trans-Atlantic prostate group. Pitfalls in the diagnosis of prostatic cancer: retrospective review of 1791 cases with clinical outcome. *Histopathology* 2007; **51**: 452-457 [PMID: 17880526 DOI: 10.1111/j.1365-2559.2007.02819.x]

22 **Bussolati G**, Alfani V, Weber K, Osborn M. Immunocytochemical detection of actin on fixed and embedded tissues: its potential use in routine pathology. *J Histochem Cytochem* 1980; **28**: 169-173 [PMID: 6986431 DOI: 10.1177/28.2.6986431]

23 **Hara K**, Ito M, Takeuchi J, Iijima S, Endo T, Hidaka H. Distribution of S-100b protein in normal salivary glands and salivary gland tumors. *Virchows Arch A Pathol Anat Histopathol* 1983; **401**: 237-249 [PMID: 6314639 DOI: 10.1007/BF00692648]

24 **Haimoto H**, Hosoda S, Kato K. Differential distribution of immunoreactive S100-alpha and S100-beta proteins in normal nonnervous human tissues. *Lab Invest* 1987; **57**: 489-498 [PMID: 3316838]

25 **Ghadially FN**. Intracytoplasmatic filaments. In: Ghadially FN, editor. Ultrastructural Pathology of the Cell and Matrix, 3rd ed. London: Butterworths, 1988: 839-936

26 **Kuroda N**, Katto K, Ohtsuki Y, Hes O, Michal M, Inoue K, Ohara M, Mizuno K, Lee GH. Hybrid sclerosing adenosis and basal cell hyperplasia of the prostate. *Med Mol Morphol* 2010; **43**: 226-230 [PMID: 21267699 DOI: 10.1007/s00795-009-0449-8]

27 **Kuroda N**, Katto K, Tamura M, Shiotsu T, Nakamura S, Ohtsuki Y, Hes O, Michal M, Inoue K, Ohara M, Mizuno K, Lee GH. Immunohistochemical application of D2-40 as basal cell marker in evaluating atypical small acinar proliferation of initial routine prostatic needle biopsy materials. *Med Mol Morphol* 2010; **43**: 165-169 [PMID: 20857265 DOI: 10.1007/s00795-008-0435-6]

28 **Gill HK**, Ioffe OB, Berg WA. When is a diagnosis of sclerosing adenosis acceptable at core biopsy? *Radiology* 2003; **228**: 50-57 [PMID: 12738875 DOI: 10.1148/radiol.2281020447]

29 **Shao S**, Yao M, Li X, Li C, Chen J, Li G, Jia C, Wu R. Conventional and contrast-enhanced ultrasound features in sclerosing adenosis and correlation with pathology. *Clin Hemorheol Microcirc* 2021; **77**: 173-181 [PMID: 32924999 DOI: 10.3233/CH-200943]

30 **Hedrick L**, Epstein JI. Use of keratin 903 as an adjunct in the diagnosis of prostate carcinoma. *Am J Surg Pathol* 1989; **13**: 389-396 [PMID: 2469333 DOI: 10.1097/00000478-198905000-00006]

31 **Devaraj LT**, Bostwick DG. Atypical basal cell hyperplasia of the prostate. Immunophenotypic profile and proposed classification of basal cell proliferations. *Am J Surg Pathol* 1993; **17**: 645-659 [PMID: 7686348 DOI: 10.1097/00000478-199307000-00001]

World Journal of Clinical Cases

Submit a Manuscript: https://www.f6publishing.com

World J Clin Cases 2022 June 26; 10(18): 6021-6031

DOI: 10.12998/wjcc.v10.i18.6021

ISSN 2307-8960 (online)

ORIGINAL ARTICLE

Retrospective Study

Value of magnetic resonance diffusion combined with perfusion imaging techniques for diagnosing potentially malignant breast lesions

Hui Zhang, Xin-Yi Zhang, Yong Wang

Specialty type: Medicine, research and experimental

Provenance and peer review: Unsolicited article; Externally peer reviewed.

Peer-review model: Single blind

Peer-review report's scientific quality classification

Grade A (Excellent): 0
Grade B (Very good): B, B
Grade C (Good): 0
Grade D (Fair): 0
Grade E (Poor): 0

P-Reviewer: Karavaş E, Turkey; Yu RQ, China

Received: December 7, 2021
Peer-review started: December 7, 2021
First decision: January 25, 2022
Revised: March 23, 2022
Accepted: April 21, 2022
Article in press: April 21, 2022
Published online: June 26, 2022

Hui Zhang, Department of Radiology, Hebei General Hospital, Shijiazhuang 050000, Hebei Province, China

Xin-Yi Zhang, Yong Wang, Department of Radiology, the First Hospital of Hebei Medical University, Shijiazhuang 050000, Hebei Province, China

Corresponding author: Yong Wang, MHSc, Department of Radiology, the First Hospital of Hebei Medical University, No. 89 Donggang Road, Shijiazhuang 050000, Hebei Province, China. wy80868@163.com

Abstract

BACKGROUND

Lesions of breast imaging reporting and data system (BI-RADS) 4 at mammography vary from benign to malignant, leading to difficulties for clinicians to distinguish between them. The specificity of magnetic resonance imaging (MRI) in detecting breast is relatively low, leading to many false-positive results and high rates of re-examination or biopsy. Diffusion-weighted imaging (DWI), combined with perfusion-weighted imaging (PWI), might help to distinguish between benign and malignant BI-RADS 4 breast lesions at mammography.

AIM

To evaluate the value of DWI and PWI in diagnosing BI-RADS 4 breast lesions.

METHODS

This is a retrospective study which included patients who underwent breast MRI between May 2017 and May 2019 in the hospital. The lesions were divided into benign and malignant groups according to the classification of histopathological results. The diagnostic efficacy of DWI and PWI were analyzed respectively and combinedly. The 95 lesions were divided according to histopathological diagnosis, with 46 benign and 49 malignant. The main statistical methods used included the Student t-test, the Mann-Whitney U-test, the chi-square test or Fisher's exact test.

RESULTS

The mean apparent diffusion coefficient (ADC) values in the parenchyma and lesion area of the normal mammary gland were $1.82 \pm 0.22 \times 10^{-3}$ mm^2/s and $1.24 \pm 0.16 \times 10^{-3}$ mm^2/s, respectively ($P = 0.021$). The mean ADC value of the malignant

group was 1.09 ± 0.23 × 10^{-3} mm^2/s, which was lower than that of the benign group (1.42 ± 0.68 × 10^{-3} mm^2/s) (P = 0.016). The volume transfer constant (Ktrans) and rate constant (Kep) values were higher in malignant lesions than in benign ones (all P < 0.001), but there were no significant statistical differences regarding volume fraction (V_e) (P = 0.866). The sensitivity and specificity of PWI combined with DWI (91.7% and 89.3%, respectively) were higher than that of PWI or DWI alone. The accuracy of PWI combined with DWI in predicting pathological results was significantly higher than that predicted by PWI or DWI alone.

CONCLUSION

DWI, combined with PWI, might possibly distinguish between benign and malignant BI-RADS 4 breast lesions at mammography.

Key Words: Magnetic resonance imaging; Breast diseases; Diffusion-weighted imaging; Perfusion-weighted imaging

©The Author(s) 2022. Published by Baishideng Publishing Group Inc. All rights reserved.

Core Tip: Lesions of breast imaging reporting and data system (BI-RADS) at mammography only appeared a wide range of risk of being malignant (2%-96%). The specificity of magnetic resonance imaging in detecting breast is relatively low. This study aimed to evaluate the value of diffusion-weighted imaging (DWI) and perfusion-weighted imaging (PWI) in diagnosing BI-RADS 4 breast lesions. The diagnostic efficacy of DWI and PWI were analyzed respectively and jointly. The results suggested DWI, combined with PWI, might possibly help distinguish benign breast lesions from malignant ones and provide clear diagnostic results for patients with potentially malignant BI-RADS 4 lesions at mammography.

Citation: Zhang H, Zhang XY, Wang Y. Value of magnetic resonance diffusion combined with perfusion imaging techniques for diagnosing potentially malignant breast lesions. *World J Clin Cases* 2022; 10(18): 6021-6031
URL: https://www.wjgnet.com/2307-8960/full/v10/i18/6021.htm
DOI: https://dx.doi.org/10.12998/wjcc.v10.i18.6021

INTRODUCTION

Breast cancer is one of the most common malignant tumors threatening women[1]. In recent years, the incidence of breast cancer has increased year by year, topping all types of cancer in Chinese women[2]. Magnetic resonance imaging (MRI) has become an essential examination method to diagnose breast lesions due to the avoidance of ionizing radiation, high soft-tissue resolution, multi-parameter imaging, multi-sequence imaging, and high sensitivity[3,4]. Nevertheless, the specificity of MRI in detecting breast is relatively low, leading to many false-positive results and high rates of re-examination or biopsy [3,4].

Novel functional MRI techniques, including diffusion-weighted imaging (DWI), perfusion-weighted imaging (PWI), and other non-invasive detection methods, have enabled the detection of pathological conditions of tissues to reach on a molecular-level, as well as the detection of functional status and change in mechanisms of organs, tissues, and cells *in vivo*[5]. DWI is considered the most effective modality for malignant tumor screening and therapeutic effect assessment for breast cancer[6-9]. PWI can be applied in detecting blood perfusion in tissues, where the perfusion imaging pattern is closely related to the density of newly-generated microvessels in tumors[10,11]. Nevertheless, these techniques have not been widely validated in clinical practice since they mainly act as auxiliary roles for assessing suspicious lesions[8,12,13]. DWI can also monitor the treatment response to neoadjuvant chemotherapy [14] and help to determine the subtypes of breast cancer[15].

According to the MRI breast imaging reporting and data system (BI-RADS) (5th edition), potentially malignant breast lesions are classified as the 4th category (BI-RADS 4) with a wide variation with regard to the risk of malignancy, from 2% to 95%[16]. BI-RADS 4 lesions could be anything from benign to malignant, resulting in the difficulties for clinicians to distinguish between them[17-20].

Therefore, the present study aimed to investigate the diagnostic efficiency of the apparent diffusion coefficient (ADC) combined with PWI in determining the nature of lesions categorized as BI-RADS 4. The results help to decide the exact nature of breast lesions before the patients undergo biopsy.

MATERIALS AND METHODS

Study design and patients

This retrospective study included patients who underwent breast MRI examination, including symptomatic patients presenting to clinic and patients detected abnormalities in regular screening, between May 2017 and May 2019 at the Department of Radiology of Hospital. The diagnostic criteria were the 5th edition of MRI BI-RADS[16].

The inclusion criteria were: (1) Age over 20 years old; (2) BI-RADS 4 based on mammography only; (3) Lesion > 5.0 mm; (4) The MRI examination of all lesions was completed before needle biopsy; and (5) The MRI examination included DWI and dynamic contrast enhancement imaging (DCE-MRI) in addition to the conventional plain scans. The exclusion criteria were: (1) Received neoadjuvant chemotherapy which might affect the MRI readings[14]; or (2) Clinical or pathological T4 lesion.

The study was reviewed and approved by the First Hospital of Hebei Medical University. The need for individual informed consent was waived by the committee.

MRI acquisition

All examinations were performed with the patients in the prone position. MRI was performed by a 1.5-T MRI scanner (Signa Excite HDxT; GE Healthcare, Waukesha, WI, United States) and a 3.0-T MRI scanner (GE Silent Discovery 750W; GE Healthcare, Waukesha, WI, United States) with an 8-channel phased-array bilateral breast coil. The scanning sequences and corresponding parameters were: (1) T2WI fat-suppressed fast spin-echo (FSE): Repetition time (TR) 6079 ms, echo time (TE) 85 ms, flip angle (FA) 111°, field-of-view (FOV) 36 × 36 mm^2, matrix size 320 × 256, number of excitation (NEX) 1.0, slice thickness (ST) 5.0 mm, scan time 2.44 s; (2) T1WI FSE: TR 697 ms, TE min full, FA 111°, FOV 36 × 36 mm^2, matrix size 320 × 256, NEX 1.0, ST 5.0 mm, scan time 1.05 s; (3) DWI: TR 2881.4 ms, TE minimum, FOV 36 × 36 mm^2, matrix size 128 × 128, ST 5.0 mm, b values 0-800 s/mm^2, scan time 2.01 s; and (4) T1WI dynamic perfusion: TR 5.5 ms, TE min full, FA 12°, FOV 34 × 34 mm^2, matrix size 160 × 150, ST 5.0 mm, 40 phase scanning, scan time 7.12 s (Figure 1). The contrast agent was gadopentetate dimeglumine (Jiangsu Hengrui Pharmaceutical Co., Ltd., China) and was administered at a dose of 0.2 mmol/kg with infusion rate of 3.0 mL/s. The intravenous injection of contrast agent began 30 s after the start of the scanning.

MRI analysis

The collected data were transmitted to the General Electric Assistant Diagnostic Workstation 4.6, and the image data were analyzed. Then two radiologists with more than 5 years of experience in breast lesion diagnosis provided an independent analysis and assessment without knowing the clinical and pathological results. A consensus was reached through discussion in case of any inconsistencies between them. Regions with enhancements in DCE-MRI sequence and high signal intensity in the DWI sequence were considered to be lesions. After obtaining the ADC map by post-processing, the ADC values were measured by manually placing the elliptic in the lesion area, and covering at least four minimum pixels, with the average value based on three measurements. Meanwhile, the volume transfer constant (K^{trans}), rate constant (K_{ep}), and extravascular extracellular volume fraction (V_e) in this region were measured (Figure 2).

Pathological features

The lesion samples gained from needle biopsy were sent to the Department of Pathology at the Hospital to obtain the pathological results. The lesions were divided into benign and malignant groups according to the classification of histopathological results. The benign group included non-hyperplasic, hyperplasic, and atypical hyperplasic lesions. The malignant group included ductal carcinoma in situ and any type of invasive carcinoma[21]. For samples with mixed pathological characteristics, the more severe lesion prevailed (Figure 3). Surgical resection was performed for all patients whose pre-surgical needle biopsy results demonstrated either malignant lesions or atypical lesions.

Statistical analysis

All data were analyzed using SPSS Version 18.0 (IBM, Armonk, NY, United States). Continuous data were presented as means ± SD or medians (range), according to the results of the Kolmogorov-Smirnov test for normal distribution, and analyzed using the Student *t*-test or the Mann-Whitney U-test, as appropriate. Categorical data were presented as numbers (percentages) and analyzed using the chi-square test or Fisher's exact test. Differences with $P < 0.05$ were considered statistically significant.

RESULTS

Characteristics of the patients and lesions

This study included 95 breast lesions in 83 female patients, of which 36 patients were in the benign

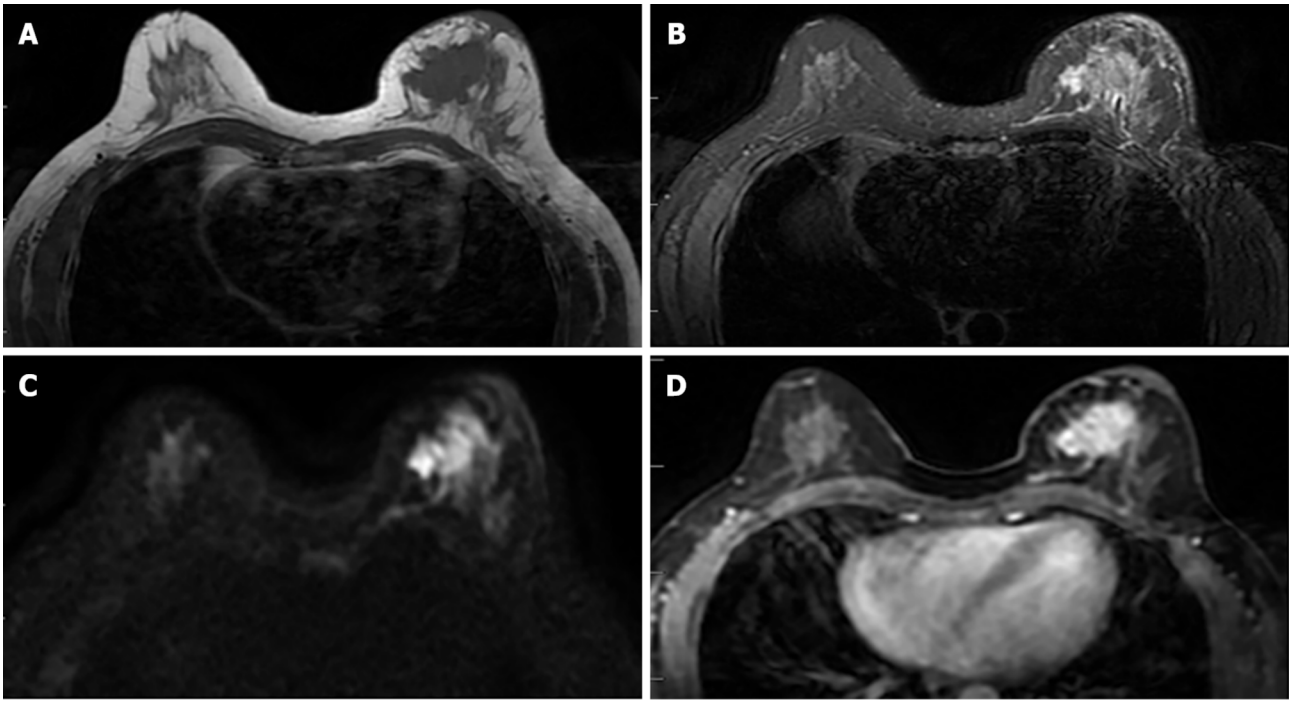

DOI: 10.12998/wjcc.v10.i18.6021 **Copyright** ©The Author(s) 2022.

Figure 1 Female, 52 years old, breast carcinoma. A and B: The left breast mass in T1WI and T2WI fat-saturated sequence is shown as a long T1 and long T2 signal shadow; C: The left breast mass is shown as a high signal in the diffusion-weighted imaging image; D: Obvious enhancement of the tumor in the transverse section of the enhanced scan.

group, and 47 patients were in the malignant group. All women were Chinese Han. There were no statistically significant differences between the benign and malignant groups in terms of age, family history, history of benign breast disease, history of marriage, history of delivery, long-term use of exogenous estrogen, alcohol abuse, and age of menarche, but there was a statistically significant difference between the groups in terms of the age of menopause (P = 0.021) (Table 1). As for the 95 lesions detected, 46 (48.4%) lesions were in the benign group, and 49 (51.6%) lesions were in the malignant group. The average size of the lesions was 2.2 cm (0.6-5.8 cm); the lesions were larger in the malignant group than in the benign group (median, 2.4 cm *vs* 1.5 cm, P = 0.007) (Table 2).

Perfusion parameters

Table 2 shows that the K^{trans} and K_{ep} values were both larger in the malignant group compared with the benign group (both P < 0.001), but there were no significant statistical differences regarding V_e (P = 0.866).

Diffusion parameters

The ADC values in the parenchyma and lesion area of the normal mammary gland were 1.82 ± 0.22 × 10^{-3} mm^2/s and 1.24 ± 0.16 × 10^{-3} mm^2/s, respectively (P = 0.021). The mean ADC value of the malignant group was 1.09 ± 0.23 × 10^{-3} mm^2/s, which was lower than that of the benign group (1.42 ± 0.68 × 10^{-3} mm^2/s) (P = 0.016). Based on the literature[22], an ADC value of 1.20 × 10^{-3} mm^2/s was used as the threshold for malignant lesions. Lesions with an ADC value lower than the threshold were considered malignant lesions, and those with an ADC value higher than the threshold were considered benign lesions (Table 3).

Diagnostic efficacy of DWI and PWI

We evaluated the diagnostic efficiency of PWI and DWI and combined examination techniques compared to the pathological results. The sensitivity and specificity of combined PWI and DWI were higher than those of PWI or DWI alone. The accuracy of combining the two test methods in predicting pathological results was also significantly higher than that predicted by PWI or DWI alone (Table 4).

DISCUSSION

BI-RADS 4 breast lesions at mammography only appeared a wide range of risk of being malignant (2%-96%)[17-20]. DWI and PWI could help discriminate benign from malignant lesions[6,10,11], but those

Table 1 Comparison of the clinical features between benign and malignant patients.

Variables	Benign (*n* = 36)	Malignant (*n* = 47)	*P* value
Age (yr)	44 (28-54)	57 (27-79)	0.238
Family history, *n* (%)	3 (9.7)	2 (3.8)	0.316
History of benign breast diseases, *n* (%)	4 (14.8)	5 (9.6)	0.673
History of marriage, *n* (%)	31 (86.1)	45 (95.7)	0.583
History of delivery, *n* (%)	29 (80.6)	42 (89.4)	0.402
Long term use of exogenous estrogen, *n* (%)	0	6 (11.8)	0.242
Alcohol abuse, *n* (%)	0	1 (1.9)	0.709
Age of menarche, *n* (%)			0.477
< 12 years old	2 (6.5)	5 (9.6)	
≥ 12 years old	29 (93.5)	47 (90.4)	
Age of menopause, *n* (%)[1]			0.021
> 55 years old	3 (9.7)	7 (13.5)	
≤ 55 years old	21 (67.7)	38 (73.1)	

[1]Patients younger than 55 and not menopausal were not included in this parameter.

Table 2 Characteristics of the lesions

Parameters		Benign (*n* = 46)	Malignant (*n* = 49)	*P* value
Lesion size (cm)		1.5 (0.6-2.7)	2.4 (1.6-5.7)	0.007
Perfusion imaging parameters	K^{trans}	0.076 ± 0.001	0.681 ± 0.013	< 0.001
	K_{ep}	0.140 ± 0.004	1.892 ± 0.021	< 0.001
	V_e	0.577 ± 0.012	0.316 ± 0.010	0.866

K^{trans}: Volume transfer constant; K_{ep}: Rate constant; V_e: Extravascular extracellular volume fraction.

techniques are mainly considered as accessory to standard imaging modalities[12]. Therefore, this study aimed to evaluate the efficiency of DWI and PWI in diagnosing breast lesions categorized as BI-RADS 4 at mammography. The results suggested that DWI, combined with PWI, might possibly distinguish between benign and malignant BI-RADS 4 breast lesions at mammography.

DWI has the advantages of short acquisition time, unnecessary for a paramagnetic contrast agent, and high sensitivity[23]. Therefore, DWI is widely used in the differential diagnosis of breast diseases, with the scanning parameters and diagnostic specificity being constantly optimized[24]. Among the new MRI techniques, DWI is considered a useful diagnostic method in differentiating benign from malignant lesions and assessing the therapeutic effect[2]. Studies showed that the ADC values of typical malignant tumors are lower than those of benign hyperplasic tissues and normal tissues[25,26]. This finding is partly attributable to the small extracellular space resulting from the high cell density of malignant tumors, which leads to the restricted diffusion of water molecules[25]. This complicated microscopic phenomenon can be partially converted into quantifiable parameters by measuring ADC values, which can thus be applied in distinguishing between different tissue sources[25,26]. In the present study, the mean ADC value of the observed lesion areas was lower than that of the normal breast tissues, and the mean ADC value of the malignant group was the lowest (except for necrotic areas). This finding is consistent with the results reported in previous studies[27,28]. Tsushima *et al*[29] found that DWI is extremely helpful for diagnosing breast cancer, which its sensitivity and specificity achieved 89% and 77%, respectively.

Many studies have been conducted on the threshold point of the ADC value used to distinguish benign lesions from malignant ones, and their conclusions differ[28,30,31]. By referring to the methods used in the literature[22] and diagnostic tests, the present study used 1.20×10^{-3} mm^2/s as the critical ADC value to distinguish benign lesions from malignant ones in the DWI examination of breast lesions. The accuracy obtained by comparison with the pathological results was approximately 73%. Using a relatively high ADC value as the critical point can effectively avoid over-diagnosis of BI-RADS 4 Lesions

Table 3 Apparent diffusion coefficient values by histopathological results, in relation to the 1.20 × 10^{-3} mm^2/s cut-off point, among the 95 lesions evaluated (mean ± SD)

Histopathological results	Number of lesions		< 1.20 × 10^{-3} mm^2/s, *n* (%)	≥ 1.20 × 10^{-3} mm^2/s, *n* (%)
Benign	46	1.42 ± 0.24	9 (19.6)	37 (80.4)
Fibrocystic hyperplasia	19	1.44 ± 0.32	4 (21.1)	15 (78.9)
Fibroadenoma	7	1.49 ± 0.27	2 (28.6)	5 (71.4)
Adenopathy	13	1.38 ± 0.26	2 (15.4)	11 (84.6)
Catheter dilatation	2	1.69 ± 0.36	1 (50.0)	1 (50.0)
Inflammation	5	1.16 ± 0.08	3 (60.0)	2 (40.0)
Malignant	49	1.08 ± 0.30	35 (71.4)	14 (28.6)
Ductal carcinoma in situ	16	1.24 ± 0.25	9 (56.3)	7 (43.7)
Invasive ductal carcinoma	24	0.92 ± 0.23	21 (87.5)	3 (12.5)
Invasive lobular carcinoma	5	1.16 ± 0.19	3 (60.0)	2 (40.0)
Neuroendocrine carcinoma	3	0.95 ± 0.67	2 (66.7)	1 (33.3)
Invasive mucinous carcinoma	1	1.84 ± 0.56	0 (0)	1 (100)

Table 4 Imaging diagnosis and pathological results of granulomatous mastitis and breast cancer by perfusion-weighted imaging and diffusion-weighted imaging

	Positive	False-positive	Negative	False-negative	Total	Sensitivity (%)	Specificity (%)	Accuracy (%)
PWI	41	8	39	7	95	85.4	83.0	84.2
DWI	35	14	37	9	95	79.5	72.5	75.8
PWI combined with DWI	44	5	42	4	95	91.7	89.3	90.5

Positive: Diagnosed malignant by magnetic resonance imaging; Negative: Diagnosed benign by magnetic resonance imaging; PWI: Perfusion-weighted imaging; DWI: Diffusion-weighted imaging.

at mammography. Except for 5.5% of the cases in this study, which were mucinous carcinomas (with an ADC value of 2.20 × 10^{-3} mm^2/s), all lesions with ADC values > 1.74 × 10^{-3} mm^2/s were nonmalignant, as indicated by the final pathological results. This critical point is close to the average of the critical values ranging from 1.60-1.81 × 10^{-3} mm^2/s, as reported by previous studies[22,28,30]. Ren *et al*[31] showed that the ADC values could be used to evaluate breast lesions' malignancy. Spick *et al*[32] also stated that DWI might partially eliminate the need for MRI-guided biopsies. They revealed that when the ADC value of 1.58 × 10^{-3} mm^2/s was used as the threshold, no false-negative occurred.

PWI is an imaging method that can clearly display microvessel density[33] and reflect the neovascularization of tumors, which is a necessary condition for tumor growth, progression, and metastasis[7,8,12,34]. The hemodynamic information that it provides has enabled quantitative analysis. The parameters include K^{trans} (which refers to the rate of the contrast agent diffusing from the inside to the outside of the blood vessel), K_{ep} (which refers to the rate of the contrast agent in the extravascular tissue space returning to the blood vessel after diffusing for a period of time), and V_e (which is the volumetric ratio of the extravascular extracellular space to the total voxel). These parameters are able to quantitatively evaluate blood perfusion in the diseased tissue[7,35], thereby enabling quantitative and differential diagnoses of lesions. In the present study, there was a significant increase in the number of blood vessels throughout the breast in sequence of PWI. The reason may be that tumor blood vessels face smaller growth resistance, and the high metabolism level of tumors gradually stimulates the regeneration of blood vessels throughout the breast. In addition, studies have shown that breast cancer with multifocal lesions, large masses, and axillary lymph node metastases have also exhibited pronounced neovascularization throughout the breast, suggesting a poor prognosis[36]. It can thus be inferred that the significant increase in the number of new blood vessels in the breast with cancerous lesions will suggest the progressive growth of malignant lesions and intramammary metastasis.

Conventional MRI scanning techniques combined with DWI and PWI can provide information on the internal structure of the breast[27], reflect the pathological characteristics of the tissue more accurately, and improve the diagnostic accuracy for breast lesions by measuring ADC values and quantitative

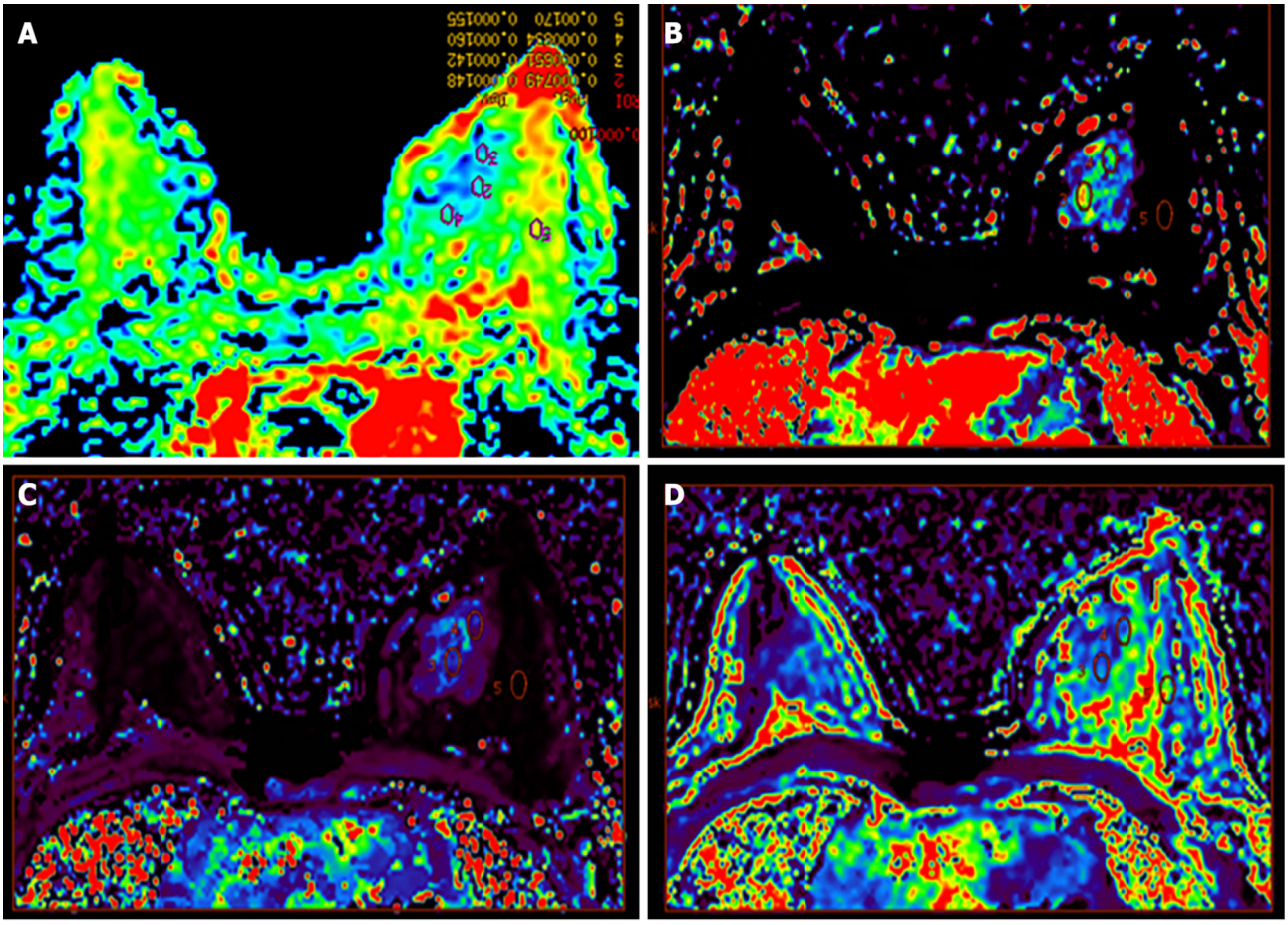

DOI: 10.12998/wjcc.v10.i18.6021 **Copyright** ©The Author(s) 2022.

Figure 2 Color image. A: The apparent diffusion coefficient (ADC) color image allows the multipoint measurement of the ADC value; B-D: Multipoint measurement of olume transfer constant (K^{trans}) (B), rate constant (K_{ep}) (C), and extravascular extracellular volume fraction (V_e) (D) of the lesions and adjacent normal tissues.

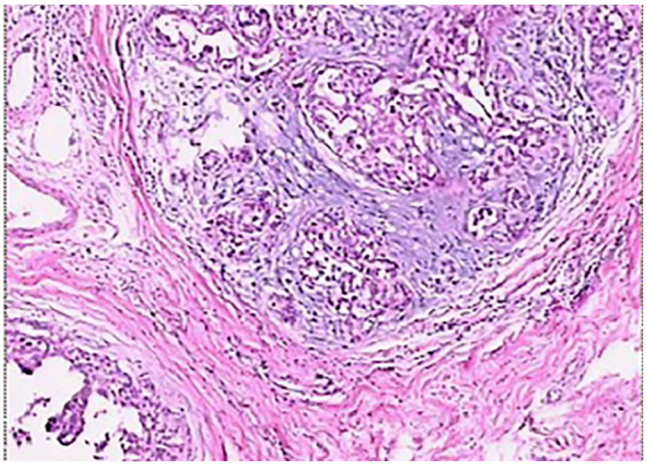

DOI: 10.12998/wjcc.v10.i18.6021 **Copyright** ©The Author(s) 2022.

Figure 3 Histopathological examination showing moderate nuclear grade ductal carcinoma in situ, with stove shape II invasive ductal carcinoma (HE × 100).

parameters of PWI[7]. This method achieves the transition from qualitative diagnosis to quantitative diagnosis, thereby associating BI-RADS 4 lesions with corresponding histopathological grades. By using a DWI sequence combined with the quantitative parameters of PWI, a pathological classification of potentially malignant lesions, which were diagnosed as BI-RADS 4 lesions by mammography, was performed in this study to improve the accuracy of imaging diagnosis and provide different clinical recommendations. The present study proved that the sensitivity and specificity of DWI combined with

PWI were higher than that of DWI and PWI alone. Nevertheless, additional studies are necessary to further confirm those results. Follow-up observations with imaging methods should be performed for those diagnosed with benign lesions, and needle biopsies should be performed, if necessary, for those diagnosed as malignant lesions.

This study has limitations. Firstly, the purpose of this study was to group BI-RADS 4 lesions at mammography based on their histological features by dividing them into two groups. Including atypical hyperplasic lesions in the benign group may result in bias, and different histological subtypes are included in the same group. As a result, the ADC values of the group may vary greatly. Secondly, two radiologists independently evaluated the slides, but the concordance was not examined. Thirdly, ultrasound data were not available for many patients because the physicians decided not to perform it, the patient refused, or it was done at another hospital, and thus could not be analyzed. Fourthly, the sample size was small, and receiver operating characteristics and multivariable analyses could not be performed. Studies with larger sample size are necessary to determine the real diagnostic value of DWI combined for PWI and determine the adequate cutoff values for the different quantitative parameters.

CONCLUSION

In conclusion, DWI, combined with PWI, might possibly help distinguish benign breast lesions from malignant ones and provide clear diagnostic results for patients with potentially malignant BI-RADS 4 lesions at mammography.

ARTICLE HIGHLIGHTS

Research background

In recent years, the incidence of breast cancer has increased year by year, topping all types of cancer in Chinese women. Novel functional magnetic resonance imaging (MRI) techniques, including diffusion-weighted imaging (DWI), perfusion-weighted imaging (PWI), and other non-invasive detection methods, have enabled the detection of pathological conditions of tissues to reach on a molecular-level, as well as the detection of functional status and change in mechanisms of organs, tissues, and cells in vivo. According to the MRI breast imaging reporting and data system (BI-RADS) (5th edition), potentially malignant breast lesions are classified as the 4th category (BI-RADS 4) with a wide variation with regard to the risk of malignancy, from 2% to 95%. The results of this study help to decide the exact nature of breast lesions before the patients undergo biopsy.

Research motivation

This study aimed to evaluate the value of DWI and PWI in diagnosing BI-RADS 4 breast lesions and analyze the diagnostic efficacy of DWI and PWI respectively and jointly, which could help to decide the exact nature of breast lesions.

Research objectives

The main objective of this study is to improve the specificity of MRI in detecting breast. MRI has become an essential examination method to diagnose breast lesions due to the avoidance of ionizing radiation, high soft-tissue resolution, multi-parameter imaging, multi-sequence imaging, and high sensitivity. When realizing the objective, the diagnostic efficiency of the apparent diffusion coefficient (ADC) combined with PWI in determining the nature of lesions categorized as BI-RADS 4 will be improved.

Research methods

This retrospective study included patients who underwent breast MRI between May 2017 and May 2019. The lesions were divided into benign and malignant groups according to the classification of histopathological results. The diagnostic efficacy of DWI and PWI were analyzed respectively and combinely.

Research results

The mean ADC value of the malignant group was lower than that of the benign group (P = 0.016). The volume transfer constant (K^{trans}) and rate constant (K_{ep}) values were higher in malignant lesions than in benign ones (all P < 0.001). The sensitivity and specificity of PWI combined with DWI (91.7% and 89.3%, respectively) were higher than that of PWI or DWI alone. Studies with larger sample size are necessary to determine the real diagnostic value of DWI combined for PWI and determine the adequate cutoff values for the different quantitative parameters.

Research conclusions

The sensitivity and specificity of combined PWI and DWI were higher than those of PWI or DWI alone. DWI, combined with PWI, might possibly help distinguish benign breast lesions from malignant ones and provide clear diagnostic results for patients with potentially malignant BI-RADS 4 lesions at mammography.

Research perspectives

To improve the accuracy of combining PWI and DWI in predicting pathological results.

FOOTNOTES

Author contributions: Zhang H and Wang Y designed the experiment. Zhang XY implemented the experiment; Zhang H and Wang Y drafted the manuscript; Wang Y was responsible for the paper.

Institutional review board statement: The study was reviewed and approved by the First Hospital of Hebei Medical University Institutional Review Board, No. 20210907.

Informed consent statement: All study participants, or their legal guardian, provided informed written consent prior to study enrollment.

Conflict-of-interest statement: The authors have no conflicts of interest to disclose.

Data sharing statement: Technical appendix, statistical code, and dataset available from the corresponding author at wy80868@163.com. Participants gave informed consent for data sharing.

Open-Access: This article is an open-access article that was selected by an in-house editor and fully peer-reviewed by external reviewers. It is distributed in accordance with the Creative Commons Attribution NonCommercial (CC BY-NC 4.0) license, which permits others to distribute, remix, adapt, build upon this work non-commercially, and license their derivative works on different terms, provided the original work is properly cited and the use is non-commercial. See: https://creativecommons.org/Licenses/by-nc/4.0/

Country/Territory of origin: China

ORCID number: Hui Zhang 0000-0002-2971-5216; Xin-Yi Zhang 0000-0001-8705-4308; Yong Wang 0000-0001-5869-2044.

S-Editor: Fan JR
L-Editor: A
P-Editor: Fan JR

REFERENCES

1 **Bray F**, Ferlay J, Soerjomataram I, Siegel RL, Torre LA, Jemal A. Global cancer statistics 2018: GLOBOCAN estimates of incidence and mortality worldwide for 36 cancers in 185 countries. *CA Cancer J Clin* 2018; **68**: 394-424 [PMID: 30207593 DOI: 10.3322/caac.21492]
2 **Wong IO**, Schooling CM, Cowling BJ, Leung GM. Breast cancer incidence and mortality in a transitioning Chinese population: current and future trends. *Br J Cancer* 2015; **112**: 167-170 [PMID: 25290086 DOI: 10.1038/bjc.2014.532]
3 **Radhakrishna S**, Agarwal S, Parikh PM, Kaur K, Panwar S, Sharma S, Dey A, Saxena KK, Chandra M, Sud S. Role of magnetic resonance imaging in breast cancer management. *South Asian J Cancer* 2018; **7**: 69-71 [PMID: 29721466 DOI: 10.4103/sajc.sajc_104_18]
4 **Mann RM**, Cho N, Moy L. Breast MRI: State of the Art. *Radiology* 2019; **292**: 520-536 [PMID: 31361209 DOI: 10.1148/radiol.2019182947]
5 **Soares JM**, Magalhães R, Moreira PS, Sousa A, Ganz E, Sampaio A, Alves V, Marques P, Sousa N. A Hitchhiker's Guide to Functional Magnetic Resonance Imaging. *Front Neurosci* 2016; **10**: 515 [PMID: 27891073 DOI: 10.3389/fnins.2016.00515]
6 **Ei Khouli RH**, Jacobs MA, Mezban SD, Huang P, Kamel IR, Macura KJ, Bluemke DA. Diffusion-weighted imaging improves the diagnostic accuracy of conventional 3.0-T breast MR imaging. *Radiology* 2010; **256**: 64-73 [PMID: 20574085 DOI: 10.1148/radiol.10091367]
7 **Baltzer P**, Mann RM, Iima M, Sigmund EE, Clauser P, Gilbert FJ, Martincich L, Partridge SC, Patterson A, Pinker K, Thibault F, Camps-Herrero J, Le Bihan D; EUSOBI international Breast Diffusion-Weighted Imaging working group. Diffusion-weighted imaging of the breast-a consensus and mission statement from the EUSOBI International Breast Diffusion-Weighted Imaging working group. *Eur Radiol* 2020; **30**: 1436-1450 [PMID: 31786616 DOI: 10.1007/s00330-019-06510-3]
8 **Iima M**, Honda M, Sigmund EE, Ohno Kishimoto A, Kataoka M, Togashi K. Diffusion MRI of the breast: Current status and future directions. *J Magn Reson Imaging* 2020; **52**: 70-90 [PMID: 31520518 DOI: 10.1002/jmri.26908]

9 **Partridge SC**, Amornsiripanitch N. DWI in the Assessment of Breast Lesions. *Top Magn Reson Imaging* 2017; **26**: 201-209 [PMID: 28961569 DOI: 10.1097/RMR.0000000000000137]

10 **Jiang L**, Lu X, Hua B, Gao J, Zheng D, Zhou Y. Intravoxel Incoherent Motion Diffusion-Weighted Imaging Versus Dynamic Contrast-Enhanced Magnetic Resonance Imaging: Comparison of the Diagnostic Performance of Perfusion-Related Parameters in Breast. *J Comput Assist Tomogr* 2018; **42**: 6-11 [PMID: 28786902 DOI: 10.1097/RCT.0000000000000661]

11 **Jia ZZ**, Shi W, Shi JL, Shen DD, Gu HM, Zhou XJ. Comparison between perfusion computed tomography and dynamic contrast-enhanced magnetic resonance imaging in assessing glioblastoma microvasculature. *Eur J Radiol* 2017; **87**: 120-124 [PMID: 28034567 DOI: 10.1016/j.ejrad.2016.12.016]

12 **Zervoudis S**, Iatrakis G, Tomara E, Bothou A, Papadopoulos G, Tsakiris G. Main controversies in breast cancer. *World J Clin Oncol* 2014; **5**: 359-373 [PMID: 25114851 DOI: 10.5306/wjco.v5.i3.359]

13 **Avendano D**, Marino MA, Leithner D, Thakur S, Bernard-Davila B, Martinez DF, Helbich TH, Morris EA, Jochelson MS, Baltzer PAT, Clauser P, Kapetas P, Pinker K. Limited role of DWI with apparent diffusion coefficient mapping in breast lesions presenting as non-mass enhancement on dynamic contrast-enhanced MRI. *Breast Cancer Res* 2019; **21**: 136 [PMID: 31801635 DOI: 10.1186/s13058-019-1208-y]

14 **Liu Z**, Li Z, Qu J, Zhang R, Zhou X, Li L, Sun K, Tang Z, Jiang H, Li H, Xiong Q, Ding Y, Zhao X, Wang K, Liu Z, Tian J. Radiomics of Multiparametric MRI for Pretreatment Prediction of Pathologic Complete Response to Neoadjuvant Chemotherapy in Breast Cancer: A Multicenter Study. *Clin Cancer Res* 2019; **25**: 3538-3547 [PMID: 30842125 DOI: 10.1158/1078-0432.CCR-18-3190]

15 **Maric J**, Boban J, Ivkovic-Kapicl T, Djilas D, Vucaj-Cirilovic V, Bogdanovic-Stojanovic D. Differentiation of Breast Lesions and Distinguishing Their Histological Subtypes Using Diffusion-Weighted Imaging and ADC Values. *Front Oncol* 2020; **10**: 332 [PMID: 32232007 DOI: 10.3389/fonc.2020.00332]

16 **American College of Radiology**. ACR BI-RADS®, Breast Imaging Reporting and Data System. Reston: American College of Radiology (2013).

17 **Elverici E**, Barça AN, Aktaş H, Özsoy A, Zengin B, Çavuşoğlu M, Araz L. Nonpalpable BI-RADS 4 breast lesions: sonographic findings and pathology correlation. *Diagn Interv Radiol* 2015; **21**: 189-194 [PMID: 25835079 DOI: 10.5152/dir.2014.14103]

18 **Liu G**, Zhang MK, He Y, Liu Y, Li XR, Wang ZL. BI-RADS 4 breast lesions: could multi-mode ultrasound be helpful for their diagnosis? *Gland Surg* 2019; **8**: 258-270 [PMID: 31328105 DOI: 10.21037/gs.2019.05.01]

19 **Bennani-Baiti B**, Dietzel M, Baltzer PA. MRI for the assessment of malignancy in BI-RADS 4 mammographic microcalcifications. *PLoS One* 2017; **12**: e0188679 [PMID: 29190656 DOI: 10.1371/journal.pone.0188679]

20 **Strobel K**, Schrading S, Hansen NL, Barabasch A, Kuhl CK. Assessment of BI-RADS category 4 Lesions detected with screening mammography and screening US: utility of MR imaging. *Radiology* 2015; **274**: 343-351 [PMID: 25271857 DOI: 10.1148/radiol.14140645]

21 **Hartmann LC**, Sellers TA, Frost MH, Lingle WL, Degnim AC, Ghosh K, Vierkant RA, Maloney SD, Pankratz VS, Hillman DW, Suman VJ, Johnson J, Blake C, Tlsty T, Vachon CM, Melton LJ 3rd, Visscher DW. Benign breast disease and the risk of breast cancer. *N Engl J Med* 2005; **353**: 229-237 [PMID: 16034008 DOI: 10.1056/NEJMoa044383]

22 **Maltez de Almeida JR**, Gomes AB, Barros TP, Fahel PE, de Seixas Rocha M. Subcategorization of Suspicious Breast Lesions (BI-RADS Category 4) According to MRI Criteria: Role of Dynamic Contrast-Enhanced and Diffusion-Weighted Imaging. *AJR Am J Roentgenol* 2015; **205**: 222-231 [PMID: 26102403 DOI: 10.2214/AJR.14.13834]

23 **Baliyan V**, Das CJ, Sharma R, Gupta AK. Diffusion weighted imaging: Technique and applications. *World J Radiol* 2016; **8**: 785-798 [PMID: 27721941 DOI: 10.4329/wjr.v8.i9.785]

24 **Thomassin-Naggara I**, De Bazelaire C, Chopier J, Bazot M, Marsault C, Trop I. Diffusion-weighted MR imaging of the breast: advantages and pitfalls. *Eur J Radiol* 2013; **82**: 435-443 [PMID: 22658868 DOI: 10.1016/j.ejrad.2012.03.002]

25 **Pereira FP**, Martins G, Carvalhaes de Oliveira Rde V. Diffusion magnetic resonance imaging of the breast. *Magn Reson Imaging Clin N Am* 2011; **19**: 95-110 [PMID: 21129637 DOI: 10.1016/j.mric.2010.09.001]

26 **Partridge SC**, Nissan N, Rahbar H, Kitsch AE, Sigmund EE. Diffusion-weighted breast MRI: Clinical applications and emerging techniques. *J Magn Reson Imaging* 2017; **45**: 337-355 [PMID: 27690173 DOI: 10.1002/jmri.25479]

27 **Pereira FP**, Martins G, Figueiredo E, Domingues MN, Domingues RC, da Fonseca LM, Gasparetto EL. Assessment of breast lesions with diffusion-weighted MRI: comparing the use of different b values. *AJR Am J Roentgenol* 2009; **193**: 1030-1035 [PMID: 19770326 DOI: 10.2214/AJR.09.2522]

28 **Brandão AC**, Lehman CD, Partridge SC. Breast magnetic resonance imaging: diffusion-weighted imaging. *Magn Reson Imaging Clin N Am* 2013; **21**: 321-336 [PMID: 23642556 DOI: 10.1016/j.mric.2013.01.002]

29 **Tsushima Y**, Takahashi-Taketomi A, Endo K. Magnetic resonance (MR) differential diagnosis of breast tumors using apparent diffusion coefficient (ADC) on 1.5-T. *J Magn Reson Imaging* 2009; **30**: 249-255 [PMID: 19629992 DOI: 10.1002/jmri.21854]

30 **Parsian S**, Rahbar H, Allison KH, Demartini WB, Olson ML, Lehman CD, Partridge SC. Nonmalignant breast lesions: ADCs of benign and high-risk subtypes assessed as false-positive at dynamic enhanced MR imaging. *Radiology* 2012; **265**: 696-706 [DOI: 10.1148/radiol.12112672]

31 **Ren C**, Zou Y, Zhang X, Li K. Diagnostic value of diffusion-weighted imaging-derived apparent diffusion coefficient and its association with histological prognostic factors in breast cancer. *Oncol Lett* 2019; **18**: 3295-3303 [PMID: 31452808 DOI: 10.3892/ol.2019.10651]

32 **Spick C**, Pinker-Domenig K, Rudas M, Helbich TH, Baltzer PA. MRI-only lesions: application of diffusion-weighted imaging obviates unnecessary MR-guided breast biopsies. *Eur Radiol* 2014; **24**: 1204-1210 [PMID: 24706105 DOI: 10.1007/s00330-014-3153-6]

33 **Shi R**, Jiang T, Si L, Li M. Correlations of magnetic resonance, perfusion-weighed imaging parameters and microvessel density in meningioma. *J BUON* 2016; **21**: 709-713 [PMID: 27569094]

34 **Katayama Y**, Uchino J, Chihara Y, Tamiya N, Kaneko Y, Yamada T, Takayama K. Tumor Neovascularization and Developments in Therapeutics. *Cancers (Basel)* 2019; **11** [PMID: 30845711 DOI: 10.3390/cancers11030316]

35 **Ryu JK**, Rhee SJ, Song JY, Cho SH, Jahng GH. Characteristics of quantitative perfusion parameters on dynamic contrast-enhanced MRI in mammographically occult breast cancer. *J Appl Clin Med Phys* 2016; **17**: 377-390 [PMID: 27685105 DOI: 10.1120/jacmp.v17i5.6091]

36 **Han M**, Kim TH, Kang DK, Kim KS, Yim H. Prognostic role of MRI enhancement features in patients with breast cancer: value of adjacent vessel sign and increased ipsilateral whole-breast vascularity. *AJR Am J Roentgenol* 2012; **199**: 921-928 [PMID: 22997388 DOI: 10.2214/AJR.11.7895]

World Journal of Clinical Cases

Submit a Manuscript: https://www.f6publishing.com

World J Clin Cases 2022 June 26; 10(18): 6032-6038

DOI: 10.12998/wjcc.v10.i18.6032

ISSN 2307-8960 (online)

ORIGINAL ARTICLE

Retrospective Study

Scar-centered dilation in the treatment of large keloids

Min Wu, Jie-Yu Gu, Ran Duan, Bo-Xuan Wei, Feng Xie

Specialty type: Surgery

Provenance and peer review: Unsolicited article; Externally peer reviewed.

Peer-review model: Single blind

Peer-review report's scientific quality classification

Grade A (Excellent): 0
Grade B (Very good): B
Grade C (Good): C
Grade D (Fair): 0
Grade E (Poor): 0

P-Reviewer: Laukkanen K, Finland; Maria Villar L, Spain

Received: January 10, 2022
Peer-review started: January 10, 2022
First decision: February 14, 2022
Revised: February 21, 2022
Accepted: April 20, 2022
Article in press: April 20, 2022
Published online: June 26, 2022

Min Wu, Jie-Yu Gu, Ran Duan, Bo-Xuan Wei, Feng Xie, Department of Plastic and Reconstructive Surgery, Shanghai Ninth People's Hospital, Shanghai JiaoTong University School of Medicine, Shanghai 200011, China

Corresponding author: Feng Xie, MD, Associate Chief Physician, Department of Plastic and Reconstructive Surgery, Shanghai Ninth People's Hospital, Shanghai JiaoTong University School of Medicine, No. 639 Zhizaoju Road, Shanghai 200011, China. xiefengdr@163.com

Abstract

BACKGROUND

Hypertrophic scars and keloid treatment is a major problem in plastic surgery. While small keloids can be treated with resection followed by radiotherapy, large keloids require treatment with a tissue expander. Conventional methods increase the need for auxiliary incisions, causing new scar hyperplasia.

AIM

To introduce a new method for the treatment of keloids with an expander.

METHODS

Between 2018 and 2021, we performed surgeries to treat large keloids in nine patients with a two-stage approach. In the first stage, an intrascar incision was made in the keloid, and a customized expander was implanted under the keloid and the surrounding normal skin. A period of 3-6 mo was allowed for skin expansion. In the second stage, after the initial incision healed, a follow-up surgery was performed to remove the expander, resect the keloid, and repair the expanded skin flap. To accomplish this, an incision was made along the scar boundary to avoid making a new surgical incision and creating new scars. Superficial radiotherapy was then performed postoperatively.

RESULTS

Two patients had anterior chest keloids. After treatment, the anterior chest incision was broken repeatedly and then sutured again after debridement. It healed smoothly without scar hyperplasia. Keloids were successfully removed in 7 patients without recurrence.

CONCLUSION

This method was performed through a keloid incision and with a custom expander embedded. After full expansion, the keloid was directly resected using a linear suture, which avoids new surgical incisions and scars and can successfully remove large-area keloids. The treatment is effective, providing new insights and

strategies for the treatment of similar large-area keloid and hypertrophic scar cases in the future.

Key Words: Expander; Keloids; Superficial radiotherapy; Intrascar incision; Treatment

©The Author(s) 2022. Published by Baishideng Publishing Group Inc. All rights reserved.

Core Tip: This paper introduces a new method for the treatment of keloids with an expander. After treatment with a single linear incision, the surgical incision was located on the keloids. Thus, because there was no additional auxiliary incision, the possibility of a new keloid was reduced.

Citation: Wu M, Gu JY, Duan R, Wei BX, Xie F. Scar-centered dilation in the treatment of large keloids. *World J Clin Cases* 2022; 10(18): 6032-6038
URL: https://www.wjgnet.com/2307-8960/full/v10/i18/6032.htm
DOI: https://dx.doi.org/10.12998/wjcc.v10.i18.6032

INTRODUCTION

Keloid treatment has always been a major problem for surgeons[1,2]. Keloids are caused by fibroblast proliferation disorders during wound healing[1,3]. Current treatments mainly include topical or oral drugs, surgical treatment, radiotherapy, and laser therapy. Specifically, these include topical (tape/ointment) and injectable adrenocorticotropic hormones, compression therapy and silica gel (application of bandages, stents, plastic clothes, among others), surgical resection, sutures, surgical resection after skin graft or flap reconstruction, and postoperative radiotherapy, among other treatments [5]. Drug injections can be used to treat small keloids, while surgical resection and superficial radiotherapy are often used to treat large keloids[5-7]. However, it is often difficult to resect keloids with large areas directly by surgery[8,9].

In 1979, the American Society of Plastic Surgeons officially recognized expander therapy was initiated in 1976, and officially recognized skin dilation as a form of expander therapy, and it has since been widely used[10,11]. Skin dilation, which entails embedding an expander and continuously pumping water to expand the normal skin and increase the area, can be used to repair skin lesions. The method is advantageous as it avoids donor site injury, has a good repair effect, and ensures the color and texture of the flap match the recipient area. Therefore, expanders have been widely used to treat hypertrophic scars and keloids in recent decades[12,13]. However, previously reported methods involved burying the expander near the scar. During skin dilation, the expanded skin flap must be rotated or pushed to repair skin lesions; thus, an auxiliary incision is needed. For patients with scar constitution, a new incision means there is a possibility for new keloid formation.

In this study, we describe a new method for treating large keloids that minimizes the need for a new surgical incision, thereby reducing the chances of new keloid formation. In this method, a direct incision was made on the keloid to form an expander bag with a capsule cavity that includes the keloid and the surrounding normal skin. After full expansion, the keloid was directly excised and the expanded flaps were pulled together and sutured linearly, minimizing the need for a new surgical incision.

MATERIALS AND METHODS

Before surgical treatment, a detailed medical history was obtained, and a physical examination was performed for each patient. The size and shape of the custom expanders were designed based on the lesion site and the shape of the surrounding normal skin. Each custom expander was 2.5 times the diameter of the lesion.

The skin expander was implanted during the first surgery stage. The patient was placed under general anesthesia, and the surgical sites were routinely disinfected. An incision, the length of the long axis of the scar, was made along the midline of the scar. The incision was not extended beyond the boundary of the scar. Based on the customized expander, the boundary of the separated expansion cavity was marked with Meilan. The boundary usually exceeded the shape of the expander by 1 cm. The full-thickness of scar tissue was cut with a blade, and taking care to maintain a uniform vertical section, the subcutaneous fat was cut down to the surface of the myometrium, and the cavity separated from the surface of the muscular membrane. During separation, the perforating vessels were electro-coagulated or ligated. The separated cavity was 1 cm wider than the boundary of the customized expander to ensure that the expander could be fully expanded without folding after implantation. Separation of the

injection pot cavity and pot mouth position and the injection pot from the expansion of the capsule cavity 10 cm was done. To achieve hard support, we ensured that the bottom of the pot was at the appropriate depth, it was easy to touch on the body surface, and the expansion was optimal. Prior to placing the expander in the separated cavity, we ensured that it had no leaks. We also checked the chassis position, flattened the expander, and placed the injection bottle that was inserted in the drainage tube in the separated cavity. We were careful not to puncture the expander during suturing.

The wound dressing was changed routinely on the second day after surgery, and the drainage tube was removed when the drainage volume was less than 20 mL (this volume was based on the size of the embedded expander and was estimated based on clinical experience). The suture was removed on the 14th day after the first surgery, and a small amount of water was injected into the cavity twice per week. The volume injected was 10% of the designed capacity of the expander; however, this was not always the case. We paid special attention to the color and tension of the expanded flap and the sensation of pain around the flap area. Therefore, if the patient was obviously uncomfortable, the tension of the flap was too high, or the color of the flap was white, the water infusion was stopped, and the site of injection was monitored over time. When the expander was filled with water to 3-4 times its designed volume, the second stage surgery to remove the keloid was commenced. Prior to initiating the second surgery, the size of the expanded flap was measured to determine whether the normal skin on both sides of the scar was sufficient to cover the chassis.

During the second-stage surgery, the expander was removed, the scar excised, and the expanded flap repaired. To achieve this, an incision was made along the scar boundary to remove the lesion from the normal tissue completely and remove the expander and injection pot. While paying attention to the treatment of both sides of the flap, the flaps were pulled towards the midline of the incision and sutured, and an appropriate drainage tube was inserted. A multi-layer tension-reduction cosmetic suture using one silk suture was required. The bottom of the flap was tethered to the rib periosteum while ensuring that there was no tension in the suture. A full subcutaneous reduction was required in patients with scar constitution.

The wound was dressed, and the drainage tube was removed as described earlier. The suture was removed between days 10 and 14 after surgery and prior to radiotherapy[14]. Radiotherapy, totaling 20 Gy, was administered in four sessions at a dose of 5 Gy per session. Radiotherapy was started on the first day post-surgery (if the first day after surgery was on the weekend, radiotherapy was suspended for two days and continued the following Monday)[15,16]. To prevent recurrence of keloids and hypertrophic scars, adequate anti-scar treatment was provided postoperatively, which included the early and effective application of reducing devices, external use of silicone gel for three months, and avoidance of foods including spicy foods, seafood, and alcohol. In addition, we ensured regular review and close postoperative follow-up of the patients.

RESULTS

The size of the keloids ranged from 2 cm × 5 cm to 15 cm × 13 cm in surgical patients (Table 1). The expansion time and designated volume of the customized expander were 3–5 mo (mean, 4 mo), and 100–800 mL (mean, 500 mL), respectively. The total volume of water injected ranged from 320–2400 mL (average, 1452 mL). Keloids were completely removed, and the surgery resulted in a linear scar. One patient had a long-term unhealed wound in the anterior chest for half a year after scar resection and radiotherapy. In this patient, the wound was directly reopened and re-sutured without further radiotherapy. This treatment resulted in smooth healing of the wound without keloid recurrence.

Total nine patients underwent keloid repair surgery, which was conducted in two stages between 2018 and 2021. In the first stage, customized expanders were implanted under the scars, and in the second stage, scar resection and expanded skin flap repair were performed. Due to the different shapes of the keloids, the customized expanders used were also different (Table 1).

The expander size ranged from 100-800 mL. The final expansion size was between 320 and 2400 mL. The water injection interval was 2 d, and each injection volume was 10% of the design capacity. When the tension of the flap was too high, a smaller volume could be injected. Expansion time in March-May, and an average of April. Representative patient cases are presented in Figure 1 and Figure 2.

DISCUSSION

Keloid-centered expansion has replaced traditional para-scar expansion. The main advantages are as follows: (1) Incisions are made in hypertrophic scars or keloids, and the wound has a strong tensile strength. This is because the healing surface includes thick scar tissue and the underlying adipose tissue. Therefore, in the process of expansion, incision dehiscence does not occur; (2) Unlike the traditional method in which the expander is embedded *via* an incision in the normal skin, this method of incision in the scar area will not add any new surgical scars, which is particularly important for people with a scar physique and does not require a new drainage tube incision. Furthermore, a previous report has

Table 1 Details of surgical patients

Patients	Age (yr)	Scar area (cm)	Dilator size (mL)	Total water injection (mL)	Location
1	23	6.5 × 4.5	200	600	Chest
2	69	15 × 10	800	2400	Back
		5 × 3	200	600	Back
3	28	15 × 13	700	2161	Chest
4	13	2 × 5	100	350	Upper limb
5	35	6 × 4	400	1200	Chest
6	32	13 × 4	100	320	Neck
7	24	10 × 6	600	1300	Chest
8	30	15 × 5	800	2400	Abdomen
9	24	11 × 6	500	1500	Chest

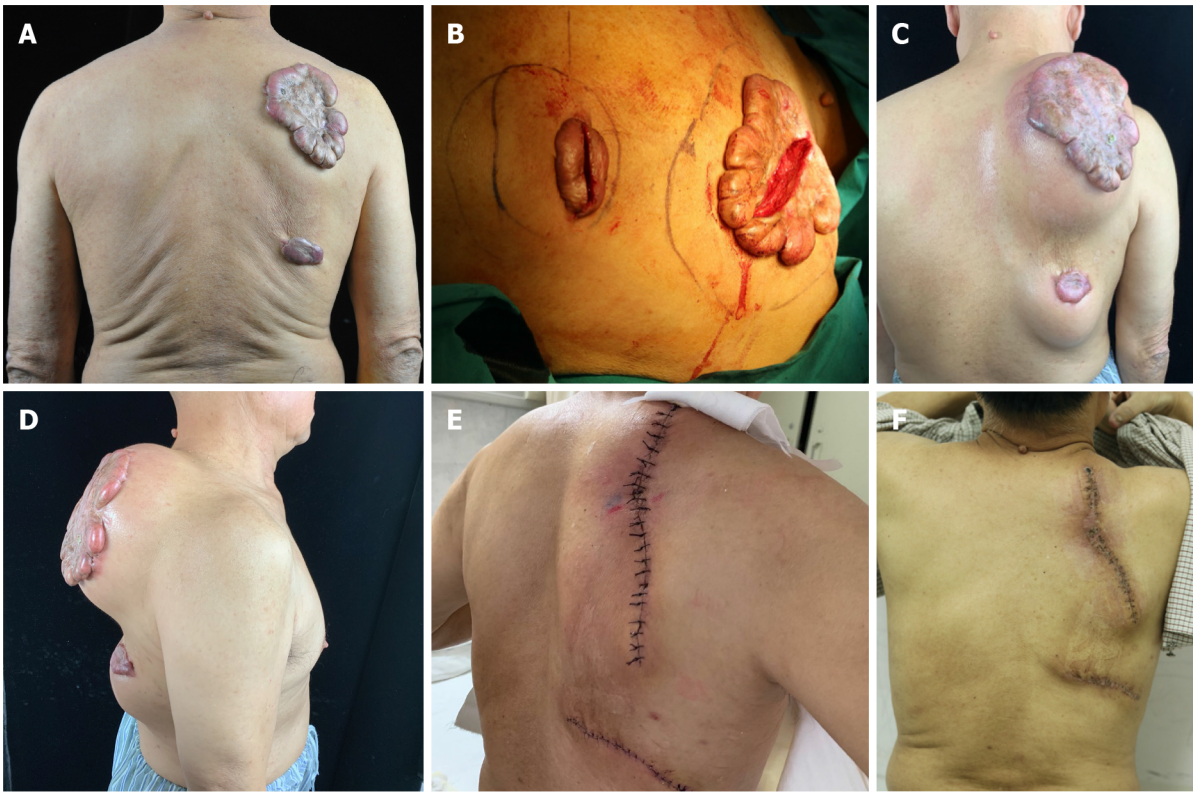

DOI: 10.12998/wjcc.v10.i18.6032 **Copyright** ©The Author(s) 2022.

Figure 1 A 69-year-old patient with keloids. A: Two prominent skin, and the edge beyond the scar base; B: In the first stage of operation, expander implantation was performed through an intrascar incision; C, D: The methylene blue line was the designed range of expander implantation; after expander implantation, normal saline was rapidly injected to dilate it; expander water injection; E: After injection of saline, the expander was removed and the expanded flap was sutured. Continuous superficial radiotherapy after the operation, for 4 d; F: Two weeks after the operation, immediate suture removal was done.

confirmed that a scar within the vicinity of the incision will not cause keloid hyperplasia[17]; and (3) During the expansion process, keloids stop developing and even partially subside due to pressure compression. This phenomenon has not been previously reported.

In this study, one patient presented with two keloids, and satisfactory results were achieved for both keloids with the keloid-centered expansion approach. In another patient, the case was complicated by poor wound healing for half a year, which manifested as epidermal erosion, exudation, and crusting. After extensive subcutaneous separation and re-suturing, the wound healed successfully. The wound healed poorly in this patient because the surgical tension was concentrated at the incision, which caused the scar at the incision to widen continuously under tension traction, and this wound was associated with the radiotherapy area. To avoid such complications, attention should be paid to the selection of an appropriate multi-gradient tension suture (specifically a flap deep and periosteum tension suture), in



DOI: 10.12998/wjcc.v10.i18.6032 **Copyright** ©The Author(s) 2022.

Figure 2 A patient with an anterior chest keloid. A: The patient with an anterior chest keloid, prominent skin lesions, and edge-invasive growth appearance; B: Scar incision after expander implantation and normal saline expansion; C: During expander removal, methylene blue was designed to remove keloid size; D: Immediately after scar excision and expander removal.

addition to the need for subcutaneous tension suture. This prevents the concentration of the flap tension on the wound.

The method of implanting the expander *via* a scar incision, as described in this report, effectively reduces the risk of additional scarring, which is a significant advantage. In addition, during the expansion process, the pressure achieved with water injection plays a role in compressing the keloids. According to clinical observations, skin expansion under keloids can prevent and reverse the pathological progress of keloids. This is another significant advantage of the keloid-centered expansion approach. After the second-stage operation to remove the lesion, the flaps were directly sutured. The resulting linear incision prevents the need for an auxiliary incision. Compared with the pedicle flap and free flap, the technical requirements and accuracy of the keloid-centered expansion approach are superior.

To repair a particular area of a keloid, custom-designed expanders are required. The diameter of a normal skin expander should be 2–3 times the keloid diameter. After expansion, the scar can be successfully removed, and the wound successfully closed. If the normal skin area to be expanded is too small, even after expansion, there will not be sufficient normal skin, and the tension will be too high to remove the scar completely when closing.

In this study, postoperative radiotherapy consisted of 20 Gy, continuous irradiation for 4-5 d, starting from the first day after surgery. A 4–5 Gy linear accelerator electron beam radiotherapy can penetrate 2-3 mm below the skin[18,19].

In the method described in this report, the surgical incision was simple, and no auxiliary incisions were required. Previous expander transfer methods included propulsion and rotation methods. An auxiliary incision is required to fully expand a hemispherical expanded flap using those methods. In this study, the expander was in the central part of the scar; thus, no auxiliary incision was needed.

The expansion process to achieve keloid compression effectively prevents the progression of keloids. However, there is also a risk of complications. After the expansion, the tension at the incision is large, and since the scar is around the incision, there is a high risk of skin damage. Therefore, after the second-stage surgery, the probability of healing is low. To mitigate this risk, a deep tension-reduction suture should be considered.

CONCLUSION

From this study of surgical patients, we present a new method, keloid-centered expansion, that we believe can successfully remove large keloids and have good prospects for healing since this method prevents the need for auxiliary incisions and reduces the risk for the formation of new keloids. The sequence of events associated with this method includes scar incision, customized expander implantation, skin expansion to remove the keloid, formation of a single linear suture incision, followed by postoperative radiotherapy.

ARTICLE HIGHLIGHTS

Research background

Current treatment modalities are classified as either conservative or surgical. Conservative treatments include intra-scar injection of anti-scar drugs, laser, external force compression, and radiotherapy, although complete curation is often not achieved. While small keloids can be directly resected followed by radiotherapy, large keloids cannot be directly resected; they require treatment with a tissue expander.

Research motivation

We present a new method, keloid-centered expansion keloid-centered expansion.

Research objectives

After treatment with a single linear incision, the surgical incision was located on the keloids. Thus, because there was no additional auxiliary incision, the possibility of a new keloid was reduced.

Research methods

In the first stage, an intrascar incision was made in the keloid, and a customized expander was implanted under the keloid and the surrounding normal skin. A period of 3-6 mo was allowed for skin expansion. In the second stage, after the initial incision healed, a follow-up surgery was performed to remove the expander, resect the keloid, and repair the expanded skin flap.

Research results

Keloids were successfully removed in seven patients using this approach without recurrence. In two patients who had anterior chest keloids, wound healing was prolonged. However, after debridement and re-suturing, the wound healed smoothly without scar hyperplasia.

Research conclusions

This method was performed through a keloid incision and with a custom expander embedded. After full expansion, the keloid was directly resected using a linear suture, which avoids new surgical incisions and scars and can successfully remove large-area keloids.

Research perspectives

Keloid treatment, especially large keloids, has always been a major problem for surgeons, and this study provides a solution for this problem, which is likely applicable for treating keloids of all sizes and for treating other hypertrophic scars as well.

FOOTNOTES

Author contributions: Xie F designed this retrospective study; Wu M wrote the manuscript; Gu JY, Duan R, and Wei WX were responsible for sorting the data.

Institutional review board statement: This study was approved by the Shanghai Ninth People's Hospital Institutional Review Board.

Informed consent statement: All study participants, or their legal guardian, provided informed written consent prior to study enrollment.

Conflict-of-interest statement: The authors report no conflict of interest.

Data sharing statement: No additional data are available.

Open-Access: This article is an open-access article that was selected by an in-house editor and fully peer-reviewed by

external reviewers. It is distributed in accordance with the Creative Commons Attribution NonCommercial (CC BY-NC 4.0) license, which permits others to distribute, remix, adapt, build upon this work non-commercially, and license their derivative works on different terms, provided the original work is properly cited and the use is non-commercial. See: https://creativecommons.org/Licenses/by-nc/4.0/

Country/Territory of origin: China

ORCID number: Min Wu 0000-0001-5462-6920; Jie-Yu Gu 0000-0001-8794-9208; Ran Duan 0000-0001-9429-0501; Bo-Xuan Wei 0000-0003-2363-2759; Feng Xie 0000-0003-3322-7271.

S-Editor: Wang JL
L-Editor: A
P-Editor: Wang JL

REFERENCES

1 **Brown JJ**, Bayat A. Genetic susceptibility to raised dermal scarring. *Br J Dermatol* 2009; **161**: 8-18 [PMID: 19508304 DOI: 10.1111/j.1365-2133.2009.09258.x]
2 **Ogawa R**. Keloid and Hypertrophic Scars Are the Result of Chronic Inflammation in the Reticular Dermis. *Int J Mol Sci* 2017; **18** [PMID: 28287424 DOI: 10.3390/ijms18030606]
3 **Robles DT**, Moore E, Draznin M, Berg D. Keloids: pathophysiology and management. *Dermatol Online J* 2007; **13**: 9 [PMID: 18328203]
4 **Lee HJ**, Jang YJ. Recent Understandings of Biology, Prophylaxis and Treatment Strategies for Hypertrophic Scars and Keloids. *Int J Mol Sci* 2018; **19** [PMID: 29498630 DOI: 10.3390/ijms19030711]
5 **Norris JE**. Superficial x-ray therapy in keloid management: a retrospective study of 24 cases and literature review. *Plast Reconstr Surg* 1995; **95**: 1051-1055 [PMID: 7732115 DOI: 10.1097/00006534-199505000-00015]
6 **Xu J**, Yang E, Yu NZ, Long X. Radiation Therapy in Keloids Treatment: History, Strategy, Effectiveness, and Complication. *Chin Med J (Engl)* 2017; **130**: 1715-1721 [PMID: 28685723 DOI: 10.4103/0366-6999.209896]
7 **Pozzi M**, Zoccali G, Drago MC, Mirri MA, Costantini M, DE Vita R. Radiotherapy following surgery in keloid treatment: our protocol. *G Ital Dermatol Venereol* 2016; **151**: 492-498 [PMID: 25907802]
8 **Bijlard E**, Kouwenberg CA, Timman R, Hovius SE, Busschbach JJ, Mureau MA. Burden of Keloid Disease: A Cross-sectional Health-related Quality of Life Assessment. *Acta Derm Venereol* 2017; **97**: 225-229 [PMID: 27378582 DOI: 10.2340/00015555-2498]
9 **Walliczek U**, Engel S, Weiss C, Aderhold C, Lippert C, Wenzel A, Hörmann K, Schultz JD. Clinical Outcome and Quality of Life After a Multimodal Therapy Approach to Ear Keloids. *JAMA Facial Plast Surg* 2015; **17**: 333-339 [PMID: 26270082 DOI: 10.1001/jamafacial.2015.0881]
10 **Radovan C**. Tissue expansion in soft-tissue reconstruction. *Plast Reconstr Surg* 1984; **74**: 482-492 [PMID: 6484035 DOI: 10.1097/00006534-198410000-00005]
11 **Austad ED**. Evolution of the concept of tissue expansion. *Facial Plast Surg* 1988; **5**: 277-279 [PMID: 3078696 DOI: 10.1055/s-2008-1064763]
12 **Jones K**, Fuller CD, Luh JY, Childs CC, Miller AR, Tolcher AW, Herman TS, Thomas CR Jr. Case report and summary of literature: giant perineal keloids treated with post-excisional radiotherapy. *BMC Dermatol* 2006; **6**: 7 [PMID: 16623939 DOI: 10.1186/1471-5945-6-7]
13 **Wolfram D**, Tzankov A, Pülzl P, Piza-Katzer H. Hypertrophic scars and keloids--a review of their pathophysiology, risk factors, and therapeutic management. *Dermatol Surg* 2009; **35**: 171-181 [PMID: 19215252 DOI: 10.1111/j.1524-4725.2008.34406.x]
14 **Cheraghi N**, Cognetta A Jr, Goldberg D. RADIATION THERAPY for the Adjunctive Treatment of Surgically Excised Keloids: A Review. *J Clin Aesthet Dermatol* 2017; **10**: 12-15 [PMID: 28979658]
15 **Kal HB**, Veen RE. Biologically effective doses of postoperative radiotherapy in the prevention of keloids. Dose-effect relationship. *Strahlenther Onkol* 2005; **181**: 717-723 [PMID: 16254707 DOI: 10.1007/s00066-005-1407-6]
16 **Gold MH**, Nestor MS, Berman B, Goldberg D. Assessing keloid recurrence following surgical excision and radiation. *Burns Trauma* 2020; **8**: tkaa031 [PMID: 33225004 DOI: 10.1093/burnst/tkaa031]
17 **Matton GE**, Tonnard PL, Monstrey SJ, Van Landuyt KH. A universal incision for tissue expander insertion. *Br J Plast Surg* 1995; **48**: 172-176 [PMID: 7735681 DOI: 10.1016/0007-1226(95)90150-7]
18 **Pampena R**, Palmieri T, Kyrgidis A, Ramundo D, Iotti C, Lallas A, Moscarella E, Borsari S, Argenziano G, Longo C. Orthovoltage radiotherapy for nonmelanoma skin cancer (NMSC): Comparison between 2 different schedules. *J Am Acad Dermatol* 2016; **74**: 341-347 [PMID: 26589877 DOI: 10.1016/j.jaad.2015.09.031]
19 **Chander SS**. Postoperative radiotherapy in high-risk postmenopausal breast cancer. *Lancet* 1999; **354**: 865-6; author reply 866 [PMID: 10485751 DOI: 10.1016/S0140-6736(05)75935-3]

World Journal of Clinical Cases

Submit a Manuscript: https://www.f6publishing.com

World J Clin Cases 2022 June 26; 10(18): 6039-6049

DOI: 10.12998/wjcc.v10.i18.6039

ISSN 2307-8960 (online)

ORIGINAL ARTICLE

Retrospective Study

Application of a novel computer-assisted surgery system in percutaneous nephrolithotomy: A controlled study

Fei Qin, Ye-Feng Sun, Xin-Ning Wang, Bin Li, Zhi-Lei Zhang, Ming-Xin Zhang, Fei Xie, Shuai-Hong Liu, Zi-Jie Wang, Yuan-Chao Cao, Wei Jiao

Specialty type: Urology and nephrology

Provenance and peer review: Unsolicited article; Externally peer reviewed.

Peer-review model: Single blind

Peer-review report's scientific quality classification

Grade A (Excellent): A
Grade B (Very good): B, B
Grade C (Good): 0
Grade D (Fair): 0
Grade E (Poor): 0

P-Reviewer: Gadelkareem RA, Egypt; Shahriari M, Iran; □urlin VM, Romania

Received: December 13, 2021
Peer-review started: December 13, 2021
First decision: February 14, 2022
Revised: March 1, 2022
Accepted: April 21, 2022
Article in press: April 21, 2022
Published online: June 26, 2022

Fei Qin, Ye-Feng Sun, Xin-Ning Wang, Bin Li, Zhi-Lei Zhang, Ming-Xin Zhang, Fei Xie, Shuai-Hong Liu, Zi-Jie Wang, Yuan-Chao Cao, Wei Jiao, Department of Urology, The Affiliated Hospital of Qingdao University, Qingdao 266000, Shandong Province, China

Corresponding author: Wei Jiao, MMed, Associate Chief Physician, Associate Professor, Deputy Director, Department of Urology, The Affiliated Hospital of Qingdao University, No. 16 Jiangsu Road, Shinan District, Qingdao 266000, Shandong Province, China.
jiaowei3929@163.com

Abstract

BACKGROUND

Most complex renal stones are managed primarily with percutaneous nephrolithotomy (PCNL). However, PCNL is still a great challenge for surgeons because of poor comprehension on complex adjacent structures. Novel techniques are required to assist in planning and navigation.

AIM

To apply and evaluate the Hisense computer-assisted surgery (CAS) system in PCNL.

METHODS

A total of 60 patients with complex renal stones were included. Thirty patients in the CAS group had three-dimensional (3D) virtual models constructed with the CAS system. The model assisted in planning and navigating in the CAS system. Thirty patients in the control group planned and navigated as standard PCNL, without the application of the CAS system. Success rate of one attempt, operation time, initial stone-free rate, decrease in hemoglobin, and complications were collected and analyzed.

RESULTS

There were no statistically significant differences in the baseline characteristics or planning characteristics. The success rate of one puncturing attempt (90% *vs* 67%, $P = 0.028$) and the initial stone-free rate (87% *vs* 63%, $P = 0.037$) were significantly higher in the CAS group. However, there were no statistically significant differences in the operation time (89.20 ± 29.60 min *vs* 92.33 ± 33.08 min, $P = 0.859$) or in the decrease in hemoglobin (11.07 ± 8.32 g/L *vs* 9.03 ± 11.72 g/L, $P = 0.300$)

between the CAS group and the control group. No statistically significant differences in the incidence of complications (Clavien-Dindo grade ≥ 2) were found.

CONCLUSION

Compared with standard PCNL, CAS-assisted PCNL had advantages in terms of the puncturing success rate and stone-free rate. The Hisense CAS System was recommended to assist in preoperative planning and intraoperative navigation for an intuitive, precise and convenient PCNL.

Key Words: Computer-assisted surgery system; Percutaneous nephrolithotomy; Three-dimensional reconstruction; Planning; Navigation

©The Author(s) 2022. Published by Baishideng Publishing Group Inc. All rights reserved.

Core Tip: Consisting of construction, display, simulation and measurement functions, the Hisense computer-assisted surgery (CAS) system is a novel and all-around software based on new generation of three-dimensional (3D) reconstruction. Compared with standard percutaneous nephrolithotomy (PCNL), CAS-assisted PCNL had advantages in terms of the puncturing success rate and stone-free rate. The CAS System was recommended to assist in preoperative planning and intraoperative navigation for an intuitive, precise and convenient PCNL.

Citation: Qin F, Sun YF, Wang XN, Li B, Zhang ZL, Zhang MX, Xie F, Liu SH, Wang ZJ, Cao YC, Jiao W. Application of a novel computer-assisted surgery system in percutaneous nephrolithotomy: A controlled study. *World J Clin Cases* 2022; 10(18): 6039-6049

URL: https://www.wjgnet.com/2307-8960/full/v10/i18/6039.htm

DOI: https://dx.doi.org/10.12998/wjcc.v10.i18.6039

INTRODUCTION

Renal stones, including large stones and multiple stones, are a common and intractable urological disease. Percutaneous nephrolithotomy (PCNL) has been recommended as the first-line treatment for renal stones that are larger than 2 cm[1,2]. In other cases of renal stones, PCNL is also an alternative treatment. However, it is difficult to achieve surgical competence in PCNL, especially for complex renal stones such as staghorn stones and multiple stones. Therefore, a great quantity of training is required for young surgeons. The study of the learning curve of a single surgeon suggested that competence in PCNL was reached after treating 60 cases and was excellent after treating 115 cases[3].

For excellent PCNL, novel techniques, including visual needles[4], three-dimensional (3D) printing [5], lasers[6], electromagnetic tracking[7] and virtual reality (VR)[8], are emerging to assist surgeons in understanding the regional anatomy and establishing percutaneous tracts. 3D reconstruction is also a novel technique[9] and has showed preliminary advantages in PCNL[10]. The structures around the stones are reconstructed from two-dimensional (2D) clinical imaging pictures to form 3D models for further display, planning and navigation. These models provide a comprehensive view to show the 3D relationship between the stones and adjacent structures, which cannot be provided by traditional 2D imaging, such as fluoroscopy, ultrasound (US) and computed tomography (CT).

The Hisense computer-assisted surgery (CAS) system, consisting of construction, display, simulation and measurement functions, is a software based on 3D reconstruction. The system has been applied in pediatric hepatectomy[11] and gastrectomy[12] and is helpful for accurate preoperative planning and intraoperative navigation. In the present study, we applied the CAS system in PCNL and first compared CAS-assisted PCNL (the CAS group) and standard PCNL (the control group) to evaluate the system.

MATERIALS AND METHODS

Patients and designs

It is a retrospective study. From October 2019 to October 2020, patients with complex renal stones, confirmed by preoperative computed tomography urography (CTU) and managed by PCNL in the Urological Department of the Affiliated Hospital of Qingdao University, were retrospectively enrolled in the study. Complex renal stones were defined as partial staghorn stones, complete staghorn stones or multiple stones. However, patients with history of operations, introduction of ureteral stents or

nephrostomy tubes, existence of other disorders in the ipsilateral kidney, or absolute operative contraindications were excluded.

Thirty patients who met the selection criteria and underwent CAS-assisted PCNL were included as the CAS group. In CAS-assisted PCNL, patients had 3D virtual models constructed with the CTU images by the CAS system (Hisense Medicine, Qingdao, China), and the model assisted in planning and navigating in the CAS system. At the same time, 103 patients met the selection criteria and underwent standard PCNL. They were ranked according to the medical record number, and the first 30 patients were included into the study as the control group in a 1:1 ratio to the patients in the CAS group using the random number method. In standard PCNL, 2D axial, sagittal and coronal images from CTU aided in planning and navigating, without the application of the CAS system.

All surgeries were performed by the same surgical team. Ethics approval was obtained from the Ethics Committee of the Affiliated Hospital of Qingdao University (QYFYWZLL26370). Informed consent was obtained from all the patients for this study.

CTU protocol

The CTU images, including the unenhanced, arterial, venous, and excretory phases, were obtained by a 64 multidetector row CT scanner (Siemens, Germany) with 1-mm step intervals. The scan delay times for the arterial, venous, and excretory phases were 25, 60, and 600-900 s, respectively, after intravenous injection of contrast material. Patients were advised to hold their breath in inspiration during the process.

Application of the Hisense CAS system

Construction of 3D virtual model: Four-phase images of the CTU were exported in Digital Imaging and Communications in Medicine format and were imported into the Hisense CAS system: (1) Segmentation: Stones, renal collecting system, ureters, renal parenchyma, renal vascular system, bottom of the thoracic cavity, spine, ribs, and skin were segmented from the images of different phases by the technique of region growing and threshold segmentation; (2) Reconstruction: The system processed the segmented structures for the 3D reconstruction of separate models using the techniques of maximum intensity projection, multiple planar reformation, curved planar reconstruction and volume rendering; (3) Combination: These separate models were registered and were integrated into a fusion model; and (4) Modification: After noise reduction, smoothing, dyeing and diaphaneity adjustments of each structure in the fusion model, a final 3D virtual model was obtained (Figure 1).

Planning for PCNL: With the simulation and measurement function of the CAS system, urological surgeons planned for the PCNL using the 3D virtual models. The planning was divided into three parts: the determination of ideal entry calyx, ideal puncture path and tract number: (1) Ideal entry calyx, where the nephoscope enters the collecting system, is defined as the calyx that is accessible to the renal pelvis and has the smallest length, the largest infundibular width, and the most "favorable calyces"[13]. A favorable calyx is defined as a calyx whose angle from the entry calyx is larger than 95°[14]. Stones in the renal pelvis and favorable calyces can be easily cleared from the ideal entry calyx. (2) The puncture path is the tract starting at the surface of the skin and ending at the boundary of the entry calyx. And ideal puncture path should have the shortest distance from the skin to the ideal entry calyx and should pass through the thinnest renal parenchyma, with the protection of adjacent vessels and organs. We moved virtual puncture path to find the ideal puncture path and recorded its depth (distance a) and direction (Figure 2). The direction was indicated by the angle between ideal puncture path and the axial plane (angle a), coronal plane (angle b), and sagittal plane (angle c). The intersection between ideal puncture path and skin is the puncture point. Then, we recorded the position of the point by the latitudinal distance to the posterior midline of the body (distance b) and the longitudinal distance to the inferior margin of the ipsilateral twelfth rib (distance c). And (3) Tract number. There are often no significant residual stones after the PCNL with one tract, based on above ideal entry calyx and puncture path. The second entry calyx and puncture path were needed to establish another tract when significant residual stones were present. The planning process of the second tract was the same as that of the first tract. A third tract was not established for the concern of increased injuries and bleeding. Repeated simulation could be performed if previous planning was not satisfactory.

Navigation for PCNL: The 3D model and PCNL plan obtained from the CAS system were applied to navigate the PCNL. During the puncture phase, we first located the actual puncture point with distances b and c. Then, we set the direction of the puncture needle by angles a, b and c. With the help of the US (Hitachi, Japan), we punctured ideal entry calyx from the actual puncture point along the direction of the puncture needle, and the puncture depth was approximately the distance a. US was mainly used to verify the position of ideal entry calyx and to adjust the puncture path. Tract number was determined as mentioned in the PCNL plan. The puncture process was performed while the patients were in inspiration. During the tract dilation phase and the stone removal phase, it was the same as a standard PCNL. During all phases, the 3D model was shown on the screen using the display function of the CAS system. The 3D model could be magnified, rotated and translated to meet surgeons' requests. Stones, the collecting system, adjacent vessels and organs could be viewed in all directions to

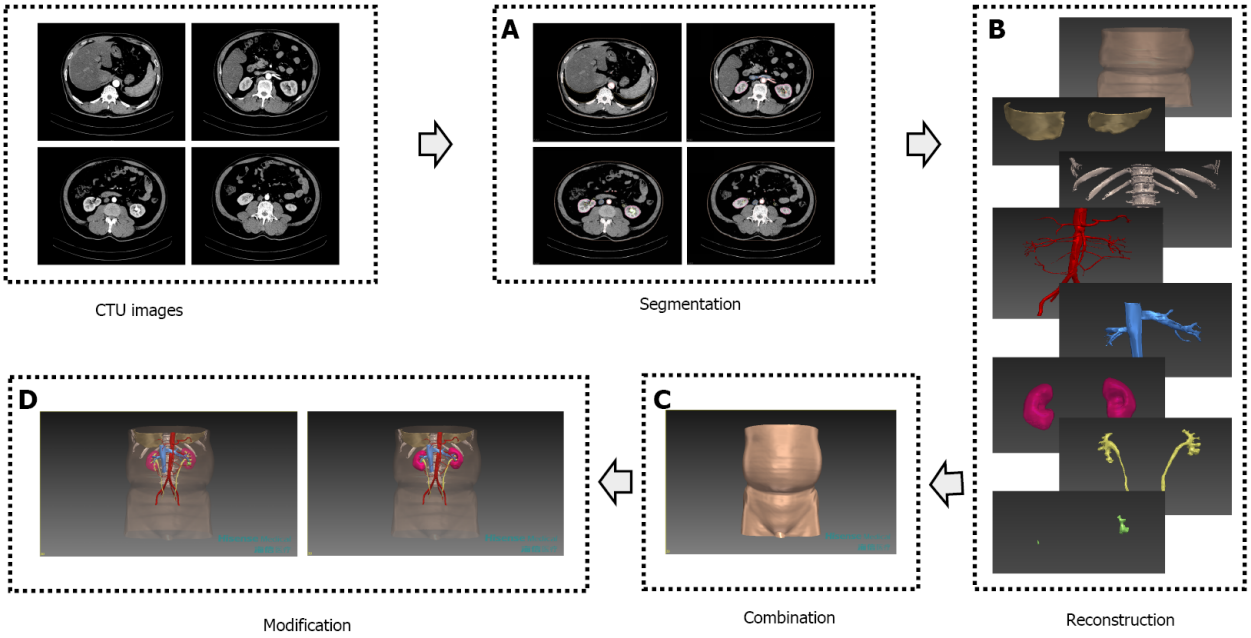

DOI: 10.12998/wjcc.v10.i18.6039 **Copyright** ©The Author(s) 2022.

Figure 1 The procedures of three-dimensional model construction by the computer-assisted surgery system. A: Different structures were segmented from different phases of CTU; B: Segmented skin, the bottom of the thoracic cavity, spine, ribs, renal arterial system, renal venous system, renal parenchyma, renal collecting system, ureters and stones were reconstructed respectively; C: In combination, reconstructed structures were registered and integrated into a fusion model; D: In modification, diaphaneity adjustment of skin, renal parenchyma and renal collecting system made it possible to observe stones.

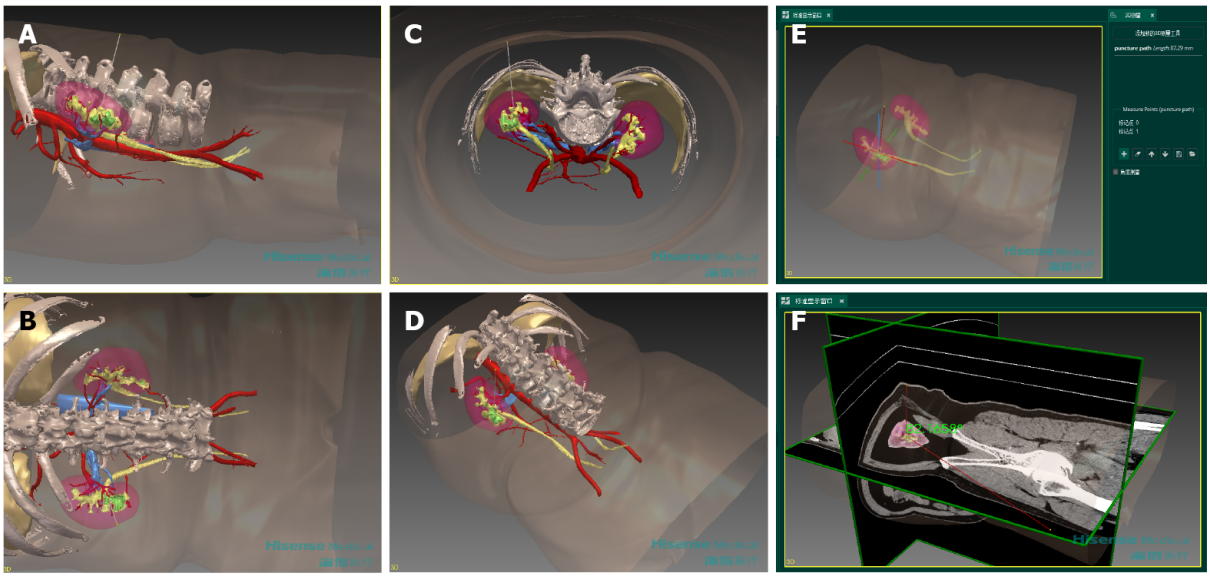

DOI: 10.12998/wjcc.v10.i18.6039 **Copyright** ©The Author(s) 2022.

Figure 2 Preoperative planning for percutaneous tracts with the three-dimensional model. Ideal puncture path in side view (A), back view (B), axial view (C) and oblique view (D) were simulated. Lengths and angles could be measured by the CAS system, taking the depth of ideal puncture path (E) and the angle between ideal puncture path and the coronal plane (F) for example.

find stones and to avoid injuries (Figure 3).

Surgical procedure

After general anesthesia, the patient was placed in the lithotomy position, and a ureteral catheter was placed for artificial hydronephrosis. Then, the patient was placed into the prone position and underwent main surgical procedure, including puncture phase, tract dilation phase and stone removal phase, with the help of the US. The tract was dilated to 24F. A 6F ureteral stent and a 14F nephrostomy tube were placed at the end of the surgery. CT was performed within 1 mo after the surgery. "Stone-

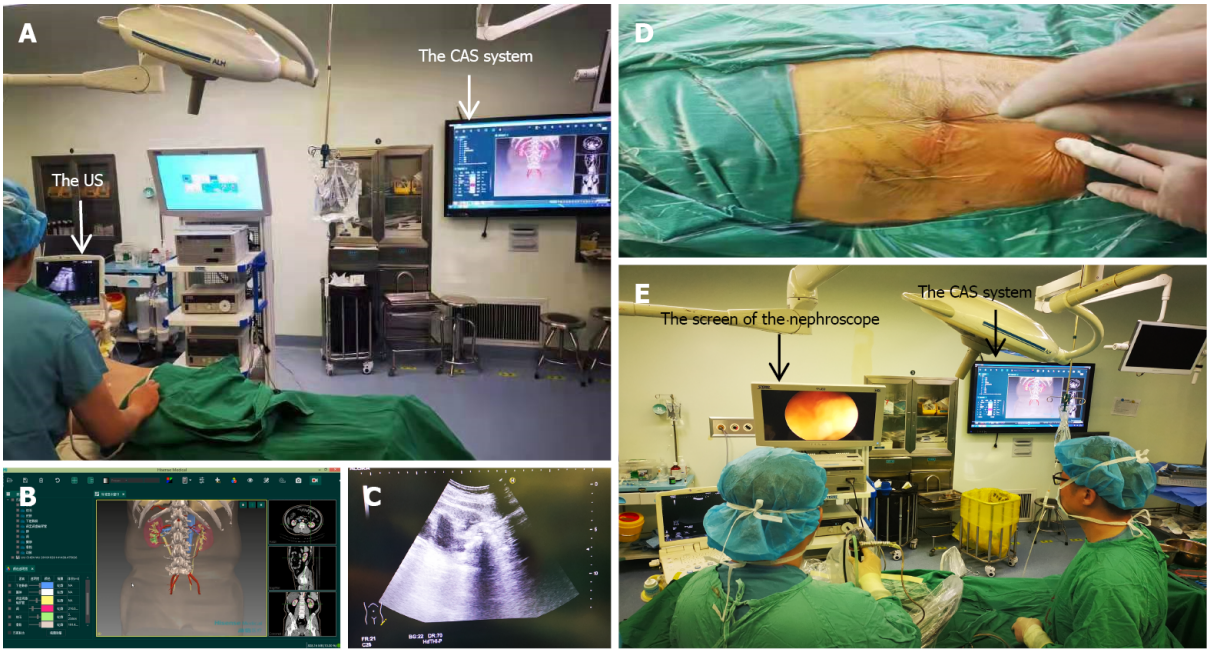

DOI: 10.12998/wjcc.v10.i18.6039 **Copyright** ©The Author(s) 2022.

Figure 3 Intraoperative navigation for percutaneous nephrolithotomy with the computer-assisted surgery system. A: Making percutaneous tracts with the help of the CAS system and the US; B: The CAS system showed the 3D model and the plan obtained preoperatively; C: The US showed puncture paths and surrounding structures in real time; D: Successful puncture was guided by parameters from preoperative planning; E: Removing stones with the reference from the CAS system.

free" was defined as no stone fragments or residual fragments present that more than 4 mm in diameter.

Data collection

Age, gender, body mass index (BMI), dilation of the collecting system, as well as side, type, density and sectional area of stones were recorded as the baseline characteristics. Entry calyx, tract length and tract number were recorded as the planning characteristics. Finally, the success rate of one attempt, operation time, initial stone-free rate, decrease in hemoglobin and complications (Clavien-Dindo grade ≥ 2) were analyzed. Initial stone-free rate was the proportion of patients who were "stone-free" after the first-stage PCNL.

Statistical analysis

Continuous data, expressed as the mean and standard deviation (SD), were analyzed by Student's *t* test or the Mann-Whitney *U* test. Categorical variables, shown as the number and percentage, were analyzed by the chi-square or Fisher's exact test. Statistical analyses were performed using SPSS version 23. $P < 0.05$ was regarded as statistically significant.

RESULTS

Sixty patients were included in the study: 30 in the CAS group and 30 in the control group. There were no statistically significant differences in age, gender, BMI, malformation of the collecting system, dilation of the collecting system, stone side, stone type, stone density or stone sectional area between the two groups (Table 1).

There were 6 upper calyces, 17 middle calyces, and 7 Lower calyces selected to be the entry calyces in the CAS group, while there were 3 upper calyces, 22 middle calyces, and 5 lower calyces selected to be the entry calyces in the control group. Most surgeries were completed with one tract (87% *vs* 90%) in the CAS group and the control group. The tract lengths in the CAS group and the control group were 76.03 ± 13.26 mm and 82.53 ± 17.58 mm, respectively. No statistically significant differences were found in the planning characteristics between the two groups (Table 2).

A total of 27/30 punctures in the CAS group and 20/30 in the control group were successful after just one attempt. The success rate of one puncturing attempt was significantly higher in the CAS group (90% *vs* 67%, $P = 0.028$). 26/30 surgeries in the CAS group and 19/30 in the control group achieved "stone-free", and the initial stone-free rate was significantly different between the two groups (87% *vs* 63%, $P = 0.037$). However, there were no statistically significant differences in the operation time (89.20 ± 29.60 min *vs* 92.33 ± 33.08 min, $P = 0.859$) or the decrease in hemoglobin (11.07 ± 8.32 g/L *vs* 9.03 ± 11.72 g/L,

Table 1 Baseline characteristics of patients and stones in the two groups

Characteristics	CAS group (*n* = 30)	Control group (*n* = 30)	*P* value
Age, yr, mean ± SD	52.30 ± 14.37	49.57 ± 13.58	0.452
Gender, *n* (%)			0.301
Male	14 (47)	18 (60)	
Female	16 (53)	12 (40)	
BMI, kg/m^2, mean ± SD	25.24 ± 3.58	25.29 ± 5.12	0.968
Dilation of the collecting system[1], *n* (%)			0.635
No or mild	18 (60)	20 (66)	
Moderate	8 (27)	5 (17)	
Severe	4 (13)	5 (17)	
Stone side, *n* (%)			0.426
Left	17 (57)	20 (67)	
Right	13 (43)	10 (33)	
Stone type, *n* (%)			0.434
Partial staghorn stone	4 (13)	8 (27)	
Complete staghorn stone	6 (20)	5 (17)	
Multiple stone	20 (67)	17 (56)	
Stone density, Hounsfield units, mean ± SD	915.15 ± 334.85	824.69 ± 245.73	0.238
Stone sectional area, mm^2, mean ± SD	562.95 ± 405.58	497.59 ± 566.88	0.174

[1]It was mild when the dilation distance of the collecting system was less than 2 cm. It was moderate when the dilation distance was between 2 cm and 4 cm. It was severe when the dilation distance was more than 4 cm. The dilation distance of the collecting system was measured when it was longest.
CAS: Computer-assisted surgery; SD: Standard deviation.

Table 2 Planning characteristics of tracts in two groups

Characteristics	CAS group (*n* = 30)	Control group (*n* = 30)	*P* value
Entry calyx[1], *n* (%)			0.413
Upper calyx	6 (20)	3 (10)	
Middle calyx	17 (57)	22 (73)	
Lower calyx	7 (23)	5 (17)	
Tract length[1], mm, mean ± SD	76.03 ± 13.26	82.53 ± 17.58	0.111
Tract number, *n* (%)			1.000
1	26 (87)	27 (90)	
2	4 (13)	3 (10)	

[1]Entry calyx and tract length were collected from the first tract if there were two tracts.
CAS: Computer-assisted surgery; SD: Standard deviation.

P = 0.300) between the CAS group and the control group. Bleeding necessitating blood transfusion was observed in 1 patient in the CAS group and 1 patient in the control group. Urinary tract infection necessitating therapeutic antibiotics or enhanced supportive therapy was observed in 2 patients in the CAS group and 2 patients in the control group. No injuries to adjacent structures were observed in the two groups. There were no statistically significant differences in the incidence of these complications (Table 3).

Table 3 Perioperative characteristics of percutaneous nephrolithotomy in two groups

Characteristics	CAS group (*n* = 30)	Control group(*n* = 30)	*P* value
Success rate of one puncturing attempt, *n* (%)	27 (90)	20 (67)	0.028
Operation time, min, mean ± SD	89.20 ± 29.60	92.33 ± 33.08	0.859
Decrease in hemoglobin, g/L, mean ± SD	11.07 ± 8.32	9.03 ± 11.72	0.300
Bleeding[1], *n* (%)	1 (3)	1 (3)	1.000
Urinary tract infection[1], *n* (%)	2 (7)	2 (7)	1.000
Injury[1], *n* (%)	0 (0)	0 (0)	-
Initial stone-free rate, *n* (%)	26 (87)	19 (63)	0.037

[1]Complications were counted and analyzed when Clavien–Dindo grade ≥ 2.
CAS: Computer-assisted surgery; SD: Standard deviation.

DISCUSSION

Most complex renal stones are managed primarily with PCNL[15]. Preoperative planning based on CTU is recommended[16], and intraoperative navigation with fluoroscopy or US is commonly used. However, PCNL is still a great challenge for surgeons because of low stone-free rate and high complication rate[17]. The most critical step to meet the challenge is the establishment of perfect tracts from the skin to the entry calyces. For higher stone free rate and lower complication rate, we applied this CAS system into PCNL, especially to establish the tract.

Traditional studies tended to perform preoperative planning with 2D CT images[18]. It was difficult to display overall 3D views in the simulation processes and the 3D precise measurements of each parameter. The surgeon had to reconstruct an overall view in mind, which relied on a long-team learning and was easily influenced by subjective judgment. The CAS system displayed a direct and objective 3D model for planning. The size, number, shape, position and adjacent structures of stones were evaluated in a panoramic view, and ideal entry calyces were selected. During the simulation, 3D puncture paths from the skin to the calyces were placed and were adjusted to obtain minimal injury to adjacent vessels and organs. It is obvious that measurement with 2D CT images cannot provide direct data of the 3D structures. The calculation method for 3D data obtained from 2D CT in PCNL was reported[19], but the process was also complex. In the CAS system, selected lengths or angles in 3D space were automatically measured and recorded with the parameters. The 3D planning from the CAS system assisted surgeons in making more precise surgeries.

The intraoperative navigation for PCNL was traditionally provided by fluoroscopy or US. The repetitive use of fluoroscopy or US was needed to make suitable percutaneous tracts. Novel techniques have helped reduce the radiation exposure and improve the accuracy during navigation, such as laser-guided puncture[6], ureteroscopy-assisted puncture[20], puncture with visual needles[4], marker-based tracking with iPADs[21] and electromagnetic tracking[7]. Navigation of the CAS system was mainly dependent on preoperative planning parameters rather than intraoperative techniques, which is different from the traditional imaging and novel techniques mentioned above. In addition, during the operation, the shape and position of stones and adjacent structures in display also gave reference to the location and adjustment of the tract. Perfect preoperative preparation and intraoperative reference reduced the repetitive use of fluoroscopy or US during the operation, especially when surgeons made percutaneous tracts. Navigation from the CAS system simplified the process for PCNL, making it more convenient. Surgeons also received less radiation exposure when the use of fluoroscopy was reduced.

The CAS system assisted PCNL in the preoperative planning and intraoperative navigation, and construction of a 3D model was a fundamental process. Initial 3D models were constructed from the excretory phase of contrast CT or CTU. Although adjacent structures were indistinct and incomplete, those models showed the relationship between stones and the collecting system, resulting in a low number of punctures[22]. The new generation of 3D reconstruction usually collects images from four phases of CTU. Structures were segmented from the phase in which they were most distinct. In particular, because of the clear display of renal arteries, segmental arteries and main branches, which did not exist in previous 3D renal pelvis model[22], injury to the renal artery system was generally avoided. In addition, noise reduction, smoothing and dyeing made structures more distinct from each other, and the transparency adjustments of the skin, kidney and collecting system made stones clearer, which improved the visual effect[23].

At present, a few studies have reported the application of the new generation of 3D reconstruction in PCNL. Tsaturyan *et al*[23] described technical details of 3D reconstruction in 3 patients. Li *et al*[9] reported 3D reconstruction in a cohort of 15 patients and provide reference in planning strategy and evaluation indicators. But these pilot studies did not include a control group. The study of Huang *et al*

[10] seemed to be the only controlled study, in which they verified the advantages of the technique in reducing number of punctures, number of tracts and volume of bleeding. Compared with our study, they had a larger sample size, but they adopted dual-source CT in the control group, which was not a standard imaging method. Besides, extra softwares were often used for post-processing procedures after 3D reconstruction in mentioned studies. 3D reconstruction and post-processing procedures were all performed in the CAS system in our study.

The perioperative characteristics showed the preliminary advantages of the CAS system. In the present study, demographic characteristics and stone characteristics that may influence the stone-free rate[24] were analyzed, and the patients in the two groups were relatively homogeneous without significant differences. Because of the absence of preoperative ipsilateral lesions or operations and the absence of second-stage surgeries, the initial stone-free rate accurately reflected the efficiency of the first-stage surgeries. The CAS group obtained a higher initial stone-free rate. Under the limitation of tract number, establishing efficient tracts to remove as many stones as possible is helpful to improve the stone-free rate[5]. We think that the display of the 3D models in the CAS system helped surgeons understand the 3D relationship between structures, which was conducive to the establishment of efficient tracts. In addition, accurate 3D measurement enabled the morphometry to be applied to the establishment of efficient tracts. For example, the angle between the entry calyx and the calyx to be reached is an independent predictive factor for accessing a particular calyx[14]. Therefore, we compared the measured data of the included angles of calyces to select ideal entry calyces. We also found a significantly higher success rate of one attempt in the CAS group, and this may be related to extra help from the CAS system. The quantitative planning data and intuitive reference of the 3D models increased the success rate of one attempt in the CAS group. Infection, bleeding and injury were major complications of PCNL[25], but most of these complications could be treated with conservative management [26]. Therefore, we focused on complications whose Clavien-Dindo grade ≥ 2. The CAS system seemed to help reduce bleeding due to the visualization of the renal vascular system, but no significant differences were found in the incidence of any complication. More patients are needed to explore the influence of the system on the development of complications.

We applied an intuitive, precise and convenient computer-assisted surgery system in PCNL and the new generation of 3D reconstruction was the key technique. The controlled study showed advantages in terms of the puncturing success rate and stone-free rate. In the future, resident training and patient care education may benefit from the system. The system and planning parameters will also promote the combination with other techniques and the application of novel techniques such as VR[8] and robot-assisted surgery[27] in PCNL. However, there are several limitations in this study. Patients were in the supine position when the CTU images were obtained, but they were in the prone position during the surgery. There was a change in the organ position between the two positions, which may alter the tract angles and injury rates[28]. Patients were advised to hold their breath for still preoperative images, but respiratory movement during the surgery could not be avoided. The system failed to provide the data and images in real time. Therefore, we reserved ultrasound to observe respiratory movement and the deformation of tissues for adjustments during surgery. In addition, further study is required due the lack of data from the tract dilation phase and stone removal phase. More patients should be included to explore the influence of the system on the development of complications. The system adds additional costs and procedures to the treatment, which need to be reduced and simplified to promote the clinical application of the system.

CONCLUSION

With multiple functions of the Hisense CAS system, an intuitive, precise and convenient PCNL could be achieved. The 3D construction of the model was the first and fundamental step, in which the new generation of 3D reconstruction was the key technique. This controlled study demonstrated the advantages of CAS-assisted PCNL in terms of the success rate of using only one puncturing attempt and the initial stone-free rate over standard PCNL. The System was recommended to assist in preoperative planning and intraoperative navigation for PCNL.

ARTICLE HIGHLIGHTS

Research background

Percutaneous nephrolithotomy (PCNL) is still a great challenge for surgeons because of poor comprehension on complex adjacent structures.

Research motivation

Novel techniques are required to assist in planning and navigation.

Research objectives
To apply and evaluate the Hisense computer-assisted surgery (CAS) system in PCNL.

Research methods
A total of 60 patients with complex renal stones were included. CAS-assisted PCNL (the CAS group) and standard PCNL (the control group) were compared in a retrospective study. Success rate of one attempt, operation time, initial stone-free rate, decrease in hemoglobin, and complications were collected and analyzed.

Research results
The success rate of one puncturing attempt (90% *vs* 67%, $P = 0.028$) and the initial stone-free rate (87% *vs* 63%, $P = 0.037$) were significantly higher in the CAS group. Compared with standard PCNL, CAS-assisted PCNL had advantages in terms of the puncturing success rate and stone-free rate.

Research conclusions
The Hisense CAS System was recommended to assist in preoperative planning and intraoperative navigation for an intuitive, precise and convenient PCNL.

Research perspectives
Consisting of construction, display, simulation and measurement functions, the CAS system is a novel and all-around software based on new generation of three-dimensional (3D) reconstruction. Compared with standard PCNL, CAS-assisted PCNL had advantages in terms of the puncturing success rate and stone-free rate. The CAS System was recommended to assist in preoperative planning and intraoperative navigation for an intuitive, precise and convenient PCNL.

FOOTNOTES

Author contributions: All authors contributed to the study conception and design; Data collection was performed by Sun YF and Zhang ZL; Data analysis was performed by Qin F, Zhang MX and Xie F; Figure collection and processing was performed by Liu SH and Wang ZJ; Cao YC and Jiao W provided clinical advice; Wang XN and Li B revised the manuscript according to comments; The first draft of the manuscript was written by Qin F and all authors commented on previous versions of the manuscript; all authors read and approved the final manuscript.

Supported by the Science and Technology Program in Chinese Medicine of Shandong Province, No. 2020M074.

Institutional review board statement: This study was reviewed and approved by the Ethics Committee of the Affiliated Hospital of Qingdao University, No. QYFYWZLL26370.

Informed consent statement: Informed consent was obtained from the patient in this study.

Conflict-of-interest statement: The authors had no conflict-of-interest to declare that are relevant to the content of this article.

Data sharing statement: The de-identified data will be shared on reasonable request to the corresponding author.

Open-Access: This article is an open-access article that was selected by an in-house editor and fully peer-reviewed by external reviewers. It is distributed in accordance with the Creative Commons Attribution NonCommercial (CC BY-NC 4.0) license, which permits others to distribute, remix, adapt, build upon this work non-commercially, and license their derivative works on different terms, provided the original work is properly cited and the use is non-commercial. See: https://creativecommons.org/Licenses/by-nc/4.0/

Country/Territory of origin: China

ORCID number: Fei Qin 0000-0002-8896-532X; Ye-Feng Sun 0000-0002-8743-8093; Xin-Ning Wang 0000-0002-7022-8073; Bin Li 0000-0001-6695-3080; Zhi-Lei Zhang 0000-0001-6801-8248; Ming-Xin Zhang 0000-0003-2606-1613; Fei Xie 0000-0002-5229-9572; Shuai-Hong Liu 0000-0001-7281-4490; Zi-Jie Wang 0000-0002-6246-2812; Yuan-Chao Cao 0000-0003-3949-168X; Wei Jiao 0000-0001-9102-4478.

S-Editor: Wu YXJ
L-Editor: A
P-Editor: Wu YXJ

REFERENCES

1 **Pradère B**, Doizi S, Proietti S, Brachlow J, Traxer O. Evaluation of Guidelines for Surgical Management of Urolithiasis. *J Urol* 2018; **199**: 1267-1271 [PMID: 29221932 DOI: 10.1016/j.juro.2017.11.111]

2 **Türk C**, Petřík A, Sarica K, Seitz C, Skolarikos A, Straub M, Knoll T. EAU Guidelines on Interventional Treatment for Urolithiasis. *Eur Urol* 2016; **69**: 475-482 [PMID: 26344917 DOI: 10.1016/j.eururo.2015.07.041]

3 **Allen D**, O'Brien T, Tiptaft R, Glass J. Defining the learning curve for percutaneous nephrolithotomy. *J Endourol* 2005; **19**: 279-282 [PMID: 15865512 DOI: 10.1089/end.2005.19.279]

4 **Zhang J**, Kang N, Jiang Y, Zhang J. Microperc with self-assembled fr 4.85 visual needle and ureteral access sheath. *J Invest Surg* 2021; 1-8 [DOI: 10.1080/08941939.2021.1902024]

5 **Xu Y**, Yuan Y, Cai Y, Li X, Wan S, Xu G. Use 3D printing technology to enhance stone free rate in single tract percutaneous nephrolithotomy for the treatment of staghorn stones. *Urolithiasis* 2020; **48**: 509-516 [PMID: 31616985 DOI: 10.1007/s00240-019-01164-8]

6 **Wu J**, Zhou P, Luo X, Hao Z, Lu C, Zhang H, Zhou T, Xu S. Novel laser positioning navigation to aid puncture during percutaneous nephrolithotomy: a preliminary report. *World J Urol* 2019; **37**: 1189-1196 [PMID: 30238400 DOI: 10.1007/s00345-018-2496-z]

7 **Rodrigues PL**, Vilaça JL, Oliveira C, Cicione A, Rassweiler J, Fonseca J, Rodrigues NF, Correia-Pinto J, Lima E. Collecting system percutaneous access using real-time tracking sensors: first pig model in vivo experience. *J Urol* 2013; **190**: 1932-1937 [PMID: 23714434 DOI: 10.1016/j.juro.2013.05.042]

8 **Farcas M**, Reynolds LF, Lee JY. Simulation-Based Percutaneous Renal Access Training: Evaluating a Novel 3D Immersive Virtual Reality Platform. *J Endourol* 2021; **35**: 695-699 [PMID: 33261507 DOI: 10.1089/end.2020.0674]

9 **Li H**, Chen Y, Liu C, Li B, Xu K, Bao S. Construction of a three-dimensional model of renal stones: comprehensive planning for percutaneous nephrolithotomy and assistance in surgery. *World J Urol* 2013; **31**: 1587-1592 [PMID: 23223963 DOI: 10.1007/s00345-012-0998-7]

10 **Huang YS**, Zhu XS, Wan GY, Zhu ZW, Huang HP. Application of simulated puncture in percutaneous nephrolithotomy. *Eur Rev Med Pharmacol Sci* 2021; **25**: 190-197 [PMID: 33506907 DOI: 10.26355/eurrev_202101_24384]

11 **Zhang G**, Zhou XJ, Zhu CZ, Dong Q, Su L. Usefulness of three-dimensional(3D) simulation software in hepatectomy for pediatric hepatoblastoma. *Surg Oncol* 2016; **25**: 236-243 [PMID: 27566028 DOI: 10.1016/j.suronc.2016.05.023]

12 **Liu H**, Wang F, Liu B, Zheng Z, Zhao J, Zhang J. Application of three-dimensional reconstruction with a Hisense computer-assisted system in upper pancreatic lymph node dissection during laparoscopic-assisted radical gastrectomy. *Asian J Surg* 2021; **44**: 730-737 [PMID: 33500172 DOI: 10.1016/j.asjsur.2020.12.034]

13 **Mishra S**, Sabnis RB, Desai M. Staghorn morphometry: a new tool for clinical classification and prediction model for percutaneous nephrolithotomy monotherapy. *J Endourol* 2012; **26**: 6-14 [PMID: 22050495 DOI: 10.1089/end.2011.0145]

14 **Guglielmetti GB**, Danilovic A, Torricelli FC, Coelho RF, Mazzucchi E, Srougi M. Predicting calyceal access for percutaneous nephrolithotomy with computed tomography multiplanar reconstruction. *Clinics (Sao Paulo)* 2013; **68**: 892-895 [PMID: 23778484 DOI: 10.6061/clinics/2013(06)27]

15 **Ghani KR**, Andonian S, Bultitude M, Desai M, Giusti G, Okhunov Z, Preminger GM, de la Rosette J. Percutaneous Nephrolithotomy: Update, Trends, and Future Directions. *Eur Urol* 2016; **70**: 382-396 [PMID: 26876328 DOI: 10.1016/j.eururo.2016.01.047]

16 **Thiruchelvam N**, Mostafid H, Ubhayakar G. Planning percutaneous nephrolithotomy using multidetector computed tomography urography, multiplanar reconstruction and three-dimensional reformatting. *BJU Int* 2005; **95**: 1280-1284 [PMID: 15892817 DOI: 10.1111/j.1464-410X.2005.05519.x]

17 **Desai M**, De Lisa A, Turna B, Rioja J, Walfridsson H, D'Addessi A, Wong C; Rosette On Behalf Of The Croes Pcnl Study Group J. The clinical research office of the endourological society percutaneous nephrolithotomy global study: Staghorn vs nonstaghorn stones. *J Endourol* 2011; **25**: 1263-1268 [DOI: 10.1089/end.2011.0055]

18 **Fang YQ**, Wu JY, Li TC, Zheng HF, Liang GC, Chen YX, Hong XB, Cai WZ, Zang ZJ, Di JM. Computer tomography urography assisted real-time ultrasound-guided percutaneous nephrolithotomy on renal calculus. *Medicine (Baltimore)* 2017; **96**: e7215 [PMID: 28614270 DOI: 10.1097/MD.0000000000007215]

19 **Akand M**, Buyukaslan A, Servi S, Civcik L. A hypothetical method for calculation of the access point, direction angle and access angle for percutaneous nephrolithotomy. *Med Hypotheses* 2019; **124**: 101-104 [PMID: 30798901 DOI: 10.1016/j.mehy.2019.02.007]

20 **Lima E**, Rodrigues PL, Mota P, Carvalho N, Dias E, Correia-Pinto J, Autorino R, Vilaça JL. Ureteroscopy-assisted Percutaneous Kidney Access Made Easy: First Clinical Experience with a Novel Navigation System Using Electromagnetic Guidance (IDEAL Stage 1). *Eur Urol* 2017; **72**: 610-616 [PMID: 28377202 DOI: 10.1016/j.eururo.2017.03.011]

21 **Rassweiler-Seyfried MC**, Rassweiler JJ, Weiss C, Müller M, Meinzer HP, Maier-Hein L, Klein JT. iPad-assisted percutaneous nephrolithotomy (PCNL): a matched pair analysis compared to standard PCNL. *World J Urol* 2020; **38**: 447-453 [PMID: 31073641 DOI: 10.1007/s00345-019-02801-y]

22 **Brehmer M**, Beckman MO, Magnusson A. Three-dimensional computed tomography planning improves percutaneous stone surgery. *Scand J Urol* 2014; **48**: 316-323 [PMID: 24521181 DOI: 10.3109/21681805.2013.876552]

23 **Tsaturyan A**, Bellin A, Barbuto S, Zampakis P, Ntzanis E, Lattarulo M, Kalogeropoulou C, Liatsikos E, Kallidonis P; Collaborators. Technical aspects to maximize the hyperaccuracy three-dimensional (HA3D™) computed tomography reconstruction for kidney stones surgery: a pilot study. *Urolithiasis* 2021; **49**: 559-566 [PMID: 33811497 DOI: 10.1007/s00240-021-01262-6]

24 **Biswas K**, Gupta SK, Tak GR, Ganpule AP, Sabnis RB, Desai MR. Comparison of STONE score, Guy's stone score and Clinical Research Office of the Endourological Society (CROES) score as predictive tools for percutaneous nephrolithotomy outcome: a prospective study. *BJU Int* 2020; **126**: 494-501 [PMID: 32506712 DOI: 10.1111/bju.15130]

25 **de la Rosette J**, Assimos D, Desai M, Gutierrez J, Lingeman J, Scarpa R, Tefekli A; CROES PCNL Study Group. The Clinical Research Office of the Endourological Society Percutaneous Nephrolithotomy Global Study: indications, complications, and outcomes in 5803 patients. *J Endourol* 2011; **25**: 11-17 [PMID: 21247286 DOI:

10.1089/end.2010.0424]
26 **Kyriazis I**, Panagopoulos V, Kallidonis P, Özsoy M, Vasilas M, Liatsikos E. Complications in percutaneous nephrolithotomy. *World J Urol* 2015; **33**: 1069-1077 [PMID: 25218854 DOI: 10.1007/s00345-014-1400-8]
27 **Oo MM**, Gandhi HR, Chong KT, Goh JQ, Ng KW, Hein AT, Tan YK. Automated Needle Targeting with X-ray (ANT-X) - Robot-assisted device for percutaneous nephrolithotomy (PCNL) with its first successful use in human. *J Endourol* 2021; **35**: e919 [PMID: 29699415 DOI: 10.1089/end.2018.0003]
28 **Marchini GS**, Berto FC, Vicentini FC, Shan CJ, Srougi M, Mazzucchi E. Preoperative planning with noncontrast computed tomography in the prone and supine position for percutaneous nephrolithotomy: a practical overview. *J Endourol* 2015; **29**: 6-12 [PMID: 25025863 DOI: 10.1089/end.2014.0299]

World Journal of Clinical Cases

Submit a Manuscript: https://www.f6publishing.com

World J Clin Cases 2022 June 26; 10(18): 6050-6059

DOI: 10.12998/wjcc.v10.i18.6050

ISSN 2307-8960 (online)

ORIGINAL ARTICLE

Retrospective Study

Influences of etiology and endoscopic appearance on the long-term outcomes of gastric antral vascular ectasia

Hyo Jin Kwon, Si Hyung Lee, Joon Hyun Cho

Specialty type: Gastroenterology and hepatology

Provenance and peer review: Unsolicited article; Externally peer reviewed.

Peer-review model: Single blind

Peer-review report's scientific quality classification

Grade A (Excellent): 0
Grade B (Very good): B, B
Grade C (Good): C
Grade D (Fair): 0
Grade E (Poor): 0

P-Reviewer: El-Nakeep S, Egypt; Govindarajan KK, India

Received: December 18, 2021
Peer-review started: December 18, 2021
First decision: January 23, 2022
Revised: January 31, 2022
Accepted: April 24, 2022
Article in press: April 24, 2022
Published online: June 26, 2022

Hyo Jin Kwon, Si Hyung Lee, Joon Hyun Cho, Division of Gastroenterology and Hepatology, Department of Internal Medicine, Yeungnam University College of Medicine, Daegu 42415, South Korea

Corresponding author: Joon Hyun Cho, MD, PhD, Associate Professor, Division of Gastroenterology and Hepatology, Department of Internal Medicine, Yeungnam University College of Medicine, 170 Hyeonchung-ro, Nam-gu, Daegu 42415, South Korea.
ygowgo96@hanmail.net

Abstract

BACKGROUND

Gastric antral vascular ectasia (GAVE) has diverse associations and presumed causes, which include liver cirrhosis, chronic kidney disease, and autoimmune disease. This heterogeneity of underlying disorders suggests that the pathogenesis of GAVE may be variable.

AIM

To compare the clinical features and long-term outcomes of GAVE according to endoscopic patterns and etiologies.

METHODS

The medical records and endoscopic images of 23 consecutive patients diagnosed with GAVE by endoscopy at Yeungnam University Hospital from January 2006 to December 2020 were retrospectively reviewed. Patients were allocated to cirrhosis (16 patients) and non-cirrhosis groups (7 patients). GAVE subtypes, as determined by endoscopy, were categorized as punctate (a diffuse, honeycomb-like appearance, 17 patients) or striped (a linear, watermelon-like appearance, 6 patients).

RESULTS

All GAVE patients with cirrhosis (16/16, 100%) had a punctate pattern by endoscopy, whereas the majority of patients (6/7, 85.7%) without cirrhosis had a striped pattern ($P < 0.001$). Overt GAVE bleeding (10/23, 43%) was significantly more common in the non-cirrhosis group than in the cirrhosis group (6/7, 85.7% *vs* 4/16, 25.0%; $P = 0.019$), and more common in the striped group than in the punctate group (5/6, 83.3% *vs* 5/17, 29.4%; $P = 0.052$). However, mean numbers of admissions due to GAVE bleeding and argon plasma coagulation (APC) sessions to address overt bleeding were similar in the cirrhosis and non-cirrhosis groups and in the punctate and striped groups. All patients with GAVE bleeding were

successfully treated by APC, and no patient died from GAVE-related blood loss during a median follow-up of 24 mo.

CONCLUSION
Punctate-type GAVE is strongly associated with liver cirrhosis, and GAVE patients without cirrhosis tend to be more prone to overt bleeding. However, the presence of cirrhosis and endoscopic patterns did not influence long-term clinical courses or outcomes in cases of overt bleeding.

Key Words: Gastric antral vascular ectasia; Cirrhosis; Endoscopy; Gastrointestinal bleeding; Argon plasma coagulation

©The Author(s) 2022. Published by Baishideng Publishing Group Inc. All rights reserved.

Core Tip: The study shows that punctate (diffuse, honeycomb)-type gastric antral vascular ectasia (GAVE) is strongly associated with liver cirrhosis, whereas striped (linear, watermelon)-type GAVE is strongly associated with non-cirrhotic underlying disease. Additionally, GAVE patients without cirrhosis tended to be more prone to overt bleeding. However, the presence of cirrhosis and endoscopic GAVE patterns did not influence clinical courses or the outcomes of overt bleeding after endoscopic APC treatment. It appears that clinical manifestations are dependent on etiologies, but that etiologies do not influence clinical courses in cases of GAVE bleeding.

Citation: Kwon HJ, Lee SH, Cho JH. Influences of etiology and endoscopic appearance on the long-term outcomes of gastric antral vascular ectasia. *World J Clin Cases* 2022; 10(18): 6050-6059
URL: https://www.wjgnet.com/2307-8960/full/v10/i18/6050.htm
DOI: https://dx.doi.org/10.12998/wjcc.v10.i18.6050

INTRODUCTION

Gastric antral vascular ectasia (GAVE), also known as "watermelon stomach", is a rare clinical condition related to upper gastrointestinal (GI) bleeding, which varies from chronic occult blood loss requiring serial transfusions to acute hemorrhage[1]. GAVE was first described by Rider *et al*[2] in 1953 and fully defined by Jabbari *et al*[3] in 1984, who described patients with hyperemic striae in gastric antrum. GAVE is characterized by a unique endoscopic appearance, which takes two forms, punctate (a diffuse, honeycomb-like appearance) and striped (a linear, watermelon-like appearance). Striped GAVE has the endoscopic appearance of red stripes radiating from antrum and converging at pylorus, whereas the punctate form is characterized by diffuse red spots indicating dilated blood vessels in antrum.

Liver cirrhosis is the most frequent underlying condition associated with GAVE and portal hypertension is seen in approximately 40% of reported cases[4,5], though GAVE may not respond to therapies directed at reducing portal pressure. In addition, GAVE has been associated with other diverse medical conditions including chronic renal failure, diabetes, and autoimmune and connective tissue disorders such as systemic lupus erythematosus, rheumatoid arthritis, and systemic sclerosis[6-10]. Thus, the heterogeneity of underlying diseases observed in GAVE patients suggests its pathogenesis may be variable[11].

Epidemiologic evidence indicating that the clinical outcomes of GAVE patients with or without cirrhosis differ is lacking. Although numerous studies have investigated GAVE and many case reports and series have been reported, little information is available on the effects of its etiologies and gross endoscopic appearances on long-term clinical courses or outcomes, especially in Asians. In this study, we aimed to determine whether the presence of cirrhosis and endoscopic patterns are related to the clinical features and course of GAVE.

MATERIALS AND METHODS

Study design and patients

This retrospective cohort study was approved by the Institutional Review Board of Yeungnam University Hospital (IRB No. 2021-10-044), which waived the requirement for written informed consent due to the retrospective nature of the study. We reviewed the medical records of 23 consecutive patients diagnosed with GAVE by endoscopy at our institution from January 2006 to December 2020. Baseline

demographic data such as gender, etiology of liver disease, and severity of liver disease (as determined using Child-Pugh scores) were collected, as were details of medical comorbidities (liver cirrhosis, chronic renal failure, autoimmune or connective tissue disease, diabetes, and others), medications [proton pump inhibitors (PPIs), non-steroidal anti-inflammatory drugs (NSAIDs), and anticoagulant and antiplatelet use], and follow-up durations. Laboratory findings such as hemoglobin levels, platelet counts, serum urea nitrogen and creatinine, serum albumin, and prothrombin activity were also reviewed. Patients were categorized into two groups based on the presence (16 patients) or absence (7 patients) of cirrhosis. Cirrhosis was diagnosed based on a combination of clinical findings, liver function tests, and computed tomographic or ultrasonographic appearances of liver and spleen. Only patients aged 18 or older were included in the analysis. Median follow-up duration was 24 mo (range 6-84 mo) in the cirrhosis group and 26 mo (range 4-96 mo) in the non-cirrhosis group.

Diagnosis and endoscopic classification

GAVE was diagnosed during upper GI endoscopy by skilled gastroenterologists. Histologic specimens were not required to differentiate GAVE from portal hypertensive gastropathy. GAVE was diagnosed primarily based on endoscopic patterns and in uncertain cases by histology[12]. Endoscopy reports and photographs were reviewed independently by two gastroenterologists (Cho JH and Kwon HJ) unaware of clinical statuses. When these two gastroenterologists disagreed regarding diagnoses, a third independent gastroenterologist (Lee SH) reviewed the information available and made final decisions. Patients were classified into one of two groups according to the two typical endoscopic appearances of GAVE, that is, to a "punctate" (diffuse, honeycomb) group (17 patients) with sharply demarcated red spots diffusely spread within antrum (Figure 1A) or a "striped" (linear, watermelon) type group (6 patients) with prominent flat or raised red stripes radiating longitudinally from pylorus to antrum (Figure 1B)[6]. During upper GI endoscopy, bleeding from GAVE lesions and the presence of other nonbleeding lesions were noted (these included lesions due to portal hypertension in patients with cirrhosis). Overt GI bleeding was defined based on the presence of symptoms, such as hematemesis, melena, or hematochezia, a change in hemodynamics, or gross bleeding by upper GI endoscopy. Median follow-up duration was 23 mo (range 6-84 mo) in the punctate group and 27 mo (range 4-96 mo) in the striped group.

Endoscopic procedure

Argon plasma coagulation (APC) treatment for GAVE consisted of electrocoagulation of all angiectatic lesions during an endoscopic session with an APC probe introduced through the working channel of an endoscope. Argon gas flow ranged from 0.8 L/min to 1 L/min, and electric power output from 50 W to 70 W. Angioectasia was managed using a combination of focal pulse and ''spray-painting'' techniques. During endoscopic sessions, argon and coagulation smoke were regularly aspirated, and coagulum on probes was removed when required. Treatment time per session varied from 20 min to 40 min. All patients received PPI therapy for 3 wk to 4 wk to promote mucosal healing after the procedure. The endpoint of treatment was defined as complete or near complete disappearance of vascular ectasia. In cases of anemia recurrence requiring transfusion of packed red blood cells or cases of overt GI bleeding recurrence, another APC session was performed. The criteria for successful APC treatment were cessation of GI bleeding and the need for transfusion. Numbers of APC sessions per patient were documented and APC treatment success rates were evaluated.

Statistical analysis

Data were analyzed using SPSS version 20.0 for Windows (SPSS Inc, Chicago, IL). GAVE patients with or without cirrhosis were compared with respect to multiple factors, which included demographics, associated underlying diseases, laboratory values, and clinical outcomes of endoscopic APC treatment. Patients with punctate or striped GAVE were also compared. Continuous variables are expressed as mean ± SD and were compared using the Student's t test or the Mann-Whitney test. Categorical variables are expressed as absolute numbers and proportions and were compared using Fisher's exact test. All statistical tests were two-sided, and statistical significance was accepted for $P < 0.05$.

RESULTS

Patient characteristics

Over the fifteen-year study period (January 2006 to December 2020), 23 patients were diagnosed with GAVE at our institution. Mean patient age was 59.8 ± 12.6 years (range 41-79) and 14 (60.9%) were male. Indications for initial endoscopy were screening for varices (8 patients), iron deficiency anemia (5), melena (8), or hematemesis (2). The etiology of cirrhosis was viral in 6 patients, alcohol in 6, autoimmune hepatitis in 1, nonalcoholic steatohepatitis in 1, and others in 2 (Table 1). The Child-Pugh classification was used to grade liver disease severity in cirrhotic patients. Eight patients with cirrhosis were classified as Child-Pugh B (50%), five as A (31.3%), and three as C (18.7%). Ten patients (62.5%) with

Table 1 Comparison of endoscopic patterns and baseline characteristics in patients with or without cirrhosis

	Cirrhosis (*n* = 16)	No cirrhosis (*n* = 7)	*P* value
Endoscopic pattern of GAVE, *n* (%)			< 0.001
Punctate (Diffuse)	16 (100)	1 (14.3)	
Stripe (Linear)	0	6 (85.7)	
Age, yr, mean ± SD	55.4 ± 12.2	69.8 ± 6.1	0.015
Gender (males/females)	12/4	2/5	0.066
BMI, kg/m^2, mean ± SD	23.4 ± 4.0	25.0 ± 4.6	0.397
Etiology of cirrhosis, *n* (%)			
Viral	6 (37.5)		
Alcohol	6 (37.5)		
Autoimmune hepatitis	1 (6.3)	NA	NA
NASH	1 (6.3)		
Cryptogenic	2 (12.5)		
Child Pugh Score, *n* (%)			
Class A	5 (31.3)		
Class B	8 (50.0)	NA	NA
Class C	3 (18.7)		
Other associated diseases, *n* (%)			
Chronic kidney disease	2 (12.5)	5 (71.4)	0.011
SLE	0	1 (14.3)	0.304
Hypertension	3 (18.8)	2 (28.6)	0.621
Diabetes mellitus	5 (31.3)	3 (42.9)	0.657
Medication, *n* (%)			
PPI use	6 (37.5)	3 (42.9)	1.000
Antiplatelet use	0	1 (14.3)	0.304
Anticoagulant use	0	1 (14.3)	0.304
Initial laboratory findings, mean ± SD			
Hemoglobin level, g/dL	7.8 ± 3.4	6.2 ± 1.6	0.494
Platelet count, k/μL	103.9 ± 73.0	176.8 ± 62.2	0.041
Total bilirubin, mg/dL	1.74 ± 1.35	1.15 ± 1.30	0.188
Albumin, g/dL	2.52 ± 0.36	3.03 ± 0.60	0.048
INR	1.23 ± 0.27	1.09 ± 0.25	0.179
BUN, mg/dL,	23.3 ± 14.0	44.9 ± 39.1	0.416
Creatinine, mg/dL	1.12 ± 0.44	3.65 ± 2.93	0.244

BMI: Body mass index; NA: Not applicable; NASH: Nonalcoholic steatohepatitis; NSAID: Nonsteroidal anti-inflammatory inhibitor drug; PPI: Proton pump inhibitor; SLE: Systemic lupus erythematosus; INR: International normalized ratio; BUN: Blood urea nitrogen.

cirrhosis had esophageal varices.

Comparison between patients with or without cirrhosis

The characteristics of patients in the cirrhosis and non-cirrhosis groups at GAVE diagnosis are summarized in Table 1. Mean age was significantly greater in the cirrhosis group (69.8 ± 6.1 *vs* 55.4 ± 12.2, P = 0.015). Men predominated in the cirrhosis group (12/16, 75.0%) and women in the non-cirrhosis group (5/7, 71.4%). Mean group body mass indices (BMIs) were not significantly different. In the non-cirrhosis group, the most common associated disease was chronic kidney disease (5/7, 71.4%),

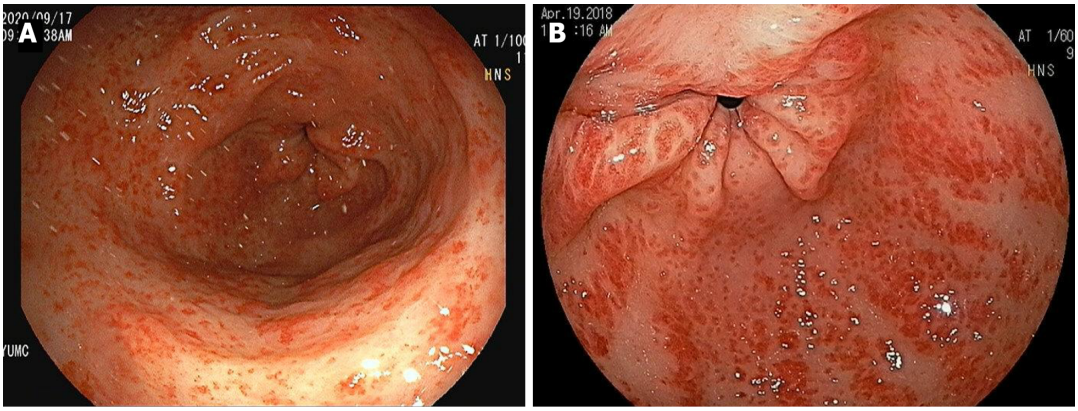

DOI: 10.12998/wjcc.v10.i18.6050 **Copyright** ©The Author(s) 2022.

Figure 1 Two main typical endoscopic views of gastric antral vascular ectasia. A: Punctate (diffuse, honeycomb)-type gastric antral vascular ectasia (GAVE) showing sharply demarcated, punctate red spots diffusely scattered in antrum; B: Striped (linear, watermelon)-type GAVE showing bright red bands radiating longitudinally from pylorus.

and this was followed by diabetes mellitus (3/7, 42.9%), and the prevalence of chronic kidney disease was significantly greater in the non-cirrhosis group (5/7, 71.4% *vs* 2/16, 12.5%; P = 0.011). The frequencies of other associated diseases, except chronic kidney disease, were similar in the two groups. Although no patient received corticosteroids or NSAIDs, 2 patients in the non-cirrhosis group were on antiplatelet or anticoagulant medication, respectively, which did not amount to a significant difference versus the cirrhotic group. As regards initial laboratory findings, platelet count and serum albumin level were significantly lower in the cirrhosis group (103.9 ± 73.0 k/μL *vs* 176.8 ± 62.2 k/μL, P = 0.041; and 2.52 ± 0.36 g/dL *vs* 3.03 ± 0.60 g/dL, P = 0.048, respectively). Mean hemoglobin levels were not significantly different in the cirrhosis and non-cirrhosis groups (7.8 ± 3.4 *vs* 6.2 ± 1.6, respectively, P = 0.494). Total bilirubin and international normalized ratio (INR) were non-significantly greater in the cirrhosis group (1.74 ± 1.35 *vs* 1.15 ± 1.30, and 1.23 ± 0.27 *vs* 1.09 ± 0.25; P = 0.188 and 0.179, respectively). Blood urea nitrogen (BUN) and serum creatinine were higher in the non-cirrhosis group (44.9 ± 39.1 *vs* 23.3 ± 14.0, and 3.65 ± 2.93 *vs* 1.12 ± 0.44, respectively), but again differences were not significant (NS, P = 0.416 and 0.244, respectively). However, group endoscopic patterns were significantly different; all patients in the cirrhosis group had punctate GAVE, whereas 6/7 patients (85.7%) in the non-cirrhosis group had striped GAVE (P < 0.001).

Comparison between endoscopic types

The characteristics of patients in the punctate and striped groups at diagnosis are summarized in Table 2. Mean age was significantly greater in the striped group (70.8 ± 6.3 *vs* 56.1 ± 12.0, P = 0.011). Men predominated in the punctate group (13/17, 76.5%), and women predominated in the striped group (5/6, 83.3%). Group BMIs were not significantly different. Sixteen of the 17 patients in the punctate group (16/17, 94.1%) had concurrent cirrhosis, whereas no patient in the striped group (0/6, 0%) had cirrhosis (P < 0.001). In the striped group, the most common associated disease was chronic kidney disease (5/6, 83.3%), which was followed by diabetes mellitus (3/6, 50%), and patients in this group had an increased prevalence of chronic kidney disease (5/6, 83.3% *vs* 2/17, 11.8%; P = 0.014). The frequencies of other associated diseases were not significantly different in the two groups. As regards initial laboratory findings, serum bilirubin was significantly higher in the punctate group (1.88 ± 1.39 *vs* 0.64 ± 0.41, P = 0.044), but creatinine was significantly higher in the striped group (4.27 ± 2.79 *vs* 1.07 ± 0.45, P = 0.034), and BUN was non-significantly higher in the striped group (51.9 ± 39.9 vs 22.5 ± 13.8, P = 0.130). Mean hemoglobin levels were similar in the punctate and striped groups (7.5 ± 3.4 *vs* 6.6 ± 1.4, P = 0.528), but platelet counts and serum albumin levels were non-significantly lower in the punctate group (114.5 ± 81.5 *vs* 159.6 ± 51.1, and 2.51 ± 0.39 *vs* 3.00 ± 0.59; P = 0.168 and 0.070, respectively). INR was non-significantly higher in the punctate group (1.23 ± 0.26 *vs* 1.08 ± 0.28, respectively, P = 0.130).

Clinical outcomes

Ten of the 23 patients (43.5%) were diagnosed with overt GAVE bleeding, and this was significantly more common in the non-cirrhosis group than in the cirrhosis group (6/7, 85.7% *vs* 4/16, 25.0%; P = 0.019, Table 3), and more common in the striped group than in the punctate group (5/6, 83.3% *vs* 5/17, 29.4%; P = 0.052, Table 4). Endoscopic APC treatment was required significantly more frequently in the non-cirrhosis group than in the cirrhosis group (6/7, 85.7% *vs* 4/16, 25.0%; P = 0.019), and more frequently required in the striped group than in the punctate group (5/6, 83.3% *vs* 5/17, 29.4%; P = 0.052). However, numbers of admissions due to GAVE bleeding were no different in the cirrhosis and non-cirrhosis groups (3.00 ± 2.45 *vs* 3.00 ± 2.83, NS) and in the punctate and striped groups (3.00 ± 2.83

Table 2 Comparison of the baseline characteristics of patients with punctate or striped patterns

	Punctate (*n* = 17)	Stripe (*n* = 6)	*P* value
Age, yr, mean ± SD	56.1 ± 12.0	70.8 ± 6.3	0.011
Gender (males/females)	13/4	1/5	0.018
BMI, kg/m^2, mean ± SD	23.5 ± 3.9	25.2 ± 2.6	0.612
Liver cirrhosis, *n* (%)	16 (94.1)	0	< 0.001
Other associated diseases, *n* (%)			
Chronic kidney disease	2 (11.8)	5 (83.3)	0.003
SLE	0	1 (16.7)	0.261
Hypertension	3 (17.6)	2 (33.3)	0.576
Diabetes mellitus	5 (29.4)	3 (50.0)	0.621
Initial laboratory findings, mean ± SD			
Hemoglobin level, g/dL	7.5 ± 3.4	6.6 ± 1.4	0.528
Platelet count, k/μL	114.5 ± 81.5	159.6 ± 51.1	0.168
Total bilirubin, mg/dL	1.88 ± 1.39	0.64 ± 0.41	0.044
Albumin, g/dL	2.51 ± 0.39	3.00 ± 0.59	0.070
INR	1.23 ± 0.26	1.08 ± 0.28	0.130
BUN, mg/dL,	22.5 ± 13.8	51.9 ± 39.9	0.130
Creatinine, mg/dL	1.07 ± 0.45	4.27 ± 2.79	0.034

BMI: Body mass index; SLE: Systemic lupus erythematosus; INR: International normalized ratio; BUN: Blood urea nitrogen.

Table 3 Comparison of the clinical outcomes of patients with or without cirrhosis

	Cirrhosis (*n* = 16)	No cirrhosis (*n* = 7)	*P* value
Overt bleeding, *n* (%)	4 (25.0)	6 (85.7)	0.019
APC treatment, *n* (%)	4 (25.0)	6 (85.7)	0.019
No. of admissions d/t GAVE bleeding, mean ± SD	3.00 ± 2.45	3.00 ± 2.83	NS
No. of APC sessions, mean ± SD	4.50 ± 4.95	4.80 ± 5.08	NS
Success of APC	4/4	6/6	NS
Surgery	0	0	NS
Death due to GAVE bleeding	0	0	NS
Follow-up, month, median (range)	24 (6-84)	26 (4-96)	NS

APC: Argon plasma cauterization; GAVE: Gastric antral vascular ectasia; NS: Not significant.

vs 3.00 ± 2.45, NS). In addition, no patient in either group needed therapy escalation to surgery. All 10 patients with GAVE bleeding underwent endoscopic APC treatment on a weekly or fortnightly basis, and all responded well to treatment. The mean numbers of APC sessions in patients with GAVE bleeding were similar in the cirrhosis and non-cirrhosis groups (4.50 ± 4.95 *vs* 4.80 ± 5.08, NS) and in the punctate and striped groups (4.00 ± 4.34 *vs* 5.25 ± 5.44, NS). Median follow-up durations were 24 mo and 26 mo in cirrhosis and non-cirrhosis groups, respectively, and 23 mo and 27 mo in punctate group and striped groups, respectively (neither intergroup difference was significant). During follow-up, 3 patients in the cirrhosis group and 1 patient in the non-cirrhosis group died of a cause other than GAVE bleeding (hepatocellular carcinoma in 1, hepatic failure in 1, and multiple organic failure in 2). No patient succumbed to GI hemorrhage.

Table 4 Comparison of the clinical outcomes of patients with punctate or striped patterns

	Punctate (*n* = 17)	Stripe (*n* = 6)	*P* value
Overt bleeding, *n* (%)	5 (29.4)	5 (83.3)	0.052
APC treatment, *n* (%)	5 (29.4)	5 (83.3)	0.052
No. of admissions d/t GAVE bleeding, mean ± SD	3.00 ± 2.83	3.00 ± 2.45	NS
No. of APC sessions, mean ± SD	4.00 ± 4.34	5.25 ± 5.44	NS
Success of APC	5/5	5/5	NS
Surgery	0	0	NS
Death due to GAVE bleeding	0	0	NS
Follow-up, month, median (range)	23 (6-84)	27 (4-96)	NS

APC: Argon plasma cauterization; GAVE: Gastric antral vascular ectasia; NS: Not significant.

DISCUSSION

The pathogenesis of GAVE is unknown but seems to be related to liver cirrhosis in most cases. Several authors have suggested that portal hypertension is the most influential contributor to the development of GAVE. Tobin *et al*[7] reported that patients with GAVE-induced gastric bleeding after bone marrow transplantation had hepatic veno-occlusive disease, which supports suggestions that portal hypertension might be a predisposing factor of GAVE. On the other hand, it has been demonstrated that GAVE lesions may develop in patients with cirrhosis independently of portal hypertension[8,11]. Indeed, Spahr *et al*[8] reported that portal decompression using a transjugular intrahepatic portosystemic shunt or a surgical end-to-side portacaval shunt was ineffective at treating GAVE bleeding. In addition to cirrhosis, several other disorders such as chronic kidney disease[9], chronic valvular, ischemic, or hypertensive heart disease, and a variety of autoimmune diseases[13], including Raynaud's phenomena, rheumatoid arthritis, primary biliary cirrhosis, and systemic sclerosis (diffuse and limited), have been also associated with the development of GAVE.

The remarkable heterogeneity of diseases associated with GAVE generates a wide array of factors that might cause angioectasia. Several factors have been suggested to play roles in the pathogenesis of GAVE. Charneau *et al*[14] reported that gastric antral motility was remarkably different in cirrhotic patients with or without GAVE. Others have suggested prostaglandin E2[15], gastrin[16], vasoactive intestinal polypeptide (VIP), and the proliferation of local neuroendocrine cells containing 5-hydroxytryptamine (5-HT)[17] are causative factors. Thus, it appears GAVE is probably caused by vasodilation and impaired motility[17] driven by these neurohumoral factors[15-18]. However, the pathophysiological changes leading to GAVE have not been fully explained[19,20]. It seems complex interplay between various factors underlies the development of vascular ectasias, and that differences in gross endoscopic appearances, *i.e.*, punctate-type or striped-type, depend on the relative influences of these factors. As described above, the assumed pathophysiology of GAVE is entirely different from that of portal hypertensive gastropathy, although at diagnosis, GAVE can be confused with this condition.

In our study, all 16 patients with cirrhosis had punctate-type GAVE and almost all patients (16/17) with punctate-type GAVE had concurrent cirrhosis. In contrast, 6 of 7 patients without cirrhosis had striped-type GAVE; the other patient had punctate-type GAVE. Thus, in this study punctate-type GAVE appeared to be associated with cirrhosis, and striped-type GAVE was not. Several reports have described linear lesions within antrum in non-cirrhotic patients and diffuse lesions in cirrhotic patients [1,6,21,22], and our results concur with these observations.

We also found that GAVE patients without cirrhosis more frequently exhibited overt bleeding and required APC treatment than those with cirrhosis. Unfortunately, we could not adjust our multivariate analysis for GI bleeding confounders due to the small number of overt GAVE bleeding cases included. Nonetheless, these observations do indicate GAVE with cirrhosis-associated nonvariceal GI bleeding is rare. However, in contrast to our results, in a retrospective study of 30 patients that underwent APC for GAVE bleeding (17 patients had cirrhosis), Lecleire *et al*[23] reported that patients with cirrhosis more frequently exhibited overt bleeding (65% *vs* 15%, $P = 0.01$), whereas patients without cirrhosis more frequently had occult bleeding as revealed by isolated iron deficiency anemia (35% *vs* 85%, $P = 0.01$). However, Wang *et al*[24] in a retrospective case-control study, reported that multivariate regression analysis adjusted for confounders showed the absence of cirrhosis best predicted active bleeding from GAVE with an odds ratio of 5.151 (95% confidence interval: 1.08-24.48, $P = 0.039$). In this previous study, of 84 GAVE patients with cirrhosis, 27 (32.1%) had overt bleeding, and of 26 patients without cirrhosis, 17 (63.4%) had overt bleeding. The reason for a significant difference between the incidences of overt bleeding according to the presence or absence of cirrhosis in GAVE remains unclear, although it has

been shown circulating neurohumoral factor levels, such as those of prostaglandin E, VIP, and 5-HT, differ in GAVE patients with or without cirrhosis[15-18]. Future studies are needed to clarify mechanistic differences between patients with or without cirrhosis in order to determine whether neurohumoral factors are responsible for clinically observed differences.

APC has been the endoscopic treatment of choice for GAVE since its introduction. In general, patients exhibit good initial response and low complication rates, but recurrent bleeding rates are usually high, and rates of 35.0% to 78.9% have been reported[25-27]. In the present study, endoscopic APC was performed in 10 patients with GAVE bleeding (4 patients had cirrhosis) and no complication was recorded after APC treatment. However, as has also been reported, 8 of the 10 patients required additional hospitalization due to GAVE bleeding after APC treatment and only two patients did not (one in the non-cirrhosis group and one in the cirrhosis group). In order to compare the clinical courses of GAVE bleeding cases with or without cirrhosis or with punctate or striped GAVE, we focused on the number of admissions due to GAVE bleeding. Although the proportion of patients with overt GAVE bleeding that received APC treatment was significantly greater among those without cirrhosis than those with cirrhosis, mean numbers of admissions due to GAVE bleeding and of APC sessions in overt bleeding patients were similar in the cirrhosis and non-cirrhosis groups and in the striped and punctate groups. These results suggest vulnerability to bleeding depends on GAVE etiology, but that clinical course after overt bleeding does not.

All patients with GAVE bleeding were successfully treated by APC. No patient needed surgery or died of GAVE-related blood loss, and mortalities during follow-up were similar in the cirrhosis and non-cirrhosis groups and in the punctate and striped groups. These findings suggest that APC is effective and safe for treating GAVE bleeding. Furthermore, the outcomes of endoscopic APC were similar regardless of endoscopic appearance or the presence of cirrhosis, which concurs with the results of a previous study[1]. Based on the above findings, we conclude that the presence of cirrhosis and endoscopic type have no influence on response to endoscopic APC treatment. We cannot explain why regardless of etiology, APC is an effective hemostatic treatment for GAVE. Indeed, the pathophysiologic features of GAVE are undetermined, and thus, open to debate.

Some limitations of the present study warrant consideration. First, some clinical data such as radiologically determined portal vein diameters and liver fibroscan data were missing due to the retrospective design of the study and lack of availability. Second, the sample size was small, especially numbers of bleedings and APC cases, and thus, it was not possible to compare study groups with respect to some variables or perform further multivariate analysis to identify risk factors of GAVE bleeding. Nevertheless, this study is one of the few to compare long-term clinical courses according to the presence or absence of cirrhosis and endoscopic type in a non-Western region.

CONCLUSION

GAVE patients without cirrhosis tended to be more prone to overt bleeding; however, the long-term clinical courses of GAVE bleeding after endoscopic APC treatment were similar irrespective of the presence of cirrhosis or endoscopic appearance. These findings suggest that the etiologies of GAVE may result in different clinical manifestations, especially bleeding, but do not influence the clinical course of GAVE bleeding. Additional studies are needed to identify the factors that play key roles in the development and clinical course of GAVE and to clarify its pathophysiologic mechanism. Furthermore, although these issues remain to be clarified, we recommend that when GAVE is diagnosed endoscopically, a careful investigation should be undertaken to determine whether liver cirrhosis and other non-cirrhotic disease processes associated with GAVE are present.

ARTICLE HIGHLIGHTS

Research background

Gastric antral vascular ectasia (GAVE) is associated with diverse medical conditions such as liver cirrhosis, chronic kidney disease, and autoimmune disease. This heterogeneity of underlying disorders suggests that the pathogenesis of GAVE may not be uniform.

Research motivation

Many studies have sought to determine whether clinical features differ in GAVE with or without cirrhosis. However, few have examined the effects of its etiologies and endoscopic patterns on long-term clinical courses or outcomes, especially in Asians.

Research objectives

To determine whether etiologies and endoscopic patterns are related to the clinical features and course of GAVE.

Research methods

A retrospective analysis of 23 consecutive patients diagnosed with GAVE from January 2006 to December 2020 was conducted. Patients were allocated to cirrhosis (16 patients) and non-cirrhosis groups (7 patients), and GAVE subtypes, as determined by endoscopy, were categorized as punctate (a diffuse, honeycomb-like appearance, 17 patients) or striped (a linear, watermelon-like appearance, 6 patients).

Research results

Punctate-type GAVE was strongly associated with liver cirrhosis, whereas striped-type GAVE was strongly associated with non-cirrhotic underlying disease. Additionally, GAVE patients without cirrhosis experienced overt bleeding more often and required APC treatment more frequently than those with cirrhosis. However, mean numbers of admissions due to GAVE bleeding and of APC sessions for overt bleeding were similar in the cirrhosis and non-cirrhosis groups and in the striped and punctate groups.

Research conclusions

GAVE etiologies may result in different clinical manifestations, especially as regards bleeding. However, etiologies and endoscopic patterns were not found to influence long-term clinical courses or treatment outcomes in cases of overt bleeding.

Research perspectives

This study is one of the few to analyze the effects of GAVE etiologies and endoscopic patterns on long-term clinical courses and outcomes. Additional studies are needed to identify those factors that play key roles in the development and clinical course of GAVE and to clarify its pathophysiologic mechanism.

FOOTNOTES

Author contributions: Cho JH and Lee SH designed the study; Kwon HJ and Cho JH performed the research; Kwon HJ and Cho JH analyzed the data; Cho JH wrote the paper; Lee SH and Cho JH revised the manuscript.

Supported by the 2020 Yeungnam University Research Grant.

Institutional review board statement: The study was reviewed and approved by the Institutional Review Board of Yeungnam University Hospital (IRB No. 2021-10-044).

Conflict-of-interest statement: There are no conflicts of interest to report.

Data sharing statement: No additional data are available.

Open-Access: This article is an open-access article that was selected by an in-house editor and fully peer-reviewed by external reviewers. It is distributed in accordance with the Creative Commons Attribution NonCommercial (CC BY-NC 4.0) license, which permits others to distribute, remix, adapt, build upon this work non-commercially, and license their derivative works on different terms, provided the original work is properly cited and the use is non-commercial. See: https://creativecommons.org/Licenses/by-nc/4.0/

Country/Territory of origin: South Korea

ORCID number: Hyo Jin Kwon 0000-0003-4214-6369; Si Hyung Lee 0000-0001-7221-7506; Joon Hyun Cho 0000-0002-3584-6300.

Corresponding Author's Membership in Professional Societies: The Korean Society of Gastroenterology.

S-Editor: Chen YL

L-Editor: A

P-Editor: Chen YL

REFERENCES

1 **Dulai GS**, Jensen DM, Kovacs TO, Gralnek IM, Jutabha R. Endoscopic treatment outcomes in watermelon stomach patients with and without portal hypertension. *Endoscopy* 2004; **36**: 68-72 [PMID: 14722858 DOI: 10.1055/s-2004-814112]

2 **RIDER JA**, KLOTZ AP, KIRSNER JB. Gastritis with veno-capillary ectasia as a source of massive gastric hemorrhage. *Gastroenterology* 1953; **24**: 118-123 [PMID: 13052170]

3 **Jabbari M**, Cherry R, Lough JO, Daly DS, Kinnear DG, Goresky CA. Gastric antral vascular ectasia: the watermelon stomach. *Gastroenterology* 1984; **87**: 1165-1170 [PMID: 6332757]

4 **Egger C**, Kreczy A, Kirchmair R, Waldenberger P, Jaschke W, Vogel W. Gastric antral vascular ectasia with portal hypertension: treatment with TIPSS. *Am J Gastroenterol* 1997; **92**: 2292-2294 [PMID: 9399773]

5 **Fisher NC**. Gastric antral vascular ectasia and its relation with portal hypertension. *Gut* 2000; **46**: 441-442 [PMID: 10733318 DOI: 10.1136/gut.46.3.440b]

6 **Sebastian S**, O'Morain CA, Buckley MJ. Review article: current therapeutic options for gastric antral vascular ectasia. *Aliment Pharmacol Ther* 2003; **18**: 157-165 [PMID: 12869075 DOI: 10.1046/j.1365-2036.2003.01617.x]

7 **Tobin RW**, Hackman RC, Kimmey MB, Durtschi MB, Hayashi A, Malik R, McDonald MF, McDonald GB. Bleeding from gastric antral vascular ectasia in marrow transplant patients. *Gastrointest Endosc* 1996; **44**: 223-229 [PMID: 8885337 DOI: 10.1016/s0016-5107(96)70155-4]

8 **Spahr L**, Villeneuve JP, Dufresne MP, Tassé D, Bui B, Willems B, Fenyves D, Pomier-Layrargues G. Gastric antral vascular ectasia in cirrhotic patients: absence of relation with portal hypertension. *Gut* 1999; **44**: 739-742 [PMID: 10205216 DOI: 10.1136/gut.44.5.739]

9 **Stefanidis I**, Liakopoulos V, Kapsoritakis AN, Ioannidis I, Eleftheriadis T, Mertens PR, Winograd R, Vamvaka E, Psychos AK, Potamianos SP. Gastric antral vascular ectasia (watermelon stomach) in patients with ESRD. *Am J Kidney Dis* 2006; **47**: e77-e82 [PMID: 16731286 DOI: 10.1053/j.ajkd.2006.02.185]

10 **Elkayam O**, Oumanski M, Yaron M, Caspi D. Watermelon stomach following and preceding systemic sclerosis. *Semin Arthritis Rheum* 2000; **30**: 127-131 [PMID: 11071584 DOI: 10.1053/sarh.2000.9623]

11 **Payen JL**, Calès P, Voigt JJ, Barbe S, Pilette C, Dubuisson L, Desmorat H, Vinel JP, Kervran A, Chayvialle JA. Severe portal hypertensive gastropathy and antral vascular ectasia are distinct entities in patients with cirrhosis. *Gastroenterology* 1995; **108**: 138-144 [PMID: 7806035 DOI: 10.1016/0016-5085(95)90018-7]

12 **Vesoulis Z**, Naik N, Maseelall P. Histopathologic changes are not specific for diagnosis of gastric antral vascular ectasia (GAVE) syndrome: a review of the pathogenesis and a comparative image analysis morphometric study of GAVE syndrome and gastric hyperplastic polyps. *Am J Clin Pathol* 1998; **109**: 558-564 [PMID: 9576573 DOI: 10.1093/ajcp/109.5.558]

13 **Sargeant IR**, Loizou LA, Rampton D, Tulloch M, Bown SG. Laser ablation of upper gastrointestinal vascular ectasias: long term results. *Gut* 1993; **34**: 470-475 [PMID: 8491392 DOI: 10.1136/gut.34.4.470]

14 **Charneau J**, Petit R, Calès P, Dauver A, Boyer J. Antral motility in patients with cirrhosis with or without gastric antral vascular ectasia. *Gut* 1995; **37**: 488-492 [PMID: 7489933 DOI: 10.1136/gut.37.4.488]

15 **Saperas E**, Pigué JM, Perez-Ayuso R, Bombi JA, Bordas JM, Sentis J, Rodés J. Comparison of snare and large forceps biopsies in the histologic diagnosis of gastric vascular ectasia in cirrhosis. *Endoscopy* 1989; **21**: 165-167 [PMID: 2776701 DOI: 10.1055/s-2007-1012933]

16 **Quintero E**, Pique JM, Bombi JA, Bordas JM, Sentis J, Elena M, Bosch J, Rodes J. Gastric mucosal vascular ectasias causing bleeding in cirrhosis. A distinct entity associated with hypergastrinemia and low serum levels of pepsinogen I. *Gastroenterology* 1987; **93**: 1054-1061 [PMID: 3498659 DOI: 10.1016/0016-5085(87)90569-5]

17 **Lowes JR**, Rode J. Neuroendocrine cell proliferations in gastric antral vascular ectasia. *Gastroenterology* 1989; **97**: 207-212 [PMID: 2785944 DOI: 10.1016/0016-5085(89)91437-6]

18 **Qureshi K**, Al-Osaimi AM. Approach to the management of portal hypertensive gastropathy and gastric antral vascular ectasia. *Gastroenterol Clin North Am* 2014; **43**: 835-847 [PMID: 25440929 DOI: 10.1016/j.gtc.2014.08.012]

19 **Selinger CP**, Ang YS. Gastric antral vascular ectasia (GAVE): an update on clinical presentation, pathophysiology and treatment. *Digestion* 2008; **77**: 131-137 [PMID: 18391491 DOI: 10.1159/000124339]

20 **Beales IL**. Watermelon stomach in the CREST syndrome. *Postgrad Med J* 1994; **70**: 766-767 [PMID: 7831185 DOI: 10.1136/pgmj.70.828.766-a]

21 **Ito M**, Uchida Y, Kamano S, Kawabata H, Nishioka M. Clinical comparisons between two subsets of gastric antral vascular ectasia. *Gastrointest Endosc* 2001; **53**: 764-770 [PMID: 11375585 DOI: 10.1067/mge.2001.113922]

22 **Fuccio L**, Mussetto A, Laterza L, Eusebi LH, Bazzoli F. Diagnosis and management of gastric antral vascular ectasia. *World J Gastrointest Endosc* 2013; **5**: 6-13 [PMID: 23330048 DOI: 10.4253/wjge.v5.i1.6]

23 **Lecleire S**, Ben-Soussan E, Antonietti M, Goria O, Riachi G, Lerebours E, Ducrotté P. Bleeding gastric vascular ectasia treated by argon plasma coagulation: a comparison between patients with and without cirrhosis. *Gastrointest Endosc* 2008; **67**: 219-225 [PMID: 18226684 DOI: 10.1016/j.gie.2007.10.016]

24 **Wang J**, Stine JG, Cornella SL, Argo CK, Cohn SM. Patients with Gastric Antral Vascular Ectasia (GAVE) Are at a Higher Risk of Gastrointestinal Bleeding in the Absence of Cirrhosis. *J Clin Transl Hepatol* 2015; **3**: 254-259 [PMID: 26807380 DOI: 10.14218/JCTH.2015.00031]

25 **Probst A**, Scheubel R, Wienbeck M. Treatment of watermelon stomach (GAVE syndrome) by means of endoscopic argon plasma coagulation (APC): long-term outcome. *Z Gastroenterol* 2001; **39**: 447-452 [PMID: 11474999 DOI: 10.1055/s-2001-15722]

26 **Yusoff I**, Brennan F, Ormonde D, Laurence B. Argon plasma coagulation for treatment of watermelon stomach. *Endoscopy* 2002; **34**: 407-410 [PMID: 11972274 DOI: 10.1055/s-2002-25287]

27 **Roman S**, Saurin JC, Dumortier J, Perreira A, Bernard G, Ponchon T. Tolerance and efficacy of argon plasma coagulation for controlling bleeding in patients with typical and atypical manifestations of watermelon stomach. *Endoscopy* 2003; **35**: 1024-1028 [PMID: 14648415 DOI: 10.1055/s-2003-44594]

World Journal of Clinical Cases

Submit a Manuscript: https://www.f6publishing.com

World J Clin Cases 2022 June 26; 10(18): 6060-6068

DOI: 10.12998/wjcc.v10.i18.6060

ISSN 2307-8960 (online)

ORIGINAL ARTICLE

Randomized Controlled Trial

Evaluation of the clinical efficacy and safety of TST33 mega hemorrhoidectomy for severe prolapsed hemorrhoids

Liu Tao, Jun Wei, Xu-Feng Ding, Li-Jiang Ji

Specialty type: Surgery

Provenance and peer review: Unsolicited article; Externally peer reviewed.

Peer-review model: Single blind

Peer-review report's scientific quality classification

Grade A (Excellent): 0
Grade B (Very good): B, B
Grade C (Good): 0
Grade D (Fair): 0
Grade E (Poor): 0

P-Reviewer: Thacoor A, United Kingdom; Yumiba T, Japan

Received: December 15, 2021
Peer-review started: December 15, 2021
First decision: January 26, 2022
Revised: February 8, 2022
Accepted: April 25, 2022
Article in press: April 25, 2022
Published online: June 26, 2022

Liu Tao, Jun Wei, Xu-Feng Ding, Li-Jiang Ji, Department of Anorectal Surgery, Changshu Hospital Affiliated to Nanjing University of Chinese Medicine, Changshu 215500, Jiangsu Province, China

Corresponding author: Li-Jiang Ji, MD, Chief Doctor, Department of Anorectal Surgery, Changshu Hospital Affiliated to Nanjing University of Chinese Medicine, No. 6 Huanghe Road, Changshu 215500, Jiangsu Province, China. ji512@163.com

Abstract

BACKGROUND

The pathogenesis of hemorrhoids is mainly anal cushion prolapse. Although the traditional treatment has a certain curative effect, it is not ideal. The remission rate of postoperative symptoms is low. Even if temporary remission is achieved, patients with hemorrhoids easily relapse after 1-2 years. The new technique of using staplers to treat prolapsed hemorrhoids has good therapeutic effects in clinical practice.

AIM

To explore the effect of TST33 mega stapler prolapse and hemorrhoid mucosal resection in the treatment of patients with severe prolapsed hemorrhoids.

METHODS

A total of 204 patients with severe prolapse hemorrhoids who were admitted to the department of anorectal in our hospital from April 2018 to June 2020 were selected, and the patients were randomly divided into group A and group B with 102 cases in each group using a randomized controlled clinical research program. Patients in Group A were treated with a TST33 mega stapler and hemorrhoid mucosal resection to treat prolapse, and patients in Group B were treated according to the Procedure for Prolapse and Hemorrhoids; the operation time, intraoperative blood loss, hospital stay, the difference in operation time, intraoperative blood loss, hospitalization time, pain degree before and after operation, degree of anal edema, anal Wexner score, and surgical complications were compared between the two groups of patients.

RESULTS

The operation time, intraoperative blood loss and hospitalization time in Group A were significantly lower than those in Group B ($P < 0.05$). The cure rate of Group A was 98.04%, compared with 95.10% cure rate of Group B, and the difference

was not statistically significant ($P > 0.05$). The visual analogue scale (VAS) at 12 h and 24 h postoperatively in Group A were significantly lower than those in Group B ($P < 0.05$). The comparison of the VAS scores between Group A and Group B at 48 h, 72 h and 96 h postoperatively revealed that the difference was not statistically significant ($P > 0.05$). One day postoperatively, the degree of perianal edema in Group A was compared with that in Group B, and the difference was not statistically significant ($P > 0.05$). Seven days postoperatively, the degree of perianal edema in Group A was significantly lower than that in Group B ($P < 0.05$). The comparison of anal Wexner scores between the two groups preoperatively and at 1 mo, 3 mo and 6 mo postoperatively showed that the difference was not statistically significant ($P > 0.05$). The Wexner scores of the two groups at 1 mo, 3 mo and 6 mo postoperatively were significantly lower than the scores preoperatively ($P < 0.05$). The postoperative complication rate of Group A was 2.94% lower than that of Group B (11.76%), which was statistically significant ($P < 0.05$).

CONCLUSION

TST33 mega anastomotic hemorrhoidectomy treatment for patients with severe prolapse hemorrhoids, leads to less postoperative pain, the rapid recovery of perianal edema and has fewer complications.

Key Words: TST33 mega stapler; Prolapse of hemorrhoids; Severe prolapsed hemorrhoids; Hemorrhoids; Circumcision

©The Author(s) 2022. Published by Baishideng Publishing Group Inc. All rights reserved.

Core Tip: Hemorrhoids are common benign perianal diseases, accounting for more than 80% of the incidence of all anorectal diseases. Severe prolapsed hemorrhoids due to the increase in hemorrhoid volume and defecation by fecal extrusion eventually lead to the fracture of anal muscle fibers.

Citation: Tao L, Wei J, Ding XF, Ji LJ. Evaluation of the clinical efficacy and safety of TST33 mega hemorrhoidectomy for severe prolapsed hemorrhoids. *World J Clin Cases* 2022; 10(18): 6060-6068
URL: https://www.wjgnet.com/2307-8960/full/v10/i18/6060.htm
DOI: https://dx.doi.org/10.12998/wjcc.v10.i18.6060

INTRODUCTION

The symptoms are more serious and the hemorrhoids generally need to be pushed back with the hand after prolapse, so severe prolapsed hemorrhoids require surgical treatment[1,2]. The procedure for prolapse and hemorrhoids (PPH) can lift and pull the anal cushion by circular resection of the rectal mucosa approximately 2–3 cm above the tooth line and anastomosis. The advantage is that the short-term therapeutic effect is still acceptable, but the PPH is prone to various complications after surgery, the recurrence rate is high, and the long-term curative effect is poor. The use of tissue-selecting therapy staplers (TSTs) has been reported, but reports are rare. To some extent, this operation reduces the disadvantages of the PPH caused by circular resection, but because of selective resection, the use of TSTs does not change the high recurrence rate after PPH. The TST33 mega stapler has an open window, and the resection tissue boundary is open, so more pathological hemorrhoids are able to be resected. Under the premise of solving PPH complications, the use of TSTs also improves the postoperative recurrence rate to a certain extent[3]. To further summarize and analyze the surgical treatment methods for patients with severe prolapsed hemorrhoids, this study compared the effect of TST33 mega staplers to provide a basis for clinical practice, which is reported as follows.

MATERIALS AND METHODS

General information

A total of 204 patients with severe prolapsed hemorrhoids that were admitted to the anorectal department of our hospital from April 2018 to June 2020 were selected and randomly divided into Group A and Group B, with 102 cases in each group, by a single-blind, randomized and controlled clinical research scheme. Inclusion criteria: (1) The age range of patients is 19 to 65 years; (2) The diagnostic criteria for patients with severe prolapsed hemorrhoids refer to the criteria in the Chinese

Guidelines for the Diagnosis and Treatment of Hemorrhoids (2020)[3]; (3) Non-circular hemorrhoids Suspended for more than half a year, reaching III and IV degree; (4) Conservative treatment for more than 3 mo is not effective; and (5) The research plan obtains the informed consent of patients and their families. The exclusion criteria were as follows: (1) Patients with a rectal tumor; (2) Patients with a perianal abscess, or anal fistula formation; (3) Patients with liver and kidney function diseases; (4) Patients with coagulation diseases; (5) Patients with a history of drug use or addiction; and (6) Patients with mental or psychological diseases.

Surgical methods

The patients in the two groups were given routine preoperative preparation, improved preoperative examination, and fasted on the day of operation. All patients were given intraspinal anesthesia, and the left lateral position was used for the operation.

Group A: For patients undergoing TST33 mega stapler hemorrhoid mucosal resection surgery, the appropriate anal mirror was selected (single opening, double opening or three opening anal mirror). The anal mirror was inserted and the inner tube was removed to expose the hemorrhoid tissue to be removed, and sutured with "0" silk sutures at the distance of 2.5-5 cm from the dentate line. Sutures were only placed in the mucosa and submucosa, a needle was placed in each opening suture, and a continuous bag was used. Sutures were only placed in the mucosa and submucosa, a needle was placed in each opening suture, and a continuous bag was used. The tail wing of the stapler was opened counterclockwise. After the head and body of the stapler were completely loosened, the head of the stapler was inserted into the anal expander. The two ends of the purse line were tightened and knotted around the central rod. The suture was exported from the symmetrical side hole of the stapler body through the suture export rod. Moderate traction was performed, the stapler was screwed clockwise, and the traction rectal tissue was pulled into the stapler nail slot. At this time, the feel knob was resistant, and the pointer of the stapler indicator window was displayed in the firing range. For female patients, surgeons paid attention to whether the posterior wall of the vagina was sutured. The stapler was hit, completing the cutting and anastomosis. For a fixed wait time of 30 s, the stapler was spun counterclockwise with a loose 3/4 circle tail, and removed. Observation of anastomotic stoma was performed if there was active bleeding Line 8' sutures were used for hemostasis. The 'cat ear' in the middle of the anastomosis was ligated with "0" silk thread. External hemorrhoid stripping to the teeth near the line parallel low ligation was performed.

Group B: The PPH was used for the treatment of hemorrhoids, and a PPH stapler was used for the treatment of internal hemorrhoids. External hemorrhoid stripping to the teeth near the line parallel low ligation was performed.

The patients in the two groups could go to the recovery unit after anesthesia recovery, and their diet gradually changed from a half-stream diet to an ordinary diet. The total infusion volume was controlled within 500 mL 6 h after the operation to reduce the incidence of urinary retention. Antibiotics were routinely used for 5 d after the operation, and dressing treatment was performed after sitting in the bath.

Observation indices and evaluation criteria

The operation time, intraoperative blood loss, hospitalization time, cure rate, pain degree, anal edema degree, anal Wexner score and surgical complications were compared between the two groups.

The criteria for healing[5] were postoperative defecation or standing for a long time and no hemorrhoid prolapse when coughing, tired, and loaded was defined as a cure.

The visual analogue scale (VAS) was used to evaluate the degree of pain[5], with 0 indicating no pain, and 10 indicating the most pain. The pain scores at 12 h, 24 h, 48 h, 72 h and 96 h postoperatively were observed.

Observe the edema around the anal margin on the 1st and 7th postoperative day. Degree I: no edema of the anal margin; degree II: mild edema of the anal margin occupies less than 1/4 circle of the perianal; degree III: edema of the anal margin occupies more than 1/4 circle of the perianal, and ≤ 1/2 circle; degree IV: Anal marginal edema occupies more than 1/2 circle perianal.

Anal Wexner score[7] evaluates the patient's preoperative and postoperative anal function, mainly from the patient's stool frequency, defecation difficulty, incomplete defecation feeling, the time required for each defecation, whether defecation requires assistance, and defecation Unsuccessful times/24 h, duration of constipation, a total score of 32 points, the higher the score, the worse the anal defecation function of patients.

Statistical analysis

In this study, measurement indices such as operation time, intraoperative blood loss and hospitalization time were tested by normal distribution, which were in accordance with the approximate normal distribution or normal distribution and are expressed as mean ± SD. The *t*-test was used for comparisons between the two groups. Non-counting data are represented by percentages, and the χ^2 test was used for comparisons. The Mann–Whitney *U* test was used for comparisons of grade counting data between the

groups. Professional SPSS 21.0 software for data processing was used, with the test level $\alpha = 0.05$.

RESULTS

Baseline data comparison of patients in the A and B groups

The baseline data for age, height, weight, course of disease, sex, prolapse of hemorrhoids, constipation, bleeding and pain were compared between Group A and Group B, and the difference was not statistically significant ($P > 0.05$, Table 1).

Comparison of surgery-related indicators between Group A and Group B

The operation time, intraoperative blood loss and hospitalization time in Group A were significantly lower than those in Group B ($P < 0.05$, Table 2).

Comparison of cure rate between Group A and Group B

The cure rate of Group A was 98.04%, compared with the cure rate of 95.10% for Group B, and the difference was not statistically significant ($P > 0.05$, Table 3).

Postoperative VAS scores for Group A and Group B

The VAS scores of patients in group A at 12 h and 24 h after operation were lower than those in group B, and the difference was statistically significant ($P < 0.05$). There was no significant difference between group A and group B at 48 h, 72 h, and 96 h after operation ($P > 0.05$), as shown in Table 4.

Comparison of postoperative perianal edema between Group A and Group B

One day postoperatively, the degree of perianal edema in Group A was compared with that in Group B, and the difference was not statistically significant ($P > 0.05$). Seven days postoperatively, the degree of perianal edema in Group A was significantly lower than that in Group B ($P < 0.05$, Table 5).

Comparison of the anal Wexner score between the two groups

Comparisons of preoperative, postoperative, 1 mo, 3 mo, and 6 mo, anal Wexner scores were made between the two groups, and the difference was not statistically significant ($P > 0.05$). The Wexner scores of the two groups at 1 mo, 3 mo and 6 mo postoperatively were significantly lower than the scores preoperatively ($P < 0.05$, Table 6).

Comparison of the complication rate between two groups

The postoperative complication rate of Group A was 2.94% lower than that of Group B (11.76%), which was statistically significant ($P < 0.05$, Table 7).

DISCUSSION

Hemorrhoids are common diseases in the anorectal system. On the one hand, the occurrence of hemorrhoids is related to varicose veins. Hemorrhoids are caused by venous congestion of the rectal submucosal and anal skin hemorrhoids[8-10]. Subnuclear prolapse aggravates venous congestion, and venous congestion aggravates the development of hemorrhoids, forming a vicious cycle. Anastomotic hemorrhoid mucosal circumcision is a traditional surgical treatment, but it has been reported that the operation has more postoperative complications and patients are prone to recurrence, mainly because the stapler used in the operation does not have enough space to remove larger amounts of rectal mucosa, resulting in incomplete resection, so the long-term effect is not good. At the same time, prolapsed hemorrhoids will lead to their own rectal elongation, expansion, volume increase, rectal muscle thinning or disappearance of pathological changes, which cannot be effectively removed and easily lead to recurrence[11,12].

Selective supraclavicular mucosal resection was improved on the basis of traditional surgical suspension and devascularization. The mucosal and submucous tissues above the supraclavicular nucleus were selectively resected, and the normal mucosal tissues between the supraclavicular nuclei were retained, so the trauma to the patients was decreased. This study found that the operation time, intraoperative blood loss and hospitalization time in Group A were lower than those in Group B, suggesting that the use of TST33 mega stapler hemorrhoid mucosal resection in the treatment of severe prolapsed hemorrhoids has reduced trauma and shorter hospitalization times, which is basically consistent with the conclusions of previous studies[13,14]. TST33 mega stapler hemorrhoid mucosal resection surgery has a large window vision, and the operation is smoother. The large window has no resection limitation, and the resection range is greater, which can fully allow for the "pulling" effect but also protect normal tissue. At the same time, the operation height is reduced. The operation height of

Table 1 Comparison of baseline data between group A and group B, *n* (%)

Basic information	Group A (*n* = 102)	Group B (*n* = 102)	t/χ^2 value	*P* value
Age (yr)	46.9 ± 8.1	45.0 ± 9.0	1.585	0.115
Height (cm)	168.1 ± 4.1	166.8 ± 5.4	1.936	0.054
Weight (kg)	66.3 ± 6.4	67.8 ± 7.8	-1.501	0.135
Course of disease (yr)	10.91 ± 1.20	11.15 ± 0.98	-1.564	0.119
Sex			1.012	0.314
Male	59 (57.84)	66 (64.71)		
Female	43 (42.16)	36 (35.29)		
Degree of hemorrhoid prolapse			1.357	0.244
III stage	69 (67.65)	61 (59.8)		
IV stage	33 (32.35)	41 (40.2)		
Constipate			3.526	0.060
Yes	41	43		
No	61	59		
Bleeding			1.225	0.268
Yes	88 (86.27)	93 (91.18)		
No	14 (13.73)	9 (8.82)		
Pain			1.079	0.299
Yes	84 (82.35)	78 (76.47)		
No	18 (17.65)	24 (23.53)		

Table 2 Comparison of surgery-related indicators between group A and group B (mean ± SD)

Groups	Operation time (min)	Intraoperative blood loss (mL)	Hospital stay (d)
Group A (*n* = 102)	17.94 ± 3.60	4.81 ± 1.03	5.8 ± 1.2
Group B (*n* = 102)	26.40 ± 4.11	10.52 ± 2.50	7.0 ± 1.4
t value	-6.396	-21.328	-7.668
P value	0.000	0.000	0.000

Table 3 Comparison of cure rate between group A and group B, *n* (%)

Groups	Cure	Get better
Group A (*n* = 102)	100 (98.04)	2 (1.96)
Group B (*n* = 102)	97 (95.10)	5 (4.90)
t value	1.331	
P value	0.249	

the PPH is 4 cm, and the operation height of the TST33 mega stapler is 2.5-3.5 cm. This height can partially remove hemorrhoid tissue and reduce the recurrence rate to a certain extent. In this study, the postoperative complication rate of Group A was 2.94% lower than that of Group B (11.76%), suggesting that TST33 mega stapler hemorrhoid mucosal resection can reduce the incidence of surgical complications in patients with severe prolapsed hemorrhoids.

This study also showed that the VAS scores at 12 h and 24 h after the operation in Group A were lower than those in Group B, suggesting that TST33 mega stapler mucosal resection for severe prolapsed hemorrhoids could significantly reduce postoperative pain. There are many influencing factors for postoperative pain. TST33 mega stapler hemorrhoid mucosal resection surgery is performed

Table 4 Postoperative visual analogue scale scores of patients in groups A and B (mean ± SD, scores)

Groups	12 h after operation	24 h after operation	48 h after operation	72 h after operation	96 h after operation
Group A (n = 102)	3.11 ± 0.98	3.30 ± 0.85	2.40 ± 0.76	1.48 ± 0.50	0.81 ± 0.30
Group B (n = 102)	3.61 ± 1.00	3.59 ± 0.98	2.58 ± 0.65	1.62 ± 0.66	0.88 ± 0.28
t value	-3.607	-2.258	-1.818	-1.708	-1.723
P value	0.000	0.025	0.071	0.089	0.086

Table 5 Comparison of the degree of perianal edema between group A and group B, n (%)

Groups	I stage	II stage	III stage	IV stage
1st day after operation				
Group A (n = 102)	91	6	3	2
Group B (n = 102)	76	15	6	5
Z value	-1.128			
P value	0.259			
7th day after operation				
Group A (n = 102)	93	6	2	1
Group B (n = 102)	80	14	5	3
Z value	-2.286			
P value	0.022			

Table 6 Comparison of anal Wexner scores between the two groups (mean ± SD, scores)

Groups	Preoperative	1 mo after surgery	3 mo after surgery	6 mo after surgery
Group A (n = 102)	22.67 ± 3.70	14.38 ± 3.36	8.74 ± 2.60	6.16 ± 1.84
Group B (n = 102)	23.25 ± 3.98	15.24 ± 3.62	9.40 ± 2.74	6.63 ± 1.81
t value	-1.078	-1.759	-1.765	-1.839
P value	0.282	0.080	0.079	0.067

Table 7 Comparison of surgical complication rates between the two groups, n (%)

Group	Anus drop	Anastomotic stenosis within 3 mo	Perianal infection	Urinary retention	Complication rate
Group A (n = 102)	3	0	0	0	3 (2.94)
Group B (n = 102)	7	3	0	2	12 (11.76)
χ^2 value					5.829
P value					0.016

above the dentate line, where the dominant nerve is mainly the visceral nerve, which is not sensitive to pain. There is less resected rectal mucosa, so the postoperative pain is relatively reduced[15]. This study also found that 7 d after the operation, the degree of perianal edema in Group A was lower than that in Group B, suggesting that TST33 mega stapler hemorrhoid mucosal resection in the treatment of severe prolapsed hemorrhoids for postoperative perianal edema was reduced to some extent, and two surgical methods for the treatment of severe prolapsed hemorrhoids can improve anal function. TST33 mega stapler hemorrhoid mucosal resection reduces the number of anastomotic nails implanted and reduces the anal bulge, thus protecting anal contraction defecation functions[16,17].

In the process of the operation, we believe that attention should be given to the following aspects. First, the appearance of a "cat ear" between anastomotic stomas after TST operation is very common. Ligation with "0" silk thread is a simple, safe and reliable method. Second, surgeons should check

whether there is bleeding in the anastomotic stoma carefully before removing the anal mirror, and the bleeding tendency should be removed to stop bleeding by "8" sutures to strengthen the anastomotic stoma. Third, the size of the resected tissue should be evaluated before the operation and the height and mode of the purse suture should be adjusted according to the need to play an individualized treatment role. Fourth, the height of the purse-string should be appropriately lowered. Choose 2.5 cm-3.5 cm on the tooth line, and remove part of the internal hemorrhoid tissue, which has a certain value for improving the postoperative curative effect[18-20].

This study analyzed the advantages of TST33 mega stapler hemorrhoid mucosal resection in the treatment of severe prolapsed hemorrhoids and showed the reduced incidence of postoperative complications, which was in line with the patient-oriented treatment concept of modern surgery and provided a certain basis for the clinical operation in the treatment of severe prolapsed hemorrhoids. However, due to the small number of cases included in this study, the lack of a large sample with a long-term follow-up and survey, the long-term efficacy and recurrence need to be further evaluated by increasing the sample size, improving the corresponding observation index, and carrying out prospective studies with in-depth analysis.

CONCLUSION

In summary, TST33 mega stapler hemorrhoid mucosal resection in the treatment of patients with severe prolapsed hemorrhoids yielded satisfactory results, less postoperative pain, perianal edema recovery block, and fewer complications.

ARTICLE HIGHLIGHTS

Research background

Although traditional treatment has certain curative effect, it is not ideal. Postoperative symptom relief rate is low. Even if temporarily relieved, hemorrhoids patients are easy to relapse.

Research motivation

In this study, the authors further summarized and analyzed the surgical treatment methods for patients with severe prolapsed hemorrhoids, and compared the effect of TST33 mega staplers to provide a basis for clinical practice.

Research objectives

This study aimed to explore the effect of TST33 mega stapler prolapse and hemorrhoid mucosal resection in the treatment of patients with severe prolapsed hemorrhoids.

Research methods

A total of 204 patients with severe prolapsed hemorrhoids that were admitted to the anorectal department of our hospital from April 2018 to June 2020 were selected and randomly divided into Group A and Group B, with 102 cases in each group, by a single-blind, randomized and controlled clinical research scheme.

Research results

This study found that the operation time, intraoperative blood loss and hospitalization time in Group A were lower than those in Group B, suggesting that the use of TST33 mega stapler hemorrhoid mucosal resection in the treatment of severe prolapsed hemorrhoids has reduced trauma and shorter hospitalization times, which is basically consistent with the conclusions of previous studies, TST33 mega stapler hemorrhoid mucosal resection surgery has a large window vision, and the operation is smoother. This study also showed that the visual analogue scale scores at 12 h and 24 h after the operation in Group A were lower than those in Group B, suggesting that TST33 mega stapler mucosal resection for severe prolapsed hemorrhoids could significantly reduce postoperative pain.

Research conclusions

TST33 mega stapler hemorrhoid mucosal resection in the treatment of severe prolapsed hemorrhoids patients yielded satisfactory results, less postoperative pain, perianal edema recovery block, and fewer complications.

Research perspectives

This study analyzed the advantages of TST33 mega stapler hemorrhoid mucosal resection in the treatment of severe prolapsed hemorrhoids and showed the reduced incidence of postoperative

complications, which was in line with the patient-oriented treatment concept of modern surgery and provided a certain basis for the clinical operation in the treatment of severe prolapsed hemorrhoids. However, due to the small number of cases included in this study, the lack of a large sample with a long-term follow-up and survey, the long-term efficacy and recurrence need to be further evaluated by increasing the sample size, improving the corresponding observation index, and carrying out prospective studies with in-depth analysis.

FOOTNOTES

Author contributions: Tao L and Wei J design the study; Ding XF drafted the manuscript, Ji L and Tao L collected the data; Tao L and Ji L analyzed and interpreted data, Tao L and Wei J revised the manuscript.

Supported by Special Project of Diagnosis and Treatment Technology for Key Clinical Diseases in Suzhou, No. LCZX202022; and Changshu Municipal Science and Technology Bureau Supporting Project, No. CS201925.

Institutional review board statement: This study was approved by the Changshu Hospital Affiliated to Nanjing University of Chinese Medicine.

Informed consent statement: All study participants, or their legal guardian, provided informed written consent prior to study enrollment.

Conflict-of-interest statement: All authors report no conflict of interest.

Data sharing statement: No additional data are available.

CONSORT 2010 statement: The authors have read the CONSORT 2010 statement, and the manuscript was checked according to the CONSORT 2010 statement.

Open-Access: This article is an open-access article that was selected by an in-house editor and fully peer-reviewed by external reviewers. It is distributed in accordance with the Creative Commons Attribution NonCommercial (CC BY-NC 4.0) license, which permits others to distribute, remix, adapt, build upon this work non-commercially, and license their derivative works on different terms, provided the original work is properly cited and the use is non-commercial. See: https://creativecommons.org/Licenses/by-nc/4.0/

Country/Territory of origin: China

ORCID number: Liu Tao 0000-0002-6962-7122; Jun Wei 0000-0002-7216-0375; Xu-Feng Ding 0000-0002-2858-375X; Li-Jiang Ji 0000-0003-4416-8334.

S-Editor: Wang JL
L-Editor: A
P-Editor: Wang JL

REFERENCES

1 **Romano G**, Cocchiara G, Maniaci S, Buscemi G, Calderone F, Gioè FP, Romano M. [The role of colonoscopy in patient follow-up after surgery for colorectal cancer. A retrospective study and review of the literature]. *G Chir* 2007; **28**: 399-402 [PMID: 17915057]
2 **Ruan N**, Chen ZH, Lin XB. [Efficacy comparison of tissue selecting therapy stapler and procedure for prolapse and hemorrhoids in the treatment of severe hemorrhoids]. *Zhonghua Wei Chang Wai Ke Za Zhi* 2013; **16**: 645-647 [PMID: 23888447]
3 **Casas-Puig V**, Bretschneider CE, Ferrando CA. Perioperative Adverse Events in Women Undergoing Concurrent Hemorrhoidectomy at the Time of Urogynecologic Surgery. *Female Pelvic Med Reconstr Surg* 2019; **25**: 88-92 [PMID: 30807406 DOI: 10.1097/SPV.0000000000000663]
4 **Zhang G**, Liang R, Wang J, Ke M, Chen Z, Huang J, Shi R. Network meta-analysis of randomized controlled trials comparing the procedure for prolapse and hemorrhoids, Milligan-Morgan hemorrhoidectomy and tissue-selecting therapy stapler in the treatment of grade III and IV internal hemorrhoids (Meta-analysis). *Int J Surg* 2020; **74**: 53-60 [PMID: 31887419 DOI: 10.1016/j.ijsu.2019.12.027]
5 **Shen K**, Wang C, Gao ZD, Jiang KW, Wang YL, Ye YJ. [Procedure for prolapse and hemorrhoids versus stapled transanal rectal resection in the treatment of grade IV hemorrhoids]. *Zhonghua Wei Chang Wai Ke Za Zhi* 2019; **22**: 1165-1169 [PMID: 31874533 DOI: 10.3760/cma.j.issn.1671-0274.2019.12.012]
6 **Ray-Offor E**, Amadi S. Hemorrhoidal disease: Predilection sites, pattern of presentation, and treatment. *Ann Afr Med* 2019; **18**: 12-16 [PMID: 30729927 DOI: 10.4103/aam.aam_4_18]
7 **Forner LB**, Beckman EM, Smith MD. Symptoms of pelvic organ prolapse in women who lift heavy weights for exercise: a

cross-sectional survey. *Int Urogynecol J* 2020; **31**: 1551-1558 [PMID: 31813038 DOI: 10.1007/s00192-019-04163-w]

8 **Percalli L**, Passalia L, Pricolo R, Riccò M. Pre-operative assessment of internal mucosal rectal prolapse in internal hemorrhoids: technical details and results from a single institution. *Acta Biomed* 2019; **90**: 308-315 [PMID: 31125011 DOI: 10.23750/abm.v90i2.6988]

9 **Mik M**, Rzetecki T, Sygut A, Trzcinski R, Dziki A. Open and closed haemorrhoidectomy for fourth degree haemorrhoids--comparative one center study. *Acta Chir Iugosl* 2008; **55**: 119-125 [PMID: 19069704 DOI: 10.2298/aci0803119m]

10 **Filingeri V**, Gravante G, Cassisa D. Clinical applications of radiofrequency in proctology: a review. *Eur Rev Med Pharmacol Sci* 2006; **10**: 79-85 [PMID: 16705953]

11 **Fan Z**, Zhang Y. Treatment of Prolapsing Hemorrhoids in HIV-Infected Patients with Tissue-Selecting Technique. *Gastroenterol Res Pract* 2017; **2017**: 1970985 [PMID: 28356909 DOI: 10.1155/2017/1970985]

12 **Lin HC**, Chen HX, He QL, Huang L, Zhang ZG, Ren DL. A Modification of the Stapled TransAnal Rectal Resection (STARR) Procedure for Rectal Prolapse. *Surg Innov* 2018; **25**: 578-585 [PMID: 30117358 DOI: 10.1177/1553350618793415]

13 **Jeong H**, Hwang S, Ryu KO, Lim J, Kim HT, Yu HM, Yoon J, Lee JY, Kim HR, Choi YG. Early Experience With a Partial Stapled Hemorrhoidopexy for Treating Patients With Grades III-IV Prolapsing Hemorrhoids. *Ann Coloproctol* 2017; **33**: 28-34 [PMID: 28289661 DOI: 10.3393/ac.2017.33.1.28]

14 **Palumbo VD**, Palumbo VD, Damiano G, Sammartano A, Messina M, Fazzotta S, Curione F, Cudia BM, Lo Monte AI. Colour Doppler-guided Haemorrhoidal Artery Ligation: a possible evolution of Transanal Haemorrhoidal Dearterialisation. *Clin Ter* 2021; **172**: 329-335 [PMID: 34247216 DOI: 10.7417/CT.2021.2337]

15 **Kuiper SZ**, Dirksen CD, Kimman ML, Van Kuijk SMJ, Van Tol RR, Muris JWM, Watson AJM, Maessen JMC, Melenhorst J, Breukink SO; Napoleon Trial Study Group. Effectiveness and cost-effectiveness of rubber band ligation versus sutured mucopexy versus haemorrhoidectomy in patients with recurrent haemorrhoidal disease (Napoleon trial): Study protocol for a multicentre randomized controlled trial. *Contemp Clin Trials* 2020; **99**: 106177 [PMID: 33080380 DOI: 10.1016/j.cct.2020.106177]

16 **Reese GE**, von Roon AC, Tekkis PP. Haemorrhoids. *BMJ Clin Evid* 2009; **2009** [PMID: 19445775]

17 **Ji L**, Li L, Weng L, Hu Y, Huang H, Wei J. Tissue selecting technique mega-window stapler combined with anal canal epithelial preservation operation for the treatment of severe prolapsed hemorrhoids: A study protocol for a randomized controlled trial. *Medicine (Baltimore)* 2020; **99**: e23122 [PMID: 33157990 DOI: 10.1097/MD.0000000000023122]

18 **Lohsiriwat V**, Wilson VG, Scholefield JH, Dashwood MR. Regional Distribution of Nitric Oxide Synthase in Human Anorectal Tissue: A Pilot Study on the Potential Role for Nitric Oxide in Haemorrhoids. *Curr Vasc Pharmacol* 2020; **18**: 43-49 [PMID: 30058493 DOI: 10.2174/1570161116666180730101532]

19 **Ng KS**, Holzgang M, Young C. Still a Case of "No Pain, No Gain"? *Ann Coloproctol* 2020; **36**: 133-147 [PMID: 32674545 DOI: 10.3393/ac.2020.05.04]

20 **Wang ZG**, Zhang Y, Zeng XD, Zhang TH, Zhu QD, Liu DL, Qiao YY, Mu N, Yin ZT. Clinical observations on the treatment of prolapsing hemorrhoids with tissue selecting therapy. *World J Gastroenterol* 2015; **21**: 2490-2496 [PMID: 25741159 DOI: 10.3748/wjg.v21.i8.2490]

World Journal of Clinical Cases

Submit a Manuscript: https://www.f6publishing.com

World J Clin Cases 2022 June 26; 10(18): 6069-6081

DOI: 10.12998/wjcc.v10.i18.6069

ISSN 2307-8960 (online)

ORIGINAL ARTICLE

Randomized Controlled Trial

Sequential chemotherapy and icotinib as first-line treatment for advanced epidermal growth factor receptor-mutated non-small cell lung cancer

Sheng-Jie Sun, Jin-Di Han, Wei Liu, Zhi-Yong Wu, Xiao Zhao, Xiang Yan, Shun-Chang Jiao, Jian Fang

Specialty type: Oncology

Provenance and peer review: Unsolicited article; Externally peer reviewed.

Peer-review model: Single blind

Peer-review report's scientific quality classification

Grade A (Excellent): 0
Grade B (Very good): B, B
Grade C (Good): 0
Grade D (Fair): D
Grade E (Poor): 0

P-Reviewer: Chiu CC, Taiwan; Roudi R, United States; Singh I, United States

Received: November 22, 2021
Peer-review started: November 22, 2021
First decision: February 7, 2022
Revised: March 13, 2022
Accepted: April 15, 2022
Article in press: April 15, 2022
Published online: June 26, 2022

Sheng-Jie Sun, Zhi-Yong Wu, Xiao Zhao, Xiang Yan, Department of Medical Oncology, The Fifth Medical Center of General Hospital of Chinese People's Liberation Army, Beijing 100039, China

Jin-Di Han, Jian Fang, Department of Internal Oncology of Chest, Beijing Cancer Hospital, Beijing 100142, China

Wei Liu, Peking Cancer Hospital Palliative Care Center, Beijing Cancer Hospital, Beijing 100142, China

Shun-Chang Jiao, Department of Oncology, The Fifth Medical Center of General Hospital of Chinese People's Liberation Army, Beijing 100039, China

Corresponding author: Shun-Chang Jiao, MD, Chief Doctor, Department of Oncology, The Fifth Medical Center of General Hospital of Chinese People's Liberation Army, No. 100 West Fourth Ring Road, Fengtai District, Beijing 100039, China. jiaosc@vip.sina.com

Abstract

BACKGROUND

Icotinib could have potential effect and tolerability when used sequentially with chemotherapy for advanced epidermal growth factor receptor (*EGFR*)-mutated non-small cell lung cancer (NSCLC).

AIM

To evaluate the efficacy and safety of chemotherapy followed by icotinib maintenance therapy as first-line treatment for advanced *EGFR*-mutated NSCLC.

METHODS

This multicenter, open-label, pilot randomized controlled trial enrolled 68 *EGFR*-mutated stage IIIB/IV NSCLC patients randomized 2:3 to the icotinib alone and chemotherapy + icotinib groups.

RESULTS

The median progression-free survival in the icotinib alone and chemotherapy + icotinib groups was 8.0 mo (95%CI: 3.84-11.63) and 13.4 mo (95%CI: 10.18-16.33), respectively (P = 0.0249). No significant differences were found in the curative

effect when considering different cycles of chemotherapy or chemotherapy regimen (all $P > 0.05$).

CONCLUSION

A sequential combination of chemotherapy and EGFR-tyrosine kinase inhibitor is feasible for stage IV *EGFR*-mutated NSCLC patients.

Key Words: Advanced stage; Chemotherapy; Epidermal growth factor receptor mutation; First-line treatment; Icotinib

©The Author(s) 2022. Published by Baishideng Publishing Group Inc. All rights reserved.

Core Tip: The combination of chemotherapy and epidermal growth factor receptor (EGFR)-tyrosine kinase inhibitor (TKI) (concomitant or intercalated) generally showed improved efficacy compared with EGFR-TKI alone as the first-line treatment for advanced non-small cell lung cancer (NSCLC). This study aimed to evaluate the efficacy and safety of chemotherapy followed by icotinib maintenance therapy as first-line treatment for advanced *EGFR*-mutated NSCLC. Sixty-eight advanced NSCLC patients were randomized 2:3 to icotinib-alone or chemotherapy plus icotinib. The chemotherapy plus icotinib group showed higher progression-free survival than the icotinib alone group. Our study suggested that the sequential combination of chemotherapy and EGFR-tyrosine kinase inhibitor is feasible for stage IV *EGFR*-mutated NSCLC patients.

Citation: Sun SJ, Han JD, Liu W, Wu ZY, Zhao X, Yan X, Jiao SC, Fang J. Sequential chemotherapy and icotinib as first-line treatment for advanced epidermal growth factor receptor-mutated non-small cell lung cancer. *World J Clin Cases* 2022; 10(18): 6069-6081

URL: https://www.wjgnet.com/2307-8960/full/v10/i18/6069.htm

DOI: https://dx.doi.org/10.12998/wjcc.v10.i18.6069

INTRODUCTION

Globally, lung cancer is the malignancy with the highest incidence and mortality. In 2018, 2.1 million new lung cancers and 1.8 million deaths were reported, with an annual age-standardized incidence rate of 22.5 per 100000 individuals and an age-standardized yearly mortality rate of 18.6 per 100000 individuals[1]. Non-small cell lung cancers (NSCLCs) represent the greatest number (85%-90%) of malignant lung tumors[2], and almost half of NSCLCs are adenocarcinomas. Adenocarcinomas display activating mutations in the epithelial growth factor receptor (*EGFR*) gene, making such cancers candidates for EGFR tyrosine kinase inhibitor (EGFR-TKI) therapy[3-5]. In Asians, individuals harboring *EGFR* mutations account for 51.4% of adenocarcinoma NSCLCs[3-5]. Currently, EGFR-TKIs are the guideline-recommended first-line treatment for advanced NSCLC with *EGFR* mutations[5].

Despite the improvement in progression-free survival (PFS) by EGFR-TKIs, acquired resistance inevitably develops after about 10 mo of treatment[3,6]. Due to the complexity of the EGFR-TKI resistance mechanisms[6-8], a combined treatment approach could be used to prevent or delay resistance development[7]. One of the combination therapies of interest and most frequently explored is chemotherapy + TKI. In clinical trials, a combination of chemotherapy and EGFR-TKI (concomitant or intercalated) generally showed improved efficacy compared with EGFR-TKI alone as the first-line treatment for advanced NSCLC[9-13]. Nevertheless, the best combinational strategy remains controversial.

In preclinical studies, compared with concurrent administration of gefitinib alone, the sequential administration of pemetrexed or paclitaxel with gefitinib exerted stronger anti-tumor activity by enhancing cell cytotoxicity[14-18]. Sequential chemotherapy followed by maintenance EGFR-TKI therapy may be a potential strategy, as suggested by recent clinical trials[19-21]. Icotinib was suggested to have potential effects and tolerability when used sequentially with chemotherapy[22-24]. Therefore, the present pilot study aimed to evaluate the efficacy and safety of different sequential combinations of chemotherapy (varying cycle number and chemotherapeutic agents), followed by icotinib maintenance *vs* icotinib alone as a first-line treatment for advanced *EGFR*-mutated NSCLC. The results might help improve the treatment strategies for these patients.

MATERIALS AND METHODS

Study design and patients

This multicenter, open-label, pilot randomized controlled trial (RCT) was conducted in four centers in China between November 2012 and July 2015. The study was carried out according to the principles of the Declaration of Helsinki and the guidelines of the Good Clinical Practice of the International Council for Harmonization. The trial was approved by the ethics committees of General Hospital of People's Liberation Army. All patients signed an informed consent form before any study procedure.

The inclusion criteria were: (1) Age 18-72 years; (2) patients with treatment-naïve advanced lung cancer having *EGFR*-sensitive mutation confirmed by pathological examinations; (3) stage IIIB or IV lung cancer; (4) Eastern Cooperative Oncology Group (ECOG) score of 0-2; (5) normal cardiac, liver, and renal functions, and routine blood test results; (6) expected survival > 3 mo; (7) negative urine pregnancy test within 7 d before screening for women of child-bearing age, and agreement to apply effective contraception measures to prevent pregnancy during and within 3 mo after the study for fertile men and women; and (8) signed informed consent forms. The exclusion criteria were: (1) Brain metastases; (2) active infection (according to the judgment of investigators); (3) major organ failure, such as decompensated cardiopulmonary failure; (4) newly developed myocardial infarction or cerebral infarction within 3 mo; (5) presence of a second malignant tumor (except for cured cervical cancer or skin cancer); (6) interstitial lung disease; or (7) pregnant or breastfeeding women.

Trial registration: ClinicalTrials.gov, NCT01665417. Registered on August 12, 2012, https://clinicaltrials.gov/ct2/show/NCT01665417.

Randomization and blinding

This study involved three randomizations. The patients were first randomized 2:3 to icotinib-alone *vs* chemotherapy + icotinib. The patients in the chemotherapy group were then randomized 1:1 to two *vs* four cycles of chemotherapy and further randomized 1:1 to pemetrexed and cisplatin (PP) *vs* docetaxel and cisplatin (DP) (Figure 1). All randomizations were carried out using a central randomization system designed by an independent biostatistician. The stratification factors after randomization included clinical stage (IIIB *vs* IV), type of *EGFR* mutation (exon 19 mutation *vs* exon 21 mutation), ECOG score (0-1 *vs* 2), and smoking status (non-smokers *vs* mild smokers *vs* regular smokers). This study was a pilot study, and the patients, treating physicians, and data assessors could not be blind to treatment allocation due to the nature of the treatments.

Treatment

Icotinib was provided by Betta Pharmaceutical Co., Ltd. (Zhejiang, China). Two or four cycles of PP (pemetrexed disodium 500 mg/m^2 iv d1, cisplatin 75 mg/m^2 iv d1, q3w) or DP (docetaxel 75 mg/m^2 iv d1, cisplatin 75 mg/m^2 iv d1, q3w) were administered to the patients assigned to the first-line chemotherapy + icotinib treatment. Icotinib hydrochloride (oral, 125 mg, tid) was used as maintenance therapy or second-line therapy until disease progression or the occurrence of severe toxicity for patients with clinical benefits or progressive disease after chemotherapy. Second-line chemotherapy after disease progression on icotinib was the crossover of the first-line chemotherapy. The chemotherapy regimen after DP/PP treatment had no restriction.

For the patients assigned to first-line icotinib treatment, 125 mg icotinib was administered orally three times per day until disease progression or the occurrence of severe toxicity. For second-line treatment, the patients received the PP (pemetrexed disodium 500 mg/m^2 iv d1, cisplatin 75 mg/m^2 iv d1, q3w) or DP (docetaxel 75 mg/m^2 iv d1, cisplatin 75 mg/m^2 iv d1, q3w) chemotherapy regimen, at the discretion of the treating physician.

Assessment

For patients on first-line chemotherapy, the tumor response was assessed after every two cycles of chemotherapy. During icotinib maintenance therapy, treatment efficacy assessment was performed 4 wk after treatment initiation and then every 6 wk until disease progression. For patients on first-line icotinib therapy, tumor response was assessed 4 wk after treatment initiation and then every 6 wk until disease progression. The tumors were assessed by plain and enhanced pulmonary computed tomography (CT) scanning, abdominal ultrasound examination, CT scanning or magnetic resonance imaging (MRI), ultrasound examination of superficial lymph nodes, brain MRI (if necessary), and emission CT (if necessary). The response to treatment was classified as complete response (CR), partial response (PR), stable disease (SD), and progressive disease (PD) according to RECIST 1.1[25]. The safety evaluation was performed using physical examinations and laboratory examinations (hematological and blood biochemical examinations). All adverse events were recorded from the informed consent until 30 d after the last dose of the study drug. The severity of the adverse events was assessed and documented according to the National Cancer Institute-Common Toxicity Criteria 3.0. The investigators judged the relationship between the adverse events and treatment.

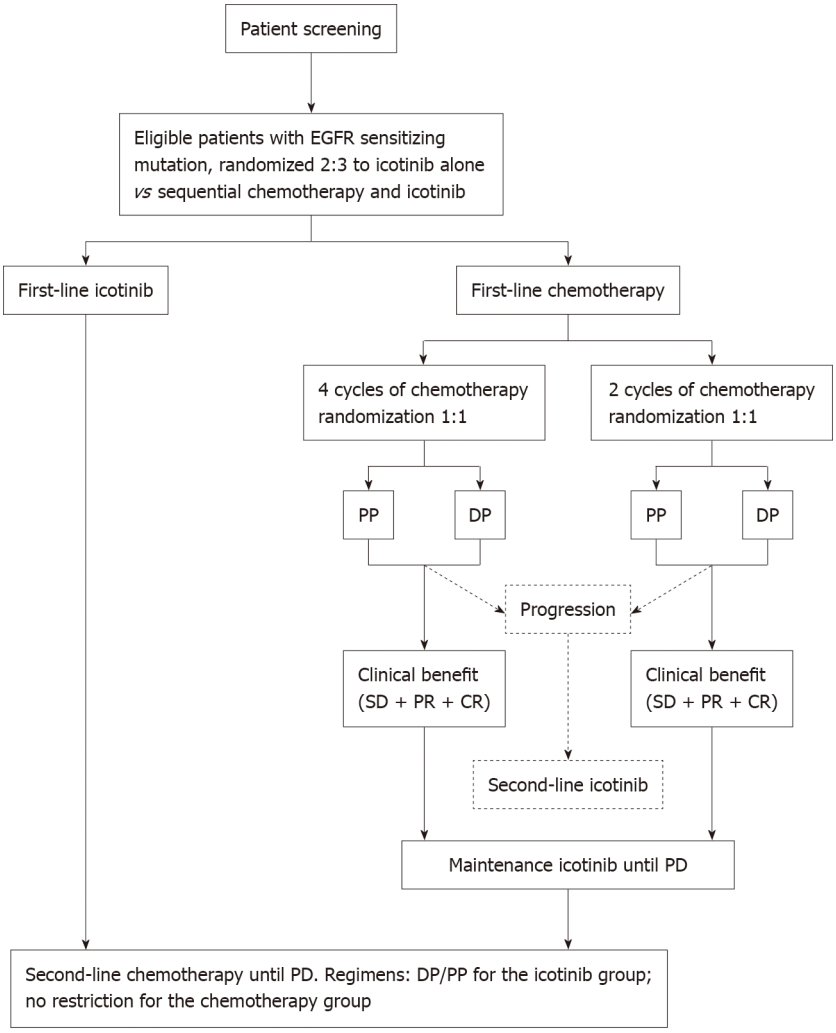

DOI: 10.12998/wjcc.v10.i18.6069 **Copyright** ©The Author(s) 2022.

Figure 1 Study design. DP: Docetaxel/cisplatin; EGFR: Epithelial growth factor receptor; PD: Progressive disease; PP: Pemetrexed/cisplatin; PR: Partial response; SD: Stable disease.

Outcomes

The study's primary endpoint was PFS, defined as the date of the start of treatment to the date of PD (per RECIST 1.1) or death, whichever occurred first. The secondary endpoint was overall survival (OS), defined as the time from the start of treatment to death. Other efficacy endpoints included overall response rate (ORR) and disease control rate (DCR). The ORR was defined as the proportion of patients achieving CR or PR, and the DCR was defined as the proportion of patients achieving CR, PR, or SD.

Statistical analysis

All analyses were performed using SAS 9.2 (SAS Institute, Inc., NC, United States). The efficacy analysis was performed in the full analysis set, defined as all randomized patients who received at least one dose of the study drug. The safety set included all randomized patients who received at least one dose of the study drug. Continuous data are presented as means ± SD and medians (ranges). Categorical data are presented as numbers (percentages). PFS and OS were analyzed using the Kaplan-Meier method and the log-rank test. The ORR and DCR were summarized as percentages and Clopper-Pearson 95%CIs. Two-sided P values of < 0.05 were considered statistically significant.

RESULTS

Characteristics of the participants

Between November 2012 and July 2015, 68 participants were recruited: 24 in the icotinib-alone group and 44 in the chemotherapy + icotinib group. The participants who received single-dose treatment (22 in the icotinib-alone group and 36 in the chemotherapy + icotinib group) were included in the analysis. All participants were randomized, and treatment was initiated. The characteristics of the participants are

shown in Table 1. All patients except one had stage IV NSCLC.

Response to treatment

Table 2 shows the responses to treatment. No participants achieved CR. In the icotinib-alone group, the ORR was 54.5% (95%CI: 32.2-75.6) and the DCR was 90.9% (95%CI: 70.8-98.9) compared with 44.1% (95%CI: 27.2-62.1) and 97.1% (95%CI: 84.7-99.9), respectively, in the chemotherapy + icotinib group.

When considering the number of chemotherapy cycles, the ORR was 47.6% (95%CI: 25.7-70.2) and the DCR was 100.0% (95%CI: 83.9-100.0) for two cycles, and the ORR was 38.5% (95%CI: 13.9-68.4) and the DCR was 92.3% (95%CI: 64.0-99.8) for four cycles. When considering the chemotherapy types, the ORR was 40.0% (95%CI: 16.3-67.7) and the DCR was 100.0% (95%CI: 78.2-100.0) for DP, and the ORR was 47.4% (95%CI: 24.4-71.1) and the DCR was 94.7% (95%CI: 74.0-99.9) for PP. When considering each chemotherapy regimen, the ORR was 33.3%-60.0%, and the DCR was 88.9%-100%.

Survival

In the icotinib group, the median follow-up was 23.1 (range, 2.5-71.9) mo. The median follow-up in the chemotherapy + icotinib group was 36.0 (range, 5.1-75.7) mo. Figures 2 and 3 present the PFS and OS, respectively. The median PFS in the icotinib-alone and chemotherapy + icotinib groups was 8.0 mo (95%CI: 3.8-11.6) *vs* 13.4 mo (95%CI: 10.2-16.3), respectively (P = 0.0249). The median OS was 23.1 (95%CI: 9.7-50.3) *vs* 36.0 mo (95%CI: 22.2-45.4), respectively (P = 0.4511). The median PFS of the participants who received two and four chemotherapy cycles was 12.1 mo *vs* 15.1 mo, and the median OS was 36.1 mo *vs* 33.9 mo, with no significant differences (PFS, P = 0.6605; OS, P = 0.9239). The PFS after two cycles of DP, two cycles of PP, four cycles of DP, and four cycles of PP was 11.9, 15.2, 15.2, and 15.1 mo, respectively; the median OS was 36.1, 28.0, 36.1, and 33.9 mo, respectively. No significant difference was observed among the different treatment regimens (PFS, P = 0.1815; OS, P = 0.9549).

Table 3 presents the treatment received after icotinib-based therapy. The treatment profile was similar in the two groups.

Treatment-related adverse events

The rates of all-grade treatment-related adverse events (TRAEs) were lower in the icotinib-alone group compared with the chemotherapy + icotinib group, and included rash (40.9% *vs* 55.9%), gastrointestinal system disorders (0.0% *vs* 82.4%), alanine transaminase elevation (27.3% *vs* 41.2%), aspartate aminotransferase elevation (13.6% *vs* 29.4%), leukopenia (0.0% *vs* 64.7%), and thrombocytopenia (0.0% *vs* 11.8%). Grade 3-4 TRAEs were not observed in the icotinib-alone group. However, grade 3-4 gastrointestinal system disorders (5.9%) and leukopenia (8.8%) were recorded in the chemotherapy + icotinib group (Table 4).

DISCUSSION

Sequential chemotherapy followed by maintenance TKI may be a potential strategy for advanced NSCLC with *EGFR* mutation. However, the optimal regimen remains to be determined. In this study, icotinib was selected because of the potential effect and tolerability of sequential chemotherapy and icotinib[22-24]. The present study indicated that the sequential combination of chemotherapy followed by icotinib improved PFS by 5.4 mo compared with icotinib alone as the first-line therapy of NSCLC. In addition, no differences were observed between two and four cycles of chemotherapy and between PP and DP. Therefore, for patients with advanced NSCLC with *EGFR* mutation, a sequential combination of chemotherapy and an EGFR-TKI is feasible. Considering the chemotherapy toxicity, the efficacy of a two-cycle chemotherapy regimen was comparable to that of a four-cycle chemotherapy regimen.

In the present study, no significant differences were observed in OS (36 mo *vs* 23.1 mo) and PFS (8.0 mo *vs* 13.4 mo), which was probably due to the small sample size or the fact of crossover of the treatment group upon disease progression. Considering the synergistic effect of EGFR-TKIs and chemotherapy in the elimination of tumor cells, as reported by some preclinical studies, gefitinib and erlotinib were combined with two chemotherapy regimens (cisplatin + gemcitabine; carboplatin + paclitaxel), thus launching four large phase III clinical studies, including INTACT 1 and 2 and TRIBUTE [26,27]. These studies showed no significant difference between chemotherapy and combined treatment groups (PFS and OS), which might be because the participants were not selected according to their *EGFR* mutation status[28]. A retrospective analysis of the OPTIMAL study on *EGFR* mutation (exon 19 deletion or exon 21 L858R mutation) showed that the OS of patients treated with chemotherapy alone was significantly lower than that of patients who received TKI and sequential chemotherapy [median OS: 11.2 *vs* 29.7 mo, HR = 2.97 (1.74-5.07)]. Although it was a retrospective analysis, it also suggested that sequential treatment with TKI and chemotherapy for selected patients with *EGFR* mutation could prolong patient OS[29]. However, a phase II clinical study in Japan, NEJ00, reported that in NSCLC patients with *EGFR* mutation, the combined therapy of gefitinib, pemetrexed, and carboplatin was significantly superior to chemotherapy followed by targeted therapy[30]. Among the 80 enrolled patients, 41 received concurrent combination therapy, while 39 also had sequential therapy. The median

Table 1 Patient characteristics

	Icotinib	Chemotherapy + icotinib	Chemotherapy + icotinib, *n* = 34			
			2DP	2PP	4DP	4PP
	n = 22	*n* = 34	*n* = 11	*n* = 10	*n* = 4	*n* = 9
Age (yr)	57.0 ± 7.4	52.7 ± 11.05	52.9 ± 11.5	49.8 ± 9.2	49.8 ± 13.7	57.1 ± 11.7
Sex						
Male	11 (50.0)	9 (26.5)	2 (18.2)	2 (20.0)	2 (50.0)	3 (33.3)
Female	11 (50.0)	25 (73.5)	9 (81.8)	8 (80.0)	2 (50.0)	6 (66.7)
Stage						
IIIB	0	1 (2.9)	0	0	0	1 (11.1)
IV	22 (100.0)	33 (97.1)	11 (100.0)	10 (100.0)	4 (100.0)	8 (88.9)
EGFR mutation						
19 Del	12 (54.5)	19 (55.9)	5 (45.5)	5 (50.0)	4 (100.0)	5 (55.6)
21 L858R	7 (31.8)	14 (41.2)	5 (45.5)	5 (50.0)	0	4 (44.4)
Other	3 (13.6)	1 (2.9)	1 (9.1)	0	0	0
Smoking						
Yes	6 (27.3)	4 (11.8)	1 (9.1)	1 (10.0)	1 (25.0)	1 (11.1)
No	15 (68.2)	30 (88.2)	10 (90.9)	9 (90.0)	3 (75.0)	8 (88.9)
Quit smoking	1 (4.5)	0	0	0	0	0
ECOG PS						
0	5 (22.7)	6 (17.6)	1 (9.1)	2 (20.0)	0	3 (33.3)
1	13 (59.1)	25 (73.5)	7 (63.6)	8 (80.0)	4 (100.0)	6 (66.7)
2	2 (9.1)	0	0	0	0	0
Other	2 (9.1)	3 (8.8)	3 (27.3)	0	0	0

Data are mean ± SD or number (%). *EGFR*: Epithelial growth factor receptor; ECOG PS: Eastern Cooperative Oncology Group performance status.

PFS was 18.3 mo *vs* 15.3 mo [HR = 0.71 (0.42-1.2), P = 0.02], and median OS was 41.9 mo *vs* 30.7 mo [HR = 0.51 (0.26-0.99), P = 0.042], respectively. The response rates in the two groups were similar (87.8% and 84.6%, respectively). Furthermore, phase II clinical studies conducted in China reported similar results for gefitinib combined with pemetrexed-based chemotherapy[31]. Based on the results of NEJ005, the phase III clinical study NEJ009 further confirmed that the efficacy of gefitinib combined with carboplatin and pemetrexed was superior to that of single-drug gefitinib treatment[32], which showed that the PFS was 20.9 mo (18.0-24.2) *vs* 11.2 mo (9.0-13.4) [HR = 0.43 (0.39-0.62), P < 0.001], and more importantly, OS was 52.2 mo *vs* 38.8 mo (HR = 0.69, P = 0.013). Subsequently, CTRI/2016/08/007149, conducted in India and almost completely similar to NEJ009, further confirmed that the efficacy of gefitinib combined with carboplatin and pemetrexed was significantly superior to that of gefitinib alone [33]. It also demonstrated that the PFS of gefitinib combined with pemetrexed-based chemotherapy was longer than 16 mo and longer than 20.9 mo in NEJ009, which was a much longer PFS than achieved by gefitinib alone. In particular, two phase III clinical trials, NEJ009 and CTRI/2016/08/007149, confirmed the benefits of OS in the combination treatment group. The studies mentioned above mainly focused on targeting, a synchronous combination of chemotherapy, or alternating sequential combination of targeting and chemotherapy. However, evidence on the use of sequential therapy based on chemotherapy followed by the target drug in *EGFR*-mutant patients is lacking. Studies at the molecular level confirmed that sequential chemotherapy with the EGFR-TKI erlotinib after docetaxel could enhance the M-phase stagnation of tumor cell division and growth, resulting in cell apoptosis. They suggested a synergistic effect between molecular targeted therapy and appropriate sequential chemotherapy. These experimental results indicated that the use of chemotherapy first to induce tumor cell stagnation and apoptosis in the M phase, followed by EGFR-TKIs to enhance this effect[34], would result in sequential therapy having a superposition effect, which might be used as a feasible option. Similar to the present study, Han *et al*[13] compared gefitinib + pemetrexed + carboplatin *vs* gefitinib alone *vs* pemetrexed + carboplatin and reported a higher ORR with the TKI + chemotherapy

Table 2 Response to treatment

	n	PR (95%CI)	SD (95%CI)	PD (95%CI)	NE (95%CI)	ORR (95%CI)	DCR (95%CI)
Icotinib	22	54.5 (32.2-75.6)	36.4 (17.2-59.3)	4.5 (0.1-22.8)	4.5 (0.1-22.8)	54.5 (32.2-75.6)	90.9 (70.8-98.9)
Chemotherapy + icotinib	34	44.1 (27.2-62.1)	52.9 (35.1-70.2)	2.9 (0.1-15.3)		44.1 (27.2-62.1)	97.1 (84.7-99.9)
2-cycle chemo	21	47.6 (25.7-70.2)	52.4 (29.8-74.3)			47.6 (25.7-70.2)	100.0 (83.9-100.0)
2DP	11	36.4 (10.9-69.2)	63.6 (30.8-89.1)			36.4 (10.9-69.2)	100.0 (71.5-100.0)
2PP	10	60.0 (26.2-87.8)	40.0 (12.2-73.8)			60.0 (26.2-87.8)	100.0 (69.2-100.0)
4-cycle chemo	13	38.5 (13.9-68.4)	53.8 (25.1-80.8)	7.7 (0.2-36.0)		38.5 (13.9-68.4)	92.3 (64.0-99.8)
4DP	4	50.0 (6.8-93.2)	50.0 (6.8-93.2)			50.0 (6.8-93.2)	100.0 (39.8-100.0)
4PP	9	33.3 (7.5-70.1)	55.6 (21.2-86.3)	11.1 (0.3-48.2)		33.3 (7.5-70.1)	88.9 (51.8-99.7)
DP	15	40.0 (16.3-67.7)	60.0 (32.3-83.7)			40.0 (16.3-67.7)	100.0 (78.2- 100.0)
PP	19	47.4 (24.4-71.1)	47.4 (24.4-71.1)	5.3 (0.1-26.0)		47.4 (24.4-71.1)	94.7 (74.0-99.9)
Total	56	48.2 (34.7-62.0)	46.4 (33.0-60.3)	3.6 (0.4-12.3)	1.8 (0.0-9.6)	48.2 (34.7-62.0)	94.6 (85.1-98.9)

DCR: Disease control rate; NE: Not evaluable; ORR: Overall response rate; PD: Progressive disease; PR: Partial response; SD: Stable disease.

Table 3 Subsequent treatments

	Icotinib	Chemotherapy + icotinib	Chemotherapy + icotinib, *n* = 34			
			2DP	2PP	4DP	4PP
	n = 22	*n* = 34	*n* = 11	*n* = 10	*n* = 4	*n* = 9
Chemotherapy	13 (59.1)	16 (47.1)	6 (54.6)	4 (40.0)	2 (50.0)	4 (44.4)
Osimertinib	10 (45.5)	17 (50.0)	6 (54.6)	4 (40.0)	2 (50.0)	5 (55.6)
Other TKI	2 (9.1)	3 (8.8)	1 (9.1)	0	0	2 (22.2)
Radiotherapy	3 (13.6)	7 (20.6)	1 (9.1)	3 (30.0)	2 (50.0)	2 (22.2)
Other	3 (13.6)	5 (14.7)	1 (9.1)	2 (20.0)	0	2 (22.2)

TKI: Tyrosine kinase inhibitor.

Table 4 Possible treatment-related adverse events

	All-grade TRAE		Grade 3-4 TRAE	
	Icotinib (*n* = 22)	Chemotherapy + icotinib (*n* = 34)	Icotinib (*n* = 22)	Chemotherapy + icotinib (*n* = 34)
Rash	9 (40.9)	19 (55.9)	0 (0.0)	0 (0.0)
Gastrointestinal system disorders	0 (0.0)	28 (82.4)	0 (0.0)	2 (5.9)
Alanine transaminase elevation	6 (27.3)	14 (41.2)	0 (0.0)	0 (0.0)
Aspartate aminotransferase elevation	3 (13.6)	10 (29.4)	0 (0.0)	0 (0.0)
Leukopenia	0 (0.0)	22 (64.7)	0 (0.0)	3 (8.8)
Thrombocytopenia	0 (0.0)	4 (11.8)	0 (0.0)	0 (0.0)

TRAE: Treatment-related adverse event.

combination than for TKI alone or chemotherapy alone (82.5% *vs* 65.9% *vs* 32.5%), with similar trends in PFS and OS. Similar results were also reported by Wen *et al*[35] and Yan *et al*[36]. Another RCT focused on first-line chemotherapy and TKI sequential treatment in patients with advanced non-squamous NSCLC[37,38]. PFS and OS were similar in the pemetrexed + cisplatin + gefitinib and gefitinib monotherapy groups in the ITT population and *EGFR*-mutated subgroup, but the sample size in the

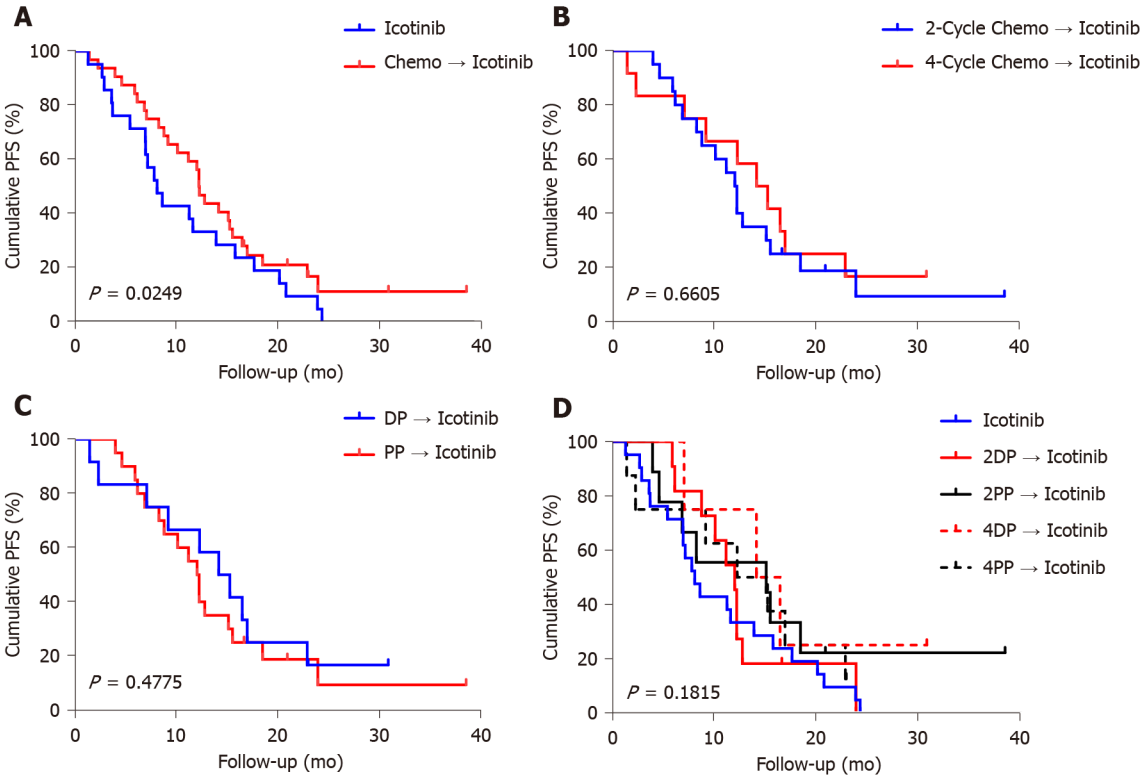

DOI: 10.12998/wjcc.v10.i18.6069 **Copyright** ©The Author(s) 2022.

Figure 2 Progression-free survival of patients. A: Progression-free survival (PFS) with icotinib *vs* chemotherapy followed by icotinib; B: PFS with two-cycle chemotherapy followed by icotinib *vs* four-cycle chemotherapy followed by icotinib; C: PFS with DP followed by icotinib *vs* PP followed by icotinib; D: PFS with icotinib *vs* various chemotherapy regimens followed by icotinib. DP: Docetaxel/cisplatin; PP: Pemetrexed/cisplatin.

EGFR-mutated subgroup was too small to draw a firm conclusion. The combination therapy may outperform the monotherapy ORR as chemotherapy and TKIs do not affect the cancer cells using the same mechanisms (*i.e.*, hitting the cells in multiple ways), and intratumor heterogeneity may be present (*i.e.*, using multiple drugs increases the likelihood of killing cells resistant to one of the drugs used). The immune system can also be activated[9,34,39,40]. Nevertheless, the PFS in the sequential treatment group in the present study was superior to that in the TKI-alone therapy group. The reason for the inconsistent results in these two studies might be that the number of patients with *EGFR* mutation in either study was small, affecting the consistency of the study results. Of note, the recent results of the FLAURA trial showed that first-line osimertinib achieved better OS and PFS than the comparator EGFR-TKIs[41], and sequential osimertinib with chemotherapy as a first-line option should be investigated. Due to the TRAE profile of osimertinib, the sequential use of chemotherapy and osimertinib could decrease the occurrence of TRAEs in the first-line treatment of NSCLC. Furthermore, the combination of EGFR-TKIs with vascular endothelial growth factor inhibitors could be a potential strategic option[42] and should also be examined.

In the present study, four cycles of chemotherapy were not better in terms of ORR, DCR, PFS, and OS compared with two cycles. Two cycles might be enough to eliminate tumor cells sensitive to chemotherapy and activate the immune system, while four cycles might lead to adverse events and decreases in blood immune cells[43]. In addition, fewer cycles could help reduce the physical, psychological, and economic burden of chemotherapy[43]. The rate of grade ≥ 3 TRAEs was 14.3% in the two-cycle subgroup and 15.4% in the four-cycle subgroup. Hence, the present study suggests similar efficacy and safety for the two- and four-cycle regimens, which could be supported by a meta-analysis that suggested no added benefit of six cycles of first-line chemotherapy compared with three and four cycles [43]. However, this study was not powered to compare two- *vs* four-cycle regimens, and additional studies are necessary to examine this point.

There are many therapeutic options in lung cancer, including chemotherapy, targeted therapy, and immunotherapy[2,44-48]. Icotinib is a promising targeted therapy for *EGFR*-mutated NSCLC[18,22-24]. The present study selected the combination of icotinib (or other EGFR-TKIs) and chemotherapy since it is the most studied combination in NSCLC, with apparent benefits in response and survival[9,18,24,34-36,49]. Still, the combination of EGFR-TKIs and immunotherapy could be a promising option for NSCLC[50-52], but some evidence suggests that immunotherapy is not effective in patients with *EGFR*-mutated NSCLC, probably because of the specific tumor microenvironment[52,53]. Indeed, early trials showed that immunotherapy monotherapy was inferior to EGFR-TKIs in *EGFR*-mutated NSCLC[52,

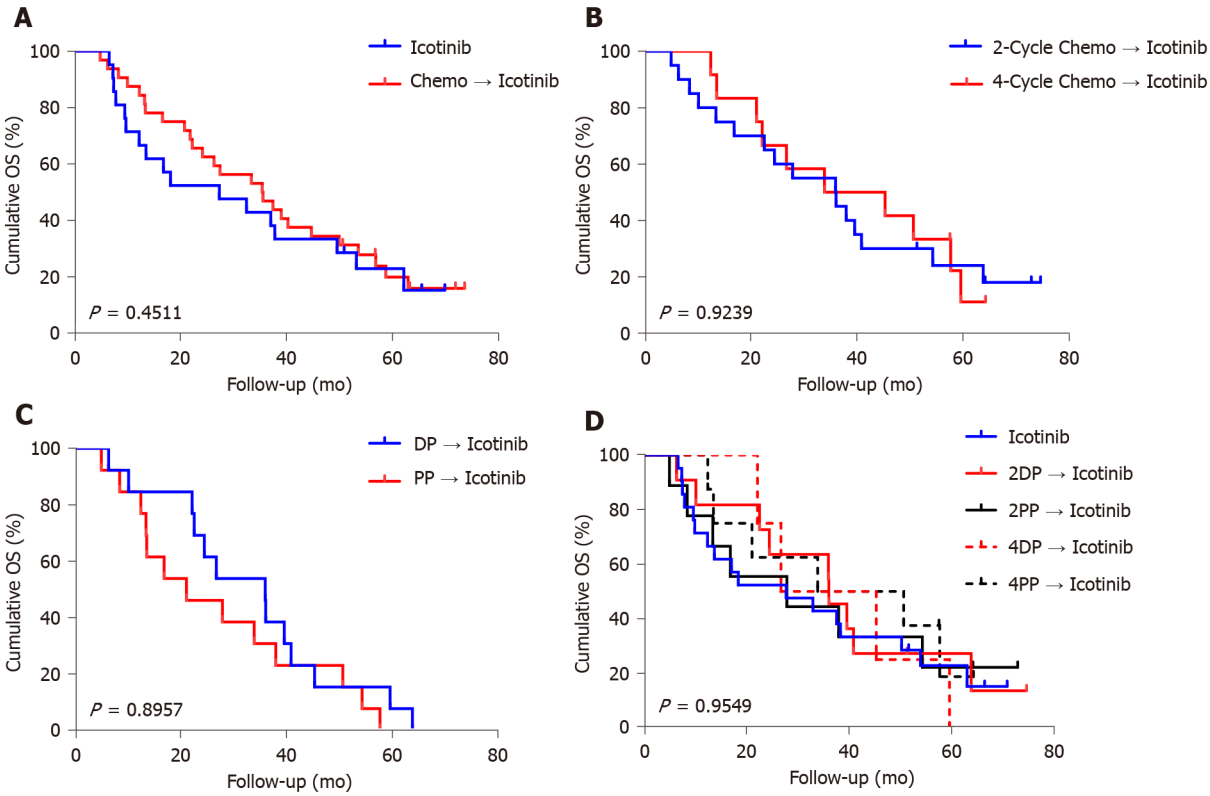

DOI: 10.12998/wjcc.v10.i18.6069 **Copyright** ©The Author(s) 2022.

Figure 3 Overall survival of patients. A: Overall survival (OS) with icotinib *vs* chemotherapy followed by icotinib; B: OS with two-cycle chemotherapy followed by icotinib *vs* four-cycle chemotherapy followed by icotinib; C: OS with docetaxel/cisplatin followed by icotinib *vs* PP followed by icotinib; D: OS with icotinib *vs* various chemotherapy regimens followed by icotinib. DP: Docetaxel/cisplatin; PP: Pemetrexed/cisplatin.

53]. Subsequent studies showed that the combination of immunotherapy with EGFR-TKIs in *EGFR*-mutated NSCLC resulted in high rates of serious AEs (33.3%-71.4% of grade 3-4 AEs)[54-56]. Therefore, additional studies are necessary before being able to use immunotherapy with EGFR-TKIs in patients with *EGFR*-mutated NSCLC.

Roviello *et al*[57] reported that EGFR-TKIs led to good outcomes in older adults with *EGFR*-mutated NSCLC. We agree that EGFR-TKIs could be a valuable and less toxic treatment option for older adults who often have difficulties with chemotherapy. Unfortunately, in the present study, the sample size was too small to be able to examine the influence of age on the treatment outcomes. Furthermore, as per the inclusion criteria, no patients > 72 years old were enrolled. Nevertheless, examining treatment options specifically in older adults is indeed a future direction for research.

This study had some limitations. This study was an exploratory study with a small sample size, and the analysis of OS had limited power. In addition, it was restricted to Chinese patients. It was an investigator-initiated trial. Only icotinib was provided, and the patients had to pay for the chemotherapy. This could have influenced recruitment. Although the trial was open to stage IIIB-IV patients, only one stage IIIB participant was actually recruited, mostly limiting the conclusions to stage IV patients. Due to the limited generalizability, the efficacy of sequential chemotherapy followed by TKI in the Caucasian population requires further investigation. Whether the results could also be generalized to non-stage IV patients remains to be examined.

CONCLUSION

For patients with stage IV NSCLC and *EGFR* mutation, sequential chemotherapy followed by TKI maintenance therapy is feasible. No significant differences were found in terms of the influence of the different number of chemotherapy cycles or different chemotherapy drugs on the curative effect, suggesting that fewer chemotherapy cycles could result in the same therapeutic effect in these specific patients.

ARTICLE HIGHLIGHTS

Research background

In 2018, 2.1 million new lung cancers and 1.8 million deaths were reported, and non-small cell lung cancers (NSCLCs) represent the greatest number (85%-90%) of malignant lung tumors. In Asians, 51.4% of epidermal growth factor receptor (*EGFR*)-mutated NSCLC was reported and EGFR-tyrosine kinase inhibitors (TKIs) have proved to be an effective treatment for this population.

Research motivation

Drug resistance always occurs after 10 mo of EGFR-TKIs treatment, and combination therapy could be an alternative to solve this difficulty. However, the most adequate combinational strategy remains controversial.

Research objectives

Some clinical studies have reported that sequential chemotherapy followed by maintenance EGFR-TKIs might be a potential strategy compared with EGFR-TKIs monotherapy. The efficacy and tolerability of icotinib has been demonstrated in many studies. Therefore, this pilot randomized controlled trial (RCT) aims to evaluate the efficacy and safety of combination therapy compared with monotherapy.

Research methods

This multicenter, open-label, pilot RCT enrolled 68 *EGFR*-mutated stage IIIB/IV NSCLC patients randomized 2:3 to the icotinib-alone and chemotherapy + icotinib groups.

Research results

A statistically significant difference was observed between the icotinib-alone and chemotherapy + icotinib groups regarding median progression-free survival (P = 0.0249). No statistically significant difference was found between two and four cycles of chemotherapy which means that the sequential combination of chemotherapy and EGFR-TKIs is feasible. Sequential chemotherapy followed by maintenance EGFR-TKIs might be a potential strategy for *EGFR*-mutated NSCLC patients; however, the optimal regimen remains to be determined.

Research conclusions

The sequential combination of chemotherapy and EGFR-TKIs could be a feasible strategy for stage IV *EGFR*-mutated NSCLC patients. It is suggested that 2-cycle sequential combination chemotherapy could have similar effectiveness to that of 4-cycle sequential combination chemotherapy in these patients.

Research perspectives

Future studies should involve a large population from multiple centers around the world to further validate the efficacy and safety of sequential treatment in *EGFR*-mutated NSCLC patients.

FOOTNOTES

Author contributions: Sun SJ, Jiao SC, and Fang J carried out the studies, participated in collecting data, and drafted the manuscript; Han JD and Liu W performed the statistical analysis and participated in its design; Wu ZY, Zhao X, and Yan X participated in the acquisition, analysis, interpretation of data and drafted the manuscript; All authors have read and approved the final manuscript.

Institutional review board statement: The study was reviewed and approved by General Hospital of People's Liberation Army.

Clinical trial registration statement: ClinicalTrials.gov, NCT01665417. Registered on August 12, 2012, https://clinicaltrials.gov/ct2/show/NCT01665417.

Informed consent statement: All patients signed an informed consent form before any study procedure.

Conflict-of-interest statement: The authors declare no conflicts of interest.

Data sharing statement: The raw dataset analyzed in the current study are available from the corresponding author on reasonable request.

Open-Access: This article is an open-access article that was selected by an in-house editor and fully peer-reviewed by external reviewers. It is distributed in accordance with the Creative Commons Attribution NonCommercial (CC BY-NC 4.0) license, which permits others to distribute, remix, adapt, build upon this work non-commercially, and license

their derivative works on different terms, provided the original work is properly cited and the use is non-commercial. See: https://creativecommons.org/Licenses/by-nc/4.0/

Country/Territory of origin: China

ORCID number: Sheng-Jie Sun 0000-0001-7010-9472; Jin-Di Han 0000-0002-0790-9802; Wei Liu 0000-0002-1534-1823; Zhi-Yong Wu 0000-0002-8763-4449; Xiao Zhao 0000-0002-8661-1480; Xiang Yan 0000-0002-3683-474X; Shun-Chang Jiao 0000-0001-8017-5342; Jian Fang 0000-0003-3697-4563.

S-Editor: Zhang H
L-Editor: Webster JR
P-Editor: Zhang H

REFERENCES

1 **Bray F**, Ferlay J, Soerjomataram I, Siegel RL, Torre LA, Jemal A. Global cancer statistics 2018: GLOBOCAN estimates of incidence and mortality worldwide for 36 cancers in 185 countries. *CA Cancer J Clin* 2018; **68**: 394-424 [PMID: 30207593 DOI: 10.3322/caac.21492]
2 **Novello S**, Barlesi F, Califano R, Cufer T, Ekman S, Levra MG, Kerr K, Popat S, Reck M, Senan S, Simo GV, Vansteenkiste J, Peters S; ESMO Guidelines Committee. Metastatic non-small-cell lung cancer: ESMO Clinical Practice Guidelines for diagnosis, treatment and follow-up. *Ann Oncol* 2016; **27**: v1-v27 [PMID: 27664245 DOI: 10.1093/annonc/mdw326]
3 **Cabanero M**, Sangha R, Sheffield BS, Sukhai M, Pakkal M, Kamel-Reid S, Karsan A, Ionescu D, Juergens RA, Butts C, Tsao MS. Management of *EGFR*-mutated non-small-cell lung cancer: practical implications from a clinical and pathology perspective. *Curr Oncol* 2017; **24**: 111-119 [PMID: 28490925 DOI: 10.3747/co.24.3524]
4 **da Cunha Santos G**, Shepherd FA, Tsao MS. EGFR mutations and lung cancer. *Annu Rev Pathol* 2011; **6**: 49-69 [PMID: 20887192 DOI: 10.1146/annurev-pathol-011110-130206]
5 **Singer J**, Irmisch A, Ruscheweyh HJ, Singer F, Toussaint NC, Levesque MP, Stekhoven DJ, Beerenwinkel N. Bioinformatics for precision oncology. *Brief Bioinform* 2019; **20**: 778-788 [PMID: 29272324 DOI: 10.1093/bib/bbx143]
6 **Morgillo F**, Della Corte CM, Fasano M, Ciardiello F. Mechanisms of resistance to EGFR-targeted drugs: lung cancer. *ESMO Open* 2016; **1**: e000060 [PMID: 27843613 DOI: 10.1136/esmoopen-2016-000060]
7 **Maione P**, Sacco PC, Casaluce F, Sgambato A, Santabarbara G, Rossi A, Gridelli C. Overcoming Resistance to EGFR Inhibitors in NSCLC. *Rev Recent Clin Trials* 2016; **11**: 99-105 [PMID: 27028971 DOI: 10.2174/1574887111666160330120431]
8 **Del Re M**, Crucitta S, Gianfilippo G, Passaro A, Petrini I, Restante G, Michelucci A, Fogli S, de Marinis F, Porta C, Chella A, Danesi R. Understanding the Mechanisms of Resistance in *EGFR*-Positive NSCLC: From Tissue to Liquid Biopsy to Guide Treatment Strategy. *Int J Mol Sci* 2019; **20** [PMID: 31416192 DOI: 10.3390/ijms20163951]
9 **Nan X**, Xie C, Yu X, Liu J. EGFR TKI as first-line treatment for patients with advanced EGFR mutation-positive non-small-cell lung cancer. *Oncotarget* 2017; **8**: 75712-75726 [PMID: 29088904 DOI: 10.18632/oncotarget.20095]
10 **Decoster L**, Giron P, Mignon S, De Grève J. The evolving first-line treatment of advanced non-small cell lung cancer harbouring epidermal growth factor receptor mutations. *Transl Lung Cancer Res* 2018; **7**: S134-S137 [PMID: 29780706 DOI: 10.21037/tlcr.2018.03.08]
11 **Sebastian M**, Schmittel A, Reck M. First-line treatment of EGFR-mutated nonsmall cell lung cancer: critical review on study methodology. *Eur Respir Rev* 2014; **23**: 92-105 [PMID: 24591666 DOI: 10.1183/09059180.00008413]
12 **Zhang C**, Leighl NB, Wu YL, Zhong WZ. Emerging therapies for non-small cell lung cancer. *J Hematol Oncol* 2019; **12**: 45 [PMID: 31023335 DOI: 10.1186/s13045-019-0731-8]
13 **Han B**, Jin B, Chu T, Niu Y, Dong Y, Xu J, Gu A, Zhong H, Wang H, Zhang X, Shi C, Zhang Y, Zhang W, Lou Y, Zhu L, Pei J. Combination of chemotherapy and gefitinib as first-line treatment for patients with advanced lung adenocarcinoma and sensitive EGFR mutations: A randomized controlled trial. *Int J Cancer* 2017; **141**: 1249-1256 [PMID: 28560853 DOI: 10.1002/ijc.30806]
14 **Wu M**, Yuan Y, Pan YY, Zhang Y. Combined gefitinib and pemetrexed overcome the acquired resistance to epidermal growth factor receptor tyrosine kinase inhibitors in non-small cell lung cancer. *Mol Med Rep* 2014; **10**: 931-938 [PMID: 24840891 DOI: 10.3892/mmr.2014.2243]
15 **Cheng H**, An SJ, Dong S, Zhang YF, Zhang XC, Chen ZH, Jian-Su, Wu YL. Molecular mechanism of the schedule-dependent synergistic interaction in EGFR-mutant non-small cell lung cancer cell lines treated with paclitaxel and gefitinib. *J Hematol Oncol* 2011; **4**: 5 [PMID: 21255411 DOI: 10.1186/1756-8722-4-5]
16 **Li T**, Ling YH, Goldman ID, Perez-Soler R. Schedule-dependent cytotoxic synergism of pemetrexed and erlotinib in human non-small cell lung cancer cells. *Clin Cancer Res* 2007; **13**: 3413-3422 [PMID: 17545550 DOI: 10.1158/1078-0432.CCR-06-2923]
17 **Giovannetti E**, Lemos C, Tekle C, Smid K, Nannizzi S, Rodriguez JA, Ricciardi S, Danesi R, Giaccone G, Peters GJ. Molecular mechanisms underlying the synergistic interaction of erlotinib, an epidermal growth factor receptor tyrosine kinase inhibitor, with the multitargeted antifolate pemetrexed in non-small-cell lung cancer cells. *Mol Pharmacol* 2008; **73**: 1290-1300 [PMID: 18187583 DOI: 10.1124/mol.107.042382]
18 **Feng X**, Zhang Y, Li T, Li Y. Sequentially administrated of pemetrexed with icotinib/erlotinib in lung adenocarcinoma cell lines *in vitro*. *Oncotarget* 2017; **8**: 114292-114299 [PMID: 29371987 DOI: 10.18632/oncotarget.23224]
19 **Kubo E**, Yamamoto N, Nokihara H, Fujiwara Y, Horinouchi H, Kanda S, Goto Y, Ohe Y. Randomized phase II study of

sequential carboplatin plus paclitaxel and gefitinib in chemotherapy-naïve patients with advanced or metastatic non-small-cell lung cancer: Long-term follow-up results. *Mol Clin Oncol* 2017; **6**: 56-62 [PMID: 28123729 DOI: 10.3892/mco.2016.1076]

20 **Choi YJ**, Lee DH, Choi CM, Lee JS, Lee SJ, Ahn JH, Kim SW. Randomized phase II study of paclitaxel/carboplatin intercalated with gefitinib compared to paclitaxel/carboplatin alone for chemotherapy-naïve non-small cell lung cancer in a clinically selected population excluding patients with non-smoking adenocarcinoma or mutated EGFR. *BMC Cancer* 2015; **15**: 763 [PMID: 26493267 DOI: 10.1186/s12885-015-1714-y]

21 **Patil VM**, Noronha V, Joshi A, Choughule AB, Bhattacharjee A, Kumar R, Goud S, More S, Ramaswamy A, Karpe A, Pande N, Chandrasekharan A, Goel A, Talreja V, Mahajan A, Janu A, Purandare N, Prabhash K. Phase III study of gefitinib or pemetrexed with carboplatin in EGFR-mutated advanced lung adenocarcinoma. *ESMO Open* 2017; **2**: e000168 [PMID: 28761735 DOI: 10.1136/esmoopen-2017-000168]

22 **Wang MC**, Liang X, Liu ZY, Cui J, Liu Y, Jing L, Jiang LL, Ma JQ, Han LL, Guo QQ, Yang CC, Wang J, Wu T, Nan KJ, Yao Y. In vitro synergistic antitumor efficacy of sequentially combined chemotherapy/icotinib in nonsmall cell lung cancer cell lines. *Oncol Rep* 2015; **33**: 239-249 [PMID: 25370413 DOI: 10.3892/or.2014.3583]

23 **Zhang Y**, Wang J, Yu Z, Ge H, Zhang LW, Feng LX. Outcomes of concurrent versus sequential icotinib therapy and chemotherapy in advanced non-small cell lung cancer with sensitive EGFR mutations. *Clin Transl Sci* 2021; **14**: 890-897 [PMID: 33382908 DOI: 10.1111/cts.12951]

24 **Zheng Y**, Fang W, Deng J, Zhao P, Xu N, Zhou J. Sequential treatment of icotinib after first-line pemetrexed in advanced lung adenocarcinoma with unknown EGFR gene status. *J Thorac Dis* 2014; **6**: 958-964 [PMID: 25093093 DOI: 10.3978/j.issn.2072-1439.2014.07.18]

25 **Nishino M**, Jackman DM, Hatabu H, Yeap BY, Cioffredi LA, Yap JT, Jänne PA, Johnson BE, Van den Abbeele AD. New Response Evaluation Criteria in Solid Tumors (RECIST) guidelines for advanced non-small cell lung cancer: comparison with original RECIST and impact on assessment of tumor response to targeted therapy. *AJR Am J Roentgenol* 2010; **195**: W221-W228 [PMID: 20729419 DOI: 10.2214/AJR.09.3928]

26 **Herbst RS**, Prager D, Hermann R, Fehrenbacher L, Johnson BE, Sandler A, Kris MG, Tran HT, Klein P, Li X, Ramies D, Johnson DH, Miller VA; TRIBUTE Investigator Group. TRIBUTE: a phase III trial of erlotinib hydrochloride (OSI-774) combined with carboplatin and paclitaxel chemotherapy in advanced non-small-cell lung cancer. *J Clin Oncol* 2005; **23**: 5892-5899 [PMID: 16043829 DOI: 10.1200/jco.2005.02.840]

27 **Johnson DH**. Targeted therapies in combination with chemotherapy in non-small cell lung cancer. *Clin Cancer Res* 2006; **12**: 4451s-4457s [PMID: 16857827 DOI: 10.1158/1078-0432.CCR-06-0095]

28 **Davies AM**, Ho C, Lara PN Jr, Mack P, Gumerlock PH, Gandara DR. Pharmacodynamic separation of epidermal growth factor receptor tyrosine kinase inhibitors and chemotherapy in non-small-cell lung cancer. *Clin Lung Cancer* 2006; **7**: 385-388 [PMID: 16800963 DOI: 10.3816/CLC.2006.n.021]

29 **Zhou C**, Wu YL, Liu X, Wang CL, Chen GY, Feng JF, Zhang SC, Wang J, Zhou SW, Ren SX, Lu S, Zhang L, Hu CP, Luo Y, Chen L, Ye M, Huang JN, Zhi XY, Zhang YP, Xiu QY. Overall survival (OS) results from OPTIMAL (CTONG0802), a phase III trial of erlotinib (E) vs carboplatin plus gemcitabine (GC) as first-line treatment for Chinese patients with EGFR mutation-positive advanced non-small cell lung cancer (NSCLC). *J Clin Oncol* 2012; **30**: 7520 [DOI: 10.1200/jco.2012.30.15_suppl.7520]

30 **Sugawara S**, Oizumi S, Minato K, Harada T, Inoue A, Fujita Y, Maemondo M, Yoshizawa H, Ito K, Gemma A, Nishitsuji M, Harada M, Isobe H, Kinoshita I, Morita S, Kobayashi K, Hagiwara K, Kurihara M, Nukiwa T. Randomized phase II study of concurrent versus sequential alternating gefitinib and chemotherapy in previously untreated non-small cell lung cancer with sensitive EGFR mutations: NEJ005/TCOG0902. *Ann Oncol* 2015; **26**: 888-894 [PMID: 25669832 DOI: 10.1093/annonc/mdv063]

31 **Yang JC**, Cheng Y, Murakami H, Yang PC, He J, Nakagawa K, Kang JH, Kim JH, Hozak RR, Nguyen TS, Zhang WL, Enatsu S, Puri T, Orlando M. A Randomized Phase 2 Study of Gefitinib With or Without Pemetrexed as First-line Treatment in Nonsquamous NSCLC With EGFR Mutation: Final Overall Survival and Biomarker Analysis. *J Thorac Oncol* 2020; **15**: 91-100 [PMID: 31605797 DOI: 10.1016/j.jtho.2019.09.008]

32 **Nakamura A**, Inoue A, Morita S, Hosomi Y, Kato T, Fukuhara T, Gemma A, Takahashi K, Fujita Y, Harada T, Minato K, Takamura K, Kobayashi K, Nukiwa T. Phase III study comparing gefitinib monotherapy (G) to combination therapy with gefitinib, carboplatin, and pemetrexed (GCP) for untreated patients (pts) with advanced non-small cell lung cancer (NSCLC) with EGFR mutations (NEJ009). *J Clin Oncol* 2018; **36**: 9005 [DOI: 10.1200/jco.2018.36.15_suppl.9005]

33 **Noronha V**, Patil VM, Joshi A, Menon N, Chougule A, Mahajan A, Janu A, Purandare N, Kumar R, More S, Goud S, Kadam N, Daware N, Bhattacharjee A, Shah S, Yadav A, Trivedi V, Behel V, Dutt A, Banavali SD, Prabhash K. Gefitinib Versus Gefitinib Plus Pemetrexed and Carboplatin Chemotherapy in EGFR-Mutated Lung Cancer. *J Clin Oncol* 2020; **38**: 124-136 [PMID: 31411950 DOI: 10.1200/JCO.19.01154]

34 **Zhang L**, Qi Y, Xing K, Qian S, Zhang P, Wu X. A novel strategy of EGFRTKI combined chemotherapy in the treatment of human lung cancer with EGFRsensitive mutation. *Oncol Rep* 2018; **40**: 1046-1054 [PMID: 29917169 DOI: 10.3892/or.2018.6499]

35 **Wen M**, Xia J, Sun Y, Wang X, Fu X, Zhang Y, Zhang Z, Zhou Y, Li X. Combination of EGFR-TKIs with chemotherapy versus chemotherapy or EGFR-TKIs alone in advanced NSCLC patients with EGFR mutation. *Biologics* 2018; **12**: 183-190 [PMID: 30555222 DOI: 10.2147/BTT.S169305]

36 **Yan X**, Wang H, Li P, Zhang G, Zhang M, Yang J, Zhang X, Zheng X, Ma Z. Efficacy of first-line treatment with epidermal growth factor receptor-tyrosine kinase inhibitor (EGFR-TKI) alone or in combination with chemotherapy for advanced non-small cell lung cancer (NSCLC) with low-abundance mutation. *Lung Cancer* 2019; **128**: 6-12 [PMID: 30642455 DOI: 10.1016/j.lungcan.2018.12.007]

37 **Yang JC**, Kang JH, Mok T, Ahn MJ, Srimuninnimit V, Lin CC, Kim DW, Tsai CM, Barraclough H, Altug S, Orlando M, Park K. First-line pemetrexed plus cisplatin followed by gefitinib maintenance therapy versus gefitinib monotherapy in East Asian patients with locally advanced or metastatic non-squamous non-small cell lung cancer: a randomised, phase 3 trial. *Eur J Cancer* 2014; **50**: 2219-2230 [PMID: 24953333 DOI: 10.1016/j.ejca.2014.05.011]

38 **Yang JC**, Srimuninnimit V, Ahn MJ, Lin CC, Kim SW, Tsai CM, Mok T, Orlando M, Puri T, Wang X, Park K. First-Line Pemetrexed plus Cisplatin followed by Gefitinib Maintenance Therapy versus Gefitinib Monotherapy in East Asian Never-Smoker Patients with Locally Advanced or Metastatic Nonsquamous Non-Small Cell Lung Cancer: Final Overall Survival Results from a Randomized Phase 3 Study. *J Thorac Oncol* 2016; **11**: 370-379 [PMID: 26725183 DOI: 10.1016/j.jtho.2015.11.008]

39 **Patil PD**, Shepherd F, Johnson DH. A Career in Lung Cancer: Pushing Beyond Chemotherapy. *Am Soc Clin Oncol Educ Book* 2019; **39**: 583-589 [PMID: 31099660 DOI: 10.1200/EDBK_239397]

40 **Lim ZF**, Ma PC. Emerging insights of tumor heterogeneity and drug resistance mechanisms in lung cancer targeted therapy. *J Hematol Oncol* 2019; **12**: 134 [PMID: 31815659 DOI: 10.1186/s13045-019-0818-2]

41 **Cheng Y**, He Y, Li W, Zhang HL, Zhou Q, Wang B, Liu C, Walding A, Saggese M, Huang X, Fan M, Wang J, Ramalingam SS. Osimertinib Versus Comparator EGFR TKI as First-Line Treatment for EGFR-Mutated Advanced NSCLC: FLAURA China, A Randomized Study. *Target Oncol* 2021; **16**: 165-176 [PMID: 33544337 DOI: 10.1007/s11523-021-00794-6]

42 **Horinouchi H**. To combine or not to combine: anti-vascular endothelial growth factor therapies in EGFR mutation positive non-small cell lung cancer. *Ann Transl Med* 2020; **8**: 554 [PMID: 32411777 DOI: 10.21037/atm.2020.01.66]

43 **Rossi A**, Chiodini P, Sun JM, O'Brien ME, von Plessen C, Barata F, Park K, Popat S, Bergman B, Parente B, Gallo C, Gridelli C, Perrone F, Di Maio M. Six versus fewer planned cycles of first-line platinum-based chemotherapy for non-small-cell lung cancer: a systematic review and meta-analysis of individual patient data. *Lancet Oncol* 2014; **15**: 1254-1262 [PMID: 25232001 DOI: 10.1016/S1470-2045(14)70402-4]

44 **Tartarone A**, Roviello G, Lerose R, Roudi R, Aieta M, Zoppoli P. Anti-PD-1 versus anti-PD-L1 therapy in patients with pretreated advanced non-small-cell lung cancer: a meta-analysis. *Future Oncol* 2019; **15**: 2423-2433 [PMID: 31237152 DOI: 10.2217/fon-2018-0868]

45 **Mohsenzadegan M**, Peng RW, Roudi R. Dendritic cell/cytokine-induced killer cell-based immunotherapy in lung cancer: What we know and future landscape. *J Cell Physiol* 2020; **235**: 74-86 [PMID: 31222740 DOI: 10.1002/jcp.28977]

46 **Petrelli F**, Ferrara R, Signorelli D, Ghidini A, Proto C, Roudi R, Sabet MN, Facelli S, Garassino MC, Luciani A, Roviello G. Immune checkpoint inhibitors and chemotherapy in first-line NSCLC: a meta-analysis. *Immunotherapy* 2021; **13**: 621-631 [PMID: 33775103 DOI: 10.2217/imt-2020-0224]

47 **Petrelli F**, Ghidini A, Luciani A. Topotecan or other agents as second-line therapy for relapsed small-cell lung cancer: A meta-analysis of randomized studies. *Mol Clin Oncol* 2021; **15**: 218 [PMID: 34476102 DOI: 10.3892/mco.2021.2383]

48 NCCN Clincal Practice Guidelines in Oncology (NCCN Guidelines). Non-Small Cell Lung Cancer. Version 2.2020. Fort Washington: National Comprehensive Cancer Network, 2019

49 **Rebuzzi SE**, Alfieri R, La Monica S, Minari R, Petronini PG, Tiseo M. Combination of EGFR-TKIs and chemotherapy in advanced EGFR mutated NSCLC: Review of the literature and future perspectives. *Crit Rev Oncol Hematol* 2020; **146**: 102820 [PMID: 31785991 DOI: 10.1016/j.critrevonc.2019.102820]

50 **Jin R**, Zhao J, Xia L, Li Q, Li W, Peng L, Xia Y. Application of immune checkpoint inhibitors in EGFR-mutant non-small-cell lung cancer: from bed to bench. *Ther Adv Med Oncol* 2020; **12**: 1758835920930333 [PMID: 32565926 DOI: 10.1177/1758835920930333]

51 **Ito T**, Nagashima H, Akiyama M, Utsumi Y, Sato H, Chiba S, Sugai M, Ube K, Mori Y, Watanabe K, Fukuhara T, Maemondo M. Treatment with immune checkpoint inhibitors after EGFR-TKIs in EGFR-mutated lung cancer. *Thorac Cancer* 2022; **13**: 386-393 [PMID: 34904383 DOI: 10.1111/1759-7714.14267]

52 **Wiest N**, Majeed U, Seegobin K, Zhao Y, Lou Y, Manochakian R. Role of Immune Checkpoint Inhibitor Therapy in Advanced *EGFR*-Mutant Non-Small Cell Lung Cancer. *Front Oncol* 2021; **11**: 751209 [PMID: 34868953 DOI: 10.3389/fonc.2021.751209]

53 **Qiao M**, Jiang T, Liu X, Mao S, Zhou F, Li X, Zhao C, Chen X, Su C, Ren S, Zhou C. Immune Checkpoint Inhibitors in EGFR-Mutated NSCLC: Dusk or Dawn? *J Thorac Oncol* 2021; **16**: 1267-1288 [PMID: 33915248 DOI: 10.1016/j.jtho.2021.04.003]

54 **Creelan BC**, Yeh TC, Kim SW, Nogami N, Kim DW, Chow LQM, Kanda S, Taylor R, Tang W, Tang M, Angell HK, Roudier MP, Marotti M, Gibbons DL. A Phase 1 study of gefitinib combined with durvalumab in EGFR TKI-naive patients with EGFR mutation-positive locally advanced/metastatic non-small-cell lung cancer. *Br J Cancer* 2021; **124**: 383-390 [PMID: 33012782 DOI: 10.1038/s41416-020-01099-7]

55 **Yang JC**, Gadgeel SM, Sequist LV, Wu CL, Papadimitrakopoulou VA, Su WC, Fiore J, Saraf S, Raftopoulos H, Patnaik A. Pembrolizumab in Combination With Erlotinib or Gefitinib as First-Line Therapy for Advanced NSCLC With Sensitizing EGFR Mutation. *J Thorac Oncol* 2019; **14**: 553-559 [PMID: 30529597 DOI: 10.1016/j.jtho.2018.11.028]

56 **Ma BBY**, Rudin CM, Cervantes A, Dowlati A. Preliminary Safety and Clinical Activity of Erlotinib Plus Atezolizumab From a Phase Ib Study in Advanced NSCLC. *Ann Oncol* 2016; **27**: ix139-ix156 [DOI: 10.1093/annonc/mdw594.005]

57 **Roviello G**, Zanotti L, Cappelletti MR, Gobbi A, Dester M, Paganini G, Pacifico C, Generali D, Roudi R. Are EGFR tyrosine kinase inhibitors effective in elderly patients with EGFR-mutated non-small cell lung cancer? *Clin Exp Med* 2018; **18**: 15-20 [PMID: 28391544 DOI: 10.1007/s10238-017-0460-7]

World Journal of Clinical Cases

Submit a Manuscript: https://www.f6publishing.com

World J Clin Cases 2022 June 26; 10(18): 6082-6090

DOI: 10.12998/wjcc.v10.i18.6082

ISSN 2307-8960 (online)

ORIGINAL ARTICLE

Randomized Clinical Trial

Impact of preoperative carbohydrate loading on gastric volume in patients with type 2 diabetes

Xin-Qiang Lin, Yu-Ren Chen, Xiao Chen, Yu-Ping Cai, Jian-Xin Lin, De-Ming Xu, Xiao-Chun Zheng

Specialty type: Medicine, research and experimental

Provenance and peer review: Unsolicited article; Externally peer reviewed.

Peer-review model: Single blind

Peer-review report's scientific quality classification

Grade A (Excellent): 0
Grade B (Very good): B, B
Grade C (Good): 0
Grade D (Fair): 0
Grade E (Poor): 0

P-Reviewer: Harsini PA, Iran; Herold M, Hungary

Received: December 22, 2021
Peer-review started: December 22, 2021
First decision: February 8, 2022
Revised: March 21, 2022
Accepted: April 21, 2022
Article in press: April 21, 2022
Published online: June 26, 2022

Xin-Qiang Lin, Department of Anesthesiology, Affiliated Hospital of Putian College, Putian Maternity and Child Care Hospital, Putian 351100, Fujian Province, China

Yu-Ren Chen, Xiao Chen, Yu-Ping Cai, Jian-Xin Lin, De-Ming Xu, Department of Anesthesiology, Affiliated Hospital of Putian College, Putian 351100, Fujian Province, China

Xiao-Chun Zheng, Department of Anesthesiology, Shenli Clinical Medical College of Fujian Medical University, Fujian Provincial Hospital, Fuzhou 350001, Fujian Province, China

Corresponding author: Xiao-Chun Zheng, MD, Professor, Department of Anesthesiology, Shenli Clinical Medical College of Fujian Medical University, Fujian Provincial Hospital, No. 134 East Street, Fuzhou 350001, Fujian Province, China. zhengxiaochun2021@163.com

Abstract

BACKGROUND

Enhanced recovery after surgery advocates that consuming carbohydrates two hours before anesthesia is beneficial to the patient's recovery. Patients with diabetes are prone to delayed gastric emptying. Different guidelines for preoperative carbohydrate consumption in patients with diabetes remain controversial due to concerns about the risk of regurgitation, aspiration and hyperglycemia. Ultrasonic gastric volume (GV) assessment and blood glucose monitoring can comprehensively evaluate the safety and feasibility of preoperative carbohydrate intake in type 2 diabetes (T2D) patients.

AIM

To evaluate the impact of preoperative carbohydrate loading on GV before anesthesia induction in T2D patients.

METHODS

Patients with T2D receiving surgery under general anesthesia from December 2019 to December 2020 were included. A total of 78 patients were randomly allocated to 4 groups receiving 0, 100, 200, or 300 mL of carbohydrate loading 2 h before anesthesia induction. Gastric volume *per* unit weight (GV/W), Perlas grade, changes in blood glucose level, and risk of reflux and aspiration were evaluated before anesthesia induction.

RESULTS

No significant difference was found in GV/W among the groups before anes-

thesia induction (P > 0.05). The number of patients with Perlas grade II and GV/W > 1.5 mL/kg did not differ among the groups (P > 0.05). Blood glucose level increased by > 2 mmol/L in patients receiving 300 mL carbohydrate drink, which was significantly higher than that in groups 1 and 2 (P < 0.05).

CONCLUSION

Preoperative carbohydrate loading < 300 mL 2 h before induction of anesthesia in patients with T2D did not affect GV or increase the risk of reflux and aspiration. Blood glucose levels did not change significantly with preoperative carbohydrate loading of < 200 mL. However, 300 mL carbohydrate loading may increase blood glucose levels in patients with T2D before induction of anesthesia.

Key Words: Type 2 diabetes; Preoperative; Carbohydrate loading; Gastric volume; Ultrasound assessment; Hyperglycemia

©The Author(s) 2022. Published by Baishideng Publishing Group Inc. All rights reserved.

Core Tip: Enhanced recovery after surgery advocates that consuming carbohydrates two hours before anesthesia is beneficial to the patient's recovery. Patients with diabetes are prone to delayed gastric emptying. Different guidelines for preoperative carbohydrate consumption in patients with diabetes remain controversial due to concerns about the risk of regurgitation, aspiration and hyperglycemia. In this study, the preoperative carbohydrate load of type 2 diabetes (T2D) patients 2 h before anesthesia induction was found by ultrasonic gastric volume assessment and blood glucose monitoring. 200 mL does not increase the risk of reflux, aspiration, and hyperglycemia, but 300 mL glucose load may cause hyperglycemia in T2D patients before induction of anesthesia.

Citation: Lin XQ, Chen YR, Chen X, Cai YP, Lin JX, Xu DM, Zheng XC. Impact of preoperative carbohydrate loading on gastric volume in patients with type 2 diabetes. *World J Clin Cases* 2022; 10(18): 6082-6090
URL: https://www.wjgnet.com/2307-8960/full/v10/i18/6082.htm
DOI: https://dx.doi.org/10.12998/wjcc.v10.i18.6082

INTRODUCTION

Enhanced recovery after surgery (ERAS) is a set of perioperative protocols to reduce complications, facilitate recovery, and decrease the length of hospitalization[1,2]. Insulin resistance is a critical complication of injury or stress. Most patients receiving surgery may develop postoperative insulin resistance. The resulting hyperglycemia is often associated with an increased risk of morbidity and mortality. ERAS recommends preoperative carbohydrate loading to decrease postoperative hyperglycemia by 50%, optimizing recovery[3-5].

More than 10% of the world population is reported to have diabetes[6], and nearly 15% of surgical patients have type 2 diabetes (T2D)[7]. Complications and hospital stays are greater in these patients than in non-diabetic patients[8,9]. Delayed gastric emptying (gastroparesis) is also more frequent in patients with diabetes[10,11]. Therefore, preoperative carbohydrate loading may adversely affect gastric volume (GV) in diabetic patients. Moreover, carbohydrate loading-induced hyperglycemia may outweigh the potential benefits of ERAS protocols in such patients. Laffin *et al*[12] found no significant difference in the hyperglycemic incidence between the groups with and without carbohydrate loading [12]. However, other studies have reported high rates of adverse outcomes, such as postoperative wound infections, cardiac events, and other complications caused by hyperglycemia, in diabetic patients receiving preoperative carbohydrate loading[13]. It is important to further study the change in blood glucose levels in diabetic patients receiving preoperative carbohydrate loading.

Perlas used ultrasound to grade GV, which was measured in the right decubitus and supine positions to assess the risk of aspiration, The visualization of gastric antrum content was scored using the Perlas grading system: Grade 0, no content visible in the supine or right lateral (RLD) position; grade 1, clear gastric fluid content only in the RLD position, but not in the supine position; and grade 2, clear gastric fluid content visible in both supine and RLD positions[14]. Perlas grade II and GV > 1.5 mL/kg have been reported to be associated with a high risk of reflux and aspiration[15,16]. Therefore, ultrasonography is used to evaluate GV both qualitatively and quantitatively. It is an economical, safe, non-invasive, and repeatable technique to assess the risk of anesthesia before surgery[17]. Data on preoperative carbohydrate loading in patients with T2D are limited[18,19]. In this study, we assessed

GV, the incidence of hyperglycemia, and the risk of gastric reflux and aspiration using ultrasonography. We also evaluated the time and dose of preoperative carbohydrates using stratified analysis. These assessments allowed us to determine the safety and feasibility of preoperative carbohydrate loading in patients with T2D.

MATERIALS AND METHODS

Inclusion and exclusion criteria

Data of adult patients (age: 40-80 years) who received surgery under general anesthesia were enrolled according to the following inclusion criteria: (1) American Society of Anesthesiologists Physical Status Classification System (ASA) classified as II-III; (2) Definite diagnosis of T2D for > 2 years; (3) Preoperative blood glucose < 10 mmol/L; (4) Glycosylated hemoglobin (HbA1c) < 8.5%; and (5) Body mass index (BMI) of 18-35 kg/m^2. Patients were excluded from the study if they had any of the following: (1) Pregnancy; (2) Cardiac or renal dysfunction; (3) Hypothyroidism; (4) Obesity (BMI > 35 kg/m^2); (5) Digestive system diseases, including gastroesophageal reflux, peptic ulcer, digestive system tumors, cholelithiasis or history of upper gastrointestinal surgery; (6) Receiving antiemetic drugs or other drugs affecting gastrointestinal motility before operation; (7) Preoperative gastrointestinal decompression or nutrition; or (8) Unwilling to participate in the study.

Patients and study design

Overall, 80 patients with T2D who received surgery under general anesthesia from December 2019 to December 2020 were enrolled in the study. Of them, 2 patients were excluded due to unclear images of the gastric antrum. Finally, 78 patients with complete follow-up data were included in the study. The flow chart of the study is presented in Figure 1. The day before surgery, patients who fulfilled the study criteria and provided written consent were randomly allocated to 4 groups. Randomization was performed using computer-generated random numbers indicating different volumes of carbohydrate loading. Patients received a clear carbohydrate drink (0, 100, 200, or 300 mL) 2 h before anesthesia induction on the day of surgery. Each group uses the same concentration of carbohydrate drink that contains 14.2 g of carbohydrate *per* 100 mL (Yichang Human Medical Food Co., Ltd.). Randomization was performed using computer-generated four-digit random numbers indicating the treatment, which were kept in sealed envelopes. An envelope was opened according to the random number from small to large based on the time sequence of inclusion of each subject. The ultrasound examiner was blinded by the study protocol, as was the staff involved in the medical procedures and data collection process. All patients received surgery under general endotracheal anesthesia. Intraoperative fluid management was limited to a glucose-free solution, and no exogenous insulin was administered. Postoperative care was standardized as clinically indicated.

Data collection and assessment

Ultrasonography was performed by an experienced investigator certified by the Chinese Health Commission. GV was assessed on the day of surgery before carbohydrate loading (T0, basal value), 2 min after carbohydrate loading (T1), and before anesthesia induction (T2). A standard convex ultrasound probe was used to scan the gastric antrum in the sagittal plane between the liver and pancreas, at first in the supine position and then in the RLD position. The gastric antrum content visualization was scored using the Perlas grading system: Grade 0, no content visible in the supine or RLD position; grade 1, clear gastric fluid content only in the RLD position, but not in the supine position; and grade 2, clear gastric fluid content visible in both supine and RLD positions[14]. The longitudinal (D1) and anteroposterior (D2) diameters of the antrum were determined, which were repeated 3 times and averaged (Figure 2). The gastric antral area (CSA) was calculated using the following formula: CSA = π × D1 × D2/4. A mathematical model was used to measure GV: 27 + 14.6 × CSA - 1.28 × age. In addition, blood glucose levels were monitored before carbohydrate loading (T0) and anesthesia induction (T2). Patients with GV *per* unit weight (GV/W) > 1.5 mL/kg were regarded as having a high risk of reflux and aspiration. Gastrointestinal decompression was performed before anesthesia induction in these patients. If the blood glucose level was > 10 mmol/L at T2, the surgery was delayed until it normalized.

Statistical analysis

The sample size was determined on the basis of the GV/W at different time periods. The average GV/W at T0, T1 and T2 in the control group was 0.66, 0.64, and 0.70 mL/kg, respectively, in our preliminary study. The values at T0, T1, and T2 in groups receiving 100 mL, 200 mL, and 300 mL carbohydrate drink were 0.45, 1.2, and 0.53 mL/kg; 0.70, 3.20, 0.85 mL/kg; and 0.65, 4.67, 0.8 mL/kg, respectively. Based on these values, we found that a sample of at least 20 patients in each group and 80 patients in total would ensure 80% power for the study to evaluate the effect of preoperative carbohydrate loading on GV. The 80% power was calculated considering a two-sided type I error of 0.05 by log-rank test and 20% loss to follow-up.

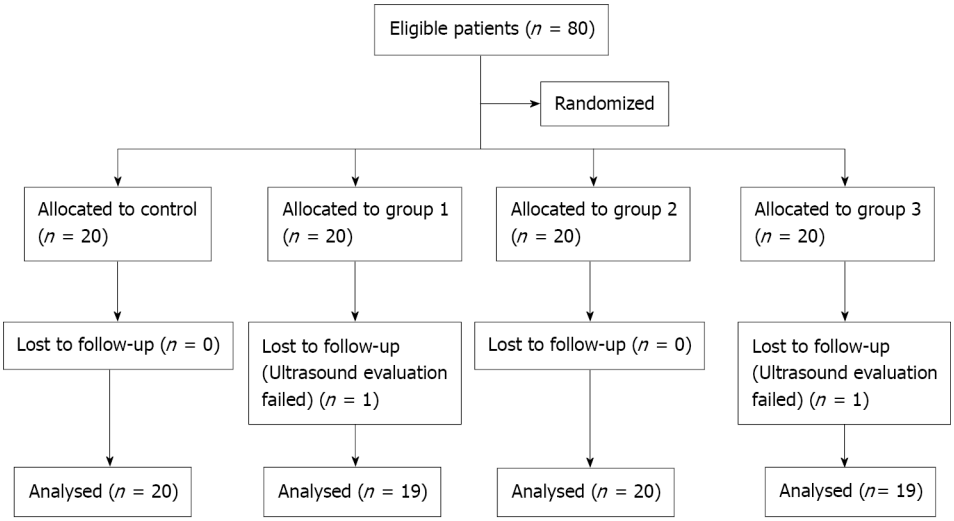

DOI: 10.12998/wjcc.v10.i18.6082 **Copyright** ©The Author(s) 2022.

Figure 1 Flow diagram of the study selection process.

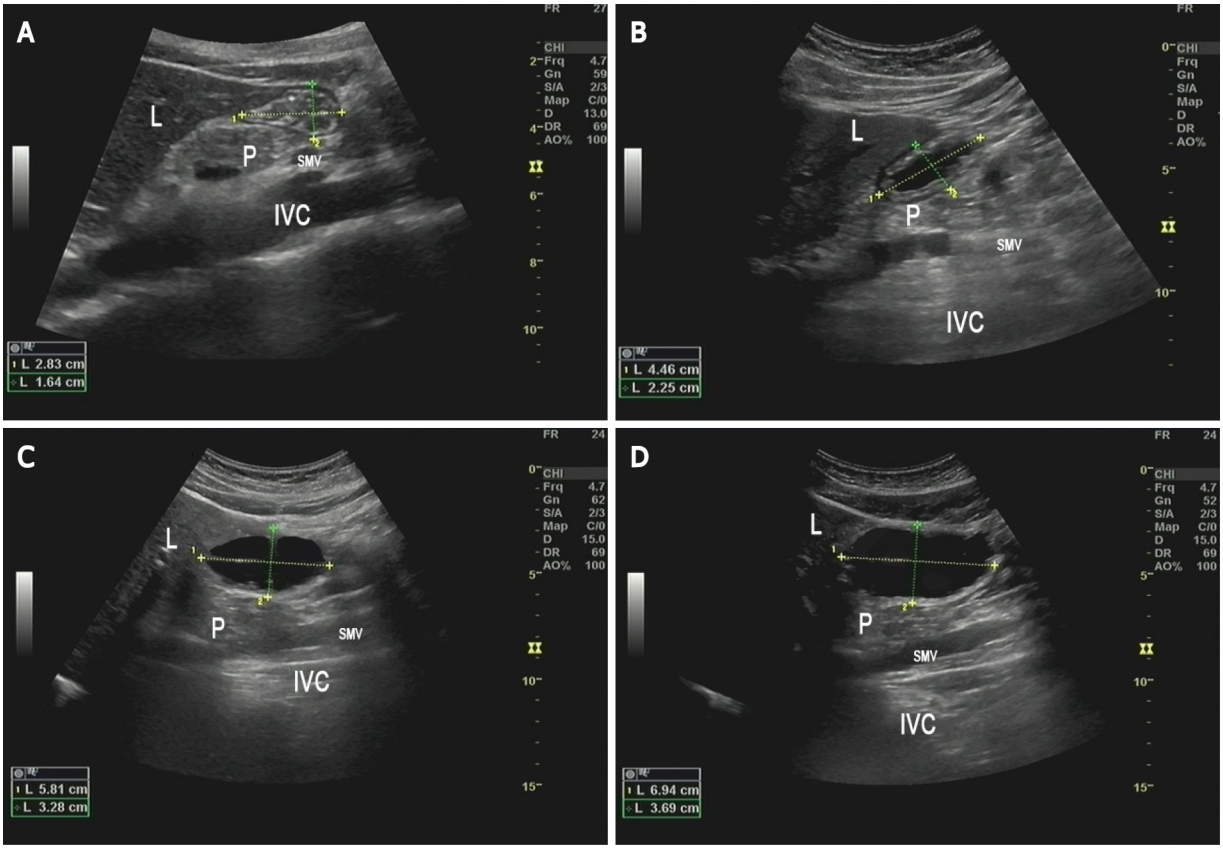

DOI: 10.12998/wjcc.v10.i18.6082 **Copyright** ©The Author(s) 2022.

Figure 2 Ultrasonic images of gastric antrum after drinking different volumes of carbohydrates. A: Control group (0 mL); B: Group 1 (100 mL); C: Group 2 (200 mL); D: Group 3 (300 mL). L: Liver; P: Pancreas; SMV: Superior mesenteric vein; IVC: Inferior vena cava.

All statistical analyses were performed in SPSS (version 24.0, IBM, New York, United States). Normally distributed continuous data are presented as mean ± SD. Categorical data are presented as frequency or rate. Age, height, weight, BMI, course of the disease, HbA1c (%), and fasting blood glucose were compared using one-way ANOVA. The ASA scores, gender, and control of blood glucose were the Chi-square test or Fisher exact test. The GV *per* unit body weight and peripheral capillary blood glucose were examined with the repeated measures analysis of variance. The Bonferroni method was applied for pairwise comparisons in the repeated measures analysis of variance. All statistical analyses were two-sided tests. A $P < 0.05$ indicated a statistically significant difference.

RESULTS

Patient characteristics

A total of 78 patients with T2D were randomly allocated to 4 groups, with the control group receiving 0 mL, group 1 receiving 100 mL, group 2 receiving 200 mL, and group 4 receiving 300 mL carbohydrate drink. All groups were well balanced for characteristics, including gender, age, BMI, height, weight, ASA grade, disease course, HbA1c, fasting blood glucose level, and control of blood glucose (Table 1).

Analysis of GV

GV was assessed at 3 different time points as described above. Gastric content was first evaluated using the Perlas A scale. No difference was observed in patients with Perlas grade II at T0 and T2 among the groups ($P > 0.05$). GV/W was increased significantly at T1 in groups 1, 2, and 3. At T2, GV/W decreased significantly, with no statistical difference observed between T0 and T2 in all the groups ($P > 0.05$) (Figure 3). Moreover, the number of patients with GV/W > 1.5 mL/kg was similar among the groups ($P > 0.05$) (Figure 3).

Analysis of blood glucose levels

The blood glucose level in all patients was tested before carbohydrate loading (T0) and anesthesia induction (T2). In groups 1, 2, and 3, blood glucose levels increased significantly at T2 compared with that at T0 ($P < 0.05$). In patients receiving 300 mL of the carbohydrate drink (group 3), the blood glucose level at T2 increased by > 2 mmol/L, which was significantly higher than that in groups 1 and 2. This finding indicates that a 300 mL carbohydrate load may increase the blood glucose level in patients with T2D before anesthesia induction (Figure 4).

DISCUSSION

Preoperative carbohydrate loading improves glycemic control and postoperative recovery in nondiabetic patients[3,4]. However, the practice of carbohydrate loading in patients with T2D is controversial because of reflux and aspiration concerns due to increased GV and delayed emptying. In our study, no difference was found in GV/W between T0 and T2 in all groups. This finding indicates that GV does not increase with a carbohydrate loading of < 300 mL. Our results are in line with those of previous studies, which reported no delay in gastric emptying in patients with T2D compared with healthy control subjects[20]. Our patients drank 14.2% liquid carbohydrates with low osmotic pressure. Delayed gastric emptying seems to affect solids rather than liquids in patients with diabetes, which can possibly explain the similar GV between T0 and T2 in our study[10,21]. Furthermore, in our study, the preoperative fasting blood glucose level was controlled less than 10 mmol/L, which may reduce the incidence of delayed gastric emptying in T2D. Previous studies have shown that severe acute hyperglycemia may lead to delayed gastric emptying[22]. In summary, carbohydrate loading of < 300 mL 2 h before anesthesia induction does not significantly affect GV in patients with T2D.

The risk of reflux and aspiration was further evaluated using Perlas grading determined by ultrasonography. Patients with Perlas grade I had < 100 mL gastric content, whereas those with grade II had obvious gastric content in both supine and RLD positions[23]. Moreover, GV/W > 1.5 mL/kg helps determine the risk of reflux and aspiration[24-26]. In our study, the number of patients with Perlas grade II and GV/W > 1.5 mL/kg did not differ among the groups. This finding further confirms that preoperative carbohydrate loading does not increase the risk of reflux and aspiration in patients with T2D. However, it should be noted that all our groups had patients with Perlas grade II and GV/W > 1.5 mL/kg. This indicates the importance of performing routine preoperative GV ultrasonography in patients with diabetes.

Change in blood glucose level was another focus of our study. In the control group, group 1 and group 2, blood glucose level increased by < 2 mmol/L after carbohydrate loading. However, in patients receiving 300 mL of the carbohydrate drink (group 3), blood glucose levels increased by 3.4 mmol/L after 2 h. Studies have shown that a change in blood glucose level of < 2 mmol/L after carbohydrate loading does not increase perioperative complications[12,27,28]. Therefore, our results support a preoperative carbohydrate loading of < 200 mL in patients with T2D, although the optimal time for preoperative carbohydrate loading remains unaddressed. Carbohydrate loading 3 h before surgery does not pose a risk for hyperglycemia or aspiration in diabetic patients[12,20]. However, some researchers do not recommend the 2-h interval between carbohydrate loading and surgery due to concerns of delayed gastric emptying[29]. In our study, carbohydrate loading 2 h before anesthesia induction did not affect GV or increase the risk of reflux and aspiration. Future studies are warranted to confirm our results.

Our study has certain limitations. First, the blood glucose level of the enrolled patients was well controlled, and their preoperative FPG was < 10 mmol/L. Further stratified analysis must be performed in patients with different levels of blood glucose and HbA1c. Second, data about primary diseases in our patients were lacking. Because primary diseases may affect GV and gastric emptying, the lack of such

Table 1 Baseline characteristics of included patients

Variables	Control	Group 1	Group 2	Group 3	χ^2	F	*P* value
ASA grade (II/III)	18/2	18/1	18/2	17/2			1.000
Gender (M/F)	12/8	10/9	8/12	12/7	2.83		0.422
Age (yr)	62.0 ± 8.8	65.6 ± 9.5	57.4 ± 9.6	62.1 ± 10.9		1.79	0.209
BMI (kg/m^2)	23.8 ± 2.3	24.3 ± 3.2	23.9 ± 2.0	25.3 ± 3.1		0.91	0.443
Height (cm)	162.5 ± 7.8	163.1 ± 6.9	165.1 ± 6.1	164.1 ± 7.4		0.39	0.759
Weight (kg)	63.5 ± 11.3	64.5 ± 8.2	65.5 ± 9.9	68.1 ± 9.9		0.60	0.623
Course of disease (yr)	9.50 ± 4.26	9.42 ± 3.91	9.15 ± 4.34	8.74 ± 4.25		0.13	0.942
HbA1c (%)	7.34 ± 0.37	7.34 ± 0.50	7.49 ± 0.46	7.46 ± 0.56		0.53	0.663
Fasting blood glucose (mmol/L)	7.35 ± 2.13	7.08 ± 1.21	6.95 ± 0.80	6.56 ± 1.20		1.03	0.386
Control of blood glucose (oral/injection of insulin)	16/4	14/5	16/4	17/2	1.76		0.568

ASA: American society of anesthesiology; BMI: Body mass index; HbA1c: Hemoglobin A1c.

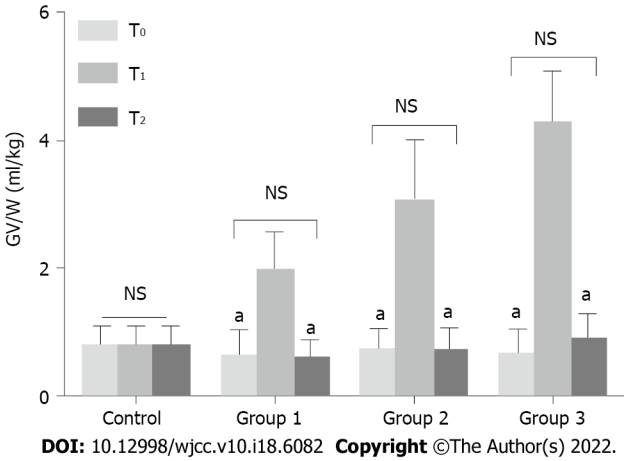

DOI: 10.12998/wjcc.v10.i18.6082 **Copyright** ©The Author(s) 2022.

Figure 3 Comparison of gastric volume *per* unit weight in four groups of patients at different time points. Gastric volume *per* unit weight (GV/W) was increased significantly at T1 in groups 1, 2, and 3. At T2, GV/W decreased significantly, with no statistical difference observed between T0 and T2 in all the groups ($^aP < 0.05$, T0 *vs* T1, T1 *vs* T2). NS: Not significant.

data could have introduced a bias in result interpretation. Finally, single-center study design and insufficient data limit further application of our results. Prospective, large-scale, randomized, and multi-centered studies are needed to further validate our results.

CONCLUSION

Preoperative carbohydrate loading < 300 mL 2 h before anesthesia induction in patients with T2D did not affect GV or increase the risk of reflux and aspiration. Blood glucose level did not significantly change with preoperative carbohydrate loading of < 200 mL. However, 300 mL carbohydrate loading may increase blood glucose levels in patients with T2D before anesthesia induction. In conclusion, it is safe for patients with T2D to drink 200 mL 14.2% carbohydrate 2 h before surgery. In the future, we will study whether preoperative consumption of 200 mL of 14.2% carbohydrate can reduce postoperative insulin resistance and promote recovery of patients.

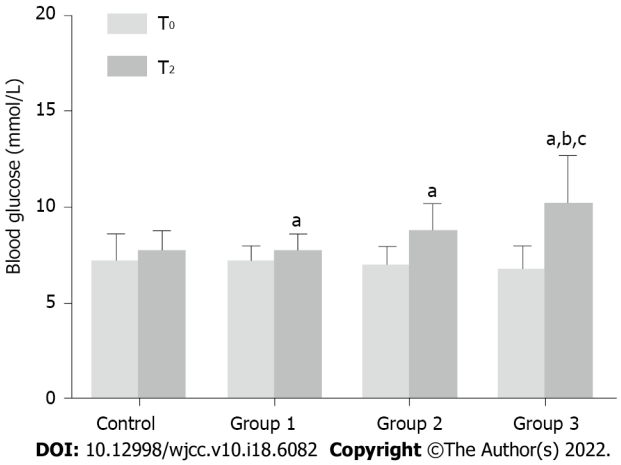

DOI: 10.12998/wjcc.v10.i18.6082 Copyright ©The Author(s) 2022.

Figure 4 Comparison of blood glucose in four groups of patients at T0 and T2. In groups 1, 2, and 3, blood glucose levels increased significantly at T2 compared with that at T0. In patients receiving 300 mL of the carbohydrate drink (group 3), the blood glucose level at T2 increased by > 2 mmol/L, which was significantly higher than that in control and group 1 ($^aP < 0.05$, T0 *vs* T2; $^bP < 0.05$, group 3 *vs* control; $^cP < 0.05$, group 3 *vs* group 1).

ARTICLE HIGHLIGHTS

Research background

More than 10% of the world's population and almost 15% of surgical patients are reported to have type 2 diabetes (T2D). Diabetic patients are prone to delayed gastric emptying due to the risk of reflux, aspiration and hyperglycemia.

Research motivation

Different guidelines for preoperative carbohydrate loading in diabetic patients are still controversial.

Research objectives

This study is conducted to evaluate the safety and feasibility of preoperative carbohydrate loading on gastric volume (GV) before anesthesia induction in T2D patients.

Research methods

Patients with T2D were randomly allocated to 4 groups receiving 0, 100, 200, or 300 mL of carbohydrate loading 2 h before anesthesia induction. Gastric volume *per* unit weight (GV/W), Perlas grade, changes in blood glucose level, and risk of reflux and aspiration were evaluated before anesthesia induction.

Research results

No significant difference was found in GV/W among the groups before anesthesia induction ($P > 0.05$). The number of patients with Perlas grade II and GV/W > 1.5 mL/kg did not differ among the groups ($P > 0.05$). Blood glucose level increased by > 2 mmol/L in patients receiving 300 mL carbohydrate drink, which was significantly higher than that in groups 1 and 2 ($P < 0.05$).

Research conclusions

Preoperative carbohydrate loading < 300 mL 2 h before anesthesia induction in patients with T2D did not affect GV or increase the risk of reflux and aspiration. Blood glucose levels did not change significantly with preoperative carbohydrate loading of < 200 mL. However, 300 mL carbohydrate loading may increase blood glucose levels in patients with T2D before induction of anesthesia.

Research perspectives

Our study illustrates the safety and recommended volume of preoperative carbohydrate loading in patients with T2D.

FOOTNOTES

Author contributions: All authors contributed to the study conception and design; Zheng XC designed the study; Material preparation, data collection and analysis were performed by Lin XQ, Chen YR and Chen X; Cai YP, Lin JX and Xu DM contributed sample collection and intellectual input; The first draft of the manuscript was written by Lin XQ and all authors commented on previous versions of the manuscript; All authors read and approved the final

manuscript; Lin XQ and Chen YR contributed equally to this study.

Supported by Natural Science Foundation of Fujian Province, No. 2019J01587.

Institutional review board statement: The present study was approved by the Ethics Committee of Putian College Affiliated Hospital, No. 201936.

Clinical trial registration statement: This study is registered at the Chinese Clinical trial registry, No. ChiCTR1900028529.

Informed consent statement: All study participants or their legal guardian provided informed written consent about personal and medical data collection prior to study enrolment.

Conflict-of-interest statement: The authors declare that they have no competing interests.

Data sharing statement: The datasets generated during and/or analyzed during the current study are not publicly available but are available from the corresponding author on reasonable request.

CONSORT 2010 statement: The authors have read the CONSORT 2010 Statement, and the manuscript was prepared and revised according to the CONSORT 2010 Statement.

Open-Access: This article is an open-access article that was selected by an in-house editor and fully peer-reviewed by external reviewers. It is distributed in accordance with the Creative Commons Attribution NonCommercial (CC BY-NC 4.0) license, which permits others to distribute, remix, adapt, build upon this work non-commercially, and license their derivative works on different terms, provided the original work is properly cited and the use is non-commercial. See: https://creativecommons.org/Licenses/by-nc/4.0/

Country/Territory of origin: China

ORCID number: Xin-Qiang Lin 0000-0001-6568-9433; Yu-Ren Chen 0000-0002-5074-4329; Xiao Chen 0000-0001-8220-0599; Yu-Ping Cai 0000-0001-6254-3332; Jian-Xin Lin 0000-0002-1699-6418; De-Ming Xu 0000-0002-6531-6124; Xiao-Chun Zheng 0000-0002-6213-0789.

S-Editor: Fan JR
L-Editor: A
P-Editor: Fan JR

REFERENCES

1 **Amer MA**, Smith MD, Herbison GP, Plank LD, McCall JL. Network meta-analysis of the effect of preoperative carbohydrate loading on recovery after elective surgery. *Br J Surg* 2017; **104**: 187-197 [PMID: 28000931 DOI: 10.1002/bjs.10408]
2 **Ljungqvist O**, de Boer HD, Balfour A, Fawcett WJ, Lobo DN, Nelson G, Scott MJ, Wainwright TW, Demartines N. Opportunities and Challenges for the Next Phase of Enhanced Recovery After Surgery: A Review. *JAMA Surg* 2021; **156**: 775-784 [PMID: 33881466 DOI: 10.1001/jamasurg.2021.0586]
3 **Wang S**, Gao PF, Guo X, Xu Q, Zhang YF, Wang GQ, Lin JY. Effect of low-concentration carbohydrate on patient-centered quality of recovery in patients undergoing thyroidectomy: a prospective randomized trial. *BMC Anesthesiol* 2021; **21**: 103 [PMID: 33823815 DOI: 10.1186/s12871-021-01323-8]
4 **Li L**, Wang Z, Ying X, Tian J, Sun T, Yi K, Zhang P, Jing Z, Yang K. Preoperative carbohydrate loading for elective surgery: a systematic review and meta-analysis. *Surg Today* 2012; **42**: 613-624 [PMID: 22581289 DOI: 10.1007/s00595-012-0188-7]
5 **Tsutsumi R**, Kakuta N, Kadota T, Oyama T, Kume K, Hamaguchi E, Niki N, Tanaka K, Tsutsumi YM. Effects of oral carbohydrate with amino acid solution on the metabolic status of patients in the preoperative period: a randomized, prospective clinical trial. *J Anesth* 2016; **30**: 842-849 [PMID: 27438627 DOI: 10.1007/s00540-016-2217-y]
6 **Bi Y**, Xu Y, Ning G. Prevalence of diabetes in Chinese adults--reply. JAMA 2014; 311: 200-201 [PMID: 24399563 DOI: 10.1001/jama.2013.283143]
7 **Albalawi Z**, Laffin M, Gramlich L, Senior P, McAlister FA. Enhanced Recovery After Surgery (ERAS®) in Individuals with Diabetes: A Systematic Review. *World J Surg* 2017; **41**: 1927-1934 [PMID: 28321553 DOI: 10.1007/s00268-017-3982-y]
8 **Darwiche G**, Almér LO, Björgell O, Cederholm C, Nilsson P. Delayed gastric emptying rate in Type 1 diabetics with cardiac autonomic neuropathy. *J Diabetes Complications* 2001; **15**: 128-134 [PMID: 11358681 DOI: 10.1016/s1056-8727(00)00143-4]
9 **Watson LE**, Phillips LK, Wu T, Bound MJ, Jones KL, Horowitz M, Rayner CK. Longitudinal evaluation of gastric emptying in type 2 diabetes. *Diabetes Res Clin Pract* 2019; **154**: 27-34 [PMID: 31238060 DOI: 10.1016/j.diabres.2019.06.010]
10 **Horowitz M**, O'Donovan D, Jones KL, Feinle C, Rayner CK, Samsom M. Gastric emptying in diabetes: clinical significance and treatment. *Diabet Med* 2002; **19**: 177-194 [PMID: 11918620 DOI: 10.1046/j.1464-5491.2002.00658.x]

11 **Horváth VJ**, Izbéki F, Lengyel C, Kempler P, Várkonyi T. Diabetic gastroparesis: functional/morphologic background, diagnosis, and treatment options. *Curr Diab Rep* 2014; **14**: 527 [PMID: 25005121 DOI: 10.1007/s11892-014-0527-8]

12 **Laffin MR**, Li S, Brisebois R, Senior PA, Wang H. The Use of a Pre-operative Carbohydrate Drink in Patients with Diabetes Mellitus: A Prospective, Non-inferiority, Cohort Study. *World J Surg* 2018; **42**: 1965-1970 [PMID: 29282506 DOI: 10.1007/s00268-017-4413-9]

13 **Sabry R**, Hasanin A, Refaat S, Abdel Raouf S, Abdallah AS, Helmy N. Evaluation of gastric residual volume in fasting diabetic patients using gastric ultrasound. *Acta Anaesthesiol Scand* 2019; **63**: 615-619 [PMID: 30609007 DOI: 10.1111/aas.13315]

14 **Perlas A**, Davis L, Khan M, Mitsakakis N, Chan VW. Gastric sonography in the fasted surgical patient: a prospective descriptive study. *Anesth Analg* 2011; **113**: 93-97 [PMID: 21596885 DOI: 10.1213/ANE.0b013e31821b98c0]

15 **Van de Putte P**, Perlas A. Ultrasound assessment of gastric content and volume. *Br J Anaesth* 2014; **113**: 12-22 [PMID: 24893784 DOI: 10.1093/bja/aeu151]

16 **Tacken MCT**, van Leest TAJ, van de Putte P, Keijzer C, Perlas A. Ultrasound assessment of gastric volumes of thick fluids: Validating a prediction model. *Eur J Anaesthesiol* 2021; **38**: 1223-1229 [PMID: 33606419 DOI: 10.1097/EJA.0000000000001465]

17 **Kruisselbrink R**, Arzola C, Jackson T, Okrainec A, Chan V, Perlas A. Ultrasound assessment of gastric volume in severely obese individuals: a validation study. *Br J Anaesth* 2017; **118**: 77-82 [PMID: 28039244 DOI: 10.1093/bja/aew400]

18 Practice Guidelines for Preoperative Fasting and the Use of Pharmacologic Agents to Reduce the Risk of Pulmonary Aspiration: Application to Healthy Patients Undergoing Elective Procedures: An Updated Report by the American Society of Anesthesiologists Task Force on Preoperative Fasting and the Use of Pharmacologic Agents to Reduce the Risk of Pulmonary Aspiration. *Anesthesiology* 2017; **126**: 376-393 [PMID: 28045707 DOI: 10.1097/ALN.0000000000001452]

19 **Smith I**, Kranke P, Murat I, Smith A, O'Sullivan G, Søreide E, Spies C, in't Veld B; European Society of Anaesthesiology. Perioperative fasting in adults and children: guidelines from the European Society of Anaesthesiology. *Eur J Anaesthesiol* 2011; **28**: 556-569 [PMID: 21712716 DOI: 10.1097/EJA.0b013e3283495ba1]

20 **Gustafsson UO**, Nygren J, Thorell A, Soop M, Hellström PM, Ljungqvist O, Hagström-Toft E. Pre-operative carbohydrate loading may be used in type 2 diabetes patients. *Acta Anaesthesiol Scand* 2008; **52**: 946-951 [PMID: 18331374 DOI: 10.1111/j.1399-6576.2008.01599.x]

21 **He XD**, Guo YM, Goyal RK. Effect of Hyperglycemia on Purinergic and Nitrergic Inhibitory Neuromuscular Transmission in the Antrum of the Stomach: Implications for Fast Gastric Emptying. *Front Med (Lausanne)* 2018; **5**: 1 [PMID: 29410956 DOI: 10.3389/fmed.2018.00001]

22 **Halland M**, Bharucha AE. Relationship Between Control of Glycemia and Gastric Emptying Disturbances in Diabetes Mellitus. *Clin Gastroenterol Hepatol* 2016; **14**: 929-936 [PMID: 26717862 DOI: 10.1016/j.cgh.2015.11.021]

23 **Perlas A**, Mitsakakis N, Liu L, Cino M, Haldipur N, Davis L, Cubillos J, Chan V. Validation of a mathematical model for ultrasound assessment of gastric volume by gastroscopic examination. *Anesth Analg* 2013; **116**: 357-363 [PMID: 23302981 DOI: 10.1213/ANE.0b013e318274fc19]

24 **Chang JE**, Kim H, Won D, Lee JM, Jung JY, Min SW, Hwang JY. Ultrasound assessment of gastric content in fasted patients before elective laparoscopic cholecystectomy: a prospective observational single-cohort study. *Can J Anaesth* 2020; **67**: 810-816 [PMID: 32314262 DOI: 10.1007/s12630-020-01668-7]

25 **Ohashi Y**, Walker JC, Zhang F, Prindiville FE, Hanrahan JP, Mendelson R, Corcoran T. Preoperative gastric residual volumes in fasted patients measured by bedside ultrasound: a prospective observational study. *Anaesth Intensive Care* 2018; **46**: 608-613 [PMID: 30447671 DOI: 10.1177/0310057X1804600612]

26 **Van de Putte P**, Vernieuwe L, Bouvet L. Gastric ultrasound as an aspiration risk assessment tool. *Indian J Anaesth* 2019; **63**: 160-161 [PMID: 30814762 DOI: 10.4103/ija.IJA_756_18]

27 **Tang X**, Li S, Wang Y, Wang M, Yin Q, Mu P, Lin S, Qian X, Ye X, Chen Y. Glycemic variability evaluated by continuous glucose monitoring system is associated with the 10-y cardiovascular risk of diabetic patients with well-controlled HbA1c. *Clin Chim Acta* 2016; **461**: 146-150 [PMID: 27502250 DOI: 10.1016/j.cca.2016.08.004]

28 **Voss AC**, Maki KC, Garvey WT, Hustead DS, Alish C, Fix B, Mustad VA. Effect of two carbohydrate-modified tube-feeding formulas on metabolic responses in patients with type 2 diabetes. *Nutrition* 2008; **24**: 990-997 [PMID: 18718737 DOI: 10.1016/j.nut.2008.06.009]

29 **Chen L**, Chen YJ, Dong HL, Feng Y, Gu XP, Huang YG, Jiang ZW, Lou WH, Liu LX, Mi WD, Ma ZL, Min S, Peng SL, Tian XD, Wang TL, Xu ZK, Xue ZG, Yao HW, Yang YM, Zhang KC, Zhu SM. Chinese expert consensus and pathway management guide for Chinese accelerated rehabilitation surgery (2018 Edition). *Zhongguo Shiyong Waike Zazhi* 2018; **38**: 1-19 [DOI: 10.19538/j.cjps.issn1005-2208.2018.01.01]

World Journal of Clinical Cases

Submit a Manuscript: https://www.f6publishing.com

World J Clin Cases 2022 June 26; 10(18): 6091-6104

DOI: 10.12998/wjcc.v10.i18.6091

ISSN 2307-8960 (online)

META-ANALYSIS

Efficacy and safety of adalimumab in comparison to infliximab for Crohn's disease: A systematic review and meta-analysis

Hua-Hua Yang, Yi Huang, Xu-Chun Zhou, Ruo-Nan Wang

Specialty type: Medicine, research and experimental

Provenance and peer review: Unsolicited article; Externally peer reviewed.

Peer-review model: Single blind

Peer-review report's scientific quality classification

Grade A (Excellent): 0
Grade B (Very good): 0
Grade C (Good): C, C
Grade D (Fair): 0
Grade E (Poor): 0

P-Reviewer: Fukata M, Japan; Ribeiro IB, Brazil

Received: December 29, 2021
Peer-review started: December 29, 2021
First decision: January 25, 2022
Revised: February 14, 2022
Accepted: April 30, 2022
Article in press: April 30, 2022
Published online: June 26, 2022

Hua-Hua Yang, Yi Huang, Xu-Chun Zhou, Department of Gastroenterology, The First Affiliated Hospital of Chongqing Medical University, Chongqing 400016, China

Ruo-Nan Wang, Department of Endocrinology, Liyuan Hospital, Tongji Medical College, Huazhong University of Science and Technology, Wuhan 430077, Hubei Province, China

Corresponding author: Xu-Chun Zhou, MD, Professor, Department of Gastroenterology, The First Affiliated Hospital of Chongqing Medical University, No. 1 Youyi Road, Yuzhong District, Chongqing 400016, China. chqxchzh@163.com

Abstract

BACKGROUND

Adalimumab (ADA) and infliximab (IFX) are the cornerstones of the treatment of Crohn's disease (CD). It remains controversial whether there is a difference in the effectiveness and safety between IFX and ADA for CD.

AIM

To perform a meta-analysis to compare the effectiveness and safety of ADA and IFX in CD.

METHODS

PubMed, Embase, Cochrane Library, and Web of Science databases were searched. Cohort studies were considered for inclusion. The primary outcomes were induction of response and remission, maintenance of response and remission, and secondary loss of response. Adverse events were secondary outcomes.

RESULTS

Fourteen cohort studies were included. There was no apparent difference between the two agents in the induction response [odds ratio (OR): 1.27, 95% confidence interval (CI): 0.93-1.74, P = 0.14] and remission (OR: 1.11, 95%CI: 0.78–1.57, P = 0.57), maintenance response (OR: 1.08, 95%CI: 0.76–1.53, P = 0.67) and remission (OR: 1.26, 95%CI: 0.87–1.82, P = 0.22), and secondary loss of response (OR: 1.01, 95%CI: 0.65–1.55, P = 0.97). Subgroup analysis revealed ADA and IFX had similar rates of response, remission, and loss of response either in anti-tumor necrosis factor-α naïve or non-naïve patients. Further, there was a similar result regardless of whether CD patients were treated with optimized therapy, including dose intensification, shortening interval, and combination immunomodulators. However, ADA had a fewer overall adverse events than IFX (OR: 0.62, 95%CI:

0.42–0.91, P = 0.02).

CONCLUSION
ADA and IFX have similar clinical benefits for anti-tumor necrosis factor-α naïve or non-naïve CD patients. Overall adverse events rate is higher in patients in the IFX group.

Key Words: Crohn disease; Adalimumab; Infliximab; Clinical efficacy; Adverse effects; Meta-analysis

©The Author(s) 2022. Published by Baishideng Publishing Group Inc. All rights reserved.

Core Tip: Differences in immunogenicity and route of administration among adalimumab (ADA) and infliximab (IFX) allow for potential variability in therapeutic properties and efficacy. However, clear recommendations have been limited due to a lack of head-to-head comparison. We conducted a meta-analysis to synthesize current results and compared the efficacy and safety of ADA and IFX. The results showed that both have similar clinical benefits for anti-tumor necrosis factor-α naïve or non-naïve Crohn's disease patients. Overall adverse events rate is higher in patients in the IFX group. ADA and IFX can be selected based on a possible history of adverse events and patient compliance.

Citation: Yang HH, Huang Y, Zhou XC, Wang RN. Efficacy and safety of adalimumab in comparison to infliximab for Crohn's disease: A systematic review and meta-analysis. *World J Clin Cases* 2022; 10(18): 6091-6104
URL: https://www.wjgnet.com/2307-8960/full/v10/i18/6091.htm
DOI: https://dx.doi.org/10.12998/wjcc.v10.i18.6091

INTRODUCTION

Crohn's disease (CD) is an incurable chronic progressive condition characterized by abdominal pain, diarrhea, and weight loss. Aminosalicylic acid preparations, glucocorticoids, immunosuppressants, and biological agents have been used for treatment. Of these, biological agents are most widely used, especially anti-tumor necrosis factor-α (anti-TNF-α) blockers, including infliximab (IFX) and adalimumab (ADA). They all have been proven effective in inducing and maintaining remission and are routinely used in the treatment of CD[1,2]. We do not know, however, which treatment should be considered the priority?

IFX, a chimeric monoclonal antibody against TNF-α, is the first approved anti-TNF-α for moderate to severe CD. ADA is a humanized monoclonal antibody against TNF-α. IFX is given by intravenous infusion every 8 wk, whereas ADA is administered subcutaneously every 4 wk. Differences in immunogenicity and route of administration among them allow for potential variability in therapeutic properties and efficacy. However, clear recommendations have been limited due to a lack of head-to-head treatment comparison. A network meta-analysis published in 2014 found that ADA may be the most efficacious agent for maintenance of remission in CD in biologic-naïve patients[3], while many new clinical practice experience studies have shown their effectiveness and safety data were comparable. Furthermore, even though there has been cumulative research, few studies have focused on secondary loss of response, anti-TNF naïve or non-naïve patients, and the benefits of treatment optimization, such as dose intensification, shortening interval, and combination with immunomodulators. We performed a meta-analysis to synthesize these results and compared the efficacy and safety of ADA and IFX.

MATERIALS AND METHODS

Our protocol was registered with PROSPERO (CRD: 42021191655). We followed the Preferred Reporting Items for the Systemic Review and Meta-Analysis guidelines.

Search retrieval

We performed literature search of electronic sources, including PubMed, Cochrane Library, Web of Science, and Embase, from initiation until October 31, 2020. No language restrictions were applied. The search terms included "Crohn disease," "adalimumab", and "infliximab" as Medical Subject Headings terms and their entry terms (Crohn disease: Crohn*; ileitis. Adalimumab: Humira; Exemptia. Infliximab: Remicade) to improve search outcomes. We also screened references of relevant articles to avoid

omissions.

Inclusion and exclusion criteria

We included cohort studies comparing ADA and IFX for treating adults with CD. Comparisons of induction of remission and response rates, maintenance of remission and response rates, secondary loss of response rates, and the incidence of adverse events were among the outcomes of included studies. Excluded studies included those conducted in the pediatric population, those that did not investigate patients with inflammatory bowel disease, and those that did not report any outcomes of interest.

Study selection

Two investigators (Yang HH and Huang Y) independently screened the titles, abstracts, and full texts of all papers to determine trial eligibility for inclusion. Investigators used a consensual approach to determine the inclusion or exclusion of selected studies after full-text assessment. Any disagreement was resolved through discussion or with a third researcher. The study characteristics were extracted independently by two authors using a standardized datasheet.

Data extraction

We collected the following variables: First author's name, year of publication, country or area, study design, number of patients, gender, median age, Montreal classification, duration of follow-up, previous treatment, and outcomes of interest. The endpoint of this meta-analysis mainly included the induction response and remission, maintenance response and remission, overall adverse events rate, severe adverse events rate, and the rate of opportunistic infections.

The outcomes of interest included: (1) Induction of clinical remission defined as Crohn's disease activity index (CDAI) < 150, Harvey Bradshaw Index (HBI) ≤ 4, or by physician's global assessment after ≤ 14 wk; (2) Induction of clinical response was defined as ΔCDAI ≥ 70, ΔHBI ≥ 2, or by physician's global assessment after ≤ 14 wk; (3) Maintenance of remission referred to clinical remission after ≤ 54 wk; (4) Maintenance of response referred to clinical response after ≤ 54 wk; (5) Secondary loss of response was defined as a reappearance of disease activity after achieving induction response, coupled with the need to change treatment, including dose intensification, the addition of an immunomodulator, or need to discontinue treatment; and (6) Secondary outcomes included a comparison of the incidence of overall adverse events, severe adverse events, and opportunistic infections in trials of maintenance therapy.

Quality assessment

One author assessed the quality of included studies through the Newcastle-Ottawa Quality Assessment Scale (NOS). High-quality studies were defined by a total score of ≥ 6.

Statistical analysis

RevMan 5.3 and Stata 16.0 software were used for statistical analysis. Odds ratio (OR) and concomitant 95% confidence interval (CI) were evaluated for the quantitative analyses. The random-effect model was used. Heterogeneity was explored by calculating I^2 and employing the Q test. An I^2 estimate > 50% and a $P < 0.05$ were regarded markers of significant heterogeneity, and its causes were investigated. We performed sensitivity analyses and subgroup analyses to detect the source of heterogeneity. $P < 0.05$ was considered to indicate a significant difference. Subgroup analyses were conducted based on the following grouping criteria: (1) Studies evaluating outcomes on anti-TNF naïve patients *vs* studies on non-naïve patients; (2) Studies evaluating outcomes on more perianal diseases in IFX group *vs* equal perianal disease in IFX and ADA group; (3) Studies evaluating primary outcomes given with treatment optimization, *i.e.* shortening the administration intervals, increasing the dose, and/or combination with immunomodulator therapy; and (4) Studies evaluating secondary outcomes at ≤ 48 wk *vs* > 48 wk. Funnel plots and Egger's test was used to test for publication bias.

RESULTS

Literature search

A preliminary search of the above database identified 2228 documents. Of these, we removed 562 duplicates, discarded 1632 studies after screening the titles and abstracts, and assessed the full text of 34 studies for eligibility. Finally, 14 cohort studies were included, and 20 were excluded. The flow diagram describes this process in detail (Figure 1).

Study characteristics

Study design, outcomes, the definition of outcomes, inclusion criteria, and follow-up time differed among the included studies. Our meta-analysis consisted of two prospective cohort studies and 12 retrospective cohort studies. Three pieces of research evaluated maintenance response or remission at 54

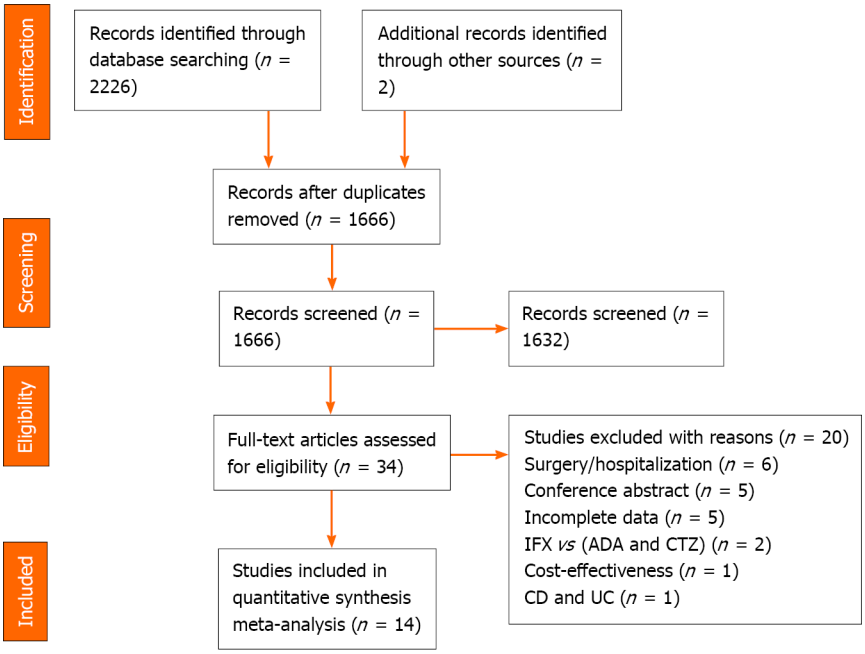

DOI: 10.12998/wjcc.v10.i18.6091 **Copyright** ©The Author(s) 2022.

Figure 1 Flow chart for literature search. IFX: Infliximab; ADA: Adalimumab; CTZ: Certolizumab; CD: Crohn's disease; UC: Ulcerative colitis.

wk[4-6], five at 48 wk[7-11], and one at 26 wk[12]. Regarding the definition of outcomes, most incorporated studies evaluated clinical response or remission by CDAI or HBI except for the study by Macaluso *et al*[10]. In addition, seven studies only included anti-TNF-naïve patients[4,7-9,12,13], and no study only included patients who failed anti-TNF treatment. Follow-up intervals across studies varied, ranging from 4 to 14 wk for induction period and 26 to 168 wk for maintenance period. The high NOS scores reflected the high quality of the enrolled studies. Thirteen studies got a score of ≥ 6, except for the study by Bau *et al*[14], which scored 5. Table 1 showed the overall characteristics of the selected studies.

Primary outcomes

Induction of response: Five studies (1040 patients) recorded induction of response[6,7,9,10,15]. No difference was shown between groups in response rates (OR: 1.27, 95%CI: 0.93–1.74, $P = 0.14$). Of the 1040 patients in five studies, 515 received ADA therapy. The heterogeneity of those studies was insignificant ($P = 0.58$, $I^2 = 0\%$) (Figure 2A). Sensitivity analysis showed no significant changes to the exclusion of any one of the studies (Supplementary Table 1). Subgroup analysis revealed no remarkable difference between groups (Table 2).

Induction of remission: When combining all four studies[6,8,9,16] reporting induction of remission data (318 on ADA therapy and 494 on IFX therapy), we found no difference between the two groups of patients (OR: 1.11, 95%CI: 0.78–1.57, $P = 0.57$). Heterogeneity was low ($P = 0.85$, $I^2 = 0\%$) (Figure 2B). Subsequent subgroup analysis showed similar results (Table 2). In sensitivity analyses, excluding any one of the studies did not significantly impact the results (Supplementary Table 1).

Maintenance of response: Of the 14 studies, seven reported the response rate in maintenance therapy[4,6,7,9-12]. A number of 1828 patients were included: 896 IFX-treated *vs* 932 ADA-treated. Data analysis showed that ADA and IFX had a similar rate of maintenance of response (OR: 1.08, 95%CI: 0.76–1.53, $P = 0.67$). Heterogeneity was significant ($P = 0.03$, $I^2 = 56\%$) (Figure 3A). Cosnes *et al*[12] evaluating response at 26 wk increased heterogeneity. In the sensitivity analysis, the result remained unchanged with the exclusion of any study (Supplementary Table 1). Subgroup analyses also showed no difference between the two groups (Table 2).

Maintenance of remission: There were 770 patients (328 on ADA therapy) available for analysis from six studies[5-9,11]. Data analysis showed that ADA and IFX had a similar rate of maintenance of remission (OR: 1.26, 95%CI: 0.87–1.82, $P = 0.22$). Heterogeneity was low ($P = 0.29$, $I^2 = 19\%$) (Figure 3B). Subgroup analyses also showed no statistical differences (Table 2). Sensitivity analysis indicated that the results were stable (Supplementary Table 1).

Secondary loss of response: Six studies with 1307 patients were included (603 receiving ADA and 704 IFX therapy)[5-7,9,12,17]. There was no statistical difference between the two treatments (OR: 1.01, 95%CI: 0.65–1.55, $P = 0.97$). Heterogeneity was notable ($P = 0.05$, $I^2 = 54\%$) (Figure 4). Heterogeneity was linked to the study by Narula *et al*[9], which found that IFX had more rate of loss of response than ADA.

Table 1 Characteristics of selected studies

Ref.	Study design	Patientinclusion criteria	ADA/IFX, *n*	Definition of remission	Definition of secondary loss of response	Induction of response/remission in wk	Maintenance of response/remission in wk	Adverse events	NOS
Zorzi *et al*[6], 2012	Retrospective	Active CD	49/44	CDAI < 150	No improvement or worsening	4/6	54	Multiple	6
Kestens *et al*[4], 2013	Retrospective	Naïve CD	100/100	NS	NS	NS	54	Multiple	9
Ma *et al*[17], 2014	Retrospective	Naïve CD	101/117	NS	Requiring dose escalation	NS	NS	NS	8
Tursi *et al*[15], 2014	Retrospective	CD	67/59	HBI ≤ 5	NS	6-14	NS	Multiple	8
Cosnes *et al*[12], 2016	Prospective	Naïve CD	264/127	CDAI < 150	Disease activity	NS	26	Multiple	8
Varma *et al*[8], 2016	Retrospective	Naïve CD	18/63	CDAI < 150	NS	12	48	Multiple	7
Narula *et al*[9], 2016	Prospective	Naïve CD	111/251	HBI < 5	Dose escalation	12	48	Multiple	8
Bau *et al*[14], 2017	Retrospective	Refractory CD	62/68	NS	NS	NS	168	Multiple	5
Otake *et al*[5], 2017	Retrospective	CD	29/39	CDAI < 150	Multiple	NS	54	NS	8
Doecke *et al* [16], 2017	Retrospective	CD	144/183	CDAI ≤ 150	NS	14	NS	NS	7
Benmassaoud *et al*[7], 2018	Retrospective	Naïve CD	77/143	HBI ≤ 4	Need for dose escalation	12	48	Multiple	8
Di Domenic-antonio *et al* [13], 2018	Retrospective	Naïve CD	505/367	NS	NS	NS	NS	Multiple	9
Macaluso *et al* [10], 2019	Retrospective	Naïve and non-naïve CD	Naïve: 214/107; non-naïve: 47/47	NS	NS	12	48	Multiple	9
Kaniewska *et al* [11], 2019	Retrospective	CD	95/82	CDAI < 150	NS	NS	48	Multiple	7

CD: Crohn's disease; ADA: Adalimumab; IFX: Infliximab; CDAI: Crohn's disease activity index; HBI: Harvey Bradshaw Index; NOS: Newcastle-Ottawa Quality Assessment Scale; NS: Not stated.

On sensitivity analyses, the results remained the same after excluding any one study (Supplementary Table 1). There was also no significant difference between ADA and IFX when subgroup analysis was done (Table 2).

Secondary outcomes

Overall adverse events: The incidence of overall adverse events was recorded in a total of eight cohort studies[4,5,7-11,14] that included 1653 patients, of which ADA was less than IFX (OR: 0.62, 95%CI: 0.42–0.91, P = 0.02). There was high heterogeneity (P = 0.04, I^2 = 53%) (Figure 5A). Subgroup analysis revealed that ADA had fewer overall adverse events than IFX in ≤ 48 wk follow-up time (OR: 0.50, 95%CI: 0.33–0.76, P = 0.001); and in anti-TNF-α-naïve patients, IFX had more adverse events (OR: 0.67, 95%CI: 0.50–0.89, P = 0.005) (Table 2). Sensitivity analysis indicated that the results were slightly unstable (Supplementary Table 1).

Severe adverse events: Our analysis of seven studies[6,8,9,11,12,14,15] with a total of 1547 patients showed ADA had a similar rate of severe adverse events with IFX (OR: 0.75, 95%CI: 0.32–1.72, P = 0.49).

Table 2 Subgroup analysis

Outcomes of interest	Subgroup analysis							
	Grouping criteria	Categories	Studies, *n*	Patients, *n*	OR	95%CI	I^2, %	*P* value
Induction of response	Anti-TNF naivety	Naïve	3	727	1.17	(0.80-1.70)	0	0.41
		Non-naïve	3	313	1.44	(0.55-3.78)	47	0.46
	Use optimization	Yes	5	1040	1.27	(0.93-1.74)	0	0.14
		No	0	0	-	-	-	-
Induction of remission	Anti-TNF naivety	Naïve	2	392	1.08	(0.68-0.72)	0	0.75
		Non-naïve	2	420	1.15	(0.67-1.96)	0	0.62
	Use optimization	Yes	3	731	1.08	(0.76-1.55)	0	0.66
		No	1	81	1.69	(0.34-8.44)	-	0.52
Maintenance of response	Anti-TNF naivety	Naïve	5	1468	1.08	(0.72-1.62)	63	0.71
		Non-naïve	3	354	1.10	(0.64-1.90)	0	0.73
	Use optimization	Yes	6	1645	1.12	(0.77-1.63)	62	0.57
		No	1	177	0.64	(0.18-2.29)	-	0.50
Maintenance of remission	Anti-TNF naivety	Naïve	3	442	1.39	(0.92-2.11)	0	0.12
		Non-naïve	3	328	1.24	(0.56-2.72)	53	0.59
	Use optimization	Yes	3	458	1.41	(0.95-2.09)	0	0.09
		No	3	312	1.18	(0.46-2.99)	55	0.73
Secondary loss of response	Anti-TNF naivety	Naïve	3	353	1.09	(0.54-2.18)	42	0.81
		Non-naïve	3	947	0.91	(0.46-1.80)	72	0.78
	Use optimization	Yes	5	1247	1.07	(0.69-1.67)	56	0.75
		No	1	53	0.48	(0.13-1.68)	54	0.99
Overall adverse events	Anti-TNF naivety	Naïve	5	1184	0.67	(0.50-0.89)	1	0.005
		Non-naïve	4	469	0.41	(0.31-1.31)	79	0.13
	Assessment time	≤ 48 wk	6	1323	0.50	(0.33-0.76)	41	0.001
		> 48 wk	2	330	1.00	(0.62-1.60)	0	0.98
Severe adverse events	Anti-TNF naivety	Naïve	3	1021	0.88	(0.40-1.92)	73	0.74
		Non-naïve	4	526	0.45	(0.03-6.51)	81	0.56
	Assessment time	≤ 48 wk	4	746	1.32	(0.80-2.19)	0	0.28
		> 48 wk	3	801	0.52	(0.09-3.05)	80	0.47
Opportunistic infections	Anti-TNF naivety	Naïve	4	1654	0.78	(0.54-1.14)	0	0.21
		Non-naïve	2	256	1.88	(0.93-3.82)	0	0.08
	Assessment time	≤ 48 wk	3	782	0.85	(0.56-1.28)	0	0.43
		> 48 wk	3	1128	1.12	(0.38-3.24)	57	0.84

anti-TNF: Anti-tumor necrosis factor; OR: Odds ratio; CI: Confidence interval.

Sensitivity analysis was performed due to notable heterogeneity (P = 0.003, I^2 = 72%) (Figure 5B). Heterogeneity mainly originated from Zorzi *et al*[6] with more severe adverse events occurring in IFX therapy. The result remained unchanged with the exclusion of any study (Supplementary Table 1). Subgroup analysis also showed similar results (Table 2).

Opportunistic infections: Six studies[4,7,9,13-15] reported side effects, with a total number of 1910 cases (ADA: IFX = 922:988). Opportunistic infections rates in the IFX and ADA groups were similar (OR: 0.96, 95%CI: 0.66-1.40, P = 0.83), and no apparent heterogeneity was detected (Figure 5C). There was no

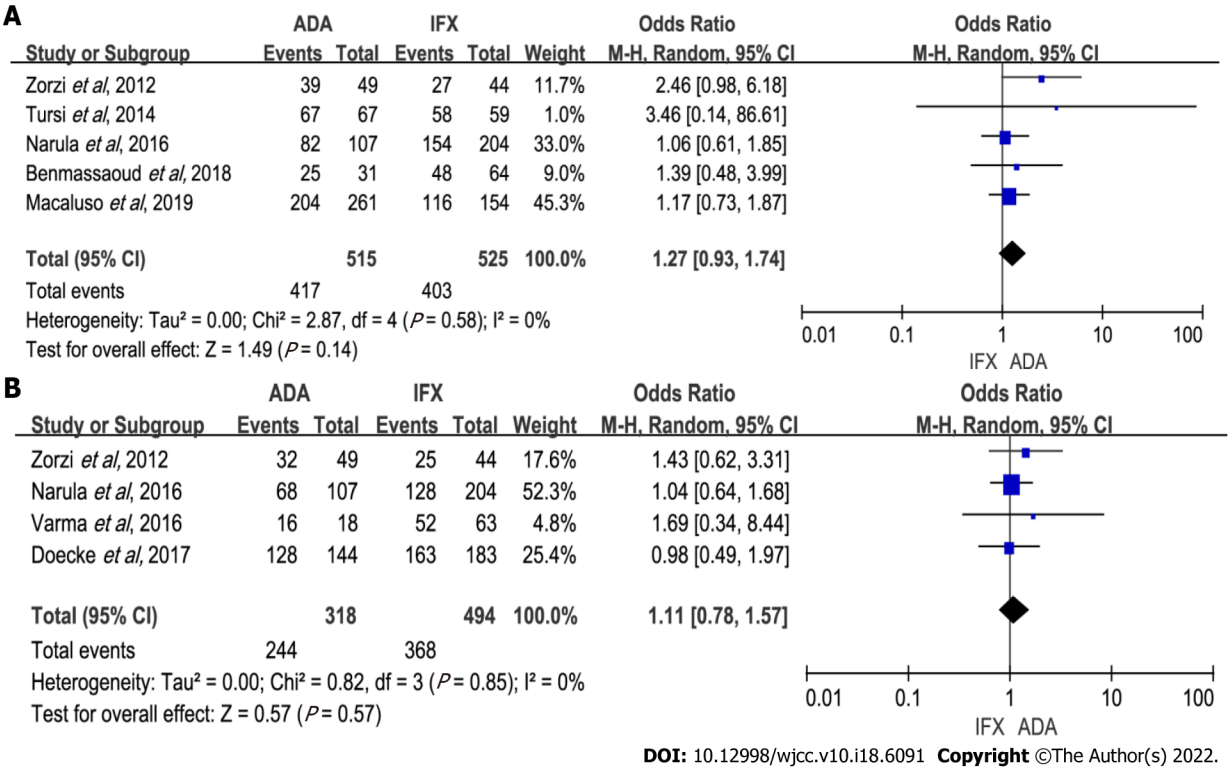

DOI: 10.12998/wjcc.v10.i18.6091 **Copyright** ©The Author(s) 2022.

Figure 2 Forest plot for induction efficacy comparing adalimumab and infliximab. A: Induction of response; B: Induction of remission. ADA: Adalimumab; IFX: Infliximab; CI: Confidence interval.

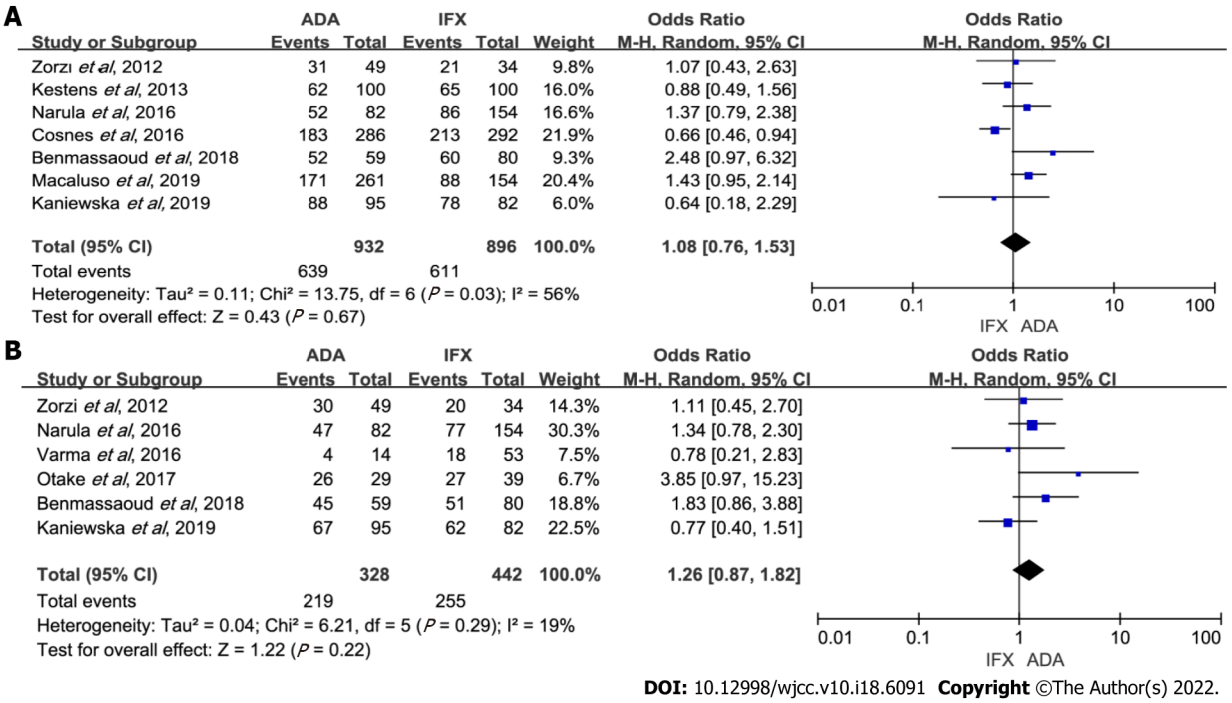

DOI: 10.12998/wjcc.v10.i18.6091 **Copyright** ©The Author(s) 2022.

Figure 3 Forest plot for maintenance efficacy comparing adalimumab and infliximab. A: Maintenance of response; B: Maintenance of remission. ADA: Adalimumab; IFX: Infliximab; CI: Confidence interval.

significant difference when subgroup analysis was done (Table 2). Sensitivity analysis showed no significant changes when any one of the studies was excluded (Supplementary Table 1).

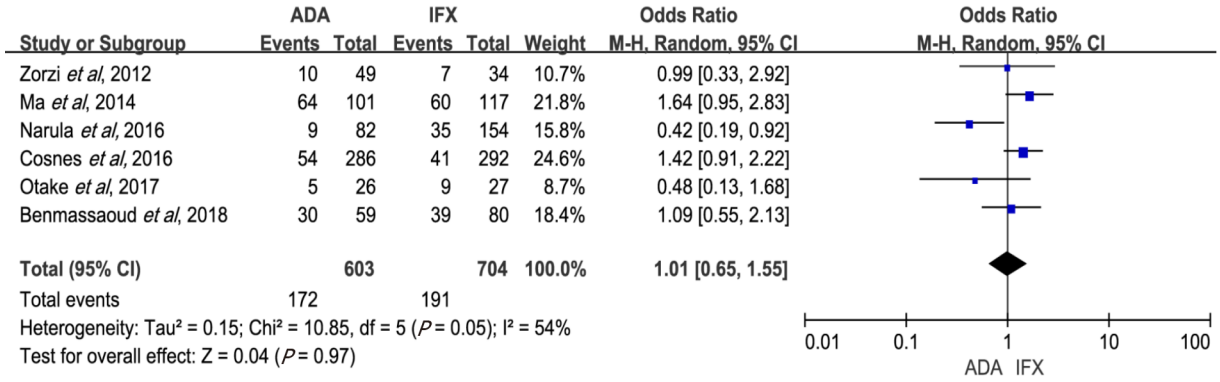

DOI: 10.12998/wjcc.v10.i18.6091 **Copyright** ©The Author(s) 2022.

Figure 4 Forest plot comparing infliximab and adalimumab for the incidence of secondary loss of response. ADA: Adalimumab; IFX: Infliximab; CI: Confidence interval.

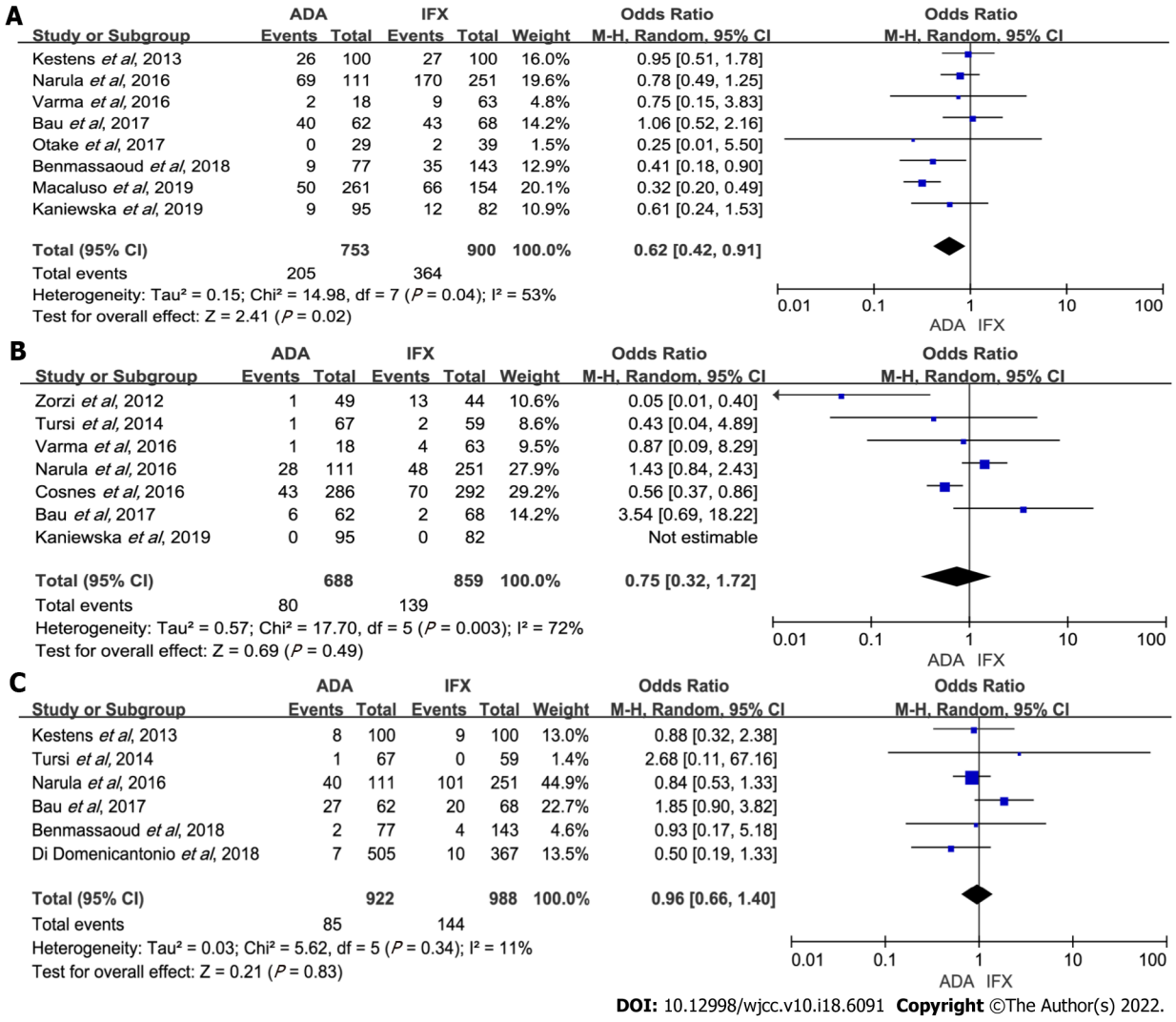

DOI: 10.12998/wjcc.v10.i18.6091 **Copyright** ©The Author(s) 2022.

Figure 5 Forest plot for comparisons of the rate of adverse events for adalimumab and infliximab. A: Overall adverse events; B: Severe adverse events; C: Opportunistic infection. ADA: Adalimumab; IFX: Infliximab; CI: Confidence interval.

Publication bias and GRADE evaluation

The symmetry of the funnel plot indicated there was no publication bias (Figure 6). The Egger's test showed no significant publication bias for maintenance of response ($P = 0.7024 > 0.05$), maintenance of remission ($P = 0.1003 > 0.05$), secondary loss of response ($P = 0.0510 > 0.05$), and overall adverse events ($P = 0.6717 > 0.05$). GRADE evidence of all outcomes was judged as "low". The results are shown in

Table 3 GRADE evidence profile

Quality assessment-No. of studies	Quality assessment-study design	Quality assessment-risk of bias	Quality assessment-inconsistency	Quality assessment-indirectness	Quality assessment-imprecision	Quality assessment-Publication bias	Summary of findings-number of patient, with IFX	Summary of findings-number of patient, with ADA	Summary of findings-effect, relative (95%CI)	Summary of findings-effect, absolute (95%CI)	Summary of findings-effect, Quality
Induction of response											
5	Observational study	Not serious	Not serious	Not serious	Not serious	Not found	403/525	417/515	OR: 1.27 (0.93-1.74)	768 *per* 1000	⊕⊕◯◯
Induction of remission											
4	Observational study	Not serious	Not serious	Not serious	Not serious	Not found	368/494	244/318	OR: 1.11 (0.78-1.57)	745 *per* 1000	⊕⊕◯◯
Maintenance of response											
7	Observational study	Not serious	Not serious	Not serious	Not serious	Not found	611/896	639/932	OR: 1.02 (0.83-1.25)	682 *per* 1000	⊕⊕◯◯
Maintenance of remission											
6	Observational study	Not serious	Not serious	Not serious	Not serious	Not found	255/442	219/328	OR: 1.26 (0.87-1.82)	577 *per* 1000	⊕⊕◯◯
Secondary loss of response											
6	Observational study	Not serious	Not serious	Not serious	Not serious	Not found	191/704	172/603	OR: 1.01 (0.65-1.55)	271 *per* 1000	⊕⊕◯◯
Overall adverse events											
8	Observational study	Not serious	Not serious	Not serious	Not serious	Not found	364/900	205/753	OR: 0.62 (0.42-0.91)	404 *per* 1000	⊕⊕◯◯
Severe adverse events											
7	Observational study	Not serious	Not serious	Not serious	Not serious	Not found	139/859	80/688	OR: 0.75 (0.32-1.72)	162 *per* 1000	⊕⊕◯◯
Opportunistic infection											
6	Observational study	Not serious	Not serious	Not serious	Not serious	Not found	144/988	85/922	OR: 0.96 (0.66-1.40)	146 *per* 1000	⊕⊕◯◯

GRADE Working Group grades of evidence: High quality (⊕⊕⊕⊕): Further research is unlikely to change our confidence in the estimate of effect; Moderate quality (⊕⊕⊕◯): Further research is likely to have an important impact on our confidence in the estimate of effect and may change the estimate; Low quality (⊕⊕◯◯): Further research is very likely to have an important impact on our confidence in the estimate of effect and is likely to change the estimate; Very low quality (⊕◯◯◯): We are very uncertain about the estimate. ADA: Adalimumab; IFX: Infliximab; OR: Odds ratio; CI: Confidence interval.

Table 3.

DISCUSSION

The immunogenicity of anti-TNF-α agents triggered the formation of anti-drug antibodies (ADAbs) specific to the agent administered. ADAbs of IFX or ADA and reduced serum concentrations in association with ADAbs together lead to decreased clinical benefit and increased adverse events. Although the immunogenicity of IFX is usually higher than that for ADA, we found both of them have similar response characteristics in CD patients. In our meta-analyses, no significant differences in primary outcomes were found between groups treated with IFX and ADA. These results were consistent with the results of most published studies[5-12,15-17]. One unexpected finding was the extent to which the overall adverse events rate of IFX was higher than that of ADA. Our meta-analysis indicated that physicians may choose on an individual basis, according to a possible history of adverse events to either IFX or ADA and to patient compliance, to give either an intravenous infusion or a self-administered subcutaneous injection.

CD is a heterogeneous disease, and the therapeutic efficacy differs between the types of disease, *e.g.*, location of disease, the existence of stenosis and/or fistula, or perianal involvement. There was no significant difference between IFX and ADA groups in the location of disease and existence of stenosis and/or fistula of included studies. However, IFX patients had more perianal diseases in the studies of Benmassaoud *et al*[7], Varma *et al*[8], Narula *et al*[9], and Cosnes *et al*[12]. Clinicians tended to choose IFX over ADA in patients with more severe disease activity or phenotypes (perianal disease) due to its intravenous administration and weight-based dosing schedule. We attempted to adjust for these differences through subgroup analysis, which led to the same conclusions (Supplementary Tables 2 and 3). Additionally, Ji *et al*[18] found the cumulative rate of nonrecurrence or aggravation of fistula at 24 mo was not significantly different between IFX and ADA groups (62.5% *vs* 83.9%, $P = 0.09$). Current evidence suggested that IFX and ADA had similar effects in patients with perianal disease.

Biologic-naïve or non-naïve patients were important factors to influence the results. It is controversial whether ADA had similar efficacy to IFX in previous anti-TNF exposure CD patients. Macaluso *et al*[10] compared clinical benefits between IFX and ADA only in biologic non-naïve CD patients and reported that there was no difference in clinical benefits at 12 wk and after 1 year ($P = 0.600$ and $P = 0.620$, respectively). A retrospective case-control study[19] found that the risk for ADAbs to IFX was higher than ADAbs to ADA when patients had prior antibodies to anti-TNF. They did not investigate clinical efficacy. However, Sasson and Ananthakrishnan[20] found that patients with high ADAbs titers exhibited similar rates of clinical efficacy to ADA therapy compared to those with low titers (at 3 mo and 12 mo $P = 0.81$ and 0.62 respectively). This may mean IFX and ADA have similar efficacy in previous anti-TNF exposed CD patients. Our findings indicated that either in naïve or non-naïve patients ADA and IFX had similar clinical response and remission. More studies conducted on previous anti-TNF exposure CD patients will be necessary.

Co-immunosuppression affected the results of the analysis. The finding that combination therapy with an immunomodulator is superior with IFX but not with ADA was reported in Kestens *et al*[4], Benmassaoud *et al*[7], and Doecke *et al*[16]. The possible reason is that IFX combined with immunomodulator treatment reduces its immunogenicity. However, clinical efficacy of ADA combination therapy did not differ from that of ADA monotherapy (71.8% *vs* 68.1% at week 26, $P = 0.63$)[21]. Therefore, more patients in the IFX group were combined with immunomodulator treatment than in the ADA group in the Narula *et al*[9] study. No change was found in results after sensitivity analysis was conducted. Patients were on concomitant immunomodulation at anti-TNF induction to improve the efficacy of the induction of the remission and discontinued co-therapy due to adverse effects or intolerability (from the beginning). When loss of response occurred, concomitant therapy was resumed (later add on). Only the Cosnes *et al*[12] study used immunomodulators later. No different results were found after sensitivity analysis was performed. Furthermore, CD patients who lost response were allowed to shorten intervals and double dosage. These optimization strategies also impacted the results. We conducted subgroup analyses comparing the outcomes between using dose optimization and not and found the clinical effect of ADA was similar to IFX.

Similar to the findings of many studies[4,10,17], the significantly higher rate of overall adverse events can be seen in patients using IFX, which could be attributed to infusion or allergic reactions. Benmassaoud *et al*[7] reported that IFX group patients were more likely to have infusion or injection reactions than ADA. A higher rate of allergic reactions in the IFX was observed in a study by Narula *et al*[9]. However, we noted that the difference did not exist in anti-TNF-α non-naïve patients and with long follow-up time. We were unable to evaluate long-term safety due to the different follow-up times of each study. Larger and long-term comparison studies will be necessary. In addition, the instability of the results also require further studies to establish these findings.

Additionally, we failed to evaluate long-term results due to the different follow-up times of each study. Inokuchi *et al*[22] performed a retrospective study to evaluate long-term prognosis. They observed that the rates of cumulative steroid-free remission rates and surgery-free did not differ significantly between the two groups after a median observation period of 64.2 mo ($P = 0.42$ and $P = 0.74$, respectively). The goal of CD treatment requires more than clinical healing. Mucosal healing and tissue healing are expected to stop disease progression and reduce recurrence. Tursi *et al*[15] found that mucosal healing and histological healing were comparable between the two groups ($P = 0.946$ and $P =$

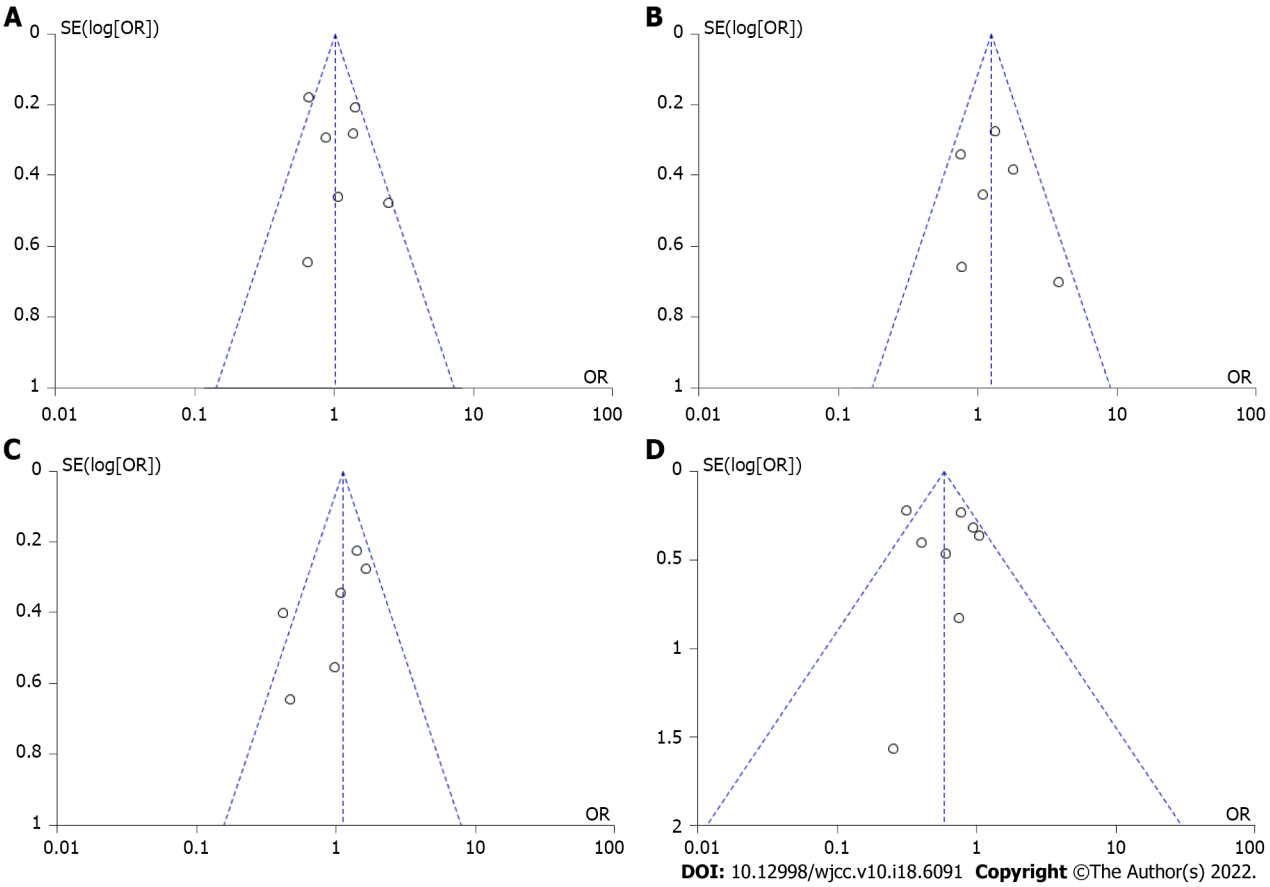

Figure 6 Funnel plot. A: Maintenance of response; B: Maintenance of remission; C: Secondary loss of response; D: Overall adverse events. OR: Odds ratio; SE: Standard error.

0.895, respectively).

Although biologic agents targeting TNF-α have achieved remarkable progress in treating CD, some patients do not respond to the induction therapy or lose response over time (secondary loss of response). The anti-drug antibodies or low serum drug concentrations play a critical part in the loss of response[23]. If ADA is superior to IFX for remission, ADA should have a lower rate of secondary loss of response than IFX. However, we failed to find a difference in the secondary loss of response between the two groups, which contradicted our hypothesis. It was further demonstrated that both have similar effects.

This work is the first direct comparison meta-analysis to evaluate the comparative effectiveness and safety of ADA and IFX in CD. Previous network meta-analyses addressed similar outcomes in the Bayesian setting indirect comparison. In our study, we enrolled comparative trial data resulting in more credible results. Furthermore, head-to-head clinical trials comparing ADA and IFX would not be feasible in the future; therefore, our studies will help guide optimal therapies.

Our current study has some limitations. First, we only included observational studies and failed to control adequately confounders, such as disease severity, disease phenotype, steroid use, *etc*. In addition to clinical benefits, we should consider other factors, such as patients' preferences and costs. Future studies are needed to address these questions.

CONCLUSION

IFX and ADA have similar response characteristics either in anti-TNF naïve and non-naïve CD patients, and ADA therapy has fewer overall adverse events. Our study indicates that IFX or ADA can be freely chosen as treatment based on physician and patient agreement. Eventually, the decision of which treatment to start may depend on factors such as patient preference and cost.

ARTICLE HIGHLIGHTS

Research background

Infliximab (IFX) is often selected as the first-line anti-tumor necrosis factor-α (TNF-α) agent for Crohn's disease (CD), despite the lack of data showing its superiority over adalimumab (ADA).

Research motivation

By comparing the effectiveness and safety between ADA and IFX, we wanted to determine if IFX or ADA is superior to the other for treatment of CD.

Research objectives

The present meta-analysis was performed to evaluate the comparative effectiveness and safety of ADA and IFX for CD to assist clinicians in making treatment choices.

Research methods

The clinical studies that compared the effectiveness or safety of ADA and IFX in the treatment of CD were searched in PubMed, Embase, Cochrane Library, and Web of Science databases.

Research results

Our meta-analysis of CD patients who were naïve or non-naïve to anti-TNF-α agents found no significant differences between IFX and ADA on many measures of effectiveness, including clinical response, clinical remission, and secondary loss of response. Interestingly, we observed a higher rate of overall adverse events in patients using IFX compared to ADA.

Research conclusions

IFX and ADA are comparable in clinical outcomes for patients with CD who are naïve or non-naïve to anti-TNF-α antagonists. However, fewer overall adverse events are noted in ADA patients.

Research perspectives

Our study provide reassurance to clinicians by synthesizing current literature suggesting that the ADA and IFX have similar effectiveness in "real-world" use. Larger, long-term, and prospective head-to-head comparison studies will be necessary to confirm these results. More research also will be necessary to explore the cost of anti-TNF-α agents.

ACKNOWLEDGEMENTS

We would like to thank all authors of the included primary studies.

FOOTNOTES

Author contributions: Yang HH and Zhou XC contributed to study design; Yang HH, Huang Y, and Wang RN contributed to the literature search; Yang HH, Huang Y, and Zhou XC participated in data extraction and analysis; Yang HH and Huang Y wrote the paper.

Conflict-of-interest statement: Nothing to disclosed.

PRISMA 2009 Checklist statement: The authors have read the PRISMA 2009 Checklist, and the manuscript was prepared and revised according to the PRISMA 2009 Checklist.

Open-Access: This article is an open-access article that was selected by an in-house editor and fully peer-reviewed by external reviewers. It is distributed in accordance with the Creative Commons Attribution NonCommercial (CC BY-NC 4.0) license, which permits others to distribute, remix, adapt, build upon this work non-commercially, and license their derivative works on different terms, provided the original work is properly cited and the use is non-commercial. See: https://creativecommons.org/Licenses/by-nc/4.0/

Country/Territory of origin: China

ORCID number: Hua-Hua Yang 0000-0002-0065-2741; Yi Huang 0000-0001-8049-1900; Xu-Chun Zhou 0000-0002-5128-3149; Ruo-Nan Wang 0000-0003-2049-6827.

S-Editor: Fan JR
L-Editor: Filipodia

P-Editor: Fan JR

REFERENCES

1 **Cushing K**, Higgins PDR. Management of Crohn Disease: A Review. *JAMA* 2021; **325**: 69-80 [PMID: 33399844 DOI: 10.1001/jama.2020.18936]

2 **Danese S**, Vuitton L, Peyrin-Biroulet L. Biologic agents for IBD: practical insights. *Nat Rev Gastroenterol Hepatol* 2015; **12**: 537-545 [PMID: 26284562 DOI: 10.1038/nrgastro.2015.135]

3 **Singh S**, Garg SK, Pardi DS, Wang Z, Murad MH, Loftus EV Jr. Comparative efficacy of biologic therapy in biologic-naïve patients with Crohn disease: a systematic review and network meta-analysis. *Mayo Clin Proc* 2014; **89**: 1621-1635 [PMID: 25441399 DOI: 10.1016/j.mayocp.2014.08.019]

4 **Kestens C**, van Oijen MG, Mulder CL, van Bodegraven AA, Dijkstra G, de Jong D, Ponsioen C, van Tuyl BA, Siersema PD, Fidder HH, Oldenburg B; Dutch Initiative on Crohn and Colitis (ICC). Adalimumab and infliximab are equally effective for Crohn's disease in patients not previously treated with anti-tumor necrosis factor-α agents. *Clin Gastroenterol Hepatol* 2013; **11**: 826-831 [PMID: 23376000 DOI: 10.1016/j.cgh.2013.01.012]

5 **Otake H**, Matsumoto S, Mashima H. Does long-term efficacy differ between infliximab and adalimumab after 1 year of continuous administration? *Medicine (Baltimore)* 2017; **96**: e6635 [PMID: 28422861 DOI: 10.1097/MD.0000000000006635]

6 **Zorzi F**, Zuzzi S, Onali S, Calabrese E, Condino G, Petruzziello C, Ascolani M, Pallone F, Biancone L. Efficacy and safety of infliximab and adalimumab in Crohn's disease: a single centre study. *Aliment Pharmacol Ther* 2012; **35**: 1397-1407 [PMID: 22519466 DOI: 10.1111/j.1365-2036.2012.05100.x]

7 **Benmassaoud A**, Al-Taweel T, Sasson MS, Moza D, Strohl M, Kopylov U, Paradis-Surprenant L, Almaimani M, Bitton A, Afif W, Lakatos PL, Bessissow T. Comparative Effectiveness of Infliximab Versus Adalimumab in Patients with Biologic-Naïve Crohn's Disease. *Dig Dis Sci* 2018; **63**: 1302-1310 [PMID: 29243105 DOI: 10.1007/s10620-017-4874-6]

8 **Varma P**, Paul E, Huang C, Headon B, Sparrow MP. A retrospective comparison of infliximab *vs* adalimumab as induction and maintenance therapy for Crohn disease. *Intern Med J* 2016; **46**: 798-804 [PMID: 26865349 DOI: 10.1111/imj.13040]

9 **Narula N**, Kainz S, Petritsch W, Haas T, Feichtenschlager T, Novacek G, Eser A, Vogelsang H, Reinisch W, Papay P. The efficacy and safety of either infliximab or adalimumab in 362 patients with anti-TNF-α naïve Crohn's disease. *Aliment Pharmacol Ther* 2016; **44**: 170-180 [PMID: 27226407 DOI: 10.1111/apt.13671]

10 **Macaluso FS**, Fries W, Privitera AC, Cappello M, Siringo S, Inserra G, Magnano A, Di Mitri R, Mocciaro F, Belluardo N, Scarpulla G, Magrì G, Trovatello A, Carroccio A, Genova S, Bertolami C, Vassallo R, Romano C, Citrano M, Accomando S, Ventimiglia M, Renna S, Orlando R, Rizzuto G, Porcari S, Ferracane C, Cottone M, Orlando A; Sicilian Network for Inflammatory Bowel Diseases [SN-IBD]. A Propensity Score-matched Comparison of Infliximab and Adalimumab in Tumour Necrosis Factor-α Inhibitor-naïve and Non-naïve Patients With Crohn's Disease: Real-Life Data From the Sicilian Network for Inflammatory Bowel Disease. *J Crohns Colitis* 2019; **13**: 209-217 [PMID: 30295785 DOI: 10.1093/ecco-jcc/jjy156]

11 **Kaniewska M**, Rosołowski M, Rydzewska G. Efficacy, tolerability, and safety of infliximab biosimilar in comparison to originator biologic and adalimumab in patients with Crohn disease. *Pol Arch Intern Med* 2019; **129**: 484-489 [PMID: 31316042 DOI: 10.20452/pamw.14901]

12 **Cosnes J**, Sokol H, Bourrier A, Nion-Larmurier I, Wisniewski A, Landman C, Marteau P, Beaugerie L, Perez K, Seksik P. Adalimumab or infliximab as monotherapy, or in combination with an immunomodulator, in the treatment of Crohn's disease. *Aliment Pharmacol Ther* 2016; **44**: 1102-1113 [PMID: 27666569 DOI: 10.1111/apt.13808]

13 **Di Domenicantonio R**, Trotta F, Cascini S, Agabiti N, Kohn A, Gasbarrini A, Davoli M, Addis A. Population-based cohort study on comparative effectiveness and safety of biologics in inflammatory bowel disease. *Clin Epidemiol* 2018; **10**: 203-213 [PMID: 29440933 DOI: 10.2147/CLEP.S150030]

14 **Bau M**, Zacharias P, Ribeiro DA, Boaron L, Steckert Filho A, Kotze PG. Safety profile of anti-TNF therapy in Crohn's disease management: A Brazilian single-center direct retrospective comparison between infliximab and adalimumab. *Arq Gastroenterol* 2017; **54**: 328-332 [PMID: 28954043 DOI: 10.1590/S0004-2803.201700000-43]

15 **Tursi A**, Elisei W, Picchio M, Penna A, Lecca PG, Forti G, Giorgetti G, Faggiani R, Zampaletta C, Pelecca G, Brandimarte G. Effectiveness and safety of infliximab and adalimumab for ambulatory Crohn's disease patients in primary gastroenterology centres. *Eur J Intern Med* 2014; **25**: 485-490 [PMID: 24631020 DOI: 10.1016/j.ejim.2014.02.010]

16 **Doecke JD**, Hartnell F, Bampton P, Bell S, Mahy G, Grover Z, Lewindon P, Jones LV, Sewell K, Krishnaprasad K, Prosser R, Marr D, Fischer J, R Thomas G, Tehan JV, Ding NS, Cooke SE, Moss K, Sechi A, De Cruz P, Grafton R, Connor SJ, Lawrance IC, Gearry RB, Andrews JM, Radford-Smith GL; Australian and New Zealand Inflammatory Bowel Disease Consortium. Infliximab vs. adalimumab in Crohn's disease: results from 327 patients in an Australian and New Zealand observational cohort study. *Aliment Pharmacol Ther* 2017; **45**: 542-552 [PMID: 27995633 DOI: 10.1111/apt.13880]

17 **Ma C**, Huang V, Fedorak DK, Kroeker KI, Dieleman LA, Halloran BP, Fedorak RN. Crohn's disease outpatients treated with adalimumab have an earlier secondary loss of response and requirement for dose escalation compared to infliximab: a real life cohort study. *J Crohns Colitis* 2014; **8**: 1454-1463 [PMID: 24947334 DOI: 10.1016/j.crohns.2014.05.007]

18 **Ji CC**, Takano S. Clinical efficacy of adalimumab *vs* infliximab and the factors associated with recurrence or aggravation during treatment of anal fistulas in Crohn's disease. *Intest Res* 2017; **15**: 182-186 [PMID: 28522947 DOI: 10.5217/ir.2017.15.2.182]

19 **Vande Casteele N**, Abreu MT, Flier S, Papamichael K, Rieder F, Silverberg MS, Khanna R, Okada L, Yang L, Jain A, Cheifetz AS. Patients With Low Drug Levels or Antibodies to a Prior Anti-Tumor Necrosis Factor Are More Likely to Develop Antibodies to a Subsequent Anti-Tumor Necrosis Factor. *Clin Gastroenterol Hepatol* 2022; **20**: 465-467.e2 [PMID: 33421628 DOI: 10.1016/j.cgh.2021.01.006]

20 **Sasson AN**, Ananthakrishnan AN. High Anti-Infliximab Antibody Titers Do Not Impact Response to Subsequent Adalimumab Treatment in Inflammatory Bowel Diseases. *Dig Dis Sci* 2021 [PMID: 34117949 DOI: 10.1007/s10620-021-07088-x]

21 **Matsumoto T**, Motoya S, Watanabe K, Hisamatsu T, Nakase H, Yoshimura N, Ishida T, Kato S, Nakagawa T, Esaki M, Nagahori M, Matsui T, Naito Y, Kanai T, Suzuki Y, Nojima M, Watanabe M, Hibi T; DIAMOND study group. Adalimumab Monotherapy and a Combination with Azathioprine for Crohn's Disease: A Prospective, Randomized Trial. *J Crohns Colitis* 2016; **10**: 1259-1266 [PMID: 27566367 DOI: 10.1093/ecco-jcc/jjw152]

22 **Inokuchi T**, Takahashi S, Hiraoka S, Toyokawa T, Takagi S, Takemoto K, Miyaike J, Fujimoto T, Higashi R, Morito Y, Nawa T, Suzuki S, Nishimura M, Inoue M, Kato J, Okada H. Long-term outcomes of patients with Crohn's disease who received infliximab or adalimumab as the first-line biologics. *J Gastroenterol Hepatol* 2019; **34**: 1329-1336 [PMID: 30724387 DOI: 10.1111/jgh.14624]

23 **Roda G**, Jharap B, Neeraj N, Colombel JF. Loss of Response to Anti-TNFs: Definition, Epidemiology, and Management. *Clin Transl Gastroenterol* 2016; **7**: e135 [PMID: 26741065 DOI: 10.1038/ctg.2015.63]

World Journal of Clinical Cases

Submit a Manuscript: https://www.f6publishing.com

World J Clin Cases 2022 June 26; 10(18): 6105-6109

DOI: 10.12998/wjcc.v10.i18.6105

ISSN 2307-8960 (online)

CASE REPORT

Successful treatment of acute relapse of chronic eosinophilic pneumonia with benralizumab and without corticosteroids: A case report

Shimon Izhakian, Barak Pertzov, Dror Rosengarten, Mordechai R Kramer

Specialty type: Respiratory system

Provenance and peer review: Unsolicited article; Externally peer reviewed.

Peer-review model: Single blind

Peer-review report's scientific quality classification

Grade A (Excellent): 0
Grade B (Very good): B
Grade C (Good): C, C
Grade D (Fair): D
Grade E (Poor): 0

P-Reviewer: Hu QD, China; Liu H, China; Pan H, China

Received: April 14, 2021
Peer-review started: April 14, 2021
First decision: September 28, 2021
Revised: November 5, 2021
Accepted: May 5, 2022
Article in press: May 5, 2022
Published online: June 26, 2022

Shimon Izhakian, Barak Pertzov, Dror Rosengarten, Mordechai R Kramer, Pulmonary Institute, Rabin Medical Center, Petach Tikva 49100, Israel

Shimon Izhakian, Barak Pertzov, Dror Rosengarten, Mordechai R Kramer, Affiliated to Sackler Faculty of Medicine, Tel Aviv University, Ramat Aviv, Israel

Corresponding author: Shimon Izhakian, MD, PhD, Doctor, Pulmonary Institute, Rabin Medical Center, No. 39 Jabotinski St., Petach Tikva 49100, Israel. shimixyz@gmail.com

Abstract

BACKGROUND

Currently, the mainstay of chronic eosinophilic pneumonia (CEP) treatment is corticosteroids, usually with a favorable response and good prognosis. However, relapse is common, requiring long-term use of corticosteroids, with risk of significant treatment-related complications. The dire need to develop new treatments for patients with CEP, who are dependent on, or resistant to corticosteroids has led to exploring novel therapies. We herein describe a patient with acute relapse of CEP, who was successfully treated with benralizumab, an IL-5Rα antagonist that has demonstrated rapid anti-eosinophil action in patients with asthma. Currently, only three recent patient reports on CEP relapse, also demonstrated successful treatment with benralizumab alone, without corticosteroids.

CASE SUMMARY

A 31-year-old non-smoking woman presented in our hospital with a 3 wk history of shortness of breath, dry cough and fever up to 38.3 °C. Laboratory examination revealed leukocytosis 10240 K/μL, eosinophilia 900 K/μL and normal values of hemoglobin, platelets, creatinine and liver enzymes. Computed tomography of the chest showed a mediastinal lymphadenopathy and consolidations in the right upper and left lower lobes. CEP was diagnosed, and the patient was treated with hydrocortisone intravenously, followed by oral prednisone, with prompt improvement. Three months later, she presented with relapse of CEP: aggravation of dyspnea, rising of eosinophilia and extension of pulmonary infiltrates on chest X-ray. She was treated with benralizumab only, with clinical improvement within 2 wk, and complete resolution of lung infiltrates following 5 wk.

CONCLUSION

Due to Benralizumab's dual mechanism of action, it both neutralizes IL-5Rα pro-eosinophil functions and triggers apoptosis of eosinophils. We therefore maintain benralizumab can serve as a reasonable therapy choice for every patient with chronic eosinophilic pneumonia and a good alternative for corticosteroids.

Key Words: Benralizumab; Eosinophilic pneumonia; Interstitial lung disease; Corticosteroid withdrawal; Case report

©The Author(s) 2022. Published by Baishideng Publishing Group Inc. All rights reserved.

Core Tip: Chronic eosinophilic pneumonia (CEP) is an idiopathic pulmonary disease, characterized by marked eosinophil accumulation in the pulmonary parenchyma. Currently, the mainstay of CEP treatment is corticosteroids. However, relapse is common, requiring long-term use of corticosteroids, with the risk of significant treatment-related adverse effects. Herein, we describe a patient with an acute CEP relapse, successfully treated with benralizumab alone, without corticosteroids. Currently, only three patients with acute relapse of CEP, were reported successfully treated with benralizumab alone, without corticosteroids. This therapy option may be particularly beneficial for patients who have previously suffered serious adverse effects from or have any contraindications to chronic corticosteroid treatment.

Citation: Izhakian S, Pertzov B, Rosengarten D, Kramer MR. Successful treatment of acute relapse of chronic eosinophilic pneumonia with benralizumab and without corticosteroids: A case report. *World J Clin Cases* 2022; 10(18): 6105-6109
URL: https://www.wjgnet.com/2307-8960/full/v10/i18/6105.htm
DOI: https://dx.doi.org/10.12998/wjcc.v10.i18.6105

INTRODUCTION

Chronic eosinophilic pneumonia (CEP) is an inflammatory lung disease, clinically characterized by isolated pulmonary involvement, with appearance of pulmonary eosinophilic infiltrates[1] that permeate the lungs, presenting symptoms include cough, fever and dyspnea[2]. Response to oral corticosteroids (OCS), the commonly administered treatment for CEP, is usually dramatic and rapid[3]. However, in approximately 50% of the patients, CEP relapses under tapering of OCS, and thus long-term OCS administration is required[3]. Unfortunately, chronic OCS treatment has a proven increased risk for treatment-related adverse effects and complications, (*e.g.*, hypertension, diabetes mellitus, osteoporosis and infections)[4]. Therefore, the dire need to develop new treatments for patients with CEP, who are dependent on, or resistant to OCS has led to exploring novel therapies. Benralizumab, an IL-5Rα antagonist has demonstrated rapid anti-eosinophil action in patients with asthma. Successful treatment with benralizumab, was also recently reported in three patients with acute relapse of CEP[5-7]. We herein describe an additional patient with an acute relapse of CEP who was successfully treated with benralizumab alone, without corticosteroids.

CASE PRESENTATION

Chief complaints

On July 26, 2020, a 31-year-old non-smoking healthy woman was evaluated in our hospital. She presented with a 3-wk history of shortness of breath, dry cough and fever up to 38.3 °C.

History of present illness

Two weeks prior to the presentation at our medical center, the patient was examined at a local emergency department for the same complaints, which had then appeared for one week. At that time, a chest X-ray showed infiltrates in the right upper and left lateral lung fields (Figure 1A). The laboratory examination revealed mild leukocytosis 11200 K/μL, eosinophilia 800 K/μL and an elevated level of serum C-reactive protein 45 mg/L. Nasopharyngeal swabs were negative for coronavirus disease 2019 (COVID-19). She was discharged home from the local hospital with recommendations for oral treatment with cefuroxime 500 mg and roxithromycin 150 mg, both twice daily for 7 days.

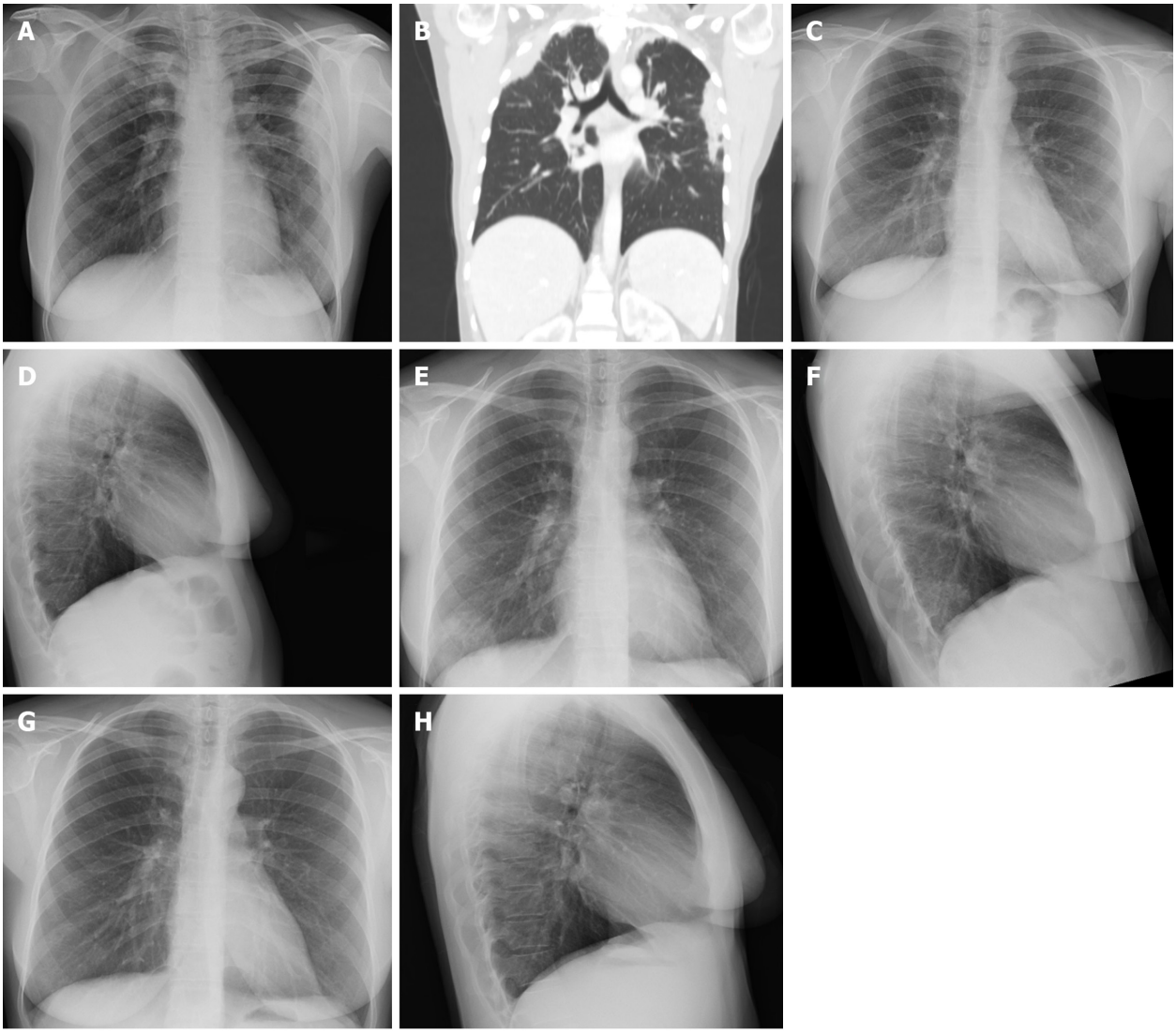

DOI: 10.12998/wjcc.v10.i18.6105 **Copyright** ©The Author(s) 2022.

Figure 1 Imaging examinations of the present patient. A: Chest X-ray (frontal view) shows infiltrates in the right upper and left lateral lung fields (two weeks prior to the patient's presentation in our hospital); B: CT of the chest (axial plain) reveals a mediastinal lymphadenopathy, and pulmonary consolidations in the right upper and left lower lobes (at first presentation); C: Chest X-ray (frontal view) and D: (lateral view) show disappearance of the pulmonary infiltrates (6 wk after the presentation); E: Chest X-ray (frontal view) and F: (lateral view) reveal a new infiltrate in the right lower lobe (4.5 mo after the presentation); G: Chest X-ray (frontal view) and H: (lateral view) reveal absorption of the infiltrate 5 wk after beginning of benralizumab treatment.

History of past illness

No specific history of past illness was reported.

Physical examination

The patient's temperature was 37.3 °C, heart rate 97 beats per minute, respiratory rate 16 breaths per minute, blood pressure 103/71 mmHg and oxygen saturation in room air 97%. On the chest examination, crepitation was detected on the left lung base. The rest of the physical examination was unrevealing.

Laboratory examinations

Abnormal laboratory findings included leukocytosis 10240 K/μL and eosinophilia 900 K/μL. Results of other routine blood tests were normal. A screening panel was negative for allergic bronchopulmonary aspergillosis, including *Aspergillus* specific immunoglobulin E and *Aspergillus fumigatus* serum precipitant. No antinuclear and anti-neutrophil cytoplasmic antibodies were detected. Serologic tests for *Toxocara*, *Strongyloides*, *Schistosoma* and *Echinococcus* were negative.

Imaging examinations

Computed tomography (CT) of the chest (axial plain) showed a mediastinal lymphadenopathy, and pulmonary consolidations in the right upper and left lower lobes (Figure 1B).

FINAL DIAGNOSIS

Eosinophilic pneumonia was diagnosed based on clinical symptoms, peripheral blood eosinophilia, peripheral lung consolidation on chest CT and prompt response to systemic glucocorticoid therapy.

TREATMENT

The patient was treated with hydrocortisone intravenously at a dosage of 100 mg three times per day, for 2 days, with rapid improvement of dyspnea and cough. The treatment was switched to oral prednisone, at a daily dosage of 40 mg, which was tapered down during the following 2 mo. On September 6, 2020, the patient was feeling well, eosinophilia had resolved, and pulmonary infiltrates no longer appeared on chest X-ray (Figures 1C and D).

OUTCOME AND FOLLOW-UP

On December 6, 2020, the patient was reevaluated, due to recurrence of dyspnea, cough and fever. Laboratory examination demonstrated blood eosinophilia 600 K/μL, white blood cells 8.8 k/micL and C-reactive protein 0.2 mg/dL. Chest X-ray revealed a new infiltrate in the right lower lobe of the frontal view (Figure 1E), which was clearer in the lateral view (Figure 1F). Acute relapse of CEP was diagnosed. We discussed with the patient treatment options, including the advantages and disadvantages of therapy with OCS *vs* anti-interleukin-5 drug, benralizumab. It was decided to start (on December 7, 2020) benralizumab subcutaneously, at a dosage of 30 mg monthly, without OCS. Following 2 wk, the patient reported significant improvement of the symptoms. One month after the first injection of benralizumab, eosinophils were zero and WBC 4 k/micL; CRP was not taken. Five weeks after the first injection, a chest X-ray was unrevealing (Figure 1G and H). Two months later, the patient received the second and third injections of benralizumab and demonstrated sustained clinical and radiographic remission of CEP.

DISCUSSION

To the best of our knowledge, we present the fourth recent report in the medical literature regarding rapid improvement of acute flare of CEP, following treatment with benralizumab, without OCS. In previous cases, benralizumab therapy was initiated after frequent, acute CEP relapses, or as an alternative after patient refusal to reinitiate OSC, due to treatment-related adverse effects. Isomoto *et al* [5] described a 58-year-old woman with CEP and a history of refractory asthma. She had three flares of her concomitant disease in the preceding year, which necessitated OCS therapy. Only for the fourth flare, her treating physician initiated a different therapy, one injection of benralizumab, which induced remission of her asthma and CEP following 16 wk. Izumo *et al*[6] described a 43-year-old healthy woman who presented with chronic cough. She was diagnosed with CEP and successfully treated with prednisolone. However, her symptoms worsened after prednisolone cessation. Following patient refusal to re-initiation of OCS, due to treatment-related adverse effects, benralizumab treatment was initiated. After 6 mo of benralizumab therapy, sustained remission of CEP was achieved. Yazawa *et al*[7] described a 70-year-old woman with a history of bronchial asthma who had dyspnea and cough for one month, and was diagnosed with CEP. She refused OCS and therefore was treated with benralizumab, which resulted in resolution of symptoms, hypoxemia and lung infiltrates. Moreover, 12 mo benralizumab maintenance treatment without OCS, provided sustained remission of CEP.

CEP is an idiopathic lung disease that is characterized by isolated pulmonary involvement, with marked eosinophil accumulation in the pulmonary parenchyma[1,2]. Therefore, we maintain benralizumab is a reasonable therapy choice for every patient with CEP. Predominately, due to its dual mechanism of action, benralizumab a humanized monoclonal antibody, as an interleukin-5 receptor α (IL-5Rα) antagonist, neutralizes the pro-eosinophil functions of IL-5R, by binding to its α subunit and by binding to FcγRIIIa receptor expressed by natural killer cells, triggers apoptosis of eosinophils *via* antibody-dependent cell-mediated cytotoxicity[8]. This therapy is especially important in patients with CEP, who present with specific clinical scenarios. As demonstrated, treatment with benralizumab may be beneficial for patients with frequent CEP relapses. Clearly, benralizumab could be the drug of choice in patients who demonstrate serious adverse effects following OCS therapy. Likewise, benralizumab therapy seems to be preferred in patients with comorbidities that are expected to be aggravated under OCS treatment.

CONCLUSION

For treatment of CEP, we maintain benralizumab can serve as a reasonable therapy choice for every patient and a good alternative for OCS.

FOOTNOTES

Author contributions: Izhakian S and Rosengarten D contributed to the acquisition and interpretation of the data; Pertzov B and Kramer MR contributed to the critical revision of the manuscript for important intellectual content; all authors contributed to the drafting of the manuscript and approved the final version.

Informed consent statement: Written informed consent was obtained from the patient for publication of this manuscript and any accompanying images.

Conflict-of-interest statement: The authors declare that they have no conflicts of interest related to this work.

CARE Checklist (2016) statement: The authors have read the CARE Checklist (2016), and the manuscript was prepared and revised according to the CARE Checklist (2016).

Open-Access: This article is an open-access article that was selected by an in-house editor and fully peer-reviewed by external reviewers. It is distributed in accordance with the Creative Commons Attribution NonCommercial (CC BY-NC 4.0) license, which permits others to distribute, remix, adapt, build upon this work non-commercially, and license their derivative works on different terms, provided the original work is properly cited and the use is non-commercial. See: https://creativecommons.org/Licenses/by-nc/4.0/

Country/Territory of origin: Israel

ORCID number: Shimon Izhakian 0000-0003-1150-1057; Barak Pertzov 0000-0002-3077-3616; Dror Rosengarten 0000-0003-1754-5878; Mordechai R Kramer 0000-0003-2376-2393.

S-Editor: Wang JL (Online Science Editor)
L-Editor: Wang TQ
P-Editor: Ma YJ

REFERENCES

1 **Suzuki Y**, Suda T. Eosinophilic pneumonia: A review of the previous literature, causes, diagnosis, and management. *Allergol Int* 2019; **68**: 413-419 [PMID: 31253537 DOI: 10.1016/j.alit.2019.05.006]
2 **Marchand E**, Reynaud-Gaubert M, Lauque D, Durieu J, Tonnel AB, Cordier JF. Idiopathic chronic eosinophilic pneumonia. A clinical and follow-up study of 62 cases. The Groupe d'Etudes et de Recherche sur les Maladies "Orphelines" Pulmonaires (GERM"O"P). *Medicine (Baltimore)* 1998; **77**: 299-312 [PMID: 9772920 DOI: 10.1097/00005792-199809000-00001]
3 **Durieu J**, Wallaert B, Tonnel AB. Long-term follow-up of pulmonary function in chronic eosinophilic pneumonia. Groupe d'Etude en Pathologie Interstitielle de la Société de Pathologie Thoracique du Nord. *Eur Respir J* 1997; **10**: 286-291 [PMID: 9042622 DOI: 10.1183/09031936.97.10020286]
4 **Naughton M**, Fahy J, FitzGerald MX. Chronic eosinophilic pneumonia. A long-term follow-up of 12 patients. *Chest* 1993; **103**: 162-165 [PMID: 8031327 DOI: 10.1378/chest.103.1.162]
5 **Isomoto K**, Baba T, Sekine A, Aiko N, Ogura T. Promising Effects of Benralizumab on Chronic Eosinophilic Pneumonia. *Intern Med* 2020; **59**: 1195-1198 [PMID: 32009090 DOI: 10.2169/internalmedicine.3606-19]
6 **Izumo T**, Kuse N, Awano N, Tone M, Jo T, Yoshimura H, Minami J, Takada K, Muto Y, Fujimoto K, Inomata M. Rapid and sustained effects of a single dose of benralizumab on chronic eosinophilic pneumonia. *Respir Med Case Rep* 2020; **30**: 101062 [PMID: 32373456 DOI: 10.1016/j.rmcr.2020.101062]
7 **Yazawa S**, Toyoshima M, Koda K, Suda T. Benralizumab as initial treatment for chronic eosinophilic pneumonia. *Allergol Int* 2021; **70**: 140-142 [PMID: 32807690 DOI: 10.1016/j.alit.2020.07.005]
8 **Kolbeck R**, Kozhich A, Koike M, Peng L, Andersson CK, Damschroder MM, Reed JL, Woods R, Dall'acqua WW, Stephens GL, Erjefalt JS, Bjermer L, Humbles AA, Gossage D, Wu H, Kiener PA, Spitalny GL, Mackay CR, Molfino NA, Coyle AJ. MEDI-563, a humanized anti-IL-5 receptor alpha mAb with enhanced antibody-dependent cell-mediated cytotoxicity function. *J Allergy Clin Immunol* 2010; **125**: 1344-1353.e2 [PMID: 20513525 DOI: 10.1016/j.jaci.2010.04.004]

World Journal of Clinical Cases

Submit a Manuscript: https://www.f6publishing.com

World J Clin Cases 2022 June 26; 10(18): 6110-6118

DOI: 10.12998/wjcc.v10.i18.6110

ISSN 2307-8960 (online)

CASE REPORT

Pembrolizumab-induced Stevens-Johnson syndrome in advanced squamous cell carcinoma of the lung: A case report and review of literature

Jing-Yi Wu, Kai Kang, Jing Yi, Bin Yang

Specialty type: Immunology

Provenance and peer review: Unsolicited article; Externally peer reviewed.

Peer-review model: Single blind

Peer-review report's scientific quality classification

Grade A (Excellent): 0
Grade B (Very good): 0
Grade C (Good): C, C
Grade D (Fair): D, D
Grade E (Poor): 0

P-Reviewer: Bos S, United Kingdom; Deshwal H, United States; Ng QX, Singapore

Received: October 10, 2021
Peer-review started: October 10, 2021
First decision: December 10, 2021
Revised: December 24, 2021
Accepted: April 30, 2022
Article in press: April 30, 2022
Published online: June 26, 2022

Jing-Yi Wu, Jing Yi, Bin Yang, Department of Thoracic Oncology, Hubei Cancer Hospital, Tongji Medical College, Huazhong University of Science and Techonology, Wuhan 430000, Hubei Province, China

Kai Kang, Department of Thoracic Oncology Surgery, Hubei Cancer Hospital, Tongji Medical College, Huazhong University of Science and Technology, Wuhan 430070, Hubei Province, China

Corresponding author: Bin Yang, MS, Academic Fellow, Academic Research, Additional Professor, Department of Thoracic Oncology, Hubei Cancer Hospital, Tongji Medical College, Huazhong University of Science and Techonology, No. 116 Zhuo Daoquan South Road, Wuhan 430000, Hubei Province, China. dlhdr2011@163.com

Abstract

BACKGROUND

For advanced lung squamous cell carcinoma, immune checkpoint inhibitors (ICIs) have been regarded as one of the optimal therapies. While immune-related adverse events (irAEs) are common in ICI treatment, cutaneous toxicities are among the most common irAEs. Most immune-related skin toxicity grades are low, and the prognosis is good. However, Stevens-Johnson syndrome (SJS) is a rare but extremely severe cutaneous adverse drug reaction with high mortality.

CASE SUMMARY

We report a rare case of SJS induced by pembrolizumab. The case involved a 68-year-old female who was diagnosed with advanced squamous cell carcinoma of the lung. SJS appeared after one cycle of immunotherapy combined with chemotherapy. After treatment with prednisone hormone symptoms, anti-infection, gamma globulin, and antipruritic agents, the skin toxicity of the patients gradually decreased and eventually disappeared. Although the antitumor treatment was stopped due to serious adverse reactions, the tumor of the patient remained stable for nearly half a year after one cycle of immune therapy combined with chemotherapy, which also corroborates the delayed effect of immunotherapy.

CONCLUSION

We believe our report can provide some references for the treatment of SJS and the treatment of immune-related adverse reactions.

Key Words: Pembrolizumab; Stevens-Johnson syndrome; Advanced squamous cell carcinoma; Lung; Immune-related adverse events; Case report

©The Author(s) 2022. Published by Baishideng Publishing Group Inc. All rights reserved.

Core Tip: Stevens-Johnson syndrome (SJS) is a rare but extremely severe cutaneous adverse drug reaction with high mortality. The case involved a 68-year-old female who was diagnosed with advanced squamous cell carcinoma of the lung. SJS syndrome appeared after one cycle of immunotherapy. After the optimal supportive treatment, skin toxicity disappeared.

Citation: Wu JY, Kang K, Yi J, Yang B. Pembrolizumab-induced Stevens-Johnson syndrome in advanced squamous cell carcinoma of the lung: A case report and review of literature. *World J Clin Cases* 2022; 10(18): 6110-6118
URL: https://www.wjgnet.com/2307-8960/full/v10/i18/6110.htm
DOI: https://dx.doi.org/10.12998/wjcc.v10.i18.6110

INTRODUCTION

Pembrolizumab is an anti-PD-1 (programmed death 1) humanized IgG4 monoclonal antibody that blocks the PD-1 receptor to enable T cell killing. Pembrolizumab, combined with chemotherapy, has shown improved efficacy in patients with advanced squamous cell carcinoma of the lung[1], with drug-related adverse events reported in 64% of patients[2]. However, adverse events of grade 3 or higher were reported in less than 10% of patients and included cutaneous side-effect cases.

Stevens-Johnson syndrome (SJS) is a severe type of pleomorphic erythema and a rare adverse mucocutaneous reaction with a mortality rate of up to 35%[3]. While SJS is characterized by maculo-papular rash – pruritus – and is often related to adverse drug reactions[4,5], the mechanism of SJS has not been determined. It has been reported that at least 200 kinds of drug reactions are related to SJS. However, cases in which anti-PD-1/anti-PD-L1 drugs contribute to SJS are rare[3]. There have been several reports of anti-PD-1/anti-PD-L1 therapy inducing SJS[6-14,15]. Here, we present our report of a rare case of pembrolizumab-associated SJS in a female patient with advanced squamous cell carcinoma of the lung.

CASE PRESENTATION

Chief complaints

The patient was a 68-year-old female without a history of smoking. On October 1st, 2020, she was admitted due to repeated cough and breathlessness for 1 mo.

History of present illness

Systemic examinations, including chest computed tomography (CT), whole abdominal CT, brain magnetic resonance imaging (MRI), bone scintigraphy, and blood tests, were performed. The test results showed that the levels of tumor markers were clearly elevated, and CT indicated a lung mass in the right lobe, several bilateral nodules, multiple mediastinal lymph nodes, and a solitary liver metastasis. Squamous cell carcinoma of the lung was diagnosed through CT-guided percutaneous needle lung biopsy, and polymerase chain reaction (PCR) revealed no epidermal growth factor receptor, anaplastic lymphoma kinase, or receptor tyrosine kinase mutations. According to the American Joint Commission on Cancer 8th edition staging system, she was clinically diagnosed with stage IVA lung squamous cell carcinoma (cT4N2M1b). According to the 2020 National Comprehensive Cancer Network guidelines, the combination of immunotherapy and chemotherapy is the best optional treatment for patients with advanced lung squamous cell carcinoma. On October 14, 2020, the patient was treated with one cycle of paclitaxel 270 mg d1 + cisplatin 120 mg d1 chemotherapy combined with pembrolizumab therapy. On November 4, 2021, which was nearly three weeks after one cycle of chemotherapy, the patient started with low fever, sore throat, and severe fatigue. Then, the patient was considered to be related to cold exposure. Penicillin treatment was used in the hospital nearby, but the patient's symptoms did not improve, which lasted for almost 5 d. On November 9th, small papules and typical erythema, accompanied by severe itchiness and general discomfort, gradually appeared on the patient's skin and were mainly distributed in the anterior chest and face. Considering the severity of the patient's

symptoms, the patient visited our hospital on November 12th. The patient's temperature was normal. The pain in her throat persisted. The physical examination of the patient showed that multiple erythematous papules could be detected on the patient's head, neck, chest, and back (covering 30% of the total body skin) (Figure 1), most of which fused to form blisters. The patient reported that these papules felt mild itchiness but painful. Eyelid edema was obvious. There were some ulcers around the lip. The patient's oral ulcers were too painful to allow her to eat anything.

History of past illness

There was no remarkable past medical history with no alcohol consumption or history of smoking.

Personal and family history

Family and personal history were unremarkable. She had no significant medical history or drug allergy.

Physical examination

A poor general condition, SCORTEN (severity-of-illness score for TEN) score of 4 points. Nikolsky's sign was positive. Koebner phenomenon was negative. Erythematous papules could be detected on the patient's head, neck, chest, and back (covering 30% of the total body skin) with mild itchy but painful symptoms. Eyelid edema was obvious. There were some ulcers around the lip. Her oral ulcers were too painful to allow her to eat anything. No other apparently positive signs were found.

Laboratory examinations

She was admitted to our hospital, and the relevant blood tests after admission are shown in Table 1 below.

Imaging examinations

Chest and abdominal CT scans showed that the primary lung lesions and liver metastases were significantly reduced, and the overall response evaluation was PR according to RECIST 1.1 (Response Evaluation Criteria in Solid Tumors).

FINAL DIAGNOSIS

We arranged an urgent consultation with a dermatologist. According to the skin and mucous membrane performance of the patient during these days, the rapid development of the disease, and history of PD-1 inhibitor use, pembrolizumab-induced SJS was diagnosed.

TREATMENT

Therefore, we immediately administered moderate- to high-potency topical steroids to treat the affected areas, oral antihistamines for pruritus and oral prednisone at 40 mg/d. After three days of treatment, the dermatologic toxicities were clearly aggravated. On November 18 (Figure 2), the rash began to spread to almost the entire body (covering more than 45% of the total body skin). The blisters were formed superficially in the epidermis with skin ulceration, and most of them had blood and fluid oozing. Part of the epidermis was peeled off from the surface of the body, exposing a moist, painful, flushed erosive surface. The oral ulcers continued to be aggravated. Both the itchiness and pain worsened, and the patient became severe (G3-4). At this point, we suspended immunotherapy, administered high potency topical steroids to the affected areas and prophylactically used antibiotics; additionally, we increased the prednisone dose to 100 mg. After three days of treatment, the cutaneous toxicities continued to worsen (Figure 3).

OUTCOME AND FOLLOW-UP

By referring to the opinions from the consultation, intravenous methylprednisolone 120 mg/d (2 mg/kg/d), gamma globulin 20 g/d, topical gentamicin, and diluted potassium permanganate were administered. Sepprayi 25 mg (recombinant human type II tumor necrosis factor receptor-antibody fusion protein, rhTNFR:Fc) was injected subcutaneously twice a week, and oral antihistamine was administered for pruritus. After a week of treatment, the dermatologic toxicities were gradually alleviated (Figure 4). Then, oral prednisone was gradually reduced, and topical drug administration continued. The treatment lasted for 3 mo, and the skin toxicity eventually disappeared (Figure 5). In terms of lung carcinoma, the pulmonary nodule was smaller than the baseline and remained stable during the 6-mo evaluation. In May 2021, the latest re-examination showed that although the patient did

Table 1 Some blood test of the patient

Time	November 18, 2021	November 26, 2021	December 1, 2021	December 7, 2020
White blood cell	10.3×10^8/L (3.5-9.5)	10.01×10^8/L (3.5-9.5)	9.28×10^8/L (3.5-9.5)	10.76×10^8/L (3.5-9.5)
Red blood cell	2.68×10^{12}/L (3.8-5.1)	3.01×10^{12}/L (3.8-5.1)	2.86×10^{12}/L (3.8-5.1)	2.63×10^{12}/L (3.8-5.1)
Hemoglobin	78 g/L (115-150)	98 g/L (115-150)	97.9 g/L (115-150)	89.3 g/L (115-150)
Thrombocyte	115×10^9/L (125-350)	124×10^9/L (125-350)	135×10^9/L (125-350)	133×10^9/L (125-350)
C-reactive protein	22.07 mg/L (0-10)		60.5 mg/L (0-10)	
Erythrocyte sedimentation rate			44 mm/h (0-22)	51 mm/h (0-22)
Procalcitonin	0.05 ng/mL (< 0.05)	0.05 ng/mL (< 0.05)	0.09 ng/mL (< 0.05)	
D-dimer	0.83 ng/mL (< 0.5 mg/L)		646 ng/mL (< 0.5 mg/L)	
Immunoglobulin G (IgG)			22.2 g/L (7.0-12.6)	
ANA reaction			Positive	
ANA drop degree			0.486	
Anti-SSA/Ro antibody			Strongly positive (+++)	
Anti-SSB			Positive (++)	
Interleukin-6			39.26 pg/mL (0-7)	



DOI: 10.12998/wjcc.v10.i18.6110 **Copyright** ©The Author(s) 2022.

Figure 1 Multiple erythematous papules can be detected on the patient's head, neck, chest and back (covering 30% of the total body skin).

not receive any antitumor treatment, the lesion remained stable.

DISCUSSION

Since the 21st century, the introduction of immunotherapy treatments has dramatically revolutionized the treatment paradigm of non-small-cell lung cancer (NSCLC)[16]. However, immune checkpoint inhibition usually leads to systemic adverse reactions, which are immune-related adverse events, mainly encompassing rash, colitis, pneumonitis, hepatitis, and thyroiditis[17]. Dermatologic toxicities seem to be the most frequently reported adverse events. SJS is a rare and severe dermatologic toxicity with high mortality[4]. The first SJS case induced by pembrolizumab in NSCLC was reported in a Japanese case[14]. Our case report is the first Chinese case of pembrolizumab-associated SJS in NSCLC.

At present, the exact mechanism of SJS remains undefined. The currently recognized theory is the T cell-mediated type IV delayed hypersensitivity reaction[18,19]. The drug triggering SJS binds the T cell receptor and MHC class I, and as a result, it leads to the massive replication of cytotoxic T cells, which



DOI: 10.12998/wjcc.v10.i18.6110 **Copyright** ©The Author(s) 2022.

Figure 2 The rash began to spread to almost all over the body (covering more than 45% of the total body skin).



DOI: 10.12998/wjcc.v10.i18.6110 **Copyright** ©The Author(s) 2022.

Figure 3 Cutaneous toxicities continued to worsen, and extensive skin ulceration was observed.

directly kill keratinocytes, and the release of granulysin, which destroys cells in the skin and the mucous membrane[20]. Yun-Shiuan's research showed that the blockade of PD-1/PD-L1 may contribute to the imbalance of the immune system, manifesting the enhancement of the T cell response and increasing the incidence of hypersensitivity[21]. During the treatment of SJS induced by ipilimumab and nivolumab in a melanoma patient[22], an increase in CD8+ T cells in the dermal epidermal junction and an increase in



DOI: 10.12998/wjcc.v10.i18.6110 **Copyright** ©The Author(s) 2022.

Figure 4 After a week of treatment, the dermatologic toxicities were gradually alleviated. A: The itchiness of the patient was significantly relieved, large blisters and ulcers basically disappeared; B: The dermis began to recover gradually.



DOI: 10.12998/wjcc.v10.i18.6110 **Copyright** ©The Author(s) 2022.

Figure 5 The patient recovered very well.

PD-L1 expression in keratinocytes were noted. Unfortunately, the biopsy analysis of our case has not been finished, and therefore, this viewpoint cannot be further confirmed. Overall, the mechanism of SJS caused by immunosuppressive drugs requires further research.

Cutaneous toxicities of immune checkpoint inhibitors might result in a longer PFS (progression-free survival) and a higher OS (overall survival) rate[23]. Bairavi and his colleagues demonstrated that NSCLC patients with one irAE and multisystem irAEs incrementally improved OS and PFS. Longer immune checkpoint inhibitor durations were an independent risk factor for the development of irAEs. In our case, it was rare that such severe AEs occurred after just one cycle of immunotherapy[24]. Susana also indicated that the median PFS was 9.49 mo in the group with irAEs *vs* 1.99 mo in the group without irAEs ($P < 0.0001$) in NSCLC treated with nivolumab[25]. In our case, the condition of the patient was stable for up to 6 mo just after one cycle of the treatment. Thus, we speculate that skin toxicities and delayed immunological effects both contributed to such a long progression-free survival time.

There is no standard treatment regimen for SJS[26], and multidisciplinary care, best supportive care, and corticosteroids are currently the most important components of its therapy[20]. By applying high-dose corticosteroids early, we can rapidly arrest SJS, while the optimal cutoff time of corticosteroids remains controversial because of its adverse drug reaction[27]. From the author's perspective, the appropriate duration of high-dose corticosteroids is within 4 wk. The combination of IVIG and steroids seems to bring better outcomes to patients with SJS[28].

In addition to corticosteroids and IVIG, drugs that suppress the immune response or inflammatory factors are also being tried in the treatment of SJS. Over the last several years, several retrospective trials have advocated the benefits of cyclosporine in the treatment of SJS/TEN[29,30]. Cyclosporine inhibits

the activation of CD4+ and CD8+ T cells in the early phase, subsequently inhibiting the secretion of granulysin, granzyme, and perforin[31]. Despite a lack of randomized control trials, cyclosporine has proven to have a mortality benefit in the treatment of SJS/TEN without a low risk of side effects. In our case, we did not use cyclosporine due to the lack of experience in the early phase of treatment for SJS. In the late phase, we used recombinant human tumor necrosis factor receptor type II-Fc fusion protein antibody as recommended by the dermatologist. The reason we used Sepprayi is that it can reduce the level of inflammatory factors, such as tumor necrosis factor-α (TNF-α), inhibiting the occurrence of hypersensitivity[32]. In our case, Sepprayi had a clear effect on the improvement of the patient's inflammatory response. However, more clinical practice and data support are needed due to limited trials.

CONCLUSION

Immunotherapy, as a new treatment in the 2010s, has a definite effect on the treatment of advanced lung cancer. However, there remain many difficulties to be overcome in the treatment of serious adverse reactions related to immunotherapy. The combination of high-dose corticosteroid shock therapy, IVIG, cyclosporine, and best supportive care might reduce mortality in the treatment of SJS. The incidence of serious immune-related skin toxicity, such as SJS, is low, but the lethality is still very high. However, there is still a long way to go for immune-related adverse events, such as predictors for adverse events and ways to prevent them in advance. In future studies, we might focus more on the prediction, prevention, and treatment of irAEs, although immunotherapy is in full swing.

FOOTNOTES

Author contributions: Wu JY and Kang K designed the study and performed the experiments; Yi J, Yang B, and Wu JY performed the experiments, analyzed the data, and wrote the manuscript; Wu JY and Kang K contributed to this article equally.

Informed consent statement: Consent was obtained from the patient for publication of this report.

Conflict-of-interest statement: The authors declare that they have no competing interests.

CARE Checklist (2016) statement: The authors have read the CARE Checklist (2016), and the manuscript was prepared and revised according to the CARE Checklist (2016).

Open-Access: This article is an open-access article that was selected by an in-house editor and fully peer-reviewed by external reviewers. It is distributed in accordance with the Creative Commons Attribution NonCommercial (CC BY-NC 4.0) license, which permits others to distribute, remix, adapt, build upon this work non-commercially, and license their derivative works on different terms, provided the original work is properly cited and the use is non-commercial. See: https://creativecommons.org/Licenses/by-nc/4.0/

Country/Territory of origin: China

ORCID number: Jing-Yi Wu 0000-0003-1886-5697; Kai Kang 0000-0002-0429-0346; Jing Yi 0000-0001-8040-9516; Bin Yang 0000-0002-2249-2590.

S-Editor: Liu JH
L-Editor: A
P-Editor: Liu JH

REFERENCES

1 **Garon EB**, Rizvi NA, Hui R, Leighl N, Balmanoukian AS, Eder JP, Patnaik A, Aggarwal C, Gubens M, Horn L, Carcereny E, Ahn MJ, Felip E, Lee JS, Hellmann MD, Hamid O, Goldman JW, Soria JC, Dolled-Filhart M, Rutledge RZ, Zhang J, Lunceford JK, Rangwala R, Lubiniecki GM, Roach C, Emancipator K, Gandhi L; KEYNOTE-001 Investigators. Pembrolizumab for the treatment of non-small-cell lung cancer. *N Engl J Med* 2015; **372**: 2018-2028 [PMID: 25891174 DOI: 10.1056/NEJMoa1501824]

2 **Kamińska-Winciorek G**, Cybulska-Stopa B, Lugowska I, Ziobro M, Rutkowski P. Principles of prophylactic and therapeutic management of skin toxicity during treatment with checkpoint inhibitors. *Postepy Dermatol Alergol* 2019; **36**: 382-391 [PMID: 31616210 DOI: 10.5114/ada.2018.80272]

3 **Micheletti RG**, Chiesa-Fuxench Z, Noe MH, Stephen S, Aleshin M, Agarwal A, Boggs J, Cardones AR, Chen JK, Cotliar J, Davis MDP, Dominguez A, Fox LP, Gordon S, Hamrick R, Ho B, Hughey LC, Jones LM, Kaffenberger BH, Kindley K, Kroshinsky D, Kwong BY, Miller DD, Mostaghimi A, Musiek A, Ortega-Loayza AG, Patel R, Posligua A, Rani M, Saluja

S, Sharon VR, Shinkai K, John JS, Strickland N, Summers EM, Sun N, Wanat KA, Wetter DA, Worswick S, Yang C, Margolis DJ, Gelfand JM, Rosenbach M. Stevens-Johnson Syndrome/Toxic Epidermal Necrolysis: A Multicenter Retrospective Study of 377 Adult Patients from the United States. *J Invest Dermatol* 2018; **138**: 2315-2321 [PMID: 29758282 DOI: 10.1016/j.jid.2018.04.027]

4 **Ma DH**, Tsai TY, Pan LY, Chen SY, Hsiao CH, Yeh LK, Tan HY, Lu CW, Chen CB, Chung WH. Clinical Aspects of Stevens-Johnson Syndrome/Toxic Epidermal Necrolysis With Severe Ocular Complications in Taiwan. *Front Med (Lausanne)* 2021; **8**: 661891 [PMID: 34055837 DOI: 10.3389/fmed.2021.661891]

5 **Xu Z**, Shen J, Yang Y, Yuan R, Xiang LF, Zhang C. Severe Cutaneous Adverse Reactions: A Single-Center Retrospective Study of 173 Patients in China. *Ann Dermatol* 2019; **31**: 545-554 [PMID: 33911647 DOI: 10.5021/ad.2019.31.5.545]

6 **Gracia-Cazaña T**, Padgett E, Calderero V, Oncins R. Nivolumab-associated Stevens-Johnson syndrome in a patient with lung cancer. *Dermatol Online J* 2021; **27** [PMID: 33865285 DOI: 10.5070/D3273052777]

7 **Logan IT**, Zaman S, Hussein L, Perrett CM. Combination Therapy of Ipilimumab and Nivolumab-associated Toxic Epidermal Necrolysis (TEN) in a Patient With Metastatic Melanoma: A Case Report and Literature Review. *J Immunother* 2020; **43**: 89-92 [PMID: 31651559 DOI: 10.1097/CJI.0000000000000302]

8 **Riano I**, Cristancho C, Treadwell T. Stevens-Johnson Syndrome-Like Reaction After Exposure to Pembrolizumab and Recombinant Zoster Vaccine in a Patient With Metastatic Lung Cancer. *J Investig Med High Impact Case Rep* 2020; **8**: 2324709620914796 [PMID: 32207346 DOI: 10.1177/2324709620914796]

9 **Robinson S**, Saleh J, Curry J, Mudaliar K. Pembrolizumab-Induced Stevens-Johnson Syndrome/Toxic Epidermal Necrolysis in a Patient With Metastatic Cervical Squamous Cell Carcinoma: A Case Report. *Am J Dermatopathol* 2020; **42**: 292-296 [PMID: 31567395 DOI: 10.1097/DAD.0000000000001527]

10 **Ryu S**, Jun I, Kim TI, Seo KY, Kim EK. Pembrolizumab-induced Stevens-Johnson Syndrome with Severe Ocular Complications. *Ocul Immunol Inflamm* 2021; 1-3 [PMID: 33826467 DOI: 10.1080/09273948.2021.1896006]

11 **Salati M**, Pifferi M, Baldessari C, Bertolini F, Tomasello C, Cascinu S, Barbieri F. Stevens-Johnson syndrome during nivolumab treatment of NSCLC. *Ann Oncol* 2018; **29**: 283-284 [PMID: 29045532 DOI: 10.1093/annonc/mdx640]

12 **Saw S**, Lee HY, Ng QS. Pembrolizumab-induced Stevens-Johnson syndrome in non-melanoma patients. *Eur J Cancer* 2017; **81**: 237-239 [PMID: 28438440 DOI: 10.1016/j.ejca.2017.03.026]

13 **Shibata A**, Yoshikawa T, Makita S, Nakagawa S, Ueda Y, Akiyama M. A case of recurrent Stevens-Johnson syndrome caused by nivolumab therapy. *Eur J Dermatol* 2019 [PMID: 31290394 DOI: 10.1684/ejd.2019.3550]

14 **Haratake N**, Tagawa T, Hirai F, Toyokawa G, Miyazaki R, Maehara Y. Stevens-Johnson Syndrome Induced by Pembrolizumab in a Lung Cancer Patient. *J Thorac Oncol* 2018; **13**: 1798-1799 [PMID: 29885481 DOI: 10.1016/j.jtho.2018.05.031]

15 **Maloney NJ**, Ravi V, Cheng K, Bach DQ, Worswick S. Stevens-Johnson syndrome and toxic epidermal necrolysis-like reactions to checkpoint inhibitors: a systematic review. *Int J Dermatol* 2020; **59**: e183-e188 [PMID: 32052409 DOI: 10.1111/ijd.14811]

16 **Horinouchi H**, Nogami N, Saka H, Nishio M, Tokito T, Takahashi T, Kasahara K, Hattori Y, Ichihara E, Adachi N, Noguchi K, Souza F, Kurata T. Pembrolizumab plus pemetrexed-platinum for metastatic nonsquamous non-small-cell lung cancer: KEYNOTE-189 Japan Study. *Cancer Sci* 2021; **112**: 3255-3265 [PMID: 34036692 DOI: 10.1111/cas.14980]

17 **Si X**, He C, Zhang L, Liu X, Li Y, Wang H, Guo X, Zhou J, Duan L, Wang M. Management of immune checkpoint inhibitor-related dermatologic adverse events. *Thorac Cancer* 2020; **11**: 488-492 [PMID: 31814310 DOI: 10.1111/1759-7714.13275]

18 **Ford M**, Sahbudin I, Filer A, Steven N, Fisher BA. High proportion of drug hypersensitivity reactions to sulfasalazine following its use in anti-PD-1-associated inflammatory arthritis. *Rheumatology (Oxford)* 2018; **57**: 2244-2246 [PMID: 30107548 DOI: 10.1093/rheumatology/key234]

19 **Venkateswaran N**, Khianey R, Generoso A. Stevens Johnson Syndrome in a Patient with Giant Cell Arteritis During Short Term Tocilizumab Therapy. *Cureus* 2020; **12**: e7662 [PMID: 32411563 DOI: 10.7759/cureus.7662]

20 **Charlton OA**, Harris V, Phan K, Mewton E, Jackson C, Cooper A. Toxic Epidermal Necrolysis and Steven-Johnson Syndrome: A Comprehensive Review. *Adv Wound Care (New Rochelle)* 2020; **9**: 426-439 [PMID: 32520664 DOI: 10.1089/wound.2019.0977]

21 **Hsu YO**, Lu KL, Fu Y, Wang CW, Lu CW, Lin YF, Chang WC, Yeh KY, Hung SI, Chung WH, Chen CB. The Roles of Immunoregulatory Networks in Severe Drug Hypersensitivity. *Front Immunol* 2021; **12**: 597761 [PMID: 33717075 DOI: 10.3389/fimmu.2021.597761]

22 **Vivar KL**, Deschaine M, Messina J, Divine JM, Rabionet A, Patel N, Harrington MA, Seminario-Vidal L. Epidermal programmed cell death-ligand 1 expression in TEN associated with nivolumab therapy. *J Cutan Pathol* 2017; **44**: 381-384 [PMID: 28000240 DOI: 10.1111/cup.12876]

23 **Wu Y**, Wu H, Lin M, Liu T, Li J. Factors associated with immunotherapy respond and survival in advanced non-small cell lung cancer patients. *Transl Oncol* 2022; **15**: 101268 [PMID: 34800914 DOI: 10.1016/j.tranon.2021.101268]

24 **de Zegher F**, Jaeken J. Endocrinology of the carbohydrate-deficient glycoprotein syndrome type 1 from birth through adolescence. *Pediatr Res* 1995; **37**: 395-401 [PMID: 7596677 DOI: 10.1001/jamaoncol.2020.5012]

25 **Cortijo-Cascajares S**, Cercós-Lletí AC, Ortiz-Pérez S, Caro-Teller JM, Ferrari-Piquero JM. Analysis of immune-mediated reactions in patients with non-small cell lung cancer treated with nivolumab and its association with effectiveness. *J Oncol Pharm Pract* 2021; 10781552211067429 [PMID: 34907812 DOI: 10.1177/10781552211067429]

26 **Park SY**, Oh IY, Kim JH, Kim HJ, Seo B, Kwon OY, Song WJ, Kwon HS, Cho YS, Moon HB, Kim TB. Therapeutic Effects of Mesenchymal Stem Cells on a Stevens-Johnson Syndrome/Toxic Epidermal Necrolysis Model. *J Korean Med Sci* 2020; **35**: e130 [PMID: 32301297 DOI: 10.3346/jkms.2020.35.e130]

27 **Lehloenya RJ**, Isaacs T, Nyika T, Dhana A, Knight L, Veenstra S, Peter J. Early high-dose intravenous corticosteroids rapidly arrest Stevens Johnson syndrome and drug reaction with eosinophilia and systemic symptoms recurrence on drug re-exposure. *J Allergy Clin Immunol Pract* 2021; **9**: 582-584.e1 [PMID: 32835874 DOI: 10.1016/j.jaip.2020.08.012]

28 **Liotti L**, Caimmi S, Bottau P, Bernardini R, Cardinale F, Saretta F, Mori F, Crisafulli G, Franceschini F, Caffarelli C. Clinical features, outcomes and treatment in children with drug induced Stevens-Johnson syndrome and toxic epidermal

necrolysis. *Acta Biomed* 2019; **90**: 52-60 [PMID: 30830062 DOI: 10.23750/abm.v90i3-S.8165]
29 **Shokeen D**. Cyclosporine in SJS/TEN management: a brief review. *Cutis* 2016; **97**: E17-E18 [PMID: 27023091]
30 **Gilbert M**, Scherrer LA. Efficacy and safety of cyclosporine in Stevens-Johnson syndrome and toxic epidermal necrolysis. *Dermatol Ther* 2019; **32**: e12758 [PMID: 30285308 DOI: 10.1111/dth.12758]
31 **González-Herrada C**, Rodríguez-Martín S, Cachafeiro L, Lerma V, González O, Lorente JA, Rodríguez-Miguel A, González-Ramos J, Roustan G, Ramírez E, Bellón T, de Abajo FJ; PIELenRed Therapeutic Management Working Group. Cyclosporine Use in Epidermal Necrolysis Is Associated with an Important Mortality Reduction: Evidence from Three Different Approaches. *J Invest Dermatol* 2017; **137**: 2092-2100 [PMID: 28634032 DOI: 10.1016/j.jid.2017.05.022]
32 **Li L**, Zhang X, Cui Y, Lu YY, Wang SX, Dong GF, Shi YZ, Luo RQ, Lei YX. [Effect of recombinant human tumor necrosis factor receptor type II-Fc fusion protein antibody on cytokines and bone metabolism in patients with juvenile idiopathic arthritis]. *Zhonghua Yi Xue Za Zhi* 2010; **90**: 2205-2208 [PMID: 21029662]

World Journal of Clinical Cases

Submit a Manuscript: https://www.f6publishing.com

World J Clin Cases 2022 June 26; 10(18): 6119-6127

DOI: 10.12998/wjcc.v10.i18.6119

ISSN 2307-8960 (online)

CASE REPORT

Hepatic epithelioid hemangioendothelioma after thirteen years' follow-up: A case report and review of literature

Wei-Fang Mo, Yu-Ling Tong

Specialty type: Gastroenterology and hepatology

Provenance and peer review: Unsolicited article; Externally peer reviewed.

Peer-review model: Single blind

Peer-review report's scientific quality classification

Grade A (Excellent): 0
Grade B (Very good): 0
Grade C (Good): C, C
Grade D (Fair): 0
Grade E (Poor): 0

P-Reviewer: Mohey NM, Egypt; Yang M, China

Received: November 25, 2021
Peer-review started: November 25, 2021
First decision: January 12, 2022
Revised: January 24, 2022
Accepted: April 22, 2022
Article in press: April 22, 2022
Published online: June 26, 2022

Wei-Fang Mo, Yu-Ling Tong, Department of General Practice, The 2nd Affiliated Hospital of Zhejiang University, School of Medicine, Hangzhou 310009, Zhejiang Province,China

Corresponding author: Yu-Ling Tong, Doctor, Assistant Professor, Department of General Practice, The 2nd Affiliated Hospital of Zhejiang University, School of Medicine, No. 88 Jiefang Road, Hangzhou 310009, Zhejiang Province, China. tongyl0313@zju.edu.cn

Abstract

BACKGROUND

Hepatic epithelioid hemangioendothelioma (EHE) is a rare vascular endothelial cell tumor of the liver, consisting of epithelioid and histiocyte-like vascular endothelial cells in mucus or a fibrotic matrix. Immunohistochemistry is usually positive for vascular markers, such as factor VIII-related antigen, CD31, and CD34. Hepatic EHE can have a varied clinical course; treatment includes liver transplantation, liver resection, chemotherapy, and radiation therapy.

CASE SUMMARY

A 46-year-old woman with abdominal discomfort and elevated serum carcinoembryonic antigen was found to have multiple low-density lesions in the liver and lung on computed tomography (CT) evaluation. An ultrasound-guided fine needle aspiration biopsy revealed a fibrous stroma with dendritic cells, containing intracellular vacuoles. Immunohistochemical staining found that the tumor cells were positive for CD34, CD31, and factor VIII-related antigen. The patient received four courses of combined chemotherapy and was followed-up for 13 years, at which time the patient was in stable condition without disease progression and a confined neoplasm, as evidenced by CT scans.

CONCLUSION

The histology and immunohistochemical characteristics of hepatic EHE are well described. Chemotherapy may be effective in patients with extrahepatic lesions.

Key Words: Epithelioid hemangioendothelioma; Liver neoplasm; Immunohistochemistry; Antineoplastic combined chemotherapy protocols; Treatment; Case report

©The Author(s) 2022. Published by Baishideng Publishing Group Inc. All rights reserved.

Core Tip: The gold standard diagnosis for hepatic epithelioid hemangioendothelioma includes epithelioid and histiocyte-like vascular endothelial cells in mucus or a fibrotic matrix, and positive vascular markers. Chemotherapy may be an effective treatment; close follow-up is necessary.

Citation: Mo WF, Tong YL. Hepatic epithelioid hemangioendothelioma after thirteen years' follow-up: A case report and review of literature. *World J Clin Cases* 2022; 10(18): 6119-6127
URL: https://www.wjgnet.com/2307-8960/full/v10/i18/6119.htm
DOI: https://dx.doi.org/10.12998/wjcc.v10.i18.6119

INTRODUCTION

Hepatic epithelioid hemangioendothelioma (EHE) is a rare malignant tumor of vascular origin, with an incidence of 0.1-0.2/100000[1,2]. Oral contraceptives, polyvinyl chloride, asbestos, thorotrast contrast medium, hepatic trauma, and viral hepatitis have been identified as risk factors for subsequent development of disease[3]. While laboratory findings always reveal abnormal liver function, tumor markers are always at normal levels. The patient described in this case report had a history of hepatitis A and normal liver function, but with a mildly elevated tumor marker [carcinoembryonic antigen (CEA) at 6.9 ng/mL]. The patient received four courses of chemotherapy and was found to remain in stable condition after 13 years of follow-up.

CASE PRESENTATION

Chief complaints

A 46-year-old woman with no significant past medical history presented at the hospital with a 1-mo history of epigastric discomfort and asthenia.

History of present illness

The patient had no other symptoms.

History of past illness

The patient had a history of acute hepatitis that had resolved without complications 20 years previously.

Personal and family history

The patient had no personal or family history of other diseases.

Physical examination

Physical examination revealed no remarkable findings.

Laboratory examinations

Laboratory testing on admission showed no abnormalities in markers of inflammation or abnormal liver function, or in peripheral blood panel or biochemical tests. Hepatitis B surface antigen (HBsAg), hepatitis B core antibody (HBcAb) and hepatitis C virus antibody (HCVAb) were negative. Tumor markers were in the normal ranges, except for a mildly elevated CEA (6.9 ng/mL; normal range: 0-5.0 ng/mL).

Imaging examinations

Abdominal ultrasound revealed multiple irregular hypoechoic lesions in the liver. Color doppler flow imaging showed spots of avascular reflective material. Contrast-enhanced computed tomography (CT) showed multiple low-density lesions in the right lobe of the liver. The largest was located in segment 8 and was 2.9 cm, 2.3 cm. Some lesions had mild-moderate enhancement during the arterial contrast-enhanced phase. The density was lower than the normal liver parenchyma during the portal vein and lag phase (Figure 1). Magnetic resonance (MR) T1-weighted images showed multiple low signal ovoid lesions in the right lobe of the liver that had a high signal on T2-weighted images (Figure 2). Chest X-rays yielded no remarkable findings. Ultrasound revealed enlarged bilateral lymph nodes in the neck, axilla, and groin.

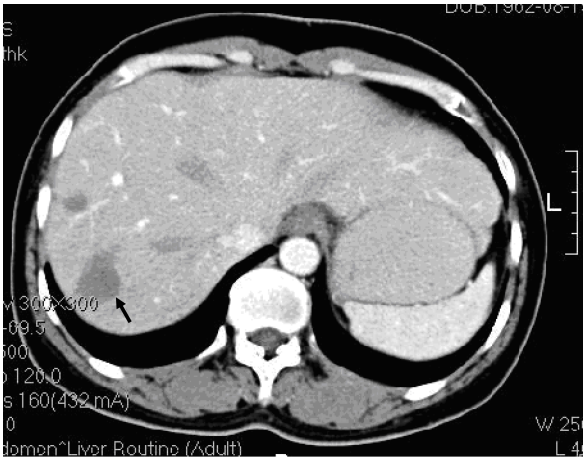

DOI: 10.12998/wjcc.v10.i18.6119 **Copyright** ©The Author(s) 2022.

Figure 1 Contrast-enhanced computed tomography. Multiple low-density lesions (black arrow) with mild-moderate peripheral enhancement are seen in the right lobe of the liver.

LABORATORY EXAMINATIONS

Laboratory testing on admission showed no abnormalities in markers of inflammation or abnormal liver function, or in peripheral blood panel or biochemical tests. HBsAg, HBcAb and HCVAb were negative. Tumor markers were in the normal ranges, except for a mildly elevated CEA (6.9 ng/mL; normal range: 0-5.0 ng/mL).

FINAL DIAGNOSIS

An ultrasound-guided fine needle aspiration biopsy revealed few hepatocytes and fibrous tissue with mildly heteromorphic spindle cell (dendritic cell) infiltration. The neoplastic cells were medium to large, with eosinophilic cytoplasm and vesicular nuclei having small, inconspicuous nucleoli. Signet ring cell-like structures were seen with intracytoplasmic lumina, occasionally containing red blood cells (Figure 3). Immunohistochemical staining indicated that the tumor cells were positive for CD31 (H12164PD590, EuroBioscience), CD34 (H12166F, EuroBioscience), and factor VIII-related antigen (FVIII-RAG, BH0012044, Goybio) (Figure 4A-C), while cells were negative for Pan Cytokeratin (CK+AFs-AE1/AE3+AF0-) (PD00330, Dako) (Figure 4D). Other results were lysozyme+-, P53+-/+ACY-ndash+ADs-, vimentin+-, EMA+-, CK8+ACY-ndash+ADs-, AFP+ACY-ndash+ADs-, CK18+ACY-ndash+ADs-, hepatocyte+ACY-minus+ADs-, CK20+ACY-minus+ADs-, and CD68+ACY-minus+ADs-,which weren't been shown in this article. Immunohistochemical staining results revealed evidence of+ACY-nbsp+ADs- endothelial differentiation, and consistent with hepatic epithelioid hemangioendothelioma (EHE).

TREATMENT

During the patient's hospital stay, she was given four cycles of combined chemotherapy with ifosfamide, cisplatin, epirubicin and recombinant human (rh) endostatin (Endostar; Simcere, Nanjing, China) injection.

OUTCOME AND FOLLOW-UP

After 13 years of follow-up, the patient remains in stable condition. A repeated CT scan found that the size of the lesions had not changed (Figure 5) and her liver function was normal.

DISCUSSION

Hepatic EHE is a rare tumor of vascular origin, with an incidence of 0.1-0.2/100000[1,2]. Fewer than 600 cases involving the liver are available in the literature, and it was first reported by Ishak *et al*[4] in 1984.

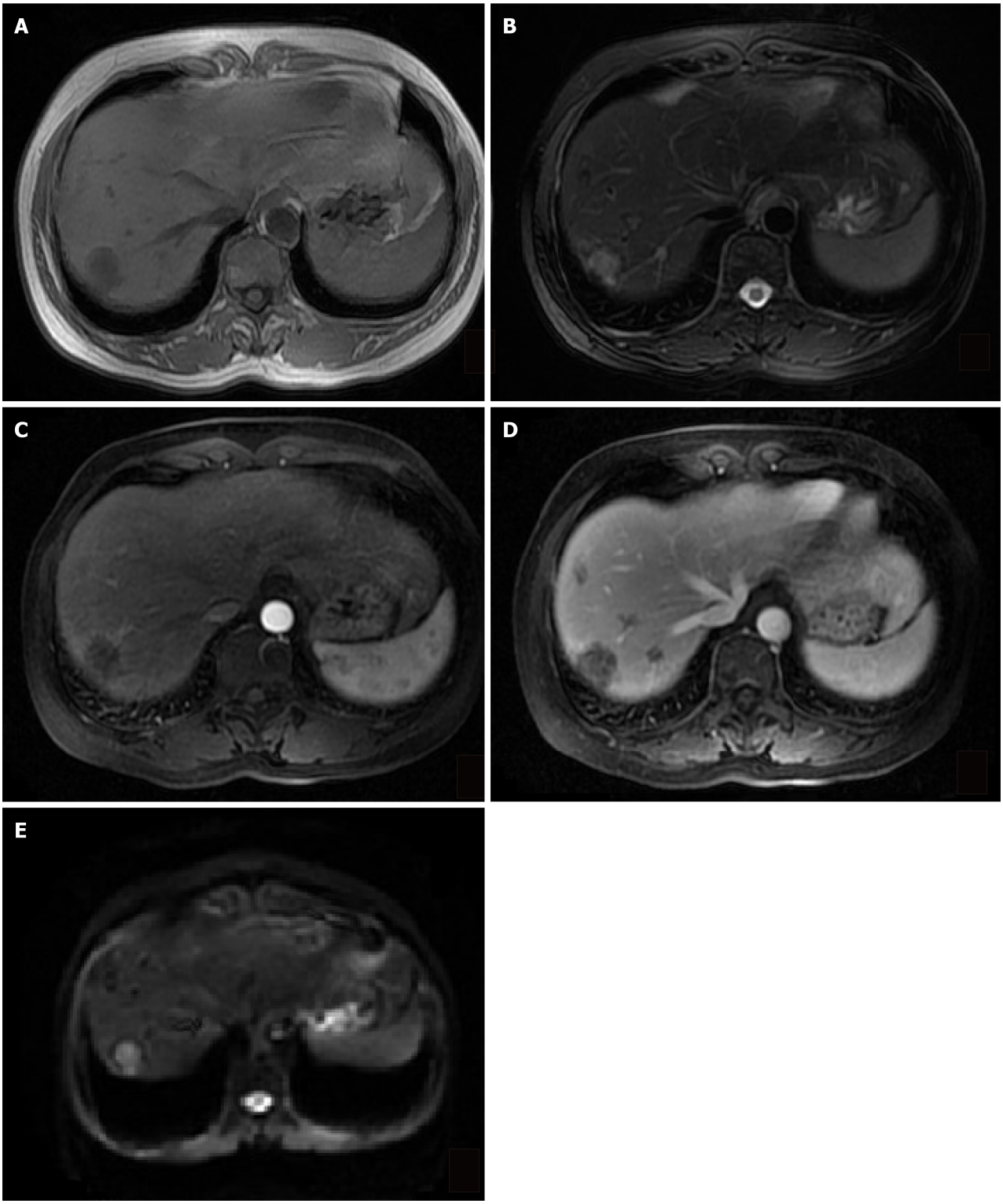

DOI: 10.12998/wjcc.v10.i18.6119 **Copyright** ©The Author(s) 2022.

Figure 2 Magnetic resonance weighted image. A: T1-weighted image shows low signal ovoid lesions in the right lobe of liver; B: The lesions have a heterogeneous high signal in the T2-weighted image; C: The largest lesion in the right lobe is mildly heterogeneous with peripheral enhancement and an arterial contrast enhancement pattern; D: Peripheral enhancement of lesions is increased in spots visible in a venous contrast enhancement pattern; E: Lesions show diffusion restriction on a diffusion-weighted image.

Hepatic EHE is as a low-to-moderate grade tumor with a malignant potential intermediate between hemangioma and hemangiosarcoma[4]. Its metastasis rate is 27%-45% and the most common tissues of origin are the lungs (81%) and celiac lymph nodes (39%)[1]. The median age has been reported as 41.7 years, with a female predominance of 3:2[3], and the clinical manifestations are variable. The most frequent symptoms are right upper quadrant pain (48.6%), hepatomegaly (20.4%), and a constitutional syndrome with progressive liver damage and weight loss (15.6%)[3]. Some patients present with Budd-

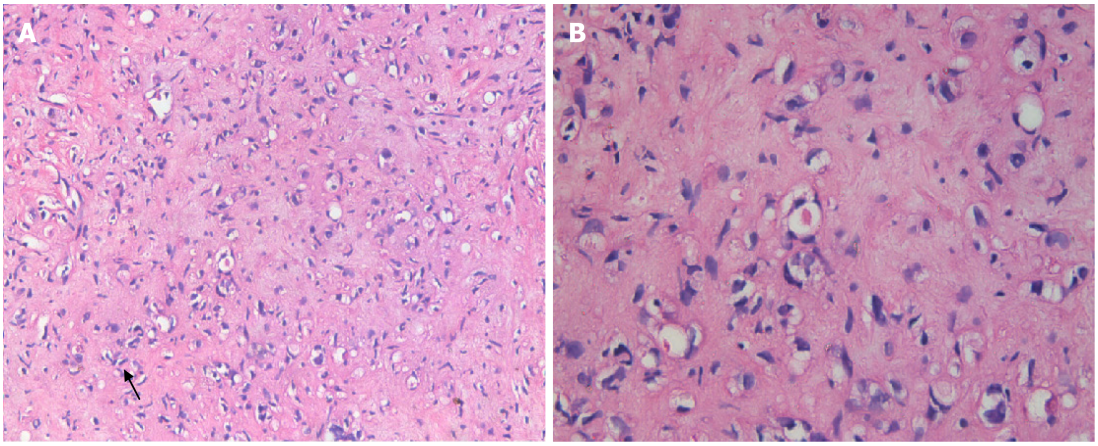

DOI: 10.12998/wjcc.v10.i18.6119 **Copyright** ©The Author(s) 2022.

Figure 3 Liver biopsy. A: Mildly heteromorphic spindle cells (dendritic cells) with interdigitating processes (hematoxylin and eosin, 200 ×); B: Intracellular vascular lumina containing a red blood cell (black arrow) (hematoxylin and eosin, 400 ×).

Chiari syndrome or liver failure, while others present with incidental findings[1,5]. Laboratory findings may reveal abnormal liver function. Nearly 75% of patients have elevated alkaline phosphatase (AKP), 2.7% have elevated alpha-fetoprotein (AFP), and 18.8% have elevated serum CEA[1,3]. Our patient had good liver function, with normal AKP, AST, ALT, and AFP. Her CEA was elevated but other markers were in their normal ranges. Oral contraceptives, polyvinyl chloride, asbestos, thorotrast contrast agent, and hepatic trauma have been identified as risk factors for subsequent disease development[3], and viral hepatitis is considered as an etiology[1,4,6]. This patient had a history of viral hepatitis A, but it had resolved without complication 20 years before she presented with hepatic EHE, making a viral etiology implausible. Because of its nonspecific manifestation, the diagnosis of hepatic EHE depends mainly on radiology and histopathology.

Most lesions are peripheral, extending to the capsular margin and are frequently hypoechoic with heterogeneous internal architecture on sonography[7,8]. On CT, lesions are almost hypodense with peripheral contrast enhancement[7,9-11]. Capsular retraction adjacent to the mass is seen in fewer than 25% of patients[9,12]. On MR, T1-weighted images of lesions frequently have a low signal and T2-weighted images have heterogeneous-increased signals. Peripheral enhancement with a thin nonenhancing rim corresponding to a narrow vascular zone can be seen with arterial contrast[7,11-13]. A lollipop sign, which is indicative of hepatic or portal veins terminating at or just within the periphery of lesions, seems to be specific for hepatic EHE[14]. The mean apparent diffusion coefficients of lesions were found to be high compared with other hepatic malignancies, which may be helpful in suggesting the diagnosis[15]. MR appears to be superior to CT, and MR with contrast may be important.

Pathologic diagnosis depends on the vascular nature of the tumor. Histologically, it is comprised of a fibrous stroma with myxohyaline areas including dendritic and epithelioid cells, often with intracellular vacuoles[1,4]. Immunohistochemical staining is positive for the expression of endothelial antigens, such as FVIII-RAG (98%), CD34 (94%), or CD31 (86%), and negative for epithelial markers[1,6]. This tumor was CD34+, vimentin+, and CD31+, and negative for epithelial markers like CK (AE1/AE3) and CK18. Podoplanin was shown to be specifically expressed in hepatic EHE (78%), and may be useful as a diagnostic marker of EHE in liver tumors[9]. Characteristic ultrastructural features include investing basal lamina, cytoplasmic intermediate filaments, Weibel–Palade bodies, and pinocytotic vesicles[4]. High cellularity, more than mitotic count, predicts an unfavorable prognosis[1,3,4]. A recent study reported that these tumors often have t(1;3) (p36.3; q25) translocations, resulting in WWTR1-CAMTA1 fusion[16]. YAP 1-TFE3 fusions have also been identified in about 10% of patients[17].

Treatment options are limited by the rarity of the tumor and currently include liver transplantation (44.8%), chemotherapy or radiotherapy (21.0%), and liver resection (9.4%), with 24.8% of patients receiving no treatment[3]. Complete liver resection should be performed if possible, but the multicentric origin of the tumor and multinodular growth make that difficult to accomplish[18]. Liver transplantation is an effective treatment for patients who are not candidates for resective surgery and those with extrahepatic manifestations or progressive liver failure[19,20]. Hepatic EHE is not sensitive to radiotherapy or chemotherapy, but some studies have found that 5-fluorouracil, doxorubicin, thalidomide, and interferon were effective[14,21,22] One-year survivals following liver transplantation, without treatment, radiotherapy or chemotherapy, and liver resection have been reported as 96%, 39.3%, 73.3%, and 100%. The corresponding 5-year rates were 54.5%, 4.5%, 30%, and 75%[3]. Hepatic EHE is of vascular origin, vascular endothelial growth (VEGF) receptors have been detected in EHE tumor cells, and VEGF has a role in tumor growth[23]. Combination treatment anti-VEGF drugs and cell cycle inhibitors, such as bevacizumab and capecitabine[24,25], pegylated liposomal doxorubicin[26], and metronomic cyclophosphaide[27] have been effective. For patients with extrahepatic lesions, it has

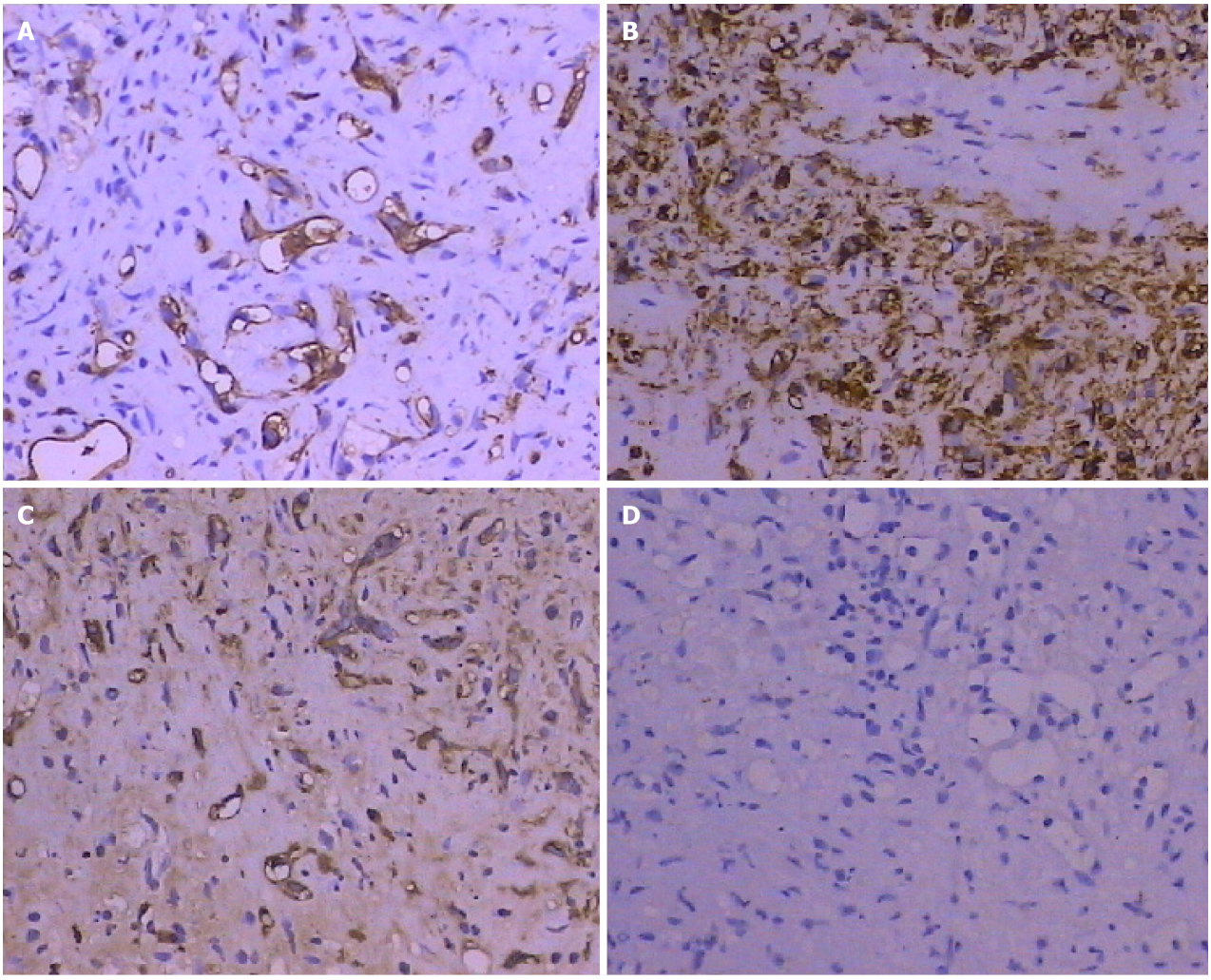

DOI: 10.12998/wjcc.v10.i18.6119 **Copyright** ©The Author(s) 2022.

Figure 4 Histopathology, immunostaining of tumor cells. A: Anti-CD31+ (200 ×); B: Anti-CD34+ (200 ×); C: Anti-factor VIII-related antigen+ (200 ×); D: Anti-CK− (Pan) (200 ×).

been reported that adjuvant chemotherapy may prevent recurrence[28].

Because the disease was multifocal in our patient, orthotopic liver transplantation may have been justified as a curative procedure. Unfortunately, a donor shortage and cost limitations made immediate transplantation unrealistic. Consequently, we choose to treat her with combined chemotherapy that included ifosfamide, cisplatin, epirubicin and rh-endostatin. rh-endostatin is purified in an *Escherichia coli* system, with an additional nine amino acid sequence of soluble protein[29]. It targets neovascular endothelial cells and has antiangiogenetic and antitumor activity. Preclinical and clinical studies showed synergistic effects of rh-endostatin and other agents that inhibit the growth of malignant tumors, with minimal toxicity[30-32]. A review by Xu *et al*[33] suggests that the combination of rh-endostatin with chemotherapy, radiotherapy, and biotherapy (*i.e.* fusion protein, or molecular-targeted therapy on cancers, *etc.*) may be the optimal strategy for cancer treatment[33]. Ling *et al*[34] reported that the antiangiogenic activity of rh-endostatin was mediated *in vitro* and *in vivo* by blocking VEGF-induced tyrosine phosphorylation of KDR/Flk-1 in endothelial cells. The vascular nature and endothelial origin of our patient's tumor led us to choose rh-endostatin for her treatment. To date, the size of her lesions has not increased, and the patient is in stable condition with normal liver function. The patient is followed-up regularly, and liver transplantation is still recommended.

CONCLUSION

In conclusion, hepatic EHE is a rare tumor, and its atypical symptoms and varied radiographic appearance make it hard to differentiate from other tumors. Diagnosis depends on histopathology. Liver resection is the treatment of choice in patients with resectable lesions, and liver transplantation is justified as a curative procedure for multinodular disease. Donor shortage and a long waiting time,

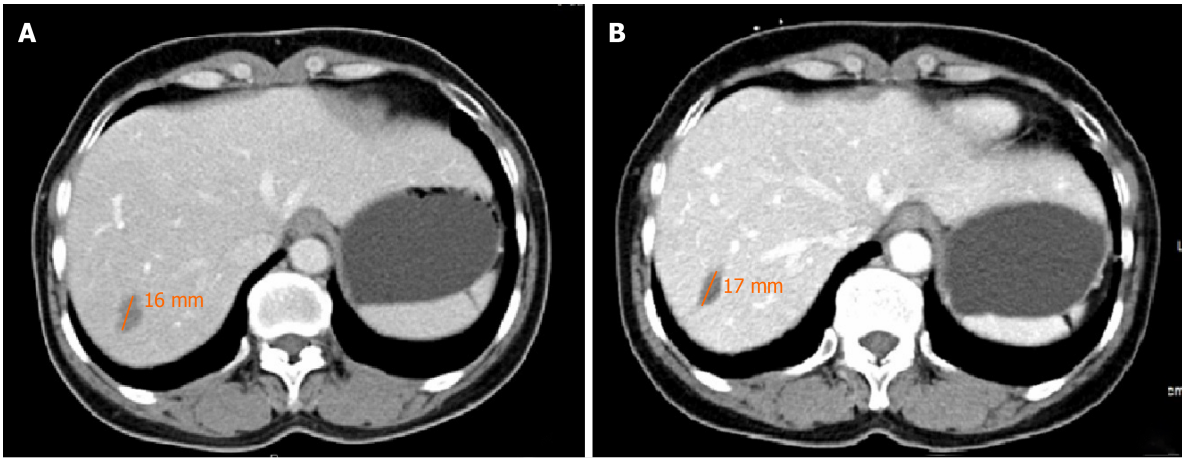

DOI: 10.12998/wjcc.v10.i18.6119 **Copyright** ©The Author(s) 2022.

Figure 5 Contrast-enhanced follow-up computed tomography scans. A: After 4 years, diameter of the low-density lesion was 16 mm; B: After 12 years, diameter of the low-density lesion was 17 mm.

among other reasons, limit the use of liver transplantation. Chemotherapy including rh-endostatin may increase the effectiveness of hepatic EHE treatment. The focus is on its therapeutic efficacy while awaiting a suitable donor liver and for patients with extrahepatic manifestations. Further research is needed.

FOOTNOTES

Author contributions: Mo WF collected the data and wrote the manuscript; Tong YL designed the report; all authors have read and approve the final manuscript.

Supported by Zhejiang Medical and Health Science and Technology Project, No. 2021429795; and Scientific Research Project of Zhejiang Education Department, No. Y202043306.

Informed consent statement: Consent was obtained from the patient, who signed a written informed consent for publication of this case report.

Conflict-of-interest statement: The authors declare that they have no competing interests.

CARE Checklist (2016) statement: The authors have read the CARE Checklist (2016), and the manuscript was prepared and revised according to the CARE Checklist (2016).

Open-Access: This article is an open-access article that was selected by an in-house editor and fully peer-reviewed by external reviewers. It is distributed in accordance with the Creative Commons Attribution NonCommercial (CC BY-NC 4.0) license, which permits others to distribute, remix, adapt, build upon this work non-commercially, and license their derivative works on different terms, provided the original work is properly cited and the use is non-commercial. See: https://creativecommons.org/Licenses/by-nc/4.0/

Country/Territory of origin: China

ORCID number: Wei-Fang Mo 0000-0003-4286-3229; Yu-Ling Tong 0000-0002-3772-9327.

S-Editor: Xing YX
L-Editor: A
P-Editor: Xing YX

REFERENCES

1 **Makhlouf HR**, Ishak KG, Goodman ZD. Epithelioid hemangioendothelioma of the liver: a clinicopathologic study of 137 cases. *Cancer* 1999; **85**: 562-582 [PMID: 10091730 DOI: 10.1002/(sici)1097-0142(19990201)85:3<562::aid-cncr7>3.0.co;2-t]

2 **Elleuch N**, Dahmani W, Aida Ben S, Jaziri H, Aya H, Ksiaa M, Jmaa A. Hepatic epithelioid hemangioendothelioma: A misdiagnosed rare liver tumor. *Presse Med* 2018; **47**: 182-185 [PMID: 29373279 DOI: 10.1016/j.lpm.2017.10.026]

3 **Mehrabi A**, Kashfi A, Fonouni H, Schemmer P, Schmied BM, Hallscheidt P, Schirmacher P, Weitz J, Friess H, Buchler MW, Schmidt J. Primary malignant hepatic epithelioid hemangioendothelioma: a comprehensive review of the literature with emphasis on the surgical therapy. *Cancer* 2006; **107**: 2108-2121 [PMID: 17019735 DOI: 10.1002/cncr.22225]

4 **Ishak KG**, Sesterhenn IA, Goodman ZD, Rabin L, Stromeyer FW. Epithelioid hemangioendothelioma of the liver: a clinicopathologic and follow-up study of 32 cases. *Hum Pathol* 1984; **15**: 839-852 [PMID: 6088383 DOI: 10.1016/s0046-8177(84)80145-8]

5 **Uchimura K**, Nakamuta M, Osoegawa M, Takeaki S, Nishi H, Iwamoto H, Enjoji M, Nawata H. Hepatic epithelioid hemangioendothelioma. *J Clin Gastroenterol* 2001; **32**: 431-434 [PMID: 11319317 DOI: 10.1097/00004836-200105000-00015]

6 **Demetris AJ**, Minervini M, Raikow RB, Lee RG. Hepatic epithelioid hemangioendothelioma: biological questions based on pattern of recurrence in an allograft and tumor immunophenotype. *Am J Surg Pathol* 1997; **21**: 263-270 [PMID: 9060595 DOI: 10.1097/00000478-199703000-00001]

7 **Lyburn ID**, Torreggiani WC, Harris AC, Zwirewich CV, Buckley AR, Davis JE, Chung SW, Scudamore CH, Ho SG. Hepatic epithelioid hemangioendothelioma: sonographic, CT, and MR imaging appearances. *AJR Am J Roentgenol* 2003; **180**: 1359-1364 [PMID: 12704052 DOI: 10.2214/ajr.180.5.1801359]

8 **Radin DR**, Craig JR, Colletti PM, Ralls PW, Halls JM. Hepatic epithelioid hemangioendothelioma. *Radiology* 1988; **169**: 145-148 [PMID: 3420251 DOI: 10.1148/radiology.169.1.3420251]

9 **Amin S**, Chung H, Jha R. Hepatic epithelioid hemangioendothelioma: MR imaging findings. *Abdom Imaging* 2011; **36**: 407-414 [PMID: 21079951 DOI: 10.1007/s00261-010-9662-0]

10 **Miller WJ**, Dodd GD 3rd, Federle MP, Baron RL. Epithelioid hemangioendothelioma of the liver: imaging findings with pathologic correlation. *AJR Am J Roentgenol* 1992; **159**: 53-57 [PMID: 1302463 DOI: 10.2214/ajr.159.1.1302463]

11 **Fulcher AS**, Sterling RK. Hepatic neoplasms: computed tomography and magnetic resonance features. *J Clin Gastroenterol* 2002; **34**: 463-471 [PMID: 11907365 DOI: 10.1097/00004836-200204000-00019]

12 **Hayashi Y**, Inagaki K, Hirota S, Yoshikawa T, Ikawa H. Epithelioid hemangioendothelioma with marked liver deformity and secondary Budd-Chiari syndrome: pathological and radiological correlation. *Pathol Int* 1999; **49**: 547-552 [PMID: 10469398 DOI: 10.1046/j.1440-1827.1999.00906.x]

13 **Van Beers B**, Roche A, Mathieu D, Menu Y, Delos M, Otte JB, Lalonde L, Pringot J. Epithelioid hemangioendothelioma of the liver: MR and CT findings. *J Comput Assist Tomogr* 1992; **16**: 420-424 [PMID: 1592925 DOI: 10.1097/00004728-199205000-00014]

14 **Alomari AI**. The lollipop sign: a new cross-sectional sign of hepatic epithelioid hemangioendothelioma. *Eur J Radiol* 2006; **59**: 460-464 [PMID: 16644166 DOI: 10.1016/j.ejrad.2006.03.022]

15 **Bruegel M**, Muenzel D, Waldt S, Specht K, Rummeny EJ. Hepatic epithelioid hemangioendothelioma: findings at CT and MRI including preliminary observations at diffusion-weighted echo-planar imaging. *Abdom Imaging* 2011; **36**: 415-424 [PMID: 20730424 DOI: 10.1007/s00261-010-9641-5]

16 **Doyle LA**, Fletcher CD, Hornick JL. Nuclear Expression of CAMTA1 Distinguishes Epithelioid Hemangioendothelioma From Histologic Mimics. *Am J Surg Pathol* 2016; **40**: 94-102 [PMID: 26414223 DOI: 10.1097/PAS.0000000000000511]

17 **Lotfalla MM**, Folpe AL, Fritchie KJ, Greipp PT, Galliano GG, Halling KC, Mounajjed T, Torres-Mora J, Graham RP. Hepatic *YAP1-TFE3* Rearranged Epithelioid Hemangioendothelioma. *Case Rep Gastrointest Med* 2019; **2019**: 7530845 [PMID: 31341686 DOI: 10.1155/2019/7530845]

18 **Haydon E**, Haydon G, Bramhall S, Mayer AD, Niel D. Hepatic epithelioid haemangioendothelioma. *J R Soc Med* 2005; **98**: 364-365 [PMID: 16055903 DOI: 10.1258/jrsm.98.8.364]

19 **Lerut JP**, Orlando G, Sempoux C, Ciccarelli O, Van Beers BE, Danse E, Horsmans Y, Rahier J, Roggen F. Hepatic haemangioendothelioma in adults: excellent outcome following liver transplantation. *Transpl Int* 2004; **17**: 202-207 [PMID: 15114438 DOI: 10.1007/s00147-004-0697-4]

20 **Nissen NN**, Cavazzoni E, Tran TT, Poordad FP. Emerging role of transplantation for primary liver cancers. *Cancer J* 2004; **10**: 88-96 [PMID: 15130268 DOI: 10.1097/00130404-200403000-00004]

21 **Bancel B**, Patricot LM, Caillon P, Ducerf C, Pouyet M. [Hepatic epithelioid hemangioendothelioma. A case with liver transplantation. Review of the literature]. *Ann Pathol* 1993; **13**: 23-28 [PMID: 8489646]

22 **Galvão FH**, Bakonyi-Neto A, Machado MA, Farias AQ, Mello ES, Diz ME, Machado MC. Interferon alpha-2B and liver resection to treat multifocal hepatic epithelioid hemangioendothelioma: a relevant approach to avoid liver transplantation. *Transplant Proc* 2005; **37**: 4354-4358 [PMID: 16387119 DOI: 10.1016/j.transproceed.2005.11.022]

23 **Kou K**, Chen YG, Zhou JP, Sun XD, Sun DW, Li SX, Lv GY. Hepatic epithelioid hemangioendothelioma: Update on diagnosis and therapy. *World J Clin Cases* 2020; **8**: 3978-3987 [PMID: 33024754 DOI: 10.12998/wjcc.v8.i18.3978]

24 **Treska V**, Daum O, Svajdler M, Liska V, Ferda J, Baxa J. Hepatic Epithelioid Hemangioendothelioma - a Rare Tumor and Diagnostic Dilemma. *In Vivo* 2017; **31**: 763-767 [PMID: 28652454 DOI: 10.21873/invivo.11128]

25 **Lau A**, Malangone S, Green M, Badari A, Clarke K, Elquza E. Combination capecitabine and bevacizumab in the treatment of metastatic hepatic epithelioid hemangioendothelioma. *Ther Adv Med Oncol* 2015; **7**: 229-236 [PMID: 26136854 DOI: 10.1177/1758834015582206]

26 **Grenader T**, Vernea F, Reinus C, Gabizon A. Malignant epithelioid hemangioendothelioma of the liver successfully treated with pegylated liposomal doxorubicin. *J Clin Oncol* 2011; **29**: e722-e724 [PMID: 21788568 DOI: 10.1200/JCO.2011.35.5891]

27 **Lakkis Z**, Kim S, Delabrousse E, Jary M, Nguyen T, Mantion G, Heyd B, Lassabe C, Borg C. Metronomic cyclophosphamide: an alternative treatment for hepatic epithelioid hemangioendothelioma. *J Hepatol* 2013; **58**: 1254-1257 [PMID: 23402747 DOI: 10.1016/j.jhep.2013.01.043]

28 **Tan Y**, Yang X, Dong C, Xiao Z, Zhang H, Wang Y. Diffuse hepatic epithelioid hemangioendothelioma with multiple splenic metastasis and delayed multifocal bone metastasis after liver transplantation on FDG PET/CT images: A case report. *Medicine (Baltimore)* 2018; **97**: e10728 [PMID: 29851777 DOI: 10.1097/MD.0000000000010728]

29 **Han Q**, Fu Y, Zhou H, He Y, Luo Y. Contributions of Zn(II)-binding to the structural stability of endostatin. *FEBS Lett* 2007; **581**: 3027-3032 [PMID: 17544408 DOI: 10.1016/j.febslet.2007.05.058]

30 **Hanna NN**, Seetharam S, Mauceri HJ, Beckett MA, Jaskowiak NT, Salloum RM, Hari D, Dhanabal M, Ramchandran R, Kalluri R, Sukhatme VP, Kufe DW, Weichselbaum RR. Antitumor interaction of short-course endostatin and ionizing radiation. *Cancer J* 2000; **6**: 287-293 [PMID: 11079167 DOI: 10.1007/s002620000128]

31 **Plum SM**, Hanson AD, Volker KM, Vu HA, Sim BK, Fogler WE, Fortier AH. Synergistic activity of recombinant human endostatin in combination with adriamycin: analysis of *in vitro* activity on endothelial cells and *in vivo* tumor progression in an orthotopic murine mammary carcinoma model. *Clin Cancer Res* 2003; **9**: 4619-4626 [PMID: 14555538 DOI: 10.1093/carcin/bgg164]

32 **Sun L**, Ye HY, Zhang YH, Guan YS, Wu H. Epidermal growth factor receptor antibody plus recombinant human endostatin in treatment of hepatic metastases after remnant gastric cancer resection. *World J Gastroenterol* 2007; **13**: 6115-6118 [PMID: 18023113 DOI: 10.3748/wjg.v13.45.6115]

33 **Xu F**, Ma Q, Sha H. Optimizing drug delivery for enhancing therapeutic efficacy of recombinant human endostatin in cancer treatment. *Crit Rev Ther Drug Carrier Syst* 2007; **24**: 445-492 [PMID: 18197781 DOI: 10.1615/critrevtherdrugcarriersyst.v24.i5.20]

34 **Ling Y**, Yang Y, Lu N, You QD, Wang S, Gao Y, Chen Y, Guo QL. Endostar, a novel recombinant human endostatin, exerts antiangiogenic effect *via* blocking VEGF-induced tyrosine phosphorylation of KDR/Flk-1 of endothelial cells. *Biochem Biophys Res Commun* 2007; **361**: 79-84 [PMID: 17644065 DOI: 10.1016/j.bbrc.2007.06.155]

World Journal of Clinical Cases

Submit a Manuscript: https://www.f6publishing.com

World J Clin Cases 2022 June 26; 10(18): 6128-6135

DOI: 10.12998/wjcc.v10.i18.6128

ISSN 2307-8960 (online)

CASE REPORT

Effectiveness and safety of ultrasound-guided intramuscular lauromacrogol injection combined with hysteroscopy in cervical pregnancy treatment: A case report

Jian-Pei Ye, Yang Gao, Li-Wei Lu, Yong-Ju Ye

Specialty type: Obstetrics and gynecology

Provenance and peer review: Unsolicited article; Externally peer reviewed.

Peer-review model: Single blind

Peer-review report's scientific quality classification

Grade A (Excellent): 0
Grade B (Very good): 0
Grade C (Good): C, C, C
Grade D (Fair): 0
Grade E (Poor): 0

P-Reviewer: Karavaş E, Turkey; Okasha H, Egypt; Socea B, Romania

Received: November 3, 2021
Peer-review started: November 3, 2021
First decision: February 21, 2022
Revised: February 23, 2022
Accepted: April 20, 2022
Article in press: April 20, 2022
Published online: June 26, 2022

Jian-Pei Ye, Department of Ultrasonography, Lishui Hospital of Traditional Chinese Medicine, Lishui 323000, Zhejiang Province, China

Yang Gao, Li-Wei Lu, Yong-Ju Ye, Department of Gynaecology, Lishui Hospital of Traditional Chinese Medicine, Lishui 323000, Zhejiang Province, China

Corresponding author: Yong-Ju Ye, Doctor, MCh, MD, MS, Chief Physician, Department of Gynaecology, Lishui Hospital of Traditional Chinese Medicine, No. 800 Zhongshan Street, Liandu District, Lishui 323000, Zhejiang Province, China. ls8558@163.com

Abstract

BACKGROUND

Cervical pregnancy is increasing in morbidity, and a definite diagnosis in early stages is challenging due to its specific onset site. Surgery is the mainstay of treatment for cervical pregnancy, but it may result in the loss of natural fertility. Therefore, it is a great challenge to pursue a safe and effective treatment for cervical pregnancy.

CASE SUMMARY

We report the case of a cervical pregnancy successfully treated by ultrasound-guided cervical-intramuscular lauromacrogol injection combined with hysteroscopy. A 23-year-old woman with minor irregular vaginal bleeding was admitted to our department with suspected ectopic pregnancy. Transvaginal ultrasound revealed a gestational sac (approximately 22 mm x 13 mm) situated in the cervical canal with a yolk sac and blood flow signals. No cardiac activity was detected. Serum beta progesterone was 17.06 ng/mL, and serum beta human chorionic gonadotropin (β-HCG) was 5077.0 IU/L. The patient was diagnosed with cervical pregnancy. She was treated by ultrasound-guided cervical-intramuscular injections of lauromacrogol (3 mL) in combination with aborting under hysteroscopic visualization. A gradual decrease in β-HCG levels and normal ultrasound findings were observed. Postoperative pathologic examination showed the presence of villi and changes in the endometrium in the secretory phase. The patient was discharged on day 6, and her β-HCG level was 0.67 mIU/mL after 1 wk. There was no statistical difference between baseline and 1-week postoperative data in terms of serum indices including liver function, renal function, and routine blood analysis after treatment. The patient subsequently

became pregnant 2 mo later and no abnormalities were detected on routine screening during pregnancy.

CONCLUSION
Ultrasound-guided cervical-intramuscular lauromacrogol injection combined with hysteroscopy may be effective and safe in the treatment of cervical pregnancy.

Key Words: Cervical pregnancy; Lauromacrogol; Hysteroscopy; Effectiveness; Safety; Case report

©The Author(s) 2022. Published by Baishideng Publishing Group Inc. All rights reserved.

Core Tip: This study reports a typical clinical case of cervical pregnancy who received a conservative treatment combining ultrasound-guided lauromacrogol injection with hysteroscopy. The effectiveness and safety of the conservative treatment were evaluated, and the patient obtained a good outcome.

Citation: Ye JP, Gao Y, Lu LW, Ye YJ. Effectiveness and safety of ultrasound-guided intramuscular lauromacrogol injection combined with hysteroscopy in cervical pregnancy treatment: A case report. *World J Clin Cases* 2022; 10(18): 6128-6135
URL: https://www.wjgnet.com/2307-8960/full/v10/i18/6128.htm
DOI: https://dx.doi.org/10.12998/wjcc.v10.i18.6128

INTRODUCTION

Cervical pregnancy is a type of ectopic pregnancy associated with induced abortion, diagnostic curettage, cesarean section, spontaneous abortion, cervical surgery, and assisted reproductive technology[1,2]. It results in increased morbidity and is diagnosed in around 0.15% of all ectopic pregnancies[3]. A definite diagnosis in the early stages is challenging due to the specific onset site. It is commonly diagnosed by ultrasound because of vaginal bleeding[4], and is often accompanied by critical medical conditions. Surgery is the mainstay in the conventional management of cervical pregnancy, but tends to cause cervical adhesions and decreased function, resulting in the loss of natural fecundity. With significant advances in clinical diagnostic techniques and a growing demand for fertility, non-invasive or minimally invasive surgery has attracted increasing attention[5]. Currently, conservative treatment combining a local injection of methotrexate (MTX) or potassium chloride, oral mifepristone, and hysteroscopy is commonly used for cervical pregnancy with good efficacy[6-9]. However, high drug doses may induce damage to liver and renal function, as well as female fertility. In this context, it is challenging to develop a conservative treatment with a good safety profile[10].

Here, we report a typical case of cervical pregnancy treated by ultrasound-guided lauromacrogol injection combined with hysteroscopy. The effectiveness and safety were evaluated and the patient had a good outcome.

CASE PRESENTATION

Chief complaints

The patient was 23 years old. She previously had five pregnancies and five abortions, including one ectopic pregnancy. She had menopause for 39 d and a little irregular vaginal bleeding for 10 d, and the last menstruation was recorded on January 23, 2020. She visited our hospital on March 2, 2020 due to similar symptoms. Her serum beta progesterone (P) was 17.06 ng/mL, and beta human chorionic gonadotropin (β-HCG) was 5077.0 IU/L. The patient was diagnosed with cervical pregnancy by transvaginal ultrasound (Figure 1) and was hospitalized.

History of present illness

The patient had menopause for 39 d and a little irregular vaginal bleeding for 10 d, and the last menstruation was recorded on January 23, 2020.

History of past illness

The patient had five intrauterine pregnancies including one tubal ectopic pregnancy, but no delivery.

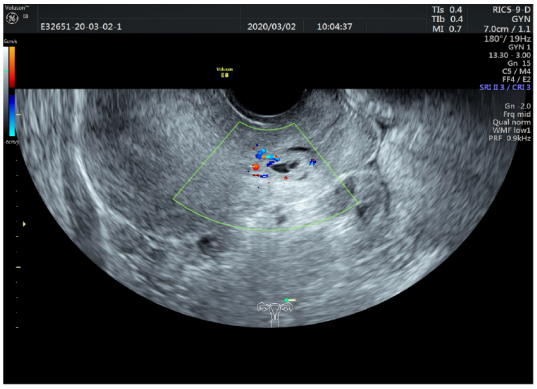

DOI: 10.12998/wjcc.v10.i18.6128 **Copyright** ©The Author(s) 2022.

Figure 1 Transvaginal ultrasound image before admission.

Personal and family history

There was no abnormality in personal and family history.

Physical examination

Physical examination showed that the patient's blood pressure was 122/83 mmHg, pulse rate was 89 bpm, temperature was 37.4°C, and respiratory rate was 20 breaths/min. Obstetrical examination findings included non-vaginal delivery, smooth vagina, slight bleeding, smooth and full cervix with no pain when held, severe uterine anteversion without tenderness, and normal bilateral fallopian tubes and ovaries.

Laboratory examinations

Serum beta progesterone was 17.06 ng/mL, and β-HCG was 5077.0 IU/L.

Imaging examinations

B-ultrasound was scheduled for the following day, and a gestational sac (approximately 22 mm x 13 mm) was situated in the cervical canal with a yolk sac and blood flow signals inside. In the meantime transvaginal ultrasound-guided tunnel puncture was thus arranged after routine disinfection using a 21G-EV type needle. Approximately 2 mL of fluid was obtained from the mass. Multiple lauromacrogol injections (3 mL) were performed targeting the cystic wall and cavity (Figure 2A). No pain or bleeding at the puncture area was observed during and after treatment. The patient was then transferred to the ward. Postoperative uterine three-dimensional B-ultrasound revealed the absence of blood flow signals around the gestational sac (Figure 2B).

FINAL DIAGNOSIS

The patient was diagnosed with cervical pregnancy.

TREATMENT

At 15:09 on March 4, aborting under hysteroscopic visualization was performed under general anesthesia with intubation. A villous tissue block (approximately 1 cm x 1.5 cm) was present and removed (around 8 g) after intramuscular injection of 3 U of pitavastatin and 1 wk with a suction tube. Further hysteroscopy revealed a rough cervical canal with a little bleeding, and balloon compression for hemostasis was provided. The procedure was uneventful and the intraoperative blood loss was approximately 50 mL. On March 5, no abnormalities were observed on B-ultrasound (Figure 3A). β-HCG was 2049.0 IU/L on March 6, 1213.0 IU/L on March 7, 496.6 IU/L on March 9, and 0.68 IU/L on March 17. No abnormalities were detected in the uterine cavity on transvaginal ultrasound on March 6, and postoperative pathologic examination on March 17 showed the presence of villi and changes in the endometrium in the secretory phase (Figure 3B).

In addition, there were no significant differences between baseline and 1-wk postoperative data with regard to serum indices including liver function, renal function, and routine blood analysis (Table 1).

During the follow-up period, the patient had normal menstruation on April 12, with a normal volume and color, which finished within 5 d (Table 2).

Table 1 Changes in routine blood index, liver function, and renal function before and one week after conservative treatment

	Before	One week after
Hemoglobin (g/L)	126	124
White blood cell count (× 10^9/L)	4.2	3.9
Platelet count (× 10^9/L)	167	184
Alanine aminotransferase (U/L)	11	18
Aspartate aminotransferase (U/L)	19	16
Creatinine (μmol/L)	49	42
Urea nitrogen (mmol/L)	3	2.6
Uric acid (μmol/L)	183	180

Ovarian function assessment: During the follow-up period, the patient had normal menstruation (normal volume and red) on April 12, which lasted 5 d (Table 2).

Table 2 Levels of serum reproductive hormones on the 5th day of menstruation

	Before (September 9, 2019)	After (May 8, 2020)
Follicle-stimulating hormone (mIU/mL)	5.53	5.89
Luteinizing hormone (mIU/mL)	4.16	6.37
Progesterone (ng/mL)	0.28	0.26
Testosterone (nmol/L)	1.28	1.34
Prolactin (ng/mL)	26.23	45.59
Estradiol (pmol/L)	121.9	292.3
Endometriosis (mm)	6	7
Antral follicle count (*n*)	7	6

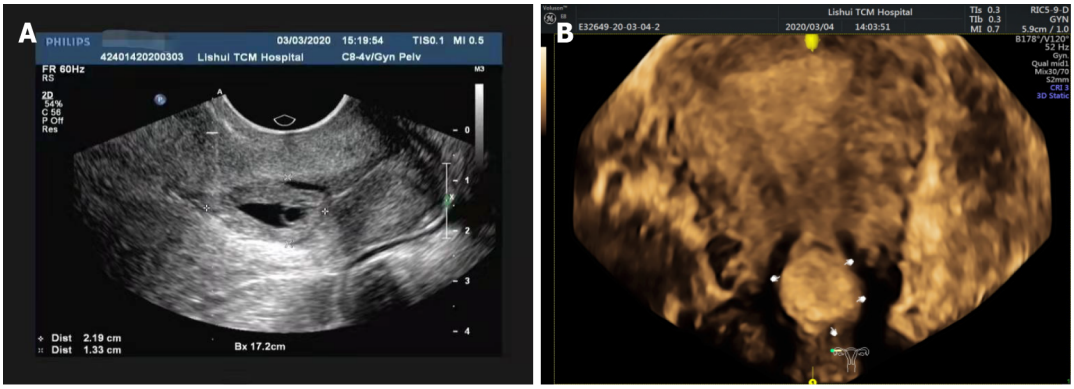

DOI: 10.12998/wjcc.v10.i18.6128 **Copyright** ©The Author(s) 2022.

Figure 2 Ultrasound-guided puncture images (A) and after puncture (B).

There were 5-7 antral follicles in the left ovary and 6-8 follicles in the right ovary. The endometrium was 11 mm thick on the 15th day of menstruation. On September 18, 2020 (day 79 of subsequent pregnancy), nuchal translucency examination suggested normal fetal development (Figure 4). No abnormalities were observed on routine screening during pregnancy. A live healthy infant was delivered on April 8, 2021.

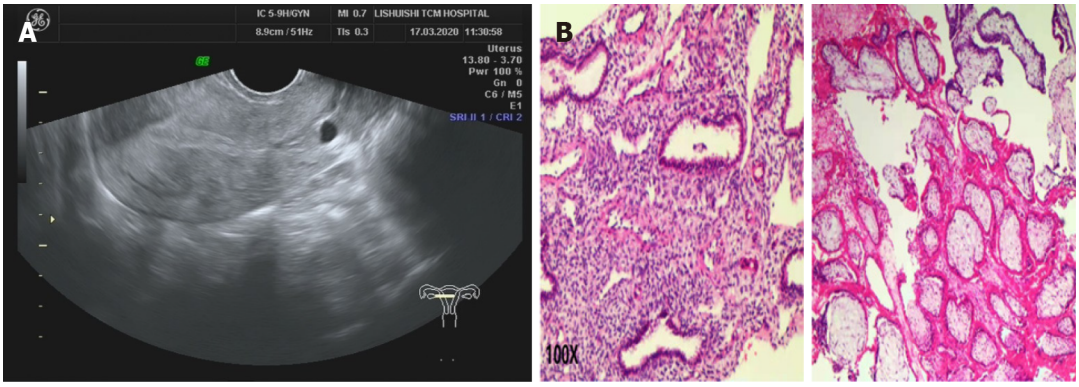

DOI: 10.12998/wjcc.v10.i18.6128 **Copyright** ©The Author(s) 2022.

Figure 3 Postoperative ultrasound (A) and pathologic examination (B).

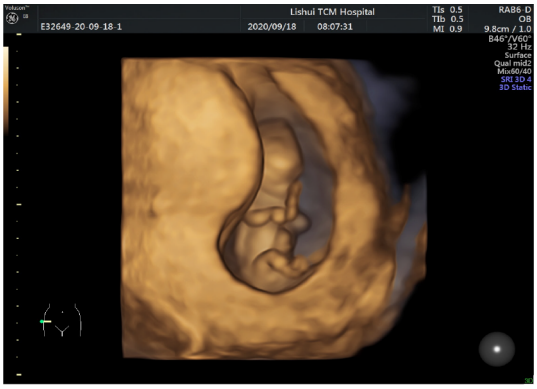

DOI: 10.12998/wjcc.v10.i18.6128 **Copyright** ©The Author(s) 2022.

Figure 4 Nuchal translucency examination.

OUTCOME AND FOLLOW-UP

Reproductive hormones, antral follicle count, and the endometrium all recovered to normal values, and no impairment of liver and renal function was observed after treatment. These findings indicate that lauromacrogol injection combined with hysteroscopy is effective and safe in the treatment of cervical pregnancy, and does not have adverse effects on fertility. Gestational and postnatal examinations showed subsequent normal fetal development. Thus, no short-term adverse effects were observed following this treatment strategy and subsequent pregnancy can be expected.

DISCUSSION

Cervical pregnancy is mainly composed of fibrous connective tissue. It can cause compromised cervical contractions and a high risk of extensive bleeding[11]. If inappropriately managed, the outcome can be catastrophic. Conventional treatment mainly includes hysterectomy. With improvements in clinical diagnostic techniques and an increasing demand for fertility, non-invasive or minimally invasive surgery is preferred by both doctors and families. Therefore, the hysterectomy rate significantly decreased from 89.5% in 1979 to 21.7% in 1994[12]. Conservative treatments mainly include MTX + curettage + interventional embolization + mifepristone or potassium chloride, local injection of vasoconstrictor, ligation of the uterus, blood vessels, and internal iliac artery, cervical cerclage, cervical Foley tube tamponade, electrosurgical excision, and radiofrequency ablation[10,13-15]. However, the safety of conservative treatment has been less studied. MTX and mifepristone are commonly used drugs with definite efficacy in the treatment of cervical pregnancy. However, in the context of a high dose, patients can develop nausea, vomiting, or impaired liver and renal function, in addition to unpredictable fertility. It was reported that a minimum 3 mo interval after MTX application is required for a subsequent pregnancy[16].

Lauromacrogol is a novel vascular sclerosant harboring hydrophilic and lyophilic groups, which conform to a directional alignment on a liquid surface to allow a significant decline in surface tension. It

is important in sclerotherapy, as it can cause sterile inflammation with the groups which can help obtain protein precipitation in several seconds and thus cause damage to the lipid bilayer of the cell membrane, thereby leading to fibrous tissue hyperplasia and adhesions[17,18]. In addition, it has great applications in digestive, cardiovascular, and nervous system diseases[19,20]. However, there is a paucity of reports on lauromacrogol as a hemostatic agent in ectopic pregnancy. Wei *et al*[21] previously adopted ultrasound-guided local lauromacrogol injection plus suction curettage in the treatment of type II cesarean scar pregnancy with a favorable therapeutic outcome, but the safety of lauromacrogol was not evaluated.

Our patient had five intrauterine pregnancies including one tubal ectopic pregnancy, but no delivery. Considering the strong will of the patient and her family for fertility preservation, an attempt was made to decrease the blood supply in the gestational sac using local injections of lauromacrogol, instead of uterine artery embolization, combined with ultrasound-guided intervention. It has been established that lauromacrogol can block the blood circulation of the embryo and cervical vein without interfering with the blood supply to the ovary. The sclerosis and hemostasis induced by lauromacrogol are mainly realized in the following two ways: Vascular lauromacrogol injection can cause direct damage to vascular endothelial cells in attached veins at the site of injection, allowing local thrombosis, the formation of a protective layer for fibrous tissue surrounding the ruptured vessels, and an increase in vascular resistance. In that way, hemostasis can be obtained by regional vascular compression contributing to decreased blood flow. In addition, lauromacrogol injection can cause superficial small areas of fibrosis in veins around the injection site, resulting in vascular compression and occlusion[22]. Here, B-ultrasound 24 h after lauromacrogol injection showed no blood supply to the gestational sac. Hysteroscopic curettage was instantly performed with a little intraoperative bleeding. This suggested the favorable vascular stiffening and rapid onset of action (3-24 h) of lauromacrogol, which greatly decreased intraoperative bleeding, shortened the time to curettage, and increased the success rate[23]. Lauromacrogol is also a type of local anesthetic that can achieve local analgesia and alleviate discomfort in patients during treatment. Polycinol injection combined with uterine curettage under ultrasound intervention for cesarean scar pregnancy has no significant effect on endometrial thickness and scar thickness in patients. After the operation, the blood supply to the uterine scar recovers well, and the menstrual recovery time is significantly shorter than that following MTX treatment. In addition, the fertility of patients can be well preserved[24].

Liver and renal function in our patient were also evaluated and showed no difference before and after treatment. Consistent with the existing literature, lauromacrogol had no adverse effects on the liver and kidneys. Similar results were observed for reproductive hormones, ovarian volume, antral follicle count, and the endometrium, resulting in a well preserved uterus and ovarian physiological functions. The patient had normal menstruation 40 d after treatment. She conceived naturally after 2 mo with normal fetal development (Figure 4) and successful delivery.

CONCLUSION

The present case demonstrated the effectiveness and safety of lauromacrogol injection plus hysteroscopy in the treatment of cervical pregnancy, which had no adverse effects on liver and renal function, fertility, and fetal development following subsequent conception. This treatment strategy deserves to be promoted and applied in the clinic. Lauromacrogol, a sclerosant used to treat cystic disease or vascular disease, has certain adverse reactions, such as low-grade fever, local pain, venous embolism, and anaphylactic reaction, most of which are mild and self-limited. However, there is a risk of serious adverse reactions during the treatment of venous disease, and the occurrence of adverse heart events should be prevented[25]. Further research on clinical indications, contraindications, and its potential as a replacement for conventional hemostatic agents and blasticidin is necessary.

FOOTNOTES

Author contributions: Ye YJ and Gao Y wrote the introduction and discussion sections; Ye YJ and Ye JP performed the review of the literature and wrote the case report; Ye YJ and Lu LW revised the manuscript.

Informed consent statement: The patient agreed to the publication of this report and provided informed consent.

Conflict-of-interest statement: The authors declare no conflicts of interest for this article.

CARE Checklist (2016) statement: The authors have read the CARE Checklist (2016), and the manuscript was prepared and revised according to the CARE Checklist (2016).

Open-Access: This article is an open-access article that was selected by an in-house editor and fully peer-reviewed by external reviewers. It is distributed in accordance with the Creative Commons Attribution NonCommercial (CC BY-

NC 4.0) license, which permits others to distribute, remix, adapt, build upon this work non-commercially, and license their derivative works on different terms, provided the original work is properly cited and the use is non-commercial. See: https://creativecommons.org/Licenses/by-nc/4.0/

Country/Territory of origin: China

ORCID number: Jian-Pei Ye 0000-0003-0675-3751; Yang Gao 0000-0002-9177-7872; Li-Wei Lu 0000-0002-1218-3647; Yong-Ju Ye 0000-0002-7269-3251.

S-Editor: Ma YJ
L-Editor: Wang TQ
P-Editor: Ma YJ

REFERENCES

1 **Hoyos LR**, Tamakuwala S, Rambhatla A, Brar H, Vilchez G, Allsworth J, Rodriguez-Kovacs J, Awonuga A. Risk factors for cervical ectopic pregnancy. *J Gynecol Obstet Hum Reprod* 2019; 101665 [PMID: 31811970 DOI: 10.1016/j.jogoh.2019.101665]
2 **Dziedzic JM**, Patel PV. Cervical Ectopic Pregnancy: A Rare Site of Implantation. *J Emerg Med* 2019; **56**: e123-e125 [PMID: 31003816 DOI: 10.1016/j.jemermed.2019.03.024]
3 **Hirakawa M**, Tajima T, Yoshimitsu K, Irie H, Ishigami K, Yahata H, Wake N, Honda H. Uterine artery embolization along with the administration of methotrexate for cervical ectopic pregnancy: technical and clinical outcomes. *AJR Am J Roentgenol* 2009; **192**: 1601-1607 [PMID: 19457824 DOI: 10.2214/AJR.08.1921]
4 **Chen YZZ**, Zhou JY. Effect of transabdomen ultrasound and transvaginal ultrasonography for diagnosing cervical ectopic pregnancy. *Zhongguo Jihua Shengyuxue Zazhi* 2020; **28**: 1621-1623+1724
5 **Han JY**, Kim H, Kim SW, Ku SY, Suh CS, Kim SH. Use of haemostatic gel in the management of cervical pregnancy: a case report. *Eur J Contracept Reprod Health Care* 2021; **26**: 167-170 [PMID: 33021850 DOI: 10.1080/13625187.2020.1824270]
6 **De La Vega GA**, Avery C, Nemiroff R, Marchiano D. Treatment of early cervical pregnancy with cerclage, carboprost, curettage, and balloon tamponade. *Obstet Gynecol* 2007; **109**: 505-507 [PMID: 17267874 DOI: 10.1097/01.AOG.0000220599.74326.94]
7 **Oliver R**, Malik M, Coker A, Morris J. Management of extra-tubal and rare ectopic pregnancies: case series and review of current literature. *Arch Gynecol Obstet* 2007; **276**: 125-131 [PMID: 17431652 DOI: 10.1007/s00404-006-0311-3]
8 **Verma U**, Goharkhay N. Conservative management of cervical ectopic pregnancy. *Fertil Steril* 2009; **91**: 671-674 [PMID: 18339381 DOI: 10.1016/j.fertnstert.2007.12.054]
9 **Petousis S**, Margioula-Siarkou C, Kalogiannidis I, Karavas G, Palapelas V, Prapas N, Rousso D. Conservative management of cervical pregnancy with intramuscular administration of methotrexate and KCl injection: Case report and review of the literature. *World J Clin Cases* 2015; **3**: 81-84 [PMID: 25610854 DOI: 10.12998/wjcc.v3.i1.81]
10 **Singh S**. Diagnosis and management of cervical ectopic pregnancy. *J Hum Reprod Sci* 2013; **6**: 273-276 [PMID: 24672169 DOI: 10.4103/0974-1208.126312]
11 **Weibel HS**, Alserri A, Reinhold C, Tulandi T. Multidose methotrexate treatment of cervical pregnancy. *J Obstet Gynaecol Can* 2012; **34**: 359-362 [PMID: 22472336 DOI: 10.1016/S1701-2163(16)35217-3]
12 **Kung FT**, Chang SY. Efficacy of methotrexate treatment in viable and nonviable cervical pregnancies. *Am J Obstet Gynecol* 1999; **181**: 1438-1444 [PMID: 10601926 DOI: 10.1016/s0002-9378(99)70389-3]
13 **Imai K**, Fukushi Y, Nishimura M, Ohara Y, Suzuki Y, Ota H, Nakajima A, Wada S, Fujino T. Combination of conservative treatment and temporary bilateral laparoscopic uterine artery clipping with hysteroscopic transcervical resection for cervical pregnancy: A retrospective study. *J Gynecol Obstet Hum Reprod* 2021; **50**: 101735 [PMID: 32251739 DOI: 10.1016/j.jogoh.2020.101735]
14 **Jachymski T**, Moczulska H, Guzowski G, Pomorski M, Piątek S, Zimmer M, Rokita W, Wielgoś M, Sieroszewski P. Conservative treatment of abnormally located intrauterine pregnancies (cervical and cesarean scar pregnancies): a multicenter analysis (Polish series). *J Matern Fetal Neonatal Med* 2020; **33**: 993-998 [PMID: 30122076 DOI: 10.1080/14767058.2018.1514009]
15 **Elmokadem AH**, Abdel-Wahab RM, El-Zayadi AA, Elrakhawy MM. Uterine Artery Embolization and Methotrexate Infusion as Sole Management for Caesarean Scar and Cervical Ectopic Pregnancies: A Single-Center Experience and Literature Review. *Can Assoc Radiol J* 2019; **70**: 307-316 [PMID: 31005344 DOI: 10.1016/j.carj.2018.12.002]
16 **Hackmon R**, Sakaguchi S, Koren G. Effect of methotrexate treatment of ectopic pregnancy on subsequent pregnancy. *Can Fam Physician* 2011; **57**: 37-39 [PMID: 21252128 DOI: 10.3399/bjgp11X549135]
17 **Kitagawa A**, Yamamoto T, Matsunaga N, Yamaji M, Ikeda S, Izumi Y, Hagihara M, Ota T, Ishiguchi T. Polidocanol Sclerotherapy Combined with Transarterial Embolization Using n-Butyl Cyanoacrylate for Extracranial Arteriovenous Malformations. *Cardiovasc Intervent Radiol* 2018; **41**: 856-866 [PMID: 29417264 DOI: 10.1007/s00270-017-1855-2]
18 **Gatz M**, Schrading S, Dirrichs T, Betsch M, Tingart M, Rath B, Kuhl C, Quack V. Topical polidocanol application in combination with static stretching in tendinopathies: a prospective pilot study. *Muscles Ligaments Tendons J* 2017; **7**: 88-97 [PMID: 28717616 DOI: 10.11138/mltj/2017.7.1.088]
19 **Ramadani A**, Jovanovska RP, Trajkovska M, Andreevski V, Calovska V, Serafimoski V, Bojadzieva S. Comparison of Argon Plasma Coagulation and Injection Therapy with Adrenalin and Polidocanol in the Management of Bleeding Angiodysplasia in Upper Gastrointestinal Tract. *Pril (Makedon Akad Nauk Umet Odd Med Nauki)* 2018; **39**: 63-68 [PMID:

30864370 DOI: 10.2478/prilozi-2018-0043]

20 **Gupta G**, Pandit RS, Jerath N, Narasimhan R. Severe life-threatening hypersensitivity reaction to polidocanol in a case of recurrent aneurysmal bone cyst. *J Clin Orthop Trauma* 2019; **10**: 414-417 [PMID: 30828217 DOI: 10.1016/j.jcot.2018.05.010]

21 **Wei SS**, Li DH, Zhang ZF, Sun WC, Jia CL. Type II caesarean scar pregnancy management by ultrasound-guided local lauromacrogol injection in combination with suction curettage: A case report. *Medicine (Baltimore)* 2020; **99**: e19743 [PMID: 32332613 DOI: 10.1097/MD.0000000000019743]

22 **Chai ZY**, Yu L, Liu MM, Zhu TW, Qi F. Evaluation of the Efficacy of Ultrasound-Guided Local Lauromacrogol Injection Combined with Aspiration for Cesarean Scar Pregnancy: A Novel Treatment. *Gynecol Obstet Invest* 2018; **83**: 306-312 [PMID: 29208846 DOI: 10.1159/000485099]

23 **Dong JJ**, Chen MZ, Yu L, Han WS. Effect of lauromacrogol combined with curettage on ulterine scar pregnancy after cesareansection. *Zhongguo Fuyou Jiankang Yanjiu* 2018; **29**: 1331-1334

24 **Sun Y**, Wei FB, Wei HJ, Liu ZN, Qiu D. Observation of long-term efficacy of polidocanol injection combined with uterine curettage in the treatment of cesarean scar pregnancy under ultrasound intervention. *Zhongguo Shiyong Yiyao* 2020; **15**: 18-20 [DOI: 10.14163/j.cnki.11-5547/r.2020.13.006]

25 **Qin YL**, Zhou J. Clinical application and adverse reactions of Lauromacrogol. *Zhongguo Jieru Yingxiang Yu Zhiliaoxue* 2020; **17**: 569-572 [DOI: 10.13929/j.issn.1672-8475.2020.09.013]

World Journal of Clinical Cases

Submit a Manuscript: https://www.f6publishing.com

World J Clin Cases 2022 June 26; 10(18): 6136-6140

DOI: 10.12998/wjcc.v10.i18.6136

ISSN 2307-8960 (online)

CASE REPORT

Carcinoma located in a right-sided sigmoid colon: A case report

Liang-Jing Lyu, Wei-Wu Yao

Specialty type: Anatomy and morphology

Provenance and peer review: Unsolicited article; Externally peer reviewed.

Peer-review model: Single blind

Peer-review report's scientific quality classification

Grade A (Excellent): 0
Grade B (Very good): B, B
Grade C (Good): 0
Grade D (Fair): 0
Grade E (Poor): E

P-Reviewer: Ding X, China; Haddadi S, Spain; Oley MH, Indonesia

Received: October 23, 2021
Peer-review started: October 23, 2021
First decision: November 18, 2021
Revised: November 27, 2021
Accepted: April 21, 2022
Article in press: April 21, 2022
Published online: June 26, 2022

Liang-Jing Lyu, Wei-Wu Yao, Department of Radiology, Tongren Hospital, Shanghai Jiao Tong University School of Medicine, Shanghai 200336, China

Corresponding author: Wei-Wu Yao, Doctor, MD, PhD, Chief Physician, Professor, Department of Radiology, Tongren Hospital, Shanghai Jiao Tong University School of Medicine, No. 1111 Xianxia Road, Shanghai 200336, China. yaoweiwuhuan@163.com

Abstract

BACKGROUND

A right-sided sigmoid colon is an extremely rare anatomic variation that should be considered as a possibility by surgeons and radiologists before surgery. Here, we report the first clinical case of a carcinoma in a right-sided sigmoid colon revealed by a preoperative computed tomography (CT).

CASE SUMMARY

A 56-year-old Chinese man was admitted to the hospital with abdominal pain. CT revealed a redundant sigmoid colon with a mass on the right side of the cecum and ascending colon. Laparoscopy confirmed an abnormal course in the descending colon and sigmoid colon. Subsequently, hemicolectomy was performed in an open manner after laparoscopic exploration. Pathological examination revealed an infiltrative mucinous adenocarcinoma with two lymph node metastases. The patient was discharged without any complications after a week. There were no signs of recurrence or metastasis during the 3-month follow-up period.

CONCLUSION

We report a rare anomaly of a right-sided sigmoid colon with carcinoma, which should be differentiated from ascending colon cancer and pericecal hernia to prevent errors and other surgical complications.

Key Words: Right-sided sigmoid colon; Sigmoid colon; Colon carcinoma; Redundant sigmoid colon; Pericecal hernia; Case report

©The Author(s) 2022. Published by Baishideng Publishing Group Inc. All rights reserved.

Core Tip: The right-sided sigmoid colon was first described by a few cadaveric studies and may not have been fully recognized by clinicians in recent years due to its relative rarity. Recognizing this variation is essential for interventional and diagnostic colonoscopy and associated surgeries. This is the first clinical case of a carcinoma located in a right-sided sigmoid colon.

Citation: Lyu LJ, Yao WW. Carcinoma located in a right-sided sigmoid colon: A case report. *World J Clin Cases* 2022; 10(18): 6136-6140
URL: https://www.wjgnet.com/2307-8960/full/v10/i18/6136.htm
DOI: https://dx.doi.org/10.12998/wjcc.v10.i18.6136

INTRODUCTION

Recognizing variations in the sigmoid colon is of key importance to surgeons and radiologists. Here, we report an atypical anatomic variation of a right-sided sigmoid colon with carcinoma, which was incidentally observed during an emergency computed tomography (CT) scan for abdominal pain. To the best of our knowledge, this is the first clinical case of a carcinoma located in a right-sided sigmoid colon detected by a preoperative CT scan. We present the following case in accordance with the CARE Reporting Checklist.

CASE PRESENTATION

Chief complaints

A 56-year-old Chinese man was admitted to our hospital with abdominal pain in the right lower quadrant for 3 days.

History of present illness

The patient had experienced irregular and formless bowel movements for three months prior to presentation at our hospital. The patient also had right lower quadrant abdominal pain, which could not be relieved after defecation. The patient had no other accompanying symptoms, including any obvious symptoms of bowel obstruction.

History of past illness

The patient had no previous surgical history.

Personal and family history

The patient did not have a history of smoking or drinking. There was no personal or family history of acute or chronic diseases.

Physical examination upon admission

The patient was 169 cm tall and weighed 65 kg. Physical examination revealed tenderness in the right lower quadrant, but no palpable mass was found.

Laboratory examinations

Laboratory tests showed moderate increases in platelets and CA724, and normal levels of white blood cells and CA199. No abnormal results were found in other biochemical tests.

Imaging examinations

CT showed an atypical location of the redundant sigmoid colon with heterogeneously enhanced circumferential wall thickening on the right side of the cecum and ascending colon (Figures 1 and 2). We reported the atypical location of the sigmoid colon with a mass, suspected the presence of a pericecal hernia, and informed the surgeons accordingly.

Colonoscopy showed an annular stricture of the sigmoid colon caused by a tumor 28 cm from the anus. Subsequent biopsy indicated malignancy.

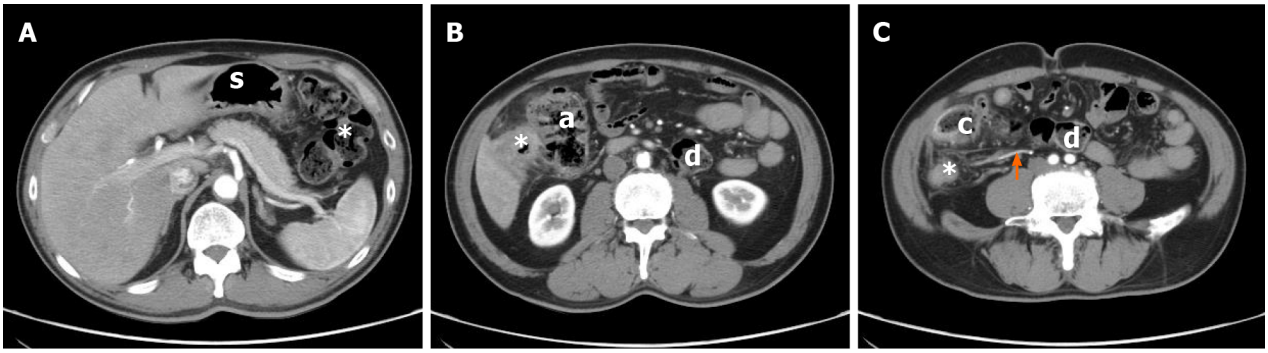

DOI: 10.12998/wjcc.v10.i18.6136 **Copyright** ©The Author(s) 2022.

Figure 1 A 56-year-old man with right-sided sigmoid colon carcinoma. A: Axial post-contrast computed tomography (CT) scan in the arterial phase demonstrates that the stomach (s) and splenic flexure of colon are normal (*); B: Axial post-contrast CT scan in the arterial phase shows the descending colon entering the peritoneum. The sigmoid colon with the tumor (*) is located on the right side of the ascending colon (a); C: Axial post-contrast CT scan in the arterial phase shows the descending colon (d) crossing to the right at the level of the L4 vertebra and continuing as the sigmoid colon (s) on the right. The tumor (*) is located in a redundant right-sided sigmoid colon. The cecum (c) is displaced toward the left at the level of the L4 transverse process instead of the right pelvic region. The inferior mesenteric artery (arrows) is shown running to the right instead of its normal left-sided course.

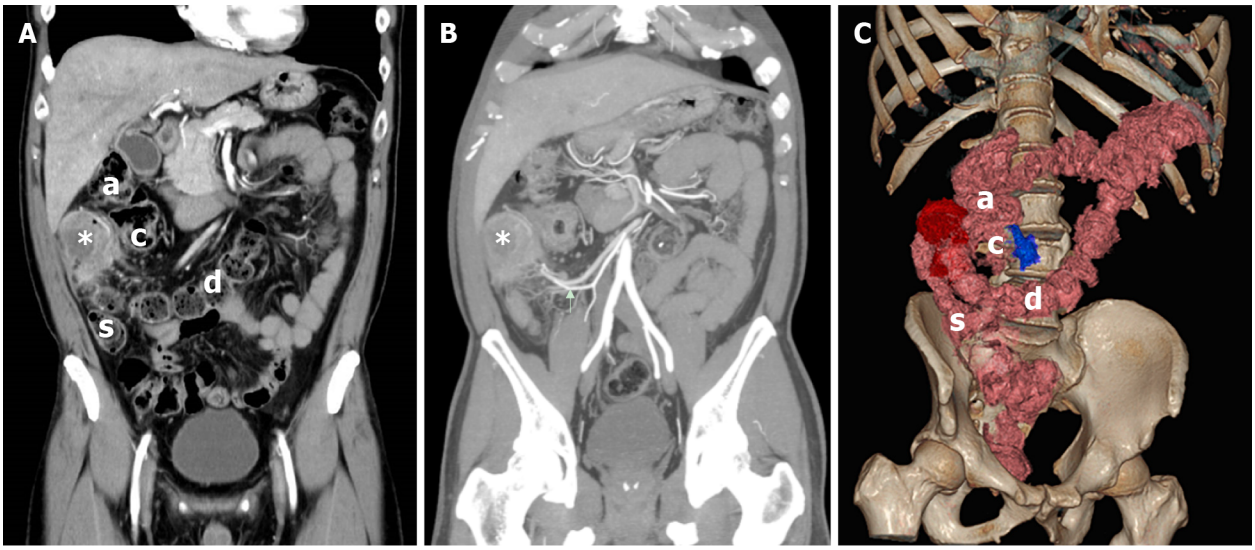

DOI: 10.12998/wjcc.v10.i18.6136 **Copyright** ©The Author(s) 2022.

Figure 2 A 56-year-old man with right-sided sigmoid colon carcinoma. A: Coronal post-contrast computed tomography (CT) scan in the arterial phase demonstrates that the descending colon (d) crosses to the right and continues as the sigmoid colon (s). The tumor (*) is located in a redundant right-sided sigmoid colon occupying the subhepatic region. The ascending colon (a) and the cecum (c) have been displaced; B: Maximum Intensity Projection (MIP) demonstrates that the tumor (*) is located in the right abdomen. The inferior mesenteric artery (arrows) is shown running to the right instead of its normal left-sided course; C: Volume Rendering Technique (VRT) demonstrates abnormal positions of both the sigmoid colon and descending colon. The descending colon (d) is shown crossing to the right and continuing as the sigmoid colon (s). The tumor (red part) is located in a redundant right-sided sigmoid colon. The ascending colon (a) and cecum (c) have been displaced. The ileocecal junction (blue part) is at the L4 level, indicating that the cecum was undescended during embryogenesis.

FINAL DIAGNOSIS

Due to inconclusive radiological signs, the patient underwent laparoscopic exploration. Intraoperatively, the surgeons detected atypical positions of both the sigmoid colon and descending colon. They converted the surgery to an open operation for safety considerations.

The surgeons found a mass that almost completely blocked the lumen of the sigmoid colon. The redundant sigmoid colon was located on the right side of the ascending colon and cecum and was supplied by the branches of the inferior mesenteric artery, which ran to the right instead of its standard left-sided course. The descending colon started at the splenic flexure and crossed to the right at the level of the L4 vertebra, and occupied the subhepatic region to continue as the sigmoid colon. The small intestine was normal. Pathological examination revealed an infiltrative mucinous adenocarcinoma with two lymph node metastases, pT4N1M0 stage IIIB (UICC-TNM: 8th edition).

TREATMENT

The surgeons performed a hemicolectomy with regional lymphadenectomy during laparotomy. No bowel perforation was observed.

OUTCOME AND FOLLOW-UP

The patient was discharged on postoperative day 7 without any complications. Moreover, there were no signs of recurrence or metastasis during the 3-month follow-up period.

DISCUSSION

The sigmoid colon shows the greatest variation in length and position[1]. The variation in length is mainly related to racial differences and a high-fiber diet[2], the position of the sigmoid colon loop is a means of adapting to the general length of the sigmoid colon[2]. A study by Saxena *et al*[3] suggested that the sigmoid colon of young children (age < 5 years) is often situated entirely on the right side for redundancy; this is not the case in adults. The presence of a right-sided sigmoid colon is very rare in adults and may be related to fixation anomalies[1], redundancy of the colon, or secondary rotation of the colon during embryogenesis[4].

In most cases of right-side colon carcinoma, the carcinoma is observed to be located in the ascending colon. In our case, circumferential wall thickening of the colon occupied the subhepatic region on the right of the ascending colon, and the ileocecal junction was displaced toward the left at the level of the L4 transverse process instead of the right pelvic region, indicating that the cecum was undescended due to midgut malrotation during embryogenesis[4]. Colonoscopy revealed a stricture 28 cm from the anus, demonstrating a sigmoid colon other than the ascending colon. The identification of the tumor location is crucial for determining the appropriate clinical course because the sigmoid colon and ascending colon have different embryological origins[5], and a recent study[6] demonstrated that right-sided colon carcinomas exhibit exophytic pathological behavior and poorer overall survival than left-sided colon carcinomas.

In the present case, the colon with wall thickening on the right side of the ascending colon was similar to a rare type of internal hernia occurring near the cecum, namely, pericecal hernia[7]. However, pericecal hernia usually involves a small bowel other than the sigmoid colon; such pericecal hernias usually produce acute intestinal obstruction, which can be confirmed by CT. In addition, it is expected that the descending colon and sigmoid colon should be observed in the standard position relative to the pericecal hernia and the inferior mesenteric artery. On CT images of the present case, no small bowel herniation or obvious dilation was observed. The descending colon crossed to the right side at the level of the L4 vertebra, where it entered the peritoneal cavity and continued as the sigmoid colon on the right side. Notably, the inferior mesenteric artery ran to the right instead of its normal left-sided course.

Shrivastava *et al*[8] first described the right-sided sigmoid colon in a cadaveric study in 2013. Flores-Ríos *et al*[9] reported a case of secondary right-sided descending and sigmoid colon caused by a wandering spleen due to laxity or abnormal development of the peritoneal ligaments, which was different from our case. Subsequently, there were two case reports[1,10] of right-sided sigmoid colons, which were discovered incidentally during surgery.

To the best of our knowledge, this is the first clinical case of carcinoma located in the right-sided sigmoid colon revealed by a preoperative CT scan and confirmed by surgery. Surgeons and radiologists should be aware of this rare variation when examining patients experiencing abdominal pain in the right lower quadrant.

The limitation of our case was the lack of appropriate intraoperative images compatible with the volume rendering image (Figure 2C), which could have provided readers with an intuitive understanding.

CONCLUSION

We report a rare anomaly of the right-sided sigmoid colon with carcinoma that could be detected by careful examination with a preoperative CT scan. This is a major congenital colon anomaly that should be recognized preoperatively and needs to be differentiated from the ascending colon and pericecal hernia to prevent errors and other surgical complications.

FOOTNOTES

Author contributions: Lyu LJ and Yao WW wrote the manuscript; all authors have read and approve the final manuscript.

Informed consent statement: Written informed consent was obtained from the patient for publication of this report.

Conflict-of-interest statement: The authors declare that they have no conflicts of interest.

CARE Checklist (2016) statement: The authors have read the CARE Checklist (2016), and the manuscript was prepared and revised according to the CARE Checklist (2016).

Open-Access: This article is an open-access article that was selected by an in-house editor and fully peer-reviewed by external reviewers. It is distributed in accordance with the Creative Commons Attribution NonCommercial (CC BY-NC 4.0) license, which permits others to distribute, remix, adapt, build upon this work non-commercially, and license their derivative works on different terms, provided the original work is properly cited and the use is non-commercial. See: https://creativecommons.org/Licenses/by-nc/4.0/

Country/Territory of origin: China

ORCID number: Liang-Jing Lyu 0000-0003-4643-9740; Wei-Wu Yao 0002-1536-9324.

S-Editor: Ma YJ
L-Editor: A
P-Editor: Ma YJ

REFERENCES

1 **Kar H**, Karasu S, Bag H, Cin N, Durak E, Peker Y, Tatar FA. Case Report of the Descending Colon Located Completely in the Right Extraperitoneal Cavity and Sigmoid Colon Located in the Right Quadrant in a Patient with a Splenic Flexure Tumor: a Rare Anomaly. *Indian J Surg* 2016; **78**: 323-325 [PMID: 27574354 DOI: 10.1007/s12262-015-1407-4]
2 **Madiba TE**, Haffajee MR. Sigmoid colon morphology in the population groups of Durban, South Africa, with special reference to sigmoid volvulus. *Clin Anat* 2011; **24**: 441-453 [PMID: 21480385 DOI: 10.1002/ca.21100]
3 **Saxena AK**, Sodhi KS, Tirumani S, Mumtaz HA, Narasimha Rao KL, Khandelwal N. Position of a sigmoid colon in right iliac fossa in children: A retrospective study. *J Indian Assoc Pediatr Surg* 2011; **16**: 93-96 [PMID: 21897567 DOI: 10.4103/0971-9261.83485]
4 **Gnansekaran D**, Prashant SA, Veeramani R, Yekappa SH. Congenital positional anomaly of descending colon and sigmoid colon: Its embryological basis and clinical implications. *Med J Armed Forces India* 2021; **77**: 241-244 [PMID: 33867645 DOI: 10.1016/j.mjafi.2019.10.006]
5 **Jess P**, Hansen IO, Gamborg M, Jess T; Danish Colorectal Cancer Group. A nationwide Danish cohort study challenging the categorisation into right-sided and left-sided colon cancer. *BMJ Open* 2013; **3** [PMID: 23793665 DOI: 10.1136/bmjopen-2013-002608]
6 **Xie X**, Zhou Z, Song Y, Wang W, Dang C, Zhang H. Differences between carcinoma of the cecum and ascending colon: Evidence based on clinical and embryological data. *Int J Oncol* 2018; **53**: 87-98 [PMID: 29658575 DOI: 10.3892/ijo.2018.4366]
7 **Inukai K**, Tsuji E, Uehara S. Paracecal hernia with intestinal ischemia treated with laparoscopic assisted surgery. *Int J Surg Case Rep* 2018; **44**: 20-23 [PMID: 29462753 DOI: 10.1016/j.ijscr.2018.02.016]
8 **Shrivastava P**, Tuli A, Kaur S, Raheja S. Right sided descending and sigmoid colon: its embryological basis and clinical implications. *Anat Cell Biol* 2013; **46**: 299-302 [PMID: 24386604 DOI: 10.5115/acb.2013.46.4.299]
9 **Flores-Ríos E**, Méndez-Díaz C, Rodríguez-García E, Pérez-Ramos T. Wandering spleen, gastric and pancreatic volvulus and right-sided descending and sigmoid colon. *J Radiol Case Rep* 2015; **9**: 18-25 [PMID: 26629290 DOI: 10.3941/jrcr.v9i10.2475]
10 **Watanabe K**, Abiko K, Tamura S, Katsumata M, Amano Y, Takao Y. Right-sided Sigmoid Colon Revealed during Laparoscopic Sacrocolpopexy. *J Minim Invasive Gynecol* 2021; **28**: 1267-1268 [PMID: 32950663 DOI: 10.1016/j.jmig.2020.09.009]

World Journal of Clinical Cases

Submit a Manuscript: https://www.f6publishing.com

World J Clin Cases 2022 June 26; 10(18): 6141-6147

DOI: 10.12998/wjcc.v10.i18.6141

ISSN 2307-8960 (online)

CASE REPORT

Subcutaneous infection caused by *Mycobacterium abscessus* following cosmetic injections of botulinum toxin: A case report

Lin Deng, Ying-Zhi Luo, Fang Liu, Xiao-Hong Yu

Specialty type: Infectious diseases

Provenance and peer review: Unsolicited article; Externally peer reviewed.

Peer-review model: Single blind

Peer-review report's scientific quality classification

Grade A (Excellent): A
Grade B (Very good): 0
Grade C (Good): C, C
Grade D (Fair): 0
Grade E (Poor): 0

P-Reviewer: Corvino A, Italy; Hosoya S, Japan; Malekzadegan A, Iran

Received: October 26, 2021
Peer-review started: October 26, 2021
First decision: December 17, 2021
Revised: December 27, 2021
Accepted: April 28, 2022
Article in press: April 28, 2022
Published online: June 26, 2022

Lin Deng, Ying-Zhi Luo, Xiao-Hong Yu, Department of Dermatology, Affiliated Hangzhou First People's Hospital, Zhejiang University School of Medicine, Hangzhou 310006, Zhejiang Province, China

Fang Liu, Department of Dermatology, Jinling Hospital, Nanjing 210002, Jiangsu Province, China

Corresponding author: Yu XH, MD, Doctor, Professor, Department of Dermatology, Affiliated Hangzhou First People's Hospital, Zhejiang University School of Medicine, No. 261 Huansha Street, Hangzhou 310006, Zhejiang Province, China. 1191656901@qq.com

Abstract

BACKGROUND

In recent years, the cosmetic intervention related infections caused by nontuberculous mycobacteria (NTM) are increasing as the informal cosmetic treatments are performed. However, many dermatologists are inexperienced in the diagnosis and management of similar cases. Here we report a case of subcutaneous infection caused by *Mycobacterium abscessus* (*M. abscessus*) following cosmetic injections of botulinum toxin.

CASE SUMMARY

A 53-year-old woman presented with multiple abscesses and nodules on her forehead and both temporal sites for half a month after cosmetic injections of botulinum toxin. Her lesions did not show any alleviation after 2-wk prescription of antibiotics. Laboratory examinations indicated that she had no sign of immunodeficiency and the whole body of computed tomography did not find any systemic infection or diseases. The pathology of skin tissue showed inflammatory cell infiltration with the negative results of Periodic acid Schiff (PAS) and Acid-fast staining and the culture yielded no microbiome. Afterwards, the puncture on abscess was performed and *M. abscessus* was successfully isolated. The pathogen was identified by acid-fast staining and DNA sequencing. The patient was treated with the strategy of clarithromycin, ofloxacin, and amikacin according to the result of drug sensitivity test and got complete remission of the lesions.

CONCLUSION

The case presents the whole process of diagnosis and management of NTM infection after cosmetic intervention and highlights the diagnostic thoughts. In a word, the mycobacterium infection should be aware in patients after cosmetic performance.

Key Words: Mycobacterium abscesses; Skin infection; Cosmetic injection; Nontuberculous mycobacteria; Case report

©The Author(s) 2022. Published by Baishideng Publishing Group Inc. All rights reserved.

Core Tip: The article reports a case of subcutaneous infection caused by *Mycobacterium abscessus* after cosmetic intervention. We present the medical history and whole process of diagnosis and management of the case and made a literature review of similar infections. The paper is trying to provide some more experience for dermatologists.

Citation: Deng L, Luo YZ, Liu F, Yu XH. Subcutaneous infection caused by *Mycobacterium abscessus* following cosmetic injections of botulinum toxin: A case report. *World J Clin Cases* 2022; 10(18): 6141-6147
URL: https://www.wjgnet.com/2307-8960/full/v10/i18/6141.htm
DOI: https://dx.doi.org/10.12998/wjcc.v10.i18.6141

INTRODUCTION

Nontuberculous mycobacteria (NTM) refer to mycobacteria other than *Mycobacterium tuberculosis* and *leprosy* with the common involved organs of the lung, bone, soft tissues, skin, and lymph nodes[1]. *Mycobacterium abscessus* (*M. abscessus*) is one of the common pathogens in NTM, which is a fast-growing mycobacterium causing skin and soft tissue infections. Meanwhile, the atypical mycobacterial infections are increasing at injection-related sites as the informal cosmetic treatments are performed, which deserves the attention of the cosmetic and medical supervision[2-4]. The case presented here is a subcutaneous infection caused by *M. abscessus* following cosmetic injections of botulinum toxin.

CASE PRESENTATION

Chief complaints

A 53-year old female patient visited our department with the complaint of multiple nodules for half a month on the forehead and both temporal sites after the injection of botulinum toxin (Figure 1A-C).

History of present illness

The lesions initially presented with erythema after 10 d of the injection then developed to nodules and abscesses after half a month. The patient did not have any concomitant symptoms such as fever, cough, fatigue, sweats, or diarrhea. She was prescribed with antibiotics for 2 wk without alleviation of the lesions.

History of past illness

The patient did not have any underlying disease or take any drugs in the past.

Personal and family history

Nothing special.

Physical examination

Physical examination indicated multiple red papules, nodules, and abscesses on the forehead and both temporal sites with a diameter of 1-3 cm.

Laboratory examinations

The routine blood, urine, and stool tests as well as kidney and liver function tests were in normal levels. The levels of C3, C4 and C-reactive protein were normal. The patient was negative for syphilis, HIV, antinuclear antibodies, and rheumatoid factor. CD3 and CD4 counts were done to check for any immunodeficiency and were within normal limits (Supplementary Table 1).

Imaging examinations

Computed tomography (CT) of the whole body did not find any systemic infection or diseases.

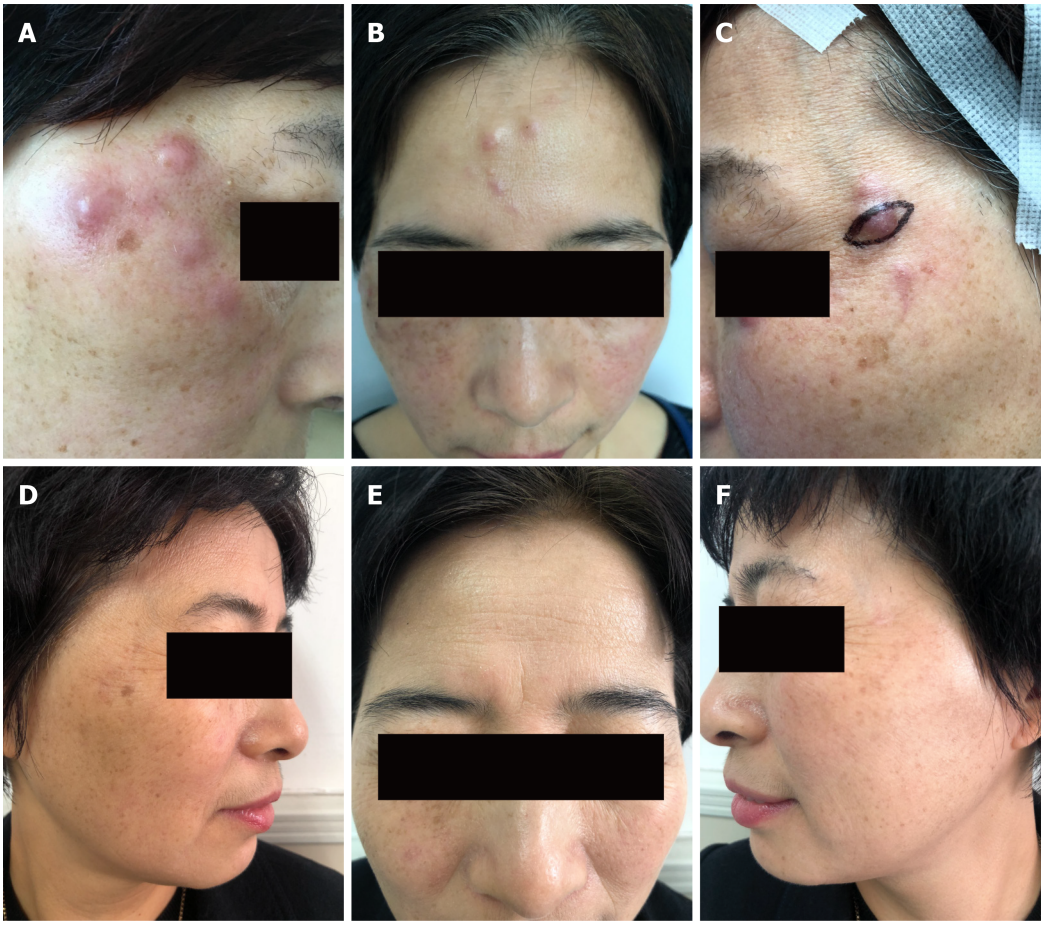

DOI: 10.12998/wjcc.v10.i18.6141 **Copyright** ©The Author(s) 2022.

Figure 1 Patient's photographs before and after treatment. A-C: Multiple red papules, nodules, and abscesses were seen on the forehead and both temporal sites with a diameter of 1 cm-3 cm; D-F: The lesions were cured after the treatment for 7 mo.

FINAL DIAGNOSIS

The patient underwent skin biopsy on the nodules of left temporal site. The pathology of skin tissue showed a large number of inflammatory cells including neutrophils, lymphocytes, and multinucleated giant cells distributed in the derma (Figure 2A and 2B). However, periodic acid Schiff (PAS) and acid-fast staining were negative. Meanwhile, the skin tissue did not yield any microbiome after culture on different media for bacteria, fungus, or mycobacterium. Considering the low biopsy- and culture-positive rate of some microorganisms, a puncture on abscess of right temporal site was further performed. Gray-white colonies were yielded after being cultured on Mycobacterium Roche's Medium (MRM) for 5 days at 35 °C (Figure 3A). Meanwhile, the pus was positive for acid-fast staining and *M. abscessus* was identified by DNA sequencing (Figure 3B). The drug sensitivity test indicated that the microbiome was sensitive to clarithromycin, moxifloxacin, azithromycin, cefoxitin, and amikacin, and was resistant to isoniazid, streptomycin, dapsone, and rifampicin (Supplementary Table 2).

TREATMENT

The patient was initially intramuscularly injected with amikacin 0.2 g and given oral clarithromycin 0.25 g twice a day for 2 wk and then adjusted to moxifloxacin 0.4 g per day and clarithromycin 0.25 g twice a day because of dizziness and vomiting caused by amikacin.

OUTCOME AND FOLLOW-UP

The patient did not show any side effects and presented complete remission of the lesions during the subsequent treatment for 7 mo (Figure 1D-F).

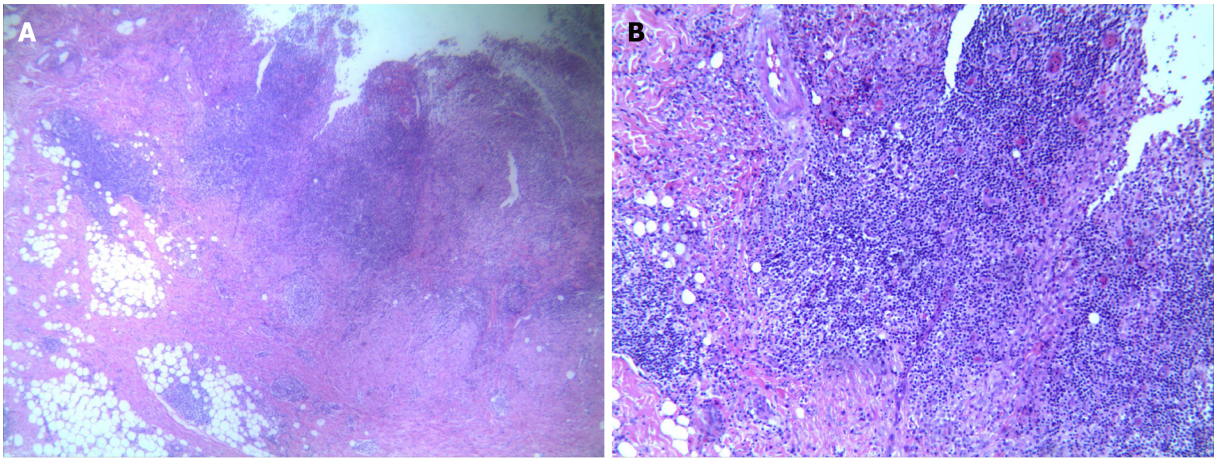

DOI: 10.12998/wjcc.v10.i18.6141 **Copyright** ©The Author(s) 2022.

Figure 2 Histopathology. The histopathology indicated a large number of mixed inflammatory cell infiltrates in the deep dermis, including neutrophils, histiocytes, and lymphocytes (A: HE × 40, B: HE × 100).

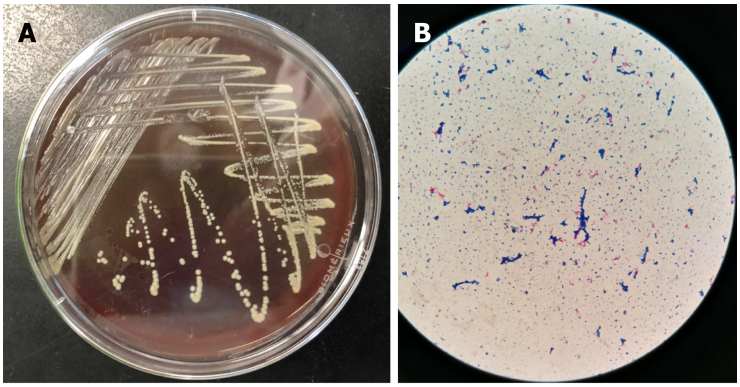

DOI: 10.12998/wjcc.v10.i18.6141 **Copyright** ©The Author(s) 2022.

Figure 3 Microbiological evidence. A: Cultures on Mycobacterium Roche's Medium yielded cream-colored, yeast-like colonies within 5 d at 35 °C; B: Scattered pink rod-shaped bacteria after acid-fast staining (× 100).

DISCUSSION

With the development of un-standard invasive performance in cosmetic industry, related iatrogenic complications are increasing in the last two decades. Injection pain, local edema, erythema, and transient nausea are common complications with mild symptoms. Life-threatening complications are rarely seen, while severe idiosyncratic reactions can cause patients to die from shock and pseudoaneurysm of the superficial temporal artery may break and cause bleeding to death[5]. Infections are also common complications, which usually can be easily cured with empiric antibiotic therapy. However, atypical mycobacterial infections are increasing these years and resistant to regular antibiotic treatment. To meet the challenge of NTM diagnosis and management, we should learn more about it. In Table 1, previous cases of mycobacterial infections caused by cosmetic performance are reviewed[2-4,6-14], the results of which are consistent with the previous studies[1]. It is common to be seen in female patients aged 25 to 45 years. This phenomenon can be attributed to the fact that these people are more often seeking invasive cosmetic performance.

The rare pathogen of *M. abscessus* is the main mycobacteria isolated from lesions cultured, which can involve the skin, soft tissue, and lymph nodes in immunocompetent or immunosuppressed patients[1,15]. The cutaneous infection caused by *M. abscessus* generally occurs following surgery, subcutaneous injection, or acupuncture[16]. Because *M. abscessus* has a hydrophobic biofilm, by which *M. abscessus* can be resistant to disinfectants and heavy metals, and lead to nosocomial infections[17]. The lesions of the patient presented here develop at the injected point of botulinum toxin. We suspected that the infection may be caused by the non-standard aseptic operation and injection, surgery, equipment contamination, or intraoperative infection. Iatrogenic infections have become one of the common causes of fast-growing mycobacterial infection because of the unstandardized aseptic operation during injection and surgery causing an increase in opportunistic infections and great pain to patients. Therefore, when managing such cases, attention should be paid to these agents.

Table 1 Patients' information statistics for subcutaneous infection caused by nontuberculous mycobacteria following cosmetic procedures

No	Ref.	Sex/Age (yr)	Duration after injection (mo/wk/d)	Skin symptoms	Site of infection	Culture	Treatment and course	Outcome
P1	The present case	F/53	Botulinum toxin (1.5 mo)	Erythematousnodules	Cheek, forehead	*M. abscessus*	Clarithromycin, moxifloxacin, amikacin 2/d (7 mo)	Cure
P2	Chen *et al* [2]	F/32	Botulinum toxin (2 mo)	Nodules and abscesses	Forehead and periorbial areas	*M. abscessus*	Clarithromycin 250 mg 2/d, rifampicin 450 mg 1/d, and ethambutol 250 mg 3/d (3 mo)	Cure
P3	Chen *et al* [2]	F/34	Botulinum toxin (10 d)	Painful papules and nodules	Lower jaw, malar, and temple regions	*M. abscessus*	Clarithromycin 250 mg 2/d, rifampicin 450 mg 1/d (6 mo)	Cure
P4	Mello *et al* [3]	F/28	Sunflower oil, deoxycholate, sinetrol, and caffeine subcutaneous application (4 wk)	Pain and erythema	Abdomen and flanks	*M. lentiflavum*	Clarithromycin, 500 mg 2/d and levofloxacin 500 mg 1/d (8 mo)	Cure
P5	Tan *et al*[4]	F/36.6 (28-45) (5 cases)	Autologous fat grafting for cosmetic breast augmentation (20 d)	Erythema, breast contour disruption, breast asymmetry	Breast	*M. Fortuitum* (2), *M. abscessus* (1), and *M. chelonei* (2)	Clarithromycin 500 mg 2/d, amikacin 800 mg 1/d, and imipenem 500 mg 4/d (54 wk) Azithromycin 500 mg 1/d, ethambutol 750 mg 1/d, rifampicin 600 mg 1/d (6 mo), and surgical debridement	Cure
P6	Yeon *et al* [6]	F/34	Botulinum toxin (3.5 mo)	Erythematousnodules	Left mandible	*M. immunogemom*	Clarithromycin 500 mg 2/d (7 m)	Cure
P7	Fang *et al* [7]	F/28	Botulinum toxin (2 wk)	Erythemaand painful nodules	Lower extremities	*M. abscessus*	Clarithromycin, moxifloxacin, and rifampicin (6 mo)	Cure
P8	Thanas arnaksorn *et al*[8]	F/42	Botulinum toxin (5 wk)	Erythematous nodules	Frontalis area and right orbicularis oculi area	Histopathologically confirmed	Clarithromycin 500 mg/d and levofloxacin500 mg/d (6 mo)	Cure
P9	Saeb-Lima *et al*[9]	F/45	Botulinum toxin (5 mo)	Erythematousplaques and nodules	Procerus muscle zone and the pars externa of orbicularis oculi muscle	Histopathologically confirmed	Clarithromycin, azithromycin, and rifampicin (40 d)	Cure
P10	Hammond *et al*[10]	F/40	Lipofilling (2 mo)	Multiple painful nodules	Buttock	*M. chelonae*	Clarithromycin 500 mg 2/d (2.5 mo), ciprofloxacin 500mg 2/d (3 mo), and surgery	Cure
P11	Yoo *et al* [11]	F/56	Filler injections (3 mo)	Nodules	Cheek	*M. volinskyi*	Doxycycline 100 mg 2/d and ciprofloxacin 750 mg 6/d (5 mo)	Cure
P12	Fiore *et al* [12]	F/31	Poly-L-lactic acid (3 mo)	Erythematous nodules	Cheek	*M. mucogenicum*	Ciprofloxacin 500 mg and clarithromycin 500 mg 2/d (6 mo)	Cure
P13	Eustace *et al*[13]	M/28	Hair transplant (2 mo)	Nodules	Sculp	*M. abscessus*	Clarithromycin 250 mg 2/d, doxycycline 100 mg 1/d (3 mo), and drainage	Cure
P14	Yang *et al* [14]	F/29	Facial injection with autologous fat (9 mo)	Abscesses	Temporal and lower orbital regions	*M. abscessus*	Moxifloxacin, clarith-romycin, and ethambutol (12 mo)	Cure

F: Female; M: Male; *M. abscessus*: *Mycobacterium abscessus*.

The skin lesions can be the initial symptoms or secondary to disseminated infections, which often present with multiple papules, herpes, nodules, erythema, or abscesses[1]. The initial symptoms of our patient presented as multiple erythema then developed to nodules and abscess. She was prescribed with multiple antibiotics but without remission of the lesions. The unspecific infection caused by fungus, *M. tuberculosis*, or NTM was suspected. Finally, the patient was diagnosed as having subcutaneous infection caused by *M. abscessus*. The golden standard for diagnosing NTM infections is histopathology and mycobacteria culture. Acid-fast staining is the most convenient and common laboratory test, while PCR sequencing and DNA chip technology have emerged as fast and accurate methods in identifying NTM[15]. However, the acid-fast staining of nodule of this patient was negative and did not yield any culture on MRM. Fortunately, the puncture fluid of abscess was positive for acid-fast staining and *M. abscessus* was yielded and identified by PCR sequencing. Therefore, once NTM infection is clinically suspected, multiple specimens should be tested by histopathology, culture, and molecular biology identification. The successful diagnosis of this patient depended on the awareness of mycobacterial infections and attitude of insistence.

NTM are intracellular colonies whose high hydrophobicity on the cell surface and cell wall permeability barrier make them resistant to traditional anti-tuberculosis drugs and difficult to treat[17]. *M. abscessus* is the most resistant strain of mycobacterium, and is highly resistant to traditional anti-tuberculosis drugs; hence, it needs to be tested for drug susceptibility when yielding positive cultures. *M. abscessus* is often sensitive to clarithromycin, amikacin, and cefoxitin. However, a single drug is easy to induce drug resistance according to the guidelines of the American Thoracic Society and the American Society of Infectious Diseases, therefore the combination of two kinds of sensitive drugs is recommended for treatment until the lesions are completely healed[18]. Meanwhile, drug susceptibility testing needs to be performed once culture of NTM is yielded to ensure the effective treatment.

CONCLUSION

NTM infection should be aware in patients with refractory lesions, particularly followed by cosmetic procedure. Moreover, the drug sensitivity test needs to be performed to obtain early diagnosis and appropriate treatment to avoid dissemination and deformity.

FOOTNOTES

Author contributions: Yu XH and Deng L were the patient' dermatologists; Deng L collected the data; Luo YZ and Liu F contributed to manuscript drafting and literature review.

Informed consent statement: Informed consent was obtained from the patient for publication of this case report.

Conflict-of-interest statement: The authors declare that they have no conflicts of interest to disclose.

CARE Checklist (2016) statement: The authors have read the CARE Checklist (2016), and the manuscript was prepared and revised according to the CARE Checklist (2016).

Open-Access: This article is an open-access article that was selected by an in-house editor and fully peer-reviewed by external reviewers. It is distributed in accordance with the Creative Commons Attribution NonCommercial (CC BY-NC 4.0) license, which permits others to distribute, remix, adapt, build upon this work non-commercially, and license their derivative works on different terms, provided the original work is properly cited and the use is non-commercial. See: https://creativecommons.org/Licenses/by-nc/4.0/

Country/Territory of origin: China

ORCID number: Lin Deng 0000-0001-9574-4632; Ying-Zhi Luo 0000-0002-9662-2562; Fang Liu 0000-0001-6961-0219; Xiao-Hong Yu 0000-0001-8932-499X.

S-Editor: Xing YX
L-Editor: Wang TQ
P-Editor: Xing YX

REFERENCES

1 **Chirasuthat P**, Triyangkulsri K, Rutnin S, Chanprapaph K, Vachiramon V. Cutaneous nontuberculous mycobacterial infection in Thailand: A 7-year retrospective review. *Medicine (Baltimore)* 2020; **99**: e19355 [PMID: 32150075 DOI: 10.1097/MD.0000000000019355]

2 **Chen X**, Jin Y, Torres KMT, Li B, Zhuo F, Ding X, Cai L, Zhang J, Zhou C. *Mycobacterium abscessus* cutaneous infection secondary to botulinum toxin injection: A report of 2 cases. *JAAD Case Rep* 2019; **5**: 982-984 [PMID: 31709291 DOI: 10.1016/j.jdcr.2019.09.017]

3 **Mello RB**, Moreira DN, Pereira ACG, Lustosa NR. Cutaneous infection by Mycobacterium lentiflavum after subcutaneous injection of lipolytic formula. *An Bras Dermatol* 2020; **95**: 511-513 [PMID: 32522448 DOI: 10.1016/j.abd.2019.11.013]

4 **Tan LC**, Li XY, Lu YG. Nontuberculous Mycobacteria Infection After Autologous Fat Grafting for Cosmetic Breast Augmentation. *Ann Plast Surg* 2020; **85**: 358-362 [PMID: 32032112 DOI: 10.1097/SAP.0000000000002234]

5 **Skaf GS**, Domloj NT, Salameh JA, Atiyeh B. Pseudoaneurysm of the superficial temporal artery: a complication of botulinum toxin injection. *Aesthetic Plast Surg* 2012; **36**: 982-985 [PMID: 22527583 DOI: 10.1007/s00266-012-9881-6]

6 **Yeon J**, Chan RCF, Fallah H. Infection with Mycobacterium immunogenum following botulinum toxin injection. *Australas J Dermatol* 2020 [PMID: 32720313 DOI: 10.1111/ajd.13406]

7 **Fang RY**, Sun QN. Mycobacterium abscessus infections following injection of botulinum toxin. *J Cosmet Dermatol* 2020; **19**: 817-819 [PMID: 31402555 DOI: 10.1111/jocd.13094]

8 **Thanasarnaksorn W**, Rattakul B, Suvanasuthi S, Sutthipisal N. Botulinum toxin type A injection-related suppurative granuloma: a case report. *J Cosmet Laser Ther* 2019; **21**: 422-424 [PMID: 31711325 DOI: 10.1080/14764172.2019.1690663]

9 **Saeb-Lima M**, Solis-Arreola GV, Fernandez-Flores A. Mycobacterial infection after cosmetic procedure with botulinum toxin a. *J Clin Diagn Res* 2015; **9**: WD01-WD02 [PMID: 26023629 DOI: 10.7860/JCDR/2015/11741.5756]

10 **Hammond SE**, Al-Bayati A, Joumblat N, Salgado CJ. Mycobacterium Chelonae Infection of the Buttocks Secondary to Lipofilling: A Case Report and Review of the Literature. *Aesthetic Plast Surg* 2017; **41**: 1150-1154 [PMID: 28526906 DOI: 10.1007/s00266-017-0890-3]

11 **Yoo SJ**, Lee KH, Jung SN, Heo ST. Facial skin and soft tissue infection caused by Mycobacterium wolinskyi associated with cosmetic proc edures. *BMC Infect Dis* 2013; **13**: 479 [PMID: 24131522 DOI: 10.1186/1471-2334-13-479]

12 **Fiore R 2nd**, Miller R, Coffman SM. Mycobacterium mucogenicum infection following a cosmetic procedure with poly-L-lactic acid. *J Drugs Dermatol* 2013; **12**: 353-357 [PMID: 23545922]

13 **Eustace K**, Jolliffe V, Sahota A, Gholam K. Cutaneous Mycobacterium abscessus infection following hair transplant. *Clin Exp Dermatol* 2016; **41**: 768-770 [PMID: 27663154 DOI: 10.1111/ced.12900]

14 **Yang P**, Lu Y, Liu T, Zhou Y, Guo Y, Zhu J, Jia C, Chen L, Yang Q. Mycobacterium abscessus Infection After Facial Injection With Autologous Fat: A Case Report. *Ann Plast Surg* 2017; **78**: 138-140 [PMID: 27220017 DOI: 10.1097/SAP.0000000000000837]

15 **Griffith DE**, Aksamit T, Brown-Elliott BA, Catanzaro A, Daley C, Gordin F, Holland SM, Horsburgh R, Huitt G, Iademarco MF, Iseman M, Olivier K, Ruoss S, von Reyn CF, Wallace RJ Jr, Winthrop K; ATS Mycobacterial Diseases Subcommittee; American Thoracic Society; Infectious Disease Society of America. An official ATS/IDSA statement: diagnosis, treatment, and prevention of nontuberculous mycobacterial diseases. *Am J Respir Crit Care Med* 2007; **175**: 367-416 [PMID: 17277290 DOI: 10.1164/rccm.200604-571ST]

16 **Suganeswari G**, Shah D, Anand AR. Intravitreal piperacillin-tazobactam in endophthalmitis caused by Mycobacterium abscessus in silico n e-filled eye: A case report. *Indian J Ophthalmol* 2020; **68**: 1471-1473 [PMID: 32587202 DOI: 10.4103/ijo.ijo_1886_19]

17 **Henry F**, Piérard-Franchimont C, Piérard GE. [Clinical case of the month. *Rev Med Liege* 2005; **60**: 7-10 [PMID: 15771310]

18 **Lyu J**, Jang HJ, Song JW, Choi CM, Oh YM, Lee SD, Kim WS, Kim DS, Shim TS. Outcomes in patients with Mycobacterium abscessus pulmonary disease treated with long-term injectable drugs. *Respir Med* 2011; **105**: 781-787 [PMID: 21211956 DOI: 10.1016/j.rmed.2010.12.012]

World Journal of Clinical Cases

Submit a Manuscript: https://www.f6publishing.com

World J Clin Cases 2022 June 26; 10(18): 6148-6155

DOI: 10.12998/wjcc.v10.i18.6148

ISSN 2307-8960 (online)

CASE REPORT

Overlapping syndrome of recurrent anti-N-methyl-D-aspartate receptor encephalitis and anti-myelin oligodendrocyte glycoprotein demyelinating diseases: A case report

Xue-Jing Yin, Li-Fang Zhang, Li-Hua Bao, Zhi-Chao Feng, Jin-Hua Chen, Bing-Xia Li, Juan Zhang

Specialty type: Clinical neurology

Provenance and peer review: Unsolicited article; Externally peer reviewed.

Peer-review model: Single blind

Peer-review report's scientific quality classification

Grade A (Excellent): 0
Grade B (Very good): B
Grade C (Good): 0
Grade D (Fair): 0
Grade E (Poor): 0

P-Reviewer: Gupta SK, India

Received: October 26, 2021
Peer-review started: October 26, 2021
First decision: March 7, 2022
Revised: March 16, 2022
Accepted: April 30, 2022
Article in press: April 30, 2022
Published online: June 26, 2022

Xue-Jing Yin, Zhi-Chao Feng, Department of Neurology, Changzhi Medical College, Changzhi 046000, Shanxi Province, China

Li-Fang Zhang, Li-Hua Bao, Jin-Hua Chen, Bing-Xia Li, Juan Zhang, Department of Neurology, Changzhi People's Hospital, Changzhi 046000, Shanxi Province, China

Corresponding author: Jinhua Chen, MM, Vice President, Chief Physician, Professor, Department of Neurology, Changzhi People's Hospital, No. 502 Changxing Middle Road, Changzhi 046000, Shanxi Province, China. cjhua0355@163.com

Abstract

BACKGROUND

Anti-N-methyl-D-aspartate receptor encephalitis (NMDARe) is capable of presenting a relapsing course and coexisting with myelin oligodendrocyte glycoprotein antibody disease, whereas it has been relatively rare. We describe a man with no history of tumor who successively developed anti-NMDARe and anti-myelin oligodendrocyte glycoprotein antibody disease.

CASE SUMMARY

A 29-year-old man was initially admitted with headache, fever, intermittent abnormal behavior, decreased intelligence, limb twitching and loss of consciousness on July 16, 2018. On admission, examination reported no abnormality. During his presentation, he experienced aggravated symptoms, and the re-examination of cranial magnetic resonance imaging (MRI) indicated punctate abnormal signals in the left parietal lobe. External examination of cerebrospinal fluid and serum results revealed serum NMDAR antibody (Ab) (-), cerebrospinal fluid NMDAR-Ab (+) 1:10 and Epstein-Barr virus capsid antigen antibody IgG (+). Due to the imaging findings, anti-NMDARe was our primary consideration. The patient was treated with methylprednisolone and gamma globulin pulse therapy, mannitol injection dehydration to reduce intracranial pressure, sodium valproate sustained-release tablets for anti-epilepsy and olanzapine and risperidone to mitigate psychiatric symptoms. The patient was admitted to the hospital for the second time for "abnormal mental behavior and increased limb movements" on December 14, 2018. Re-examination of electroencephalography and cranial MRI showed no abnormality. The results of autoimmune encephalitis antibody revealed that serum NMDAR-Ab was weakly positive and cerebrospinal fluid

NMDAR-Ab was positive. Considering comprehensive recurrent anti-NMDARe, the patient was treated with propylene-hormone pulse combined with immunosuppressive agents (mycophenolate mofetil), and the symptoms were relieved. The patient was admitted for "hoarseness and double vision" for the third time on August 23, 2019. Re-examination of cranial MRI showed abnormal signals in the medulla oblongata and right frontal lobe, and synoptophore examination indicated concomitant esotropia. The patient's visual acuity further decreased, and the re-examination of cranial MRI + enhancement reported multiple scattered speckled and patchy abnormal signals in the medulla oblongata, left pons arm, left cerebellum and right midbrain, thalamus. The patient was diagnosed with an accompanying demyelinating disease. Serum anti-myelin oligodendrocyte glycoprotein 1:10 and NMDAR antibody 1:10 were both positive. The patient was diagnosed with myelin oligodendrocyte glycoprotein antibody-related inflammatory demyelinating disease of the central nervous system complicated with anti-NMDARe overlap syndrome. The patient was successfully treated with methylprednisolone, gamma globulin pulse therapy and rituximab treatment. The patient remained asymptomatic and follow-up MRI scan 6 mo later showed complete removal of the lesion.

CONCLUSION

We emphasize the rarity of this antibody combination and suggest that these patients may require longer follow-up due to the risk of recurrence of two autoimmune disorders.

Key Words: Autoimmune encephalitis; Recurrent anti-N-methyl-D-aspartate receptor encephalitis; Myelin oligodendrocyte glycoprotein; Psoriasis; Case report

©The Author(s) 2022. Published by Baishideng Publishing Group Inc. All rights reserved.

Core Tip: Here we present a man with autoimmune encephalitis in whom antibodies against N-methyl-D-aspartate receptor and myelin oligodendrocyte glycoprotein were sequentially detected. This is the first recurrent N-methyl-D-aspartate receptor encephalitis case in the literature for which antibodies of N-methyl-D-aspartate receptor and myelin oligodendrocyte glycoprotein were positive simultaneously and both supratentorial and infratentorial cranial magnetic resonance imaging were involved. Also, the patient responded very well with the optic nerve injury and encephalitis completely recovering. Psoriasis detected at the 6-mo follow-up may also be an immune-related disease, but the mechanism is unknown.

Citation: Yin XJ, Zhang LF, Bao LH, Feng ZC, Chen JH, Li BX, Zhang J. Overlapping syndrome of recurrent anti-N-methyl-D-aspartate receptor encephalitis and anti-myelin oligodendrocyte glycoprotein demyelinating diseases: A case report. *World J Clin Cases* 2022; 10(18): 6148-6155
URL: https://www.wjgnet.com/2307-8960/full/v10/i18/6148.htm
DOI: https://dx.doi.org/10.12998/wjcc.v10.i18.6148

INTRODUCTION

In several individuals, anti-N-methyl-D-aspartate receptor encephalitis (anti-NMDARe) may occur with myelin oligodendrocyte glycoprotein (MOG) antibody disease sequentially or simultaneously[1-3]. However, there have been few reports of recurrent anti-NMDARe with MOG antibody disease overlap syndrome worldwide. We present a case of a young man initially admitted with headache, fever, behavioral abnormalities and intellectual decline, followed by hoarseness, blurred vision, disturbance of consciousness as well as seizures. Magnetic resonance imaging (MRI) involved multiple regions (*e.g.*, the parietal lobe, frontal lobe, midbrain, thalamus, cerebellum and medulla oblongata). From this case, we recommend the simultaneous detection of viruses, autoimmune encephalitis-associated antibodies and central nervous system demyelination-associated antibodies for patients suspected of having central nervous system demyelinating disease or anti-NMDARe. The aim is to increase the understanding of autoimmune encephalitis overlap syndrome as their clinical and prognostic features may differ from those of single-antibody disease.

CASE PRESENTATION

Chief complaints

A 29-year-old man presented to the Neurology Department of our hospital complaining of headache, fever, intermittent abnormal behavior, decreased intelligence, limb twitching and loss of consciousness. During his presentation, he experienced aggravated symptoms.

The patient was admitted to the hospital for the second time for abnormal mental behavior and increased limb movements.

The patient was admitted for hoarseness and double vision for the third time. During his presentation, the patient's visual acuity further decreased.

History of present illness

The patient began to experience symptoms of headache, fever, nausea and vomiting 7 d before admission. He experienced limb weakness, intermittent behavioral abnormalities and decreased intelligence 4 d before admission. He experienced limb twitching and loss of consciousness 2 d before admission.

History of past illness

The patient had a history of previous surgery for otitis media.

Personal and family history

The daughter of the uncle in the family suffered from lupus erythematosus.

Physical examination

First admission: Clear consciousness, poor orientation to time, place and personality, poor numeracy and unremarkable physical examination.

Second admission: Intermittent clear consciousness, uncooperative rest of nervous system.

Third admission: Horizontal movement of the eyeball was limited, nystagmus to the left in left vision, nystagmus to the right in right vision, vertical nystagmus in upper and lower visions, decreased lateral acupuncture sensation in bilateral face, weak closure of left eyelid, less sensitive corneal reflex, left central facial paralysis, less powerful elevation of right soft palate, left deviation of uvula, left muscle strength grade 4, less stable finger and nose, decreased tendon reflexes in four extremities and positive Babinski sign on the left side were identified.

Laboratory examinations

First admission: Mycobacterium tuberculosis antibody detection reported no abnormality. Cerebrospinal fluid examination revealed: white blood cells 40 × 10^6/L; total protein 0.4 g/L; glucose 3.12 mol/L; and chloride 126.9 mmol/L. External examination of cerebrospinal fluid and serum results revealed: serum NMDAR antibody (Ab) (-); cerebrospinal fluid NMDAR-Ab (+) 1:10; cerebrospinal fluid herpes simplex virus antibody (HSVI, II IgG, IgM) (-); rubella virus antibody (RVIgG, IgM) (-); cytomegalovirus (CMVIgG, IgM) (-); Epstein-Barr virus (EBV) early antigen antibody IgG, IgM, IgA (-); EBV virus capsid antigen antibody IgM, IgA (-); and EBV virus capsid antigen antibody IgG (+).

Second admission: The results of autoimmune encephalitis antibody were serum NMDAR-Ab weakly positive and cerebrospinal fluid NMDAR-Ab positive.

Third admission: Serum anti-MOG (+) 1:10 and NMDAR antibody (+) 1:10 were examined.

Imaging examinations

First admission: Head MRI, chest X-ray and electroencephalography were normal. Re-examination of cranial MRI showed punctate abnormal signals in the left parietal lobe (Figure 1A).

Second admission: Examination of electroencephalography and cranial MRI showed no abnormality (Figure 1B).

Third admission: Examination of cranial MRI showed abnormal signals in the medulla oblongata and right frontal lobe (Figure 1C), and synoptophore examination indicated concomitant esotropia. In such a period, the re-examination of cranial MRI + enhancement reported multiple scattered speckled and patchy abnormal signals in the medulla oblongata, left pons arm, left cerebellum and right midbrain (Figure 1D-F).

MULTIDISCIPLINARY EXPERT CONSULTATION

Lin Wang, MD, Chief Physician, Department of Neurology, Beijing Xuanwu Hospital. The patient confirmed the diagnosis of anti-NMDARe for first admission. The patient should undergo medical treatment with methylprednisolone and gamma globulin pulse therapy and olanzapine to improve sleep. In addition, this patient required regular re-examination of electroencephalography.

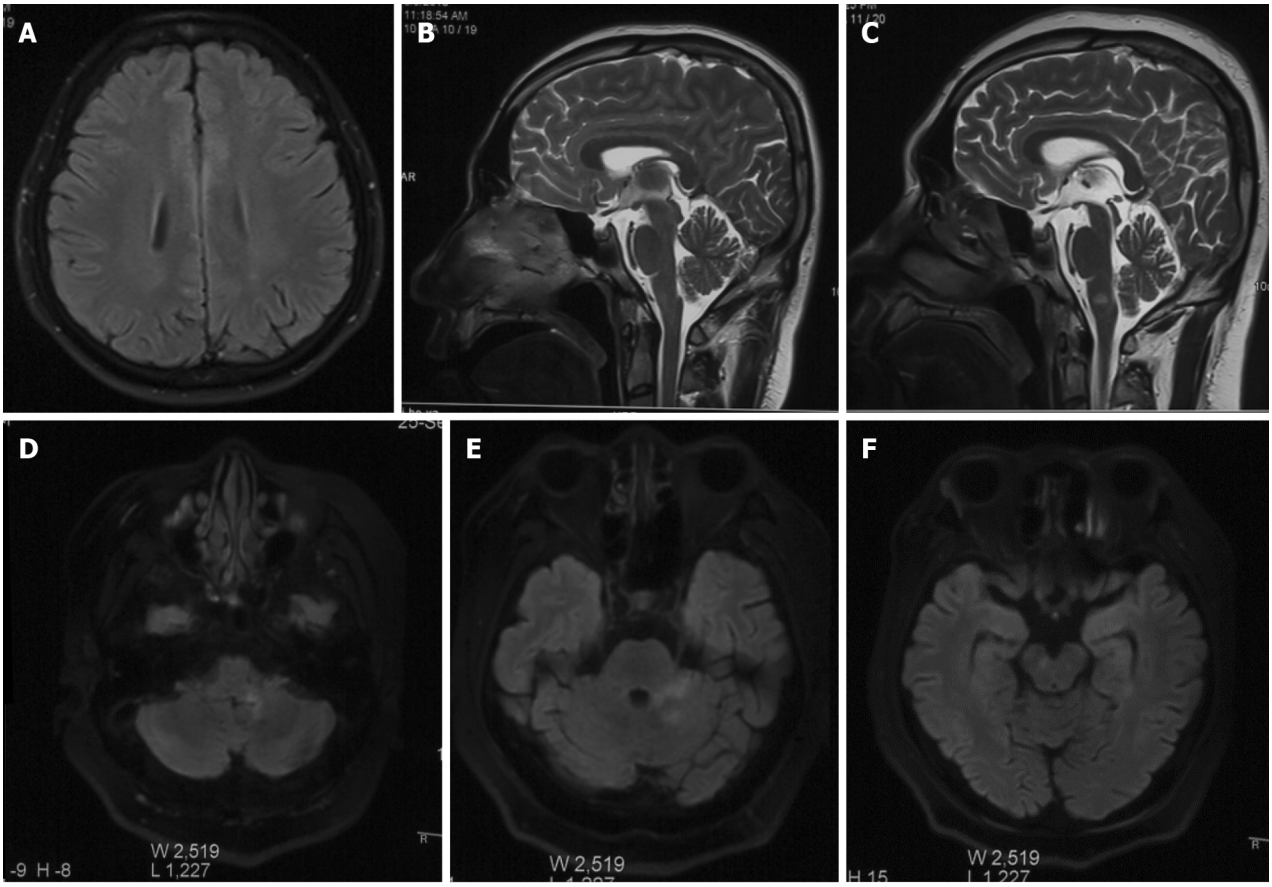

DOI: 10.12998/wjcc.v10.i18.6148 **Copyright** ©The Author(s) 2022.

Figure 1 Imaging changes in the pathogenesis of overlapping syndrome. A: Punctate abnormality in left parietal lobe (first episode); B: Normal sagittal position; C: High signal intensity was identified in the medulla oblongata in the T2 sagittal view; D: High signal intensity was identified in the left medulla oblongata and cerebellum of Flair; E: Flair showed hyperintensity in the left pontine arm and left cerebellum; F: Flair showed hyperintensity in the right midbrain.

Hongzhi Guan, MD, Professor and Chief, Department of Central Nervous System Infection, Beijing Xiehe Hospital. The patient confirmed the diagnosis of recurrent anti-NMDARe for second admission. The patient had psychiatric symptoms, language disorder, autonomic dysfunction and other symptoms in this attack, which were considered to be comprehensive recurrent type. First, the presence of tumors in the patient's body was assessed, gamma globulin and hormone pulse therapy were standardized in those without tumors, and the hormone dose was reduced to 75 mg, 1 tablet every 2 wk. At the same time, according to the consensus, immunosuppressant (mofetil) 1-2 mg/d, orally for at least 1 year, antiepileptic treatment with sodium valproate and olanzapine increased to 2 mg/time to control psychiatric symptoms.

FINAL DIAGNOSIS

The final diagnosis of the presented case was MOG antibody-related inflammatory demyelinating disease of the central nervous system complicated with anti-NMDARe overlap syndrome.

TREATMENT

The patient underwent medical treatment with methylprednisolone and gamma globulin pulse therapy and olanzapine to improve sleep after the first admission. The patient was assessed to be tumor-free at the second admission and given standard gamma globulin and steroid pulse therapy with a steroid dose reduced to 75 mg, 1 tablet every 2 wk. At the same time, according to the consensus, immunosuppressive agents (mofetil) 1-2 mg/d, orally for at least 1 year and antiepileptic treatment with sodium valproate and olanzapine increased to 2 mg/time to control psychiatric symptoms was prescribed. At the last admission, the patient was successfully treated with methylprednisolone, gamma globulin pulse therapy and rituximab treatment.

OUTCOME AND FOLLOW-UP

The patient had an uneventful clinical course, whilst dexamethasone was decreased progressively until its cessation. At the follow-up visit 1 year after hospital discharge, the patient was asymptomatic. An MRI scan showed complete removal of the lesion. However, we observed scattered red rashes on both upper limbs and trunk. Since dermoscopy showed scattered red spots and plaque changes on the glans penis and ventral surface of the extremities and a few scales, the diagnosis of psoriasis was considered. Halometasone ointment was applied externally.

DISCUSSION

The concept of anti-NMDARe was first introduced in 2007 by Dalmau *et al*[4]. MOG antibodies are related to demyelinating diseases of the central nervous system. Therefore, the concept of MOG antibody-related demyelinating diseases of the central nervous system (MOG antibody disease) was proposed[6,7]. Some patients suffering anti-NMDARe have positive serum MOG antibody, and some patients suffering MOG antibody have positive cerebrospinal fluid anti-NMDAR antibody, which is called MOG antibody disease with anti-NMDARe overlap syndrome (MNOS)[1,8,9]. In several individuals, anti-NMDARe may occur with MOG antibody disease sequentially or simultaneously[1-3]. However, there have been rare reports of recurrent anti-NMDARe with MOG antibody disease overlap syndrome worldwide.

Encephalitis is a neurological disorder caused by diffuse or multiple inflammatory lesions of the brain parenchyma. Among them, autoimmune encephalitis generally refers to a type of encephalitis mediated by autoimmune mechanisms[10]. At present, the proportion of autoimmune encephalitis accounts for 10%-20% of encephalitis cases, of which anti-NMDARe is the most common, accounting for about 80% [11,12]. Autoimmune encephalitis should be differentiated from central nervous system infections caused by herpes simplex encephalitis, epidemic encephalitis B, neurosyphilis, bacteria, fungi, parasites, Creutzfeldt-Jakob disease and the presence or absence of opportunistic infectious diseases associated with immunosuppressive or anti-tumor agents[13,14].

Cerebrospinal fluid antibodies were negative in the acute phase of the above infectious diseases[15]. In this case, relevant examinations such as cerebrospinal fluid cytology, culture, virus, antibody, cranial MRI, electroencephalogram, tumor screening [tumor markers, chest computed tomography, scrotum, both kidneys, hepatobiliary b-ultrasound] and positron emission tomography-computed tomography were perfected for differential significance[9,16]. We report a young man who initially presented with headache, fever and epilepsy as the first symptoms, followed by behavioral abnormalities, intellectual decline, dyskinesia and decreased autonomic function in accordance with the course of "bimodal encephalitis" reported in the literature[17]. Combined with cerebrospinal fluid NMDAR antibody (+) 1:10, EBV viral capsid antigen antibody IgG (+), negative tumor screening program and other examinations, it was considered to be anti-NMDARe secondary to non-tumor viral encephalitis. The disadvantage of this case is that metagenomic next-generation sequencing was not further refined to identify the presence of other bacterial or viral infections.

Five months after improvement of treatment, the patient once again developed psychiatric symptoms and increased limb movements, and the cerebrospinal fluid NMDAR antibody (+) was 1:10. Given the definition of recurrent anti-NMDARe, *i.e.* new symptoms not able to be explained by other reasons or aggravation of original symptoms were identified 2 mo after the improvement of NMDARe treatment[2,10], the diagnosis of recurrent anti-NMDARe could be confirmed. Subsequently, the patient developed hoarseness and double vision, and the re-examination of cranial MRI + enhancement indicated new lesions. On the whole, anti-NMDARe was not related to optic nerve damage and sensory disturbance in clinical practice, and patients suffering demyelinating diseases of the central nervous system are considered to be combined with MRI and clinical manifestations. The detection of serum MOG antibody indicated MOG (+) 1:10, by complying with the diagnostic criteria of MOG antibody disease[18]. Then diagnosis of anti-NMDARe with MOG antibody disease overlap syndrome was confirmed.

Characteristics of this case include: (1) Etiology: it has been reported in the literature that anti-NMDARe is related to tumors, but the incidence of tumors detected in patients suffering MNOS is small, and the prognosis is good[2,10,19]. The present patient agreed with previous literature reports in which no tumor was detected during a 2-year course; (2) Affected population: MOG antibody disease and anti-NMDARe are usually more common in women, and the incidence of MNOS in children is higher than that in adults[1,5,9]. However, the patient in this case was an adult male, it was relatively rare; (3) Clinical manifestations: the clinical symptoms of recurrent anti-NMDARe are mild, overall manifested as a single symptom, which is mild when recurrent[10,20]. Nevertheless, this patient was inconsistent with existing literature reports, showing psychiatric symptoms, language impairment and autonomic dysfunction. At the time of recurrence, he displayed considerable clinical symptoms, *i.e.* comprehensive recurrent anti-NMDARe; (4) MRI findings: the cranial MRI of patients suffering anti-NMDARe may be unremarkable, or there may be only scattered cortical and subcortical dot-like abnormalities[4,20]. The first two episodes in this patient were consistent with the findings in previous

reports. All patients suffering MNOS will have supratentorial lesions and less infratentorial lesions[1], but both supratentorial and infratentorial cranial MRI were involved in this patient; (5) Prognosis: the optic nerve injury and encephalitis of this patient recovered completely, thereby not complying with the findings of Titulaer *et al*[2], who found that patients suffering MNOS had a delayed recovery from demyelinating disease and a more pronounced residual deficit; and (6) Concomitant disease: At present, anti-NMDARe secondary to EBV-related viral encephalitis has not been reported worldwide, and psoriasis was reported by dermatoscopy during the 6-mo follow-up of the patient. Psoriasis[21] is an immune-mediated polygenic genodermatosis, which may be the result of a combination of genetic, environmental and immunological factors. To the best of the authors' knowledge, there have been no reported related cases worldwide.

CONCLUSION

In clinical practice, simultaneous detection of viruses, autoimmune encephalitis-related antibodies and central nervous system demyelination-related antibodies is recommended for patients suffering from suspected central nervous system demyelinating disease or anti-NMDARe. First, when the patient has a typical course of "bimodal symptoms," *i.e.* the first peak has "fever, psycho-behavioral abnormalities, epilepsy" as the symptoms and the second peak has "psycho-behavioral abnormalities, memory loss, dyskinesia, autonomic dysfunction" as the primary symptoms to consider autoimmune encephalitis secondary to viral encephalitis. Second, when anti-NMDARe patients are identified to develop symptoms involving the optic nerve and spinal cord (*e.g.*, decreased visual acuity, limb motor or sensory impairment), the coexistence of MOG antibody disease should be considered. Third, when patients suffering MOG antibody disease develop encephalitis symptoms (*e.g.*, psycho-behavioral abnormalities or cognitive impairment) and novel lesions are seen on cranial MRI, anti-NMDARe coexistence should be considered.

ACKNOWLEDGEMENTS

We thank the patient for consenting to our reporting of this case.

FOOTNOTES

Author contributions: Yin XJ, Bao LH and Li BX, were the patient's physician, reviewed the literature and contributed to manuscript drafting; Feng ZC and Zhang J performed and analyzed the magnetic resonance imaging; Zhang LF and Chen JH were responsible for the revision of the manuscript for important intellectual content; All authors issued final approval for the version to be submitted.

Supported by Health Commission of Shanxi Province Issued "Four Approval" Scientific and Technological Innovation Projects in 2020, No. 2020XM38.

Informed consent statement: Informed written consent was obtained from the patient for publication of this report and any accompanying images.

Conflict-of-interest statement: The authors declare that they have no conflict of interest.

CARE Checklist (2016) statement: The authors have read the CARE Checklist (2016), and the manuscript was prepared and revised according to the CARE Checklist (2016).

Open-Access: This article is an open-access article that was selected by an in-house editor and fully peer-reviewed by external reviewers. It is distributed in accordance with the Creative Commons Attribution NonCommercial (CC BY-NC 4.0) license, which permits others to distribute, remix, adapt, build upon this work non-commercially, and license their derivative works on different terms, provided the original work is properly cited and the use is non-commercial. See: https://creativecommons.org/Licenses/by-nc/4.0/

Country/Territory of origin: China

ORCID number: Xue-Jing Yin 0000-0002-4365-3699; Li-Fang Zhang 0000-0002-7925-2686; Li-Hua Bao 0000-0001-9509-3171; Zhi-Chao Feng 0000-0002-5547-3388; Jin-Hua Chen 0000-0002-0231-3786; Bing-Xia Li 0000-0001-6554-0284; Juan Zhang 0000-0002-3925-1507.

S-Editor: Liu JH
L-Editor: Filipodia

P-Editor: Liu JH

REFERENCES

1 **Fan S**, Xu Y, Ren H, Guan H, Feng F, Gao X, Ding D, Fang F, Shan G, Guan T, Zhang Y, Dai Y, Yao M, Peng B, Zhu Y, Cui L. Comparison of myelin oligodendrocyte glycoprotein (MOG)-antibody disease and AQP4-IgG-positive neuromyelitis optica spectrum disorder (NMOSD) when they co-exist with anti-NMDA (N-methyl-D-aspartate) receptor encephalitis. *Mult Scler Relat Disord* 2018; **20**: 144-152 [PMID: 29414288 DOI: 10.1016/j.msard.2018.01.007]

2 **Titulaer MJ**, Höftberger R, Iizuka T, Leypoldt F, McCracken L, Cellucci T, Benson LA, Shu H, Irioka T, Hirano M, Singh G, Cobo Calvo A, Kaida K, Morales PS, Wirtz PW, Yamamoto T, Reindl M, Rosenfeld MR, Graus F, Saiz A, Dalmau J. Overlapping demyelinating syndromes and anti–N-methyl-D-aspartate receptor encephalitis. *Ann Neurol* 2014; **75**: 411-428 [PMID: 24700511 DOI: 10.1002/ana.24117]

3 **Sarigecili E**, Cobanogullari MD, Komur M, Okuyaz C. A rare concurrence: Antibodies against Myelin Oligodendrocyte Glycoprotein and N-methyl-d-aspartate receptor in a child. *Mult Scler Relat Disord* 2019; **28**: 101-103 [PMID: 30590238 DOI: 10.1016/j.msard.2018.12.017]

4 **Dalmau J**, Tüzün E, Wu HY, Masjuan J, Rossi JE, Voloschin A, Baehring JM, Shimazaki H, Koide R, King D, Mason W, Sansing LH, Dichter MA, Rosenfeld MR, Lynch DR. Paraneoplastic anti-N-methyl-D-aspartate receptor encephalitis associated with ovarian teratoma. *Ann Neurol* 2007; **61**: 25-36 [PMID: 17262855 DOI: 10.1002/ana.21050]

5 **Pérez CA**, Agyei P, Gogia B, Harrison R, Samudralwar R. Overlapping autoimmune syndrome: A case of concomitant anti-NMDAR encephalitis and myelin oligodendrocyte glycoprotein (MOG) antibody disease. *J Neuroimmunol* 2020; **339**: 577124 [PMID: 31837635 DOI: 10.1016/j.jneuroim.2019.577124]

6 **Reindl M**, Waters P. Myelin oligodendrocyte glycoprotein antibodies in neurological disease. *Nat Rev Neurol* 2019; **15**: 89-102 [PMID: 30559466 DOI: 10.1038/s41582-018-0112-x]

7 **Rojc B**, Podnar B, Graus F. A case of recurrent MOG antibody positive bilateral optic neuritis and anti-NMDAR encephalitis: Different biological evolution of the two associated antibodies. *J Neuroimmunol* 2019; **328**: 86-88 [PMID: 30599296 DOI: 10.1016/j.jneuroim.2018.12.003]

8 **Weber MS**, Derfuss T, Metz I, Brück W. Defining distinct features of anti-MOG antibody associated central nervous system demyelination. *Ther Adv Neurol Disord* 2018; **11**: 1756286418762083 [PMID: 29623106 DOI: 10.1177/1756286418762083]

9 **Abboud H**, Probasco JC, Irani S, Ances B, Benavides DR, Bradshaw M, Christo PP, Dale RC, Fernandez-Fournier M, Flanagan EP, Gadoth A, George P, Grebenciucova E, Jammoul A, Lee ST, Li Y, Matiello M, Morse AM, Rae-Grant A, Rojas G, Rossman I, Schmitt S, Venkatesan A, Vernino S, Pittock SJ, Titulaer MJ; Autoimmune Encephalitis Alliance Clinicians Network. Autoimmune encephalitis: proposed best practice recommendations for diagnosis and acute management. *J Neurol Neurosurg Psychiatry* 2021; **92**: 757-768 [PMID: 33649022 DOI: 10.1136/jnnp-2020-325300]

10 **Dalmau J**, Armangué T, Planagumà J, Radosevic M, Mannara F, Leypoldt F, Geis C, Lancaster E, Titulaer MJ, Rosenfeld MR, Graus F. An update on anti-NMDA receptor encephalitis for neurologists and psychiatrists: mechanisms and models. *Lancet Neurol* 2019; **18**: 1045-1057 [PMID: 31326280 DOI: 10.1016/S1474-4422(19)30244-3]

11 **Armangue T**, Spatola M, Vlagea A, Mattozzi S, Cárceles-Cordon M, Martinez-Heras E, Llufriu S, Muchart J, Erro ME, Abraira L, Moris G, Monros-Giménez L, Corral-Corral Í, Montejo C, Toledo M, Bataller L, Secondi G, Ariño H, Martínez-Hernández E, Juan M, Marcos MA, Alsina L, Saiz A, Rosenfeld MR, Graus F, Dalmau J; Spanish Herpes Simplex Encephalitis Study Group. Frequency, symptoms, risk factors, and outcomes of autoimmune encephalitis after herpes simplex encephalitis: a prospective observational study and retrospective analysis. *Lancet Neurol* 2018; **17**: 760-772 [PMID: 30049614 DOI: 10.1016/S1474-4422(18)30244-8]

12 **Graus F**, Titulaer MJ, Balu R, Benseler S, Bien CG, Cellucci T, Cortese I, Dale RC, Gelfand JM, Geschwind M, Glaser CA, Honnorat J, Höftberger R, Iizuka T, Irani SR, Lancaster E, Leypoldt F, Prüss H, Rae-Grant A, Reindl M, Rosenfeld MR, Rostásy K, Saiz A, Venkatesan A, Vincent A, Wandinger KP, Waters P, Dalmau J. A clinical approach to diagnosis of autoimmune encephalitis. *Lancet Neurol* 2016; **15**: 391-404 [PMID: 26906964 DOI: 10.1016/S1474-4422(15)00401-9]

13 **Armangue T**, Leypoldt F, Málaga I, Raspall-Chaure M, Marti I, Nichter C, Pugh J, Vicente-Rasoamalala M, Lafuente-Hidalgo M, Macaya A, Ke M, Titulaer MJ, Höftberger R, Sheriff H, Glaser C, Dalmau J. Herpes simplex virus encephalitis is a trigger of brain autoimmunity. *Ann Neurol* 2014; **75**: 317-323 [PMID: 24318406 DOI: 10.1002/ana.24083]

14 **Xu CL**, Liu L, Zhao WQ, Li JM, Wang RJ, Wang SH, Wang DX, Liu MY, Qiao SS, Wang JW. Anti-N-methyl-D-aspartate receptor encephalitis with serum anti-thyroid antibodies and IgM antibodies against Epstein-Barr virus viral capsid antigen: a case report and one year follow-up. *BMC Neurol* 2011; **11**: 149 [PMID: 22126669 DOI: 10.1186/1471-2377-11-149]

15 **Berger B**, Pytlik M, Hottenrott T, Stich O. Absent anti-N-methyl-D-aspartate receptor NR1a antibodies in herpes simplex virus encephalitis and varicella zoster virus infections. *Int J Neurosci* 2017; **127**: 109-117 [PMID: 26887329 DOI: 10.3109/00207454.2016.1147447]

16 **Ellul M**, Solomon T. Acute encephalitis - diagnosis and management. *Clin Med (Lond)* 2018; **18**: 155-159 [PMID: 29626021 DOI: 10.7861/clinmedicine.18-2-155]

17 **Shu Y**, Qiu W, Zheng J, Sun X, Yin J, Yang X, Yue X, Chen C, Deng Z, Li S, Yang Y, Peng F, Lu Z, Hu X, Petersen F, Yu X. HLA class II allele *DRB1*16:02* is associated with anti-NMDAR encephalitis. *J Neurol Neurosurg Psychiatry* 2019; **90**: 652-658 [PMID: 30636700 DOI: 10.1136/jnnp-2018-319714]

18 **Jarius S**, Paul F, Aktas O, Asgari N, Dale RC, de Seze J, Franciotta D, Fujihara K, Jacob A, Kim HJ, Kleiter I, Kümpfel T, Levy M, Palace J, Ruprecht K, Saiz A, Trebst C, Weinshenker BG, Wildemann B. MOG encephalomyelitis: international recommendations on diagnosis and antibody testing. *J Neuroinflammation* 2018; **15**: 134 [PMID: 29724224 DOI: 10.1186/s12974-018-1144-2]

19 **Ishikawa N**, Tajima G, Hyodo S, Takahashi Y, Kobayashi M. Detection of autoantibodies against NMDA-type glutamate

receptor in a patient with recurrent optic neuritis and transient cerebral lesions. *Neuropediatrics* 2007; **38**: 257-260 [PMID: 18330842 DOI: 10.1055/s-2007-1004521]

20 **Titulaer MJ**, McCracken L, Gabilondo I, Armangué T, Glaser C, Iizuka T, Honig LS, Benseler SM, Kawachi I, Martinez-Hernandez E, Aguilar E, Gresa-Arribas N, Ryan-Florance N, Torrents A, Saiz A, Rosenfeld MR, Balice-Gordon R, Graus F, Dalmau J. Treatment and prognostic factors for long-term outcome in patients with anti-NMDA receptor encephalitis: an observational cohort study. *Lancet Neurol* 2013; **12**: 157-165 [PMID: 23290630 DOI: 10.1016/S1474-4422(12)70310-1]

21 **Boehncke WH**, Schön MP. Psoriasis. *Lancet* 2015; **386**: 983-994 [PMID: 26025581 DOI: 10.1016/S0140-6736(14)61909-7]

World Journal of Clinical Cases

Submit a Manuscript: https://www.f6publishing.com

World J Clin Cases 2022 June 26; 10(18): 6156-6162

DOI: 10.12998/wjcc.v10.i18.6156

ISSN 2307-8960 (online)

CASE REPORT

Liver transplantation for late-onset ornithine transcarbamylase deficiency: A case report

Xiao-Hui Fu, Yu-Hui Hu, Jian-Xiang Liao, Li Chen, Zhan-Qi Hu, Jia-Lun Wen, Shu-Li Chen

Specialty type: Genetics and heredity

Provenance and peer review: Unsolicited article; Externally peer reviewed.

Peer-review model: Single blind

Peer-review report's scientific quality classification

Grade A (Excellent): 0
Grade B (Very good): 0
Grade C (Good): C, C
Grade D (Fair): D
Grade E (Poor): 0

P-Reviewer: Enosawa S, Japan; Topal U, Turkey

Received: October 28, 2021
Peer-review started: October 28, 2021
First decision: December 27, 2021
Revised: January 10, 2022
Accepted: April 22, 2022
Article in press: April 22, 2022
Published online: June 26, 2022

Xiao-Hui Fu, Yu-Hui Hu, Shu-Li Chen, Department of Inherited Metabolic Disorders, The Affiliated Hospital of China Medical University and Shenzhen Children's Hospital, Shenzhen 518038, Guangdong Province, China

Jian-Xiang Liao, Li Chen, Zhan-Qi Hu, Jia-Lun Wen, Department of Neurology, The Affiliated Hospital of China Medical University and Shenzhen Children's Hospital, Shenzhen 518038, Guangdong Province, China

Corresponding author: Shu-Li Chen, PhD, Chief Doctor, Department of Inherited Metabolic Disorders, The Affiliated Hospital of China Medical University and Shenzhen Children's Hospital, No. 7019 Yitian Road, Futian District, Shenzhen 518038, Guangdong Province, China. 13008803656@163.com

Abstract

BACKGROUND

Ornithine transcarbamylase deficiency (OTCD) is an X-linked inherited disorder and characterized by marked elevation of blood ammonia. The goal of treatment is to minimize the neurological damage caused by hyperammonemia. OTCD can be cured by liver transplantation (LT). Post-transplant patients can discontinue anti- hyperammonemia agents and consume a regular diet without the risk of developing hyperammonemia. The neurological damage caused by hyperammonemia is almost irreversible.

CASE SUMMARY

An 11.7-year-old boy presented with headache, vomiting, and altered consciousness. The patient was diagnosed with late-onset OTCD. After nitrogen scavenging treatment and a protein-free diet, ammonia levels were reduced to normal on the third day of admission. Nevertheless, the patient remained in a moderate coma. After discussion, LT was performed. Following LT, the patient's blood ammonia and biochemical indicators stabilized in the normal range, he regained consciousness, and his nervous system function significantly recovered. Two months after LT, blood amino acids and urine organic acids were normal, and brain magnetic resonance imaging showed a decrease in subcortical lesions.

CONCLUSION

LT can significantly improve partial neurological impairment caused by late-onset OTCD hyperammonemic encephalopathy, and LT can be actively considered when early drug therapy is ineffective.

Key Words: Ornithine transcarbamylase deficiency; Urea cycle disorder; Hyperammonemic encephalopathy; Liver transplantation; Case report

©The Author(s) 2022. Published by Baishideng Publishing Group Inc. All rights reserved.

Core Tip: There are differing views on the timing of liver transplantation (LT) for ornithine transcarbamylase deficiency (OTCD) and whether it makes sense to perform LT in a patient with severe neurological impairment. We report a case of late-onset OTCD with severe neurological impairment, whose nervous system function recovered after LT. In late-onset OTCD patients with severe neurological impairment, LT can be considered.

Citation: Fu XH, Hu YH, Liao JX, Chen L, Hu ZQ, Wen JL, Chen SL. Liver transplantation for late-onset ornithine transcarbamylase deficiency: A case report. *World J Clin Cases* 2022; 10(18): 6156-6162
URL: https://www.wjgnet.com/2307-8960/full/v10/i18/6156.htm
DOI: https://dx.doi.org/10.12998/wjcc.v10.i18.6156

INTRODUCTION

Ornithine transcarbamylase deficiency (OTCD) is the most common urea cycle disorder, with an incidence of approximately 1/56500 to 1/80000 reported in the literature[1-4]. The 2019 Urea Cycle Disorders Diagnosis and Management guidelines recommend liver transplantation (LT) for patients with severe urea cycle disorders who do not have severe neurological impairment and have stable metabolic status[5]. Opinions regarding LT for children with pre-existing severe brain damage differ as LT does not restore pre-existing neurological damage and due to the high risk of LT in children with acute encephalopathy; there is no experience regarding the extent to which neurological damage can be restored after surgery[5]. We report a patient with late-onset OTCD with good neurological recovery after LT.

CASE PRESENTATION

Chief complaints

An 11.7-year-old boy was admitted to our hospital due to headache, vomiting and altered mental status.

History of present illness

Two days before admission, the patient complained of a headache without obvious inducement, accompanied by vomiting 25 times. The headache did not improve with cold medication. He became unconscious 12 h before admission, and relevant tests were completed at a referring hospital. His blood ammonia was > 500 μmol/L. He was referred to our hospital for further treatment.

History of past illness

The patient was the product of a first pregnancy and first birth (G1P1) mother, and delivered by cesarean section at term with a birth weight of 3.0 kg. His perinatal condition was unremarkable, with no history of asphyxia. He was generally healthy and developed normally for a child of the same age. Prior to this episode, the family was not aware that the patient had OTCD.

Personal and family history

The patient had no significant family history. No patients in the family had OTCD or symptoms associated with the disease.

Physical examination

On physical examination, he was in a moderate comatose state [Glasgow coma score (GSC) 6] and was unresponsive to sound. His eyes could not be closed, the pupils were equally large and round, about 3 mm in diameter, and light reflex was delayed. There were no significant abnormalities on cardiopulmonary or abdominal examinations. Muscle strength in the limbs could not be tested, muscle tone was normal, and all pathological signs were negative.

Laboratory examinations

Laboratory tests showed a significantly elevated blood ammonia level (Table 1). Liver function and coagulation times were abnormal. Blood tandem mass spectrometry showed moderately elevated glutamine. Citrulline and arginine were in the normal range. Urine organic acid gas phase mass spectrometry showed that uracil and orotic acid levels were elevated. Blood ammonia levels during the first week of admission are shown in Figure 1. During the remainder rest of his hospital stay, levels were in the normal range.

Whole exome gene testing revealed the *OTC* gene exon2 hemizygote variant c.119G > A (p.R40H), inherited from his mother. The missense mutation was located in the well-studied exon functional domain without benign variation [Pathogenic moderate (PM) 1]. The frequencies of all normal population databases (dsSNP, 1000 genomes) were less than 0.0005 (PM2). This is a variant with different amino acid changes at the same locus reported in the literature as pathogenic variants (PM5). Pathogenic missense mutations of this gene are common, and benign missense mutations are rare [Pathogenic supporting (PP) 2]. The literature reported that variant to caused impaired gene function as show by *in vitro* functional assays [Pathogenic strong (PS) 3]. In summary, according to American College of Medical Genetics (ACMG)guidelines, this variant is likely pathogenic (PM1 + PM2 + PM5 + PP2 + PS3).

Imaging examinations

Brain magnetic resonance imaging (MRI) revealed that large patches of symmetrical high signal shadows on T2 weighted imaging (T2WI) and fluid attenuated inversion recovery in the cerebral hemispheres, and diffusion WI (DWI) revealed a significant high signal, more pronounced in the bilateral dorsal thalamus, caudate nucleus, lenticular nucleus, insula, cingulate gyrus and frontal lobe into the cortex at the falx.

FINAL DIAGNOSIS

Hyperammonemic encephalopathy and ornithine transcarbamylase deficiency.

TREATMENT

After admission, the patient underwent continuous hemodiafiltration (Disposable hemodialysate filter and supporting pipeline, Prismaflex M100 set, Gambro Industries, Meyzieu, France; blood flow velocity 150-300 mL/min, replacement velocity 1000-2500 mL/h, dialysis velocity 1500-5000 mL/h) to lower the blood ammonia level. The impairment of consciousness worsened, and the repeat blood ammonia level was 511.72 μmol/L. Within a few hours, he fell into a severe coma (GSC 3) and developed central respiratory failure. We immediately provided ventilation, reduced intracranial pressure (mannitol and hypertonic sodium), nitrogen scavenger agents including sodium benzoate and arginine, antibiotics to inhibit ammonia production by intestinal bacteria, along with multiple nutritional support treatments.

On day 3, blood ammonia decreased to normal and was maintained in the normal range for the remainder of the hospital stay. The continuous hemodiafiltration parameters (blood flow velocity 120 mL /min, replacement velocity 500 mL/h, dialysis velocity 2500 mL/h) were gradually adjusted downwards. On day 6, the patient discontinued hemodiafiltration. On day 7, the patient's consciousness changed from deep coma to moderate coma. On day 12, the patient was weaned from the ventilator; however, he remained in a moderate coma.

On day 31, modified piggyback orthotopic LT (anastomosis of the donor inferior vena cava to the recipient inferior vena cava) was performed, the donor was deceased. Postoperatively, the patient was treated with tacrolimus, sodium mescaline, and methylprednisolone. On day 35 (day 4 after surgery), the patient was conscious (opened eyes autonomously, obeyed commands, verbal response was "T"). A repeat brain MRI more than 2 mo after transplantation showed that the previous subcortical lesions had largely disappeared; however, hydrocephalus was worse (Figure 2). He was discharged after 3 mo and underwent abdominal ventricular drainage at another hospital.

OUTCOME AND FOLLOW-UP

At follow-up, 6 mo after surgery, he could sit, squat, and walk smoothly on his own. He could say simple superlatives, and his command execution rate was approximately 30%. He showed poor emotional control and a greater temper to his parents; however, he was gentler to strangers and his brother.

Table 1 Laboratory data

Parameter	On admission	After LT	Reference range
Blood ammonia, μmol/L	461.2 ↑	51.2	14-65
Blood lactic acid, mmol/L	4.47 ↑	0.78	0.5-2.2
APTT, s	37.3	24.1	26.1-40.7
PT, s	23.1 ↑	12.6	9.3-12.9
INR	2.030 ↑	1.10	0.72-1.15
Fibrinogen, g/L	1.88	2.36	1.57-3.93
ALT, U/L	73 ↑	44 ↑	0-40
AST, U/L	50 ↑	31	0-40
ALP, U/L	564 ↑	126	40-500
GGT, U/L	15	107 ↑	0-50
TBIL, μmol/L	30.8 ↑	4.0	0.9-17.1
IBIL, μmol/L	25.6 ↑	1.8	2-17
Albumin, g/L	45.5	41.9	35-55
Serum creatinine, μmol/L	63.5	42.3	64-104
Serum uric acid, μmol/L	442.90 ↑	365.6	90-420
Ceruloplasmin	24.4	absent	22-322
Blood amino acids			
Glutamine, μmol/L	66.28 ↑	15.83	1.0-55.0
Citrulline, μmol/L	14.7	14.19	5.50-45.00
Arginine, μmol/L	13.57	5.38	1.00-70.00
Urine organic acid			
Uracil, mmol/molCr	29.4 ↑	0.0	0.0-8.0
Urinary orotic acid, mmol/molCr	123.3 ↑	0.0	0.0-2.0

↑: Higher than the reference value; LT: Liver transplantation; APTT: Activated partial thromboplastin time; PT: Prothrombin time; INR: International normalized ratio; ALT: Alanine aminotransaminase; AST: Aspartate aminotransferase; ALP: Alkaline phosphatase; GGT: γ-glutamyl transpeptidase; TBIL: Total bilirubin; IBIL: Indirect bilirubin.

DISCUSSION

OTCD can develop at any age. Depending on the time of onset, OTCD can be divided into the neonatal-onset type and the late-onset type (age of onset > 28 d)[6]. Patients with neonatal onset usually present in the first few hours and days after birth with severe disease and high mortality. The clinical presentation of late-onset disease varies widely, with no specific clinical manifestations before initial onset. Acute onset of late-onset OTCD can be induced by infection, prolonged fasting, or fatigue. The outcome for conservative treatment is poor in patients with hyperammonemia crisis, and 5-year survival is approximately 45%[7].

Outcomes in urea cycle disorders are related to blood ammonia levels and the duration of the coma. According to a European questionnaire, patients with blood ammonia levels > 300 μmol/L or peak blood ammonia levels > 480 μmol/L during the first episode suffered neurological dysfunction[8]. Although patients with late-onset OTCD generally have better outcomes than those with neonatal onset, there is a higher incidence of residual neurological damage, and the mortality rate for late-onset OTCD with coma on the first episode is high. In a follow-up study that included 90 OTCD cases, 18 patients had coma as their first presentation and 6 of them died[9]. Among 16 genetically confirmed cases of late-onset OTCD reported in the Chinese literature[10], nine died shortly after hospital admission, suggesting the disease's aggressive nature at acute onset. In our case, the patient was physically fit and had normal development before the presentation. Headache and vomiting were the primary manifestations; these symptoms were not taken seriously until the onset of unconsciousness, which delayed the treatment. Although blood ammonia levels reduced to the normal range after aggressive treatment, neurological damage did not improve with the normalization of blood ammonia. The patient was in a

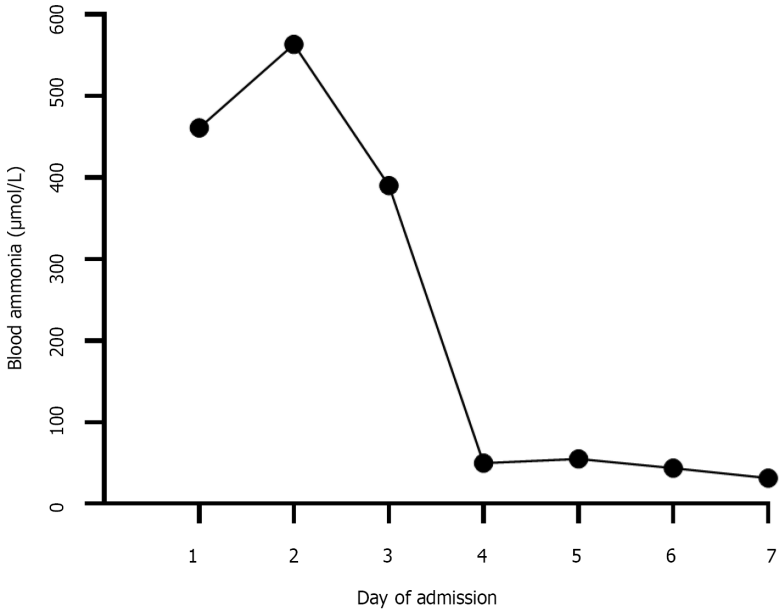

DOI: 10.12998/wjcc.v10.i18.6156 **Copyright** ©The Author(s) 2022.

Figure 1 Blood ammonia changes during the first week of admission.

moderate coma before LT.

OTCD is treated with a low-protein diet and long-term oral ammonia-lowering medications. LT is the radical treatment for OTCD. After LT, patients no longer need to restrict their diet or take nitrogen scavenging agents[5]. Statistics on LT in patients with urea circulation disorders show that the 5-year survival rate of patients after LT can exceed 90%[11,12]. There is no consensus regarding the indications or timing of LT. It is now believed that LT should be performed in all patients with neonatal onset to prevent neurological damage[13]. The indications and timing of LT for late-onset OTCD must be determined by the clinical symptoms, including poor drug efficacy, recurrent episodes of hyperammonemia, growth retardation, and inability to strictly control the diet[14]. Although post-transplant patients require long-term immunosuppressive drugs, there is evidence that OTCD patients who underwent LT have a better quality of life than those who did not and no longer risked death due to sudden-onset hyperammonemia[11,15].

The present patient had an acute onset, a long duration of hyperammonemia, severe brain damage, and was in a moderate coma before LT. Therefore, the optimal time window for LT was missed, and the choice of LT and the extent to which the patient would recover from neurological damage after transplantation were a concern for his physicians and parents. Most LTs for OTCD patients are carried out in the context of stable metabolism, and there are few reports of LT in patients with severe neurological injury. Nevertheless, given the patient's inability to regain consciousness, we performed LT, and he was conscious 4 d later. After LT, he did not take nitrogen scavenging agents, and blood ammonia, liver, and kidney function biochemistry were maintained in the normal range at regular follow-up. Kawagishi *et al*[16] reported a patient who underwent LT for recurrent hyperammonemia due to late-onset OTCD, and blood ammonia was maintained in the normal range without further nitrogen scavenging agents after surgery. Nevertheless, at 16 mo after surgery showed no change in subcortical lesions. Brain MRI in our patient was repeated about 2 mo after surgery, and suggested a significant reduction in abnormal cranial signals compared with the previous MRI, indicating that LT was effective in the treatment of this patient, However, brain MRI showed that hydrocephalus had progressed and brain atrophy was present, suggesting that some neurological damage may not be reversed after LT.

Several studies have shown that LT could be used as a radical treatment which significantly improves the quality of life[11,17]. However, it is not clear whether LT is beneficial for OTCD patients who already have severe neurological damage. This case report suggests that LT can be attempted in children with late-onset OTCD, even if severe neurological impairment is already present. Neurological recovery after LT in this patient was unexpected; the recovery of higher functions such as emotional control and spatial thinking require long-term rehabilitation training and psychotherapy, and its effects need to be observed during follow-up.

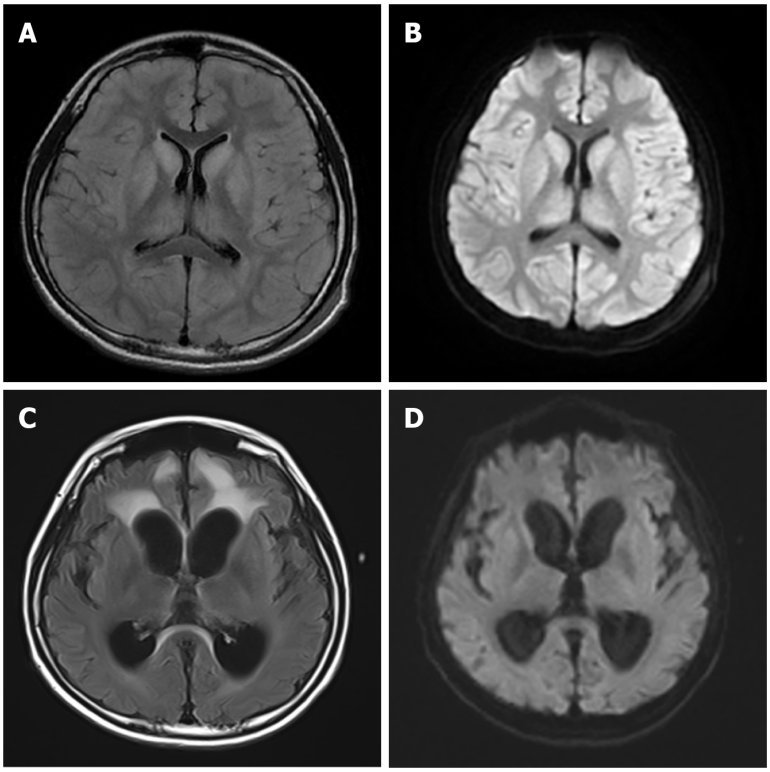

DOI: 10.12998/wjcc.v10.i18.6156 **Copyright** ©The Author(s) 2022.

Figure 2 Brain magnetic resonance imaging. A: On admission, brain magnetic resonance imaging (MRI), T2 fluid attenuated inversion recovery (FLAIR) imaging showed a large symmetrical high signal, more pronounced in the bilateral dorsal thalamus, caudate nucleus, lenticular nucleus, insula, cingulate gyrus and frontal lobe into the cortex at the falx; B: On admission, a high signal was observed on diffusion weighted imaging (DWI) of bilateral dorsal thalamus, caudate nucleus, lenticular nucleus, insula, frontal lobe into the cortex at the falx; C: Two months after liver transplantation (LT), brain MRI, T2 FLAIR imaging showed that the cerebral sulcus fissure was widened and deepened bilaterally in the cerebral hemispheres, and the cortex was atrophied, with a patchy high signal in the frontal lobes bilaterally; D: Two months after LT, brain MRI, DWI did not show any significant abnormal signal, and the abnormal signal in the original bilateral cerebral hemispheric cortex, dorsal thalamus, basal ganglia area, insula, cingulate gyrus, and frontal and temporal lobes was no longer obvious.

CONCLUSION

In summary, patients with late-onset OTCD and acute hyperammonemic encephalopathy are at high risk, and LT can significantly improve the neurological damage caused by this disease. As a radical cure for OTCD, LT should be considered more aggressively.

FOOTNOTES

Author contributions: Hu YH, Liao JX, Chen L, Hu ZQ and Wen JL were responsible for the treatment and management of the patient; Fu XH and Chen SL collected the patient's clinical data and wrote the paper; all authors were involved in writing the manuscript and read and approved the final manuscript.

Supported by the Sanming Project of Medicine in Shenzhen, No. SZSM201812005.

Informed consent statement: Informed written consent was obtained from the patient for the publication of this report and any accompanying images.

Conflict-of-interest statement: The authors declare that they have no conflict of interest.

CARE Checklist (2016) statement: The authors have read the CARE Checklist (2016), and the manuscript was prepared and revised according to the CARE Checklist (2016).

Open-Access: This article is an open-access article that was selected by an in-house editor and fully peer-reviewed by external reviewers. It is distributed in accordance with the Creative Commons Attribution NonCommercial (CC BY-NC 4.0) license, which permits others to distribute, remix, adapt, build upon this work non-commercially, and license their derivative works on different terms, provided the original work is properly cited and the use is non-commercial. See: https://creativecommons.org/Licenses/by-nc/4.0/

Country/Territory of origin: China

ORCID number: Xiao-Hui Fu 0000-0002-9000-224X; Yu-Hui Hu 0000-0002-6989-2460; Jian-Xiang Liao 0000-0001-9769-3365; Li Chen 0000-0002-9029-9581; Zhan-Qi Hu 0000-0001-5926-3962; Jia-Lun Wen 0000-0002-1399-5890; Shu-Li Chen 0000-0001-9989-6414.

S-Editor: Guo XR
L-Editor: Webster JR
P-Editor: Guo XR

REFERENCES

1 **Wilcken B**. Problems in the management of urea cycle disorders. *Mol Genet Metab* 2004; **81** Suppl 1: S86-S91 [PMID: 15050980 DOI: 10.1016/j.ymgme.2003.10.016]
2 **Summar ML**, Koelker S, Freedenberg D, Le Mons C, Haberle J, Lee HS, Kirmse B, European registry and network for intoxication type metabolic diseases (E-IMD). The incidence of urea cycle disorders. *Mol Genet Metab* 2013; **110**: 179-180 [PMID: 23972786 DOI: 10.1016/j.ymgme.2013.07.008]
3 **Dionisi-Vici C**, Rizzo C, Burlina AB, Caruso U, Sabetta G, Uziel G, Abeni D. Inborn errors of metabolism in the Italian pediatric population: a national retrospective survey. *J Pediatr* 2002; **140**: 321-327 [PMID: 11953730 DOI: 10.1067/mpd.2002.122394]
4 **Kido J**, Nakamura K, Mitsubuchi H, Ohura T, Takayanagi M, Matsuo M, Yoshino M, Shigematsu Y, Yorifuji T, Kasahara M, Horikawa R, Endo F. Long-term outcome and intervention of urea cycle disorders in Japan. *J Inherit Metab Dis* 2012; **35**: 777-785 [PMID: 22167275 DOI: 10.1007/s10545-011-9427-0]
5 **Häberle J**, Burlina A, Chakrapani A, Dixon M, Karall D, Lindner M, Mandel H, Martinelli D, Pintos-Morell G, Santer R, Skouma A, Servais A, Tal G, Rubio V, Huemer M, Dionisi-Vici C. Suggested guidelines for the diagnosis and management of urea cycle disorders: First revision. *J Inherit Metab Dis* 2019; **42**: 1192-1230 [PMID: 30982989 DOI: 10.1002/jimd.12100]
6 **Division of genetics and metabolism**, Child diseases and health care branch, Chinese association for maternal and child health. Consensus on diagnosis and treatment of ornithine trans-carbamylase deficiency. *Zhejiang Daxue Xuebao Yixueban* 2020; **49**: 539-547 [PMID: 33210478 DOI: 10.3785/j.issn.1008-9292.2020.04.11]
7 **Wakiya T**, Sanada Y, Mizuta K, Umehara M, Urahasi T, Egami S, Hishikawa S, Fujiwara T, Sakuma Y, Hyodo M, Murayama K, Hakamada K, Yasuda Y, Kawarasaki H. Living donor liver transplantation for ornithine transcarbamylase deficiency. *Pediatr Transplant* 2011; **15**: 390-395 [PMID: 21585627 DOI: 10.1111/j.1399-3046.2011.01494.x]
8 **Enns GM**. Neurologic damage and neurocognitive dysfunction in urea cycle disorders. *Semin Pediatr Neurol* 2008; **15**: 132-139 [PMID: 18708004 DOI: 10.1016/j.spen.2008.05.007]
9 **Brassier A**, Gobin S, Arnoux JB, Valayannopoulos V, Habarou F, Kossorotoff M, Servais A, Barbier V, Dubois S, Touati G, Barouki R, Lesage F, Dupic L, Bonnefont JP, Ottolenghi C, De Lonlay P. Long-term outcomes in Ornithine Transcarbamylase deficiency: a series of 90 patients. *Orphanet J Rare Dis* 2015; **10**: 58 [PMID: 25958381 DOI: 10.1186/s13023-015-0266-1]
10 **Sun Y**, Li XM, Zhang TX, Li DL, Ji KQ, Yan CZ, Zhao YY. Clinical research of two cases of late-onset ornithine carbamoyltransferase deficiency. *Zhonghua Shenjingke Zazhi* 2019; **52**: 399-405 [DOI: 10.3760/cma.j.issn.1006-7876.2019.05.007]
11 **Morioka D**, Kasahara M, Takada Y, Shirouzu Y, Taira K, Sakamoto S, Uryuhara K, Egawa H, Shimada H, Tanaka K. Current role of liver transplantation for the treatment of urea cycle disorders: a review of the worldwide English literature and 13 cases at Kyoto University. *Liver Transpl* 2005; **11**: 1332-1342 [PMID: 16237708 DOI: 10.1002/Lt.20587]
12 **Molema F**, Martinelli D, Hörster F, Kölker S, Tangeraas T, de Koning B, Dionisi-Vici C, Williams M; additional individual contributors of MetabERN. Liver and/or kidney transplantation in amino and organic acid-related inborn errors of metabolism: An overview on European data. *J Inherit Metab Dis* 2021; **44**: 593-605 [PMID: 32996606 DOI: 10.1002/jimd.12318]
13 **Kido J**, Matsumoto S, Mitsubuchi H, Endo F, Nakamura K. Early liver transplantation in neonatal-onset and moderate urea cycle disorders may lead to normal neurodevelopment. *Metab Brain Dis* 2018; **33**: 1517-1523 [PMID: 29948653 DOI: 10.1007/s11011-018-0259-6]
14 **Wakiya T**, Sanada Y, Urahashi T, Ihara Y, Yamada N, Okada N, Ushijima K, Otomo S, Sakamoto K, Murayama K, Takayanagi M, Hakamada K, Yasuda Y, Mizuta K. Impact of enzyme activity assay on indication in liver transplantation for ornithine transcarbamylase deficiency. *Mol Genet Metab* 2012; **105**: 404-407 [PMID: 22264779 DOI: 10.1016/j.ymgme.2011.12.019]
15 **Foschi FG**, Morelli MC, Savini S, Dall'Aglio AC, Lanzi A, Cescon M, Ercolani G, Cucchetti A, Pinna AD, Stefanini GF. Urea cycle disorders: a case report of a successful treatment with liver transplant and a literature review. *World J Gastroenterol* 2015; **21**: 4063-4068 [PMID: 25852294 DOI: 10.3748/wjg.v21.i13.4063]
16 **Kawagishi N**, Satoh K, Enomoto Y, Akamatsu Y, Sekiguchi S, Satoh A, Fujimori K, Takasago Y, Ito T, Ohura T, Satomi S. Improved quality of life and unchanged magnetic resonance brain imaging after living donor liver transplantation for late-onset ornithine transcarbamylase deficiency: report of a case. *Surg Today* 2005; **35**: 1087-1091 [PMID: 16341494 DOI: 10.1007/s00595-005-3071-y]
17 **Kasahara M**, Sakamoto S, Horikawa R, Koji U, Mizuta K, Shinkai M, Takahito Y, Taguchi T, Inomata Y, Uemoto S, Tatsuo K, Kato S. Living donor liver transplantation for pediatric patients with metabolic disorders: the Japanese multicenter registry. *Pediatr Transplant* 2014; **18**: 6-15 [PMID: 24283623 DOI: 10.1111/petr.12196]

World Journal of Clinical Cases

Submit a Manuscript: https://www.f6publishing.com

World J Clin Cases 2022 June 26; 10(18): 6163-6167

DOI: 10.12998/wjcc.v10.i18.6163

ISSN 2307-8960 (online)

CASE REPORT

Disseminated strongyloidiasis in a patient with rheumatoid arthritis: A case report

Jin-Hao Zheng, Lu-Yu Xue

Specialty type: Critical care medicine

Provenance and peer review: Unsolicited article; Externally peer reviewed.

Peer-review model: Single blind

Peer-review report's scientific quality classification

Grade A (Excellent): 0
Grade B (Very good): 0
Grade C (Good): C
Grade D (Fair): 0
Grade E (Poor): 0

P-Reviewer: Ahmed OM, Egypt

Received: October 28, 2021
Peer-review started: October 28, 2021
First decision: March 7, 2022
Revised: March 16, 2022
Accepted: April 22, 2022
Article in press: April 22, 2022
Published online: June 26, 2022

Jin-Hao Zheng, Lu-Yu Xue, Department of Critical Care Medicine, Huashan Hospital Affiliated to Fudan University, Shanghai 200040, China

Corresponding author: Lu-Yu Xue, Doctor, Occupational Physician, Department of Critical Care Medicine, Huashan Hospital Affiliated to Fudan University, No. 12 Middle Urumqi Road, Shanghai 200040, China. icuxueluyu@163.com

Abstract

BACKGROUND

Strongyloidiasis is usually a chronic infection but it can develop into a fatal disease in immunosuppressed patients.

CASE SUMMARY

A 68-year-old male with rheumatoid arthritis was treated with a variety of immunosuppressants for the past 3 years. Recently, the patient presented with a partial small-bowel obstruction, petechia, coughing and peripheral neuropathy. The diagnosis was difficult to clarify in other hospitals. Our hospital found *Strongyloides stercoralis* larvae with active movement in the routine stool and sputum smears. The diagnosis of disseminated strongyloidiasis was established. Ivermectin combined with albendazole was used for treatment. The patient responded to therapy and was discharged.

CONCLUSION

This case underscores the importance of comprehensive differential diagnosis in immunocompromised patients.

Key Words: Strongyloidiasis; Rheumatoid arthritis; Immunosuppressants; Small-bowel obstruction; Ivermectin; Albendazole; Case report

©The Author(s) 2022. Published by Baishideng Publishing Group Inc. All rights reserved.

Core Tip: Strongyloidiasis is usually a chronic infection but it can develop into a fatal disease in immunosuppressed patients. Here, we present a case of an immunocompromised patient with disseminated strongyloidiasis that was ignored by other hospitals. We discuss the challenges of diagnosis and the treatment. Since the disease was widespread, ivermectin combined with albendazole was used for treatment. This case underscores the importance of comprehensive differential diagnosis in immunocompromised patients.

Citation: Zheng JH, Xue LY. Disseminated strongyloidiasis in a patient with rheumatoid arthritis: A case report. *World J Clin Cases* 2022; 10(18): 6163-6167
URL: https://www.wjgnet.com/2307-8960/full/v10/i18/6163.htm
DOI: https://dx.doi.org/10.12998/wjcc.v10.i18.6163

INTRODUCTION

Strongyloidiasis is a disease caused by the human pathogenic parasitic roundworm *Strongyloides stercoralis* (*S. stercoralis*). Most larvae are excreted in the stool but re-infection or self-infection can occur when the mature larvae burrow into the intestinal wall or the anal tissue. *S. stercoralis* infections can become chronic and even fatal in immunosuppressed patients[1]. This report describes the clinical features of disseminated strongyloidiasis in an immunosuppressed patient as well as the diagnosis and treatment.

CASE PRESENTATION

Chief complaints

A 68-year-old male with repeated multi-joint pain for 3 years, abdominal pain and abdominal distension for 2 mo and progressive difficulty in swallowing, coughing, hoarseness and dysphonia for 1 wk.

History of present illness

The patient with rheumatoid arthritis was treated successively using a variety of immunosuppressants (methylprednisolone, tocilizumab, adalimumab, rituximab) for the past 3 years. Recently, the patient received treatment in several hospitals for a partial small-bowel obstruction of unknown origin which reoccurred repeatedly after treatment. As the patient's condition worsened, new symptoms appeared including petechia, progressive difficulty in swallowing, coughing, hoarseness and dysphonia. A neurologist considered peripheral neuropathy because electromyography indicated peripheral nerve axonal damage. High-dose intravenous immunoglobulin therapy (2 g/kg over 5 d) was not effective, so plasmapheresis was recommended. At the same time, a parasite was detected in the stool, however, the species was neither identified nor treated. Due to the progress of bulbar palsy, the patient was referred to our hospital.

History of past illness

Diabetic history: Diabetic history for several years, maximum 18 mmol/L. Taking insulin medication, blood sugar is unsatisfactory for control.

Personal and family history

The patient had no specific personal and family history.

Physical examination

Upon admission, he displayed weight loss, stable vital signs, hoarseness, dysarthria, wet rales audible in both lungs, weak bowel sounds, muscle strength grade 3 in all limbs and diminished tendon reflexes.

Laboratory examinations

His biochemistry panel was as follows: K of 3.4 mmol/L, Na of 129 mmol/L, Ca of 1.88 mmol/L, and albumin of 25 g/L. Stool-Rt and sputum smears tested positive for *S. stercoralis* larvae with active movement (Figure 1).

Imaging examinations

A chest CT showed bilateral infiltrates indicating pneumonia. Echocardiography showed impaired movement of the left ventricular myocardium (EF 42%).

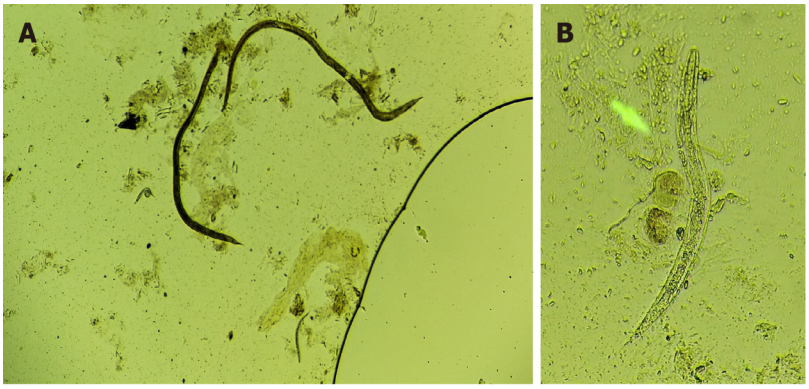

DOI: 10.12998/wjcc.v10.i18.6163 **Copyright** ©The Author(s) 2022.

Figure 1 Larva of *Strongyloides stercoralis* separated from the stool of the patient. A: 10 × 10; B: 10 × 40.

FINAL DIAGNOSIS

The diagnosis of disseminated strongyloidiasis was established.

TREATMENT

After 1 wk of treatment with albendazole 400 mg tid and other supportive treatments, the sputum smear was still positive. The addition of ivermectin 0.2 mg/kg/d × 2 d every 2 wk was then given. On day 4 of ivermectin treatment, the sputum smear and stool tested negative for intestinal parasites. After 2 wk of comprehensive treatment, the patient's mental state gradually improved and muscle strength of the limbs recovered. After 6 wk of hospitalization, his abdominal pain and all previously mentioned symptoms except for the joint pain had dissipated. The patient was discharged and given a small dose of methylprednisolone + methotrexate + celecoxib to control the rheumatoid arthritis and relieve the joint pain. We used albendazole for 4 wk total and ivermectin for a total of 6 wk[2].

OUTCOME AND FOLLOW-UP

At 3 mo after discharge, a follow-up chest CT and electromyography showed lung and cardiac function had recovered.

DISCUSSION

Strongyloidiasis is a zoonotic intestinal parasitosis caused by *S. stercoralis*. It is estimated that 30–100 million people are infected worldwide with this parasite[3]. Most infected individuals are asymptomatic or present with intermittent symptoms[4]. Immunosuppressed patients can develop hyperinfection syndrome and disseminated nematode disease which have high mortality rates[5-7]. Strongyloidiasis has been reported following concomitant tocilizumab and methylprednisolone treatment[8]. Some case reports suggest that paralytic ileus may be caused by massive intestinal infestation with *S. stercoralis*[9].

Our case has two important clinical features. First, the patient had a history of immunosuppression and subsequently developed clinical symptoms (*e.g.*, intestinal obstruction, pneumonia and petechia). The patient's heart was also affected. Previous hospitals detected the presence of parasites but focused instead on the neurological manifestations. We confirmed the presence of *S. stercoralis* larvae in the patient's stool and sputum[10]. Second, the patient presented with choking and hoarseness at the time of diagnosis. Head, neck, mediastinal MRI, cerebrospinal fluid and other examinations found no evidence of neurological invasion. Therefore, we considered two possibilities: (1) Nutritional deficiencies in vitamin B1, vitamin B12 and folic acid due to long periods of fasting, causing malabsorption and intestinal obstruction which can lead to peripheral neuropathy[11]; and (2) Neurotoxic biological agents (*e.g.*, TNF inhibitors, anti-IL-6 receptor antibody), which can cause peripheral neuropathy in approximately 42% of cases[12].

The Centers for Disease Control and Prevention and World Health Organization recommend ivermectin as the first choice for strongyloidiasis. In endemic areas, a combination of albendazole and ivermectin is recommended[13], and Moxidectin has also been tried as a treatment[14]. Repeated or extended dosing is preferred until worms are no longer detected[15]. Considering that the patient was

still taking low-dose methylprednisolone and methotrexate tablets for rheumatoid arthritis, we adopted a multi-dose and long course of treatment. At the 3 mo follow-up, no recurrence of the disease was detected, so the treatment was effective.

CONCLUSION

This case highlights important considerations for patients receiving immunosuppressive therapy. It is necessary to improve medical workers' awareness of strongyloidiasis to avoid delays in diagnosis and ensure adequate management of infected patients.

FOOTNOTES

Author contributions: Zheng JH designed the study, analyzed the data and wrote the manuscript; Xue LY contributed to study conception and design and revision of the manuscript.

Informed consent statement: Informed consent was obtained from the patient. The participant consented to the submission of the case report to the Journal.

Conflict-of-interest statement: The authors have no conflicts of interest to declare that are relevant to the content of this article.

CARE Checklist (2016) statement: The authors have read the CARE Checklist(2016), and the manuscript was prepared and revised according to the CARE Checklist(2016).

Open-Access: This article is an open-access article that was selected by an in-house editor and fully peer-reviewed by external reviewers. It is distributed in accordance with the Creative Commons Attribution NonCommercial (CC BY-NC 4.0) license, which permits others to distribute, remix, adapt, build upon this work non-commercially, and license their derivative works on different terms, provided the original work is properly cited and the use is non-commercial. See: https://creativecommons.org/Licenses/by-nc/4.0/

Country/Territory of origin: China

ORCID number: Jin-Hao Zheng 0000-0003-0864-5156; Lu-Yu Xue 0000-0001-8773-7088.

S-Editor: Ma YJ
L-Editor: Filipodia
P-Editor: Ma YJ

REFERENCES

1 **Khieu V**, Srey S, Schär F, Muth S, Marti H, Odermatt P. Strongyloides stercoralis is a cause of abdominal pain, diarrhea and urticaria in rural Cambodia. *BMC Res Notes* 2013; **6**: 200 [PMID: 23688049 DOI: 10.1186/1756-0500-6-200]
2 **Hofmann D**, Smit C, Sayasone S, Pfister M, Keiser J. Optimizing moxidectin dosing for Strongyloides stercoralis infections: Insights from pharmacometric modeling. *Clin Transl Sci* 2022; **15**: 700-708 [PMID: 34889057 DOI: 10.1111/cts.13189]
3 **Schär F**, Trostdorf U, Giardina F, Khieu V, Muth S, Marti H, Vounatsou P, Odermatt P. Strongyloides stercoralis: Global Distribution and Risk Factors. *PLoS Negl Trop Dis* 2013; **7**: e2288 [PMID: 23875033 DOI: 10.1371/journal.pntd.0002288]
4 **Olsen A**, van Lieshout L, Marti H, Polderman T, Polman K, Steinmann P, Stothard R, Thybo S, Verweij JJ, Magnussen P. Strongyloidiasis--the most neglected of the neglected tropical diseases? *Trans R Soc Trop Med Hyg* 2009; **103**: 967-972 [PMID: 19328508 DOI: 10.1016/j.trstmh.2009.02.013]
5 **Marcos LA**, Terashima A, Canales M, Gotuzzo E. Update on strongyloidiasis in the immunocompromised host. *Curr Infect Dis Rep* 2011; **13**: 35-46 [PMID: 21308453 DOI: 10.1007/s11908-010-0150-z]
6 **Comelli A**, Mangioni D, Scaramella L, Maraschini A, Gaudino C, Folli C, Ceriotti F, Triulzi F, Canetta C, Gori A, Bandera A. Strongyloides stercoralis central nervous system dissemination in a migrant misdiagnosed with eosinophilic granulomatosis with polyangiitis. *J Travel Med* 2022; **29** [PMID: 34718667 DOI: 10.1093/jtm/taab177]
7 **Mah J**, Lieu A, Holmes E, Vaughan S. A case of disseminated strongyloidiasis after multiple courses of immunosuppression. *CMAJ* 2022; **194**: E89-E92 [PMID: 35074835 DOI: 10.1503/cmaj.211056]
8 **Lier AJ**, Tuan JJ, Davis MW, Paulson N, McManus D, Campbell S, Peaper DR, Topal JE. Case Report: Disseminated Strongyloidiasis in a Patient with COVID-19. *Am J Trop Med Hyg* 2020; **103**: 1590-1592 [PMID: 32830642 DOI: 10.4269/ajtmh.20-0699]
9 **Yoshida H**, Endo H, Tanaka S, Ishikawa A, Kondo H, Nakamura T. Recurrent paralytic ileus associated with strongyloidiasis in a patient with systemic lupus erythematosus. *Mod Rheumatol* 2006; **16**: 44-47 [PMID: 16622724 DOI: 10.1007/s10165-005-0447-1]

10 **Buonfrate D**, Fittipaldo A, Vlieghe E, Bottieau E. Clinical and laboratory features of Strongyloides stercoralis infection at diagnosis and after treatment: a systematic review and meta-analysis. *Clin Microbiol Infect* 2021; **27**: 1621-1628 [PMID: 34325063 DOI: 10.1016/j.cmi.2021.07.016]
11 **Morís G**. Inflammatory bowel disease: an increased risk factor for neurologic complications. *World J Gastroenterol* 2014; **20**: 1228-1237 [PMID: 24574797 DOI: 10.3748/wjg.v20.i5.1228]
12 **Spagnoli C**, Pisani F, Di Mario F, Leandro G, Gaiani F, De' Angelis GL, Fusco C. Peripheral neuropathy and gastroenterologic disorders: an overview on an underrecognized association. *Acta Biomed* 2018; **89**: 22-32 [PMID: 30561392 DOI: 10.23750/abm.v89i9-S.7956]
13 **Henriquez-Camacho C**, Gotuzzo E, Echevarria J, White AC Jr, Terashima A, Samalvides F, Pérez-Molina JA, Plana MN. Ivermectin versus albendazole or thiabendazole for Strongyloides stercoralis infection. *Cochrane Database Syst Rev* 2016; CD007745 [PMID: 26778150 DOI: 10.1002/14651858.CD007745.pub3]
14 **Bisoffi Z**, Buonfrate D. Moxidectin: an ally to ivermectin for treating Strongyloides stercoralis? *Lancet Infect Dis* 2021; **21**: 1060-1061 [PMID: 33798488 DOI: 10.1016/S1473-3099(20)30718-0]
15 **Mejia R**, Nutman TB. Screening, prevention, and treatment for hyperinfection syndrome and disseminated infections caused by Strongyloides stercoralis. *Curr Opin Infect Dis* 2012; **25**: 458-463 [PMID: 22691685 DOI: 10.1097/QCO.0b013e3283551dbd]

World Journal of Clinical Cases

Submit a Manuscript: https://www.f6publishing.com

World J Clin Cases 2022 June 26; 10(18): 6168-6174

DOI: 10.12998/wjcc.v10.i18.6168

ISSN 2307-8960 (online)

CASE REPORT

CYP27A1 mutation in a case of cerebrotendinous xanthomatosis: A case report

Zhao-Ran Li, Yu-Ling Zhou, Qi Jin, Yin-Yin Xie, Hong-Mei Meng

Specialty type: Neurosciences

Provenance and peer review: Unsolicited article; Externally peer reviewed.

Peer-review model: Single blind

Peer-review report's scientific quality classification

Grade A (Excellent): 0
Grade B (Very good): B
Grade C (Good): 0
Grade D (Fair): D
Grade E (Poor): 0

P-Reviewer: Parry AH, India; Wiratnaya IGE, Indonesia

Received: November 4, 2021
Peer-review started: November 4, 2021
First decision: March 7, 2022
Revised: March 15, 2022
Accepted: April 21, 2022
Article in press: April 21, 2022
Published online: June 26, 2022

Zhao-Ran Li, Yu-Ling Zhou, Qi Jin, Yin-Yin Xie, Hong-Mei Meng, Department of Neurology, The First Hospital of Jilin University, Changchun 130000, Jilin Province, China

Corresponding author: Hong-Mei Meng, PhD, Doctor, Department of Neurology, The First Hospital of Jilin University, No. 71 Xinmin Street, Chaoyang District, Changchun 130000, Jilin Province, China. menghm@jlu.edu.cn

Abstract

BACKGROUND

Cerebrotendinous xanthomatosis (CTX) is a rare autosomal recessive metabolic disease caused by mutations in *CYP27A1*. It has a low incidence rate, insidious onset, and diverse clinical manifestations. It can be easily misdiagnosed and can go unrecognized by clinicians, leading to delayed treatment and worsened patient outcomes.

CASE SUMMARY

A 38-year-old male was admitted to our hospital with a history of unabating unstable posture and difficulty in walking for more than 30 years. Subsequently based on the patient's medical history, clinical symptoms, magnetic resonance imaging and gene sequencing results, he was finally diagnosed with CTX. Due to the low incidence rate of the disease, clinicians have insufficient knowledge of it, which makes the diagnosis process more tortuous and prolongs the diagnosis time.

CONCLUSION

Prompt diagnosis and treatment of CTX improve patient outcomes.

Key Words: Cerebrotendinous xanthomatosis; *CYP27A1*; Sterol 27-hydroxylase; c.380G>; c.1563dupA; Case report

©The Author(s) 2022. Published by Baishideng Publishing Group Inc. All rights reserved.

Core Tip: Cerebrotendinous xanthomatosis (CTX) is a rare disease for which prompt diagnosis and treatment improve patient outcomes. In addition, unreported new mutation and previously reported mutation were found in this patient. Thus, it provides new data for the further study of the pathogenesis of CTX and enriches the pathogenic mutation spectrum of *CYP27A1*.

Citation: Li ZR, Zhou YL, Jin Q, Xie YY, Meng HM. *CYP27A1* mutation in a case of cerebrotendinous xanthomatosis: A case report. *World J Clin Cases* 2022; 10(18): 6168-6174
URL: https://www.wjgnet.com/2307-8960/full/v10/i18/6168.htm
DOI: https://dx.doi.org/10.12998/wjcc.v10.i18.6168

INTRODUCTION

Cerebrotendinous xanthomatosis (CTX) is a rare autosomal recessive lipid deposition disorder characterized by systemic signs and neurological dysfunction[1]. CTX is a treatable genetic metabolic disease, and early diagnosis and treatment can delay the progression of the disease to a considerable extent[2]. We report a case of CTX caused by mutations at two sites in *CYP27A1*. This case report will help clinicians to better understand CTX and its presentation, leading to early diagnosis and treatment, thereby improving the quality of life of patients.

CASE PRESENTATION

Chief complaints

A 38-year-old male was admitted to our hospital with a history of unabating postural instability and difficulty in walking for more than 30 years.

History of present illness

The patient was first brought for treatment at the age of 5 years. Clinical documentation at that time reported that the patient had exhibited unabating postural instability and difficulty in walking that did not improve with rest. He also exhibited cognitive impairment and irritability.

History of past illness

Since childhood, the patient experienced frequent episodes of chronic diarrhea lasting multiple weeks. At the age of 11 years, the patient underwent bilateral cataract surgery. At the age of 36 years, the patient presented with bilateral masses on the Achilles tendons coupled with thickening of the Achilles tendons.

Personal and family history

The patient had no specific personal and family medical history.

Physical examination

Neurological examination revealed gait ataxia, increased muscle tension in both lower limbs, bilateral hyperreflexia of the Achilles and knee tendons, a bilateral positive Babinski sign, and bilateral positive ankle clonus, indicating that the pyramidal tracts were damaged bilaterally. In addition, the patient also presented with arched feet and egg-sized, hard, painless lumps in both achilles tendons (Figure 1).

Laboratory examinations

Blood lipid level examination revealed a total cholesterol concentration of 4.03 mmol/L (reference range: 2.60–5.20 mmol/L).

Imaging examinations

Magnetic resonance imaging (MRI) (Figure 2A and B) of the brain showed T2-weighted and FLAIR imaging hyperintensity in the bilateral cerebellar dentate nuclei. Electroencephalography showed abnormal slow-wave activity, composed of θ and δ waves, bilaterally in the posterior regions. MRI (Figure 2C and D) of the right ankle indicated fusiform swelling and abnormal signals in the Achilles tendons.

Genetic testing

Based on the patient's medical history, clinical manifestations, and imaging analyses, it was unclear if

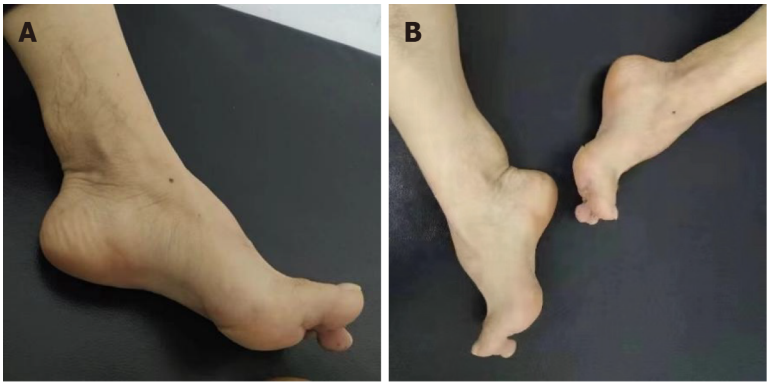

DOI: 10.12998/wjcc.v10.i18.6168 **Copyright** ©The Author(s) 2022.

Figure 1 These two pictures (A, B) showed arched feet and egg-sized, hard, painless lumps in both achilles tendons.

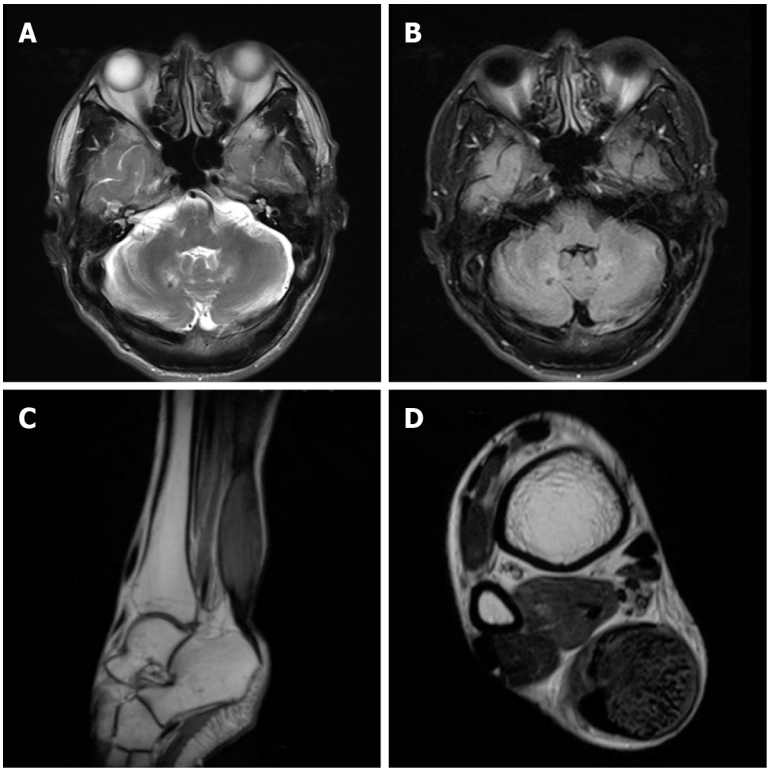

DOI: 10.12998/wjcc.v10.i18.6168 **Copyright** ©The Author(s) 2022.

Figure 2 Magnetic resonance imaging. A, B: Magnetic resonance imaging (MRI) of the brain showed T2-weighted and FLAIR imaging hyperintensity in the bilateral cerebellar dentate nuclei; C, D: MRI of the right ankle showed fusiform swelling and abnormal signals in the achilles tendons.

CTX was involved, and gene sequencing was required to confirm the diagnosis. After informing the patient, the patient was eager to identify the underlying cause and had hopes for treatment; therefore he agreed to undergo gene sequencing analyses. Genomic DNA was extracted from the peripheral blood cells of the patient, and first-generation sequencing of the exon coding region of *CYP27A1* revealed that the gene had a compound heterozygous mutation of c.380G>A (Figure 3) and c.1563dupA (Figure 4). Further examination demonstrated that the mother and sister of the patient were carriers of the c.1563dupA mutation.

FINAL DIAGNOSIS

Based on the patient's medical history, clinical manifestations, auxiliary examinations and gene sequencing results, the diagnosis of CTX was confirmed.

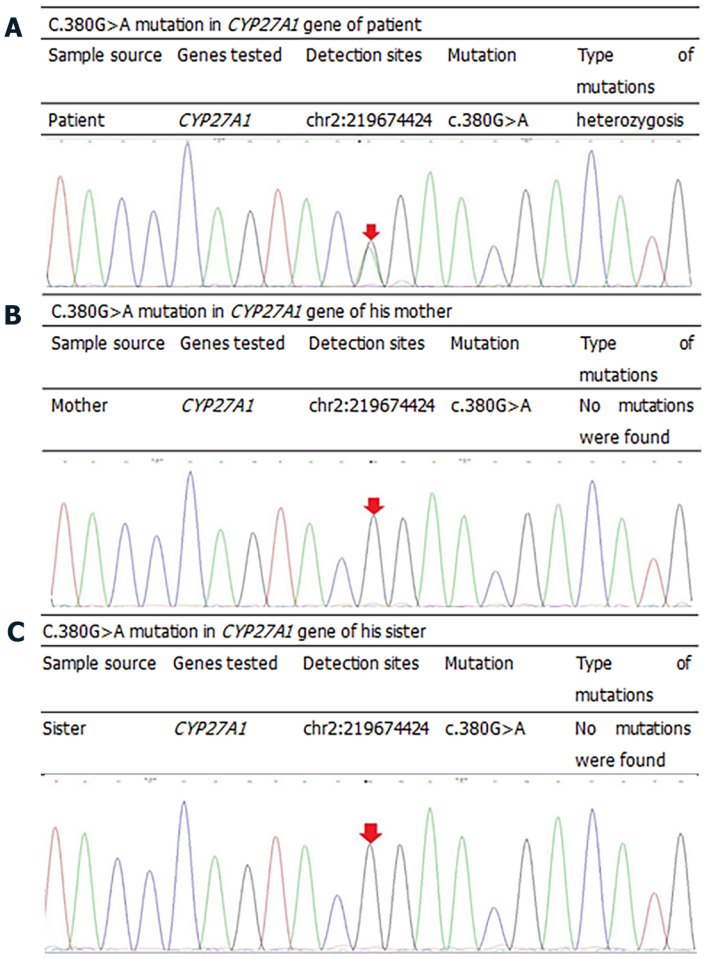

DOI: 10.12998/wjcc.v10.i18.6168 **Copyright** ©The Author(s) 2022.

Figure 3 C.380G>A mutation in *CYP27A1* gene of patient and his families. A: Patient; B: Mother; C: Sister.

TREATMENT

After the diagnosis of CTX, the patient was prescribed chenodeoxycholic acid (CDCA) at 250 mg three times per day and instructed to adhere to a low-cholesterol diet.

OUTCOME AND FOLLOW-UP

After 1 year of treatment, the patient felt that the symptoms of weakness in both lower limbs had improved slightly, but he did not report any additional changes. The patient reported no adverse reactions to CDCA.

DISCUSSION

The main cause of CTX is sterol 27-hydroxylase deficiency caused by the mutation of *CYP27A1*[3]. *CYP27A1* encodes sterol 27-hydroxylase and is the only gene known to be associated with CTX[4]. Sterol 27-hydroxylase is involved in the biosynthesis of primary bile acids, including cholic acid and CDCA [5]. Sterol 27-hydroxylase deficiency obstructs the synthesis of primary bile acids, which causes the accumulation of bile acid synthesis pathway intermediates and derivative metabolites such as cholesterol and cholestanol. These substances are easily deposited in various lipophilic tissues, and therefore, they are more common in the brain, lens, and tendons[6]. They can negatively influence the function of cellular calcium channels, destroy the stability of cell membranes, and initiate the apoptosis pathway[7].

Currently, CTX is considered a rare disease, as are only a few hundred reported cases worldwide. However, we believe that this value is likely underestimated owing to the diversity of symptoms and the frequent delay in diagnosis. Consequently, the number of CTX cases is likely to be considerably far

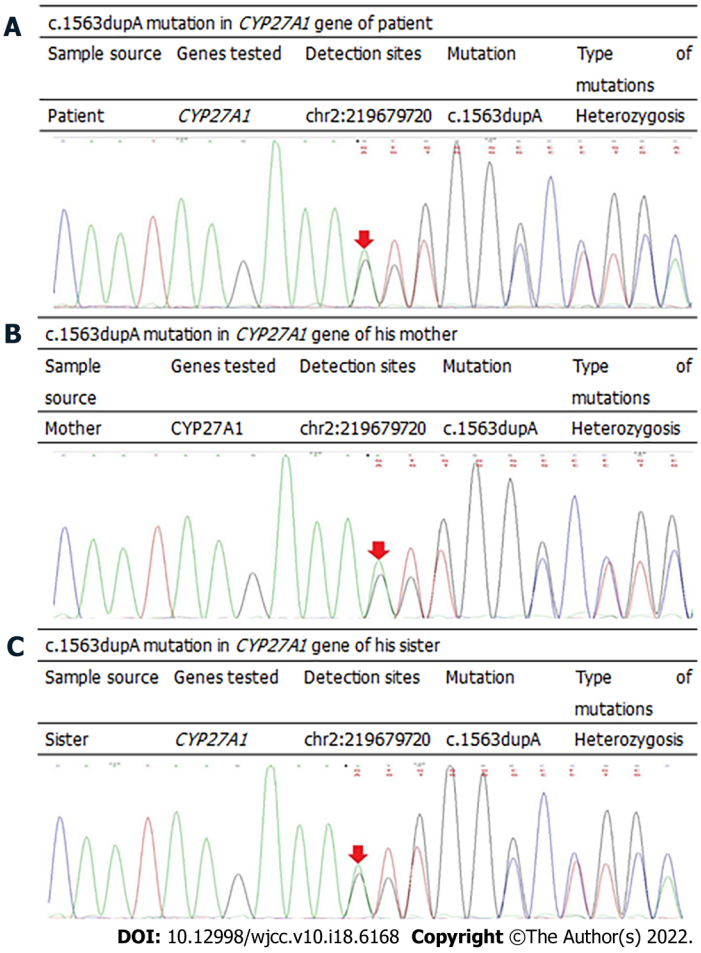

DOI: 10.12998/wjcc.v10.i18.6168 **Copyright** ©The Author(s) 2022.

Figure 4 c.1563dupA mutation in *CYP27A1* gene of patient and his families. A: Patient; B: Mother; C: Sister.

higher than that reported. The primary manifestations of CTX are infant-onset chronic refractory diarrhea, juvenile-onset bilateral cataracts, tendinous xanthomas, and progressive neurological dysfunction[8]. Neurophenotypes include ataxia, pyramidal tract signs, cognitive impairment, and peripheral neuropathy[8]. When the above symptoms are unexplained by common diseases at any age, the possibility of CTX should be considered, and further examinations should be performed. In the case of our patient, almost all the aforementioned symptoms occurred, although they varied in age at presentation. The constellation of symptoms observed in our patient caused us to consider CTX before other possible diseases.

There are no recognized diagnostic criteria for CTX; thus, clinicians must make their diagnoses based on medical history, family history, and clinical characteristics, following which the diagnosis must be confirmed by performing blood biochemistry tests, plasma cholesterol assessment, MRI, and gene sequencing. Our patient's gene sequencing results showed two mutation sites in *CYP27A1*: c.380G>A located on exon 2 and c.1563dupA located on exon 9. Among these, the mutation site c.380G>A has been reported previously[9], but the c.1563dupA mutation is novel and yet to be reported. As our patient possesses a known pathogenic mutation in *CYP27A1*, we are currently unable to determine whether the new gene mutation is pathogenic; further research is needed to confirm the same. In addition, the biochemical diagnosis of CTX is based on the increase in serum cholestanol and urine bile alcohols levels[4]. The typical imaging findings indicating the prevalence of CTX include T2-weighted and FLAIR imaging hyperintensity in the dentate nucleus[10]. The current case supports the inclusion of high signal intensity of the two dentate nuclei on MRI as a typical feature of CTX[11]. The typical imaging manifestations of CTX are high signal in T2 weighted imaging and FLAIR imaging of dentate nucleus.

In CTX treatment, there is currently no clear treatment plan, and the condition can be treated symptomatically based on the different clinical manifestations. Bile acid supplements, such as CDCA, provide a source of primary bile acids, which can inhibit the synthesis of bile acids through a negative feedback mechanism, thereby prevent the accumulation of cholesterol and cholestanol[12]. Consequently, early oral bile acid supplement treatment is recommended[13]. In addition, cataract extraction is common performed in these patients, and xanthoma can be surgically removed.

Our patient was prescribed CDCA replacement therapy. At a follow-up visit 6 months post-treatment, the symptoms of the patient had improved slightly. Based on previous studies, we understand that the clinical process of CTX is progressive[14]. Saussy *et al*[14] compared three cases of CTX and concluded that early and uninterrupted treatment can delay progression of the disease, avert nervous system involvement, and improve the quality of life of patients. Once the neurological symptoms are completely determined, the therapeutic effect will be considerably reduced.

CONCLUSION

Herein, we reported a case where first-generation sequencing of *CYP27A1* was performed in a patient with CTX, leading to the detection of an unreported new mutation as well as a previously reported mutation. Consequently, this case provides new data for further examination of the pathogenesis of CTX and enriches the pathogenic mutational spectrum of *CYP27A1*. In addition, the diagnosis of our patient helped him to receive genetic counseling and guidance regarding fertility. We hope that our case report enables other clinicians to more deeply understand the diagnosis and treatment of CTX, leading to early diagnoses and treatment and improved patient prognoses.

ACKNOWLEDGEMENTS

We would like to thank the patient and the patient's family.

FOOTNOTES

Author contributions: Li ZR acquired patient information and prepared the manuscript; Zhou YL prepared the Figure; Jin Q and Xie YY checked the literature and proposed the idea of publishing this case study; Meng HM reviewed and edited the manuscript; and All authors read and approved the final manuscript.

Informed consent statement: Informed consent was obtained from the patient. The participant consented to the submission of the case report to the Journal.

CARE Checklist (2016) statement: The authors have read the CARE Checklist (2016), and the manuscript was prepared and revised according to the CARE Checklist (2016).

Open-Access: This article is an open-access article that was selected by an in-house editor and fully peer-reviewed by external reviewers. It is distributed in accordance with the Creative Commons Attribution NonCommercial (CC BY-NC 4.0) license, which permits others to distribute, remix, adapt, build upon this work non-commercially, and license their derivative works on different terms, provided the original work is properly cited and the use is non-commercial. See: https://creativecommons.org/Licenses/by-nc/4.0/

Country/Territory of origin: China

ORCID number: Zhao-Ran Li 0000-0002-0048-8398; Yu-Ling Zhou 0000-0002-9155-111X; Qi Jin 0000-0002-5966-9118; Yin-Yin Xie 0000-0002-8749-2831; Hong-Mei Meng 0000-0001-6418-7300.

S-Editor: Ma YJ
L-Editor: A
P-Editor: Ma YJ

REFERENCES

1 **Dell'Aversano Orabona G**, Dato C, Oliva M, Ugga L, Dotti MT, Fratta M, Gisonni P. Multi-imaging study in a patient with cerebrotendinous xanthomatosis: radiology, clinic and pathology correlation of a rare condition. *BJR Case Rep* 2020; **6**: 20190047 [PMID: 32201602 DOI: 10.1259/bjrcr.20190047]
2 **Degrassi I**, Amoruso C, Giordano G, Del Puppo M, Mignarri A, Dotti MT, Naturale M, Nebbia G. Case Report: Early Treatment With Chenodeoxycholic Acid in Cerebrotendinous Xanthomatosis Presenting as Neonatal Cholestasis. *Front Pediatr* 2020; **8**: 382 [PMID: 32766184 DOI: 10.3389/fped.2020.00382]
3 **Salen G**, Steiner RD. Epidemiology, diagnosis, and treatment of cerebrotendinous xanthomatosis (CTX). *J Inherit Metab Dis* 2017; **40**: 771-781 [PMID: 28980151 DOI: 10.1007/s10545-017-0093-8]
4 **Koyama S**, Sekijima Y, Ogura M, Hori M, Matsuki K, Miida T, Harada-Shiba M. Cerebrotendinous Xanthomatosis: Molecular Pathogenesis, Clinical Spectrum, Diagnosis, and Disease-Modifying Treatments. *J Atheroscler Thromb* 2021;

28: 905-925 [PMID: 33967188 DOI: 10.5551/jat.RV17055]

5 **Hong X**, Daiker J, Sadilek M, DeBarber AE, Chiang J, Duan J, Bootsma AH, Huidekoper HH, Vaz FM, Gelb MH. Toward newborn screening of cerebrotendinous xanthomatosis: results of a biomarker research study using 32,000 newborn dried blood spots. *Genet Med* 2020; **22**: 1606-1612 [PMID: 32523054 DOI: 10.1038/s41436-020-0846-x]

6 **Parry AH**, Wani AH, Bashir M, Gojwari TA. Cerebrotendinous xanthomatosis - A case report. *Indian J Radiol Imaging* 2019; **29**: 332-334 [PMID: 31741606 DOI: 10.4103/ijri.IJRI_444_18]

7 **Baghbanian SM**, Mahdavi Amiri MR, Majidi H. Cerebrotendinous xanthomatosis revisited. *Pract Neurol* 2021; **21**: 243-245 [PMID: 33853856 DOI: 10.1136/practneurol-2020-002895]

8 **Verrips A**, Dotti MT, Mignarri A, Stelten BML, Verma S, Federico A. The safety and effectiveness of chenodeoxycholic acid treatment in patients with cerebrotendinous xanthomatosis: two retrospective cohort studies. *Neurol Sci* 2020; **41**: 943-949 [PMID: 31863326 DOI: 10.1007/s10072-019-04169-8]

9 **Watts GF**, Mitchell WD, Bending JJ, Reshef A, Leitersdorf E. Cerebrotendinous xanthomatosis: a family study of sterol 27-hydroxylase mutations and pharmacotherapy. *QJM* 1996; **89**: 55-63 [PMID: 8730343 DOI: 10.1093/oxfordjournals.qjmed.a030138]

10 **Mignarri A**, Dotti MT, Federico A, De Stefano N, Battaglini M, Grazzini I, Galluzzi P, Monti L. The spectrum of magnetic resonance findings in cerebrotendinous xanthomatosis: redefinition and evidence of new markers of disease progression. *J Neurol* 2017; **264**: 862-874 [PMID: 28324197 DOI: 10.1007/s00415-017-8440-0]

11 **Cao LX**, Yang M, Liu Y, Long WY, Zhao GH. Chinese patient with cerebrotendinous xanthomatosis confirmed by genetic testing: A case report and literature review. *World J Clin Cases* 2020; **8**: 5446-5456 [PMID: 33269283 DOI: 10.12998/wjcc.v8.i21.5446]

12 **Gerrish AC**, Gaba S. Case 239: Cerebrotendinous Xanthomatosis. *Radiology* 2017; **282**: 916-921 [PMID: 28218883 DOI: 10.1148/radiol.2016150707]

13 **Pierre G**, Setchell K, Blyth J, Preece MA, Chakrapani A, McKiernan P. Prospective treatment of cerebrotendinous xanthomatosis with cholic acid therapy. *J Inherit Metab Dis* 2008; **31** Suppl 2: S241-S245 [PMID: 19125350 DOI: 10.1007/s10545-008-0815-z]

14 **Saussy K**, Jain N, Murina A. Cerebrotendinous xanthomatosis: A report of 3 cases. *JAAD Case Rep* 2020; **6**: 1205-1207 [PMID: 33294542 DOI: 10.1016/j.jdcr.2020.10.012]

World Journal of Clinical Cases

Submit a Manuscript: https://www.f6publishing.com

World J Clin Cases 2022 June 26; 10(18): 6175-6183

DOI: 10.12998/wjcc.v10.i18.6175

ISSN 2307-8960 (online)

CASE REPORT

Postoperative multiple metastasis of clear cell sarcoma-like tumor of the gastrointestinal tract in adolescent: A case report

Wen-Peng Huang, Li-Ming Li, Jian-Bo Gao

Specialty type: Gastroenterology and hepatology

Provenance and peer review: Unsolicited article; Externally peer reviewed.

Peer-review model: Single blind

Peer-review report's scientific quality classification

Grade A (Excellent): 0
Grade B (Very good): B
Grade C (Good): 0
Grade D (Fair): D
Grade E (Poor): 0

P-Reviewer: Gabazza EC, Japan; Hashimoto K, Japan

Received: November 3, 2021
Peer-review started: November 3, 2021
First decision: November 19, 2021
Revised: November 25, 2021
Accepted: March 29, 2022
Article in press: March 29, 2022
Published online: June 26, 2022

Wen-Peng Huang, Li-Ming Li, Jian-Bo Gao, Department of Radiology, The First Affiliated Hospital of Zhengzhou University, Zhengzhou 450052, Henan Province, China

Corresponding author: Jian-Bo Gao, PhD, Academic Research, Chairman, Chief Doctor, Instructor, Department of Radiology, The First Affiliated Hospital of Zhengzhou University, No. 1 East Jianshe Road, Zhengzhou 450052, Henan Province, China.
jianbogaochina@163.com

Abstract

BACKGROUND

Clear cell sarcoma-like tumor of the gastrointestinal tract (CCSLGT) is a rare malignant gastrointestinal mesenchymal soft tissue tumor. Its genetic feature is *EWSR1* gene rearrangement. Histologically, it is often accompanied by a varying number of CD68-positive osteoclast-like giant cells. CCSLGT mostly occurs in the small intestinal wall of young people and children. In terms of clinical manifestations, there is no significant difference between it and other gastrointestinal tumors, and the diagnosis depends on immunohistochemistry and gene detection.

CASE SUMMARY

A 16-year-old man developed dizziness and fatigue 2 mo ago, and 10 d ago showed progressive exacerbation of paroxysmal epigastric pain and stopped flatulence and defecation. Computed tomography showed a soft tissue mass in the distal ileum. After complete resection of the lesion, it was diagnosed by combined immunohistochemical and genetic examination as CCSLGT. After surgery, the patient gradually developed lymph node, liver, lung, bone, left thigh, pleura and adrenal metastasis. The survival time was 4 years and 8 mo.

CONCLUSION

Whole abdominal computed tomography enhancement is recommended for patients with gastrointestinal symptoms. There is no effective treatment for CCSLGT with multiple metastases *via* the lymphatic system and bloodstream after surgical resection.

Key Words: Clear cell sarcoma-like tumor of the gastrointestinal tract; Metastasis; X-ray computed tomography; Case report

©The Author(s) 2022. Published by Baishideng Publishing Group Inc. All rights reserved.

Core Tip: Clear cell sarcoma-like tumor of the gastrointestinal tract (CCSLGT) is a rare malignant mesenchymal tumor with unique morphological, immunophenotypic and molecular genetic characteristics. Its clinical manifestations are unspecific, and the diagnosis depends on immunohistochemistry and gene testing. Positron emission tomography/computed tomography is recommended for patients with CCSLGT, which can provide functional and metabolic information in addition to anatomical information, and effectively reduce missed lesions. Currently, there is no effective treatment for CCSLGT.

Citation: Huang WP, Li LM, Gao JB. Postoperative multiple metastasis of clear cell sarcoma-like tumor of the gastrointestinal tract in adolescent: A case report. *World J Clin Cases* 2022; 10(18): 6175-6183
URL: https://www.wjgnet.com/2307-8960/full/v10/i18/6175.htm
DOI: https://dx.doi.org/10.12998/wjcc.v10.i18.6175

INTRODUCTION

Clear cell sarcoma-like tumor of the gastrointestinal tract (CCSLGT) is a rare malignant mesenchymal soft tissue tumor that can occur in any part of the gastrointestinal tract, mostly in the small intestinal wall, followed by the stomach, colon and peritoneum[1,2]. Zambrano *et al*[3] first reported in 2003 that, because of the characteristic appearance of osteoclast-like giant cells in the tumor, they believed that this type of tumor had some but not all of the characteristics of soft tissue clear cell sarcoma. The etiology and pathogenesis of CCSLGT are not clear. Its genetic feature is *EWSR1* gene rearrangement, which is seen in 81% of cases[4]. Histologically, CCSLGT shows diffuse sheet-like or irregular nest-like arrangement of interstitial tumor cells infiltrating the mucosal and plasma layers of the gastrointestinal wall, with visible pseudopapillary and pseudokryoid mass structures, mucus-like interstitium and focal necrosis, lightly stained or transparent cytoplasm, small or inconspicuous nucleoli, active mitosis, and scattered distribution of osteoblast-like multinucleated giant cells in about 50% of cases[5-7]. Immunohistochemistry was characterized by positive expression of Smur100 protein and SOX-10, but no expression of melanocyte markers such as HMB45 and Melan A. Dense secretory granules were seen in the ultrastructure, but no melanosomes were seen, suggesting neuroendocrine differentiation. CCSLGT is more common in young people and children; the age of onset is 5-81 years; there is no gender difference; the tumor can invade the serosa and even involve the surrounding organs; and the clinical manifestations are not significantly different from those of other gastrointestinal tumors. We here report a case of an adolescent with CCSLGT who developed multiple metastases in mesenteric lymph nodes, liver, lung, bone, left inner thigh, pleura, mediastinum, hilar lymph nodes, and adrenal gland after surgery, and had a poor prognosis with survival of no more than 5 years despite aggressive antitumor therapy. As far as we know, there are few reports in the English-language literature of multiple metastases in adolescent patients with CCSLGT after extensive resection. Clinicians should consider its highly invasive biological behavior and follow-up closely with whole-body imaging.

CASE PRESENTATION

Chief complaints

A 16-year-old man had dizziness and fatigue without obvious cause 2 mo ago. After strenuous exercise 15 d ago, dizziness was aggravated, with nausea and tinnitus.

History of present illness

Laboratory test results at a local hospital showed neutrophils (6.35×10^9/L, normal level 1.80×10^9-6.30×10^9/L), erythrocytes (3.91×10^{12}/L, normal level 4.80×10^9–5.80×10^9/L), platelets (486×10^{12}/L, normal level 100×10^9-300×10^9/L), high sensitivity C-reactive protein (188.0 mg/L, normal level 0.5-10 mg/L), fecal occult blood test positive, and gastroscopy suggested erosive gastritis. No obvious abnormality was found on colonoscopy. The patient was diagnosed with gastrointestinal bleeding and hemorrhagic anemia. The patient presented with tolerable paroxysmal epigastric pain 10 d prior to hospital visit, but the abdominal pain worsened progressively when eating 10 h previously, and he came to our hospital for medical treatment. He had normal spirit and appetite, poor sleep, and normal defecation and urination, and a weight loss of 3 kg.

History of past illness

The patient was in good health.

Personal and family history

The patient had no family history of hereditary diseases.

Physical examination

On admission, he had pressure pain in the wall of the upper abdomen, and no rebound tenderness, bowel sounds at 8 beats/min.

Laboratory examinations

Laboratory test results showed elevated fibrinogen (5.72 g/L, normal level 2–4 g/L), but no obvious abnormality was found in tumor markers.

Imaging examinations

Abdominal digital radiography did not show any dilated loop of bowel to suggest bowel obstruction (Figure 1). Further contrast-enhanced computed tomography (CT) of the abdomen and pelvis showed obvious localized thickening of the ileal wall in the right lower abdomen, with soft tissue density mass, involving the intestinal wall with a length of approximately 4.1 cm, plain scan CT value of approximately 59 HU (Figure 2A), arterial phase CT value of approximately 78 HU (Figure 2B) and venous phase CT value of approximately 97 cm (Figure 2C), showing moderate uniform progressive enhancement. Multiplanar reformation (MPR) images showed that the mass in the intestinal wall grew inwards. The thickness of the mass was approximately 2.4 cm, and resulted in luminal narrowing. Several enlarged lymph nodes could be seen at the root of the mesentery, and the largest was approximately 2.8 cm in diameter (Figure 2D).

FINAL DIAGNOSIS

Combined with pathological morphology, immunohistochemistry and gene detection, the tumor was diagnosed as CCSLGT.

TREATMENT

The patient underwent resection of the small intestinal masses. During the operation, a solid and hard protuberant tumor was located in the ileum approximately 15 cm from the ileocecal part. The tumor of about 5 cm × 3.5 cm × 2 cm invaded the whole layer of the intestine; did not invade the surrounding organs; enlarged lymph nodes were seen at the root of the mesentery, with a size about 2 cm × 1 cm; dark red content could be seen in the distal intestine, and old bleeding was considered; and no abnormality was found in the liver and pelvis. The tumor and part of the small intestine were removed at 5 cm from both ends of the lesion, and the mesenteric and perienteric fat lymph nodes were dissected. The postoperative specimens were sent for pathological examination. Under light microscopy, the tumor cells were diffusely arranged and separated by a slender fibrous septum (Figure 3A). Immunohistochemical detection: AE1/AE3 (-), CK7 (focal ±), Smur100 (+) (Figure 3B), MelanA (-), HIB45 (-), CD34 (vascular +) (Figure 3C), CD117 (-), Dog-1 (-), CDX-2 (-), Villin (-), CK8/18 (-), LCA (-), CD10 (-), TFE-3 (-), SMA (-), desmin (-), MyoD1 (pulp ±), myogenin (pulp ±), NSE (pulp ±), Ki-67 (30% +) (Figure 3D). Fluorescence *in situ* hybridization (FISH) detected 100 tumor cells, and the number of positive cells for fluorescent labeling was 46%. Reverse transcription polymerase chain reaction regarding *EWS/ATF1* was positive to confirm our FISH experiment. According to the interpretation criteria, this case had *EWSR1* gene breakage (Figure 3E).

OUTCOME AND FOLLOW-UP

The patient was followed up regularly without adjuvant treatment. After 13 mo, he stopped defecation and flatulence and came to our hospital because of intermittent severe abdominal pain. CT examination showed multiple enlarged lymph nodes at the root of the mesentery (Figure 4A). Clinicians considered metastasis and carried out abdominal exploration. Tumors of 6.0 cm × 4.0 cm × 3.0 cm and 1.5 cm × 1.0 cm × 0.5 cm were found at the root of the retroperitoneal small intestine.

After surgical resection, the specimens were sent for pathological examination, combined with medical history and immunohistochemistry in accordance with CCSLGT mesenteric lymph node metastasis. Ultrasonography (US) 27 mo after the operation showed that the intrahepatic echo was hyperechoic (Figure 4B), and the internal echo was inhomogeneous, with a size of about 1.4 cm × 1.2 cm. There was no obvious blood flow signal on color Doppler flow imaging. Ultrasound-guided percutaneous hepatic space-occupying biopsy and radiofrequency ablation were performed, and the left lobe

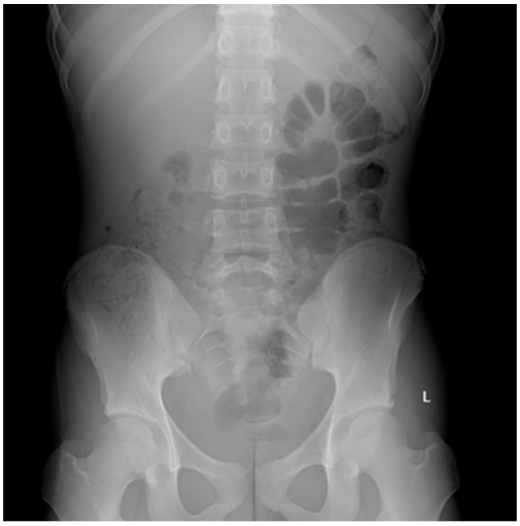

DOI: 10.12998/wjcc.v10.i18.6175 **Copyright** ©The Author(s) 2022.

Figure 1 Digital radiography. There was no obvious manifestation of intestinal obstruction.

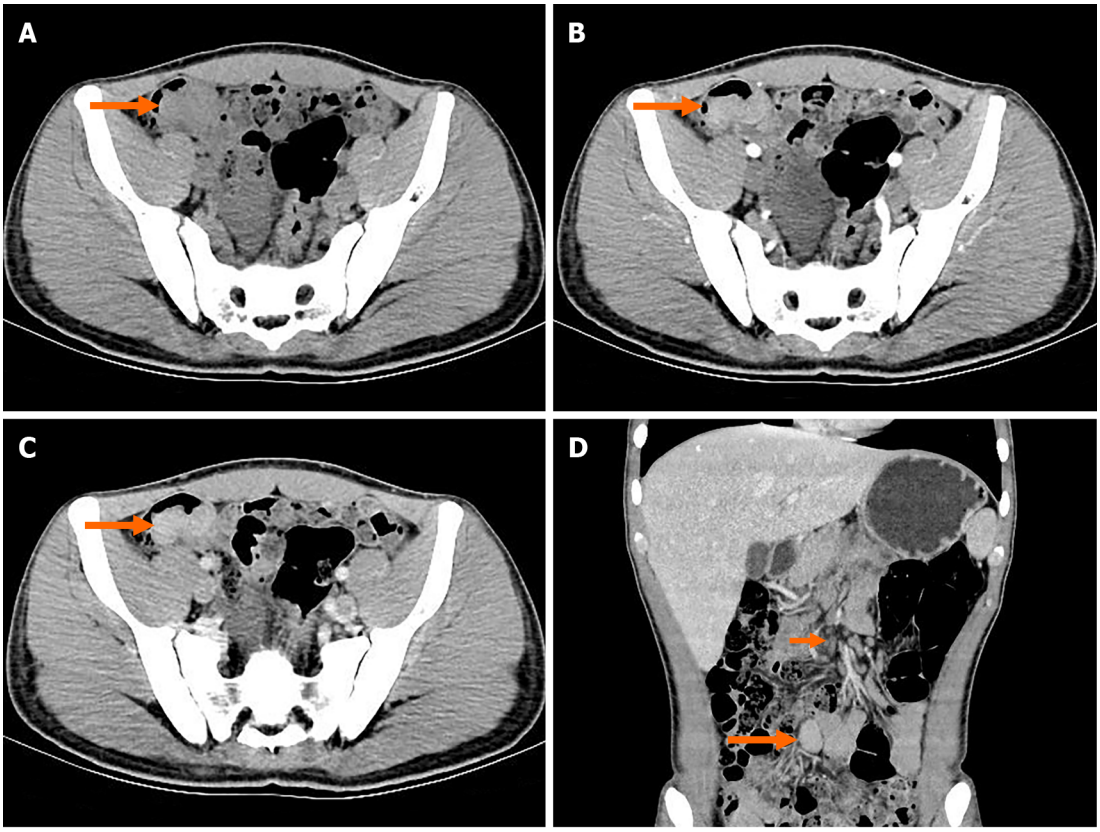

DOI: 10.12998/wjcc.v10.i18.6175 **Copyright** ©The Author(s) 2022.

Figure 2 Preoperative computed tomography. A: Obvious localized thickening of ileal wall in the right lower abdomen; B: The mass showed mild enhancement in the arterial phase; C: The mass showed moderate homogeneous progressive enhancement during the venous phase; D: The venous coronal images showed that the mass of the intestinal wall grew into the intestinal cavity; the intestinal cavity was obviously narrowed; and the lymph nodes at the root of the mesentery were enlarged.

nodules were ablated with hyperechoic coverage. The postoperative specimens were sent for pathological examination, which was consistent with CCSLGT liver metastasis. CT examination at 32 mo after the operation showed multiple solid and well-defined nodules in both lungs, and a patchy and nodular low-density mass in the liver, with unclear boundary, contrast enhancement in the ring but no obvious enhancement in the center (Figure 4C). The enlarged lymph nodes at the root of the mesentery were enlarged and increased compared with before.

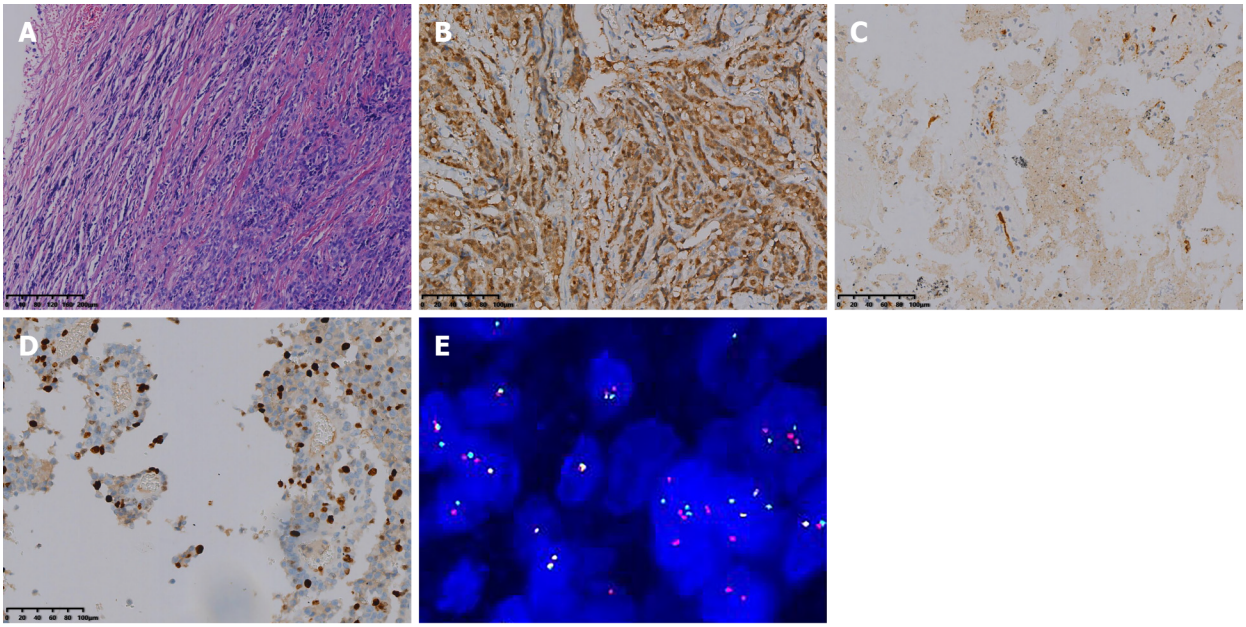

DOI: 10.12998/wjcc.v10.i18.6175 **Copyright** ©The Author(s) 2022.

Figure 3 Optical microscopy and molecular pathology fluorescence *in situ* hybridization. A: The tumor cells were diffusely arranged, separated by a slender fibrous diaphragm [hematoxylin and eosin (HE) 200×]; B: Immunohistochemical staining revealed S-100 positivity (Envision, 200×); C: Immunohistochemical staining revealed CD34 positivity (Envision, 200×); D: Immunohistochemical staining revealed 30% positivity for Ki-67 (Envision, 200×); E: total of 100 tumor cells were detected and counted, and the number of positive cells was 46%. *EWSR1* gene breakage occurred in this case.

Contrast-enhanced US showed multiple areas of solid inhomogeneous hypoechogenicity adjacent to the superior mesenteric artery with clear boundaries. The larger areas were about 3.6 cm × 2.9 cm, and the enhancement was slow and uneven. Solid inhomogeneous areas of hypoechogenicity of 1.3 cm × 1.2 cm and 2.2 cm × 1.9 cm were seen under the capsule of the right anterior lobe and posterior lobe of the liver, respectively. The boundary was unclear, the arterial phase showed circular enhancement, and the enhancement in the portal vein and delayed phases decreased. Ultrasound-guided lymph node biopsy and radiofrequency ablation of enlarged lymph nodes adjacent to the superior mesenteric artery and radiofrequency ablation of liver space were performed. Postoperative pathology combined with medical history and immunohistochemistry were consistent with CCSLGT superior mesenteric artery parames-enteric lymph node metastasis.

At 35 mo after the operation, the patient found a mass on the inside of the left thigh, with hard texture, poor range of motion, traction-like pain in the left thigh, and tension in the posterior lumbar muscles with fluctuating pain, passive posture and limited activity, which lasted for 1 h. The symptoms gradually worsened. Magnetic resonance imaging (MRI) of lumbar vertebrae showed low signal intensity in T12, L1 and L3 vertebrae, slightly high signal intensity in T2-weighted imaging, and high signal intensity in L3 vertebrae on turbo inversion recovery magnitude fat pressing sequence (Figure 4D).

Whole-body ^{99m}Tc-methylene diphosphonate bone scintigraphy showed increased radiotracer uptake in L3 vertebral body (Figure 5), and bone metastasis was considered. The patient was treated regularly with intensity-modulated radiotherapy. CT showed more lesions in the liver, unclear cystic-solid, low-density, space-occupying lesion on the inner side of the left thigh, and uneven circular enhancement (Figure 4E). The maximum dimension was about 3.3 cm × 2.9 cm. Ultrasound-guided puncture biopsy and radiofrequency ablation of the mass in the medial thigh and radiofrequency ablation of the liver were performed. Postoperative pathology combined with morphology, immunohistochemistry and previous medical history were consistent with CCSLGT medial metastasis of the left thigh.

Thirty-nine months after the operation, the patient came to our hospital with recurrent fever, cough and expectoration for > 1 mo. The body temperature fluctuated from 38.0 to 39.5 °C. CT examination showed more multiple small nodules in both lungs than before (Figure 4F).

Forty-three months after the operation, pelvic MRI showed multiple diffuse restricted high signals in the bilateral inguinal area and adjacent iliac vessels, with mild MRI enhancement (Figure 4G). Re-examination by CT showed that the nodule of the left lower lobe was significantly enlarged and the boundary was unclear (Figure 6A). The size of the nodule was 2.5 cm × 3.5 cm, with mild inhomogeneous enhancement, and the left pleural soft tissue nodule showed enhancement (Figure 6B). Bilateral inguinal lymph nodes were enlarged and there was a small amount of fluid density in bilateral pleura and pericardium.

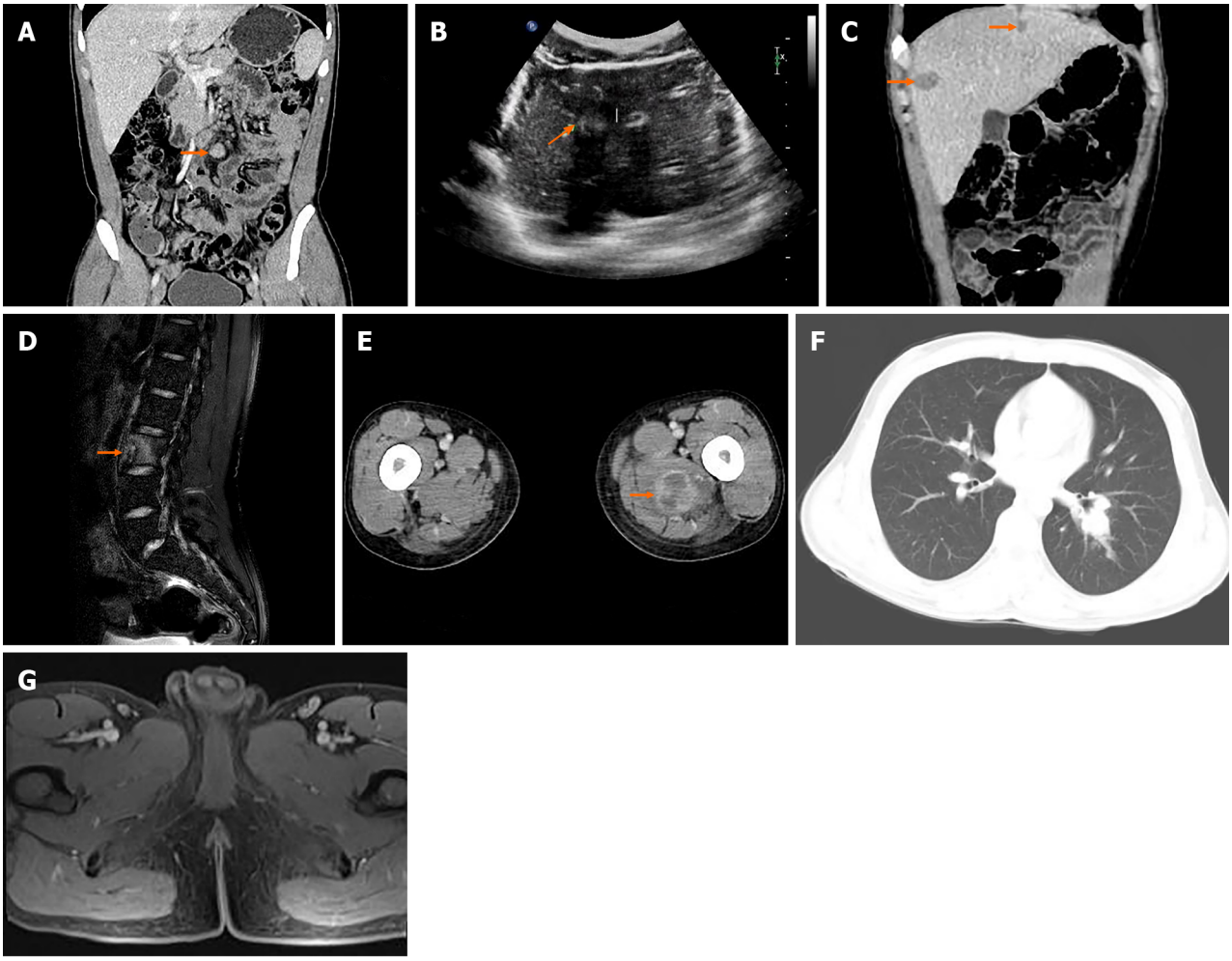

DOI: 10.12998/wjcc.v10.i18.6175 **Copyright** ©The Author(s) 2022.

Figure 4 Images at 13 mo, 27 mo, 32 mo, 35 mo, 39 mo, and 43 mo after surgery. A: Computed tomography 13 mo after surgery, multiple enlarged lymph nodes were seen at the root of the mesentery; B: Ultrasonography 27 mo after surgery, there was a higher echo with a clear boundary in the liver, and the internal echo was not uniform; C: Computed tomography 32 mo after surgery, there were multiple patchy and nodular low-density space-occupying lesions in the liver, the boundary was not clear, the ring was slightly enhanced, but there was no obvious enhancement in the center; D: Magnetic resonance imaging 35 mo after surgery, L3 vertebrae showed high signal intensity on turbo inversion recovery magnitude fat pressing sequence; E: Computed tomography 35 mo after surgery, the mass on the inner side of the left thigh showed inhomogeneous circular enhancement and the boundary was unclear; F: Computed tomography 39 mo after surgery, there were multiple small nodules in both lungs, the larger of which was located in the lower lobe of the left lung, with a diameter of ~1.9 cm; G: Magnetic resonance imaging 43 mo after surgery, multiple mild enhanced signals in bilateral inguinal area and adjacent iliac vessels.

CT examination at 50 mo after the operation showed an irregular mass in the lower lobe of the left lung, which was significantly larger in size than before (Figure 6C) and moderate enhancement (Figure 6D). Other nodules in both lungs were enlarged and increased in number, with multiple mediastinal, left hilar, and axillary lymphadenopathy (Figure 6E). Soft tissue nodules in the left pleura were enlarged, low-density soft tissue masses were seen in the left adrenal gland with a diameter of approximately 2.3 cm, and the boundary was unclear, moderately reinforced in a circular pattern (Figure 6F), with small pleural and pericardial effusion.

At 56 mo after the operation, the patient died of multiple metastases of CCSLGT.

DISCUSSION

The most common clinical manifestations of CCSLGT are abdominal pain, intestinal obstruction, accompanied by varying degrees of anemia, nausea, vomiting, weight loss and fatigue[2-4]. This patient was in good health, had no family history of tumors, and the symptoms were atypical at the beginning, because the primary tumor of the small intestine was rare. After an occult blood test was positive, the patient was examined by gastroscopy and colonoscopy, but not by enteroscopy. He was diagnosed with erosive gastritis with gastrointestinal bleeding, no small intestinal lesions were found, and antitumor treatment was delayed. Later, the patient developed paroxysmal epigastric pain, stopped flatulence and defecation, and no intestinal obstruction was found by digital radiography. Further CT enhancement

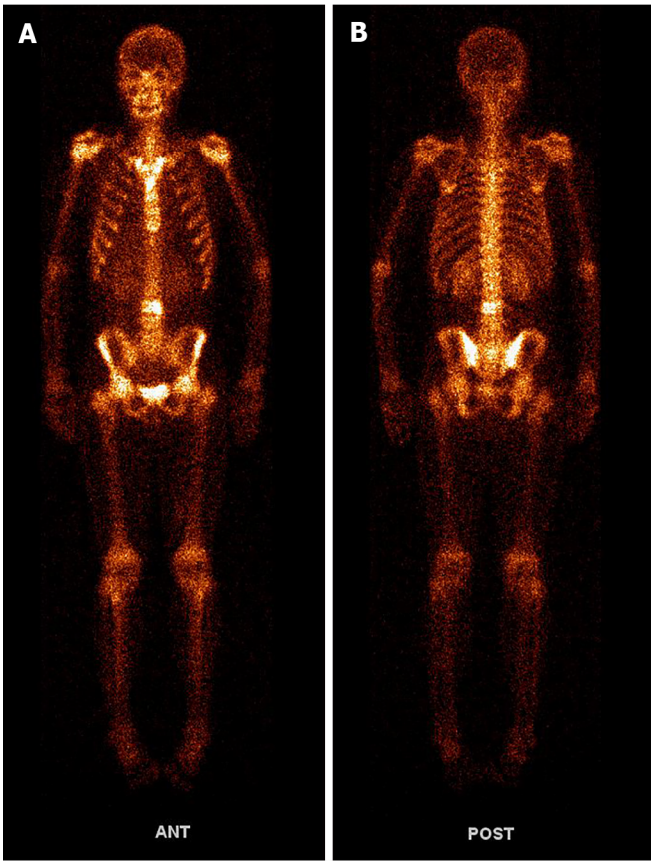

DOI: 10.12998/wjcc.v10.i18.6175 **Copyright** ©The Author(s) 2022.

Figure 5 Whole-body ^{99m}Tc-methylene diphosphonate bone scan imaging 35 mo after surgery. A: Anterior posterior position image; B: Posterior anterior position image.

found a space-occupying soft tissue mass in the ileum. Therefore, patients with gastrointestinal symptoms should be examined by CT, which is beneficial for the detection of lesions in other parts of the body. The median diameter of CCSLGT is 45 mm, ranging from 15 mm to 135 mm. In general, it is multinodular and can be accompanied by hemorrhage, necrosis or cystic changes[4]. The present case was consistent with reports in the literature.

Histologically, tumor cells infiltrate between the walls of the gastrointestinal tract, often into the mucous membrane and serous layer, forming mucosal ulcers. CCSLGT consists of medium-sized tumor cells arranged in flaky or irregular nest-like structures separated by a slender fibrous diaphragm, pseudopapillary, pseudoglandular and pseudochrysanthemum-shaped structures and myxoid stroma, and occasionally pseudoangioma-like structures. Osteoclast-like multinucleated giant cells are scattered in approximately 50% of the cases[5-7]. Mitotic activity is significantly active in these tumors, accompanied by typical focal necrosis[8]. Stockman *et al*[7] reviewed and analyzed 16 cases of CCSLGT, and found that the tumor showed neurodifferentiation potential and expressed neuroendocrine markers, indicating that gastrointestinal CCS originated from neuroectodermal precursor cells and may have lost the ability of melanocyte differentiation. Therefore, a new name was proposed, malignant gastrointestinal neuroectodermal tumor.

The imaging findings of CCSLGT have rarely been reported. CT examination of our patient showed that the peripheral wall of the intestinal canal in the distal part of the right lower abdominal ileum was localized and thickened, the density was uniform, and no calcification or cystic necrosis was found. After MPR, the tumor showed strong invasive growth into the intestine, a clear boundary, obvious narrowing of the intestinal cavity and moderate progressive enhancement, which was different from that of traditional sarcomas. It may be associated with the presence of mucoid stroma in the tumor pathological tissue, which makes the contrast medium enter the tumor tissue slowly. Pathologically, the tumor invaded the whole layer of the intestinal wall, and the peri-intestinal fat was clear on CT images, and no invasion was found.

CCSLGT in the small intestine should be differentiated from small intestinal stromal tumor, small intestinal adenocarcinoma and small intestinal lymphoma. Small intestinal stromal tumors often occur in the jejunum, with characteristic expression of CD117. CT shows irregular or circular thickening of the intestinal wall, or manifested as a round or lobulated mass protruding from the intestinal lumen. The enhanced mass or thickened intestinal wall showed mild to moderate enhancement. CT of small intestinal adenocarcinoma shows irregular or circular thickening of the intestinal wall, irregular mucous

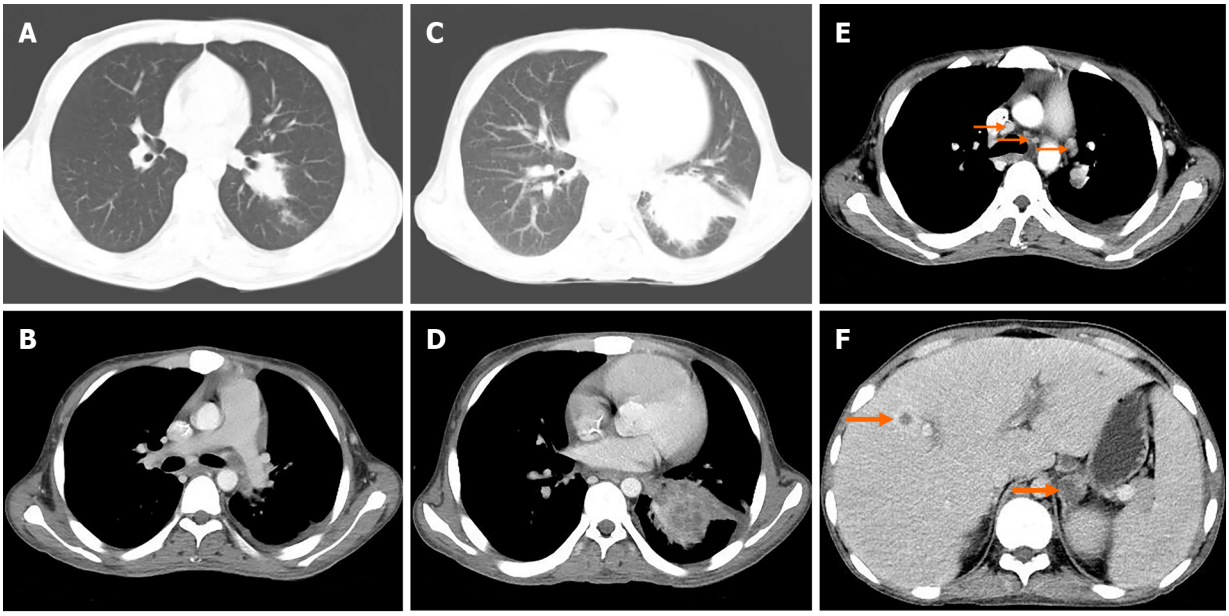

DOI: 10.12998/wjcc.v10.i18.6175 **Copyright** ©The Author(s) 2022.

Figure 6 Computed tomography 43 mo (A-B) and 50 mo (C-F) after surgery. A: The nodule of the lower lobe of the left lung was obviously enlarged, and the boundary was not clear. The size was about 2.5 cm × 3.5 cm; B: The soft tissue nodule of the left pleura showed slight enhancement, with a small amount of fluid density in the left pleural cavity; C: The irregular mass in the lower lobe of the left lung was significantly larger than before, with a size of about 8.2 cm × 5.7 cm; D: After enhancement, the focus showed moderate enhancement; E: Multiple enlarged lymph nodes in mediastinum, left hilum and left axilla; F: Low-density soft tissue mass of the left adrenal gland with unclear boundary and moderate circular enhancement.

membrane, or localized soft tissue masses protruding into the intestinal lumen, and mild to moderate enhancement of the mass or thickened intestinal wall. Most small intestinal lymphomas show diffuse uniform thickening of the intestinal wall, the involved intestinal segment is long and some of them show single or multiple polypoid masses protruding into the intestinal cavity, and most of them show mild to moderate homogeneous enhancement.

CCSLGT has highly invasive biological behavior, and local recurrence and distant metastasis readily occur in the later stage. Regional lymph nodes, lungs, bones and liver are the main sites of metastasis [9]. Currently, there is no effective treatment, and the main treatment is surgical resection. Even after treatment, CCSLGT usually relapses in a wide range of metastatic nodules and visceral diseases[10]. After extensive surgical resection, metastasis of mesenteric lymph nodes, liver, lung, bone, medial left thigh, pleura, mediastinum, hilar lymph nodes and adrenal gland gradually appeared in the present patient, indicating that CCSLGT metastasizes through lymph nodes and blood. Although our patient received active antitumor therapy, the survival time was < 5 years and his prognosis was poor. Disappointingly, conventional adriamycin-based chemotherapy for other non-small round cell soft tissue sarcomas is ineffective, and there is no report that postoperative radiotherapy and chemotherapy are helpful; therefore, larger prospective studies are needed to determine the best treatment options [11]. Although there are currently no effective treatments for this highly aggressive tumor, future targeted therapies that inhibit the function of the *EWSR1–CREB1* fusion oncogene or its associated downstream pathways may be effective in treating the disease. CT can accurately locate CCSLGT and provide the characteristics of lesion size, shape, internal structure and growth. It is of value in observing invasion of adjacent tissues and organs and lymph nodes, and distant metastasis. Positron emission tomography/CT is recommended for patients with CCSLGT, which can provide functional metabolic information beyond anatomical images and effectively reduce missed lesions.

CONCLUSION

In summary, Whole abdominal CT enhancement is recommended for patients with gastrointestinal symptoms. CCSLGT is a rare malignant mesenchymal tumor with unique morphological, there is no effective treatment for CCSLGT with systemic multiple metastases *via* the lymphatic system and bloodstream after surgical resection. immunophenotypic and molecular genetic characteristics. The clinical manifestations are not specific, and the diagnosis depends on immunohistochemistry and gene detection. Currently, there is no effective treatment. Clinicians should consider its highly aggressive biological behavior, follow it closely, and recommend regular postoperative whole-body imaging to reduce missed lesions. The diagnosis of this young patient with CCSLGT was clear. After active

antitumor treatment, the metastatic focus *in vivo* is still progressing, the survival time is short, and the prognosis is poor.

FOOTNOTES

Author contributions: Huang WP acquired and analysed of the work, drafted the manuscript, imaging data collection and analysis; Li LM edited the manuscript; Gao JB wrote and reviewed and edited the manuscript; all authors met the requirements for authorship for the submitted version and agreed to its submission.

Informed consent statement: The study was approved by the Institutional Review Board at The First Affiliated Hospital of Zhengzhou University. Participant gave written consent to participate in the study.

Conflict-of-interest statement: The authors declare that they have no competing interests.

CARE Checklist (2016) statement: The authors have read the CARE Checklist (2016), and the manuscript was prepared and revised according to the CARE Checklist (2016).

Open-Access: This article is an open-access article that was selected by an in-house editor and fully peer-reviewed by external reviewers. It is distributed in accordance with the Creative Commons Attribution NonCommercial (CC BY-NC 4.0) license, which permits others to distribute, remix, adapt, build upon this work non-commercially, and license their derivative works on different terms, provided the original work is properly cited and the use is non-commercial. See: https://creativecommons.org/Licenses/by-nc/4.0/

Country/Territory of origin: China

ORCID number: Wen-Peng Huang 0000-0002-9104-1494; Li-Ming Li 0000-0002-2910-9742; Jian-Bo Gao 0000-0003-2621-3701.

S-Editor: Ma YJ
L-Editor: A
P-Editor: Ma YJ

REFERENCES

1 **Taminelli L**, Zaman K, Gengler C, Peloponissios N, Bouzourene H, Coindre JM, Hostein I, Guillou L. Primary clear cell sarcoma of the ileum: an uncommon and misleading site. *Virchows Arch* 2005; **447**: 772-777 [PMID: 16021514 DOI: 10.1007/s00428-005-0019-y]
2 **Huang W**, Zhang X, Li D, Chen J, Meng K, Wang Y, Lu Z, Zhou X. Osteoclast-rich tumor of the gastrointestinal tract with features resembling those of clear cell sarcoma of soft parts. *Virchows Arch* 2006; **448**: 200-203 [PMID: 16220298 DOI: 10.1007/s00428-005-0051-y]
3 **Zambrano E**, Reyes-Mugica M, Franchi A, Rosai J. An osteoclast-rich tumor of the gastrointestinal tract with features resembling clear cell sarcoma of soft parts: reports of 6 cases of a GIST simulator. *Int J Surg Pathol* 2003; **11**: 75-81 [PMID: 12754623 DOI: 10.1177/106689690301100202]
4 **Green C**, Spagnolo DV, Robbins PD, Fermoyle S, Wong DD. Clear cell sarcoma of the gastrointestinal tract and malignant gastrointestinal neuroectodermal tumour: distinct or related entities? *Pathology* 2018; **50**: 490-498 [PMID: 29970252 DOI: 10.1016/j.pathol.2018.05.001]
5 **Askan G**, Kombak FE, Seven IE, Basturk O. Clear Cell Sarcoma-Like Tumor of the Gastrointestinal Tract. *J Gastrointest Cancer* 2019; **50**: 651-656 [PMID: 29623567 DOI: 10.1007/s12029-018-0069-4]
6 **Wang J**, Thway K. Clear cell sarcoma-like tumor of the gastrointestinal tract: an evolving entity. *Arch Pathol Lab Med* 2015; **139**: 407-412 [PMID: 25724038 DOI: 10.5858/arpa.2013-0547-RS]
7 **Stockman DL**, Miettinen M, Suster S, Spagnolo D, Dominguez-Malagon H, Hornick JL, Adsay V, Chou PM, Amanuel B, Vantuinen P, Zambrano EV. Malignant gastrointestinal neuroectodermal tumor: clinicopathologic, immunohistochemical, ultrastructural, and molecular analysis of 16 cases with a reappraisal of clear cell sarcoma-like tumors of the gastrointestinal tract. *Am J Surg Pathol* 2012; **36**: 857-868 [PMID: 22592145 DOI: 10.1097/PAS.0b013e31824644ac]
8 **Gahanbani Ardakani A**, Boyle DJ, Elton C. Gastrointestinal clear cell sarcoma-like tumour of the ascending colon. *Ann R Coll Surg Engl* 2016; **98**: e37-e39 [PMID: 26890846 DOI: 10.1308/rcsann.2016.0073]
9 **Hisaoka M**, Ishida T, Kuo TT, Matsuyama A, Imamura T, Nishida K, Kuroda H, Inayama Y, Oshiro H, Kobayashi H, Nakajima T, Fukuda T, Ae K, Hashimoto H. Clear cell sarcoma of soft tissue: a clinicopathologic, immunohistochemical, and molecular analysis of 33 cases. *Am J Surg Pathol* 2008; **32**: 452-460 [PMID: 18300804 DOI: 10.1097/PAS.0b013e31814b18fb]
10 **Thway K**, Judson I, Fisher C. Clear cell sarcoma-like tumor of the gastrointestinal tract, presenting as a second malignancy after childhood hepatoblastoma. *Case Rep Med* 2014; **2014**: 984369 [PMID: 24715928 DOI: 10.1155/2014/984369]
11 **Kawai A**, Hosono A, Nakayama R, Matsumine A, Matsumoto S, Ueda T, Tsuchiya H, Beppu Y, Morioka H, Yabe H; Japanese Musculoskeletal Oncology Group. Clear cell sarcoma of tendons and aponeuroses: a study of 75 patients. *Cancer* 2007; **109**: 109-116 [PMID: 17133413 DOI: 10.1002/cncr.22380]

World Journal of Clinical Cases

Submit a Manuscript: https://www.f6publishing.com

World J Clin Cases 2022 June 26; 10(18): 6184-6191

DOI: 10.12998/wjcc.v10.i18.6184

ISSN 2307-8960 (online)

CASE REPORT

Toripalimab combined with targeted therapy and chemotherapy achieves pathologic complete response in gastric carcinoma: A case report

Rui Liu, Xia Wang, Zhi Ji, Ting Deng, Hong-Li Li, Yan-Hui Zhang, Yu-Chong Yang, Shao-Hua Ge, Le Zhang, Ming Bai, Tao Ning, Yi Ba

Specialty type: Medicine, research and experimental

Provenance and peer review: Unsolicited article; Externally peer reviewed.

Peer-review model: Single blind

Peer-review report's scientific quality classification

Grade A (Excellent): 0
Grade B (Very good): 0
Grade C (Good): C, C
Grade D (Fair): 0
Grade E (Poor): E

P-Reviewer: Arigami T, Japan; Lal A, United States; Marickar F, India

Received: November 5, 2021
Peer-review started: November 5, 2021
First decision: February 14, 2022
Revised: February 28, 2022
Accepted: April 22, 2022
Article in press: April 22, 2022
Published online: June 26, 2022

Rui Liu, Xia Wang, Zhi Ji, Ting Deng, Hong-Li Li, Yan-Hui Zhang, Yu-Chong Yang, Shao-Hua Ge, Le Zhang, Ming Bai, Tao Ning, Yi Ba, National Clinical Research Center for Cancer, Key Laboratory of Cancer Prevention and Therapy, Tianjin's Clinical Research Center for Cancer, Tianjin Medical University Cancer Institute and Hospital, Tianjin 300000, China

Corresponding author: Rui Liu, Doctor, Chief Doctor, National Clinical Research Center for Cancer, Key Laboratory of Cancer Prevention and Therapy, Tianjin's Clinical Research Center for Cancer, Tianjin Medical University Cancer Institute and Hospital, North Huanhu West Road, Sports Institute, Hexi District, Tianjin 300000, China. ruiliu688@126.com

Abstract

BACKGROUND

Neoadjuvant or perioperative chemotherapy combined with surgery can reduce postoperative recurrence and improve the long-term survival rate of patients with locally advanced resectable gastric carcinoma. Nivolumab combined with chemotherapy has been recommended by the National Comprehensive Cancer Network guidelines as a first-line therapy for advanced gastric carcinoma/adenocarcinoma of the gastroesophageal junction and serves as the basis for immunotherapy combined with chemotherapy to become a neoadjuvant therapy. Herein, we report a case in which pathologic complete response was achieved by neoadjuvant administration of toripalimab, Herceptin, and docetaxel, oxaliplatin, calcium folinate, and fluorouracil (FLOT) chemotherapy followed by surgery for human epidermal growth factor receptor 2 (HER2)- and programmed death-ligand 1 (PD-L1)-positive locally advanced gastric carcinoma. We hope that this case will shed some light on neoadjuvant therapy for gastric carcinoma.

CASE SUMMARY

The patient was diagnosed with locally advanced adenocarcinoma of the cardia. Immunohistochemistry of the baseline tissues suggested that the tissues were HER2- (fluorescent *in situ* hybridization) and PD-L1-positive (combined positive score = 1). The patient underwent surgery following a four-cycle neoadjuvant therapy comprising Herceptin, toripalimab, and FLOT chemotherapy. The postoperative pathological findings showed mild atypical hyperplasia of the local glands with chronic mucosal inflammation (proximal stomach), no clear residual tumor (tumor regression grade 0), no regional lymph node metastasis, and

negative upper and lower cut ends. The levels of tumor markers were reduced to normal levels after re-examination. With good postoperative recovery, the four-cycle preoperative chemotherapy was continued at the same dosage as that previously administered. After the treatment, the patient was monitored every 3 mo with a follow-up of 12 mo (4 times). As of February 27, 2022, he was in a good condition without disease progression. The clinical trial registration number is E2019401.

CONCLUSION

There are many ongoing studies on neoadjuvant immunotherapy combined with chemotherapy or radiotherapy; however, most of these studies are phase II studies with small cohorts. According to the results of some current studies, these combined regimens have shown promising results in terms of efficacy and safety. However, the clinical efficacy and safety of the neoadjuvant therapies used in these combined regimens need to be confirmed by additional prospective phase III clinical trials, and further exploration of molecular markers for effective populations is required.

Key Words: Toripalimab; Targeted therapy; Chemotherapy; Perioperative management; Gastric carcinoma; Case report

©The Author(s) 2022. Published by Baishideng Publishing Group Inc. All rights reserved.

Core Tip: We report a case in which pathologic complete response was achieved by neoadjuvant administration of toripalimab, Herceptin, and docetaxel, oxaliplatin, calcium folinate, and fluorouracil chemotherapy followed by surgery for human epidermal growth factor receptor 2- and programmed death-ligand 1-positive locally advanced gastric carcinoma. We hope that this case will shed some light on neoadjuvant therapy for gastric carcinoma.

Citation: Liu R, Wang X, Ji Z, Deng T, Li HL, Zhang YH, Yang YC, Ge SH, Zhang L, Bai M, Ning T, Ba Y. Toripalimab combined with targeted therapy and chemotherapy achieves pathologic complete response in gastric carcinoma: A case report. *World J Clin Cases* 2022; 10(18): 6184-6191
URL: https://www.wjgnet.com/2307-8960/full/v10/i18/6184.htm
DOI: https://dx.doi.org/10.12998/wjcc.v10.i18.6184

INTRODUCTION

Gastric carcinoma has a high incidence in China. Surgery might be a radical cure for gastric carcinoma; however, it is limited to only early-stage gastric carcinoma (stage I). The 5-year survival rate of patients with locally advanced gastric carcinoma (late stage) is 30%–50%[1], even with an extended area of resection and lymph node dissection. Many studies have confirmed that the combination of adjuvant/neoadjuvant chemotherapy/chemoradiotherapy can improve patients' prognosis, enhance R0 resection rates, reduce distant metastases and recurrence rates, and improve survival rates through tumor downstaging[2-4]. In the European randomized controlled phase III AIO-fluorouracil (FLOT)-4 trial, resectable gastric carcinoma patients received either the FLOT (docetaxel, oxaliplatin, calcium folinate, and fluorouracil) or epirubicin, cisplatin, and fluorouracil (ECF) regimen before and after surgery. The results showed that the FLOT regimen had better efficacy, higher R0 resection rate, better disease-free survival (DFS), and better overall survival (OS) than the ECF regimen, which laid the foundation for the FLOT regimen to become a new standard perioperative therapy for advanced gastric carcinoma. Therefore, a regimen that combines surgery with neoadjuvant or perioperative chemotherapy has been recommended by the guidelines of the Chinese Society of Clinical Oncology, the European Society for Medical Oncology, and the National Comprehensive Cancer Network (NCCN).

The KEYNOTE-059[5] and ATTRACTION-02[6] trials have suggested that programmed death-1 (PD-1) inhibitors are effective for advanced gastric carcinoma/adenocarcinoma of the gastroesophageal junction. The United States Food and Drug Administration (FDA) and the National Medical Products Administration have approved the indications for pembrolizumab in patients with a programmed death-ligand 1 (PD-L1) combined positive score (CPS) ≥ 1 and nivolumab in the third-line and posterior-line treatment of advanced gastric carcinoma. The CheckMate-649[7] and ATTRACTION-04[8] trials have revealed that nivolumab plus chemotherapy has significantly better efficacy than chemotherapy alone in the first-line treatment of advanced gastric carcinoma/adenocarcinoma. In China, as the first approved immunotherapy targeting PD-1, toripalimab (JS001) induces the endocytosis of PD-1, reduces the expression of PD-1 on the membrane surface, and relieves the immunosuppression of T cells, thereby achieving strong antitumor effects. In 2020, the American Society of Clinical Oncology reported

the clinical response and biomarker analysis of first-line toripalimab combined with standard chemotherapy for solid tumors in a phase II cohort study[9]. The study found that the objective response rate (ORR) was 54.5%, the disease control rate was 84.8%, and the duration of response was 8.3 mo. Moreover, in the randomized controlled phase III KEYNOTE-585[10] trial, which is currently enrolling patients, therapy-naive patients with locally advanced gastric carcinoma/adenocarcinoma of the gastroesophageal junction in the experimental group will receive pembrolizumab combined with neoadjuvant chemotherapy before surgery and pembrolizumab combined with adjuvant chemotherapy after surgery, whereas those in the control group will receive placebo combined with chemotherapy.

Human epidermal growth factor receptor 2 (HER2), also known as erythroblastic oncogene B2 (ERBB2), is a proto-oncogenic protein encoded by the *ERBB2* gene on human chromosome 17. Tyrosine kinase receptor that binds to the membrane is a protein product of this gene. This receptor can promote cell proliferation and inhibit apoptosis, leading to neoplasm formation[11]. *HER2* overexpression or amplification is found in 13%–22% of patients with gastric carcinoma or adenocarcinoma of the esophagogastric junction[12]. Immunohistochemistry (IHC) staining and fluorescent *in situ* hybridization (FISH) are recommended by the guidelines for the detection of *HER2* overexpression in patients with advanced gastric adenocarcinoma. In 2010, trastuzumab was approved by the FDA as a first-line drug in combination chemotherapy for HER2-positive gastric carcinoma. In another study[13], preliminary results were obtained for combined immunotherapy, trastuzumab, and chemotherapy for gastric carcinoma/esophageal cancer/adenocarcinoma of the esophagogastric junction. The study found that the 6-mo progression-free survival (PFS) rate was 75%, the ORR was 91%, the median PFS was 13 mo, and the median OS was 27.3 mo. The above data were better than the previous data for HER2-positive advanced gastric carcinoma.

In this study, we report a case in which pathologic complete response (pCR) was achieved by neoadjuvant toripalimab, Herceptin, and FLOT chemotherapy followed by surgery for HER2- and PD-L1-positive locally advanced gastric carcinoma. We hope to provide more evidence for neoadjuvant therapies in gastric carcinoma patients by reporting this case.

CASE PRESENTATION

Chief complaints

A 63-year-old male patient experienced dysphagia, poor appetite, night sweats, and fatigue on July 2, 2020, and sought medical attention at the Hulunbuir People's Hospital in Inner Mongolia, China.

History of present illness

On July 22, 2020, gastroscopy revealed protuberant lesions in the cardia and fundus; bite biopsy revealed adenocarcinoma of the cardia (Figure 1A); IHC revealed HER2 positivity (2+, FISH was recommended); *in situ* hybridization revealed *EBER* (−); and FISH revealed *HER2* positivity (Figure 1B).

History of past illness

The patient has been suffering from hepatitis B virus (HBV) infection for more than 30 years, without history of hypertension, coronary heart disease, diabetes, or tuberculosis.

Personal and family history

The patient's family history is not applicable.

Physical examination

The tissues obtained from the bite biopsy were tested for PD-1, revealing CPS positivity (CPS = 1) (Figure 1C) and TPS negativity.

Laboratory examinations

On July 22, 2020, gastroscopy revealed protuberant lesions in the cardia and fundus; bite biopsy revealed adenocarcinoma of the cardia; IHC revealed HER-2 positivity (2+, FISH was recommended); *in situ* hybridization revealed *EBER* (−); and FISH revealed *HER2* positivity. Next-generation sequencing (NGS) revealed tumor protein p53 (*TP53*) c.329G>C p.Arg110Pro (abundance 33.82%), and *ERBB2* copy number amplification (n = 4.5).

Imaging examinations

On July 30, 2020, a computed tomography (CT) scan was performed (Figure 2A).

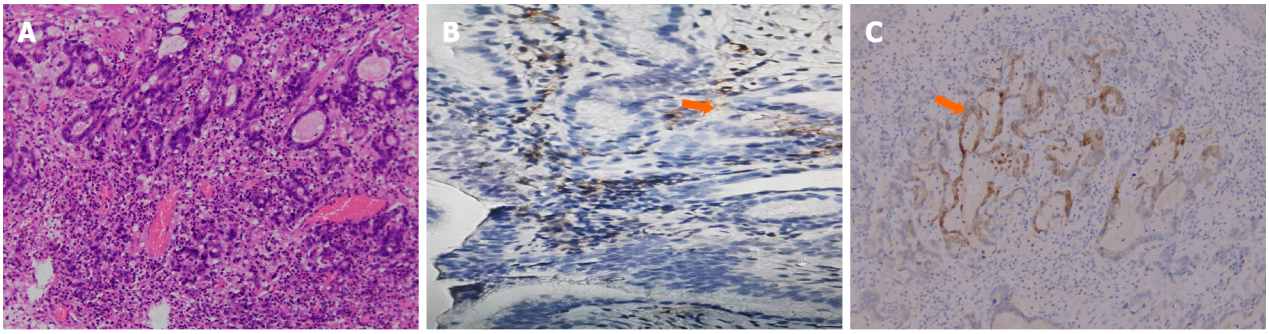

DOI: 10.12998/wjcc.v10.i18.6184 **Copyright** ©The Author(s) 2022.

Figure 1 Histology and immunohistochemistry images. A: Histology; B: Positivity for programmed death-ligand 1 (combined positive score = 1); C: Positivity for human epidermal growth factor receptor 2.

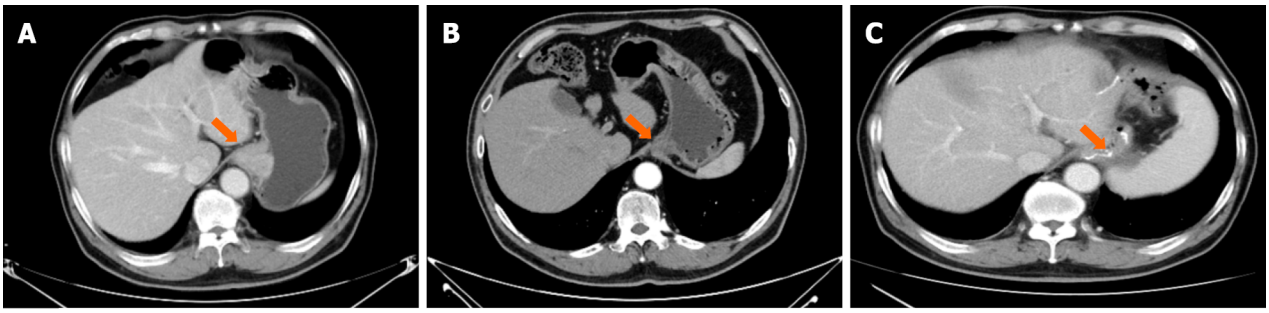

DOI: 10.12998/wjcc.v10.i18.6184 **Copyright** ©The Author(s) 2022.

Figure 2 Computed tomography images. A: Baseline; B: After neo-adjuvant therapy; C: After surgery.

FINAL DIAGNOSIS

(1) Thickened wall of the cardia and adjacent lesser curvature of the stomach, suggestive of carcinoma of the cardia, and invaded fundus and multiple lymph nodes in the hepatogastric ligament region, for which clinical and endoscopic examination needed to be performed; (2) Multiple cysts in the liver; (3) Cyst of the right kidney; (4) Slightly thickened left adrenal gland, with follow-up visits recommended; (5) Prostatic calcification; (6) Subpleural ground-glass opacity in the right lung and scattered nodules and granules on the pleura of both lungs and under the interlobar pleura, with follow-up visits recommended; and (7) A dot-like compact shadow on the 5th right rib, for which follow-up visits were recommended.

TREATMENT

From July 30, 2020 to September 2020, four-cycle targeted therapy, chemotherapy, and immunotherapy were administered. The specific regimen was as follows: Trastuzumab: 420 mg in the first cycle and 280 mg in the second cycle; docetaxel: 90 mg, ivd, d1; oxaliplatin: 150 mg, ivd, d1; calcium folinate: 700 mg, ivd, d1; fluorouracil: 4800, civ, 46 h; and toripalimab: 240 mg, ivd, d2; Q2W. Grade I gastrointestinal reaction occurred and improved after symptomatic treatment.

The imaging findings (CT on October 15, 2020, compared with that on July 30, 2020) after the four cycles of therapy were as follows (Figure 2B): The wall thickness of the cardia and adjacent lesser curvature was less than that before therapy; lymph nodes in the hepatogastric ligament region were reduced in size; and subpleural infiltration in the right lower lobe was more absorbed. No other significant changes were noted. Upper gastrointestinal tract radiography revealed carcinoma of the cardia.

Under general anesthesia, the patient underwent laparoscopic radical D2 gastrectomy for gastric carcinoma on October 23, 2020. Surgical findings revealed a neoplasm at the fundus of the stomach from the cardia, which presented as a 4 cm × 2 cm ulcer with local serosal invasion. No significantly enlarged lymph nodes were found around the stomach. The lesions presented post-chemotherapy scar-like changes. Multiple small lymph nodes were noted around the stomach, most of which were post-chemotherapy changes. The postoperative pathological findings revealed focal (proximal stomach) mild atypical glandular hyperplasia with chronic mucosal inflammation, no clear residual tumor (tumor

regression grade 0), no regional lymph node metastasis, and negative upper and lower cut ends. The grading was as follows: Station 1 0/9, Station 2 0/6, Station 3A 0/12, Station 3B 0/2, Station 4SA soft tissue (−), Station 4SB 0/1 and soft tissue (−), Station 4D 0/2, Station 5 soft tissue (−), Station 6 0/1, Station 7 soft tissue (−), Station 8 soft tissue (−), Station 9 0/4, Station 12A soft tissue (−), Station 19 0/1, and Station 20 0/2. No circulating tumor microemboli or circulating tumor cells were detected. A retest of tumor markers showed a return to normal levels.

OUTCOME AND FOLLOW-UP

With good postoperative recovery, the postoperative CT film (performed on November 16, 2020, Figure 2C) was stored, and the four-cycle chemotherapy regimen was continued at the same dosage as that administered previously. Until February 27, 2022, the patient was examined quarterly for 12 mo (4 times), and he was in a good condition without disease progression. The timeline of this case report is indicated in Figure 3.

DISCUSSION

In a study of combined immunotherapy and trastuzumab treatment for HER2-positive gastric carcinoma[13], 25 patients received immunotherapy and targeted therapy as the initial treatment and chemotherapy in the second cycle, whereas 12 patients received immunotherapy, targeted therapy, and chemotherapy as the initial treatment. In the initial treatment, no significant difference was observed in PFS and 12-mo OS between the 25-patient and 12-patient groups. While in our case, the patient did not receive chemotherapy in the initial treatment; more specifically, the patient received Herceptin and toripalimab in the first cycle and chemotherapy in the second cycle. Previous studies have found no difference in survival between groups receiving chemotherapy and groups not receiving chemotherapy in the initial treatment. Our study suggested that, for HER2-positive gastric carcinoma patients, it is worthy to further evaluate whether the first-line "de-chemotherapy" can be carried out with a large cohort sample.

It is believed that the basis for immunotherapy to benefit HER2-positive patients is that trastuzumab induces antibody-dependent cell-mediated cytotoxicity, improves the presentation of tumor antigens, and paves the way for immune reaction of tumors[14]. Clinical data also show that HER2-positive breast cancer has more types of tumor-infiltrating lymphocytes than average, which demonstrates the importance of trastuzumab in immunity induction[15]. In addition, studies have confirmed that trastuzumab can increase the expression level of PD-L1 in immune cells of patients with breast cancer [16]. Combined with the encouraging clinical outcome of this patient, it is promising to investigate the systemic immune responses in depth, for instance, the lymphocyte infiltration, immune marker dynamics, and functional cytokine secretion. Moreover, this patient has been infected with HBV for many years, which may have an impact on his immune system. Large cohorts are necessary to draw conclusions regarding this aspect if feasible.

There are many ongoing studies of neoadjuvant immunotherapy combined with chemotherapy or radiotherapy; however, most of these studies are phase II studies with small cohorts. According to some of the results reported thus far, these combined regimens have shown promising efficacy and safety[17-19] (Table 1). Many studies have shown that chemotherapy can: (1) Boost the release of damage-associated molecular patterns from tumor cells and improve tumor cell immunogenicity; and (2) Elevate the levels of major histocompatibility complex molecules and enhance tumor antigen presentation[20]. Additionally, chemotherapy promotes the expression of PD-1/PD-L1 through a variety of signaling pathways. Therefore, in this case, chemotherapy and immunotherapy were applied for the patient before the surgical removal. For gastric carcinoma, first-line immunotherapy combined with chemotherapy is recommended by NCCN guidelines for patients with a PD-L1 CPS ≥ 5. However, the CheckMate 649 study[7] suggested that nivolumab combined with chemotherapy improves the OS and DFS of all patients, including those with a CPS ≥ 5 and CPS ≥ 1. In line with this, our patient's IHC results revealed PD-L1 with a CPS of 1. More prospective cohort studies are needed to determine the selection of biomarkers in neoadjuvant therapies involving immunotherapy and chemotherapy.

Apart from the above aspects, *TP53* is a crucial tumor suppressor gene, and *TP53* mutation occurs at an incidence of approximately 45% in gastric carcinoma[21]. The efficacy of immunotherapy varies with the *TP53* mutation. According to the retrospective meta-analysis mentioned above, *TP53* mutation was negatively correlated with the patients' OS with either colon cancer or gastric carcinoma who received immunotherapy but was positively correlated with the efficacy of immunotherapy for lung cancer[21]. In this study, *TP53* c.329G>C p.Arg110Pro mutation was detected using NGS in the baseline tissues of the patient. Therefore, additional prospective cohort studies are required to conclude and explore the correlation between *TP53* mutation and the efficacy of immunotherapy for gastric carcinoma.

Table 1 Summary of neoadjuvant immunotherapies for gastric carcinoma

Regimen	Neoplasm	Number of participants	pCR rate	MPR	Ref.
Camrelizumab plus FOLFOX	Locally advanced gastric carcinoma and adenocarcinoma of the esophagogastric junction	26	2 (9%)	8 (36%)	[17]
Sintilimab plus FLOT	Gastric and adenocarcinoma of the esophagogastric junction	17	3/17 (17.6%)	10/17 (58.8%)	[18]
Sintilimab plus CapeOX	Locally advanced resectable gastric/adenocarcinoma of the esophagogastric junction	26	6/26 (23.1%)	14/26 (53.8%)	[19]

MPR: Mannose 6-phosphate receptors; pCR: Pathologic complete response.

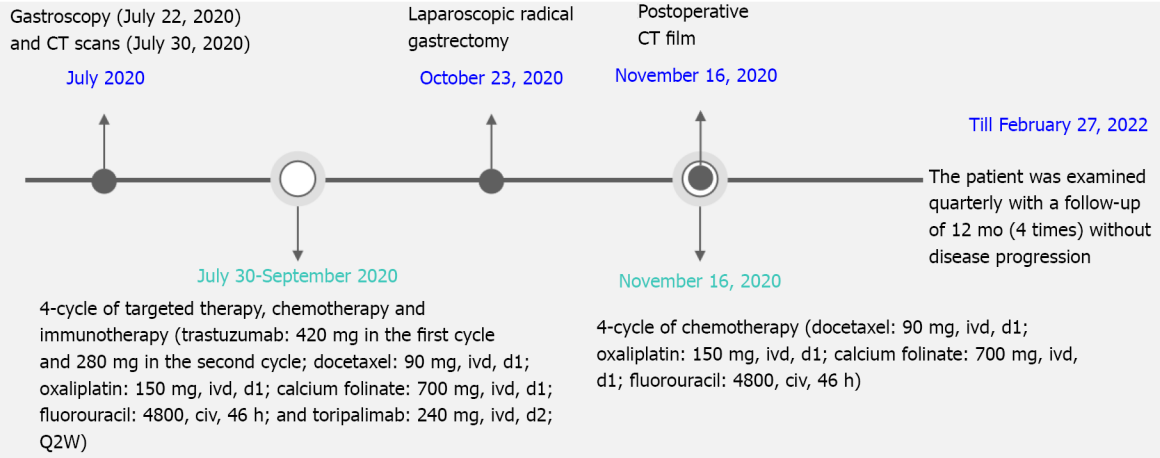

DOI: 10.12998/wjcc.v10.i18.6184 **Copyright** ©The Author(s) 2022.

Figure 3 Timeline of this case report. CT: Computed tomography.

CONCLUSION

Here, we demonstrated that in a patient with HER2-positive locally advanced gastric carcinoma, there was scope for resection; therefore, a regimen composed of Herceptin, chemotherapy, and immunotherapy was carefully selected to achieve higher efficacy and better surgical resection. The patient was administered with the perioperative regimen comprising Herceptin, FLOT, and toripalimab. The postoperative pathological findings revealed that this regimen led to complete tumor response and the levels of tumor biomarkers returned to normal. Furthermore, no circulating tumor cell was detected and no significant immune-related adverse effects were noted, demonstrating that this regimen had sufficient efficacy and safety. The four-cycle chemotherapy was continued postoperatively and completed in the patient, in line with the principle of "effective treatment should be continued if the symptoms are relieved". This patient is currently in the quarterly follow-up period. A previous study suggested that the ability to achieve postoperative pCR in patients with neoadjuvant therapy is positively correlated with longer durations of survival[22]. Thus far, all tumors have been removed from this patient using this regimen, and we hope that this regimen will lead to long-time survival benefits.

FOOTNOTES

Author contributions: Liu R designed the experiments, processed the data, applied for fund support, and wrote the first draft; Wang X performed the data collection; Ji Z, Deng T, Li HL, Zhang YH, Yang YC, Ge SH, Zhang L, Bai M and Ning T performed the data analysis; Ba Y modified the article.

Supported by Chinese Research Hospital Association, No. Y2019FH-DTCC-SC3.

Informed consent statement: Informed written consent was obtained from the patient for the publication of this report and any accompanying images.

Conflict-of-interest statement: Nothing to disclose.

CARE Checklist (2016) statement: The authors have read the CARE Checklist (2016), and the manuscript was prepared and revised according to the CARE Checklist (2016).

Open-Access: This article is an open-access article that was selected by an in-house editor and fully peer-reviewed by external reviewers. It is distributed in accordance with the Creative Commons Attribution NonCommercial (CC BY-NC 4.0) license, which permits others to distribute, remix, adapt, build upon this work non-commercially, and license their derivative works on different terms, provided the original work is properly cited and the use is non-commercial. See: https://creativecommons.org/Licenses/by-nc/4.0/

Country/Territory of origin: China

ORCID number: Rui Liu 0000-0003-1287-2589; Xia Wang 0000-0002-2935-0691; Zhi Ji 0000-0002-2935-0692; Ting Deng 0001-0002-2935-0694; Hong-Li Li 0000-0002-8476-0936; Yan-Hui Zhang 0002-0002-3546-0876; Yu-Chong Yang 0000-0002-2935-0698; Shao-Hua Ge 0001-0002-2935-7642; Le Zhang 0001-0002-2935-0699; Ming Bai 0000-0002-2935-0666; Tao Ning 0000-0002-2935-0654; Yi Ba 0000-0002-2935-0634.

S-Editor: Fan JR
L-Editor: Wang TQ
P-Editor: Fan JR

REFERENCES

1 **Sehdev A**, Catenacci DV. Perioperative therapy for locally advanced gastroesophageal cancer: current controversies and consensus of care. *J Hematol Oncol* 2013; **6**: 66 [PMID: 24010946 DOI: 10.1186/1756-8722-6-66]
2 **Cunningham D**, Allum WH, Stenning SP, Thompson JN, Van de Velde CJ, Nicolson M, Scarffe JH, Lofts FJ, Falk SJ, Iveson TJ, Smith DB, Langley RE, Verma M, Weeden S, Chua YJ, MAGIC Trial Participants. Perioperative chemotherapy *vs* surgery alone for resectable gastroesophageal cancer. *N Engl J Med* 2006; **355**: 11-20 [PMID: 16822992 DOI: 10.1056/NEJMoa055531]
3 **Ychou M**, Boige V, Pignon JP, Conroy T, Bouché O, Lebreton G, Ducourtieux M, Bedenne L, Fabre JM, Saint-Aubert B, Genève J, Lasser P, Rougier P. Perioperative chemotherapy compared with surgery alone for resectable gastroesophageal adenocarcinoma: an FNCLCC and FFCD multicenter phase III trial. *J Clin Oncol* 2011; **29**: 1715-1721 [PMID: 21444866 DOI: 10.1200/JCO.2010.33.0597]
4 **Schuhmacher C**, Gretschel S, Lordick F, Reichardt P, Hohenberger W, Eisenberger CF, Haag C, Mauer ME, Hasan B, Welch J, Ott K, Hoelscher A, Schneider PM, Bechstein W, Wilke H, Lutz MP, Nordlinger B, Van Cutsem E, Siewert JR, Schlag PM. Neoadjuvant chemotherapy compared with surgery alone for locally advanced cancer of the stomach and cardia: European Organisation for Research and Treatment of Cancer randomized trial 40954. *J Clin Oncol* 2010; **28**: 5210-5218 [PMID: 21060024 DOI: 10.1200/JCO.2009.26.6114]
5 **Fuchs CS**, Doi T, Jang RW, Muro K, Satoh T, Machado M, Sun W, Jalal SI, Shah MA, Metges JP, Garrido M, Golan T, Mandala M, Wainberg ZA, Catenacci DV, Ohtsu A, Shitara K, Geva R, Bleeker J, Ko AH, Ku G, Philip P, Enzinger PC, Bang YJ, Levitan D, Wang J, Rosales M, Dalal RP, Yoon HH. Safety and Efficacy of Pembrolizumab Monotherapy in Patients With Previously Treated Advanced Gastric and Gastroesophageal Junction Cancer: Phase 2 Clinical KEYNOTE-059 Trial. *JAMA Oncol* 2018; **4**: e180013 [PMID: 29543932 DOI: 10.1001/jamaoncol.2018.0013]
6 **Kang YK**, Boku N, Satoh T, Ryu MH, Chao Y, Kato K, Chung HC, Chen JS, Muro K, Kang WK, Yeh KH, Yoshikawa T, Oh SC, Bai LY, Tamura T, Lee KW, Hamamoto Y, Kim JG, Chin K, Oh DY, Minashi K, Cho JY, Tsuda M, Chen LT. Nivolumab in patients with advanced gastric or gastro-oesophageal junction cancer refractory to, or intolerant of, at least two previous chemotherapy regimens (ONO-4538-12, ATTRACTION-2): a randomised, double-blind, placebo-controlled, phase 3 trial. *Lancet* 2017; **390**: 2461-2471 [PMID: 28993052 DOI: 10.1016/S0140-6736(17)31827-5]
7 **Janjigian YY**, Shitara K, Moehler M, Garrido M, Salman P, Shen L, Wyrwicz L, Yamaguchi K, Skoczylas T, Campos Bragagnoli A, Liu T, Schenker M, Yanez P, Tehfe M, Kowalyszyn R, Karamouzis MV, Bruges R, Zander T, Pazo-Cid R, Hitre E, Feeney K, Cleary JM, Poulart V, Cullen D, Lei M, Xiao H, Kondo K, Li M, Ajani JA. First-line nivolumab plus chemotherapy *vs* chemotherapy alone for advanced gastric, gastro-oesophageal junction, and oesophageal adenocarcinoma (CheckMate 649): a randomised, open-label, phase 3 trial. *Lancet* 2021; **398**: 27-40 [PMID: 34102137 DOI: 10.1016/S0140-6736(21)00797-2]
8 **Kang YK**, Chen LT, Ryu MH, Oh DY, Oh SC, Chung HC, Lee KW, Omori T, Shitara K, Sakuramoto S, Chung IJ, Yamaguchi K, Kato K, Sym SJ, Kadowaki S, Tsuji K, Chen JS, Bai LY, Oh SY, Choda Y, Yasui H, Takeuchi K, Hirashima Y, Hagihara S, Boku N. Nivolumab plus chemotherapy *vs* placebo plus chemotherapy in patients with HER2-negative, untreated, unresectable advanced or recurrent gastric or gastro-oesophageal junction cancer (ATTRACTION-4): a randomised, multicentre, double-blind, placebo-controlled, phase 3 trial. *Lancet Oncol* 2022; **23**: 234-247 [PMID: 35030335 DOI: 10.1016/S1470-2045(21)00692-6]
9 **Ren C**, Wei XL, Xu N, Shen L, Dai GH, Yuan XL, Chen Y, Yang SJ, Shi JH, Hu XC, Lin XY, Zhang QY, Feng JF, Ba Y, Liu YP, Liu W, Shu YQ, Xu RH, Shanghai Junshi Biosciences. Clinical response and biomarker analysis of a phase II basket trial of toripalimab, a PD-1 mAb in combination with standard chemotherapy as a first-line treatment for patients with solid tumors. *2020 ASCO Annual Meeting I* 2020; **38**: 15 [DOI: 10.1200/JCO.2020.38.15_suppl.e15083]
10 **Bang YJ**, Van Cutsem E, Fuchs CS, Ohtsu A, Tabernero J, Ilson DH, Hyung WJ, Strong VE, Goetze TO, Yoshikawa T,

Tang LH, Hwang PMT, Webb N, Adelberg D, Shitara K. KEYNOTE-585: Phase III study of perioperative chemotherapy with or without pembrolizumab for gastric cancer. *Future Oncol* 2019; **15**: 943-952 [PMID: 30777447 DOI: 10.2217/fon-2018-0581]

11 **Ménard S**, Pupa SM, Campiglio M, Tagliabue E. Biologic and therapeutic role of HER2 in cancer. *Oncogene* 2003; **22**: 6570-6578 [PMID: 14528282 DOI: 10.1038/sj.onc.1206779]

12 **Grillo F**, Fassan M, Sarocchi F, Fiocca R, Mastracci L. HER2 heterogeneity in gastric/gastroesophageal cancers: From benchside to practice. *World J Gastroenterol* 2016; **22**: 5879-5887 [PMID: 27468182 DOI: 10.3748/wjg.v22.i26.5879]

13 **Janjigian YY**, Maron SB, Chatila WK, Millang B, Chavan SS, Alterman C, Chou JF, Segal MF, Simmons MZ, Momtaz P, Shcherba M, Ku GY, Zervoudakis A, Won ES, Kelsen DP, Ilson DH, Nagy RJ, Lanman RB, Ptashkin RN, Donoghue MTA, Capanu M, Taylor BS, Solit DB, Schultz N, Hechtman JF. First-line pembrolizumab and trastuzumab in HER2-positive oesophageal, gastric, or gastro-oesophageal junction cancer: an open-label, single-arm, phase 2 trial. *Lancet Oncol* 2020; **21**: 821-831 [PMID: 32437664 DOI: 10.1016/S1470-2045(20)30169-8]

14 **Melero I**, Berman DM, Aznar MA, Korman AJ, Pérez Gracia JL, Haanen J. Evolving synergistic combinations of targeted immunotherapies to combat cancer. *Nat Rev Cancer* 2015; **15**: 457-472 [PMID: 26205340 DOI: 10.1038/nrc3973]

15 **Savas P**, Loi S. Investigating the positive relationship between tumor-infiltrating lymphocytes and trastuzumab therapy. *Immunotherapy* 2014; **6**: 803-805 [PMID: 25290412 DOI: 10.2217/imt.14.60]

16 **Chaganty BKR**, Qiu S, Gest A, Lu Y, Ivan C, Calin GA, Weiner LM, Fan Z. Trastuzumab upregulates PD-L1 as a potential mechanism of trastuzumab resistance through engagement of immune effector cells and stimulation of IFNγ secretion. *Cancer Lett* 2018; **430**: 47-56 [PMID: 29746929 DOI: 10.1016/j.canlet.2018.05.009]

17 **Liu Y**, Han G, Li H. Camrelizumab combined with FOLFOX as neoadjuvant therapy for resectable locally advanced gastric and gastroesophageal junction adenocarcinoma. *J Clin Oncol* 2020; **38** suppl 15: 4536

18 **Li N**, Li Z, Fu Q, Zhang B, Luo S. Phase II study of sintilimab combined with FLOT regimen for neoadjuvant treatment of gastric or gastroesophageal junction (GEJ) adenocarcinoma. *J Clin Oncol* 2021; **39** suppl 3: 216 [DOI: 10.1200/JCO.2021.39.3_suppl.216]

19 **Jiang H**, Yu X, Kong M, Ma Z, Zhou D, Wang W, Wang H, Li N, He K. Sintilimab plus oxaliplatin/capecitabine (CapeOx) as neoadjuvant therapy in patients with locally advanced, resectable gastric (G)/esophagogastric junction (GEJ) adenocarcinoma. *J Clin Oncol* 2021; **39** suppl 3: 211 [DOI: 10.1200/JCO.2021.39.3_suppl.211]

20 **Heinhuis KM**, Ros W, Kok M, Steeghs N, Beijnen JH, Schellens JHM. Enhancing antitumor response by combining immune checkpoint inhibitors with chemotherapy in solid tumors. *Ann Oncol* 2019; **30**: 219-235 [PMID: 30608567 DOI: 10.1093/annonc/mdy551]

21 **Li L**, Li M, Wang X. Cancer type-dependent correlations between TP53 mutations and antitumor immunity. *DNA Repair (Amst)* 2020; **88**: 102785 [PMID: 32007736 DOI: 10.1016/j.dnarep.2020.102785]

22 **Topalian SL**, Taube JM, Pardoll DM. Neoadjuvant checkpoint blockade for cancer immunotherapy. *Science* 2020; **367** [PMID: 32001626 DOI: 10.1126/science.aax0182]

World Journal of Clinical Cases

Submit a Manuscript: https://www.f6publishing.com

World J Clin Cases 2022 June 26; 10(18): 6192-6197

DOI: 10.12998/wjcc.v10.i18.6192

ISSN 2307-8960 (online)

CASE REPORT

Presentation of Boerhaave's syndrome as an upper-esophageal perforation associated with a right-sided pleural effusion: A case report

Ni Tan, Yin-Hua Luo, Guang-Cai Li, Yi-Lin Chen, Wei Tan, Yue-Hua Xiang, Liang Ge, Di Yao, Ming-Hua Zhang

Specialty type: Gastroenterology and hepatology

Provenance and peer review: Unsolicited article; Externally peer reviewed.

Peer-review model: Single blind

Peer-review report's scientific quality classification

Grade A (Excellent): A
Grade B (Very good): 0
Grade C (Good): C
Grade D (Fair): 0
Grade E (Poor): 0

P-Reviewer: Choi YS, South Korea; He D, China

Received: November 7, 2021
Peer-review started: November 7, 2021
First decision: January 11, 2022
Revised: January 18, 2022
Accepted: April 29, 2022
Article in press: April 29, 2022
Published online: June 26, 2022

Ni Tan, Guang-Cai Li, Yi-Lin Chen, Wei Tan, Yue-Hua Xiang, Liang Ge, Di Yao, Ming-Hua Zhang, Pulmonary and Critical Care Medicine, Central Hospital of Tujia and Miao Autonomous Prefecture, Hubei University of Medicine, Enshi Autonomous Prefecture 445000, Hubei Province, China

Yin-Hua Luo, Cardiovascular Disease Center, Central Hospital of Tujia and Miao Autonomous Prefecture, Hubei University of Medicine, Enshi Autonomous Prefecture 445000, Hubei Province, China

Corresponding author: Ming-Hua Zhang, MD, Chief Doctor, Doctor, Pulmonary and Critical Care Medicine, Central Hospital of Tujia and Miao Autonomous Prefecture, Hubei University of Medicine, Blog 158, WuYang, Street, Enshi Autonomous Prefecture 445000, Hubei Province, China. 1115295145@qq.com

Abstract

BACKGROUND

Spontaneous esophageal rupture or Boerhaave's syndrome is a rare and acute disease with a high incidence of misdiagnosis and mortality. Here, we aimed to explore the clinical characteristics, diagnosis, treatment, and prognosis of spontaneous esophageal rupture, and to analyze the causes of misdiagnosis during the treatment of spontaneous esophageal rupture.

CASE SUMMARY

The clinical features of the patient with spontaneous esophageal rupture misdiagnosed earlier as pleural effusion were retrospectively analyzed and the reasons for misdiagnosis are discussed based on a current review of the literature. The patient was admitted to a local hospital due to shortness of breath accompanied by vomiting and abdominal distension for five hours. Based on the computed tomography (CT) scan analysis, clinically, right pleural effusion was diagnosed. However, the patient was unwilling to undergo right closed thoracic drainage. The patient also had intermittent fevers against infection, and during the course of treatment, he complained of chest pain, following which, he was transferred to our hospital. Grapefruit-like residue drainage fluid was observed. Re-examination of the chest CT scans suggested the presence of spontaneous perforation in the upper left esophagus. Therefore, the patient underwent an urgent esophageal hiatus repair. Unfortunately, the patient died of infection and respiratory failure

due to progressive dyspnea after surgery.

CONCLUSION
Spontaneous esophageal rupture is a rare disease associated with high fatality. The patients do not present typical clinical symptoms and the disease progresses rapidly. This case report highlights the importance of a dynamic review of chest CT scan, not only for the initial identification of segmental injury but also for prioritizing subsequent treatment strategies. Moreover, we have presented some clues for clinicians to recognize and diagnose spontaneous esophageal rupture at rare sites (upper-esophageal segment) through this case report of spontaneous esophageal rupture that caused the patient's death. We have also summarized the reasons for the misdiagnosis and lessons learned.

Key Words: Spontaneous esophageal rupture; Chest computed tomography; Upper-esophageal perforation; Right-sided pleural effusion; Misdiagnosis; Case report

©The Author(s) 2022. Published by Baishideng Publishing Group Inc. All rights reserved.

Core Tip: Spontaneous esophageal rupture is a rare disease associated with high fatality. We report a case of spontaneous esophageal rupture misdiagnosed earlier as pleural effusion at an early stage and investigated the causes of its misdiagnosis, along with our experience during diagnosis and treatment. This case report also highlights the importance of a dynamic chest computed tomography review, not only for initial identification of the injured segment but also for prioritizing subsequent treatment strategies. Moreover, we also provide clues for clinicians to recognize and diagnose spontaneous esophageal rupture at a rare site (upper-esophageal segment) by reporting this case.

Citation: Tan N, Luo YH, Li GC, Chen YL, Tan W, Xiang YH, Ge L, Yao D, Zhang MH. Presentation of Boerhaave's syndrome as an upper-esophageal perforation associated with a right-sided pleural effusion: A case report. *World J Clin Cases* 2022; 10(18): 6192-6197
URL: https://www.wjgnet.com/2307-8960/full/v10/i18/6192.htm
DOI: https://dx.doi.org/10.12998/wjcc.v10.i18.6192

INTRODUCTION

Spontaneous esophageal rupture refers to the full-thickness rupture of the esophageal wall caused by indirect trauma, non-foreign bodies, non-esophageal, and/or adjacent organ disease; it is also known as Boerhaave's syndrome[1]. While the incidence of this disease is low, it is easily misdiagnosed at an early stage and progresses rapidly. After the occurrence of an esophageal rupture, due to negative pressure in the pleural cavity, the stomach contents easily enter the mediastinum and thorax, which often causes serious mediastinum infection and empyema in the early stages. If not treated promptly, severe sepsis rapidly develops into multiple organ failure and even death, which is an emergency during thoracic surgery[2]. Therefore, the associated mortality rate is extremely high. Thus, correctly diagnosing spontaneous esophageal rupture in the early stage is of great importance for the survival of patients with spontaneous esophageal rupture.

Herein, we report a case of spontaneous esophageal rupture misdiagnosed earlier as pleural effusion at an early stage and investigated the causes of its misdiagnosis, along with our experience during diagnosis and treatment. We also highlight the importance of reviewing dynamic chest computed tomography (CT) scans for the diagnosis of spontaneous esophageal rupture.

CASE PRESENTATION

Chief complaints

An 84-year-old male was admitted to a local hospital, with complaints of shortness of breath, abdominal distension, and vomiting.

History of present illness

The patient was admitted to a local hospital, with complaints of shortness of breath, abdominal distension, and vomiting. He did not vomit again during his stay at the hospital.

Based on the evidence, the patient was diagnosed with pleural effusion and recommended to undergo right closed thoracic drainage; however, the patient's family refused given his advanced age. Therefore, antibiotics were prescribed to prevent infection. However, after treatment, blood inflammatory indicators were significantly elevated and did not improve [white blood cell (WBC) count: 19.40 × 10^9/L; C-reactive protein (CRP): 304.90 mg/L] (Table 1). The patient also suffered from intermittent fevers and over time, complained of chest pain. After eight days, the patient was transferred to our hospital.

After admission, the patient agreed to undergo right closed thoracic drainage and grapefruit-like residue drainage fluid was observed (Figure 1C). During the physical examination, subcutaneous emphysema of the right chest wall with crepitus was detected.

History of past illness

The patient had no history of lung diseases.

Personal and family history

No similar disease was identified in his family.

Physical examination

His vital signs were stable and no other specific symptoms were noted.

Laboratory examinations

The initial routine blood examination results showed that both WBC count and CRP levels were slightly elevated (WBC: 12.15 x 10^9/L, CRP: 13.96 mg/L, Table 1).

During hospitalization, laboratory tests also indicated an increase in inflammatory markers.

Imaging examinations

The chest CT scan showed the presence of a small amount of fluid in the right pleural cavity (Figure 1A). Thus, chest CT scanning was repeated. Right-sided pleural effusion with right lung distension insufficiency and perforation of the upper left esophagus were observed (Figure 1B).

FINAL DIAGNOSIS

Considering the above signs and symptoms, the patient was diagnosed with spontaneous perforation of the upper left esophagus, and an urgent esophageal hiatus repair was performed.

TREATMENT

During surgery, a right lateral thoracic incision was made. The patient's right chest wall, muscles, and fascia were severely congested and edematous, along with a ruptured esophagus (Figure 1D).

OUTCOME AND FOLLOW-UP

Unfortunately, due to deterioration of his condition, the patient died from infection and respiratory failure.

DISCUSSION

Spontaneous esophageal rupture, a rare and life-threatening disease, was first reported by Rokicki M in 1724, and to date, a mere 50 cases have been reported in the literature[3]. Based on an epidemiological survey for this disease in Iceland, it has a low incidence of 31 per million per year[4]. Moreover, several studies confirm that men are more prone to morbidity than women and that the highest risk group included those in the 40-60 years age group[5]. Spontaneous esophageal rupture caused by vomiting followed by a large meal often precipitates secondary bacterial infections, which contribute to 50% of the total mortality[6]. Therefore, early diagnosis and surgical treatment are important in the treatment of this disease.

Although many cases of spontaneous esophageal rupture have been reported, the lack of specific symptoms of this condition continues to pose a challenge[7]. Mackler's triad comprising an acute presentation of retching or vomiting, lower chest pain, and surgical emphysema, is a clinical manifestation with relatively high specificity for the diagnosis of spontaneous esophageal rupture.

Table 1 Changes in laboratory indices during the patient's hospital stay

Date	T (℃)	WBC	GR%	N	Hb	CRP	PCT	cTnI	Myo	BNP	Antibiotic
February 26, 2021[1]	36.1	12.15	86.2	10.5	108	13.96		132.7	154.5	40.6	Unclear
March 5, 2021[1]	38	19.4	93.7	18.2	95	304.9	6.51	27.7	151.2	325.9	Unclear
March 7, 2021[2]	37.8	20.36	95.5	19.4	84	211.24	31.26			5816	Imipenem+ Linezolid
March 9, 2021[2]	36.8	15.44	92.8	14.3	76	163.9	9.37			4354	Imipenem+ Linezolid
March 10, 2021[2]	36.9	13.88	89.3	12.4	81	177.82	7.28				Imipenem+ Linezolid+ Fluconazole
March 13, 2021[2]	36.6	10.78	95	10.2	94						Sulperazon
March 15, 2021[2]	36.9	10.3	90.2	9.3	83						Sulperazon
March 19, 2021[2]	36.5	16.62	95.8	15.9	78						Sulperrazon

[1]The date of the patient's admission to the local hospital.

[2]The date of the patient's admission to our hospital.

Abbreviation: T: Temperature; WBC: White Blood Cell; Neu%: The percentage of Neutrophils; N: Neutrophil; Hb: Hemoglobin; CRP: C-reactive protein; PCT: Procalcitonin; cTnI: Cardiac Troponin I; Myo: Myoglobin; BNP: Brain Natriuretic Peptide.

However, its incidence is only about 14%[8,9]. Other signs, which are non-specific, including hemodynamic blood instability or the presence of the Hammer sign-on auscultation, can also help in diagnosing the disease[10]. As secondary infection can irritate adjacent organs, symptoms including abdominal pain, nausea, chest tightness, shortness of breath, and dyspnea can also occur. In addition, elevated cardiac biomarkers and amylase also make it difficult to differentiate it from pericarditis, myocardial infarction, peptic ulcer, and other conditions. For patients with clinical suspicion of the disease, early chest CT examination is particularly important as it shows the manifestation of mediastinal or free peritoneal air as the first sign.

To the best of our knowledge, spontaneous esophageal rupture often occurs in the thoracic esophagus and its incidence in the upper thoracic esophagus is relatively rare. The reasons for this are broadly described as follows: the myometrium of the esophagus is divided into two, the inner ring and the outer longitudinal layer. Approximately 2 mm thick elastic fibers are sandwiched between the two layers. Owing to the lack of coherence in the anatomical structure of the esophagus, a sudden rise in intraesophageal pressure (up to 290 mmHg) can lead to rupture at this altered anatomical structure of the esophagus[11]. While esophageal rupture occurs most commonly in the lower third of the left thoracic segment of the esophagus (80%), it is less frequent in the right esophagus, the upper thoracic, and ventral segments of the esophagus[12]. Among the physical signs, right pleural effusion is also uncommon. In the case of the upper thoracic esophageal perforation, prevertebral or subcutaneous air may be present[13]. Herein, we reported in detail, a case of a spontaneous esophageal rupture in the upper thoracic esophagus, with no obvious signs and symptoms in the early stage. Due to the lack of an early dynamic chest CT review, this disease was misdiagnosed.

Collectively, the reasons for the misdiagnosis were as follows: first, the on-admission chest CT report was only suggestive of a right-sided hydropneumothorax, inconsistent with CT presentation in most reports; additionally, chest pain began later during the course of disease progression, along with a lack of other typical manifestations. Finally, upper thoracic esophageal perforation is a rare site of esophageal rupture and the dynamic chest CT scan was not reviewed during hospitalization, thereby leading to early misdiagnosis and a consequent delay in appropriate treatment.

CONCLUSION

This case report highlights the importance of a dynamic chest CT review, not only for initial identification of the injured segment but also for prioritizing subsequent treatment strategies. Moreover, we also provide clues for clinicians to recognize and diagnose spontaneous esophageal rupture at a rare site (upper-esophageal segment) by reporting this case of spontaneous esophageal rupture and summarizing the reasons for its misdiagnosis.

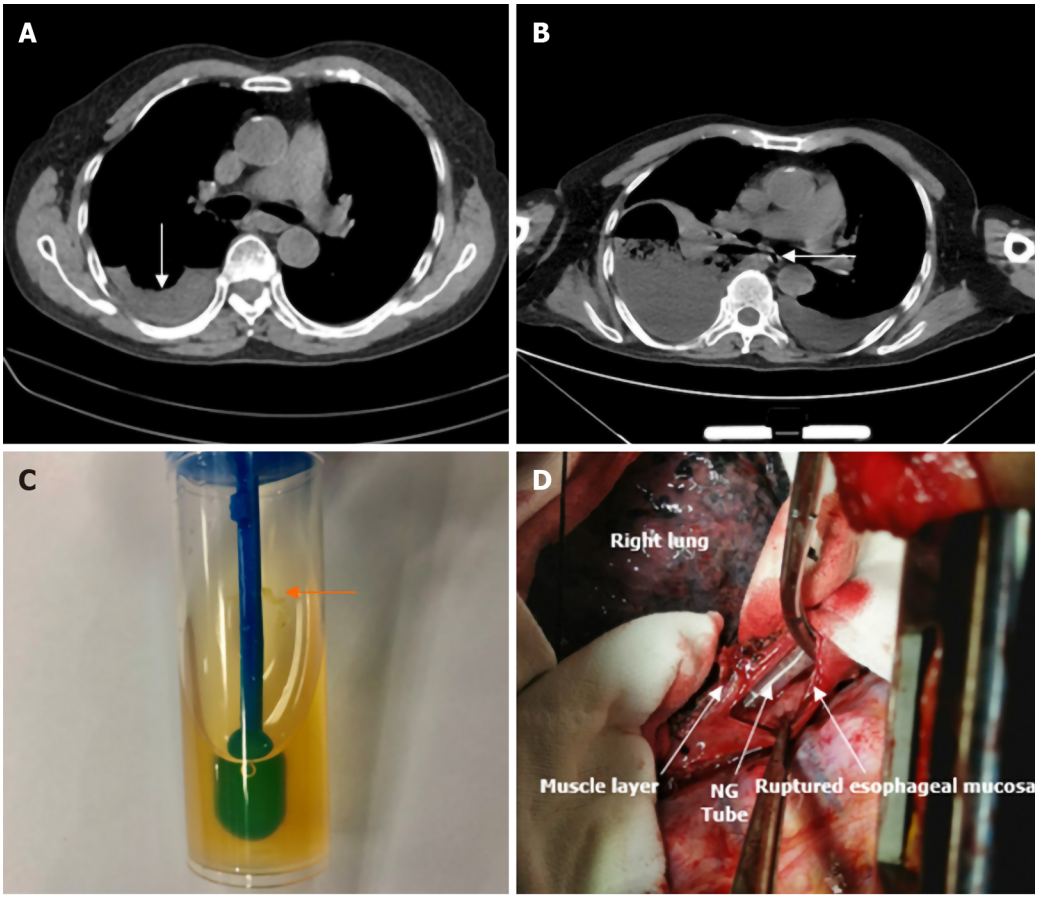

DOI: 10.12998/wjcc.v10.i18.6192 **Copyright** ©The Author(s) 2022.

Figure 1 Computed tomography. A: The chest computed tomography (CT) scan showed a small amount of fluid in the right pleural cavity; B: Chest CT was repeated: right-sided pleural effusion and perforation of the upper left esophagus were observed; C: Grapefruit-like residue drainage liquid was seen; D: The surgery showed the ruptured esophagus with nasogastric tube (NG tube) exposure.

FOOTNOTES

Author contributions: All authors made substantial contributions to conception and design, acquisition of data, or analysis and interpretation of data; took part in drafting the article or revising it critically for important intellectual content; agreed to submit to the current journal; gave final approval of the version to be published; and agree to be accountable for all aspects of the work.

Supported by the Natural Science Foundation of Hubei Province, No. 2019CFB798.

Informed consent statement: The patient has provided informed consent for publication of the case. A copy of the written consent is available for review from the Editor-in-Chief of this journal.

Conflict-of-interest statement: The authors have no conflicts of interest in relation to this work.

CARE Checklist (2016) statement: The authors have read the CARE Checklist (2016), and the manuscript was prepared and revised according to the CARE Checklist (2016).

Open-Access: This article is an open-access article that was selected by an in-house editor and fully peer-reviewed by external reviewers. It is distributed in accordance with the Creative Commons Attribution NonCommercial (CC BY-NC 4.0) license, which permits others to distribute, remix, adapt, build upon this work non-commercially, and license their derivative works on different terms, provided the original work is properly cited and the use is non-commercial. See: https://creativecommons.org/Licenses/by-nc/4.0/

Country/Territory of origin: China

ORCID number: Ni Tan 0000-0002-7591-0143; Yin-Hua Luo 0000-0003-4381-7048; Guang-Cai Li 0000-0002-9728-0197; Yilin Chen 0000-0003-1969-9854; Wei Tan 0000-0001-7625-5518; Yue-Hua Xiang 0000-0002-9526-5778; Liang Ge 0000-0003-2147-7652; Di Yao 0000-0002-6966-0416; Ming-Hua Zhang 0000-0003-4577-626X.

S-Editor: Ma YJ

L-Editor: Webster JR
P-Editor: Ma YJ

REFERENCES

1 **Maurya VK**, Sharma P, Ravikumar R, Bhatia M. Boerhaave's syndrome. *Med J Armed Forces India* 2016; **72**: S105-S107 [PMID: 28050085 DOI: 10.1016/j.mjafi.2015.12.004]
2 **Garas G**, Zarogoulidis P, Efthymiou A, Athanasiou T, Zacharakis E. Spontaneous esophageal rupture as the underlying cause of pneumothorax: early recognition is crucial. *Journal of Thoracic Disease* 2014 [DOI: 10.1016/s0041-3879(50)80042-9]
3 **Rokicki M**, Rokicki W, Rydel M. Boerhaave's Syndrome- Over 290 Yrs of Surgical Experiences. *Polski przeglad chirurgiczny* 2016 [DOI: 10.1515/pjs-2016-0077]
4 **Vidarsdottir H**, Blondal S, Alfredsson H, Geirsson A, Gudbjartsson T. Oesophageal perforations in Iceland: a whole population study on incidence, aetiology and surgical outcome. *Thoracic & Cardiovascular Surgeon* 2010 [DOI: 10.1055/s-0030-1250347]
5 **Marshall W B**. Boerhaave syndrome: a case report. *AANA Journal* 2002 [DOI: 10.14744/scie.2018.92485]
6 **Brauer R B**, Liebermann-Meffert D, Stein H J, Bartels H, Siewert JR. Boerhaave's syndrome: analysis of the literature and report of 18 new cases. *Diseases of the Esophagus* 1997 [DOI: 10.1093/dote/10.1.64]
7 **Wang J**, Wang D, Chen J. Diagnostic challenge and surgical management of Boerhaave's syndrome: a case series. *J Med Case Rep* 2021; **15**: 553 [PMID: 34749789 DOI: 10.1186/s13256-021-03080-1]
8 **Spapen J**, De Regt J, Nieboer K, Verfaillie G, Honoré PM, Spapen H. Boerhaave's Syndrome: Still a Diagnostic and Therapeutic Challenge in the 21st Century. *Case Rep Crit Care* 2013; **2013**: 161286 [PMID: 24829816 DOI: 10.1155/2013/161286]
9 **Carrozza F**, Dragean C. Spontaneous Esophageal Rupture or Boerhaave's Syndrome. *J Belg Soc Radiol* 2020; **104**: 1 [PMID: 31976387 DOI: 10.5334/jbsr.1882]
10 **O'Kelly F**, Lim KT, Cooke F, Ravi N, Reynolds JV. An unusual presentation of Boerhaave Syndrome: a case report. *Cases J* 2009; **2**: 8000 [PMID: 19830042 DOI: 10.4076/1757-1626-2-8000]
11 **Maier A**, Pinter H, Anegg U, Fell B, Sankin O, Tomaselli F. Boerhaave's syndrome: a continuing challenge in thoracic surgery. Hepatogastroenterology 2001 [DOI: 10.1016/s1010-7940(00)00592-3]
12 **Rassameehiran S**, Klomjit S, Nugent K. Right-sided hydropneumothorax as a presenting symptom of Boerhaave's syndrome (spontaneous esophageal rupture). *Proc (Bayl Univ Med Cent)* 2015; **28**: 344-346 [PMID: 26130884 DOI: 10.1080/08998280.2015.11929269]
13 **Korn O**, Oñate JC, López R. Anatomy of the Boerhaave syndrome. *Surgery* 2007; **141**: 222-228 [PMID: 17263979 DOI: 10.1016/j.surg.2006.06.034]

World Journal of Clinical Cases

Submit a Manuscript: https://www.f6publishing.com

World J Clin Cases 2022 June 26; 10(18): 6198-6204

DOI: 10.12998/wjcc.v10.i18.6198

ISSN 2307-8960 (online)

CASE REPORT

Camrelizumab-induced anaphylactic shock in an esophageal squamous cell carcinoma patient: A case report and review of literature

Kai Liu, Jian-Feng Bao, Tao Wang, Hao Yang, Bao-Ping Xu

Specialty type: Allergy

Provenance and peer review: Unsolicited article; Externally peer reviewed.

Peer-review model: Single blind

Peer-review report's scientific quality classification

Grade A (Excellent): 0
Grade B (Very good): B
Grade C (Good): C
Grade D (Fair): 0
Grade E (Poor): 0

P-Reviewer: Costa T, Portugal; Trabelsi M, Tunisia

Received: November 9, 2021
Peer-review started: November 9, 2021
First decision: December 27, 2021
Revised: January 13, 2022
Accepted: April 22, 2022
Article in press: April 22, 2022
Published online: June 26, 2022

Kai Liu, Department of Radiotherapy, Traditional Chinese Hospital of Lu'an affiliated to Anhui University of Traditional Chinese Medicine, Lu'an 237000, Anhui Province, China

Jian-Feng Bao, Department of Immuno-logy, Xixi Hospital of Hangzhou affiliated to Zhejiang University of Traditional Chinese Medicine, Hangzhou 310023, Zhejiang Province, China

Tao Wang, Department of Urology, Zhongshan Hospital of Traditional Chinese Medicine Affiliated to Guangzhou University of Chinese Medicine, Zhongshan 528401, Guangdong Province, China

Hao Yang, Bao-Ping Xu, Department of Critical Care Medicine, Traditional Chinese Hospital of Lu'an affiliated to Anhui University of Traditional Chinese Medicine, Lu'an 237000, Anhui Province, China

Corresponding author: Bao-Ping Xu, MD, Professor, Department of Critical Care Medicine, Traditional Chinese Hospital of Lu'an affiliated to Anhui University of Traditional Chinese Medicine, No. 76 Renmin Road, Lu'an 237000, Anhui Province, China. xu131406@qq.com

Abstract

BACKGROUND

Camrelizumab (SHR-1210), an immune checkpoint inhibitor, is clinically used as a therapeutic option for various types of tumors. However, reports of adverse reactions associated with camrelizumab are gradually increasing. Anaphylactic shock due to camrelizumab has not been reported previously, until now. We report here, for the first time, a case of anaphylactic shock associated with camrelizumab in a patient with esophageal squamous cell carcinoma.

CASE SUMMARY

An 84-year-old male esophageal cancer patient received radiotherapy and chemotherapy 11 years ago. He was diagnosed with advanced esophageal squamous cell carcinoma with liver metastasis (TxN1M1) and received the first immunotherapy (camrelizumab 200 mg/each time, once every 3 wk) dose in December 2020, with no adverse reactions. Three weeks later, a generalized rash was noted on the chest and upper limbs; palpitations and breathing difficulties with a sense of dying occurred 10 min after the patient had been administered with the second camrelizumab therapy. Electrocardiograph monitoring revealed a 70 beats/min pulse rate, 69/24 mmHg (1 mmHg = 0.133 kPa) blood pressure, 28

breaths/min respiratory rate, and 86% pulse oximetry in room air. The patient was diagnosed with anaphylactic shock and was managed with intravenous fluid, adrenaline, dexamethasone sodium phosphate, calcium glucosate, and noradrenaline. Approximately 2 h after treatment, the patient's anaphylactic shock symptoms had been completely relieved.

CONCLUSION
Due to the widespread use of camrelizumab, attention should be paid to anti-programmed cell death 1 antibody therapy-associated hypersensitivity or anaphylactic shock.

Key Words: Camrelizumab; Anaphylactic shock; Anti-programmed cell death one antibodies; Immunotherapy; Case report

©The Author(s) 2022. Published by Baishideng Publishing Group Inc. All rights reserved.

Core Tip: Since its approval in 2019 by the National Drug Administration, camrelizumab (SHR-1210), a programmed cell death 1 inhibitor, is in wide clinical use as a therapeutic option for various tumor types. Until now, allergic reactions induced by camrelizumab have been rarely reported from various studies. For the first time, we report a case of camrelizumab-induced anaphylactic shock in a patient with esophageal squamous cell carcinoma.

Citation: Liu K, Bao JF, Wang T, Yang H, Xu BP. Camrelizumab-induced anaphylactic shock in an esophageal squamous cell carcinoma patient: A case report and review of literature. *World J Clin Cases* 2022; 10(18): 6198-6204
URL: https://www.wjgnet.com/2307-8960/full/v10/i18/6198.htm
DOI: https://dx.doi.org/10.12998/wjcc.v10.i18.6198

INTRODUCTION

Since its approval in 2019 by the National Drug Administration, camrelizumab (SHR-1210), an immune checkpoint inhibitor (ICI), is in wide clinical use as a therapeutic option for various tumor types[1]. However, reports of camrelizumab-associated adverse reactions are increasing gradually, with any organ or tissue being affected. Reactive cutaneous capillary endothelial proliferation is the most common adverse event that is associated with camrelizumab, with an incidence accounting for about two-thirds of all patients treated with camrelizumab[2]. It is followed by immune-related hepatitis, pneumonia, and myocarditis among other clinical complications[3,4]. Until now, allergic reactions induced by ICIs have been reported in various studies[5,6].

As a relatively new programmed cell death 1 (PD-1) inhibitor, camrelizumab-induced anaphylactic shock has not yet been reported. We report here, for the first time, a case of camrelizumab-induced anaphylactic shock in a patient being treated for esophageal squamous cell carcinoma.

CASE PRESENTATION

Chief complaints

An 84-year-old male patient (163 cm in height, 41 kg in weight) presenting with esophageal cancer was administered with radiotherapy and chemotherapy 11 years prior, after which he got better.

History of present illness

In December 2020, the patient was diagnosed with advanced esophageal squamous cell carcinoma with liver metastasis, classified as stage TxN1M1. Based on the 2020 Chinese Society of Clinical Oncology guidelines, the patient was administered the first immunotherapeutic (camrelizumab 200 mg/each time + 0.9% NS 100 mL, intravenous infusion, q3w) and did not exhibit any adverse reactions. On January 12, 2021, the patient was admitted to the hospital for the second time to be administered the same therapy. On January 19, 2021, the patient was introduced to intravenous infusions of camrelizumab. However, 10 min after initiating intravenous camrelizumab, he suddenly developed a generalized rash in the chest and upper limbs. He also experienced chest tightness without chest pain, palpitations, and breathing difficulties with a sense of dying.

History of past illness

The patient had a previous medical history free of allergy.

Personal and family history

The patient had no significant personal or family history.

Physical examination

Electrocardiograph (ECG) monitoring revealed a pulse rate of 70 beats/min, blood pressure of 69/24 mmHg, a respiratory rate of 28 breaths/min, and a pulse oximetry of 86% in room air (no other medication was administered concomitantly). The patient presented with drowsiness and weakened cardiac sounds as well as a weak major arterial pulse.

Laboratory examinations

Blood analysis revealed white blood cell count of 7.04 × 10^9/L, neutrophil count of 2.81 × 10^9/L (normal range: 2.0-7.5 × 10^9/L), neutrophil percentage of 39.90%, red blood cell count of 2.35 × 10^{12}/L, hemoglobin level of 66.00 g/L (normal range: 110-160 g/L), platelet count of 219.00 × 10^9/L (normal range: 100-300 × 10^9/L), C-reactive protein level of 31.61 mg/L (normal range: < 0.5 mg/L), potassium level of 2.12 mmol/L (normal range: 3.5-5.0 mmol/L), chloride level of 117.80 mmol/L (normal range: 96-108 mmol/L), and calcium level of 1.41 mmol/L (normal range: 2.0-2.6 mmol/L). Markers of renal function and levels of cardiac enzyme and troponin were normal.

Imaging examinations

ECG (Figure 1) revealed a sinus rhythm. Enhanced computed tomography scan revealed chronic inflammation of the right lower lobe with left-side pleural slight effusion (Figure 2).

FINAL DIAGNOSIS

Based on the findings from the examination and investigations, we first considered the possibility of anaphylactic shock.

TREATMENT

The intravenous camrelizumab infusion was stopped immediately. In lieu, treatment was begun with corticoids, adrenaline, norepinephrine and intravenous fluid. Continuous supplementation of intravenous potassium and calcium were also provided.

OUTCOME AND FOLLOW-UP

The patient reported his chest tightness to be significantly relieved. He also experienced no shortness of breath, palpitations, or discomfort. The upper limbs and chest rash subsided rapidly, at approximately 2 h after treatment. ECG monitoring revealed a pulse rate of 78 beats/min, blood pressure of 112/68 mmHg, respiratory rate of 19 breaths/min, and pulse oximetry of 99% (oxygen absorption at 2 L/min).

On January 20, 2021, biochemical examination revealed that serum potassium and calcium levels were normal. The basic treatment was continued, without repeated anaphylactic shock. It is very unfortunate, however, that the patient refused to return to use of the camrelizumab, due to his excessive fear of anaphylactic shock, even after the physician provided a sufficient explanation. As such, we consulted the published literature and found switching to another type of anti-PD-1 antibody to be a feasible alternative. Indeed, such an approach has been successfully reported, with patients exhibiting relatively good clinical effects without allergic reactions[5,6].

Another type of anti-PD-1 antibody, nivolumab, is an ICI with a similar mechanism of action that is effective for treatment. The adverse e□ect profile of nivolumab is similar to those of camrelizumab, so the drugs related to the prevention of allergic reactions should be administered as premedication 30 min prior to the nivolumab infusion. The drawback is that it is very expensive and, in China, it is not covered by insurance reimbursement plans. Therefore, the patient rejected the physician's suggestion to replace the immunotherapy drugs. The patient was discharged on January 23, 2021.

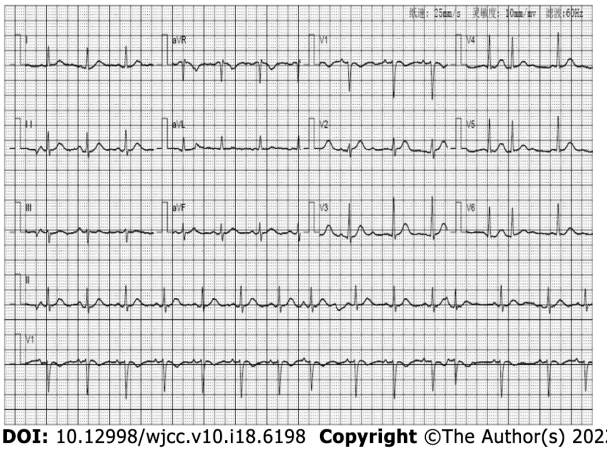

DOI: 10.12998/wjcc.v10.i18.6198 **Copyright** ©The Author(s) 2022.

Figure 1 Electrocardiograph revealed a sinus rhythm.

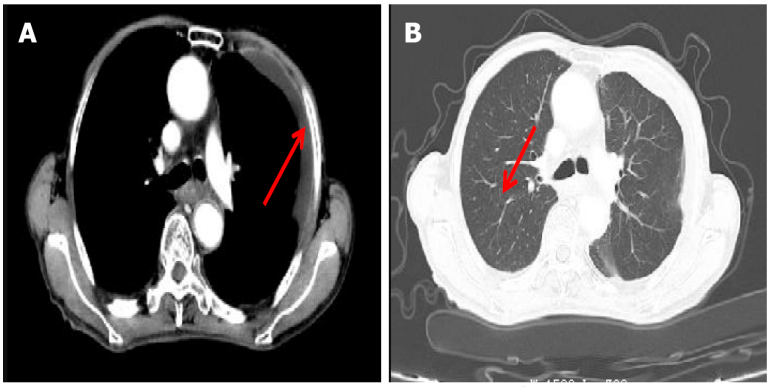

DOI: 10.12998/wjcc.v10.i18.6198 **Copyright** ©The Author(s) 2022.

Figure 2 Enhanced computed tomography scan revealed chronic inflammation. A: Left-side pleural slight effusion; B: Chronic inflammation of the right lower lobe.

DISCUSSION

Anaphylactic shock is a serious life-threatening acute systemic hypersensitivity reaction that is characterized by rapid development of life-threatening bronchospasms, or respiratory failure, or cardiovascular abnormalities. Sometimes, it is accompanied by general urticaria, erythema, and skin itch [7,8]. The symptoms associated with anaphylactic shock usually occur within minutes or less than 1 h after administration of the precipitating drug and result from activation of tissue mast cells and blood basophils, which release histamine and other inflammatory mediators[8]. Drug-induced anaphylactic shock accounts for a significantly high mortality rate among in-patients. Therefore, if not handled in time, it is often life-threatening[9].

Camrelizumab is a humanized PD-1 inhibitor that was developed by Jiangsu Hengrui Medicine Co. Ltd.[10]. It blocks the binding between programmed death ligand 1 and programmed death ligand 2 by targeting PD-1, thereby inhibiting tumor cell evasion from the immune system and ultimately causing an anti-tumor effect[11]. Camrelizumab has been clinically approved for the treatment of various tumors, including relapsed or refractory classical Hodgkins lymphoma, esophageal squamous cell carcinoma, hepatocellular carcinoma, and non-small cell lung cancer, among others[1,12]. Camrelizumab has therapeutic effects and has been shown to clinically improve various tumors, while having a manageable safety profile[13-17]. Moreover, it has exhibited potential anti-tumor effects in patients who failed chemotherapy or in those who are resistant to chemotherapy, while having an acceptable toxicity profile[18,19]. Due to the widespread application of camrelizumab, it has the potential to become a routine option for tumor immunotherapy[10]. However, camrelizumab-associated adverse events, including common reactive cutaneous capillary endothelial proliferation[2], immune-related hepatitis and pneumonia[3], immune-associated myocarditis[4], abnormal hepatic functions, anemia, and diarrhea[20], among others, have been reported. Most camrelizumab-associated adverse events are mild and can be regulated by interrupting treatment[20]. Camrelizumab-associated anaphylactic shock is rare but potentially fatal. Only two studies have reported on hypersensitivities induced by anti-programmed death ligand 1 agents[5,6]. Camrelizumab-associated allergic reactions or anaphylactic shock have never

been reported previously. Therefore, the understanding of allergic reactions or anaphylactic shock caused by immune preparations such as camrelizumab is limited, which may create the potential for delays in identification and management during the early stages of hypersensitivity. This can lead to a life-threatening outcome. Here, we provide the first report of camrelizumab-associated anaphylactic shock, which should arouse the interest of clinicians.

Adverse reactions for this case were evaluated according to the national adverse drug reaction Evaluation Standard of China[21]. Our patient experienced sudden-onset of the anaphylactic shock, within 10 min after intravenous injection of the camrelizumab infusion, implying an obvious time correlation between camrelizumab administration and development of the adverse event. Although there is no description of anaphylactic shock adverse events in the instructions for camrelizumab, it has been reported that serious hypersensitivities can occur after administration of the same anti-PD-1 or anti-programmed death ligand 1 agents, such as nivolumab[5,6]. Anaphylactic shock is a special manifestation of anaphylactic reactions; therefore, based on the above evidence, it can be considered that camrelizumab may cause hypersensitivities, including anaphylactic shock. After withdrawal of camrelizumab and administration of related treatments (*e.g.*, oxygen inhalation, anti-allergies, stable blood pressure treatment, and fluid resuscitation) were initiated, out patient's blood pressure returned to normal, chest tightness symptoms were significantly relieved, and all his other medications were continued while he gradually improved after 3 h. Since then, the patient has not had symptoms of anaphylactic shock. In addition, the patient had no history of drug anaphylaxis, and there were no changes in the use of other drugs before and after the occurrence of anaphylactic shock. The patient did not experience anaphylactic shock again after stopping the camrelizumab treatment; this allowed us to exclude the association of anaphylactic shock for the other drugs he was taking. Since his Naranjo Adverse Drug Reaction Probability Scale score was 5[22], we concluded that the anaphylactic shock was most likely caused by the camrelizumab administration.

Infections can aggravate or induce the occurrence of severe allergic reactions. About 1.3% to 11.0% of adults with severe allergic reactions have infectious etiologies[23]. These allergic reactions may be attributed to the immunoglobulin G produced during infection[24,25]. The patient had no adverse reactions after the first camrelizumab therapy, and the second treatment plan was the same as the initial treatment. He had been admitted to the hospital due to esophageal tumor accompanied by lung infection. After anti-infection treatment, findings of routine blood tests, including white blood cell and neutrophil counts, were normal, while C-reactive protein levels decreased from 116.16 to 70.35 mg/L. Computed tomography of the patient's lungs showed that his lesions were improved, while his lung infections had come under control. The patient suffered a sudden anaphylactic shock after second camrelizumab administration. Although the infection was controlled, the C-reactive protein levels remained elevated, implying that the inflammatory medium in the body had not been removed completely, which may have been one of the inducing factors of anaphylactic shock. Therefore, for patients with mixed infections, clinicians should be cautious in their application of camrelizumab.

Solvent mediums and drug configurations play an important role in hypersensitivity or anaphylactic shock. Camrelizumab is a powder, requiring suspension for injection. The drug manual requires that every 200 mg of camrelizumab be dissolved in 5 mL of sterilized injection water. For this, the sterile injection water is slowly added along the wall of the bottle containing the camrelizumab powder and dissolved by slow vortexing, to avoid direct sprinkling of water droplets on the surface of the powder. Then, the compound solution is extracted to make a 100 mL 0.9% sodium chloride solution or 5% glucose injection in an infusion bag dilution for intravenous administration by drip over a 30-minutes period. For our patient, the drug was prepared in strict accordance with these instructions, and the patient had no allergic reaction during the first dose. Therefore, neither the drug configuration nor solvent factors explain the patient's anaphylactic shock.

Individual factors also lead to the occurrence of allergic diseases. Epidemiologically, most anaphylactic shock cases occur in the older population, with higher risks among those aged over 70 years[26]. The mortality rate for females is lower than that of males[9]. Our patient was an 84-year-old male with esophageal squamous cell carcinoma and liver metastases. Therefore, he was at a high risk of anaphylactic shock.

Due to its increased clinical use, camrelizumab-associated hypersensitivity or anaphylactic shock should arouse the attention of clinicians. There are limited specific treatments for anaphylactic shock in clinical practice. Therefore, early identification is very important[27]. Generally, drugs that may cause anaphylactic shock should be immediately discontinued. Open venous channels, oxygen inhalation, and ECG monitoring should be performed[28]. Epinephrine is often administered for anaphylactic shock, which can excite α receptors and constrict peripheral blood vessels[29]. Rapid intravenous fluids can restore the effective blood volume, and generally about 250-500 mL of the fluids are recommended. Vasoactive drugs, including norepinephrine and dopamine, are recommended if blood pressure cannot be maintained after fluid resuscitation[30]. Secondly, glucocorticoids and histamine receptor antagonists should be administered as anti-allergic treatments. In cases of severe dyspnea and laryngeal edema, emergency organ intubation and tracheotomy are required[28]. It has not been conclusively determined whether immunotherapy should be restarted after the occurrence of anaphylactic shock. Studies reported continuous immunotherapeutic administration after successfully trying desensitization therapy. However, re-anaphylactic shock and failure of desensitization treatment can occur during

desensitization[6,31], and the safety and efficacy of desensitization therapy for patients with anaphylactic shock both need to be verified further. Switching to another immunotherapeutic drug is, thus, recommended. This approach has been applied successfully in previous studies, with the reported patients exhibiting relatively good clinical effects without allergic reactions[5,6].

CONCLUSION

Due to widespread use of camrelizumab, attention should be paid to anti-PD-1 blockade treatment-associated hypersensitivity or anaphylactic shock. We have reported herein a case of camrelizumab-induced anaphylactic shock in a patient with esophageal squamous cell carcinoma. Strengthening the monitoring of adverse drug reactions and identification of allergic reactions caused by camrelizumab treatment in the early stages should be taken into consideration by clinicians.

FOOTNOTES

Author contributions: Xu BP and Liu K designed the study and drafted the manuscript; Wang T and Yang H collected and analyzed the data; Xu BP and Bao JF revised the manuscript critically for important intellectual content; all authors reviewed and approved the final manuscript.

Supported by the National Natural Science Foundation of China, No. 81873317; the Natural Science Foundation of Zhejiang, No. LSY19H030002; and the Science and Technology Projects of Hangzhou City, No. 20181228Y22.

Informed consent statement: Informed written consent was obtained from the patient for the publication of this report and any accompanying images.

Conflict-of-interest statement: The authors declare that they have no conflict of interest.

CARE Checklist (2016) statement: The authors have read the CARE Checklist (2016), and the manuscript was prepared and revised according to the CARE Checklist (2016).

Open-Access: This article is an open-access article that was selected by an in-house editor and fully peer-reviewed by external reviewers. It is distributed in accordance with the Creative Commons Attribution NonCommercial (CC BY-NC 4.0) license, which permits others to distribute, remix, adapt, build upon this work non-commercially, and license their derivative works on different terms, provided the original work is properly cited and the use is non-commercial. See: https://creativecommons.org/Licenses/by-nc/4.0/

Country/Territory of origin: China

ORCID number: Kai Liu 0000-0001-8279-0760; Jian-Feng Bao 0000-0001-1130-8057; Tao Wang 0000-0003-1152-8399; Hao Yang 0000-0001-5334-3603; Bao-Ping Xu 0000-0001-6257-2766.

S-Editor: Guo XR
L-Editor: A
P-Editor: Guo XR

REFERENCES

1 **Markham A**, Keam SJ. Correction to: Camrelizumab: First Global Approval. *Drugs* 2019; **79**: 1497 [PMID: 31446564 DOI: 10.1007/s40265-019-01191-0]
2 **Wang F**, Qin S, Sun X, Ren Z, Meng Z, Chen Z, Chai X, Xiong J, Bai Y, Yang L, Zhu H, Fang W, Lin X, Chen X, Li E, Wang L, Yan P, Zou J. Reactive cutaneous capillary endothelial proliferation in advanced hepatocellular carcinoma patients treated with camrelizumab: data derived from a multicenter phase 2 trial. *J Hematol Oncol* 2020; **13**: 47 [PMID: 32393323 DOI: 10.1186/s13045-020-00886-2]
3 **Tan Y**, Ye Y, Chen L. Fatal immune-related hepatitis with intrahepatic cholestasis and pneumonia associated with camrelizumab: A case report and literature review. *Open Med (Wars)* 2021; **16**: 553-557 [PMID: 33869777 DOI: 10.1515/med-2021-0267]
4 **Wang F**, Sun X, Qin S, Hua H, Liu X, Yang L, Yang M. A retrospective study of immune checkpoint inhibitor-associated myocarditis in a single center in China. *Chin Clin Oncol* 2020; **9**: 16 [PMID: 32279526 DOI: 10.21037/cco.2020.03.08]
5 **Choi B**, McBride A, Scott AJ. Treatment with pembrolizumab after hypersensitivity reaction to nivolumab in a patient with hepatocellular carcinoma. *Am J Health Syst Pharm* 2019; **76**: 1749-1752 [PMID: 31612928 DOI: 10.1093/ajhp/zxz189]
6 **Sáenz de Santa María García M**, Noguerado-Mellado B, Rojas-Pérez-Ezquerra P, Prieto-García A, Bartolomé-Zavala B, Tornero P. First case of allergy to nivolumab. *J Allergy Clin Immunol Pract* 2017; **5**: 1140-1141 [PMID: 28284782 DOI: 10.1016/j.jaip.2017.01.015]

7 **Gouel-Cheron A**, Neukirch C, Kantor E, Malinovsky JM, Tacquard C, Montravers P, Mertes PM, Longrois D. Clinical reasoning in anaphylactic shock: addressing the challenges faced by anaesthesiologists in real time: A clinical review and management algorithms. *Eur J Anaesthesiol* 2021; **38**: 1158-1167 [PMID: 33973926 DOI: 10.1097/EJA.0000000000001536]

8 **Limsuwan T**, Demoly P. Acute symptoms of drug hypersensitivity (urticaria, angioedema, anaphylaxis, anaphylactic shock). *Med Clin North Am* 2010; **94**: 691-710, x [PMID: 20609858 DOI: 10.1016/j.mcna.2010.03.007]

9 **Liu FC**, Chiou HJ, Kuo CF, Chung TT, Yu HP. Epidemiology of Anaphylactic Shock and its Related Mortality in Hospital Patients in Taiwan: A Nationwide Population-Based Study. *Shock* 2017; **48**: 525-531 [PMID: 28498295 DOI: 10.1097/SHK.0000000000000899]

10 **Song H**, Liu X, Jiang L, Li F, Zhang R, Wang P. Current Status and Prospects of Camrelizumab, A Humanized Antibody Against Programmed Cell Death Receptor 1. *Recent Pat Anticancer Drug Discov* 2021; **16**: 312-332 [PMID: 33563158 DOI: 10.2174/1574892816666210208231744]

11 **Su H**, Yu C, Ma X, Song Q. Combined immunotherapy and targeted treatment for primary alveolar soft part sarcoma of the lung: case report and literature review. *Invest New Drugs* 2021; **39**: 1411-1418 [PMID: 33765213 DOI: 10.1007/s10637-021-01105-6]

12 **Wang CY**, Sheng CC, Ma GL, Xu D, Liu XQ, Wang YY, Zhang L, Cui CL, Xu BH, Song YQ, Zhu J, Jiao Z. Population pharmacokinetics of the anti-PD-1 antibody camrelizumab in patients with multiple tumor types and model-informed dosing strategy. *Acta Pharmacol Sin* 2021; **42**: 1368-1375 [PMID: 33154554 DOI: 10.1038/s41401-020-00550-y]

13 **Wang P**, Fang X, Yin T, Tian H, Yu J, Teng F. Efficacy and Safety of Anti-PD-1 Plus Anlotinib in Patients With Advanced Non-Small-Cell Lung Cancer After Previous Systemic Treatment Failure-A Retrospective Study. *Front Oncol* 2021; **11**: 628124 [PMID: 33791214 DOI: 10.3389/fonc.2021.628124]

14 **Liu Y**, Wang C, Li X, Dong L, Yang Q, Chen M, Shi F, Brock M, Liu M, Mei Q, Liu J, Nie J, Han W. Improved clinical outcome in a randomized phase II study of anti-PD-1 camrelizumab plus decitabine in relapsed/refractory Hodgkin lymphoma. *J Immunother Cancer* 2021; **9** [PMID: 33820822 DOI: 10.1136/jitc-2021-002347]

15 **Chen X**, Qin S, Gu S, Ren Z, Chen Z, Xiong J, Liu Y, Meng Z, Zhang X, Wang L, Zou J. Camrelizumab plus oxaliplatin-based chemotherapy as first-line therapy for advanced biliary tract cancer: A multicenter, phase 2 trial. *Int J Cancer* 2021; **149**: 1944-1954 [PMID: 34309846 DOI: 10.1002/ijc.33751]

16 **Liao R**. Effectiveness of anti-PD-1 for hepatocellular carcinoma. *Lancet Oncol* 2020; **21**: e293 [PMID: 32502446 DOI: 10.1016/S1470-2045(20)30170-4]

17 **Zhang W**, Yan C, Gao X, Li X, Cao F, Zhao G, Zhao J, Er P, Zhang T, Chen X, Wang Y, Jiang Y, Wang Q, Zhang B, Qian D, Wang J, Zhou D, Ren X, Yu Z, Zhao L, Yuan Z, Wang P, Pang Q. Safety and Feasibility of Radiotherapy Plus Camrelizumab for Locally Advanced Esophageal Squamous Cell Carcinoma. *Oncologist* 2021; **26**: e1110-e1124 [PMID: 33893689 DOI: 10.1002/onco.13797]

18 **Fan Y**, Zhao J, Wang Q, Huang D, Li X, Chen J, Fang Y, Duan J, Zhou C, Hu Y, Yang H, Zhou J, Lin X, Wang L, Wang Z, Xu Y, Zhang T, Shi W, Zou J, Wang J. Camrelizumab Plus Apatinib in Extensive-Stage SCLC (PASSION): A Multicenter, Two-Stage, Phase 2 Trial. *J Thorac Oncol* 2021; **16**: 299-309 [PMID: 33166719 DOI: 10.1016/j.jtho.2020.10.002]

19 **Cong X**, Chen J, Zheng W. The combination of camrelizumab and apatinib obtained ongoing partial remission for a patient with osimertinib-resistant non-small cell lung cancer: case report. *Ann Palliat Med* 2021; **10**: 3469-3474 [PMID: 33040541 DOI: 10.21037/apm-19-462]

20 **Huang J**, Xu J, Chen Y, Zhuang W, Zhang Y, Chen Z, Chen J, Zhang H, Niu Z, Fan Q, Lin L, Gu K, Liu Y, Ba Y, Miao Z, Jiang X, Zeng M, Fu Z, Gan L, Wang J, Zhan X, Liu T, Li Z, Shen L, Shu Y, Zhang T, Yang Q, Zou J; ESCORT Study Group. Camrelizumab *vs* investigator's choice of chemotherapy as second-line therapy for advanced or metastatic oesophageal squamous cell carcinoma (ESCORT): a multicentre, randomised, open-label, phase 3 study. *Lancet Oncol* 2020; **21**: 832-842 [PMID: 32416073 DOI: 10.1016/S1470-2045(20)30110-8]

21 **Li B**, Gao R, Li R, Lu F, Zi MJ, Li QN, Tang XD. Causal determination of the adverse events and adverse drug reactions in drug clinical trials. *Zhongguo Xinyao Zazhi* 2014; **23**: 1465-1470 [DOI: CNKI: SUN: ZXYZ.0.2014-12-026]

22 **Naranjo CA**, Busto U, Sellers EM, Sandor P, Ruiz I, Roberts EA, Janecek E, Domecq C, Greenblatt DJ. A method for estimating the probability of adverse drug reactions. *Clin Pharmacol Ther* 1981; **30**: 239-245 [PMID: 7249508 DOI: 10.1038/clpt.1981.154]

23 **Jiang NN**, Yin J. Trigger Factors and Mechanism of Anaphylaxis. Zhonghua Linchuangmianyi He Biantaifanying Zazhi 2016; 10: 269-275 [DOI: 10.3969/j.issn.1673-8705.2016.03.015]

24 **Mazur N**, Patterson R, Perlman D. A case of idiopathic anaphylaxis associated with respiratory infections. *Ann Allergy Asthma Immunol* 1997; **79**: 546-548 [PMID: 9433372 DOI: 10.1016/S1081-1206(10)63064-5]

25 **Custovic A**, Murray C, Simpson A. Allergy and infection: understanding their relationship. *Allergy* 2005; **60** Suppl 79: 10-13 [PMID: 15842227 DOI: 10.1111/j.1398-9995.2005.00851.x.]

26 **Park HK**, Kang MG, Yang MS, Jung JW, Cho SH, Kang HR. Epidemiology of drug-induced anaphylaxis in a tertiary hospital in Korea. *Allergol Int* 2017; **66**: 557-562 [PMID: 28291680 DOI: 10.1016/j.alit.2017.02.008]

27 **Takazawa T**, Oshima K, Saito S. Drug-induced anaphylaxis in the emergency room. *Acute Med Surg* 2017; **4**: 235-245 [PMID: 29123869 DOI: 10.1002/ams2.282]

28 **Müller-Werdan U**, Werdan K. [Anaphylactic shock]. *Anaesthesist* 1997; **46**: 549-563 [PMID: 9297387 DOI: 10.1007/s001010050436]

29 **Bennett MJ**, Hirshman CA. Epinephrine for anaphylactic shock. *JAMA* 1985; **253**: 510-511 [PMID: 3968781 DOI: 10.1001/jama.1985.03350280066012]

30 **Brown SG**. The pathophysiology of shock in anaphylaxis. *Immunol Allergy Clin North Am* 2007; **27**: 165-175, v [PMID: 17493496 DOI: 10.1016/j.iac.2007.03.003]

31 **Kim KW**, Chung S, Lee SY, Yoon SS, Kang HR. Successful Infusion of Obinutuzumab by Desensitization: A Case of Anaphylactic Shock During Desensitization. *J Investig Allergol Clin Immunol* 2020; **30**: 457-459 [PMID: 32376522 DOI: 10.18176/jiaci.0581]

World Journal of Clinical Cases

Submit a Manuscript: https://www.f6publishing.com

World J Clin Cases 2022 June 26; 10(18): 6205-6210

DOI: 10.12998/wjcc.v10.i18.6205

ISSN 2307-8960 (online)

CASE REPORT

Nontraumatic convexal subarachnoid hemorrhage: A case report

Hong-Liang Chen, Bin Li, Chao Chen, Xiao-Xuan Fan, Wen-Bin Ma

Specialty type: Clinical neurology

Provenance and peer review: Unsolicited article; Externally peer reviewed.

Peer-review model: Single blind

Peer-review report's scientific quality classification

Grade A (Excellent): 0
Grade B (Very good): 0
Grade C (Good): C, C
Grade D (Fair): 0
Grade E (Poor): 0

P-Reviewer: Diana F, Italy; Nag DS, India

Received: November 14, 2021
Peer-review started: November 14, 2021
First decision: December 10, 2021
Revised: December 17, 2021
Accepted: April 29, 2022
Article in press: April 29, 2022
Published online: June 26, 2022

Hong-Liang Chen, Bin Li, Chao Chen, Wen-Bin Ma, Department of Neurology, Binzhou Medical University Hospital, Binzhou 256600, Shandong Province, China

Xiao-Xuan Fan, Department of Clinical Medicine, Binzhou Medical University, Binzhou 256600, Shandong Province, China

Corresponding author: Wen-Bin Ma, MD, Associate Professor, Department of Neurology, Binzhou Medical University Hospital, No. 661 Huanghe 2nd Road, Binzhou 256600, Shandong Province, China. mawbin@163.com

Abstract

BACKGROUND

Nontraumatic convexal subarachnoid hemorrhage (cSAH) is a rare type of atypical subarachnoid hemorrhage. It mainly presents as a focal and transient neurological deficit with similar manifestations as transient ischemic attack.

CASE SUMMARY

We report a case of a 64-year-old man who visited the hospital with paroxysmal left-sided numbness and weakness is presented in this study. Computed tomography examination indicated a high-density image of the right frontal-parietal sulcus. Digital subtraction angiography showed severe stenosis at the right anterior cerebral artery A2-A3 junction (stenosis rate approximately 70%).

CONCLUSION

The findings of this case indicate that anterior cerebral artery stenosis may lead to the occurrence of cSAH.

Key Words: Nontraumatic convexal subarachnoid hemorrhage; Subarachnoid hemorrhage; Transient ischemic attack; Artery atherosclerosis stenosis; Case report

©The Author(s) 2022. Published by Baishideng Publishing Group Inc. All rights reserved.

Core Tip: This is a rare case of convexal subarachnoid hemorrhage (cSAH) with transient ischemic attack as the first presentation. We reported the whole course. This case indicated the clinical characteristics, laboratory findings, imaging examinations and adjustment of treatment and discussed the possible relation between anterior cerebral artery stenosis and the occurrence of cSAH.

Citation: Chen HL, Li B, Chen C, Fan XX, Ma WB. Nontraumatic convexal subarachnoid hemorrhage: A case report. *World J Clin Cases* 2022; 10(18): 6205-6210
URL: https://www.wjgnet.com/2307-8960/full/v10/i18/6205.htm
DOI: https://dx.doi.org/10.12998/wjcc.v10.i18.6205

INTRODUCTION

Nontraumatic convexal subarachnoid hemorrhage (cSAH) is a subtype of atypical SAH. Its bleeding site is mainly confined to one or more cerebral hemisphere convexocortical sulci with high incidence in the central sulcus. It does not affect the brain parenchyma, basal cistern, or interhemispheric fissure. It is characterized by low hemorrhage, and only the local cerebral cortex is involved. In addition, it is not associated with typical symptoms such as severe headache and meningeal irritation. In the present study, a case of a cSAH patient with transient ischemic attack (TIA) and a summary of relevant literature are presented.

CASE PRESENTATION

Chief complaints

A 64-year-old male was admitted to the hospital after experiencing paroxysmal left-sided numbness and weakness for 4 d.

History of present illness

These symptoms occurred 2-3 times a day and lasted approximately 20 min each time.

History of past illness

The patient had a clinical history of ischemic stroke and no history of hypertension, diabetes, coronary heart disease, or major trauma.

Personal and family history

The patient had no history of smoking or drinking, and no family history.

Physical examination

The systolic and diastolic blood pressure of the patient during admission was 130/80 mmHg. The patient presented with paroxysmal left hemiplegia without obvious inducement. The left limb could not move during the attack and was accompanied by numbness and discomfort on the left face, trunk, upper, and lower limbs; and the patient presented with dizziness. The National Institute of Health Stroke Scale score of the patient was 0.

Laboratory examinations

Routine clinical biochemistry showed normal results.

Imaging examinations

Computed tomography (CT) examination was performed during admission and showed a high-density image of the right frontal-parietal sulcus. Magnetic resonance imaging examination showed a slight increase in the T1 flair and a high T2 flair. Diffusion-weighted imaging (DWI) revealed high signal intensity, whereas susceptibility weighted imaging (SWI) showed slightly increased signal intensity in the right frontal lobe. Machine records activity results indicated short local stenosis of the right anterior cerebral artery of the A3 segment, and magnetic resonance venography revealed a thin contrast in the left transverse sinus and left sigmoid sinus (Figure 1). Severe stenosis was observed in the right anterior cerebral artery A2-A3 junction (stenosis rate approximately 70%), and mild stenosis was observed in the distal end of A3 (stenosis rate approximately 30%) through digital subtraction angiography (DSA) (Figure 2).

MULTIDISCIPLINARY EXPERT CONSULTATION

There is no multidisciplinary expert consultation.

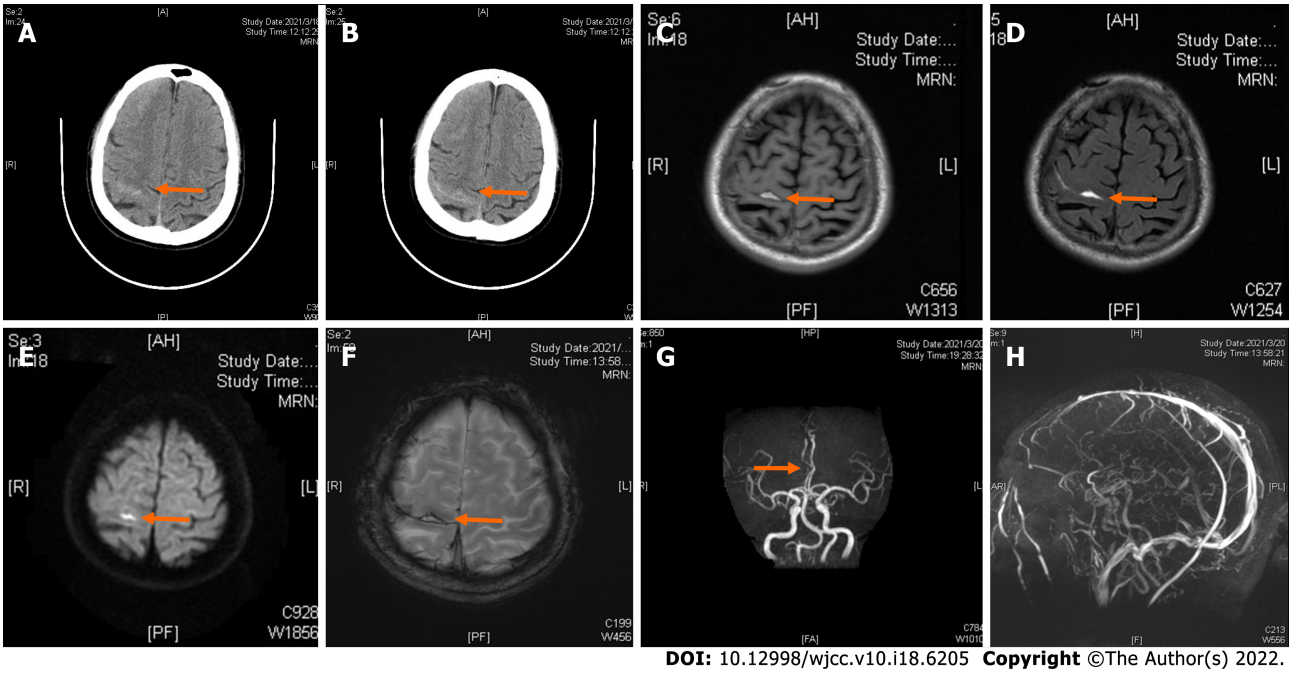

DOI: 10.12998/wjcc.v10.i18.6205 **Copyright** ©The Author(s) 2022.

Figure 1 Computed tomography imaging. A and B: Axial computed tomography images showing a high-density image of right frontal-parietal sulcus; C: Magnetic resonance imaging showing slightly elevated T1-flair; D: Elevated T2-flair; E: Diffusion-weighted imaging revealed high signal intensity; F: Susceptibility weighted imaging showing slightly increased signal intensity in the right frontal; G: Machine records activity showing short local stenosis of the right anterior cerebral artery of A3 segment; H: Magnetic resonance venography revealed a thinner contrast in the left transverse sinus and left sigmoid sinus.

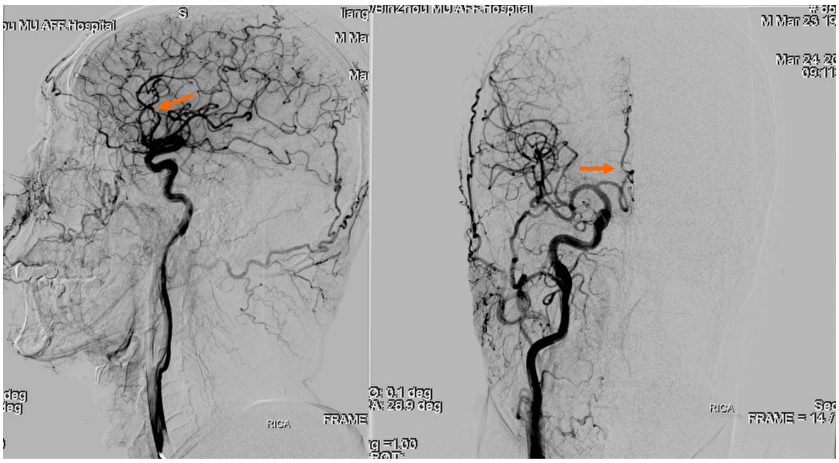

DOI: 10.12998/wjcc.v10.i18.6205 **Copyright** ©The Author(s) 2022.

Figure 2 Digital subtraction angiography showing severe stenosis in the right anterior cerebral artery A2-A3 junction.

FINAL DIAGNOSIS

The complete evidence supported the final diagnosis of cSAH.

TREATMENT

The patient was given blood pressure monitoring, cerebrovascular spasm prevention (nimodipine), cerebral protection, and other treatments.

OUTCOME AND FOLLOW-UP

The range of brain CT-showed bleeding was significantly reduced compared to the previous range after

9 d. The patient had no recurrence of paroxysmal left-sided numbness and weakness.

DISCUSSION

cSAH is a subtype of atypical SAH. Approximately 49% of patients with SAH present with TIA-like symptoms; therefore, the actual annual incidence is more than 5.1 cases in every 100000 people[1]. The etiology of cSAH is highly correlated with age, hypertension, coronary heart disease, and diabetes. Common causes of cSAH include cerebral amyloidosis (CAA), reversible cerebral vasoconstriction syndrome (RCVS), cortical vein thrombosis (CoVT), intracranial large artery atherosclerosis stenosis or occlusion, moyamoya disease, and vasculitis. Notably, CAA is the main cause, accounting for approximately 39% of all cSAH cases[1]. Transient sensorimotor dysfunction (TFNE) is the main symptom in cSAH patients above 60 years of age, and CAA is the common cause of disease, followed by intracranial atherosclerosis stenosis or occlusion[2,3]. In contrast, headache is the main clinical manifestation in patients under 60 years of age, whereas rCVS and CoVT are the main causes of cSAH in these patients [3]. Nakajima *et al*[4-5] reported that more than half of patients with cSAH presented with cerebral vascular occlusion and TFNE and were often misdiagnosed with transient cerebral ischemia. Notably, CAA is a progressive age-related cerebrovascular disease. The severity of the disease increases with age due to deposition of amyloid beta protein in the cortex and leptomeningeal vessels, which is the main cause of cSAH. A previous study reported that TFNE is the main characteristic clinical manifestation of CAA-induced cSAH, followed by cortical superficial siderosis (CSS) and rebleeding[6]. The incidence of hypercholesterolemia is lower in patients with CAA-induced cSAH than in patients with TIA. Cholesterol is negatively correlated with the incidence of nontraumatic intracerebral hemorrhage and aneurysmal hemorrhage[5]. Symptoms of cSAH are paroxysmal and include TIA attacks, seizures, and TFNE. This indicates that TIA attacks can occur as a result of ischemic infarction or may occur as a clinical manifestation of hemorrhagic stroke.

A previous study reported that hyperacute arterial ischemic stroke occurs in patients within 4.5 h and 6 days after a concurrent rate of cSAH 0.5%[4]. Acute changes in hemodynamics and damage to the blood brain barrier may be important mechanisms for the occurrence of cSAH. The incidence of SAH is associated with cerebrovascular disease risk factors such as hypertension, coronary heart disease, and diabetes, and this relationship can be explained by collateral circulation. ICA stenosis or occlusion and MCA stenosis or occlusion can promote the formation of Willis circle and the opening of PIA meningostomy vessels, respectively[7-8].

CT scan is important for the diagnosis of cSAH. However, the sensitivity of CT decreases after a period of time. Notably, flair is highly sensitive to hemorrhage in the cerebral convexity cortex sulcus and is more effective in the diagnosis of acute and subacute SAH than plain CT scans. DWI and SWI are characterized by high sensitivity and accuracy in the diagnosis of SAH. Cerebrospinal fluid examination cannot confirm the diagnosis of cSAH; however, it helps in determining the etiology of the disease[9]. Notably, DSA is performed to further confirm the diagnosis when the cause of disease cannot be determined through noninvasive examination. Studies report that cSAH may be a marker of vascular fragility and a major risk factor for future lobar hemorrhage[10]. Cortical or watershed subarachnoid hemorrhage may be the result of excessive cerebral perfusion. High-grade stenosis is always a sign of hemodynamic compromise, and collateral circulation might be a predictor of excessive cerebral perfusion[11]. The clinical and imaging findings of the patient in the present study indicate a positive diagnosis of cSAH and rule out the possibility of CAA. The cause of the disease was initially considered to be atherosclerotic stenosis of the large cerebral artery; however, later severe stenosis of the anterior cerebral artery was considered the cause of the present case. It is speculated that the pathogenesis may be severe stenosis of the anterior cerebral artery, which can cause compensatory dilation and vulnerability of cortical lateral branch vessels in the corresponding region, when hemodynamic changes occur, such as a sudden increase in intracranial perfusion pressure, resulting in the rupture of the leptic lateral branch circulation vessels that have already undergone expansion or increased permeability, resulting in bleeding, or the arrival of embolus to the fragile collateral vessels causing blood vessel rupture and causing a small amount of bleeding, which as indicated by DSA examination. Intracranial artery stenosis/occlusion caused by cSAH is common in MCA. In summary, the findings of the present study indicate that ACA stenosis may lead to the occurrence of cSAH.

cSAH is treated using different treatment strategies depending on the cause of the disease. Antiplatelet therapy is used for intracranial artery stenosis or occlusion caused by arteriosclerosis, nimodipine is administered for reversible cerebral vasoconstriction syndrome, and steroid hormone is given for the treatment of vasculitis. Symptomatic therapy for cSAH includes reduction of intracranial pressure, anti-epilepsy drugs, and administration of drugs for lowering blood pressure. The prognosis of cSAH depends on the cause, and most patients present with good prognosis. However, CAA-induced intracranial hemorrhage is recurrent and associated with poor prognosis[12].

CONCLUSION

Symptoms of cSAH are complex and not easily detected during clinical investigations. The cause of the disease should be explored to minimize missed diagnosis and misdiagnosis.

FOOTNOTES

Author contributions: Ma WB conceived the study, participated in its design and draft the manuscript; Li B, Chen C and Fan XX collected data; Chen HL helped to draft the manuscript; all authors read and approved the final manuscript.

Supported by Research Fund of the Department of Science and Technology of Shandong Province, China, No. 2019WS328.

Informed consent statement: Written informed consent was obtained from the patient for publication of this case report.

Conflict-of-interest statement: The authors declare no conflict of interest.

CARE Checklist (2016) statement: The authors have read the CARE Checklist (2016), and the manuscript was prepared and revised according to the CARE Checklist (2016).

Open-Access: This article is an open-access article that was selected by an in-house editor and fully peer-reviewed by external reviewers. It is distributed in accordance with the Creative Commons Attribution NonCommercial (CC BY-NC 4.0) license, which permits others to distribute, remix, adapt, build upon this work non-commercially, and license their derivative works on different terms, provided the original work is properly cited and the use is non-commercial. See: https://creativecommons.org/Licenses/by-nc/4.0/

Country/Territory of origin: China

ORCID number: Hong-Liang Chen 0000-0001-9434-9796; Bin Li 0000-0002-8721-4356; Chao Chen 0000-0003-0417-3809; Xiao-Xuan Fan 0000-0003-4912-6774; Wen-Bin Ma 0000-0001-5030-0093.

S-Editor: Xing YX
L-Editor: A
P-Editor: Xing YX

REFERENCES

1 **Khurram A**, Kleinig T, Leyden J. Clinical associations and causes of convexity subarachnoid hemorrhage. *Stroke* 2014; **45**: 1151-1153 [PMID: 24496391 DOI: 10.1161/STROKEAHA.113.004298]
2 **Kumar S**, Goddeau RP Jr, Selim MH, Thomas A, Schlaug G, Alhazzani A, Searls DE, Caplan LR. Atraumatic convexal subarachnoid hemorrhage: clinical presentation, imaging patterns, and etiologies. *Neurology* 2010; **74**: 893-899 [PMID: 20231664 DOI: 10.1212/WNL.0b013e3181d55efa]
3 **Martínez-Lizana E**, Carmona-Iragui M, Alcolea D, Gómez-Choco M, Vilaplana E, Sánchez-Saudinós MB, Clarimón J, Hernández-Guillamon M, Munuera J, Gelpi E, Gómez-Anson B, de Juan-Delago M, Delgado-Mederos R, Montaner J, Ois A, Amaro S, Blesa R, Martí-Fàbregas J, Lleó A, Fortea J. Cerebral amyloid angiopathy-related atraumatic convexal subarachnoid hemorrhage: an ARIA before the tsunami. *J Cereb Blood Flow Metab* 2015; **35**: 710-717 [PMID: 25735919 DOI: 10.1038/jcbfm.2015.25]
4 **Nakajima M**, Inatomi Y, Yonehara T, Hirano T, Ando Y. Nontraumatic convexal subarachnoid hemorrhage concomitant with acute ischemic stroke. *J Stroke Cerebrovasc Dis* 2014; **23**: 1564-1570 [PMID: 24630829 DOI: 10.1016/j.jstrokecerebrovasdis.2013.12.046]
5 **Stanton JED**, Chandratheva A, Wilson D, Hostettler IC, Islam S, Werring DJ. Clinical features distinguish cerebral amyloid angiopathy-associated convexity subarachnoid haemorrhage from suspected TIA. *J Neurol* 2020; **267**: 133-137 [PMID: 31583428 DOI: 10.1007/s00415-019-09558-9]
6 **Charidimou A**, Jäger RH, Fox Z, Peeters A, Vandermeeren Y, Laloux P, Baron JC, Werring DJ. Prevalence and mechanisms of cortical superficial siderosis in cerebral amyloid angiopathy. *Neurology* 2013; **81**: 626-632 [PMID: 23864315 DOI: 10.1212/WNL.0b013e3182a08f2c]
7 **Sato T**, Sakai K, Mimori M, Komatsu T, Sakuta K, Terasawa Y, Umehara T, Omoto S, Mitsumura H, Murakami H, Shimizu T, Matsushima S, Iguchi Y. Convexity Subarachnoid Hemorrhage Accompanied by Hyperacute Ischemic Stroke. *Cerebrovasc Dis* 2020; **49**: 70-78 [PMID: 31910410 DOI: 10.1159/000505013]
8 **Chandra RV**, Leslie-Mazwi TM, Oh D, Mehta B, Yoo AJ. Extracranial internal carotid artery stenosis as a cause of cortical subarachnoid hemorrhage. *AJNR Am J Neuroradiol* 2011; **32**: E51-2; author reply E53 [PMID: 21349955 DOI: 10.3174/ajnr.A2456]
9 **Refai D**, Botros JA, Strom RG, Derdeyn CP, Sharma A, Zipfel GJ. Spontaneous isolated convexity subarachnoid

hemorrhage: presentation, radiological findings, differential diagnosis, and clinical course. *J Neurosurg* 2008; **109**: 1034-1041 [PMID: 19035716 DOI: 10.3171/JNS.2008.109.12.1034]

10 **Raposo N**, Charidimou A, Roongpiboonsopit D, Onyekaba M, Gurol ME, Rosand J, Greenberg SM, Goldstein JN, Viswanathan A. Convexity subarachnoid hemorrhage in lobar intracerebral hemorrhage: A prognostic marker. *Neurology* 2020; **94**: e968-e977 [PMID: 32019785 DOI: 10.1212/WNL.0000000000009036]

11 **Diana F**, Frauenfelder G, Botto A, Saponiero R, Romano DG. Cerebral hyperperfusion syndrome after intracranial stenting: Case report and systematic review. *Interv Neuroradiol* 2021; **27**: 843-849 [PMID: 33884930 DOI: 10.1177/15910199211011860]

12 **Usmani N**, Ahmad FU, Koch S. Convexity subarachnoid hemorrhage in ischemic stroke. *J Neurol Sci* 2015; **348**: 259-261 [PMID: 25498843 DOI: 10.1016/j.jns.2014.11.031]

World Journal of Clinical Cases

Submit a Manuscript: https://www.f6publishing.com

World J Clin Cases 2022 June 26; 10(18): 6211-6217

DOI: 10.12998/wjcc.v10.i18.6211

ISSN 2307-8960 (online)

CASE REPORT

Growth hormone ameliorates hepatopulmonary syndrome and nonalcoholic steatohepatitis secondary to hypopituitarism in a child: A case report

Xiao-Yuan Zhang, Ke Yuan, Yan-Lan Fang, Chun-Lin Wang

Specialty type: Medicine, research and experimental

Provenance and peer review: Unsolicited article; Externally peer reviewed.

Peer-review model: Single blind

Peer-review report's scientific quality classification

Grade A (Excellent): 0
Grade B (Very good): 0
Grade C (Good): C, C, C
Grade D (Fair): 0
Grade E (Poor): 0

P-Reviewer: Aktas S, Turkey; Govindarajan KK, India; Soresi M, Italy

Received: November 13, 2021
Peer-review started: November 13, 2021
First decision: March 7, 2022
Revised: March 25, 2022
Accepted: April 22, 2022
Article in press: April 22, 2022
Published online: June 26, 2022

Xiao-Yuan Zhang, Ke Yuan, Yan-Lan Fang, Chun-Lin Wang, Department of Pediatrics, The First Affiliated Hospital, Zhejiang University School of Medicine, Hangzhou 310003, Zhejiang Province, China

Corresponding author: Chun-Lin Wang, Doctor, PhD, Chief Doctor, Professor, Department of Pediatrics, The First Affiliated Hospital, Zhejiang University School of Medicine, No. 79 Qingchun Road, Hangzhou 310003, Zhejiang Province, China. hzwangcl@zju.edu.cn

Abstract

BACKGROUND

Craniopharyngioma is a benign tumor that usually develops in children; however, it is located in the center and close to sensitive structures, such as the pituitary gland and hypothalamus. As the hypothalamus plays a crucial role in the homeostasis of anterior pituitary hormone synthesis, damage to the hypothalamus leads to multiple pituitary hormone deficiencies and non-alcoholic fatty liver disease, including hepatopulmonary syndrome (HPS). HPS has limited treatment and poor prognosis.

CASE SUMMARY

A girl aged 13 years and 6 mo underwent surgery for craniopharyngioma 6 years prior. Right craniotomy was performed with total resection *via* the corpus callosum approach, and the tumor at the base was approximately 3.5 cm × 3.5 cm × 4.0 cm. At 1 year postoperatively, she exhibited abdominal distension and weakness, and the laboratory tests revealed fatty liver disease. Thereafter, she had not visited the outpatient clinic for 2 years. Two years ago, she developed decreased activity endurance, severe cyanosis, chest tightness, wheezing, and intermittent and recurrent low fever after mild physical labor. Hepatobiliary ultrasonography, liver biopsy, and contrast echocardiography of the right heart showed cirrhosis and multiple pituitary hormone deficiencies, indicating HPS. After 1 year of treatment with recombinant human growth hormone, the liver function and oxygenation improved; she did not undergo liver transplantation.

CONCLUSION

Craniopharyngioma surgery can easily cause hypopituitarism, which can lead to nonalcoholic steatohepatitis and HPS in children. Early growth hormone therapy is important to improve the prognosis of these diseases.

Key Words: Craniopharyngioma; Nonalcoholic fatty liver disease; Hypopituitarism; Hepatopulmonary syndrome; Growth hormone; Children; Case report

©The Author(s) 2022. Published by Baishideng Publishing Group Inc. All rights reserved.

Core Tip: Hepatopulmonary syndrome (HPS) is a serious complication of chronic liver disease with a poor prognosis. Currently, liver transplantation is the only available treatment; however, severe hypoxemia before transplantation is a high risk factor for postoperative death. We present a case of postoperative craniopharyngioma in a child with nonalcoholic steatohepatitis and HPS secondary to hypopituitarism. The patient's liver function and hypoxemia were improved by growth hormone replacement therapy, and liver transplantation was expected to be avoided.

Citation: Zhang XY, Yuan K, Fang YL, Wang CL. Growth hormone ameliorates hepatopulmonary syndrome and nonalcoholic steatohepatitis secondary to hypopituitarism in a child: A case report. *World J Clin Cases* 2022; 10(18): 6211-6217
URL: https://www.wjgnet.com/2307-8960/full/v10/i18/6211.htm
DOI: https://dx.doi.org/10.12998/wjcc.v10.i18.6211

INTRODUCTION

Nonalcoholic steatohepatitis and hepatopulmonary syndrome (HPS) are rare in children with secondary pituitary insufficiency after surgery for craniopharyngioma. Craniopharyngioma and treatment sequelae may lead to polypituitary insufficiency, which further affects the hormone secretion in the body. Endocrine diseases also cause nonalcoholic fatty liver disease (NAFLD)[1]. This report aims to further elucidate the clinical characteristics of nonalcoholic steatohepatitis (NASH) and HPS caused by hypothalamic-pituitary dysfunction after surgery for craniopharyngioma and the improvement of this disease after hormone replacement therapy, which has great significance in the clinical prognosis.

CASE PRESENTATION

Chief complaints

The chief complaints were liver enlargement for 4 years, activity loss for 2 years, and cyanosis for more than 1 year.

History of present illness

A female patient aged 13 years and 6 mo was diagnosed with craniopharyngioma 6 years prior and underwent surgical resection without postoperative hormone replacement therapy. She had weakness after the surgery, and multiple laboratory tests revealed hypernatremia and hyperchloremia. The maximum serum sodium level was 176 mmol/L, which was improved by infusion of glucose, and the lowest sodium level was reduced to approximately 155 mmol/L. Four years ago, abdominal distension due to liver enlargement was noted, and B-ultrasound examination suggested fatty liver disease. The patient had severe cyanosis, chest tightness, wheezing, intermittent fever, and progressive exacerbation after mild physical labor for more than 1 year. Oxygen saturation fluctuated around 85% under high-flow oxygen inhalation. Hepatobiliary ultrasonography, liver biopsy, and contrast echocardiography of the right heart revealed cirrhosis and HPS.

History of past illness

The patient had no history of hypertension, diabetes, or heart disease. She had undergone surgery for craniopharyngioma 6 years ago.

Personal and family history

The patient was born to a G1P1 mother at full term. The patient's parents are alive, healthy, and divorced. The patient does not have siblings.

Physical examination

Under atmospheric inhalation, oxygen saturation (SpO_2) mostly fluctuated at around 70%. Cyanosis of the face and lips was noted. The heart rate was 124 beats/min, respiration was 26 breaths/min, blood

pressure was 96/46 mmHg, height was 141.5 cm (-2.5 SD), and weight was 41.85 kg (-0.5 SD). The skin sclera did not have obvious yellow staining, and acanthosis nigricans was noted around the neck and axillae. No abnormality was found during cardiopulmonary auscultation, and the abdomen was soft but enlarged with palpable spleen and liver. Examination of the nervous system was negative, double breasts were in stage B1, pubic hair was in stage PH1, and no axillary hair was found.

Laboratory examinations

The patient exhibited hypernatremia (serum sodium level, 167 mmol/L; normal range, 135–145 mmol/L), mild liver function abnormality (alanine aminotransferase level, 67 U/L, normal range, 7–40 U/L; aspartate aminotransferase level, 93 U/L, normal range, 13–40 U/L; γ-glutamyltranspeptidase, 107 U/L, normal range, 7–45 U/L; total bilirubin level, 45.1 μmol/L, normal range, 0.0–21 μmol/L; total biliary acid level, 22.3 μmol/L, normal range, 0.0–10.0 μmol/L; indirect bilirubin level, 33.6 μmol/L, normal range, 3-14 μmol/L; triglyceride level, 2.53 mmol/L, normal range, 0.3–1.7 mmol/L), abnormal renal function (creatinine level, 79 μmol/L; normal range, 15–77 μmol/L), and high blood ammonia level (94 μmol/L; normal range, 10–47 μmol/L). The patient had hypopituitarism and multiple pituitary hormone deficiencies (Table 1). However, the coagulation function, immune function, and Epstein-Barr virus and cytomegalovirus levels were normal. The hepatitis series, including hepatitis A virus, hepatitis B virus, hepatitis C virus, hepatitis D virus, and hepatitis E virus, were normal.

Imaging examinations

Echocardiography of the right heart revealed a diffuse arteriovenous shunt in the lung (grade III > 100/frame), which was consistent with HPS (Figure 1A). Abdominal ultrasonography revealed bile duct dilatation, cirrhosis, and splenomegaly (Figure 1B). Biopsy of the liver parenchyma showed loss of lobular structure, formation of regenerated nodules, swelling of the hepatocytes, mild steatosis (20%), fibroseptal bile duct hyperplasia, and fibrous tissue hyperplasia. The diagnostic view showed nodular cirrhosis (considering the origin of NASH) (Figure 2). The liver vasculature of computed tomography angiography revealed cirrhotic hepatosplenomegaly and portal hypertension, spongiform changes in the left portal artery, mild varicose veins in the lower esophagus, and splenic-renal shunt. Magnetic resonance cholangiopancreatography did not show abnormal changes in the pancreatic duct. The pituitary magnetic resonance imaging that included the conventional plain scan and dynamic contrast-enhanced scan showed postoperative changes in craniopharyngioma.

FINAL DIAGNOSIS

The final diagnoses were liver cirrhosis, HPS, hypopituitarism, and electrolyte imbalance.

TREATMENT

The patient received multiple hormone replacement and desmopressin therapies: Growth hormone (GH) (4 IU qn), thyroid hormone (levothyroxine sodium hydrate, 50 μg/d), corticosteroid (hydrocortisone, 15 mg/d), and desmopressin (Minirin, 0.05 mg/d). Moreover, the patient received symptomatic oxygen inhalation and calcium and potassium supplementation.

OUTCOME AND FOLLOW-UP

Oxygen saturation improved significantly after 1 mo of GH treatment and currently fluctuated at around 92% for low-flow nasal catheter oxygen. Liver function was reduced to the normal range, hypernatremia improved, and total bilirubin, indirect bilirubin, total bile acid, and lipid levels were significantly improved. During regular follow-up, it was found that liver transplantation was not required.

DISCUSSION

Craniopharyngioma is a rare primary brain tumor that originates from ectopic embryonic remnants of the craniopharyngeal duct or squamous epithelial cells. Its incidence is 0.5–2 cases *per* million persons *per* year, with peaks in childhood/adolescence (8 years) and adulthood (40–50 years)[2,3]. Although histologically defined as a benign tumor, craniopharyngioma often compresses nearby key structures, such as the optic neurohypophysis or hypothalamus[4,5]. Postoperative complications of craniopharyngioma, especially endocrine dysfunction, have a high incidence and mainly manifest as

Table 1 Laboratory examinations results

Variable	Value
IGF-1 (220.0-972.0 ng/mL)	170
TSH (0.35-4.94 mIU/L)	1.05
FT3 (2.43-6.01 pmol/L)	3.9
FT4 (9.01-19.05 pmol/L)	7.94
ACTH (8 am, pg/mL)	< 5.00
Cortisol (8 am, 5-25 μg/dL)	< 1.00
LH (1.8-11.78 mIU/mL,)	0.09
FSH (3.03-8.08 mIU/mL)	< 0.05
Testosterone (10.83-56.94 ng/dL)	< 3.82
Estradiol (21-251 pg/mL)	< 10.00
Progesterone (0.00-0.30 ng/mL)	< 0.10
Prolactin (5.18-26.53 ng/mL)	44.60

IGF-1: Insulin-like growth factor-I; TSH: Thyroid stimulating hormone; FT3: Free triiodothyronine; FT4: Free thyroxine; ACTH: Adrenocorticotropic hormone; LH: Luteinizing hormone; FSH: Follicle stimulating hormone.

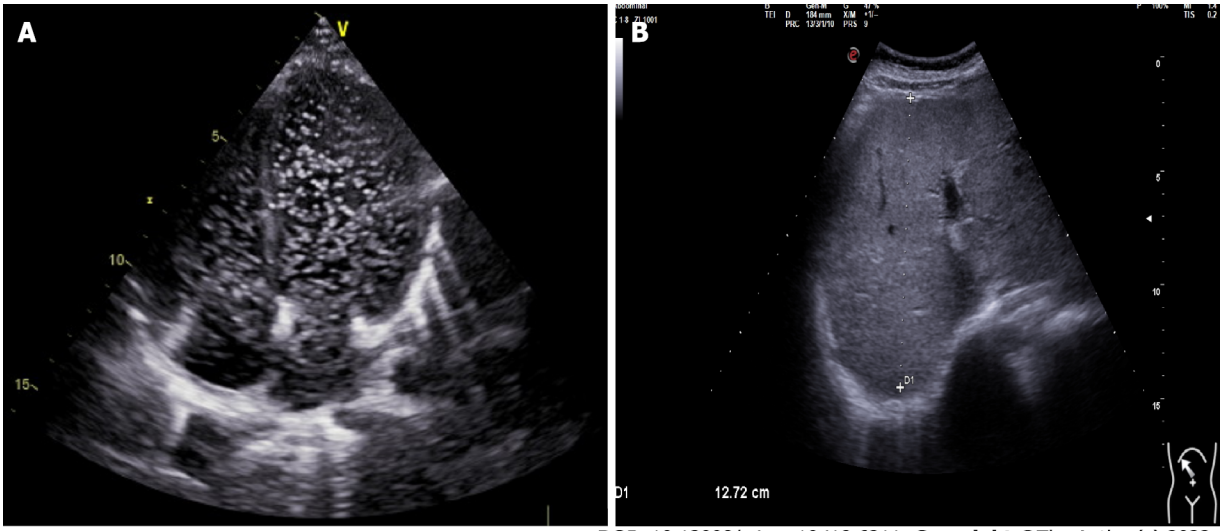

DOI: 10.12998/wjcc.v10.i18.6211 **Copyright** ©The Author(s) 2022.

Figure 1 Ultrasonography. A: Right echocardiography revealed diffuse arteriovenous shunt in the lung (grade III > 100/frame), consistent with hepatopulmonary syndrome; B: Abdominal ultrasound displayed bile duct dilatation, cirrhosis, and splenomegaly.

intractable diabetes insipidus hypothalamic-pituitary insufficiency, severe electrolyte disorder, and neuropsychological defects, which seriously affect the quality of life of children.

NAFLD is a chronic liver disease worldwide, and its incidence is increasing with the prevalence of obesity, diabetes, and metabolic syndrome. Statistically, the global incidence is 25%[6]. NAFLD is histologically classified into NAFLD and NASH, cirrhosis, and hepatocellular carcinoma. NAFLD and NASH are associated with hypothalamic hypopituitarism, but their pathogeneses remain unclear, and an increasing number of studies have found that the development of NASH is closely related to endocrine hormone abnormalities[7]. In children, it is caused by craniopharyngioma or pituitary adenoma and sequelae of treatment, leading to hypothyroidism, adrenal insufficiency, hypogonadotropism, and GH deficiency[8]. Adams *et al*[9] reported 21 cases of NAFLD, among which 15 were secondary after brain tumor surgery (approximately 71%), suggesting that brain tumor near the pituitary hypothalamus is an important cause of NAFLD. More than 50% (eight cases) of these tumors were craniopharyngiomas, suggesting the importance of careful diagnosis and exclusion of this type of tumor in the presence of clinically unexplained NAFLD[9]. Jung *et al*[10] reported the case of a 19-year-old girl diagnosed with craniopharyngioma who developed hypothalamic obesity, NAFLD, and

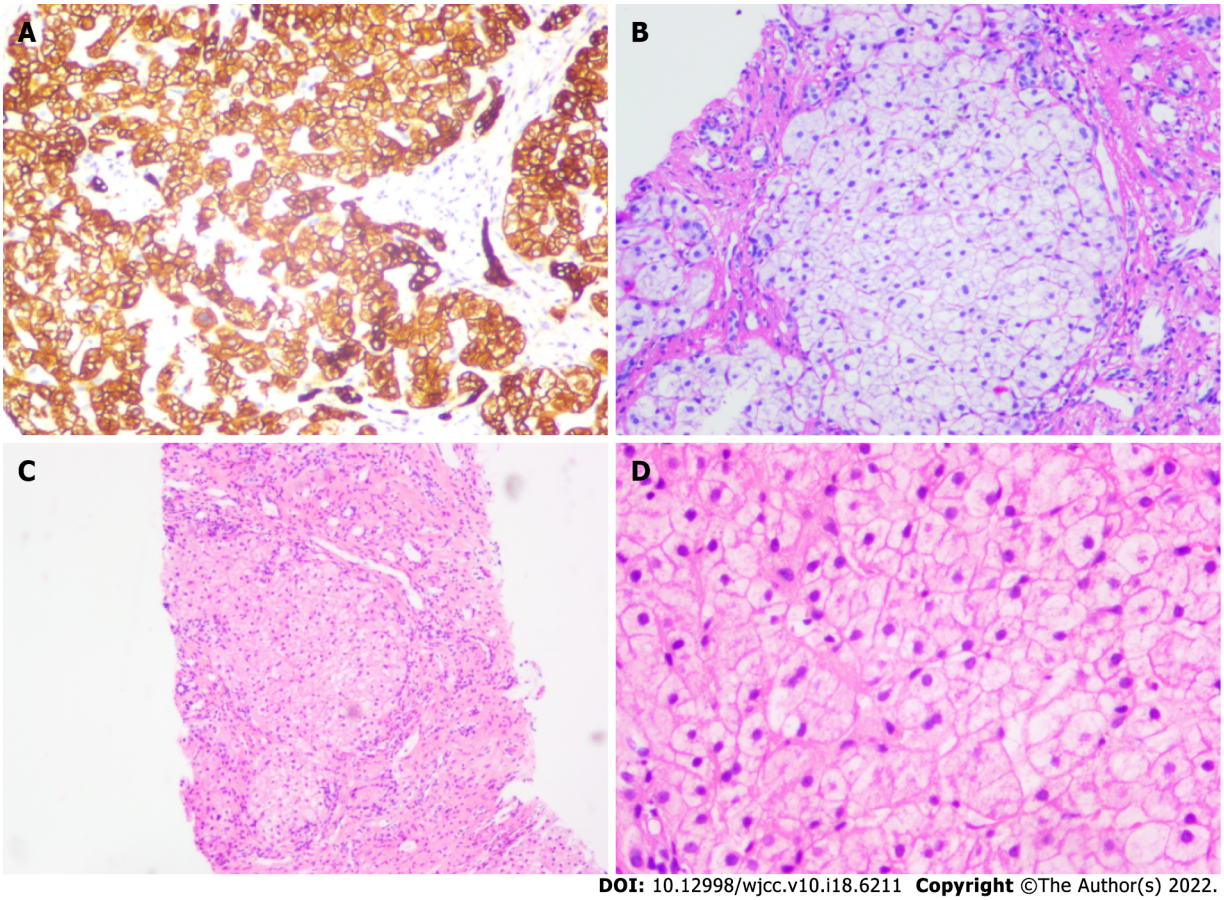

DOI: 10.12998/wjcc.v10.i18.6211 **Copyright** ©The Author(s) 2022.

Figure 2 Pathological images of liver biopsy. A: Immunohistochemical staining for CK818 (× 200); B: dPAS staining (× 200); C: HE staining (× 50); D: HE staining (× 200). Nodular cirrhosis (consider the origin of nonalcoholic steatohepatitis).

progression to HPS after tumor resection[10]. Recently, studies on patients with hypothalamic-pituitary involvement after craniopharyngioma have found that the prevalence of NAFLD in children is approximately 3%–10%, while the incidence of NAFLD caused by hypothalamic-pituitary damage after craniopharyngioma has increased to approximately 50%[11,12]. Previously, it was generally believed that the risk factors for NAFLD were excessive fructose intake, insulin resistance, and metabolic syndrome, followed by oxidative stress injury and endoplasmic reticulum stress, adipocytokine, mitochondrial dysfunction, and bisphenol A intake[13,14].

In a retrospective study that reported the association between hypopituitarism, hypothalamic dysfunction, and NAFLD, NAFLD was found in 2.3% of patients with hypopituitarism and hypothalamic obesity[15]. Moreover, a recent analysis of long-term outcomes after childhood-onset craniopharyngioma found that 1 of 32 patients (3%) died of cirrhosis[16].

The risk of progression from childhood simple fatty liver to adult cirrhosis and liver failure is low, and the natural course of NAFLD in patients with hypothalamic and pituitary dysfunction may be more aggressive than that in the general population. Therefore, children with craniopharyngioma should be closely followed postoperatively, especially for liver function and pituitary hormone levels. Some scholars have reported NASH 4 years after pituitary tumor resection, accompanied by dyspnea and hypoxemia, which eventually developed into HPS[17]. HPS is a serious complication of chronic liver disease, which includes three main characteristics: Abnormal liver function, pulmonary telangiectasia (shunt), and hypoxemia[18]. It is a progressive disease that is a complication of cirrhosis or portal hypertension. The main clinical manifestations are dyspnea and cyanosis. At this point, the exact pathogenesis of HPS is still unclear, and is most likely thought to occur due to vasodilatation caused by nitric oxide[19], which increases pulmonary blood flow and cardiac output, leading to pulmonary ventilation-perfusion mismatch and arteriovenous shallows, ultimately making it difficult for oxygen molecules to bind with hemoglobin, and resulting in hypoxemia[20,21]. Currently, liver transplantation is the accepted treatment. Despite successful liver transplantation, NAFLD has a high recurrence rate. Therefore, the prospects for the treatment of NAFLD and HPS secondary to craniopharyngioma are not optimistic, and the need for liver transplantation should be carefully considered. We present the case of a 13-year-old girl with hypopituitarism following surgery for craniopharyngioma; particularly, GH deficiency resulted in slow-progressive NASH, which progressed to cirrhosis, and HPS was eventually diagnosed. After GH replacement therapy, liver biochemical indexes and hypoxemia were significantly

improved. Therefore, it is speculated that GH may provide a new approach for the treatment of HPS in the future. An 11-year-old boy from Japan was reported to have developed hypopituitarism after surgical resection of a pituitary tumor and subsequently progressed to NASH and HPS. He underwent living-donor liver transplantation at 15 years of age and developed NAFLD again 1 year after transplantation; GH replacement therapy improved liver function, which stabilized to the normal range during 10 years of follow-up[17]. Kodama *et al*[22] and Torii *et al*[23] reported that GH replacement therapy improved NASH and HPS[22,23]. A 29-year-old man with pituitary stalk interruption syndrome progressed slowly to HPS, and after 14 mo of treatment with recombinant human GH, the liver function and hypoxemia improved, and liver fibrosis did not progress[24].

Recent studies have demonstrated an increased prevalence of NASH in adult patients with GH deficiency and improvement in liver function impairment after GH replacement therapy. Although it is unclear whether GH replacement therapy directly or indirectly reduces oxidative stress in the liver, GH has antioxidant stress effects *in vivo*. GH can directly reduce adipogenesis in liver cells and simultaneously regulate the production of IGF1, which can induce cell senescence and inactivate hepatic stellate cells, thus improving liver fibrosis[25].

CONCLUSION

Craniopharyngioma in children likely damages the pituitary gland and leads to hypopituitarism, regardless of its unique location or treatment with surgery or radiotherapy. Hypopituitarism in children is likely to develop into NASH, cirrhosis, and even HPS. In this study, GH replacement therapy significantly improved liver function, metabolic status, and hypoxemia, providing new clinical support for the early diagnosis and treatment of NASH and HPS in children with hypopituitarism.

FOOTNOTES

Author contributions: Zhang XY and Wang CL conceived and designed the study; Zhang XY and Yuan K provided clinical research; Zhang XY wrote the paper; Zhang XY, Yuan K, Fang YL, and Wang CL reviewed and edited the manuscript; all authors read and approved the manuscript.

Informed consent statement: Informed written consent was obtained from the patient for the publication of this report and any accompanying images.

Conflict-of-interest statement: The authors declare that they have no conflicts of interest related to this manuscript.

CARE Checklist (2016) statement: The authors have read the CARE Checklist (2016), and the manuscript was prepared and revised according to the CARE Checklist (2016).

Open-Access: This article is an open-access article that was selected by an in-house editor and fully peer-reviewed by external reviewers. It is distributed in accordance with the Creative Commons Attribution NonCommercial (CC BY-NC 4.0) license, which permits others to distribute, remix, adapt, build upon this work non-commercially, and license their derivative works on different terms, provided the original work is properly cited and the use is non-commercial. See: https://creativecommons.org/Licenses/by-nc/4.0/

Country/Territory of origin: China

ORCID number: Xiao-Yuan Zhang 0000-0003-1607-2490; Ke Yuan 0000-0002-0458-3683; Yan-Lan Fang 0000-0001-6579-417X; Chun-Lin Wang 0000-0002-4273-1341.

S-Editor: Fan JR
L-Editor: Wang TQ
P-Editor: Fan JR

REFERENCES

1 **Marino L**, Jornayvaz FR. Endocrine causes of nonalcoholic fatty liver disease. *World J Gastroenterol* 2015; **21**: 11053-11076 [PMID: 26494962 DOI: 10.3748/wjg.v21.i39.11053]
2 **Lustig RH**. Hypothalamic obesity after craniopharyngioma: mechanisms, diagnosis, and treatment. *Front Endocrinol (Lausanne)* 2011; **2**: 60 [PMID: 22654817 DOI: 10.3389/fendo.2011.00060]
3 **Eveslage M**, Calaminus G, Warmuth-Metz M, Kortmann RD, Pohl F, Timmermann B, Schuhmann MU, Flitsch J, Faldum A, Müller HL. The Postopera tive Quality of Life in Children and Adolescents with Craniopharyngioma. *Dtsch Arztebl Int* 2019; **116**: 321-328 [PMID: 31219033 DOI: 10.3238/arztebl.2019.0321]

4 **Müller HL**. Craniopharyngioma. *Endocr Rev* 2014; **35**: 513-543 [PMID: 24467716 DOI: 10.1210/er.2013-1115]
5 **Chen X**, Tong Y, Shi Z, Chen H, Yang Z, Wang Y, Chen L, Yu J. Noninvasive molecular diagnosis of craniopharyngioma with MRI-based radiomics approach. *BMC Neurol* 2019; **19**: 6 [PMID: 30616515 DOI: 10.1186/s12883-018-1216-z]
6 **Kim U**, Kim N, Shin HY. Modeling Non-Alcoholic Fatty Liver Disease (NAFLD) Using "Good-Fit" Genome-Editing Tools. *Cells* 2020; **9** [PMID: 33271878 DOI: 10.3390/cells9122572]
7 **Singeap AM**, Stanciu C, Huiban L, Muzica CM, Cuciureanu T, Girleanu I, Chiriac S, Zenovia S, Nastasa R, Sfarti C, Cojocariu C, Trifan A. Association between Nonalcoholic Fatty Liver Disease and Endocrinopathies: Clinical Implications. *Can J Gastroenterol Hepatol* 2021; **2021**: 6678142 [PMID: 33505943 DOI: 10.1155/2021/6678142]
8 **Gilliland T**, Dufour S, Shulman GI, Petersen KF, Emre SH. Resolution of non-alcoholic steatohepatitis after growth hormone replacement in a pediatric liver transplant patient with panhypopituitarism. *Pediatr Transplant* 2016; **20**: 1157-1163 [PMID: 27762491 DOI: 10.1111/petr.12819]
9 **Adams LA**, Feldstein A, Lindor KD, Angulo P. Nonalcoholic fatty liver disease among patients with hypothalamic and pituitary dysfunction. *Hepatology* 2004; **39**: 909-914 [PMID: 15057893 DOI: 10.1002/hep.20140]
10 **Jung D**, Seo GH, Kim YM, Choi JH, Yoo HW. Hepatopulmonary syndrome caused by hypothalamic obesity and nonalcoholic fatty liver disease after surgery for craniopharyngioma: a case report. *Ann Pediatr Endocrinol Metab* 2018; **23**: 51-55 [PMID: 29609450 DOI: 10.6065/apem.2018.23.1.51]
11 **Hoffmann A**, Bootsveld K, Gebhardt U, Daubenbüchel AM, Sterkenburg AS, Müller HL. Nonalcoholic fatty liver disease and fatigue in long-term survivors of childhood-onset craniopharyngioma. *Eur J Endocrinol* 2015; **173**: 389-397 [PMID: 26088821 DOI: 10.1530/EJE-15-0422]
12 **Della Corte C**, Mazzotta AR, Nobili V. Fatty liver disease and obesity in youth. *Curr Opin Endocrinol Diabetes Obes* 2016; **23**: 66-71 [PMID: 26702852 DOI: 10.1097/MED.0000000000000221]
13 **Sandlers Y**, Shah RR, Pearce RW, Dasarathy J, McCullough AJ, Dasarathy S. Plasma Krebs Cycle Intermediates in Nonalcoholic Fatty Liver Disease. *J Clin Med* 2020; **9** [PMID: 31979094 DOI: 10.3390/jcm9020314]
14 **Paradies G**, Paradies V, Ruggiero FM, Petrosillo G. Oxidative stress, cardiolipin and mitochondrial dysfunction in nonalcoholic fatty liver disease. *World J Gastroenterol* 2014; **20**: 14205-14218 [PMID: 25339807 DOI: 10.3748/wjg.v20.i39.14205]
15 **Simoneau-Roy J**, O'Gorman C, Pencharz P, Adeli K, Daneman D, Hamilton J. Insulin sensitivity and secretion in children and adolescents with hypothalamic obesity following treatment for craniopharyngioma. *Clin Endocrinol (Oxf)* 2010; **72**: 364-370 [PMID: 19486023 DOI: 10.1111/j.1365-2265.2009.03639.x]
16 **Sterkenburg AS**, Hoffmann A, Gebhardt U, Warmuth-Metz M, Daubenbüchel AM, Müller HL. Survival, hypothalamic obesity, and neuropsychological/psychosocial status after childhood-onset craniopharyngioma: newly reported long-term outcomes. *Neuro Oncol* 2015; **17**: 1029-1038 [PMID: 25838139 DOI: 10.1093/neuonc/nov044]
17 **Fujio A**, Kawagishi N, Echizenya T, Tokodai K, Nakanishi C, Miyagi S, Sato K, Fujimori K, Ohuchi N. Long-term survival with growth hormone replacement after liver transplantation of pediatric nonalcoholic steatohepatitis complicating acquired hypopituitarism. *Tohoku J Exp Med* 2015; **235**: 61-67 [PMID: 25744617 DOI: 10.1620/tjem.235.61]
18 **Kim KY**, Kim TH, Lee JM, Yi NJ, Kim HY, Moon JS, Ko JS. Clinical outcomes and risk factors of hepatopulmonary syndrome in children. *Sci Rep* 2021; **11**: 4134 [PMID: 33603173 DOI: 10.1038/s41598-021-83785-x]
19 **Fallon MB**. Mechanisms of pulmonary vascular complications of liver disease: hepatopulmonary syndrome. *J Clin Gastroenterol* 2005; **39**: S138-S142 [PMID: 15758649]
20 **Lv Y**, Fan D. Hepatopulmonary Syndrome. *Dig Dis Sci* 2015; **60**: 1914-1923 [PMID: 25732713 DOI: 10.1007/s10620-015-3593-0]
21 **Ikubo Y**, Kasai H, Sugiura T, Saito T, Shoji H, Sakao S, Kasahara Y, Tanabe N, Tatsumi K. Pulmonary Hypertension that Developed During Treatment for Hepatopulmonary Syndrome and Pulmonary Arteriovenous Malformation. *Intern Med* 2019; **58**: 1765-1769 [PMID: 30799344 DOI: 10.2169/internalmedicine.1993-18]
22 **Kodama K**, Ichihara A, Seki Y, Ikarashi Y, Sagawa T, Kogiso T, Taniai M, Tokushige K. Characteristics of NAFLD Based on Hypopituitarism. *Can J Gastroenterol Hepatol* 2020; **2020**: 8814435 [PMID: 33102399 DOI: 10.1155/2020/8814435]
23 **Torii N**, Ichihara A, Mizuguchi Y, Seki Y, Hashimoto E, Tokushige K. Hormone-replacement Therapy for Hepatopulmonary Syndrome and NASH Associated with Hypopituitarism. *Intern Med* 2018; **57**: 1741-1745 [PMID: 29910217 DOI: 10.2169/internalmedicine.0027-17]
24 **Ji W**, Nie M, Mao JF, Zhang HB, Wang X, Wu XY. Growth hormone cocktail improves hepatopulmonary syndrome secondary to hypopituitarism: A case report. *World J Clin Cases* 2021; **9**: 4852-4858 [PMID: 34222458 DOI: 10.12998/wjcc.v9.i18.4852]
25 **Takahashi Y**. The Role of Growth Hormone and Insulin-Like Growth Factor-I in the Liver. *Int J Mol Sci* 2017; **18** [PMID: 28678199 DOI: 10.3390/ijms18071447]

World Journal of Clinical Cases

Submit a Manuscript: https://www.f6publishing.com

World J Clin Cases 2022 June 26; 10(18): 6218-6226

DOI: 10.12998/wjcc.v10.i18.6218

ISSN 2307-8960 (online)

CASE REPORT

Vancomycin dosing in an obese patient with acute renal failure: A case report and review of literature

Kun-Yan Xu, Dan Li, Zhen-Jie Hu, Cong-Cong Zhao, Jing Bai, Wen-Li Du

Specialty type: Pharmacology and pharmacy

Provenance and peer review: Unsolicited article; Externally peer reviewed.

Peer-review model: Single blind

Peer-review report's scientific quality classification

Grade A (Excellent): 0
Grade B (Very good): B
Grade C (Good): C, C
Grade D (Fair): 0
Grade E (Poor): 0

P-Reviewer: Katip W, Thailand; Kothan S, Thailand; Muthu S, India

Received: November 23, 2021
Peer-review started: November 23, 2021
First decision: January 11, 2022
Revised: January 19, 2022
Accepted: April 22, 2022
Article in press: April 22, 2022
Published online: June 26, 2022

Kun-Yan Xu, Dan Li, Jing Bai, Wen-Li Du, Department of Pharmacy, Fourth Hospital of Hebei Medical University, Shijiazhuang 050011, Hebei Province, China

Zhen-Jie Hu, Cong-Cong Zhao, Department of Intensive Care Unit, Fourth Hospital of Hebei Medical University, Shijiazhuang 050011, Hebei Province, China

Corresponding author: Jing Bai, Associate Chief Pharmacist, Department of Pharmacy, Fourth Hospital of Hebei Medical University, No. 12 Jiankang Road, Chang'an District, Shijiazhuang 050011, Hebei Province, China. baijing619@163.com

Abstract

BACKGROUND

Vancomycin is the most commonly used drug for methicillin-resistant *Staphylococcus aureus*. The empirical clinical doses of vancomycin based on non-obese patients may not be optimal for obese ones.

CASE SUMMARY

This study reports a case of vancomycin dosing adjustment in an obese patient (body mass index 78.4 kg/m^2) with necrotizing fasciitis of the scrotum and left lower extremity accompanied with acute renal failure. Dosing adjustment was performed based on literature review and factors that influence pharmacokinetic parameters are analyzed. The results of the blood drug concentration monitoring confirmed the successful application of our dosing adjustment strategy in this obese patient. Total body weight is an important consideration for vancomycin administration in obese patients, which affects the volume of distribution and clearance of vancomycin. The alterations of pharmacokinetic parameters dictate that vancomycin should be dose-adjusted when applied to obese patients. At the same time, the pathophysiological status of patients, such as renal function, which also affects the dose adjustment of the patient, should be considered.

CONCLUSION

Monitoring vancomycin blood levels in obese patients is critical to help adjust the dosing regimen to ensure that vancomycin concentrations are within the effective therapeutic range and to reduce the incidence of renal injury.

Key Words: Vancomycin; Obesity; Acute renal failure; Pharmacokinetics; Case report

©The Author(s) 2022. Published by Baishideng Publishing Group Inc. All rights reserved.

Core Tip: We report the medical records of dose adjustment of vancomycin in an obese patient (body weight 240 kg), including the dose adjustment protocol in acute renal injury. This article also reviews the current literature on the application of vancomycin in the obese population and provides recommendations on how to make dose adjustments based on available evidence.

Citation: Xu KY, Li D, Hu ZJ, Zhao CC, Bai J, Du WL. Vancomycin dosing in an obese patient with acute renal failure: A case report and review of literature. *World J Clin Cases* 2022; 10(18): 6218-6226
URL: https://www.wjgnet.com/2307-8960/full/v10/i18/6218.htm
DOI: https://dx.doi.org/10.12998/wjcc.v10.i18.6218

INTRODUCTION

Since 1980, the prevalence of obesity has more than doubled worldwide. It is estimated that by 2030, 60% of the world's adult population will be classified as obesity[1]. In the United States from 2013 to 2014, the prevalence of obesity was 35.0% for male and 40.4% for female adults, and there was a significant linear increasing trend among women in the prevalence of obesity from 2005 through 2014 [2]. Obesity has also become a major public health burden in China. Over the past 40 years, the prevalence of obesity has increased significantly. The nationally representative survey showed that more than half of the Chinese adults are obese according to the Chinese standards[3]. The increased prevalence of obesity poses a challenge for clinicians to deliver optimized doses of antimicrobial drugs in the intensive care unit. Obesity is a key risk factor for community and hospital-acquired infections[4], and increases risks of incidence and mortality compared to non-obese individuals[5]. It may affect the pharmacokinetics of antimicrobial agents, particularly in patients requiring high-dose antimicrobial therapy[6], and can also influence the immune response and increase susceptibility to infections[7], resulting in a high risk of infection in obese patients[8]. As a consequence, clinicians are increasingly facing severely obese patients requiring antibiotic treatment. However, few studies have summarised the published data and provided clinical guidance for effective dosing in these patients.

Since the early 1980s, as the number of methicillin-resistant *Staphylococcus aureus* (MRSA) infections began to increase, vancomycin has become the drug of first choice for this microbial infection[9]. Vancomycin belongs to glycopeptide antibiotic which acts by inhibiting bacterial cell wall synthesis[10]. It is the most widely used antibiotic worldwide for the treatment of severe Gram-positive bacterial infections[11]. The binding of vancomycin to protein is approximately 50% to 55%[10]. The volume of distribution is 0.4-1 L/kg[9]. Vancomycin is primarily cleared *via* renal excretion[12]. The actual body weight of obese subjects increases the chance of vancomycin exposure and the incidence of vancomycin-associated nephrotoxicity[13]. Therefore, dose adjustment is required when vancomycin is used in obese patients, because of the effect of obesity on vancomycin pharmacokinetic parameters. One study shows that therapeutic drug monitoring (TDM) significantly improves the clinical curative effect and reduces the incidence of nephrotoxicity in patients treated with vancomycin[14].

Although the pharmacokinetics of vancomycin in the general population is well-described, to the best of our knowledge, only a few studies have investigated the effect of vancomycin dose in the obese population. This study reports the medical records of dose adjustment of vancomycin in an obese patient weighing up to 240 kg, including the dose adjustment protocol in the acute renal injury. This article also reviews the current literature on the application of vancomycin in the obese population and provides recommendations on how to make dose adjustments based on the available evidence.

CASE PRESENTATION

Chief complaints

A 40-year-old man was referred to our intensive care unit (ICU), with the complaints of chest tightness and shortness of breath with no obvious cause for 3 mo.

History of present illness

In November 2020, the patient reported chest tightness and shortness of breath with no obvious cause. Three days later, the patient's symptoms aggravated with abdominal distension and edema of both lower limbs. He was admitted to the ICU of a local hospital for acute respiratory failure. After 2 wk of treatment, the patient still had persistent fever and was transferred to the ICU of our hospital on November 18, 2020.

History of past illness

The patient had suffered from hypertension for 3 years and erysipelas of the right lower extremity for 2 years.

Personal and family history

The patient had no specific personal or family history.

Physical examination

The patient's height and body weight were 175 cm and 240 kg, respectively. The patient had necrotizing fasciitis of the scrotum and left lower extremity, and large brown skin pigmentation of the left calf, and two approximately 2-cm surgical incisions with built-in gauze drainage and cloudiness drainage fluid were visible in the left thigh and the middle of the left calf (Figure 1).

Laboratory examinations

The culture of secretion revealed *Staphylococcus hemolyticus* at a local hospital.

Imaging examinations

There were no abnormal imaging data findings.

FINAL DIAGNOSIS

The final diagnoses were: (1) Sepsis; (2) Acute respiratory distress syndrome; (3) Pneumonia; (4) Heart failure; (5) Necrotizing fasciitis of the scrotum and left lower extremity; and (6) Severe obesity.

TREATMENT

The patient had pulmonary infection and *Staphylococcus hemolyticus* was detected in his secretion at the local hospital. His initial serum creatinine was 63.3 μmol/L and creatinine clearance (CrCl) was greater than 90 mL/min. Based on the patient's history and drug sensitivity testing results, intravenous levofloxacin 0.75 g/d and tigecycline 0.2 g/d were started empirically for anti-infection treatment. Then, linezolid 0.6 g intravenous injection every 12 h was prescribed to replace levofloxacin, and the patient's temperature decreased to normal after 3 d of treatment. On November 27, the patient developed a high fever (temperature up to 40.2 °C), and his high-sensitivity C-reactive protein (hs-CRP) rose to 183.51 mg/L (Table 1). Considering the infection from the lower extremity and the scrotum, the patient received enhanced drainage and dressing change. Meanwhile, the culture of sputum and scrotal revealed *Acinetobacter baumannii*. The linezolid was subsequently discontinued and intravenous infusion of vancomycin was started. Because the patient was severely obese, after reviewing the literature, we determined the dosing regimen of a loading dose (vancomycin administered as continuous infusion of 2 g over 2 h) and a maintenance dose (vancomycin 1 g infused over 60 min every 8 h). The vancomycin blood trough concentration was 11.7 μg/mL after the patient had received three doses of vancomycin. The patient developed acute renal failure due to the aggravation of infection, the serum creatinine levels showed a gradual increase, and the vancomycin trough concentration was greater than 20 μg/mL (up to 34.3 μg/mL). We then adjusted the vancomycin administration dose according to the blood drug concentration monitoring. On December 16, continuous renal replacement therapy (CRRT) was used because of anuria of the patient. Given using continuous veno-venous hemodiafiltration mode, we adjusted the vancomycin administration dose to 1 g every 12 h, during which vancomycin blood drug concentration fluctuated between 10 and 20 μg/mL.

OUTCOME AND FOLLOW-UP

The treatment produced significant improvement in the patient's respiratory status and the infection. Vancomycin and CRRT treatment were subsequently discontinued on December 24. Two days later, the patient was transferred out of the ICU to continue treatment. He was well with no further complaints at the routine 1-mo follow-up.

DISCUSSION

In recent years, body mass index (BMI) is a world-accepted grading method to assess the degree of

Table 1 Changes of indicators during the patient's hospitalization

Check item/date	November 19	November 28	December 1	December 11	December 16	December 20	December 25
White blood cell count (× 10^9/L)	5.50	9.59	8.16	14.02	35.29	20.19	7.71
Neutrophil percentage (%)	62.6	75.80	75.00	85.60	85.90	82.20	68.30
Procalcitonin(ng/mL)	0.130	0.190	0.190	9.170	53.760	4.930	1.160
High-sensitivity C-reactive protein(mg/L)	183.51	194.91	140.00	68.80	99.00	22.30	8.91
Serum creatinine (μmol/L)	67.8	61.8	48.9	266.8	453.1 (CRRT)	120.9 (CRRT)	264.1 (CRRT)

CRRT: Continuous renal replacement therapy.



DOI: 10.12998/wjcc.v10.i18.6218 **Copyright** ©The Author(s) 2022.

Figure 1 Infection of the left leg in the obese patient.

obesity. According to the criteria of the guideline, obesity is defined as a BMI of 30.0 kg/m^2 or higher [15]. Based on the body weight and height of this patient, his BMI was calculated to be 78.4 kg/m^2, which met the threshold for obesity. Numerous physiopathological changes occur in obese individuals, including changes in distribution (V_d) and renal excretion[16].

Vancomycin is a time-dependent antibiotic and a number of factors influence its clinical activity, including variable tissue distribution, dose size, and clearance rate[17]. One study showed that total body weight (TBW) influenced the V_d and clearance (CL) of vancomycin (Table 2)[18]. As expected, obesity is a known factor affecting drug pharmacokinetics[19]. Vancomycin, as a hydrophilic drug, is able to penetrate and distribute, to a certain extent, in adipose tissues, thereby increasing the V_d[20]. A large retrospective study by Ducharme *et al*[21] showed that the V_d was greater in obese subjects than in normal subjects by examining pharmacokinetics of vancomycin in 704 patients. Blouin and his colleagues[22] also demonstrated statistically significant differences in weight-indexed V_d between two groups of subjects. A recent study suggests that V_d changes in obese patients can be ascribed to the physicochemical properties of the drugs in most cases[23]. In addition, the degree of the V_d depends on the lipophilicity, hydrophilicity, protein binding, and molecular weight of the antibiotic[24]. In the obese population, higher cardiac output and blood volume may increase blood flow, and lead to larger V_d[25]. Edema combined with fluid resuscitation can increase the V_d of different antibacterial agents in obese, critically ill patients[26].

Previous studies indicated that CL of vancomycin was much higher in the obese population, especially in young obese patients, and they required high doses to obtain adequate trough concentrations[9]. Han *et al*[27] demonstrated that obese adults exhibited higher drug clearance rates than non-obese ones. Unlike V_d, the physicochemical properties of drugs have little effect on CL, which is largely controlled by physiological processes[23]. The change in clearance was mainly attributed to an increase in kidney mass and renal blood flow in obese subjects[28]. Greater glomerular filtration rate and renal perfusion in obese individuals increase the CL of vancomycin[29]. At the same time, greater renal volume, hypertrophy of the renal unit, and hydrostatic pressure of the glomerulus were also associated

Table 2 Literature on dose adjustment analysis of vancomycin in obese patients

Title (year)	Design	Results	Conclusions	Ref.
Pharmacokinetics of vancomycin in extremely obese patients with suspected or confirmed staphylococcus aureus infections (2015)	Prospective pharmacokinetic study To assess vancomycin pharmacokinetic parameters in obese patients *n* = 31	When the minimum inhibitory concentration (MIC) was 1 μg/ml, the probability of the concentration-time curve (AUC)/MIC rate of 400 for vancomycin at 4000 to 5000 mg/d was 93%	V_d and clearance of vancomycin were affected by total body weight, respectively	Adane *et al* [18]
Vancomycin pharmacokinetics in a patient population: effect of age, gender, and body weight (1994)	Retrospective review Comparative pharmacokinetics of vancomycin using steady-state peak and trough serum concentrations *n* = 704	V_d is 0.69 L/kg IBW in normal females compared with 0.58 in men The V_d for obese women and men was 1.17 and 0.90 L/kg IBW respectively	Vancomycin dosing can be improved by adapting the initial estimates of V_d in obese people	Ducharme *et al*[21]
Vancomycin pharmacokinetics in normal and morbidly obese subjects (1982)	An uncontrolled study Vancomycin pharmacokinetics was determined in normal and morbidly obese populations *n* = 10	Significant differences in mean terminal half-life and volume of distribution values between normal and morbidly obese individuals Strong correlations between TBW and V_d and total body clearance	TBW should be used for dosing of vancomycin in obese individuals	Blouin *et al* [22]
Vancomycin dosing in critically ill patients: robust methods for improved continuous-infusion regimens (2011)	A retrospective data collection To perform a pharmacokinetic analysis of vancomycin in subjects *n* = 206	Patients with a creatinine clearance of 100 ml/min/1.73 m^2 should receive a continuous infusion at least 35 mg/kg/d to maintain target concentrations	TBW should be considered for the initial dose The maintenance dose can be directed by creatinine clearance	Roberts *et al*[39]
Dosing vancomycin in the super obese: less is more (2018)	Retrospective study Determining an experiential vancomycin dosing strategy for obese individuals *n* = 346	Maintenance dose > 4500 mg/d is not required in obese patients to reach the pharmacodynamic AUC target	Using AUC-targeted TDM can optimize the treatment of obese adults	Crass *et al* [40]
The pharmacokinetics of vancomycin during the initial loading dose in patients with septic shock (2016)	A prospective, non-comparative study To investigate the pharmacokinetics of vancomycin in patients with early septic shock *n* = 12	The two-compartmental first-order elimination model The mean ± SD of the total vancomycin clearance (3.70 ± 1.25 L/h) was higher than in patients with non-septic shock There was no increase in the volume of the central compartment (8.34 ± 4.36 L) or the volume of peripheral compartment (30.99 ± 7.84 L) compared to patients with non-septic shock	In the early stages of septic shock, the total clearance of vancomycin increased, while the volumes of distribution of the central and peripheral compartments did not increase	Katip *et al* [52]
Multicenter evaluation of vancomycin dosing: emphasis on obesity (2008)	A random sampling Patients receiving vancomycin were categorised by body mass index and randomly chosen from the computer-generated query *n* = 421	Adequate initial doses were achieved in 93.9% of overweight patients and 27.7% of obese patients	The patient receives a weight-based dose	Hall *et al* [53]
Performance of a vancomycin dosage regimen developed for obese patients (2012)	Retrospective review Comparison of original and revised dosing regimens for achieving target serum trough concentrations and occurrence of nephrotoxicity in obese subjects *n* = 138	Revised strategy resulted in a higher frequency of target troughs	Compared with the original strategy, the revised strategy improved the attainment of target trough concentrations with minimal nephrotoxicity	Reynolds *et al*[54]

V_d: Distribution; TBW: Total body weight; IBW: Ideal body weight; TDM: Therapeutic drug monitoring; AUC: Concentration-time curve; MIC: Minimum

inhibitory concentration.

with greater CL of vancomycin in the obese group[30]. Vancomycin is a hydrophilic drug with predominant renal excretion. Furthermore, augmented renal clearance (ARC), defined as a creatinine clearance more than or equal to 130 mL/min/1.73 m^2, refers to enhanced elimination of hydrophilic solutes by the kidneys[31]. The results indicate that ARC has been described in the obese, non-critically ill patient[32], and is a common finding in critically ill patients with normal plasma creatinine concentrations[33].

The option of vancomycin loading doses is dependent on the estimate of the V_d. Pharmacokinetic research had demonstrated that vancomycin V_d increases with increasing TBW[34]. The physicochemical properties of drugs lead us not to define a universal body-size parameter for the distribution and clearance of drugs. As a consequence, the body weight was used in dose selection for drug administration[35]. One guideline states that a reasonable approach to the initial dose of vancomycin in obese individuals is to increase the loading dose to 20 to 25 mg/kg TBW and to decrease the maintenance dose, then adjust the dose according to TDM[36]. The 2020 Infectious Diseases Society of America (IDSA) consensus recommends the use of a TBW-based loading dose of 20 to 25 mg/kg in obese adults with severe infections, and considers capping doses of 3000 mg as the most practical dosing regimen [37].

Data have shown an excellent correlation between TBW and CL[38]. Thus, the empirical maintenance dose of vancomycin is dependent on the estimated CL[39]. The initial maintenance doses of vancomycin can be calculated by vancomycin CL and target AUC for obese population[18,40]. The 2020 IDSA consensus points out that the mean vancomycin CL in obese patients is approximately 6 L/h, which corresponds to an AUC of approximately 500 mg·h/L at a daily dose of 3000 mg. The empirical vancomycin maintenance dose for obese adults should not exceed 4500 mg/d because vancomycin CL rarely goes beyond 9 L/h[37].

The pharmacodynamic parameter that best predicts the efficacy of vancomycin is the ratio of the area under the curve (AUC) to the minimum inhibitory concentration (MIC)[9]. In adult patients with suspected or definitive serious MRSA infection, the AUC/MIC ratio (assuming a vancomycin MIC of 1 mg/L) with targets between 400 and 600 was recommended in the American Society of Health-System Pharmacists (ASHP) 2020 guideline[37]. Based on the historical difficulty of AUC estimation in clinical practice, previous expert guidelines recommended monitoring trough concentrations as a surrogate marker for the AUC/MIC ratio[41]. The 2020 Evidence-based Guideline for Therapeutic Drug Monitoring of Vancomycin recommends maintaining vancomycin steady-state trough concentrations at 10–20 mg/L to achieve clinical efficacy and improve patient safety[42].

CRRT is a common treatment for critically ill patients with acute renal injury[43]. With advances in hemodialysis membrane technology, vancomycin is cleared substantially by effective and high-flux dialyzers[44]. Therefore, vancomycin dosing regimens for CRRT need to be changed, but there is no mention of CRRT dosing recommendations in the latest FDA-approved vancomycin package insert[45]. V_d may be increased in CRRT patients compared to healthy individuals with normal kidney function [46]. During CRRT treatment, vancomycin CL remains a near-steady-state condition over the dosing interval, although vancomycin CL may decline over time as a result of hemodialysis filter plugging[46]. Vancomycin CL is closely related to the flow rate of ultrafiltration/dialysis solution[47]. The recommended loading dose for patients receiving CRRT is based on the actual TBW, at the dose of 20 to 25 mg/kg[48]. In order to achieve the generation of steady-state concentrations between 15 and 20 mg/L, a maintenance dose of 400 to 650 mg/12 h of vancomycin at an ultrafiltration flow rate of 30-40 mg/kg/h is recommended for most critically ill patients[49]. Due to the unstable clinical situation, vancomycin concentration must be strictly monitored in critical patients[50].

In summary, we report a case of adjusting the blood concentration of vancomycin with enhanced effectiveness in an obese patient. The initial TBW of the patient with normal renal function was 240 kg. Thus, the patient should receive an initial TBW-based load of 6 to 7.2 g of vancomycin every day. However, the dose of vancomycin is greater than 4 g/d, which increases the risk of nephrotoxicity[51]. Following the recommended dose limit of 3 g, the patient received an initial TBW-based loading dose of 2 g and a maintenance dose of 1 g of vancomycin every 8 h. The initial serum concentration of 11.7 μg/mL was obtained, after the patient had received three doses of vancomycin. The serum concentration demonstrated that the dosing regimen is reasonable. Due to acute renal failure with reduced urine output or even anuria, intravenous injection of vancomycin at 3 g/d led to a blood concentration of vancomycin that was higher than 20 μg/mL. We immediately reduced the dose of vancomycin and monitored the blood concentration of the drug. On the 29th day, the patient was treated with CRRT, the dosage regimen of vancomycin was 1 g every 12 h considering the clearance of vancomycin by CRRT, and the blood concentration was 13.3 μg/mL. The final blood concentration of vancomycin was maintained in the range of 10 to 20 mg/L.

CONCLUSION

The clinical dose of drugs administered is generally determined based on the results of pharmacokinetic studies and clinical trial studies in non-obese patients, which may not be optimal in obese individuals. Hence, the difference in pharmacokinetics of different drugs between obese and non-obese patients must be considered during drug treatment. Obesity is also associated with physiological changes that can alter the pharmacokinetics of vancomycin, and the selection of the dose of vancomycin administered needs to take into account the effect of the body weight of patients. Furthermore, both the loading dose and the maintenance dose are different from non-obese patients. During treatment, we should make appropriate dose adjustments based on the patient's therapeutic drug monitoring and renal function. At the same time, altered pharmacokinetics of antibacterial drugs may require dose individualization to achieve target concentrations. Adjustment of loading dose and maintenance dose is critical for the antibiotic treatment in obese patients using vancomycin. Unfortunately, limited data are available analyzing vancomycin concentrations in obese patients.

ACKNOWLEDGEMENTS

We thank the intensive care unit multidisciplinary team of the Fourth Hospital of Hebei Medical University for their treatment support.

FOOTNOTES

Author contributions: Bai J and Du WL conceived the manuscript; Xu KY drafted the manuscript; Li D monitored blood vancomycin concentrations; Hu ZJ was involved in drug therapy; Zhao CC was responsible for the patient.

Supported by the Hebei Natural Science Foundation of China, No. H2019206614.

Informed consent statement: Informed written consent was obtained from the patient for publication of this report and any accompanying images.

Conflict-of-interest statement: The authors declare that they have no conflict of interest to disclose.

CARE Checklist (2016) statement: The authors have read the CARE Checklist (2016), and the manuscript was prepared and revised according to the CARE Checklist (2016).

Open-Access: This article is an open-access article that was selected by an in-house editor and fully peer-reviewed by external reviewers. It is distributed in accordance with the Creative Commons Attribution NonCommercial (CC BY-NC 4.0) license, which permits others to distribute, remix, adapt, build upon this work non-commercially, and license their derivative works on different terms, provided the original work is properly cited and the use is non-commercial. See: https://creativecommons.org/Licenses/by-nc/4.0/

Country/Territory of origin: China

ORCID number: Kun-Yan Xu 0000-0002-5416-9288; Dan Li 0000-0002-5863-6234; Zhen-Jie Hu 0000-0002-9528-8371; Cong-Cong Zhao 0000-0002-1298-6351; Jing Bai 0000-0002-2717-6458; Wen-Li Du 0000-0002-4208-0008.

S-Editor: Xing YX
L-Editor: Wang TQ
P-Editor: Xing YX

REFERENCES

1 **Kelly T**, Yang W, Chen CS, Reynolds K, He J. Global burden of obesity in 2005 and projections to 2030. *Int J Obes (Lond)* 2008; **32**: 1431-1437 [PMID: 18607383 DOI: 10.1038/ijo.2008.102]
2 **Flegal KM**, Kruszon-Moran D, Carroll MD, Fryar CD, Ogden CL. Trends in Obesity Among Adults in the United States, 2005 to 2014. *JAMA* 2016; **315**: 2284-2291 [PMID: 27272580 DOI: 10.1001/jama.2016.6458]
3 **Pan XF**, Wang L, Pan A. Epidemiology and determinants of obesity in China. *Lancet Diabetes Endocrinol* 2021; **9**: 373-392 [PMID: 34022156 DOI: 10.1016/S2213-8587(21)00045-0]
4 **Huttunen R**, Syrjänen J. Obesity and the risk and outcome of infection. *Int J Obes (Lond)* 2013; **37**: 333-340 [PMID: 22546772 DOI: 10.1038/ijo.2012.62]
5 **El-Solh A**, Sikka P, Bozkanat E, Jaafar W, Davies J. Morbid obesity in the medical ICU. *Chest* 2001; **120**: 1989-1997 [PMID: 11742933 DOI: 10.1378/chest.120.6.1989]

6 **Genoni G**, Prodam F, Marolda A, Giglione E, Demarchi I, Bellone S, Bona G. Obesity and infection: two sides of one coin. *Eur J Pediatr* 2014; **173**: 25-32 [PMID: 24146165 DOI: 10.1007/s00431-013-2178-1]

7 **Hainer V**, Zamrazilová H, Kunešová M, Bendlová B, Aldhoon-Hainerová I. Obesity and infection: reciprocal causality. *Physiol Res* 2015; **64**: S105-S119 [PMID: 26680472 DOI: 10.33549/physiolres.933130]

8 **Falagas ME**, Kompoti M. Obesity and infection. *Lancet Infect Dis* 2006; **6**: 438-446 [PMID: 16790384 DOI: 10.1016/S1473-3099(06)70523-0]

9 **Rybak M**, Lomaestro B, Rotschafer JC, Moellering R Jr, Craig W, Billeter M, Dalovisio JR, Levine DP. Therapeutic monitoring of vancomycin in adult patients: a consensus review of the American Society of Health-System Pharmacists, the Infectious Diseases Society of America, and the Society of Infectious Diseases Pharmacists. *Am J Health Syst Pharm* 2009; **66**: 82-98 [PMID: 19106348 DOI: 10.2146/ajhp080434]

10 **Schilling A**, Neuner E, Rehm SJ. Vancomycin: a 50-something-year-old antibiotic we still don't understand. *Cleve Clin J Med* 2011; **78**: 465-471 [PMID: 21724929 DOI: 10.3949/ccjm.78a.10168]

11 **Marsot A**, Boulamery A, Bruguerolle B, Simon N. Vancomycin: a review of population pharmacokinetic analyses. *Clin Pharmacokinet* 2012; **51**: 1-13 [PMID: 22149255 DOI: 10.2165/11596390-000000000-00000]

12 **Polso AK**, Lassiter JL, Nagel JL. Impact of hospital guideline for weight-based antimicrobial dosing in morbidly obese adults and comprehensive literature review. *J Clin Pharm Ther* 2014; **39**: 584-608 [PMID: 25203631 DOI: 10.1111/jcpt.12200]

13 **Choi YC**, Saw S, Soliman D, Bingham AL, Pontiggia L, Hunter K, Chuang L, Siemianowski LA, Ereshefsky B, Hollands JM. Intravenous Vancomycin Associated With the Development of Nephrotoxicity in Patients With Class III Obesity. *Ann Pharmacother* 2017; **51**: 937-944 [PMID: 28709394 DOI: 10.1177/1060028017720946]

14 **Ye ZK**, Tang HL, Zhai SD. Benefits of therapeutic drug monitoring of vancomycin: a systematic review and meta-analysis. *PLoS One* 2013; **8**: e77169 [PMID: 24204764 DOI: 10.1371/journal.pone.0077169]

15 **Jensen MD**, Ryan DH, Apovian CM, Ard JD, Comuzzie AG, Donato KA, Hu FB, Hubbard VS, Jakicic JM, Kushner RF, Loria CM, Millen BE, Nonas CA, Pi-Sunyer FX, Stevens J, Stevens VJ, Wadden TA, Wolfe BM, Yanovski SZ, Jordan HS, Kendall KA, Lux LJ, Mentor-Marcel R, Morgan LC, Trisolini MG, Wnek J, Anderson JL, Halperin JL, Albert NM, Bozkurt B, Brindis RG, Curtis LH, DeMets D, Hochman JS, Kovacs RJ, Ohman EM, Pressler SJ, Sellke FW, Shen WK, Smith SC Jr, Tomaselli GF; American College of Cardiology/American Heart Association Task Force on Practice Guidelines; Obesity Society. 2013 AHA/ACC/TOS guideline for the management of overweight and obesity in adults: a report of the American College of Cardiology/American Heart Association Task Force on Practice Guidelines and The Obesity Society. *Circulation* 2014; **129**: S102-S138 [PMID: 24222017 DOI: 10.1161/01.cir.0000437739.71477.ee]

16 **Janson B**, Thursky K. Dosing of antibiotics in obesity. *Curr Opin Infect Dis* 2012; **25**: 634-649 [PMID: 23041773 DOI: 10.1097/QCO.0b013e328359a4c1]

17 **Rybak MJ**. The pharmacokinetic and pharmacodynamic properties of vancomycin. *Clin Infect Dis* 2006; **42** Suppl 1: S35-S39 [PMID: 16323118 DOI: 10.1086/491712]

18 **Adane ED**, Herald M, Koura F. Pharmacokinetics of vancomycin in extremely obese patients with suspected or confirmed Staphylococcus aureus infections. *Pharmacotherapy* 2015; **35**: 127-139 [PMID: 25644478 DOI: 10.1002/phar.1531]

19 **Hanrahan TP**, Lipman J, Roberts JA. Antibiotic dosing in obesity: a BIG challenge. *Crit Care* 2016; **20**: 240 [PMID: 27506812 DOI: 10.1186/s13054-016-1426-y]

20 **Grace E**. Altered vancomycin pharmacokinetics in obese and morbidly obese patients: what we have learned over the past 30 years. *J Antimicrob Chemother* 2012; **67**: 1305-1310 [PMID: 22382471 DOI: 10.1093/jac/dks066]

21 **Ducharme MP**, Slaughter RL, Edwards DJ. Vancomycin pharmacokinetics in a patient population: effect of age, gender, and body weight. *Ther Drug Monit* 1994; **16**: 513-518 [PMID: 7846752 DOI: 10.1097/00007691-199410000-00013]

22 **Blouin RA**, Bauer LA, Miller DD, Record KE, Griffen WO Jr. Vancomycin pharmacokinetics in normal and morbidly obese subjects. *Antimicrob Agents Chemother* 1982; **21**: 575-580 [PMID: 7081978 DOI: 10.1128/AAC.21.4.575]

23 **Hanley MJ**, Abernethy DR, Greenblatt DJ. Effect of obesity on the pharmacokinetics of drugs in humans. *Clin Pharmacokinet* 2010; **49**: 71-87 [PMID: 20067334 DOI: 10.2165/11318100-000000000-00000]

24 **Hites M**, Taccone FS. Optimization of antibiotic therapy in the obese, critically ill patient. *Réanimation* 2015; **24**: 278-294

25 **Durand C**, Bylo M, Howard B, Belliveau P. Vancomycin Dosing in Obese Patients: Special Considerations and Novel Dosing Strategies. *Ann Pharmacother* 2018; **52**: 580-590 [PMID: 29262697 DOI: 10.1177/1060028017750084]

26 **Alobaid AS**, Hites M, Lipman J, Taccone FS, Roberts JA. Effect of obesity on the pharmacokinetics of antimicrobials in critically ill patients: A structured review. *Int J Antimicrob Agents* 2016; **47**: 259-268 [PMID: 26988339 DOI: 10.1016/j.ijantimicag.2016.01.009]

27 **Han PY**, Duffull SB, Kirkpatrick CM, Green B. Dosing in obesity: a simple solution to a big problem. *Clin Pharmacol Ther* 2007; **82**: 505-508 [PMID: 17952107 DOI: 10.1038/sj.clpt.6100381]

28 **Lemmens HJ**, Ingrande J. Pharmacology and obesity. *Int Anesthesiol Clin* 2013; **51**: 52-66 [PMID: 23797645 DOI: 10.1097/AIA.0b013e31829a4d56]

29 **Chagnac A**, Weinstein T, Korzets A, Ramadan E, Hirsch J, Gafter U. Glomerular hemodynamics in severe obesity. *Am J Physiol Renal Physiol* 2000; **278**: F817-F822 [PMID: 10807594 DOI: 10.1152/ajprenal.2000.278.5.F817]

30 **Eknoyan G**. Obesity, diabetes, and chronic kidney disease. *Curr Diab Rep* 2007; **7**: 449-453 [PMID: 18255009 DOI: 10.1007/s11892-007-0076-5]

31 **Udy AA**, Roberts JA, Boots RJ, Paterson DL, Lipman J. Augmented renal clearance: implications for antibacterial dosing in the critically ill. *Clin Pharmacokinet* 2010; **49**: 1-16 [PMID: 20000886 DOI: 10.2165/11318140-000000000-00000]

32 **Hites M**, Taccone FS, Wolff F, Maillart E, Beumier M, Surin R, Cotton F, Jacobs F. Broad-spectrum β-lactams in obese non-critically ill patients. *Nutr Diabetes* 2014; **4**: e119 [PMID: 24956136 DOI: 10.1038/nutd.2014.15]

33 **Udy AA**, Baptista JP, Lim NL, Joynt GM, Jarrett P, Wockner L, Boots RJ, Lipman J. Augmented renal clearance in the ICU: results of a multicenter observational study of renal function in critically ill patients with normal plasma creatinine concentrations*. *Crit Care Med* 2014; **42**: 520-527 [PMID: 24201175 DOI: 10.1097/CCM.0000000000000029]

34 **Smit C**, Wasmann RE, Goulooze SC, Wiezer MJ, van Dongen EPA, Mouton JW, Brüggemann RJM, Knibbe CAJ.

Population pharmacokinetics of vancomycin in obesity: Finding the optimal dose for (morbidly) obese individuals. *Br J Clin Pharmacol* 2020; **86**: 303-317 [PMID: 31661553 DOI: 10.1111/bcp.14144]

35 **Pai MP**. Drug dosing based on weight and body surface area: mathematical assumptions and limitations in obese adults. *Pharmacotherapy* 2012; **32**: 856-868 [PMID: 22711238 DOI: 10.1002/j.1875-9114.2012.01108.x]

36 **Meng L**, Mui E, Holubar MK, Deresinski SC. Comprehensive Guidance for Antibiotic Dosing in Obese Adults. *Pharmacotherapy* 2017; **37**: 1415-1431 [PMID: 28869666 DOI: 10.1002/phar.2023]

37 **Rybak MJ**, Le J, Lodise TP, Levine DP, Bradley JS, Liu C, Mueller BA, Pai MP, Wong-Beringer A, Rotschafer JC, Rodvold KA, Maples HD, Lomaestro BM. Therapeutic monitoring of vancomycin for serious methicillin-resistant Staphylococcus aureus infections: A revised consensus guideline and review by the American Society of Health-System Pharmacists, the Infectious Diseases Society of America, the Pediatric Infectious Diseases Society, and the Society of Infectious Diseases Pharmacists. *Am J Health Syst Pharm* 2020; **77**: 835-864 [PMID: 32191793 DOI: 10.1093/ajhp/zxaa036]

38 **Bauer LA**, Black DJ, Lill JS. Vancomycin dosing in morbidly obese patients. *Eur J Clin Pharmacol* 1998; **54**: 621-625 [PMID: 9860149 DOI: 10.1007/s002280050524]

39 **Roberts JA**, Taccone FS, Udy AA, Vincent JL, Jacobs F, Lipman J. Vancomycin dosing in critically ill patients: robust methods for improved continuous-infusion regimens. *Antimicrob Agents Chemother* 2011; **55**: 2704-2709 [PMID: 21402850 DOI: 10.1128/AAC.01708-10]

40 **Crass RL**, Dunn R, Hong J, Krop LC, Pai MP. Dosing vancomycin in the super obese: less is more. *J Antimicrob Chemother* 2018; **73**: 3081-3086 [PMID: 30203073 DOI: 10.1093/jac/dky310]

41 **Liu C**, Bayer A, Cosgrove SE, Daum RS, Fridkin SK, Gorwitz RJ, Kaplan SL, Karchmer AW, Levine DP, Murray BE, J Rybak M, Talan DA, Chambers HF; Infectious Diseases Society of America. Clinical practice guidelines by the infectious diseases society of america for the treatment of methicillin-resistant Staphylococcus aureus infections in adults and children. *Clin Infect Dis* 2011; **52**: e18-e55 [PMID: 21208910 DOI: 10.1093/cid/ciq146]

42 **He N**, Su S, Ye Z, Du G, He B, Li D, Liu Y, Yang K, Zhang X, Zhang Y, Chen X, Chen Y, Chen Z, Dong Y, Gu J, Guo D, Guo R, Hu X, Jiao Z, Li H, Liu G, Li Z, Lv Y, Lu W, Miao L, Qu J, Sun T, Tong R, Wang L, Wang M, Wang R, Wen A, Wu J, Wu X, Xu Y, Yang Y, Yang F, Zhan S, Zhang B, Zhang C, Zhang H, Zhang J, Zhang W, Zhao L, Zhao R, Zhao W, Zhao Z, Zhou W, Zeng XT, Zhai S. Evidence-based Guideline for Therapeutic Drug Monitoring of Vancomycin: 2020 Update by the Division of Therapeutic Drug Monitoring, Chinese Pharmacological Society. *Clin Infect Dis* 2020; **71**: S363-S371 [PMID: 33367582 DOI: 10.1093/cid/ciaa1536]

43 **Clark WR**, Mueller BA, Alaka KJ, Macias WL. A comparison of metabolic control by continuous and intermittent therapies in acute renal failure. *J Am Soc Nephrol* 1994; **4**: 1413-1420 [PMID: 8161723 DOI: 10.1681/ASN.V471413]

44 **Pallotta KE**, Manley HJ. Vancomycin use in patients requiring hemodialysis: a literature review. *Semin Dial* 2008; **21**: 63-70 [PMID: 18251960 DOI: 10.1111/j.1525-139X.2007.00333.x]

45 **Mueller BA**, Smoyer WE. Challenges in developing evidence-based drug dosing guidelines for adults and children receiving renal replacement therapy. *Clin Pharmacol Ther* 2009; **86**: 479-482 [PMID: 19844225 DOI: 10.1038/clpt.2009.150]

46 **van de Vijsel LM**, Walker SA, Walker SE, Yamashita S, Simor A, Hladunewich M. Initial vancomycin dosing recommendations for critically ill patients undergoing continuous venovenous hemodialysis. *Can J Hosp Pharm* 2010; **63**: 196-206 [PMID: 22478979 DOI: 10.4212/cjhp.v63i3.915]

47 **Covajes C**, Scolletta S, Penaccini L, Ocampos-Martinez E, Abdelhadii A, Beumier M, Jacobs F, de Backer D, Vincent JL, Taccone FS. Continuous infusion of vancomycin in septic patients receiving continuous renal replacement therapy. *Int J Antimicrob Agents* 2013; **41**: 261-266 [PMID: 23312601 DOI: 10.1016/j.ijantimicag.2012.10.018]

48 **Kellum JA**, Lameire N; KDIGO AKI Guideline Work Group. Diagnosis, evaluation, and management of acute kidney injury: a KDIGO summary (Part 1). *Crit Care* 2013; **17**: 204 [PMID: 23394211 DOI: 10.1186/cc11454]

49 **Li Q**, Liang F, Sang L, Li P, Lv B, Tan L, Liu X, Chen W. Pharmacokinetics of and maintenance dose recommendations for vancomycin in severe pneumonia patients undergoing continuous venovenous hemofiltration with the combination of predilution and postdilution. *Eur J Clin Pharmacol* 2020; **76**: 211-217 [PMID: 31734748 DOI: 10.1007/s00228-019-02755-5]

50 **Chaijamorn W**, Jitsurong A, Wiwattanawongsa K, Wanakamanee U, Dandecha P. Vancomycin clearance during continuous venovenous haemofiltration in critically ill patients. *Int J Antimicrob Agents* 2011; **38**: 152-156 [PMID: 21636256 DOI: 10.1016/j.ijantimicag.2011.04.010]

51 **Lodise TP**, Lomaestro B, Graves J, Drusano GL. Larger vancomycin doses (at least four grams per day) are associated with an increased incidence of nephrotoxicity. *Antimicrob Agents Chemother* 2008; **52**: 1330-1336 [PMID: 18227177 DOI: 10.1128/AAC.01602-07]

52 **Katip W**, Jaruratanasirikul S, Pattharachayakul S, Wongpoowarak W, Jitsurong A, Lucksiri A. The pharmacokinetics of vancomycin during the initial loading dose in patients with septic shock. *Infect Drug Resist* 2016; **9**: 253-260 [PMID: 27920562 DOI: 10.2147/IDR.S121513]

53 **Hall RG 2nd**, Payne KD, Bain AM, Rahman AP, Nguyen ST, Eaton SA, Busti AJ, Vu SL, Bedimo R. Multicenter evaluation of vancomycin dosing: emphasis on obesity. *Am J Med* 2008; **121**: 515-518 [PMID: 18501233 DOI: 10.1016/j.amjmed.2008.01.046]

54 **Reynolds DC**, Waite LH, Alexander DP, DeRyke CA. Performance of a vancomycin dosage regimen developed for obese patients. *Am J Health Syst Pharm* 2012; **69**: 944-950 [PMID: 22610026 DOI: 10.2146/ajhp110324]

World Journal of Clinical Cases

Submit a Manuscript: https://www.f6publishing.com

World J Clin Cases 2022 June 26; 10(18): 6227-6233

DOI: 10.12998/wjcc.v10.i18.6227

ISSN 2307-8960 (online)

CASE REPORT

Insulinoma after sleeve gastrectomy: A case report

Miry Lobaton-Ginsberg, Pilar Sotelo-González, Claudia Ramirez-Renteria, Fany Gabriela Juárez-Aguilar, Aldo Ferreira-Hermosillo

Specialty type: Endocrinology and metabolism

Provenance and peer review: Unsolicited article; Externally peer reviewed.

Peer-review model: Single blind

Peer-review report's scientific quality classification

Grade A (Excellent): 0
Grade B (Very good): B
Grade C (Good): C, C
Grade D (Fair): 0
Grade E (Poor): 0

P-Reviewer: Ding XJ, China; Zhou ST, China

Received: December 13, 2021
Peer-review started: December 13, 2021
First decision: January 8, 2022
Revised: January 24, 2022
Accepted: April 28, 2022
Article in press: April 28, 2022
Published online: June 26, 2022

Miry Lobaton-Ginsberg, Facultad de Medicina, Universidad Anáhuac México Norte, Mexico City 52786, Mexico

Pilar Sotelo-González, Servicio de Endocrinología, Hospital de Especialidades, Centro Médico Nacional Siglo XXI, IMSS, Mexico City 06720, Mexico

Claudia Ramirez-Renteria, Aldo Ferreira-Hermosillo, Unidad de Investigación Médica en Enfermedades Endocrinas, Instituto Mexicano del Seguro Social, Mexico City 06720, Mexico

Fany Gabriela Juárez-Aguilar, Servicio de Anatomía Patológica, Hospital de Especialidades del Centro Médico Nacional Siglo XXI, IMSS, Mexico City 06720, Mexico

Corresponding author: Aldo Ferreira-Hermosillo, MD, MSc, Research Scientist, Unidad de Investigación Médica en Enfermedades Endocrinas, Instituto Mexicano del Seguro Social, 330 Cuauhtémoc, Doctores, Mexico City 06720, Mexico. aldo.nagisa@gmail.com

Abstract

BACKGROUND

Laparoscopic sleeve gastrectomy (LSG) has been proposed as an effective and durable treatment for severe obesity and glucose metabolism disorders, and its prevalence has increased from 5% to 37% since 2008. One common complication after bariatric surgery is a postprandial hyperinsulinemic hypoglycemic state. While rare, insulinomas can cause this state, where symptoms are more common in the fasting state; thus, evaluation of insulin secretion is needed. Until now, there have been no reports of insulinoma after LSG.

CASE SUMMARY

We describe the case of a 43-year-old woman who was referred to the obesity clinic 2 years after LSG was performed. She had symptoms of hypoglycemia predominantly in the fasting state and documented hypoglycemia of less than 30 mg/dL, which are compatible with Whipple's triad. Initially, dumping syndrome was suspected, but after a second low fasting plasma glucose was documented, a 72-h fasting test was performed that tested positive. Computed tomography and endoscopic ultrasound were performed, identifying the presence of a homogeneous hypoechoic semioval tumoral lesion in the pancreas. The diagnosis was compatible with insulinoma. After laparoscopic enucleation of the insulinoma, the symptoms and hypoglycemia disappeared. The histopathological report described a well-differentiated grade 2 neuroendocrine tumor with positive chromogranin and synaptophysin and Ki67 immunopositivity in 4% of the neoplastic cells.

CONCLUSION
Insulinoma after LSG is a rare condition, and clinicians must be aware of it, especially if the patient has hypoglycemic symptoms during the fasting state.

Key Words: Insulinoma; Hypoglycemia; Bariatric surgery; Glucagon-like peptide 1 amide; Neuroendocrine tumors; Case report

©The Author(s) 2022. Published by Baishideng Publishing Group Inc. All rights reserved.

Core Tip: Neuroglycopenic symptoms compatible with Whipple's triad were identified in a woman 2 years after laparoscopic sleeve gastrectomy, predominantly occurring in the fasting state. After discarding late dumping syndrome, a 72-h fasting test was performed and tested positive. Imaging techniques documented the presence of a tumoral lesion in the pancreas, compatible with insulinoma. After laparoscopic enucleation of the insulinoma, the symptoms were relieved. When hypoglycemia occurs after bariatric surgery, evaluation of insulin secretion is needed to conduct a correct diagnostic approach. Follow-up must be performed by a multidisciplinary team.

Citation: Lobaton-Ginsberg M, Sotelo-González P, Ramirez-Renteria C, Juárez-Aguilar FG, Ferreira-Hermosillo A. Insulinoma after sleeve gastrectomy: A case report. *World J Clin Cases* 2022; 10(18): 6227-6233
URL: https://www.wjgnet.com/2307-8960/full/v10/i18/6227.htm
DOI: https://dx.doi.org/10.12998/wjcc.v10.i18.6227

INTRODUCTION

The obesity pandemic has become a great topic of interest due to its implications for quality of life, comorbidities, increasing mortality, and the economic impact on health services worldwide[1]. Bariatric surgery (BS) is an effective and durable treatment for severe obesity and glucose metabolism disorders, with laparoscopic Roux-Y gastric bypass surgery (RYGB) being the most common procedure[2,3]. Nevertheless, laparoscopic sleeve gastrectomy (LSG) has been proposed as a procedure capable of achieving the same goals, but with fewer complications[4].

A common complication in BS is the development of a postprandial hyperinsulinemic hypoglycemic state[5]. Hypoglycemia is defined as a glucose level below 70 mg/dL according to the American Diabetes Association guidelines[6]. The possible causes of hypoglycemia in patients who had undergone BS include late dumping syndrome, nesidioblastosis and, rarely, insulinoma[5,7]. Up to 40 cases of nesidioblastosis have been reported after RYGB, and only one case has been reported after sleeve gastrectomy [8,9]. To our knowledge, there are few reports of insulinoma after BS[10] but no reports after LSG. The purpose of these case reports is to inform clinicians that patients with neuroglycopenic symptoms during the fasting state could have hypoglycemia caused by insulinoma, which is not only due to late dumping syndrome.

A review of the medical literature for insulinoma and hypoglycemia after BS was performed in PubMed. We searched "insulinoma", "hypoglycemia", "sleeve gastrectomy", "RYGB", "glucagon-like peptide 1 (GLP-1)", and "ghrelin" and a combination of the above terms including all dates up to October 2021. Herein, we present the case of a 43-year-old woman referred to the obesity clinic due to neuroglycopenic symptoms caused by an insulinoma 2 years after a sleeve gastrectomy.

CASE PRESENTATION

Chief complaints

A 43-year-old woman was referred to the obesity clinic due to neuroglycopenic symptoms caused by an insulinoma 2 years after a sleeve gastrectomy.

History of present illness

In March 2020, 2 years after LSG was performed, the patient developed neuroglycopenic symptoms including short-term memory loss, lingual nerve paresthesia, and nonspecific visual alterations predominantly during the morning in a fasting state. These symptoms were suppressed with food intake. Two months later, she visited a physician who documented fasting plasma glucose of 27 mg/dL, and in June 2020, the symptoms occurred more frequently, and she gained 14 kg. In the beginning, late dumping symptoms were suspected, but in September 2020, fasting plasma glucose of 30 mg/dL was docu-

mented, so she was hospitalized for the evaluation of hypoglycemia in a 72-h supervised fast test. She had baseline plasma glucose of 67 mg/dL, nonsuppressed insulin of 16.4 IU/mL, and C-peptide of 3.64 ng/mL. In the first hour after initiation, she developed Whipple's triad symptoms, and her lab results detected plasma glucose of 38 mg/dL, insulin of 25.9 IU/mL, and C-peptide of 4.31 ng/mL. Thus, it was decided to stop the protocol and initiate 1000 mL of 20% glucose solution in 12 h.

History of past illness

In 2002, the patient was diagnosed with obesity and dyslipidemia (high triglycerides and cholesterol with low HDL) and treated with improvements in diet, physical activity, and statins without weight control. In 2016, a gastric balloon was placed, and although her body mass index (BMI) in 2018 was 34.4 kg/m^2, LSG was performed.

Personal and family history

The patient had no specific personal or family history.

Physical examination

After LSG, the patient weighed 74 kg, and her BMI was 32 kg/m^2. The physical examination showed no obvious cardiovascular or respiratory abnormalities. The abdomen was soft, and the only sign was the presence of postsurgery scars.

Laboratory examinations

Upon hospitalization prior to the surgery, the patient's hemoglobin A1c level was 4.8% (normal range: < 5.7%). The C-peptide value was normal at 3.64 ng/mL (1.1-4.4 ng/mL), and insulin was mildly elevated at 16.40 μUI/mL (3.21-16.30 μUI/mL). Lipid levels indicated dyslipidemia with total cholesterol of 224 mg/dL and LDL-c of 142.8 mg/dL. Other biochemical parameters were normal and only an iron deficiency anemia was documented. Thyroid function was normal, with TSH 2.46 μUI/mL (0.27-4.20 μUI/mL), FT4 1.06 ng/dL (0.93-1.70 ng/dL), and cortisol level 15.04 ug/dL (3.70-19.40 μg/dL), all within the normal range.

Imaging examinations

Computed tomography (CT) demonstrated the presence of a focal asymmetric reinforcement area in the head of the pancreas (Figure 1A). Endoscopic ultrasound showed the presence of a tumoral lesion in the pancreas in close proximity to the main pancreatic duct and splenomesenteric confluence without evidence of invasion (Figure 1B and C).

FINAL DIAGNOSIS

The final diagnosis was insulinoma. This was confirmed by histology and immunohistochemistry of the tumor (Figure 2).

TREATMENT

After a surgery consultation, a laparoscopic insulinoma enucleation was performed without complications. No other tumors were identified in the upper abdomen.

OUTCOME AND FOLLOW-UP

Histopathological findings revealed a well-differentiated neuroendocrine grade 2 tumor with free edges. Immunohistochemical studies confirmed positive chromogranin and synaptophysin as well as a proliferative activity (Ki67) in 4% of neoplastic cells.

After surgery, the neuroglycopenic symptoms were relieved, and the patient had no hypoglycemic events. Her current treatment is diet and physical activity, targeting a BMI of 31.1 kg/m^2.

DISCUSSION

Since 2013, 468609 BSs have been performed worldwide[2]. LSG was initially introduced as a first-stage restrictive procedure to a more complex definitive one. At present, it is performed as a stand-alone BS [7]. Since 2008, the prevalence of the LSG procedure has increased from 5% to 37% worldwide[2], but in Mexico, it is performed only in 13% of patients, whereas LRYGB is performed in 85.8%, with a bypass/

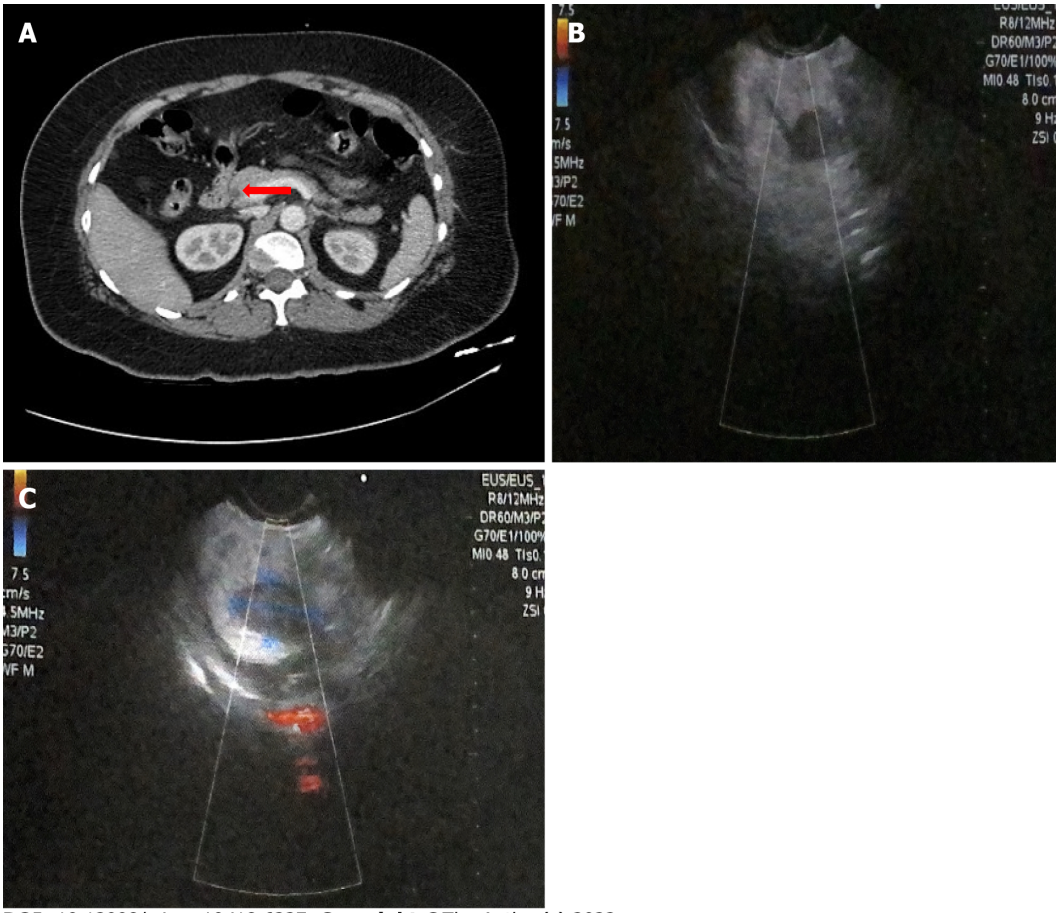

DOI: 10.12998/wjcc.v10.i18.6227 **Copyright** ©The Author(s) 2022.

Figure 1 Imaging examinations. A: Computed tomography image for neuroendocrine tumor. The orange arrow indicates a focal asymmetric reinforcement area of 11 mm × 14 mm of 145 HU in the head of the pancreas; B and C: Endoscopic ultrasound images indicating the presence of a homogeneous hypoechoic semioval tumoral lesion in the pancreas, with well-defined borders measuring 2.1 cm × 1.2 cm, in close apposition to the main pancreatic duct and splenomesenteric confluence without evidence of invasion.

sleeve ratio of 7:1. In our center, LSG accounts for 20% of total BSs (200 procedures since 2010).

LSG comprises vertical longitudinal resection of the greater gastric curve that includes the fundus, body, and antrum as well as the formation of a tubular conduit with a capacity of < 100 mL. Weight loss is achieved by restrictive and humoral effects[8,11].

Hypoglycemia is a well-documented complication after BS. Papamargaritis *et al*[12,13] recorded a study where 33% of patients experienced severe hypoglycemia a year after LSG due to late dumping symptoms, which usually occurs 1-3 h after a high-carbohydrate meal triggering a hyperinsulinemic response. Since 2005, up to 40 cases of nesidioblastosis after RYGB have been reported[8], and only one case after LSG was documented in 2019 by Kim *et al*[9]. While rare, insulinomas have been reported after BS. Mulla *et al*[10] described seven cases of insulinoma, one patient with pancreatic neuroendocrine tumor, and one patient with insulinoma and pancreatic neuroendocrine tumor after BS, 78% of whom were women. In these cases, hypoglycemia was more common in the fasting state.

The mechanism of the post-BS hyperinsulinemic hypoglycemic state and the changes in beta cell proliferation are not fully understood. In the LSG, the faster transit of undigested nutrients to the distal gastrointestinal tract due to rapid gastric emptying upregulates the production of GLP-1 secreted by enteroendocrine L cells in the distal intestine. This increase can normalize blood glucose and regulate insulin synthesis and proinsulin gene expression, as well as glucagon and somatostatin secretion[3]. GLP-1 has multiple beneficial effects on β cells, including an increase in their number by inhibiting apoptosis and enhancing neogenesis as well as promoting its proliferation. In a study carried out in 2016 by Xu *et al*[14], it was found that a chemically modified GLP-1 (mGLP-1) analog promotes the proliferation of pancreatic mouse β cells, upregulating the expression of cyclin E, CDK2, Bcl-2, Bax, and p21. The cyclin E-CDK2 complex plays an important role in the regulation of the G1 phase of the G1/S cell cycle, while p21 is a universal cyclin-dependent kinase (CKI) inhibitor. Meanwhile, the *Bcl-2* and *Bax* genes, two important members of the *Bcl-2* gene family, have opposite functions, inhibiting or promoting cell apoptosis, respectively[14].

An increase in ghrelin levels has been observed a year after BS[15]. Ghrelin and the type 1a ghrelin receptor (GHS-R1A) are expressed in different types of neuroendocrine tumors. Recently, Wu *et al*[16]

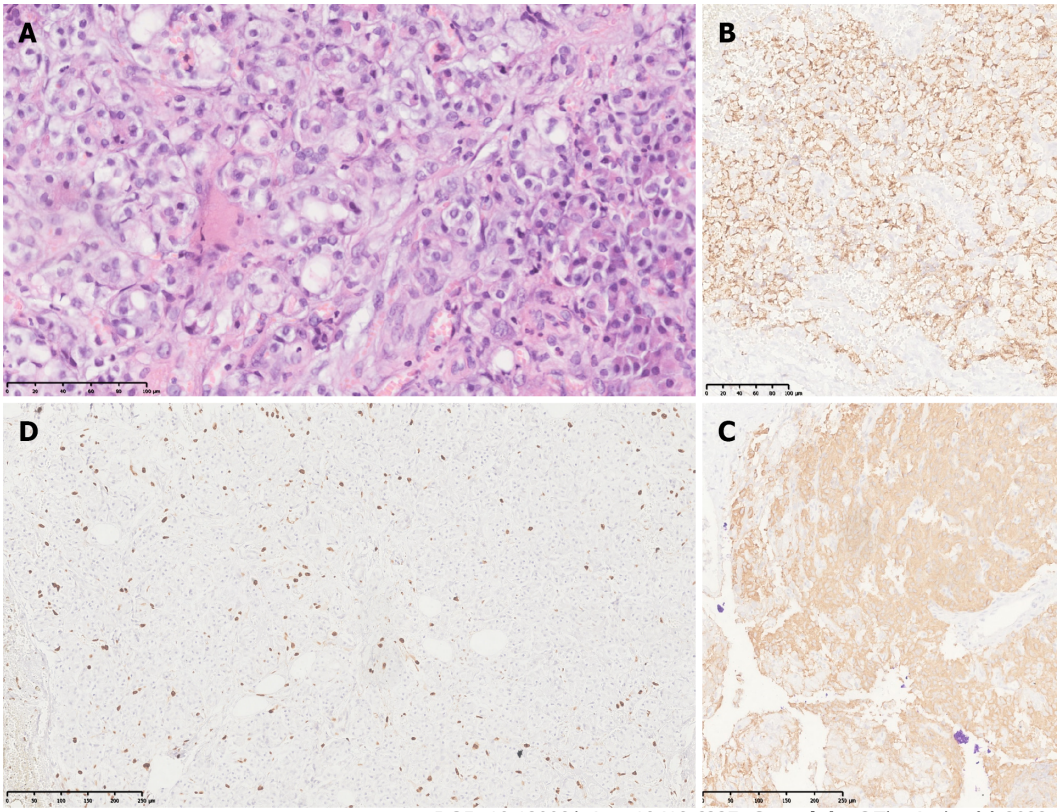

DOI: 10.12998/wjcc.v10.i18.6227 **Copyright** ©The Author(s) 2022.

Figure 2 Histology and immunohistochemistry of the tumor. A: Hematoxylin and eosin photomicrograph (40 ×) showing neoplastic cells presenting uniformly round nuclei with granular chromatin (salt and pepper image), typical of neuroendocrine cells with extensive eosinophilic cytoplasm; B and C: Photomicrographs of immunohistochemical staining for chromogranin (B) and synaptophysin (C) (10 ×). Neoplastic cells show strong immunopositivity for both markers in the cytoplasm, which corroborates the neuroendocrine lineage of the neoplasia; D: Immunohistochemical staining for Ki67 (cell proliferation index). Strong nuclear immunopositivity is seen in approximately 4% of neoplastic cells. The tumor was classified as grade 2, according to the 2019 WHO classification.

found that GHS-R1a was found in 60% of insulinomas, suggesting that ghrelin may act through autocrine or paracrine pathways. The proliferative effects of ghrelin and its association with insulinoma have not been studied, although there is a clinical case report where a ghrelin-producing neuroendocrine tumor was transformed into an insulinoma[17].

The diagnosis of hypoglycemia after BS is challenging. The first step after identifying the presence of symptoms is to verify their relationship to hypoglycemia. A detailed clinical history must be performed to identify family or personal history of neuroendocrine tumors, if patients are taking any hypoglycemic medication such as sulfonylureas or if the symptoms are more common in fasting state, as in our case.

In a stepwise manner, biochemical analysis must be performed to rule out other causes[18]. Plasma glucose, insulin, C-peptide, proinsulin, beta-hydroxybutyrate, and cortisol levels should be measured. The development of provocative studies such as a 72-h fasting test is also recommended[10,18]. The goal is to determine whether beta-cell peptides are appropriately suppressed during hypoglycemia. If autonomous insulin secretion is identified, insulinoma should be suspected[10,18]. The next step is to determine the anatomical localization and to exclude other tumors. Multidetector contrast-enhanced imaging CT or dual phase helical CT with thin sections are the preferred initial imaging options. In patients in whom noninvasive radiologic techniques are negative or to improve the sensitivity for identifying an insulinoma, endoscopic ultrasound (EUS) must be performed. EUS has 80%-92% sensitivity for detecting tumors as small as 5 mm. Additionally, EUS-guided fine needle aspiration allows pathologic confirmation in 57% of patients. If the techniques mentioned above fail to detect the tumor, selective arteriography and intra-arterial calcium stimulation tests with hepatic venous sampling can be performed. They should be used only as a last resort because they are invasive techniques[5,10]. In our case, we performed CT and EUS that allowed us to identify insulinoma.

Finally, histopathologic and immunohistochemical confirmation is necessary to classify the type of tumor and to determine the patient's follow-up[19].

The definitive treatment for insulinoma comprises complete surgical resection. However, there are other treatment options such as octreotide or EUS-guided alcohol tumor ablation, radiofrequency ablation (RFA), or embolization[20]. There is superior short-term recovery, shorter length of stay, decreased hemorrhage, and improved cosmesis when performing minimally invasive pancreatic resection compared to open pancreatic surgery[10]. However, the technique used depends on the size, extension, localization, and type of lesion. Atypical resection, including enucleation and partial or

middle pancreatectomy, has the advantage of pancreatic parenchyma preservation, thereby reducing the risk of late exocrine and/or endocrine insufficiency[20]. As in the case of our patient, when the lesion was small, benign, solitary, and superficial and when the pancreatic duct was not involved, the best surgical approach was laparoscopic enucleation[21]. It is important to note that positive resection margins are not associated with increased recurrence rates[10].

CONCLUSION

This is the first case of insulinoma after sleeve gastrectomy. Although this is a very rare case, clinicians must be aware of it, especially if the patient has hypoglycemic symptoms during the fasting state.

FOOTNOTES

Author contributions: Lobaton-Ginsberg M participated in the conception and design of the report and wrote the paper; Sotelo-González MP made substantial contributions to the acquisition, analysis, and interpretation of the patient data and helped write the paper; Juárez-Aguilar FG performed the histopathological and immunohistochemical report; Ramírez-Rentería C and Ferreira-Hermosillo A were involved in the coordination and design of the report and the revision of the manuscript; all authors read and approved the final manuscript.

Informed consent statement: Informed written consent was obtained from the patient for the publication of this report and any accompanying images.

Conflict-of-interest statement: The authors declare that they have no conflict of interest to disclose.

CARE Checklist (2016) statement: The authors have read the CARE Checklist (2016), and the manuscript was prepared and revised according to the CARE Checklist (2016).

Open-Access: This article is an open-access article that was selected by an in-house editor and fully peer-reviewed by external reviewers. It is distributed in accordance with the Creative Commons Attribution NonCommercial (CC BY-NC 4.0) license, which permits others to distribute, remix, adapt, build upon this work non-commercially, and license their derivative works on different terms, provided the original work is properly cited and the use is non-commercial. See: https://creativecommons.org/Licenses/by-nc/4.0/

Country/Territory of origin: Mexico

ORCID number: Miry Lobaton-Ginsberg 0000-0001-8227-087X; Pilar Sotelo-González 0000-0002-4132-5093; Claudia Ramirez-Renteria 0000-0003-3025-8339; Fany Gabriela Juárez-Aguilar 0000-0002-6204-3677; Aldo Ferreira-Hermosillo 0000-0002-5159-9856.

S-Editor: Chen YL
L-Editor: Wang TQ
P-Editor: Chen YL

REFERENCES

1 **Molina-Ayala M**, Rodríguez-González A, Albarrán-Sánchez A, Ferreira-Hermosillo A, Ramírez-Rentería C, Luque-de León E, Bosco-Garate I, Laredo-Sánchez F, Contreras-Herrera R, Mac Gregor-Gooch J, Cuevas-García C, Mendoza-Zubieta V. [Clinical and biochemical characteristics of patients with morbid obesity at the time of hospital admission and one year after undergoing bariatric surgery]. *Rev Med Inst Mex Seguro Soc* 2016; **54** Suppl 2: S118-S123 [PMID: 27561014]

2 **Belligoli A**, Sanna M, Serra R, Fabris R, Pra' CD, Conci S, Fioretto P, Prevedello L, Foletto M, Vettor R, Busetto L. Incidence and Predictors of Hypoglycemia 1 Year After Laparoscopic Sleeve Gastrectomy. *Obes Surg* 2017; **27**: 3179-3186 [PMID: 28547566 DOI: 10.1007/s11695-017-2742-2]

3 **Guilbert L**, Joo P, Ortiz C, Sepúlveda E, Alabi F, León A, Piña T, Zerrweck C. Safety and efficacy of bariatric surgery in Mexico: A detailed analysis of 500 surgeries performed at a high-volume center. *Rev Gastroenterol Mex (Engl Ed)* 2019; **84**: 296-302 [PMID: 29933896 DOI: 10.1016/j.rgmx.2018.05.002]

4 **Yang J**, Gao Z, Williams DB, Wang C, Lee S, Zhou X, Qiu P. Effect of laparoscopic Roux-en-Y gastric bypass versus laparoscopic sleeve gastrectomy on fasting gastrointestinal and pancreatic peptide hormones: A prospective nonrandomized trial. *Surg Obes Relat Dis* 2018; **14**: 1521-1529 [PMID: 30449509 DOI: 10.1016/j.soard.2018.06.003]

5 **Malik S**, Mitchell JE, Steffen K, Engel S, Wiisanen R, Garcia L, Malik SA. Recognition and management of hyperinsulinemic hypoglycemia after bariatric surgery. *Obes Res Clin Pract* 2016; **10**: 1-14 [PMID: 26522879 DOI: 10.1016/j.orcp.2015.07.003]

6 **American Diabetes Association**. 6. Glycemic Targets: *Standards of Medical Care in Diabetes-2021*. *Diabetes Care* 2021;

44: S73-S84 [PMID: 33298417 DOI: 10.2337/dc21-S006]
7 **Natoudi M**, Panousopoulos SG, Memos N, Menenakos E, Zografos G, Leandros E, Albanopoulos K. Laparoscopic sleeve gastrectomy for morbid obesity and glucose metabolism: a new perspective. *Surg Endosc* 2014; **28**: 1027-1033 [PMID: 24185751 DOI: 10.1007/s00464-013-3275-y]
8 **Service GJ**, Thompson GB, Service FJ, Andrews JC, Collazo-Clavell ML, Lloyd RV. Hyperinsulinemic hypoglycemia with nesidioblastosis after gastric-bypass surgery. *N Engl J Med* 2005; **353**: 249-254 [PMID: 16034010 DOI: 10.1056/NEJMoa043690]
9 **Kim A**, Snaith JR, Mahajan H, Holmes-Walker DJ. Nesidioblastosis following laparoscopic sleeve gastrectomy. *Clin Endocrinol (Oxf)* 2019; **91**: 906-908 [PMID: 31465534 DOI: 10.1111/cen.14083]
10 **Mulla CM**, Storino A, Yee EU, Lautz D, Sawnhey MS, Moser AJ, Patti ME. Insulinoma After Bariatric Surgery: Diagnostic Dilemma and Therapeutic Approaches. *Obes Surg* 2016; **26**: 874-881 [PMID: 26846121 DOI: 10.1007/s11695-016-2092-5]
11 **Gjeorgjievski M**, Imam Z, Cappell MS, Jamil LH, Kahaleh M. A Comprehensive Review of Endoscopic Management of Sleeve Gastrectomy Leaks. *J Clin Gastroenterol* 2021; **55**: 551-576 [PMID: 33234879 DOI: 10.1097/MCG.0000000000001451]
12 **Papamargaritis D**, Koukoulis G, Sioka E, Zachari E, Bargiota A, Zacharoulis D, Tzovaras G. Dumping symptoms and incidence of hypoglycaemia after provocation test at 6 and 12 months after laparoscopic sleeve gastrectomy. *Obes Surg* 2012; **22**: 1600-1606 [PMID: 22773085 DOI: 10.1007/s11695-012-0711-3]
13 **Scarpellini E**, Arts J, Karamanolis G, Laurenius A, Siquini W, Suzuki H, Ukleja A, Van Beek A, Vanuytsel T, Bor S, Ceppa E, Di Lorenzo C, Emous M, Hammer H, Hellström P, Laville M, Lundell L, Masclee A, Ritz P, Tack J. International consensus on the diagnosis and management of dumping syndrome. *Nat Rev Endocrinol* 2020; **16**: 448-466 [PMID: 32457534 DOI: 10.1038/s41574-020-0357-5]
14 **Xu F**, Wang KY, Wang N, Li G, Liu D. Bioactivity of a modified human Glucagon-like peptide-1. *PLoS One* 2017; **12**: e0171601 [PMID: 28152036 DOI: 10.1371/journal.pone.0171601]
15 **Navarro García MI**, González-Costea Martínez R, Torregrosa Pérez N, Romera Barba E, Periago MJ, Vázquez Rojas JL. Fasting ghrelin levels after gastric bypass and vertical sleeve gastrectomy: An analytic cohort study. *Endocrinol Diabetes Nutr (Engl Ed)* 2020; **67**: 89-101 [PMID: 31680051 DOI: 10.1016/j.endinu.2019.07.004]
16 **Wu HY**, Li NS, Song YL, Bai CM, Wang Q, Zhao YP, Xiao Y, Yu S, Li M, Chen YJ. Plasma levels of acylated ghrelin in patients with insulinoma and expression of ghrelin and its receptor in insulinomas. *Endocrine* 2020; **68**: 448-457 [PMID: 32124259 DOI: 10.1007/s12020-020-02233-4]
17 **Chauhan A**, Ramirez RA, Stevens MA, Burns LA, Woltering EA. Transition of a pancreatic neuroendocrine tumor from ghrelinoma to insulinoma: a case report. *J Gastrointest Oncol* 2015; **6**: E34-E36 [PMID: 25830049 DOI: 10.3978/j.issn.2078-6891.2014.113]
18 **Sheehan A**, Patti ME. Hypoglycemia After Upper Gastrointestinal Surgery: Clinical Approach to Assessment, Diagnosis, and Treatment. *Diabetes Metab Syndr Obes* 2020; **13**: 4469-4482 [PMID: 33239898 DOI: 10.2147/DMSO.S233078]
19 **Patti ME**, Goldfine AB, Hu J, Hoem D, Molven A, Goldsmith J, Schwesinger WH, La Rosa S, Folli F, Kulkarni RN. Heterogeneity of proliferative markers in pancreatic β-cells of patients with severe hypoglycemia following Roux-en-Y gastric bypass. *Acta Diabetol* 2017; **54**: 737-747 [PMID: 28512677 DOI: 10.1007/s00592-017-1001-2]
20 **Okabayashi T**, Shima Y, Sumiyoshi T, Kozuki A, Ito S, Ogawa Y, Kobayashi M, Hanazaki K. Diagnosis and management of insulinoma. *World J Gastroenterol* 2013; **19**: 829-837 [PMID: 23430217 DOI: 10.3748/wjg.v19.i6.829]
21 **Liu J**, Zhang CW, Hong DF, Wu J, Yang HG, Chen Y, Zhao DJ, Zhang YH. Laparoscope resection of retroperitoneal ectopic insulinoma: a rare case. *World J Gastroenterol* 2015; **21**: 4413-4418 [PMID: 25892896 DOI: 10.3748/wjg.v21.i14.4413]

World Journal of Clinical Cases

Submit a Manuscript: https://www.f6publishing.com

World J Clin Cases 2022 June 26; 10(18): 6234-6240

DOI: 10.12998/wjcc.v10.i18.6234

ISSN 2307-8960 (online)

CASE REPORT

Primary intestinal lymphangiectasia presenting as limb convulsions: A case report

Yun Cao, Xiao-Hong Feng, Hai-Xiang Ni

Specialty type: Gastroenterology and hepatology

Provenance and peer review: Unsolicited article; Externally peer reviewed.

Peer-review model: Single blind

Peer-review report's scientific quality classification

Grade A (Excellent): 0
Grade B (Very good): 0
Grade C (Good): C
Grade D (Fair): D
Grade E (Poor): 0

P-Reviewer: Choudhery MS, Pakistan; Panteris V, Greece

Received: November 26, 2021
Peer-review started: November 26, 2021
First decision: January 24, 2022
Revised: March 15, 2022
Accepted: April 29, 2022
Article in press: April 29, 2022
Published online: June 26, 2022

Yun Cao, Xiao-Hong Feng, Hai-Xiang Ni, Department of Endocrinology, The First Affiliated Hospital of Zhejiang Chinese Medical University (Zhejiang Provincial Hospital of Traditional Chinese Medicine), Hangzhou 310006, Zhejiang Province, China

Corresponding author: Xiao-Hong Feng, MD, Associate Professor, Department of Endocrinology, The First Affiliated Hospital of Zhejiang Chinese Medical University (Zhejiang Provincial Hospital of Traditional Chinese Medicine), No. 54 Youdian Road, Hangzhou 310006, Zhejiang Province, China. feng_xiaohong2021@163.com

Abstract

BACKGROUND

Primary intestinal lymphangiectasia (PIL) is a rare protein-losing enteropathy characterized by abnormally dilated lymphatic structures, resulting in leakage of lymph (rich in protein, lymphocytes, and fat) from the intestinal mucosal and submucosal layers and thus hypoproteinemia, lymphopenia, hypolipidemia, and pleural effusion.

CASE SUMMARY

A 19-year-old Chinese male patient complained of recurrent limb convulsions for the last 1 year. Laboratory investigations revealed low levels of calcium and magnesium along with hypoproteinemia and high parathyroid hormone levels, whereas gastroscopy exhibited chronic non-atrophic gastritis and duodenal lymphatic dilatation. Subsequent gastric biopsy showed moderate chronic inflammatory cell infiltration distributed around a small mucosal patch in the descending duodenum followed by lymphatic dilatation in the mucosal lamina propria, which was later diagnosed as PIL. The following appropriate medium-chain triglycerides nutritional support significantly improved the patient's symptoms.

CONCLUSION

Since several diseases mimic the clinical symptoms displayed by PIL, like limb convulsions, low calcium and magnesium, and loss of plasma proteins, it is imperative to conduct a detailed analysis to avoid any misdiagnosis while pinpointing the correct clinical diagnosis and simultaneously ruling out other clinical aspects in the reported cases without any past disease history. A careful assessment should always be made to ensure an accurate diagnosis in a timely manner so that the patient can be delivered quality health services for a positive health outcome.

Key Words: Protein-losing enteropathy; Primary intestinal lymphangiectasia; Limb convulsions; Adult; Case report

©The Author(s) 2022. Published by Baishideng Publishing Group Inc. All rights reserved.

Core Tip: In this case report, a 19-year-old Chinese male patient complained of recurrent limb convulsions for 1 year. Laboratory investigations revealed low levels of calcium and magnesium along with hypoproteinemia and high parathyroid hormone levels, but the patient had no limbs edema, which is rear in primary intestinal lymphangiectasia cases. Differential diagnosis is difficult in such case. Careful analysis and examination results finally enabled the patient to receive effective treatment after a definite diagnosis.

Citation: Cao Y, Feng XH, Ni HX. Primary intestinal lymphangiectasia presenting as limb convulsions: A case report. *World J Clin Cases* 2022; 10(18): 6234-6240
URL: https://www.wjgnet.com/2307-8960/full/v10/i18/6234.htm
DOI: https://dx.doi.org/10.12998/wjcc.v10.i18.6234

INTRODUCTION

Intestinal lymphangiectasia (IL) is a rare protein-losing enteropathy[1], characterized by small intestinal lymphatic drainage obstruction, chylous ascites, and villi distortion that further cause lymphatic congestion and elevate the lymphatic pressure, thereby resulting in leakage of lymph liquid into the small intestinal lumen. IL can be categorized into two forms, primary IL (PIL) and secondary IL (SIL). PIL, first reported by Milroy in 1892, is more common in children and adolescents, though rarely, it can also occur in adults and has a tendency to occur sporadically with an unknown etiology. Waldmann *et al*[2] in 1961 after demonstrating protein loss quantification by ^{51}Cr-labelled albumin revealed that the lymphatic vessels present in the mucosal and submucosal layers of the small intestine were abnormally dilated to varying degrees. Hence, this diagnosis came into existence.

The incidence of PIL is likely to be related to lymphatic dysplasia in infants which is more frequently diagnosed in children (less than 3 years old), but also in adolescents and even elderly cases[3]. Although in most cases lymphatic dilation is typically seen in the descending duodenum, lymphatic dilation in the small intestine is usually mild and segmental, and secondary causes should be excluded. In this case report, a 19-year-old adult man complained of limb convulsions for the past 1 year, which after further investigations, was later identified as PIL. The following medium-chain triglycerides (MCT) nutritional support improved the patient's condition.

CASE PRESENTATION

Chief complaints

A 19-year-old Chinese male patient complained of recurrent limb convulsions for the past 1 year.

History of present illness

The patient experienced recurrent limb convulsions and numbness with an unknown medical history in the absence of any aggravating factors like joint inflammation, edema, headache, dizziness, nausea and vomiting, abdominal distention, pain, or diarrhea, leading to a gradual weight loss by five kilograms, but due to the ignorance of the patient as well as his family, no further treatment was initiated. But 1 wk ago, his symptoms, comprising of limb convulsions and numbness, got so aggravated that he visited the community hospital in April 2021 for a thorough examination that was preceded by laboratory investigations that showed reduced levels of blood calcium 1.50 mmol/L (1.95 mmol/L after correction, normal range: 2.08-2.6 mmol/L), magnesium 0.49 mmol/L (normal range: 0.75-1.02 mmol/L), potassium 3.38 mmol/L (normal range: 3.5-5.5 mmol/L), and albumin 17.27 g/L (normal range: 40-55 g/L) while displaying increased parathyroid hormone (PTH) 113.0 pg/mL (normal range: 15-65 pg/mL). The patient had blood phosphorus at 1.12 mmol/L, TSH at 2.5 mIU/L, and a positive fecal occult blood test (FOBT). He was supplemented with albumin, calcium gluconate injections, and potassium magnesium aspartate. Henceforth, the persistent symptoms like limb convulsions and numbness were relieved after symptomatic treatment for 1 week. He went to the Endocrinology Department of our hospital for a further definite diagnosis.

History of past illness

The patient was healthy until the age of 18, with no trauma or any history of tumor.

Personal and family history

The patient was born by spontaneous labor at term, was breastfed in infancy, and had normal physical and cognitive development as his peers along with good academic performance. However, he had a history of hemorrhoids but did not have any long-term chronic abdominal pain and diarrhea in adolescence. His parents were healthy while denying any history of familial genetic disease, psychosis, and infection in the older family generations.

Physical examination

The patient's height was 174 cm, weight was 52 kg, and body mass index was 17.18 kg/m^2. He did not exhibit widening of either eye distance or base of the nose-bridge and small external ear while his abdomen was flat and soft, with no abdominal tenderness or rebound pain, non-palpable liver and spleen, normal bowel sounds, and limb strength. Especially, no concave edema was found in both lower limbs, whereas the Babinski's sign, Chvostek's sign, and Trousseau's sign were negative (Figure 1).

Laboratory examinations

The results of blood biochemistry were: Calcium 2.37 mmol/L (normal range: 2.08-2.6 mmol/L), magnesium 0.73 mmol/L (normal range: 0.75-1.02 mmol/L), potassium 4.19 mmol/L, phosphorus 1.19 mmol/L, parathyroid hormone 16.7 pg/mL (normal range: 15-65 pg/ mL), and albumin 25.2 g/L (normal range: 40-55 g/L). The FOBT was positive (1+).

The results of routine blood tests were: White blood cell count 3.8 x 10^9/L, lymphocyte count 0.41 x 10^9/L (normal range: 1.1 x 10^9/L-3.2 x 10^9/L), and lymphatic percentage 10.4% (normal range: 20%-50%)

The results of fat-soluble vitamin tests were: Vitamin A 0.28 μg/mL (normal range: 0.30-0.70 μg/mL), 25-hydroxyvitamin D 5.28 ng/mL (< 20 ng/mL suggesting deficiency), vitamin E 4.49 μg/mL (normal range: 0.30-0.70 μg/mL), and vitamin K1 0.12 ng/mL (normal range: 0.20-2.50 ng/mL).

The results of immunological tests were: Immunoglobulin (Ig)A 0.49 g/L (normal range: 0.82-4.53 g/L), IgG 1.44 g/L (normal range: 7.51-15.6 g/L), IgM 0.18 g/L(normal range: 0.46-3.04 g/L), complement (C)3 0.67 g/L (normal range: 0.79-1.52 g/L), C4 0.15 g/L (normal range: 0.16-0.38 g/L); transferrin 1.42 g/L (normal range: 2.0-3.6 g/L); copper orchid protein 10.70 mg/dL (normal range: 22-58 mg/dL); B cell count (CD19+) 38 x 10^6/L (normal range: 50 x 10^6/L-670 x 10^6/L), T cell count (CD3+CD45+) 179 x 10^6/L(normal range: 470 x 10^6/L-3270 x 106 /L), T helper count (CD3+CD4+) 46 x 10^6/L (normal range: 200 x 10^6/L-1820 x 10^6/L), T inhibitory cell count (CD3+CD8+) 120 x 10^6/L (normal range: 130 x 10^6/L-1350 x 10^6/L); the number of NK cells was normal.

The HIV + RPR panel was Negative, and blood and stool IBD screening showed no obvious abnormalities.

The patient had normal liver and kidney function, thyroid function, thyroglobulin, thyroglobulin antibody, and thyroid peroxidase antibody. The results of endocrine tests were: ACTH: 8 am 13.2 ng/L, 4 pm 12.6 ng/L, 0 am 5.3 ng/L; cortisol: 8 am 174.3 nmol/L, 4 pm 102.7 nmol/L, 0 am < 25 nmol/L; follicle stimulating hormone 5.98 IU/L, luteinizing hormone 7.74 IU/L, estradiol 98.38 pmol/L, testosterone 27.56 nmol/L; insulin-like growth factor-1 208 μg/L, and insulin-like growth factor binding protein-3 4.8 mg/L. Tumor markers, ANA spectrum, ANCA, rheumatoid factor, ESR, and hepatic fibrosis were all in the normal range. Urine immunoglobulin light chain, 24-h urine protein, and 24-h urine calcium within the normal range.

Imaging examinations

B-mode ultrasound imaging of the parathyroid gland revealed a hypo-echoic nodule with a clear boundary and regular shape along with few blood vessels (Figure 2). An MRI examination exhibited no obvious abnormality while an abnormal-signal nodule was found in front of the right middle abdominal psoas muscle, which was considered as an enlarged lymph node followed by a scanty exudate at the abdominal and pelvic cavity, along with cortical soft tissue edema. Capsule endoscopy showed the flat composition of duodenal mucosal villi with no obvious abnormality in the jejunal or ileal mucosa. Gastroscopy exhibited chronic non-atrophic gastritis and duodenal lymphatic dilatation (Figure 3). Subsequent gastric biopsy showed moderate chronic inflammatory cell infiltration distributed around a small mucosal patch in the descending duodenum followed by lymphatic dilatation in the mucosal lamina propria (Figure 4).

FINAL DIAGNOSIS

Finally, the patient was diagnosed with PIL (Figures 3 and 4).



DOI: 10.12998/wjcc.v10.i18.6234 **Copyright** ©The Author(s) 2022.

Figure 1 Normal lower limbs. No edema of the lower limbs was observed in the 19-year-old patient in this case.

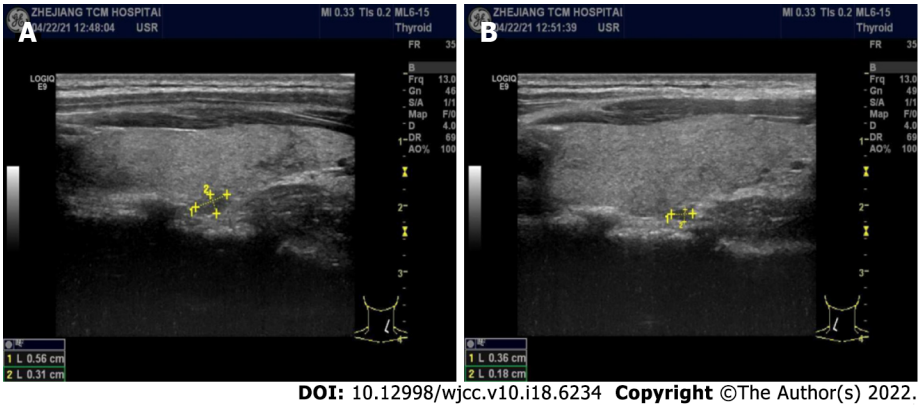

DOI: 10.12998/wjcc.v10.i18.6234 **Copyright** ©The Author(s) 2022.

Figure 2 Parathyroid gland ultrasound images. Hypoechoic nodules can be seen in the parathyroid gland, 0.56 cm x 0.31 cm on the right (A) and 0.36 cm x 0.18 cm on the left (B), with a clear boundary, regular shape, and few blood flow signals.

TREATMENT

The patient was treated with a low-fat, high-protein, light diet which contains 1800 calorie each day, and with MCT powder supplement, calcium supplement, and vitamin D supplement.

OUTCOME AND FOLLOW-UP

The patient returned to the clinic 3 mo later, and showed no symptoms of convulsion of the limbs. Meanwhile, blood calcium and albumin in the laboratory examination increased compared with the values before.

DISCUSSION

The clinical manifestations of PIL are diverse as they may cause dilatation of the intestinal lymphatic vessels, leading to loss of lymph fluid into the gastrointestinal tract. While it is mainly characterized by



DOI: 10.12998/wjcc.v10.i18.6234 **Copyright** ©The Author(s) 2022.

Figure 3 Gastroscopic image. Multiple white spots and patches can be clearly seen in the duodenum.

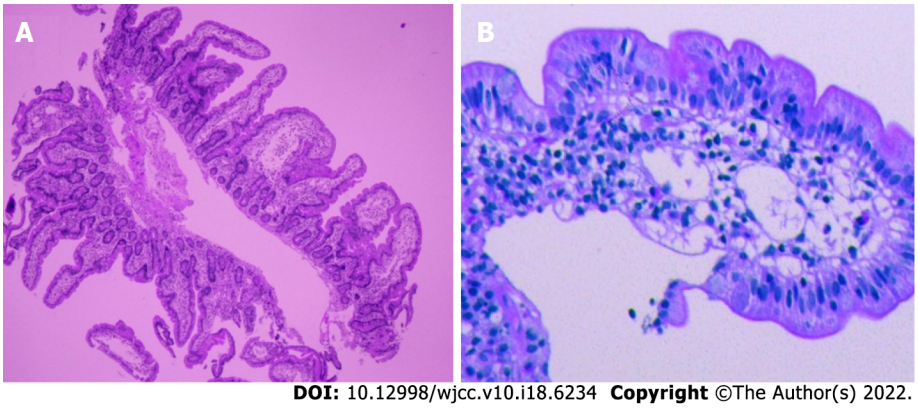

DOI: 10.12998/wjcc.v10.i18.6234 **Copyright** ©The Author(s) 2022.

Figure 4 Gastroscopic pathological images. A: Moderate chronic inflammatory cell infiltration distributed around a small mucosal patch in the descending duodenum (25 × magnification); B: The descending duodenum followed by lymphatic dilatation in the mucosal lamina propria (400 × magnification).

edema of varying degrees, it can also manifest as pleural effusion, pericarditis, chylous ascites, diarrhea, fat vitamin deficiency, weight loss, and other symptoms occurring in severe cases. In our case, due to unknown past medical history, diagnosing and providing prompt treatment were initially challenging as there was no clear history of diarrhea and abdominal pain, limb convulsions, or disease symptoms in childhood. The now obvious limb convulsions first appeared when the patient was 18 years of age and manifested themselves as hypocalcemia, hypomagneemia, and hypoproteinemia, along with elevated PTH levels. Due to similar propensity and characteristics, this disease can easily mimic pseudohypoparathyroidism (PHP) and some other similar diseases in internal medicine, which might lead to misdiagnosis and a plethora of unpleasant side effects. Therefore, the foremost thing that is recommended is to reach a definite diagnosis for a positive outcome.

Laboratory tests at presentation suggested hypocalcemia, hypomagneemia, hypoproteinemia, and lymphocytopenia. Further investigation revealed elevated PTH, decreased vitamin D, low immunoglobulinemia, and positive FOBT. First, the patient had hypocalcemia and hypomagnesemia, and the convulsions of the limbs were relieved by treatment with calcium gluconate and potassium magnesium aspartate. Elevated PTH and hypoproteinemia gave us the impression of renal insufficiency, but subsequent negative results of renal function and urinary protein precluded this diagnosis. Laboratory tests revealed normal liver function and negative rheumatoid and tumor markers, so we focused on the parathyroid gland. According to B-ultrasonography, hyperplasia of nodules, elevated PTH, and hypocalcemia were suggested, which first promoted us to consider a disease of endocrinology.

PHP is a genetic disease in which peripheral cells are resistant to PTH[4]. The central link of the disease is PTH resistance, which leads to high blood phosphorus and activation disorders of 25-(OH)D3, eventually leading to hypocalcaemia. Although this disease is common in women but more severe in men, the reported patients showed symptoms at 2 years of age, which became more obvious after the age of 10 but can rarely be seen in people aged 20 years or above. Tetany and intracranial calcification are usually the most common clinical manifestations and imaging features of PHP. PHP patients with

vitamin D deficiency have more severe clinical symptoms, and vitamin D deficiency increases the risk of autoimmune disease. Vitamin D is mainly synthesized in the skin of the body, and then converted into 25-(OH)D by the hydroxylation of 25-hydroxylase (CYP27A1) in the liver, which is the main form of vitamin D in the circulation. 25-(OH)D binds to vitamin D binding protein into the blood circulation and generates active metabolite 1,25-(OH)2D under the catalysis of renal 1αhydroxylase (CYP27B1). 1,25-(OH)2D acts on the intestine, kidney, and bone to regulate the metabolism of calcium and phosphorus. In the small intestine, 1,25-(OH)2D promotes the absorption of calcium and phosphorus, and serum 25-(OH)D is inversely proportional to PTH. When the serum 25-(OH)D level decreases, blood calcium decreases and PTH increases. The increased PTH stimulates the activity of 1αhydroxylase and increases the efficiency of 25-(OH)D conversion to 1,25-(OH)2D. In addition, PTH also normalizes blood calcium levels by stimulating osteoclast proliferation, and increasing bone absorption and calcium release. In this case, the patient had low calcium, with a compensatory increase of PTH, and the blood phosphorus level was within the normal range during the onset. The reexamination of PTH returned to normal during the further correction of low calcium, proving that it was a secondary factor, so PHP could be excluded. Parathyroid nodules were also considered nonfunctional.

Considering the possibility of protein-loss enteropathy, subsequent gastroscopy revealed duodenal lymphatic dilation, confirming our assessment. IL could be divided into primary and secondary types. Primary IL is a congenital lesion with an ambiguous incidence rate and disease mechanism though occurring more sporadically despite the involvement of genetic factors in the pathogenesis[5], whereas secondary IL can be caused by several factors as autoimmune diseases (*i.e.*, Crohn's disease[6], ulcerative colitis[7], and Henoch-Schonlein purpura), tumors (such as non-Hodgkin's lymphoma[8]), infections (such as rotavirus), portal hypertension, constrictive pericarditis[9], trauma, or surgical injury [10]. In our case report, Crohn's disease was first excluded as FOBT results showed 1+ repeatedly while blood and stool IBD screening was negative. As the patient had a previous history of hemorrhoids, the anorectal department considered it as hemorrhoid bleeding after the consultation.

Some PIL patients are found with abnormal immune system responses in which the decrease of B cells is manifested by the decreasing IgG, IgA, and IgM levels[11]. Some previous studies also reported that PIL patients' peripheral blood samples contain a very low number of $CD4^+$ T cells[12] that were significantly lesser than B cells, while the remaining $CD4^+$ T cells became highly differentiated and sensitized, thereby showing poor proliferation[13]. It was also observed that the patient's T lymphocytes kept on decreasing in varying degrees in this case. Further evidence will be necessary to determine whether T lymphocytes mediate the immune functions in the intestine, and further lead to the occurrence and development of the disease.

Since the PIL etiology is ambiguous and standardized treatment is inadequate, a study by Alfano *et al* [14] revealed that the primary goal of PIL treatment is to reduce protein loss, maintain circulating blood volume, and inhibit excessive tissue fluid production, thereby indicating that pharmacological treatment is the first-line treatment prescribed in the clinic. In the gastrointestinal tract, MCT is decomposed into glycerol and medium-chain fatty acids that are directly absorbed in the portal vein blood flow by small intestinal epithelial cells without going through lymphatic vessels, thus reducing the pressure in lymphatic vessels, lymph leakage, and protein loss. Incorporating an MCT-rich diet in daily life could significantly improve the symptoms and long-term mortality of PIL patients, although it might not improve the inherent lymphatic abnormalities; thus, the patients might need to take the required medications for a longer period of time.

CONCLUSION

Based on this case, PIL as a potential diagnosis should be considered even in the absence of any adolescent-illness history for adults with recurrent limb convulsions, low calcium and magnesium, hypoproteinemia, and high PTH levels. MCT diet, as a dietary supplement, can effectively improve the clinical symptoms of PIL patients while providing pharmacotherapy after the final diagnosis was made by a thorough detailed analysis.

FOOTNOTES

Author contributions: Cao Y and Feng XH contributed to literature review and manuscript drafting; Cao Y and Ni HX contributed to patient management and data analysis; and all authors approved the final article and assured all the questions regarding the accuracy of the article.

Informed consent statement: The patient consented to his case being published anonymously.

Conflict-of-interest statement: The authors declare that they have no conflicts of interest to disclose.

CARE Checklist (2016) statement: The authors have read the CARE Checklist (2016), and the manuscript was

prepared and revised according to the CARE Checklist (2016).

Open-Access: This article is an open-access article that was selected by an in-house editor and fully peer-reviewed by external reviewers. It is distributed in accordance with the Creative Commons Attribution NonCommercial (CC BY-NC 4.0) license, which permits others to distribute, remix, adapt, build upon this work non-commercially, and license their derivative works on different terms, provided the original work is properly cited and the use is non-commercial. See: https://creativecommons.org/Licenses/by-nc/4.0/

Country/Territory of origin: China

ORCID number: Yun Cao 0000-0002-8788-6312; Xiao-Hong Feng 0000-0002-8991-9384; Hai-Xiang Ni 0000-0002-7005-4851.

S-Editor: Ma YJ
L-Editor: Wang TQ
P-Editor: Ma YJ

REFERENCES

1 **Vardy PA**, Lebenthal E, Shwachman H. Intestinal lymphagiectasia: a reappraisal. *Pediatrics* 1975; **55**: 842-851 [PMID: 1134884]
2 **Waldmann TA**, Steinfeld JL, Dutcher TF, Davidson JD, Gordon RS. The role of the gastrointestinal system in "idiopathic hypoproteinemia". *Gastroenterology* 1961; **41**: 197-207 [PMID: 13782654 DOI: 10.1016/S0016-5085(19)35130-3]
3 **Dong J**, Xin J, Shen W, Wen T, Chen X, Sun Y, Wang R. CT Lymphangiography (CTL) in Primary Intestinal Lymphangiectasia (PIL): A Comparative Study with Intraoperative Enteroscopy (IOE). *Acad Radiol* 2019; **26**: 275-281 [PMID: 29885759 DOI: 10.1016/j.acra.2018.04.023]
4 **Bastepe M**. The GNAS locus and pseudohypoparathyroidism. *Adv Exp Med Biol* 2008; **626**: 27-40 [PMID: 18372789 DOI: 10.1007/978-0-387-77576-0_3]
5 **Wen J**, Tang Q, Wu J, Wang Y, Cai W. Primary intestinal lymphangiectasia: four case reports and a review of the literature. *Dig Dis Sci* 2010; **55**: 3466-3472 [PMID: 20198428 DOI: 10.1007/s10620-010-1161-1]
6 **Steinfeld JL**, Davidson JD, Gordon RS, Greene FE. The mechanism of hypoproteinemia in patients with regional enteritis and ulcerative colitis. *Am J Med* 1960; **29**: 405-415 [PMID: 13834226 DOI: 10.1016/0002-9343(60)90036-x]
7 **Ungaro R**, Babyatsky MW, Zhu H, Freed JS. Protein-losing enteropathy in ulcerative colitis. *Case Rep Gastroenterol* 2012; **6**: 177-182 [PMID: 22679407 DOI: 10.1159/000338191]
8 **Chieng JH**, Garrett J, Ding SL, Sullivan M. Clinical presentation and endoscopic features of primary gastric Burkitt lymphoma in childhood, presenting as a protein-losing enteropathy: a case report. *J Med Case Rep* 2009; **3**: 7256 [PMID: 19830151 DOI: 10.4076/1752-1947-3-7256]
9 **Petersen VP**, Hastrup J. Protein-losing enteropathy in constrictive pericarditis. *Acta Med Scand* 1963; **173**: 401-410 [PMID: 13942764 DOI: 10.1111/j.0954-6820.1963.tb17423.x]
10 **Hourigan SK**, Anders RA, Mitchell SE, Schwarz KB, Lau H, Karnsakul W. Chronic diarrhea, ascites, and protein-losing enteropathy in an infant with hepatic venous outflow obstruction after liver transplantation. *Pediatr Transplant* 2012; **16**: E328-E331 [PMID: 22489846 DOI: 10.1111/j.1399-3046.2012.01686.x]
11 **Heresbach D**, Raoul JL, Genetet N, Noret P, Siproudhis L, Ramée MP, Bretagne JF, Gosselin M. Immunological study in primary intestinal lymphangiectasia. *Digestion* 1994; **55**: 59-64 [PMID: 7509299 DOI: 10.1159/000201124]
12 **Fuss IJ**, Strober W, Cuccherini BA, Pearlstein GR, Bossuyt X, Brown M, Fleisher TA, Horgan K. Intestinal lymphangiectasia, a disease characterized by selective loss of naive CD45RA+ lymphocytes into the gastrointestinal tract. *Eur J Immunol* 1998; **28**: 4275-4285 [PMID: 9862365 DOI: 10.1002/(SICI)1521-4141(199812)28:12<4275::AID-IMMU4275>3.0.CO;2-P]
13 **Grant E**, Junker A. Nine-year-old girl with lymphangiectasia and chest pain. *Pediatr Infect Dis J* 2005; **24**: 659, 663-664 [PMID: 15999019 DOI: 10.1097/01.inf.0000168847.56321.cb]
14 **Alfano V**, Tritto G, Alfonsi L, Cella A, Pasanisi F, Contaldo F. Stable reversal of pathologic signs of primitive intestinal lymphangiectasia with a hypolipidic, MCT-enriched diet. *Nutrition* 2000; **16**: 303-304 [PMID: 10758368 DOI: 10.1016/s0899-9007(00)00223-9]

World Journal of Clinical Cases

Submit a Manuscript: https://www.f6publishing.com

World J Clin Cases 2022 June 26; 10(18): 6241-6246

DOI: 10.12998/wjcc.v10.i18.6241

ISSN 2307-8960 (online)

CASE REPORT

Esophagogastric junctional neuroendocrine tumor with adenocarcinoma: A case report

Zhen-Zhen Kong, Lu Zhang

Specialty type: Medicine, research and experimental

Provenance and peer review: Unsolicited article; Externally peer reviewed.

Peer-review model: Single blind

Peer-review report's scientific quality classification

Grade A (Excellent): 0
Grade B (Very good): 0
Grade C (Good): C, C, C
Grade D (Fair): D, D
Grade E (Poor): 0

P-Reviewer: Casella C, Italy; Chiba H, Japan; Hunasanahalli Giriyappa V, India; Mohamed SY, Egypt; Viswanath Y, United Kingdom

Received: November 30, 2021
Peer-review started: November 30, 2021
First decision: March 11, 2022
Revised: March 16, 2022
Accepted: April 27, 2022
Article in press: April 27, 2022
Published online: June 26, 2022

Zhen-Zhen Kong, Lu Zhang, Department of Gastroenterology, The First Affiliated Hospital of Zhejiang Chinese Medical University, Hangzhou 310000, Zhejiang Province, China

Corresponding author: Lu Zhang, Department of Gastroenterology, The First Affiliated Hospital of Zhejiang Chinese Medical University, No. 54 Post Road, Shangcheng District, Hangzhou 310000, Zhejiang Province, China. zl06302021@163.com

Abstract

BACKGROUND

At present, cases of esophageal neuroendocrine tumors combined with cardia adenocarcinoma are extremely rare worldwide, and there are no clinical reports. Herein, we describe such a case for clinical reference.

CASE SUMMARY

The presence of cardia cancer and esophageal neuroendocrine tumors in a single patient has not yet been reported. The patient in this case underwent prompt endoscopic treatment and additional surgical resection. Pathology revealed the following: The distance between the cardia cancer and the esophageal neuroendocrine tumors was small, approximately 3 mm. Vascular invasion was observed. The esophageal neuroendocrine tumor was determined to be grade G3. According to the treatment guidelines, after the patient received an explanation of their condition, additional surgical procedures were provided in a timely manner. Early detection and early treatment can successfully prolong survival and improve the quality of life of patients.

CONCLUSION

Early detection and early treatment can successfully prolong survival and improve the quality of life of such patients.

Key Words: Esophageal neuroendocrine tumor; Cardia moderately differentiated adenocarcinoma; Endoscopic treatment; Surgery; Pathology; Case report

©The Author(s) 2022. Published by Baishideng Publishing Group Inc. All rights reserved.

Core Tip: Cases of esophageal neuroendocrine tumors combined with moderately differentiated gastric cardia adenocarcinoma are very rare. Pathology is the gold standard for diagnosis. Endoscopy and additional surgical resection proved to be successful in our case. Early detection and early treatment are both of great significance to the life and health of patients. Considering the successful resection of this case, we provide this case report to serve as a clinical reference.

Citation: Kong ZZ, Zhang L. Esophagogastric junctional neuroendocrine tumor with adenocarcinoma: A case report. *World J Clin Cases* 2022; 10(18): 6241-6246
URL: https://www.wjgnet.com/2307-8960/full/v10/i18/6241.htm
DOI: https://dx.doi.org/10.12998/wjcc.v10.i18.6241

INTRODUCTION

At present, cases of esophageal neuroendocrine tumors (NETs) combined with cardia adenocarcinoma are extremely rare worldwide. The presence of cardia cancer and esophageal NETs (E-NETs) in a single patient has not yet been reported. Herein, we describe such a case for clinical reference.

CASE PRESENTATION

Chief complaints

A 76-year-old man was hospitalized due to the presence of a cardia mass.

History of present illness

Previous gastroscopy showed a 0-IIa-like cardia lesions and chronic atrophic gastritis with erosions. The pathological examination revealed the following: Tubular adenoma with high-grade intraepithelial neoplasia; mild chronic atrophic gastritis of the antrum; intestinal metaplasia; and *Helicobacter pylori* infection (Figure 1).

History of past illness

The patient's medical history was unremarkable.

Personal and family history

The patient's personal/family history was unremarkable.

Physical examination

No remarkable characteristics were found during the physical examination.

Laboratory examinations

The laboratory results were all normal.

Imaging examinations

Previous gastroscopy showed a 0-IIa-like lesion of the cardia and chronic atrophic gastritis with erosions. Enhanced computed tomography scan of the full abdomen was performed after hospitalization, which revealed that the local gastric wall of the gastric cardia was slightly thickened, no significantly enlarged lymph node shadow was seen around the cardia, and the rest of the region appeared unchanged (Figures 2-4).

FINAL DIAGNOSIS

The final diagnosis was differentiated cardia adenocarcinoma and E-NET (G3).

TREATMENT

Endoscopic submucosal dissection and surgical resection were performed.

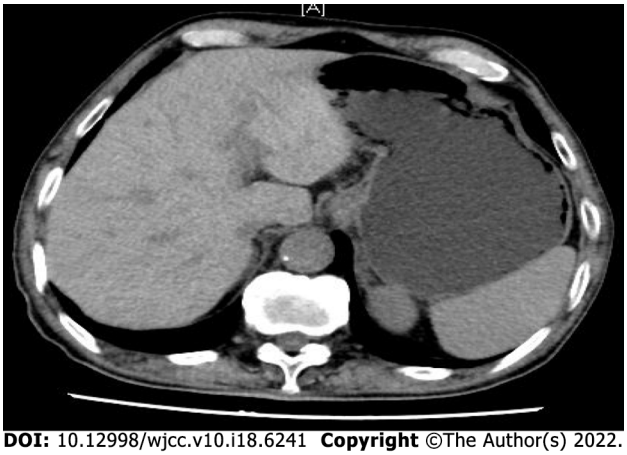

DOI: 10.12998/wjcc.v10.i18.6241 **Copyright** ©The Author(s) 2022.

Figure 1 Full abdominal enhanced computed tomography.

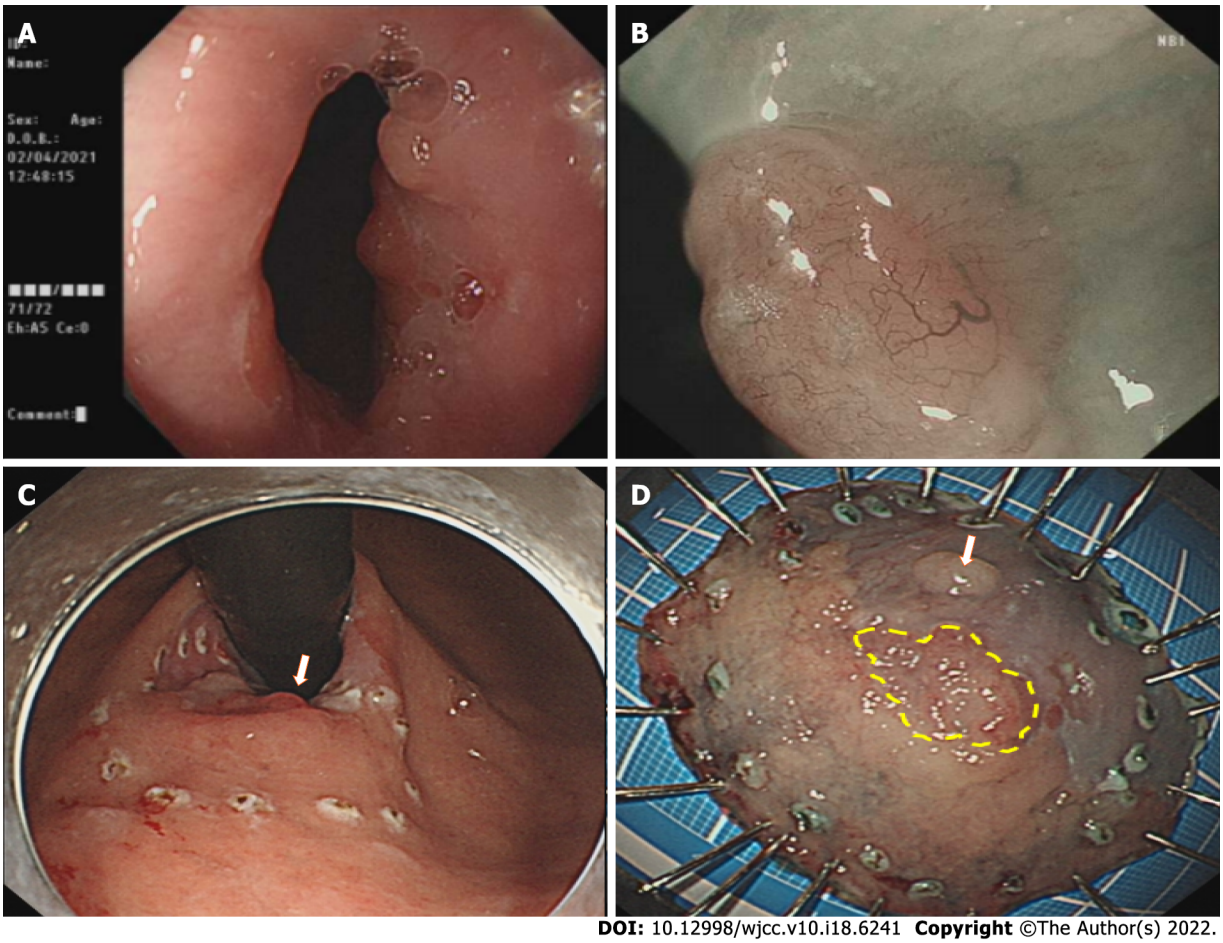

DOI: 10.12998/wjcc.v10.i18.6241 **Copyright** ©The Author(s) 2022.

Figure 2 Endoscopic submucosal dissection. A: Cardia mass; B: Submucosal injection; C: Tick to mark the lesion area; D: Lesion specimen.

OUTCOME AND FOLLOW-UP

The patient was in good general condition without obvious discomfort (Figures 5 and 6).

DISCUSSION

NENs are a group of highly heterogeneous tumors originating from neuroendocrine cells. They can occur in many parts of the body but are most often found in the digestive system, followed by the lungs.

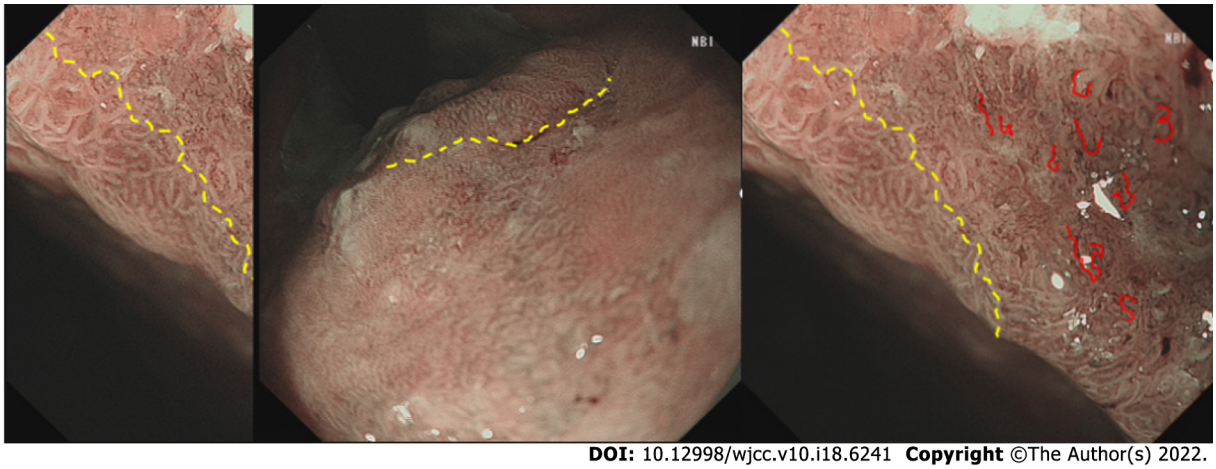

DOI: 10.12998/wjcc.v10.i18.6241 **Copyright** ©The Author(s) 2022.

Figure 3 Narrow-band imaging.

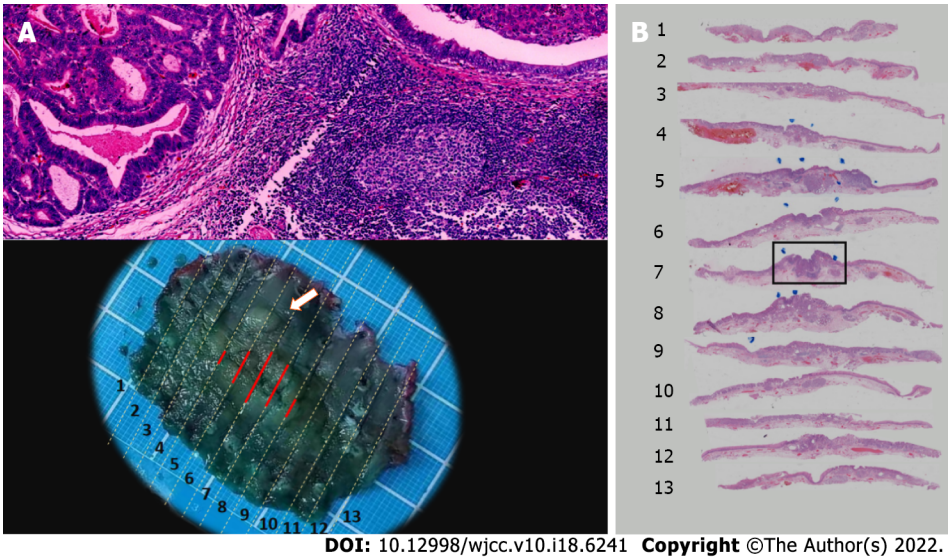

DOI: 10.12998/wjcc.v10.i18.6241 **Copyright** ©The Author(s) 2022.

Figure 4 Pathology of cardia endoscopic submucosal dissection specimens. A: Moderately differentiated adenocarcinoma of the cardia; B: Esophageal neuroendocrine tumors (G3).

E-NETs are very rare[1], accounting for only 1.4% of all gastrointestinal pancreatic tumors[2] and 0.15%-2.80% of all esophageal tumors[3]. This is due to the poor development of the neuroendocrine system in this area of the body[2]. The incidence rate varies across countries[4]; these tumors are more commonly found in Asian countries than in Western countries[5]. Studies have found that smoking (present in 49%) and drinking (present in 31%) may be a high-risk factor[6,7]. At present, cases of E-NETs combined with cardia adenocarcinoma are extremely rare worldwide, and there are no clinical reports.

Pathology is the gold standard for the diagnosis of NETs. The proliferation activity of tumor cells can be evaluated by the number of mitotic figures or the Ki-67 index. According to the 2019 WHO classification standards, NETs are divided into three grades: G1, G2, and G3. The classification criteria are as follows: G1 is defined as < 2 mitotic cells/10 high-power fields (HPFs), G2 as 2-20 cells/10 HPFs, and G3 as > 20 cells/10 HPFs. The Ki-67 index is classified as follows: G1, ≤ 2%; G2, 3%-20%; and G3, > 20%[8]. When the Ki-67 index is inconsistent with the mitotic cell classification, it can instead be classified as high or low. DAXX/ATRX and p53/RB mutations can be used to distinguish G3 NETs from neuroendocrine carcinomas (NECs). According to the guidelines, NETs are < 1 cm in size, are grade G1/G2, have a low metastasis rate (< 3%), and do not infiltrate into the muscularis propria (T1 stage). Thus, they are suitable for endoscopic treatment. For tumors or NECs more than 2 cm in diameter, the metastasis rate can reach as high as 60% to 80%, so radical resection is the first choice.

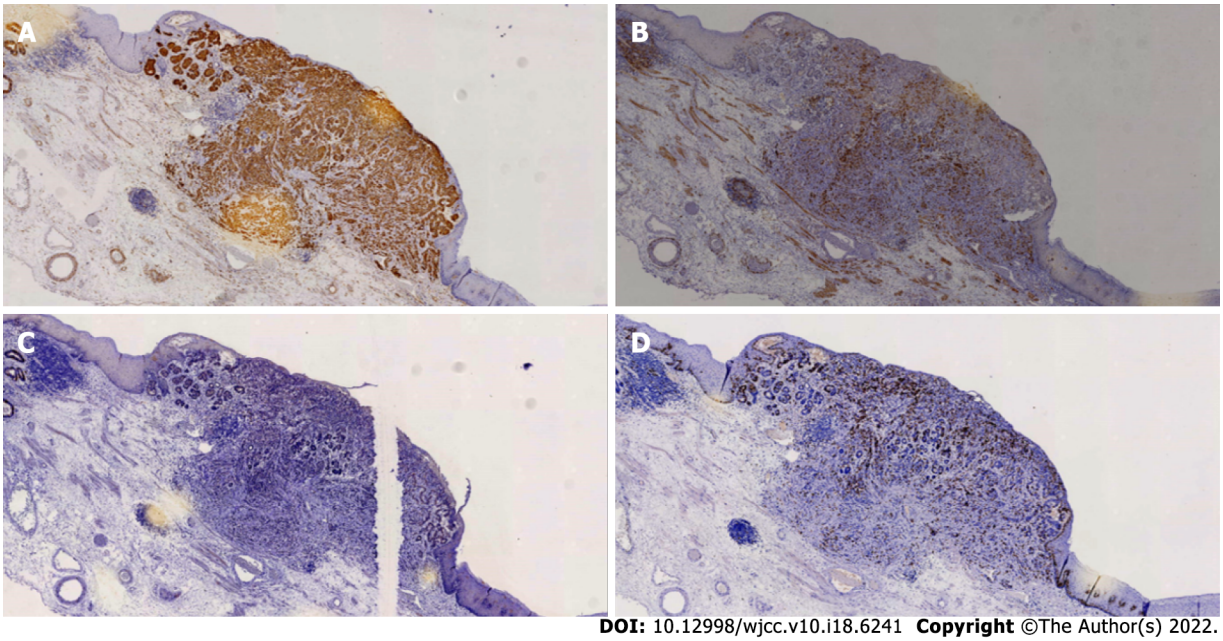

DOI: 10.12998/wjcc.v10.i18.6241 **Copyright** ©The Author(s) 2022.

Figure 5 Immunohistochemical staining of esophageal neuroendocrine tumors. A: Syn; B: CD56; C: CgA; D: Ki-67 (25%+).

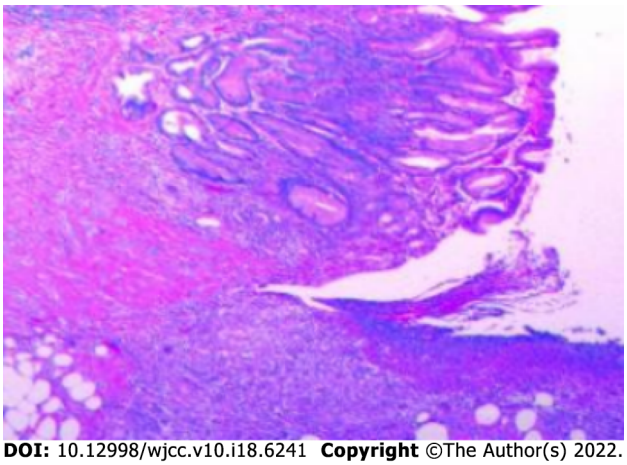

DOI: 10.12998/wjcc.v10.i18.6241 **Copyright** ©The Author(s) 2022.

Figure 6 Representative pathology of excised gastric specimens.

CONCLUSION

A case of cardia adenocarcinoma combined with E-NETs has not yet been reported. In our patient, after timely endoscopic treatment, pathology revealed that the distance between the cardia cancer and the E-NETs was small, approximately 3 mm, vascular invasion was observed, and the E-NET was determined to be grade G3. According to the treatment guidelines, after the patient received an explanation of their condition, additional surgical procedures were provided in a timely manner. Complete resection of the lesion significantly improved the patient's quality of life.

FOOTNOTES

Author contributions: Kong ZZ was involved in writing the article; Zhang L was involved in the conception of the study; all authors read and approved the final manuscript.

Supported by Zhejiang Provincial Department of Health Clinical Research Application Project, No. 2022KY924; and General Project of Zhejiang Provincial Department of Health, No. 2021KY835.

Informed consent statement: Informed written consent was obtained from the patient for publication of this report and any accompanying images.

Conflict-of-interest statement: The authors declare that they have no conflicts of interest to disclose.

CARE Checklist (2016) statement: The authors have read the CARE Checklist (2016), and the manuscript was prepared and revised according to the CARE Checklist (2016).

Open-Access: This article is an open-access article that was selected by an in-house editor and fully peer-reviewed by external reviewers. It is distributed in accordance with the Creative Commons Attribution NonCommercial (CC BY-NC 4.0) license, which permits others to distribute, remix, adapt, build upon this work noncommercially, and license their derivative works on different terms, provided the original work is properly cited and the use is noncommercial. See: https://creativecommons.org/Licenses/by-nc/4.0/

Country/Territory of origin: China

ORCID number: Zhen-Zhen Kong 0000-0002-2177-0974; Lu Zhang 0000-0001-7726-4846.

S-Editor: Fan JR
L-Editor: Wang TQ
P-Editor: Fan JR

REFERENCES

1 **Chin YP**, Lai WF, Chiang MT, Chang SC. Esophageal neuroendocrine tumor with initial presentation as painless forehead and neck masses: A case report. *Medicine (Baltimore)* 2017; **96**: e9282 [PMID: 29390385 DOI: 10.1097/MD.0000000000009282]
2 **Lee CG**, Lim YJ, Park SJ, Jang BI, Choi SR, Kim JK, Kim YT, Cho JY, Yang CH, Chun HJ, Song SY; Neuroendocrine tumor study group. The clinical features and treatment modality of esophageal neuroendocrine tumors: a multicenter study in Korea. *BMC Cancer* 2014; **14**: 569 [PMID: 25098730 DOI: 10.1186/1471-2407-14-569]
3 **Weinberg JS**, Suki D, Hanbali F, Cohen ZR, Lenzi R, Sawaya R. Metastasis of esophageal carcinoma to the brain. *Cancer* 2003; **98**: 1925-1933 [PMID: 14584076 DOI: 10.1002/cncr.11737]
4 **Egashira A**, Morita M, Kumagai R, Taguchi KI, Ueda M, Yamaguchi S, Yamamoto M, Minami K, Ikeda Y, Toh Y. Neuroendocrine carcinoma of the esophagus: Clinicopathological and immunohistochemical features of 14 cases. *PLoS One* 2017; **12**: e0173501 [PMID: 28288180 DOI: 10.1371/journal.pone.0173501]
5 **Sorbye H**, Welin S, Langer SW, Vestermark LW, Holt N, Osterlund P, Dueland S, Hofsli E, Guren MG, Ohrling K, Birkemeyer E, Thiis-Evensen E, Biagini M, Gronbaek H, Soveri LM, Olsen IH, Federspiel B, Assmus J, Janson ET, Knigge U. Predictive and prognostic factors for treatment and survival in 305 patients with advanced gastrointestinal neuroendocrine carcinoma (WHO G3): the NORDIC NEC study. *Ann Oncol* 2013; **24**: 152-160 [PMID: 22967994 DOI: 10.1093/annonc/mds276]
6 **Wu IC**, Chu YY, Wang YK, Tsai CL, Lin JC, Kuo CH, Shih HY, Chung CS, Hu ML, Sun WC, Wang JP, Wang HP. Clinicopathological features and outcome of esophageal neuroendocrine tumor: A retrospective multicenter survey by the digestive endoscopy society of Taiwan. *J Formos Med Assoc* 2021; **120**: 508-514 [PMID: 32600867 DOI: 10.1016/j.jfma.2020.06.024]
7 **Huang Q**, Wu H, Nie L, Shi J, Lebenthal A, Chen J, Sun Q, Yang J, Huang L, Ye Q. Primary high-grade neuroendocrine carcinoma of the esophagus: a clinicopathologic and immunohistochemical study of 42 resection cases. *Am J Surg Pathol* 2013; **37**: 467-483 [PMID: 23426118 DOI: 10.1097/PAS.0b013e31826d2639]
8 **Nagtegaal ID**, Odze RD, Klimstra D, Paradis V, Rugge M, Schirmacher P, Washington KM, Carneiro F, Cree IA; WHO Classification of Tumours Editorial Board. The 2019 WHO classification of tumours of the digestive system. *Histopathology* 2020; **76**: 182-188 [PMID: 31433515 DOI: 10.1111/his.13975]

World Journal of Clinical Cases

Submit a Manuscript: https://www.f6publishing.com

World J Clin Cases 2022 June 26; 10(18): 6247-6253

DOI: 10.12998/wjcc.v10.i18.6247

ISSN 2307-8960 (online)

CASE REPORT

Foreign body granuloma in the tongue differentiated from tongue cancer: A case report

Zhen-Hua Jiang, Ran Xv, Li Xia

Specialty type: Medicine, general and internal

Provenance and peer review: Unsolicited article; Externally peer reviewed.

Peer-review model: Single blind

Peer-review report's scientific quality classification

Grade A (Excellent): 0
Grade B (Very good): B, B
Grade C (Good): 0
Grade D (Fair): 0
Grade E (Poor): 0

P-Reviewer: Saleem S, Pakistan; Zahed M, Iran

Received: December 7, 2021
Peer-review started: December 7, 2021
First decision: January 25, 2022
Revised: February 12, 2022
Accepted: April 20, 2022
Article in press: April 20, 2022
Published online: June 26, 2022

Zhen-Hua Jiang, Ran Xv, Li Xia, Department of Otolaryngology - Head and Neck Surgery, Mianyang Central Hospital, School of Medicine, University of Electronic Science and Technology of China, Mianyang 621000, Sichuan Province, China

Corresponding author: Li Xia, MD, Chief Doctor, Department of Otolaryngology - Head and Neck Surgery, Mianyang Central Hospital, School of Medicine, University of Electronic Science and Technology of China, No. 12 Changjia Lane, Mianyang 621000, Sichuan Province, China. hsialy@sina.com

Abstract

BACKGROUND

Embedded foreign bodies in the tongue are rarely seen in clinical settings. An untreated foreign body can cause a granuloma which often presents as an enlarged tongue mass. However, if foreign body ingestion status is unknown, physical examination and magnetic resonance imaging (MRI) tend to lead to suspicion of tongue cancer, especially in older patients. Thus, differential diagnosis of an enlarged tongue mass is important, especially because it is closely related to the choice of treatment method.

CASE SUMMARY

A 61-year-old woman was admitted to the hospital with pain and noticeable swelling in the tongue that had persisted for over 1 mo. She had no previous medical history. MRI revealed abnormal signal intensities that were indicative of a neoplasm. Thus, the oral surgeon and radiologist arrived at a primary diagnosis of tongue cancer. The patient visited the Ear Nose and Throat Department for further consultation and underwent an ultrasound examination of the tongue. The ultrasonography was consistent with a linear hyperechoic foreign body which was indicative of an embedded foreign body (bone) in the tongue, even though the patient denied any history of foreign body ingestion. Complete surgical enucleation of the lesion was conducted. The mass which included a fish bone was completely removed. The post-operative pathological examination confirmed that the mass was a granuloma containing collagen fibers, macrophages and chronic inflammatory cells. The patient recovered without complications over a 2 mo follow-up period.

CONCLUSION

We report a rare case of foreign body granuloma in the tongue that was primarily diagnosed as tongue cancer. The MRI and ultrasound examinations revealed a

piece of bone in the left lateral aspect of the tongue. The granuloma, which contained a fish bone, was completely removed *via* surgery and confirmed *via* biopsy. Differential diagnosis of the enlarged tongue mass was critical to the selection of treatment method.

Key Words: Tongue; Foreign body; Granuloma; Cancer; Differential diagnosis; Case report

©The Author(s) 2022. Published by Baishideng Publishing Group Inc. All rights reserved.

Core Tip: This case report concerns an older adult referred to our Ear Nose and Throat Department with an enlarged tongue mass and a primary diagnosis of tongue cancer after magnetic resonance imaging (MRI). A review of the MRI data and oral ultrasound examination diagnosed a foreign body granuloma, confirmed by surgery and postoperative pathological examination. Oral ultrasound and/or computed tomography are critical in terms of differential diagnosis; certain MRI features may provide clues guiding diagnosis of a foreign body granuloma.

Citation: Jiang ZH, Xv R, Xia L. Foreign body granuloma in the tongue differentiated from tongue cancer: A case report. *World J Clin Cases* 2022; 10(18): 6247-6253
URL: https://www.wjgnet.com/2307-8960/full/v10/i18/6247.htm
DOI: https://dx.doi.org/10.12998/wjcc.v10.i18.6247

INTRODUCTION

The introduction of a foreign body into the tongue can occasionally occur as food is being chewed. In most situations this can lead to pain, swelling and irritation[1]. Such foreign bodies can usually be identified and diagnosed *via* visual inspection, especially if they are not buried in the muscle layer[2]. A clear history of foreign body introduction into the mouth, as well as a timely visit to the physician, can be conducive to the diagnosis[3]. Penetration of the tongue by a foreign substance can cause an acute inflammatory response and foreign bodies that remain in place may elicit a granulomatous inflammatory response[4]. The cause of granuloma in the tongue can be difficult to ascertain, especially without a clear history of foreign body ingestion. In this paper, we describe the case of a foreign body granuloma in the tongue of a Chinese woman. The initial diagnosis was tongue cancer but further examination revealed a foreign body in the tongue which was removed *via* surgery.

CASE PRESENTATION

Chief complaints

A 61-year-old woman was admitted to the Ear Nose and Throat (ENT) Department of our hospital complaining of pain and noticeable swelling of the tongue.

History of present illness

The patient sought out a general practitioner because of pain and noticeable swelling in the tongue that persisted for over 1 mo. She was given a short course of antibiotics which provided no symptom relief. The patient was referred to the Department of Stomatology, where an oral surgeon prescribed oral maxillofacial magnetic resonance imaging (MRI). The imaging revealed abnormal signal intensities, as shown in Figure 1, which are indicative of tongue cancer. The patient then visited the ENT Department for further consultation.

History of past illness

The patient had no previous medical history.

Personal and family history

There was no specific personal and family history.

Physical examination

Intraoral examination showed mild swelling in a longitudinal 2 cm × 1.5 cm area on the left lateral aspect of the tongue. A hardened nodule with an ill-defined margin was found on the tongue. The nodule was the same color as the surrounding tongue tissue (normal color) and no clearly identifiable

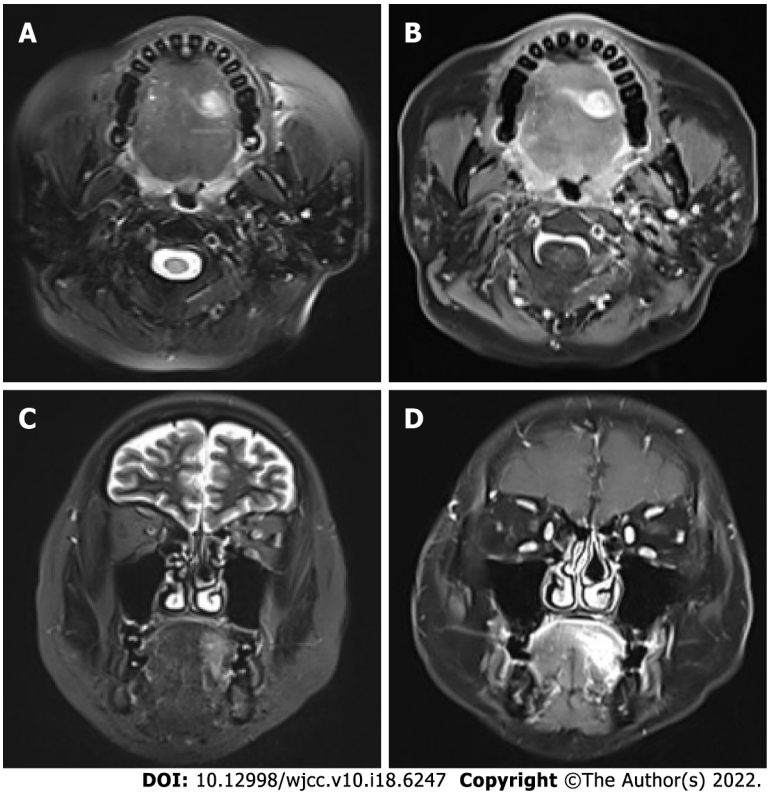

DOI: 10.12998/wjcc.v10.i18.6247 **Copyright** ©The Author(s) 2022.

Figure 1 Magnetic resonance imaging indicated an abnormal signal intensity on the left side of the tongue. A-D: T2-weighted magnetic resonance imaging (MRI) revealed a hyperintense shadow and contrast-enhanced T1-weighted MRI obvious enhancement of the mass in the transverse (A and B) and coronal planes (C and D). Scale bar: 2 cm.

foreign bodies were observed on the tongue as shown in Figure 2.

Laboratory examinations

The results of routine tests of complete blood count, kidney function and liver function were normal.

Imaging examinations

The oral maxillofacial MRI showed abnormal and ill-defined signal intensities on the left side of the tongue (size: 1.6 cm × 1.2 cm × 2.0 cm; Figure 1) and multiple swollen cervical lymph nodes (up to 0.7 cm in size, in the submaxillary region and carotid sheath). The primary diagnosis was tongue cancer as reported by the specialists in the Department of Radiology. However, the doctors in the ENT Department reviewed the MRI images and considered the possibility of foreign body granuloma for two reasons. First, granuloma and cancer can have similar imaging features; and second, the shadow seemed to indicate that the tongue tissue was protected from foreign bodies, as shown by images taken in the transverse plane. During the initial clinical interview the patient denied a history of foreign body ingestion. To differentiate between the two possibilities, further examinations were conducted.

Further diagnostic work-up

The patient was referred for ultrasound examination of the tongue. The ultrasound device used a linear probe with a 13-MHz transducer. The acoustic picture was consistent with a linear hyperechoic foreign body, specifically a piece of bone, as shown in Figure 3. When asked about the possibility of fish bone ingestion or another foreign body in the tongue, the patient could not recall whether she had recently eaten fish. However, her daughter recalled that a meal containing fish (with bones) might have been served to the patient 2 mo prior to seeking medical assistance. Complete surgical enucleation of the lesion was then conducted. The mass with the fish bone was completely removed without compromising the capsule (Figure 4A), and no hemorrhagic accident occurred. The fish bone was 1.5 cm in length (Figure 4B). Post-operative pathological examination showed that the lesion was a granuloma containing collagen fibers, macrophages and chronic inflammatory cells.

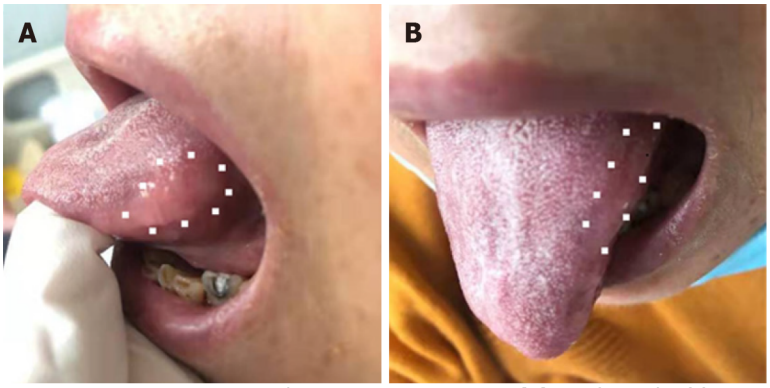

DOI: 10.12998/wjcc.v10.i18.6247 **Copyright** ©The Author(s) 2022.

Figure 2 Irregular ill-defined nodule on the left side. A-B: The tongue was of normal color on visual clinical examination in sagittal section (A) and transverse section (B). The dots indicate the margins of the nodule.

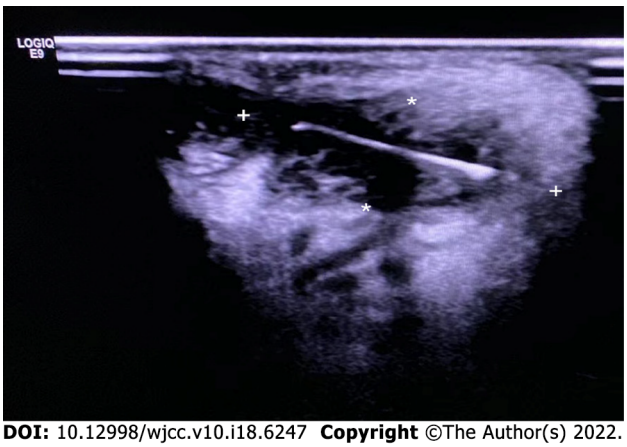

DOI: 10.12998/wjcc.v10.i18.6247 **Copyright** ©The Author(s) 2022.

Figure 3 Ultrasound examination of the tongue. Ultrasonography revealed an object of hyperechoic linear density, suggestive of an embedded foreign body (stars).

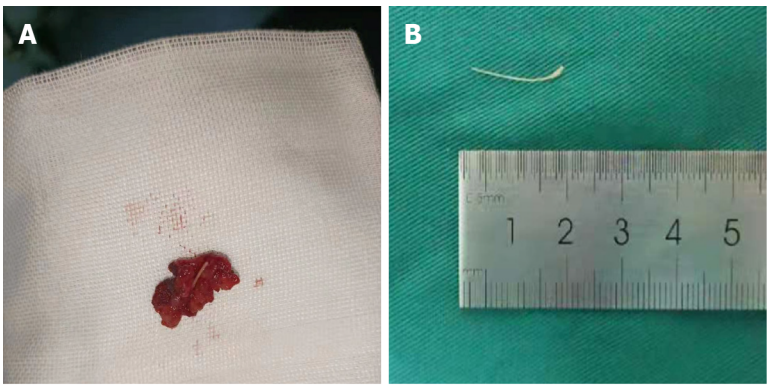

DOI: 10.12998/wjcc.v10.i18.6247 **Copyright** ©The Author(s) 2022.

Figure 4 The foreign body. A: Total enucleation without removal of the fish bone; B: The fish bone after removal.

FINAL DIAGNOSIS

Foreign body (fish bone) granuloma in the tongue.

TREATMENT

After the surgery, the patient received antibiotics (ceftriaxone) with systemic steroids and the post-operative recovery was uneventful. The patient was discharged on the third post-operative day.

OUTCOME AND FOLLOW-UP

The patient recovered well and there were no complications during the 2-mo follow-up period.

DISCUSSION

A diagnosis of tongue cancer is often considered in older adults with an enlarged tongue nodule/mass and localized pain[5]. The many differential diagnoses of a tongue mass include an inflammatory lesion and schwannoma[1]. A diagnosis of a granuloma attributable to an embedded foreign body is rare when there is no clear history of foreign body ingestion or oral trauma[6]. In the present case, the differential diagnosis of an irregular nodule with a smooth surface included cavernous hemangioma, anaplastic large-cell lymphoma, endophytic squamous cell carcinoma and Kaposi sarcoma of the tongue[7-10]. Differential diagnosis is important as cancer treatment and enucleation of a foreign body granuloma differ greatly in terms of surgical preparation, operation, tongue reconstruction and patient consultation [11-13].

MRI is the preferred diagnostic modality for evaluating tongue cancer because abnormal MRI signals have been strongly associated with pathological findings[14]. However, MRI is not an ideal modality for differentiating tongue cancer from embedded foreign body granuloma with foreign body[15]. The signals associated with tongue cancer are hyperintensity in a T2-weighted image (WI) and heterogeneous enhancement in an enhanced T1 WI, similar to granuloma[14,16]. In the present case, the fish bone (shown by hypointense signals in both the T1 and T2 WIs) was difficult to detect by MRI[17], and not surprisingly the primary diagnosis of tongue cancer was consistent with the abnormalities found in the tongue by MRI and with the swollen cervical lymph nodes. Besides this, shifting of metal fragments under the effects of MRI can result in potential damage of vital structures. If the doubt of a metal foreign body is present, the contraindications of MRI should be considered[18].

Several studies used ultrasound to detect a suspected embedded foreign body in the tongue[3,4,6]. The foreign bodies, which included a pequi spine, metal wire, and fish bone were visualized and localized accurately, demonstrating the utility of ultrasound for guiding therapeutic interventions. Multislice computerized tomography (CT) and cone beam CT also seem useful for visualizing embedded foreign bodies, although CTs have poor performance in terms of detecting wood[15]. Thus, when an embedded foreign body is suspected in a patient with an enlarged tongue mass, ultrasonography and CT can play an important role in the differential diagnosis[19].

In our case, the lesion was "walled off" on transverse images (Figure 2). This might indicate that the mass was "delimited" by a capsule. A similar sign was observed in an early case report of a patient with foreign body granuloma[16]. Thus, this sign might be a useful indicator of the need for further examinations (other than MRI). However, this issue requires further investigation.

CONCLUSION

We reported the case of a woman with an enlarged tongue mass initially diagnosed with tongue cancer. The ENT specialists reviewed the MRI data and corrected the diagnosis to 'foreign body in the tongue' based on oral ultrasound examination. The granuloma containing the fish bone was completely removed during surgery and post-operative pathological examination confirmed that the lesion was a granuloma. In cases with an enlarged tongue mass, oral ultrasound and/or CT examinations are important for differential diagnosis, to facilitate selection of the appropriate treatment method.

ACKNOWLEDGEMENTS

The authors acknowledge the colleagues for participating in this study. We are deeply indebted to the patient who participated in this study.

FOOTNOTES

Author contributions: Xu R was the patient's doctor in charge, reviewed the literature and contributed to manuscript drafting; Jiang ZH operated on the patient and contributed to manuscript drafting; Xia L reviewed the literature and was responsible for the revision of the manuscript for important intellectual content; All authors issued final approval for the version to be submitted.

Supported by the Research Start-up Grant for Talent of Mianyang Central Hospital of China, No. 2021YJRC-001; and the Applied Technique Research and Development Program of Mianyang City of China, No. 2019YFZJ022.

Informed consent statement: Informed written consent was obtained from the patient for publication of this report and any accompany images.

Conflict-of-interest statement: The authors declare that they have no conflict of interest.

CARE Checklist (2016) statement: The authors have read the CARE Checklist (2016), and the manuscript was prepared and revised according to the CARE Checklist (2016).

Open-Access: This article is an open-access article that was selected by an in-house editor and fully peer-reviewed by external reviewers. It is distributed in accordance with the Creative Commons Attribution NonCommercial (CC BY-NC 4.0) license, which permits others to distribute, remix, adapt, build upon this work non-commercially, and license their derivative works on different terms, provided the original work is properly cited and the use is non-commercial. See: https://creativecommons.org/Licenses/by-nc/4.0/

Country/Territory of origin: China

ORCID number: Zhen-Hua Jiang 0000-0001-5239-9154; Ran Xv 0000-0002-5381-111X; Li Xia 0000-0002-5529-884X.

S-Editor: Ma YJ
L-Editor: Filipodia
P-Editor: Ma YJ

REFERENCES

1 **Patel KS**. Foreign body in the tongue: an unusual site for a common problem. *J Laryngol Otol* 1991; **105**: 849-850 [PMID: 1753199 DOI: 10.1017/s0022215100117529]
2 **Kumagai K**, Hirose Y, Yoshida S. Woman With Foreign Body on Her Tongue. *Ann Emerg Med* 2018; **72**: e121-e122 [PMID: 30454805 DOI: 10.1016/j.annemergmed.2018.06.028]
3 **Pigott DC**, Buckingham RB, Eller RL, Cox AJ. Foreign body in the tongue: a novel use for emergency department ultrasonography. *Ann Emerg Med* 2005; **45**: 677-679 [PMID: 15940107 DOI: 10.1016/j.annemergmed.2004.12.030]
4 **Pereira RMA**, de Oliveira Afonso Pereira PC, Rodrigues VC, de Andrade LFB, de Carvalho EM, Júnior HM. Foreign Body Granuloma in the Tongue by a Pequi Spine. *Case Rep Dent* 2020; **2020**: 8838250 [PMID: 33224535 DOI: 10.1155/2020/8838250]
5 **Tagliabue M**, Belloni P, De Berardinis R, Gandini S, Chu F, Zorzi S, Fumagalli C, Santoro L, Chiocca S, Ansarin M. A systematic review and meta-analysis of the prognostic role of age in oral tongue cancer. *Cancer Med* 2021; **10**: 2566-2578 [PMID: 33760398 DOI: 10.1002/cam4.3795]
6 **Lin CJ**, Su WF, Wang CH. A foreign body embedded in the mobile tongue masquerading as a neoplasm. *Eur Arch Otorhinolaryngol* 2003; **260**: 277-279 [PMID: 12750919 DOI: 10.1007/s00405-002-0549-8]
7 **Kripal K**, Rajan S, Ropak B, Jayanti I. Cavernous hemangioma of the tongue. *Case Rep Dent* 2013; **2013**: 898692 [PMID: 24073342 DOI: 10.1155/2013/898692]
8 **Fatahzadeh M**, Schwartz RA. Oral Kaposi's sarcoma: a review and update. *Int J Dermatol* 2013; **52**: 666-672 [PMID: 23679875 DOI: 10.1111/j.1365-4632.2012.05758.x]
9 **Mangold AR**, Torgerson RR, Rogers RS. Diseases of the tongue. *Clin Dermatol* 2016; **34**: 458-469 [PMID: 27343960 DOI: 10.1016/j.clindermatol.2016.02.018]
10 **Tang W**, Wang Y, Yuan Y, Tao X. Assessment of tumor depth in oral tongue squamous cell carcinoma with multiparametric MRI: correlation with pathology. *Eur Radiol* 2022; **32**: 254-261 [PMID: 34255162 DOI: 10.1007/s00330-021-08148-6]
11 **Mannelli G**, Arcuri F, Agostini T, Innocenti M, Raffaini M, Spinelli G. Classification of tongue cancer resection and treatment algorithm. *J Surg Oncol* 2018; **117**: 1092-1099 [PMID: 29432642 DOI: 10.1002/jso.24991]
12 **Konishi M**, Fujita M, Shimabukuro K, Wongratwanich P, Verdonschot RG, Kakimoto N. Intraoral Ultrasonographic Features of Tongue Cancer and the Incidence of Cervical Lymph Node Metastasis. *J Oral Maxillofac Surg* 2021; **79**: 932-939 [PMID: 33031775 DOI: 10.1016/j.joms.2020.09.006]
13 **Teo DT**, Loy AH, Goh YH, Chan YM. Head and neck cancer after foreign body ingestion. *Ann Acad Med Singap* 2004; **33**: 379-381 [PMID: 15175786 DOI: 10.1159/000225582]
14 **Ong CK**, Chong VF. Imaging of tongue carcinoma. *Cancer Imaging* 2006; **6**: 186-193 [PMID: 17208674 DOI: 10.1102/1470-7330.2006.0029]

15 **Javadrashid R**, Fouladi DF, Golamian M, Hajalioghli P, Daghighi MH, Shahmorady Z, Niknejad MT. Visibility of different foreign bodies in the maxillofacial region using plain radiography, CT, MRI and ultrasonography: an in vitro study. *Dentomaxillofac Radiol* 2015; **44**: 20140229 [PMID: 25426703 DOI: 10.1259/dmfr.20140229]
16 **Chen H**. A tongue granuloma due to a fishbone mimicking a neoplasm: ultrasound-guided differential diagnosis. *Ultraschall Med* 2011; **32** Suppl 1: S1-S2 [PMID: 21225550 DOI: 10.1055/s-0030-1270593]
17 **Wang A**, Zhou Y, Huang Q. A fish bone induced aortic arch pseudoaneurysm in a male patient: A case report. *Medicine (Baltimore)* 2019; **98**: e16486 [PMID: 31335713 DOI: 10.1097/MD.0000000000016486]
18 **Caraiani C**, Petresc B, Dong Y, Dietrich CF. Contraindications and adverse effects in abdominal imaging. *Med Ultrason* 2019; **21**: 456-463 [PMID: 31765455 DOI: 10.11152/mu-2145]
19 **Kim JP**, Kwon OJ, Shim HS, Kim RB, Kim JH, Woo SH. Analysis of Clinical Feature and Management of Fish Bone Ingestion of Upper Gastrointestinal Tract. *Clin Exp Otorhinolaryngol* 2015; **8**: 261-267 [PMID: 26330922 DOI: 10.3342/ceo.2015.8.3.261]

World Journal of Clinical Cases

Submit a Manuscript: https://www.f6publishing.com

World J Clin Cases 2022 June 26; 10(18): 6254-6260

DOI: 10.12998/wjcc.v10.i18.6254

ISSN 2307-8960 (online)

CASE REPORT

Modified endoscopic ultrasound-guided selective N-butyl-2-cyanoacrylate injections for gastric variceal hemorrhage in left-sided portal hypertension: A case report

Jian Yang, Yan Zeng, Jun-Wen Zhang

Specialty type: Gastroenterology and hepatology

Provenance and peer review: Unsolicited article; Externally peer reviewed.

Peer-review model: Single blind

Peer-review report's scientific quality classification

Grade A (Excellent): 0
Grade B (Very good): B, B
Grade C (Good): C, C
Grade D (Fair): 0
Grade E (Poor): 0

P-Reviewer: Afify S, Egypt; Garbuzenko DV, Russia; Garbuzenko DV, Russia; Martino A, Italy

Received: December 12, 2021
Peer-review started: December 12, 2021
First decision: February 8, 2022
Revised: February 9, 2022
Accepted: April 22, 2022
Article in press: April 22, 2022
Published online: June 26, 2022

Jian Yang, Jun-Wen Zhang, Department of Gastroenterology, The First Affiliated Hospital of Chongqing Medical University, Chongqing 400016, China

Yan Zeng, Department of Psychology, The Second Affiliated Hospital of Chongqing Medical University, Chongqing 400010, China

Corresponding author: Jun-Wen Zhang, MD, Chief Doctor, Professor, Department of Gastroenterology, The First Affiliated Hospital of Chongqing Medical University, No. 1 Youyi Road, Yuzhong District, Chongqing 400016, China. 959308413@qq.com

Abstract

BACKGROUND

Left-sided portal hypertension (LSPH), also known as sinistral portal hypertension or regional portal hypertension, refers to extrahepatic portal hypertension caused by splenic vein obstruction or stenosis. N-butyl-2-cyanoacrylate (NBC) has been widely used in the endoscopic hemostasis of portal hypertension, but adverse events including renal or pulmonary thromboembolism, mucosal necrosis and gastrointestinal (GI) bleeding may occur after treatment. Herein, we report successfully managing gastric variceal (GV) hemorrhage secondary to LSPH using modified endoscopic ultrasound (EUS)-guided selective NBC injections.

CASE SUMMARY

A 35-year-old man was referred to our hospital due to an upper GI hemorrhage. Gastroscopy revealed GV hemorrhage and computed tomography venography (CTV) confirmed LSPH. The patient requested endoscopic procedures and rejected surgical therapies including splenectomy. EUS-guided selective NBC injections were performed and confluences of gastric varices were selected as the injection sites to reduce the injection dose. The "sandwich" method using undiluted NBC and hypertonic glucose was applied. No complications occurred. The patient was followed up regularly after discharge. Three months later, the follow-up gastroscopy revealed firm gastric submucosa with no sign of NBC expulsion and the follow-up CTV showed improvements in LSPH. No recurrent GI hemorrhage was reported during this follow-up period.

CONCLUSION

EUS-guided selective NBC injection may represent an effective and economical treatment for GV hemorrhage in patients with LSPH.

Key Words: Left-sided portal hypertension; Endoscopic ultrasound; Selective; N-butyl-2-cyanoacrylate; Gastric varices; Case report

©The Author(s) 2022. Published by Baishideng Publishing Group Inc. All rights reserved.

Core Tip: Gastric variceal (GV) hemorrhage caused by left-sided portal hypertension (LSPH) is a severe complication. Endoscopic ultrasound (EUS)-guided procedures for GV hemorrhage demonstrated beneficial results in reducing complication risks. Herein, we report the successful management of GV hemorrhage secondary to LSPH using EUS-guided selective N-butyl-2-cyanoacrylate injection which proved the effectiveness and safety of this method. This case is the first report choosing confluences of gastric varices as injection sites to reduce the injection dose and postoperative complications in patients with LSPH.

Citation: Yang J, Zeng Y, Zhang JW. Modified endoscopic ultrasound-guided selective N-butyl-2-cyanoacrylate injections for gastric variceal hemorrhage in left-sided portal hypertension: A case report. *World J Clin Cases* 2022; 10(18): 6254-6260
URL: https://www.wjgnet.com/2307-8960/full/v10/i18/6254.htm
DOI: https://dx.doi.org/10.12998/wjcc.v10.i18.6254

INTRODUCTION

Left-sided portal hypertension (LSPH), also known as sinistral portal hypertension or regional portal hypertension, refers to extrahepatic portal hypertension caused by splenic vein obstruction or stenosis [1-3]. LSPH accounts for about 5% of extrahepatic portal hypertension and is characterized by isolated gastric varices (GVs) and normal liver functions[3]. Pancreatic diseases are the major causes of LSPH. Most patients with LSPH have no obvious clinical symptoms and they are often diagnosed during the endoscopic examination after gastrointestinal (GI) bleeding. Therefore, LSPH should be considered in patients with pancreatic diseases who develop unexplained GI hemorrhage[1,4].

Gastric variceal (GV) hemorrhage leads to significant mortality in patients with portal hypertension. Although N-butyl-2-cyanoacrylate (NBC) has been widely used in the endoscopic hemostasis of portal hypertension, the early expulsion of NBC and the resultant hemorrhage is not uncommon[5]. Compared with conventional endoscopic injection, endoscopic ultrasound (EUS)-guided procedures in patients with GV bleeding demonstrated better diagnostic capability and clinical efficacy[6,7].

Herein, we report the successful management of GV hemorrhage secondary to LSPH using modified EUS-guided selective NBC injection.

CASE PRESENTATION

Chief complaints

A 35-year-old man was referred to our hospital due to an upper GI hemorrhage.

History of present illness

A few hours before admission, the patient had no apparent reason for one occurrence of sudden vomiting of blood mixed with stomach contents and the amount was estimated to be about 50-100 mL. He denied melena and syncope.

History of past illness

Nine months previously, this patient was admitted to our hospital due to persistent upper abdominal pain. He was diagnosed with severe acute pancreatitis (SAP) and underwent EUS-guided drainage of a pancreatic walled-off necrosis. He also had a 6-year history of hypertension and took enalapril regularly.

Personal and family history

This patient had a 10-year smoking history (a pack per day) and has not quit smoking. He denied alcoholism and taking nonsteroidal anti-inflammatory drugs.

Physical examination

After admission, physical examination revealed no abnormality except for 130/91 mmHg blood pressure.

Laboratory examinations

No apparent abnormalities were found in the emergency blood analysis.

Imaging examinations

After admission, gastroscopy confirmed GV hemorrhage (IGV1 by Sarin classification), and no esophageal varices or portal hypertensive gastropathy was found (Figure 1). Abdominal computed tomography venography (CTV) revealed stenosis of the proximal superior mesenteric vein, invisible proximal splenic vein and increased collateral circulations (Figure 2). Neither a portal vein thrombosis nor a splenorenal shunt was detected.

FINAL DIAGNOSIS

LSPH and GV hemorrhage.

TREATMENT

The patient requested endoscopic procedures and rejected surgical therapies including splenectomy. EUS-guided selective NBC injections were performed for the treatment and prophylaxis of GV hemorrhage.

A linear Pentax echoendoscope (Hoya Co., Tokyo, Japan) and the color Doppler flow imaging were employed to determine the puncture site. EUS revealed an enlarged portal vein without cavernous transformation (Figure 3A). The confluences of GVs were selected as the injection sites to reduce the injection dose. A 22-gauge needle (Boston Scientific Co., Natick, MA, United States) was used to perform the puncture into the selected GVs (Figure 3B). The "sandwich" method using undiluted NBC (0.5 mL/ampoule; Beijing Compont Medical Devices Co., Beijing, China) and hypertonic glucose was applied (Figure 3C). A total of 2 mL of NBC was injected into three different confluences of GVs. Hyperechoic fillings and decreased blood flow signals were observed after injections (Figure 3D).

OUTCOME AND FOLLOW-UP

The patient fasted for 1 d after the procedure. No complications, including ectopic embolism, fever and post-injection GI bleeding occurred. The patient was followed up regularly after discharge. Three months later, the follow-up gastroscopy revealed no sign of NBC expulsion (Figure 4) and follow-up CTV showed improvements in LSPH (Figure 5). No recurrent GI hemorrhage and other complications were reported during the 3-mo follow-up.

DISCUSSION

Pancreatic diseases such as pancreatitis and pancreatic tumors are the most common etiology of LSPH [3,8]. The anatomical proximity between the splenic vein and the pancreas makes the splenic vein more susceptible to pancreatic diseases. When pancreatic disease obstructs the splenic vein flow, the pressure of the left portal vein system increases and blood flows retrogradely through the short and posterior gastric veins and the gastroepiploic veins, which would lead to GVs. In patients with acute pancreatitis, infected walled-off necrosis was one of the risk factors for LSPH and early anticoagulation could not wholly prevent its occurrence[8]. In this case, the patient had a history of SAP and infected pancreatic necrosis which may be responsible for his LSPH. About 20% of patients with portal hypertension may develop GVs[9], and although LSPH is a rare cause of upper GI hemorrhage, GV hemorrhage in patients with LSPH secondary to pancreatic disease is not uncommon. Liu *et al*[10] reported that about 15.3% of LSPH patients had complicated bleeding GVs and the death risk is relatively higher when recurrent GV hemorrhage occurs so this is worthy of attention.

It is well known that splenectomy is the most effective treatment for LSPH. However, transjugular intrahepatic portosystemic shunt, balloon retrograde transvenous obliteration, endoscopic injection sclerotherapy (EIS) and endoscopic NBC injection were reported effective for patients who are not suitable or unwilling to choose surgery[11]. Although endoscopic NBC injection therapy has been proven minimally invasive and effective[12], conventional endoscopic NBC injections may also cause

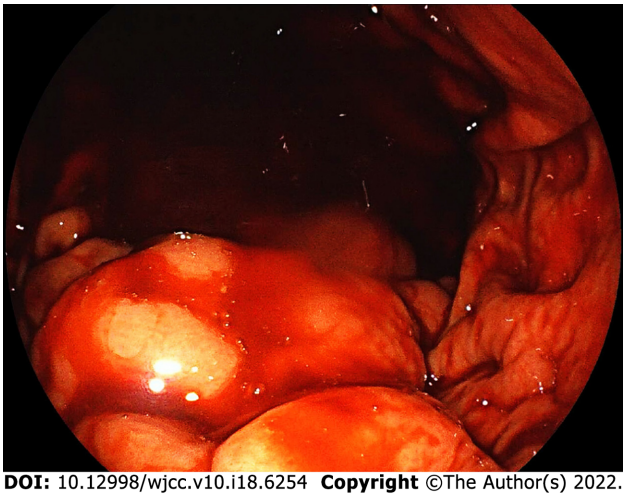

DOI: 10.12998/wjcc.v10.i18.6254 **Copyright** ©The Author(s) 2022.

Figure 1 Gastroscopic image. Gastroscopy revealed gastric variceal with signs of recent bleeding in the absence of active bleeding.

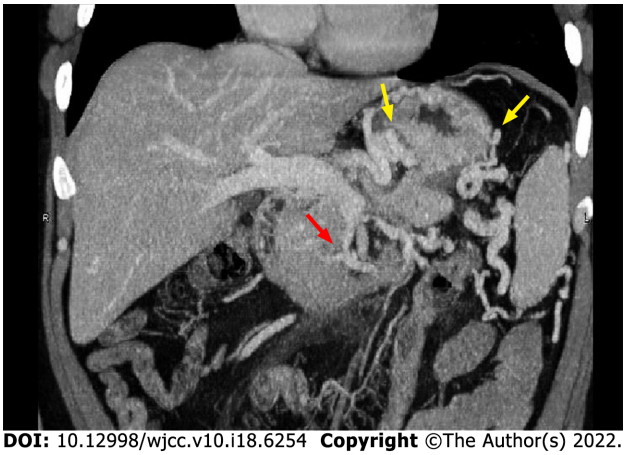

DOI: 10.12998/wjcc.v10.i18.6254 **Copyright** ©The Author(s) 2022.

Figure 2 Abdominal computed tomography venography image. Computed tomography venography revealed stenosis of the proximal superior mesenteric vein (red arrow), invisible proximal splenic vein, and increased collateral circulations (yellow arrows).

severe complications including renal or pulmonary thromboembolism, fever, severe pain caused by intraperitoneal injection, mucosal necrosis at the injection site and GI bleeding[13]. As reported in recent years, an EUS-guided hemostasis treatment, including injection of NBC or in combination with coils, injection of thrombin or absorbable gelatin sponge, and clip-assisted endoscopic NBC injection, demonstrated promising results in reducing complication risks[14,15].

Modified EUS-guided selective NBC injection was applied for three distinct advantages in this present case. First, a reduced NBC dose may result in a lower occurrence of post-operational GI bleeding and ectopic embolism. EUS can also provide the detection of submucosal GVs, their confluences and real-time effectiveness evaluation for GV obliteration[7]. These advantages make it possible to identify and select confluences of gastric varices which were in the direction of bleeding gastric vessels and used as injection sites to reduce the injection dose. Although EUS-guided coil injection is reported superior to conventional NBC injection in terms of rebleeding after treatment[16], it was believed that a reduced dose of NBC would be injected into GVs in the modified EUS-guided selective NBC injection, which would lead to lower chances of post-injection ulcer and GI hemorrhage. Besides, reduced NBC dose may result in a similar lower occurrence of ectopic embolism in selective NBC injection as in the coils-combined injection method and clip-assisted injection method. Second, there would be no additional risk of radioactive exposure; coils and metal clips were not used in this modified injection procedure, which decreased the cost of endoscopic procedures. Third, selective NBC injection demonstrated a faster and firmer obliteration effect in GV hemorrhage than thrombin and absorbable gelatin sponge injections, making NBC injection more suitable than other procedures for acute GV bleeding. NBC rarely causes vascular necrosis and was reported superior to EIS in the hemostasis rate for GV bleeding[17]. Thus, EUS-guided selective NBC injection was performed for this patient based on the above factors and the result was adequate. Despite all these advantages, the operation time of EUS-guided selective NBC injection seemed a little longer than that of conventional

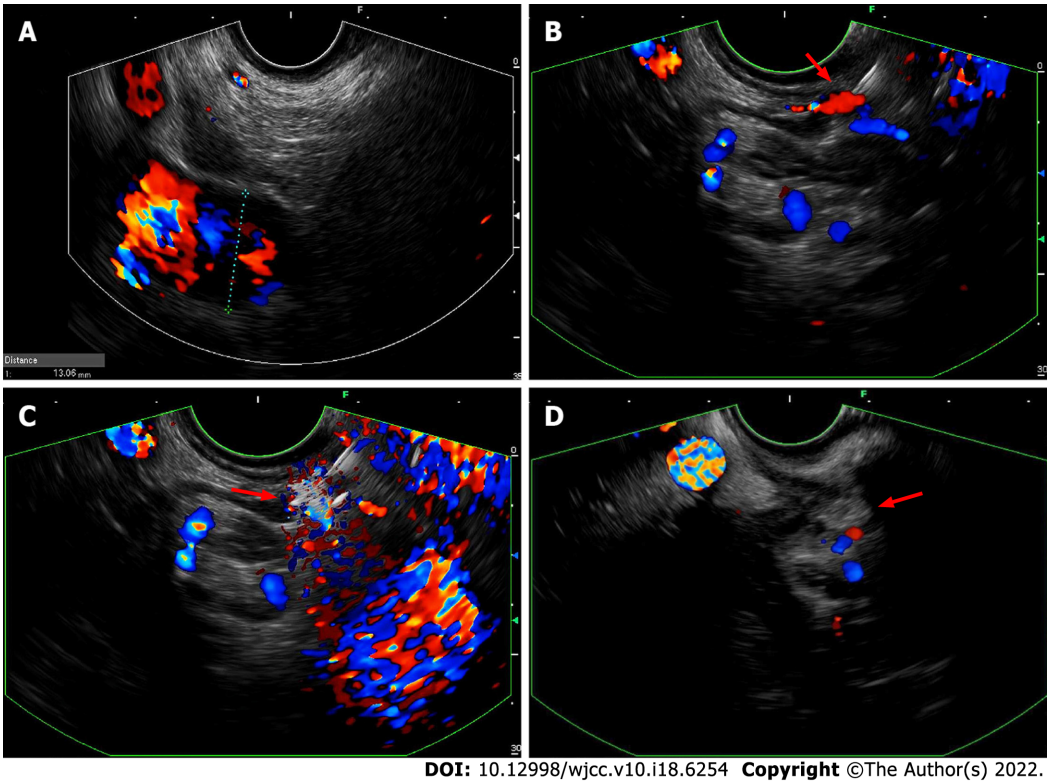

DOI: 10.12998/wjcc.v10.i18.6254 **Copyright** ©The Author(s) 2022.

Figure 3 Endoscopic ultrasound images. A: Endoscopic ultrasound revealed an enlarged portal vein; B: A confluence of gastric varices was identified and selected as the injection site (red arrow); C: Undiluted N-butyl-2-cyanoacrylate (red arrow) was injected into the selected gastric varix *via* a 22-gauge needle; D: Hyperechoic fillings (red arrow) and decreased blood flow signals were observed after injections.

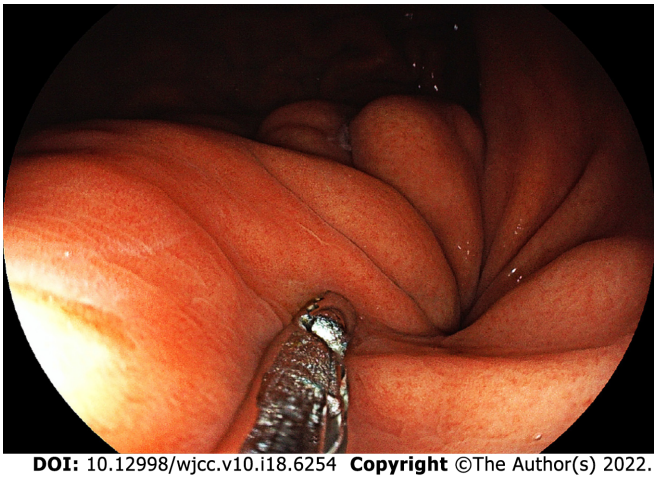

DOI: 10.12998/wjcc.v10.i18.6254 **Copyright** ©The Author(s) 2022.

Figure 4 Gastroscopic image. With the help of biopsy forceps, the follow-up gastroscopy revealed firm gastric submucosa and no sign of N-butyl-2-cyanoacrylate expulsion.

endoscopic NBC injection due to time consumption to confirm confluences of GVs during the EUS procedure. Additional cases are needed to verify our findings and compare the efficacies and complications of different embolization methods guided by EUS. Currently, this described technique is recommended to be used only in hemodynamically stable patients. To the best of our knowledge, this case is the first report choosing confluences of gastric varices as injection sites to reduce the injection dose and postoperative complications in patients with LSPH.

CONCLUSION

Modified EUS-guided selective NBC injection may represent an effective and economical treatment for

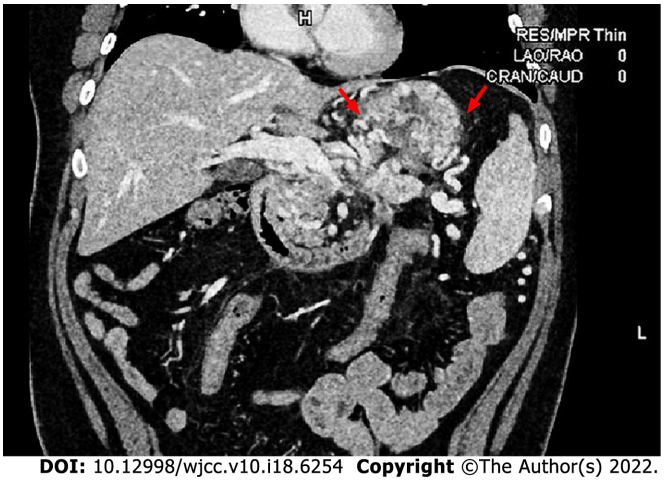

DOI: 10.12998/wjcc.v10.i18.6254 **Copyright** ©The Author(s) 2022.

Figure 5 Computed tomography venography image. Compared with the results before the operation (Figure 2), follow-up computed tomography venography revealed improvements in left-sided portal hypertension and collateral circulations (red arrows).

GV hemorrhage in patients with LSPH.

FOOTNOTES

Author contributions: Yang J, Zeng Y and Zhang JW designed the research study; Yang J and Zhang JW performed the endoscopic procedures; Yang J and Zeng Y performed the literature search, analyzed the data and wrote the manuscript; All authors have read and approved the final manuscript.

Informed consent statement: All study participants, or their legal guardian, provided informed written consent prior to study enrollment.

Conflict-of-interest statement: The authors declare that they have no conflict of interest.

CARE Checklist (2016) statement: The authors have read the CARE Checklist (2016), and the manuscript was prepared and revised according to the CARE Checklist (2016).

Open-Access: This article is an open-access article that was selected by an in-house editor and fully peer-reviewed by external reviewers. It is distributed in accordance with the Creative Commons Attribution NonCommercial (CC BY-NC 4.0) license, which permits others to distribute, remix, adapt, build upon this work non-commercially, and license their derivative works on different terms, provided the original work is properly cited and the use is non-commercial. See: https://creativecommons.org/Licenses/by-nc/4.0/

Country/Territory of origin: China

ORCID number: Jian Yang 0000-0001-8170-0727; Yan Zeng 0000-0003-4935-1306; Jun-Wen Zhang 0000-0003-2911-598X.

Corresponding Author's Membership in Professional Societies: Chinese Society of Gastroenterology.

S-Editor: Zhang H
L-Editor: Filipodia CL
P-Editor: Zhang H

REFERENCES

1 **Zheng K**, Guo X, Feng J, Bai Z, Shao X, Yi F, Zhang Y, Zhang R, Liu H, Romeiro FG, Qi X. Gastrointestinal Bleeding due to Pancreatic Disease-Related Portal Hypertension. *Gastroenterol Res Pract* 2020; **2020**: 3825186 [PMID: 32308674 DOI: 10.1155/2020/3825186]

2 **Xie CL**, Wu CQ, Chen Y, Chen TW, Xue HD, Jin ZY, Zhang XM. Sinistral Portal Hypertension in Acute Pancreatitis: A Magnetic Resonance Imaging Study. *Pancreas* 2019; **48**: 187-192 [PMID: 30629031 DOI: 10.1097/MPA.0000000000001242]

3 **Köklü S**, Coban S, Yüksel O, Arhan M. Left-sided portal hypertension. *Dig Dis Sci* 2007; **52**: 1141-1149 [PMID: 17385040 DOI: 10.1007/s10620-006-9307-x]

4 **Fernandes A**, Almeida N, Ferreira AM, Casela A, Gomes D, Portela F, Camacho E, Sofia C. Left-Sided Portal Hypertension: A Sinister Entity. *GE Port J Gastroenterol* 2015; **22**: 234-239 [PMID: 28868415 DOI: 10.1016/j.jpge.2015.09.006]

5 **Cheng LF**, Wang ZQ, Li CZ, Cai FC, Huang QY, Linghu EQ, Li W, Chai GJ, Sun GH, Mao YP, Wang YM, Li J, Gao P, Fan TY. Treatment of gastric varices by endoscopic sclerotherapy using butyl cyanoacrylate: 10 years' experience of 635 cases. *Chin Med J (Engl)* 2007; **120**: 2081-2085 [PMID: 18167180]

6 **Mohan BP**, Chandan S, Khan SR, Kassab LL, Trakroo S, Ponnada S, Asokkumar R, Adler DG. Efficacy and safety of endoscopic ultrasound-guided therapy versus direct endoscopic glue injection therapy for gastric varices: systematic review and meta-analysis. *Endoscopy* 2020; **52**: 259-267 [PMID: 32028533 DOI: 10.1055/a-1098-1817]

7 **Hammoud GM**, Ibdah JA. Utility of endoscopic ultrasound in patients with portal hypertension. *World J Gastroenterol* 2014; **20**: 14230-14236 [PMID: 25339809 DOI: 10.3748/wjg.v20.i39.14230]

8 **Li H**, Yang Z, Tian F. Clinical Characteristics and Risk Factors for Sinistral Portal Hypertension Associated with Moderate and Severe Acute Pancreatitis: A Seven-Year Single-Center Retrospective Study. *Med Sci Monit* 2019; **25**: 5969-5976 [PMID: 31400275 DOI: 10.12659/MSM.916192]

9 **Sarin SK**, Lahoti D, Saxena SP, Murthy NS, Makwana UK. Prevalence, classification and natural history of gastric varices: a long-term follow-up study in 568 portal hypertension patients. *Hepatology* 1992; **16**: 1343-1349 [PMID: 1446890 DOI: 10.1002/hep.1840160607]

10 **Liu Q**, Song Y, Xu X, Jin Z, Duan W, Zhou N. Management of bleeding gastric varices in patients with sinistral portal hypertension. *Dig Dis Sci* 2014; **59**: 1625-1629 [PMID: 24500452 DOI: 10.1007/s10620-014-3048-z]

11 **Al-Khazraji A**, Curry MP. The current knowledge about the therapeutic use of endoscopic sclerotherapy and endoscopic tissue adhesives in variceal bleeding. *Expert Rev Gastroenterol Hepatol* 2019; **13**: 893-897 [PMID: 31389265 DOI: 10.1080/17474124.2019.1652092]

12 **Chevallier O**, Guillen K, Comby PO, Mouillot T, Falvo N, Bardou M, Midulla M, Aho-Glélé LS, Loffroy R. Safety, Efficacy, and Outcomes of N-Butyl Cyanoacrylate Glue Injection through the Endoscopic or Radiologic Route for Variceal Gastrointestinal Bleeding: A Systematic Review and Meta-Analysis. *J Clin Med* 2021; **10** [PMID: 34070534 DOI: 10.3390/jcm10112298]

13 **Lim YS**. Practical approach to endoscopic management for bleeding gastric varices. *Korean J Radiol* 2012; **13** Suppl 1: S40-S44 [PMID: 22563286 DOI: 10.3348/kjr.2012.13.S1.S40]

14 **Zhang M**, Li P, Mou H, Shi Y, Tuo B, Jin S, Sun R, Wang G, Ma J, Zhang C. Clip-assisted endoscopic cyanoacrylate injection for gastric varices with a gastrorenal shunt: a multicenter study. *Endoscopy* 2019; **51**: 936-940 [PMID: 31378856 DOI: 10.1055/a-0977-3022]

15 **Bhat YM**, Weilert F, Fredrick RT, Kane SD, Shah JN, Hamerski CM, Binmoeller KF. EUS-guided treatment of gastric fundal varices with combined injection of coils and cyanoacrylate glue: a large U.S. experience over 6 years (with video). *Gastrointest Endosc* 2016; **83**: 1164-1172 [PMID: 26452992 DOI: 10.1016/j.gie.2015.09.040]

16 **Bazarbashi AN**, Wang TJ, Jirapinyo P, Thompson CC, Ryou M. Endoscopic Ultrasound-Guided Coil Embolization With Absorbable Gelatin Sponge Appears Superior to Traditional Cyanoacrylate Injection for the Treatment of Gastric Varices. *Clin Transl Gastroenterol* 2020; **11**: e00175 [PMID: 32677809 DOI: 10.14309/ctg.0000000000000175]

17 **Oho K**, Iwao T, Sumino M, Toyonaga A, Tanikawa K. Ethanolamine oleate versus butyl cyanoacrylate for bleeding gastric varices: a nonrandomized study. *Endoscopy* 1995; **27**: 349-354 [PMID: 7588347 DOI: 10.1055/s-2007-1005712]

World Journal of Clinical Cases

Submit a Manuscript: https://www.f6publishing.com

World J Clin Cases 2022 June 26; 10(18): 6261-6268

DOI: 10.12998/wjcc.v10.i18.6261

ISSN 2307-8960 (online)

CASE REPORT

Management of type IIIb dens invaginatus using a combination of root canal treatment, intentional replantation, and surgical therapy: A case report

Jing Zhang, Na Li, Wu-Li Li, Xian-Yu Zheng, Song Li

Specialty type: Dentistry, oral surgery and medicine

Provenance and peer review: Unsolicited article; Externally peer reviewed.

Peer-review model: Single blind

Peer-review report's scientific quality classification

Grade A (Excellent): 0
Grade B (Very good): B
Grade C (Good): C
Grade D (Fair): 0
Grade E (Poor): 0

P-Reviewer: Abu Hasna A, Brazil; Memis S, Turkey

Received: December 17, 2021
Peer-review started: December 17, 2021
First decision: January 26, 2022
Revised: February 8, 2022
Accepted: April 21, 2022
Article in press: April 21, 2022
Published online: June 26, 2022

Jing Zhang, Na Li, Wu-Li Li, Xian-Yu Zheng, Song Li, Stomatological Hospital and College, Key Laboratory of Oral Diseases Research of Anhui Province, Anhui Medical University, Hefei 230032, Anhui Province, China

Corresponding author: Song Li, PhD, Doctor, Professor, Stomatological Hospital and College, Key Laboratory of Oral Diseases Research of Anhui Province, Anhui Medical University, No. 69 Meishan Road, Hefei 230032, Anhui Province, China. 3197053337@qq.com

Abstract

BACKGROUND

Type IIIb dens invaginatus (DI) with a lateral canal located at the mid-third of the root is rarely reported. Here, we report a rare case of type IIIb DI in the left upper anterior tooth with a lateral canal that led to persistent periodontitis.

CASE SUMMARY

A 15-year-old female patient presented with a chief complaint of pain associated with recurrent labial swelling in the area of the left anterior tooth. A diagnosis of type IIIb DI and chronic periodontitis was made. Intentional replantation was performed after conventional endodontic treatment failed. After 6 mo, the patient was asymptomatic, but a sinus tract was observed. Cone-beam computed tomography images showed bone loss in the mesial of the mid-root. Based on methylene blue staining and microscopy images, the lateral foramen located at the middle third of the root was surgically treated. After 3 years of follow-up, the clinical findings and radiographic assessment presented a favorable prognosis of bone healing without root absorption or ankylosis.

CONCLUSION

Type IIIb DI with a lateral canal can be successfully treated by root canal treatment, intentional replantation, and surgical therapy.

Key Words: Dens invaginatus; Intentional replantation; Surgical therapy; Lateral canal; Case report

©The Author(s) 2022. Published by Baishideng Publishing Group Inc. All rights reserved.

Core Tip: Type IIIb dens invaginatus (DI) with a lateral canal located at the mid-third of the root is first reported. Here, we report a rare case of type IIIb DI in the left upper anterior tooth with a lateral canal that led to persistent periodontitis and it was successfully treated by a combination of root canal treatment, intentional replantation, and surgical therapy.

Citation: Zhang J, Li N, Li WL, Zheng XY, Li S. Management of type IIIb dens invaginatus using a combination of root canal treatment, intentional replantation, and surgical therapy: A case report. *World J Clin Cases* 2022; 10(18): 6261-6268
URL: https://www.wjgnet.com/2307-8960/full/v10/i18/6261.htm
DOI: https://dx.doi.org/10.12998/wjcc.v10.i18.6261

INTRODUCTION

Dens invaginatus (DI) is a dental developmental anomaly resulting from enamel enfolding into the dental papilla prior to calcification. DI occurs more often in permanent maxillary lateral incisors and less frequently in mandibular anterior and deciduous teeth[1]. Clinically, pits lined with enamel defects and dentin invaginated into the dental/teeth with DI are susceptible to caries due to microorganism accumulation, easily leading to pulp necrosis and periapical inflammation[2]. However, DI may be easily overlooked due to the absence of clinical signs of malformation.

The most widely known classification of DI into three types was made by Oehler[3] in 1957 based on the extent of invagination from the crown into the root. Type III is the most complicated form due to the more extreme anatomical complexity. Type IIIa refers to invagination penetrating through the root and forming a lateral foramen as a pseudoforamen, while type IIIb refers to invagination extending through the root with an apical foramen. There is usually no communication with the pulp, which lies compressed within the wall around the invagination process. However, to our knowledge, this is the first report of a tooth of type IIIb DI infected *via* a lateral canal.

DI poses a great challenge in endodontic treatment due to the development of malformations with distortion of the teeth. Canal irregularities and invagination may prevent mechanical and chemical preparation. Due to the anatomic variations of the complex root canal morphologies, various treatment options have been proposed, including sealing of the invagination, root canal treatment, intentional replantation, periapical microsurgery, and extraction[4-6]. Here, we report a complex case of type IIIb DI with a lateral canal. After endodontic treatment, intentional replantation, and periapical microsurgery, the clinical findings and radiographic assessment presented a favorable prognosis of effective periapical healing at a 3-year follow-up assessment.

CASE PRESENTATION

Chief complaints

A 15-year-old female patient presented to the Department of Endodontics, Anhui Medical University, China with a chief complaint of pain associated with recurrent labial swelling in the area of the left anterior tooth for the past 6 mo. The patient reported that she had undergone endodontic treatment 1 mo earlier with symptom recurrence.

History of present illness

The patient presented to the Department of Endodontics, Anhui Medical University, China, with a chief complaint of pain associated with recurrent labial swelling in the area of the left anterior tooth for the past 6 mo.

History of past illness

The patient reported that she had undergone endodontic treatment 1 mo earlier with symptom recurrence.

Personal and family history

The patient had a noncontributory personal and family history.

Physical examination

Oral examination revealed fluctuating buccal swelling with a sinus at the apical area (Figure 1A). Tooth 22 showed an intact crown with a palatal access cavity (Figure 1B). Sensitivity to vertical percussion and negativity to palpation and electric pulp testing were observed, whereas the response of adjacent teeth

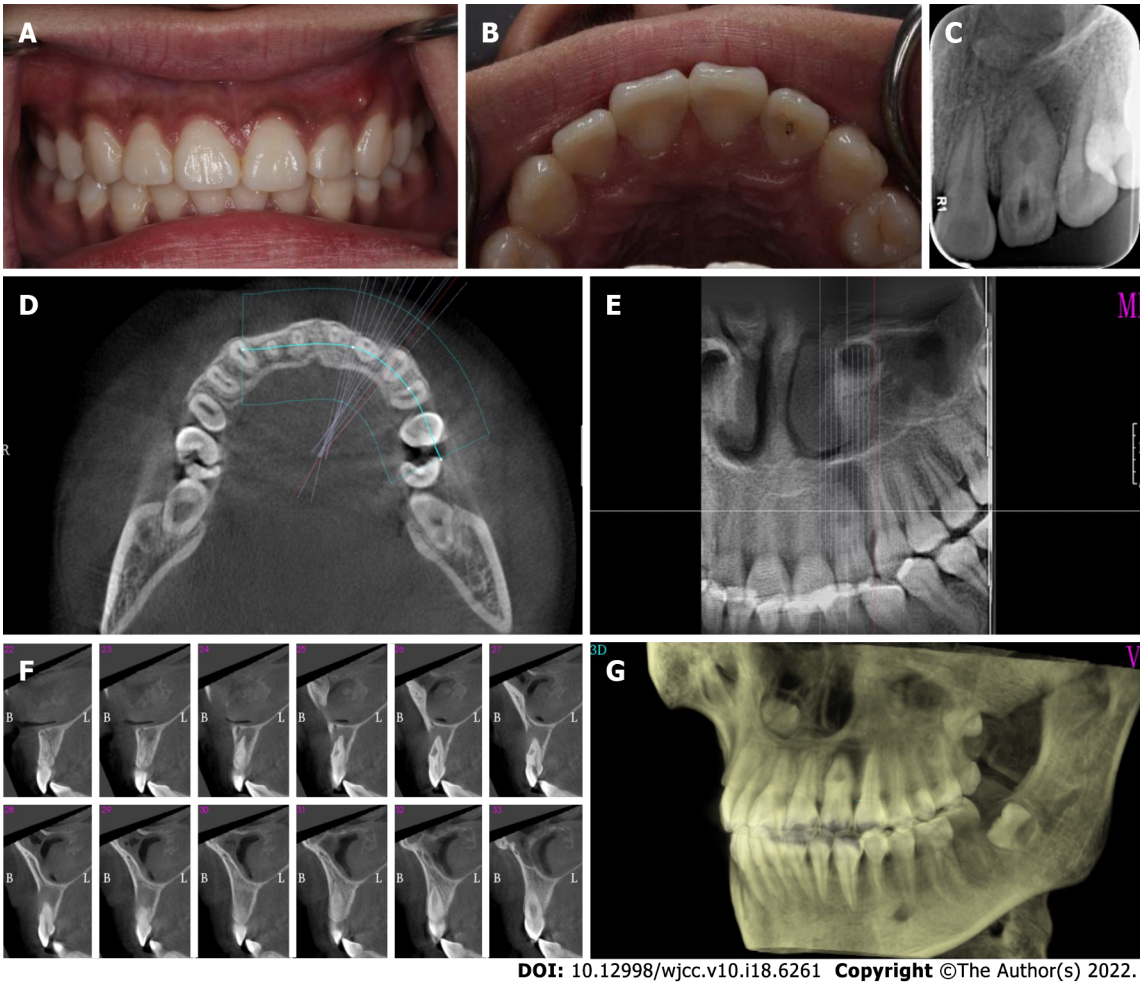

DOI: 10.12998/wjcc.v10.i18.6261 **Copyright** ©The Author(s) 2022.

Figure 1 Preoperative photograph of the left upper anterior teeth. A: Labial view showing an intact left lateral incisor with a sinus on the distobuccal aspect; B: Palatal view showing tooth 22 with an access cavity; C: Radiograph showing the presence of dens invaginatus (DI) associated with a large periapical lesion; D-F: Cone-beam computed tomography images: Transverse view showing radiolucency surrounding tooth 22 (D), coronal view showing a DI extending to the apex of the root (E), and sagittal sections showing DI with a large periapical radiolucency (F); G: Three-dimensional reconstruction indicating loss of labial cortical plate.

was normal. The periodontal probing depths were within the normal range with slight mobility. Radiography showed an invagination of dentin lined by enamel into the pulpal space, expanded space in the middle of the teeth with a large periapical radiolucent lesion, and the presence of bone resorption (Figure 1C).

Laboratory examinations

The patient's blood test results were all normal.

Imaging examinations

A cone-beam computed tomography (CBCT) scan showed invagination extending from the crown into the root with an apical foramen associated with a large periapical radiolucent lesion, which caused variation in the main root canal. A well-defined unilocular periapical radiolucent lesion was observed. Sagittal CBCT images showed that a loop-shaped chamber separated the main root canal (Figure 1D-G).

FINAL DIAGNOSIS

A diagnosis of type IIIb DI and chronic periodontitis was made.

TREATMENT

Under rubber dam isolation, the temporary filling was removed, and access to the main and invaginated

canals was completed. Pulp vitality in the main canal and dens invaginatus canal confirmed necrosis. The total length of the canals was estimated to be 19 mm, and the canals were then thoroughly prepared to apical size 30 by the crown-down technique with a NiTi file. A large volume of pale-yellowish fluid drained from the canal. Following thorough irrigation with 5.25% sodium hypochlorite (NaOCl), the root canals were dried with paper points, and calcium hydroxide paste was placed into the two canals (Figure 2A). The coronal access was sealed with a 3-mm-thick temporary restorative material. The patient was scheduled to return after 2 wk.

Intentional replantation

As endodontic therapy failed and the aberrant anatomic structure hampered adequate disinfection and obturation, the patient was informed that root canal retreatment could not clean out the infected pulp tissue clearly and obturation could not seal the pseudo canal tightly. Intentional replantation and surgical treatment were chosen as the next treatment. After discussing the risk and the financial cost, her parents chose to perform intentional replantation at the 2-wk follow-up appointment (Figure 2B). The patient received 500 mg amoxicillin and 400 mg ibuprofen 30 min before surgery and was instructed to rinse with 0.2% chlorhexidine gluconate solution. After local anesthesia, a minimal portion of tooth 22 was extracted without any fracture. The crown was held by saline-soaked wet gauze to keep the teeth moist and to minimize damage to the periodontal ligament (PDL) (Figure 2C). Under the dental operating microscope, the apex of the tooth was resected with a high-speed handpiece for 3 mm, and the foramen was clearly and deeply prepared by ultrasonic tips. iBoot BP (Innovative BioCeramix Inc., Vancouver, Canada) was placed to completely seal the retrograde cavity (Figure 2D). Then, the tooth was gently replanted into the socket and fixed by a wire and composite resin splint (Figure 2E). The extraoral times were limited to under 13 min. A radiograph was taken to confirm that the depth of iBoot BP was approximately 5 mm (Figure 2F). After the surgery was performed, amoxicillin (500 mg, 3 times per day) was administered for 3 d to prevent wound infection. The patient was instructed to maintain a soft diet and use a 0.2% chlorhexidine gluconate oral rinse for 2 wk.

Two weeks after the procedure, the patient returned, and the wire and composite resin splint were removed. After removal of the temporary restorative material under rubber dam isolation, calcium hydroxide paste in the root canals was cleared by ultrasonication. After drying the canals with paper points, the canals were fully obturated with gutta percha, and iRoot BP (Innovative BioCeramix Inc.) was performed using a vertical condensation technique. Subsequently, tooth 22 was restored using acid-etch and composite resin Z350 (3M ESPE, MN, United States).

Unfortunately, 6 mo later, the patient returned pain-free, but the swelling (sinus tract) in the buccal maxillary region reappeared (Figure 3A and B). A gutta percha point in the draining sinus revealed point tracking to a large periapical lesion associated with the mesial surface of tooth 22 (Figure 3C and D).

Surgical treatment

The patient refused the extraction and had a strong desire to preserve natural tooth 22. The patient and her parents agreed to perform endodontic microsurgery as a last resort to seal the lateral canal in the mesial of tooth 22. After local anesthesia, a full-thickness triangular mucoperiosteal flap was made to expose the mesial area of tooth 22. The root surface was stained with methylene blue to identify the lateral foramen. An L-shaped pit on the mid-root surface was observed, which was then prepared with an ultrasonic tip and obturated with iRoot BP (Figure 3E and F). The granulomatous tissues were curetted, and the surgical region was irrigated with 0.9% saline. Finally, the flap was repositioned and sutured. The sutures were removed after 2 wk.

OUTCOME AND FOLLOW-UP

At the 3-year recall evaluation, the patient had no painful symptoms. The radiograph image presented complete healing of the periapical lesion around the tooth root. Continuity of the periodontal ligament was observed, and intercortical bone had formed completely without any root resorption or ankylosis (Figure 4).

DISCUSSION

Treatment for DI varies depending on the invagination type, anatomy of the canal, level of pulp involvement, and morphology of the apex. To our knowledge, this is the first report of an infection of type IIIb DI with a lateral canal resulting in the persistence of periapical damage. Microorganism contamination in the invagination easily inflames the pulp irreversibly and even causes pulp necrosis both in the main canal and the invagination canal, especially in patients with type III DI. In patients with type IIIa DI, endodontic treatment should be performed on the canals as if they were two independent canals[6]. In patients with type IIIb, some authors recommend removing the extremely

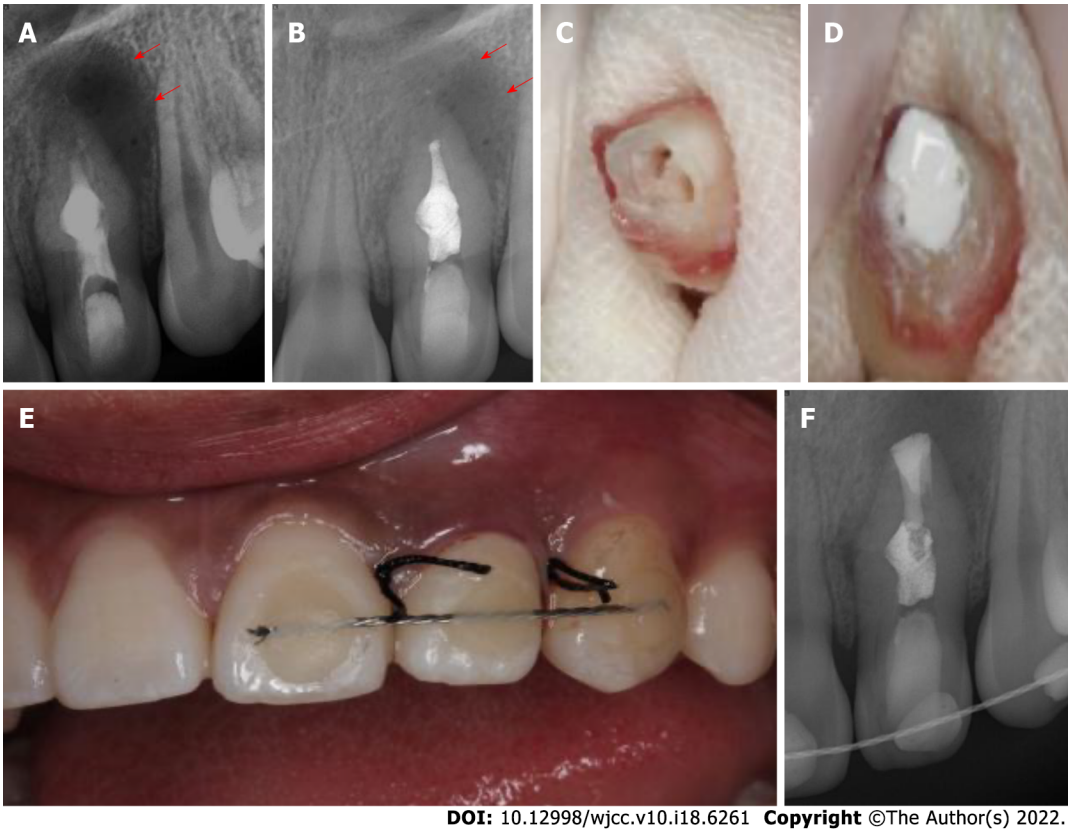

DOI: 10.12998/wjcc.v10.i18.6261 **Copyright** ©The Author(s) 2022.

Figure 2 Canal disinfection and intentional replantation. A: Radiographic image showing that tooth 22 was placed with hydroxide paste; B: Radiographic image of tooth 22 at the 2-wk recall; C: Tooth 22 was extracted, and the apex of the tooth was resected; D: Obturation of root canal space and retroseal of the apex with iRoot BP; E: Replantation of tooth 22 with a composite resin splint; F: Radiographic image of the replantation of tooth 22 (red arrow indicates the boundaries of the lesion).

large anomalous invagination using ultrasonic instruments and combining the two canals as one space to allow for complete and sufficient disinfection[7]. The removal of the single and large canal was followed by obturation with mineral trioxide aggregate in the apical third. However, the elimination of invagination severely compromised the strength of the tooth and increased the risk of tooth fracture. Martins *et al*[7] reported that three Fibercore posts were applied to the root canal to reinforce the thin root wall. In this reported case, the invaginated cavity occupied the center of the canal and adhered labially to the canal wall. Removal of the invaginated hard tissue was impractical. Such removal would cause a thin outer shell of dentine to remain, which may result in a poor prognosis.

Successful root canal treatment is based on the complete removal of all infections in the entire root canal system[8]. However, due to the anatomical impediments of type IIIb DI that restrict instrument cleaning and sufficient shaping, chemomechanical preparation cannot effectively eliminate all the infected tissues in the main canal or the invagination canal, including lateral canals and apical ramifications[9]. This would cause root canal treatment to occasionally fail, resulting in the persistence of periapical damage. Since a conventional root canal, as the first alternative, had already been initiated and failed in this patient, surgical endodontic or intentional replantation was the second treatment option instead of tooth extraction[10].

Intentional replantation is defined as deliberate extraction of the teeth and visual endodontic manipulation followed by reinsertion back into the original socket. The advantages of intentional replantation are that the major procedure is performed visually and that it benefits inaccessible areas, including the morphological variation in type IIIb DI[11]. A recent systematic review demonstrated that the survival rate of intentional replantation was 90%[12]. In a retrospective study of ten cases of type IIIb DI with apical periodontitis treated by intentional replantation, the survival rate was 80%[13]. Due to its high survival rate, low invasiveness, and cost-effectiveness, intentional replantation is regarded as a reliable and viable treatment when root canal treatment fails. PDL is important for the success of intentional replantation. Yu *et al*[14] reported that PDL cells remained alive within 15 to 20 min, which was crucial for the ability of PDL cells to attach to the alveolus. In this patient, we limited the extraoral time to 13 min, leading to successful periradicular healing.

Unfortunately, the sinus tract in the buccal maxillary region was noted at six recall evaluations. In the initial radiograph, we focused on the morphological variation of DI and periapical infection while ignoring the lateral infection caused by organisms in the lateral canal. Considering the patient's wishes and with the aid of methylene blue staining, surgical treatment was attempted as the last resort to

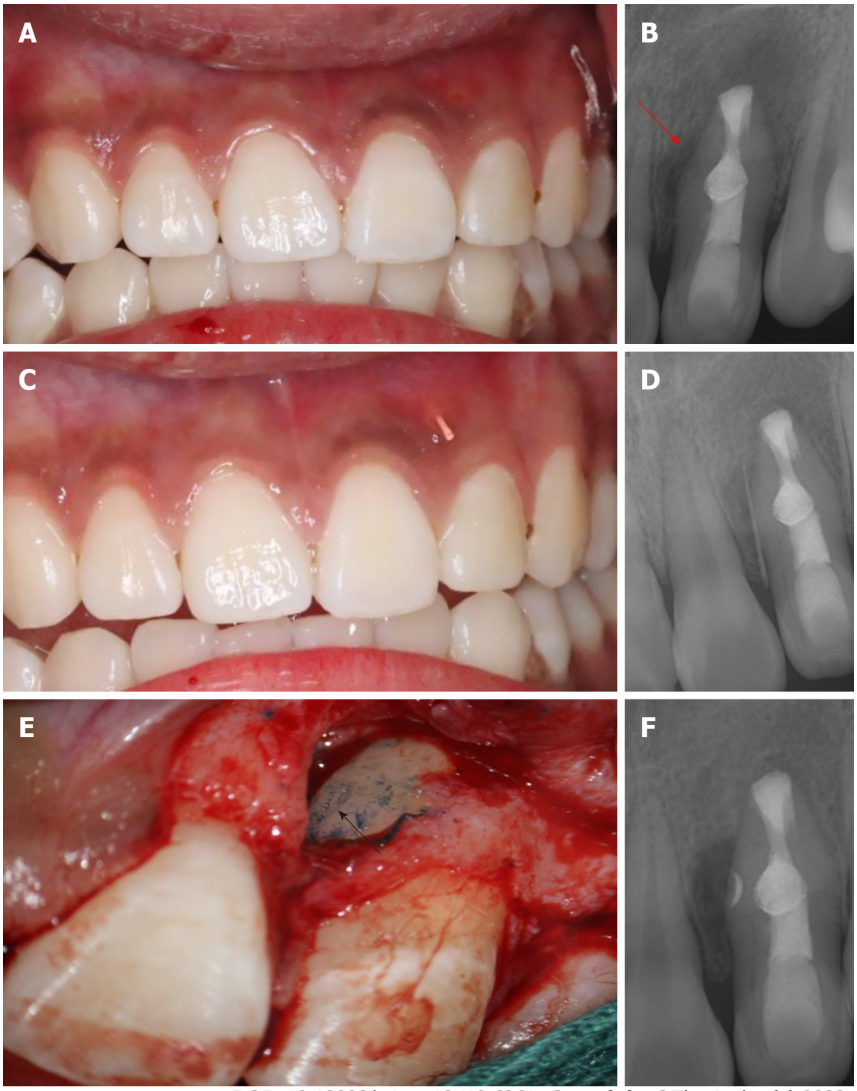

DOI: 10.12998/wjcc.v10.i18.6261 **Copyright** ©The Author(s) 2022.

Figure 3 Intraoral examination after 6 mo and surgical treatment. A: Labial view showing the left lateral incisor with a sinus on the mesiobuccal aspect; B: Radiograph image showing enlargement of a large periapical radiolucency (red arrow) around the mid-root of tooth 22; C: A gutta percha was placed into the sinus of tooth 22; D: Radiograph of tooth 22 with a gutta percha point in the sinus tract; E: Surgical confirmation of the L-shaped pit on the mid-root surface (black arrow); F: Postoperative radiograph.

obturate the lateral canal. Lateral canals are accessory canals that usually extend vertically to the main canal. They are not easily visible in preoperative radiographs[9]. Ricucci *et al*[9] assessed 500 representative extracted teeth that were scanned by microcomputed tomography. The authors found that lateral canals occurred more frequently in the apical third of the root than in the middle of the root. The shape and tortuosity of the lateral canals may vary among different teeth. Most of the lateral canals were curved and not circular, as reported in this patient, which increased the complexity of the treatment. The median diameter of the lateral canals is 67 μm, while the diameter of the main canals is two to three times larger[15,16]. Therefore, apical periodontitis occurs far more frequently than lateral periodontitis.

Some studies have reported that periradicular inflammation has no relationship with unfilled lateral canals[17], and some authors have argued that an insufficiently obturated lateral canal can lead to endodontic treatment failure. This was attributed to the patency of the lateral canal and microbiological involvement[18]. Kim and Kratchman[19] recommended resecting at least 3 mm of apical root to eliminate 98% of apical ramifications and 93% of lateral canals that exist within 3 mm of the root end. However, in this patient, the foramen of the later canal was located at the middle third of the root. Therefore, removal of 3 mm of root end by surgical treatment would not have benefited lateral periodontitis healing. To our knowledge, this is the first report of a tooth of type IIIb DI infected *via* the lateral canal located at the middle of the root.

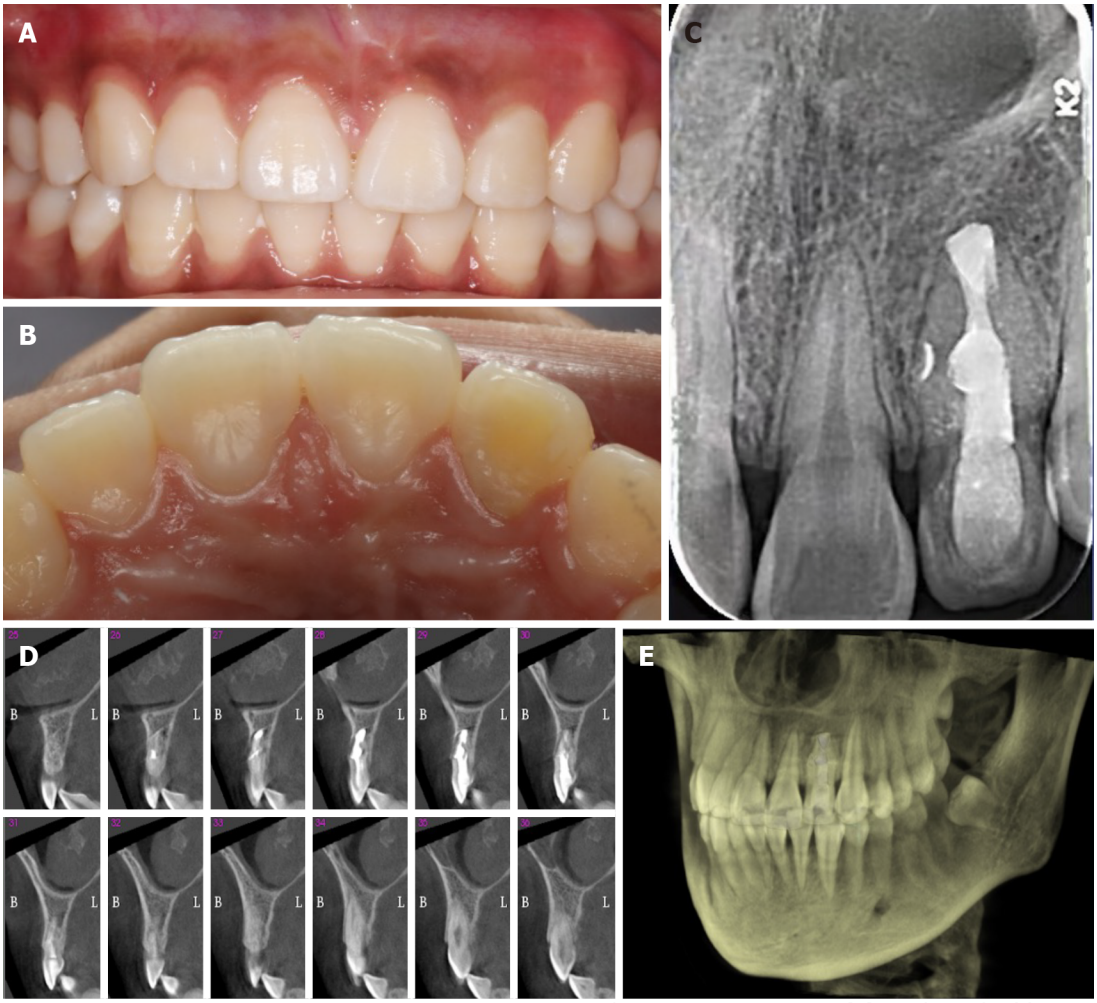

DOI: 10.12998/wjcc.v10.i18.6261 **Copyright** ©The Author(s) 2022.

Figure 4 Follow-up photographs and radiograph. A: Three-year recall labial view; B: Three-year recall palatal view; C: Three-year recall radiograph. The obturated lateral canal was visualized; D: Sagittal sections showing bony healing; E: Three-dimensional reconstruction indicating continuous bony plates.

CONCLUSION

Type IIIb DI has a variety of atypical internal morphologic complexities, which presents a great challenge for treatment in the clinic. This reported case highlights the significance of awareness of type IIIb DI with a lateral canal in the middle of the root. This result indicated that complex type IIIb DI can be successfully treated by a combination of intentional replantation and surgical treatment when conventional endodontic therapy fails.

FOOTNOTES

Author contributions: Zhang J, Li N, and Li WL analyzed and interpreted the imaging findings; Zhang J and Zheng XY reviewed the literature and drafted the manuscript; Li S was the patient's dentist and was responsible for the revision of the manuscript; all authors issued final approval for the version to be submitted.

Supported by Health and Medical Research Fund of the Food and Health Bureau, Hong Kong, China, No. 06171376; Natural Science Foundation of Anhui Province, China, No. 2008085MH255; and Scientific Research Funding of Anhui Medical University, China, No.2020xkj148.

Informed consent statement: Consent was obtained from the patient's parents for publication of this report.

Conflict-of-interest statement: The authors declare that they have no conflicts of interest to disclose.

CARE Checklist (2016) statement: The authors have read the CARE Checklist (2016), and the manuscript was prepared and revised according to the CARE Checklist (2016).

Open-Access: This article is an open-access article that was selected by an in-house editor and fully peer-reviewed by external reviewers. It is distributed in accordance with the Creative Commons Attribution NonCommercial (CC BY-NC 4.0) license, which permits others to distribute, remix, adapt, build upon this work non-commercially, and license their derivative works on different terms, provided the original work is properly cited and the use is non-commercial. See: https://creativecommons.org/Licenses/by-nc/4.0/

Country/Territory of origin: China

ORCID number: Jing Zhang 0000-0002-2774-8110; Na Li 0000-0002-0091-7797; Wu-Li Li 0000-0002-3684-7057; Xian-Yu Zheng 0000-0002-1631-8641; Song Li 0000-0003-1736-2852.

S-Editor: Yan JP
L-Editor: Wang TQ
P-Editor: Yan JP

REFERENCES

1 **Alkadi M**, Almohareb R, Mansour S, Mehanny M, Alsadhan R. Assessment of dens invaginatus and its characteristics in maxillary anterior teeth using cone-beam computed tomography. *Sci Rep* 2021; **11**: 19727 [PMID: 34611255 DOI: 10.1038/s41598-021-99258-0]
2 **Vier-Pelisser FV**, Pelisser A, Recuero LC, Só MV, Borba MG, Figueiredo JA. Use of cone beam computed tomography in the diagnosis, planning and follow up of a type III dens invaginatus case. *Int Endod J* 2012; **45**: 198-208 [PMID: 21978185 DOI: 10.1111/j.1365-2591.2011.01956.x]
3 **Oehlers FA**. Dens invaginatus (dilated composite odontome). I. Variations of the invagination process and associated anterior crown forms. *Oral Surg Oral Med Oral Pathol* 1957; **10**: 1204-18 contd [PMID: 13477660 DOI: 10.1016/0030-4220(57)90077-4]
4 **Ozbas H**, Subay RK, Ordulu M. Surgical retreatment of an invaginated maxillary central incisor following overfilled endodontic treatment: a case report. *Eur J Dent* 2010; **4**: 324-328 [PMID: 20613922]
5 **Kumar H**, Al-Ali M, Parashos P, Manton DJ. Management of 2 teeth diagnosed with dens invaginatus with regenerative endodontics and apexification in the same patient: a case report and review. *J Endod* 2014; **40**: 725-731 [PMID: 24767572 DOI: 10.1016/j.joen.2013.10.030]
6 **Agrawal PK**, Wankhade J, Warhadpande M. A Rare Case of Type III Dens Invaginatus in a Mandibular Second Premolar and Its Nonsurgical Endodontic Management by Using Cone-beam Computed Tomography: A Case Report. *J Endod* 2016; **42**: 669-672 [PMID: 26874642 DOI: 10.1016/j.joen.2016.01.001]
7 **Martins JNR**, da Costa RP, Anderson C, Quaresma SA, Corte-Real LSM, Monroe AD. Endodontic management of dens invaginatus Type IIIb: Case series. *Eur J Dent* 2016; **10**: 561-565 [PMID: 28042276 DOI: 10.4103/1305-7456.195176]
8 **Gallacher A**, Ali R, Bhakta S. Dens invaginatus: diagnosis and management strategies. *Br Dent J* 2016; **221**: 383-387 [PMID: 27713460 DOI: 10.1038/sj.bdj.2016.724]
9 **Ricucci D**, Siqueira JF Jr. Fate of the tissue in lateral canals and apical ramifications in response to pathologic conditions and treatment procedures. *J Endod* 2010; **36**: 1-15 [PMID: 20003929 DOI: 10.1016/j.joen.2009.09.038]
10 **Siqueira JF Jr**, Rôças IN, Hernández SR, Brisson-Suárez K, Baasch AC, Pérez AR, Alves FRF. Dens Invaginatus: Clinical Implications and Antimicrobial Endodontic Treatment Considerations. *J Endod* 2022; **48**: 161-170 [PMID: 34902355 DOI: 10.1016/j.joen.2021.11.014]
11 **Peer M**. Intentional replantation - a 'last resort' treatment or a conventional treatment procedure? *Dent Traumatol* 2004; **20**: 48-55 [PMID: 14998415 DOI: 10.1046/j.1600-4469.2003.00218.x]
12 **Mainkar A**. A Systematic Review of the Survival of Teeth Intentionally Replanted with a Modern Technique and Cost-effectiveness Compared with Single-tooth Implants. *J Endod* 2017; **43**: 1963-1968 [PMID: 29061358 DOI: 10.1016/j.joen.2017.08.019]
13 **Li N**, Xu H, Kan C, Zhang J, Li S. Retrospective Study of Intentional Replantation for Type IIIb Dens Invaginatus with Periapical Lesions. *J Endod* 2022; **48**: 329-336 [PMID: 34999093 DOI: 10.1016/j.joen.2021.12.010]
14 **Yu YH**, Kim M, Kratchman S, Karabucak B. Surgical management of lateral lesions with intentional replantation in single-rooted mandibular first premolars with radicular groove: 2 case reports. *J Am Dent Assoc* 2022 [PMID: 35078591 DOI: 10.1016/j.adaj.2021.09.012]
15 **Ponce EH**, Vilar Fernández JA. The cemento-dentino-canal junction, the apical foramen, and the apical constriction: evaluation by optical microscopy. *J Endod* 2003; **29**: 214-219 [PMID: 12669885 DOI: 10.1097/00004770-200303000-00013]
16 **Xu T**, Tay FR, Gutmann JL, Fan B, Fan W, Huang Z, Sun Q. Micro-Computed Tomography Assessment of Apical Accessory Canal Morphologies. *J Endod* 2016; **42**: 798-802 [PMID: 26975416 DOI: 10.1016/j.joen.2016.02.006]
17 **Barthel CR**, Zimmer S, Trope M. Relationship of radiologic and histologic signs of inflammation in human root-filled teeth. *J Endod* 2004; **30**: 75-79 [PMID: 14977300 DOI: 10.1097/00004770-200402000-00003]
18 **Dammaschke T**, Witt M, Ott K, Schäfer E. Scanning electron microscopic investigation of incidence, location, and size of accessory foramina in primary and permanent molars. *Quintessence Int* 2004; **35**: 699-705 [PMID: 15470993]
19 **Kim S**, Kratchman S. Modern endodontic surgery concepts and practice: a review. *J Endod* 2006; **32**: 601-623 [PMID: 16793466 DOI: 10.1016/j.joen.2005.12.010]

World Journal of Clinical Cases

Submit a Manuscript: https://www.f6publishing.com

World J Clin Cases 2022 June 26; 10(18): 6269-6276

DOI: 10.12998/wjcc.v10.i18.6269

ISSN 2307-8960 (online)

CASE REPORT

Clivus-involved immunoglobulin G4 related hypertrophic pachymeningitis mimicking meningioma: A case report

Yang Yu, Liang Lv, Sen-Lin Yin, Cheng Chen, Shu Jiang, Pei-Zhi Zhou

Specialty type: Medicine, research and experimental

Provenance and peer review: Unsolicited article; Externally peer reviewed.

Peer-review model: Single blind

Peer-review report's scientific quality classification

Grade A (Excellent): A
Grade B (Very good): B
Grade C (Good): C
Grade D (Fair): 0
Grade E (Poor): 0

P-Reviewer: Khan S, India; Velá zquez-Saornil J, Spain

Received: December 13, 2021
Peer-review started: December 13, 2021
First decision: February 14, 2022
Revised: February 23, 2022
Accepted: April 22, 2022
Article in press: April 22, 2022
Published online: June 26, 2022

Yang Yu, Department of Neur-osurgery, West China Hospital, Sichuan University, Chengdu 610041, Sichuan Province, China

Liang Lv, Sen-Lin Yin, Cheng Chen, Shu Jiang, Pei-Zhi Zhou, Department of Neur-osurgery, West China Hospital, Sichuan University, Chengdu 610041, Sichuan Province, China

Corresponding author: Pei-Zhi Zhou, MD, Associate Professor, Surgeon, Department of Neurosurgery, West China Hospital, Sichuan University, No. 37 Guoxue Alley, Chengdu 610041, Sichuan Province, China. peizhizhou@126.com

Abstract

BACKGROUND

Immunoglobulin G4 related disease (IgG4-RD) is a fibroinflammatory disease with markedly elevated serum IgG4 levels and fibrous tissue proliferation, accompanied by numerous plasma cells. IgG4 related hypertrophic pachymeningitis (IgG4-RHP) is relatively rare and indistinguishable from other phymatoid diseases before the operation. The risk of long-term immunosuppression needs to be balanced with disease activity.

CASE SUMMARY

A 40-year-old man presented with headache and bilateral abducent paralysis. He was also diagnosed with pulmonary tuberculosis 10 years ago and was on regular treatment for the same. Before the operation and steroid therapy, the patient was suspected of having tubercular meningitis at a local hospital. A clivus lesion was found *via* brain magnetic resonance imaging (MRI) at this presentation. He was preliminarily diagnosed with meningioma and underwent Gamma Knife Surgery. Transnasal endoscopic resection was performed to treat deterioration of nerve function. Postoperative pathologic examination suggested IgG4-RD. Moreover, the serum IgG4 was elevated at 1.90 g/L (reference range: 0.035-1.500 g/L). After steroid therapy for 2 mo, the lesion size diminished on MRI, and the function of bilateral abducent nerves recovered.

CONCLUSION

IgG4-RHP is relatively rare and indistinguishable before the operation. Elevated serum IgG4 levels and imaging examination help in the diagnosis of IgG4-RHP. Surgery is necessary when lesions progress and patients start to develop cranial nerve function deficit.

Key Words: Immunoglobulin G4 related disease; Hypertrophic pachymeningitis; Immu-noglobulin G4 related hypertrophic pachymeningitis; Clivus; Case report

©The Author(s) 2022. Published by Baishideng Publishing Group Inc. All rights reserved.

Core Tip: Immunoglobulin G4 related disease (IgG4-RD) is a fibroinflammatory disease with markedly elevated serum IgG4 levels and fibrous tissue proliferation, accompanied by numerous plasma cells. It is known to affect multiple organs. IgG4-related hypertrophic pachymeningitis (IgG4-RHP) is relatively rare and indistinguishable from IgG4-RD before the operation. Herein, we present a rare case of IgG4-RHP with intact magnetic resonance imaging and pathologic images. The case highlighted the differential diagnosis with other phymatoid lesions such as meningioma, fungal infection, and tuberculosis and the importance of comprehensive multidisciplinary treatment. Surgery becomes necessary when lesions progress and patients start to develop cranial nerve function deficit.

Citation: Yu Y, Lv L, Yin SL, Chen C, Jiang S, Zhou PZ. Clivus-involved immunoglobulin G4 related hypertrophic pachymeningitis mimicking meningioma: A case report. *World J Clin Cases* 2022; 10(18): 6269-6276
URL: https://www.wjgnet.com/2307-8960/full/v10/i18/6269.htm
DOI: https://dx.doi.org/10.12998/wjcc.v10.i18.6269

INTRODUCTION

Immunoglobulin G4 related disease (IgG4-RD) was initially noticed in patients with autoimmune pancreatitis in 2001 and formally named in 2010, classified as sarcoidosis with different manifestations in several organs and the same pathological characteristics[1,2]. The main characteristic of IgG4-RD is elevated levels of serum IgG4. Moreover, the lesions are often tumescent with abundant IgG4-positive plasma cells and fibrosis. Such inflammatory lesions can be seen in the pancreas, kidney, lungs, salivary glands, and other organs. Specifically, the conditions of IgG4-RD in the central nervous system are meningitis and hypophysitis[3]. As for the IgG4-related hypertrophic pachymeningitis (IgG4-RHP), the clinical and imaging manifestation is similar to that of meningioma, posing a challenge for preoperative diagnosis[4,5]. Additionally, the time and scope of operation should be considered carefully. Finally, this disease is related to some bacterial infections, such as tuberculosis. And we need to weight the pros and cons between these infections and corticosteroid therapy for IgG4-RD. Herein, we report a rare case with IgG4-RHP at the clivus area mimicking meningioma and discuss the relevant literature.

CASE PRESENTATION

Chief complaints

A 40 year-old man was admitted for headache, bilateral temporal visual field defect, and limited abduction in both eyes.

History of present illness

Five years before the present admission, the patient started to experience discontinuous and aggravating headache. Owing to symptomatic deterioration, the patient was admitted to the neurology department of a local hospital. Because the patient also had a history of pulmonary tuberculosis, he was suspected of having tuberculosis meningitis and treated with anti-tuberculosis drugs at the local hospital. However, the symptom did not alleviate. Upon presentation to our hospital, the patient underwent a brain magnetic resonance imaging (MRI) scan that showed the presence of a clival lesion measuring 2.6 × 1 cm^2 with isointense signal on T1-weighted (T1WI) and T2-weighted (T2WI) imaging; accordingly, he was diagnosed with meningioma. The lesion was homogenously enhanced on contrast MRI with a dural tail sign (Figure 1). Because there was no cranial nerve function defect, the patients chose to undergo Gamma Knife Surgery at a dose of 11 Gy at the 45% isodose line, and regular follow-up was planned.

History of past illness

The patient had suffered from pulmonary tuberculosis 11 years ago and accepted standard anti-tuberculosis treatment for 1 year.

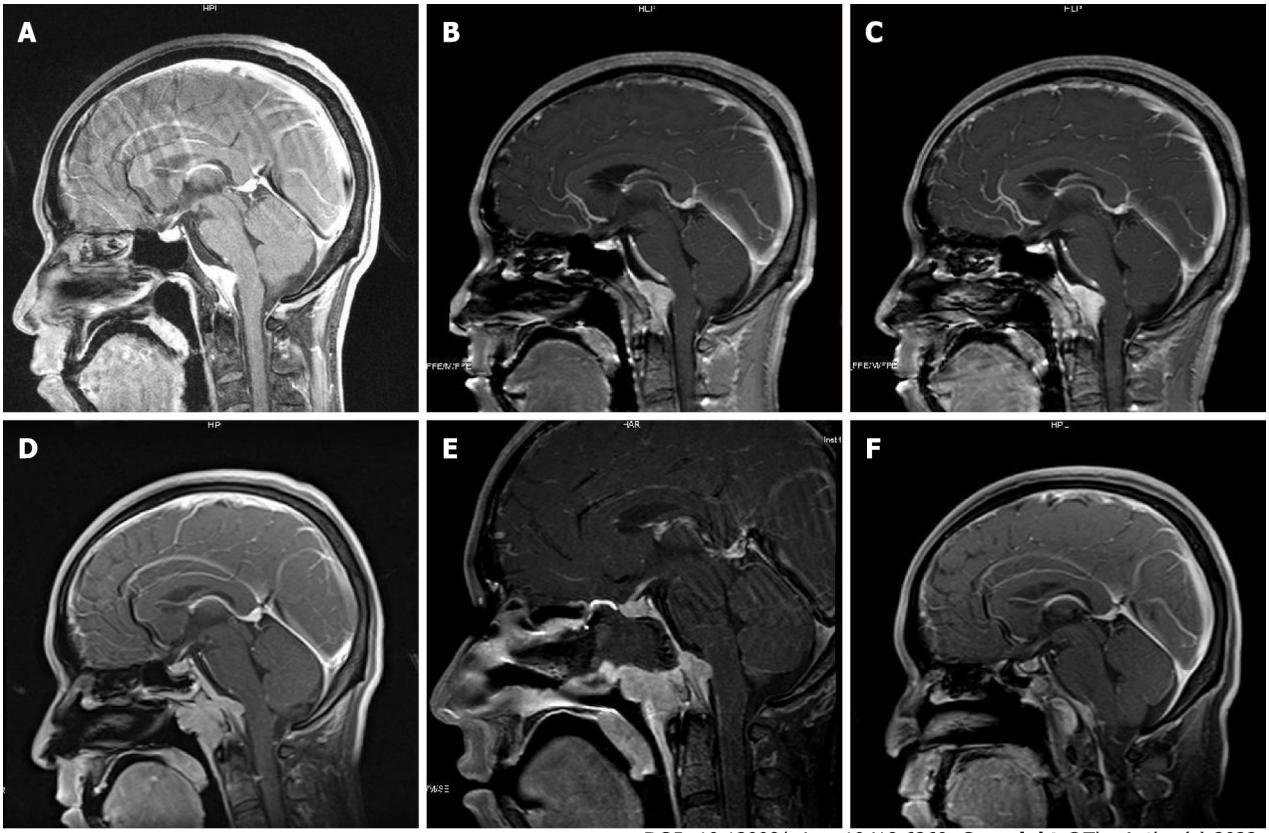

DOI: 10.12998/wjcc.v10.i18.6269 **Copyright** ©The Author(s) 2022.

Figure 1 Lesion alteration on the sagittal view. A: This image shows the condition when the patient was first admitted to the tuberculosis department diagnosed as having a meningioma (December 2016); B: Before the performance of Gamma Knife Surgery (March 2017); C: Six months after the performance of Gamma Knife Surgery (September 2017); D: Preoperative image (November 2019); E: Postoperative image (January 2020); F: Two months after operation (March 2020).

Personal and family history

No other particular personal and family history was reported.

Physical examination

This patient showed right abducens paralysis, hoarse voice, bitemporal hemianopsia, and slight swallowing difficulty. No other positive signs were found.

Laboratory examinations

Lumbar puncture was performed and we found that the number of karyocytes (mainly mononuclear cells) and protein levels in cerebrospinal fluid had risen (Table 1).

After pathological results showed IgG4-RD, further systemic evaluation was performed to find other lesions associated with IgG4-RD. The serum IgG level was 17.20 g/L (reference range: 8.00-15.50 g/L), and the serum level of IgG4 was 1.90 g/L (reference range: 0.035-1.500 g/L). Tuberculosis associated gamma interferon release assay showed positive results with TB-IGRA (T-N) at 414.21 pg/mL.

Imaging examinations

After admission, routine laboratory testing and preoperative preparation were carried out. A repeat brain MRI scan showed that the lesion became larger, measured 3.8 cm × 2.9 cm × 2.9 cm, and compressed the adjacent brain stem (Figure 1). Further, small pneumatoceles in the upper lobe of the right lung were detected by thorax computed tomography (CT). Moreover, the examination of visual field confirmed binocular hemianopia (Figure 2). No other positive results were found.

FINAL DIAGNOSIS

The postoperative pathology confirmed the proliferation of fibrous tissue accompanied by numerous lymphocytes and plasma cells, which is displayed in Figure 3. Immunohistochemical staining showed positive results for CD138 and IgG4. Gene rearrangement test showed negative results for IgH. Thus,

Table 1 Examination results of cerebral fluid through the years

	2014	2016	2020
General characters	Normal	Normal	Normal
Karyocytes (10^6/L)	120	90	1
Mononuclear cells (%)	97.0	92.0	-
Multinucleate cells (%)	3.0	8.0	-
Pus cells	Unseen	Unseen	Unseen
Protein quantification (g/L)	1.02	0.69	0.55
Glucose (mmol/L)	2.55	4.07	3.95
Chloride (mmol/L)	127.2	124.4	127
Acid-fast bacillus	None	None	None
Ink staining	None	None	None
Gram staining	None	None	None
Fungal and bacterial culture	Undone	Negative	Negative
TB-DNA	Undone	Negative	Negative

Reference value: Karyocytes (< 10 × 10^6/L), pus cells (none), protein quantification (0.15-0.45 g/L), glucose (2.5-4.4 mmol/L), and chloride (120-130 mmol/L).

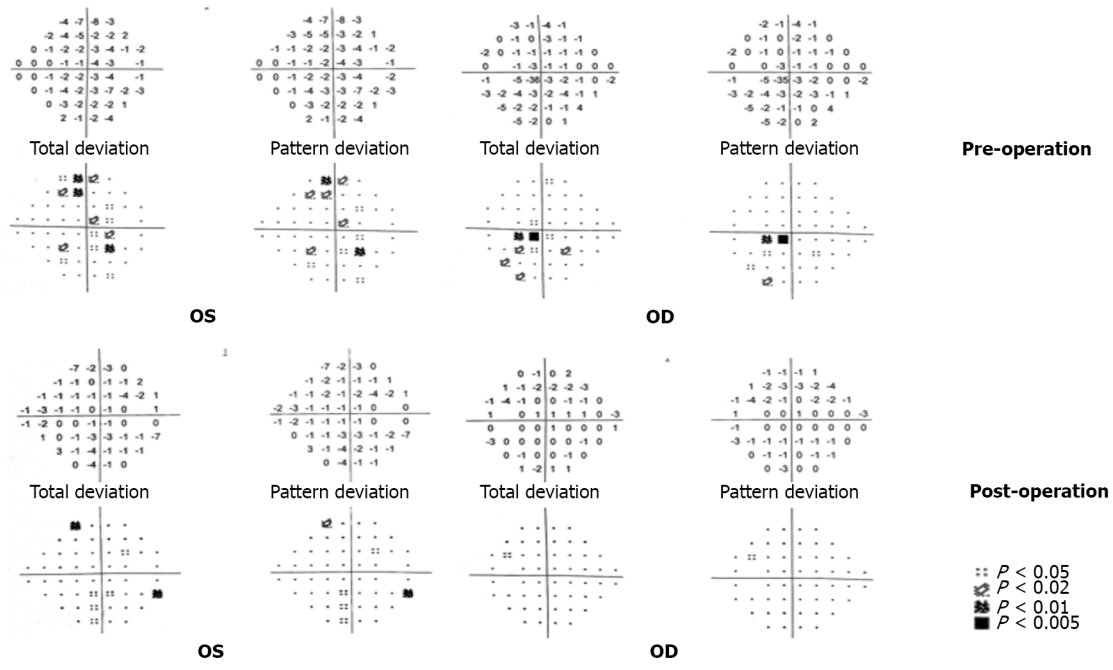

DOI: 10.12998/wjcc.v10.i18.6269 **Copyright** ©The Author(s) 2022.

Figure 2 Examination of visual field before and after the operation. The alteration of the visual field before and after the operation is shown. The second row is the result at 4 mo after the operation.

IgG4-RD was finally diagnosed.

TREATMENT

The patient underwent transnasal endoscopic approach resection which aimed to partially remove the lesion for pathology analysis and alleviate the headache caused by meningeal tension. During the operation, we found that the lesion extended to the sphenoid sinus and nasopharynx without a clear

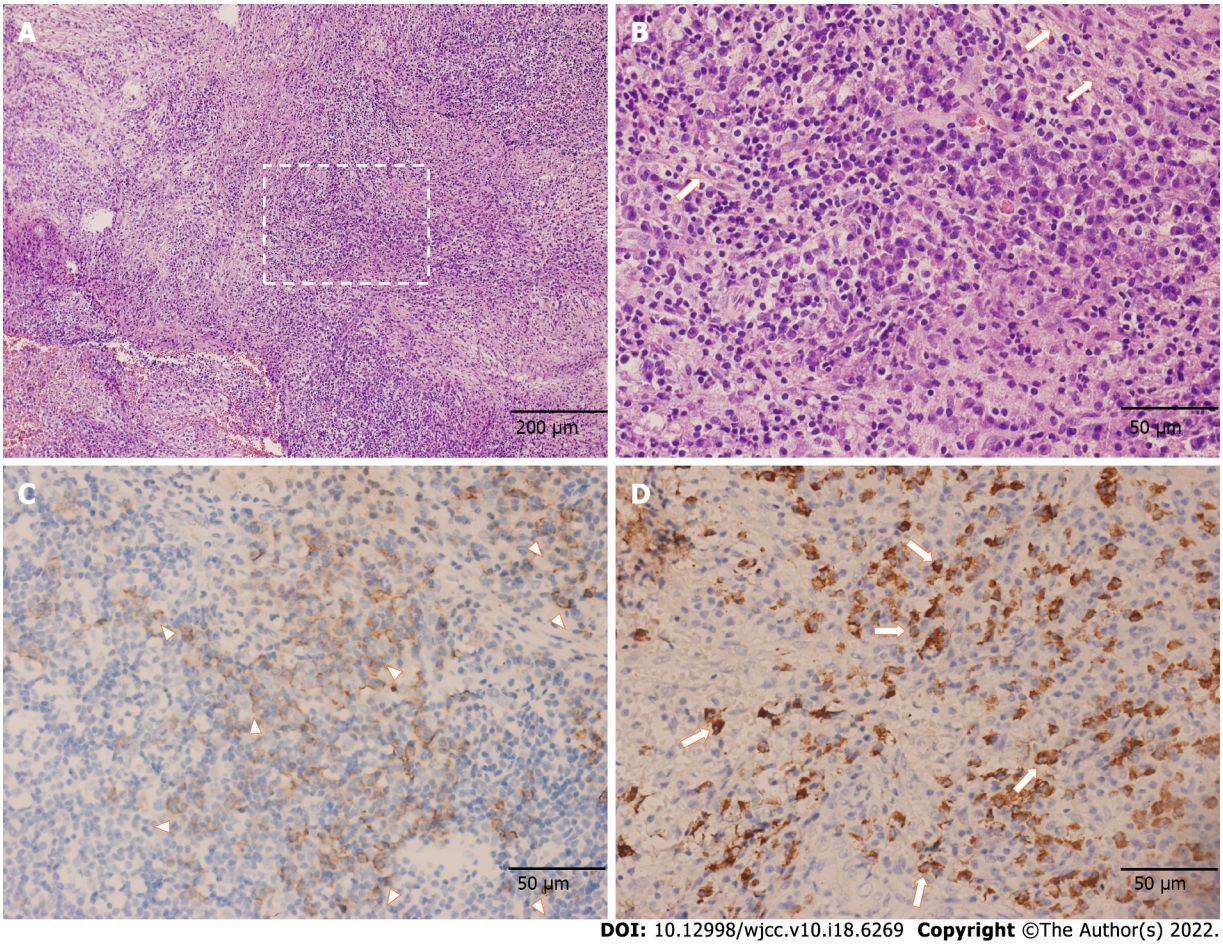

DOI: 10.12998/wjcc.v10.i18.6269 **Copyright** ©The Author(s) 2022.

Figure 3 Pathological features of the resection part indicating the diagnosis of immunoglobulin G4 related hypertrophic pachymeningitis. A and B: Proliferation of fibrous tissue accompanied by numerous lymphocytes and plasma cells as shown by hematoxylin and eosin staining (A: × 100; B: × 400); C: Immunohistochemical staining exhibited an increased number of CD138-positive plasma cells (× 400); D: Large number of immunoglobulin G4-positive plasma cells as shown by immunohistochemical staining [~200 *per* high power field (× 400)].

boundary. Notably, the local mucosa was edematous and tight. The clivus bone had been partially damaged, and the clivus epidural was thicker. The intraoperative frozen section examination revealed the proliferation of spindle cells accompanied by many lymphocytes and plasma cells.

For the diagnosis of IgG4-RD, solu medrol was administrated at a dose of 80 mg *per* day, and methotrexate was administrated at 10 mg every week. Famotidine, calcium carbonate, and vitamin D3 tablets were prescribed against adverse reactions during the treatment. After discharge from the hospital, the solu medrol was tapered over 4 wk to 50 mg *per* day.

OUTCOME AND FOLLOW-UP

The patient confirmed that his headache and hoarse voice gradually improved after 1 mo. The follow-up was arranged 3 mo after the operation, which showed that the abduction movement could be achieved for binocular vision. Brain MRI showed that the residual lesion obviously shrunk (Figure 1). The change for bilateral visual fields is displayed in Figure 2.

DISCUSSION

IgG4-RD is a condition that affects multiple organs, and its clinical manifestations often vary across different organs. Reportedly, several kinds of bacterial infection can be causative factors for this disease related to stimulation with Toll-like receptor ligands[6,7]. Several previous studies have also reported the comorbidity of IgG4-RD with tuberculosis, as seen in our patient[8-11].

IgG4-RD of the CNS is mainly related to IgG4-related hypertrophic pachymeningitis and hypophysitis. Among them, IgG4-RHP is relatively rare, with the primary clinical manifestation of headache and other nerve function disabilities. Moreover, it was apparent that the cranial nerve

function could partially recover once the disease was in remission. At the first onset of the disease, multi-organ disease is not widespread (57%)[6]. Therefore, regular follow-up and systemic evaluation is crucial.

Through this case, we summarize the differential diagnoses of IgG4-RHP, such as meningioma, tuberculosis meningitis, fungal meningitis, and metastatic tumor. Furthermore, the complete MRI images showed the lesion alteration during treatment. However, there are limited reports of this rare disease in the literature. Higher evidence-based studies are needed to promote the diagnosis and treatment of IgG4-RHP.

Measuring the serum concentration of IgG4, radiological examination, and pathological screening are important for diagnosis. It is difficult to distinguish IgG4-RHP and meningioma before the operation and pathologic examination. The serum level of IgG4 can facilitate diagnosis, but it does not always show an increase. As reported by Wallace *et al*[12], the sensitivity and specificity of serum IgG4 were 90% and 60%, respectively. Moreover, the negative predictive value and positive predictive value of the serum IgG4 assay were 96% and 34%, respectively, which could be helpful and convenient to exclude the diagnosis of IgG4-RD related to the CNS[12]. It is also helpful to distinguish tuberculosis and IgG4-RD based on the fact that serum IgG4 does not significantly increase in tuberculosis[13]. Further, imaging results could be a crucial clue for preoperative diagnosis. Lumbar puncture provides the necessary information for differentiation from CNS infections and malignant tumors. IgG4 levels in cerebrospinal fluid have been reported to be elevated[14]. However, the concentration of IgG4 in cerebrospinal fluid could not distinguish this disease from other inflammatory pachymeningitis[6].

Radiology examination plays an essential role in diagnosis. The lesion could be observed as linear dural thickening or a bulging mass. The linear dural thickened lesion appears both in the brain and spine. The tumoral lesion is frequently located in the clivus area. The heterogeneity was observed on MRI because of active inflammation. Typically, T1WI MRI would exhibit a hyperintense or isointense signal. Hypertrophic pachymeningitis usually shows thickening meninges and hypointensity on T2WI MRI, while it would become relative hyperintense when the inflammation aggravates[3,4,6,7,15]. The lesion would be homogenously enhanced on enhanced MRI. In this case, the lesion showed an isointensite signal on T1WI and T2WI and was homogenously enhanced on contrast MRI with a dural tail sign. CT showed that the skull was involved apparently and the lesion appeared hyperdense when contrast-enhanced CT was performed. In case of a meningioma, CT frequently displays that the lesion is isodense or has slightly higher density with a round, leafy, or flat shape[3,6]. Calcification becomes visible in some tumors[6]. Meningioma has similar characteristics as an IgG4-RHP lesion. T1WI often shows isointense or mildly hypointense signal, and T2WI usually shows isointense or mildly hyperintense signal. Besides, the meningioma could be markedly characterized by the tail of the meninges.

It is advisable to focus on some characteristics to help distinguish between meningioma and IgG4-RHP. We noticed that the symptoms of IgG4-RHP were severe and diverse, while those of meningioma were not as varied. These symptoms were due to inflammatory irritation and compression of the adjacent nerves and dura mater[16]. Another characteristic of IgG4-RHP was that the tail signal was broader than meningioma on MRI for the diffuse inflammation along with the dura mater. The meningioma lesion seems relatively confined and phymatoid compared with IgG4-RHP. Moreover, the IgG4-RHP lesion frequently involves extracranial parts.

Other diseases, such as metastatic tumors and fungal infections, should also be considered. It was observed that metastatic tumors could spread and proliferate along the meninges, causing various severe symptoms. In this situation, the history of malignant tumor provided clues to the diagnosis. Likewise, a CNS fungal infection can show similar features, which can be identified by examining the cerebrospinal fluid.

CNS tuberculosis is another antidiastole. Patients with tuberculous meningitis often have a fever, headache, and focal neurological symptoms. And tuberculous meningitis is often secondary to pulmonary or intestinal tuberculosis. As for radiology examination, CT often exhibits nodular or punctate calcifications and hydrocephalus, and enhanced scans are often accompanied by meningeal strengthening. MRI frequently shows a hypointense T1WI signal and hyperintense T2WI signal. The enhancement scan could display irregular bar or nodular strengthening lesions of the meninges. Cerebrospinal fluid is essential for the diagnosis of tuberculous meningitis. Moreover, TB-IGRA could facilitate this diagnosis.

The purpose of the operation was not only to perform a biopsy but also to alleviate symptoms. We know that the lesion would stretch meninges and then cause headache. Similarly, the lesion compresses cranial nerves to cause relevant symptoms. The resection can reduce meningeal tension, release compression, and finally alleviate headache and nerve deficits. Further, it is suitable to use the transnasal endoscopic approach for a clival lesion in IgG4-RHP. When the lesion is too broad to remove completely, it is sensible to leave some parts in order to maintain the integrity of the dura mater, which can prevent severe complications such as cerebrospinal fluid leakage and intracranial infection.

Glucocorticoids and immunosuppressants can be used for the non-surgical treatment, such as prednisolone (0.6 mg/kg/d) for 4 wk. The dose of steroid was gradually decreased through 3-6 mo and the dose was finally maintained at 2.5 to 5.0 mg/d for 3 years[17]. Other immunosuppressants should be considered, such as methotrexate, cyclophosphamide, mycophenolate mofetil, and azathioprine[6,7].

Another consensus recommended utilizing calcium carbonate and vitamin D3 tablets to prevent glucocorticoid-induced osteoporosis[18,19]. Additionally, it is essential to exclude some latent infections before using glucocorticoids and immunosuppressants. In this case, the patient had a history of tuberculosis and we performed the chest CT and TB-IGRA to ensure the absence of any current underlying infection. In future, when similar patients with the imaging characteristics described in this report are encountered, measurement of serum IgG4 levels may be helpful for diagnosis.

CONCLUSION

IgG4-RHP is a relatively rare disease that seems complicated to diagnose preoperatively. The purpose of surgery is to obtain the specimens required for pathological examination and plan the follow-up treatment. It is essential to perform a rigorous follow-up and systematic assessment of the whole body.

FOOTNOTES

Author contributions: Yu Y collected the data, contacted with the patient, and wrote the manuscript; Lv L wrote and revised the manuscript; Chen C and Yin SL made the revision to the primary manuscript; Jiang S and Zhou PZ supervised the whole work and made the operation.

Supported by 1·3·5 Project for Disciplines of Excellence–Clinical Research Incubation Project, West China Hospital, Sichuan University, No. 2019HXFH018.

Informed consent statement: Informed written consent was obtained from the patient for publication of this report and any accompanying images.

Conflict-of-interest statement: The authors declare that they have no conflict of interest to disclose.

CARE Checklist (2016) statement: The authors have read the CARE Checklist (2016), and the manuscript was prepared and revised according to the CARE Checklist (2016).

Open-Access: This article is an open-access article that was selected by an in-house editor and fully peer-reviewed by external reviewers. It is distributed in accordance with the Creative Commons Attribution NonCommercial (CC BY-NC 4.0) license, which permits others to distribute, remix, adapt, build upon this work non-commercially, and license their derivative works on different terms, provided the original work is properly cited and the use is non-commercial. See: https://creativecommons.org/Licenses/by-nc/4.0/

Country/Territory of origin: China

ORCID number: Yang Yu 0000-0002-9901-1310; Liang Lv 0000-0002-5524-7014; Sen-Lin Yin 0000-0003-2241-3749; Cheng Chen 0000-0002-7540-1306; Shu Jiang 0000-0002-6700-7560; Pei-Zhi Zhou 0000-0002-8017-5833.

S-Editor: Fan JR
L-Editor: Wang TQ
P-Editor: Fan JR

REFERENCES

1 **Hamano H**, Kawa S, Horiuchi A, Unno H, Furuya N, Akamatsu T, Fukushima M, Nikaido T, Nakayama K, Usuda N, Kiyosawa K. High serum IgG4 concentrations in patients with sclerosing pancreatitis. *N Engl J Med* 2001; **344**: 732-738 [PMID: 11236777 DOI: 10.1056/nejm200103083441005]

2 **Takahashi H**, Yamamoto M, Suzuki C, Naishiro Y, Shinomura Y, Imai K. The birthday of a new syndrome: IgG4-related diseases constitute a clinical entity. *Autoimmun Rev* 2010; **9**: 591-594 [PMID: 20457280 DOI: 10.1016/j.autrev.2010.05.003]

3 **Wallace ZS**, Carruthers MN, Khosroshahi A, Carruthers R, Shinagare S, Stemmer-Rachamimov A, Deshpande V, Stone JH. IgG4-related disease and hypertrophic pachymeningitis. *Medicine (Baltimore)* 2013; **92**: 206-216 [PMID: 23793110 DOI: 10.1097/MD.0b013e31829cce35]

4 **Tang H**, Ding G, Xiong J, Zhu H, Hua L, Xie Q, Gong Y. Clivus Inflammatory Pseudotumor Associated with Immunoglobulin G4-Related Disease. *World Neurosurg* 2018; **118**: 71-74 [PMID: 29966794 DOI: 10.1016/j.wneu.2018.06.174]

5 **Cha YJ**, Lee SK, Chang JH, Kim SH. Report of a rare case of atypical lymphoplasmacyte-rich meningioma in the tentorium mimicking idiopathic hypertrophic pachymeningitis. *Brain Tumor Pathol* 2016; **33**: 216-221 [PMID: 26902101 DOI: 10.1007/s10014-016-0254-8]

6 **Lu LX**, Della-Torre E, Stone JH, Clark SW. IgG4-related hypertrophic pachymeningitis: clinical features, diagnostic

criteria, and treatment. *JAMA Neurol* 2014; **71**: 785-793 [PMID: 24733677 DOI: 10.1001/jamaneurol.2014.243]

7 **Stone JH**, Zen Y, Deshpande V. IgG4-related disease. *N Engl J Med* 2012; **366**: 539-551 [PMID: 22316447 DOI: 10.1056/NEJMra1104650]

8 **Bae K**, Jung An H, Jeon KN, Hyun Song D, Kim SH, Kim HC. Coexistence of nontuberculous mycobacterium and IgG4-related disease in a solitary pulmonary nodule: A case report. *Medicine (Baltimore)* 2019; **98**: e18179 [PMID: 31770270 DOI: 10.1097/MD.0000000000018179]

9 **Bajema KL**, Daniel JC, Hussain S, Dworkin RJ. IgG4-related pulmonary and salivary disease associated with pulmonary tuberculosis. *Ann Am Thorac Soc* 2014; **11**: 1165-1167 [PMID: 25238001 DOI: 10.1513/AnnalsATS.201406-229LE]

10 **Kawano M**, Yamada K, Kakuchi Y, Ito K, Hamano R, Fujii H, Inoue R, Matsumura M, Takahira M, Zen Y, Yachie A, Nakashima A, Yamagishi M. A case of immunoglobulin G4-related chronic sclerosing sialadenitis and dacryoadenitis associated with tuberculosis. *Mod Rheumatol* 2009; **19**: 87-90 [PMID: 18855098 DOI: 10.1007/s10165-008-0127-z]

11 **Imai T**, Yumura W, Takemoto F, Kotoda A, Imai R, Inoue M, Hironaka M, Muto S, Kusano E. A case of IgG4-related tubulointerstitial nephritis with left hydronephrosis after a remission of urinary tract tuberculosis. *Rheumatol Int* 2013; **33**: 2141-2144 [PMID: 22218636 DOI: 10.1007/s00296-011-2271-6]

12 **Wallace ZS**, Mattoo H, Carruthers M, Mahajan VS, Della Torre E, Lee H, Kulikova M, Deshpande V, Pillai S, Stone JH. Plasmablasts as a biomarker for IgG4-related disease, independent of serum IgG4 concentrations. *Ann Rheum Dis* 2015; **74**: 190-195 [PMID: 24817416 DOI: 10.1136/annrheumdis-2014-205233]

13 **Araujo Z**, Giampietro F, Rivas-Santiago B, Luna-Herrera J, Wide A, Clark W, de Waard JH. Patients exposed to Mycobacterium tuberculosis infection with a prominent IgE response. *Arch Med Res* 2012; **43**: 225-232 [PMID: 22564424 DOI: 10.1016/j.arcmed.2012.04.002]

14 **Zhao Y**, Xu J. Imaging features, clinicopathological analysis and diagnostic strategy of IgG4-related hypertrophic pachymeningitis. *Ann Palliat Med* 2020; **9**: 2551-2558 [PMID: 32819129 DOI: 10.21037/apm-19-452]

15 **Detiger SE**, Karim F, Monserez D, Verdijk R, van Hagen M, Paridaens D, van Laar J. IgG4-Related Disease of Skull Base: Case Series of 3 Patients with Headache. *World Neurosurg* 2020; **134**: 536-539 [PMID: 31669684 DOI: 10.1016/j.wneu.2019.10.111]

16 **Tokushige S**, Matsuura H, Hideyama T, Tamura K, Maekawa R, Shiio Y. Hypertrophic Pachymeningitis as a Potential Cause of Headache Associated with Temporal Arteritis. *Intern Med* 2016; **55**: 523-526 [PMID: 26935376 DOI: 10.2169/internalmedicine.55.5340]

17 **Kamisawa T**, Okazaki K, Kawa S, Shimosegawa T, Tanaka M; Research Committee for Intractable Pancreatic Disease and Japan Pancreas Society. Japanese consensus guidelines for management of autoimmune pancreatitis: III. Treatment and prognosis of AIP. *J Gastroenterol* 2010; **45**: 471-477 [PMID: 20213336 DOI: 10.1007/s00535-010-0221-9]

18 **Park SY**, Gong HS, Kim KM, Kim D, Kim HY, Jeon CH, Ju JH, Lee SS, Park DA, Sung YK, Kim SW. Korean Guideline for the Prevention and Treatment of Glucocorticoid-induced Osteoporosis. *J Bone Metab* 2018; **25**: 195-211 [PMID: 30574464 DOI: 10.11005/jbm.2018.25.4.195]

19 **Buckley L**, Guyatt G, Fink HA, Cannon M, Grossman J, Hansen KE, Humphrey MB, Lane NE, Magrey M, Miller M, Morrison L, Rao M, Robinson AB, Saha S, Wolver S, Bannuru RR, Vaysbrot E, Osani M, Turgunbaev M, Miller AS, McAlindon T. 2017 American College of Rheumatology Guideline for the Prevention and Treatment of Glucocorticoid-Induced Osteoporosis. *Arthritis Rheumatol* 2017; **69**: 1521-1537 [PMID: 28585373 DOI: 10.1002/art.40137]

World Journal of Clinical Cases

Submit a Manuscript: https://www.f6publishing.com

World J Clin Cases 2022 June 26; 10(18): 6277-6282

DOI: 10.12998/wjcc.v10.i18.6277

ISSN 2307-8960 (online)

CASE REPORT

De novo brain arteriovenous malformation formation and development: A case report

Huan Huang, Xue Wang, An-Na Guo, Wei Li, Ren-Hua Duan, Jun-Hao Fang, Bo Yin, Dan-Dong Li

Specialty type: Clinical neurology

Provenance and peer review: Unsolicited article; Externally peer reviewed.

Peer-review model: Single blind

Peer-review report's scientific quality classification

Grade A (Excellent): A
Grade B (Very good): 0
Grade C (Good): C
Grade D (Fair): 0
Grade E (Poor): 0

P-Reviewer: Almzeogi MA, Serbia; Medina SM, Bolivia

Received: January 13, 2022
Peer-review started: January 13, 2022
First decision: March 23, 2022
Revised: April 1, 2022
Accepted: April 27, 2022
Article in press: April 27, 2022
Published online: June 26, 2022

Huan Huang, Xue Wang, An-Na Guo, Department of Radiology, The Second Affiliated Hospital and Yuying Children's Hospital of Wenzhou Medical University, Wenzhou 325000, Zhejiang Province, China

Wei Li, Ren-Hua Duan, Jun-Hao Fang, Bo Yin, Dan-Dong Li, Department of Neurosurgery, The Second Affiliated Hospital and Yuying Children's Hospital of Wenzhou Medical University, Wenzhou 325000, Zhejiang Province, China

Corresponding author: Dan-Dong Li, MD, Neurosurgeon, Department of Neurosurgery, The Second Affiliated Hospital and Yuying Children's Hospital of Wenzhou Medical University, No. 108 Xueyuan West Road, Wenzhou 325000, Zhejiang Province, China.
andonglmn@163.com

Abstract

BACKGROUND

Brain arteriovenous malformation (AVM), an aberrant vascular development during the intrauterine period, is traditionally considered a congenital disease. Sporadic reports of cases of *de novo* AVM formation in children and adults have challenged the traditional view of its congenital origin.

CASE SUMMARY

In this report, we have presented the case of a child with a *de novo* brain AVM. Magnetic resonance imaging and magnetic resonance angiography of the brain showed no AVM at the age of 5 years and 2 mo. Brain AVM was first detected in this child at the age of 7 years and 4 mo. The brain AVM was significantly advanced, and hemorrhage was seen for the first time at the age of 12 years and 8 mo. There was further progression in the AVM, and hemorrhage occurred again at the age of 13 years and 5 mo. Genetic analysis of this patient revealed a mutation in the *NOTCH2* (p.Asp473Val) gene.

CONCLUSION

In short, our case has once again confirmed the view that brain AVM is an acquired disease and is the result of the interaction of genes, environment, and molecules.

Key Words: *De novo* arteriovenous malformation; Angiogenesis; Hemorrhage; *NOTCH2*; Case report

©The Author(s) 2022. Published by Baishideng Publishing Group Inc. All rights reserved.

Core Tip: Brain arteriovenous malformation (AVM) is one of the main causes of spontaneous cerebral hemorrhage in children. At present, the mechanism of the occurrence and development of AVM is not clear, and there have been very few case reports that have documented the progression of a *de novo* brain AVM. In this report, we present the case of a child with a *de novo* brain AVM. Brain AVM was first detected in this child at the age of 7 years and 4 mo and was significantly advanced and hemorrhaging at the age of 12 years and 8 mo. Genetic analysis of this patient revealed a mutation in the *NOTCH2* (p.Asp473Val) gene.

Citation: Huang H, Wang X, Guo AN, Li W, Duan RH, Fang JH, Yin B, Li DD. *De novo* brain arteriovenous malformation formation and development: A case report. *World J Clin Cases* 2022; 10(18): 6277-6282
URL: https://www.wjgnet.com/2307-8960/full/v10/i18/6277.htm
DOI: https://dx.doi.org/10.12998/wjcc.v10.i18.6277

INTRODUCTION

Brain arteriovenous malformation (AVM) is one of the main causes of spontaneous cerebral hemorrhage in children[1] and accounts for 30%-50% of spontaneous cerebral hemorrhage in children[1,2]. It is generally believed that AVM is a kind of congenital vascular disease[3]. The abnormality is formed in the third to fourth week of embryonic development, when the length is about 40-80 mm, during the process of cerebrovascular development and manifests as abnormal coiled and interlaced vascular clusters[4]. Arteries and veins are directly connected by malformed vascular clusters. At present, the mechanism of the occurrence and development of AVM is not clear, and there have been very few case reports that have documented the progression of a *de novo* brain AVM[5-7]. Here, we have documented for the first time a case of a child with a *de novo* brain AVM that progressed and ruptured twice within 6 years. We have also reported for the first time the potential role of heterozygous mutations in the *NOTCH2* gene in the pathogenesis of AVM.

CASE PRESENTATION

Chief complaints

A 15-year-old boy was admitted to the hospital in November 2019 with complaints of an acute headache for 3 h.

History of present illness

The child presented with a sudden severe headache for 3 h with no inducing factors. He was conscious and had no history of nausea, dizziness, or fever.

History of past illness

The boy had normal growth and development and no history of other special diseases. In August 2011, the child presented at another hospital with complaints of a headache for more than 1 wk. At that time, magnetic resonance imaging (MRI), magnetic resonance angiography (MRA), and magnetic resonance venography (MRV) were performed. The scans revealed that there was no vascular abnormality, abnormal signal intensity, or any other findings suggestive of an AVM (Figure 1A-C). At that time, the doctor did not administer any treatment, and the headache was ameliorated by itself. In October 2013, the child again presented at another hospital with headache and nausea for 2 d. His MRA scan revealed a small right temporal AVM, the size of which was 6.2 mm × 1.9 mm (Figure 1C). Digital subtraction angiography revealed the presence of a suspicious lesion in the right temporal lobe (Figure 1D). The boy was treated for headaches and was not examined further. In February 2019, the boy presented at our hospital complaining of a sudden headache and vomiting for 2 h. He was conscious when he came to our hospital. His Glasgow coma scale score was 14, and National Institutes of Health Stroke Scale score was 1. Computed tomography of the head demonstrated acute intracerebral hemorrhage in the right temporal lobe. The MRA revealed a small AVM in the right temporal lobe (Figure 1E). Symptomatic treatment was given to the child during hospitalization, and gamma knife radiosurgery was suggested. Unfortunately, the child's parents rejected radiotherapy.

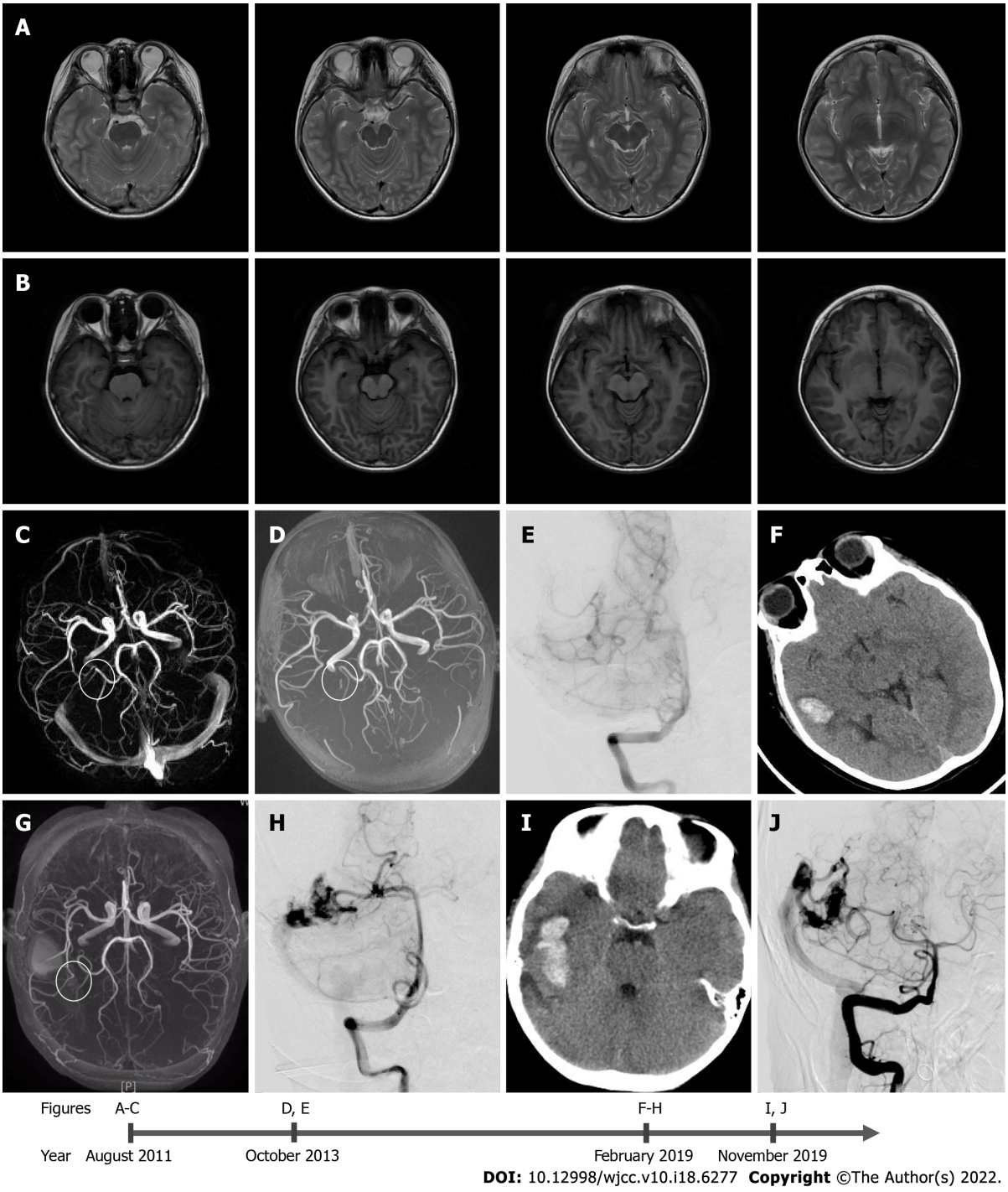

DOI: 10.12998/wjcc.v10.i18.6277 **Copyright** ©The Author(s) 2022.

Figure 1 Diagnostic images from August 2011 to November 2019. A-C: T1 (A) and T2 (B) weighted images of magnetic resonance imaging, and (C) magnetic resonance angiography (MRA) done in August 2011, at the age of 5 years and 2 mo. There is no evidence of vascular lesion; D and E: The results of (D) MRA and (E) the first anteroposterior digital subtraction angiography (DSA) performed in October 2013, indicating *de novo* arteriovenous malformation; F-H: The results of (F) the head computed tomography (CT) scan, (G) MRA, and (H) the second DSA, which were performed in February 2019; I and J: Results from (I) the post-hemorrhage non-contrast head CT scan depicting blood in the right temporal lobe and (J) the third DSA, which were performed in November 2019.

Personal and family history

The patient did not have any personal or family history of brain AVM.

Physical examination

The patient was conscious when examined at our hospital in November 2019. His Glasgow coma scale score was 15 and his National Institutes of Health Stroke Scale score was 1.

Laboratory examinations

Laboratory examinations showed no significant abnormality.

Imaging examinations

A small AVM within the right temporal lobe was visualized in the MRA (Figure 1G), and cerebral angiogram revealed the presence of a 21.6 mm × 21.2 mm right temporal AVM, which was supplied by the inferior temporal branches of the right posterior cerebral artery. Venous drainage occurred through superficial cerebellar veins into the right sigmoid sinus. It was classified as Spetzler-Martin grade 1 (Figure 1H).

In November 2019, computed tomography of the head demonstrated the presence of an acute intracerebral hemorrhage in the right temporal lobe (Figure 1I). Digital subtraction angiography displayed abnormal vascular clusters, which were slightly larger than those seen 10 mo ago. The size of these clusters was 24.3 mm × 22.8 mm. The AVM was classified as a Spetzler-Martin grade 1 (Figure 1J).

Further diagnostic work-up

After receiving consent from the child's parents, we conducted genetic analysis for the child and his parents. We discovered a mutation that might be related to the incidence of AVM, *NOTCH2* heterozygous mutation [NM_024408.3; c.1418A>T; p.Asp473Val]. The mutation was only found in the child.

FINAL DIAGNOSIS

Brain AVM, Spetzler-Martin grade 1.

TREATMENT

The parents refused to conduct further interventional treatment. Supportive treatment was administered during the hospitalization period, and the boy was discharged after 10 d in good clinical condition.

OUTCOME AND FOLLOW-UP

The clinical condition of the child was good during the final follow-up, which was performed on January 2021. The child was in good general condition at the time. After January 2021, he was lost to follow-up.

DISCUSSION

The patient underwent MRI, MRA, and MRV scans in August 2011, at the age of 5 years and 2 mo for nonspecific headaches. No abnormal vascular lesions or secondary signs of brain AVM were observed. A brain AVM was first identified in October 2013. Bleeding occurred for the first time in February 2019 and occurred again in November 2019. The malformed vascular clusters progressed significantly during this period. No risk factors were associated with AVM in this case. Literature review revealed that most of the reported AVM cases had underlying pathology, and only a few of them had no cause of *de novo* AVM[5,8]. Our case report is the first to define the progression and eventual rupture within 6 years following its primary discovery. We also report for the first time that heterozygous mutations in the *NOTCH2* gene might be playing a role in the pathogenesis of AVM.

Currently, the pathogenesis of brain AVM is not clearly understood. The imbalance of some signal molecules during embryonic development is believed to be the most likely reason for no capillary formation between the arteries and veins[9]. This balance is dependent on the strict regulation of various angiogenic factors, and any interference for these automatic regulation factors may lead to the formation of AVM[10,11]. There was no high-risk factor for AVM in this case, and the only high-risk factor that may have a relation in the development of AVM was the heterozygous mutation of the *NOTCH2* gene. The NOTCH2 protein is the receptor of the Notch signaling pathway, and its activity can directly affect Notch signaling[12]. However, the Notch signaling pathway has complex and context-dependent effects on angiogenesis[13,14]. Studies have demonstrated that abnormal activation of Notch signaling in human brain AVM was associated with AVM bleeding[15]. The inhibition and activation of Notch signaling were both associated with AVM formation. The mutation in this case (p.Asp473Val) was first described by Gilbert *et al*[16]. The mutation is located in exon 8, and exon 8 encodes the epidermal growth factor-12 domain of *NOTCH2*[16,17]. Unfortunately, there has been no research on the effect of this mutation on the function of the NOTCH2 protein.

CONCLUSION

We report for the first time a case of *de novo* AVM formation in a child, which progressed and eventually ruptured within 6 years. Our case contests the traditional view that brain AVM is congenital, and our case once again confirms the view that brain AVM is an acquired disease that is the result of an interaction of genes, environment, and molecules.

ACKNOWLEDGEMENTS

We thank the Department of Neurosurgery and the Department of Radiology of The Second Affiliated Hospital and Yuying Children's Hospital of Wenzhou Medical University for the diagnosis and treatment of the patient.

FOOTNOTES

Author contributions: Li DD was in charge of case review and preparation of the manuscript; Huang H, Wang X, Guo AN, and Li W collected clinical opinions regarding this case and drafted the manuscript; Duan RH, Fang JH, and Yin B participated in the coordinating the manuscript; Huang H and Li DD revised the manuscript; All authors read and approved the final manuscript.

Supported by the Science and Technology Program of Wenzhou, China, No. Y20190145 to Huan Huang; and the Beijing New Health Industry Development Foundation, No. XM2020-02-002 to Bo Yin.

Informed consent statement: Written informed consent was obtained from the patient's parents.

Conflict-of-interest statement: The authors declare there are no conflicts of interest.

CARE Checklist (2016) statement: The authors have read the CARE Checklist (2016), and the manuscript was prepared and revised according to the CARE Checklist (2016).

Open-Access: This article is an open-access article that was selected by an in-house editor and fully peer-reviewed by external reviewers. It is distributed in accordance with the Creative Commons Attribution NonCommercial (CC BY-NC 4.0) license, which permits others to distribute, remix, adapt, build upon this work non-commercially, and license their derivative works on different terms, provided the original work is properly cited and the use is non-commercial. See: https://creativecommons.org/Licenses/by-nc/4.0/

Country/Territory of origin: China

ORCID number: Huan Huang 0000-0001-8842-2424; Xue Wang 0000-0001-6178-6316; An-na Guo 0000-0003-3631-1401; Wei Li 0000-0002-3401-0077; Ren-Hua Duan 0000-0003-2776-7060; Jun-Hao Fang 0000-0002-1395-0756; Bo Yin 0000-0002-5487-0197; Dan-Dong Li 0000-0003-4973-8818.

S-Editor: Gong ZM
L-Editor: Filipodia
P-Editor: Gong ZM

REFERENCES

1 **Sison V**, Stackhouse T, Breeze R, Hall T, McKenzie P, Tartaglia N. Arteriovenous Malformation in a Youth with Atypical Autism Symptoms. *J Child Dev Disord* 2017; **3** [PMID: 28989994 DOI: 10.4172/2472-1786.100042]
2 **Jimenez JE**, Gersey ZC, Wagner J, Snelling B, Ambekar S, Peterson EC. Role of follow-up imaging after resection of brain arteriovenous malformations in pediatric patients: a systematic review of the literature. *J Neurosurg Pediatr* 2017; **19**: 149-156 [PMID: 27911246 DOI: 10.3171/2016.9.PEDS16235]
3 **Leblanc GG**, Golanov E, Awad IA, Young WL; Biology of Vascular Malformations of the Brain NINDS Workshop Collaborators. Biology of vascular malformations of the brain. *Stroke* 2009; **40**: e694-e702 [PMID: 19834013 DOI: 10.1161/STROKEAHA.109.563692]
4 **Mullan S**, Mojtahedi S, Johnson DL, Macdonald RL. Embryological basis of some aspects of cerebral vascular fistulas and malformations. *J Neurosurg* 1996; **85**: 1-8 [PMID: 8683257 DOI: 10.3171/jns.1996.85.1.0001]
5 **Santos R**, Aguilar-Salinas P, Entwistle JJ, Aldana PR, Beier AD, Hanel RA. De Novo Arteriovenous Malformation in a Pediatric Patient: Case Report and Review of the Literature. *World Neurosurg* 2018; **111**: 341-345 [PMID: 29294397 DOI: 10.1016/j.wneu.2017.12.145]
6 **Chen W**, Choi EJ, McDougall CM, Su H. Brain arteriovenous malformation modeling, pathogenesis, and novel therapeutic targets. *Transl Stroke Res* 2014; **5**: 316-329 [PMID: 24723256 DOI: 10.1007/s12975-014-0343-0]

7 **Florian IA**, Beni L, Moisoiu V, Timis TL, Florian IS, Balaşa A, Berindan-Neagoe I. 'De Novo' Brain AVMs-Hypotheses for Development and a Systematic Review of Reported Cases. *Medicina (Kaunas)* 2021; **57** [PMID: 33652628 DOI: 10.3390/medicina57030201]

8 **Yeo JJ**, Low SY, Seow WT, Low DC. Pediatric de novo cerebral AVM: report of two cases and review of literature. *Childs Nerv Syst* 2015; **31**: 609-614 [PMID: 25537110 DOI: 10.1007/s00381-014-2609-y]

9 **Storkebaum E**, Quaegebeur A, Vikkula M, Carmeliet P. Cerebrovascular disorders: molecular insights and therapeutic opportunities. *Nat Neurosci* 2011; **14**: 1390-1397 [PMID: 22030550 DOI: 10.1038/nn.2947]

10 **Achrol AS**, Guzman R, Varga M, Adler JR, Steinberg GK, Chang SD. Pathogenesis and radiobiology of brain arteriovenous malformations: implications for risk stratification in natural history and posttreatment course. *Neurosurg Focus* 2009; **26**: E9 [PMID: 19409010 DOI: 10.3171/2009.2.FOCUS0926]

11 **Ma L**, Guo Y, Zhao YL, Su H. The Role of Macrophage in the Pathogenesis of Brain Arteriovenous Malformation. *Int J Hematol Res* 2015; **1**: 52-56 [PMID: 26495437 DOI: 10.17554/j.issn.2409-3548.2015.01.12]

12 **Wang MM**. Notch signaling and Notch signaling modifiers. *Int J Biochem Cell Biol* 2011; **43**: 1550-1562 [PMID: 21854867 DOI: 10.1016/j.biocel.2011.08.005]

13 **Gridley T**. Notch signaling in vascular development and physiology. *Development* 2007; **134**: 2709-2718 [PMID: 17611219 DOI: 10.1242/dev.004184]

14 **Murphy PA**, Lu G, Shiah S, Bollen AW, Wang RA. Endothelial Notch signaling is upregulated in human brain arteriovenous malformations and a mouse model of the disease. *Lab Invest* 2009; **89**: 971-982 [PMID: 19546852 DOI: 10.1038/labinvest.2009.62]

15 **Wang LJ**, Xue Y, Huo R, Yan Z, Xu H, Li H, Wang J, Zhang Q, Cao Y, Zhao JZ. N6-methyladenosine methyltransferase METTL3 affects the phenotype of cerebral arteriovenous malformation *via* modulating Notch signaling pathway. *J Biomed Sci* 2020; **27**: 62 [PMID: 32384926 DOI: 10.1186/s12929-020-00655-w]

16 **Gilbert MA**, Bauer RC, Rajagopalan R, Grochowski CM, Chao G, McEldrew D, Nassur JA, Rand EB, Krock BL, Kamath BM, Krantz ID, Piccoli DA, Loomes KM, Spinner NB. Alagille syndrome mutation update: Comprehensive overview of JAG1 and NOTCH2 mutation frequencies and insight into missense variant classification. *Hum Mutat* 2019; **40**: 2197-2220 [PMID: 31343788 DOI: 10.1002/humu.23879]

17 **Duan Z**, Li FQ, Wechsler J, Meade-White K, Williams K, Benson KF, Horwitz M. A novel notch protein, N2N, targeted by neutrophil elastase and implicated in hereditary neutropenia. *Mol Cell Biol* 2004; **24**: 58-70 [PMID: 14673143 DOI: 10.1128/MCB.24.1.58-70.2004]

World Journal of Clinical Cases

Submit a Manuscript: https://www.f6publishing.com

World J Clin Cases 2022 June 26; 10(18): 6283-6288

DOI: 10.12998/wjcc.v10.i18.6283

ISSN 2307-8960 (online)

CASE REPORT

Coinfection of *Streptococcus suis* and *Nocardia asiatica* in the human central nervous system: A case report

Ying-Ying Chen, Xin-Hong Xue

Specialty type: Clinical neurology

Provenance and peer review: Unsolicited article; Externally peer reviewed.

Peer-review model: Single blind

Peer-review report's scientific quality classification

Grade A (Excellent): 0
Grade B (Very good): B
Grade C (Good): 0
Grade D (Fair): D
Grade E (Poor): 0

P-Reviewer: Keikha M, Iran; Sachu A, India

Received: December 17, 2021
Peer-review started: December 17, 2021
First decision: January 18, 2022
Revised: February 19, 2022
Accepted: April 21, 2022
Article in press: April 21, 2022
Published online: June 26, 2022

Ying-Ying Chen, Xin-Hong Xue, Department of Neurology, Liaocheng People's Hospital, Liaocheng 252000, Shandong Province, China

Corresponding author: Xin-Hong Xue, Doctor, Additional Professor, Department of Neurology, Liaocheng People's Hospital, No. 67, Dongchang West Road, Liaocheng 252000, Shandong Province, China. chenaz323232@126.com

Abstract

BACKGROUND

Streptococcus suis (*S. suis*) is an anthropozoonotic pathogen that shows clinical manifestations of meningitis, septicemia, and arthritis in infected humans. *Nocardia* is another type of anthropozoonotic bacteria, with clinical manifestations of skin, lung, and brain abscesses in infected humans. Few intracranial infections caused by *S. suis* or *Nocardia* have been reported. To the best of our knowledge, no study has reported a patient with simultaneous intracranial infection by *S. suis* and *Nocardia*.

CASE SUMMARY

A 66-year-old male presented at Liaocheng People's Hospital (Liaocheng, Shandong Province, China) reporting dizziness with nausea and vomiting. Metagenomic next-generation sequencing (mNGS) was performed on cerebrospinal fluid for examination, and the patient was diagnosed with suppurative meningitis caused by *S. suis* infection. He received anti-infection treatment with penicillin sodium and ceftriaxone. The patient's condition initially improved but then deteriorated. Further mNGS of cerebrospinal fluid revealed both *S. suis* and *Nocardia*. Imaging examination revealed a brain abscess. Furthermore, a mixed infection of *S. suis* and *Nocardia* was detected in the patient's central nervous system. The patient was treated with antibiotics and sulfamethoxazole. He was discharged after his condition improved.

CONCLUSION

This case shows that the disease can be recurrent in patients with intracranial infection of a rare pathogen. The possibility of mixed infection should also be considered, especially in patients treated with immunosuppressive agents. mNGS of cerebrospinal fluid is a supplement to conventional microbial pathogen identification methods. Patients with unknown pathogen diagnosis, early extensive use of antibiotics and infection with rare pathogens can be diagnosed by the combination of conventional methods and mNGS of cerebrospinal fluid.

Key Words: *Streptococcus suis*; *Nocardia*; Meningitis; Brain abscess; Case report

©The Author(s) 2022. Published by Baishideng Publishing Group Inc. All rights reserved.

Core Tip: *Streptococcus suis* (*S. suis*) meningitis is rare in the neurology department. *S. suis* combined with *Nocardia* is also rare, and intracranial infection of atypical pathogens is difficult to identify. *Streptococcus* cultivation requires high nutrition. In addition, the difficulty of cultivating *S. suis* makes the clinical identification more challenging and usually prolongs therapies. mNGS can be utilized to determine pathogens in the early phase of illness.

Citation: Chen YY, Xue XH. Coinfection of *Streptococcus suis* and *Nocardia asiatica* in the human central nervous system: A case report. *World J Clin Cases* 2022; 10(18): 6283-6288
URL: https://www.wjgnet.com/2307-8960/full/v10/i18/6283.htm
DOI: https://dx.doi.org/10.12998/wjcc.v10.i18.6283

INTRODUCTION

Streptococcus suis (*S. suis*) is a facultative anaerobic gram-positive bacterium located in the nasal cavity, tonsils, upper respiration tract and gastrointestinal tract of pigs. This microbe can be transmitted through contact, the respiratory tract and the digestive tract[1]. It enters the human body, spreads through the blood to the epithelial cells of the choroid plexus in the brain and crosses the blood-brain barrier, resulting in intracranial infection. The common complications of *S. suis* infection are hearing loss and vestibular dysfunction[2]. Since the first case in Denmark in 1968, over 1600 mankind *S. suis* infections have been documented in 30 nations across the globe, especially in Southeastern Asian countries[3]. *S. suis* is divided into 35 serotypes (Types 1-34 and Type 1/2), as per the different antigenicity of the capsular polysaccharide; the common serotypes with strong pathogenicity to pigs are Type 1, Type 2, Type 1/2, Type 7 and Type 9[4].

Nocardia is a gram-positive aerobic bacterium and an opportunistic pathogen. It is widely distributed in soil and water and mainly invades the human body through respiratory tract inhalation and damaged skin. Infection by *Nocardia* leads to abscesses of the respiratory system, skin and central nervous system as well as systemic disseminated infection. At least 100 species of *Nocardia* have been identified; the medically relevant strains include *Nocardia asteroides*, *Nocardia brasiliensis*, *Nocardia farcinica*, *etc.*

Few cases of simultaneous infection with *S. suis* and *Nocardia* have been reported. The current case was an elderly male patient who had *S. suis* meningitis with a *Nocardia* brain abscess, and metagenomic next-generation sequencing (mNGS) of cerebrospinal fluid confirmed the coinfection of *S. suis* and *Nocardia*. The present research was accepted by the Ethical Board of Liaocheng People's Hospital, and the publication of clinical data was approved by the patient's family[5,6].

CASE PRESENTATION

Chief complaints

A 66-year-old hospitalized male who complained of dizziness.

History of present illness

The patient developed dizziness, nausea, and vomiting 4 d prior. The vomit was non-brown-colored stomach contents, accompanied by confusion, headache, and hearing loss in both ears. One day prior, his dizziness aggravated, and he presented to the hospital.

History of past illness

The man was healthy, with no specific diseases.

Physical examination

Body temperature 38.5 °C, heart rate 66 bpm, and blood pressure 210/110 mmHg. The patient reported blurred consciousness, binaural hearing loss, signs of meningeal irritation displayed by neck rigidity, positive Kernig's and Lesage's signs, normal muscular strength and limb muscle tension, and negative pathologic signs.

Laboratory examinations

On admission, the patient's examination results were completely normal, including leukocyte count, hypersensitive C-reactive protein, procalcitonin, electrolytes, liver and kidney function tests and coagulation function tests. On the second day of hospitalization, cerebrospinal fluid examination showed 62.9 × 10^3 white blood cells (WBCs)/μL, with a protein level of 8036 mg/L, glucose level of 3.8 mmol/L and chloride ion concentration of 139 mmol/L. The cerebrospinal fluid pressure was 270 mm H_2O; in routine examination of the cerebrospinal fluid, the appearance was light yellow and slightly muddy; the Pandy test was positive, with 2.4 × 10^8/L karyocytes, 51% neutrophils, and 69% lymphocytes. Biochemical examination of cerebrospinal fluid revealed a total protein content > 1.07 g/L (normal, approximately 0.15-0.40 g/L), dextrose level of 1.87 mmol/L (normal, approximately 2.5-4.4 mmol/L), chloride level of 114.60 mmol/L (normal, approximately 120-132 mmol/L), body temperature of 38.5 °C, heart rate of 66 bpm, and blood pressure of 210/110 mmHg. The patient reported blurred consciousness and binaural hearing loss. He had signs of meningeal irritation in the form of neck stiffness and positive Kernig's and Lesage's signs.

After 5 d, cerebrospinal fluid was extracted by lumbar puncture and subjected to mNGS. The result revealed *S. suis* (with 1884 detected sequences), and the relative abundance was 93.27%. No pathogens were found by routine methods such as cerebrospinal fluid culture or blood culture.

We then performed lumbar puncture every week to extract cerebrospinal fluid and examined inflammatory indices, with cerebrospinal fluid culture and blood culture performed.

After 37 d, the patient's condition worsened. We repeated mNGS of cerebrospinal fluid, and the results revealed *S. suis* (the number of detected sequences was 130) and *Nocardia asiatica* (the number of detected sequences was 31598). The results of the seven cerebrospinal fluid examinations are shown in Table 1, and the etiological examination of the cerebrospinal fluid is shown in Table 2.

FINAL DIAGNOSIS

The initial diagnosis on admission was intracranial infection. Coinfection of *S. suis* and *Nocardia* infection was the final diagnosis.

TREATMENT

The sufferer was hospitalized and finished routine examination, and he received lumbar puncture on the second day after admission. The routine culture, staining and bacterial examinations of cerebrospinal fluid were negative. According to the biochemical results of cerebrospinal fluid, we considered bacterial meningitis and empirically gave the patient ceftriaxone 2 g once a day. After 5 d of treatment, the patient's condition did not improve significantly, and he still had dizziness, nausea and vomiting. Physical examination revealed a clear mind, poor spirit, positive meningeal stimulation sign, normal muscular strength and limb muscle tension, and negative pathologic signs on both sides. The outcomes showed that the *S. suis* sequence was detected; the number of sequences identified was 1884, and the relative abundance was 93.27%. The patient was diagnosed with suppurative meningoencephalitis caused by *S. suis* infection. The treatment plan was adjusted as follows: ceftriaxone 2 g q12h plus penicillin sodium 4 million units q6h intravenous drip, combined with the hormone dexamethasone 10 mg qd and *Ginkgo biloba* extract 70 mg bid to improve the patient's hearing. The patient's temperature gradually returned to normal, and the patient had no symptoms other than binaural hearing loss. After 37 d of treatment, the patient had a fever again, the body temperature reached 38.8 °C, and severe headache occurred. Laboratory examination showed that the WBC count registered 7.8 × 10^9/L (referential range: 4-10 × 10^9/L), and the neutrophil percentage registered 73.5% (referential range: 40%-75%). Subsequently, considering that the patient had drug resistance or that the patient's condition was repeated, we continued to apply the antibiotics ceftriaxone 2 g q12h and penicillin sodium 4 million units q6h. Nevertheless, his body temperature increased persistently, and our team discovered that he displayed neck stiffness again. Therefore, our team finished lumbar puncture. Cerebrospinal fluid test revealed a WBC content of 34 × 10^6 WBC/μL, a protein content of 4470 mg/L, a GLU content of 2.48 mmol/L, and a chloride ion level of 124.40 mmol/L. *Nocardia* was identified in the cerebrospinal fluid *via* mNGS on day 2. At the time, our team thought that *Nocardia* meningitis was rare, that the probability of *Nocardia* endocranial infection was low, and that the probability of contamination was high. Therefore, our team didn't modify the therapeutic regimen. Subsequently, his body temperature still presented a fluctuation between 38 °C and 39 °C. Just when we were overwhelmed, we discussed with neurologists, infectious disease specialists and hematologists, considering that the patient's central nervous system was reinfected with *Nocardia*, and developed a treatment plan: ceftriaxone, penicillin sodium, and compound sulfamethoxazole oxazole tablets combined with anti-infective therapy. His body temperature restored to normal on the 2nd day posterior to the modification of the therapeutic regimen. After 65 d, his clinical symptoms improved. The patient was discharged from the hospital.

Table 1 The results of 6 cerebrospinal fluid samples from the patient after admission to our hospital

Date	Color	Opening pressure (mmH_2O)	Nucleated cells ($\times 10^6$/L)	Neutrophils (%)	The lymphocytes (%)	Protein (g/L)	Glucose (mmol/L)	Chloride (mmol/L)
On admission	Yellowish	270	240	51	28	1.07	1.87	114.60
Day 5	Yellowish	90	620	30	69	2.07	3.36	119.70
Day 14	Yellowish	150	142	38	20	1.09	2.70	119.80
Day 23	Clear	180	30	35	40	1.01	3.01	122.80
Day 37	Clear	210	32	6	63	0.86	2.48	124.20
Day 65	Clear	130	15	1	59	<0.4	2.79	128.50
One year later	Clear	120	0	0	0	0.13	3.5	125.50

Table 2 Etiological test results of cerebrospinal fluid

Date	Bacterial colonies	The sequence number	Bacterial species	The sequence number	Note
Day 5 of symptom onset	*Streptococcus*	1884	*Streptococcus suis*	1884	Pathogenic microorganism
Day 37 of symptom onset	*Nocardia*	31598	*Nocardia asiatica*	28621	Pathogenic microorganism
Day 37 of symptom onset	*Streptococcus*	130	*Streptococcus suis*	1130	Pathogenic microorganism
Day 65 of symptom onset	*Staphylococcus*	314	*Staphylococcus cohnii*	28	Background microorganism
One year later	*Staphylococcus*	180	*Staphylococcus cohnii*	5	Background microorganism

After returning home, he continued to take compound sulfamethoxazole tablets trimethoprim-sulfamethoxazole (TMP-SMX), with TMP 80 mg and SMX 400 mg 2 tablets/time, 2 times/d for a total of 12 mo until the 1-year follow-up.

OUTCOME AND FOLLOW-UP

At the 1-year follow-up, the patient had left hearing loss in both ears and could work normally.

DISCUSSION

The current patient frequently consumed pork and was infected with *S. suis* after eating contaminated pork. His drinking history and diabetes history are risk factors for *S.suis* infection[7]. *Nocardia* infection can occur in patients taking immunosuppressant hormones and by *S. suis*, which destroys the blood-brain barrier. Brain computed tomography scan of the brain of the patient led to the diagnosis of *Nocardia* infection of the central nervous system. During infection, the pathogen enters the brain tissue through the lumbar puncture wound, resulting in brain abscess[8].

There was no improvement in binaural hearing impairment at the 1-year follow-up. Animal studies have shown that hearing impairment is related to suppurative labyrinthitis caused by the invasion of *S. suis* in the subarachnoid space to the external lymph through the cochlear aqueduct, which leads to the disturbance of inner ear microcirculation and the direct invasion of the cochlear nerve by *S. suis*[9]. Hearing impairment affects the daily life of patients, and questions regarding how to predict, prevent and treat hearing impairment are urgent problems that remain to be solved.

The patient's condition initially improved after the initial treatment for *S. suis* and then deteriorated. We speculated that the patient was not sensitive to the current treatment and that there might be drug-resistant strains of *S. suis*. Therefore, we repeated mNGS and found that the counts of *S. suis* deoxyribonucleic acid (DNA) decreased (from 1884 to 130), which confirmed that our treatment was effective. We also identified 31598 *Nocardia* sequences by mNGS. Therefore, we concluded that the deterioration of the patient's condition was caused by intracranial infection with *Nocardia*, and the patient was diagnosed with coinfection of *S. suis* and *Nocardia*. After the treatment plan was adjusted to penicillin sodium combined with ceftriaxone and sulfamethoxazole, the patient's systemic and nervous system symptoms improved within a few weeks. The number of leukocytes decreased gradually, and the

proportion of multiple nuclei cells decreased significantly, as observed in the re-examination of cerebrospinal fluid. The patient's condition improved, and the mNGS results obtained at the time were consistent with the clinical situation.

mNGS is a multi-faceted technique which can determine pathogenic agents more quickly and accurately in contrast to conventional approaches and can even offer novel enlightenment regarding illness propagation, virulence, and antibiotic tolerance. In contrast to conventional identification approaches which can merely identify some target pathogenic agents, mNGS is a shotgun sequence identification approach of ribonucleic acids (RNAs) and DNAs from clinic specimens, in which the entire DNAs or RNAs of the specimen to be examined are blended and subjected to sequencing, and the data are afterwards contrasted with the pathogenic agent data base to acquire pathogen categorization data. Such approach can identify substantial pathogenic agents in a run in 48 h. The pathogenic agent profiles involve nearly every virus, bacterium, fungus, and parasite which is capable of infecting sufferers. The detailed description of the materials and approaches for mNGS were presented by supplemental material.

There were no pathogenic bacteria found in the multiple evaluations of blood culture, cerebrospinal fluid culture and smears, which may be related to the extensive use of cephalosporins in the early stage of treatment. mNGS quickly and accurately diagnoses pathogens without the influence of antibiotic treatment[10]. mNGS detects pathogenic pathogens, including rare pathogens, more appropriately than traditional detection methods. mNGS also determines all DNA/RNA genome information in a sample in a single run and allows for the identification and typing of all pathogens without specific primers, which can play an important role in the diagnosis and treatment of complex and mixed infectious diseases with repeated negative clinical routine examinations. Rapid detection and identification offer the opportunity for treatment at early stages of disease, which helps control the condition, shorten recovery time, improve the prognosis and shorten the hospital stay duration. Therefore, mNGS can provide reliable and effective evidence for the diagnosis and treatment of CNS infectious diseases, with certain clinical application value[7].

CONCLUSION

In the case of intracranial infection with rare pathogens, if the disease continues during treatment, clinicians should also consider coinfection more than the possibility of drug resistance. mNGS of cerebrospinal fluid can accurately and quickly diagnose pathogen infection in the nervous system in rare cases of infections of multiple pathogens. Based on the number of reads and relative abundance, mNGS could be used for semiquantitative detection, which can evaluate the therapeutic effect to a certain extent in addition to its important diagnostic value.

ACKNOWLEDGEMENTS

The authors are very grateful to the patient for participating in this study.

FOOTNOTES

Author contributions: Chen YY reviewed the literature, analyzed the patient data and wrote the manuscript; Xue XH and Chen YY were responsible for data collection; All the authors read and approved the final manuscript.

Informed consent statement: Informed written consent was obtained from the patient for publication of this report and any accompanying images.

Conflict-of-interest statement: The authors declare that they have no conflicts of interest.

CARE Checklist (2016) statement: The authors have read the CARE Checklist (2016), and the manuscript was prepared and revised according to the CARE Checklist (2016).

Open-Access: This article is an open-access article that was selected by an in-house editor and fully peer-reviewed by external reviewers. It is distributed in accordance with the Creative Commons Attribution NonCommercial (CC BY-NC 4.0) license, which permits others to distribute, remix, adapt, build upon this work non-commercially, and license their derivative works on different terms, provided the original work is properly cited and the use is non-commercial. See: https://creativecommons.org/Licenses/by-nc/4.0/

Country/Territory of origin: China

ORCID number: Ying-Ying Chen 0000-0002-0668-4285; Xin-Hong Xue 0000-0003-0034-3831.

S-Editor: Chang KL
L-Editor: A
P-Editor: Chang KL

REFERENCES

1 **Lun ZR**, Wang QP, Chen XG, Li AX, Zhu XQ. Streptococcus suis: an emerging zoonotic pathogen. *Lancet Infect Dis* 2007; **7**: 201-209 [PMID: 17317601 DOI: 10.1016/S1473-3099(07)70001-4]
2 **Jover-García J**, López-Millán C, Gil-Tomás JJ. Emerging infectious diseases: Streptococcus suis meningitis. *Rev Esp Quimioter* 2020; **33**: 385-386 [PMID: 32766669 DOI: 10.37201/req/055.2020]
3 **Goyette-Desjardins G**, Auger JP, Xu J, Segura M, Gottschalk M. Streptococcus suis, an important pig pathogen and emerging zoonotic agent-an update on the worldwide distribution based on serotyping and sequence typing. *Emerg Microbes Infect* 2014; **3**: e45 [PMID: 26038745 DOI: 10.1038/emi.2014.45]
4 **Hlebowicz M**, Jakubowski P, Smiatacz T. Streptococcus suis Meningitis: Epidemiology, Clinical Presentation and Treatment. *Vector Borne Zoonotic Dis* 2019; **19**: 557-562 [PMID: 30855223 DOI: 10.1089/vbz.2018.2399]
5 **Brown-Elliott BA**, Brown JM, Conville PS, Wallace RJ Jr. Clinical and laboratory features of the Nocardia spp. based on current molecular taxonomy. *Clin Microbiol Rev* 2006; **19**: 259-282 [PMID: 16614249 DOI: 10.1128/CMR.19.2.259-282.2006]
6 **Wilson JW**. Nocardiosis: updates and clinical overview. *Mayo Clin Proc* 2012; **87**: 403-407 [PMID: 22469352 DOI: 10.1016/j.mayocp.2011.11.016]
7 **Wilson MR**, Sample HA, Zorn KC, Arevalo S, Yu G, Neuhaus J, Federman S, Stryke D, Briggs B, Langelier C, Berger A, Douglas V, Josephson SA, Chow FC, Fulton BD, DeRisi JL, Gelfand JM, Naccache SN, Bender J, Dien Bard J, Murkey J, Carlson M, Vespa PM, Vijayan T, Allyn PR, Campeau S, Humphries RM, Klausner JD, Ganzon CD, Memar F, Ocampo NA, Zimmermann LL, Cohen SH, Polage CR, DeBiasi RL, Haller B, Dallas R, Maron G, Hayden R, Messacar K, Dominguez SR, Miller S, Chiu CY. Clinical Metagenomic Sequencing for Diagnosis of Meningitis and Encephalitis. *N Engl J Med* 2019; **380**: 2327-2340 [PMID: 31189036 DOI: 10.1056/NEJMoa1803396]
8 **Abu-Gazala M**, Engel A, Stern A, Guralnik L. An unusual case of nocardiosis presented as a mediastinal mass in an immunocompetent patient. *Am J Respir Crit Care Med* 2014; **189**: 492-493 [PMID: 24528321 DOI: 10.1164/rccm.201308-1546LE]
9 **Feng Y**, Zhang H, Wu Z, Wang S, Cao M, Hu D, Wang C. Streptococcus suis infection: an emerging/reemerging challenge of bacterial infectious diseases? *Virulence* 2014; **5**: 477-497 [PMID: 24667807 DOI: 10.4161/viru.28595]
10 **Salzberg SL**, Breitwieser FP, Kumar A, Hao H, Burger P, Rodriguez FJ, Lim M, Quiñones-Hinojosa A, Gallia GL, Tornheim JA, Melia MT, Sears CL, Pardo CA. Next-generation sequencing in neuropathologic diagnosis of infections of the nervous system. *Neurol Neuroimmunol Neuroinflamm* 2016; **3**: e251 [PMID: 27340685 DOI: 10.1212/NXI.0000000000000251]

World Journal of Clinical Cases

Submit a Manuscript: https://www.f6publishing.com

World J Clin Cases 2022 June 26; 10(18): 6289-6297

DOI: 10.12998/wjcc.v10.i18.6289

ISSN 2307-8960 (online)

CASE REPORT

Dilated left ventricle with multiple outpouchings — a severe congenital ventricular diverticulum or left-dominant arrhythmogenic cardiomyopathy: A case report

Xin Zhang, Run-Yu Ye, Xiao-Ping Chen

Specialty type: Cardiac and cardiovascular systems

Provenance and peer review: Unsolicited article; Externally peer reviewed.

Peer-review model: Single blind

Peer-review report's scientific quality classification

Grade A (Excellent): 0
Grade B (Very good): B
Grade C (Good): C
Grade D (Fair): 0
Grade E (Poor): 0

P-Reviewer: Mishra AK, United States; Wang H, United States

Received: December 26, 2021
Peer-review started: December 26, 2021
First decision: March 7, 2022
Revised: March 20, 2022
Accepted: April 24, 2022
Article in press: April 24, 2022
Published online: June 26, 2022

Xin Zhang, Run-Yu Ye, Xiao-Ping Chen, Department of Cardiology, West China Hospital, Sichuan University, Chengdu 610041, Sichuan Province, China

Corresponding author: Xiao-Ping Chen, MD, Chief Doctor, Cardiology Department, West China Hospital, Sichuan University, No. 37 Guoxue Alley, Wuhou District, Chengdu 610041, Sichuan Province, China. xiaopingchen111@126.com

Abstract

BACKGROUND

Left-dominant arrhythmogenic cardiomyopathy (LDAC) is a relatively rare disease characterized by poor prognosis that exacerbates the incidence of sudden cardiac death and ventricular arrhythmias. Clinically, LDAC is constantly overlooked or misdiagnosed as myocardial infarction, myocarditis, and dilated cardiomyopathy, owing to atypical and nonspecific clinical manifestations at an early stage.

CASE SUMMARY

A 57-year-old woman was diagnosed with sinus bradycardia and chronic bifascicular block during a health check. She occasionally experienced mild chest pain and paroxysmal palpitation during activity in the past 2 years. Comprehensive auxiliary examinations, including electrocardiogram, echocardiography, coronary computerized tomography angiography, and magnetic resonance imaging, revealed that she had LDAC instead of congenital ventricular diverticulum. The physicians prescribed standard oral therapy for heart failure and implantable cardioverter-defibrillator. Consequently, her left ventricular systolic function and symptoms remained stable at the 2-year follow-up after discharge.

CONCLUSION

Based on this case, clinicians need to be aware of LDAC in patients with localized left ventricular lesions and multiple electrocardiographic abnormalities. Multimodality cardiovascular imaging is effective in identification of multiple types of cardiomyopathy and cardiac inner structures.

Key Words: Congenital ventricular diverticulum; Left-dominant arrhythmogenic cardiomyopathy; Magnetic resonance imaging; Case report

©The Author(s) 2022. Published by Baishideng Publishing Group Inc. All rights reserved.

Core Tip: Left-dominant arrhythmogenic cardiomyopathy is a relatively rare disease, characterized by poor prognosis. We present a case with a dilated left ventricle that manifested with reduced ejection fraction, multiple outpouchings, left chest leads low voltage, and fragmented QRS. Multimodality cardiovascular imaging diagnosed the patient with left-dominant arrhythmogenic cardiomyopathy instead of congenital ventricular diverticulum. This case alerts clinicians to be aware of left-dominant arrhythmogenic cardiomyopathy in patients with localized left ventricular lesions and multiple electrocardiographic abnormalities.

Citation: Zhang X, Ye RY, Chen XP. Dilated left ventricle with multiple outpouchings — a severe congenital ventricular diverticulum or left-dominant arrhythmogenic cardiomyopathy: A case report. *World J Clin Cases* 2022; 10(18): 6289-6297
URL: https://www.wjgnet.com/2307-8960/full/v10/i18/6289.htm
DOI: https://dx.doi.org/10.12998/wjcc.v10.i18.6289

INTRODUCTION

Left-dominant arrhythmogenic cardiomyopathy (LDAC) is a non-hypertrophic, non-hypertensive, and non-valvular progressive cardiomyopathy with fibrofatty myocardium infiltration that prominently occurs in the left ventricle[1]. LDAC might present with ventricular outpouching, which makes it difficult to differentiate from congenital ventricular diverticulum from the echocardiography[2]. Here, we present a case of LDAC with left chest leads low voltage, fragmented QRS (f-QRS), left ventricle (LV) dilation, LV systolic impairment, LV outpouchings, and late gadolinium enhancement of LV myocardium, which was finally diagnosed using multimodality cardiovascular imaging.

CASE PRESENTATION

Chief complaints

A 57-year-old woman, presenting with a dilated left ventricle, reduced ejection fraction, and chronic bifascicular block, was referred to the cardiology department, West China Hospital, on December 10, 2019.

History of present illness

She occasionally experienced mild chest pain and paroxysmal palpitation during activity in the past 2 years. Her exercise capacity was also mildly reduced. She did not manifest symptoms of fatigue, dizziness, syncope, peripheral edema, and abdominal distention.

History of past illness

The patient had neither prior medical comorbidities nor addictions.

Personal and family history

Her father had a premature sudden cardiac death at the age of 40.

Physical examination

The patient showed good nutrition, active position, clear mind, fluent language, and was cooperative in examination. Examinations on her whole skin and mucous membrane revealed no yellow staining, cyanosis, and bleeding spots. She had a blood pressure and resting heart rate of 120/68 mmHg and 60 beats per min, respectively, and auscultation of both lungs was normal with neither dry nor wet rales. The apical pulse was located 0.5 cm lateral to the midclavicular line on the left side of the fifth rib, while her heart rhythm was regular. The first and second heart sounds were basically normal, without extra and splitting of the heart sound. No valvular murmurs were detected in any of the auscultation areas. In addition, she did not exhibit any physical signs of heart failure, including edema, ascites, jugular venous distention, and hepatojugular reflux.

Laboratory examinations

Results from the routine blood test and plasma biochemical examinations, including kidney and liver

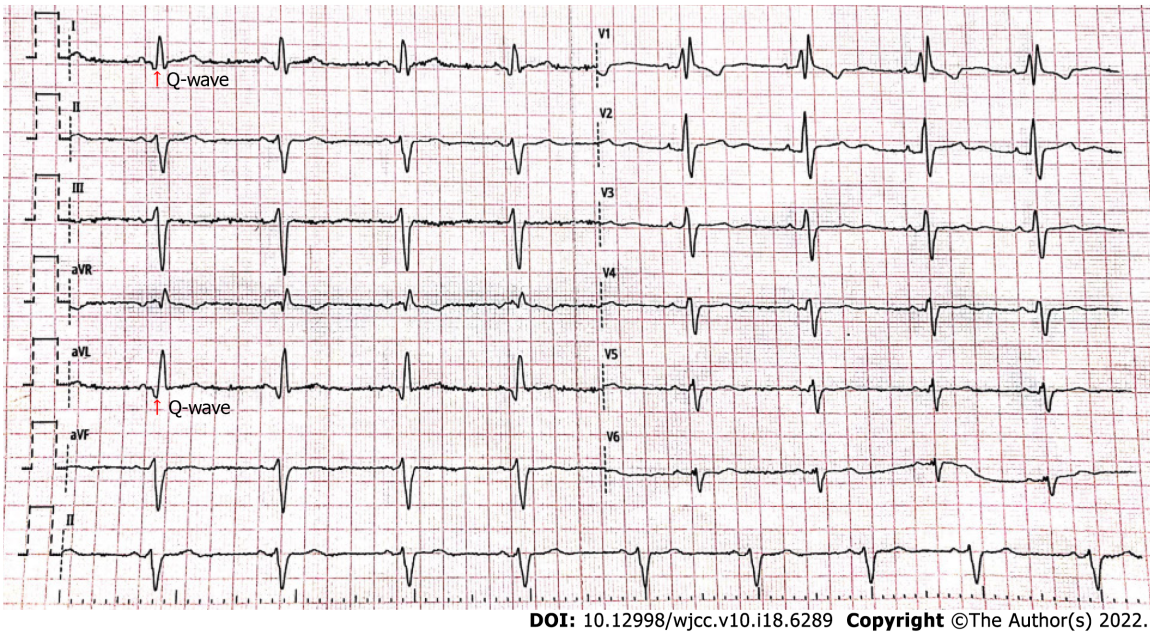

DOI: 10.12998/wjcc.v10.i18.6289 **Copyright** ©The Author(s) 2022.

Figure 1 Routine 12-leads electrocardiogram results of the patient under this study. Electrocardiogram showed left anterior branch block, complete right bundle branch block, high sidewall (I, AVL) abnormal Q wave, and left chest leads low voltage (V4-6) with poor R wave progression.

A

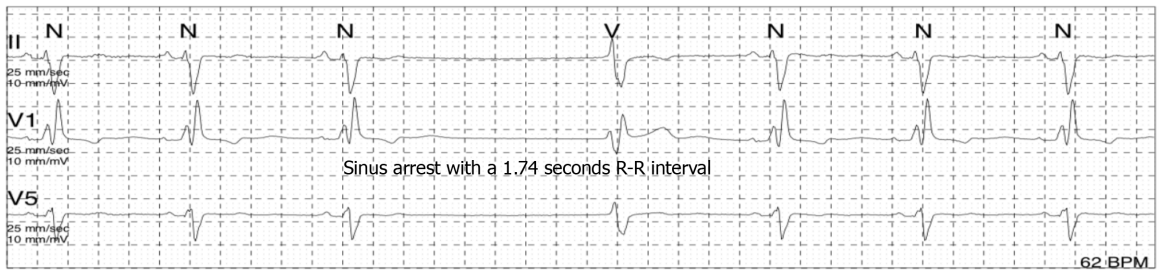

B

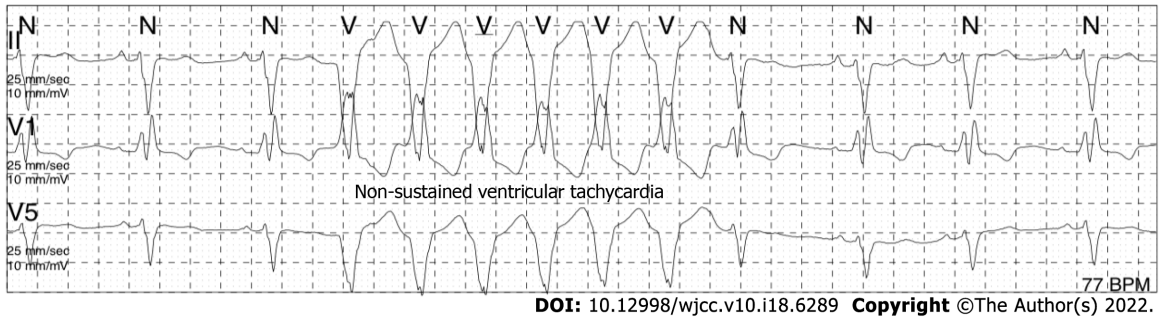

DOI: 10.12998/wjcc.v10.i18.6289 **Copyright** ©The Author(s) 2022.

Figure 2 Sinus arrest (A) and ventricular tachycardia (B) recorded in Holter monitoring for this case.

function, glucose, lipid, and electrolyte, were normal. Similarly, thyroid function, kappa and lambda urine free light chains as well as coagulation profile and autoimmune antibodies were also within the normal range. The plasma N-terminal fragment of the pro-brain natriuretic peptide was 325 ng/L.

Imaging examinations

The electrocardiogram (Figure 1) revealed left anterior branch block, complete right bundle branch block (RBBB), high sidewall abnormal Q wave, and left chest leads (V4-V6) low voltage with poor R wave progression. On the other hand, Holter monitoring (Figures 2 and 3) revealed sinus arrest with a 1.74 s R-R interval, multisource premature ventricular beats, non-sustained ventricular tachycardia with an RBBB pattern, and f-QRS in leads V3-V6. Transthoracic echocardiography (TTE) showed a dilated LV with a diameter of 60 mm as well as a reduced LV ejection fraction of 35% and a left ventricular apex cystic outpouching (12 mm × 13 mm) that displayed synchronous contractility (Figure 4A-C).

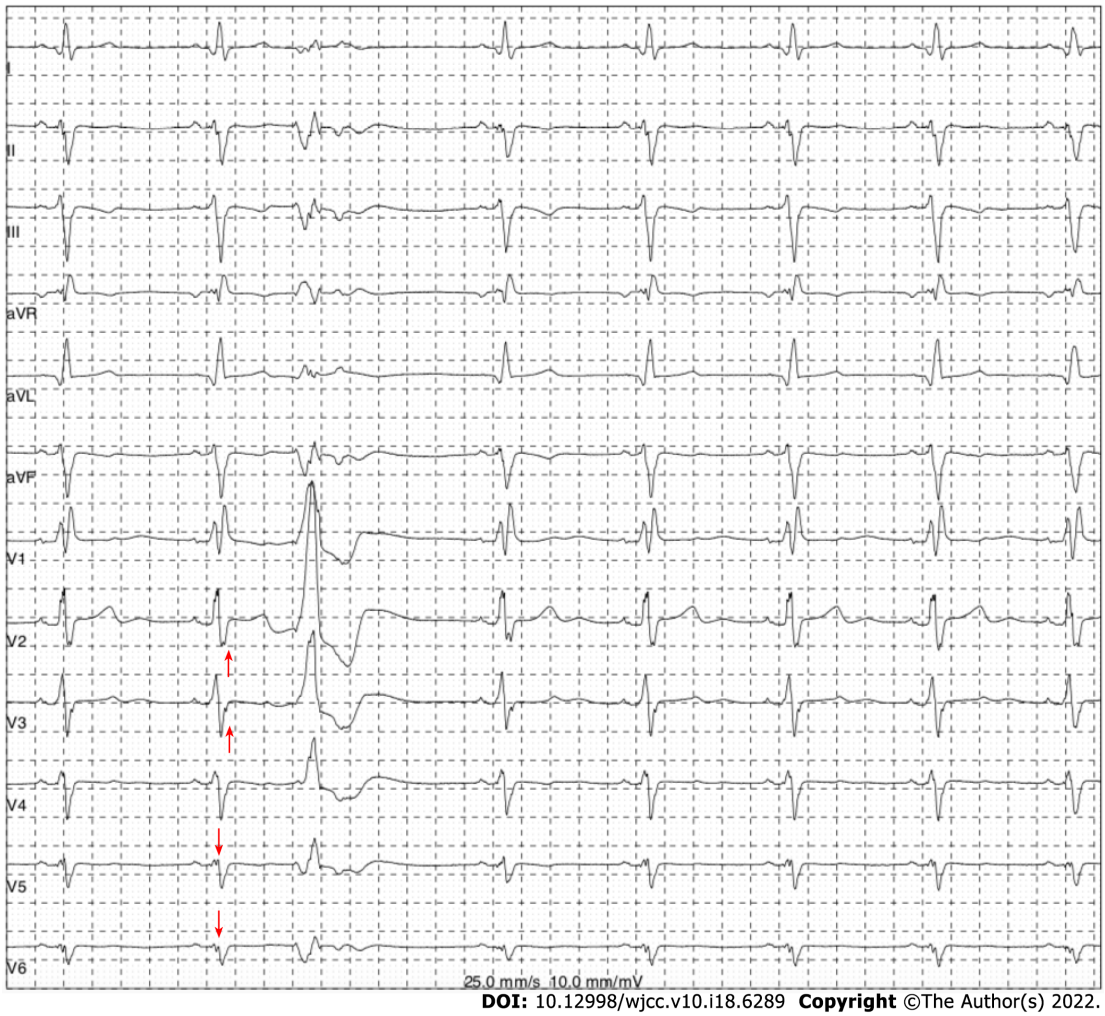

DOI: 10.12998/wjcc.v10.i18.6289 **Copyright** ©The Author(s) 2022.

Figure 3 Fragmented QRS and ventricular premature beats recorded in Holter monitoring for this case. Holter monitoring showed ventricular premature beats with a right bundle branch block pattern and fragmented QRS in leads V3-V6 (marked using red arrows).

Myocardial contrast echocardiography revealed contractile outpouching without obvious filling defects (Figure 4D). Coronary computerized tomography angiography (CCTA) revealed right dominant coronary artery circulation without obvious stenosis, LV multiple outpouchings, uneven thickness of the LV wall (Figure 5A, B, E, and F), hypodense region (CT value -90~-114 HU) at localized myocardium of LV septum (Figure 5C), and free wall (Figure 5D). These findings were consistent with profiles of fatty tissue infiltration. In addition, we used cardiac magnetic resonance imaging (CMRI) to evaluate the cardiac structure, bilateral ventricular function, segmental movement, and tissue characterization in the patient. CMRI results revealed LV dilatation, abnormal activity of the LV wall (Figure 6A and B), an outpouching at the LV apex, and a low signal in the septum myocardium midwall after contrast injection (Figure 6C). Moreover, late gadolinium enhancement in the midwall of the left ventricular septum and free wall myocardium were also evident (Figure 6D).

Genetic testing

High-throughput sequencing revealed no genetic variation with high clinical phenotype correlation and sufficient evidence of pathogenicity.

FINAL DIAGNOSIS

These findings highly pointed to LDAC.

TREATMENT

After comprehensive evaluation of the patient, we prescribed sacubitril valsartan sodium tablets (50 mg

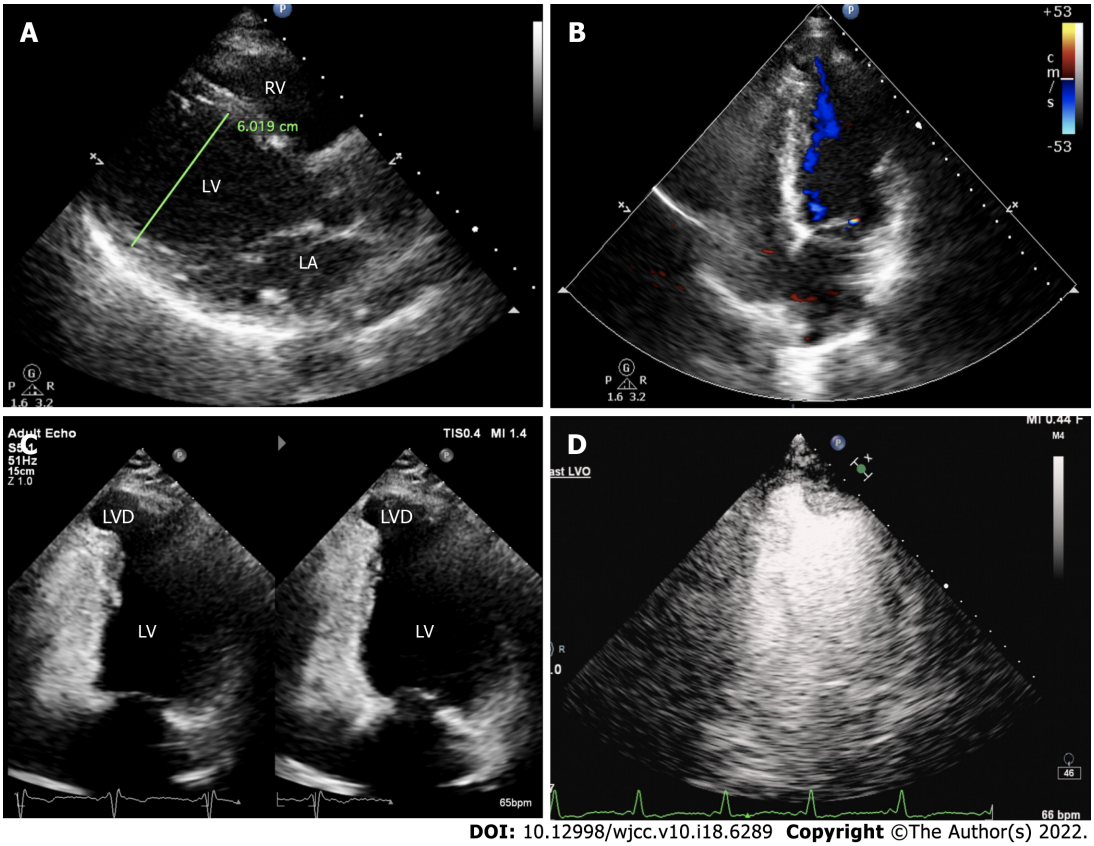

DOI: 10.12998/wjcc.v10.i18.6289 **Copyright** ©The Author(s) 2022.

Figure 4 Transthoracic echocardiography results of the patient under this study. A: Long-axis view of the left ventricle at the end of diastole. The left ventricle was dilated with a diameter of 60 mm; B: Cystic outpouching in the left ventricular apical septum on the apical four-chamber view and intra-cystic blood flow signals were seen during systole; C: Cystic outpouching had an approximate size of 12 mm × 13 mm with a continuous muscle wall, while its activity synchronized with ventricular contraction and diastole; D: Myocardial contrast echocardiograph revealed no obvious filling defect in the cystic structure.

bid) and spironolactone (20 mg qd). We did not administer a beta-blocker in this case, owing to multiple atrioventricular conduction abnormalities. In addition, she was given low-dose thiazide diuretics when needed to relieve edema and congestion symptoms. Three months later, her left ventricular size and systolic function had not changed compared to baseline. Consequently, she was subjected to an implantable cardioverter-defibrillator after full discussion in our department.

OUTCOME AND FOLLOW-UP

Two years later, we re-evaluated her symptoms and clinical indexes and found that the symptoms improved after taking standard oral medication for ejection fraction reduced heart failure. The pacemaker program did not record sustained ventricular tachycardia or ventricular fibrillation. Echocardiography revealed that left ventricular size and systolic function were almost similar to 2 years prior to treatment.

DISCUSSION

This case affirms the need for clinicians to be aware of LDAC in patients with localized left ventricular lesions and multiple electrocardiographic abnormalities. Notably, multimodality cardiovascular imaging and electrocardiogram (ECG) should be considered in this situation.

The patient in the present case revealed various ECG abnormalities, including sinus node dysfunction, chronic bifascicular block, abnormal Q wave, left chest leads low voltage (V4-6), poor R wave progression in leads V4-V6, and f-QRS in leads V3-V6. These were all indicative of left ventricular myocardial abnormality and extensive conduction system disorder. f-QRS, which has been defined as the presence of additional R' waves or a notch in the R or S wave in two contiguous leads[3], indicates myocardial scarring and represents distortion of signal conduction as well as depolarization processes within ventricles[4]. Previous studies have shown that f-QRS is an independent predictor for cardiac events, ventricular arrhythmias, and sudden cardiac death[5]. Notably, it has been detected in patients

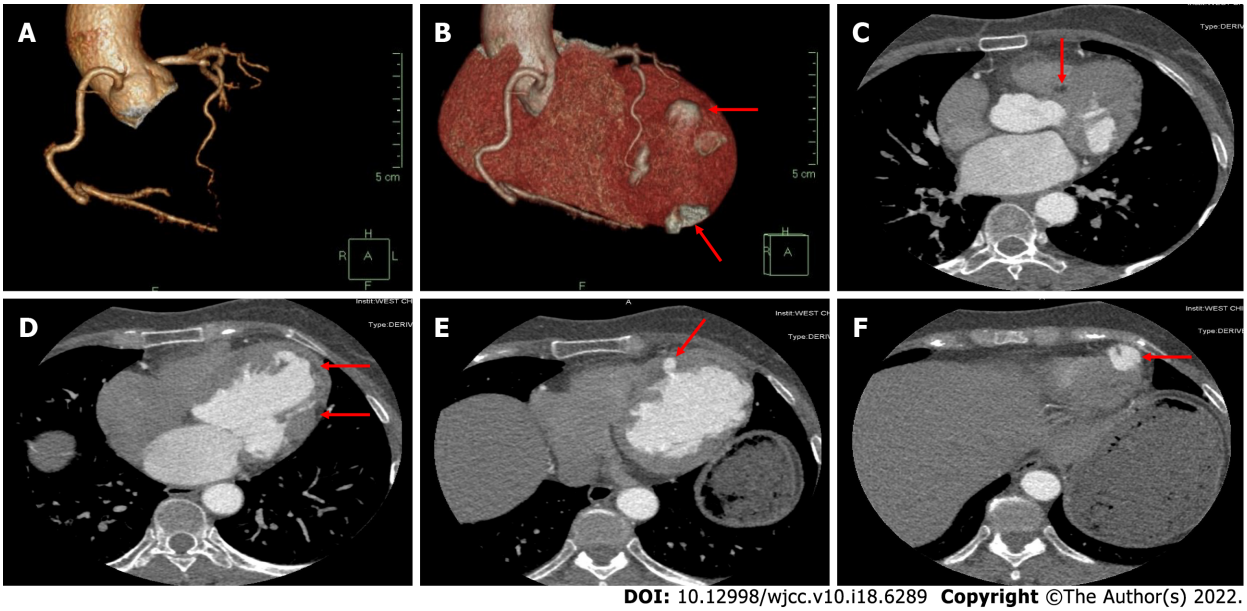

DOI: 10.12998/wjcc.v10.i18.6289 **Copyright** ©The Author(s) 2022.

Figure 5 Coronary computerized tomography angiography results of the patient under this study. A: Three-dimensional reconstruction of coronary arteries and right dominant coronary artery circulation showed no obvious stenosis; B: Three-dimensional reconstruction of the heart showed multiple outpouchings on the left ventricular wall; C: The left ventricular septum myocardium exhibited uneven enhancement. The degree of enhancement is shown by the red arrow and was lower than that of the surrounding tissue, computed tomography value -90 HU; D: Uneven enhancement in the left ventricle free wall myocardium. The degree of enhancement is shown by the red arrow and was lower than that of the surrounding tissue, computed tomography value -114 HU; E: The left ventricular wall exhibited a disordered structure. The uneven thickness of the ventricular wall and local diverticulum is denoted by the red arrow; F: Diverticulum in the apex of the left ventricle is shown by the red arrow.

with various structural heart or primary electrical diseases, such as Brugada syndrome, arrhythmogenic right ventricular dysplasia, and acquired long QT syndrome[6]. Therefore, careful differential diagnosis for cardiomyopathy was imperative for the patient in the present case. Furthermore, there is a need to consider multimodality cardiovascular imaging.

CMRI combined with CCTA is effective in identification of multiple types of cardiomyopathy and cardiac inner structures. Initially, we considered the left ventricular apex outpouching with a thick wall, narrow communication, and synchronous contractility to be a diverticulum based on evidence from echocardiography and myocardial contrast echocardiography. However, CCTA and CMRI generated more details for differential diagnosis. Previous studies have shown that CCTA, a noninvasive approach, can effectively distinguish outpouchings caused by myocardial infarction and ischemic cardiomyopathy related to occlusion (or lack thereof) of the coronary arteries[7,8]. Furthermore, CMRI has a unique advantage in identifying cardiomyopathy. Black blood with T1 and T2 sequences as well as dynamic bring blood were used to evaluate the cardiac structure, tissue characterization, bilateral ventricular function, and segmental movement. In addition, delayed enhancement imaging following administration of gadolinium can result in more information on fibrosis, scarring, and fat infiltration in the local myocardium[9]. In the present case, CCTA and CMRI results revealed LV septum and free wall local myocardium replaced by fatty tissue as well as LV midwall late gadolinium enhancement, multiple LV outpouchings, and uneven thickness of the LV wall, without stenosis of coronary arteries. These abnormalities were accompanied by non-sustained ventricular tachycardia with an RBBB pattern and f-QRS in the left chest leads. Consequently, we considered that this patient had arrhythmogenic cardiomyopathy.

Arrhythmogenic cardiomyopathy refers to a category of non-hypertrophic, non-hypertensive, and non-valvular progressive cardiomyopathy with fibrofatty myocardium infiltration[10]. Previous studies have classified arrhythmogenic cardiomyopathy into classical arrhythmogenic right ventricular cardiomyopathy, LDAC, and biventricular involvement categories[11]. The patient in the present study was eventually diagnosed with LDAC. LDAC, which was first described by Sen-Chowdhry *et al*[1] in 2008, has been easily overlooked or misdiagnosed as myocardial infarction, myocarditis, and dilated cardiomyopathy in clinical practice. Notably, LDAC is a relatively rare disease. For example, it accounted for less than 0.15% of 35845 consecutive patients who were referred for CMRI examinations in Fuwai Hospital (Beijing, China), National Center for Cardiovascular Diseases[12].

Clinically, LDAC patients mainly manifest palpitations, presyncope, exertional dyspnea, and chest pain with normal coronary angiography, with only a handful of cases found to be asymptomatic[12,13]. Patients with LDAC have poor prognosis. For example, Feliu *et al*[13] found that 32.4% of all LDAC patients studied manifested major adverse cardiovascular events, which were mainly accompanied by sudden cardiac death and ventricular arrhythmias, during a mean follow-up of 3.74 years.

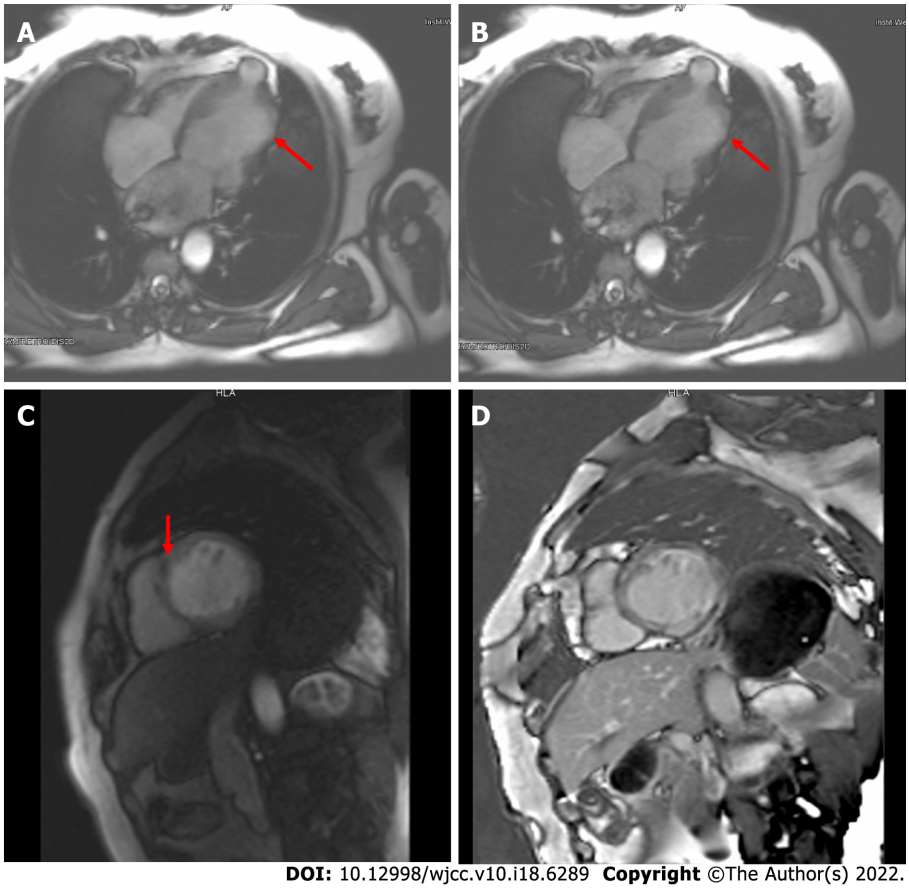

DOI: 10.12998/wjcc.v10.i18.6289 **Copyright** ©The Author(s) 2022.

Figure 6 Cardiac magnetic resonance imaging results of the patient under this study. A and B: Four-chamber cine images at end-diastole (A) and end-systole (B) showed left ventricular dilatation, abnormal activity of the ventricular wall (arrows indicate severely diminished contractility), and outpouching at the left ventricular apex; C: Short-axis first-pass perfusion showed a low signal at the midwall of the septum myocardium; D: Short-axis delayed enhancement imaging demonstrated diffuse stripes of hyperenhancement in the midwall of the left ventricular septum and free wall myocardium.

At present, no specific diagnostic criteria exist for LDAC. In 2008, Dr. Chowdhry established the following initial diagnostic features of LDAC: (1) Arrhythmia: sustained or non-sustained ventricular tachycardia; (2) Imaging: (a) LV aneurysms; and (b) mild LV dilation and/or systolic impairment; (3) Biopsy/CMRI: (a) cardiomyocyte loss with fibrofatty replacement on histology; and (b) extensive late gadolinium enhancement of LV myocardium (with subepicardial/midmyocardial distribution); and (4) Unexplained T-wave inversion in V5, V6 ± V4, I, and AVL[1]. Recently, Corrado *et al*[11] suggested that the following elements should be considered as LDAC: (1) ECG changes, such as low QRS voltages in limb leads and inverted T waves in the inferolateral leads; (2) Ventricular arrhythmias with an RBBB pattern; and (3) Structural and functional imaging features consistent with 'hypokinetic and fibrotic LV.' Interestingly, the ultrasonographer initially misdiagnosed the patient in the present study as congenital ventricular diverticulum (CVD), according to the left ventricular apex cystic outpouching displaying synchronous contractility with the corresponding cardiac chamber.

CVD, first described in 1816, was often asymptomatic and incidentally detected during a regular physical check-up. Generally, the left ventricular diverticulum was in a thick wall, comprising endocardium, myocardium, and pericardium, with a narrow communication between the cavity and ventricular and displayed synchronous contractility with the LV[14]. This was likened to an appendix originating from the ventricle. The left ventricular diverticulum has an average size that varies from 0.5 cm to as large as 8.0-9.0 cm[15]. Notably, the left ventricular diverticulum not only has low prevalence, as evidenced by 0.4%-2.2% across different studies[16], but has also been associated with occurrence of other congenital abnormalities, including septal defects, dextrocardia, and pulmonary stenosis. Generally, CVD combined with midline thoraco-abdominal congenital abnormalities, diaphragmatic and sternal defects, and partial absence of diaphragmatic pericardium is referred to as Cantrell's syndrome[17].

CVD has the atypical and nonspecific clinical manifestations at an early stage, namely arrhythmias, cardiac rupture, heart failure, and embolism[18,19], which make it easily confused with LDAC. However, some of these features can be adopted during the differential diagnosis between CVD and LDAC. First, most CVD are single and located at the cardiac apex[20,21]. Second, the left ventricular wall exhibits neither signal alterations nor signs of necrosis or fibrous tissue in CVD cases[22]. Third, CVD patients exhibit more frequent extracardiac anomalies than those with LDAC[19]. Fourth, the size

of CVD does not change over time, suggesting a benign course[23]. However, the patient in the present study not only manifested multiple left ventricular outpouchings but also exhibited uneven-thickness left ventricular wall with multiple flaky fatty infiltrations. This interesting case indicates that clinicians should not ignore LDAC upon detecting left ventricle outpouching on TTE.

Although myocardial biopsy is the gold standard diagnostic criterion, this patient refused this invasive examination. After comprehensively analyzing a combination of the medical history and positive clues on auxiliary examinations, including ECG, TTE, CCTA, and CMRI, the specialists in our department unanimously diagnosed the patient with LDAC. She was subsequently administered with standard oral therapy for heart failure with reduced ejection fraction and implantable cardioverter-defibrillator. The patient was very satisfied with the process of diagnosis, treatment, and follow-up.

CONCLUSION

LDAC is a relatively rare disease, which requires multimodality cardiovascular imaging for diagnosis. CMRI combined with CCTA is an excellent approach for identification of multiple types of cardiomyopathy and cardiac inner structures. From the present case, clinicians are advised to consider LDAC in patients with localized left ventricular lesions and multiple electrocardiographic abnormalities.

ACKNOWLEDGEMENTS

The authors thank the radiology department of West China Hospital, Sichuan University for technical support. Second, we thank Dr. Jerry, PhD from the Home for researchers editorial team for editing the language of this manuscript.

FOOTNOTES

Author contributions: Zhang X and Ye RY contributed equally to this article; Zhang X and Ye RY were the patient's cardiologists, reviewed the literature, and contributed to manuscript drafting; Chen XP was responsible for the revision of the manuscript for important intellectual content; All authors issued final approval for the version to be submitted.

Supported by Chengdu Science and Technology Bureau, China, No. 2020-YF05-00290-SN.

Informed consent statement: Written informed consent was obtained from the patient for the publication of this case report and the accompanying images.

Conflict-of-interest statement: The authors declare that they have no competing interests to declare.

CARE Checklist (2016) statement: The authors have read the CARE Checklist (2016), and the manuscript was prepared and revised according to the CARE Checklist (2016).

Open-Access: This article is an open-access article that was selected by an in-house editor and fully peer-reviewed by external reviewers. It is distributed in accordance with the Creative Commons Attribution NonCommercial (CC BY-NC 4.0) license, which permits others to distribute, remix, adapt, build upon this work non-commercially, and license their derivative works on different terms, provided the original work is properly cited and the use is non-commercial. See: https://creativecommons.org/Licenses/by-nc/4.0/

Country/Territory of origin: China

ORCID number: Xin Zhang 0000-0003-3305-3144; Run-Yu Ye 0000-0001-8245-0774; Xiao-Ping Chen 0000-0001-7172-8216.

S-Editor: Gong ZM
L-Editor: Filipodia
P-Editor: Gong ZM

REFERENCES

1 **Sen-Chowdhry S**, Syrris P, Prasad SK, Hughes SE, Merrifield R, Ward D, Pennell DJ, McKenna WJ. Left-dominant arrhythmogenic cardiomyopathy: an under-recognized clinical entity. *J Am Coll Cardiol* 2008; **52**: 2175-2187 [PMID: 19095136 DOI: 10.1016/j.jacc.2008.09.019]

2 **Andreini D**, Conte E, Casella M, Mushtaq S, Pontone G, Dello Russo A, Nicoli F, Carità P, Catto V, Vettor G, Gasperetti

A, Sommariva E, Rizzo S, Basso C, Tondo C, Pepi M. Cardiac magnetic resonance features of left dominant arrhythmogenic cardiomyopathy: differential diagnosis with myocarditis. *Int J Cardiovasc Imaging* 2022; **38**: 397-405 [PMID: 34546457 DOI: 10.1007/s10554-021-02408-8]

3 **Jain R**, Singh R, Yamini S, Das MK. Fragmented ECG as a risk marker in cardiovascular diseases. *Curr Cardiol Rev* 2014; **10**: 277-286 [PMID: 24827794 DOI: 10.2174/1573403x10666140514103451]

4 **Brohet C**. Fragmentation of the QRS complex: the latest electrocardiographic craze? *Acta Cardiol* 2019; **74**: 185-187 [PMID: 30950722 DOI: 10.1080/00015385.2019.1600827]

5 **Haukilahti MA**, Eranti A, Kenttä T, Huikuri HV. QRS Fragmentation Patterns Representing Myocardial Scar Need to Be Separated from Benign Normal Variants: Hypotheses and Proposal for Morphology based Classification. *Front Physiol* 2016; **7**: 653 [PMID: 28082919 DOI: 10.3389/fphys.2016.00653]

6 **Ratheendran AC**, Subramanian M, Bhanu DK, Prabhu MA, Kannan R, Natarajan KU, Saritha Sekhar S, Thachathodiyil R, Harikrishnan MS, Pai PG. Fragmented QRS on electrocardiography as a predictor of myocardial scar in patients with hypertrophic cardiomyopathy. *Acta Cardiol* 2020; **75**: 42-46 [PMID: 30602338 DOI: 10.1080/00015385.2018.1547355]

7 **Al'Aref SJ**, Min JK. Cardiac CT: current practice and emerging applications. *Heart* 2019; **105**: 1597-1605 [PMID: 31142595 DOI: 10.1136/heartjnl-2018-314229]

8 **Ramsey BC**, Fentanes E, Choi AD, Branch KR, Thomas DM. Myocardial Assessment with Cardiac CT: Ischemic Heart Disease and Beyond. *Curr Cardiovasc Imaging Rep* 2018; **11**: 16 [PMID: 29963220 DOI: 10.1007/s12410-018-9456-2]

9 **Yoneyama K**, Kitanaka Y, Tanaka O, Akashi YJ. Cardiovascular magnetic resonance imaging in heart failure. *Expert Rev Cardiovasc Ther* 2018; **16**: 237-248 [PMID: 29478345 DOI: 10.1080/14779072.2018.1445525]

10 **Towbin JA**, McKenna WJ, Abrams DJ, Ackerman MJ, Calkins H, Darrieux FCC, Daubert JP, de Chillou C, DePasquale EC, Desai MY, Estes NAM 3rd, Hua W, Indik JH, Ingles J, James CA, John RM, Judge DP, Keegan R, Krahn AD, Link MS, Marcus FI, McLeod CJ, Mestroni L, Priori SG, Saffitz JE, Sanatani S, Shimizu W, van Tintelen JP, Wilde AAM, Zareba W. 2019 HRS expert consensus statement on evaluation, risk stratification, and management of arrhythmogenic cardiomyopathy. *Heart Rhythm* 2019; **16**: e301-e372 [PMID: 31078652 DOI: 10.1016/j.hrthm.2019.05.007]

11 **Corrado D**, van Tintelen PJ, McKenna WJ, Hauer RNW, Anastastakis A, Asimaki A, Basso C, Bauce B, Brunckhorst C, Bucciarelli-Ducci C, Duru F, Elliott P, Hamilton RM, Haugaa KH, James CA, Judge D, Link MS, Marchlinski FE, Mazzanti A, Mestroni L, Pantazis A, Pelliccia A, Marra MP, Pilichou K, Platonov PGA, Protonotarios A, Rampazzo A, Saffitz JE, Saguner AM, Schmied C, Sharma S, Tandri H, Te Riele ASJM, Thiene G, Tsatsopoulou A, Zareba W, Zorzi A, Wichter T, Marcus FI, Calkins H; International Experts. Arrhythmogenic right ventricular cardiomyopathy: evaluation of the current diagnostic criteria and differential diagnosis. *Eur Heart J* 2020; **41**: 1414-1429 [PMID: 31637441 DOI: 10.1093/eurheartj/ehz669]

12 **He J**, Xu J, Li G, Zhou D, Li S, Zhuang B, Chen X, Duan X, Li L, Fan X, Huang J, Yin G, Jiang Y, Wang Y, Zhao S, Lu M. Arrhythmogenic Left Ventricular Cardiomyopathy: A Clinical and CMR Study. *Sci Rep* 2020; **10**: 533 [PMID: 31953454 DOI: 10.1038/s41598-019-57203-2]

13 **Feliu E**, Moscicki R, Carrillo L, García-Fernández A, Martínez Martínez JG, Ruiz-Nodar JM. Importance of cardiac magnetic resonance findings in the diagnosis of left dominant arrythmogenic cardiomyopathy. *Rev Esp Cardiol (Engl Ed)* 2020; **73**: 885-892 [PMID: 31992505 DOI: 10.1016/j.rec.2019.12.004]

14 **Srichai MB**, Hecht EM, Kim DC, Jacobs JE. Ventricular diverticula on cardiac CT: more common than previously thought. *AJR Am J Roentgenol* 2007; **189**: 204-208 [PMID: 17579172 DOI: 10.2214/AJR.06.1223]

15 **Ohlow MA**. Congenital left ventricular aneurysms and diverticula: definition, pathophysiology, clinical relevance and treatment. *Cardiology* 2006; **106**: 63-72 [PMID: 16612072 DOI: 10.1159/000092634]

16 **Sharma A**, Kumar S. Overview of left ventricular outpouchings on cardiac magnetic resonance imaging. *Cardiovasc Diagn Ther* 2015; **5**: 464-470 [PMID: 26675616 DOI: 10.3978/j.issn.2223-3652.2015.11.02]

17 **Vazquez-Jimenez JF**, Muehler EG, Daebritz S, Keutel J, Nishigaki K, Huegel W, Messmer BJ. Cantrell's syndrome: a challenge to the surgeon. *Ann Thorac Surg* 1998; **65**: 1178-1185 [PMID: 9564963 DOI: 10.1016/s0003-4975(98)00089-7]

18 **Ohlow MA**. Congenital left ventricular aneurysms and diverticula: an entity in search of an identity. *J Geriatr Cardiol* 2017; **14**: 750-762 [PMID: 29581714 DOI: 10.11909/j.issn.1671-5411.2017.12.005]

19 **Ohlow MA**, von Korn H, Lauer B. Characteristics and outcome of congenital left ventricular aneurysm and diverticulum: Analysis of 809 cases published since 1816. *Int J Cardiol* 2015; **185**: 34-45 [PMID: 25782048 DOI: 10.1016/j.ijcard.2015.03.050]

20 **Restrepo CS**, Lane MJ, Murillo H. Cardiac aneurysms, pseudoaneurysms, and diverticula. *Semin Roentgenol* 2012; **47**: 262-276 [PMID: 22657116 DOI: 10.1053/j.ro.2011.11.011]

21 **Cresti A**, Cannarile P, Aldi E, Solari M, Sposato B, Franci L, Limbruno U. Multimodality Imaging and Clinical Significance of Congenital Ventricular Outpouchings: Recesses, Diverticula, Aneurysms, Clefts, and Crypts. *J Cardiovasc Echogr* 2018; **28**: 9-17 [PMID: 29629254 DOI: 10.4103/jcecho.jcecho_72_17]

22 **Romagnoli A**, Ricci A, Morosetti D, Fusco A, Citraro D, Simonetti G. Congenital left ventricular diverticulum: Multimodality imaging evaluation and literature review. *J Saudi Heart Assoc* 2015; **27**: 61-67 [PMID: 25544824 DOI: 10.1016/j.jsha.2014.07.004]

23 **Scagliola R**, Rosa GM, Seitun S. Cardiac Outpouchings: Definitions, Differential Diagnosis, and Therapeutic Approach. *Cardiol Res Pract* 2021; **2021**: 6792643 [PMID: 34567801 DOI: 10.1155/2021/6792643]

World Journal of Clinical Cases

Submit a Manuscript: https://www.f6publishing.com

World J Clin Cases 2022 June 26; 10(18): 6298-6306

DOI: 10.12998/wjcc.v10.i18.6298

ISSN 2307-8960 (online)

CASE REPORT

Spontaneous healing of complicated crown-root fractures in children: Two case reports

Zi-Ling Zhou, Lei Gao, Shu-Kai Sun, Hong-Shi Li, Cai-Di Zhang, Wen-Wen Kou, Zheng Xu, Li-An Wu

Specialty type: Medicine, research and experimental

Provenance and peer review: Unsolicited article; Externally peer reviewed.

Peer-review model: Single blind

Peer-review report's scientific quality classification

Grade A (Excellent): 0
Grade B (Very good): B, B
Grade C (Good): C, C
Grade D (Fair): D, D
Grade E (Poor): E

P-Reviewer: Abu Hasna A, Brazil; Hamzah SH, Malaysia; Heboyan A, Armenia; Kukiattrakoon B, Thailand; Mehta V, India; Nath SG, India; Slutzky Goldberg I, Israel

Received: December 25, 2021
Peer-review started: December 25, 2021
First decision: February 8, 2022
Revised: February 21, 2022
Accepted: April 27, 2022
Article in press: April 27, 2022
Published online: June 26, 2022

Zi-Ling Zhou, Lei Gao, Shu-Kai Sun, Cai-Di Zhang, Wen-Wen Kou, Department of Pediatric Dentistry, School of Stomatology, Fourth Military Medical University, Xi'an 710032, Shaanxi Province, China

Hong-Shi Li, Institute of Stomatology, The General Air Force Hospital of PLA, Beijing 110142, China

Zheng Xu, The Center for Pediatric Dentistry, Department of Pediatric Dentistry, University of Washington, Seaatle, WA 98115, United States

Li-An Wu, Department of Pediatric Dentistry, School of Stomatology, The Fourth Military Medical University, Xi'an 710032, Shaanxi Province, China

Corresponding author: Li-An Wu, PhD, Professor, Department of Pediatric Dentistry, School of Stomatology, The Fourth Military Medical University, No. 145 Changle West Road, Xincheng District, Xi'an 710032, Shaanxi Province, China. lianwu@fmmu.edu.cn

Abstract

BACKGROUND

Complicated crown-root fracture is considered a severe dental trauma and is unlikely to heal without treatment. Usually, dentists have to remove the loose coronal fragment of the fractured tooth and treat the remaining part with multidisciplinary approaches. However, we observed spontaneous healing of fracture in two pediatric cases with a history of complicated crown-root fractures over 4 years ago.

CASE SUMMARY

In case 1, a 12-year-old boy complained of pain at tooth 11 following an accidental fall 1 d ago. Clinical examination showed a crack line on the crown of tooth 11. Cone beam computed tomography (CBCT) images of tooth 11 showed signs of hard tissue deposition between the fractured fragments. The patient recalled that tooth 11 had struck the floor 1 year ago without seeking any other treatment. In case 2, a 10-year-old girl fell down 1 d ago and wanted to have her teeth examined. Clinical examination showed a fracture line on the crown of tooth 21. CBCT images of tooth 21 also showed signs of hard tissue deposition between the fractured fragments. She also had a history of dental trauma 1 year ago and her tooth 11 received dental treatment by another dentist. According to her periapical radiograph at that time, tooth 21 was fractured 1 year ago and the fracture was overlooked by her dentist. Both of these two cases showed spontaneous healing of

complicated crown-root fractures. After over 4 years of follow-up, both fractured teeth showed no signs of abnormality.

CONCLUSION
These findings may provide new insights and perspectives on the management and treatment of crown-root fractures in children.

Key Words: Dental trauma; Complicated crown-root fracture; Spontaneous healing; Children; Case report

©The Author(s) 2022. Published by Baishideng Publishing Group Inc. All rights reserved.

Core Tip: Crown-root fracture is a severe dental trauma involving the enamel, dentin, cementum, and periodontal ligament. The mobile coronal fragment usually needs to be removed or reattached with bonding agent depending on the extent of the injury. Spontaneous healing with hard tissues has been rarely reported in crown-root fracture so far. In this report, we present two clinical cases with spontaneous healing of complicated crown-root fractures of permanent central incisors in children with over 4 years of follow-up, which may provide new insights and perspectives on the management and treatment of crown-root fractures.

Citation: Zhou ZL, Gao L, Sun SK, Li HS, Zhang CD, Kou WW, Xu Z, Wu LA. Spontaneous healing of complicated crown-root fractures in children: Two case reports. *World J Clin Cases* 2022; 10(18): 6298-6306
URL: https://www.wjgnet.com/2307-8960/full/v10/i18/6298.htm
DOI: https://dx.doi.org/10.12998/wjcc.v10.i18.6298

INTRODUCTION

Crown-root fracture originates from the crown and extends apically in an oblique direction[1]. It is usually caused by fall, fight, traffic accident, or foreign bodies[2]. It is reported that the incidences of crown-root fractures are 2% in the deciduous teeth and 5% in the permanent dentition[3]. According to the International Association of Dental Traumatology (IADT) guidelines for the management of traumatic dental injuries, the options for the treatment of complicated crown-root fractures with pulpal exposure include partial pulpotomy, root canal therapy, gingivectomy, orthodontic extrusion, surgical extrusion, root submergence, and extraction with immediate or delayed implant-retained crown restoration or a conventional bridge[4]. Due to the complexity of crown-root fracture, its treatment is not always the same and different dentists may choose different treatments.

In this report, we present two clinical cases with spontaneous healing of complicated crown-root fractures of permanent central incisors in children. In both of these two cases, the fractured fragments healed spontaneously with hard tissue deposition around the fracture lines, which suggested that dentists may have more treatment options when dealing with crown-root fracture.

CASE PRESENTATION

Chief complaints

Case 1: A 12-year-old boy was referred to our department complaining of pain at his maxillary right central incisor following an accidental fall 1 d ago.

Case 2: A 10-year-old girl visited our department with her parents after she fell 1 d ago, complaining of pain at her maxillary left central incisor.

History of present illness

Case 1: The patient recalled that this tooth once struck the floor when he fell approximately 1 year ago, and he did not seek any treatment then due to the absence of symptoms.

Case 2: According to the patient's dental history, tooth 11 was fractured 1 year ago and was treated with injectable Root Canal Paste (Vitapex, Morita, Japan) for apexification and composite resin being placed in chamber by a local general dentist. During the examination after that injury, the general dentist did not find any responsive sign and symptoms of injury for tooth 21.

History of past illness

Case 1: The patient was medically healthy without taking any medications.

Case 2: Medical history of this patient was noncontributory.

Personal and family history

Cases 1 and 2: There were no specific family health histories.

Physical examination

Case 1: Clinical examination showed that tooth 11 was responsive to palpation and had bleeding from the gingival crevice (Figure 1A) but showed no displacement and no increased mobility. Using a dental probe without any pressure, a crack line was detected on the crown of tooth 11, which was slightly below the gingival margin. Cold test showed no response.

Case 2: Extra-oral examinations were normal. Intra-oral examination showed that there was a complicated crown fracture in tooth 11 with discolored crown and pulp chamber being filled by resin from the lingual surface. Tooth 21 exhibited class I mobility and a facial fracture line below the gingival margin was detected by a probe without any pressure. Tooth 21 was responsive to cold test and palpation (Figure 1B).

Imaging examinations

Case 1: Cone beam computed tomography (CBCT) images showed an oblique crown-root fracture line extending from the labial surface of the tooth 11 to the palatal alveolar ridge, which is approximately 3.8 mm below the palatal gingival margin. Surprisingly, the images also showed signs of hard tissue deposition between the fractured fragments (Figure 2).

Case 2: CBCT images of tooth 21 showed an oblique crown-root fracture line starting from the labial surface and extending palatally below the alveolar ridge for approximately 3.5 mm beneath the palatal gingival margin (Figure 3), which resulted in the abnormal mobility of the coronal fragment. Interestingly, it also showed signs of hard tissue deposition at the pulpal side between the fractured fragments, indicating a healing process for the pre-existing fracture in tooth 21. Upon reviewing the radiographs taken 1 year ago after the first injury, the fracture line on tooth 21 was noticed (Figure 4). Since the patient never complained of any symptoms on tooth 21, and the periapical radiograph showed no signs of abnormality, the fracture was overlooked by the general dentist.

FINAL DIAGNOSIS

Case 1

Based on the history and findings of the imaging examinations, tooth 11 was diagnosed as complicated crown-root fractures (old fracture spontaneous healing).

Case 2

Based on the history and findings of the imaging examinations, tooth 11 was diagnosed as complicated crown fractures and tooth 21 was diagnosed as complicated crown-root fractures (old fracture spontaneous healing).

TREATMENT

Case 1

At this point, since there were no other signs and clinical symptoms, and the coronal fragment was not loose, the patient was recommended to wear a mandible occlusal pad for 2 wk with periodical revisit and special attention of not re-injuring the tooth (Figure 5A).

Case 2

During the current visit, tooth 21 was stabilized with a flexible fiber splint (RTD Quartz Splint™, France, Figure 5B) and a mandible occlusal pad was placed for 2 wk. Three months later, the splint was removed and the root canal of tooth 11 was completed after obturation with gutta-percha and sealer (Figure 5C and D). Tooth 11 was then restored with resin composite 1 wk later (Figure 5E). Tooth 21 showed normal mobility and normal response in the pulp sensibility test. There were no discoloration or radiographic signs of periapical lesions at this point and no further treatment was applied.



DOI: 10.12998/wjcc.v10.i18.6298 **Copyright** ©The Author(s) 2022.

Figure 1 Initial intraoral photographs. A: Case 1, bleeding from the gingival crevice of tooth 11; B: Case 2, complicated crown fracture in tooth 11 with discolored crown and pulp chamber filled by resin, and mild inflammation in the marginal gingiva of teeth 11 and 21; C: Case 1, tooth 11 taken 1 yr later.

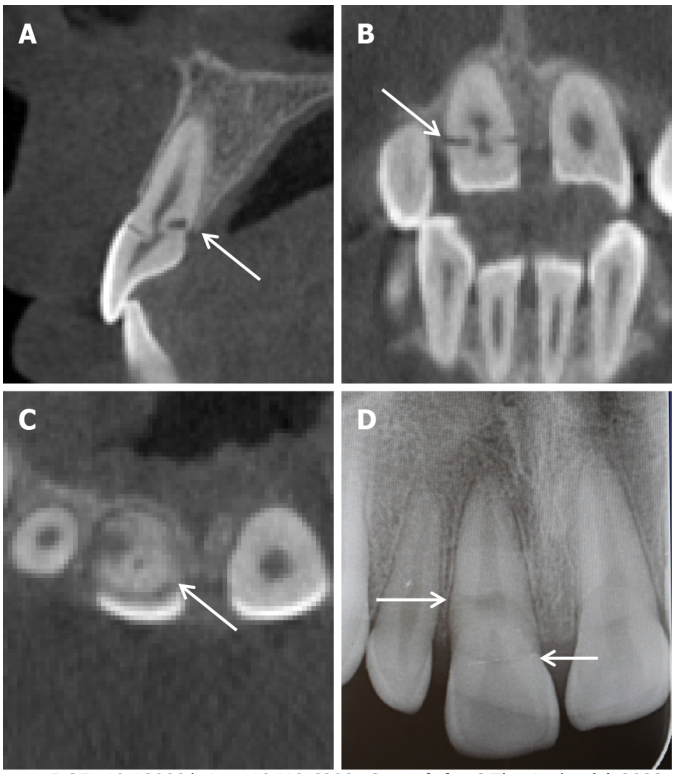

DOI: 10.12998/wjcc.v10.i18.6298 **Copyright** ©The Author(s) 2022.

Figure 2 Cone beam computed tomography and periapical radiograph images showing an oblique crown-root fracture from the labial surface of the tooth 11 to the palatal alveolar ridge, which had signs of healing. A: Sagittal; B: Coronal; C: Cross-sectional; D: Periapical.

OUTCOME AND FOLLOW-UP

Case 1

During the periodical monitoring of the pulp condition every 3 mo for 1 year, the tooth showed normal color and mobility and became responsive to pulp sensibility test (Figure 1C). Radiographic examination revealed that the fracture line became blurred gradually (Figure 6A). The patient was followed annually for 3 years, and there were no signs of abnormality on tooth 11. The periapical radiographs also appeared to be normal (Figure 6B-D).

Case 2

At 1-year follow up visit, tooth 21 remained stable and was responsive to pulp test. The periapical radiograph of tooth 21 revealed no signs of periapical abnormality and no significant change of the fracture line (Figure 7A). The patient was not followed until 4 years later. Clinical examination on tooth 21 revealed no sign of abnormality. The coronal fragment was not loose, and the CBCT image of tooth 21 showed signs of healing (Figure 7B-D).

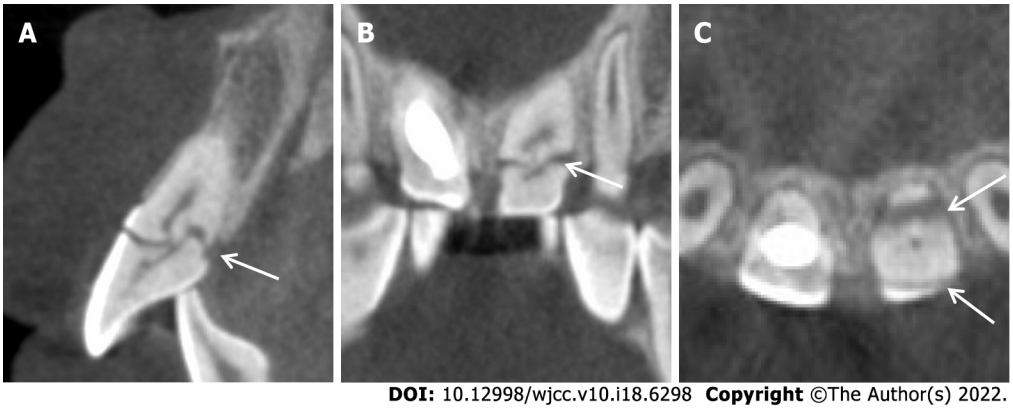

DOI: 10.12998/wjcc.v10.i18.6298 **Copyright** ©The Author(s) 2022.

Figure 3 Cone beam computed tomography images showing an oblique crown-root fracture from the labial surface of the tooth 21 with hard tissue deposition at the pulpal side across the fracture line. A: Sagittal; B: Coronal; C: Cross-sectional.

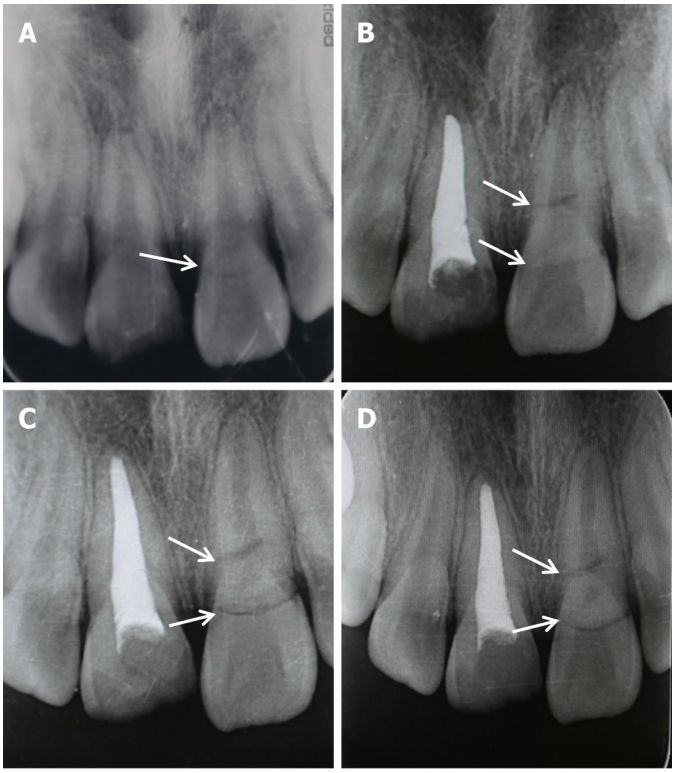

DOI: 10.12998/wjcc.v10.i18.6298 **Copyright** ©The Author(s) 2022.

Figure 4 Periapical radiographs. A: Periapical radiograph of teeth 11 and 21 after the first injury 1 yr ago showed fracture on tooth 21; B-D: Periapical radiographs of teeth 11 and 21 after tooth 11 was treated with apexification. The fracture line on tooth 21 became more evident over the time (B: 3 mo after initial injury; C: 6 mo after initial injury; D: 9 mo after initial injury).

DISCUSSION

Crown-root fracture is a severe dental trauma involving the enamel, dentin, cementum, and periodontal ligament[5,6]. According to the classifications of Andreasen, it can be classified as complicated crown-root fracture if there is pulpal involvement and non-complicated crown-root fracture if there is no pulpal involvement[7]. In the case of complicated crown-root fracture, complications, *e.g.*, pulp necrosis, apical periodontitis, and root resorption, may occur if the pulp is left untreated[8,9]. The mobile coronal fragment usually needs to be removed or reattached with bonding agent depending on the extent of the injury. Multidisciplinary care is usually required for the treatment of crown-root fracture. While relatively common in root fractures, spontaneous healing with hard tissues has been rarely reported in crown-root fracture so far[10-12]. This is probably due to the severe pulp injury and the connections of the fracture in the coronal portion with the oral cavity, leading to inevitable microbial contamination in the pulp and subsequent pulpal necrosis[13-15].

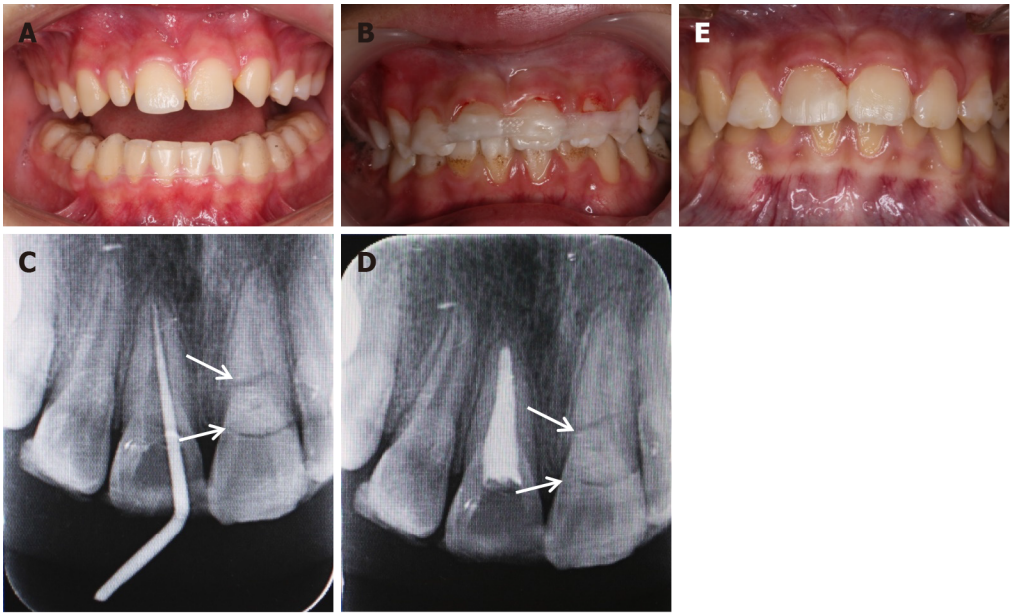

DOI: 10.12998/wjcc.v10.i18.6298 **Copyright** ©The Author(s) 2022.

Figure 5 Treatment photographs. A: Intraoral photograph after wearing a mandible occlusal pad; B: Tooth 21 was stabilized with a fiber splint; C and D: Completion of root canal therapy for tooth 11; E: Tooth 11 was restored with resin composite.

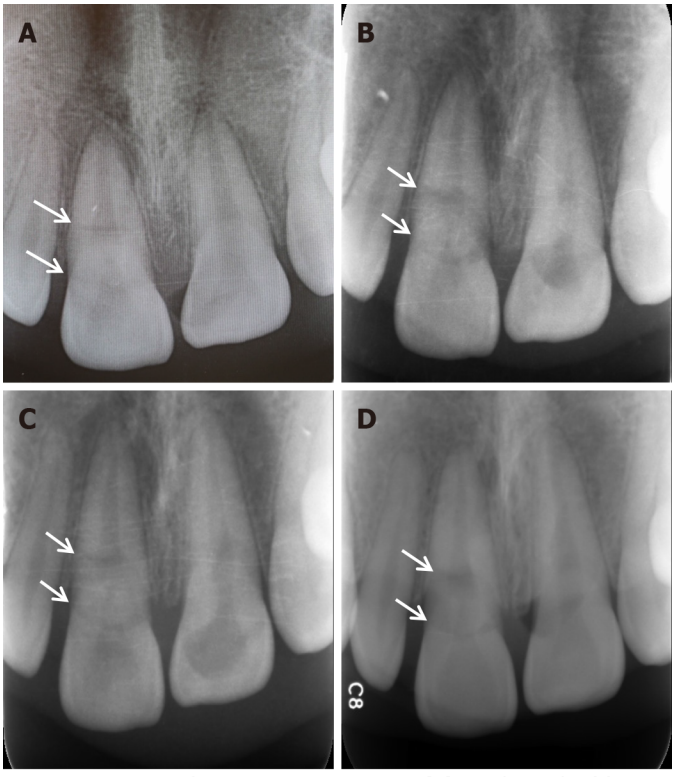

DOI: 10.12998/wjcc.v10.i18.6298 **Copyright** ©The Author(s) 2022.

Figure 6 Periapical radiographs. A-D: Periapical radiographs of tooth 11 taken 1 (A), 2 (B), 3 (C), and 4 yr later (D).

Inorganic compound accounts for 95% of the enamel[16], and fracture on the enamel is unlikely to heal. That is the reason why the enamel fragments were still separated by a narrow radiolucent line in the CBCT images, and we can still detect a fracture on the labial surface of the enamel clinically. To some extent, the two cases are analogous to root fractures in the cervical third except for the fracture on the enamel. Healing of crown-root fractures is the healing of the dentine and cementum, which is similar to the healing of root fractures. According to Andreasen and Hjorting-Hensen, healing of root fractures can be classified into four types[17]: (1) Calcified tissue wound healing; (2) Healing by interposition of connective tissue; (3) Healing by interposition of bone and connective tissue; and (4)



DOI: 10.12998/wjcc.v10.i18.6298 **Copyright** ©The Author(s) 2022.

Figure 7 Periapical radiograph and cone beam computed tomography images. A: Periapical radiograph of teeth 11 and 21 taken 9 mo after the restoration of tooth 11; B-D: Sagittal (B), coronal (C), and cross-sectional (D) cone beam computed tomography images taken 4 yr later showing sign of repair.

Healing by interposition of granulation tissue. The most desirable outcome is the calcified tissue wound healing. In these two cases, it is likely that calcified tissue wound healing occurred since CBCT showed deposition of radiopaque tissues between the separated fragments. In addition, both teeth exhibited response in the pulp test during the follow-up examination, which can demonstrate the reparative dentin formation and calcified tissue wound healing.

Due to the bacterial invasion from the gingival sulcus, the reported incidence of tooth survival for root fractures in the cervical third is only 30%[18]. In these two cases, the fracture was closer to gingival sulcus than most root fractures, and the labial fracture lines were located in the gingival sulcus. Thus, it is intriguing how and why the pulp survived in these two cases. Based on the age of the patients, it is possible that the initial injuries occurred during the later phase of the maxillary central incisors eruption when the tooth roots were still immature. At that moment, the cervical region of the enamel was still covered by the junctional epithelium, which seals the fracture from the oral cavity. The junctional epithelium and the pulp also contain immune cells (*e.g.*, neutrophils, lymphocytes, macrophages, and mast cells) that can protect the pulp against the microbes near the gingival sulcus[16,19]. Moreover, pulpal vitality after injury might be maintained by the stability of the oblique fracture line, which is in consistent with our clinical finding that there is no severe displacement of coronal fragment after injury. Finally, the immature teeth have more sufficient blood supply with a large amount of stem cells that can promote and accelerate healing. All these favorable factors provided an ideal circumstance to maintain the vitality of the pulp. The vital pulp and the intact periodontal ligament contain large number of odontoblasts and cementoblasts[19], which might contribute to the deposition of hard tissue matrix between the fragments and the healing of the fractures.

There are still some limitations in this study. The use of the mandibular pad in treatments was not based on the IADT guidelines. Instead, the treatment was based on a previous study[20]. Further research is needed to compare different treatments.

CONCLUSION

In this case report, we observed hard tissue healing without any intervention in two pediatric cases of crown-root fracture, suggesting that spontaneous healing with hard tissue deposition may occur in pediatric patients with complicated crown-root fractures and minimal displacement. It should be emphasized that conservative treatments with regular follow-up should be preferred for cases of children after trauma.

FOOTNOTES

Author contributions: Zhou ZL, Gao L and Wu LA performed the dental treatment; Zhou ZL, Sun SK, Zhang CD and Kou WW reviewed the literature, and contributed to the drafting of the manuscript; Xu Z, Li HS and Wu LA were responsible for the revision of the manuscript for important intellectual content; all authors issued final approval for the version to be submitted.

Supported by National Natural Science Foundation of China, No. 81771095; Shaanxi Provincial Key R&D Program, China, No. 2021KWZ-26; and State Key Laboratory of Military Stomatology, No. 2020ZA01.

Informed consent statement: Informed written consent was obtained from the patients' parents for publication of this report and any accompanying images.

Conflict-of-interest statement: The authors declare that they have no conflict of interest to report.

CARE Checklist (2016) statement: The authors have read the CARE Checklist (2016), and the manuscript was prepared and revised according to the CARE Checklist (2016).

Open-Access: This article is an open-access article that was selected by an in-house editor and fully peer-reviewed by external reviewers. It is distributed in accordance with the Creative Commons Attribution NonCommercial (CC BY-NC 4.0) license, which permits others to distribute, remix, adapt, build upon this work non-commercially, and license their derivative works on different terms, provided the original work is properly cited and the use is non-commercial. See: https://creativecommons.org/Licenses/by-nc/4.0/

Country/Territory of origin: China

ORCID number: Zi-Ling Zhou 0000-0002-9739-766X; Lei Gao 0000-0001-9828-8994; Shu-Kai Sun 0000-0002-2123-977X; Hong-Shi Li 0000-0003-3331-4957; Cai-Di Zhang 0000-0001-8395-2231; Wen-Wen Kou 0000-0002-2693-0965; Zheng Xu 0000-0002-9028-7935; Li-An Wu 0000-0001-8909-328X.

S-Editor: Gao CC
L-Editor: Wang TQ
P-Editor: Gao CC

REFERENCES

1 **Mokhtari S**, Hajian S, Sanati I. Complicated Crown-root Fracture Management Using the 180-degree Rotation Method. *Int J Clin Pediatr Dent* 2019; **12**: 247-250 [PMID: 31708624 DOI: 10.5005/jp-journals-10005-1625]
2 **Andreasen JO**, Andreasen FM, Andresson L. Textbook and Color Atlas of Traumatic Injuries to the Teeth. 4th ed. Oxford: Blackwell Publishing, 2007
3 **Andreasen JO**. Etiology and pathogenesis of traumatic dental injuries. A clinical study of 1,298 cases. *Scand J Dent Res* 1970; **78**: 329-342 [PMID: 4394635 DOI: 10.1111/j.1600-0722.1970.tb02080.x]
4 **Diangelis AJ**, Andreasen JO, Ebeleseder KA, Kenny DJ, Trope M, Sigurdsson A, Andersson L, Bourguignon C, Flores MT, Hicks ML, Lenzi AR, Malmgren B, Moule AJ, Pohl Y, Tsukiboshi M; International Association of Dental Traumatology. International Association of Dental Traumatology guidelines for the management of traumatic dental injuries: 1. Fractures and luxations of permanent teeth. *Dent Traumatol* 2012; **28**: 2-12 [PMID: 22230724 DOI: 10.1111/j.1600-9657.2011.01103.x]
5 **Alves MD**, Tateyama MA, Pavan N, Queiroz AF, Nunes M, Endo MS. Multidisciplinary Approach to Complicated Crown-root Fracture Treatment: A Case Report. *Oper Dent* 2021 [PMID: 34963000 DOI: 10.2341/20-015-S]
6 **Sanaei-Rad P**, Hajihassani N, Jamshidi D. Management of a complex traumatic dental injury: Crown, crown-root, and root fracture. *Clin Case Rep* 2020; **8**: 2504-2509 [PMID: 33363767 DOI: 10.1002/ccr3.3191]
7 **Yu H**, Zhu H. The management of a complicated crown-root fracture incorporating modified crown-lengthening surgery. *Br Dent J* 2021; **230**: 217-222 [PMID: 33637921 DOI: 10.1038/s41415-021-2653-4]
8 **Marcenes W**, al Beiruti N, Tayfour D, Issa S. Epidemiology of traumatic injuries to the permanent incisors of 9-12-year-old schoolchildren in Damascus, Syria. *Endod Dent Traumatol* 1999; **15**: 117-123 [PMID: 10530154 DOI: 10.1111/j.1600-9657.1999.tb00767.x]
9 **Heboyan AG**, Vardanyan AR, Avetisyan AA, Margaryan MM, Azatyan VY, Yesayan LK, Sharimanyan LA, Martirosyan KH. Rare clinical case of tooth root external resorption as a delayed post-traumatic complication. *New Armenian Med J* 2018; **12**: 92-97
10 **Artvinli LB**, Dural S. Spontaneously healed root fracture: report of a case. *Dent Traumatol* 2003; **19**: 64-66 [PMID: 12656859 DOI: 10.1034/j.1600-9657.2003.00111.x]
11 **Görduysus M**, Avcu N, Görduysus O. Spontaneously healed root fractures: two case reports. *Dent Traumatol* 2008; **24**: 115-116 [PMID: 18173680 DOI: 10.1111/j.1600-9657.2007.00497.x]
12 **Ranka M**, Shah J, Youngson C. Root fracture and its management. *Dent Update* 2012; **39**: 530-532, 535 [PMID: 23167202 DOI: 10.12968/denu.2012.39.8.530]
13 **Andreasen FM**, Andreasen JO. Root fractures. Textbook and Color atlas of traumatic injuries to the teeth. 3rd ed.

Copenhagen: Munksgaard, 1994: 279-313
14 **Trope M**, Chivian N, Sigurdsson A, Vann W. Traumatic injuries. In: Cohen S, Burns RC. Pathways of the pulp. 8th ed. St. Louis: Mosby, 2002: 603-649
15 **Marinčák D**, Doležel V, Přibyl M, Voborná I, Marek I, Šedý J, Žižka R. Conservative Treatment of Complicated Crown Fracture and Crown-Root Fracture of Young Permanent Incisor-A Case Report with 24-Month Follow-Up. *Children (Basel)* 2021; **8** [PMID: 34572157 DOI: 10.3390/children8090725]
16 **Zero DT**, Zandona AF, Vail MM, Spolnik KJ. Dental caries and pulpal disease. *Dent Clin North Am* 2011; **55**: 29-46 [PMID: 21094717 DOI: 10.1016/j.cden.2010.08.010]
17 **Andreasen JO**, Hjorting-Hansen E. Intraalveolar root fractures: radiographic and histologic study of 50 cases. *J Oral Surg* 1967; **25**: 414-426 [PMID: 5231441 DOI: 10.1177/00220345670460066601]
18 **Abbott PV**. Diagnosis and Management of Transverse Root Fractures. *J Endod* 2019; **45**: S13-S27 [PMID: 31623913 DOI: 10.1016/j.joen.2019.05.009]
19 **Lindhe J**, Lang NP, Karring T. Clinical periodontology and implant dentistry. 5th ed. Oxford: Blackwell Publishing, 2008
20 **Zhang HW**, Li Y, Zhang Z. The clinical study of vacuum-formed jaw-pillow used for teeth fixing in children with traumatic anterior teeth. *Yati Yasui Yazhoubing Xue Zazhi* 2014; **34**: 488-490

World Journal of Clinical Cases

Submit a Manuscript: https://www.f6publishing.com

World J Clin Cases 2022 June 26; 10(18): 6307-6313

DOI: 10.12998/wjcc.v10.i18.6307

ISSN 2307-8960 (online)

CASE REPORT

Thyroid follicular renal cell carcinoma excluding thyroid metastases: A case report

Si-Cheng Wu, Xi-Ya Li, Bang-Jie Liao, Kun Xie, Wei-Min Chen

Specialty type: Medicine, research and experimental

Provenance and peer review: Unsolicited article; Externally peer reviewed.

Peer-review model: Single blind

Peer-review report's scientific quality classification

Grade A (Excellent): 0
Grade B (Very good): B, B
Grade C (Good): C
Grade D (Fair): 0
Grade E (Poor): 0

P-Reviewer: Bari SU, India; Moez R, Tunisia

Received: December 31, 2021
Peer-review started: December 31, 2021
First decision: February 21, 2022
Revised: March 16, 2022
Accepted: April 21, 2022
Article in press: April 21, 2022
Published online: June 26, 2022

Si-Cheng Wu, Xi-Ya Li, Bang-Jie Liao, Kun Xie, Wei-Min Chen, Department of Urology, The First Affiliated Hospital of Nanchang University, Nanchang 330036, Jiangxi Province, China

Corresponding author: Wei-Min Chen, Doctor, Chief Doctor, Surgeon, Surgical Oncologist, Department of Urology, The First Affiliated Hospital of Nanchang University, No. 17 Yongwai Zhengjie, Nanchang 330036, Jiangxi Province, China. cwmncdxyfy@126.com

Abstract

BACKGROUND

Thyroid follicular renal cell carcinoma is a special type of renal cell carcinoma newly recognized in recent years. It has attracted attention because of its unique histology, immunophenotype, and clinical characteristics. It has a very low incidence, and the number of case reports available for review is limited. Moreover, a thyroid mass with type of tumour is rare.

CASE SUMMARY

We report a case of a renal mass with a bilateral thyroid mass that was accidentally discovered in a 60-year-old man during physical examination. B-mode ultrasound showed a hypoechoic mass in the middle and lower parenchyma of the right kidney, and computed tomography showed an iso-density shadow tumour in the right kidney. Contrast agents had a significant continuous enhancement effect on the tumour, and the enhancement was not uniform. After partial nephrectomy, pathological analysis was performed to rule out the possibility that the renal tumour was caused by thyroid tumour metastasis. Needle biopsy of the thyroid tumour confirmed that the renal cell carcinoma was not related to the thyroid tumour. The patient was alive at the last postoperative follow-up.

CONCLUSION

This is the third published case in which thyroid tumour biopsy was performed to confirm that thyroid follicular renal cell carcinoma is not thyroid related.

Key Words: Renal cell carcinoma; Thyroid follicular renal cell carcinoma; Kidney; Thyroid tumour metastasis; Case report

©The Author(s) 2022. Published by Baishideng Publishing Group Inc. All rights reserved.

Core Tip: This is only the third published report combined with a thyroid tumor biopsy to confirm that thyroid follicular renal cell carcinoma is not thyroid related. In addition to the typical pathologic features of this tumor, our patient had radiographic features that were different from those previously reported.

Citation: Wu SC, Li XY, Liao BJ, Xie K, Chen WM. Thyroid follicular renal cell carcinoma excluding thyroid metastases: A case report. *World J Clin Cases* 2022; 10(18): 6307-6313
URL: https://www.wjgnet.com/2307-8960/full/v10/i18/6307.htm
DOI: https://dx.doi.org/10.12998/wjcc.v10.i18.6307

INTRODUCTION

Renal cell carcinoma (RCC) is a malignant tumour that originates from the renal parenchymal urothelial system and accounts for approximately 80%-85% of all malignant renal tumours. It is one of the most common tumours in the urinary system, second only to prostate cancer and bladder cancer[1]. Thyroid follicular RCC (TFRCC) is a rare new subtype of primary RCC that is not a true carcinoma originating from the thyroid gland. Although it is histologically similar to thyroid follicular carcinoma, TFRCC lacks typical thyroid markers. The rarity of these tumours limits our understanding of them, leading to misdiagnosis and inappropriate treatment. Here, we report the case of a 60-year-old man who presented with lower back and abdominal pain. Imaging examination revealed lesions in the right kidney and bilateral thyroid gland. Based on postoperative pathological examination findings, renal metastasis of the thyroid carcinoma was excluded.

CASE PRESENTATION

Chief complaints

A 60-year-old man presented with a > 1-mo history of right lower back and abdominal pain.

History of present illness

The 60-year-old man presented with a > 1-mo history of right lower back and abdominal pain. Computed tomography (CT) revealed small solid nodules under the capsule in the middle and lower part of the right kidney, leading to the suspicion of small RCC.

History of past illness

The patient had a 10-year history of diabetes. He did not take his medicine regularly and had poor blood glucose control.

Personal and family history

The patient had no relevant personal or family history.

Physical examination

The patient's vital signs were normal.

Laboratory examinations

Laboratory examinations on admission revealed a carbohydrate antigen 19-9 level of 99.98 μmol/mL and creatinine level of 73.5 μmol/L (postoperative creatinine level: 79.1 μmol/L). The glomerular filtration rate in the left and right kidneys was 34.88 and 34.89 mL/min, respectively.

Imaging examinations

Ultrasound showed a round hypoechoic mass measuring approximately 0.9 × 0.8 cm in the middle and lower parenchyma of the right kidney; however, there was no obvious blood flow signal in the mass. Computed tomography angiography revealed a small nodular iso-density shadow (approximately 1 cm in diameter) in the middle parenchyma of the right kidney that protruded to the edge of the kidney. An enhanced scan showed continuous and obvious enhancement during the arterial phase. However, the enhancement was not uniform, and there were no abnormal tumour-supplying blood vessels (Figure 1). Ultrasound of the thyroid gland performed in our hospital on 5 January 2021 showed bilateral thyroid nodules (TI-RADS3 class).



DOI: 10.12998/wjcc.v10.i18.6307 **Copyright** ©The Author(s) 2022.

Figure 1 A small nodular iso-density shadow was observed in the middle parenchyma of the right kidney, with a diameter of about 1 cm, protruding to the kidney edge. Plain scan (A), Enhanced scan (B), Delayed contrast-enhanced scan (C), computed tomography three-dimensional imaging (D and E).

FINAL DIAGNOSIS

Postoperative pathology showed: Part of the renal tissue, 2.1 cm × 1.5 cm × 1.5 cm in size, had been cut in half in the clinic. Analysis of the tissue section revealed a nodular body measuring 1.2 cm × 1.0 cm × 0.6 cm; it was greyish-yellow or greyish white, slightly tough, and had slightly unclear boundaries. Moreover, it contained free adipose tissue (5.5 cm × 3.3 cm × 1.2 cm) and was not in contact with lymph nodes. Microscopy revealed glandular, cystic follicular, or papillary tumour cells of uniform size. The cytoplasm was medium stained, lightly stained, or empty bright, and the nucleus was round or slightly irregular with small nucleoli and red-stained lumen. Immunohistochemistry showed CK (3+); EMA) (+); Vimentin (+); PAX-8 (+); CK7 (+); Ki67 (2%+); P504S (+); E-cd (+); CD117 (-); CD10 (+); RCC (-); Calponin (-); TTF-1 (-); TG (-); TFE3 (weak+); S-100 (-); WT-1 (-); CA9 (-). Therefore, TFRCC of the right kidney was considered (Figure 2).

TREATMENT

Laparoscopic partial nephrectomy was performed in December 2020. The patient recovered well after surgery and was discharged after 3 d. Fine-needle biopsy of the thyroid nodules was performed in 2021, and revealed no obvious pathological abnormalities .

OUTCOME AND FOLLOW-UP

The patient underwent re-examination on 30 March 2021, and the CT scan showed that the right kidney had changed after partial nephrectomy, but there were no other abnormalities. At the last follow-up, the patient was alive and healthy.

DISCUSSION

Previously, TFRCC was known as thyroid-like follicular carcinoma of the kidney or thyroid follicular carcinoma-like renal tumour, a special type of RCC with thyroid follicular carcinoma-like histomorphology. This rare, new type of RCC was described in detail at the 2012 International Society of Urological Pathology. In 2016, the World Health Organization Classification of Urological Oncology reclassified renal tumour subtypes, and TFRCC was listed as a 'tentative renal cell carcinoma' due to its extremely low incidence rate and small number of cases available for review[2]. This type of tumour was first described by Angell[3] in 1996. Immunohistochemical staining of the reported cases showed positive expression of TG and TTF-1 in tumour cells, although no space-occupying lesions were detected by thyroid examination. However, considering that papillary thyroid carcinoma can develop lymph node or distant metastasis with very small primary foci, we believe that the first case of TFRCC was reported in an abstract published by Amin[4] in 2004 and in a case report published by Jung[5] in 2006. Thus far, approximately 41 cases have been reported[6].

Due to its rarity, the pathogenic factors of TFRCC are unclear. Recent studies have found that a previous history of malignant tumour and chemotherapy, especially the use of a platinum-based chemotherapy regimen, significantly increased the risk of TFRCC, but the relationship between the mutual development needs to be determined in future studies[7]. Moreover, relevant genetic data on TFRCC are limited. In only a few groups of genetic tests, there were obvious genetic changes in TFRCC, but the chromosomal changes were significantly different to each other, and the genetic changes were

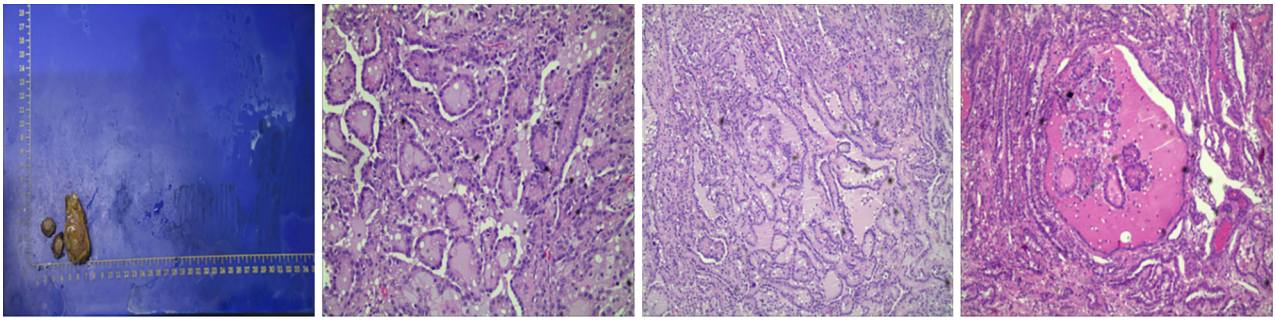

DOI: 10.12998/wjcc.v10.i18.6307 **Copyright** ©The Author(s) 2022.

Figure 2 Part of the renal tissue, 2.1 cm × 1.5 cm × 1.5 cm in size, with a nodular body and part of the free adipose tissue, without contact with obvious lymph nodes. Microscopically, the tumor cells were glandular, cystic follicular, or papillary, and the cell size was uniform. The cytoplasm was medium, light stained or empty bright, and the nucleus was round or slightly irregular, with small nucleoli and red stain in the lumen. Original magnification: 100 ×; scale bar: 100 μm.

not consistent with those of other known types of RCC[8]. More cases and studies are needed to find causative factors and genes.

The existing case data suggest that the disease mainly occurs in women. Currently, the youngest reported case pertains to a 10-year-old child[9] in whom the right side was more affected than the left side. The clinical symptoms are not obvious and most lack specificity; they are found accidently during physical examination. In most symptomatic patients, symptoms manifest as gross haematuria and abdominal pain, while some patients show hypertension[10,11,12], repeated urinary stimulation symptoms[12,13], weight loss[13], and other symptoms(Table 1). For the preoperative diagnosis of common RCC, CT is the first choice. However, for TFRCC, preoperative ultrasound seems to be more accurate than CT in visualizing the mass. On plain CT, cystic-solid changes are usually seen with high-density shadow, clear boundary, haemorrhage, and necrosis. Most of them show weak enhancement on enhanced scan, which is different to the obvious enhancement of other types. Moreover, eggshell-like calcification has been observed around the tumour, while the calcification in other types of RCC generally appears in the centre of the tumour. However, in our case, plain CT showed a moderate density shadow, while an enhanced scan showed continuous obvious uneven enhancement, inhomogeneous enhancement, and no obvious calcification, which was rarely seen in previous case reports. Magnetic resonance imaging generally shows a high signal on T1-weighted imaging and a low signal on T2-weighted imaging compared to the signal in the renal parenchyma. These characteristic imaging findings may have a certain suggestive value for preoperative consideration of TFRCC; however, pathological and immunological examination need to be performed for diagnosis.

Macroscopically, most of the tumours are clear with a false capsule and both cystic and solid, with occasional bleeding, necrosis, or cystic degeneration. The section has a medium texture and is greyish white to greyish yellow, which differs from the multi-coloured appearance of clear cell RCC. Microscopically, the most prominent feature of the tumour is the formation of the thyroid follicular carcinoma-like structure, and the follicular cavity is filled with a red dye colloid-like substance, which is similar to thyroid colloid-like substance. The cytoplasm of the tumour cells is bichromatic or eosinophilic and empty and bright, the nucleus is round and oval, and the heteromorphism is not obvious. Occasionally, the nuclear groove can be seen, the mitotic image is rare, and the Fuhrman grade is mainly grade 2. Most cases show positive expression of CK, CK7, vimentin, and EMA; negative expression of the thyroid markers TTF-1 and TG; and low Ki-67 proliferation index[14]. In our case, the tumour was solid, its boundary was unclear, the other histological characteristics were similar to those previously reported, and the Ki-67 proliferation index was 2%. The degree of malignancy of the tumour was low, and the postoperative recovery was good.

The pathological diagnosis should be differentiated from thyroid carcinoma with renal metastasis and ovarian monodermal teratoma with renal metastasis, and the history can not completely exclude the primary TFRCC. The immunohistochemical markers TTF-1 and TG have important value in differential diagnosis. However, in poorly differentiated or sarcomatoid-differentiated thyroid carcinoma, TG and TTF-1 are absent, which can be distinguished according to whether there is a primary tumour. In addition, attention should be paid to the differentiation with renal thyroidisation[11], other nephrogenic tumours[12], and atrophic kidney[15]. It is not difficult to distinguish them in combination with clinical and histological characteristics. Our patient had bilateral thyroid mass; therefore, we needed to rule out the possibility that the kidney lesion was metastasized by thyroid carcinoma. Thyroid cancer often metastasises to the bone, lung, and liver and rarely to the kidney. There are <30 reported cases of renal metastasis of thyroid cancer origin, and the expression of TTF-1 and TG is both positive and strongly positive[16,17]. The specimens from our patient were repeatedly examined by the Pathology Department in our hospital, and both TTF-1 and TG continued to be absent. Therefore, the possibility of thyroid origin was ruled out, and TFRCC was presumed to be the primary tumour in the kidney. The

Table 1 Comparison of the features of 41 cases with metastatic and non-metastatic thyroid-like follicular carcinoma of the kidney reported from 2006 to 2022

Features	Non-metastatic (*n* = 34)	Metastatic (*n* = 7)
Age (yr), mean ± SD (range)	41.7 ± 17 (10-83)	42.6 ± 14 (27-68)
Female sex	18/33 (55%; 1 unknown)	4/7 (57%)
Clinical presentation		
Incidental	24 (71%)	4 (57%)
Flank pain/haematuria	10 (29%)	3 (43%)
History of malignancy (other sites)	8 (24%)	1 (14%)
Tumour characteristics		
Size (cm), mean ± SD (range)	4.2 ± 2.3 (1.1-11.8)	5.3 ± 2.3 (3.5-10)
Right/left sided	17/16 (1 unknown)	5 2
Necrosis	9 (24%)	3 (43%)
Ki-67 proliferation index	1% to 30% (*n* = 6)	6% (*n* = 1)
pT stage		
1a	20	3
1b	10	3
2a	1	0
2b	2	0
Immunohistochemical features		
CK7	24/25 (96%)	5/6 (83%)
CK20	3/14 (21%)	2/4 (50%)
CD10	4/23 (17%)	1/5 (20%)
Vimentin	20/25 (80%)	3/4 (75%)
PAX8	10/11 (91%)	3/4 (75%)
Site of metastasis	-	Bone (2), lung (3), lymph node (2)
Follow-up period (mo)	22.1 ± 19.8	30.6 ± 28.8
Disease/death at follow-up	0	2 (28%)

diagnosis was then confirmed by thyroid tumour biopsy, similar to the method used in the case reported by Cai[16] and Tretiakova[13].

TFRCC has a certain degree of invasiveness, up to T3, and can have retroperitoneal lymph node metastasis and distant metastasis such as skull and meninges[6]. These tumours may metastasise through the blood-derived pathway, but the degree of malignancy is generally low. Surgical resection is the main treatment, which is supplemented by postoperative follow-up. Surgical methods include radical nephrectomy, partial nephrectomy, and resection of the metastatic lesion, which can be performed even if distant metastasis occurs. Except for a few patients with dedifferentiation of sarcomatoid areas[18] or with highly malignant cells[8], there is currently no clear clinicopathological feature that can predict the occurrence of metastasis and its poor outcome. There are limited reports on adjuvant therapy after surgery. At present, surgery is selected according to the general guidelines for RCC, and its unique treatment scheme needs to be actively explored in clinical practice to avoid unnecessary over-treatment and ensure the quality of life of patients. Following effective treatment, patients do not easily relapse, have a good prognosis, and can achieve long-term survival.

CONCLUSION

In summary, TFRCC is a rare subtype of low-grade malignant renal cell carcinoma with certain invasiveness, which usually occurs in young and middle-aged women. Its clinical and imaging manifestations have certain suggestive value, with unique morphological and immunohistochemical

characteristics. The diagnosis depends on pathology and immunohistochemistry, and surgical resection is the preferred treatment. The overall prognosis is good, but there is a certain malignant potential, which needs long-term and close follow-up. If the disease progresses, the treatment plan for metastatic RCC should be considered. Due to the low incidence of TFRCC, there are few studies on this tumour; therefore, further studies are needed to enhance understanding and provide valuable information for diagnosis and treatment. No recurrence or metastasis was found in our case; however, further observation is needed in terms of survival time.

FOOTNOTES

Author contributions: Wu S and Xie K contributed equally to this work; Wu S, Li X, Liao B, Xie K and Chen W designed the research study; Wu S, Li X, Xie K and Liao B performed the research; Wu S and Xie K contributed new reagents and analytic tools; Li X, Xie K and Liao B analyzed the data and wrote the manuscript; all authors have read and approved the final manuscript.

Supported by Natural Science Foundation of Jiangxi Province, No. 2010GZY0806.

Informed consent statement: Consent was obtained from the patient and his family for publication of this report.

Conflict-of-interest statement: The authors declare that there are no conflicts of interest.

CARE Checklist (2016) statement: The authors have read the CARE Checklist (2016), and the manuscript was prepared and revised according to the CARE Checklist (2016).

Open-Access: This article is an open-access article that was selected by an in-house editor and fully peer-reviewed by external reviewers. It is distributed in accordance with the Creative Commons Attribution NonCommercial (CC BY-NC 4.0) license, which permits others to distribute, remix, adapt, build upon this work non-commercially, and license their derivative works on different terms, provided the original work is properly cited and the use is non-commercial. See: https://creativecommons.org/Licenses/by-nc/4.0/

Country/Territory of origin: China

ORCID number: Si-Cheng Wu 0000-0003-3429-1849; Xi-Ya Li 0000-0002-9017-1203; Bang-Jie Liao 0000-0002-8892-0180; Kun Xie 0000-0003-0628-2128; Wei-Min Chen 0000-0001-5634-4417.

S-Editor: Wang LL
L-Editor: Webster JR
P-Editor: Wang LL

REFERENCES

1 **Siegel RL**, Miller KD, Fuchs HE, Jemal A. Cancer Statistics, 2021. *CA Cancer J Clin* 2021; **71**: 7-33 [DOI: 10.3322/caac.21654]
2 **Moch H**, Cubilla AL, Humphrey PA, Reuter VE, Ulbright TM. The 2016 WHO Classification of Tumours of the Urinary System and Male Genital Organs-Part A: Renal, Penile, and Testicular Tumours. *Eur Urol* 2016; **70**: 93-105 [PMID: 26935559 DOI: 10.1016/j.eururo.2016.02.029]
3 **Angell SK**, Pruthi R, Freiha FS. Primary thyroidlike carcinoma of the kidney. *Urology* 1996; **48**: 632-635 [PMID: 8886074 DOI: 10.1016/S0090-4295]
4 **Amin MB**, Gupta R, Ondrej H, McKenney JK, Michal M, Young AN, Paner GP, Junker K, Epstein JI. Primary thyroid-like follicular carcinoma of the kidney: report of 6 cases of a histologically distinctive adult renal epithelial neoplasm. *Am J Surg Pathol* 2009; **33**: 393-400 [PMID: 19047894 DOI: 10.1097/PAS.0b013e31818cb8f5]
5 **Jung SJ**, Chung JI, Park SH, Ayala AG, Ro JY. Thyroid follicular carcinoma-like tumor of kidney: a case report with morphologic, immunohistochemical, and genetic analysis. *Am J Surg Pathol* 2006; **30**: 411-415 [PMID: 16538064 DOI: 10.1097/01.pas.0000194745.10670.dd]
6 **Agrawal V**, Neyaz Z, Kapoor R. Thyroid-Like Follicular Carcinoma of the Kidney With Oncocytic Cells: A Case Report and Review of Metastatic and Non-metastatic Tumors. *Int J Surg Pathol* 2020; **28**: 913-917 [PMID: 32484016 DOI: 10.1177/1066896920930283]
7 **Dong L**, Huang J, Huang L, Shi O, Liu Q, Chen H. Thyroid-Like Follicular Carcinoma of the Kidney in a Patient with Skull and Meningeal Metastasis: A Unique Case Report and Review of the Literature. *Medicine (Baltimore)* 2016; **95**: e3314 [DOI: 10.1097/md.0000000000003314]
8 **Ko JJ**, Grewal JK, Ng T, Lavoie JM, Thibodeau ML, Shen Y, Mungall AJ, Taylor G, Schrader KA, Jones SJM, Kollmannsberger C, Laskin J, Marra MA. Whole-genome and transcriptome profiling of a metastatic thyroid-like follicular renal cell carcinoma. *Cold Spring Harb Mol Case Stud* 2018; **4** [PMID: 30446580 DOI: 10.1101/mcs.a003137]
9 **de Jesus LE**, Fulgêncio C, Leve T, Dekermacher S. Thyroid-like follicular carcinoma of the kidney presenting on a 10 year-old prepubertal girl. *Int Braz J Urol* 2019; **45**: 834-842 [PMID: 31063281 DOI:

10.1590/S1677-5538.IBJU.2018.0471]

10 **Wang H**, Yu J, Xu Z, Li G. Clinicopathological study on thyroid follicular carcinoma-like renal tumor related to serious hypertension: Case report and review of the literature. *Medicine (Baltimore)* 2017; **96**: e6419 [DOI: 10.1097/md.0000000000006419]

11 **Wu Y**, Huang F, Zhou X, Yu S, Tang Q, Li S, Wang J, Chen L. Hypoxic Preconditioning Enhances Dental Pulp Stem Cell Therapy for Infection-Caused Bone Destruction. *Tissue Eng Part A* 2016; **22**: 1191-1203 [PMID: 31329527 DOI: 10.1089/ten.tea.2016.0086.correx]

12 **Zhang Y**, Yang J, Zhang M, Meng Z, Song W, Yang L, Li L, Wang D, Shi T. Thyroid follicular carcinoma-like renal tumor: A case report and literature review. *Medicine (Baltimore)* 2018; **97**: e10815 [PMID: 29794767 DOI: 10.1097/MD.0000000000010815]

13 **Tretiakova MS**, Kehr EL, Gore JL, Tykodi SS. Thyroid-Like Follicular Renal Cell Carcinoma Arising Within Benign Mixed Epithelial and Stromal Tumor. *Int J Surg Pathol* 2020; **28**: 80-86 [PMID: 31342803 DOI: 10.1177/1066896919863478]

14 **Eble JN**, Delahunt B. Emerging entities in renal cell neoplasia: thyroid-like follicular renal cell carcinoma and multifocal oncocytoma-like tumours associated with oncocytosis. *Pathology* 2018; **50**: 24-36 [PMID: 29132724 DOI: 10.1016/j.pathol.2017.09.005]

15 **Herlitz L**, Hes O, Michal M, Tretiakova M, Reyes-Múgica M, Nguyen JK, Troxell ML, Przybycin CG, Magi-Galluzzi C, McKenney JK. "Atrophic Kidney"-like Lesion: Clinicopathologic Series of 8 Cases Supporting a Benign Entity Distinct From Thyroid-like Follicular Carcinoma. *Am J Surg Pathol* 2018; **42**: 1585-1595 [PMID: 30285996 DOI: 10.1097/PAS.0000000000001157]

16 **Cai DM**, Wang HY, Jiang Y, Parajuly SS, Tian YE, Ma BY, et al. Primary follicular thyroid carcinoma metastasis to the kidney and widespread dissemination: A case report. *Oncol Lett* 2016; **11**: 3293-3297 [DOI: 10.3892/ol.2016.4417]

17 **Cavalcante A**, Kuwano AY, Costa-Matos A, Spanholi EF, Souza T, Mascarenhas FM. Thyroid-like follicular carcinoma of the kidney - Case report. *Urol Case Rep* 2017; **15**: 36-38 [PMID: 28948155 DOI: 10.1016/j.eucr.2017.08.005]

18 **Jenkins TM**, Rosenbaum J, Zhang PJ, Schwartz LE, Nayak A, Cooper K, Tickoo SK, Lal P. Thyroid-Like Follicular Carcinoma of the Kidney With Extensive Sarcomatoid Differentiation: A Case Report and Review of the Literature. *Int J Surg Pathol* 2019; **27**: 678-683 [PMID: 31032708 DOI: 10.1177/1066896919845490]

World Journal of Clinical Cases

Submit a Manuscript: https://www.f6publishing.com

World J Clin Cases 2022 June 26; 10(18): 6314-6318

DOI: 10.12998/wjcc.v10.i18.6314

ISSN 2307-8960 (online)

CASE REPORT

Appendiceal bleeding: A case report

Sheng-Yue Zhou, Mao-Dong Guo, Xiao-Hua Ye

Specialty type: Medicine, research and experimental

Provenance and peer review: Unsolicited article; Externally peer reviewed.

Peer-review model: Single blind

Peer-review report's scientific quality classification

Grade A (Excellent): 0
Grade B (Very good): B, B
Grade C (Good): 0
Grade D (Fair): 0
Grade E (Poor): 0

P-Reviewer: Bhusal U, Nepal; Kumar S, India

Received: December 31, 2021
Peer-review started: December 31, 2021
First decision: January 23, 2022
Revised: January 27, 2021
Accepted: April 24, 2022
Article in press: April 24, 2022
Published online: June 26, 2022

Sheng-Yue Zhou, Mao-Dong Guo, Xiao-Hua Ye, Department of Gastroenterology, Affiliated Jinhua Hospital, Zhejiang University School of Medicine, Jinhua 321000, Zhejiang Province, China

Corresponding author: Xiao-Hua Ye, MD, Deputy Director, Department of Gastroenterology, Affiliated Jinhua Hospital, Zhejiang University School of Medicine, No. 365 Renmin East Road, Jinhua 321000, Zhejiang Province, China. yexiaohuare@qq.com

Abstract

BACKGROUND

Acute lower gastrointestinal bleeding is common in clinical practice, and the colon is responsible for the majority of cases. However, appendiceal bleeding is an extremely rare cause. Appendiceal bleeding due to vascular diseases, such as angiodysplasia and Dieulafoy's lesion, may result in massive lower gastrointestinal bleeding. Appendectomy is a reliable and effective option for treatment.

CASE SUMMARY

A 32-year-old male presented to our hospital with hematochezia that had lasted for 6 h, with approximately 600-800 mL bloody stools and loss of consciousness for a few seconds. Persistent bleeding from the orifice of the appendix was observed by colonoscopy. Following the new diagnosis of appendiceal bleeding, the patient was treated by an emergency laparoscopic appendectomy. Finally, the patient was pathologically diagnosed with appendiceal Dieulafoy's lesion. The patient was uneventfully discharged, and follow-up 2 wk later showed no evidence of rebleeding.

CONCLUSION

Although appendiceal bleeding is a rare cause of acute lower gastrointestinal bleeding, clinicians should consider it during differential diagnosis.

Key Words: Appendix; Gastrointestinal hematochezia; Lower gastrointestinal tract; Vascular malformations; Case report

©The Author(s) 2022. Published by Baishideng Publishing Group Inc. All rights reserved.

Core Tip: Appendiceal bleeding is a rare cause of acute lower gastrointestinal bleeding. Appendiceal bleeding due to vascular diseases, such as angiodysplasia and Dieulafoy's lesion, may result in massive lower gastrointestinal bleeding. Appendectomy is a reliable and effective option for treatment.We report a case of lower gastrointestinal bleeding due to appendiceal Dieulafoy's lesion. The patient recovered well after an emergency laparoscopic appendectomy. Clinicians should consider appendiceal bleeding during differential diagnosis.

Citation: Zhou SY, Guo MD, Ye XH. Appendiceal bleeding: A case report. *World J Clin Cases* 2022; 10(18): 6314-6318
URL: https://www.wjgnet.com/2307-8960/full/v10/i18/6314.htm
DOI: https://dx.doi.org/10.12998/wjcc.v10.i18.6314

INTRODUCTION

The common causes of lower gastrointestinal bleeding are mostly known to be diseases of the colon, rectum, and terminal ileum[1]. However, appendiceal bleeding as the origin is extremely rare. Diverticulum, angiodysplasia, inflammation, and neoplasm are the usual etiologies for appendiceal bleeding[2,3]. Vascular diseases, such as angiodysplasia and Dieulafoy's lesion, are one of the most common causes of massive bleeding and sometimes can be life-threatening[1,4]. We report herein a case of lower gastrointestinal bleeding due to appendiceal Dieulafoy's lesion, with a literature review.

CASE PRESENTATION

Chief complaints

A 32-year-old male presented to the emergency department of our hospital with hematochezia that had lasted for 6 h.

History of present illness

The patient reported having experienced approximately 600-800 mL bloody stools before presentation to the hospital. The patient also reported having experienced loss of consciousness for a few seconds. No other gastrointestinal symptoms, such as nausea, vomiting, or abdominal pain, were experienced during the process. The patient denied past history of hematochezia.

History of past illness

The patient had been previously diagnosed with hemorrhoids and hypertension, but was taking no medications.

Personal and family history

The personal and family history-taking revealed no information relevant to the current case.

Physical examination

The patient's temperature was 36.5 °C, heart rate was 95 beats per minute, respiratory rate was 20 breaths per minute, blood pressure (measured with electronic cuff) was 147/105 mmHg, and oxygen saturation in room air was 99%. The physical examination showed an anemic appearance, without any other pathological signs.

Laboratory examinations

The laboratory tests showed that hemoglobin was 102 g/L (normal range: 130-175 g/L), revealing a mild anemia. Other routine relevant examinations, such as platelet counts and for markers of coagulation function, and liver and renal function, yielded normal findings. Unfortunately, the patient passed bloody stools again 1 d after conservative treatment in our department, with his hemoglobin level dropping to 86 g/L.

Imaging examinations

An emergency colonoscopy was performed, and extended up to the terminal ileum. During the procedure, blood clots in the cecum were first washed out and we were then able to observe a large quantity of fresh blood oozing out of the appendiceal orifice (Figure 1A). In addition, contrast-enhanced abdominal computed tomography (CT) scan showed a high-density area in the appendix without any

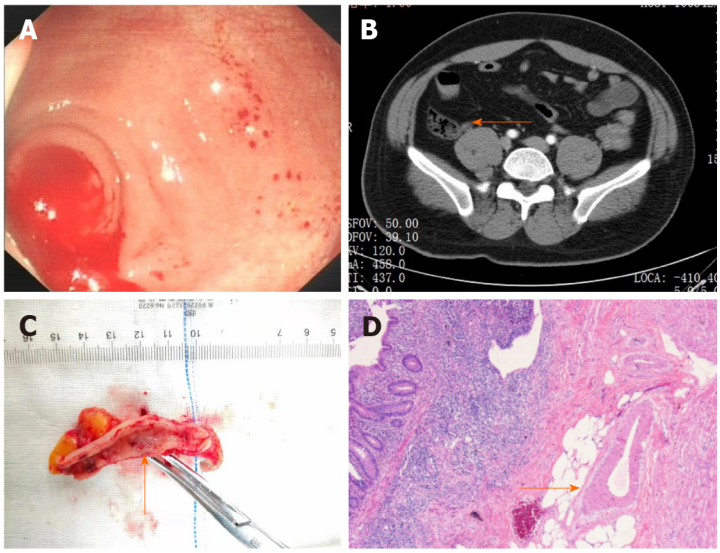

DOI: 10.12998/wjcc.v10.i18.6314 **Copyright** ©The Author(s) 2022.

Figure 1 Appendiceal bleeding caused by Dieulafoy's lesion. A: Colonoscopy showed active bleeding from the appendiceal orifice after blood clots were flushed out of the ileocecal junction; B: Enhanced abdominal computed tomography showed a high-density area in the appendix, revealing the possibility of appendiceal bleeding (arrow); C: Macroscopic pathological observation showed a vessel stump on the mucosa of the appendix (arrow); D: Microscopic pathological examination showed a caliber-persistent artery in the submucosa of the appendix (arrow).

signs of acute appendicitis, tumor, or diverticulum (Figure 1B).

FINAL DIAGNOSIS

Bleeding of the appendix.

TREATMENT

We suspected that the source of bleeding was the appendix, which prompted an emergency laparoscopic appendectomy. During that surgery, no signs of acute appendicitis or diverticulitis were observed; however, a large amount of blood clots was observed through the longitudinal incision of the appendix. A vessel stump was also found on the mucosa of the appendix (Figure 1C). Pathologically, a caliber-persistent artery was detected near the vessel stump of the mucosa surface, corresponding to Dieulafoy's lesion within the appendix (Figure 1D).

OUTCOME AND FOLLOW-UP

The patient had no recurrent hematochezia or melena, and was discharged from the hospital 6 d after the surgery. Follow-up 2 wk later showed no evidence of rebleeding.

DISCUSSION

Acute lower gastrointestinal bleeding is commonly encountered in clinical practice, with colon being responsible for the majority of cases[1]. Appendiceal bleeding, on the other hand, is an extremely rare cause, and as such may be missed or misdiagnosed.Although lower gastrointestinal bleeding is generally less severe than upper gastrointestinal bleeding - with spontaneous cessation of the bleeding occurring in most cases, appendiceal bleeding attributed to vascular diseases, such as angiodysplasia and Dieulafoy's lesion, may result in massive lower gastrointestinal bleeding and sometimes can be life-threatening[1,4]. As a clinician, having an awareness of appendiceal bleeding is significant. A literature search of relevant articles on the PubMed/MEDLINE database, from January 1977 to November 2021, was conducted, using the key words of "appendix bleeding" or "appendix hemorrhage". Six articles regarding appendiceal bleeding due to vascular diseases were identified (Table 1)[5-10].

Table 1 Cases of appendiceal bleeding caused by vascular diseases

Case	Age/sex	Chief complaint	Hemoglobin, g/L	Techniques	Treatment	Pathology	Ref.
1	21/female	Massive hematochezia	106	Endoscopy	Appendectomy	Dieulafoy's lesion	[5]
2	72/male	Hematochezia	126	Endoscopy	Appendectomy	Angiodysplasia	[6]
3	68/male	Massive hematochezia	82	Endoscopy	Appendectomy	Dieulafoy's lesion	[7]
4	41/male	Melena	Not reported	Endoscopy	Appendectomy	Atypical florid vascular proliferation	[8]
5	76/female	Massive hematochezia	52	Angiography	Vessel embolization and appendectomy	Angiodysplasia	[9]
6	42/male	Melena	77	Endoscopy	Appendectomy	Vascular malformation	[10]
Our case	32/male	Massive hematochezia	86	Endoscopy	Appendectomy	Dieulafoy's lesion	

The average age of the included cases was 50.3 years (range: 21-76 years). In terms of sex, 5 males and 2 females are reported on herein. Similar to previous reports, the most likely cause of hospitalization was massive hematochezia, rather than melena[3]. Pathological analyses showed the main vascular factors of appendiceal bleeding to be angiodysplasia and Dieulafoy's lesion. Dieulafoy's lesion is caused by an abnormal artery that fails to diminish to the minute size of the mucosal capillary microvasculature [11]. The most common location of Dieulafoy's lesion is the stomach. Others have reported Dieulafoy's lesion in the esophagus, duodenum, small intestine, colon, and rectum[12-15]; however, an appendiceal Dieulafoy's lesion is extremely rare. Among the included publications, there were only 2 cases of appendiceal bleeding due to Dieulafoy's lesion published in English language[5,7], with ours being the third case.

Several modalities, such as colonoscopy, contrast-enhanced abdominal CT, and angiography, can be applied in diagnosing appendiceal bleeding[2,3,9]. In our case, colonoscopy directly revealed the active bleeding from the appendiceal orifice. For such cases, emergency colonoscopy for acute lower gastrointestinal bleeding should be utilized, at least to the terminal ileum. In addition, the orifice of the appendix should be carefully observed. Contrast-enhanced abdominal CT is useful in evaluating diverticulum, neoplasm, or acute inflammation. Although mesenteric artery angiography requires bleeding of more than 0.5 mL/min, vessel embolization is feasible in controlling acute bleeding[9].

A reliable and effective choice of treatment for appendiceal bleeding is appendectomy[2]. Other attempts, including vessel embolization and endoscopic therapy (therapeutic barium enema and endoclips), have been reported as successful for controlling bleeding[9,16,17]; however, the risk of acute appendicitis and rebleeding after vessel embolization and endoscopic therapy are unmanageable, and the patient may still require an appendectomy[9,17]. Studies for the feasibility of vessel embolization and endoscopic therapy continue to be warranted.

CONCLUSION

We present a treatment experience of appendiceal bleeding caused by Dieulafoy's lesion. Although appendiceal bleeding is a rare cause of acute lower gastrointestinal bleeding, clinicians should consider it during differential diagnosis.

FOOTNOTES

Author contributions: Zhou SY designed and drafted the manuscript; Guo MD performed the colonoscopy; Ye XH revised the manuscript for important intellectual content; and all authors approved the final version of the manuscript.

Supported by the Natural Science Foundation of Zhejiang Province, No. LQ19H030003; and Key Project of Jinhua Science and Technology Bureau, No. 2018A32022.

Informed consent statement: Consent was obtained from the patient for publication of this report and any accompanying images.

Conflict-of-interest statement: The authors declare that they have no conflict of interest.

CARE Checklist (2016) statement: The authors have read the CARE Checklist (2016), and the manuscript was prepared and revised according to the CARE Checklist (2016).

Open-Access: This article is an open-access article that was selected by an in-house editor and fully peer-reviewed by external reviewers. It is distributed in accordance with the Creative Commons Attribution NonCommercial (CC BY-NC 4.0) license, which permits others to distribute, remix, adapt, build upon this work non-commercially, and license their derivative works on different terms, provided the original work is properly cited and the use is non-commercial. See: https://creativecommons.org/Licenses/by-nc/4.0/

Country/Territory of origin: China

ORCID number: Sheng-Yue Zhou 0000-0001-5808-2545; Mao-Dong Guo 0000-0003-4016-0773; Xiao-Hua Ye 0000-0002-8358-4093.

S-Editor: Wang JJ
L-Editor: A
P-Editor: Wang JJ

REFERENCES

1 **Marion Y**, Lebreton G, Le Pennec V, HournaE, Viennot S, Alves A. The management of lower gastrointestinal bleeding. *J Visc Surg* 2014; **151**: 191-201 [PMID: 24768401 DOI: 10.1016/j.jviscsurg.2014.03.008]
2 **Maeda Y**, Saito S, Ohuchi M, Tamaoki Y, Nasu J, Baba H. Appendiceal bleeding in an elderly male: a case report and a review of the literature. *Surg Case Rep* 2021; **7**: 147 [PMID: 34160703 DOI: 10.1186/s40792-021-01234-3]
3 **Chen W**, Qiu H, Yang X, Zhang J. Appendix Bleeding with Painless Bloody Diarrhea: A Case Report and Literature Review. *Open Med (Wars)* 2019; **14**: 735-739 [PMID: 31637304 DOI: 10.1515/med-2019-0084]
4 **Hoedema RE**, Luchtefeld MA. The management of lower gastrointestinal hemorrhage. *Dis Colon Rectum* 2005; **48**: 2010-2024 [PMID: 16175326 DOI: 10.1007/s10350-005-0138-1]
5 **Xue M**, Weng WH, Wang LJ. An Unusual Cause of Acute Massive Lower Gastrointestinal Bleeding. *Gastroenterology* 2020; **158**: 1550-1551 [PMID: 31560906 DOI: 10.1053/j.gastro.2019.08.057]
6 **Choi JM**, Lee SH, Ahn BK, Baek SU. Hematochezia due to Angiodysplasia of the Appendix. *Ann Coloproctol* 2016; **32**: 117-119 [PMID: 27437394 DOI: 10.3393/ac.2016.32.3.117]
7 **Reynolds JK**, Mejia VA. Appendiceal Dieulafoy lesion: an unusual cause of massive lower gastrointestinal bleeding. *Am Surg* 2015; **81**: E18-E19 [PMID: 25569049]
8 **Gu MJ**, Choi JH, Kim SH. Atypical florid vascular proliferation in appendix: a diagnostic dilemma. *DiagnPathol* 2013; **8**: 12 [PMID: 23347775 DOI: 10.1186/1746-1596-8-12]
9 **Kyokane T**, Akita Y, Katayama M, Kitagawa Y, Sato T, Shichino S, Nimura Y. Angiodysplasia of the appendix. *Am J Gastroenterol* 2001; **96**: 242-244 [PMID: 11197261 DOI: 10.1111/j.1572-0241.2001.03385.x]
10 **So JB**, Alexander DJ, Chong AP, Goh PM. Laparoscopic appendicectomy in the management of acute lower gastrointestinal bleeding. *GastrointestEndosc* 1995; **42**: 488-489 [PMID: 8566644 DOI: 10.1016/s0016-5107(95)70056-0]
11 **Dieulafoy G**. Exulceratio simplex. *Bull Acad Med* 1898; **39**: 49-84
12 **Inayat F**, Ullah W, Hussain Q, Hurairah A. Dieulafoy's lesion of the oesophagus: a case series and literature review. *BMJ Case Rep* 2017; **2017** [PMID: 28062437 DOI: 10.1136/bcr-2016-218100]
13 **Inayat F**, Amjad W, Hussain Q, Hurairah A. Dieulafoy's lesion of the duodenum: a comparative review of 37 cases. *BMJ Case Rep* 2018; **2018** [PMID: 29472423 DOI: 10.1136/bcr-2017-223246]
14 **Malik A**, Inayat F, Goraya MHN, Almas T, Ishtiaq R, Malik S, Tarar ZI. Jejunal Dieulafoy's Lesion: A Systematic Review of Evaluation, Diagnosis, and Management. *J Investig Med High Impact Case Rep* 2021; **9**: 2324709620987703 [PMID: 33472441 DOI: 10.1177/2324709620987703]
15 **Inayat F**, Ullah W, Hussain Q, Abdullah HMA. Dieulafoy's lesion of the colon and rectum: a case series and literature review. *BMJ Case Rep* 2017; **2017** [PMID: 29070617 DOI: 10.1136/bcr-2017-220431]
16 **Chung IH**, Kim KH. A case of successful colonoscopic treatment of acute appendiceal bleeding by endoclips. *J Korean Soc Coloproctol* 2011; **27**: 329-332 [PMID: 22259749 DOI: 10.3393/jksc.2011.27.6.329]
17 **Smith EJ**, Coventry C, Taylor J, De'ath H, Haque A. A case of endovascular management to gain control of a lower gastrointestinal haemorrhage caused by appendiceal artery bleeding. *J Surg Case Rep* 2021; **2021**: rjab204 [PMID: 34123349 DOI: 10.1093/jscr/rjab204]

World Journal of Clinical Cases

Submit a Manuscript: https://www.f6publishing.com

World J Clin Cases 2022 June 26; 10(18): 6319-6324

DOI: 10.12998/wjcc.v10.i18.6319

ISSN 2307-8960 (online)

CASE REPORT

Spontaneous healing after conservative treatment of isolated grade IV pancreatic duct disruption caused by trauma: A case report

Ming-Zhen Mei, Yu-Feng Ren, Yi-Ping Mou, Yuan-Yu Wang, Wei-Wei Jin, Chao Lu, Qi-Cong Zhu

Specialty type: Medicine, general and internal

Provenance and peer review: Unsolicited article; Externally peer reviewed.

Peer-review model: Single blind

Peer-review report's scientific quality classification

Grade A (Excellent): A
Grade B (Very good): 0
Grade C (Good): C
Grade D (Fair): 0
Grade E (Poor): 0

P-Reviewer: Lin F, China; Verde F, Italy

Received: January 15, 2022
Peer-review started: January 15, 2022
First decision: April 8, 2022
Revised: April 10, 2022
Accepted: April 24, 2022
Article in press: April 24, 2022
Published online: June 26, 2022

Ming-Zhen Mei, Departments of General Surgery, Tiantai Campus of Zhejiang Provincial People's Hospital, Taizhou 317200, Zhejiang Province, China

Yu-Feng Ren, Yi-Ping Mou, Yuan-Yu Wang, Wei-Wei Jin, Chao Lu, Qi-Cong Zhu, Department of General Surgery, Cancer Center, Division of Gastrointestinal and Pancreatic Surgery, Zhejiang Provincial People's Hospital, Affiliated People's Hospital, Hangzhou Medical College, Hangzhou 310014, Zhejiang Province, China

Yu-Feng Ren, Yi-Ping Mou, Yuan-Yu Wang, Wei-Wei Jin, Chao Lu, Qi-Cong Zhu, Key Laboratory of Gastroenterology of Zhejiang Province, Hangzhou 310014, Zhejiang Province, China

Corresponding author: Yuan-Yu Wang, MD, PhD, Chief Doctor, Professor, Department of General Surgery, Cancer Center, Division of Gastrointestinal and Pancreatic Surgery, Zhejiang Provincial People's Hospital, Affiliated People's Hospital, Hangzhou Medical College, No. 158 Shangtang Road, Gongshu District, Hangzhou 310014, Zhejiang Province, China.
lywyy1979@126.com

Abstract

BACKGROUND

Trauma is a common cause of pancreatic duct disruption. Surgical treatment is recommended in current clinical guidelines for adult pancreatic injury because non-surgical treatments have higher risks of serious complications or even death compared with surgical treatment.

CASE SUMMARY

A 22-year-old woman was admitted to Tiantai People's Hospital of Zhejiang Province after 1-h duration of abdominal pain and distension following trauma. The diagnosis was "traumatic pancreatic rupture". The patient's symptoms were not severe, her vital signs were stable, and signs of peritonitis were not obvious. Therefore, conservative treatment could be considered, with the possibility of emergency surgery if necessary. After 2 mo of conservative treatment with duct drainage, the pancreatic duct healed spontaneously with no significant complications.

CONCLUSION

We report a case of pancreatic duct disruption in the head and neck caused by trauma that was treated conservatively and healed spontaneously, providing a new choice for clinical practice. For isolated pancreatic injury with rupture of the pancreatic duct in the head and neck, conservative treatment under close obse-

rvation is feasible.

Key Words: Trauma; Pancreatic ducts; Conservative treatment; Drainage; Case report

©The Author(s) 2022. Published by Baishideng Publishing Group Inc. All rights reserved.

Core Tip: In this study, we report a case of pancreatic duct disruption in the head and neck caused by trauma that was treated conservatively and which healed spontaneously, providing a new basis for clinical practice. For isolated pancreatic injury with rupture of the pancreatic duct in the head and neck, conservative treatment under close observation is feasible.

Citation: Mei MZ, Ren YF, Mou YP, Wang YY, Jin WW, Lu C, Zhu QC. Spontaneous healing after conservative treatment of isolated grade IV pancreatic duct disruption caused by trauma: A case report. *World J Clin Cases* 2022; 10(18): 6319-6324
URL: https://www.wjgnet.com/2307-8960/full/v10/i18/6319.htm
DOI: https://dx.doi.org/10.12998/wjcc.v10.i18.6319

INTRODUCTION

Trauma is a common cause of pancreatic duct disruption. Surgical treatment is recommended in current clinical guidelines for adult pancreatic injury because, compared with surgical treatment, non-surgical treatments have higher risks of serious complications or even death[1,2]. In this study, we report a case of pancreatic duct disruption in the head and neck caused by trauma that was treated conservatively and which healed spontaneously.

CASE PRESENTATION

Chief complaints

A 22-year-old female patient was admitted to Tiantai People's Hospital of Zhejiang Province on 13 July 2020 after 1-hour duration of abdominal pain and distension following trauma.

History of present illness

The patient experienced sudden-onset persistent and unbearable abdominal pain, radiating to the lower back, with abdominal distension and nausea, and without vomiting, coma, dizziness, headache, chest tightness, shortness of breath, bloody vomiting, or hemoptysis. The trauma resulted from impact with bicycle handlebars on the upper abdomen during an electrical bicycle accident 1 h earlier.

She had no other complaints. Her sleep and appetite were normal, and her excretion and egestion were both normal.

History of past illness

The patient had an unremarkable medical history.

Personal and family history

The patient grew up in her locality, denied any contact with contaminated water or radiation exposure, and did not smoke or consume alcohol. She had no gestational history, and her annual menstruation cycle was 13/year (q 4-6 wk/duration: 20-30 d).

Physical examination

Physical examination findings on admission: body temperature: 37.2 ℃, respiratory rate: 20 breaths/min, blood pressure: 118/63 mmHg, and heart rate: 103 beats/min. The patient had a clear mind, low mood, flat and soft abdomen, tenderness in the upper abdomen, no obvious rebound pain, bowel sounds: 2/min, and no shifting dullness. No other significant abnormalities were observed.

Laboratory examinations

Serum amylase concentration: 1258 U/L (upper limit of normal: 135 U/L), white blood cell count: 17.8 × 10^9/L, neutrophils: 82%, red blood cell count: 4.51 × 10^{12}/L, hemoglobin: 143 g/L, platelet count: 211 × 10^9/L, C-reactive protein: < 0.499 mg/L, and procalcitonin: < 0.02 ng/mL; liver and kidney function was



DOI: 10.12998/wjcc.v10.i18.6319 **Copyright** ©The Author(s) 2022.

Figure 1 Contrast-enhanced abdominal computed tomography, which shows a morphologically smooth pancreatic neck/head with small lamellar high-density shadows at the anterior edge, with no significant enhancement.

normal, the levels of plasma lactate was normal.

Imaging examinations

Abdominal computed tomography (CT): The pancreatic head/neck was full in shape, and small lamellar high-density shadows were seen at the anterior edge, with a CT value of 64 HU. There was no edema and thickening of bilateral anterior renal fascia and no peritoneal or retroperitoneal effusion. The lesion was not significantly enhanced during contrast-enhanced CT, and some surrounding low-density exudative shadows were observed (Figure 1).

FINAL DIAGNOSIS

The diagnosis was "traumatic pancreatic rupture".

TREATMENT

The patient was informed that her condition was critical, and there were indications for emergency surgery; however, the patient's symptoms were not severe, her vital signs were stable, and signs of peritonitis were not obvious. Therefore, conservative treatment could be considered, with the possibility of emergency surgery if necessary. The patient was then treated with fasting, gastrointestinal decompression, acid control, digestive enzyme inhibition, anti-inflammation, and fluid replacement. After treatment, her abdominal pain was relieved. Abdominal CT on 14 July 2020 revealed lamellar high-density shadows in the pancreatic head and neck, with no significant increase in fluid collection, and with obvious exudative shadows around the pancreas; fluid accumulation was evident in the abdominal cavity. Conservative treatment was continued, and the patient's condition gradually improved. A naso-intestinal tube was placed for enteral feeding on 20 July 2020, which was well-tolerated. Repeat ultrasonography on 23 July 2020 revealed local fluid collection in the neck of the pancreas measuring approximately 60 mm × 46 mm × 38 mm and no obvious fluid accumulation in the abdominal cavity. Therefore, catheter drainage of the peripancreatic fluid collection was performed, and approximately 300 mL of pale bloody fluid was removed. Repeat abdominal CT on 24 July 2020 revealed local dissection of the pancreatic head/neck, encapsulated effusion in the form of a pseudocyst measuring 17 mm × 31 mm, and a small amount of fluid in the abdominopelvic cavity (Figure 2). The patient was transferred to Zhejiang Provincial People's Hospital for follow-up treatment on 27 July 2020, during which inflammatory indices were normal, and serum total amylase reached a maximum of 932 U/L (upper limit of normal: 135 U/L), with no significant fluid exiting the drain. Abdominal CT was repeated and revealed that the pancreatic head/neck was morphologically swollen, with increased surrounding encapsulated fluid. Ultrasound-guided peripancreatic catheter drainage by transperitoneal was performed again, and 300 mL of clear pancreatic fluid was removed. The serum amylase concentration decreased to normal after this drainage. On 24 August 2020, puncture pancreatography visualized the distal pancreatic duct. On 25 August 2020, endoscopic retrograde cholangiopancreatography (ERCP) was performed to place a pancreatic duct stent. The pancreatic duct in the pancreatic head was circular in shape and was not connected with the pancreatic duct in the pancreatic body/tail. Therefore, the pancreatic duct stent could not be placed.

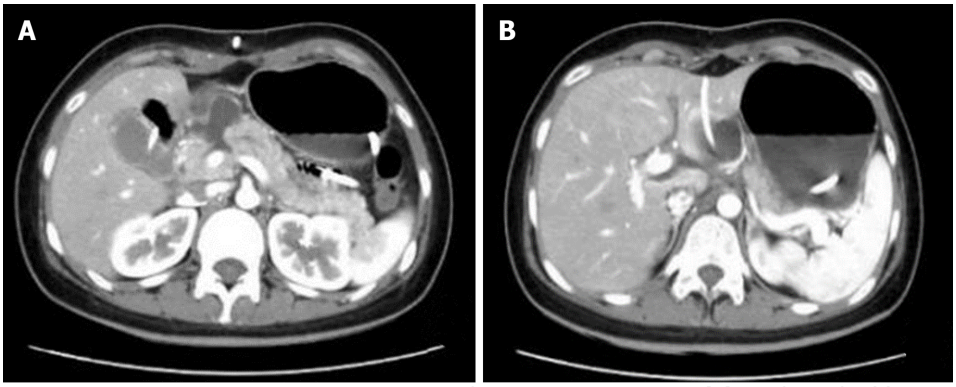

DOI: 10.12998/wjcc.v10.i18.6319 **Copyright** ©The Author(s) 2022.

Figure 2 Abdominal computed tomography. A: Localized rupture of the pancreatic head/neck; B: A pseudocyst, drained with a catheter.

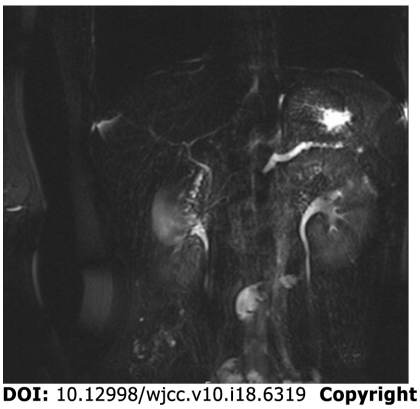

DOI: 10.12998/wjcc.v10.i18.6319 **Copyright** ©The Author(s) 2022.

Figure 3 Magnetic resonance cholangiopancreatography showing a slightly dilated pancreatic duct in the pancreatic tail.

OUTCOME AND FOLLOW-UP

The main pancreatic duct was not dilated by transpuncture tube angiography, and there was no obvious liquid dark areas around the pancreas; therefore, the puncture drain was removed. Re-examination on 10 November 2020 revealed that the patient had no discomfort and no abnormalities on physical examination. The serum amylase concentration was 44 U/L. Magnetic resonance cholangiopancreatography (MRCP) suggested slightly dilated pancreatic ducts in the pancreatic tail (Figure 3).

DISCUSSION

The pancreas is a retroperitoneal organ with a deep and hidden location, and pancreatic injury occurs in only 0.4%-6.0% of abdominal trauma cases[1]. The pancreas is located in front of the first and second lumbar vertebrae; therefore, injury is often caused by direct action on the spine owing to crushing force from the upper abdomen, mostly sustained in the pancreatic body. Approximately 39% of pancreatic injuries are associated with pancreatic duct disruption[2]. Isolated pancreatic injury is even more rare, comprising less than 3% of cases[3].

The level of serum amylase has little significance for the early diagnosis of pancreatic trauma. Serum amylase cannot be increased in about 40% of patients, and it can also be increased in non-pancreatic injury and intestinal injury[4]. Adamson *et al*[5] conducted a retrospective study on 1821 patients with trauma. The level of serum amylase or lipase increased in 116 patients, and only 8 patients finally identified pancreatic trauma. The significance of serum amylase or lipase in the diagnosis of pancreatic trauma is limited, and it also depends on the necessary imaging examination. Currently, CT is the first-line technique for evaluating pancreatic injury. CT is easy to perform, and its high imaging quality, clear display of the pancreatic contours and peripancreatic bleeding, and the option for multiplanar reconstruction, can achieve a diagnostic accuracy rate of > 80%. However, there are limitations in the diagnosis of pancreatic duct disruption, and the accuracy rate needs to be improved by dynamic review [6]. In this case, we performed dynamic CT review to clarify the presence of pancreatic duct disruption. According to the American Association for the Surgery of Trauma (AAST) classification of pancreatic

Table 1 American Association for the Surgery of pancreatic trauma for the pancreas

Grade[1]	Type of injury	Description of injury
I	Hematoma	Minor contusion without duct injury
	Laceration	Superficial laceration without duct injury
II	Hematoma	Major contusion without duct injury or tissue loss
	Laceration	Major laceration without duct injury or tissue loss
III	Laceration	Distal transection or parenchymal injury with duct injury
IV	Laceration	Proximal transection or parenchymal injury involving ampulla
V	Laceration	Massive disruption of pancreatic head

[1]Advances one grade for multiple injuries up to grade III.

injuries, injuries involving the pancreatic duct are classified as grade III or IV injuries, as outlined in Table 1[7]. For hemodynamically stable patients, MRCP can be performed when further clarification of pancreatic duct integrity is needed during follow-up treatment. MRCP has the advantages of being noninvasive and providing accurate pancreatic duct imaging. In this case, complete rupture of pancreatic neck was well established by computed tomography (Figure 2A), so we did not perform MRCP. ERCP can lead to a series of complications, such as bleeding, perforation, and iatrogenic pancreatitis, and is more often used for treatment. This patient's admission serum amylase concentration was significantly elevated, and the diagnosis of pancreatic duct disruption was confirmed when the elevated amylase finding was combined with the dynamic CT review.

The management of pancreatic injuries is controversial and based on small retrospective studies. There are no randomized studies addressing this issue. Based on the available class III evidence, the Eastern Association for the Surgery of Trauma recommended drainage for Grade 1 and Grade 2 injuries and resection with drainage for Grade 3 or higher[8]. Siboni *et al*[3] study found nonoperative management of minor isolated pancreatic injuries is associated with lower mortality and shorter hospital stay than operative management. However, in severe trauma, nonoperative management is associated with higher mortality and longer hospital stays than operative management[3].

Mohseni *et al*[9] research showed pancreatic resection for the treatment of grade III and IV penetrating pancreatic injury is not associated with a significant decrease in mortality but is associated with a significant increase in hospital length of stay. Drainage alone of the pancreatic bed may be a viable option, even for high-grade injuries[9]. For traumatic pancreatic injury, the optimal treatment strategy can be formulated only when the patient's vital signs, abdominal signs, degree of pancreatic injury, and the presence of surrounding organ injury are considered comprehensively.

Recently, the use of endoscopic stenting of the pancreatic duct for the successful treatment of pancreatic duct disruption has been increasingly reported[10]. In a recently published report showing patients with pancreatic trauma who had received pancreatic stents undergoing ERCP 0-15 d after the trauma, the stents were removed after 4-8 wk and at follow-up between 6-24 mo. Endoscopic stent treatment may avoid emergency pancreatic resection and should always be considered in the management of patients with traumatic pancreatic duct injury[11]. When the patient is admitted to our hospital, the condition of this case was stable, so we did not chose pancreatic duct stent implantation. Compared with pancreatic resection, which is highly invasive and affects patients' quality of life, endoscopic treatment is undoubtedly a new treatment strategy and is gradually gaining more attention.

CONCLUSION

In this case, after 2 mo of conservative treatment with duct drainage, the pancreatic duct healed spontaneously with no significant complications. This case provides a new consideration for clinical practice: In isolated pancreatic injury with rupture of the pancreatic duct in the head and neck, conservative treatment under close observation is feasible. In young and fit populations with stable hemodynamics, no signs of peritonitis, and no obvious active bleeding on abdominal CT, conservative treatment can be considered first, combined with dynamic CT review and fluid drainage. Endoscopic pancreatic duct stenting can then be considered if appropriate because, in some cases, the pancreatic duct can heal spontaneously.

FOOTNOTES

Author contributions: Mei MZ and Ren YF have contributed equally to this work; Mei MZ and Ren YF made substantial contributions to acquisition of data, analysis, and interpretation of data; Mou YP, Wang YY, Jin WW, Lu C, and Zhu QC made substantial contributions to the conception, acquisition of data, analysis, and interpretation of data; all authors have been involved in drafting the manuscript and revising it critically for important intellectual content; All authors read and approved the final manuscript and take public responsibility for appropriate portions of the content and agree to be accountable for all aspects of work.

Supported by Traditional Chinese medicine Science and Technology Project of Zhejiang Province, No. 2020ZB029.

Informed consent statement: Written informed consent was obtained from the patient for the publication of this case report and the accompanying images.

Conflict-of-interest statement: The authors declare that they have no competing interests.

CARE Checklist (2016) statement: The authors have read the CARE Checklist (2016), and the manuscript was prepared and revised according to the CARE Checklist (2016).

Open-Access: This article is an open-access article that was selected by an in-house editor and fully peer-reviewed by external reviewers. It is distributed in accordance with the Creative Commons Attribution NonCommercial (CC BY-NC 4.0) license, which permits others to distribute, remix, adapt, build upon this work non-commercially, and license their derivative works on different terms, provided the original work is properly cited and the use is non-commercial. See: https://creativecommons.org/Licenses/by-nc/4.0/

Country/Territory of origin: China

ORCID number: Ming-Zhen Mei 0000-0003-0673-5748; Yu-Feng Ren 0000-0003-4605-2271; Yi-Ping Mou 0000-0002-0778-6022; Yuan-Yu Wang 0000-0001-8462-7211; Wei-Wei Jin 0000-0002-2974-9598; Chao Lu 0000-0003-0050-1086; Qi-Cong Zhu 0000-0003-3281-7288.

S-Editor: Gong ZM
L-Editor: Filipodia
P-Editor: Gong ZM

REFERENCES

1 **Feliciano DV**. Abdominal Trauma Revisited. *Am Surg* 2017; **83**: 1193-1202 [PMID: 29183519]
2 **Ding WW**, Wang K, Liu BC, Xi FC, Wang ZM, Li WQ, Li JS. Management of pancreatic trauma: A report of 136 cases. *Zhongguo Shiyong Waike Zazhi* 2018; **38**: 782-785
3 **Siboni S**, Kwon E, Benjamin E, Inaba K, Demetriades D. Isolated blunt pancreatic trauma: A benign injury? *J Trauma Acute Care Surg* 2016; **81**: 855-859 [PMID: 27537506 DOI: 10.1097/TA.0000000000001224]
4 **Mahajan A**. Current Status of Role of Serum Amylase and Lipase to Triage Blunt Pancreatic Trauma? *J Clin Diagn Res* 2016; **10**: PL02 [PMID: 28050447 DOI: 10.7860/JCDR/2016/24265.8838]
5 **Adamson WT**, Hebra A, Thomas PB, Wagstaff P, Tagge EP, Othersen HB. Serum amylase and lipase alone are not cost-effective screening methods for pediatric pancreatic trauma. *J Pediatr Surg* 2003; **38**: 354-7; discussion 354
6 **Li RH**. Manifestations and Diagnostic Value of Multi-slice Spiral CT in Patients with Emergency Pancreatic Trauma. *Zhongguo CT He MRI Zazhi* 2017; **15**: 88-90 [DOI: 10.3969/j.issn.1672-5131.2017.03.029]
7 **Coccolini F**, Kobayashi L, Kluger Y, Moore EE, Ansaloni L, Biffl W, Leppaniemi A, Augustin G, Reva V, Wani I, Kirkpatrick A, Abu-Zidan F, Cicuttin E, Fraga GP, Ordonez C, Pikoulis E, Sibilla MG, Maier R, Matsumura Y, Masiakos PT, Khokha V, Mefire AC, Ivatury R, Favi F, Manchev V, Sartelli M, Machado F, Matsumoto J, Chiarugi M, Arvieux C, Catena F, Coimbra R; WSES-AAST Expert Panel. Duodeno-pancreatic and extrahepatic biliary tree trauma: WSES-AAST guidelines. *World J Emerg Surg* 2019; **14**: 56 [PMID: 31867050 DOI: 10.1186/s13017-019-0278-6]
8 **Bokhari F**, Phelan H, Holevar M, Brautigam R, Collier B, Como JJ, Clancy K, Cumming JK, Cullinane D, Smith L; on behalf of the Eastern Association for the Surgery of Trauma Practice Management and Guidelines. EAST Guidelines for the Diagnosis and Management of Pancreatic Trauma. Published 2009. Accessed June 6, 2016. Available from: http://www.east.org/education/practicemanagement-guidelines/pancreatic-trauma-diagnosis-and-management-of-pancreatic-trauma
9 **Mohseni S**, Holzmacher J, Sjolin G, Ahl R, Sarani B. Outcomes after resection versus non-resection management of penetrating grade III and IV pancreatic injury: A trauma quality improvement (TQIP) databank analysis. *Injury* 2018; **49**: 27-32 [PMID: 29173964 DOI: 10.1016/j.injury.2017.11.021]
10 **Kottapalli DC**, Devashetty S, Suryanarayana VR, Kilari M, Ismail MD, Mathew P, Chetty PK. Complete pancreatic duct disruption in an isolated pancreatic injury: successful endoscopic management. *Oxf Med Case Reports* 2016; **2016**: 44-46 [PMID: 26989493 DOI: 10.1093/omcr/omw010]
11 **Björnsson B**, Kullman E, Gasslander T, Sandström P. Early endoscopic treatment of blunt traumatic pancreatic injury. *Scand J Gastroenterol* 2015; **50**: 1435-1443 [PMID: 26096464 DOI: 10.3109/00365521.2015.1060627]

World Journal of Clinical Cases

Submit a Manuscript: https://www.f6publishing.com

World J Clin Cases 2022 June 26; 10(18): 6325-6332

DOI: 10.12998/wjcc.v10.i18.6325

ISSN 2307-8960 (online)

CASE REPORT

Pneumonia and seizures due to hypereosinophilic syndrome—organ damage and eosinophilia without synchronisation: A case report

Tetsuro Ishida, Tomonori Murayama, Seiju Kobayashi

Specialty type: Clinical neurology

Provenance and peer review: Unsolicited article; Externally peer reviewed.

Peer-review model: Single blind

Peer-review report's scientific quality classification

Grade A (Excellent): 0
Grade B (Very good): B
Grade C (Good): C
Grade D (Fair): 0
Grade E (Poor): 0

P-Reviewer: Fazilat-Panah D, Iran; Shuang WB, China

Received: February 3, 2022
Peer-review started: February 3, 2022
First decision: March 23, 2022
Revised: March 29, 2022
Accepted: April 30, 2022
Article in press: April 30, 2022
Published online: June 26, 2022

Tetsuro Ishida, Department of Psychiatry, Hokujinkai Ishibashi Hospital, Otaru 047-8585, Japan

Tomonori Murayama, Department of Psychiatry, Kushiro Red Cross Hospital, Kushiro 085-8512, Japan

Seiju Kobayashi, Department of Psychiatry, Shinyukai Nakae Hospital, Sapporo 001-0022, Japan

Corresponding author: Tetsuro Ishida, MD, Chief Doctor, Department of Psychiatry, Hokujinkai Ishibashi Hospital, 3-7-7 Nagahashi, Otaru 047-8585, Japan.
teturoisida@yahoo.co.jp

Abstract

BACKGROUND

Hypereosinophilic syndrome (HES) is a condition characterized by increased eosinophil proliferation in the bone marrow, as well as tissue eosinophilia, often causing organ damage. The cause of the disease is unknown. Initial symptoms include fatigue, cough, shortness of breath, myalgia, angioedema, fever, and pneumonia. In addition to the respiratory symptoms, damage to the central nervous system can lead to severe seizures. Here, we report a case with pneumonia and complex partial seizures secondary to HES.

CASE SUMMARY

A 94-year-old woman was admitted to our hospital for heart failure and bloody stools. After admission, she also showed symptoms of pneumonia. Non-contrast computed tomography of the chest showed pleural effusion and infiltrative shadows. Lower gastrointestinal endoscopy showed multiple ulcers in the sigmoid colon. Blood analyses showed marked eosinophilia (eosinophils 1760/mm^3, total leukocytes 6850/mm^3). Initial treatment with furosemide 20 mg/d and prednisolone 25 mg/d relieved these symptoms. However, the patient subsequently experienced localised epileptic seizures characterized by bilateral eyelid twitching and eyes rolling upwards, without generalized convulsions, and respiratory arrest occurred. Electroencephalography showed spikes and waves. Non-contrast magnetic resonance imaging of the brain showed extensive periventricular hyperintensity. With administration of levetiracetam 1000 mg/d the epileptic seizures disappeared. However, the patient's consciousness remained impaired, and her pneumonia worsened again. Two weeks later, she died of pneumonia.

CONCLUSION
HES symptoms are variable and atypical, and the level and timing of eosinophilia and organ damage are often discordant.

Key Words: Case report; Hypereosinophilic syndrome; Pneumonia; Seizures; Prednisolone; Levetiracetam

©The Author(s) 2022. Published by Baishideng Publishing Group Inc. All rights reserved.

Core Tip: Although there are diagnostic criteria for hypereosinophilic syndrome, the various degrees of organ damage and hypereosinophilia often make diagnosis difficult in clinical practice. In addition, the organ damage and blood changes do not always occur concurrently. Therefore, clinicians must consider many differential diagnoses, especially when patients present with atypical symptoms and disease course. Early initiation of treatment is no less important than an accurate diagnosis, and the balance between the two should be considered according to the patient's condition as well as the level and quality of medical resources available at the hospital.

Citation: Ishida T, Murayama T, Kobayashi S. Pneumonia and seizures due to hypereosinophilic syndrome—organ damage and eosinophilia without synchronisation: A case report. *World J Clin Cases* 2022; 10(18): 6325-6332
URL: https://www.wjgnet.com/2307-8960/full/v10/i18/6325.htm
DOI: https://dx.doi.org/10.12998/wjcc.v10.i18.6325

INTRODUCTION

Hypereosinophilic syndrome (HES) is a marked blood and tissue eosinophilia of unknown aetiology with a variety of clinical manifestations. Since 1975, the disease has been defined by three criteria: (1) Blood eosinophilia ≥ 1500/mm^3 for longer than 6 mo (or death before 6 mo associated with signs and symptoms of hypereosinophilic disease); (2) Lack of evidence for parasitic, allergic, or other known causes of eosinophilia; and (3) Presumptive signs of organ involvement, such as heart failure, gastrointestinal dysfunction, central nervous system abnormalities, fever, or weight loss[1].

However, there are several problems with these criteria. First, according to these criteria, clinicians must wait 6 mo to diagnose a patient with multiple organ involvement. Second, an increase in eosinophils does not necessarily correlate with organ damage. Some patients may have a marked increase in eosinophils but only mild symptoms, while others may have a mild increase in eosinophils but significant organ damage[2]. Therefore, two diagnostic criteria have now been proposed to replace the classic three: (1) Blood eosinophilia of greater than 1500/mm^3 on at least two occasions or evidence of prominent tissue eosinophilia associated with symptoms and marked blood eosinophilia; and (2) Exclusion of secondary causes of eosinophilia, such as parasitic or viral infections, allergic diseases, drug-induced or chemical-induced eosinophilia, hypoadrenalism, and neoplasia[3]. However, this revision of the diagnostic criteria does not solve all the problems in the diagnosis and treatment of HES. We anticipate that this case will aid in the diagnosis and treatment of similar cases.

CASE PRESENTATION

Chief complaints

A 94-year-old Asian woman presented to our hospital for dyspnoea and wet cough. She also had abdominal pain and bloody stools. She was admitted to our hospital with a diagnosis of heart failure and sigmoid colon ulceration (day 1).

History of present illness

Her respiratory distress started during the night 1 d before presentation. It improved after 1 h and was still mild over the next morning and evening hours. However, 22 h later, her symptom got worse again during the night.

History of past illness

The patient had no chronic illnesses such as hypertension, diabetes, or asthma, and no history of cancer. She was a non-smoker and did not habitually drink alcohol. She had a well-balanced diet and lived a healthy lifestyle.

Personal and family history

There was no specific history.

Physical examination

The patient was 148 cm tall, weighed 42 kg, and her vital signs were as follows: blood pressure 111/43 mmHg; pulse 90/min; respiratory rate 14/min; and SpO_2 98% (room air). On chest auscultation, her heart rhythm was regular and no heart murmur was found. However, auscultation of respiratory sounds found wheezing. Her abdomen was flat and soft and abdominal auscultation found neither increased nor decreased intestinal peristalsis. There was no rebound tenderness or abdominal guarding. However, there was intermittent and spontaneous abdominal pain and bloody stools. Her eyelid conjunctiva did not show jaundice or pallor. Her oral and nasal cavities and skin surfaces showed no abnormal findings. Her upper limbs showed no abnormalities. However, her lower extremities showed indurated oedema.

Laboratory examinations

On day 1, her rapid antigen tests using a throat swab were negative for influenza A and B and COVID-19. Her electrocardiogram (ECG) showed no abnormalities on admission and on loss of consciousness on day 108. In her blood analyses, there were no abnormalities in the electrolyte, glucose, lipid, liver function, and renal function parameters. The antinuclear antibody (ANA) titre at 1:40 serum dilution was positive but staining patterns at 1:40 serum dilution was negative for homogeneous, discrete speckled, speckled, nucleolar, and peripheral staining. Anti-neutrophil cytoplasmic antibody (ANCA) and HIV tests were negative. On day 32, the patient's IgE level was slightly high at 237 IU/mL (normal: 27.54–138.34), but her IgG, IgA, and IgM levels were normal. Blood analyses also showed that eosinophils and brain natriuretic peptide (BNP) levels were high. The highest values for each were 1760/mm^3 on day 26 for eosinophils and 738.1 pg/mL on day 1 for BNP (Figures 1 and 2). The blood and sputum taken on day 26 were negative on culture for bacteria or fungi and no parasites were found. However, on day 109, blood culture was positive for methicillin-resistant Staphylococcus epidermidis, and the β-D-glucan level was high (316.0 pg/mL). On day 128, blood tests showed normal levels of ammonia. The patient's post-consciousness EEG showed spikes and waves in Fp1, F1, C3, P3, and O1 (Figure 3). Her echocardiogram showed no thrombi in the atria or ventricles.

Imaging examinations

Non-contrast computed tomography imaging of the patient's chest showed bilateral pleural effusions and infiltrative shadows (Figure 4). Her gastrointestinal endoscopy showed multiple ulcers in the sigmoid colon (Figure 5). Histopathological examination showed colonic gland prolapse, vitrification of the stroma, and an infiltration of inflammatory cells, but no evidence of malignant transformation. Non-contrast magnetic resonance imaging of the patient's head showed extensive periventricular hyperintensity (Figure 6).

MULTIDISCIPLINARY EXPERT CONSULTATION

Norihisa Okuda MD, Vice-president and Chief, Department of Respiratory Medicine, Hokujinkai Ishibashi Hospital

The patient's eosinophils in the blood tests exceeded 1500/mm^3 only once, but she had high eosinophils multiple times without meeting this threshold. Additionally, it was clear that the eosinophilic infiltrate was causing serious damage to the nervous, respiratory, cardiovascular, and digestive systems. We should not have delayed the initiation of her treatment any longer to meet the classical diagnostic criteria. Biopsies of organs other than her sigmoid colon were considered for a more precise examination and imatinib initiation was considered for more effective treatment, but both were too invasive for the elderly patient. Given that she and her family did not wish to undergo these tests and treatments, we did not pursue these options. Although Japan is a country with some of the richest medical resources in the world, the hospital where the patient was admitted had no intensive care unit or specialists in collagen diseases and autoimmune diseases, and the same is true for other similar rural hospitals. The use of limited medical resources is an important issue in this country as in the rest of the world.

FINAL DIAGNOSIS

The patient was diagnosed with epileptic seizures and pneumonia caused by HES.

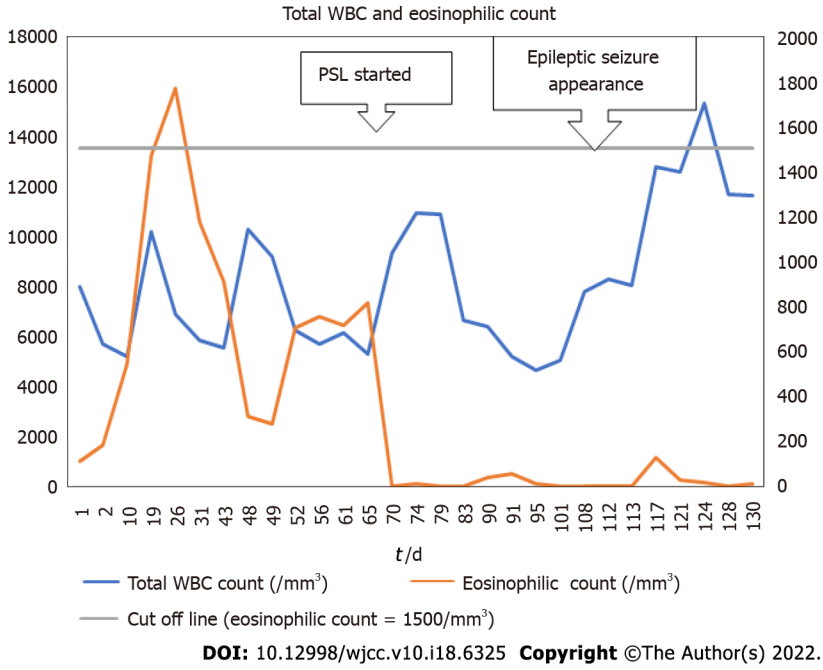

DOI: 10.12998/wjcc.v10.i18.6325 **Copyright** ©The Author(s) 2022.

Figure 1 The patient's serial blood test results showing changes in total white blood cells and eosinophil count. The eosinophil count was automatically calculated from the ratio of eosinophils to total white blood cells. When the ratio was less than 0.1%, it was counted as 0. WBC: White blood cells; PSL: Prednisolone.

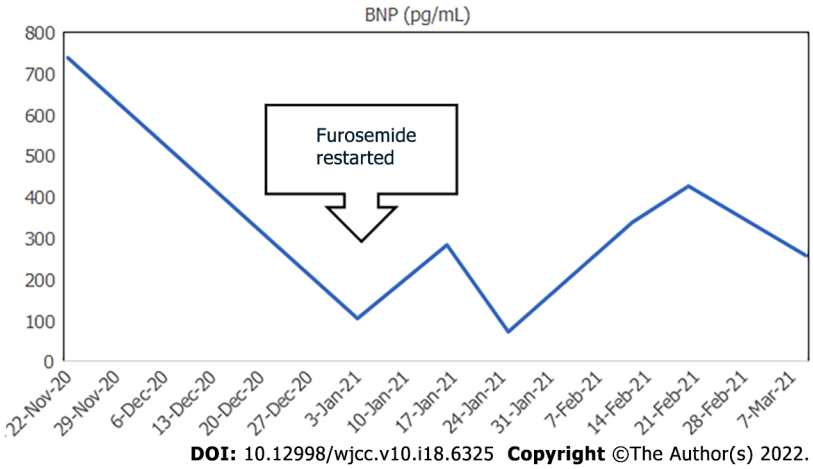

DOI: 10.12998/wjcc.v10.i18.6325 **Copyright** ©The Author(s) 2022.

Figure 2 Serial changes in the patient's brain natriuretic peptide values. BNP: Brain natriuretic peptide.

TREATMENT

In addition to rehabilitation, the patient was treated with furosemide for heart failure, ceftazidime and vancomycin and fungard and PSL for pneumonia and levetiracetam (LEV) for seizures.

OUTCOME AND FOLLOW-UP

Furosemide 20 mg/d for 10 d from the day of admission (day 1) relieved her congestive heart failure symptoms for a period of time. A diet suitable for digestion and absorption made her bloody stools and abdominal pain disappear. Rehabilitation, including gait training and flexibility exercises to prevent loss of range of motion and contractures throughout the body, was also initiated. However, from day 56, her congestive heart failure symptoms recurred, and pneumonia also appeared. Treatment with 20 mg/d furosemide was restarted from that day, but without effect. Ceftazidime 2 g/d was also ineffective in treating the pneumonia. On day 68, the patient was diagnosed with HES and treatment with prednisolone (PSL) 25 mg/d was started. After that, the pneumonia and heart failure symptoms gradually

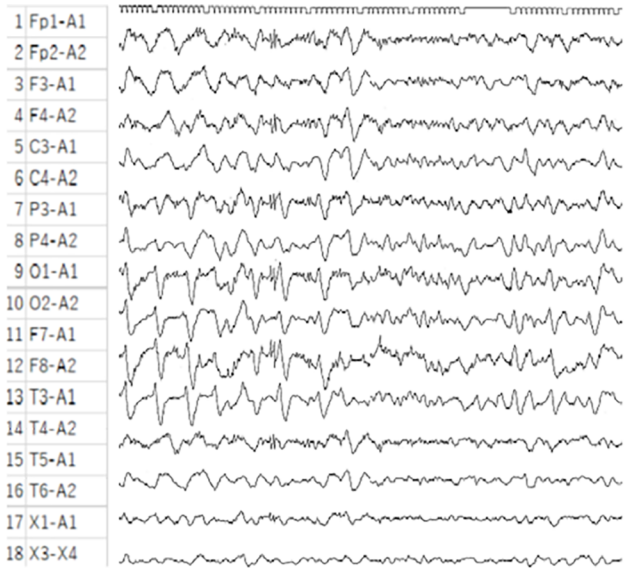

DOI: 10.12998/wjcc.v10.i18.6325 **Copyright** ©The Author(s) 2022.

Figure 3 The patient's post loss of consciousness electroencephalogram showing a slow wave indicative of a clinical epileptic seizure.

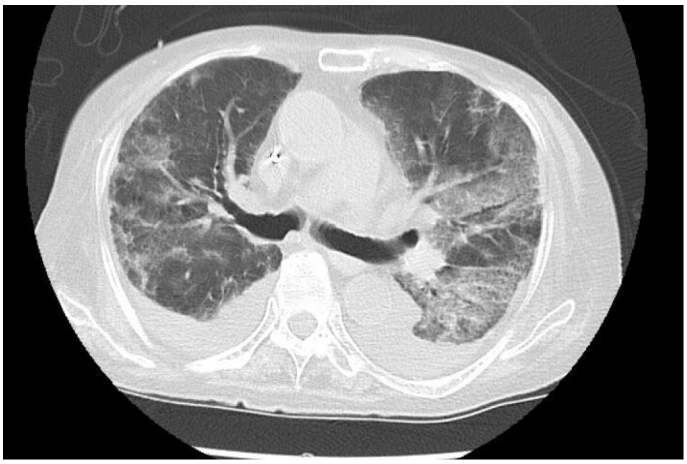

DOI: 10.12998/wjcc.v10.i18.6325 **Copyright** ©The Author(s) 2022.

Figure 4 Non-contrast computed tomography image of the patient's chest showing bilateral pleural effusions and infiltrative shadows.

improved, so the PSL was gradually reduced to 15 mg/d. Her rehabilitation was also resumed. However, on day 108, her eyes suddenly rolled upwards, and she showed eyelid twitching and loss of consciousness. Her breathing stopped and her SpO_2 dropped to 70% (room air). Oxygen therapy (reservoir mask: 10 L/min) was started immediately. Diazepam 10 mg intramuscular injection was also given and after 5 minutes her SpO_2 improved to 90% (reservoir mask: 10 L/min) and her seizures stopped. LEV 1000 mg/d was started and subsequently, the seizures did not recur. However, her state of consciousness continued to be unfavourable on the Glasgow Coma Scale, E2 V2 M4[4]. Her respiratory status also improved reaching SpO_2 90% (nasal cannula: O_2 1L), but not higher. On day 109, fungard 50 mg/d, vancomycin 1 g/d and ceftazidime 2 g/d were started and her PSL was increased to 30 mg/d. However, her pneumonia continued to worsen, and she died of pneumonia on day 135.

DISCUSSION

First, we will discuss diagnosis of HES. As mentioned at the beginning of this report, the diagnostic requirement for HES is a blood eosinophil count ≥ 1500/mm^3 for at least 6 mo according to the classical diagnostic criteria or measured at least twice according to the diagnostic criteria proposed by Simon *et al* [3]. In this case, neither of these criteria were met at the time the diagnosis was made. In our case, the patient's blood eosinophil count exceeded 1500/mm^3 only once and this did not necessarily coincide with the most severe period of organ damage. Some clinicians suggested that we should have waited

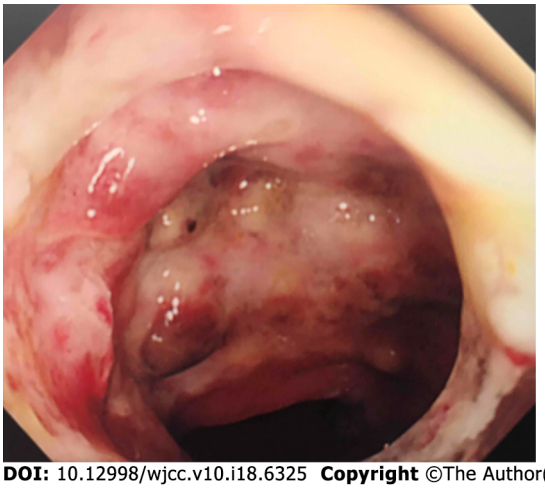

DOI: 10.12998/wjcc.v10.i18.6325 **Copyright** ©The Author(s) 2022.

Figure 5 Gastrointestinal endoscopy image showing multiple mucosal ulcers in the sigmoid colon.

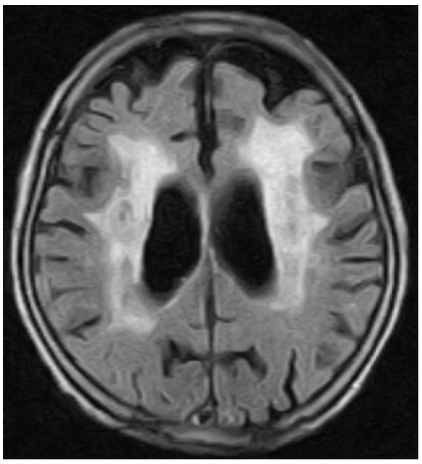

DOI: 10.12998/wjcc.v10.i18.6325 **Copyright** ©The Author(s) 2022.

Figure 6 Non-contrast magnetic resonance imaging of the patient's head showing extensive periventricular hyperintensity.

until her eosinophil count had risen again and her symptoms had worsened before deciding on a diagnosis. However, as stated in the Multidisciplinary Expert Consultation, we needed to start her treatment as soon as possible. This was considered a higher priority than meeting the strict diagnostic criteria. In addition, the disease course in this case meets the criterion of "or death before 6 mo associated with signs and symptoms of hypereosinophilic disease" listed in the supplementary information in the classical criteria[3]. Heart failure, sigmoid colon ulceration, pneumonia, and epilepsy signified damage to each of these organs in our patient. Therefore, the diagnosis of HES in this case was appropriate. With regard to treatment, the focus is on PSL. As is well known, PSL is a drug that needs to be tapered off, not stopped abruptly. Furthermore, a longer PSL treatment course is commonly required for eosinophilic pneumonia. However, in this case, given the early decline in the eosinophil count after initiation of PSL therapy, perhaps it should have been tapered or stopped earlier.

Next, we would like to discuss the diagnosis and treatment of epilepsy. Common causes of loss of consciousness in older people include heart disease, autonomic disorders, other conditions such as anaemia, ischaemia and varicose veins, or anticholinergic drugs[5]. Our patient had congestive heart failure at the time of admission, but her condition improved. She did not have any blood clots identified that could have caused cerebral embolism. Her vital signs, including blood pressure and ECG, were normal. Therefore, it was considered unlikely that the loss of consciousness was due to circulatory problems. Her post-consciousness electroencephalogram (EEG) suggested that there were epileptic discharges around the left anterior frontal lobe, motor cortex, central sulcus, sensory cortex, and visual cortex. The rather unremarkable EEG findings compared with the clinical findings may be because this EEG was done after the LEV treatment was started. The epileptic discharges may have been more intense before the administration of antiepileptic drugs. We were not able to do rapid or continuous monitoring EEG at our hospital. In diagnosing and treating her epilepsy, we were forced to prioritise life-saving treatment over rigorous diagnosis.

Regarding the seizure type, her epilepsy was most likely a complex partial seizure. Complex partial seizures are more likely to occur in older adults and cause disorientation, but they do not cause tonic or clonic seizures[6]. The fact that LEV treatment was effective in preventing the seizure symptoms was also one of the reasons for the diagnosis. However, the presence of eyelid twitching also suggests that her seizure type may have been absence seizures. Absence seizures are generally more common in young children and have a shorter duration of disorientation. However, if the seizure is an atypical absence seizure, the disturbance of consciousness may be prolonged. In Japan, LEV may be administered at doses of up to 3000 mg/d. However, in this case, the patient was elderly, and it was feared that increasing the dose of LEV might cause side effects such as malignant syndrome. The LEV dose was not increased because there were no obvious epileptic seizures after the start of LEV at a dose of 1000 mg/d. In this case, the patient's loss of consciousness was prolonged even after an intramuscular injection of 10 mg diazepam and was, therefore, considered to be benzodiazepine-refractory. LEV, fosphenytoin, and valproic acid are suitable for the treatment of epilepsy which does not improve with benzodiazepines. In elderly patients, there is no difference in the safety or therapeutic efficacy between these three drugs[7]. LEV was chosen in this case because it can be started intravenously and can be seamlessly transferred to the oral route if oral medication becomes available later. We considered hepatic encephalopathy as a possible cause of our patient's impaired consciousness, but this was ruled out by the normal blood ammonia levels and the fact that the EEG showed no triphasic waves.

While all ANA staining patterns were negative, the ANA titre was positive at 1:40 dilution. This result indicates that our patient may have had a collagen disease. Therefore, we needed to differentiate the collagen diseases with eosinophilia granulomatosis with polyangiitis (EPGA) and polyarteritis nodosa (PAN), from HES. EPGA, formerly known as Churg–Strauss syndrome, is characterised by asthma, eosinophilia of the blood and tissues, and small vessel vasculitis. The clinical symptoms are variable but can be divided into two main subtypes: The "vasculitis" type, which is positive for ANCA and shows glomerulonephritis, purpura, and inflammation of multiple peripheral nerves. The other is the "eosinophilic" type, which is negative for ANCA but is characterised by a markedly high level of eosinophils and damage in the lungs and myocardium[8]. This case is similar to the "eosinophilic" type, but EPGA is less likely to cause central nervous system damage such as seizures.

PAN is a vasculitis that targets medium-sized arteries and leads to multi-organ failure. The target organs include the heart and the gastrointestinal tract. We note that damage to the central nervous system has also been reported[9]. However, damage to the lungs has rarely been reported[10]. The present case is not typical but is similar to both EPGA and PAN. However, the pathological findings in the sigmoid colon did not show the features of either of these diseases.

In terms of brain imaging findings, the differential diagnosis in this case also includes cerebral amyloid angiopathy (CAA). The Modified Boston Criteria for CAA are based on imaging and pathological findings. The disease can be classified as: (1) Definite CAA; (2) Probable CAA with supporting pathology; (3) Probable CAA; and (4) Possible CAA. The novelty of this criteria is that (3) and (4) do not require a pathological examination[11]. In this case, at the request of the patient and her family, no pathological examination of the brain tissue was performed after her death. Generally, the hallmark of CAA on brain imaging is multiple sporadic lesions confined to the cerebral cortex, cortico-subcortical junction grey matter, and subcortical white matter. However, some subtypes of CAA, such as cerebral amyloid angiopathy-related inflammation (CAA-ri), present with mass-like lesions as in this case[12]. CAA-ri is known to respond well to treatment with steroids and immunosuppressive drugs. In this case, treatment was given with the expectation that the patient might be diagnosed with CAA-ri. There is a report that CAA-ri can cause seizures[13], which seems to be consistent with the symptoms in this case. However, there are no previous studies on its frequency. Similar cases need to be studied in the future.

CONCLUSION

HES can cause damage to many organs and has an undulating disease course. Therefore, HES must be differentiated from other diseases such as EPGA, PAN, and CAA. In this case, the diagnosis was more difficult because of the time lag between the various clinical symptoms and the eosinophilia. The focus of treatment was to determine the appropriate dose and duration of PSL and LEV therapy. We conclude that this case report can be used as a reference for the diagnosis and treatment of similar cases.

ACKNOWLEDGEMENTS

This study was conducted at Iwanai Kyokai Hospital (209-2, Aza-Takadai, Iwanai-cho, Iwanai-gun, Hokkaido 045-0013, Japan). We are grateful to the patient who gave her consent to take part in this study. We would also like to thank Dr. Kawasaki, Dr. Yamazaki, and Dr. Kuroda in the Department of Internal Medicine at Iwanai Kyokai Hospital for their help and support. We thank Leah Cannon, PhD, from Edanz (https://jp.edanz.com/ac) for editing a draft of this manuscript.

FOOTNOTES

Author contributions: Ishida T was the patient's primary care physician and contributed to the literature review and manuscript preparation; Murayama T and Kobayashi S reviewed the literature and contributed to the preparation of the manuscript; and All authors gave their approval for the final version to be submitted.

Informed consent statement: Informed written consent was obtained from the patient for publication of this report and any accompanying images.

Conflict-of-interest statement: The authors declare that they have no conflicts of interest.

CARE Checklist (2016) statement: The authors have read the CARE Checklist (2016), and the manuscript was prepared and revised according to the CARE Checklist (2016).

Open-Access: This article is an open-access article that was selected by an in-house editor and fully peer-reviewed by external reviewers. It is distributed in accordance with the Creative Commons Attribution NonCommercial (CC BY-NC 4.0) license, which permits others to distribute, remix, adapt, build upon this work non-commercially, and license their derivative works on different terms, provided the original work is properly cited and the use is non-commercial. See: https://creativecommons.org/Licenses/by-nc/4.0/

Country/Territory of origin: Japan

ORCID number: Tetsuro Ishida 0000-0002-8513-2373; Tomonori Murayama 0000-0003-2371-8421; Seiju Kobayashi 0000-0002-1557-1426.

S-Editor: Ma YJ
L-Editor: A
P-Editor: Ma YJ

REFERENCES

1 **Chusid MJ**, Dale DC, West BC, Wolff SM. The hypereosinophilic syndrome: analysis of fourteen cases with review of the literature. *Medicine (Baltimore)* 1975; **54**: 1-27 [PMID: 1090795]
2 **Klion AD**, Bochner BS, Gleich GJ, Nutman TB, Rothenberg ME, Simon HU, Wechsler ME, Weller PF; The Hypereosinophilic Syndromes Working Group. Approaches to the treatment of hypereosinophilic syndromes: a workshop summary report. *J Allergy Clin Immunol* 2006; **117**: 1292-1302 [PMID: 16750989 DOI: 10.1016/j.jaci.2006.02.042]
3 **Simon HU**, Rothenberg ME, Bochner BS, Weller PF, Wardlaw AJ, Wechsler ME, Rosenwasser LJ, Roufosse F, Gleich GJ, Klion AD. Refining the definition of hypereosinophilic syndrome. *J Allergy Clin Immunol* 2010; **126**: 45-49 [PMID: 20639008 DOI: 10.1016/j.jaci.2010.03.042]
4 **Teasdale G**, Jennett B. Assessment of coma and impaired consciousness. A practical scale. *Lancet* 1974; **2**: 81-84 [PMID: 4136544 DOI: 10.1016/s0140-6736(74)91639-0]
5 **Berrut G**, Hommet C, Beauchet O. [Loss of consciousness in the elderly]. *Psychol Neuropsychiatr Vieil* 2007; **5**: 101-120 [PMID: 17556217]
6 **Collins NS**, Shapiro RA, Ramsay RE. Elders with epilepsy. *Med Clin North Am* 2006; **90**: 945-966 [PMID: 16962851 DOI: 10.1016/j.mcna.2006.06.002]
7 **Chamberlain JM**, Kapur J, Shinnar S, Elm J, Holsti M, Babcock L, Rogers A, Barsan W, Cloyd J, Lowenstein D, Bleck TP, Conwit R, Meinzer C, Cock H, Fountain NB, Underwood E, Connor JT, Silbergleit R; Neurological Emergencies Treatment Trials; Pediatric Emergency Care Applied Research Network investigators. Efficacy of levetiracetam, fosphenytoin, and valproate for established status epilepticus by age group (ESETT): a double-blind, responsive-adaptive, randomised controlled trial. *Lancet* 2020; **395**: 1217-1224 [PMID: 32203691 DOI: 10.1016/S0140-6736(20)30611-5]
8 **Trivioli G**, Terrier B, Vaglio A. Eosinophilic granulomatosis with polyangiitis: understanding the disease and its management. *Rheumatology (Oxford)* 2020; **59**: iii84-iii94 [PMID: 32348510 DOI: 10.1093/rheumatology/kez570]
9 **de Boysson H**, Guillevin L. Polyarteritis Nodosa Neurologic Manifestations. *Neurol Clin* 2019; **37**: 345-357 [PMID: 30952413 DOI: 10.1016/j.ncl.2019.01.007]
10 **De Virgilio A**, Greco A, Magliulo G, Gallo A, Ruoppolo G, Conte M, Martellucci S, de Vincentiis M. Polyarteritis nodosa: A contemporary overview. *Autoimmun Rev* 2016; **15**: 564-570 [PMID: 26884100 DOI: 10.1016/j.autrev.2016.02.015]
11 **Greenberg SM**, Charidimou A. Diagnosis of Cerebral Amyloid Angiopathy: Evolution of the Boston Criteria. *Stroke* 2018; **49**: 491-497 [PMID: 29335334 DOI: 10.1161/STROKEAHA.117.016990]
12 **Silek H**, Erbas B. Cerebral Amyloid Angiopathy Related Inflammation Presenting as Steroid Responsive Brain Mass. *Turk Neurosurg* 2020; **30**: 629-631 [PMID: 30649812 DOI: 10.5137/1019-5149.JTN.22592-18.3]
13 **Ii Y**, Tomimoto H. [Inflammatory cerebral amyloid angiopathy]. *Brain Nerve* 2015; **67**: 275-285 [PMID: 25846442 DOI: 10.11477/mf.1416200132]

World Journal of Clinical Cases

Submit a Manuscript: https://www.f6publishing.com

World J Clin Cases 2022 June 26; 10(18): 6333-6337

DOI: 10.12998/wjcc.v10.i18.6333

ISSN 2307-8960 (online)

CASE REPORT

Creutzfeldt-Jakob disease presenting with bilateral hearing loss: A case report

Seunghee Na, Se A Lee, Jong Dae Lee, Eek-Sung Lee, Tae-Kyeong Lee

Specialty type: Clinical neurology

Provenance and peer review: Unsolicited article; Externally peer reviewed.

Peer-review model: Single blind

Peer-review report's scientific quality classification

Grade A (Excellent): A
Grade B (Very good): B
Grade C (Good): 0
Grade D (Fair): 0
Grade E (Poor): 0

P-Reviewer: Wang YJ, China; Xie Q, China

Received: February 9, 2022
Peer-review started: February 9, 2022
First decision: March 23, 2022
Revised: March 24, 2022
Accepted: April 22, 2022
Article in press: April 22, 2022
Published online: June 26, 2022

Seunghee Na, Department of Neurology, Incheon St. Mary's Hospital, The Catholic University of Korea, Incheon 21431, South Korea

Se A Lee, Jong Dae Lee, Department of Otorhinolaryngology-Head and Neck Surgery, Soonchunhyang University Bucheon Hospital, Bucheon 14584, South Korea

Eek-Sung Lee, Tae-Kyeong Lee, Department of Neurology, Soonchunhyang University Bucheon Hospital, Bucheon 14584, South Korea

Corresponding author: Eek-Sung Lee, MD, PhD, Assistant Professor, Department of Neurology, Soonchunhyang University Bucheon Hospital, 170, Jomaru-ro, Bucheon 14584, South Korea. eeksung@schmc.ac.kr

Abstract

BACKGROUND

Sporadic Creutzfeldt-Jakob disease (sCJD) is a prion disease characterized as a fatal transmissible neurodegenerative disorder. Dizziness is often the first presenting symptom of sCJD, but hearing loss as an early manifestation is very rare.

CASE SUMMARY

A 76-year-old man presented with bilateral sudden hearing impairment and dizziness for 10 d. He was taking medications for hypertension and diabetes. He denied any difficulty with activities of daily living or hearing impairment before the onset of symptoms. Pure tone audiometry showed bilateral severe hearing impairment. Brain magnetic resonance imaging (MRI) and laboratory tests were within normal limits. Given his diagnosis of sudden sensory hearing loss, the patient received corticosteroid treatment but it was ineffective. Two weeks later, he complained of aggravated gait impairment, disorientation, and cognitive impairment. Repeat brain MRI showed diffuse cortical high signal intensities on diffusion-weighted imaging. In cerebrospinal fluid analysis, the real-time quaking-induced conversion assay was positive, and 14-3-3 protein was detected in the by western blotting. Considering all the data, we diagnosed probable sCJD, and the patient's symptoms rapidly progressed into akinetic mutism.

CONCLUSION

For patients with abrupt bilateral hearing impairment, especially in the elderly, various differential diagnoses, including sCJD, should be considered.

Key Words: Case report; Creutzfeldt-Jakob disease; Bilateral hearing loss; Diffusion-

weighted imaging; Real-time quaking-induced conversion assay

©The Author(s) 2022. Published by Baishideng Publishing Group Inc. All rights reserved.

Core Tip: Hearing impairment as an initial manifestation of Creutzfeldt-Jakob disease is rare. However, it should be regarded as a differential diagnosis in an elderly patient with bilateral hearing impairment unresponsive to standard corticosteroid treatment. Repeat brain imaging including diffusion-weighted imaging and cerebrospinal fluid analysis will be helpful for diagnosis.

Citation: Na S, Lee SA, Lee JD, Lee ES, Lee TK. Creutzfeldt-Jakob disease presenting with bilateral hearing loss: A case report. *World J Clin Cases* 2022; 10(18): 6333-6337
URL: https://www.wjgnet.com/2307-8960/full/v10/i18/6333.htm
DOI: https://dx.doi.org/10.12998/wjcc.v10.i18.6333

INTRODUCTION

Sporadic Creutzfeldt-Jakob disease (sCJD) is a prion disease characterized as a fatal transmissible neurodegenerative disorder[1]. The key features of sCJD are rapidly progressive dementia and diverse symptoms including myoclonus, pyramidal and extrapyramidal symptoms, cerebellar disturbance, visual symptoms, and akinetic mutism. Among them, it is known that the most commonly reported presenting symptom is cognitive decline. In other presentations, dizziness is also often the first presenting symptom of sCJD, but hearing loss as an early manifestation is very rare[2]. Herein, we report a case of acute bilateral sensorineural hearing loss as the first manifestation of sCJD.

CASE PRESENTATION

Chief complaints

A 76-year-old man presented with bilateral sudden hearing impairment and dizziness for 10 d.

History of present illness

The hearing impairment first developed on the left side and then rapidly progressed to bilateral. He also reported dizziness that was aggravated by positional changes and accompanied by a slight gait imbalance, but he could walk without assistance.

History of past illness

He was taking medications for hypertension and diabetes for over ten years. He denied any difficulty with activities of daily living or hearing impairment before the onset of symptoms.

Personal and family history

No special history of personal and family.

Physical examination

The patient revealed no spontaneous nystagmus or gaze-evoked nystagmus. The bedside head impulse test was unremarkable. The other cranial nerves were unremarkable, and there was no limb ataxia.

Laboratory examinations

Laboratory tests including routine blood tests, autoimmune studies, thyroid function tests, and antibodies of the paraneoplastic syndrome were unremarkable except for an HbA1c of 8.1% and hyperglycemia. Pure tone audiometry (PTA) showed bilateral severe hearing impairment (Figure 1).

Imaging examinations

Brain magnetic resonance imaging (MRI) was within normal limits (Figure 2A).

Further diagnostic work-up

Given his diagnosis of sudden sensory hearing loss, the patient received corticosteroid treatment (prednisolone 60 mg/d for 10 d and tapering) but it was ineffective. Two weeks later, however, he complained of aggravated gait impairment, word-finding difficulty, disorientation, and cognitive

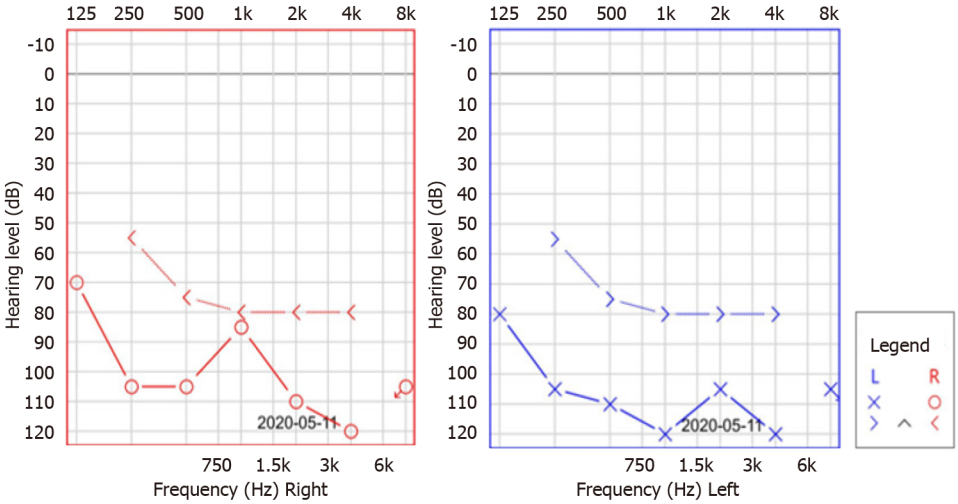

DOI: 10.12998/wjcc.v10.i18.6333 **Copyright** ©The Author(s) 2022.

Figure 1 Pure tone audiometry. Pure tone audiometry revealed severe bilateral low- and high-frequency hearing loss.

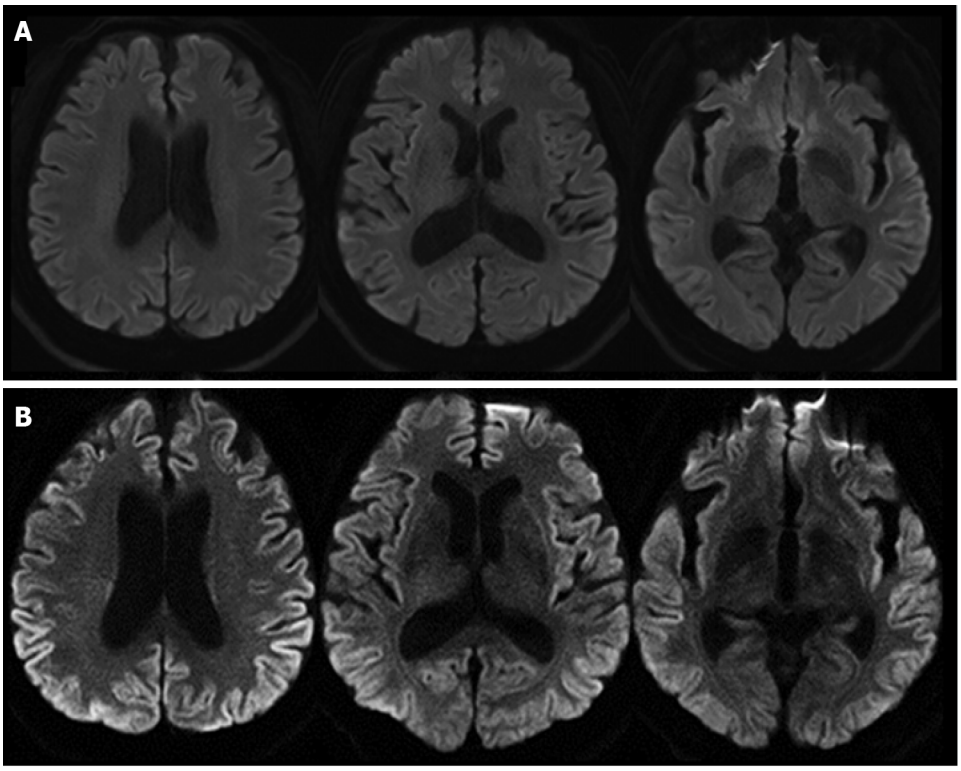

DOI: 10.12998/wjcc.v10.i18.6333 **Copyright** ©The Author(s) 2022.

Figure 2 Findings of brain magnetic resonance imaging. A: The initial brain magnetic resonance imaging (MRI). The initial brain diffusion-weighted imaging was unremarkable; B: The follow-up brain MRI. The follow-up brain diffusion-weighted imaging showed high signal intensities in the bilateral frontal, temporal, parietal, and occipital cortices.

impairment. Repeat brain MRI showed high signal intensities in the frontal, temporal, parietal, and occipital cortices on diffusion-weighted imaging (Figure 2B). Cerebrospinal fluid (CSF) analysis revealed normal concentrations of protein and glucose without pleocytosis. However, the real-time quaking-induced conversion (RT-QuIC) assay was positive, and 14-3-3 protein was detected in the CSF by western blotting.

FINAL DIAGNOSIS

Considering all the data, we diagnosed probable sCJD. The amended diagnostic criteria added that the combination of cognitive decline, positive CSF RT-QuIC, and one or more typical CJD symptoms can draw the diagnosis of probable sCJD[3]. Because he had never undertaken neurosurgery dealing with a dura mater and the genetic analysis revealed that there was no mutation or polymorphism of the prion gene, we excluded the possibility of familial CJD or iatrogenic CJD. Moreover, our patient revealed a positive RT-QuIC test and met the criteria of probable sCJD.

TREATMENT

Because of the characteristics of sCJD, the intractable rapidly progressive dementia[1], he received conservative care.

OUTCOME AND FOLLOW-UP

The patient's symptoms rapidly progressed into akinetic mutism within only two months after the onset of bilateral hearing impairment.

DISCUSSION

This patient presented with an abrupt onset of bilateral hearing impairment and dizziness as the first manifestation of sCJD. Although he only complained of otologic symptoms and was diagnosed initially with bilateral sensorineural hearing loss, the patient then developed additional neurologic symptoms including cognitive decline and prominent gait imbalance, which rapidly progressed. The amended diagnostic criteria of sCJD area that the combination of positive CSF RT-QuIC and progressive cognitive impairment or any of typical CJD symptoms can draw the diagnosis of probable sCJD[3]. Our patient revealed a positive RT-QuIC test and met the criteria of probable sCJD. The possibilities of familial or iatrogenic CJD were excluded because there was no mutation or polymorphism of the prion gene and he had no history of epidemiological evidence. Although the etiology of sCJD has been unknown, many researchers assumed that the prion disease might be initiated by the stochastic misfolded cellular prion protein or mutations in the prion protein gene at ongoing neurogenesis areas[4].

Hearing impairment as an early symptom of sCJD has been described in a few reports[5,6]. Those patients were elderly, older than 65 years, and first complained of only suddenly developed bilateral hearing impairment and subjective unsteadiness. Our patient's hearing loss were also bilateral and unresponsive to steroid treatment. Postmortem studies in sCJD have revealed that the prion protein deposition in the brainstem is symmetrical and starts in the early stage of sCJD[7]. These neuropathologic characteristics account for the bilaterality of the hearing impairment in patients with sCJD.

The authors of a previous report conducted a brain MRI at the initial presentation, and it was within normal limit[5]. Our patient showed imaging findings that reflected his complaints and symptoms of sCJD. At his first visit when he complained of only hearing impairment and vague dizziness, the brain MRI was unremarkable. After other symptoms developed, however, repeat brain MRI revealed characteristic high signal intensities of the bilateral cerebral cortices, which were a clue for the diagnosis of sCJD.

Among the presenting symptoms of our patient, the dizziness was nonspecific and vague, but the hearing impairment was abrupt and very severe. Furthermore, the hearing difficulty was broad, from low to high frequency. When a patient with cognitive decline is suspected of having hearing difficulty, an appropriate evaluation is difficult because laboratory tests, such as pure tone audiometry, cannot be obtained without patient cooperation, and an accurate history of onset time and the pattern of the hearing impairment is needed. In sCJD, the most common presenting symptom is cognitive decline[3]. Thus, even if hearing impairment occurs in the early stage of sCJD, evaluations for the presence of hearing symptoms and otologic function under rapidly progressive cognitive decline are difficult. In our patient, however, the history of hearing impairment and the result of PTA were reliable because the patient did not complain of cognitive impairment at presentation.

CONCLUSION

The patient presented with sudden onset hearing impairment and dizziness, followed by progressive cognitive impairment and confusion. Repeat brain MRI revealed characteristic findings of sCJD, and the

RT-QuIC test was positive. For patients with abrupt bilateral hearing impairment, especially in the elderly, various differential diagnoses, including sCJD, should be considered. Moreover, when sCJD is suspected, close follow-up with thorough history taking and neurologic examinations and repeated workups that include brain diffusion-weighted imaging and CSF analysis will be helpful.

FOOTNOTES

Author contributions: Lee ES conceived and designed the study; Lee TK provided supervision; Lee ES and Lee collected the data; Lee SN wrote the first draft of the manuscript; Lee SA and Lee JD edited and contributed to critical revision; and All authors read and approved the final version of the manuscript for submission.

Supported by National Research Foundation of Korea, No. 2019R1C1C1006539.

Informed consent statement: The authors declare that this single case report has been performed in accordance with the ethical standards laid down in the 1964 Declaration of Helsinki.

Conflict-of-interest statement: The authors declare that they have no conflict of interest.

CARE Checklist (2016) statement: The authors have read the CARE Checklist (2016), and the manuscript was prepared and revised according to the CARE Checklist (2016).

Open-Access: This article is an open-access article that was selected by an in-house editor and fully peer-reviewed by external reviewers. It is distributed in accordance with the Creative Commons Attribution NonCommercial (CC BY-NC 4.0) license, which permits others to distribute, remix, adapt, build upon this work non-commercially, and license their derivative works on different terms, provided the original work is properly cited and the use is non-commercial. See: https://creativecommons.org/Licenses/by-nc/4.0/

Country/Territory of origin: South Korea

ORCID number: Seunghee Na 0000-0001-8578-8578; Se A Lee 0000-0002-6263-1903; Jong Dae Lee 0000-0003-2866-9841; Eek-Sung Lee 0000-0003-3517-8207; Tae-Kyeong Lee 0000-0001-6913-4689.

Corresponding Author's Membership in Professional Societies: Korean Neurological Association.

S-Editor: Ma YJ
L-Editor: A
P-Editor: Ma YJ

REFERENCES

1 **Collins SJ**, Lawson VA, Masters CL. Transmissible spongiform encephalopathies. *Lancet* 2004; **363**: 51-61 [PMID: 14723996 DOI: 10.1016/S0140-6736(03)15171-9]
2 **Rabinovici GD**, Wang PN, Levin J, Cook L, Pravdin M, Davis J, DeArmond SJ, Barbaro NM, Martindale J, Miller BL, Geschwind MD. First symptom in sporadic Creutzfeldt-Jakob disease. *Neurology* 2006; **66**: 286-287 [PMID: 16434680 DOI: 10.1212/01.wnl.0000196440.00297.67]
3 **Hermann P**, Laux M, Glatzel M, Matschke J, Knipper T, Goebel S, Treig J, Schulz-Schaeffer W, Cramm M, Schmitz M, Zerr I. Validation and utilization of amended diagnostic criteria in Creutzfeldt-Jakob disease surveillance. *Neurology* 2018; **91**: e331-e338 [PMID: 29934424 DOI: 10.1212/WNL.0000000000005860]
4 **Iacono D**, Ferrari S, Gelati M, Zanusso G, Mariotto S, Monaco S. Sporadic Creutzfeldt-Jakob Disease: Prion Pathology in Medulla Oblongata-Possible Routes of Infection and Host Susceptibility. *Biomed Res Int* 2015; **2015**: 396791 [PMID: 26457299 DOI: 10.1155/2015/396791]
5 **Bigelow DC**, Eisen MD, Yen DM, Saull SC, Solomon D, Schmidt DE. Otolaryngological manifestations of Creutzfeldt-Jakob disease. *Arch Otolaryngol Head Neck Surg* 1998; **124**: 707-710 [PMID: 9639484 DOI: 10.1001/archotol.124.6.707]
6 **Salazar R**, Cerghet M, Ramachandran V. Bilateral hearing loss heralding sporadic Creutzfeldt-Jakob disease: a case report and literature review. *Otol Neurotol* 2014; **35**: 1327-1329 [PMID: 25122149 DOI: 10.1097/MAO.0000000000000485]
7 **Iwasaki Y**, Hashizume Y, Yoshida M, Kitamoto T, Sobue G. Neuropathologic characteristics of brainstem lesions in sporadic Creutzfeldt-Jakob disease. *Acta Neuropathol* 2005; **109**: 557-566 [PMID: 15933870 DOI: 10.1007/s00401-005-0981-0]

World Journal of Clinical Cases

Submit a Manuscript: https://www.f6publishing.com

World J Clin Cases 2022 June 26; 10(18): 6338-6340

DOI: 10.12998/wjcc.v10.i18.6338

ISSN 2307-8960 (online)

LETTER TO THE EDITOR

Stem cells as an option for the treatment of COVID-19

Maria Veronica Cuevas-González, Juan Carlos Cuevas-González

Specialty type: Medicine, research and experimental

Provenance and peer review: Invited article; Externally peer reviewed.

Peer-review model: Single blind

Peer-review report's scientific quality classification

Grade A (Excellent): 0
Grade B (Very good): B
Grade C (Good): C
Grade D (Fair): 0
Grade E (Poor): 0

P-Reviewer: Al-Omari B, United Arab Emirates; Emran TB, Bangladesh

Received: February 6, 2022
Peer-review started: February 6, 2022
First decision: March 23, 2022
Revised: April 1, 2022
Accepted: May 12, 2022
Article in press: May 12, 2022
Published online: June 26, 2022

Maria Veronica Cuevas-González, Institute of Biomedical Sciences, Universidad Autonoma de Ciudad Juarez, Juarez 32310, Chihuahua, Mexico

Juan Carlos Cuevas-González, Institute of Biomedical Sciences, Autonomous University of Ciudad Juárez, Ciudad Juarez 32310, Chihuahua, Mexico

Corresponding author: Juan Carlos Cuevas-González, PhD, Academic Research, Institute of Biomedical Sciences, Autonomous University of Ciudad Juárez, Av. Benjamín Franklin No. 4650, Zona Pronaf Condominio La Plata, Ciudad Juarez 32310, Chihuahua, Mexico. cuevas_gonzalez@hotmail.com

Abstract

The application of stem cells is among the many strategies currently available for the treatment of multiple diseases. Stem cells are characterized as undifferentiated cells that have the ability to differentiate towards multiple lineages and self-renewal, among other attributes. Since the first umbilical cord stem cell transplant for the treatment of Fanconi anemia, the use of stem cells for the treatment of multiple diseases, including coronavirus disease 2019, has increased, showing promising results that require evaluation through research studies that include a longer follow-up time. Therefore, the main objective of this Letter is to provide an update on the use of stem cells in the treatment of severe acute respiratory syndrome coronavirus 2, as well as identify the main challenges and limitations presented by this type of therapy.

Key Words: COVID-19; Stem cells; Multiple diseases; Undifferentiated cells; Appropriate treatment; Cytokines granulocyte-macrophage colony-stimulating factor

©The Author(s) 2022. Published by Baishideng Publishing Group Inc. All rights reserved.

Core Tip: The stem-cell-derived microvesicles improve the oxygenation conditions of patients, thereby avoiding mechanical oxygenation methods. They demonstrate the ability to modulate the inflammatory response by reducing the levels of proinflammatory cytokines within the first few hours of their intravenous application because these microvesicles contain cytokines, growth factors, and microRNAs, which function as anti-inflammatory agents.

Citation: Cuevas-González MV, Cuevas-González JC. Stem cells as an option for the treatment of COVID-19. *World J Clin Cases* 2022; 10(18): 6338-6340
URL: https://www.wjgnet.com/2307-8960/full/v10/i18/6338.htm
DOI: https://dx.doi.org/10.12998/wjcc.v10.i18.6338

TO THE EDITOR

The current pandemic we are experiencing due to coronavirus disease 2019 (COVID-19) undoubtedly represents a significant challenge for medical and research domains. The magnitude of the disease is evident with millions of lives lost; therefore, the need to find appropriate treatment is urgent. One of the main effects that this type of virus triggers in the human body is the overproduction of pro-inflammatory cytokines [interleukins (ILs)], such as IL-1α/β, IL-2, IL-6, IL-12, interferon (IFN)-α/β/γ, and the anti-tumor necrosis factor (TNF), which cause damage to multiple organs[1]. Zheng[2] published a very interesting study in which they carried out a review of the effects of stem cells in the treatment of severe acute respiratory syndrome coronavirus 2 (SARS-CoV-2). It covers the ability of stem cells to secrete immunomodulatory factors and to improve the adverse effects of respiratory syndrome by reducing fibrosis.

Since the first umbilical cord stem cell transplant for the treatment of Fanconi anemia[3], the use of stem cells for the treatment of multiple diseases, including COVID-19, has increased. Among the various positive effects of stem cells is their capacity for immunoregulation by controlling inflammatory processes. The evidence we have on the use of stem cells for the SARS-CoV-2 infection is from transplanting mesenchymal cord cells by intravenous infusion, in which there is a significant decrease in the cytokines granulocyte-macrophage colony-stimulating factor, IFN-γ, IL-5, IL-6, IL-7, TNF-α, TNF-, platelet-derived growth factor-BB, and RANTES, which in turn decrease the mortality rate and the recovery time of patients[4]. Also, the application of umbilical stem cells has shown—through imaging analysis—that it improves the damage to lung tissue by reducing the solid component, which may be related to fibrosis[5].

Stem cells influence the regulation of cytokine expression by promoting the polarization of macrophages from a pro-inflammatory to an anti-inflammatory phenotype through the production of different types of cytokines, such as prostaglandin E2, TNF-stimulated gene 6 protein lactate, kynurenic acid, and spermidine, all of which in turn have an effect on the adaptive immune system by preventing the activation of effector T cells and promoting the regulation of regulatory T cells[6].

The efficacy and safety of the application of stem-cell-derived microvesicles have also been evaluated, which improve the oxygenation conditions of patients, thereby avoiding mechanical oxygenation methods and demonstrating the ability to modulate the inflammatory response by reducing the levels of proinflammatory cytokines within the first few hours of their intravenous application[7]. This is because these microvesicles contain cytokines, growth factors, and microRNAs that function as anti-inflammatory agents[8].

Although clinical trials have shown that stem-cell-based therapy has great advantages that have a direct impact on the survival of patients with severe disease, there are significant technical and biological limitations with this type of therapy: (1) The methods of obtaining stem cells—for example, those that come from adults; and (2) The quantity and quality of these stem cells depend on the age of the donor and their exposure to environmental stress, which could affect cell proliferation and differentiation[9]. Obtaining stem cells is still a challenge due to the lack of consensus of ethics committees. Another major challenge is the *in vitro* manipulation given to the cells: Keeping them in expansion for long periods of time can limit the characteristics of the cells regarding their regeneration potential and genomic stability[10].

The conclusion of this Letter is that although encouraging results have been obtained, we believe it is necessary to continue with long-term clinical trials that (1) Include a greater number of patients that allow adequate evaluation; (2) Design studies with a longer follow-up time, months or years, which allows an adequate assessment of the possible biological risks of the application of stem cells; and (3) Include the evaluation of molecular studies in order to analyze the gene expression of stem cells within the body These three clinical trial points will aid in obtaining approval from the international institutions that sanction the use of medical drugs (including stem cells).

FOOTNOTES

Author contributions: Cuevas-González MV and Cuevas-González JC wrote the manuscript.

Conflict-of-interest statement: None.

Open-Access: This article is an open-access article that was selected by an in-house editor and fully peer-reviewed by

external reviewers. It is distributed in accordance with the Creative Commons Attribution NonCommercial (CC BY-NC 4.0) license, which permits others to distribute, remix, adapt, build upon this work non-commercially, and license their derivative works on different terms, provided the original work is properly cited and the use is non-commercial. See: https://creativecommons.org/Licenses/by-nc/4.0/

Country/Territory of origin: Mexico

ORCID number: Maria Veronica Cuevas-González 0000-0003-3112-4893; Juan Carlos Cuevas-González 0000-0002-6981-8025.

S-Editor: Fan JR
L-Editor: Filipodia
P-Editor: Fan JR

REFERENCES

1 **Yang B**, Fan J, Huang J, Guo E, Fu Y, Liu S, Xiao R, Liu C, Lu F, Qin T, He C, Wang Z, Qin X, Hu D, You L, Li X, Wang T, Wu P, Chen G, Zhou J, Li K, Sun C. Clinical and molecular characteristics of COVID-19 patients with persistent SARS-CoV-2 infection. *Nat Commun* 2021; **12**: 3501 [PMID: 34108465 DOI: 10.1038/s41467-021-23621-y]
2 **Zheng ZX**. Stem cell therapy: A promising treatment for COVID-19. *World J Clin Cases* 2021; **9**: 11148-11155 [PMID: 35071545 DOI: 10.12998/wjcc.v9.i36.11148]
3 **Charitos IA**, Ballini A, Cantore S, Boccellino M, Di Domenico M, Borsani E, Nocini R, Di Cosola M, Santacroce L, Bottalico L. Stem Cells: A Historical Review about Biological, Religious, and Ethical Issues. *Stem Cells Int* 2021; **2021**: 9978837 [PMID: 34012469 DOI: 10.1155/2021/9978837]
4 **Lanzoni G**, Linetsky E, Correa D, Messinger Cayetano S, Alvarez RA, Kouroupis D, Alvarez Gil A, Poggioli R, Ruiz P, Marttos AC, Hirani K, Bell CA, Kusack H, Rafkin L, Baidal D, Pastewski A, Gawri K, Leñero C, Mantero AMA, Metalonis SW, Wang X, Roque L, Masters B, Kenyon NS, Ginzburg E, Xu X, Tan J, Caplan AI, Glassberg MK, Alejandro R, Ricordi C. Umbilical cord mesenchymal stem cells for COVID-19 acute respiratory distress syndrome: A double-blind, phase 1/2a, randomized controlled trial. *Stem Cells Transl Med* 2021; **10**: 660-673 [PMID: 33400390 DOI: 10.1002/sctm.20-0472]
5 **Shi L**, Huang H, Lu X, Yan X, Jiang X, Xu R, Wang S, Zhang C, Yuan X, Xu Z, Huang L, Fu JL, Li Y, Zhang Y, Yao WQ, Liu T, Song J, Sun L, Yang F, Zhang X, Zhang B, Shi M, Meng F, Song Y, Yu Y, Wen J, Li Q, Mao Q, Maeurer M, Zumla A, Yao C, Xie WF, Wang FS. Effect of human umbilical cord-derived mesenchymal stem cells on lung damage in severe COVID-19 patients: a randomized, double-blind, placebo-controlled phase 2 trial. *Signal Transduct Target Ther* 2021; **6**: 58 [PMID: 33568628 DOI: 10.1038/s41392-021-00488-5]
6 **Shi Y**, Wang Y, Li Q, Liu K, Hou J, Shao C. Immunoregulatory mechanisms of mesenchymal stem and stromal cells in inflammatory diseases. *Nat Rev Nephrol* 2018; **14**: 493-507 [PMID: 29895977 DOI: 10.1038/s41581-018-0023-5]
7 **Sengupta V**, Sengupta S, Lazo A, Woods P, Nolan A, Bremer N. Exosomes Derived from Bone Marrow Mesenchymal Stem Cells as Treatment for Severe COVID-19. *Stem Cells Dev* 2020; **29**: 747-754 [PMID: 32380908 DOI: 10.1089/scd.2020.0080]
8 **Yu B**, Zhang X, Li X. Exosomes derived from mesenchymal stem cells. *Int J Mol Sci* 2014; **15**: 4142-4157 [PMID: 24608926 DOI: 10.3390/ijms15034142]
9 **Brown C**, McKee C, Bakshi S, Walker K, Hakman E, Halassy S, Svinarich D, Dodds R, Govind CK, Chaudhry GR. Mesenchymal stem cells: Cell therapy and regeneration potential. *J Tissue Eng Regen Med* 2019; **13**: 1738-1755 [PMID: 31216380 DOI: 10.1002/term.2914]
10 **Saleh FA**, Ghazzawi J. Clinical update on the use of mesenchymal stem cells in COVID-19. *Am J Transl Res* 2021; **13**: 12195-12205 [PMID: 34956446]



Published by **Baishideng Publishing Group Inc**
7041 Koll Center Parkway, Suite 160, Pleasanton, CA 94566, USA
Telephone: +1-925-3991568
E-mail: bpgoffice@wjgnet.com
Help Desk: https://www.f6publishing.com/helpdesk
https://www.wjgnet.com



© 2022 Baishideng Publishing Group Inc. All rights reserved.